ITTC2024

30TH INTERNATIONAL TOWING TANK CONFERENCE

22–27 SEPTEMBER 2024 | HOBART TASMANIA AUSTRALIA

PROCEEDINGS OF THE 30TH ITTC

VOLUME 1

TABLE OF CONTENTS

VOLUME 1

PREFACE

It is our great pleasure and honour to warmly welcome all the participants to the 30th International Towing Tank Conference in Hobart, Tasmania. As the first meeting was held in 1932, this marks the first time in its 98-year history that the full conference is being held in Australia.

Lutruwita (the name given by it's Indigenous peoples to the land we now call Tasmania) has been inhabited by humans for around 40,000 years. The Indigenous peoples (Palawa kani; Palawa or Pakana) remained predominantly isolated from the rest of Australia when the land-bridge become flooded through sea rise around 8000 years ago. The Indigenous peoples of Lutruwita have for many thousands of years, passed from generation to generation the knowledge of constructing watercraft including bark canoes. Such canoes were used to journey around coastal Tasmania and its offshore islands.

Tasmania is an island state of Australia; located 240 kilometres south of the Australian mainland and is separated from it by the Bass Strait. The state encompasses the main island of Tasmania, the 26th-largest island in the world, and the surrounding 1000 islands. It is Australia's least populous state, with less than 600,000.

Over its long history, the ITTC has addressed both core hydrodynamic business and lead the field in evaluating new innovations. These pioneering technologies hold a direct relevance to Tasmania, being as it is at the forefront of these emerging technologies. Tasmania is a world leader in the building of high-speed aluminium catamaran ferries. Moreover, it is currently building the largest fully-battery operated ferry of its type in the world. Teams in Tasmania are pioneering marine renewable energy research, and its industry is at the forefront of aquaculture implementation. Hobart is the functional hub for pioneering Antarctic and Southern Ocean research; and strives to serve as a world-class gateway for servicing the South. Most well-known in the maritime world, Hobart is the finish line for the world-famous annual Sydney-Hobart yacht race that starts on Boxing Day each year.

The world has thrown many challenges in the last few years, with many institutions having to adapt to the new normal. The ITTC has tackled the same challenges head on. The "Future of the ITTC" working group have worked diligently to consider how the ITTC can meet the needs of its members and to innovate new ways of working. The working groups have each in their own way adapted to the challenges of remote working and digital meetings. I would like to take the opportunity to thank all the committees that have worked so hard and passionately over the last three years; typically undertaken above and beyond their daily duties.

I welcome you to Tasmania and I wish you an enjoyable and rewarding conference.

Tasmania, 12th September 2024

Michael Woodward
Executive Committee - 30th Conference Chairman

CONFERENCE ORGANISING COMMITTEE

MICHAEL WOODWARD

Executive Committee - 30th Conference Chairman

GREGOR MACFARLANE

Australian Maritime College

SECRETARIAT

ESTELLE HUDSON

AMC Search

EDITORS

MICHAEL WOODWARD

Executive Committee - 30th Conference Chairman

GREGOR MACFARLANE

Australian Maritime College

THANK YOU TO OUR SUPPORTERS

UNIVERSITY of TASMANIA
AMC
Australian Maritime College

AMCS
AMC SEARCH

THANK YOU TO OUR SPONSORS

hr wallingford

QUALISYS
Motion Capture Systems

VHT VAN HALTEREN TECHNOLOGIES

30TH INTERNATIONAL TOWING TANK CONFERENCE
22–27 SEPTEMBER 2024 | HOBART TASMANIA AUSTRALIA

REPORT OF THE EXECUTIVE COMMITTEE

1.1 INTRODUCTION

The roles and responsibilities of the Executive Committee are defined in the ITTC Rules and include:

- Implementing the decisions of the Full Conference
- Representing ITTC between Conferences
- Appointing chairmen and members of Technical Committees and Groups
- Replacing members of technical committees and groups as necessary between Conferences
- Accepting new member organisations to the ITTC
- Appointing members of the Advisory Council and reviewing the members on a regular basis
- Appointing the ITTC Secretary
- Managing the finances
- Approving the host, arrangements and associated costs and registration fees for the Conference
- Reporting on its activities to the Full Conference

During the 30th ITTC, the Executive Committee has performed its duties in accordance with the above. The Executive Committee has worked together with the Advisory Council on the presentation of recommendations to be adopted by the 30th Full Conference.

2. OBITUARIES

2.1 Dr. Ulderico Bulgarelli

Dr. Ulderico Bulgarelli, widely known as Paolo, an applied mathematician deeply involved in ship hydrodynamics for part of his life, passed away on January 22nd, 2024.

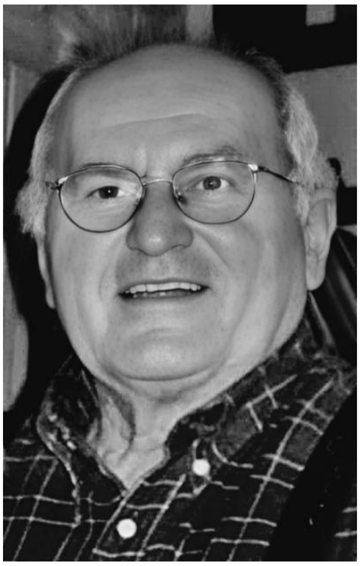

Paolo started his scientific career in the late 1960s, at the “Mauro Picone” Institute for Calculus Applications, National Research Council of Italy (CNR). There he had fruitful cooperation with leading scientists in numerical analysis and scientific computing, followed, in the 1970s, by long term scholarships at prestigious institutions abroad, like the Mathematical Institute of the Polish Academy of Sciences, Warsaw, Poland, the Department of Computer Sciences, University of Wisconsin, Madison, USA, and the Department of Mathematics, University of Texas, Arlington, USA.

In the 1980s, his teaching activity in mathematics extended to fluid mechanics, starting with a course in computational fluid dynamics for PhD students at the University of L'Aquila. It was the initial stage for the development of a mathematical-numerical modelling research group for fluid dynamics that will change the course of ship hydrodynamics in Italy. In fact, with the advice and support of Prof. Renzo Piva, University of Rome La Sapienza, in 1986 Paolo moved to INSEAN, the so-called “Naval Tank”, the national ship model basin. The activities of the institute were then limited to conventional model testing of naval and commercial vessels. There, with little funding by the Ministry of Transport, Paolo started to set up a research group that, in few years, made INSEAN a worldwide recognised leading institution in ship hydrodynamic research: they were "on the map", as David Taylor director, Bill Morgan, once said.

Paolo has long been active in the ITTC community, serving in technical activities (he was a member of the Resistance and Flow Committee in the 19th, 20th and 21st ITTC, of the Resistance Committee in the 22nd ITTC) and on governance bodies (as a member of the Executive Committee and Advisory Council in the 24th, 25th and 26th ITTC).

Paolo retired in 2009. On 1st January 2011, INSEAN became part of the CNR (where it all started fifty years earlier), subsequently taking its current name "Institute of Marine Engineering" (INM).

Paolo was a scientific father for many researchers: he asked for the best and, at the same time, encouraged us to look at the "pieces of the puzzle that remain". He always invited, as Nobel Prize winner Elias Canetti said: "Don't always get to the end. There's a lot in between!".

2.2 Prof. Knut Minsaas

Knut Minsaas was born in Trondheim, Norway, on December 17, 1936. He passed away on March 12, 2022, at the age of 85.

Completing his education in Naval Architecture at the Norwegian University of Science and Technology in 1961, Knut Minsaas conducted his master's thesis at the Ship Model Basin in Trondheim (now SINTEF Ocean), focusing on ducted propellers. The following year, he began his employment at the same institution. Throughout his professional life, Knut Minsaas diligently engaged in research and development concerning resistance and propulsion systems for ships and high-speed vessels.

In 1967, his compendium "Propeller Theory" was published, later recognized as a seminal work within SINTEF Ocean. Subsequently, he contributed to numerous scientific studies and publications. In 1997, Knut Minsaas commenced his tenure as a Professor in ship hydrodynamics at the Norwegian University of Science and Technology, NTNU.

Internationally oriented in his professional endeavors, Knut Minsaas possessed an exceptional grasp of the scientific literature in his field, often reaching far back in time. He actively participated in various international conferences and forums, notably the ITTC. Serving on the Cavitation Committee for the 18th and 19th ITTC (1984-1990) and as a member of the Waterjet Committee for the 21st ITTC (1993-1996).

He demonstrated a unique ability to apply theoretical principles in practical analysis and design. His contributions to the development of hydrofoil catamarans for Norwegian shipyards in the 1980s earned him SINTEF's research award.

Knut Minsaas will be deeply missed, particularly by his family and colleagues at SINTEF Ocean and NTNU. Renowned for his warm-hearted demeanor, ability to spread good cheer, and his unwavering dedication to his profession, he left an indelible mark. A curious individual with a keen interest in new ideas spanning technology, history, and politics, conversations with Knut were always enriching and engaging.

Kourosh Koushan on behalf of SINTEF Ocean

2.3 Prof. Shen Hong-cui

Prof. Shen Hong-cui, former technical director of China Ship Scientific Research Center (CSSRC), passed away at the age of 83 on January 25th 2023.

Born in Shanghai on September 19th 1940, Prof. Shen got his bachelor degree from Shanghai Jiaotong University in 1963. He joined the Ship Model Test Institute of China (later CSSRC) in the same year. He served as technical staff in the towing tank during his early career, and then worked as director of Ship Overall Performance Department of CSSRC. He was promoted to be technical director of CSSRC in 1993. He retired from CSSRC in 2005, but he was soon invited by CSSRC to be an adviser and he devoted himself to CSSRC until December 2022.

Since 1993, Prof. Shen had been a member of the 21st ITTC Resistance & Flow Committee. He joined the 22nd ITTC Executive Committee, representing East Asia. As local organizing committee chair of second half of 22nd ITTC Full Conference (Seoul/Shanghai), he hosted the conference events in China from September 9th to 11th, 1999. It was the first time that ITTC held its full conference in China. As representative of CSSRC in ITTC, he joined the 23rd ITTC Advisory Council.

Prof. Shen Hong-cui was a very famous research scholar in hydrodynamics, especially in resistance and propulsion performance of ships, turbulence boundary layer theory and its application on underwater vehicles. He was granted Special Allowance by the State Council of China. He received seven National Science & Technology Awards. He was also a great tutor who had instructed 18 students for master's and Ph. D degrees.

We extend deepest condolences to Prof. Shen’s family and mourn the loss of a great colleague.

Prof. He Chun-rong on behalf of

China Ship Scientific Research Center

2.4 Antonio Baquero Mayor

Antonio Baquero Mayor died in Madrid the 18th of February of 2023 at the age of 73.

Antonio, graduated of the Universidad Politécnica de Madrid (UPM-ETSIN), has been one of the most significant Naval Architects of the El Pardo Model Basin (CEHIPAR) and a long-time supporter of the ITTC and CRS community; from 1981 to 1990 he was a member of the ITTC Manoeuvring Committee and part of the Cooperative Research Ships (CRS) Steering Group at various periods from 1995 to 2003.

Antonio Baquero was the author of many rigorous technical papers yet easy-to-understand motivated by a strong academical vocation as he always arranged his work at the CEHIPAR tanks with university teaching within the UPM-ETSIN in Madrid and the United States.

Hard worker at CEHIPAR since 1979, he developed his professional activity within several departments, starting as head of the Manoeuvring Basin to later dedicate the main part of his professional life to the Research and Development of Hydrodynamics.

At all the stages of his working life he was committed to promote the passion for hydrodynamics among young naval architects. His greatest legacy is the large group of well-prepared in hydrodynamics professionals he left behind and that will always miss him.

2.5 Jaakko Pylkkänen

Jaakko Pylkkänen was born in Helsinki in 1943 and died on 31st December 2021.

He was M.Sc. in Naval Architecture from Helsinki University of Technology 1968, and in 1977, he defended his doctoral thesis "A Theoretical Study of a Propeller with Skew and Rake, An Application of the Asymptotic Matching Technique."

In 1991, he became professor in hydrodynamics at Helsinki University of Technology, and from 1984 to 2007, he was employed by the VTT Ship Laboratory as Senior Scientist.

In ITTC context, Jaakko was member of the Propulsion Committee of the 20th and 21st ITTC and Chairman of the same committee of the 22nd ITTC.

2.6 David Clarke

Dr David Clarke (BSc, PhD, DSc, Ceng, FRINA)

Dr David Clarke passed away on 29 August 2024 after a short illness in his hometown, South Shields, Northeast England. He was very well-known to many generations of ITTC members and delegates through his sterling contributions as the chairman, secretary and member of various Technical, Advisory and Executive committees.

He was born in 1938 in Sunderland. Following his DLC degree in Loughborough (1960), David obtained his BSc degree in Aeronautics at Imperial College, London (1961), and this was followed by a PhD degree (1976) in the field of Ship Manoeuvring and control from the same university as a part-time student, while he was employed by the British Ship Building Research Association (BSRA) in Wallsend, Newcastle upon Tyne. Before joining the BSRA in 1963, he worked for the Bristol Aircraft Company on the TSR2 project, which was followed by a short spell at Palmers Ship Yard.

Later, in his teaching career at Newcastle University, he obtained a certificate in Teaching and Learning in Higher Education (1997) as well as a distinguished DSc degree (2002) based on his invaluable contributions in the field of manoeuvring and control of ships. In addition to these academic qualifications, Dr Clarke also had a CEng degree (1971), and he was accepted as a Fellow of the RINA (1980).

Dr Clarke joined the BSRA in 1963, where he became the Senior Manager of Hydrodynamics until 1992. During this period, he went through the transformation of the BSRA to British Maritime Technology (BMT Ltd) in 1985 by amalgamation with the National Physical Laboratory (NPL) in Teddington. During his BSRA/BMT employment period, Dr Clarke was responsible for initiating and managing research activities on a wide range of topics, including marine hydrodynamics, structures, and other naval architectural topics. In particular, he carried out research into ship manoeuvring and control over many years. In the same period, together with his team, Dr Clarke initiated the pioneering Analogue Computer-based, real-time and interactive simulation using fully non-linear ship motion equations, which allowed them to conduct more realistic harbour simulations for many major stakeholder shipping companies. In the late 1980s, the analogue simulation system was transformed into a digital one by Dr Clarke's team in BMT, also using pioneering transputer-based digital parallel processing and Ocaml programming language, which led to the development of the well-known REMBRANDT system of BMT in those days. Dr Clarke also took leading roles in chairing several technical committees at IMO (through MEPC) and ITTC (through the Executive, Advisory, Manoeuvring and Symbols & Terminology Committees). He was also the secretary to the Executive Committee of ITTC, with which the School of Marine Science and Technology at Newcastle University was closely involved with the organisation of the 24th ITTC Conference in Edinburgh in September 2005. During his teaching days at Newcastle University, Dr Clarke contributed to lecturing on Marine Dynamics, Ship Structures, Planing Craft and Dynamic Positioning lectures. In the same period and after his retirement, he also lectured on Marine Dynamics at the Naval Architecture and Marine Engineering Department of the University of Strathclyde in Glasgow and Newcastle Universities as a visiting lecturer.

During his teaching career, Dr Clarke conducted pioneering research activities through four years of the national Engineering Physics and Science Research Council (EPSRC) funded managed programme (MOSES project) concerned with the effect of trailing vortices on the calculation of ship stability derivatives. He also made significant contributions to the EU Framework Programmes, especially in manoeuvring and controlling Azimuthing Podded propulsor-driven ships (e.g. through FP5-OPTIPOD and FASTPOD projects) and supervised a number of PhD students in the Newcastle and Strathclyde Universities.

Through his activities in industry and academia, Dr Clarke made profound contributions to the development and progress of the contemporary IMO ship manoeuvring criteria, as well as establishing close collaboration between the ITTC and IMO by preparing the proposal in 2005 for the ITTC to become the non-governmental organisation (NGO) with the observer status to IMO.

There are many people through ITTC, academic institutions, and the maritime industry who will have fond memories of David Clarke for his friendship with his witty character and his invaluable technical contributions to the manoeuvring and control of ships through the legacy of his published work. He is survived by his wife, Elizabeth, his daughters, Helen and Caroline, and his son Simon.

3. COMMITTEE MEMBERSHIP

Membership of the 30th Executive Committee has been the following:

ITTC Association Chairman: Kourosh Koushan, SINTEF Ocean, Norway

Northern Europe representative: Claus D. Simonsen, FORCE Technology, Denmark

Central Europe representative: Janou Hennig, HSVA, Germany

Southern Europe representative: Lanfranco Benedetti, CNR-INM, Italy

Pacific Islands representative: Toru Katayama, Osaka Metropolitan University, Japan

North and West Asia representative: Chunrong He, CSSRC, China

South and East Asia representative: Yonghwan Kim, Seoul National University, Korea

Americas representative: Art Reed, NSWCCD, USA.

Non-voting ex-officio members of the Executive Committee were:

Michael Woodward, Australian Maritime College, Australia, as Chairman of the 30th Conference

Gerhard Strasser, Vienna Model Basin, Austria, as Advisory Council Chairman,

Didier Fréchou, DGA Hydrodynamics, France, as past Chairman,

Aage Damsgaard, FORCE Technology, Denmark, as ITTC Secretary.

4. COMMITTEE MEETINGS

Due to the continued COVID threat, the first three EC meetings were held virtually. Finally, in September 2023, it was again possible to meet physically, in Seoul, Korea, and then in April 2024 in Wageningen, The Netherlands. Further virtual meetings are foreseen before the final physical meeting at the conference in Tasmania September 2024.

The first meeting was held virtually during the 29th Conference. The committee reviewed the actions following the Conference and the ITTC.A General Assembly.

The General Assembly had voted on two changes to the Statutes, the first allowing members not having physical test facilities, the second dividing East Asia into two areas, North and West Asia, and South and East Asia, respectively, and changing the number of Executive Committee members accordingly. The first item was considered to constitute a change of the aims of the Association, which required a quorum of two thirds of the members to be present. As this was not the case, an Extraordinary General Assembly was required to decide on the change. The second item just required that a majority of the members present voted in favour, which was the case.

The General Assembly had elected Kourosh Koushan as chairman of ITTC.A.

The committee appointed Kourosh Koushan as chairman of the Working Group on the Future of ITTC, the continuation of which had been endorsed by the Full Conference.

The ITTC.A Extraordinary General Assembly was held as an Outlook voting in December 2021. 61 members voted, 44 in favour and 17 against the proposed change allowing members not operating physical test facilities.

The second committee meeting was planned to be held in Japan, hosted by NMRI. However, as COVID travel restrictions were not yet lifted everywhere, it was decided to hold a virtual meeting.

Yonghwan Kim was elected Vice Chairman of the Executive Committee.

Two non-experimental organisations had applied for membership of ITTC following the opening for such organisations. The applications were on hold because the criteria for accepting them had not been decided. The committee agreed on these criteria and on creating a membership application form to be used by such organisations.

The WG on the Future of ITTC reported on its activities, including the above-mentioned criteria for membership of non-experimental organisations, the possibility of establishing an ITTC Journal, cooperation with ISO, IMO and classification societies, and payment by non-members for access to ITTC documents.

Five members of Technical Committees had been replaced since the conference.

The effect of sanctions on Russia on work in the Technical Committees was discussed. One out of four committees with Russian members had experienced problems caused by this, and no contact could be established with the Russian AC member. It was decided to await further development.

The Advisory Council Chairman continues to participate in IMO MEPC meetings, and the Executive Committee accepted to cover the associated expenses.

The secretary presented audited accounts for the 29th ITTC secretariat and the status of fee payments for the 30th ITTC. The option to pay the fee annually had been chosen by 17 members. As it increases the administrative burden and bank costs, this number should hopefully not increase.

The 30th Conference arrangements and programme were discussed, as well as the venue for the 31st Conference, which will be held in Central Europe.

The ITTC Secretary announced that after having served for six periods, this period would be his last. The Advisory Council Chairman would send the job description to the AC members and invite candidates.

The third meeting was an intermediate virtual meeting held in February 2023 to catch up on some critical issues.

The performance of the Resistance and Propulsion Committee was a matter of great concern, and possible actions were discussed.

Further progress on the possible ITTC Journal and other ways of publishing ITTC work were presented.

The sanctions on Russia were causing increased impact on Technical Committee work and action might be required in order to avoid too much disruption.

The cooperation with ISSC has not been functioning well, so ITTC has presented a new proposal to ISSC for organising the joint committee. The answer is awaited.

Two candidates for the position as ITTC Secretary had been identified. However, neither of the two met the two fundamental criteria for the ITTC Secretary, i.e. being employed and supported by an Advisory Council member, and having experience with ITTC. No decision was made, and the search will continue.

The Advisory Council Chairman declared that he was willing to serve another period.

The fourth meeting was held physically in Seoul, Korea, hosted by Seoul National University with the support of Hanwha Ocean and Hyundai.

Several members were absent and had asked if they could be represented by a proxy. It was accepted this time, but the Executive Committee decided that proxies shall not be allowed.

The committee discussed a proposal by the AC Working Group on Correlation on further actions to be initiated with the participation of all ITTC members. The committee was authorised to proceed with asking members to test the method for speed/power prediction at different drafts prepared by the Working Group and to develop a guideline. However, for the moment, the method should be kept internal in ITTC.

The problems in the Resistance and Propulsion Committee, now enhanced because of the resignation of the Chairman, were again discussed, and it was endeavoured to find a solution.

On proposal by the Working Group on the Future of ITTC, it was decided that all procedures and guidelines, in addition to being copyrighted, shall include the information for DOI registration. DOI registration will then be followed up during the 31st ITTC.

It was also decided that, in the future, ITTC documents shall not be freely available to non-members. An arrangement with a pay wall shall be organised during the 31st ITTC.

Furthermore, it was decided that a survey shall be performed among ITTC members on the interest in publishing ITTC related work in an ITTC Journal.

ISSC has not responded to ITTC's proposal for organising the future cooperation, so ITTC will terminate the participation in the joint committee and remove any mention of the cooperation from the ITTC website.

Further details on the arrangements for the 30th Conference were presented. The budget and proposed registration fee was accepted by the commission. Area Representatives were asked to identify observers to be invited and send the information to the organisers.

The committee accepted the proposal from Central Europe that the 31st Conference should be hosted by University of Ghent, Belgium.

The Advisory Council proposed John Koch Nielsen, FORCE Technology, Denmark, as the next ITTC Secretary. He will be supported by FORCE Technology in his work, but has no former experience with ITTC. The present ITTC Secretary will make sure that he is properly introduced to the work as secretary and to the functioning of ITTC.

The fifth meeting was held physically in Wageningen, The Netherlands, hosted by MARIN.

Some Technical Committees had reported in their progress reports that they intended to or had already submitted papers to conferences or workshops on subjects related to their work in the Technical Committee. To make it clear that publication of the ITTC work shall first be done at the ITTC Conference, the committee will propose a revision of the ITTC Rules and the ITTC.A Statues regarding this. In addition, this rule shall be included in the Terms of Reference for the committees.

The committee had observed that quite few of the about 35 participants in the AC meeting had participated actively in the discussions. Suggestions were made how to increase the active involvement of the participants.

The subject of an ITTC Journal and publication of ITTC work was again on the agenda. Some committee members mentioned that we should be careful that ITTC was not being seen as an academic organisation by the industry.

The committee reviewed and accepted the structure of Technical Committees for the next period proposed by AC.

The budget for the 31st ITTC was presented and slightly adjusted. Based on this budget, the committee will propose to keep the present membership fee.

Some items were not covered in this meeting, so it was decided to arrange an intermediate meeting to take care of these.

The sixth meeting was held virtually as a TEAMS meeting in May 2024.

The meeting covered the items which were not finished at the previous meeting, and also reviewed the first draft of the EC report to the Conference.

5. COMMITTEE ACTIVITIES

5.1 Revision of ITTC Rules

The committee decided to recommend to the 30th Full Conference to revise the ITTC Rules to clearly define the issues of copyright and publication of work performed in the Technical Committees. In addition, the revisions will resolve some small differences between the ITTC Rules and the ITTC.A Statues.

The present version of the Rules is found as Procedure 1.0-01 in the 2021 version of the Quality Systems Manual, and the proposed revised Rules are included as an appendix in the Proceedings of this Conference.

5.2 Revision of ITTC.A Statutes

As a consequence of the proposed revision of the ITTC Rules, a number of revisions of the ITTC.A Statutes are required.

The proposed revised Statutes are included in Appendixes to the Proceedings of this Conference.

5.3 Appointment of ITTC.A Chairman

The Executive Committee has sent all members the invitation of candidates for the position as Chairman of ITTC.A to be elected at the General Assembly. The deadline for proposing candidates is after the publication of this report.

The present Chairman Prof. Kourosh Koushan, SINTEF Ocean, Norway, is willing to continue.

5.4 Criteria for non-experimental organisations to be member of ITTC

At the 29th Full Conference, it was decided to accept that organisations that do not operate physical experimental facilities could become members of ITTC. The Executive Committee decided that the applicant shall:

- carry out work in support of the designers, builders and operators of ships and marine installations
- document related R&D activity
- work with verification and/or validation and/or collecting full scale data related to ships and marine installations
- be willing to share knowledge and data
- perform related projects as a main part of the business
- document conducting related projects at least for the last 3 years.
- have at least 2 dedicated employees working full or main portion of their time with related projects
- be a liable company or an accredited academic institution
- be in possession of self-developed and or licensed recognized software for analysis and/or simulation in related projects.

5.5 Committees and Tasks of the 31st ITTC

Based on input from the technical committees, AC members, ITTC members and the Executive Committee Working Group on the Future of ITTC, the Advisory Council prepared the document proposing the structure and Terms of Reference of technical committees and groups of the 31st ITTC enclosed as an appendix to the Proceedings of this Conference.

5.6 Changes in ITTC Membership

The following new members of ITTC have been approved during this period (or late last period):

- Technomar, Brazil, as the first non-experimental organisation allowed according to the revised ITTC Rules
- NSTL India
- TCOMS, Singapore.

Membership was terminated for the following:

- University College Cork, Ireland
- Indian Institute of Technology Madras, India
- Technical University Delft, The Netherlands
- Oregon State University, USA.

The membership of Krylov Institute was put on hold due to the sanctions against Russia.

Several members have changed their Designated Representatives. The member information as known by the secretariat on 1st May 2024 is included as an appendix to the Proceedings of this Conference.

The total number of members is 103.

5.7 Changes in Advisory Council Membership

One additional member has been accepted in the Advisory Council, DSME, Korea, later changed to Hanwha Ocean. The Advisory Council now has 40 members.

The membership of Krylov Institute is on hold due to the sanctions on Russia.

5.8 Changes in Technical Committee Membership

The Executive Committee has endorsed a number of changes of membership of the technical committees. An appendix to the Proceedings includes a list of all past and present members of the committees of the 30th ITTC.

Due to the sanctions on Russia, membership of Technical Committees was terminated for all Russian members. The consequence was that some of the tasks given to the Technical Committees could not be performed.

5.9 Advisory Council Membership Review

During this period, approximately half of the Advisory Council members were reviewed using the evaluation form that was revised during the 27th ITTC. All the organisations reviewed were accepted as members.

One member, VTT, Finland, decided to withdraw from the Advisory Council after this period as their model tank facility was being decommissioned.

5.10 ITTC Secretary

As the ITTC Secretary during the past six ITTC periods decided to step down, the Advisory Council invited candidates to take this position. Two candidates were put forward, but one of them later withdrew the candidature. Consequently, the Advisory Council recommended to the Executive Committee to appoint John Koch Nielsen, FORCE Technology, Denmark, as ITTC Secretary.

5.11 ITTC Website

The website is continuously updated with member information and provides links to ITTC Recommended Procedures and Guidelines, Symbols and Terminology, Dictionary, and the Sample QA Manual.

The website furthermore holds the Proceedings of all ITTC Conferences and the Catalogue of Facilities. Under the News menu, you will find the ITTC News, and under Miscellaneous, other relevant information may be found. The menu Benchmark Data holds links to the available benchmark data.

The password protected Member's area holds information for the Executive Committee and Advisory Council and has been very useful for the preparations for and follow-up after the meetings.

5.12 ISBN and ISSN Number on Publications

In 2020, the ITTC Association registered as publisher at the Swiss ISBN Agency. The association bought a quota of 1000 ISBN numbers for 861,60 CHF that can be assigned to digital and printed publications. After publication, a copy of the published document must be submitted to the Swiss National Library.

The request of the ISSN (International Standard Serial Number) assignment for the ITTC proceedings series is in progress.

5.13 DOI Registration of Procedures and Guidelines

As part of the efforts of making ITTC documents better known to the public, the committee decided that all Technical Procedures and Guidelines shall be DOI registered. This implies that they shall identify the authors and include an abstract and, preferably, keywords. The Quality Systems Group has designed a new layout of the documents to accommodate this information.

5.14 IMO Activities

The ITTC AC Chairman attended the following meetings, with travel and hotel costs paid by ITTC:

MEPC 76 (Marine Environment Protection Committee): 10 to 17 June 2021

MEPC 77: 22 to 26 November 2021

MEPC 78: 6 to 10 June 2022

MEPC 79: 12 to 16 December 2022

MEPC 80: 3 to 7 July 2023

The following submissions have been made by ITTC:

MEPC 78/6 Updated ITTC Recommended Procedures and Guidelines concerning the determination and verification of EEDI

MEPC 79/6 Draft amendments to the 2014 Guidelines on survey and certification of the Energy Efficiency Design Index (EEDI)

SDC 8/INF.2 Physical background and mathematical models for stability failures of the Second-Generation Intact Stability Criteria (prepared by the Stability in Waves Committee)

SDC 10/INF.5 Review of the 2014 Guidelines for the reduction of underwater noise from commercial shipping to address adverse impacts on marine life (MEPC.1/ Circ.833)(2014 Guidelines) and identification of next steps (prepared by the SC on Cavitation and Noise)

SDC 10/INF.7 ITTC support to the trial application of direct stability assessment within the Second-Generation Intact Stability Criteria (prepared by the Stability in Waves Committee)

Several members of ITTC participate via the member states to IMO.

5.15 ISO Activities

The Advisory Council Chairman and the Full Scale Ship Performance Committee has participated actively in the revision of the ISO speed/power sea trial standard 15016.

5.16 IEC Activities

The SC on Ocean Renewable Energy represents ITTC in the liaison with IEC TC 114 in order to harmonise ITTC procedures and guidelines and IEC standards on marine energy conversion systems.

5.17 ITTC Accounts

The final accounts of the 29th ITTC and the projected accounts for the 30th ITTC are shown below. All amounts are in USD. The accounts for the 29th ITTC were checked and approved by the internal auditors Marco Ferrando, University of Genova, and R. U. Franz von Bock und Polach, Technical University of Hamburg.

Account item	30th projected	29th Final
ITTC fee	70,000	85,175
AC fee	120,000	150,150
Financial income	0	2,670
Total income	190,000	237,995
Secretariat hours	110,000	119,621
Secretariat expenses	10,000	4,916
IMO/ISO activities	10,000	17,735
Support to Conference	6,000	6,000
Financial costs	1,500	1,510
Website	2,000	1,981
ITTC Association	15,000	15,093
Total costs	154,500	166,856
Net Result	35,500	71,140
Total equity capital	135,587	100,087

5.18 Budget for 31st ITTC

The proposed budget (in USD) for the 31st ITTC is shown below. The budget is based on the assumption that the ITTC membership fee is kept unchanged 225 USD annually and the additional fee for AC membership is unchanged 1,000 USD annually.

Account item	31st ITTC Budget
ITTC fee	69,525
AC fee	120,000
Financial income	0
Total income	189,525
Secretariat hours	117,000
Secretariat expenses	10,000
IMO/ISO activities	8,000
Support to Conference	6,000
Website	3,000
ITTC Association	10,000
Financial costs	1,500
Miscellaneous costs	15,000
Total costs	170,500
Net Result	19,025

6. RECOMMENDATIONS TO THE FULL CONFERENCE

The Executive Committee recommends the following to the Full Conference:

- Adopt the new and revised procedures and guidelines prepared by the technical committees and group as listed in the report of the Quality Systems Group
- Delete and remove the procedures and guidelines from the ITTC Recommended Procedures and Guidelines, as being obsolete as listed in the report of the Quality Systems Group
- Adopt the revised Register of ITTC Recommended Procedures and Guidelines as prepared by the Quality Systems Group
- Adopt the revised ITTC Rules as reflected in the revised procedure 1.0-01
- Adopt the committee structure and Terms of Reference for the 31st ITTC as presented in the appendix to the Proceedings of this Conference
- Accept the proposed chairs and members of the technical committees and groups
- Accept that the Executive Committee continues the Working Group on the Future of ITTC

- Accept that the Executive Committee pursues the idea of an ITTC Journal and encourages members to publish their work in this
- Accept University of Ghent as host of the 31st ITTC Full Conference and Guillaume Delefortrie as chairman of the conference
- Accept Mr. John Koch Nielsen, FORCE Technology, as ITTC Secretary for the 31st ITTC
- Accept the continued involvement of ITTC in IMO and to support this activity financially
- Accept the formal liaison with ISO and IEC on subjects relevant to ITTC
- Accept the proposed budget for the 31st ITTC and general membership fee of 225 USD annually and an additional fee of 1000 USD annually for Advisory Council members.

7. RECOMMENDATIONS TO THE ITTC.A GENERAL ASSEMBLY

The Executive Committee recommends the following to the ITTC.A General Assembly:

- Adopt the revised Statutes and Articles of ITTC.A
- Accept the person proposed and communicated by the Executive Committee in the invitation to the general Assembly as the next Chairman of the ITTC Association
- Accept internal auditors that will be named at the General Assembly.

30TH INTERNATIONAL TOWING TANK CONFERENCE
22–27 SEPTEMBER 2024 | HOBART TASMANIA AUSTRALIA

REPORT OF THE ADVISORY COUNCIL

ADVISORY COUNCIL

1. MEMBERSHIP AND MEETINGS

The membership of the 30th Advisory Council consisted of 40 organisations. One new organisation, Aker Arctic, Finland, was admitted to the Advisory Council.

Prof. Gerhard Strasser, Vienna Model Basin, was elected Chairman and Prof. Daisuke Kitazawa, University of Tokyo, Vice Chairman. The ITTC Secretary, Mr. Aage Damsgaard, is acting as Secretary of the Advisory Council.

The first meeting was planned to be held in Japan in September 2022, but due to the continued COVID-threat, it was held as a virtual meeting. The focus of the meeting was the review of the progress of the technical committee activities, and the response to the committees. Some of the Technical Committees had apparently had a very slow start, possibly due to the COVID-situation, and special actions were initiated to follow up on these.

AC had initiated a Working Group to investigate the speed/power predictions at different drafts, named the AC WG on Correlation. The group presented a report on their initial findings and were commissioned to continue the work.

The second meeting was held physically in Seoul, Korea, and was attended by representatives of ten out of twelve Technical Committees and Groups in addition to 32 out of 40 AC members. In addition, some of the Area Representatives of EC, which are not AC members, attended the meeting.

The progress of the Technical Committees was reviewed and was in general satisfactory. However, one committee had serious problems, partly due to the resignation of the chairman, and particular attention was given to that committee in order to improve the situation.

The Chairperson of the AC WG on Correlation presented the report on the results of their work and recommendations for further action. A lengthy debate followed, and it was agreed that the WG should develop a test that should be tried by all AC members before a conclusion could be drawn.

Among other subjects discussed was the cooperation with ISSC, which is not working, continuation of the involvement in IMO, and recommendation of the next ITTC Secretary. As there is just one candidate, AC recommends John Koch Nielsen, FORCE Technology, as the next ITTC Secretary.

The third meeting was again a physical meeting hosted by MARIN, The Netherlands. 31 of the 40 AC members attended and the four EC members that are not AC members also attended.

Apart from reviewing the general progress of the technical committees, focus was on the review of the final drafts of technical procedures and guidelines submitted by the committees. In total, approximately 90 new or revised procedures and guidelines were reviewed, and more than half of them were sent back to the committees for further corrections.

The second important item on the agenda was the decision on the structure of committees of the 31st ITTC and preparation of the Terms of Reference (TOR) for these committees. Input to the first draft of the TOR was prepared by the AC Working Groups, but as the meeting had been reduced to 1 ½ days against the usual 2 ½ days, it was not possible to prepare a complete draft for further discussion. Hence, it was decided to convene a TEAMS meeting to review and discuss the TOR. It was also decided that the committees shall not be required to review all technical procedures and guidelines. The TOR shall define clearly which of them must be revised and the committees may recommend which of them they wish to revise. An important decision was that a Group shall be established to resolve overlaps between procedures and guidelines, particularly with respect to description of environmental conditions.

Finally, a lengthy discussion took place over the outcome and recommendations of the AC WG on Correlation, in particular the proposed Guideline on Evaluating Power Ratio between Drafts. The consensus was that review of the guideline was closely linked to performing the test also suggested by the WG, and as just 11 of the AC members had performed that test, it was decided to extend the deadline to end July and arrange a TEAMS meeting mid-August to decide.

The fourth meeting was the virtual meeting to review the draft TOR for the next committees and groups. Approximately 33 persons attended the meeting and many corrections to the second draft of the TOR were suggested. It was decided that further reviews and corrections will be handled by mail communications, and that the final version will be reviewed at the virtual meeting planned for mid-August.

The fifth meeting was the virtual meeting held on 16th August 2024 with two main items on the agenda, viz. finalization of the Terms of Reference for the next committees and conclusion on the work performed by the AC WG on Correlation.

A few changes to the Terms of Reference were agreed, and they can be submitted to the conference organizer.

The procedure for predicting the speed/power curve at different drafts proposed by the AC WG was discussed at length. One solution was to publish it as a draft guideline with a note of concern to be formulated. This will be further discussed at the next AC meeting to be held on the first day of the conference.

The sixth and last meeting of AC will be held at the 30th Conference in Tasmania.

2. ACTIVITIES OF THE ADVISORY COUNCIL

2.1 Kick-off Meeting with Technical Committees

The kick-off meeting with technical committees implemented at the 26th Conference was held as a virtual meeting as the rest of the conference, with participation of the AC Chairman, the ITTC Secretary and the QSG Chairman, and the new TC Chairmen participating in the virtual conference.

2.2 Review of the Work of the Technical Committees and Groups

One of the main tasks of AC is to review the progress of the Technical Committees, partly by reviewing the progress reports submitted by the committees, but in some cases supplemented with direct contact to the committee chairs. Due to the continued COVID situation, some of the committees had a very slow start on their work, but all but one caught up during the second year.

The technical committees and group submitted more than 80 revised or new procedures for review by the Advisory Council and proposed a number of procedures to be deleted. With such a large number of documents, it is evident that keeping deadlines, as well as maintaining a high standard of the procedures is crucial. During this period, more than half of all “final” procedures had to be returned to the committees for further corrections following the last AC review, and some even had to go back to the committees once more. Should the AC review procedures have been taken literally, all these procedures would have been postponed to the next period.

In the review of procedures and guidelines, it became evident that a considerable number of overlaps and inconsistencies exist between different procedure and guidelines dealing with similar subjects, e.g. environmental conditions. In order to try to resolve this, AC decided to propose an Group on Overlap for the next period.

2.3 Advisory Council Working Groups

As in the recent periods, the work of the Advisory Council was organised in five working groups, each dealing specifically with the work of selected committees. This time the distribution of committees between the AC working groups was as shown in the table below.

WG 1	WG 2	WG 3	WG 4
SC on Combined CFD/EFD Methods	Resistance and Propulsion	Manoeuvring	Ocean Engineering
SC Ice	Full Scale Ship Performance	Seakeeping	SC Ocean Renewable Energy
SC Cavitation and Noise	SC Wind Propulsed and Wind Assisted Ships	Stability in Waves	

The work of the Quality Systems Group was monitored by WG 5.

The main responsibilities of the working groups are to review committee progress reports, review procedures and guidelines and define the Terms of Reference for the next committees. In order to use the time at the AC meetings efficiently, the working groups as far as possible perform their review before the meetings. This is of course possible, only, if the documents are submitted timely by the committees. The meetings are then used to consolidate the comments resulting from the review in discussions with the entire AC and preparing responses to the committees.

2.4 ITTC Recommended procedures

A total of about 90 procedures and guidelines were prepared by the committees and group, some new, some with major revisions and most with minor revisions. The report from the Quality Systems Group contains a detailed account of the work with procedures and guidelines.

In addition to the revisions of the contents of the procedures and guidelines, all had a new title page layout, including information required for DOI registration, which is planned to take place during the next period.

The proposed new Register of ITTC Recommended Procedures and Guidelines has been published on the ITTC website.

2.5 Technical Committees for the 31st ITTC

AC reviewed the structure of technical committees and groups and decided that most of the Specialist Committees could be closed and the work be continued in other technical committees. As the combination of resistance and propulsion into one committee had not been a success due to the excessive number of tasks, it was decided to separate them again. Several procedures contain the same subjects with diverging recommendations, so it was decided to form a Group on Overlap to resolve this.

As decided by the 29th Full Conference, there is no longer a distinguishment between the permanent committees and Specialist Committees. They are all named Technical Committees. The following Technical Committees are proposed for the 31st ITTC:

- Resistance
- Propulsion
- Manoeuvring
- Seakeeping
- Ocean Engineering
- Stability in Waves
- Full Scale Ship Performance
- Cavitation and Noise
- Ice
- Wind Powered and Wind Assisted Ships

The following Groups were proposed:

- Quality Systems Group
- Group on Overlap

2.6 Appointment of new ITTC Secretary

The AC Chairman had issued an advertisement to find a new ITTC Secretary to replace Mr. Aage Damsgaard, who had announced his resignation after this period. Two candidates applied, Prof. Marco Ferrando, University of Genova, and Mr. John Koch Nielsen, FORCE Technology. Neither of the two candidates meet the two formal requirements, which are being employed by an AC member and having experience with ITTC.

Later on, Prof. Ferrando withdrew his application as he was assigned to some new duties at the university, that would not allow him to dedicate the required time to the secretary job. Consequently, AC decided to recommend to the EC to propose John Koch Nielsen as the next ITTC Secretary, to be approved by the Full Conference.

2.7 Cooperation with IMO

The Advisory Council, represented by its Chairman, has continued to actively be involved in activities concerning EEDI and GHG-emissions.

3. OFFICERS FOR THE 30TH ITTC ADVISORY COUNCIL

Prof. Gerhard Strasser was reappointed as Chairman for the 31st ITTC Advisory Council and Prof. Daisuke Kitazawa as Vice Chairman.

ITTC2024

30TH INTERNATIONAL TOWING TANK CONFERENCE
22–27 SEPTEMBER 2024 | HOBART TASMANIA AUSTRALIA

REPORT OF THE QUALITY SYSTEMS GROUP

Quality Systems Group

1. INTRODUCTION

1.1 Membership and Meetings

The members of the Quality Systems Group of the 30th ITTC are:

Prof. Marco Ferrando (Chair)
University of Genoa
Via Balbi 5, 16126 Genoa, ITALY

Weimin Chen
Shanghai Ship and Shipping Research Institute (SSSRI)
No. 600, Minsheng Road, Pudong New Area, Shanghai, CHINA

Gregory Grigoropoulos
National Technical University of Athens
9 Heroon Polytechniou, 15773 Zografou
GREECE

Dr. Spyros Hirdaris, CEng FRINA FSNAME
ABS Hellenic SM LLC.
1, Sachtouri & Navarinou Str. | Kallithea, Athens – 176 74 | GREECE

Kwang-Jun Paik
Inha University
2N491, Inha-ro 100, Michuhol-gu, Incheon 22212, ROK

Chengsheng Wu
China Ship Scientific Research Centre (CSSRC)
No. 222, Shanshui East Road, Wuxi City, Jiangsu province, CHINA

Daisuke Kitazawa
University of Tokyo
5-1-5 Kashiwanoha, Kashiwa, Chiba 2778574, JAPAN

Prof. Tahsin Tezdogan
University of Southampton
Boldrewood Campus, Burgess Road
SO16 7QF Southampton, UK

Joel T. Park, Ph. D., FASME (Secretary)
Naval Surface Warfare Center Carderock Division (NSWCCD)
9500 MacArthur Boulevard
Code 852, Bldg. 18, Rm 201F
West Bethesda, MD 20817-5700, USA

Prof. Joel Sales Sena Jr.
LabOceano - Brazilian Ocean Technology Laboratory
Parque Tecnológico do Rio, Rua Paulo Emídio Barbosa, 485 Quadra 7-a, Rio de Janeiro
BRAZIL

Quality Systems Group meetings have been held during the work period:

No in person meetings have been held. The work was performed by video conferences and mail exchange

1.2 Tasks

The recommendations for the work of the Quality Systems Group as given by the 29th ITTC were as follows:

1. During the first six months after the conference:

A) Perform a detailed review of all ITTC Recommended Procedures and Guidelines for compliance with ITTC quality requirements with regard to format, references, symbols, terminology, uncertainty analysis and parameter lists.
B) Either update the procedures in these aspects or cooperate with the relevant committee on these updates.
C) Submit the updated procedures to the Advisory Council (AC) before 31.12.2021.

2. During the first six months after the conference:

A) Perform a detailed review of all uncertainty analysis procedures for compliance with ITTC quality requirements about format, references, symbols, terminology and parameter lists.
B) Check that all uncertainty analysis procedures contain a worked example based on the current versions of model test procedures.
C) Cooperate with the relevant technical committees on updating the procedures, including a worked example.
D) Submit a status report on this task to the Advisory Council before 31.12.2021, updating expected to be completed before 30.06.2022.

3. Review the titles and numbering of technical procedures and propose changes, if any, for approval by the Advisory Council before 31.12.2021.
4. Maintain the Register of ITTC Recommended Procedures and Guidelines.
5. Introduce New Uncertainty Analyses Guidelines to include data anomalies in Machine Learning Algorithms for Autonomous and Intelligent ships.
6. Observe the development or revision of ISO Standards regarding Quality Control.
7. Update the ITTC Symbols and Terminology List.
8. Update the Uncertainty Analysis section of the Symbols & Terminology List.
9. Update the ITTC Dictionary of Hydromechanics.
10. Expand the content of current ITTC dictionary version, considering CFD, MASS, etc.
11. Support the technical committees dealing with stochastic processes with guidance on development, revision, and update of procedures for the inclusion of confidence bands on their computational and experimental results.
12. Observe BIPM/JCGM standards for uncertainty analysis, in particular the uncertainty analysis terminology.
13. Review developments in metrology theory and uncertainty analysis and issue appropriate procedures.
14. Setup an effective way to collect benchmark data.
15. Upload all the collected and verified benchmark data into the ITTC benchmark data repository.
16. Liaise with relevant technical committees to complete a questionnaire about the demand and use of benchmarks, not to be limited to model scale.
17. Cooperate with technical committees to establish the ITTC benchmarks, including definition, raw data, data format, etc.

18. Prepare a procedure on the internal calibration of steel rulers or a practical way to check length measurement.

2. PERFORMED TASKS

2.1 Perform a detailed review of all ITTC Recommended Procedures and Guidelines for compliance with ITTC quality requirements with regard to format, references, symbols, terminology, uncertainty analysis and parameter lists.

A detailed review of the documents under the paragraph 7.5 Process Control of the Quality Systems Manual - Version 2021 has been undertaken.

114 documents have been analysed and checked against procedure 4.2.3-01-01 Guide for the Preparation of ITTC Recommended Procedures.

Procedure 4.2.3-01-01 prescribed a rigid scheme for ITTC Procedures.

The outcome of the review is produced in detail in Appendix A. and summarized as follows:

No. of documents	Structure of documents
14	slightly different
65	different
35	strongly different

and <u>not a single document is fully compliant with the prescribed structure</u>.

Following this, the AC decided to modify procedure 4.2.3-01-01 Guide for the Preparation of ITTC Recommended Procedures.

AC decided also that a complete revision of all procedures and guidelines to follow the ITTC standard would not be possible this term. It will be part of the Terms of Reference for the next term.

As regards Procedures/guidelines missing the Parameters/Symbols paragraph AC decided to ask the concerned committees to fill in missing symbols in this term.

2.2 Perform a detailed review of all uncertainty analysis procedures for compliance with ITTC quality requirements about format, references, symbols, terminology and parameter lists.

A detailed review of the uncertainty analysis procedures under the paragraph 7.5 Process Control of the Quality Systems Manual - Version 2021 has been undertaken.

The elements of the review included the following six items:

- Format
- References
- Terminology
- Symbols
- Parameters List
- Example

A total of 113 procedures was reviewed and a summary is included in Appendix B. . Three of the six items (Example, Reference, and Symbol) are included as columns in the appendix. Additional discussion is in the Comment column.

2.3 Review the titles and numbering of technical procedures and propose changes, if any, for approval by the Advisory Council before 31.12.2021.

The review of numbering, titles, and classification of the documents under the paragraph 7.5 Process Control of the Quality Systems Manual - Version 2021 has been undertaken.

Procedures in the following table were found to have a wrong classification since their content is rather a Guideline than a Procedure.

7.5-02-01-03	P	Fresh Water and Seawater Properties
7.5-02-05-04.1	P	Excerpt of ISO 2631, Seasickness and Fatigue
7.5-03-02-02	P	Benchmark Database for CFD Validation for Resistance and Propulsion

Following this their classification has been changed.

As regards Procedure

7.5-02-05-05	P	Evaluation and Documentation of HSMV

the document is a rather a Guideline than a Procedure and its classification has been changed. The name was misleading and has been changed into: Evaluation and Documentation of High-Speed Marine Vehicle (HSMV) Manoeuvrability

Procedure

7.5-02-05-06	P	HSMV Structural Loads

had a misleading name that has been changed into: High-Speed Marine Vehicle (HSMV) Model Tests for Prediction of Structural Loads

The AC concurred on the need to implement the proposed changes that are being finalised during this conference.

The Resistance and Propulsion committee suggested that guideline 7.5-02-03-02.5 Experimental Wake Scaling Methods could be renamed "Experimental Wake Scaling Methods for a Cavitation Test" and renumbered to sit within the 7.5-02-03-03 Cavitation section.

The suggestion was accepted and a new guideline 7.5-02-03-03.10 Experimental Wake Scaling Methods for a Cavitation Test has been added to the Register.

2.4 Maintain the Register of ITTC Recommended Procedures and Guidelines.

During the second meeting the Advisory Council decided that on the front page of all ITTC Recommended Procedures and Guidelines there should be a remark regarding copyright. Additional to this, there should be provided a placeholder for the DOI Number.

Following this request the front page of Procedures/Guidelines has been updated and substituted to the existing one in most of the updated documents.

Accordingly, also procedure 4.2.3-01-01 Guide for the Preparation of ITTC Recommended Procedures and Work instruction 4.2.3-01-03 Work Instruction for Formatting ITTC Recommended Procedures have been updated.

As an example of the new format requirements application Guideline 7.5-02-01-03 Fresh Water and Seawater Properties has been updated.

The revision of the Manual of ITTC Recommended Procedures and Guidelines included 81 documents:

- 2 existing procedures were deleted.
- 7 new Procedures/Guidelines have been approved.
- 72 existing procedures have been reviewed or updated.
- 34 cover pages have been updated to the new format.
- Procedures 7.5-02-02-01 Resistance Tests and 7.5-02-03-01.4 1978 ITTC Performance Prediction Method have been corrected for small typographic errors.

The table of "Revision Outcomes" is illustrated in Appendix C.

2.5 Introduce New Uncertainty Analyses Guidelines to include data anomalies in

Machine Learning Algorithms for Autonomous and Intelligent ships.

Task 5 has not been performed. This task was proposed by QSG following a suggestion of Ahmed Derradji-Aouat, the only QSG member with the relevant expertise. No member of the current QSG possess the required knowledge and AC agreed to postpone this task.

2.6 Observe the development or revision of ISO Standards regarding Quality Control.

The member of the QCG GG organized the 42nd ISO/TC8 Plenary Meeting in Athens during September 18-22, 2023. The active Sub-Committees (SC) and Working Groups (WG) and their context within ISO/TC8 are listed in the following two tables (the published standards of the SCs are given in parentheses):

SC1	Maritime Safety (56)
SC2	Marine Environment Protection (32)
SC3	Piping and Machinery (57)
SC4	Outfitting and Deck Machinery (80)
SC6	Navigation and Ship Operations (42)
SC7	Inland Navigation Vessels (34)
SC8	Ship Design (66)
SC11	Intermodal & Short Sea Shipping (8)
SC12	Large Yachts (12)
SC13	Marine Technology (15)
SC25	Maritime GHG reduction (4)

GHG: Greenhouse gas

WG3	Special Offshore Structures and Support Vessels
WG4	Maritime Security
WG6	Ship Recycling
WG8	Liquid and Gas Fuelled Vessels
WG10	Smart Shipping
WG11	Dredger
WG12	Aquatic Nuisance Species
WG14	Maritime Education and Training

During this meeting the development trends of maritime standards were discussed by representative of various stakeholders (shipowners, class societies, shipbuilders). Reduction of polluting emissions, alternative fuels, sustainable energy resources and automation affect directly ship operation. To this goal standards for the following items must be developed or updated:

- Alternative fuels (biofuels, synthetic fuels, green fuels, hydrogen, ammonia, methanol)
- Carbon capture on board
- Transportation of CO_2, or its transformation to other substances.
- Transportation of H_2, NH_3 and biofuels.
- Use of various Energy Saving Devices.
- Air-Assisted Propulsion (sails, kite, Flettner rotors)
- Alternative auxiliary propulsion devices (flapping foils, ducts etc.)
- Digitalization and onboard information
- AI-driven operations onboard
- Cyber-security in data handling and transfer
- Electrification in ship operation

- Other ISO/TCs of interest to ITTC are:
  - ISO/TC188 Small Craft (97 published standards; 14 of them refer on personal safety equipment)
  - ISO/TC204 Intelligent Transport Systems (340 published standards)
  - ISO /TC43 Acoustics (221 published standards)
  - ISO/TC067 Materials, equipment and offshore structures for petroleum, petrochemical and natural gas industries (203 published standards; 22 of them refer to Offshore structures and 6 to Arctic operations)

Finally, an ongoing discussion is occurring in the ISO/TC8/SC6/WG17 enhanced by representatives from ITTC for updating ISO15016:2015 on Speed/Power Trials Procedure & Analysis.

2.7 Update the ITTC Symbols and Terminology List.

During meeting 30:2 the Advisory Council decided that additional to the symbols in the symbols list also acronyms can be given. To this effect QSG has been requested to add a relevant column in the Symbols and Terminology List replacing the existing column named Computer Symbol.

An acronyms list is incompatible with the table format in ITTC (2021a). A separate table of acronyms has been prepared for ITTC (2021a):

Acronym	Definition
AC	Advisory Council
EC	Executive Council
BIPM	Bureau International des Poids et Mesures
CFD	Computational fluid dynamics
EFD	Experimental fluid dynamics
ESD	Energy Saving Device
GUM	Guide to the expression of Uncertainty in Measurement
HSMV	High-speed marine vehicle
IMO	International Maritime Organization
ISO	International Organization for Standardization
JCGM	Joint Committee for Guides in Metrology
JCGM-WG1	JCGM Working Group 1
JCGM-WG2	JCGM Working Group 2
LDV	Laser Doppler velocimetry
MSC	Marine Safety Committee
NMI	National Metrology Institute
PIV	Particle imaging velocimetry
QSG	Quality Systems Group
SPIV	Stereo-PIV
TC	Technical committee
UV	Underwater vehicle
V&V	Verification and validation
VIM	International vocabulary of metrology
VIM	Vortex induced motion
VIV	Vortex induced vibration

A section on verification and validation (V&V) should be added. The V&V equation as provided by ASME (2009) is as follows:

$$E = S - D \tag{1}$$

where E is the validation error, S is the simulation result, and D is the experimental data. The V&V ITTC procedures appear to follow this definition but do not reference ASME (2009). The procedures should be consistent. In some locations the definition is reversed: $E = D - S$. Example V&V ITTC procedures are ITTC (2021b, c) 7.5-03-01-01 and 7.5-03-04-02. ITTC (2021c) 7.5-03-04-02 has been reviewed by QSG for the Manoeuvring Committee.

The equations written using Math Type were transformed into MS Equation format.

2.8 Update the Uncertainty Analysis section of the Symbols & Terminology List.

The uncertainty symbols list is on pages 5 through 12 in section 1.1.1 Uncertainty of ITTC (2021a). This table contains numerous errors and should be replaced with Annex J of JCGM 100:2008. This table has been revised to align with the contents of JCGM 100:2008-Annex J

2.9 Update the ITTC Dictionary of Hydromechanics.

The ITTC structured dictionary and alphabetical dictionary have been reviewed and the following corrections have been made:

The year of the version in the upper right corner was written as 202 or 2017, so it has been corrected to 2021. These dictionaries are updated this year, so finally they are revised to 2024.

Some formulas and variables were written in the old equation editor, so they were rewritten in the new equation editor. Also, some variables have been changed to italics.

Some pages were written in two columns, so they were all changed to one column. The order of some figures has been adjusted accordingly.

Regarding links to figures, the links with misaligned figure numbers and links to different figures have been corrected. In Chapter 9, links to figures have been inserted as in the other chapters.

Some typos and omissions have been corrected.

The descriptions such as "(which see)" and others have been found. They will be removed as extraneous in the future.

2.10 Expand the content of current ITTC dictionary version, considering CFD, MASS, etc.

Explanation of keywords related to Computational Fluid Dynamics (CFD) has been add-ed. Keywords were extracted from 12 CFD-related procedures from 7.5-03-01-01 to 7.5-03-04-02. Keywords explained in other chapters of existing dictionaries were omitted. In the end, 76 keywords were extracted and explained with reference to specialized books on CFD. These keywords are first consolidated into ITTC structured dictionary, and the overall index of titles is updated. It is then integrated into the ITTC alphabetical dictionary.

2.11 Support the technical committees dealing with stochastic processes with guidance on development, revision, and update of procedures for the inclusion of confidence bands on their computational and experimental results.

No request has been received on this topic.

QSG assisted in reviewing procedure 7.5-02-05-03.3, revised by the Resistance and Propulsion Committee, as regard Uncertainty Analysis matters.

QSG also assisted Specialist Committee on Ice about an UA procedure for ice resistance tests.

2.12 Observe BIPM/JCGM standards for uncertainty analysis, in particular the uncertainty analysis terminology.

The international standard for uncertainty analysis is the Guide to the expression of Uncertainty in Measurement or GUM. The GUM is managed by the Joint Committee for Guides in Metrology (JCGM) of the Bureau International des Poids et Mesures (BIPM) in Sèvres, France. The JCGM consists of two working groups. Working Group 1 (WG1) manages the GUM, while Working Group 2 (WG2) manages the International Vocabulary of Metrology (VIM).

The GUM consists of the following six (6) documents with details in the References. The web page for downloading JCGM documents is as follows:
https://www.bipm.org/en/committees/jc/jcgm/publications .

JCGM 100:2008
JCGM 101:2008
JCGM 102:2011
JCGM 106:2012
JCGM GUM-1:2023
JCGM GUM-6:2020

WG1 is in the process of developing two revisions with a new numbering system. The following information is from the WG1 Newsletter dated May 2024. JCGM-1:2023 replaces JCGM 104:2009.

JCGM GUM-5:202x "Guide to the expression of uncertainty in measurement – Part 5: Examples of uncertainty evaluation." A draft is expected by spring 2024.

JCGM GUM-7:202x "Guide to the expression of uncertainty in measurement – Part 7: Propagation of distributions using a Monte

Carlo method." This document will be a re-publication of JCGM 101:2008. An advanced working draft is under discussion.

The JCGM 200:2012 (VIM) is being revised. A draft of the 4th Edition dated July 2023 is being reviewed.

2.13 Review developments in metrology theory and uncertainty analysis and issue appropriate procedures.

New ITTC uncertainty procedures are not provided for this report. A number of journals contain information on metrology and an uncertainty analysis. The number of papers is very large. Summarizing the papers would be a challenge. The following is a list with links to some journals:

1. Metrologia. A journal of BIPM. Volumes 58-60 (2021-2023) has about 16 relevant articles: https://iopscience.iop.org/journal/0026-1394
2. Journal of Verification, Validation, and Uncertainty Quantification. A journal of the American Society of Mechanical Engineers (ASME): https://asmedigitalcollection.asme.org/verification
3. Ocean Engineering. An Elsevier publication: https://www.sciencedirect.com/journal/ocean-engineering

ASME has an annual conference on Verification, Validation, and Uncertainty Quantification (VVUQ). No technical papers are published. The web page for the most recent conference is https://event.asme.org/VandV

2.14 Setup an effective way to collect benchmark data.

2.14.1 Definition

Benchmark model, either physical or numerical, is a standardized model to calibrate the results from model test configuration or numerical simulations. The main significance of Benchmark model is to provide a recognized benchmark for evaluating and comparing the performance and effects of ships at various stages, including design, construction, and operation. It can serve as a foundation for researching and developing new methods, based on validation and verification.

Currently, ITTC is paying more attention on benchmark. "benchmark", the word became common in TOR, and most of the committee has at least one task related to benchmark.

General Terms：All committees shall endeavor to identify benchmark data and submit these to the ITTC Secretary for inclusion in the benchmark data repository on the ITTC website.

Resistance and Propulsion Committee: the committee report should include sections on new benchmark data; conduct a benchmark study.

Manoeuvring Committee: collect the benchmark data

Seakeeping Committee: the committee report should include sections on new benchmark data; organize a benchmark experimental campaign

Ocean Engineering Committee: the committee report should include sections on new benchmark data; develop specifications for a benchmark test, and the benchmark study may also include CFD comparisons

Stability in waves Committee: the committee report should include sections on new benchmark data; continue the identification of benchmark data for validation of stability-in-waves predictions

Full-Scale Ship Performance Committee: the committee report should include sections on new benchmark data; collect full scale data obtained through relevant benchmark tests

Specialist Committee on Ocean Renewable Energy: Assess level of support for a benchmark study of comparisons

Specialist Committee on Cavitation and Noise: Review the currently available CFD benchmark data

Specialist Committee on Ice: continue work on uncertainty analysis including conducting benchmarking study among ice model basins.

Specialist Committee on Combined CFD and EFD Methods: review the outcome of ongoing CFD benchmark campaigns; develop a standard process of performing a CFD benchmark study within ITTC.

2.14.2 Data type

Regarding as the data type, it may combine with two aspects.

The first aspect is related to profession, which includes resistance, propulsion, seakeeping ability, manoeuvrability, cavitation, offshore, etc. All those typically include a complete set of design parameters, such as main dimensions, parameters, body lines, geometry, as well as major equipment and propulsion systems, like main engines, propulsion systems, and steering devices, etc. It also includes a series of data of ship performance which deprived from model test or numerical simulations, as well as sea trail data.

The second aspect is scope. That is international and regional benchmark for different purpose. International benchmarking data, as a second variant of a Korean VLCC KVLCC2, a Korean container ship KCS, a Japan Bulk Carrier JBC are widely used to verify the performance of new measuring system or new simulation method, while regional benchmarking data are normally for specific research or purpose, as Joint industry project. Some results from Joint Industrial Projects (JIP) could also be used widely after authorized.

2.14.3 Data source

At present, the benchmark data can be mainly downloaded from internet.

Some are from international conference and adopted as benchmark data for various validation and verification. Such as KVLCC, KCS, and JBC, are widely used in many international workshops for calibrations.

Some are from specific project or joint industry project, for a certain research purpose, such as the Joint Research Project JORES project [https://jores.net].

All those data could be defined as benchmark.

2.14.4 Sharing mechanism

Benchmark data normally created from international conference and could be acquired for free. While some benchmark data are obtained from business demand with confidential agreement therefore, they could only be shared within a small-scale party. Therefore, an effective sharing mechanism shall be established within ITTC.

2.14.5 Maintenance and support

Furthermore, a specific group is needed to maintain the benchmark. As learned that benchmark repository has already existed in ITTC website, therefore, it is easy for ITTC member to reach the access. Since many committees have the task related to benchmark, the outputs could be shared in a mutual agreed framework.

2.14.6 Conclusions

The establishment of a benchmark requires a clear understanding of the research needs and objectives. After collecting and cleaning data for a particular type of ship, the characteristic parameters and specifications of the benchmark ship are determined. The benchmark ship should possess the typical characteristics of its ship type but should not have specific features assigned by a particular shipbuilder or operator, making it a common standard. Once established, a benchmark ship can be widely used and studied by researchers and ship designers. This process involves accumulating data from relevant water tank tests and numerical simulations.

Currently, lots of research has been performed related with full-scale ships; therefore, to establish a database is essential with full scale data, which is more useful compared with model scale. All the ITTC community have to work on it step by step.

2.14.7 Question

For the future work, since many technical committees are working on benchmark, the data format and data standard shall be established in the first place.

Meanwhile, data collection and classification shall also be paid more attention.

Last but not least, benchmark work needs support from all technical committee. An operational mechanism shall be discussed.

2.15 Upload all the collected and verified benchmark data into the ITTC benchmark data repository.

Two series benchmark data have been investigated, and the data has also been collected.

- Gothenburg 2010 Workshop on Numerical Ship Hydrodynamics was held in Gothenberg on 8-10 December 2010 and the purpose has been to assess the performance of contemporary CFD codes used in hydrodynamic. The addressed designs were:
    - a US combatant DTMB5415 with 5 different cases
    - a Korean container ship KCS with 9 different cases
    - a second variant of a Korean VLCC KVLCC2 with 7 different cases
- Tokyo 2015 Workshop on CFD in Ship Hydrodynamics was held in Tokyo on December 2-4, 2015, with the objective to compare results of state-of-the-art numerical methods for a number of well specified test cases to assess the capabilities of the methods and to find the best way forward. The addressed designs were:
    - Japan Bulk Carrier JBC with 9 different cases
    - KRISO Container Ship KCS with 5 different cases
    - ONR Tumblehome model 5613 ONRT with 3 different cases

All the data is ready, an upload procedure is needed.

Test cases	Series No.	JBC 1	KCS 2	ONRT 3
Calm water： Resistance				
w/o ESD: resistance, sinkage and trim	1	1.1	2.1*	
With ESD: resistance, sinkage and trim	2	1.2		
w/o ESD: time-averaged velocity field, turbulence, wave pattern	3	1.3		
with ESD: time-averaged velocity field, turbulence	4	1.4		
w/o ESD: thrust, torque, sinkage and trim	5	1.5	2.5*	
Calm water: Self-propulsion				
with ESD: thrust, torque, sinkage and trim	6	1.6		
w/o ESD: time-averaged velocity field, turbulence	7	1.7	2.7*	

Test cases	Series No.	JBC 1	KCS 2	ONRT 3
with ESD: time-averaged velocity field, turbulence	8	1.8		
Calm water: Free Self-propulsion				
thrust, torque, sinkage and trim	9			3.9
Regular wave: head waves				
motion response, added resistance	10		2.10	
Regular wave: other headings				
motion response, added resistance	11		2.11	
Regular wave: head waves				
thrust, torque, RPS, motion response, speed loss	12			3.12
Regular wave: other headings				
thrust, torque, RPS, motion response, speed loss	13			3.13

ESD: Energy Saving Device

2.16 Liaise with relevant technical committees to complete a questionnaire about the demand and use of benchmarks, not to be limited to model scale.

In order to investigate the demand and use of benchmark, a questionnaire was issued and sent to the ITTC community to learn about what is focused and what is concerned.

Eight (8) questions are listed in the questionnaire. Herein, the results are summarized.

<u>Kind of benchmark (Demand of the benchmark)</u>

- Question：What are your interests on benchmark data?

Answer: Most of the participants show their interests on benchmark data related with resistance, seakeeping, manoeuvrability, CFD, full scale.

<u>Data type of benchmark (Demand of the benchmark)</u>

- Question：What are your interests on the data type of the benchmark?

Answer: Most of the participants show their interests on raw data, geometry, analysed data, tables. The choice of Mesh and Figures is in second place.

<u>Source of data</u>

- Question: What is the effective and feasible way to collect the benchmark data?

Answer: Colleagues, publications, conference, and internet are all the best choices.

<u>Application of Benchmark</u>

- Question: What is your purpose to use benchmark data?

Answer: Main purpose is to calibrate the model test results and calibrate the CFD results. Comparison of extrapolation method, calibration of geometry and calibration of CFD calculation policy take the second place.

<u>Sharing of benchmark</u>

- Question: What kind of way you like to share the benchmark with others?

Answer: Most participants would like to share on request of independent email or from ITTC benchmark repository. Publications, conference, internet is the second choice.

<u>Data sharing</u>

- Question: What kind of data you like to share with others?

Answer: Analysed data, tables and figures are selected mostly. Raw data, geometry and mesh may not be widely accepted yet.

Sharing of working mechanism

- Question: What is your idea to work with ITTC community to develop benchmark?

Answer: Most of the participants choose to work with TC. Part of them would like to work with AC and liaise with QSG.

Participation to benchmark work

- Question: Would you like to take part in the research work about benchmark?
- Answer: Most of the participants are willing to join such work.

Conclusions:

Almost all the participants show strong interests on the benchmark data.

Lots of participants are concerned with the ITTC repository.

Most of participants would like to work with TC to develop benchmark data.

Most of participants would like to take part in the work related with benchmark data.

2.17 Cooperate with technical committees to establish the ITTC benchmarks, including definition, raw data, data format, etc.

Since most of the TC have their own benchmarking work within TOR, less work could be done by QSG.

Communication between QSG and CFD/EFD has been established and benchmark research has been investigated on bow wave breaking experiments for CFD and EFD. And the essay has been published in 34th Symposium on Naval Hydrodynamics Washington, D.C., June 26 – July 1, 2022, with title "KCS Unsteady Bow Wave Breaking Experiments for Physics and CFD Validation".

2.18 Prepare a procedure on the internal calibration of steel rulers or a practical way to check length measurement.

Work Instructions 7.6-02-01 has been prepared to guide the verification of a new steel ruler or for the verification of a ruler in production or in service.

3. CONCLUSIONS

For the purpose of the format, a complete revision of all procedures and guidelines to follow the ITTC standard is required, with special attention in including the Parameters/Symbols paragraph.

During the second meeting the Advisory Council decided that additional to the symbols in the symbols list also acronyms can be given. Acronyms are not to be in equations. Furthermore, a separate table of acronyms not connected to ITTC Symbols is recommended.

The list of symbols for Uncertainty Analysis should be expanded.

Consideration should be given by the Conference to new emerging technologies in artificial intelligence (such as machine learning techniques) respect to data quality assessment.

Consideration should be given by the Conference to further development of liaison with International Ship and Offshore Structures Congress (ISSC) for the purpose harmonization and common understanding of the state of the art in Uncertainty Analysis.

4. RECOMMENDATIONS TO THE 30TH ITTC

The 30th ITTC Quality Systems Group recommends the following:

Adopt the revised procedures and guidelines and work instructions:

- 4.2.3-01-01 – Guide for the Preparation of ITTC Recommended Procedures
- 4.2.3-01-03 - Work Instruction for Formatting ITTC Recommended Procedures
- 7.5-02-01-03 - Fresh Water and Seawater Properties
- 7.6-02-01 – Verification of Steel Rulers

5. RECOMMENDATIONS FOR FUTURE WORK

1. Maintain the Register of ITTC Recommended Procedures and Guidelines.
2. Introduce New Uncertainty Analyses Guidelines to include data anomalies in Machine Learning Algorithms for Autonomous and Intelligent ships.
3. Observe the development or revision of ISO Standards regarding Quality Control.
4. Update the ITTC Symbols and Terminology List.
5. Harmonize the uncertainty symbols list with Annex J of JCGM 100:2008
6. Update the ITTC Dictionary of Hydromechanics.
7. Support the technical committees dealing with stochastic processes with guidance on development, revision, and update of procedures for the inclusion of confidence bands on their computational and experimental results.
8. Observe BIPM/JCGM standards for uncertainty analysis, in particular the uncertainty analysis terminology.
9. Review developments in metrology theory and uncertainty analysis and issue appropriate procedures.
10. Upload all the collected and verified benchmark data into the ITTC benchmark data repository.
11. Cooperate with technical committees to establish the ITTC benchmarks, including definition, raw data, data format, etc.

6. REFERENCES

ASME, 2009, “Standard for Verification and Validation in Computational Fluid Dynamics and Heat Transfer,” American Society of Mechanical Engineers, New York, ASME V&V 20.

ITTC, 2021a, “ITTC Symbols and Terminology List, Version 2021,” 29th International Towing Tank Conference.

ITTC, 2021b, “Uncertainty Analysis in CFD Verification and Validation, Methodology and Procedures,” Revision 04, 29th International Towing Tank Conference, ITTC 75-03-01-01.

ITTC, 2021c, “Validation and Verification of RAMS Solutions in the Prediction of Manoeuvring Capabilities,” Revision 02, 29th International Towing Tank Conference, ITTC 75-03-04-02.

JCGM 100:2008, “Guide to the expression of uncertainty in measurement, GUM 1995, with minor modifications,” Joint Committee for Guides in Metrology (JCGM), Bureau International des Poids et Mesures (BIPM), Sèvres, France.

JCGM 101:2008, “Evaluation of measurement data — Supplement 1 to the “Guide to the expression of uncertainty in measurement” — Propagation of distributions using a Monte Carlo method,” Joint Committee for Guides in Metrology (JCGM), Bureau International des Poids et Mesures (BIPM), Sèvres, France.

JCGM 102:2011, “Evaluation of measurement data — Supplement 2 to the ‘Guide to the expression of uncertainty in measurement' — Extension to any number of output quantities," Joint Committee for Guides in Metrology (JCGM), Bureau International des Poids et Mesures (BIPM), Sèvres, France.

JCGM 106:2012, "Evaluation of measurement data — The role of measurement uncertainty in conformity assessment," Joint Committee for Guides in Metrology (JCGM), Bureau International des Poids et Mesures (BIPM), Sèvres, France. JCGM GUM-1:2023 "Guide to the expression of uncertainty in measurement – Part 1: Introduction." Publication is anticipated for early 2024.

JCGM GUM-1:2023 "Guide to the expression of uncertainty in measurement – Part 1: Introduction." Joint Committee for Guides in Metrology (JCGM), Bureau International des Poids et Mesures (BIPM), Sèvres, France.

JCGM GUM-6:2020, "Guide to the expression of uncertainty in measurement — Part 6: Developing and using measurement models," Joint Committee for Guides in Metrology (JCGM), Bureau International des Poids et Mesures (BIPM), Sèvres, France.

JCGM 200:2012, "International vocabulary of metrology – Basic and general concepts and associated terms (VIM)," 3rd Edition, Joint Committee for Guides in Metrology (JCGM), Bureau International des Poids et Mesures (BIPM), Sèvres, France.

Appendix A. OUTCOME OF THE REVIEW OF ITTC RECOMMENDED PROCEDURES AND GUIDELINES FOR COMPLIANCE WITH ITTC QUALITY REQUIREMENTS

Number		Title	Effective Date	Revision	§ 1. PURPOSE	§ 2. DESCRIP-TION	§ 3 VALIDATION	§ 4 PARAM/SYM B	§ 5 REFER-ENCES	§ = paragraph NA=Not Appl.
7.5-01		**TEST PREPARATION**								
7.5-01-01		**Ship Models**								
7.5-01-01-01	P	Ship Models	2017	4	√	in § 3	NA	in § 2	in § 4	Structure different
7.5-01-02		**Propeller Models**								
7.5-01-02-01	P	(Terminology and Nomenclature for Propeller Geometry) Deleted	2017	Deleted						
7.5-01-02-02	P	Propeller Model Accuracy	2017	1	√	wrong name	NA	in § 3	√	Structure different
7.5-01-03		**Instrumentation, Calibration**								
7.5-01-03-01	P	Uncertainty Analysis, Instrument Calibration	2017	2	√	in various §	NA	missing	in § 8	Structure **strongly different**
7.5-01-03-02	P	Uncertainty Analysis, Laser Doppler Velocimetry Calibration	2008	0	√	in various §	embedded in text	in § 7	in § 8	Structure **strongly different**
7.5-01-03-03	G	Guideline on the Uncertainty Analysis for Particle Image Velocimetry	2014	1	√	in various §	embedded in text	missing	in § 7	Structure **strongly different**
7.5-01-03-04	G	Benchmark for PIV(2C) and SPIV(3C) setups	2017	1	√	in various §	NA	missing	in § 6	Structure **strongly different**
7.5-02		**TESTING AND EXTRAPOLATION METHODS**								
7.5-02-01		General								
7.5-02-01-01	P	Guide to the Expression of Uncertainty in Experimental Hydrodynamics	2014	2	√	in various §	in various §	√	in § 18	Structure **strongly different**
7.5-02-01-02		(Uncertainty Analysis in EFD, Guidelines for Resistance Towing Tank Tests) Replaced by 7.5-02-02-02	2011	Deleted						
7.5-02-01-03	P	Fresh Water and Seawater Properties	2011	2	wrong name	in various §	in various §	in § 6	√	Structure different
7.5-02-01-04	G	Guideline on Best Practices for the Applications of PIV/SPIV in Towing Tanks and Cavitation Tunnels	2014	0	√	missing	NA	missing/NA	in § 12	Structure **strongly different**

Number		Title	Effective Date	Revision	§ 1. PURPOSE	§ 2. DESCRIP-TION	§ 3 VALIDATION	§ 4 PARAM/SYMB	§ 5 REFER-ENCES	§ = paragraph NA=Not Appl.
7.5-02-01-05	G	(Model-Scale Propeller Cavitation Noise Measurements) Moved to 7.5-02-03-03.9	2021	Deleted						
7.5-02-01-06	P	Determination of a type A uncertainty estimate of a mean value from a single time series measurement	2021	1	√	√	missing	missing	in § 6	Structure different
7.5-02-01-07	G	Guideline to Practical Implementation of Uncertainty Analysis	2021	1	√	NA	NA	missing	in § 7	Structure different
7.5-02-01-08	P	Single Significant Amplitude and Confidence Intervals for Stochastic Processes	2017	0	√	in various §	NA	missing	in § 8	Structure different
7.5-02-02		**Resistance**								
7.5-02-02-01	P	Resistance Tests	2021	5	√	in § 3	in § 4	in § 2	√	Structure different
7.5-02-02-02	G	General Guidelines for Uncertainty Analysis in Resistance Tests	2021	3	√	NA	NA	int § 6	in § 7	Structure different
7.5-02-02-02.1	G	Example for Uncertainty Analysis of Resistance Tests in Towing Tanks	2021	1	√	in various §	NA	missing	in § 6	Structure different
7.5-02-02-02.2	G	Practical Guide for Uncertainty Analysis of Resistance Measurements in Routine Tests	2021	1	√	wrong name	embedded in various §	missing	in § 6	Structure strongly different
7.5-02-02-03	G	Resistance and Propulsion Test and Performance Prediction with Skin Frictional Drag Reduction Techniques	2017	0	√	in various §	NA	in § 2	in § 7	Structure strongly different
7.5-02-02-04		Wave Profile Measurement and Wave Pattern Resistance Analysis	2021	0	√	in § 3	in § 6	in § 2	in § 7	Structure strongly different
7.5-02-03		**Propulsion**								
7.5-02-03-01		**Performance**								
7.5-02-03-01.1	P	Propulsion/ Bollard pull Test	2021	6	√	in § 3	Partly mentioned in § 4	in § 2	√	Structure slightly different
7.5-02-03-01.2	P	(Uncertainty Analysis Example for Propulsion Test) Deleted	2021	Deleted						
7.5-02-03-01.3	P	Podded Propulsor Tests and Extrapolation	2021	2	√	√	NA	missing	√	Structure different
7.5-02-03-01.4	P	1978 ITTC Performance Prediction Method	2021	5	√	√	Full scale data	in § 2.2	in § 4	Structure slightly different
7.5-02-03-01.5	G	Predicting Powering Margins	2017	2	√	in various §	NA	in § 2	√	Structure strongly different
7.5-02-03-01.6	G	Hybrid Contra-Rotating Shaft Pod Propulsors Model Test	2017	1	√	in § 3	Partly mentioned in § 4	in § 2	√	Structure different
7.5-02-03-01.7	P	Performance Prediction Method for Unequally Loaded, Multiple Propeller Vessels	2021	1	√	√	Partly mentioned in § 2	in § 2	in § 4	Structure strongly different

Number		Title	Effective Date	Revision	§ 1. PURPOSE	§ 2. DESCRIP-TION	§ 3 VALIDATION	§ 4 PARAM/SYMB	§ 5 REFER-ENCES	§ = paragraph NA=Not Appl.
7.5-02-03-01.8	G	Scaling Method for ship wake fraction with pre-swirl devices	2021	0	√	√	NA	in § 2	in § 3	Structure **strongly different**
7.5-02-03-02		**Propulsor**								
7.5-02-03-02.1	P	Open Water Test	2021	4	√	in § 3, named procedure	in § 4	in § 2	√	Structure **strongly different**
7.5-02-03-02.2	P	(Uncertainty Analysis, Example for Open Water Test) Deleted	2021	Deleted						
7.5-02-03-02.3	P	Nominal Wake Measurements by LDV, Model Scale Experiments	2014	1	√	in § 3, named differently	NA	in § 2	missing	Structure **strongly different**
7.5-02-03-02.4	P	Nominal Wake Measurement by a 5-Hole Pitot Tube	2011	1	√	in § 4	UA in § 5	in § 2	in § 6	Structure **strongly different**
7.5-02-03-02.5	G	Experimental Wake Scaling Methods	2017	1	√	In various §	in § 7	in § 2	in § 8	Structure **strongly different**
7.5-02-03-03		**Cavitation**								
7.5-02-03-03.1	P	Model-Scale Cavitation Test	2017	4	√	wrong name	in § 4	in § 3	missing	Structure **different**
7.5-02-03-03.2	P	Description of Cavitation Appearances	2014	2	√	wrong name	in § 4	in § 3	missing	Structure **different**
7.5-02-03-03.3	P	Cavitation Induced Pressure Fluctuations Model Scale Experiments	2014	5	√	wrong name	in § 4	in § 3	missing	Structure **different**
7.5-02-03-03.4	P	Cavitation Induced Pressure Fluctuations Numerical Prediction Methods	2014	2	√	wrong name	in § 4	in § 3	√	Structure **slightly different**
7.5-02-03-03.5	P	Cavitation Induced Erosion on Propellers, Rudders and Appendages Model Scale Experiments	2011	2	√	wrong name	in§ 5	in § 3	in § 6	Structure **different**
7.5-02-03-03.6	G	Podded Propulsor Model Scale Cavitation Test	2011	2	√	wrong name	NA	√	missing	Structure **different**
7.5-02-03-03.7	P	Prediction of Cavitation Erosion Damage for Unconventional Rudders or Rudders Behind Highly-Loaded Propellers	2017	1	√	wrong name	in § 6	missing	in § 7	Structure **different**
7.5-02-03-03.8	P	Modelling the Behaviour of Cavitation in Waterjets	2008	0	√	wrong name	missing	missing	√	Structure **strongly different**
7.5-02-03-03.9	G	Model-Scale Propeller Cavitation Noise Measurements	2021	2	√	wrong name	in § 5	√	in § 6	Structure **different**
7.5-02-04		**Ice Testing**								
7.5-02-04-01	G	General Guidance and Introduction to Ice Model Testing	2021	3	√	wrong name	Benchmark tests	in § 2.5	in § 4	Structure **different**
7.5-02-04-02	P	Test Methods for Model Ice Properties	2021	3	√	wrong name	missing	in § 1.3	in § 11	Structure **strongly different**

Number		Title	Effective Date	Revision	§ 1. PURPOSE	§ 2. DESCRIP-TION	§ 3 VALIDATION	§ 4 PARAM/SYM B	§ 5 REFER-ENCES	§ = paragraph NA=Not Appl.
7.5-02-04-02.1	P	Resistance Tests in Ice	2017	2	√	wrong name	in § 4 Bench-mark tests	missing	missing	Structure strongly differ-ent
7.5-02-04-02.2	P	Propulsion Tests in Ice	2017	1	√	wrong name	in § 4	in § 3	missing	Structure differ-ent
7.5-02-04-02.3	PC	Manoeuvring Tests in Ice	2021	1	√	wrong name	in § 5	√	in § 6	Structure differ-ent
7.5-02-04-02.4	P	(Tests in Deformed Ice) Deleted	2017	Deleted						
7.5-02-04-02.5	P	Experimental Uncertainty Analysis for Ship Resistance in Ice Tank Testing	2005	0	√	In various §	in § 8	missing	in § 9	Structure strongly differ-ent
7.5-02-04-03	G	Guidelines for Modelling of Complex Ice En-vironments	2021	1	√	In various §	NA	missing	in § 9	Structure strongly differ-ent
7.5-02-05		**High Speed Marine Vehicles**								
7.5-02-05-01	P	High Speed Marine Vehicles Resistance Test	2017	3	√	in § 3	in § 5	in § 2	in § 6	Structure differ-ent
7.5-02-05-02	P	High Speed Marine Vehicle Propulsion Test	2017	3	√	wrong name	in § 4	in § 3	√	Structure differ-ent
7.5-02-05-03.1	P	Waterjet Propulsive Performance Prediction - Propulsion Test and Extrapolation	2011	2	√	√	√	missing	in § 4	Structure differ-ent
7.5-02-05-03.2	P	Waterjet System Performance	2017	2	√	√	√	missing	in § 4	Structure differ-ent
7.5-02-05-03.3	P	Uncertainty Analysis - Example for Waterjet Propulsion Test	2017	2	√	in § 3	NA	in § 2	in § 4	Structure differ-ent
7.5-02-05-04	P	Seakeeping Tests	2021	2	√	wrong name	in § 4	in § 3	√	Structure differ-ent
7.5-02-05-04.1	P	Excerpt of ISO 2631, Seasickness and Fatigue	1999	0	√	NA	NA	NA	missing	Structure strongly differ-ent
7.5-02-05-05	P	Evaluation and Documentation of HSMV	2014	2	√	√	NA	in § 3	√	Structure strongly differ-ent
7.5-02-05-06	P	HSMV Structural Loads	2021	1	√	wrong name	in § 4	in § 3	√	Structure strongly differ-ent
7.5-02-05-07	P	(Dynamic Instability Tests) Withdrawn	2021	Deleted						
7.5-02-06		**Manoeuvrability**								
7.5-02-06-01	P	Free Running Model Tests	2021	4	√	√	in § 5 Bench-mark tests	in § 3	in § 5	Structure differ-ent
7.5-02-06-02	P	Captive Model Test Procedure	2021	6	√	In various §	in § 5	missing	in § 6	Structure differ-ent
7.5-02-06-03	P	Validation of Manoeuvring Simulation Mod-els	2021	4	√	In various §	in § 4	missing	√	Structure differ-ent

Number		Title	Effective Date	Revision	§ 1. PURPOSE	§ 2. DESCRIP-TION	§ 3 VALIDATION	§ 4 PARAM/SYMB	§ 5 REFER-ENCES	§ = paragraph NA=Not Appl.
7.5-02-06-04	P	Uncertainty Analysis for manoeuvring predictions based on captive manoeuvring tests	2021	3	√	In various §	Example in Appendixes	missing	in § 4	Structure different
7.5-02-06-05	G	Uncertainty Analysis for free running model tests	2021	2	wrong name	In various §	wrong name	missing	in § 8	Structure different
7.5-02-06-06	G	Benchmark Data for Validation of Manoeuvring Predictions	2021	0	√	In various §	NA	missing	√	Structure different
7.5-02-06-07	G	Captive Model Test for Underwater Vehicles	2021	0	√	in § 4	in § 5	in § 2	in § 6	Structure different
7.5-02-07		**Loads and Responses**								
7.5-02-07-01		**Environmental Modelling**								
7.5-02-07-01.1	G	Laboratory Modelling of Multidirectional Irregular Wave Spectra	2017	1	√	In various §	NA	in § 3	in § 6	Structure different
7.5-02-07-01.2	G	Laboratory Modelling of Waves	2021	1	√	In various §	NA	missing	in § 4	Structure different
7.5-02-07-01.3	G	(Guidelines for Modelling of Complex Ice Environments) Moved to 7.5-02-04-03	2021	Deleted						
7.5-02-07-01.4	P	Confidence Intervals for Significant Wave Height and Modal Period	2017	0	√	In various §	NA	missing	in § 4	Structure different
7.5-02-07-01.5	G	Laboratory Modelling of Wind	2021	0	√	In various §	NA	missing	√	Structure different
7.5-02-07-01.6	G	Laboratory Modelling of Currents	2021	0	√	In various §	NA	missing	in § 6	Structure different
7.5-02-07-02		**Seakeeping**								
7.5-02-07-02.1	P	Seakeeping Experiments	2021	7	√	√	in § 4	in § 3	√	Structure slightly different
7.5-02-07-02.2	P	Predicting of Power Increase in Irregular Waves from Model Tests	2021	6	√	In various §	in § 7	in § 6	in § 8	Structure different
7.5-02-07-02.3	P	Experiments on Rarely Occurring Events	2021	6	√	wrong name	in § 4	in § 3 no symbols	√	Structure slightly different
7.5-02-07-02.4	P	(Validation of Seakeeping Computer Codes in the Frequency Domain) Deleted	2014	Deleted						
7.5-02-07-02.5	P	Verification and Validation of Linear and Weakly Nonlinear Seakeeping Computer Codes	2021	3	√	In various §	in § 7 Benchmark tests	missing	in § 8	Structure different
7.5-02-07-02.6	P	Global Loads Seakeeping Procedure	2021	2	√	wrong name	in § 4	in § 3	√	Structure slightly different
7.5-02-07-02.7	P	Sloshing Model Tests	2021	1	√	wrong name	in § 4	in § 3	√	Structure slightly different
7.5-02-07-02.8	P	Calculation of the weather factor f_w for decrease of ship speed in waves	2021	1	√	In various §	in § 7 Benchmark tests	in § 2	in § 8	Structure strongly different
7.5-02-07-03		**Ocean Engineering**								
7.5-02-07-03.1	P	Floating Offshore Platform Experiments	2021	3	√	wrong name	in § 4	in § 3	√	Structure slightly different

Number		Title	Effective Date	Revision	§ 1. PURPOSE	§ 2. DESCRIPTION	§ 3 VALIDATION	§ 4 PARAM/SYMB	§ 5 REFERENCES	§ = paragraph NA=Not Appl.
7.5-02-07-03.10	G	Guideline for VIV Testing	2021	1	√	in § 5	UA in § 6	in § 3	in § 7	Structure different
7.5-02-07-03.11	G	Guideline for Model Tests of Stationary Multi-Bodies Operating in Close Proximity	2021	1	√	√	UA in § 4	in § 3	√	Structure slightly different
7.5-02-07-03.12	G	Uncertainty Analysis for a Wave Energy Converter	2021	1	√	in various §	example in § 8	missing	in § 9	Structure strongly different
7.5-02-07-03.13	G	Guideline for VIM Testing	2021	1	√	in § 5	UA in § 6	missing	in § 7	Structure strongly different
7.5-02-07-03.14	P	Analysis Procedure of Model Tests in Irregular Waves	2021	1	√	wrong name	described in §4	in § 3 but variables are not listed	√	Structure different
7.5-02-07-03.15	G	Uncertainty analysis - Example for horizontal axis turbines	2021	1	√	in various §	NA	partly in §5.1 wrong name	in § 6	Structure different
7.5-02-07-03.16	G	Model Construction of Offshore Systems	2021	0	√	in various §	partly described in §6	in § 2.1	in § 8	Structure different
7.5-02-07-03.17	G	Uncertainty Analysis for Model Testing of Offshore Wind Turbines	2021	0	√	in various §	example in §4	missing	√	Structure different
7.5-02-07-03.18	G	Practical guidelines for numerical modelling of wave energy converters	2021	0	√	in various §	in § 6.3	missing	in § 7	Structure different
7.5-02-07-03.2	P	Analysis Procedure for Model Tests in Regular Waves	2021	3	√	wrong name	NA	in § 3	in § 6	Structure different
7.5-02-07-03.3	P	(Model Tests on Tanker-Turret Systems) Deleted	2014	Deleted						
7.5-02-07-03.4	P	(Active Hybrid Model Tests of Floating Offshore Structures with Mooring Lines) Deleted	2021	Deleted						
7.5-02-07-03.5	P	Passive Hybrid Model Tests of Floating Offshore Structures with Mooring Lines	2021	3	√	√	in § 4	in § 3	in § 6	Structure slightly different
7.5-02-07-03.6	P	Dynamic Positioning System Model Test Experiments	2021	2	√	in § 3	UA in § 5	in § 2 no symbols	in § 6	Structure different
7.5-02-07-03.7	G	Wave Energy Converter Model Test Experiments	2021	2	√	in § 3	UA in § 3.7	missing	in § 4	Structure different
7.5-02-07-03.8	P	Model Tests for Offshore Wind Turbines	2021	2	in § 2	in § 4	UA in § 4.4	missing	√	Structure strongly different
7.5-02-07-03.9	P	Model Tests for Current Turbines	2021	2	√	in § 3	UA in § 3.6	√	√	Structure slightly different
7.5-02-07-04		**Stability**								
7.5-02-07-04.1	P	Model Tests on Intact Stability	2008	2	√	in various §	described in §4	missing	missing	Structure different
7.5-02-07-04.2	P	Model Tests on Damage Stability in Waves	2017	3	√	√	described in §4	in § 3 but variables are not listed	√	Structure slightly different
7.5-02-07-04.3	G	Predicting the Occurrence and Magnitude of Parametric Rolling	2021	3	√	in various §	example in Appendix	in § 6	in § 7	Structure different

Number		Title	Effective Date	Revision	§ 1. PURPOSE	§ 2. DESCRIP-TION	§ 3 VALIDATION	§ 4 PARAM/SYMB	§ 5 REFER-ENCES	§ = paragraph NA=Not Appl.
7.5-02-07-04.4	P	Simulation of Capsize Behaviour of Damaged Ships in Irregular Beam Seas	2021	3	√	in various §	in §4	missing	√	Structure different
7.5-02-07-04.5	P	Estimation of Roll Damping	2021	1	√	in various §	in §5	in Appendix B	in § 7	Structure different
7.5-02-07-04.6	P	Extrapolation for Direct Stability Assessment in Waves	2021	0	√	in various §	embedded in text	in § 5	in § 6	Structure different
7.5-02-07-04.7	P	Inclining Tests	2021	0	√	in various §	§4	NA	in § 8	Structure different
7.5-03		**CFD**								
7.5-03-01		**General**								
7.5-03-01-01	P	Uncertainty Analysis in CFD, Verification and Validation Methodology and Procedures	2021	4	√	in various §	NA	missing	in § 6	Structure different
7.5-03-01-02	G	Quality Assurance in Ship CFD Application	2021	2	√	in § 3	in § 4-5	missing	in § 6	Structure different
7.5-03-01-03	P	(CFD User's Guide) Deleted	2021	deleted						
7.5-03-01-04	P	(CFD Verification) Deleted	2021	deleted						
7.5-03-02		**Resistance and Flow**								
7.5-03-02-01	P	Uncertainty Analysis in CFD, Examples for Resistance and Flow	2017	1	√	in various §	in § 2.3 and 2.4	missing	in § 3	Structure different
7.5-03-02-02	P	Benchmark Database for CFD Validation for Resistance and Propulsion	2021	2	√	√	NA	missing	in § 3	Structure different
7.5-03-02-03	G	Practical Guidelines for Ship CFD Applications	2014	1	different name	in various §	in § 4.2	missing in § 2.3.1, § 2.3.6	√	Structure different
7.5-03-02-04	G	Practical Guidelines for Ship Resistance CFD	2021	1	different name	√	NA	missing	√	Structure slightly different
7.5-03-02-05	G	Use of CFD methods to calculate wind resistance coefficient	2021	0	different name	in various §	in § 8	in § 2	in § 9	Structure strongly different
7.5-03-03		**Propulsion**								
7.5-03-03-01	G	Practical Guidelines for Ship Self-propulsion CFD	2014	0	different name	in various §	in § 6	missing	in § 7	Structure strongly different
7.5-03-03-02	G	Practical Guidelines for RANS Calculation of Nominal Wakes	2014	0	different name	In various §	in § 3.4	missing	in § 4	Structure strongly different
7.5-03-04		**Manoeuvrability**								
7.5-03-04-01	G	Guideline on Use of RANS Tools for Manoeuvring Prediction	2021	2	√	√	in § 4 Examples	missing	√	Structure slightly different
7.5-03-04-02	G	Validation and Verification of RANS Solutions in the Prediction of Manoeuvring Capabilities	2021	2	√	In various §	in § 5	missing	in § 6	Structure strongly different
7.5-04		**Full Scale Measurements**								
7.5-04-01		**Speed and Power Trials**								

Number		Title	Effective Date	Revision	§ 1. PURPOSE	§ 2. DESCRIP-TION	§ 3 VALIDATION	§ 4 PARAM/SYMB	§ 5 REFER-ENCES	§ = paragraph NA=Not Appl.
7.5-04-01-01.1	P	Preparation, Conduct and Analysis of Speed/Power Trials	2021	7	√	in various §	NA	in Appendix L	in § 13	Structure **strongly different**
7.5-04-01-01.2	P	(Analysis of Speed/Power Trial Data) Merged into 7.5-04-01-01.1	2017	deleted						
7.5-04-02		**Manoeuvrability**								
7.5-04-02-01	P	Full Scale Manoeuvring Trials Procedure	2021	3	√	in various §	in § 4, wrong name	in § 3 no symbols	√	Structure **different**
7.5-04-02-02	G	UV Full Scale Manoeuvring Trials	2021	0	√	in various §	in § 4, wrong name	in § 3 no symbols	√	Structure **different**
7.5-04-03		**Ice Testing**								
7.5-04-03-01	IP	Ship Trials in Ice	1999	0	√	in various §	in § 4	in § 3 no symbols	missing	Structure **different**
7.5-04-04		**Hydrodynamic Noise**								
7.5-04-04-01	G	Underwater Noise from Ships, Full Scale Measurements	2021	2	√	in various §	missing	missing	in § 6	Structure **strongly different**
7.5-04-05		**Model-ship correlation**								
7.5-04-05-01	G	Guideline on the determination of model-ship correlation factors	2021	1	different name	in § 3	NA	in § 2	in § 4	Structure **different**
7.6-01		**Measuring Equipment**								
7.6-01-01	P	Control of Inspection, Measuring and Test Equipment	1999	0	√	in various §	NA	missing	missing	Structure **strongly different**

Appendix B. OUTCOME OF THE REVIEW OF UNCERTAINTY ANALYSIS PROCEDURES FOR COMPLIANCE WITH ITTC QUALITY REQUIREMENTS.

No.	Rev	Year	Example	Reference	Symbol	Comment
7.5-01-01-01	4	2017	n	n	n	Expand to include model measurements with uncertainty estimates
7.5-01-02-01						Deleted
7.7-01-02-02	1	2017	n	n	n	Expand to include model measurements with uncertainty estimates
7.5-01-03-01	2	2017	y	y	y	
7.5-01-03-02	0	2008	y	y	y	Update GUM reference
7.5-01-03-03	1	2014	n	n	n	Discusses UA in general terms but has no UA references or examples
7.5-01-03-04	1	2017	n	n	n	Benchmark tests should include UA
7.5-02-01-01	2	2014	y	y	y	Add prediction limit and add 7.5-02-01-07 as reference
7.5-02-01-03	2	2011	y	y	y	
7.5-02-01-04	0	2014	n	n	n	No uncertainty analysis or UA reference. Symbols and nomenclature unique to PIV.
7.5-02-01-06	1	2021	y	y	y	
7.5-02-01-07	1	2021	y	y	y	
7.5-02-01-08	0	2017	y	y	n	UA not applicable. Var and SSA not in the symbols list. Distinction should be made between confidence and prediction intervals.
7.5-02-02-01	5	2021	n	n	y	UA and examples covered in separate procedures. Depth *Fr* should be corrected as Fr_h.
7.5-02-02-02	3	2021	y	y	y	UA for resistance test, but no model test results. Example is separate procedure that has been revised.
7.5-02-02-02.1	1	2021	y	y	y	Revision in review. This procedure was revised and is an example of a resistance test.
7.5-02-02-02.2	1	2021	y	y	y	UA for resistance test, but no model test results. Example as separate procedure has been deleted, and reference should be deleted. Reference list should be updated.
7.5-02-02-04	0	2021	n	y	y	Only has UA references.
7.5-02-03-01.1	6	2021	n	y	y	Only has UA references.
7.5-02-03-01.3	2	2021	n	n	y	
7.5-02-03-01.4	5	2021	n	n	y	On page 8, physical units should be in regular font. Nm should be N·m.
7.5-02-03-01.5	2	2017	n	n	y	No uncertainty analysis or UA reference. Reference list is numerical and should be alphabetical.
7.5-02-03-01.6	1	2017	n	n	y	States UA procedures should be followed. Nm should be N·m.
7.5-02-03-01.7	1	2021	n	n	y	No UA or reference. Nm should be N·m.
7.5-02-03-01.8	0	2021	n	n	y	No UA or reference.
7.5-02-03-02.1	4	2021	n	y	y	Only has UA references. Nm should be N·m.
7.5-02-03-02.3	1	2014	n	n	n	Only generic discussion of UA. Symbols may be unique to LDV and not reviewed in detail.

No.	Rev	Year	Example	Reference	Symbol	Comment
7.5-02-03-02.4	1	2011	n	n	n	Outdated discussion of UA. Pitch and yaw symbols not consistent with ITTC. Procedure should be revised.
7.5-02-03-02.5	1	2017	n	n	n	
7.5-03-01-01	4	2021	n	y	n	Current GUM referenced. V&V consistent with ASME. Symbols consist with ASME. ITTC Symbols not relevant. How to include in ITTC Symbols should be reviewed.
7.5-03-01-02	2	2021	n	n	n	Procedure does not reference the GUM. A section title is Assessment of total uncertainty. Total uncertainty is not in the GUM. The appropriated terminology is combined and expanded uncertainty
7.5-03-02-01	1	2017	y	n	n	Procedure should be updated. Does not reference GUM. Equation numbers start with (33) and should begin with (1). Coleman and Steele (1999) in text is out of date and not in Reference list.
7.5-03-02-03	1	2014	n	n	y	Procedure should be updated. Does not reference GUM. Equation numbers start with (33) and should begin with (1). Coleman and Steele (1999) in text is out of date and not in Reference list.
7.5-03-02-04	1	2021	n	n	y	
7.5-03-02-05	0	2021	n	n	y	
7.5-03-03-01	0	2014	n	n	y	Equation numbers are all (0) and should be renumbered. References should be updated. V&V section is vague and should be updated with information from 7.5-03-03-03.
7.5-03-03-02	0	2014	y	n	y	Procedure has numerical example but no uncertainty analysis. V&V section is general. Reference list should be updated and include 7.5-03-01-01.
7.5-03-04-01	2	2021	y	n	y	Up to date procedure with several examples. No discussion of UA or V&V. ITTC 7.5-03-04-02 is effectively a companion procedure and should be included in the Reference list.
7.5-03-04-02	2	2021	y	y	y	ITTC procedures should be added to Reference list. This procedure is effectively a companion to 7.5-03-04-01 and should be included as a Reference.

Appendix C. OUTCOME OF THE MANUAL OF ITTC RECOMMENDED PROCEDURES AND GUIDELINES MAINTENANCE.

New/ Rev./ Del	Number	P /G	Title	Effec-tive Date
R	4.2.3-01-01	P	Guide for the Preparation of ITTC Recommended Procedures	2024
R	4.2.3-01-03	W	Work Instruction for Formatting ITTC Recommended Procedures	2024
R	7.5-01-01-01	P	Ship Models	2024
R	7.5-02-01-03	G	Fresh Water and Seawater Properties	2024
R	7.5-02-01-04	GC	Guideline on Best Practices for the Applications of PIV/SPIV in Towing Tanks and Cavitation Tunnels	2024
R	7.5-02-01-08	P	Single Significant Amplitude and Confidence Intervals for Stochastic Processes	2024
N	7.5-02-01-09	P	Avoiding self-repeating effect in time-domain numerical simulation of ship motion	2024
N	7.5-02-01-10	P	Procedure of Estimation of Frequency of Random Events by Direct Counting	2024
N	7.5-02-01-11	P	Statistical Validation of Extrapolation Methods for Time Domain Numerical Simulation of Ship Motions	2024
R	7.5-02-03-01.8	G	Scaling Method for ship wake fraction with pre-swirl devices	2024
N	7.5-02-03-01.9	G	Guidelines for Predicting the power saving of a wind propulsion ship on a route at design stage	2024
D	7.5-02-03-02.5	G	(Experimental Wake Scaling Methods) - Moved to 7.5-02-03-03.10	2024
R	7.5-02-03-03.1	P	Model-Scale Cavitation Test	2024
R	7.5-02-03-03.2	P	Visual Description and Measurement of Cavitation Events	2024
R	7.5-02-03-03.3	P	Cavitation Induced Pressure Fluctuations Model Scale Experiments	2024
R	7.5-02-03-03.4	P	Cavitation Induced Pressure Fluctuations Numerical Prediction Methods	2024
R	7.5-02-03-03.5	P	Cavitation Induced Erosion on Propellers and Rudders, Model Scale Experiments and Numerical Guidance	2024
R	7.5-02-03-03.6	G	Podded Propulsor Model Scale Cavitation Test	2024
D	7.5-02-03-03.7	P	(Prediction of Cavitation Erosion Damage for Unconventional Rudders or Rudders Behind Highly Loaded Propellers) Merged in 7.5-02-03-03.5	2024
R	7.5-02-03-03.8	P	Modelling the Behaviour of Cavitation in Waterjets	2024
R	7.5-02-03-03.9	G	Model-Scale Propeller Cavitation Noise Measurements	2024
R	7.5-02-04-02	P	Test Methods for Model Ice Properties	2024
R	7.5-02-04-02.1	P	Resistance Tests in Ice	2024
R	7.5-02-04-02.3	PC	Manoeuvring Tests in Ice	2024
R	7.5-02-04-03	G	Guidelines for Modelling of Complex Ice Environments	2024
R	7.5-02-05-01	P	High Speed Marine Vehicles Resistance Test	2024
R	7.5-02-05-04	P	HSMV Seakeeping Tests	2024
R	7.5-02-05-04.1	G	Excerpt of ISO 2631-1&3:1985, Seasickness and Fatigue	2024
R	7.5-02-05-05	G	Evaluation and Documentation of HSMV Manoeuvrability	2024
R	7.5-02-05-06	P	HSMV Model Tests for Prediction of Structural Loads	2024
R	7.5-02-06-01	P	Free Running Model Tests	2024
R	7.5-02-06-02	P	Captive Model Test Procedure	2024
R	7.5-02-06-03	P	Validation of Manoeuvring Simulation Models	2024
R	7.5-02-06-04	P	Uncertainty Analysis for manoeuvring predictions based on captive manoeuvring tests	2024
R	7.5-02-06-05	G	Uncertainty Analysis for free running model tests	2024
R	7.5-02-06-06	G	Benchmark Data for Validation of Manoeuvring Predictions	2024
R	7.5-02-06-07	G	Captive Model Test for Underwater Vehicles	2024
R	7.5-02-07-01.4	P	Confidence Intervals for Significant Wave Height and Modal Period	2024

R	7.5-02-07-01.5	G	Laboratory Modelling of Wind	2024
R	7.5-02-07-01.6	G	Laboratory Modelling of Currents	2024
R	7.5-02-07-02.1	P	Seakeeping Experiments	2024
R	7.5-02-07-02.2	P	Predicting of Power Increase in Irregular Waves from Model Tests	2024
R	7.5-02-07-02.3	P	Experiments on Rarely Occurring Events	2024
R	7.5-02-07-02.5	P	Verification and Validation of Linear and Weakly Nonlinear Seakeeping Computer Codes	2024
R	7.5-02-07-02.6	P	Global Loads Seakeeping Procedure	2024
R	7.5-02-07-02.7	P	Sloshing Model Tests	2024
R	7.5-02-07-02.8	P	Calculation of the weather factor f_w for decrease of ship speed in waves	2024
R	7.5-02-07-03.5	P	Passive Hybrid Model Tests of Floating Offshore Structures with Mooring Lines	2024
R	7.5-02-07-03.6	P	Dynamic Positioning System Model Test Experiments	2024
R	7.5-02-07-03.7	G	Wave Energy Converter Model Test Experiments	2024
R	7.5-02-07-03.8	P	Model Tests for Offshore Wind Turbines	2024
R	7.5-02-07-03.9	P	Model Tests for Current Turbines	2024
R	7.5-02-07-03.11	G	Guideline for Model Tests of Stationary Multi-Bodies Operating in Close Proximity	2024
R	7.5-02-07-03.12	G	Uncertainty Analysis for a Wave Energy Converter	2024
R	7.5-02-07-03.15	G	Uncertainty analysis - Example for horizontal axis turbines	2024
R	7.5-02-07-03.16	G	Model Construction of Offshore Systems	2024
R	7.5-02-07-03.17	G	Uncertainty Analysis for Model Testing of Offshore Wind Turbines	2024
R	7.5-02-07-03.18	G	Practical guidelines for numerical modelling of wave energy converters	2024
R	7.5-02-07-04.1	P	Model Tests on Intact Stability	2024
R	7.5-02-07-04.2	P	Model Tests on Damage Stability in Waves	2024
R	7.5-02-07-04.3	G	Predicting the Occurrence and Magnitude of Parametric Rolling	2024
R	7.5-02-07-04.4	P	Simulation of Capsize Behaviour of Damaged Ships in Irregular Beam Seas	2024
R	7.5-02-07-04.5	P	Estimation of Roll Damping	2024
N	7.5-02-07-04.8	P	Computational procedure for instantaneous GZ curve during time-domain numerical simulation in irregular waves	2024
R	7.5-03-01-01	P	Uncertainty Analysis in CFD, Verification and Validation Methodology and Procedures	2024
R	7.5-03-02-01	P	Uncertainty Analysis in CFD, Examples for Resistance and Flow	2024
R	7.5-03-02-02	G	Benchmark Database for CFD Validation for Resistance and Propulsion	2024
R	7.5-03-02-03	G	Practical Guidelines for Ship CFD Applications	2024
R	7.5-03-02-04	G	Practical Guidelines for Ship Resistance CFD	2024
R	7.5-03-02-05	G	Guideline on the CFD-based Determination of Wind Resistance Coefficients	2024
R	7.5-03-03-01	G	Practical Guidelines for Ship Self-propulsion CFD	2024
R	7.5-03-03-02	G	Practical Guidelines for RANS Calculation of Nominal Wakes	2024
R	7.5-03-04-01	G	Guideline on Use of RANS Tools for Manoeuvring Prediction	2024
R	7.5-03-04-02	G	Validation and Verification of RANS Solutions in the Prediction of Manoeuvring Capabilities	2024
R	7.5-04-01-01.1	P	Preparation, Conduct and Analysis of Speed/Power Trials	2024
N	7.5-04-01-02	P	Conduct and Analysis of Sea Trial for Wind Assisted Ships	2024
R	7.5-04-02-01	P	Full Scale Manoeuvring Trials	2024
R	7.5-04-02-02	G	UV Full Scale Manoeuvring Trials	2024
R	7.5-04-03-01	G	Guidelines for Ship Trials in Ice	2024
R	7.5-04-04-01	G	Underwater Noise from Ships, Full Scale Measurements	2024
N	7.6-02-01	W	Verification of Steel Rulers	2024
R	4.2.3-01-01	P	Guide for the Preparation of ITTC Recommended Procedures	2024

ITTC2024

30TH INTERNATIONAL TOWING TANK CONFERENCE
22–27 SEPTEMBER 2024 | HOBART TASMANIA AUSTRALIA

REPORT OF THE RESISTANCE AND PROPULSION COMMITTEE

RESISTANCE & PROPULSION COMMITTEE

1. INTRODUCTION

1.1 Membership and Meetings

The members of the Resistance and Propulsion Committee of the 30th ITTC were:

- Nicholas Dawson (Chair)
  QinetiQ,
  UK
- Bryson Metcalf (Secretary)
  NSWC Carderock Division,
  USA
- Tokihiro Katsui
  Kobe University,
  JAPAN
- Yasuhiko Inukai
  Japan Maritime United Corporation,
  JAPAN
- Kwang-Soo Kim
  KRISO,
  SOUTH KOREA
- Byoung-Guk Kim
  Hanwha Ocean Company,
  SOUTH KOREA
- Matteo Diez
  CNR-INM,
  ITALY
- Stefano Gaggero
  University di Genova,
  ITALY
- Weichao Shi
  Newcastle University,
  UK
- Renchuan Zhu,
  Shanghai Jao-Tong University,
  CHINA
- Nikolaj Larsen (Former Chair, departed committee 2023)
  FORCE Technology,
  DENMARK

Three in-person committee meetings were held during the work period:

- The first meeting was held at FORCE Technology, in Copenhagen, Denmark, on the 9th – 10th November 2022.
- The second meeting was held at Kobe University in Kobe, Japan, on the 8th – 9th June 2023.
- The third meeting was held at CRN-INM in Rome, Italy between 31st January – 1st February 2024.

Additional video meetings were conducted to enable the participation of those who were unable to attend the in-person meetings and to try to maintain progress between meetings.

1.2 Tasks

The recommendations for the work of the Resistance and Propulsion Committee as given by the 29th ITTC were as follows:

1. Update the state-of-the-art for predicting the performance of different ship concepts emphasizing developments since the 2021 ITTC Full Conference. The committee report should include sections on:

A) The potential impact of new technological developments on the ITTC, including, for example new types of hull and propeller coatings, propulsors, rudders.
B) New experimental techniques and extrapolation methods.
C) New benchmark data.
D) Practical applications of computational methods to performance predictions and scaling.
E) The need for R&D for improving methods of model experiments, numerical modelling and full-scale measurements.

2. Review ITTC Recommended Procedures relevant to resistance and propulsion, and

A) Identify any requirements for changes in the light of current practice, and, if approved by the Advisory Council, update them,
B) Identify the need for new procedures and outline the purpose and contents of these.

3. Rewrite procedure 7.5-02-03-01.2, Uncertainty Analysis, Example for Propulsion Test (old procedure deleted 2021), complying with current ITTC guidelines for uncertainty analysis. Include a worked example complying with current ITTC procedures for propulsion tests. Cooperate closely with the Quality Systems Group
4. Rewrite procedure 7.5-02-03-02.2, Uncertainty Analysis, Example for Open Water Test (old procedure deleted 2021), complying with current ITTC guidelines for uncertainty analysis. Include a worked example complying with current ITTC procedures for open water tests. Cooperate closely with the Quality Systems Group.
Update procedure 7.5-02-05-03.3, Uncertainty Analysis, Example for Water Jet Propulsion Test, complying with current ITTC guidelines for uncertainty analysis. Include a worked example complying with current ITTC procedures for water jet propulsion tests. Cooperate closely with the Quality Systems Group.
5. Conduct a benchmark study focusing on the effect of Re at model scale and scaling methods for full scale prediction. CFD calculations would be run at a range of Re at model scale and full scale, along with openwater model tests at a range of Re. The study could use two propellers that were provided for the previous benchmark study run by the 28th ITTC.
6. Investigation of the issue of laminar effects in self-propulsion test of propeller with low blade area.

A) Conduct a survey how ITTC members tackle this issue, and which scaling method they use for low blade area propellers.
B) Investigate the sufficiency of conduction two open water tests at different Reynolds numbers for full scale extrapolation. C) Review literature on the subject.
C) Suggest modification to recommended procedures.

7. Investigation of the issue of extrapolation of model tests with ducted propellers to full scale according to different Re-numbers. Identify the need and change relevant procedures if necessary.
8. Update of the Load variation test method in 7.5–0203–01.4 "1978 ITTC Performance Prediction Method"

A) Review of the Load Variation Test method, considering a wider range of resistance and develop a new method if necessary.
B) Review the effectiveness of shallow water effects in Load Variation Test method and develop of a new method if necessary.

9. Monitor the experience of ITTC members using CFD-based form factors and, if necessary, update the Recommended Procedures accordingly. This includes the correlation with sea trial data, numerical friction line, how to handle a submerged transom, the possibility to handle separation in model scale by deriving model and full scale form factors. Continue the comparative studies on CFD methods for form factor derivation.
10. Investigation of the requirements for the testing and numerical evaluation of high-speed marine vessels. Address the need of updating the relevant procedures.
11. Investigation into the use of CFD methods in scaling of model test results for a more precise speed-power prediction. The issues with high priority are:

A) Propeller open water scaling
B) Difference in Reynolds number at selfpropulsion and open water test, laminar effect in self-propulsion test
C) Effective wake scaling
D) Scaling of immersed transoms
E) Energy saving devices

12. Investigation of measurement and prediction methods for breaking waves.
13. Investigation of the scaling of sinkage and trim in deep water, as well as their effect on the form factor.
14. Investigation of the scale effects of ships advancing through shallow/restricted waters, in particular scaling of sinkage.
15. Developments in hull and propeller model manufacturing. Investigate the advances in additive manufacturing techniques and novel materials. Investigate the use of 3D scanning techniques to validate the model geometry in view of updating the procedures.
16. Guidelines for model testing of coatings; in particular, skin friction reducing and air lubrication systems, including scaling laws.
17. Review of CFD methods for roughness effects and recommend best practice; in particular, in terms of wall resolved as well as wall function methods.
18. Identify the necessity of guidelines for CFD methods, model tests and scaling for energy saving devices.
19. Investigation of the issue of powering and resistance for slower speed submerged vehicles due to the resurgence of UUV (Unmanned Underwater Vehicle) and AUV (Autonomous Underwater Vehicle). The UUV’s and AUV’s can be plagued by the added drag of appendages, sensors and add-ons. They can have much greater impact on performance (% wise) than typical submerged vehicles (torpedo/subs) since UUV’s and AUV’s typically operate at much slower speeds. The community would benefit with a better correction for Cf than the flat plate curve. Identify the need and, if necessary, update the procedures to better handle transition issues that would be present in these lower Re submerged vehicles.

Unfortunately, due to the limited resources of the R&P committee it was not possible to complete all actions and some have been recommended to be undertaken by the following committee.

2. STATE OF THE ART

2.1 New Benchmark Data

2.1.1 JoRes Project

One of the most significant sources of benchmark data in recent years is the "Joint Research Project: Numerical Methods Validation For Designing and Building More Advanced and Energy Efficient Ships". This is a €1.5M project, self-funded by the participants and contributors, which is a global initiative to develop validation cases.

The International Maritime Organisation (IMO) has set ambitious targets for the maritime sector to significantly reduce Greenhouse Gas (GHG) emissions. The IMO's goal of achieving net zero emissions by 2050 will require a combination of energy efficiency optimisation and the use of carbon-neutral fuels. The JoRes project noted that efficiency optimisation can only be achieved using digital simulations, which require validation.

The availability of appropriate full-scale data for comparison has long been an issue for both CFD validation and for making assessments of Correlation Allowance, hull fouling allowances and so on. The JoRes project aims to address this issue, by making a large dataset publically available. This phase of the JoRes project is already complete, and the project organisers have state that all the results and the geometry files will be made publically available on 1 December 2024 and will include trials data of:

- General cargo vessel
- Tanker
- Twin-screw RoRo ferry
- Cruise liner
- Tug boat
- Bulk Carrier

In addition to full-scale trials data, the project has also been collecting data on hull and propeller fouling, hull roughness, and other aspects which are considered critical to resistance and propulsion of ships.

2.1.2 GATERS project

The Gate Rudder System (GATERS) project has also published results of full scale trials data, which is of relevance to a number of areas of interest to the ITTC community. The objective of the GATERS project was to "Design, Manufacture and Install a Retrofit Gate Rudder System". Aimed at the retrofit market as well as for new-builds, the Gate Rudder System (GRS) intends to improve the flow around an existing propeller, reducing tip losses and parasitic drag.

Full scale trials were conducted on vessels with both gate rudder systems and conventional rudder systems. As a retrofit system, the GATERS project believe that fuel savings of up to 10% are possible in calm water conditions, rising to 15% savings in a normal sea state, when compared to a conventional rudder system. If savings of even half this magnitude can be achieved in practice then it would be expected that this technology will become of significant interest over the next decade. It will be important for anyone conducting CFD simulations to design a GRS to have robustly validated their processes, as the cost-benefit analysis of whether to fit the system or not would be affected by the accuracy of the results. The availability of model and full scale data, both with and without a gate rudder system fitted could make this dataset particularly valuable, as it can be used to validate standard CFD processes as well as those applicable to this particular type of Energy Saving Device (ESD).

3. PROCEDURES

Three updated procedures were accepted by the Quality Systems Group of the 30th ITTC for publication at this time. These were:

- 7.5-01-01-01 Ship Models
- 7.5-02-03-01.8 Energy Saving Devices
- 7.5-02-05-01 High Speed Marine Vehicles

Corrections were minor in nature and focussed upon ensuring consistency with other Recommended Procedures and Guidelines.

A number of other procedures were deemed insufficiently complete by the Quality Systems Group and will be passed to the next committee for completion.

3.1 A REVIEW OF SCALING METHODS FOR SHIP WAKE FRACTION WITH PRE-SWIRL DEVICES

A comprehensive review was completed of Guideline 7.5-02-03-01.8 – *Scaling method for ship wake fraction with pre-swirl devices*.

The relevance of Energy Saving Devices (ESD), especially in the case of refitting of existing ships, is continuously increasing due to the need of comply with stricter requirements in terms of the efficiency and carbon footprint of ships. Typical ESDs are Pre- and Post- Swirl Stator (PSS), Pre-Swirl Ducts (PSD), Wake Equalizing Ducts (WED), Propeller Boss Cap Fins (PBCF), Vane Wheels, Contra-Rotating Propellers (CRP) and their possible combinations.

Among these devices, those exploiting the pre-swirling effect (PSS and PSD) appear to be the most promising, especially when applied to ships with high blockage coefficients. Although the performance varies according to ship type and operating condition, the energy reduction effect is estimated to be about 3% to 7% (Dang *et al.*, 2012, Lee *et al.*, 1992, Mewis and Guiard, 2011, Shin *et al.*, 2013, Kim *et al.*, 2015, Koushan *et al.*, 2020, Furcas and Gaggero, 2021, Gaggero and Martinelli, 2022, Nicorelli *et al.*, 2023). The working principle (the generation of a counter swirl flow to the propeller that corresponds to a local blade loading, a consequent reduction of the rate of revolution for the required thrust and the final reduction of delivered power) poses several questions concerning the extrapolation to full-scale. The original ITTC 1978 method was developed for conventional ships and showed limitations when applied to ships equipped with pre-swirl devices (Lee, 2015). The ITTC 1999 method adopted a different scaling procedure by distinguishing the axial and the tangential component of the wake to the propeller. However, it was never included in the recommended procedures and guidelines despite being introduced in the 22nd ITTC final report of the Specialist Committee on Unconventional Propulsors (ITTC 1999). Current ITTC recommended procedures and guidelines (ITTC 2021) adopt a modified extrapolation methodology to account in a more reasonable way for the angle of attack to the propeller based on the work of Kim *et al.* (2017). In this method, the axial and tangential velocity components are scaled separately: the axial wake (being viscous in nature) is scaled according to ITTC 1978, while the tangential component (being mainly potential in nature) following the assumptions of ITTC 1999, is not scaled:

$$w_{SS} = (t_{MS} + 0.04) + (w_{MS\,axial} - t_{MS} - 0.04)\frac{C_{FS} + C_A}{C_{FM}} + w_{MS\,tangential}$$

$$w_{MS\,axial} = w_{MO} + (w_{MS} - w_{MO}) \cdot F_x$$

$$w_{MS\,tangential} = (w_{MS} - w_{MO}) \cdot F_t$$

The most relevant modification, introduced by ITTC 2021, is the use of two weighting factors, F_x and F_t, to account for the importance of axial and tangential components of the velocity field to the propeller based on the type of the device.

Kim *et al.* (2017) suggested values for these weighting factors based on a limited number of ships and ESD types (KCS and KVLCC ships equipped with a Pre-Swirl Stator and a Pre-Swirl Duct respectively), as shown in Table 1.

Table 1 - Factors of axial and tangential coefficients for ITTC 2021 scaling procedure. From Kim et a. (2017) and ITTC 7.5-02-03-01.8

ESD type	F_x	F_t
PSS	0.3	0.7
PSD	0.8	0.2

Some other recent studies widened the range of test cases and pointed out the necessity for systematic analyses, as suggested in the ITTC procedure, to refine the proposed extrapolation method.

Nicorelli *et al.* (2023) applied several extrapolation procedures (ITTC 1978, ITTC 1999 and ITTC 2021) to three devices specifically designed by a simulation-based optimization method for the Duisburg Test Case (DTC). The design was carried out at full-scale using a combination of BEM and RANSE analyses. Fully resolved RANSE analyses at both model and full scale allowed comparison with ITTC extrapolation methods. In the study, a PSD, a PSS and a WED were analysed in order to span over the entire range of pure axial/mixed/pure tangential functioning of the devices.

In addition, as one of the activities of the ITTC Resistance and Propulsion Committee, a similar analysis was extended to two additional PSS (a two- and a three-fins design), which geometries were available to the Committee. These devices were also designed using optimization based methodologies (Furcas and Gaggero, 2021) and model- and full-scale fully resolved RANSE analyses were employed for comparison with ITTC wake extrapolation procedures.

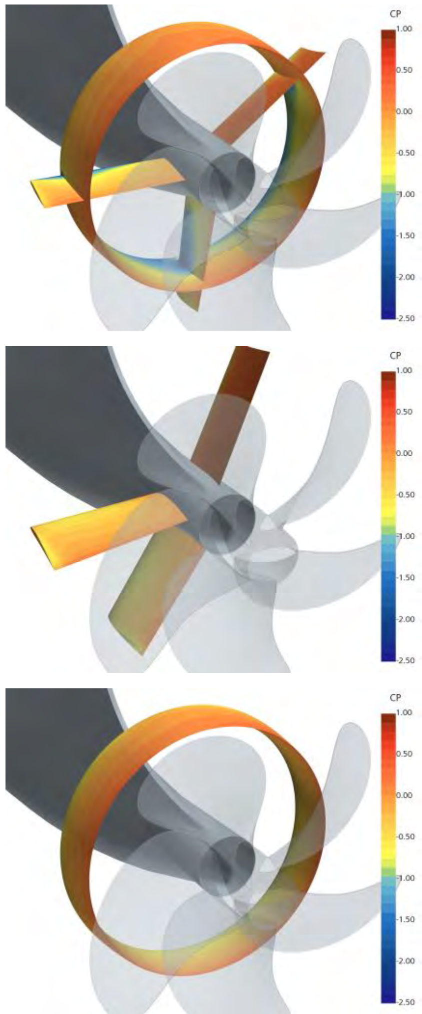

Figure 1 - Pre-Swirl Duct, Pre-Swirl Stator and Wake Equalizing Duct for the DTC hull from Nicorelli and Gaggero (2023)

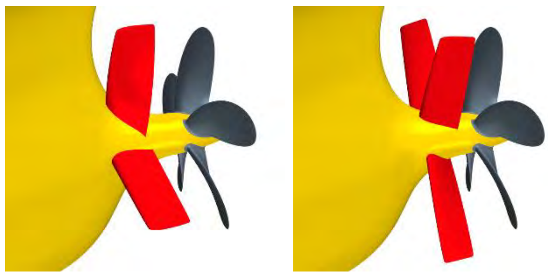

Figure 2 - Two- and Three-fins Pre-Swirl Stators for the JBC hull, from Furcas and Gaggero (2021)

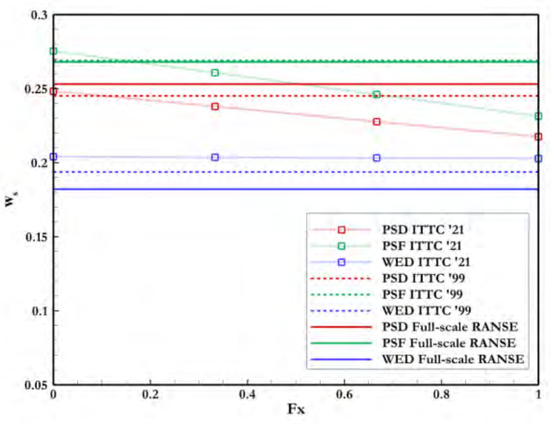

Figure 3 - Full-scale effective wake fractions (W_S) using several extrapolation methods compared to full-scale RANSE calculations; Influence of the axial/tangential coefficient of the ITTC 2021 procedure. DTC test case adapted from Nicorelli and Gaggero (2023)

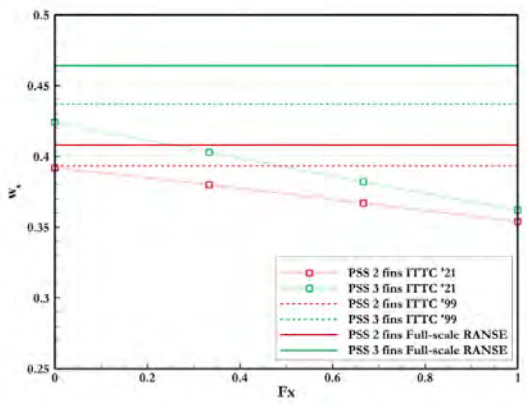

Figure 4 - Full-scale effective wake fractions (W_S) using several extrapolation methods compared to full-scale RANSE calculations; Influence of the axial/tangential coefficient of the ITTC 2021 procedure. JBC test case from ITTC Resistance and Propulsion Committee

The results of the CFD calculations showed that the coefficients suggested by the ITTC 2021 would benefit from further investigation. ITTC 2021 full-scale wake of DTC equipped with the pure swirling device (Pre-Swirl Stator) matches with the full-scale RANSE prediction with a weight of axial wake F_x equal to 0.18 ($F_t = 0.82$) compared to the 0.3 (and 0.7) suggested by the procedure. For the Japan Bulk Carrier, ITTC 2021 full-scale extrapolations are closer to fully resolved RANSE (Pre-Swirl Stator, regardless number of blades) when the axial component of the scaling procedure is set to 0. Mixed devices (Pre-Swirl Ducts) compare better with CFD when the axial component of the wake (which should be dominant due to the presence of the duct) is weighted by a factor equal to 0.1 (rather than the 0.7 of the procedure). Pure axial devices like the WED are substantially overestimated with respect to full scale RANSE analyses if compared to the results of the ITTC 1999 procedure.

Table 2 - Extrapolated and calculated full-scale wake fractions. (form factor = 0.094, $C_A = 0$, [1] $F_X = 0.8$, $F_T = 0.2$; [2] $F_X = 0.3$, $F_T = 0.7$; [3] $F_X = 1$, $F_T = 0$), DTC test case, from Nicorelli and Gaggero (2023)

	ITTC'78 (no ESD)	**ITTC'99 with ESD**
Reference	0.197	-
PSD 3p	-	0.245
PSS 3p	-	0.268
WED	-	0.194
	ITTC'21 with ESD	**Full-scale RANSE**
Reference	-	0.180
PSD 3p	0.224[1]	0.253
PSS 3p	0.262[2]	0.268
WED	0.203[3]	0.182

Table 3 - Extrapolated and calculated full-scale wake fractions. (form factor = 0.2, $C_A = 0$, [1] $F_X = 0.3$, $F_T = 0.7$), JBC test case.

	ITTC'78 (no ESD)	**ITTC'99 with ESD**
Reference	0.350	-
PSS 2p	-	0.414
PSS 3p	-	0.459
	ITTC'21 with ESD	**Full-scale RANSE**
Reference	-	0.313
PSS 2p	0.403[1]	0.408
PSS 3p	0.427[1]	0.464

Based on these results, which are not themselves conclusive due to the scarcity of configurations/combination of ESD and ship types, further investigations on the most appropriate extrapolation strategy for ship wakes affected by the presence of ESDs are recommended for future ITTC activities. Because of the difficulties of obtaining sharable geometries, a benchmark using available ships and non-commercial ESD designs would be preferred.

4. BENCHMARK STUDY ON THE EFFECT OR RE AT MODEL SCALE AND SCALING METHODS FOR FULL SCALE PREDICTION

The 28th ITTC initiated comparative CFD studies on conventional and unconventional (tip rake) propellers. A benchmark study, focusing on the effect of Re at model scale and on the scaling method for full scale, was proposed during the 29th ITTC as a task for the following ITTC. During the 30th ITTC, the benchmark was arranged and disseminated. Results collected by the Resistance and Propulsion Committee are collected in the following sections.

The two propellers adopted for the benchmark were, again, the VP1306 (aka PPTC) and the tip rake propeller P1727 (aka PPTC_2), kindly made available by SVA Potsdam (https://www.sva-potsdam.de/en/ittc-benchmark/). This choice was dictated by the availability of these geometries for easy sharing among participants. Additionally, several benchmarking activities have been already carried out on these propellers.

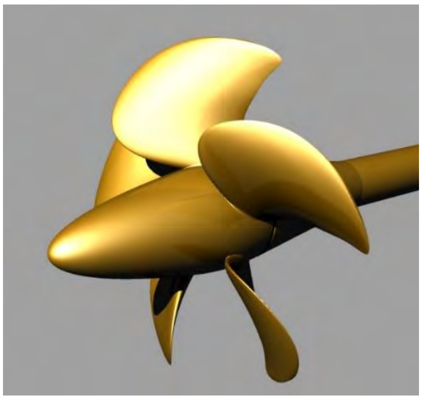

Figure 5 - 3D view of the PPTC propeller, “closed gap” version

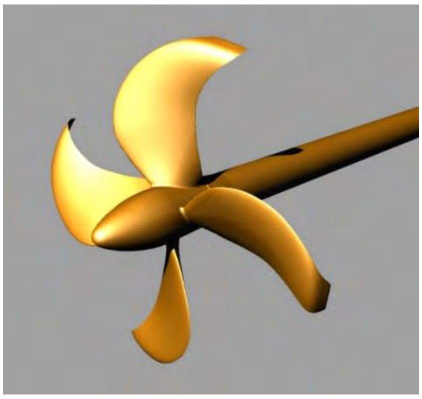

Figure 6 - 3D view of the PPTC_2 propeller, “closed gap” version

For the benchmark, contributors were requested to perform calculations at both model and full scale. Model scale results were collected for four different rates of revolution of the propellers, covering a relatively large range of testing conditions typical of towing tank/cavitation tunnel experiments.

Detailed instructions were provided to limit as much as possible uncertainties on the computational domain and numerical setup (domain size, use of transition sensitive turbulence model and turbulence intensity). Data were collected in dedicated questionnaires.

Table 4 - Functioning conditions – PPTC propeller

	Model Scale	*Full Scale*
Diameter [m]	0.25	3
rps	[10; 12.5; 15; 17.5]	4.33
Avg. $Re_{0.75r/R}$	0.6 to 1.05 $*10^6$	$36*10^6$

Table 5 - Functioning conditions – PPTC_2 propeller

	Model Scale	*Full Scale*
Diameter [m]	0.2386	7.5
rps	[12; 15; 18; 21]	3.21
Avg. $Re_{0.75r/R}$	0.36 to 0.64 $*10^6$	$86*10^6$

Only six institutions sent data. Since some of them performed analyses using different tools and setups (transition sensitive and fully turbulent models), in total 10 sets of results for the conventional and 8 for the non-conventional propellers are available. StarCCM+, Fluent, CFX and OpenFOAM were the preferred computational tools for the analyses. MARIN used its in-house ReFRESCO code. Most of the calculations were presented using transition sensitive turbulence model (Gamma-based) with wall-resolved boundary layer (y+<<1) at model scale. Some participants sent data using only fully turbulent analyses at model scale, employing wall-functions (y+>40) and utilising only a limited number of prism layers. For transition sensitive analyses in most of cases the turbulence intensity was fixed equal to 1% on the propeller plane. For some participants, this was the value set at the inlet boundary, leading to a smaller value on the propeller plane due to decay. Other participants made use of decay controlling techniques (calibration of inlet value to achieve the required intensity on the propeller plane, turbulence intensity sources to counteract the turbulent decay). Only one participant performed calculations with a custom turbulence intensity (1.5%) based on its own experience.

Collected data were compared with model scale experiments (when available) and against each other. Scale effects were addressed by computing percentage differences of full-scale data ($_{fs}$) with respect to model scale ($_{ms}$) results:

The thrust and torque coefficient corrections are given by the following:

$$\Delta K_T = \frac{K_{Tfs} - K_{Tms}}{K_{Tms}}$$

$$\Delta K_Q = \frac{K_{Qfs} - K_{Qms}}{K_{Qms}}$$

The format of these formulae mean that a positive value of Δ corresponds to an increase in performance at full scale. Please note that this convention is opposite to what is typically assumed in ITTC procedures for scaling of the thrust coefficient.

Table 6 - Overview of the participants

Institute	VP1304	P1727
Samsung Heavy Industries	✓	✓
University of Genoa	✓	✓
INTA – CEHIPAR	✓	✓*
Akashima Laboratory	✓	✓
Japan Marine United Corporation	✓	✓
MARIN	✓*	

* not the entire set of rps

4.1 Results for the conventional propeller VP1304

The general trends of the results for the conventional propeller are similar to those observed by the 28th ITTC. By looking at the calculations at 15 rps, for which model scale experimental results are available from SVA POTSDAM, it is possible to observe a certain underestimation of thrust, which is more pronounced at higher advance coefficients. Calculations using transition sensitive models are generally closer to experiments while the few fully turbulent analyses tend to underestimate the thrust up to 10% at the design point (design advance coefficient of 1.269). Torque is generally better predicted. When transition sensitive models are employed the general trend is a slight overestimation at lower advance coefficients and a slight underestimation at high advance coefficients. Fully turbulent analyses under-predict the torque over almost the entire range of realistic conditions.

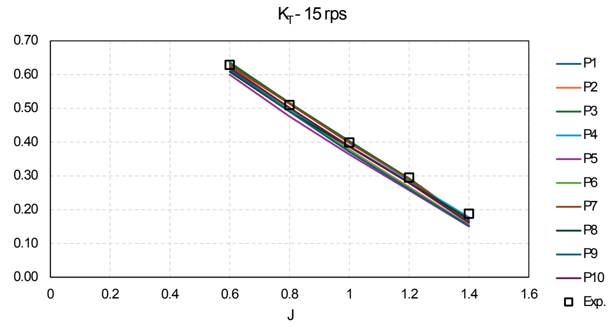

Figure 7 - Thrust coefficient at the rate of revolution (15rps) of experiments. Results for VP1304

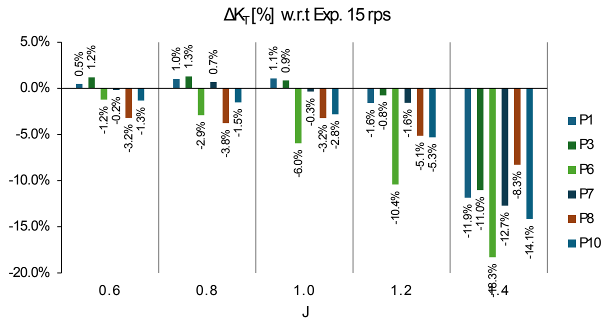

Figure 10 - Percentage difference (Thrust) with respect to experiments at 15 rps - transition sensitive analyses Results for VP1304

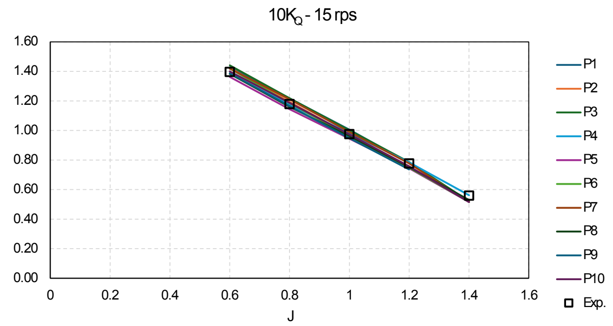

Figure 8 - Torque coefficient at the rate of revolution (15rps) of experiments. Results for VP1304

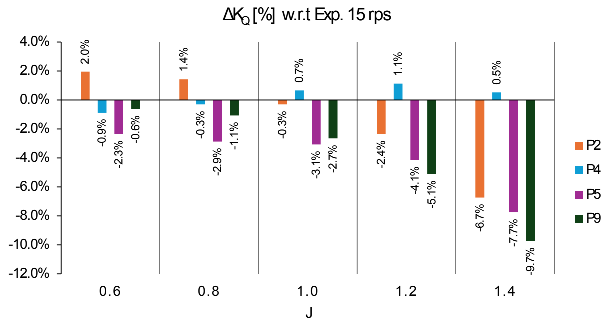

Figure 11 - Percentage difference (Torque) with respect to experiments at 15 rps - fully turbulent analyses

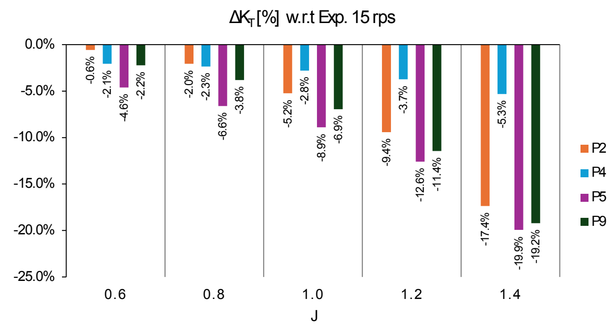

Figure 9 - Percentage difference (Thrust) with respect to experiments at 15 rps - fully turbulent analyses

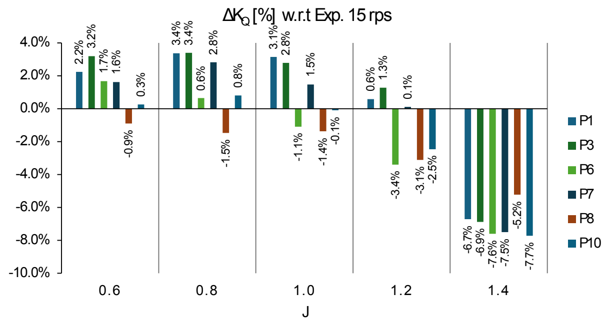

Figure 12 - Percentage difference (Torque) with respect to experiments at 15 rps - transition sensitive analyses Results for VP1304.

Full scale data seem to have less deviation for both thrust and torque, with the exception of two outliers (one significantly overestimated, one significantly underestimated).

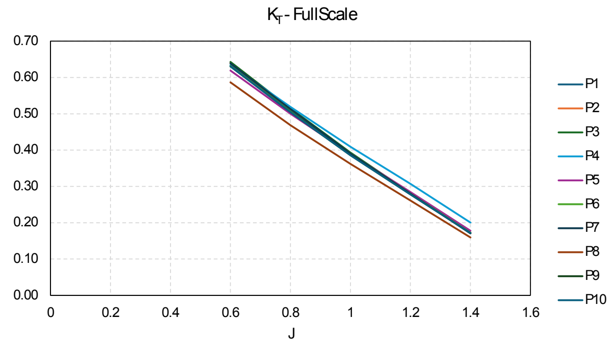

Figure 13 - Full-scale thrust coefficient of VP1304

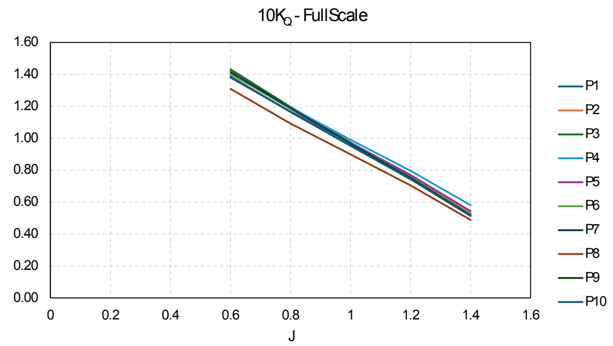

Figure 14 - Full-scale torque coefficient of VP1304

The resulting model-to-ship scaling is affected by non-negligible uncertainties, especially if the entire set of rotational rates is addressed. Two main features can be observed when relating data with the numerical models employed for the analyses. With the use of transition sensitive models (see data P1, P3, P7 and P8), model scale calculations, at most Reynolds numbers in the selected range, tend to predict values of model scale thrust and torque higher than those at full scale (using fully turbulent models). This results in scale corrections which are negative (based on the sign assumption of previous equations) for both thrust and torque. This is contrary to what is usually accepted (i.e. increased thrust and decreased torque at full-scale, due to the lower frictional coefficient). Reasons for this behaviour can be found in the "cambering effect" of radial streamlines, if laminar flow is occurring at model scale, which changes the lift coefficient of the blade sections. If significant laminar flow is present then abrupt separation characteristics can also cause a substantial increase in the sectional pressure drag. Transition sensitive calculations with the 1.5% turbulence intensity level (P10) mitigate this tendency, due to a large extension of the turbulent region at model scale, resulting in a model scale thrust that is more similar to the fully turbulent full scale data, at least for some loading conditions.

Scaling to full-scale, starting from model scale fully turbulent analyses, is in line with usual expectations, showing the generally accepted increase of thrust. Also, the values of torque are sometimes increased (whereas a decrease would typically be expected), but of a smaller amount compared to thrust, which then leads to an increase in the predicted open-water efficiency.

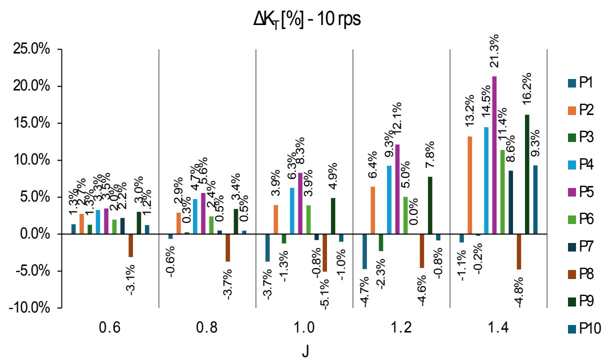

Figure 15 - Predicted scale effect (Thrust) for VP1304 at 10 rps (600 rpm)

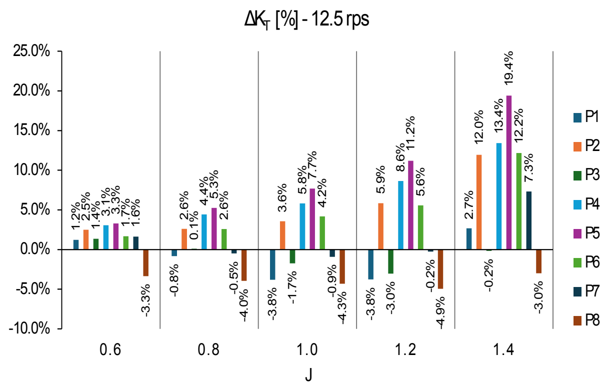

Figure 16 - Predicted scale effect (Thrust) for VP1304 at 12.5 rps (750 rpm)

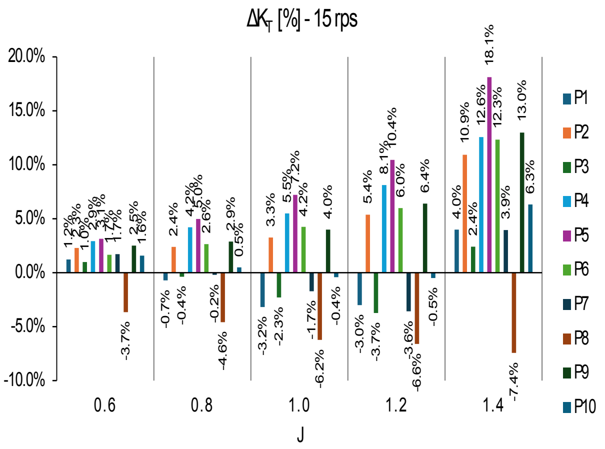

Figure 17 - Predicted scale effect (Thrust) for VP1304 at 15 rps (900 rpm)

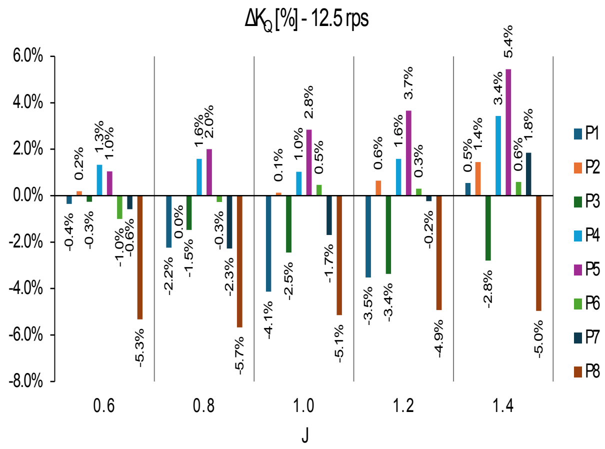

Figure 20 - Predicted scale effect (Torque) for VP1304 at 12.5 rps (750 rpm)

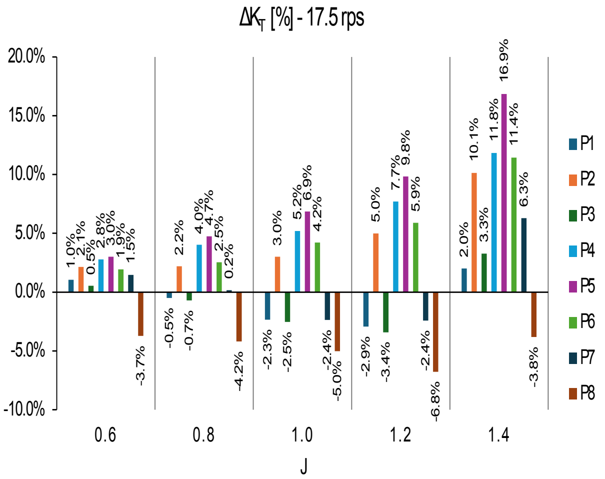

Figure 18 - Predicted scale effect (Thrust) for VP1304 at 17.5 rps (1050 rpm)

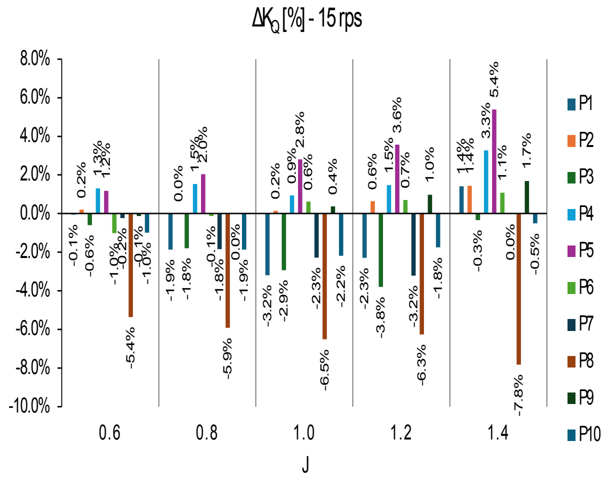

Figure 21 - Predicted scale effect (Torque) for VP1304 at 15 rps (900 rpm)

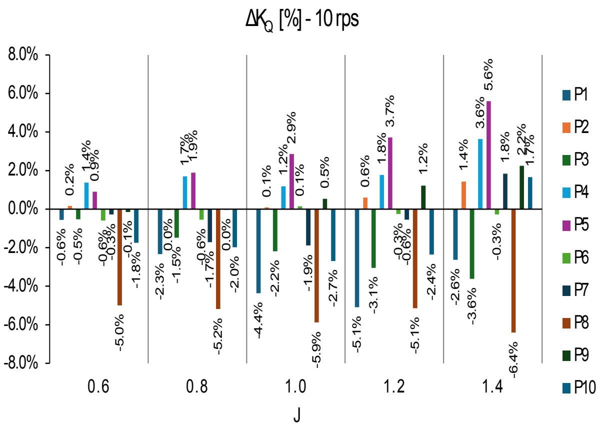

Figure 19 - Predicted scale effect (Torque) for VP1304 at 10 rps (600 rpm)

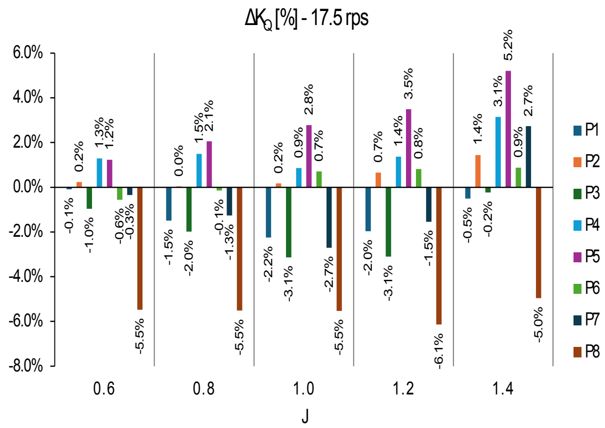

Figure 22 - Predicted scale effect (Torque) for VP1304 at 17.5 rps (1050 rpm)

Compared to usual ITTC-based scaling, CFD analyses generally overestimate the model-to-full scale effects by a significant margin. Regardless of the "sign" of the correction, numerical calculations predict variations between model and full scale of the order of 2-6%, on average, depending on J for both thrust and torque. ITTC '78 corrections are significantly lower, smaller than 0.2% (thrust) and 0.5% (torque) when computed using the suggested blade surface roughness of 30 x10^{-6} m (ITTC – Recommended Procedures and Guidelines - 7.5 – 02-03 – 01.4, effective date 2021 – rev. 05)

Also, when compared with data obtained having greatly reduced values of surface roughness (all the full scale CFD calculations were carried out using smooth surfaces, i.e. not employing roughness sensitive wall functions or corrections), the suggested scaled values from the ITTC procedure, especially for the thrust coefficient, are substantially lower than what is observed from the CFD calculations.

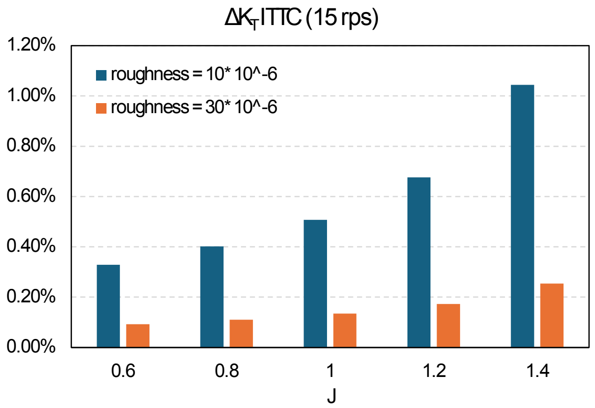

Figure 23 - ITTC scale effect (Thrust) for VP1304 at 15 rps (900 rpm)

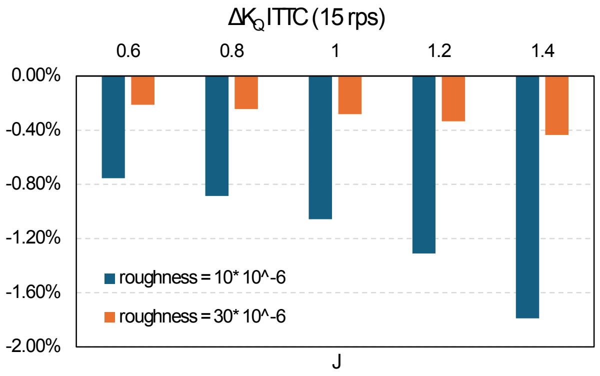

Figure 24 - ITTC scale effect (Torque) for VP1304 at 15 rps (900 rpm)

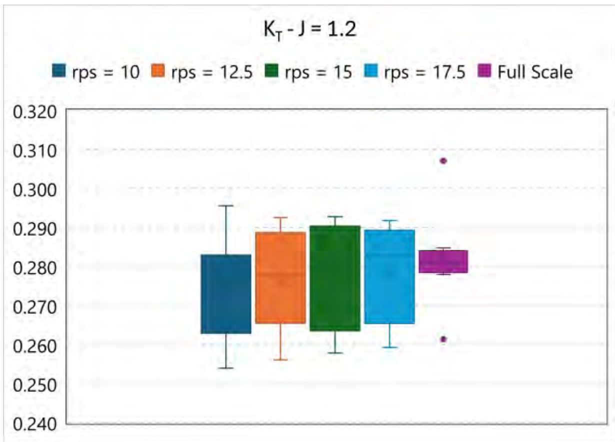

Figure 25 – Thrust coefficient statistics (mean/max/min/upper and lower quartile) at the design advance coefficient for VP1304

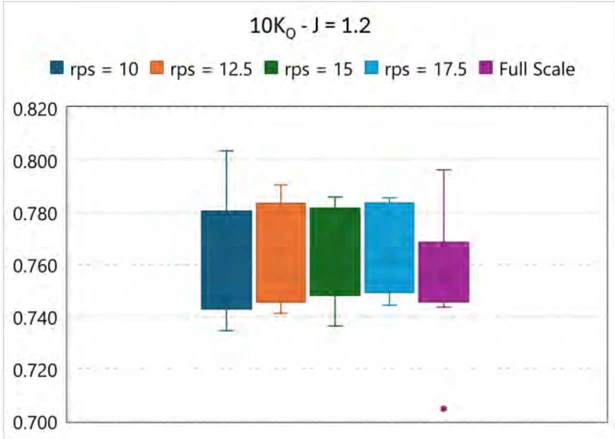

Figure 26 – Torque coefficient statistics (mean/max/min/upper and lower quartile) at the design advance coefficient for VP1304

4.2 Results for the unconventional propeller P1727

Results for the unconventional P1727 propeller confirm the trends observed for VP1304. Also, in this case, the comparison with the experimental data at 18 rps shows a certain deviation of calculations which, in this case, are equally over- and under- predicted. Overall, also for this propeller and its range of Reynolds numbers (lower than the previous tests case), calculations employing transition sensitive models are closer to experiments (1-2%) while fully turbulent calculations predict, on average, deviation up to 10% (underestimation) at the design point.

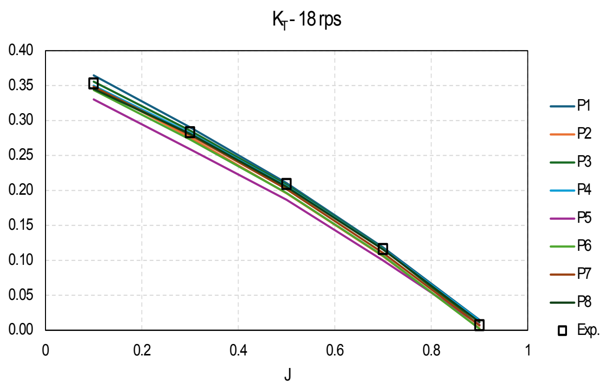

Figure 27 - Thrust coefficient at the rate of revolution (15 rps) of experiments. Results for P1727

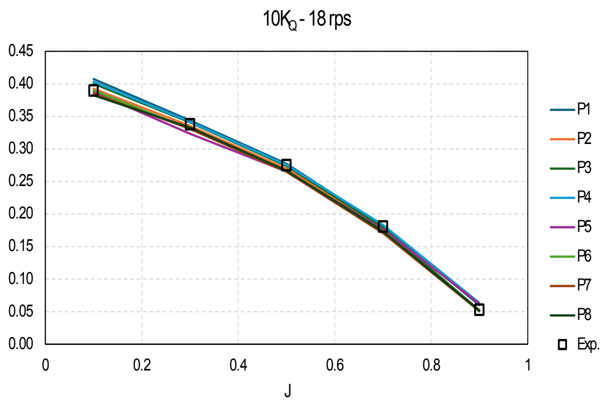

Figure 28 - Torque coefficient at the rate of revolution (15rps) of experiments. Results for P1727

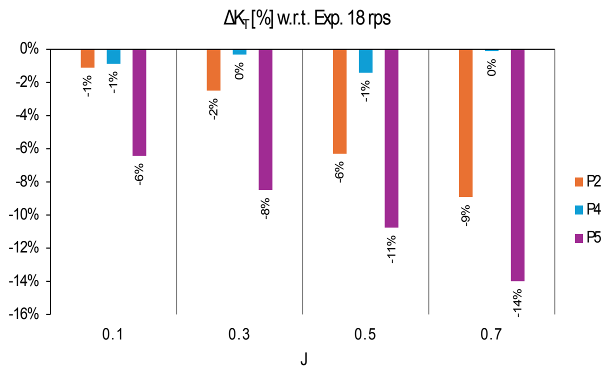

Figure 29 - Percentage difference (Thrust) with respect to experiments at 18 rps - fully turbulent analyses

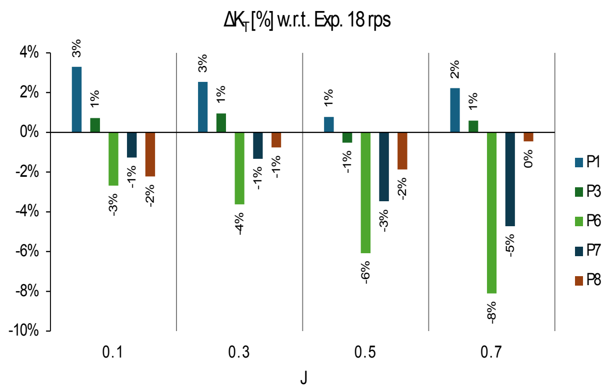

Figure 30 - Percentage difference (Thrust) with respect to experiments at 18 rps - transition sensitive analyses Results for P1727

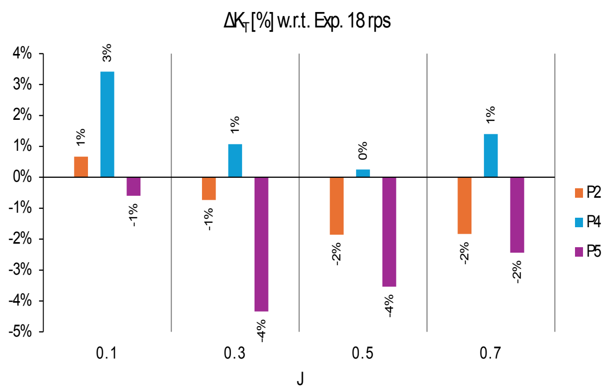

Figure 31 - Percentage difference (Torque) with respect to experiments at 18 rps - fully turbulent analyses

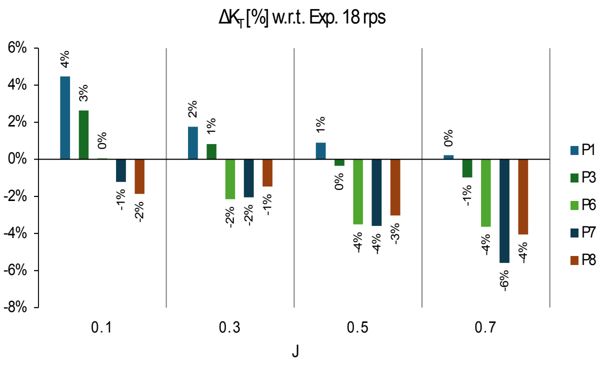

Figure 32 - Percentage difference (Torque) with respect to experiments at 18 rps - transition sensitive analyses Results for P1727

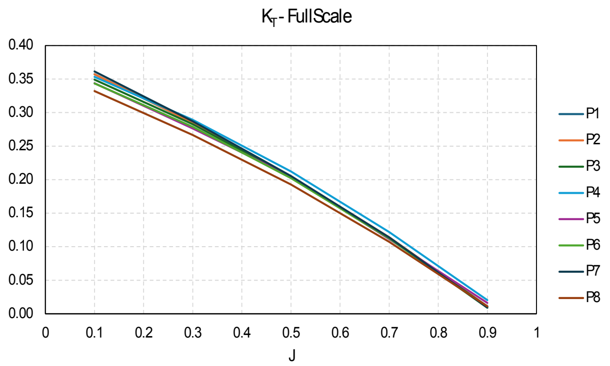

Figure 33 - Full-scale thrust coefficient of P1727

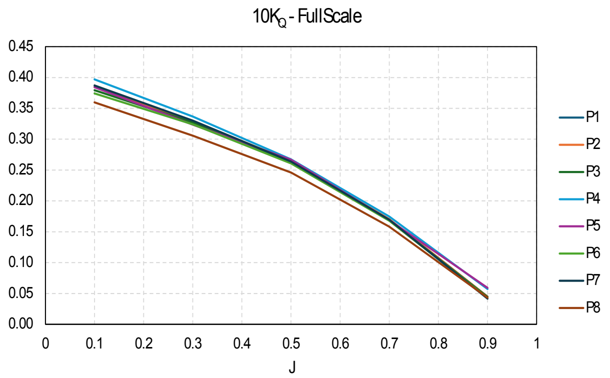

Figure 34 - Full-scale torque coefficient of P1727

In contrast, the full-scale data appear to be more scattered than what was observed for VP1304, which leads to even more complex trends. As a general statement, full scale scaling starting from fully turbulent model scale results shows increase of K_T and proportionally smaller Δ value (usually a decrease) of K_Q. Analyses with the transition sensitive models generally repeat the trends seen with VP1304. However, in some cases, it is possible to observe both decrease and increase of thrust correction from model to ship size as the advance coefficient varies, which is believed to principally due to the variation in Re as the rate of revolutions is varied..

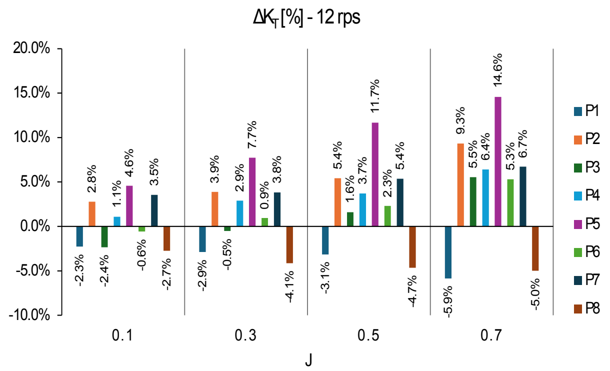

Figure 35 - Predicted scale effect (Thrust) for P1727 at 12 rps (720 rpm)

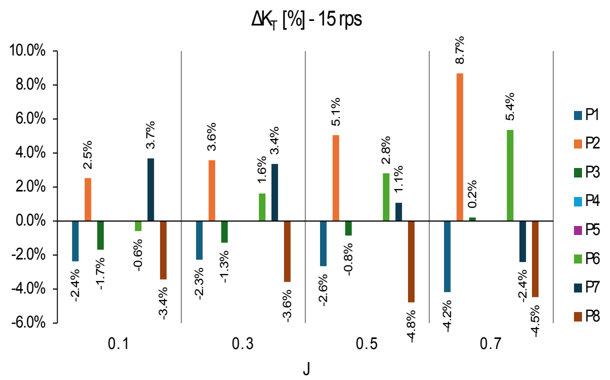

Figure 36 - Predicted scale effect (Thrust) for P1727 at 15 rps (900 rpm)

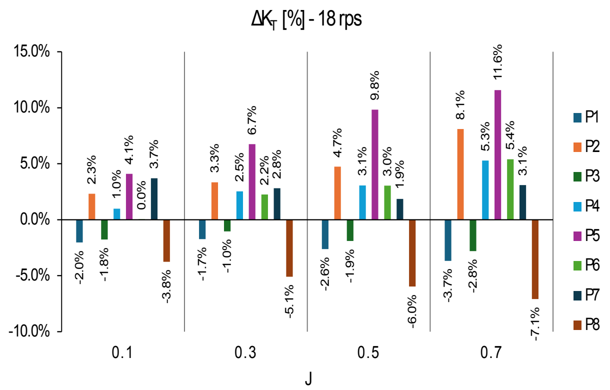

Figure 37 - Predicted scale effect (Thrust) for P1727 at 18 rps (1080 rpm)

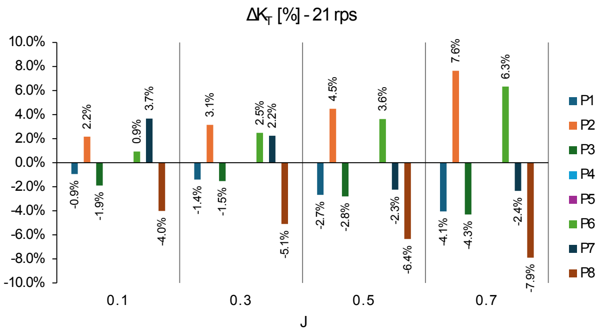

Figure 38 - Predicted scale effect (Thrust) for P1727 at 21 rps (1260 rpm)

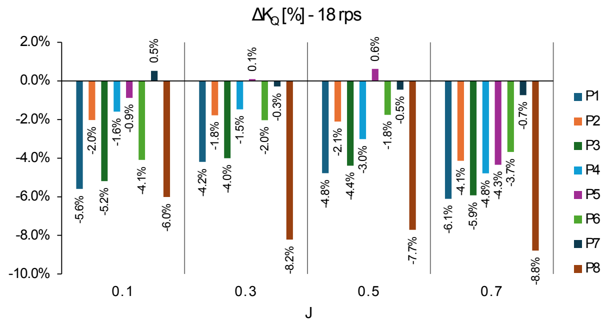

Figure 41 - Predicted scale effect (Torque) for P1727 at 18 rps (1080 rpm)

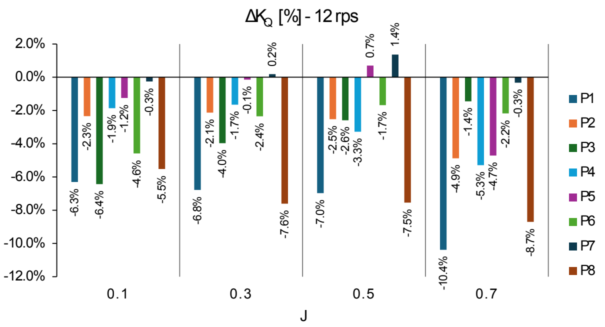

Figure 39 - Predicted scale effect (Torque) for P1727 at 12 rps (720 rpm)

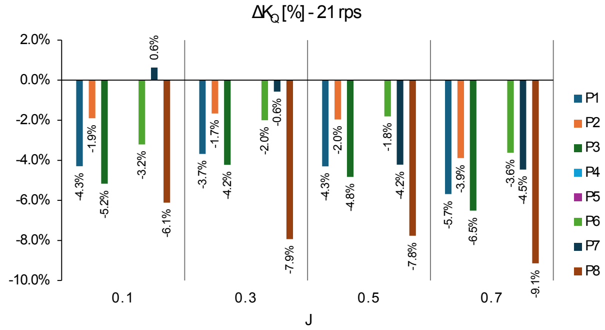

Figure 42 - Predicted scale effect (Torque) for P1727 at 21 rps (1260 rpm)

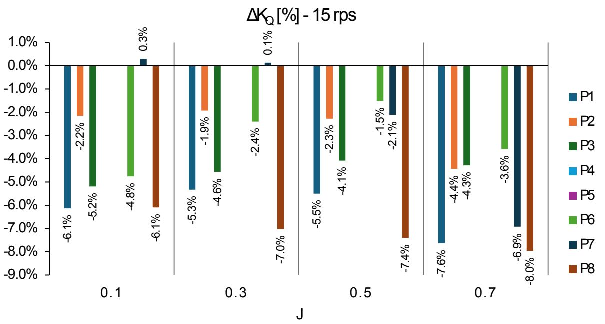

Figure 40 - Predicted scale effect (Torque) for P1727 at 15 rps (900 rpm)

The comparison with the ITTC ’78 scaling method shows the same inconsistencies observed for the conventional propeller. CFD predicted scale correction are far higher than standard ITTC values which, even in the case of hydraulically smooth surfaces (closer to numerical calculations), are three or four times smaller.

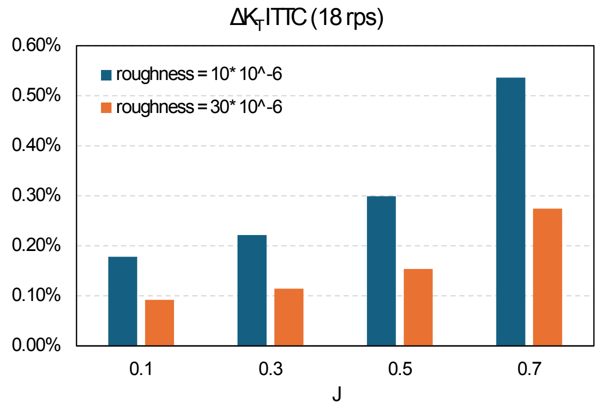

Figure 43 - ITTC scale effect (Thrust) for P1727 at 18 rps

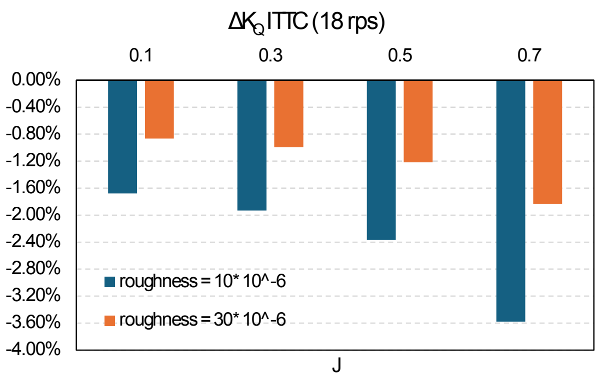

Figure 44 - ITTC scale effect (Torque) for P1727 at 18 rps

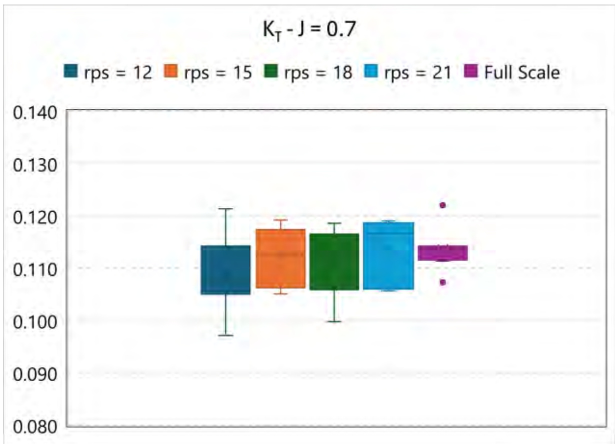

Figure 45 – Thrust coefficient statistics (mean/max/min/upper and lower quartile) at the design advance coefficient for P1727

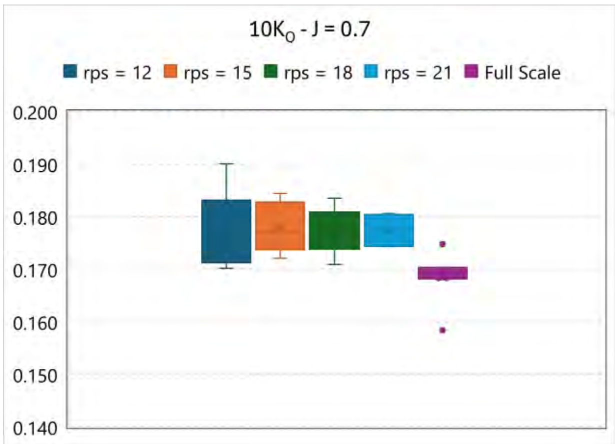

Figure 46 – Torque coefficient statistics (mean/max/min/upper and lower quartile) at the design advance coefficient for P1727

4.3 Final considerations

The analyses carried out for the geometries proposed by the benchmark show a certain number of small uncertainties, especially at model scale, that when taken in combination may lead to a significantly different assessment of the scaling effect. The use of transition sensitive calculations permits, in general, more accurate prediction of the model scale performance, since the underestimation of thrust and torque observed with fully turbulent analyses is substantially reduced. The high sensitivity to inflow conditions (not always available from experimental data) and the turbulence decay process (or how to control it), however, raise the question of whether an accurate full-scale prediction can be made from model-scale data (Kerkvliet *et al*. 2024) without knowing the results *a priori* (i.e. blade streamlines through paint flow tests or, more roughly, measured open water performance) for a calibration of the turbulence intensity parameters. The high sensitivity to turbulence intensity, shown in some additional calculations of the participants, as well as in recent papers (Gaggero, 2020, Rubino and Abdel Maksoud, 2024, Kerkvliet *et al.* 2024), may explain the unexpected behaviour of K_T and K_Q scaling behaviour when model scale calculations are performed at very low turbulence intensity and Re number without any feedback in terms of real behaviour of the flow over the blades. Slightly higher turbulence intensity may determine completely different scaling, moreover dependent on the propeller geometry, nullifying the efforts for a poorly calibrated numerically based scaling approach/tool. This makes the topic still worth of additional investigations. Better controlled model scale experiments to validate numerical tools (including measurement or recording of the inflow turbulence intensity level) may be useful. Fully-turbulent model scale measurements using non-intrusive tripping (Kerkvliet *et al.* 2024), on the other hand, may provide better characterization of the open water propeller performance thanks to the low numerical uncertainty and improved similarity with full-scale flow regimes.

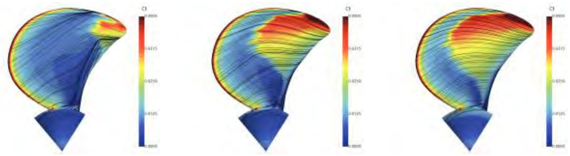

Turb. Int. = 1%   Turb. Int. = 1.4%   Turb. Int. = 1.8%

Figure 47 - VP1304 skin friction coefficient and streamlines at the design advance coefficient as a function of turbulence intensity (15 rps, from additional calculations of Participant 3).

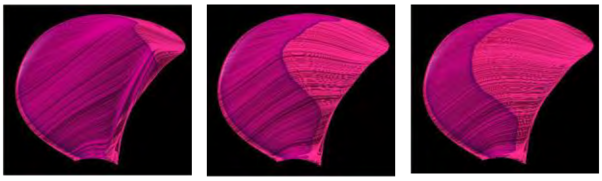

Turb. Int. = 1%   Turb. Int. = 1.4%   Turb. Int. = 2%

Figure 48 - VP1304 skin friction coefficient and streamlines at the design advance coefficient as a function of turbulence intensity (15 rps, from additional calculations of Participant 10).

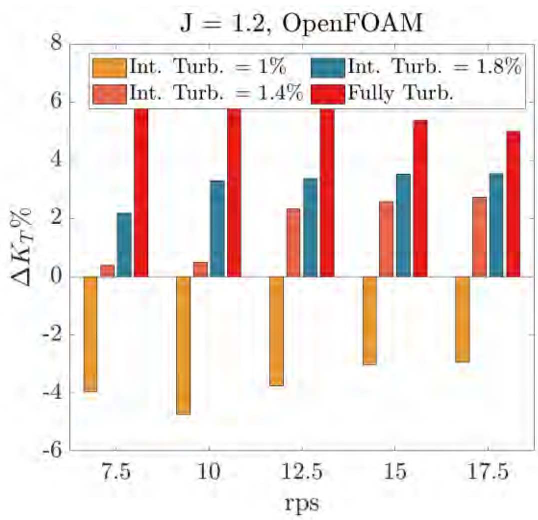

Figure 49 - Scale effect on thrust coefficient for VP1304 at the design advance coefficient as a function of rate of revolution and turbulence intensity at the propeller plane (from additional calculations of one of the participants).

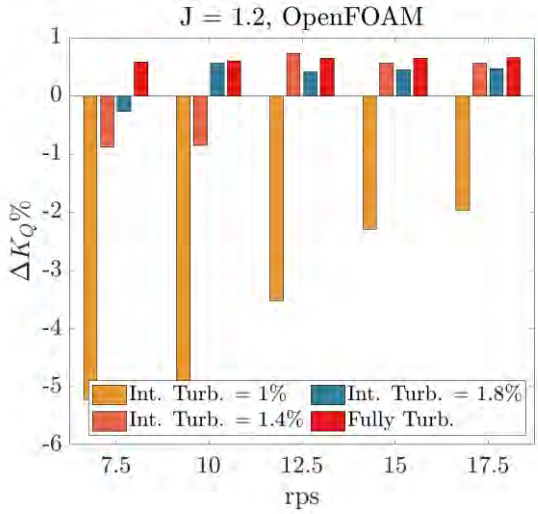

Figure 50 - Scale effect on torque coefficient for VP1304 at the design advance coefficient as a function of rate of revolution and turbulence intensity at the propeller plane (from additional calculations of one of the participants).

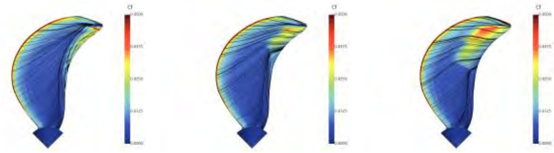

Turb. Int. = 1%   Turb. Int. = 1.4%   Turb. Int. = 1.8%

Figure 51 - P1727 skin friction coefficient and streamlines at the design advance coefficient as a function of the turbulence intensity (18 rps, from additional calculations of one of the participants)

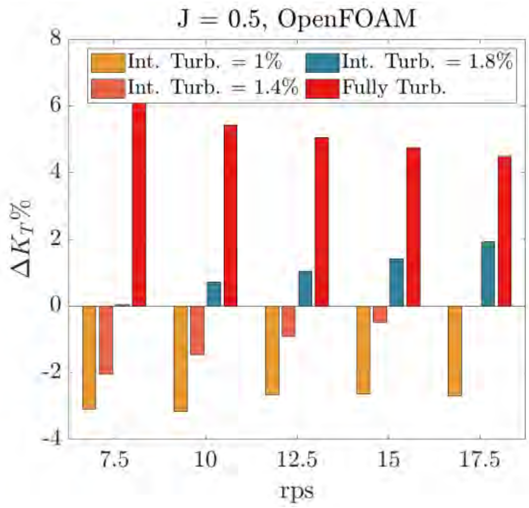

Figure 52 - Scale effect on thrust coefficient for P1727 at the design advance coefficient as a function of rate of revolution and turbulence intensity at

the propeller plane (from additional calculations of one of the participants)

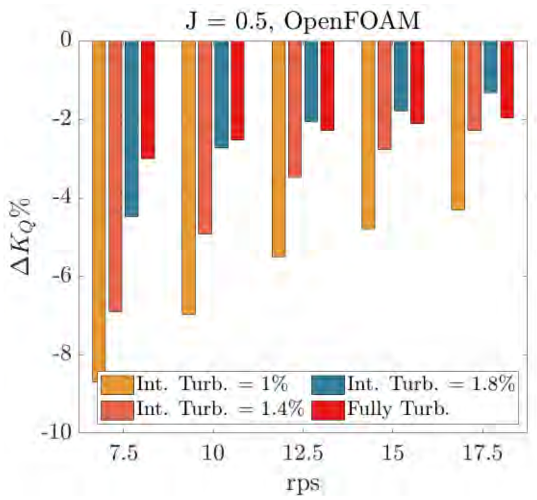

Figure 53 - Scale effect for P1727 at the design advance coefficient as a function of rate of revolution and turbulence intensity at the propeller plane (from additional calculations of one of the participants)

5. INVESTIGATION OF THE ISSUE OF LAMINAR EFFECTS IN SELF-PROPULSION TEST OF PROPELLER WITH LOW BLADE AREA

5.1 Introduction

Self-propulsion tests are often conducted at Reynolds Numbers (Re) lower than desirable, because many recent propellers have low blade area and short chord lengths in order to achieve high efficiency. The low Re can lead to an unexpected reduction in the calculated relative-rotative efficiency, η_R, which leads to difficulty when attempting to use the current scaling procedure as described in the ITTC '78 Performance Prediction Method.

While this is not a new problem, as there have been many discussions under previous ITTC committees, the trend towards low operating ship speeds and the pursuit of even smaller efficiency gains to reduce greenhouse gas emissions give this problem even greater importance in the current world.

Firstly, a survey was conducted to find out how ITTC members tackle this issue. Subsequently, a literature review was conducted, investigating how these low Re effects could be addressed.

5.2 Survey results

The committee conducted a survey on three topics: A) Self-Propulsion Test (SPT), B) Propeller Open water Test (POT) and C) Propeller scaling procedure. Fifteen organizations responded. The geographical region and organizational type of the respondents are shown below.

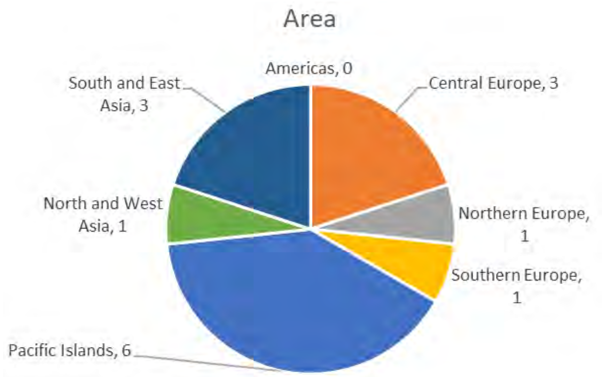

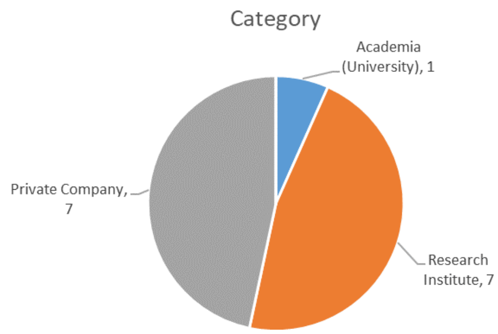

<u>A. Self-propulsion test</u>

A1. Have you ever had any problems with a self-propulsion test due to low Re?

- More than half of the respondents answered "YES".

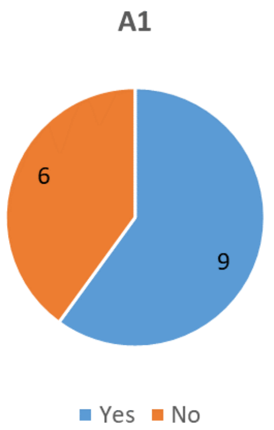

A2. Please let us know what problem you encountered and what Re was then.

- Self-propulsion factors, especially η_R, were unreasonable.
- Measurement values significantly scattered.
- Re was below 2×10^5.

A3. Please let us know how you dealt with the problem.

- Enlarge dimension of a ship model.
- Check with a conventional large blade area propeller.
- Check with a 2-POT method.
- The η_R obtained at the highest Froude number was used as a constant value.
- Apply a turbulent stimulator.

A4. Please let us know the typical value of length of the model ship, the diameter of the model propeller and the minimum speed of the model ship in a self-propulsion test, and whether a design propeller or a stock propeller was used.

- The length of model ranges from 4m to 12 m. Models of length 7 m to 8 m were most typical.
- The diameter of the model propellers range from 0.2 m to 0.3m.
- The minimum towing speed ranges from 0.8m/s to 2m/s. 1m/s being the most common.
- Most of the respondents use both stock and design propellers depending on the scale and extent of the testing programme.

A5. It is recommended in ITTC Recommended Procedure 7.5-02-03-02.1 that; *The propeller open water tests should be conducted at least at two Reynolds Numbers; one should be at the Reynolds Number used for the evaluation of the propulsion test, which should be not lower than* 2×10^5 *and the other should be as high as possible*. It is recommended that the open water characteristics at low Re are used to analysis the self-propulsion test. Do you follow the recommendation? If your answer is YES, please let us know which Re you select. (eg. The exact same as the self-propulsion test or specific value like 3×10^5 regardless of actual Re at self-propulsion test) If your answer is NO, please let us know the reason.

- Most of the respondents answered “No”.
- The flow in behind condition is assumed to be turbulent (i.e. different from POT).
- The database of model-ship correlations has been established based on the self-propulsion factors using the Propeller Open Water Characteristics (POWC) at the high Re.
- POT at multiple Re is expensive.
- The measurement values of the POW at the low Re are unsteady.
- There is no universal view which Re is appropriate to represent the behind condition.

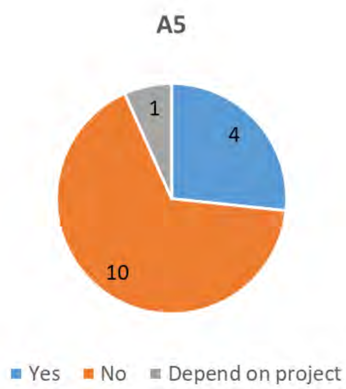

A6. Do you have any idea to solve problems with a self-propulsion test due to low Re?

- Carry out repeated tests and take longer measurements.
- Increase the size of a model ship.
- Use a 2-POT method.

- Use turbulence stimulators.
- Use a stock propeller with larger blade area.
- Carry out POT with simulated inflow turbulence (2-3% of turbulent intensity).

<u>B. Open water test</u>

B1. Have you ever had any problems with an open water test due to low Re?

- More than half of the respondents answered "NO".

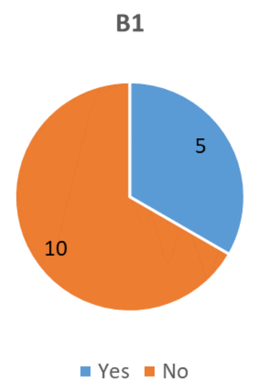

B2. Please let us know what problem you encountered and what the Re was.

- Poor reproducibility.
- Very different from the CFD simulation.

B3. Please let us know how you dealt with the problem.

- Use the most reasonable value from the repeated tests.
- Use turbulence stimulators.

B4. It is recommended in RP 7.5-02-03-02.1 that the open water characteristics at highest Re are used for full scale power prediction. Do you follow the recommendation?

- Most of the respondents answered "Yes".

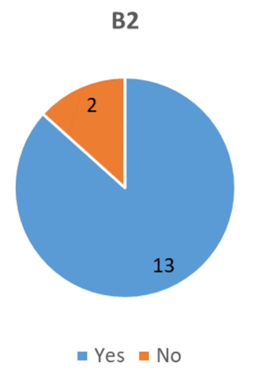

B5. Do you conduct an open water test at multiple Re each time in order to investigate the Re dependency?

- More than half of the respondents answered "Yes".

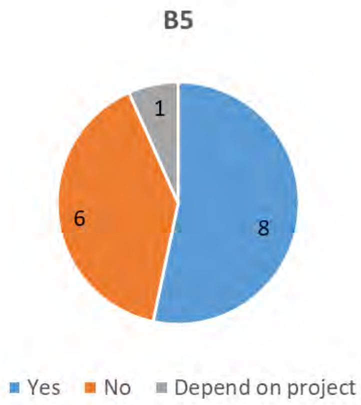

B6. Do you think the minimum Re, 2×10^5, in the present ITTC procedure is sufficient for obtaining the stable open water characteristics?

- More than half of the respondents answered "NO".
- Large laminar effect remains at Re of 2×10^5.
- The minimum should be higher than 5×10^5.
- Re should be above the transition from laminar to turbulent flow.
- A fixed value is not reasonable due to the plurality of different propeller designs.

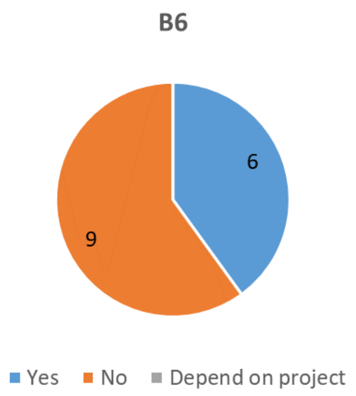

C. Propeller scaling procedure

C1. Do you scale an open water characteristics at model test for full scale power prediction?

- More than half of the respondents answered "NO".
- Model-ship correlation factors have been established based on the procedure using no scaled propeller open-water curve.
- There is no reasonable simple method considering the change of K_T.
- The propeller open-water curve at the highest Re can represent the full scale propeller open-water curve.

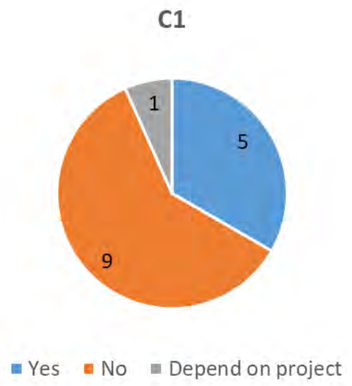

C2. Which kind of a scaling method do you use? (ex. ITTC-78, own procedure)

- All the respondents except one stated that they use the "ITTC '78 method".

C3. Please let us know on what Re is based when scaling.

- The highest Re

C4. Have you ever had any problems with scaling?

- Most of the respondents answered "NO".

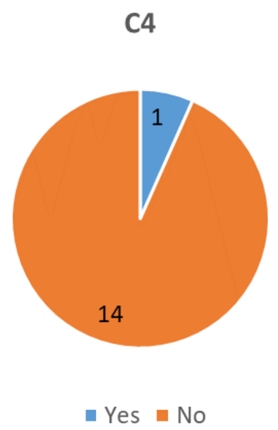

C5. Please let us know what problem you encountered and what Re was then.

- The scaled down propeller open-water curve did not correspond to the measured one at low Re.

C6. Please let us know how you dealt with the problem.

- Apply a 2-POT method.

Summary

According to the survey, more than half of the respondents have problems with the self-propulsion test, while not as many have problems with open-water test or the scaling method. Thus, the focus of the literature review was placed upon investigating the problems with the self-propulsion test. The problems that many organizations consider are as follows.

- Self-propulsion factors obtained, especially η_R, are unreliable.
- Measurement accuracy is reduced due to small measurement quantities.

Because the latter is highly dependent on the facility's dynamometer specification, the literature regarding the former was reviewed. The problem arises from an inconsistence in the propeller characteristics, i.e. the boundary layer regime on the blade surface, between open water and behind condition.

Thus, the direct solution to this problem is to make the open water characteristics used for self-propulsion factor analysis as similar as possible to the behind condition.

There are two approaches. One is to use a 2-POT method and the other is to use turbulence stimulation techniques.

5.3 2-Propeller Open-water Test method

The 2-POT method uses the propeller open-water curve at the same or similar Re as the self-propulsion test for analysis of the model-scale self-propulsion data and then uses the high Re propeller open-water curve data to make the full-scale powering predictions. This method is based on the assumption that the flow characteristics on the blade in the behind condition are similar to those in the open water condition at the same or similar Re. In contrast, a 1-POT method uses the same high Re propeller open-water curve for both the self-propulsion analysis and the full-scale powering predictions.

The effectiveness of the 2-POT method has long been studied. One of the earliest studies was by Tamura et al (1977). They concluded that the 2-POT method is preferable to the 1-POT method to obtain reasonable self-propulsion factors, i.e. effective wake ratio and η_R, by observing the flow patterns on the blade in both the open water and behind conditions and by comparing the results against self-propulsion factors analysed using propeller open-water curve using turbulent stimulators.

More recent studies by Hasuike et al. (2017) and Lücke et al. (2017) were introduced in the report of the 29th ITTC Resistance and Propulsion committee (2021). They performed CFD calculations to investigate the flow on the blade, in addition to the paint tests included in many previous studies, and clearly showed the mixed state of laminar and transitional flow at model-scale, which is different from fully turbulent flow at full-scale. The superiority of the 2-POT method over the 1-POT method was confirmed by highlighting similarities in the flow regime between open water and behind conditions at low Re.

Li et al. (2019) investigated transitional flows and their impact on performance prediction. Similar to the studies by Hasuike et al. (2017) and Lücke et al. (2017), their study included propeller open-water test, self-propulsion test, paint flow visualisation tests and CFD analysis on three propellers: one with a small blade area and two with large blade areas. An unexpected decrease in η_R was only observed for the propeller with the smallest blade area when analysed using the 1-POT method. Although high turbulence intensity and inhomogeneous propeller inflow in behind condition may stabilize the flow on the blade, thereby delaying or preventing flow separation, they were probably insufficient to prevent separation for the smallest blade propeller, which had a steeper negative pressure gradient at the trailing edge than the large blade propellers. Analysing η_R using the propeller open-water curve at high Re with reduced flow separation could result in an unexpected reduction in η_R. They concluded that the reason for the too low η_R was not only the difference in Re between the propeller open-water test and the self-propulsion test, but also the difference in the degree of flow separation. The 2-POT method can be a solution to the issue of too low η_R, but they noted that careful calibration work is needed to identify an appropriate Re for the self-propulsion analysis, as Lücke et al. (2017) used propeller open-water curve data at 40% higher Re, considering the difference in flow characteristics between propeller open-water test and self-propulsion test.

Although various studies have shown the effectiveness of the 2-POT method, and it being recommended in the ITTC Recommended Procedure 7.5-02-03-02.1, many organizations don't use it for the reasons outlined in the survey results.

One of the reasons is the assumption that the flow in behind condition is fully turbulent, unlike in open water. However, this is not clearly supported by the aforementioned studies.

Challenges related to measurement precision for small quantities and inconveniences associated with changes in model-ship correlation factors may also contribute to the reluctance to use the 2-POT method. In addition, an unusual drop of η_R is not evident in all cases. As shown in Lücke et al. (2017) and Li et al. (2019), whether or not the reduction in η_R occurs depends heavily on the particular design of the propeller, e.g. blade area, section profile and chord width load distribution.

However, when the reduction in η_R does occur, the application of the 2-POT method can be highly beneficial. Therefore, it is recommended to perform the propeller open-water test at multiple Reynolds numbers, particularly for propellers with a low blade area ratios and short chord length sections.

5.4 Turbulence Stimulation

The second potential solution is a turbulent stimulator. Turbulence stimulation aims to create similar flow patterns on the blades in both open water and behind conditions and both at model-scale and full-scale conditions, i.e. encourage a fully turbulent flow regime.

As well as the 2-POT method described previously, the effectiveness of turbulence stimulation is well established and proven. The 14th ITTC Propeller committee (1975) investigated the influence of turbulence stimulation on self-propulsion factors and recommended as follows;

"*As mentioned above, not only the correlation method but also the test technique used in testing propellers are important to obtain good correlation between the ship and model. For that the propeller surface should have turbulent flow. Since it is difficult to perform the propeller open water test at a sufficiently high Rn, turbulence stimulation should be introduced for the propeller blades. Considerable work on turbulence stimulation has been devoted to model ships, but very little to model propellers. Cooperative work may be needed to obtain a standard method for stimulating turbulence on the propeller surface. Also, flow survey will be necessary on the propeller surface in the self-propulsion tests.*"

Around the same time as the 14th ITTC (1975), various research was conducted on turbulent stimulators, e.g. Suzuki(1974), Tamura et al. (1977), Tsuda et al. (1978), Ishii et al (1983). They reported the successful transition from a laminar flow to turbulent flow by applying trip wires, sand roughness and studs near the leading edge. Turbulent stimulators can stabilize values of η_R by ensuring consistent flow regime between the open-water test and the self-propulsion test and by mitigating changes in propeller open-water curve with Re. Contradicting these results, studies by Boorsma (2000) and Lücke et al. (2017) suggested that the presence of stimulators did not significantly alter the flow compared to conditions without them, remaining predominantly laminar. They showed that artificial roughening at the leading edge does not consistently induce turbulent flow at model scale. These contradictory results indicate the difficulty in determining the optimal size and location of turbulators, which are highly dependent on the propeller geometry. In addition to the uncertainty associated with making the flow turbulent, a significant decrease in efficiency due to turbulators themselves poses a practical obstacle to their use.

Addressing this issue, Bart Schuiling et al. (2024) introduced a novel turbulent stimulator as shown in Figure 54.

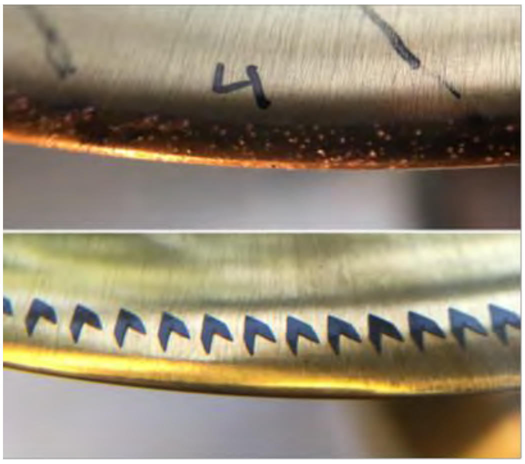

Figure 54 - Sand roughness (top) and novel turbulators (bottom), Bart Schuiling et al. (2024)

It is believed that this method can efficiently trip the flow from laminar to turbulent by generating vortices which resembles the hairpin-like vortical structures crucial to the boundary layer transition process, and with minimal additional drag. As shown in Figure 54 arch-shaped seals made from vinyl foil were attached discretely at the leading edge. Contrary to sand roughness widely used as stimulators on propulsors, the geometry of the turbulators can be accurately defined using CAD, which ensures precise and easy application. The paint test, which utilized also a novel technique using ultra-violet photography, revealed that applying the novel turbulators could successfully trip the flow as shown in Figure 55. They confirmed that the turbulators could mitigate the laminar flow separation for a small blade area propeller, resulting in a smaller change in efficiency as Re was varied. The parasitic drag of the elements was also investigated by varying the height of the element and it was found that penalty on both open water efficiency and thrust coefficient were typically of the order of 0.1% to 0.6%. Although not mentioned in the paper, the novel turbulence stimulators are expected to solve the problem with the prediction of too low η_R.

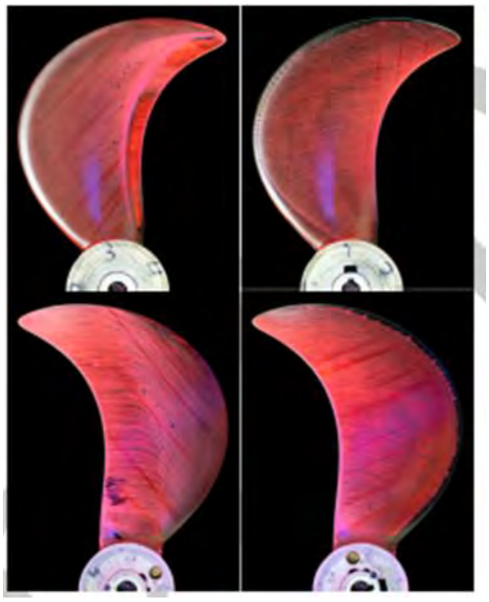

Figure 55 - Comparison of flow patterns without turbulators (left) and with turbulators (right), Bart Schuiling et al. (2024)

The introduction of a new technique is challenging because it requires a change in the model-ship correlation factors that each test facility has accumulated over time. However, accurately predicting full-scale performance and developing the most efficient full-scale propeller is crucial if the IMO's targets on reducing greenhouse gas emissions are to be met. MARIN, the organisation where Schuiling & Kerkvliet work, is running a Joint Industrial Project called "Tripping" to develop new scale corrections for propellers using their novel turbulators. According to the website of Tripping (2024), this project will involve extensive model testing and CFD simulation. This project is in line with the aforementioned recommendation by 14th ITTC Propeller committee (1975) and therefore deserves particular attention in the near future.

6. INVESTIGATION OF THE ISSUE OF EXTRAPOLOATION OF MODEL TESTS WITH DUCTED PROPELLERS TO FULL SCALE ACCORDING TO DIFFERENT REYNOLDS NUMBERS

Studies on the extrapolation to full scale of the performance of ducted propellers are particularly scarce. Only a few studies, based on CFD calculations, are available (Bhattacharyya *et al.*, 2015, 2016a, 2016b) and are limited to propulsors equipped with accelerating nozzles (Nozzle 19A and Nozzle 37). No published data are available for decelerating nozzle configurations.

As one of the activities of the Resistance and Propulsion Committee, some additional CFD analyses on both accelerating and decelerating type ducted propulsors were carried out. Following the guidelines of the benchmark on open propeller performance scaling, the investigation accounted for the influence of turbulence models, turbulence intensity and model scale rate of revolution for two geometries available within the Committee and taken from the EU Funded BESST Project (Gaggero *et al.* 2013).

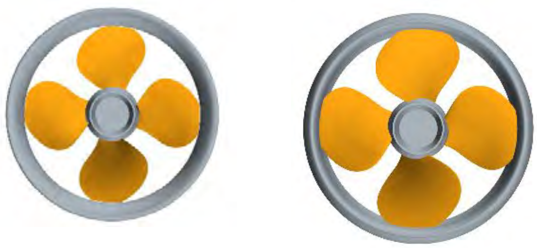

Figure 56 - Accelerating (left) and decelerating (right) ducted propellers

Analyses were repeated at model scale using the fully turbulent SST k-ω turbulence model and the γ-Reθ turbulence sensitive method (three levels of turbulence intensity at the propeller plane). Four advance coefficients at five different choices of rate of revolutions were considered to investigate the influence of propeller loading in a range of functioning conditions typical of model scale experiments. Full-scale values were obtained only using the fully turbulent model.

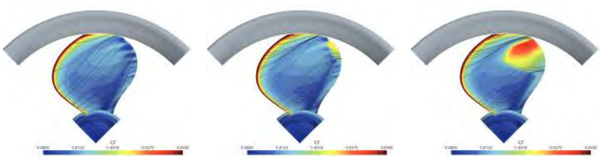

Turb. Int. = 1% Turb. Int. = 1.4% Turb. Int. = 1.8%

Figure 57 - Accelerating ducted propeller: skin friction coefficient and streamlines at the design advance coefficient as a function of the turbulence intensity (15 rps)

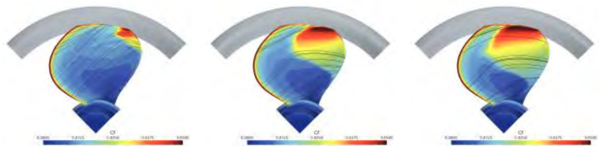

Turb. Int. = 1% Turb. Int. = 1.4% Turb. Int. = 1.8%

Figure 58 - Decelerating ducted propeller: skin friction coef-ficient and streamlines at the design advance coefficient as a function of the turbulence intensity (15 rps).

The limited analyses on ducted propellers show very similar trends and the complexity of phenomena observed for the open propellers. Also, in this case there is a strong influence of the inflow conditions on the model scale predicted performance which make the realization of robust scaling methodologies based on model scale CFD a very demanding task and require, first of all, detailed and accurate model scale measurements to understand the role of flow turbulence.

For this choice of geometries, the accelerating ducted propeller seems less prone to transition to turbulence, even at relatively high values (1.8%) of turbulence intensity estimated in correspondence of the propeller disk. This corresponds, as in the case of open propellers, to computed values (transition sensitive models) of thrust realized by the propulsor blades that are substantially higher at model scale than at full scale.

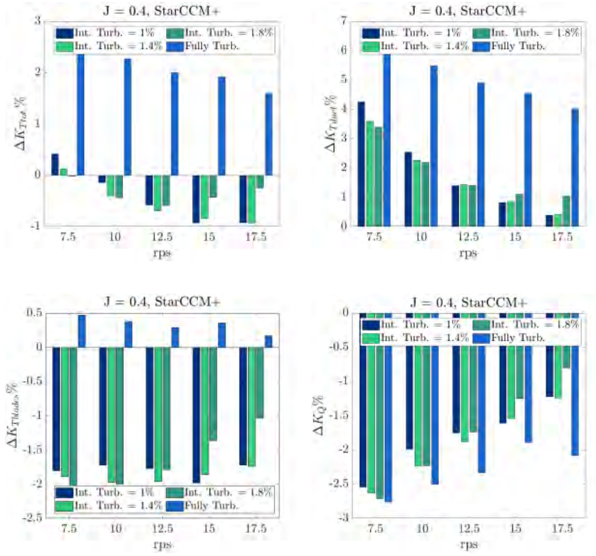

Figure 59 – Scale effect at J = 0.4 for the Accelerating ducted propeller (total thrust, thrust of the duct alone, thrust of the blades alone, total torque)

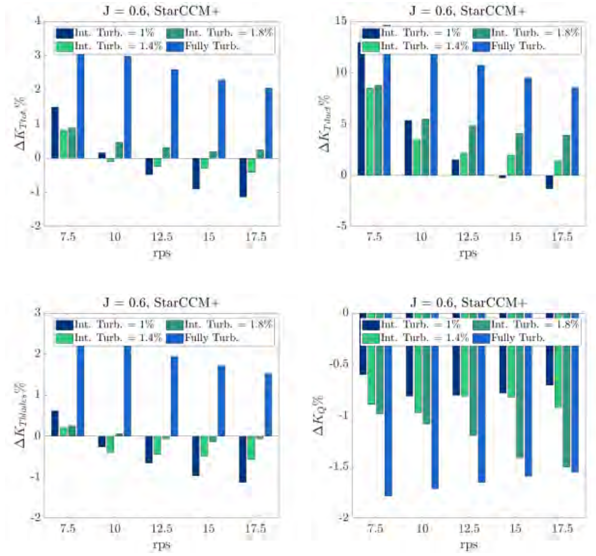

Figure 61 – Scale effect at J = 0.6 for the Decelerating ducted propeller (total thrust, thrust of the duct alone, thrust of the blades alone, total torque)

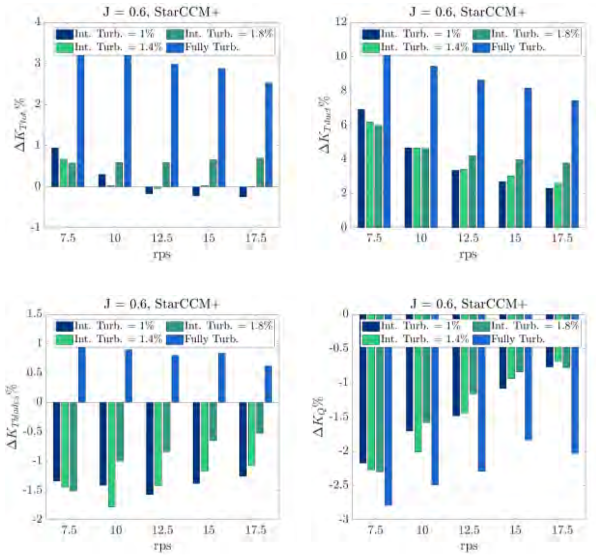

Figure 60 – Scale effect at J = 0.6 for the Accelerating ducted propeller (total thrust, thrust of the duct alone, thrust of the blades alone, total torque)

This trend is less evident for the decelerating ducted propeller, for which a reduction of the delivered thrust is observed only for combinations of very low turbulence intensity levels at highly loaded conditions (low J). In contrast, at high J values, when the decelerating nozzle produces a resistance and the increase of the static pressure inside the duct is higher, the scaling of torque change signs.

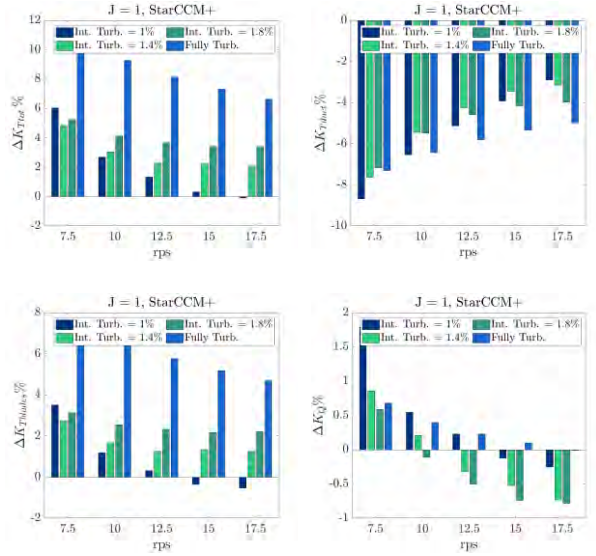

Figure 62 – Scale effect at J = 1.0 for the Decelerating ducted propeller (total thrust, thrust of the duct alone, thrust of the blades alone, total torque). Note that at J = 1 the duct produces a drag

7. UPDATE OF THE LOAD VARIATION TEST METHOD IN 1978 ITTC PERFORMANCE PREDICTION METHOD

7.1.1 Introduction

The Load Variation Test is carried out to assess the variation of propulsion performance such as the efficiency, speed of revolution, propeller torque and thrust due to a change of the ship's resistance for a particular speed.

In the current procedure 7.5-02-03-01.4, the rate of revolutions is varied to provide a self-propulsion point corresponding to the calm water resistance plus an additional allowance of between -10 to +20%. However, there is concern that this range may be insufficient, according to the new Minimum Propulsion Power requirements of the IMO. It is suggested that the appropriate range may be different according to the application fields and ship type, size and draft. Therefore it is necessary to re-examine the recommended range of the Load Variation Test.

The results of Load Variation Test can be applied to the following scenarios.

- Speed/power trials
- Operational performance
- IMO Minimum propulsion power
- IMO EEDI f_w

The characteristics of the application fields are summarized in Table 7. In this review, the most appropriate range for the Load Variation Rest is investigated in the speed/power trial condition.

Table 7 - Characteristics of application fields for load variation test

Application fields	Speed	Environment	Testing stage	Analysis
Speed/power trials	65~100% of MCR	BF5~6	Sea Trials	Real seas -> calm water
Operational performance	Operation range	Depends on operation area	Sea Trials	Real seas -> calm water
Minimum propulsion power	2knots	BF7~8	Design stage	Calm water -> real seas
EEDI fw	≒design speed	BF6	Design stage	Calm water -> real seas

7.1.2 Methodology

The speed and power trial study investigated 19 ships across 4 different types and a range of appropriate sizes, as shown in Table 8. Design and ballast drafts were selected as test conditions at each trial speed corresponding to NCR.

Table 8 - Ship types and sizes

Type	Size (Δ or capacity)
Bulker	10, 60, 176 k Te
Tanker	37, 50, 75, 115, 157, 320 k Te
Container	3600, 8600, 11000, 20000 TEU
Gas Carrier	4, 12, 80, 138, 174, 200 k Te

For environmental disturbance, wind and wave loads were considered. The detailed conditions of environmental load calculation are summarized in Table 9.

Table 9 - Conditions of environmental load calculation

Item	Value
Significant wave height	Visual observation limit*
Modal wave period	Statistics on North Pacific ocean (Bales, 1983)
Wave direction	0~180deg
Wave spectrum	ITTC spectrum
Irregular wave type	Long crested
Added resistance formula	STAWAVE2*, SNNM*
Wind speed	Statistics on North Pacific ocean (Bales, 1983)
Wind direction	0~180deg
Wind resistance coefficient	ITTC chart

*Recommended ITTC Procedure 7.5-04-01-01.1

When using the SNNM formula in the range $\lambda/L < 0.3$, the value of the added resistance coefficient at $\lambda/L = 0.3$ was used instead of the value from original formula. This was done because it is difficult to validate the empirical formula for $\lambda/L < 0.3$ due to limitations on measurement accuracy. Furthermore, the full-scale values of added resistance coefficient at short wavelengths can be lower than that measured at model-scale (Sigmund and Moctar (2018)), as illustrated in Figure 63.

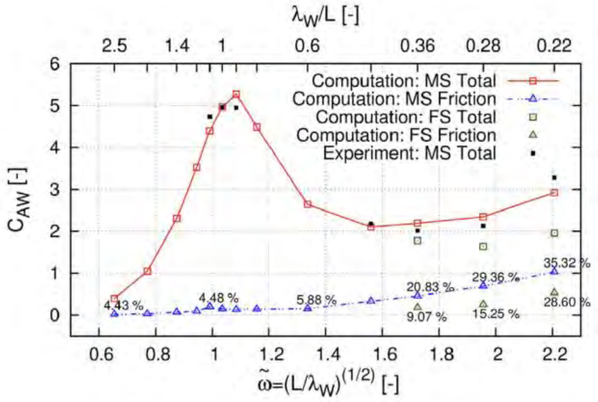

Figure 63 Computed and measured coefficients of total and frictional added resistance at model and full-scale (Sigmund and Moctar, 2018).

7.1.3 Results of speed & power trials investigation

The calculation results are shown in Figure 64 to Figure 67 and Table 10 to Table 11. Although there are differences depending on the type of ship and the method of analysing the added resistance in waves, the maximum added resistance ratio is typically about 30% and the minimum added resistance ratio is typically about -3.5%. In these tables R_0 denotes the resistance in calm water.

Table 10 – Max. added resistance ratio ($\Delta R_{max}/R_0$)

Method		Range [%]	Avg. [%]
Wind	Wave		
ITTC chart	STAWAVE-2	16~36	27
ITTC chart	SNNM	19~40	32

Table 11 – Min. added resistance ratio ($\Delta R_{min}/R_0$)

Method		Range [%]	Avg. [%]
Wind	Wave		
ITTC chart	STAWAVE-2	-7.3~-1.5	-4.1
ITTC chart	SNNM	-5.7~1.3	-3.0

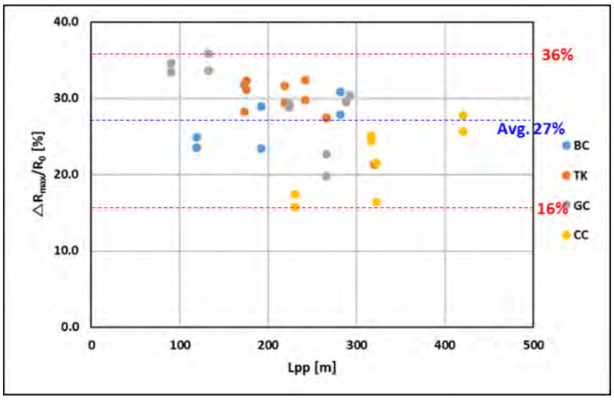

Figure 64 Max. added resistance ratio (STA-WAVE-2)

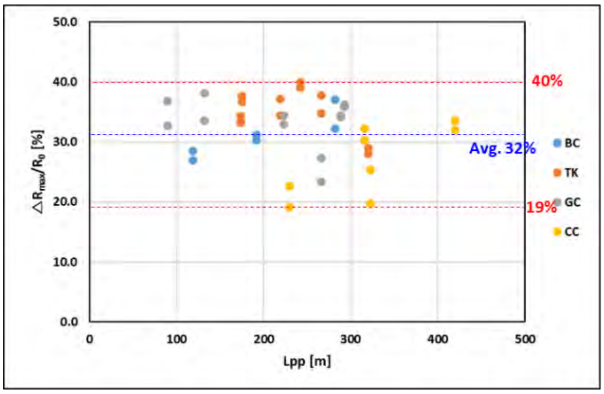

Figure 65 Max. added resistance ratio (SNNM)

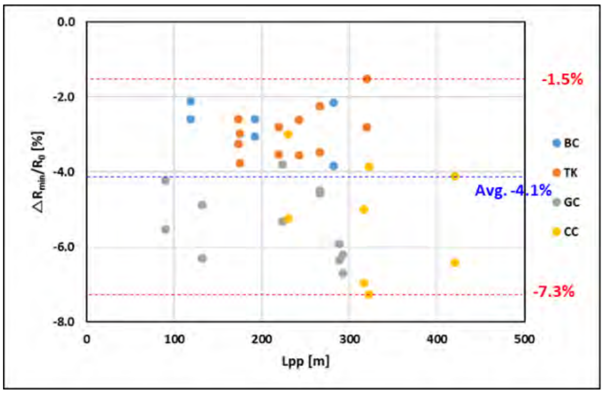

Figure 66 Min. added resistance ratio (STAWAVE-2)

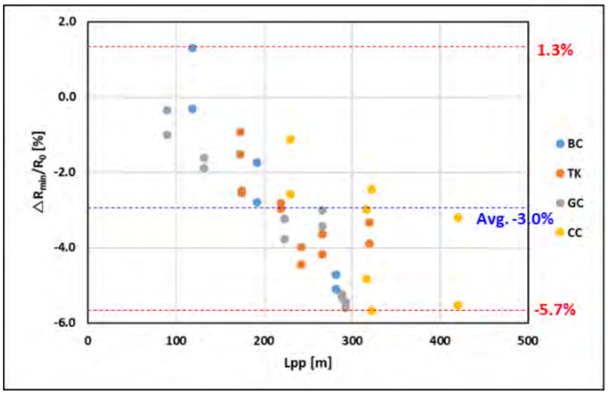

Figure 67 Min. added resistance ratio (SNNM)

There is no clear trend in the maximum added resistance according to the length of the ship. This is because as the length of the ship increases, the significant wave height and wind speed determined by the visual observation limit also increases. The difference due to a change in draft of a vessel does not appear to be particularly large, because, as draught reduces from the design condition to the ballast condition the windage area increases by a corresponding amount. The resulting increase in the wind resistance compensates, to some degree, for the decrease in the added resistance in waves.

7.1.4 Conclusion

The range of the Load Variation Test in Procedure 7.5-02-03-01.4, when applied to the analysis of speed/power trials, should be adjusted so that its maximum limit is 40% of the resistance in calm water.

7.2 Investigation of Self-propulsion Factors for Evaluation of Minimum Propulsion Power in Adverse Conditions

7.2.1 Introduction

IMO MEPC has been regulating the minimum propulsion power by providing a guideline to ensure safe operation of ships in adverse conditions since 2013, when EEDI began to be applied. The guideline has been revised several times and the adverse conditions are defined according to the length between perpendiculars of the ship, as shown in Table 12.

Table 12 - Definition of adverse conditions

Ship length [m]	H_S [m]	T_P [s]	V_W [m/s]
Less than 200	4.5	7.0 to 15.0	19.0
$200 \leq L_{PP} \leq 250$	Linear interpolation		Linear interpolation
More than 250	6.0		22.6

*H_S is significant wave height, T_P is peak wave period, and V_W is mean wind speed.

The guideline suggests two assessments:

- Assessment level 1 – minimum power lines assessment
- Assessment level 2 – minimum power assessment.

If it fulfils either of these assessments then the ship is considered to have sufficient power. These assessments are applied to bulk carriers, tankers and combination carriers with a size equal to or greater than 20,000 DWT.

In assessment level 2, the default conservative values for self-propulsion factors are provided as $w = 0.15$ and $t = 0.1$. These values were suggested by China, as shown in in Figure 68 (see reference IMO MEPC 72/5/9), and adopted to the guideline at MEPC 76. To check whether the default conservative values are reasonable, the model test was performed in KRISO, through the following method.

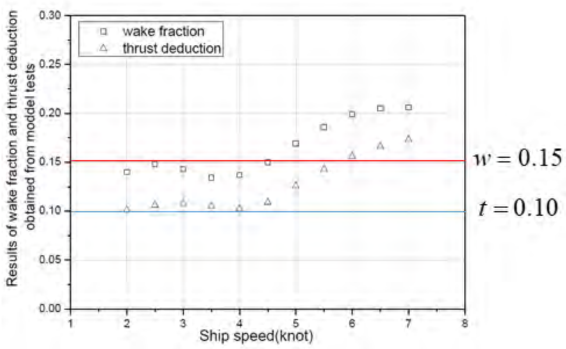

Figure 68 - Model test results of wake fraction and thrust deduction factor at low speeds (IMO MEPC 72/5/9, 2018)

7.2.2 Test conditions of self-propulsion for minimum propulsion power assessment

Test conditions for evaluating minimum propulsion power are similar to load variation test in that they evaluate propulsion performance considering realistic seaway, but the degree of load change and advance speed are significantly different. And the results of load variation test are normally used for speed/power trial correction, which converts propulsion performance from real seas to calm water. However, evaluating minimum propulsion power has the opposite process of converting from calm water to real seas.

Table 13 - Comparison of test conditions

	Load variation test	Minimum propulsion power
Advance speed	Normally corresponding to 65% ~ 100% MCR	2knots
Load range ($\Delta R/R_0$)	-10 ~ 20%	≫1,000%
Conversion	From real seas to calm water	From calm water to real seas

The model test under low speed of 2 knots and highly overload condition is similar to the model test in ice condition. For the evaluation of minimum propulsion power, the model test is carried out through the overload test defined in

ITTC Recommended Procedures 7.5-02-04-02.2 (Propulsion Tests in Ice).

7.2.3 Method to obtain self-propulsion factors

For the evaluation of minimum propulsion power, self-propulsion factors of full-scale ships are required. The self-propulsion factors of model-scale are obtained from the model test results with the advance speed applying Froude similarity and extrapolated to full-scale.

By the following assumptions, it can be obtained the self-propulsion factors of full-scale at 2 knots.

- The correlation between towing force (F_X) and thrust (T_M) is linear. The towing force measured during self-propulsion is equal to the resistance of the model ship when the measured propeller thrust is zero at low speed range.
- The flow characteristics of the propeller blade in self-propelled condition is defined only by the propeller Reynolds number, ignoring the turbulent flow characteristics developed along hull surface.
- The thrust deduction factor is considered as constant for the variations of the propeller loading.
- As advance speed decreases, the boundary layer thickness increases due to the decrease of Reynolds number and the effect of ship wave can be ignored.

To find the self-propulsion point, the following equation is used to calculate the towing force considering the skin friction correction and the additional resistance.

$$F_X = F_{D,skin} - \frac{R_{Add}}{\lambda^3}\frac{\rho_M}{\rho_S} \tag{1}$$

In the above equation, R_{Add} is the added resistance of full-scale at 2 knots. The value is calculated from the guideline for minimum propulsion power. The added resistance in adverse conditions is, in general, significantly larger than the calm water resistance at 2 knots.

The thrust deduction factor is obtained according to 1978 ITTC method.

$$t = \frac{T_M + F_X - R_C}{T_M} \tag{2}$$

Using the assumptions, the thrust deduction factor also can be obtained using linear relation of the thrust and the towing force.

$$t = 1 + \frac{\Delta F_X}{\Delta T_M} = 1 + 1/\left(\frac{\Delta T_M}{\Delta F_X}\right) \tag{3}$$

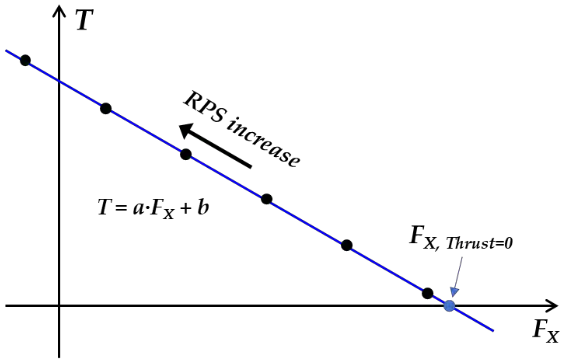

Figure 69 - Correlation between towing force and thrust

When calculating wake fraction of model-scale, it shall be used that the test results of propeller open water with propeller Reynolds number same as that in self-propulsion test. Propeller Reynolds number is defined in ITTC Recommended Procedure 7.5-02-03-02.1 (Open Water Test).

$$Re_{0.7} = \frac{c_{0.7}\sqrt{V_A^2 + (0.7\pi n D)^2}}{\upsilon} \tag{4}$$

For calculating propeller Reynolds number in self-propulsion test, the wake fraction is assumed initially and then an iterative calculation is performed until the wake fraction and propeller Reynolds number converge. In the iterative calculation process, test results of propeller open water with various propeller Reynolds number and advance ratio are also used.

The wake fraction in full-scale is obtained according to 1978 ITTC method with w_{TM} and t.

7.2.4 Characteristics of self-propulsion factors in adverse conditions

To investigate the characteristics of self-propulsion factors, KVLCC2 (300,000 DWT tanker) and KSUPRAMAX (66,000 DWT bulk carrier) were used. Propeller Open Water (POW) tests at various blade Reynolds numbers were performed, and the characteristics of wake fraction were analysed using two different POW results. One is the POW results with the high propeller Reynolds number (High $Re_{0.7}$), which is normally used for the extrapolation to full-scale. The other is that of the lower Reynolds number ($Re_{0.7}$) matched with the Reynolds number of the self-propulsion point during the propulsion test.

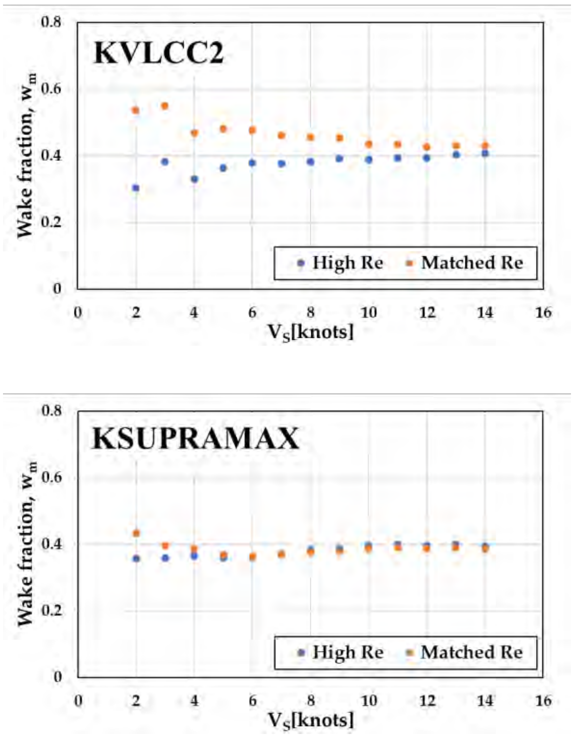

Figure 70 - Calculated wake fraction at model-scale

From the results of Matched $Re_{0.7}$ in Figure 70 it was confirmed that the wake fraction in model-scale increased at low speed range, which was consistent with the previous assumption.

To evaluate the minimum propulsion power, the self-propulsion factors calculated by the results of Matched $Re_{0.7}$ are extrapolated to full-scale.

As shown in Figure 71, the wake fraction and thrust deduction factor showed the same tendency in full-scale. As the speed decreased, the self-propulsion factors also decreased. However, comparing the results with the values at 2knots suggested in the guideline, the wake fraction is higher than $w = 0.15$ and the thrust deduction factor is lower than $t = 0.1$.

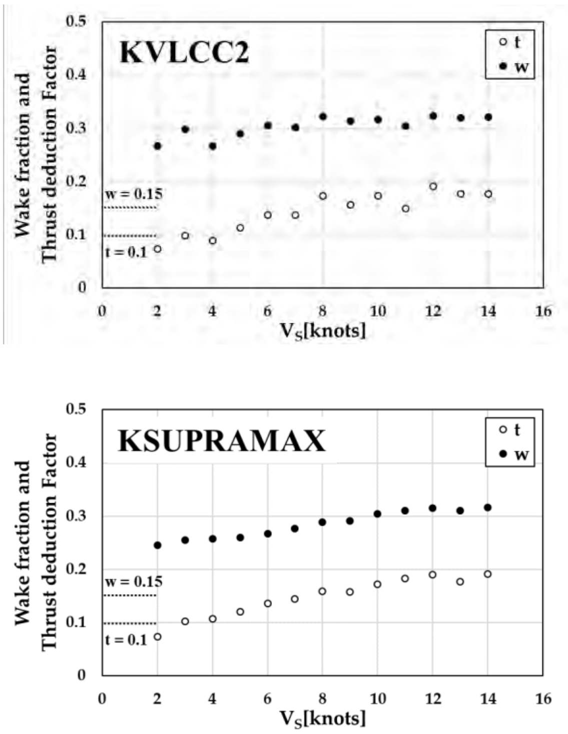

Figure 71 - Calculated wake fraction at full-scale

As shown in Table 8~9, the minimum propulsion power was evaluated using the self-propulsion factors from model test. And the assessment result was compared with that of the self-propulsion factors from the guideline. The required brake horsepower deduced from the model tests less than that of the guideline by about 5% in the both ships.

Table 14 - Minimum propulsion power assessment for KVLCC2

Item [unit]	Guideline	Model test	Diff.
X_S [kN]	35	35	
X_W [kN]	339	339	
X_d [kN]	824	824	
X_r [kN]	40	39	
X_T [kN]	1,238	1,237	
EHP [kW]	1,274	1,273	
J [-]	0.123	0.109	
w [-]	**0.150**	**0.268**	
t [-]	**0.100**	**0.075**	
η_O [-]	0.193	0.171	
η_H [-]	1.059	1.264	
η_R [-]	1.000	1.000	
η_D [-]	0.205	0.216	
RPM	43.1	42.2	-2.2 %
T [kN]	1,375	1,337	-2.8 %
Q^{req} [kN-m]	1,391	1,347	-3.2 %
P_B^{req} [kW]	**6,282**	**5,949**	**-5.3 %**

Table 15 - Minimum propulsion power assessment for KSUPRAMAX

Item [unit]	Guideline	Model test	Diff.
X_S [kN]	15	15	
X_W [kN]	188	188	
X_d [kN]	334	334	
X_r [kN]	18	17	
X_T [kN]	555	555	
EHP [kW]	571	571	
J [-]	0.114	0.103	
w [-]	**0.150**	**0.246**	
t [-]	**0.100**	**0.074**	
η_O [-]	0.171	0.155	
η_H [-]	0.159	1.228	
η_R [-]	1.000	1.000	
η_D [-]	0.181	0.190	
RPM [rev/min]	76.6	75.0	-2.1 %
T [kN]	617	599	-2.9 %
Q^{req} [kN-m]	398	386	-3.0 %
P_B^{req} [kW]	**3,191**	**3,031**	**-5.0 %**

8. INVESTIGATION OF THE REQUIREMENTS FOR TESTING AND NUMBERICAL EVALUATION OF HIGH-SPEED MARINE VESSELS

The Committee discussed the requirements for testing and numerical evaluation of high-speed marine vessels and addressed the need to update the relevant procedures.

Attention focussed on specific needs associated with properly manufacturing, measuring and reporting the transom radius geometry. Namely, the Committee reviewed synergetic experimental and computational studies (see Lee et al., 2021) highlighting the effect that the transom radius has upon the running trim and sinkage of the model. In this regard, it was found useful to recommend that the model manufacturer should pay particular attention, when finishing the model, to ensure that geometric features including boundaries of transom sterns remain well-defined with sharp edges. It was also recommended that the model documentation should include details of transom sterns and record the transom radius.

Accordingly, revisions were made to the relevant procedures, namely ITTC Recommended Procedure and Guidelines 7.5-01-01-01 Ship Models and 7.5-02-05-01 High Speed Marine Vehicles Resistance Test.

9. INVESTIGATION OF MEASUREMENT AND PREDICTION METHODS FOR BREAKING WAVES

9.1 Introduction

Even though ship resistance in calm water can be well predicted, it is still challenging to accurately resolve the flow field, especially for the breaking wave phenomenon of high-speed surface ships. For a large-scale ship, the bow wave is usually unstable and irregular, which is often accompanied by wave breaking and intense water-air mixture. Therefore, the problem of bow wave breaking is one of the main focuses (Li et al. (2022b)).

As shown in Figure 72, depending on the shape of a bow and for sufficiently high ship speeds, spilling and/or plunging breaking occurs, inducing vortices and scars. The waterline entrance angle and ship speed are thought to have a considerable impact on the breaking type of bow waves. Depending on the appearance of stability at the crest, the breaking waves can be classified as plunging breaking waves or spilling breaking waves (see reference Olivieri et al. (2007), Jin (2022)).

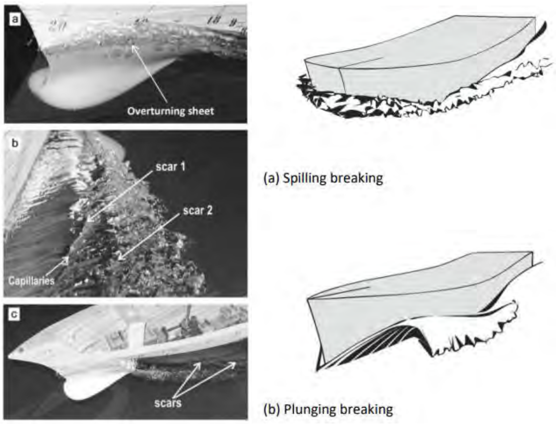

Figure 72 - Bow breaking waves & Classification of the bow wave breaking, Olivieri et al. (2007), Jin (2022)

For task 13 of the 30th ITTC Resistance & Propulsion committee, a literature study was undertaken to investigate the measurement and prediction methods for breaking waves. The literature search focused on resistance and propulsion papers published in the last 5 years containing keywords; ‘breaking waves’, ‘bow wave’, ‘ships’, etc.. The reviewed papers were broken down into two categories; experimental observations and numerical simulations.

9.2 Experimental observations

Vera Hengelmolen et al. (2022) studied the effect of bow wave breaking on added resistance by combining visual observations with resistance tests. Their research introduced a dynamic waterline detection method involving stereo vision, to capture the relative wave elevation in the bow region of the ship. By placing stereo camera arrangements inside the hull of a semi-transparent ship, the waterline can be tracked using an edge detection algorithm at each moment in time. By performing resistance tests on the Delft Systematic Dead rise Series ship model no. 523, the added resistance was observed to be proportional to the relative wave height squared. Figure 73 shows the experimental setup of relative wave height measurements and Figure 74 shows the example of the waterline detection and waterline mapped to be plotted on the 3D hull model.

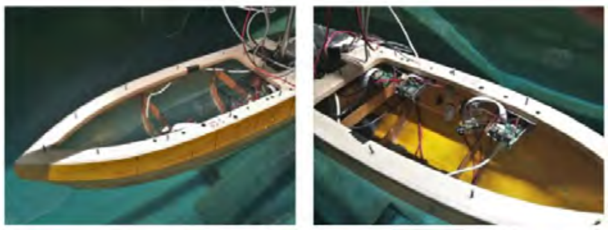

Figure 73 - Experimental setup of wave height measurement, Vera Hengelmolen et al. (2022)

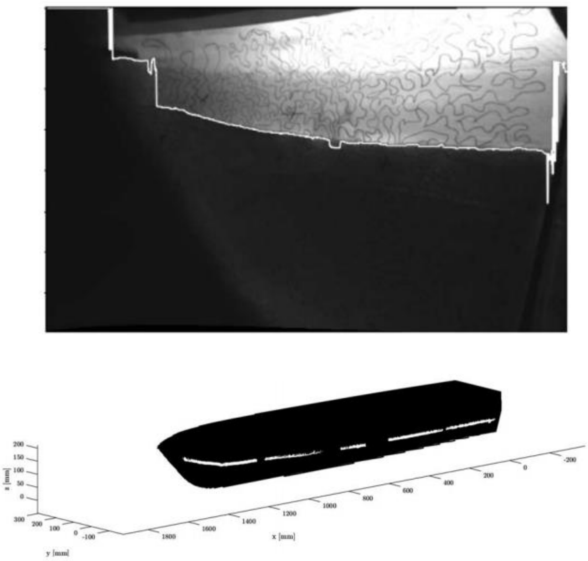

Figure 74 - Waterline detection, Vera Hengelmolen et al. (2022)

Mallat et al. (2022) summarized the breaking wave bubble measurement around ship model using an optical probe measurement and PIV technique. Using an optical probe they locally measured the size and the velocity of the bubbles generated by breaking waves around a ship model in calm water and regular waves in a circulating flume tank. They also performed a comparison with more classical bubble detection results obtained using image tracking methods. They suggested that the two methods provide complementary results for bubble characteristics. Figure 75 shows the experimental setup of the bubble measurement study by using optical probe and PIV cameras. Figure 76 show a time sequence of images of the same taken over one wave period viewed from the bottom of the circulating flume tank. The tip of the optical probe is visible on these figure (green circle).

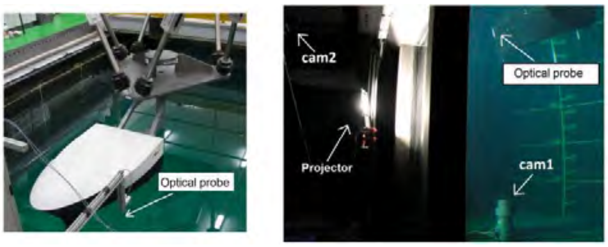

Figure 75 - Experimental setup, Mallat et al. (2022)

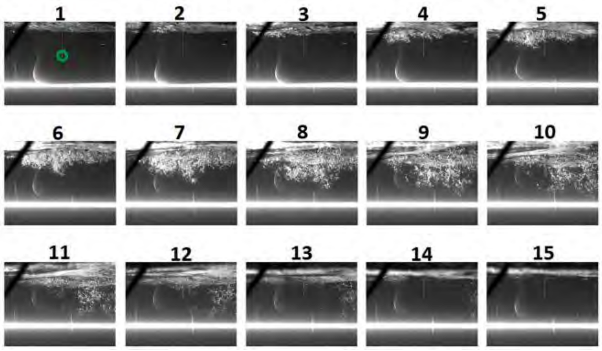

Figure 76 - Images in the (x,z) plane from camera for a wave period with bubbles, Mallat et al. (2022)

Jacobi et al. (2022) presented velocity measurements using PIV, together with a reconstruction of hydrodynamic pressures for the analysis of fast ships. Stereoscopic PIV measurements with a towed underwater PIV system were conducted during towing tank tests to obtain the velocity field in the bow region of a fast ship at speeds up to Fr=0.8. Figure 77 shows the ship model mounted to a hexapod next to the stereoscopic PIV system.

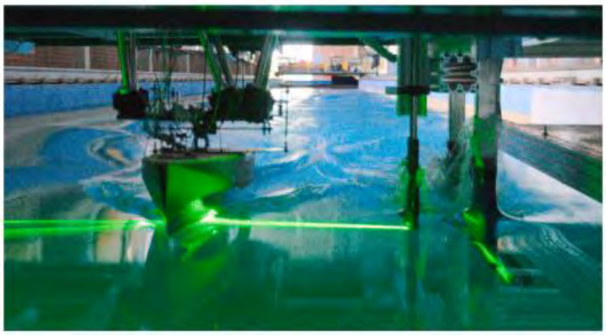

Figure 77 - Experimental setup, Jacobi et al. (2022)

They implemented the post-processing procedure for the pressure reconstruction, including the solution of the Poisson equation, into the open-source CFD package OpenFOAM. Their results show that the PIV method is capable of capturing the flow characteristics in the bow region of a fast ship and, in addition, that it can be used together with the pressure Poisson equation to obtain the hydrodynamic pressure field. The pressure fields reconstructed from the velocity field captured by the PIV system are presented in Figure 78, where they are compared to the numerical results for three selected time-steps during the downward motion of the ship hull.

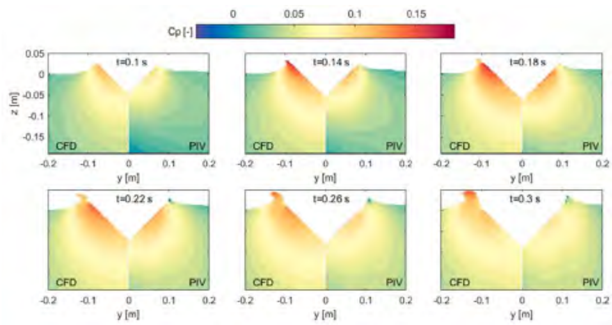

Figure 78 - Distribution of phase-averaged pressure fields at six selected time instants during the downward motion of the ship model, performing oscillatory motions at f = 1 Hz with an amplitude of a = 0.035 m. Comparison of experimental with numerical results, Jacobi et al. (2022)

Regarding the wider range of flow kinematics in breaking wave, systematic analysis to investigate the effects of breaking waves impacting on marine structures has been of recent interest in green water research. Fontes et al. (2022) presented an experimental investigation of the kinematics of consecutive green water events generated with incident wave trains, particularly during their formation and interaction with the bow of a fixed structure. These events include Plunging-Dam-Break (PDB) and Hammer-Fist (HF) types of green water. These event types were also reported by Greco et al. (2007) in experiments using regular wave trains in a wave flume but did not include flow kinematics.

The experimental campaign by Fontes et al. (2022), consisting of incident wave trains of different steepness, was carried out using a fixed, rectangular bow installed in the wave flume of the Institute of Engineering at the National Autonomous University of Mexico. In the experiments, each wave train consisted of consecutive wave cycles that approached the bow of the structure, thus generating consecutive green water events. The flow kinematics during the formation of representative PDB and HF types of consecutive green water events, were experimentally investigated using Particle Image Velocimetry (PIV) methods. The evolution of the kinematics of PBD and HF type events was analysed to understand the flow behaviour as they are generated at bow of the structure. Figure 79 illustrates the flow kinematics during the generation of HF type green water events.

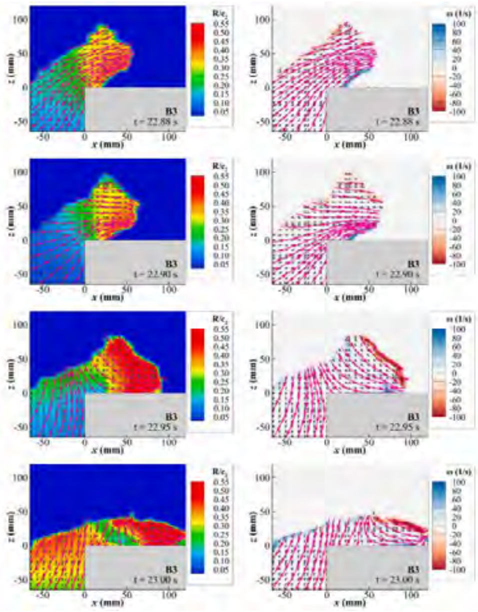

Figure 79 - Evolution of flow kinematics during the generation of a representative HF type green water event, Fontes et al. (2022)

9.3 Numerical approaches

Focusing on the wave-breaking phenomena of high-speed ships, Wang et al. (2020) performed numerical simulations to investigate the wave breaking phenomenon around high-speed ships. To resolve the flow field around a KRISO Container ship (KCS) model, they used both, Unsteady Reynolds-Averaged Navier-Stokes (URANS) simulations and Delayed Detached Eddy Simulation (DDES) approaches. Additionally, they used high-resolution, Volume of Fluid (VOF) techniques in OpenFOAM to capture the free surface. In their paper, the breaking wave phenomena was resolved by both URANS and DDES for Froude numbers greater than 0.35. The predicted URANS and DDES bow wave results were compared with experimental measurements conducted at the China Ship Scientific Research Center (CSSRC).

Figure 80 shows the comparison of the simulated wave patterns in high-speed conditions with the experimental measurements.

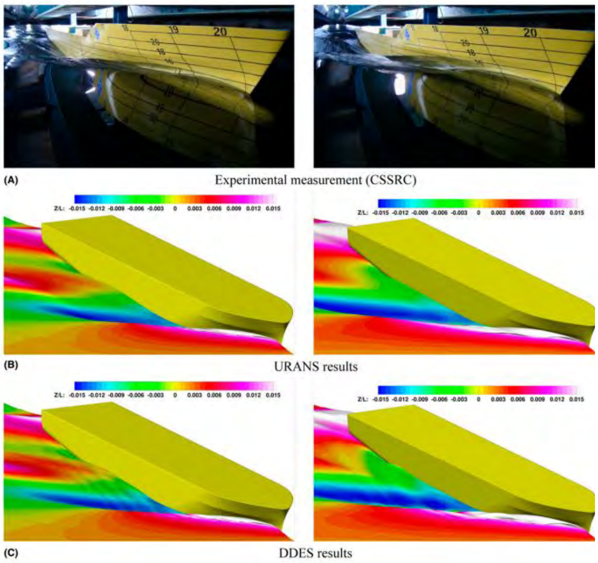

Figure 80 - Comparison of wave patterns (left column: Fn=0.35, right column: Fn=0.40): (A) Experimental measurement (CSSRC); (B) URANS results (C); DDES results, Wang et al. (2020)

The Fn = 0.40 cases shows more violent breaking bow waves more consistent with the experimental results. The DDES results provided more complex results illustrating the process of the overturning and breaking bow wave, and also captured some small-scale free surface features.

They presented axial vorticity distributions at different transverse cross sections to illustrate the different predictions of the breaking bow waves made using URANS and DDES methods. Five sections with x/Lpp equal to 0.05, 0.10, 0.15, 0.20, and 0.25 are presented in Figure 81 to illustrate the breaking wave phenomena.

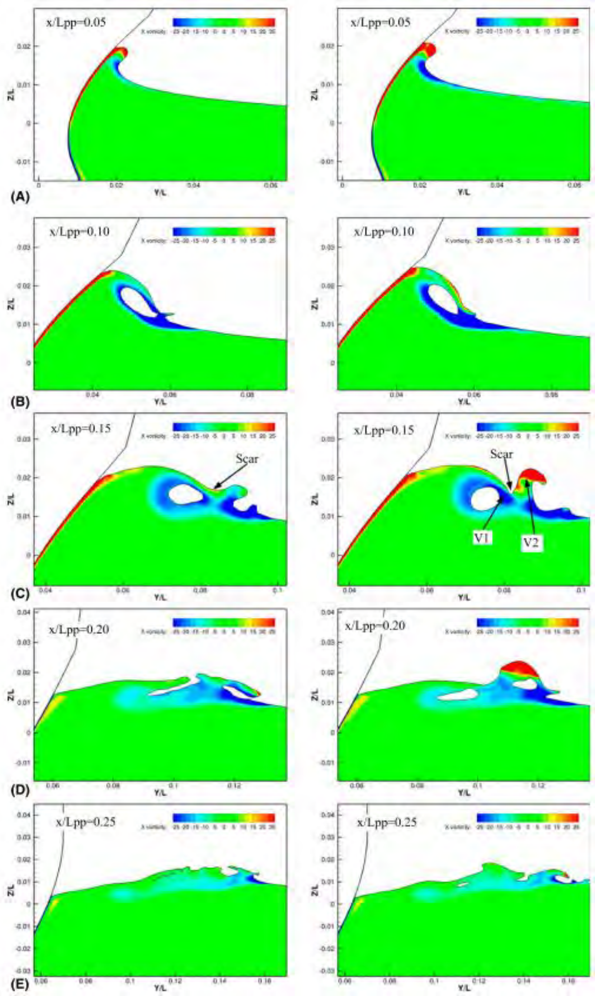

Figure 81 - Axial vorticity distribution (left column: URANS results, right column: DDES results), Wang et al. (2020)

The variation between the URANS and DDES wave fields and vorticity were mainly concentrated near the free surface. As shown in Figure 81-A, the initial plunger was generated because of the interaction between gravity and inertial forces when the hull blocks the inflow. A second plunger can be seen in Figure 81-C (x/Lpp=0.15), where it can be seen that the axial vorticity distributions predicted by DDES and URANS show significant differences. These differences are the main cause of the different shapes of breaking waves. Scars can be observed in the bow wave region from both URANS and DDES results due to counter-rotating vortex pairs (V1 and V2). In the far field region of Figure 81-C (x/Lpp=0.25), dissipation of the vorticity in the URANS results is noticeable compared with the DDES results. Consequently, the free surface is smoother in the URANS computations.

Another publication focusing on breaking waves by Wu et al. (2021) studied the breaking bow wave of the David Taylor Model Basin (DTMB) surface combatant model under different trim angles at Fr = 0.35 using Delayed Detached Eddy Simulation (DDES). The approach was adopted to study the breaking bow wave features, such as plunging jet and air entrainment. DDES was chosen because it has been shown that RANS methods average the N-S equation by time, smoothing out the turbulent pulsations in the flow field (Wilson et al., 2007). Wu's research delves into the influence of hull trim angle on breaking bow waves through simulations of different trim conditions (1 degree trim by bow, a model test condition, and 1 degree trim by stern). They compared and analysed the wave contour, free surface outline, vorticity field and velocity field at several transverse cross sections. Figure 82 shows the numerical representation of the bow waves generated by different trim angles.

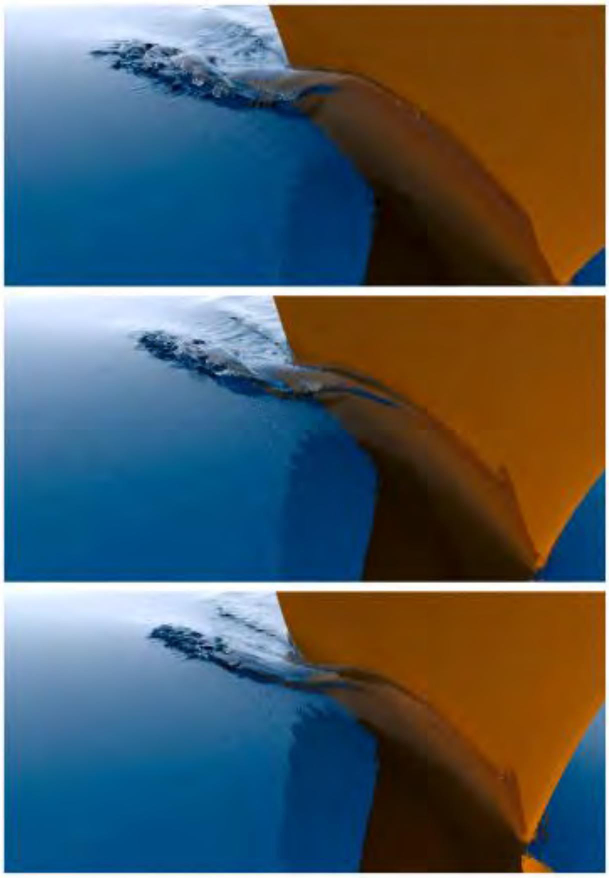

Figure 82 - Close-up view of the bow waves in the three cases (top; 1 deg. trim by bow, middle; model test condition, bot-tom; 1 deg. trim by stern), Wu et al. (2021)

Their results showed that trim by the bow makes free surface steeper and wave amplitude larger in the breaking bow wave region. They presented that the reason is that trim by the bow enlarges the attack angle of the bow, thus energizing the bow wave and generating a more violent free surface on the breaking bow wave.

To accurately capture the complex free surface of the breaking waves, it has been suggested that higher order two phase solvers in numerical simulations are needed. Jin (2021) presented a new two-phase flow solver for the analysis and prediction of complex ship flows through an investigation of breaking bow waves and built an air-water boundary layer model to overcome the discontinuity over the two-phase interface in his PhD thesis. He developed a combined Volume of Fluid (VOF) and immersed boundary method to simulate two-phase flows with high density ratio. The interface was captured using the VOF method, and a new boundary layer was built on the lighter phase side by an immersed boundary method. The new solver was used to study breaking bow waves generated by a wedge-shape bow and the KRISO Container Ship (KCS). Jin (2021) showed this method improves the robustness and stability of two-phase flow simulations, and higher accuracy can be obtained on a relatively coarse grid compared to the original VOF method.

Li et al. (2022a) introduced another interface capturing method to simulate the ship-induced breaking waves with high-accuracy VOF (volume of fluid) schemes using the un-structured THINC (tangent of hyperbola for interface capturing) type scheme. Particularly, an extension version of THINC/QQ (THINC method with quadratic surface representation and Gaussian quadrature), namely, THINC/QQ-SF (THINC/ QQ extended for split-face unstructured cells) was used in their works. By numerical simulation for model DTMB 5415 under Fn=0.35, they showed that the combination of THINC/QQ-SF and HRIC can better capture the wave breaking details with less numerical diffusion, and the reliability of the resistance prediction is higher, compared with original VOF-HRIC. Figure 12 shows the comparisons of the breaking wave interface near the DTMB 5415 bow with the original VOF-HRIC scheme and the new scheme illus-trating the benefit of the combination VOF scheme of THINC/QQ-SF and HRIC (high-resolution interface capturing).

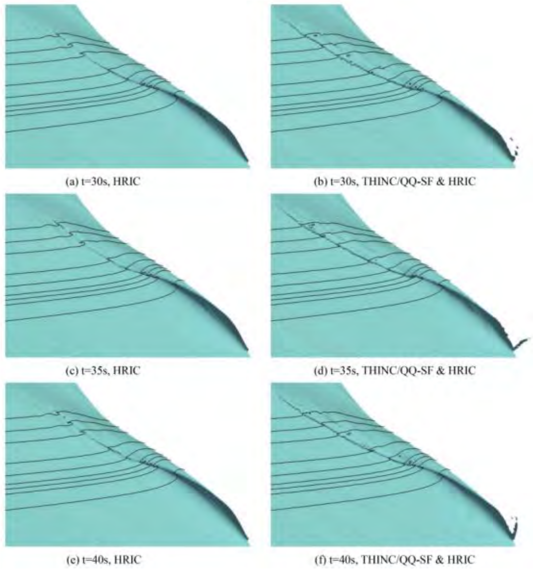

Figure 83 - Comparisons of the interface near the DTMB 5415 bow, Li et al. (2022a)

Figure 12: Comparisons of the interface near the DTMB 5415 bow, Li et al. (2022a)

Wang et al. (2023) investigated nonlinear ship waves by implementing the Longitudinal Cut Method (LCM) and Wake Survey Analysis Method (WSAM) in a computational fluid dynamics (CFD) simulation. LCM is wave pattern analysis by and the wake survey analysis method (WSAM) is the viscous resistance measurement method. The wave pattern resistance (Rwp) prediction of the LCM method was validated using a Series 60 Cb= 0.6 ship model. WASM was performed on a wall-sided model, incorporating the local adaptive mesh refinement (LAMR) and surface tension models to capture nonlinear bow waves. Far and near-field wave patterns and momen-tum loss resistance (RML) were compared with the experiment as shown in Figure 84.

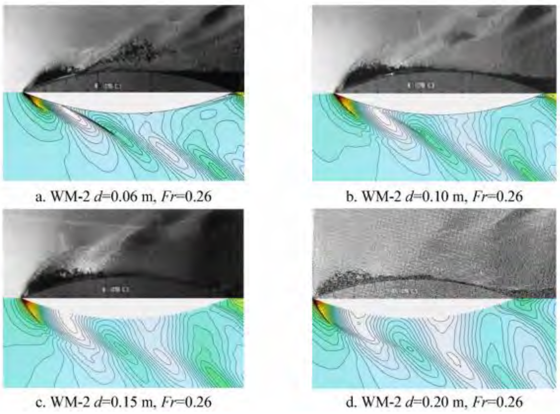

Figure 84 - Measured (top) and computed (bottom) wave patterns of WM-2 at Fr = 0.26 , Wang et al. (2023)

In their paper, they stated that it is meaningful to evaluate the nonlinearity in ship waves (Rn_w) by numerical simulation, considering the high-cost and complexity of conducting such an experiment. Their paper focuses on the analysis and evaluation of the resistance due to the nonlinearity of the waves and consequently provides some insights to evaluate the nonlinearity in ship waves to further understand their underlying mechanisms.

9.4 Concluding remarks

Breaking waves are important to ship engineers. Violent breaking bow waves, including spray, foam and bubbles, have significant impact on many aspects of ship design, such as increased hull resistance, inaccurate prediction of the added resistance in waves, and a substantial additional source of radar signature for naval craft. It also directly affects the motion and dynamic response of ships, local structural strength, and also ship manoeuvrability. The understanding of how waves break around the bow of a ship is important to the design of advanced ‘green’ ships, the development of energy saving techniques, structural safety, vibration reduction and noise control. To gain a better understanding of the physical phenomena for high-speed ships, extensive experimental studies have been conducted worldwide to try to explain the mechanism of breaking waves and to provide abundant computational fluid dynamics (CFD) validation data (Li at al.(2022b)).

In previous studies, the features of breaking bow waves are observed via experiment method. Experimental observations on bow waves mainly focused on the wave height or the velocity fields by using surface visualization techniques (aluminium powder and tracking particles), capacitance wires, 5-hole pitot tubes, underwater cameras etc. Recently, thanks to the development of the high-speed camera, video equipment can now be used to record the process of wave breaking, to capture the typical flow structures and to record the locations of bow wave run-up. PIV technology can also be employed to measure the velocity/pressure field and to determine the evolution of vortical flow fields around the ship.

The hydrodynamic phenomena involved in ship flows are usually discovered by experimental observation and then investigated further by conducting numerical simulations. Experimental measurements are still considered to be the most reliable methods to evaluate the breaking bow wave, however, there are many limitations with experimental measurements.

The experimental measurements are highly dependent upon experimental conditions and involve time consuming procedures for test measurement system preparation and experiment execution. Due to the high cost in both money and time, the observation is usually limited to benchmark ships or simplified geometries (Jin (2021)).

Traditionally, ship wave systems are described by potential flow theories without taking in to account the influence of viscosity. Nonlinear potential flow methods are suitable for modelling steep waves up to the point of breaking but have limited ability to capture the spray and bubbles associated with breaking waves.

In recent years, with the rapid development of High-Performance Computing (HPC) systems, Computational Fluid Dynamics (CFD) approach are widely used to conduct flow field simulations. Most of the previous numerical studies are based on the Reynolds-Averaged Navier-Stokes (RANS) equations. Using RANS codes, the overturning of bow wave and jet splashing can be captured while details of the turbulent flow field cannot be well resolved due to the time-averaging operator. Therefore, the Delayed Detached Eddy Simulation (DDES) approach, combined with a higher order two-phase solver to accurately capture the free-surface, has been prevalent in the simulation of breaking bow waves. However, the high computational cost of this approach limits its widespread use. Therefore, simulation with adaptive mesh refinement may be a good approach, which can greatly improve the computational efficiency of massively parallel computations of two-phase mixed flow (Li et al. (2022b)).

10. DEVELOPMENTS IN HULL AND PROPELLER MANUFACTURING

In the age of Artificial Intelligence, Autonomous Vehicles and other '4th Industrial Revolution' technologies, there have also been developments in Additive Manufacturing (AM) which are potentially applicable in the production of ship and propeller models. Physical model testing requires the manufacture of low volume or bespoke parts to extremely tight tolerances, which can be challenging to achieve in a cost-effective manner and drives up testing costs. With no need for moulds or fixed tooling, each part produced by AM can be unique, which lends itself perfectly to the manufacture of bespoke components. In recent years, the introduction of large scale / large format AM machines allows ever larger components to be manufactured, including the production of complete ship models.

10.1 Developments in Additive Manufacturing (AM) processes for metals

10.1.1 Background

GE Aviation started conducting research into AM techniques in the early 1990s and by 2012 its work with Morris Technologies enabled it to manufacture a radical new injector nozzle, which would have been extremely difficult and uneconomical to produce using conventional manufacturing techniques. GE realised the significance of its new manufacturing capability and decided to bring future development in-house and bought out its collaborator. By 2015 GE Aviation had improved its AM techniques and processes sufficiently that they could be used to produce over 25% of its new 'Catalyst' turboprop engine. The technology born from Rapid Prototyping had evolved into a fully-fledged production capability, capable of forming high precision parts from complex metal alloys suitable for use in safety critical aviation components.

In 2010 the American Society for Testing and Materials (ASTM) released a set of standards which split up the range of AM processes into seven categories [ASTM standard F2792-12; Standard Terminology for Additive Manufacturing Technologies;2012], covering methods of manufacture for both plastics and metals. In 2015 the ASTM standard was incorporated into ISO/ASTM 52900, which uses the same seven categories of AM processes (ISO/ASTM 52900:2021).

In 2017, the world's first class approved 3D printed propeller was unveiled at Damen Shipyards in the Netherlands. The 1.35 m diameter propeller, named WAAMpeller, was manufactured by Rotterdam Additive Manufacturing Lab (RAMLAB) and was a collaborative project between RAMLAB, Damen shipyards group, Promarin, Autodesk and Bureau Veritas. The first propeller was manufactured for demonstration purposes, but the second propeller was tested on a tug and passed all acceptance criteria.

The propeller was subsequently accredited by Bureau Veritas for use on Damen's Stan Tug 1606 class, making it the first AM propeller to be accredited for operational use. 3D printing of the 'WAAMpeller' is shown in Figure 85.

Figure 85 - Printing WAAMpeller (courtesy RAM-LAB)

Another benchmark research project was conducted in South Korea by Det Norske Veritas (DNV), Hyundai Heavy Industries (HHI), Korea Institute of Industrial Technology (KITECH) and SY Metal Co. Ltd. (SYMETAL). A report on the project was published by Govindaraj et al (2021). SYMETAL manufactured a 2 m diameter 4-bladed propeller and a 0.7 m long sacrificial propeller blade using the WAAM process. Both the propeller and the single test blade were subjected to dye-penetrant testing with no flaws being detected. Four test coupons were subsequently cut from the sacrificial blade; two aligned with the build layer direction and two perpendicular to the build layer direction. The four coupons were subjected to material composition and mechanical properties tests, and the results showed were highly consistent. Both material properties and composition control exceeded DNV Ship Rule requirements and DNV accepted WAAM as a method suitable for the manufacture of Ship Propellers. DNV updated their 'Rules for Classification of Ships' in July 2021 (effective 1 Jan 2023), with the inclusion of a new section on Additively Manufactured Materials.

The 'Realisation and Demonstration of Advanced Material Solutions for Sustainable and Efficient Ships' (RAMSSES) project also used WAAM to produce a hollow propeller blade and is currently ongoing. Testing was conducted on a samples of a number of materials, including Cupro-Aluminium and Martensitic or Duplex Steels. The materials testing again showed that the WAAM method produced more consistent material properties than traditional casting methods (which typically vary through thickness of the casting).

Det Norske Veritas (DNV) released an updated version its metal Additive Manufacturing Standard DNV-ST-B203 in 2022. It covers qualification and production requirements for the most established metal AM processes, including Directed Energy Deposition (DED), Powder Bed Fusion (PBF) and Binder Jetting (BJT).

A comprehensive review of different materials and techniques was presented by Bergsma et al at the High Performance Marine Vehicle (HIPER) conference in 2016 [3D-Printing and the Maritime Construction Sector, Bergsma, van der Zalm, Pruyn, HIPER 2016, Cortana, Italy]. An overview of a limited number of relevant processes and developments to metal 3D printing is given below.

10.1.2 Wire Arc Additive Manufacturing, also known as DED-Arc

The use of WAAM in the shipbuilding industry was summarised by Tasdemir and Nohut (2021).

Wire Arc Additive Manufacture (WAAM) was developed from welding processes and uses an electric arc as the heat source and the metal wire as the raw material. The part is built up sequentially by adding material using a robotic arm. WAAM is now also referred to as Directed Energy Deposition – Arc (DED-Arc) in accordance with the ISO/ASTM naming convention.

WAAM can achieve a high deposition rate compared to many other AM techniques and the material properties are considered excellent, partly because the high temperature deposition of new material heat treats the layers deposited previously. However, tight tolerances are not currently possible, so it is necessary to build the part oversize and then use conventional subtractive machining strategies (i.e. CNC milling) to achieve necessary tolerances.

WAAM offers the potential for cost and lead time reductions for Ship's propellers, together with increased material efficiency, since it is able to produce very near net shape preforms without the need for complex tooling, moulds or dies. However, WAAM can currently only produce "near net shape" components, and CNC machining is required to produce the final geometry to acceptable tolerances. While WAAM could be used for model scale propellers, the relatively small cost of the raw material billet relative to the total manufacture cost and the fact that 3 or 5-axis CNC machining is required to complete the propeller mean that it is unlikely to have significant advantages at model scale.

10.1.3 Powder Bed Fusion (PBF)

Powder Bed Fusion (PBF) creates the part in a basin filled with metal powder, which is melted using a high energy source to build the solid structure layer-by-layer. A variety of different energy sources are currently used to melt the powder, which include Laser (L) and Electron Beam (EB). The excess powder is then recycled. L-PBF is also known as Selective Laser Melting (SLM) or Direct Metal Laser Sintering (DMLS),

These two methods (L-PBF and EB-PBF) are two of the manufacturing techniques pioneered by GE Aviation. GE Aviation state that L-PBF can produce complex parts with complex geometries to exceptional levels of precision. EB-PBF is stated by GE Aviation as being able to produce dimensionally accurate parts that need to be produced quickly and efficiently, while delivering parts with low residual stresses (the part is usually heat treated in the printer after printing to remove residual thermal stresses). Both these methods are potentially suitable for model scale production of finished propellers and components, however the cost of the machines and powders is high and it is considered difficult to get parts right first time.

In 2022 DNV reported that a joint project between Kongsberg Maritime and SLM Solutions produced a hollow thruster blade with a titanium internal honeycomb structure. The blade is currently undergoing fatigue testing, which is a known concern relating to parts produced using PBF methods.

10.1.4 Blown Powder Technology (BPT)

BPT uses a similar theory to PBF, but instead of forming the part in a basin full of powder, the powder is transported to the melt pool by adding it to the inert gas flow used to shield the arc.

A relatively new technique, BPT has the advantage of being able to change metallurgy through the deposition process, so that different layers of metals can be laid down which are well bonded to one another. This technology enables multi-layered components to be fabricated which would be impossible with conventional manufacturing techniques.

10.1.5 Binder Jetting

Binder Jetting Technology (BJT) is another AM technique which can produce metallic parts, however it cannot produce parts with the same structural properties as WAAM, PBF or BPT. Porosity and structural integrity are considered significant considerations when considering BJT, as is shrinkage of the part during sintering.

BJT produces parts using metal powder within a basin and a printing head (similar to an ink-jet printer) applies the binding agent to bond the powder particles together. After all layers have been laid down, the part can be sintered at high temperature to fuse the metal particles together. However, the sintering process can cause shrinkage of up to 20% and can sometimes also result in warping or sagging. Control of dimensional tolerances is therefore difficult its applicability to parts requiring tight tolerances may be limited.

10.2 Developments in Additive Manufacturing processes for plastics

In comparison to AM processes for metal components, those for plastics are relatively well developed and are already commonly used in hydrodynamic model testing. As far back as 2016 the Ship-Technology.com website reported that Hamburg Ship Model Basin (HSVA) used 3D printers to create vessel appendages and energy saving devices and HSVA stated that "it's quite widespread in the model basins". A straw poll of the R&P committee members showed that while a large number of different techniques are currently being used to produce hull models, a significant number already use 3D printing to produce appendages such as rudders, fin stabilisers, transom wedges, waterjet housings etc. Member organisations have also been experimenting with coating components, in order to improve surface finish and also the structural integrity of the component. Treatments include coating with epoxy, or thermal spraying of metallic coatings, though little work has been published to date.

A number of member organisations are currently investigating 3D printing manufacturing techniques for the production of ship hull models, even for relatively large models of up to 10 m in length. While the manufacturing tolerances appear in line with ITTC guidelines, members have also expressed concern that model stiffness may not be as good as that of traditional model manufacturing techniques. To provide additional structural stiffness, two different organisations have 3D printed material around aluminium beam reinforcement, which has apparently worked well.

One of the most advanced attempts at 3D printing an entire ship model has been conducted at the Naval Surface Warfare Center, Carderock Division (NSWCCD). A detailed description of their work is provided below:

10.3 Applications of AM in model and component manufacture for hydrodynamic testing.

10.3.1 Hull manufacture capability development by Naval Surface Warfare Center Carderock Division

Mosqueda et al (2024) presented results from a new model fabrication technique illustrating the effectiveness of a large-scale additively manufactured hull model.

The hull form used was a representative geometry of the Arleigh Burke Class Destroyer during its Pre-Contract design phase, the geometry of which will be better known to the ITTC community by its original design designation DTMB 5415. This geometry was previously used by the ITTC for comparative resistance testing by the hydrodynamic community and has also been used for a number of computational workshops, such as the Gothenburg 2000 CFD workshop (Larsson et al, 2003). This geometry exists in the public domain, allowing for future studies and validation tests to be conducted with open-source data within the naval hydrodynamics and tow tank testing communities.

Models 5617 and 5796 were manufactured and tested to evaluate the feasibility of using an additively manufactured model for future experimental testing purposes at the Naval Surface Warfare Center Carderock Division (NSWCCD). The models were used to conduct a resistance test to determine if the additively manufactured model can withstand the structural stresses of a carriage test and reproduce results from a traditionally manufactured fiberglass model. AM technology provides the potential for significant cost and time savings to be achieved from a construction, rigging, and testing standpoint.

Tests were be conducted in August and September, 2023 at the David Taylor Model Basin (DTMB) on Carriage 1 located in West Bethesda, Maryland.

The AM hull was fabricated under contract by Airtech International using a Large-Scale Additive Manufacturing (LSAM) machine developed by Thermwood, Inc., which is shown in Figure 86.

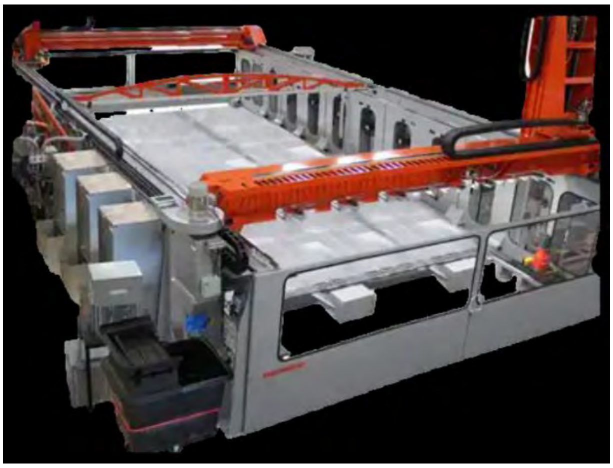

Figure 86: LSAM 1540 additive and subtractive machine (https://www.thermwood.com/lsam_home.htm)

This technology features both additive and subtractive capabilities allowing for large-scale, tight-tolerance parts to be created quickly and at a low per part cost. LSAM uses a "Near Net Shape" approach to part production where the part is first printed at high speed slightly larger than needed, then trimmed to the final size and shape using a 5-axis milling head on the same machine. LSAM can process parts from virtually any thermoplastic composite material, including high temperature materials that are ideal for moulds and tooling that must operate at elevated temperatures. A number of recycled materials are also available. LSAM's unique printing system produces parts that are solid, fully fused, vacuum tight and virtually void free, due to the compression roller that compacts the layers together after material deposition. LSAM systems can print in three orientations:

- Horizontal Layer Printing (HLP). Standard printing from the machine table.
- Vertical Layer Printing (VLP) option. Vertical Layer Printing allows parts to be printed that are as long as the machine table.
- Angle Layer Printing (ALP) option. Angle Layer Printing is the ability to print at a 45-degree angle.

Each print orientation has advantages and limitations for a particular part design. The ability to perform all three options using the same machine provides maximum print flexibility.

The objective of the presented work was to assess the feasibility of using an additively manufactured model for future model making and testing purposes. Specifically, they compared results from a LSAM model (5796) to a geometrically-similar fiberglass model (5617). , both constructed to a dimension ratio of 1:24.824.

The assessment included the hydrodynamic performance characteristics through calm water resistance tests, the geometric accuracy and repeatability of model fabrication, and assessment of rudimentary level material characteristics during testing. The material characteristic assessment included model/material water intake/absorption, hull crack development, and the presence and magnitude of hull deformation while testing.

The model appendage suite consists of a bow sonar dome, bilge keels, skeg, struts, and twin rudders with rudder shoes. Of the listed appendages, removable components include the bilge keels, struts, and rudders, which were fabricated using Stereolithography (SLA) 3D printing technology out of Accura 60 resin, and the dummy prop shafting which was fabricated using a 5/8 inch diameter hollow brass tube. Detailed dimensional characteristics of Model

5617 and Model 5796 were provided with waterline lengths of 18.77 feet (5.721 m) and a draught of 0.81 feet (0.247 m).

Turbulence tripping was achieved by installing 1/8th inch diameter by 1/10th inch projected length cylindrical studs placed approximately 0.5%*LPP aft of the stem spaced one inch apart. Studs around the sonar dome were placed in the transverse plane at the area of maximum sonar dome breadth.

Model 5617, originally built in 2002 by NSWCCD , was constructed of a fiberglass outer hull with mahogany internal structure, plywood bulkheads, and RenShape medium-high density polyurethane mounting pads. A photograph of Model 5617 is provided in Figure 87.

Figure 87: Photograph of Model 5617.

Model 5796 was built in 2022 by Airtech Int. for the current effort. The bare hull model was 3D printed using LSAM technology with a modified ABS material with 20% carbon-fiber infill reinforcement published by Airtech International (2021). The hull was printed using the ALP orientation at a 45-degree angle as shown in Figure 88.

Figure 88. Angled Layer Printing (ALP) LSAM Model 5796.

The build was completed in three separate sections and subsequently bonded together prior to final machining due to the complexity of the overhanging geometries. Section 1 is the forward part of the hull from the tip of the bow to approximately station 0.5, section #2 a small region on the lower forward part of the sonar dome, and section #3 is the remaining bulk geometry of the hull, from station 0.5 to the end of the stern. A photograph of Model 5796 as delivered from Airtech Int. showing the different sections is provided in Figure 89.

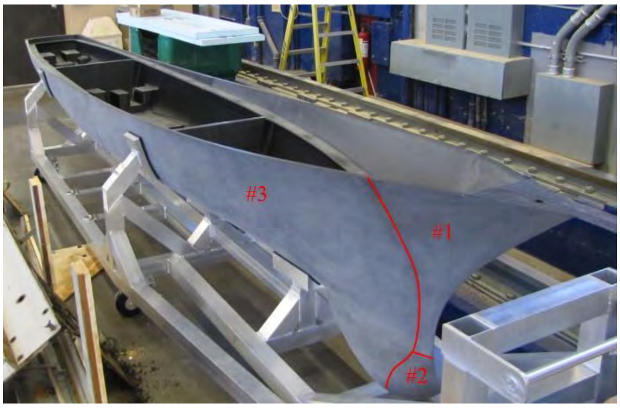

Figure 89. Model 5796 as delivered showing different sections.

After delivery of Model 5796, NSWCCD, installed the appendages (bilge keels, rudders, struts, propeller shafting), painted the outer hydrodynamic surface and sealed the joints between the hull sections. A photograph of Model 5796 after all additional work was completed is provided in Figure 90.

Figure 90. Photograph of Model 5796.

Laser scans of both models were conducted by the NSWCCD metrology department. Model 5617 was scanned, prior to testing, in an inverted orientation while resting on a layup table with elevated pedestals. Model 5796 was scanned in this same orientation, in a right-side-up orientation while in its cradle prior to testing, and again after testing in the inverted orientation. The intent of these scans was to ensure that LSAM technology can produce a model that is geometrically as accurate, if not more accurate, than historical model fabrication practices.

When constructing a model using LSAM technology, it is recommended to incorporate a flat-machined surface on the model that can be easily referenced as a datum plane when comparing point cloud metrology surface measurements to the source geometry. This technique allows for a more accurate assessment of the model geometry and the information can be used to guide future design decisions when building models for experimental testing purposes. The results of the surface deviation contour plots are shown in Figure 91 and Figure 92.

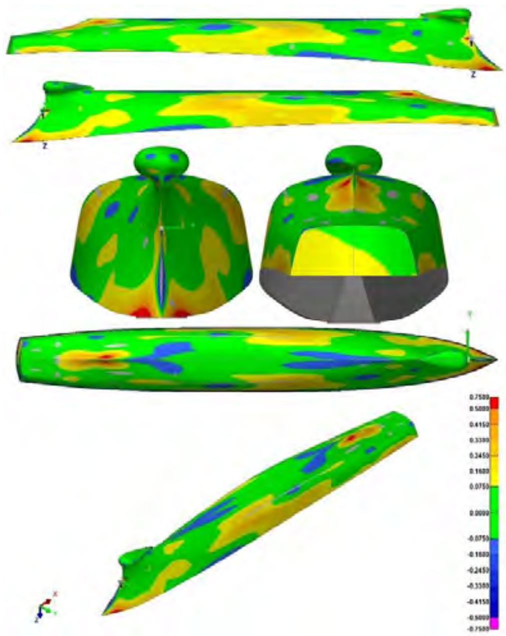

Figure 91. Model 5617 (GRP) – Pre-test Inverted. Contour plots of model surface deviation using best-fit method at 60% acceptance criteria.

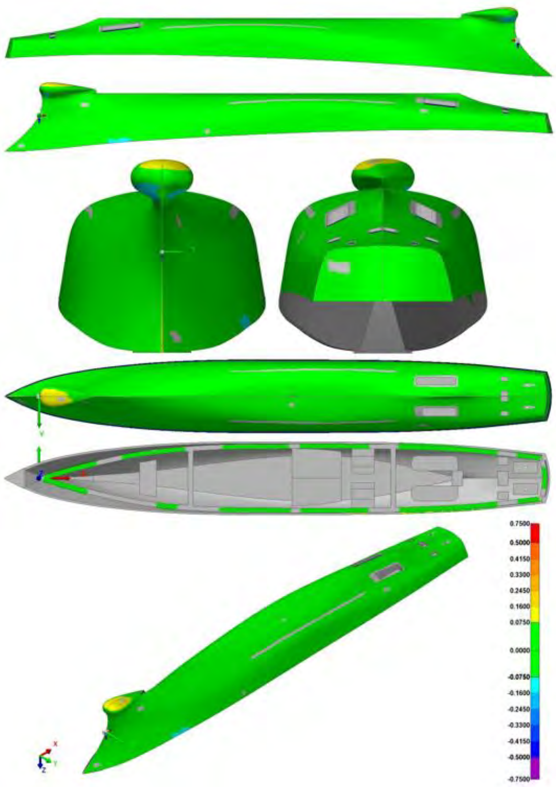

Figure 92 - Model 5796 (LSAM) - Post-Test, Inverted, Contour plots of model surface deviation using best-fit method at 60% acceptance criteria

The contour plot levels range from ±0.75in but show that the geometric accuracy of the hydrodynamic surfaces of the LSAM Model 5796 was far superior to that of the fiberglass Model 5617 and passed all scanning tolerance criteria, with measurements falling within ±0.075 in. The author suggested that additional hull form measurements be conducted periodically over the next several years and/or decades to assess the impacts on the model of long-term exposure to changing temperatures and humidity in the stored environment. Although, considering the low build cost and the ability to recycle the build materials, storing models for long durations may not be necessary.

Both Models 5617 and 5796 were outfitted with the same set of resistance testing and deflection measurement instrumentation. The resistance and the side force of the models were measured using linear transducer block gauges positioned at the forward tow point below the heave staff. The predicted full-scale effective power (EHP) indicated good agreement between both models as well as with historical data from Borda, G. G., et al. (1984) and Longo and Stern (1998). The deviation between the predicted EHP for the LSAM and the fiberglass model is shown in Figure 93.

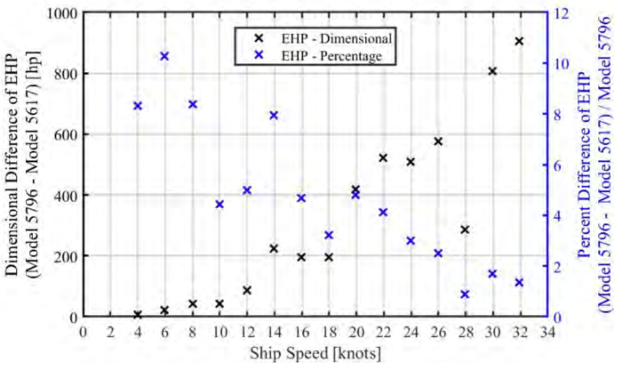

Figure 93. Deviation of EHP between LSAM and fiberglass models

The ship rise at L/LPP = 0.3, 0.5, and 0.7 and trim indicated acceptable underway model attitude was achieved with minimal impact on resistance measurements. The predicted ship rise for each model is shown in Figure 94.

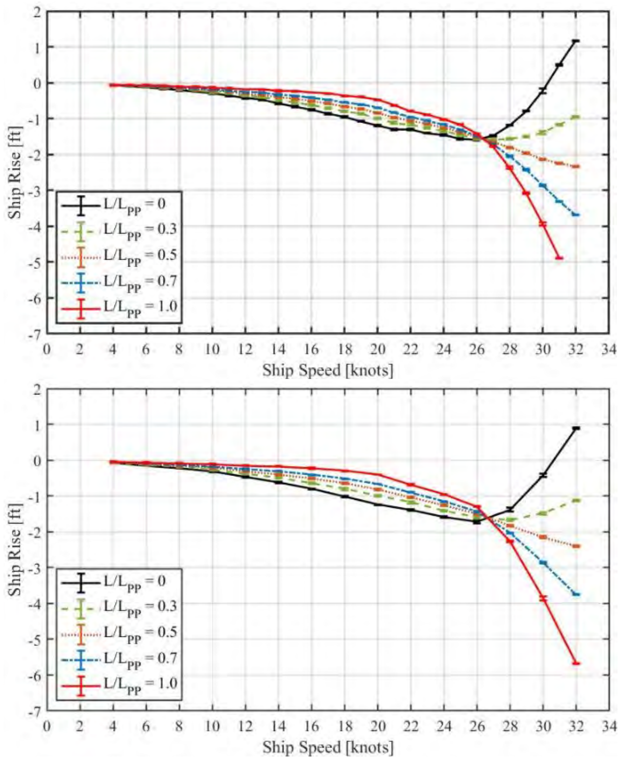

Figure 94. Prediction of ship rise for LSAM (top) and fiberglass (bottom) models

To quantify any deflection, or model hogging/sagging at various speeds while underway, the deflection of both models was determined by using a set of vertical and horizontal string potentiometer measurements positioned along the length of the hull. There were 5 vertical string potentiometers at the longitudinal positions indicated in Figure 94. These included two required for measuring running sinkage and trim at FP ($L/L_{pp}=0$) and AP ($L/L_{pp}=1$), and an additional 3 located nominally at the two internal bulkhead locations of Model 5796 and at the longitudinal center of gravity (LCG). Three horizontal string potentiometers were used to measure the deflection across the breadth of the model, at the top of the gunwhales. The measurements for both models were within the uncertainty of the string potentiometer sensors, however it was observed that the variance of measurements on Model 5796 were narrower than those measured on Model 5617 as shown in Figure 95.

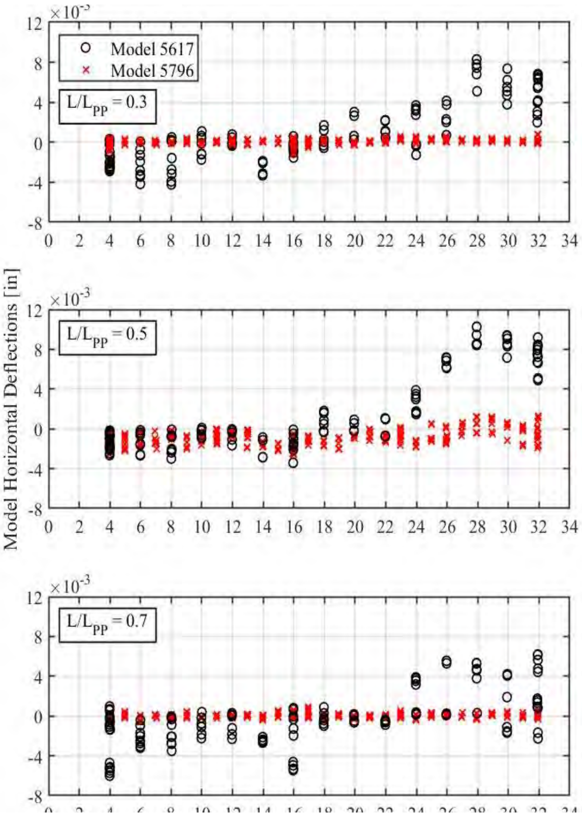

Figure 95. Model horizontal deflections at L/LPP = 0.3, 0.5, 0.7 AFP.

Additionally, water absorption and/or hull crack development were assessed throughout the duration of testing by weighing and inspecting the model at the start and end of each testing day. These measurements resulted in insignificant findings for water absorption but deflection measurements illustrated a more flexible fiberglass model as shown in Figure 96.

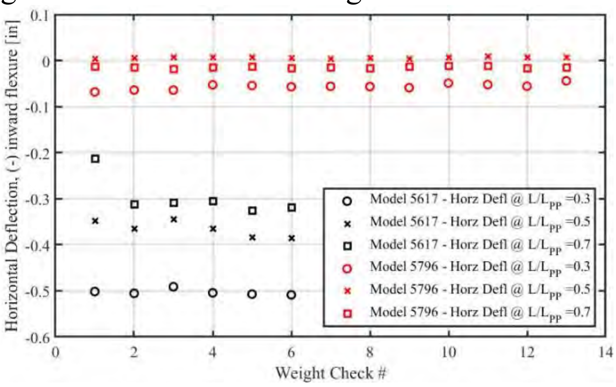

Figure 96. Horizontal deflections during model weight checks.

As the model was lifted to measure the weight it was found that the fiberglass model deformed inward from the lifting straps significantly relative to the LSAM model. Horizontal deflection measurements at L/LPP = 0.3, 0.5, and 0.7 suggest that the LSAM Model 5796 was slightly more rigid than Model 5617, however due to the differences in the age of the two models and the designs of the as-tested internal structures, it cannot be stated conclusively that an LSAM model is an improvement in this regard.

Based on the experience of using an LSAM model, the author included a list of design considerations for future LSAM model fabrication efforts as follows;

- All mounting holes, reference planes, scribe markings, etc. should be completed during initial model construction while model is in the original LSAM coordinate system.
- Coat the inner hull with an epoxy/hardening compound to protect against scratches and scrapes.
- Install metal threaded inserts, suitable for plastic materials, into all holes for all critical bolted joints, or for joints where repeated disassembly is required.
- During model construction phase, scribe a centerline along length of hull and mark all known or anticipated markings on hull while model is in original LSAM coordinate system.
- Include a flat plane relative to keel at the bow and stern of the model to provide measurable reference planes relative to the keel.
- Include a common reference plane along the length of the model to provide a datum plane for alignment of laser scan point cloud for geometry verification measurements.
- Hull geometry should be constructed without hollow voids to avoid spaces that could retain water without awareness.

- Design sufficient internal structure (bulkheads and longitudinals) to provide desired stiffness for your application.

- For models used in dynamic measurements (i.e. seakeeping and manoeuvring tests) consider a hull design for a near target dynamic mass property configuration with minimized total displacement.

Provided the quantitative and qualitative information, the author stated the overall feasibility of an additively manufactured surface ship model was deemed acceptable for tow tank resistance testing in calm water. A significant savings in cost and time-to-procure the model was achieved and is expected to improve further over time as lessons are learned and recommended design suggestions are employed.

10.3.2 Manufacture and testing of a 3D printed propeller at University of Genoa

Cilia et al (2019) conducted a cavitation test using a propeller printed in stainless steel and compared the results with data for the same propeller manufactured from bronze. The purpose of the programme was to determine whether a printed propeller could be accurate enough and strong enough that it would be suitable to conduct a cavitation experiment.

Initially they assessed material suitability for the production of the test propeller, considering a range of plastics and metals. Their preliminary assessment concluded that all the plastics would be insufficiently stiff and that tip deformation would not be expected to remain within ITTC guidelines. They also concluded that all the metals would be considered suitable for manufacture.

10 stainless blades were printed using a Renishaw AM-250 printer, and six were selected for metrological assessment. Limited ‘high precision’ measurements were obtained for each blade (three sections, twenty points per section) to determine the accuracy to which the manufacture had been achieved. They noted that:

- There was a generalized lack of material in the printed blades.
- Tip geometry fell far outside ITTC tolerances, with a high standard deviation.
- The worst measurement points were at the leading and trailing edges, which is also partly due to the difficulty in measuring these locations.
- The printed blades were less consistent than the machined blades.

They noted that the propeller blades did not conform to accepted ITTC tolerances, but considered that it was still worthwhile to conduct a cavitation inception test on the printed propeller, to determine what degree of difference would be found relative to their baseline historic data. Differences in hydrodynamic performance were found to be significant, with notable reduction in K_T, K_Q and η_O. They also showed that the propulsive coefficients were significantly different even at low load conditions, indicating that differences may be due to the as-manufactured geometry and not to deflections under load.

When conducting cavitation inception assessments, they noted that the 3D printed blades showed significant variation in cavitation inception indices. They attributed most of this variation to the lack of consistency in blade geometry, such as flat spots, squared leading edges with knuckles, incorrect surface curvature etc.

Overall, they concluded that they had identified a number of critical issues with their manufacturing process which had affected the accuracy of their printed propeller and would need to be resolved in future attempts.

10.3.3 AM manufacture and testing of 3D printed plastic and metal propellers at University of Naples Federico II

Staiano et al (2018), at the University of Naples, manufactured three propellers using AM techniques and conducted open water propeller tests. Two were printed from engineering grade plastics using Fused Deposition Moulding. The third propeller was manufactured using Direct Metal Laser Sintering (DMLS / L-PBF) from AlSi10Mg Aluminium alloy. Data were compared with benchmark data of INSEAN.

A comprehensive assessment of build accuracy was undertaken using both a high-resolution Laser scanner, together with surface roughness measurements. The standard deviation of the distance between measured point cloud data and the nominal CAD data surface was found to be 0.14 mm for the DMLS propeller. Assuming a normal distribution of points around the mean, this would mean that more than 30% of the measurement points showed discrepancy in excess of 0.14 mm. The plastic propellers showed even greater discrepancy from the design intent, particularly around the blade tips, with a standard deviation in excess of 0.50 mm. They attributes some of the discrepancy to thermal stresses and shrinkage of the plastic as it cooled. They also noted that the DMLS propeller showed rotational symmetry in its error characteristics, indicating that the geometrical errors were consistent between blades, whereas the plastic propellers showed rotational asymmetry. A key factor noted by the authors was that the DMLS propeller had a significantly higher level of surface roughness than is typically seen with conventional manufacturing techniques.

The authors reported that the propulsive coefficients presented showed significant differences to the benchmark data. They stated that future work will be undertaken to study the effect of roughness on the hydrodynamic performance of propellers. No comments were made on the corrections used when processing the data.

10.4 Conclusions

Significant advances in Additive Manufacture have been made over the last 10 years, with the development of many techniques which can now be considered suitable for use in model manufacture for hydrodynamic model testing.

The Additive/Subtractive LSAM system developed by Thermwood and demonstrated by NSWCCD shows very exciting promise, achieving tolerances which easily meet ITTC guidelines. The structural integrity of the complete model also appears to be at least equal to conventional manufacture techniques. Full exploitation of such a build technique would require some rethinking of conventional build approaches, to include the printing of all mounting points for propulsion and data acquisition equipment (dynamometers, force gauges etc). This new manufacturing methodology has the potential to significantly reduce model build and fit-out times, if the high initial cost of purchase of the machine can be overcome.

Additive manufacturing techniques for propellers are less well developed, although there are some methods which show promise. Some of the techniques already accredited by Classification Societies have significant advantage at full scale, where custom moulds and casting formers are needed. At model scale, however, the availability of high-quality solid billets of the necessary size and material renders some of these techniques (e.g. WAAM) redundant, since 5-axis machining is also required to produce the final part. The PBF family of AM methods are considered by the AM industry to be the most mature technologies and also have the largest market share. However, DMLS (L-PBF) machines can be difficult to operate and a process of trial and error is sometimes required before producing accurate and functional parts. To be cost-effective in hydrodynamic model testing it is required that a propeller model is created right-first-time, which makes new technologies difficult and costly to implement. Nonetheless, developments are rapidly continuing in this field and it must be considered only a matter of time before some of these new techniques are ready and cost-effective for the manufacture of bespoke model-scale propellers. Future developments in this field should be closely monitored.

11. GUIDELINES FOR MODEL TESTING OF COATINGS

11.1 Model testing of coatings to evaluate the hydrodynamic frictional performance

There are several options to investigate the hydrodynamic frictional characteristics of coating surfaces by model testing, e.g., velocity profile method, rotating disk method, towed plate method and so on. In any of those cases, it is necessary to obtain the roughness function for the coating surface at actual ship scale roughness Reynolds number, in order to evaluate the frictional characteristics of the coatings when they are installed to actual ships.

The mean velocity profile near the smooth wall surface has logarithmic region which is given by equation (1). The surface roughness causes a downward shift ΔU^+ in log-law which is so-called roughness function given in eq. (2). The roughness function is a function of roughness Reynolds number k^+ which is defined as $k^+ = u_\tau k_S/\nu$ where k_S is the roughness length scale. Once $\Delta U^+ = \Delta U^+(k^+)$ is obtained for a given rough surface, we can estimate the additional frictional resistance due to surface roughness, by using the boundary layer similarity law or by conducting CFD calculations with wall-function based boundary condition considering roughness function.

$$U^+ = \frac{1}{\kappa}\ln(y^+) + B \tag{1}$$

$$U^+ = \frac{1}{\kappa}\ln(y^+) + B - \Delta U^+ \tag{2}$$

11.1.1 Velocity profile method

The velocity profile method directly measures the mean velocity profile in turbulent boundary layer of coated rough surface and obtains the roughness function by determining the frictional velocity in some way. Schultz and Myers (2003) measured the velocity profile of flat plate flow using LDV in a closed-circuit water tunnel. Fig.1 shows the schematic of the flat plate test fixture. In their study, the friction velocity, u_τ, for the smooth surface was obtained by Clauser chart method, and for the rough surfaces, u_τ was obtained using a procedure based on the modified Clauser chart method given by Perry and Li (1990).

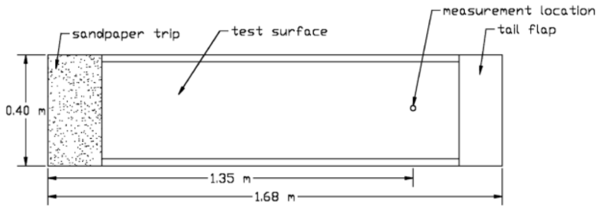

Figure 97 - Schematic of the flat plate test fixture for the velocity profile method by Schultz and Myers (2003)

11.1.2 Rotating disk method

Schultz and Myers (2003) conducted rotating disk experiments and obtained the roughness functions for several rough surfaces. A schematic of the rotating disk facility is shown in Fig. 2. This method measures the torque coefficients C_m for the smooth and rough disks for various rates of revolution and the roughness functions are calculated indirectly using the similarity law analysis of Granville (1982). This procedure involves comparing the C_m values of smooth and rough disks at the same value of $Re_R(C_m)^{1/2}$. The resulting equations for k^+ and ΔU^+ are given in eq. (3) and (4), respectively.

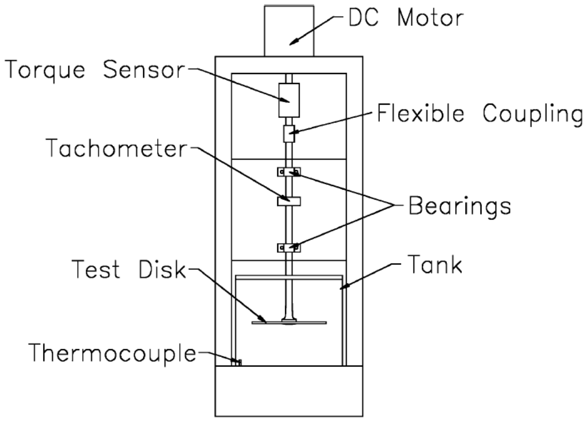

Figure 98 - Schematic of rotating disk test apparatus by Schultz and Myers (2003)

$$k^+ = \left(\frac{k}{R}\right)\sqrt{\frac{5}{8\pi}}Re_R\sqrt{C_m} \times \left\{1 - \left[\frac{2}{\kappa} - \Delta U^{+\prime}\right]\left(\frac{C_m}{40\pi}\right)_R\right\} \tag{3}$$

$$\Delta U^+ = \sqrt{\frac{8\pi}{5}}\left[\left(\frac{1}{\sqrt{C_m}}\right)_S - \left(\left(\frac{1}{\sqrt{C_m}}\right)_R\right)\right] + \frac{\Delta U^{+\prime}}{5} \tag{4}$$

11.1.3 Towed plate method

The towed plate method measures the frictional resistance coefficients C_F of flat plate with smooth and rough surfaces. Figure 99 shows the experimental setup of Schultz and Myers (2003) research. The roughness functions for the towed plate data are calculated using the similarity law analysis of Granville (1987). This procedure involves comparing the C_F values of smooth and rough plates at the same value of $Re_L C_F$. The resulting equations for k^+ and ΔU^+ are given in eq. (5) and (6), respectively.

$$k^+ = \left(\frac{k}{L}\right)\left(\frac{Re_L C_F}{2}\right)\left(\sqrt{\frac{2}{C_F}}\right)_R \times \left[1 - \frac{1}{\kappa}\left(\sqrt{\frac{C_F}{2}}\right)_R + \frac{1}{\kappa}\left(\frac{3}{2\kappa} - \Delta U^+\right)\left(\frac{C_F}{2}\right)_R\right] \tag{5}$$

$$\Delta U^+ = \left(\sqrt{\frac{2}{C_F}}\right)_S - \left(\sqrt{\frac{2}{C_F}}\right)_R - 19.7\left[\left(\sqrt{\frac{C_F}{2}}\right)_S - \left(\sqrt{\frac{C_F}{2}}\right)_R\right] - \frac{1}{\kappa}\Delta U^{+\prime}\left(\sqrt{\frac{C_F}{2}}\right)_R \tag{6}$$

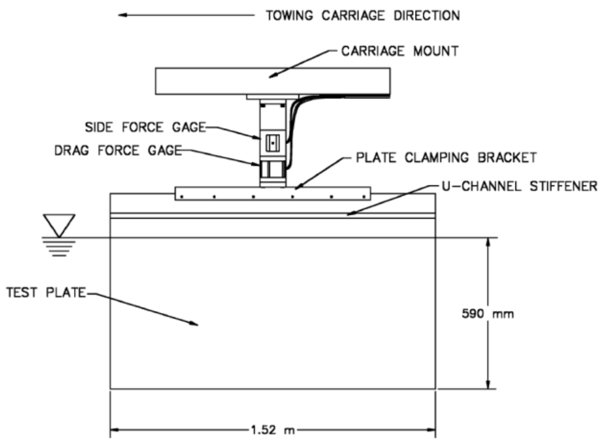

Figure 99 - Schematic of the flat plate test fixture for the towed plate method by Schultz and Myers (2003)

Schultz and Myers (2003) have compared three roughness determination methods which are velocity profile method, rotating disk method and towed plate method for two types of sandpaper and epoxy surface. Figure 100 shows the measured roughness functions for each of the test surfaces using the three determination methods and the comparison with the Grigson's and Schlichting's roughness functions. The authors concluded as follows, "The results for the velocity profile and towed plate methods show good agreement for all surfaces, with the epoxy surface following a Colebrook-type roughness function and the sandpaper surfaces following a Nikuradse-type roughness function. Although the tests using the rotating disk method were carried out at much higher Reynolds numbers, the results for the sandpaper rough surfaces agree within their uncertainty with a Nikuradse-type roughness function in the fully rough regime, while the results for the epoxy surface agree with a Colebrook-type roughness function."

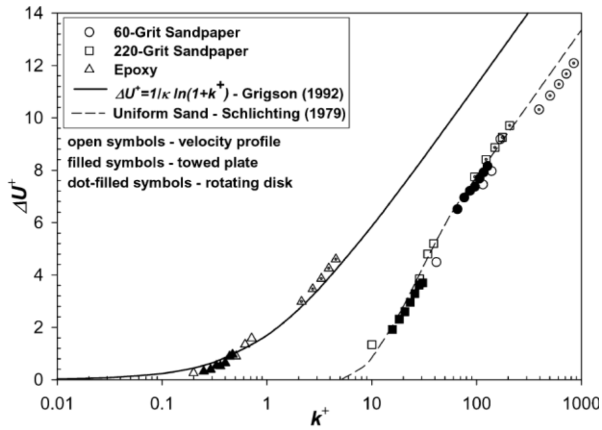

Figure 100 - Roughness function for the test surfaces obtained using the three methods by Schultz and Myers (2003)

Schultz also investigated the frictional resistance of antifouling coating systems by towed plate method. The roughness function for the un-fouled coatings shows reasonable agreement with a Colebrook-type roughness function when $k_S = 0.17R_a$ ($R_a$is a simple multiple of the centreline average height) is used as the roughness length scale shown in Figure 101.

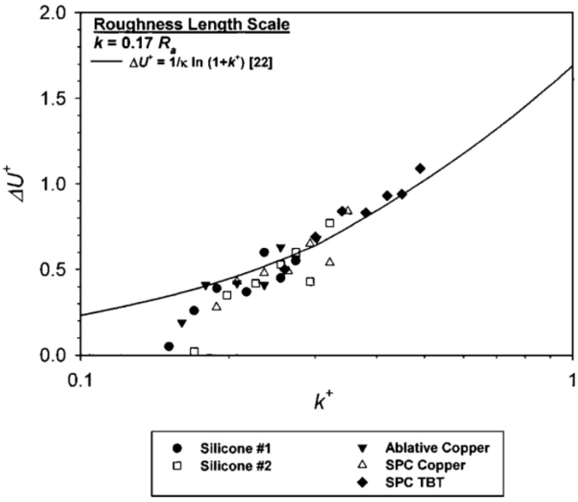

Figure 101 - Roughness function for the AF test surfaces in the cleaned condition. (Schlutz 2004)

Demirel et. al. (2014) calculated frictional resistance of smooth and rough surface flat plate using CFD in the same condition with Schultz's experiments (2004). The Colebrook-type roughness function of Grigson (1992) was employed in the wall-function of the solver and the roughness length scale was set in $k_S = 0.17R_a$ as Schlutz recommended. The calculated frictional coefficients showed good agreement with experimental results. This indicates that the roughness function and roughness length scale for antifouling (AF) coatings shown by Schultz are appropriate for use at model scale. Demirel *et al* also calculated the frictional resistance coefficients of flat plate at ship scale Reynolds number. The percentage increase in frictional resistance coefficients due to the AF coatings' roughness varies between 3.77% and 6.10%.

Yeginbayeva and Atlar (2018) presented experimental data on the boundary layer and drag characteristics of antifouling coating systems with different finishes. The coating types investigated were linear-polishing polymers, foul-release and controlled-depletion polymers. Their method is so-called velocity profile method which uses LDV in a large circulating water tunnel. The Krogstad's method was used to estimate the friction velocity, which is required to obtain the roughness functions for each coating surface. The measured roughness functions of tested surfaces displayed a monotonic behaviour of Colebrook-type Grigson's roughness function against the roughness Reynolds number. The range of roughness Reynolds number is relatively higher than the other experimental results. The roughness length scales defined by the peak-to-trough height ($k_S = 0.14R_t$) and combination of root mean square roughness and spatial distribution of height parameters ($k_S = 0.4R_q(1+\lambda_a)^{0.05}$) presented a satisfactory correlation with ΔU^+ in the transitionally rough flow regimes. (Fig. 6, 7)

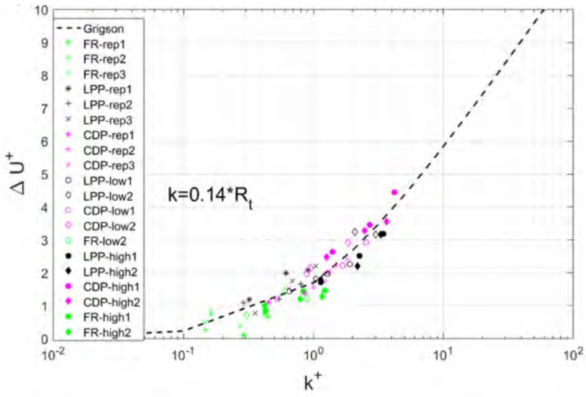

Figure 102 - Roughness function results for FR, LPP and CDP types with normal and mimicked hull finishes by using R_t. (Yeginbayeva and Atlar 2018)

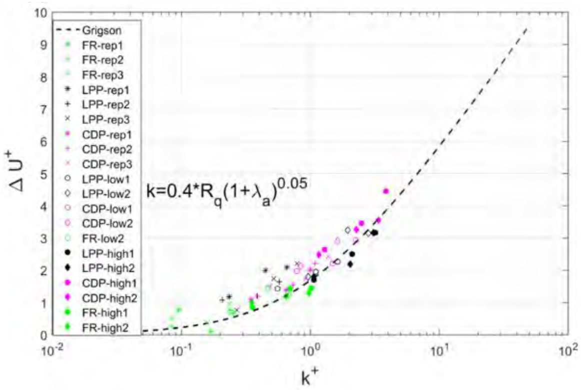

Figure 103 - Roughness function results for FR, LPP and CDP types with normal and mimicked hull finishes by using a correlation based on R_q and λ_a (Yeginbayeva and Atlar 2018)

As mentioned above, frictional characteristics have been investigated in detail at model scale. However, the behaviour of the roughness functions for coating surfaces at actual ship scale roughness Reynolds number region is still not sufficiently clear. As pointed out by Schlutz (2004), in order to obtain the roughness functions at higher roughness Reynolds number region, the rotation disk method is appropriate. Therefore, it is needed to investigate the frictional characteristics of coating surfaces in detail at higher roughness Reynolds number region using rotating devices, such as rotating disk and rotating cylinder (Katsui et. al. 2018) for the more accurate estimation of actual ship's frictional resistance.

11.2 Frictional drag reduction by air lubrication systems

The attempt to reduce the hydrodynamic frictional resistance such as ships and pipelines by air lubrication systems has a long history. Murai (2014) reviewed the research history of this topic comprehensively and exposited recent understandings of drag reduction mechanism.

According to Murai, the air lubrication-based drag reduction techniques are categorized into three kinds, which are bubble drag reduction (BDR), gas layer drag reduction (GLDR) and gas cavity drag reduction (GCDR). BDR works with action of dispersed bubbles inside the boundary layer. GLDR relies on replacement of highly shearing liquid with gas in the form of froths or long gas films. GCDR occurs when backward step provides a large gas single-phase space. Fig. 8 shows the schematic of three kinds of air lubrication.

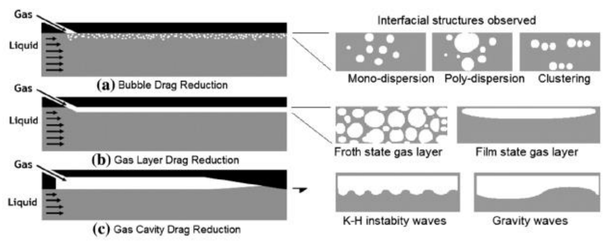

Figure 104 - Three types of frictional drag reduction enabled by gas injection. a Bubble drag reduction, b Gas layer drag reduction, c Gas cavity drag reduction (Murai 2014)

In order to apply the air lubrication-based drag reduction systems to engineering applications, it is necessary to understand the physical mechanism of drag reduction, including the scale effects. However, as Murai pointed out, "Understanding of the mechanism of transition allows reasonable design of drag reduction and improved performance. Unfortunately, the mechanism in use of bubbles is not explained by a couple of dimensionless parameters. What we see from data available today is a series of correlations among the liquid flow speed, gas flow rate, mean bubble size, and drag reduction ratio for a number of different flow configurations." Figure 105 represents a rough sketch of a drag reduction mechanism diagram as proposed by Murai. The parameter "G" in this figure is the sensitivity of the drag reduction per unit void fraction which is defined in eq. (7).

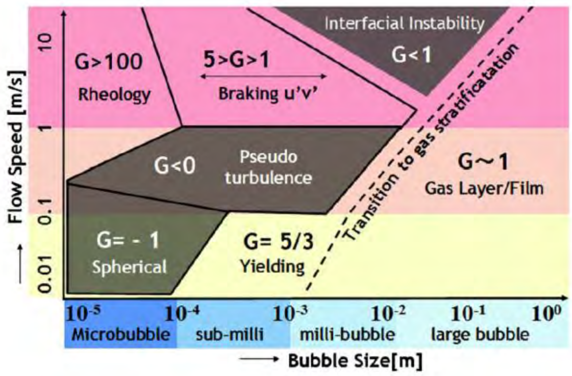

Figure 105 - Transition diagram of the drag reduction mech-anism owing to bubble injection (Murai 2014)

$$G = \frac{\frac{\Delta D}{D}}{\alpha} = \frac{1}{\alpha}\left\{1 - \frac{C_f}{C_{f0}}(1-\alpha)\right\} \qquad (7)$$

Where, ΔD, D, and α are original drag without air injection, reduced drag with air injection, and void fraction respectively. The lines that separate the domain into seven regions are determined from experimental data. Thus, the lines can be termed as transition lines of the dominant drag reduction mechanism.

On the other hand, the air lubrication system has been already installed to the actual ship and its energy-saving effects were confirmed by sea trial test (Mizoguchi et. al. 2010). The size of the ship is 162m in length, 38m in breadth and 4.5/6.37m in draft. The achieved net energy-saving effect was 12% at the maximum air blow-off rate. Although, we have to know the scaling law of drag reduction rate by the air lubrication system to estimate the actual ship performance from the model experiments accurately, we still don't have sufficient understanding on it. Therefore, it is important to accumulate the experimental data at ship scale Reynolds number using large sized model to investigate the scaling law for the drag reduction by air lubrication method.

Tanaka et. al. (2022) investigated the frictional drag reduction by bubble injection by means of model experiments using a 36 m length flat-bottom model ship. The towing speed is up to 8.0 m/s, with which Reynolds number reaches $2.9*10^8$. The resistance of the model ship and the distribution of the local wall shear stress on the entire bottom plate was measured. They have found out that the local wall shear stress has a profile that decays with the downstream distance depending on the air flow rate. Considering this feature, they have presented a formula describing the streamwise transition of the ratio of the friction coefficient and proposed a method of predicting the drag reduction for a full-scale ship.

It is still needed to accumulate the experimental data on drag reduction by air lubrication at ship scale Reynolds number to find out the behaviour of the air. If the air behaviour in turbulent boundary layer at full scale can be modelled, we can also utilize CFD technique to estimate the actual ship performance.

12. TOR18 – REVIEW CFD METHODS FOR ROUGHNESS EFFECTS

12.1 CFD methods for roughness effects using wall-function method

This procedure uses the relation between velocity and surface shear stress, the so-called log-law including roughness effects shown in eq. (1) at the 1st layer cell center point from the surface. And once the friction velocity is known, the value of k and omega are defined based on asymptotic behaviour at the near wall, eq. (2) and (3) (Wilcox 2006). ΔU^+in eq. (1) is called the roughness function, which represents a downward shift in the log-law caused by to the momentum deficit in the boundary layer due to roughness. The roughness function is generally defined as a function of roughness Reynolds number $k^+ = u_\tau k_s/\nu$ and has logarithmic behavior in terms of k^+ for usual sand-grain roughness. k_s means roughness length scale and it is defined to be the roughness height for the sand-grain roughness. In ship hydrodynamics, t hull surface roughness is mainly split into two categories: painted surface roughness and roughness due to bio-fouling. The characteristics of those two types of roughness are different from sand-grain roughness. Therefore, it is necessary to know the roughness function itself or roughness length scale for each roughness. Demirel et al. (2017) and Song et al. (2019, 2020, 2021) have shown the effect that biofouling has on ship resistance using CFD with wall function method considering the roughness function. They have used the roughness functions shown in eq. (4) with the roughness length scale for each roughness conditions shown in Table 1 and 2. Demirel et al. (2014) also calculated the added frictional resistance due to antifouling coatings over flat plate using the wall function method. The roughness function proposed by Grigson was used and the roughness length scale (sand-grain equivalent roughness height) was defined as $k_s = 0.17R_a$, based on measured average roughness height R_a for each coating. Table 3 shows the comparison of calculated and measured C_F at model scale Reynolds number by Demirel et al. Calculated skin friction coefficients agree with measured ones.

$$\frac{U}{u_\tau} = \frac{1}{\kappa}\ln\frac{u_\tau y}{\nu} + B - \Delta U^+ \tag{1}$$

$$k = \frac{{u_\tau}^2}{\sqrt{\beta^*}} \tag{2}$$

$$\omega = \frac{k^{\frac{1}{2}}}{{\beta^*}^{\frac{1}{4}}\kappa y} \tag{3}$$

$$\Delta U^+ = \begin{cases} 0 & \text{for } k^+ < 3 \\ \frac{1}{\kappa}\ln(0.26k^+)^{\sin\left[\frac{\pi}{2}\frac{\log\left(\frac{k^+}{3}\right)}{\log(5)}\right]} & \text{for } 3 < k^+ < 15 \\ \frac{1}{\kappa}\ln(0.26k^+) & \text{for } \rightarrow 15 < k^+ \end{cases} \tag{4}$$

Table 16 - Roughness length scale k_s for coating and fouling shown by Demirel et al. (2017)

A range of representative coating and fouling conditions [6].

Description of condition	NSTM rating[a]	k_s (μm)	Rt_{50} (μm)
Hydraulically smooth surface	0	0	0
Typical as applied AF coating	0	30	150
Deteriorated coating or light slime	10–20	100	300
Heavy slime	30	300	600
Small calcareous fouling or weed	40–60	1000	1000
Medium calcareous fouling	70–80	3000	3000
Heavy calcareous fouling	90–100	10000	10000

[a] NSTM [44].

Table 17 - Roughness length scale k_s for fouling conditions shown by Song et al. (2019)

Roughness length scales of test surfaces, adapted from Demirel et al. (2017a).

Test surface	Barnacle type	Surface coverage (%)	Barnacle height *h* (mm)	Representative sand-grain roughness height k_G (μm)
B10%	Big	10%	5	174
B20%	Big	20%	5	489
M10%	Medium	10%	2.5	84
M20%	Medium	20%	2.5	165
M40%	Medium	40%	2.5	388
M50%	Medium	50%	2.5	460
S10%	Small	10%	1.25	24
S20%	Small	20%	1.25	63
S40%	Small	40%	1.25	149
S50%	Small	50%	1.25	194

The advantage of using the wall-function method is that the roughness function can be directly applied to the wall boundary condition. After the roughness function is obtained, it is easy to apply it to the wall boundary condition. The roughness functions of hull coatings are investigated by many researchers so far (Yeginbayeva et. al. 2018, Atencio et. al. 2019). However, the relation between the roughness function and surface profile of coatings unclear, especially for ship scale roughness Reynolds number, because the characteristics of roughness profile have many variations and roughness length scale changes depending on it. Therefore, further investigations on roughness functions for coating rough surfaces are needed.

Table 18 - Comparison of CF at model scale Reynolds number by Demirel et al. (2014)

Table 8
The comparison of C_F values at $Re = 5.5 \times 10^6$.

Surface	C_F (CFD)	C_F (experiment)	Difference (%)
Smooth	0.003185	0.003226	−1.26
Silicone 1	0.003460	0.003374	2.54
Silicone 2	0.003481	0.003426	1.60
Ablative Copper	0.003470	0.003401	2.04
SPC Copper	0.003491	0.003438	1.55
SPC TBT	0.003551	0.003500	1.45

12.2 CFD methods for roughness effects using wall resolved method

In the wall resolved CFD using k-omega SST turbulence model, which is widely used in ship flow CFD, the modified wall boundary conditions of omega or k and omega are applied to simulate the effects of the surface roughness. Wilcox (2006) showed a modified wall boundary condition of omega for rough surface which is shown in eq. (5) and (6). Hellsten (1998) introduced a lower limit of k^+which depends on y^+ as an extension of Wilcox's method. Hellsten's wall boundary conditions are shown in eq. (5), (7) and (8). In the method proposed by Knopp et. al. (2009), the modified wall boundary condition not only for omega, but also for k are introduced for the rough surface shown in eq. (9) - (11). Aupoix also has shown the wall boundary conditions of k and omega for rough surface based on Grigson's representation of Colebrook's results.

- Wall boundary condition of omega for rough surface proposed by Wilcox (2006)

$$\omega = \frac{{u_\tau}^2}{\nu} S_R \tag{5}$$

$$S_R = \begin{cases} \left(\dfrac{200}{k^+}\right)^2 \\ \qquad \text{for } k^+ \leq 5 \\ \dfrac{100}{k^+} + \left[\left(\dfrac{200}{k^+}\right)^2 - \dfrac{100}{k^+}\right] e^{5-k^+} \\ \qquad \text{for } 5 < k^+ \end{cases} \tag{6}$$

- Hellsten's modification of Wilcox's wall boundary condition of omega for rough surface (1998)

$$k^+ = \max\left(k^+, 4.3{y^+}^{0.85}\right) \tag{7}$$

$$S_R = \begin{cases} \left(\dfrac{50}{k^+}\right)^2 & k^+ \leq 25 \\ \dfrac{100}{k^+} & 25 < k^+ \end{cases} \tag{8}$$

- Wall boundary condition of omega and k for rough surface proposed by Knopp (2009)

$$\omega = \min\left(\frac{u_\tau}{\sqrt{\beta}\kappa d_0}, \frac{60\nu}{\beta y^2}\right) \tag{9}$$

$$k = \min\left(1, \frac{k^+}{90}\right)\frac{{u_\tau}^2}{\sqrt{\beta}} \tag{10}$$

$$\begin{aligned} d_0 = 0.03k_s \min\left(1, \left(\frac{k^+}{30}\right)^{\frac{2}{3}}\right) \\ \times \min\left(1, \left(\frac{k^+}{45}\right)^{\frac{1}{4}}\right) \\ \times \min\left(1, \left(\frac{k^+}{60}\right)^{\frac{1}{4}}\right) \end{aligned} \tag{11}$$

- Wall boundary condition of omega and k for rough surface proposed by Aupoix (2014)

$$\omega = \min\left(\left(\begin{array}{c} \frac{300}{k^{+2}}\left(\tanh\left(\frac{15}{4k^+}\right)\right)^{-1} \\ +\frac{191}{k^+}\left(1-\exp\left(-\frac{k^+}{250}\right)\right) \end{array}\right)\frac{{u_\tau}^2}{\nu}, \frac{60\nu}{\beta y^2}\right) \tag{12}$$

$$k = \max\left(0, \frac{1}{\sqrt{\beta}}\left(\left(\frac{\log\left(\frac{k^+}{30}\right)}{\log(10)} + \left(1-\tanh\left(\frac{k^+}{125}\right)\right)\right) \times \tan\left(\frac{k^+}{125}\right)\right)\right) \times {u_\tau}^2 \tag{13}$$

Orych et al. (2022) showed a comparison of calculated frictional resistance of flat plate and ship with wall boundary conditions proposed by Hellsten, Knopp and Aupoix. The flat plate results are shown in Figure 106. They pointed out that "The performance of the selected roughness models shows that Aupoix-Colebrook yields the most reasonable results when compared to extrapolated model scale experiments and another CFD method."

The wall resolved method itself predicts turbulent boundary layer flow with higher accuracy than wall function method. On the other hand, in case of the calculation with rough wall surface, the wall resolved method requires the complicated wall boundary conditions for turbulent parameter omega and k compared with wall function method. Also, the relation between the roughness function and roughness Reynolds number k^+ is not clear. As well as the wall function method, wall resolved method also needs appropriate roughness length scale k_s for various kind of rough surface in ship scale roughness Reynolds number.

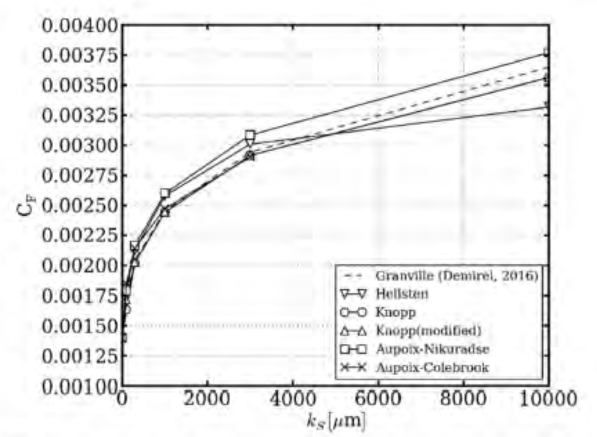

Fig. 18. Roughness model comparison for a flat plate at Re = 2.89 × 10⁹, k-ω SST, k_s range 0–10 000 μm.

Figure 106 - Comparison of calculated CF with various wall boundary conditions for rough surface (Wall resolved calculations) by Orych et al. (2022)

13. IDENTIFY THE NECESSITY OF GUIDELINES FOR CFD METHODS, MODEL TESTS AND SCALING FOR ENERGY SAVING DEVICES

Many different kinds of Energy Saving Devices (ESD) have already been developed, which makes the creation of generic guidelines for CFD and/or model tests extremely difficult. A classification system for the different ESDs is proposed below, which is a first step towards the creation of guidelines for testing and scaling processes.

Depending on the working principle, existing and emerging energy saving devices can be categorised into five areas:

- Hull resistance reduction measures,
- Propeller flow conditioning devices,
- Propeller/hub modifications,
- Manoeuvring energy saving devices
- Renewable energy assisted propulsion

These categories are broken down further in Figure 107.

They vary in general location with respect to the vessel as shown in Figure 108.

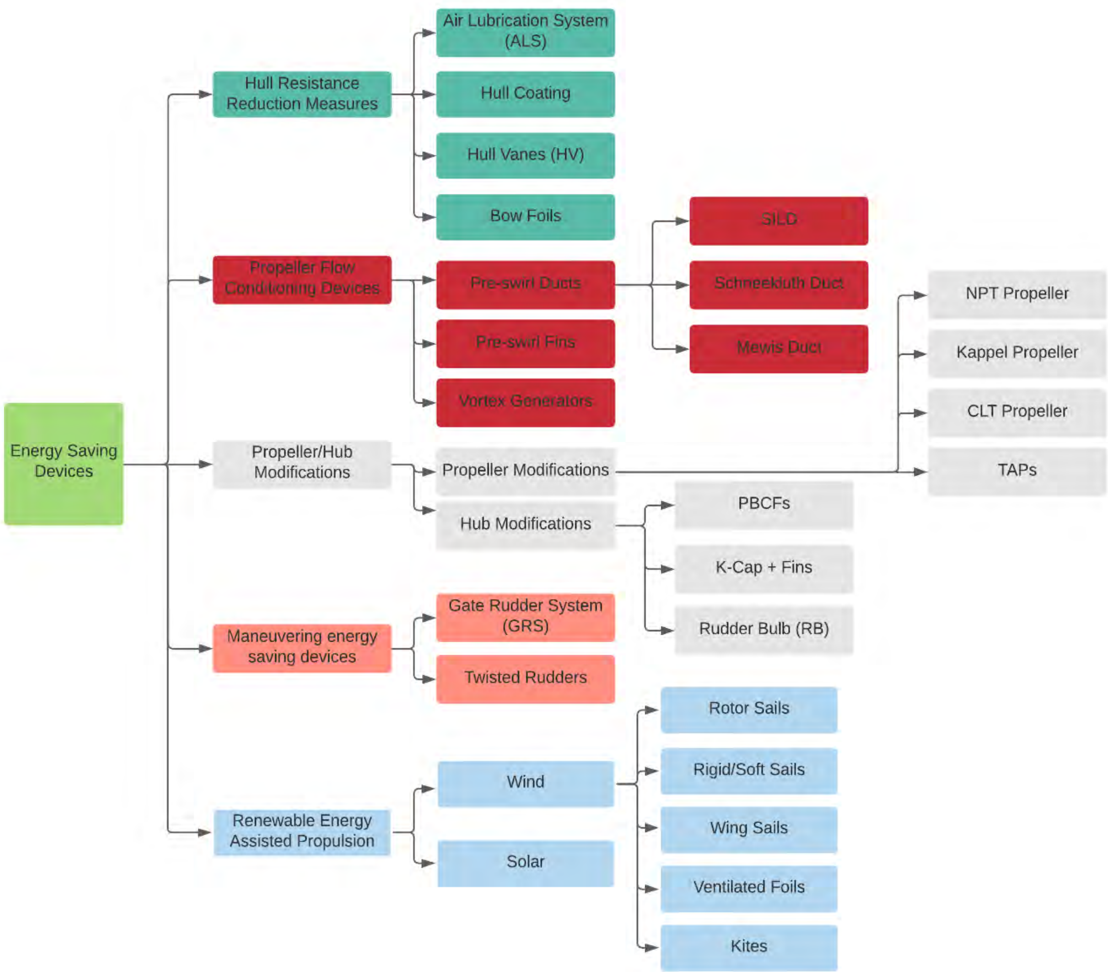

Figure 107 - Categorisation of existing and emerging energy saving devices (ESDs)

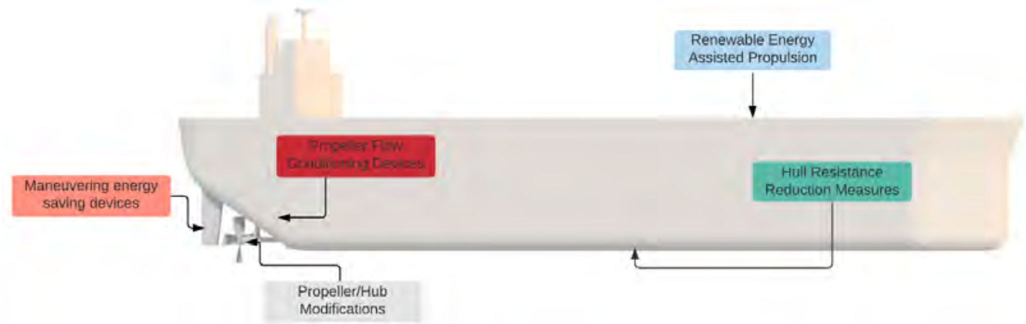

Figure 108 - General application of energy saving devices (ESDs) for a location point of view

Due to the different working principles, it is not considered feasible to develop a uniform approach to test their performance and predict the performance for full-scale conditions. Therefore, the following sessions discuss the scaling methods according to the categories.

13.1.1 Hull Resistance Reduction Measures

In shipping, a large part of the fuel is used to overcome hydrodynamic forces, up to 85% (Ahmadzadehtalatapeh and Mousavi, 2015), hence reducing hull resistance is the most direct way to save energy. To date, three major approaches have been released into the commercial sector which include air lubrication, hull coatings and hull appendages (e.g. hull vane or bow foil). Depending on their working principles, they affect the skin frictional coefficients, wave making resistance, form factor, or wetted surface area. It has been summarised as below:

- Skin frictional coefficients: coating applications, air lubrications.
- Wave making resistance: hull vane, bow foil.
- Form factor: hull vane, bow foil.
- Wetted surface area: air lubrication.

Detailed quantification of the effect of the individual technologies is needed for the scaling of the energy saving devices.

13.1.2 Propeller Flow Conditioning Devices

Propeller flow conditioning devices refer to devices installed upstream of the propeller which improve the flow into the propeller. The devices include pre-swirl duct, pre-swirl fins, wake equalizing duct and vortex generators. The scaling of these devices needs to consider the impact on wake fraction, thrust deduction and form factor. In the situation that the device provides additional thrust (by recovering 'wasted' energy), it should be considered as part of the propulsion system.

At ITTC 2021, the guideline was adopted for the scaling of the pre-swirl fin devices. Two methods have been proposed. However, due to the complexity of the devices, the application of such methods depends on the specific device type with limited application until now.

13.1.3 Propeller/Hub Modification

Propeller/hub modifications include development in novel propeller design to improve the performance of the propellers and the new propeller hub design to recover energy behind the propeller (e.g. Propeller Boss Cap Fins). The effect of these devices must be included in the propeller open water tests and the scaling should be combined with the propeller open scaling. However, full scale trials of propeller boss cap fins have not always shown the performance improvements predicted by model tests and detailed analysis is required, Kimura & Ando (2019).

13.1.4 Manoeuvring Energy Saving Devices

Manoeuvring Energy Saving Devices are those innovations on rudders to integrate the manoeuvring devices with the propulsion system. The typical devices include Gate rudder, twisted rudder, rudder bulb and rudder with fins. So far, the devices is developed to provide additional thrust for ships, which also affects the rudder resistance. When additional thrust is generated by these devices, they shall be considered to be an integral part of the propulsion unit when considering scaling approaches, i.e. considering rudder resistance to be a component of the hull resistance shall be avoided.

13.1.5 Renewable Energy Assisted Propulsion

Renewable Energy Assisted Propulsion refers to devices using wind or solar energy to either propel the vessel or to provide additional energy that can be used to power the ship's energy saving. Devices using wind energy to produce additional propulsion force include wind sails, Flettner rotors and other wind assisted propulsion devices. The scaling of the performance of such devices shall consider the reduced propeller thrust requirement, leading to different thrust deduction factor, propeller operation and efficiency. It should also consider the effect on the resistance of the ship, such as the effect of an additional yaw angle. For devices like wind turbines or solar panels, which only provide additional energy to the ship's power system, the devices have minor hydrodynamic impact.

13.1.6 CFD application on scaling of the energy saving devices.

As discussed previously, depending on the principle of the energy saving devices, different parameters can be affected by the application of the energy saving devices. Until now, there is no unified approach for the scaling of energy saving devices. It has to discussed retrospectively regarding to individual devices. At the moment, most research has been conducted by using CFD for the full-scale performance prediction. However, the results are not well benchmarked and validated to provide a guideline for CFD modelling for energy saving devices. General guidelines for hull and propeller modelling have been followed, as summarised in Table 19 below. Further research is required conducted in this area to develop the best practice and to assist in the formulation of ITTC guidelines for appropriate modelling of energy saving devices.

Table 19 - Typical CFD modelling approaches and parameters for model and full scale modelling

	Model Scale	Full Scale
Size: Ship length	3-8 m	50-300m
Size: Propeller Dia	150mm-250mm	2-6m
Size: ESD typical reference length	150mm-250mm	2-6m
Turbulence model	SST k-w Realisable K-e	SST k-w Realisable K-e
Wall modelling	Wall function: low Y+	Wall function: high Y+
Y+	1-5 or above 30	above 30
Mesh: near wall	Follow the Y+ guide regarding individual components: propeller, hull, ESD.	
Mesh: Free-surface	Monitor Kelvin wave development Resolve the wave length in 50-80 cells and the wave height in 20 cells	
Time step	Dominated by propeller: propeller advances between 0.5 and 2 degrees per time step (Recommended by ITTC 7.5-03-03-01) Special attention is needed if the propeller is interacting with ESDs.	

14. CONCLUSIONS AND RECOMMENDATIONS

14.1 State of the Art

The work of the JoRes project should be reviewed when it is published in December 24, to determine how the data contained within it can be used by the ITTC to improve its recommended guidelines and procedures.

The work of the GATERS project should also be reviewed, to determine how its data could be used for the assessment of the gate rudders. The large efficiency improvements claimed by the project make this type of Energy Saving Device of particular relevance to the IMO's goals for greenhouse gas reduction, and the availability of both geometric data and full-scale trials data may allow a robust scaling process to be developed.

14.2 Procedures

The following three updated procedures should be adopted by the 30th ITTC:

- 7.5-01-01-01 Ship Models
- 7.5-02-03-01.8 Energy Saving Devices
- 7.5-02-05-01 High Speed Marine Vehicles

The procedures which were only able to be partially completed by the 30th ITTC R&P committee should be completed and reviewed by the 31st ITTC. In particular, the background work done on updating the ITTC's 1978 Performance Prediction Method should be considered a priority, together with the uncertainty analysis worked example which goes with it.

The Waterjet propulsion test uncertainty analysis should also be completed and released. A new dataset, which includes data collected from pressure tappings, is required in order for this to be undertaken.

The review of the *Scaling methods for ships fitted with pre-swirl devices* procedure highlighted that further work and investigation into this type of ESD is required. Since many of these devices are considered to be proprietary, a benchmark using non-commercial ESD designs should be generated and used. However, the use of a non-commercial design may limit the potential for conducting full scale validation, which would be of great value when considering the relatively small improvements in efficiency that these ESDs can create.

14.3 Benchmark study on the effect of Re at model scale and scaling methods for full-scale prediction

The results of CFD simulations conducted by a number of participants showed significant variability between their results, which was potentially of a similar order of magnitude to the scale effects the study was attempting to characterise.

The variability raises the question of whether an accurate full-scale prediction can be made from model-scale data (Schuiling/Kerkvliet *et al* 2024), without knowing the results *a priori* to enable correct calibration of turbulence intensity parameters.

The production of best practice guidelines for conducting CFD simulations of Propeller Open Water Test (POT) should be considered by the ITTC.

Benchmark experimental data for CFD validation of POT would benefit greatly by the inclusion of turbulence intensity measurements and flow visualisation techniques such as paint flow tests.

Fully turbulent model-scale measurements using non-intrusive tripping (Schuiling/Kirkvliet 2024) may provide better characterization of the full-scale open water performance due to the improved similarity with full-scale flow regimes. The work of the 'Tripping' Joint Industry Project (www.marin.nl/jips/tripping) should be monitored carefully. Further work on this topic should be well integrated with the investigation of laminar flow effects in self-propulsion test.

14.4 Investigation of the issue of laminar effects in self-propulsion test of propeller with low blade area

A significant number of participants in the study reported having issues with low Re during self-propulsion tests. Recent work by Hasuike (2017) and Lucke (2017) showed mixed laminar and transitional flow at model scale, which is different to the fully turbulent flow expected at full scale. The superiority of the 2-POT method was confirmed by highlighting the similarities in the flow regime between open water and behind conditions at low Reynolds number.

It is recommended to conduct the propeller open-water test at multiple Reynolds numbers, particularly for propellers with low blade area ratios. This should provide better understanding of the asymptotic convergence of the propulsive coefficients.

The work of the Tripping Joint Industry Project should be monitored carefully. The novel turbulent stimulator design of Schuiling & Kerkvliet may help alleviate the issue of laminar flow at model scale, both for propeller open water testing and also in the self-propulsion testing.

14.5 Investigation of the issue of extrapolation of model tests with ducted propellers to full-scale according to different Reynolds numbers

Very limited published data are available on the extrapolation to full scale of ducted propeller performance. A small CFD study conducted by a member of the committee showed similar, if not greater, sensitivity to inflow turbulence intensity level to that of an open water propeller.

It is recommended that the problem of Reynolds number sensitivity for a ducted propeller is deferred until the effects of Reynolds number and laminar-turbulent transitional flow on open propellers is better understood.

14.6 Update of the load variation test method in 1978 ITTC Performance Prediction method

A review of procedure 7.5-02-03-01.4 – *1978 ITTC Performance Prediction Method* found that the formula for relative rotative efficiency (η_R) was incorrect when using a torque identity approach.

The correct formula for η_R, using a torque identity, is:

$$\eta_R = \frac{K_{TM}}{K_{TQM}}$$

Where K_{TM} is the thrust coefficient from the self-propulsion test. K_{TQM} is read from the propeller open water diagram, by using the torque identity to find the advance ratio where K_{QM} intersects the torque curve and reading off the thrust coefficient at the same advance ratio.

The IMO's minimum propulsion power requirements for safe passage have resulted in a change to recommended range of added resistance allowances. A small study of the added resistance in waves for a number of different vessel types indicate that the historically used load variation test allowance of -10% to +20% is insufficient.

It is recommended that, particularly at low speed, testing organisations should increase the range of the load variation test to -10% to +40%.

Added resistance in waves can have non-linear effects, particularly above 30%. Care should be taken to ensure that appropriate data is collected, and also that data are interpolated correctly. Additionally, care should be taken to ensure that air draw into the propellers does not occur when testing at highly overloaded conditions.

To bring the ITTC's 1978 Performance Prediction Method procedure in line with other procedures was found to require more work than originally anticipated. Significant work was done on this update, but it was not completed in time for release in the 30th ITTC. It is recommended that this work is continued by the 31st ITTC.

14.7 Investigation of the requirements for the testing and numerical evaluation of high-speed marine vessels

The flow around the lower edge of a transom stern was noted to affect the running sinkage and trim during testing. This characteristic will affect both physical model experiments and CFD studies.

It was recommended that the sharpness of the transom edge of a physical model is measured using edge gauges and recorded in the model's documentation.

14.8 Investigation of measurement and prediction methods for breaking waves

A range of different techniques were documented for experimental characterisation and measurement of breaking waves, focussing on the behaviour around the bow of a vessel.

Experimental techniques ranged from the use of transparent and semi-transparent models, with cameras viewing from inside the model, to Particle Image Velocimetry (sometimes stereoscopic PIV) based techniques. It was noted, however, that experimental measurements are highly dependent upon experimental conditions and are extremely time consuming, so observations are usually limited to benchmark ships or simplified test cases.

Numerical techniques continue to advance, due to ever increasing computational power. CFD techniques include Unsteady RANS (URANS), Delayed Detached Eddy Simulation

(DDES). In addition to changes in the underlying computational solvers, academic effort has also made progress on higher-order interface capturing schemes. The DDES method, combined with higher order two-phase schemes have been prevalent in recent academic work. However, the computational cost of this approach limits its widespread use and these techniques are generally considered to still be in development.

14.9 Developments in hull and propeller manufacturing

Significant advances have been made in Additive Manufacturing (AM) over recent years, and it is commonly used for the manufacture of appendages by the ITTC community.

Recent work conducted around the world has been investigating the feasibility of printing entire ship models up to 10 m in length. Some organisations have expressed concern about model rigidity and have needed to add aluminium beam reinforcement.

A study conducted by NSWCCD, to be reported by Mosqueda et al (2024), showed that Large Scale Additive Manufacturing (LSAM) of a ship model can achieve standard ITTC model build tolerances. The LSAM manufacturing technique pioneered by Thermwood Inc. appears extremely promising for future model building, which could reduce lead time for model manufacture and also reduce costs.

AM techniques for metals have also made huge advances over recent years, but trial studies indicate that the technology may not yet be sufficiently mature that it can be used for propeller manufacture at this time. The Powder Bed Fusion class of techniques hold the most promise, but are difficult to get right first time. The cavitation testing and open water testing of AM propellers conducted at two Italian universities is exciting, but showed differences in hydrodynamic and cavitation performance when compared to benchmark data. Developments in this field should continue to be monitored, as it must only be a matter of time before processes suitable for model scale propeller manufacture become available.

14.10 Guidelines for model testing of coatings

It was not possible to develop robust guidelines for the model testing of coatings, because insufficient published literature exists at this time. However, a review of the current state-of-the-art was conducted in this field.

Techniques documented included velocity profile method, rotating disk method, towed plate method. The frictional characteristics have been investigated in detail at model scale. However, the behaviour of the roughness functions for coating surfaces at ship scale roughness Reynolds numbers is still not sufficiently clear. As pointed out by Schultz (2004) the rotating disc and rotating drum techniques have potential to investigate the frictional characteristics of coating surfaces at higher roughness Reynolds number regions. Further work is required before guidelines can be issued by the ITTC.

Frictional drag reduction by air lubrication techniques were also reviewed. Air lubrication techniques have already been implemented on ships and shown to provide net energy savings (Mizoguchi *et al* 2010), however a clear understanding of all the flow phenomena is not yet possible. Monitoring of the work in this field should be continued, because this type of technology could be fundamental if the IMO is to achieve its stated goals of achieving net zero greenhouse gas emissions by 2050.

14.11 Review CFD methods for roughness effects

A review of wall-function methods was conducted, including a literature review of recent published work in this field. The roughness functions of hull coatings have been investigated by a number of researchers, however the relationship between the roughness function and the surface profile of coatings is still unclear, especially for ship scale roughness Reynolds numbers. Further investigations on roughness functions for coating rough surfaces are needed.

For wall-resolved CFD techniques, the review focussed on the k-omega SST turbulence model, because this is widely used in CFD simulations of ship resistance and propulsion. Typically, modified k and omega boundary conditions are applied to simulate the effects of surface roughness. Orych et al (2022) showed a comparison of calculated frictional resistance of flat plate and ship with a variety of wall boundary conditions. Orych's work showed that the Aupoix-Colebrook method yields the most reasonable results when compared to extrapolated model scale experiments and more detailed CFD methods.

While wall-resolved techniques predict turbulent boundary layer flow with higher accuracy than wall function methods, the relationship between the roughness function and the roughness Reynolds number k+ is still not clear. The wall-resolved method also needs appropriate roughness length scale for various types of rough surfaces at ship scales. Further work is still required in this field, in order to determine best practice.

14.12 Identify the necessity of guidelines for CFD methods, model tests and scaling processes for Energy Saving Devices

A huge variety of Energy Saving Devices are currently being developed which makes the creation of generic guidelines difficult. Individual guidelines are likely to be required for specific techniques, such as: frictional resistance reduction; energy recovery devices such as hull vanes; propulsion efficiency improvements via inflow conditioning devices or gate rudders; renewable energy assisted propulsion systems such as Flettner rotors, sails or kites. It should be noted, however, that some of these ESDs interact with other parts of the ship system, so a holistic approach may be required. Additionally, many of the systems exhibit considerable scale effects and savings predicted by model tests cannot always be realised at full scale. Full scale testing of ESDs is therefore required and some work is being undertaken in this field. Determining a robust and reliable scaling process is essential, because many of these techniques would be expected to only give small improvements in efficiency.

Two new guidelines have been prepared by the ITTC Specialist Committee on Wind Powered Ships:

- Guideline for predicting the power saving of wind powered ships
- Conduct and analysis of sea trial for wind-assisted ships.

The 31st Resistance and Propulsion committee should review these documents and incorporate any additional requirements into the self-propulsion test guideline and into the 1978 ITTC Performance Prediction Method, if appropriate.

15. REFERENCES

Ahmadzadehtalatapeh, M., Mousavi, M., "A review on the Drag Reduction Methods of she Ship Hulls for Improving the Hydrodynamic Performance", International Journal of Maritime Technology, Vol 4 (2015) : 51-64

Airtech International, 2021, "Material Properties Specifications Data Sheet. Dahltram_S-150CF-EN".

Atencio, B. N., Chernoray, V., 2019, "A resolved RANS CFD approach for drag characterization of antifouling paints", Ocean Engineering 171, 519–532.

Aupoix, B., 2014. Wall roughness modelling with k-w STT model. In: 10th International ERCOFTAC Symposium on Engineering Turbulence Modelling and Measurements, Sep 2014. MARBELLA, Spain.

Bart, S., Maarten, K., Douwe R., 2024, "An Experimental Study on Visualisation and Passive Control of Model Propeller Boundary Layers", Eighth International Symposium on Marine Propulsors smp'24, Berlin, Germany.

Bhattacharyya, A., Krasilnikov, V., and Steen, S., 2015, "Scale effects on a 4-bladed propeller operating in ducts of different design in open water" In Proceedings of the Forth International Symposium on Marine Propulsors SMP2015, Austin, Texas, USA.

Bhattacharyya, A., Krasilnikov, V., and Steen, S., 2016a, "Scale effects on open water characteristics of a controllable pitch propeller working within different duct designs" Ocean Engineering, 112, 226-242.

Bhattacharyya, A., Krasilnikov, V., and Steen, S., 2016b, "A CFD-based scaling approach for ducted propellers" Ocean engineering, 123, 116-130.

Boorsma, A., 2000, "Improving full scale ship powering performance predictions by application of propeller leading edge roughness", Master of Science Thesis, University of Technology, Delft.

Borda, G. G., et al., 1984, "Resistance, Powering Optimum Rudder Angle Experiments on a 465.9 Foot (142 m) Guided Missile Destroyer (DDG-51) Represented by Model 5415-1 and Fixed Pitch Propellers 4876 and 4877 (U)," DTNSRDC/SPD-0200-08.

Cilia, T., Beretta, D., Gualeni, P., Tani, G., Vivani, M., "Additive Manufacturing Application to a Ship Propeller Model for Experimental Activity in the Cavitation Tunnel", Journal of Ship Production and Design, Bol. 35, No.4, November 2019, pp 364-373.

Dang J., Dong G., Chen H., 2012, "An exploratory study on the working principle of energy saving devices (ESDs): PIV, CFD investigations ad ESD design guidelines", Proceedings of the ASME 31st International Conference on Offshore Mechanics and Arctic Engineering (OMAE), Rio the Janeiro, Brasil.

Demirel, Y. K., Khorasanchi, M., Turan, O., Incecik, A., Schultz, M. P., 2014, "A CFD model for the frictional resistance prediction of antifouling coatings", Ocean Engineering 89, 21–31.

Demirel, Y. K., Turan,O., Incecik, A., 2017, "Predicting the effect of biofouling on ship resistance using CFD", Applied Ocean Research 62, 100–118.

Eça, L., Hoekstra, M., 2011, "Numerical aspects of including wall roughness effects in the SST k-ω eddy-viscosity turbulence model", Comp Fluids 40:299–314.

Fontes, J.V.H., Martínez-Flores, A., Hernandez, I.D., Mendoza, E., Silva, R., 2022, "Flow Kinematics in the Generation of Different Types of Green Water Events with Incident

Wave Trains", Ocean Engineering, 258: 111519.

Furcas, F., Gaggero, S., 2021 "Pre-Swirl Stators design using a coupled BEM-RANSE approach" Ocean Engineering, vol. 222, Article Number 108579.

Gaggero, S. 2020 "Influence of laminar-to-turbulent transition on model scale propeller performances. Part I: fully wetted conditions", Ship and Offshore Structures, 17(4), pp. 772–791.

Gaggero, S. and Martinelli, M., 2022, "Pre-Swirl fins design for improved propulsive performances: application to fast twin-screw passenger ships" Journal of Ocean Engineering and Marine Energy, vol. 9.

Gaggero, S., Rizzo, C. M., Tani, G., and Viviani, M., 2013 "Design, analysis and experimental characterization of a propeller in decelerating duct", In Third International Symposium on Marine Propulsors (SMP2013), Launceston, Tasmania, Australia.

Govindrak, R.B., Junghans, E., Andersen, I., ki Lim, Y., Lindstrom, P., "Additive manufactured marine component – Ni Al bronze propeller", Procedia Structural Integrity, 34:20-25.

Hengelmolen, V. and Wellens, P. R., 2022, "An Experimental Study on Added Resistance Focused on the Effects of Bow Wave Breaking and Relative Wave Measurements", International Shipbuilding Progress, 69: 61-89.

Hellsten, A., 1998, "Some Improvements in Menter's K-Omega SST Turbulence model", 29th AIAA, Fluid Dynamics Conference. Fluid Dynamics and Co-located Conferences, https://doi.org/10.2514/6.1998-2554.

Hasuike N., Okazaki M., Okazaki A., Fujiyama K., 2017, "Scale effects of marine propellers in POT and self propulsion test conditions", Fifth International Symposium on Marine Propulsors smp'17, Espoo, Finland.

Ishii, N., Yagi, H., Yuasa, H., 1983, "Model Testing of Propeller Cavitation Roughening the Leading Edge of Blades", Journal of the Society of Naval Architects of Japan, 153.

ITTC, 1975, "Report of Propeller Committee", 14th ITTC Full Conference Proceedings, Ottawa, Canada.

ITTC, 2021, "Report of Propeller and Resistance Committee", 29th ITTC Full Conference Proceedings.

Jacobi, G., Thill, C.H., Huijsmans, R.H.M., 2022, "Pressure Reconstruction from PIV Measurements in the Bow Region of a Fast Ship", Ocean Engineering, 252: 110318.

Jin, Q., 2022, "A Combined Volume of Fluid and Immersed Boundary Method for Simulations of Ship Bow Breaking Waves", PhD Thesis, University of Southampton.

Kerkvliet, M., Baltazar, J., Schuiling, B. and Eça, L., 2024 "A Numerical Study on Model Propeller Performance Prediction Including Transitional and Passively Controlled Boundary Layer Considerations", Proceedings of the 8th International Symposium on Marine Propulsors, Berlin, Germany.

Kim, J.H., Choi, J.E., Choi, B.J., Chung, S.H., and Seo, H.W., 2015, "Development of energy-saving devices for a full slow-speed ship through improving propulsion performance" International Journal of Naval Architecture and Ocean Engineering, vol.7, no. 2, pp 390-398.

Kim, M.C., Shin, Y.J., Lee, W.J., Lee, J.H., 2017, "Study on extrapolation method for self-propulsion test with pre-swirl device" Proceedings of the International Symposium on Marine Propulsion, Espoo, Finland.

Kimura, K., Ando, S., "A Method to predict Full Scale Performance of the Propeller Boss Cap

Fins", Sixth International Symposium on Marine Propulsors, SMP 19, Rome, Italy.

Knopp, T., Eisfeld, B., Calvo, J. B., 2009, "A new extension for k-ω turbulence model to account for wall roughness", Int. J. Heat Fluid Flow 30 (1), 54-65, 101016/jiheatfluidflow200809009.

Koushan, K., Krasilnikov, V., Nataletti, M., Sileo, L., and Spence, S., 2020 "Experimental and Numerical Study of Pre-Swirl Stators PSS" Journal of Marine Science and Engineering, vol. 8.

Larsson, L. Stern, F. Bertram, V., "Benchmarking of Computational Fluid Dynamics for Ship Flows: The Gothenburg 2000 Workshop", Journal of Ship Research 47 (01): 63-81, 2003

Lee, E.J., Mousaviraad, M., Weil, C.R., Jiang, M.J., Fullerton, A.M. and Stern, F., 2021, Assessment of experiments and CFD for the semi-planing R/V Athena Model in calm water, *Ocean Engineering*, Vol. 236, p.109254.

Lee J.T., Kim M.C., Suh J.C., Kim S.H., Choi J.K., 1992 "Development of preswirl stator-propeller system for Improvement of Propulsion Efficiency: a Symmetric Stator Propulsion System", Journal of the Society of Naval Architects of Korea, vol. 41, no. 3, pp. 13-21

Lee, W.J., 2015 "Study on Full-Scale Performance Prediction for Pre-Swirl Device Model Test Results", Ph.D. Thesis, Pusan National University

Li, C., Duan, W-Y., Zhao, B-B., 2022a, "Breaking Wave Simulations for a High-Speed Surface Vessel with Hybrid THINC and HRIC Schemes", Applied Ocean Research, 25: 103257.

Li, D-Q, Lindell, P, Werner, Sücke T., 2019, "Transitional flow on model scale propellers and their likely influence on performance prediction", Sixth International Symposium on Marine Propulsors smp'19, Rome, Italy.

Li, Z., Zhang, X-S., Wan, D-C., 2022b, "Research Progress on the Hydrodynamic Performance of Water-Air-Bubble Mixed Flows Around a Ship", Journal of Hydrodynamics, 34(2): 171-188.

Longo, J., & Stern, F., 1998, "Resistance, Sinkage and Trim, Wave Profile, and Nominal Wake Tests and Uncertainty Assessment for DTMB Model 5512." Paper presented at the SNAME 25th American Towing Tank Conference, Iowa City, Iowa, USA.

Lücke T., Streckwall H., 2017, "Experience with Small Blade Area Propeller Performance", Fifth International Symposium on Marine Propulsors smp'17, Espoo, Finland.

Mallat, B., Germain,G., Billard, J-Y., Gabillet, C. 2022, "Breaking Wave Bubble Measurements Around Ship Model by Optical Probe", Ocean Engineering, 246: 110438.

MARIN, 2024, "Tripping JIP", Retrieved April 8,2024 from https://www.marin.nl/en/jips/tripping, .

Mewis F. and Guiard T., 2011, "Mewis duct – New development, solutions and conclusions", Proceedings of the 2nd International Symposium on Marine Propulsors, Hamburg, Germany.

Mosqueda, K., (2024), "Large Scale Additively Manufactured Model Feasibility Study and Resistance Experiments", NSWCCD-80-TR-2024-001.

Nicorelli, G., Villa, D. and Gaggero, S., 2023, "Pre-Swirl Ducts, Pre-Swirl Fins and Wake-Equalizing Ducts for the DTC Hull: Design and Scale Effects", Journal of Marine Science and Engineering, vol. 11 no.5

Olivieri, A., Pistani, F., Wilson, R., Campana, E.F., Stern, F., A., 2007, "Scars and Vortices

Induced by Ship Bow and Shoulder Wave Breaking", Journal of Fulid Engineering ASME, 129: 1445-1459.

Orych, M, Werner, S., Larsson, L., 2022, "Roughness effect modelling for wall resolved RANS – Comparison of methods for marine hydrodynamics", Ocean Engineering 266, 112778.

Rubino, G. and Abdel-Maksoud, M., 2024, "Model- and Full-Scale Tip-Rake Marine Propellers: Analysis of the Scale Effects in Open Water", Proceedings of the 8th International Symposium on Marine Propulsors, Berlin, Germany.

Shin H.J., Lee J.S., Lee K.H., Han M.R., Hur E.B., Shin S.C., 2013, "Numerical and experimental investigation of conventional and unconventional preswirl duct for VLCC", International Journal of Naval Architecture and Ocean Engineering, vol. 5, no. 2, pp 413-430.

Song, S., Demirel, Y. K., Atlar, M., 2019, "An investigation into the effect of biofouling on the ship hydrodynamic characteristics using CFD", Ocean Engineering 175, 122–137.

Song, S., Demirel, Y. K., Atlar, M., Dai, S., Day, S., Turan, O., 2000, "Validation of the CFD approach for modelling roughness effect on ship resistance", Ocean Engineering 200.

Song, S., Ravenna, R., Dai, S., Muscat-Fenech, C. D., Tani, G., Demirel, Y. K., Atlar, M., Day, S., Incecik, A., 2021, "Experimental investigation on the effect of heterogeneous hull roughness on ship resistance", Ocean Engineering 223.

Staiano, G., Gloria, A., Ausanio, G., Lanzotti, A., Pensa, C., Martorelli, M., "Experimental study on hydrodynamic performances of naval propellers to adopt new additive manufacturing process", International Journal on Interactive Design and Manufacturing (2018) 12:1-14

Suzuki, T., 1974, "Effect of Turbulence Stimulating Device on the Results of Propeller Open Water and Self-propulsion Tests",

Tasdemir, A., Nohut, S., "An overview of wire arc additive manufacturing (WAAM) in shipbuilding industry", Ships and Offshore Structures, 16:7, 797-814.

Wang, J., Ren, Z., Wan, D-C., 2020, "Study of a Container Ship with Breaking Waves at High Froude Number Using URANS and DDES Methods", Journal of Ship Research, 1-11.

Wang, X., Zhu, R., Jiang,Y., 2023, "Numerical investigation on nonlinear ship waves by LCM and WSAM", Ocean Engineering, 284: 115076.

Wilcox, D. C., 2006, "Turbulence modeling for CFD Third Edition", DCW Industries, Inc.

Wilson, R., Carrica, P., and Stern, F., 2007, "Simulation of Ship Breaking Bow Waves and Induced Vorticies and Scars", International Journal for Numerical Methods in Fluids, 54-4: 419-451.

Wu, D., Wang, J., Wan, D-C., 2021, "Delayed detached eddy simulation method for breaking bow waves of a surface combatant model with different trim angle", Ocean Engineering, 242: 110177.

Yeginbayeva, I. A., Atlar, M., 2018, "An experimental investigation into the surface and hydrodynamic characteristics of marine coatings with mimicked hull roughness ranges", Biofouling, 34:9, 1001-1019.

ITTC2024
30TH INTERNATIONAL TOWING TANK CONFERENCE
22–27 SEPTEMBER 2024 | HOBART TASMANIA AUSTRALIA

REPORT OF THE MANOEUVRING COMMITTEE

1. INTRODUCTION

1.1 Membership and Meetings

The members of the Manoeuvring Committee (MC) of the 30th ITTC are:

- Prof. Dr. Xide Cheng (Chair). Wuhan University of Technology, CHINA
- Dr. Zhiming Yuan (Secretary). Universities of Glasgow and Strathclyde, UK
- Ms. Janne Flensborg Otzen. FORCE Technology, DENMARK
- Dr. Takashi Kishimoto. Akishima Laboratories (Mitsui Zosen) Inc, JAPAN
- Dr. Youngjae Sung. Hyundai Maritime Research Institute, REPUBLIC OF KOREA
- Dr. Maciej Reichel. Gdansk University of Technology, POLAND
- Dr. Dobrin V. Efremov. Bulgarian Ship Hydrodynamics Centre, BULGARIA
- Dr. Andrea Serani. National Research Council-Institute of Marine Engineering, ITALY
- Prof. Heather Peng. Memorial University Newfoundland, CANADA
- Dr. Shawn Aram. Naval Surface Warfare Center Carderock Division, USA
- Dr. Dong Jin Yeo. Korea Research Institute of Ships and Ocean Engineering, REPUBLIC OF KOREA

Four committee meetings have been held during the work period:

- The first meeting (online), January 10-12, 2022;
- The second meeting (online), 30th November - 1st December, 2022;
- The third meeting (in-person), 20-21 July, 2023, KRISO, Daejeon, Korean
- The fourth meeting (in-person), 9-11 January, 2024, Strathclyde, Glasgow, UK.

Due to COVID impacts, MC also held more than ten breakout online meetings during this term.

1.2 Tasks

The recommendations for the work of the Manoeuvring Committee as given by the 30th ITTC were as follows:

1) Update the state-of-the-art for predicting the manoeuvring behaviour of ships, emphasizing developments since the 2021 ITTC Conference. The committee report should include sections on:
   a. The potential impact of new technological developments on the ITTC, such as unmanned ship and autonomous navigation
   b. New experiment techniques and extrapolation methods
   c. The practical applications of computational methods to manoeuvring predictions and scaling, including CFD methods

d. The need for R&D for improving methods of model experiments, numerical modelling and full-scale measurements

2) During the first year, Recommended Procedures manoeuvring, and
a. Identify any requirements for changes in the light of current practice and, if approved by the Advisory Council, update them,
b. Identify the need for new procedures and outline the purpose and contents of these.

3) Update procedure 7.5-02-06-05 “Uncertainty Analysis for Free Running Model Tests” complying with current ITTC guidelines for uncertainty analysis. Cooperate closely with the Quality Systems Group.

4) Survey the state of the art of the development of autonomous navigation technology such as the application of artificial intelligence schemes, and investigate potential impact to ITTC, including the impact to autopilot of full-scale ships.

5) Update 7.5-02-06-02, “Captive Model Test”, particularly with specific attention to the treatment of amplitudes, frequencies, and inertial coefficients and to have a single integrated example for uncertainty analysis, based on the SIMMAN results.

6) Update 7.5-02-06-03 “Validation of Manoeuvring Simulation Models”, reflecting the outcome of SIMMAN and any other new developments.

7) Continue the work with underwater vehicles towards and complete the guidelines, extending to submarines and ROV’s, if possible.

8) Update the guidelines proposed by Special Committee on Manoeuvring in Waves of the 29th term, collaborating with the Seakeeping Committee.

9) Support and collaborate with SIMMAN group for post processing and analysis of the submitted results and collect the benchmark data for the validation of numerical methods of ship manoeuvring, including the wave induced forces and moments in waves.

10) Validate the Level 2 - Minimum Power Assessment of the Draft Amendments to Guidelines (MEPC.1/Circ.850/Rev.3).

11) Collect benchmark data for
a. Underwater vehicles
b. Inland navigation
c. Model-scale vessels with a documented full-scale variant

12) Survey the captive test in waves and collect the data of the hydrodynamic forces acting on the ship in waves, which can be used for the validation and application of simulation tools, including
a. Oblique towing test data in waves
b. Circular motion test data in waves
a. PMM test data in waves
b. Rudder force data in waves when ship is moving straight ahead

13) Investigate its implications on manoeuvrability of the effect of novel devices and clean fuel technology on available installed power, in wind and waves.

2. STATE OF THE ART

2.1 Experimental Measurements

2.1.1 Shallow, Restricted and Confined Waterways

Recent studies provide invaluable insights into various aspects of maritime navigation, including the effects of mud layers, ship-to-ship interactions, and the impact of canal and quay geometries on ship manoeuvrability. The following papers collectively contribute to a deeper understanding of the complexities involved in maritime transportation in specialized environments.

Delefortrie et al. (2022a) presented a focused study on the influence of fluid mud on ship squats. Through an extensive series of towing tank tests, the research demonstrates that the presence of a mud layer significantly increases squat, especially at smaller drift angles. The experimental results led to the development of a correction term for existing empirical squat prediction formulas, accounting for the unique impact of mud layers. This study is particularly relevant for navigating ships in environments with fluidized mud layers, providing essential insights for safe and efficient manoeuvring in such challenging conditions.

Böttner and Kondziella (2022) explored the dynamics of ship-to-ship interactions in shallow and confined waters. Their model test study reveals that the forces exerted on moored containerships by passing vessels increase more than quadratically with the speed of the passing ship, highlighting the significant impact of speed reduction in managing these interaction forces. The study also emphasizes the amplified longitudinal interaction forces due to the presence of a quay wall, with reduced sway forces. These findings are instrumental for improving the safety and management of ship movements in such challenging navigational environments, particularly given the trend towards larger vessels.

Ley et al. (2022) presented a comprehensive examination of the hydrodynamic interactions between passing and moored ships in confined canal environments. The research, utilizing scale model tests, focuses on the dynamic response of moored ships to passing vessels in a canal port setting. Key findings include the identification of significant rope tension forces on the moored ships, influenced by various factors such as the speed of the passing ship, rope stiffness, and pretension. The study reveals that the hydrodynamic forces induced by passing ships are considerable and must be factored into the design and operation of mooring systems in similar canal port scenarios.

Mehr et al. (2022) focused on the impact of water depth on the rolling behaviour of large vessels. The study utilizes model tests to determine how different water depths affect the roll natural period and damping coefficient. The findings indicate that for a depth-to-draft ratio greater than 2.0, changes in water depth do not significantly influence these parameters. However, when this ratio is less than 2.0, both the roll period and damping coefficient increase exponentially with decreasing water depth. This study offers crucial insights into ship stability and safety in shallow waters, a significant consideration for large commercial vessels operating in such environments.

Okuda et al. (2022) examined how the direction of propeller rotation (inward or outward) affects the manoeuvrability of twin-propeller and twin-rudder ships. The paper presents results from free-running model tests, including turning, zigzag, stopping, and crabbing manoeuvres in both deep and shallow water conditions. A key finding is that the propeller rotation direction significantly influences crabbing performance in shallow water. Specifically, ships with outward rotating propellers demonstrate better manoeuvrability in these conditions. This research provides valuable insights for the design and operation of twin-propeller, twin-rudder ships, particularly in terms of propeller rotation direction and its impact on manoeuvrability in shallow waters.

Verwilligen et al. (2022) presented a comprehensive analysis of the impact of bank effects on ship manoeuvrability in confined channels. The study combines model-scale towing tank tests with full-scale measurements to assess the influence of bank effects on a bulk carrier navigating through the Canal Ghent-Terneuzen. Key findings highlight the significant impact of canal geometry and bank presence on ship behaviour, including alterations in manoeuvring and squatting. The research underscores the importance of considering bank effects in the design and operation of navigation channels, especially for large vessels in confined waterways, to ensure safe and efficient maritime operations.

Delefortrie et al. (2022c) presented an in-depth exploration of how various barge configurations affect the manoeuvring behaviour of push convoys. Using a 6 Degrees of Freedom (DOF) manoeuvring model, the research evaluates multiple configurations for factors such as number of barges, draft, and position of the pusher in both deep and shallow waters. The findings from captive model tests, validated through fast time simulation runs and real-time simulations with experienced skippers, demonstrate that barge configuration significantly impacts manoeuvrability. These insights are essential for designing and operating inland waterways and push convoys.

Esferra et al. (2021) investigated the hydrodynamic interactions between passing and moored ships. The research, using scale model simulations, focuses on the Santos Port and explores the effects of different navigational conditions on the mooring lines of docked ships. The findings emphasize the significant strain on mooring systems induced by passing ships, especially in the right margin trajectory close to the dock. The study offers valuable insights into mooring system performance under varying conditions of ship passage, highlighting the critical need for effective mooring strategies in ports to ensure the safety and stability of docked vessels.

Hachiya et al. (2022) investigated the impacts of a false bottom in a towing tank on the hydrodynamic forces acting on a ship model. The research, conducted with a KCS model, reveals that in a false bottom setup, both lateral force and yaw moment are reduced compared to a true bottom setup, with the difference growing more pronounced at shallower depths. The study also proposes and preliminarily tests countermeasures against this false bottom effect, using computational fluid dynamics (CFD) simulations to assess their effectiveness. This research provides valuable insights for accurate hydrodynamic force measurements in ship model testing, particularly in shallow water environments.

Delefortrie et al. (2023) provided an in-depth analysis of shallow water effects on ship manoeuvrability using experimental fluid dynamics (EFD), focusing on cases from SIMMAN 2020. The study utilizes historical test data and new trials to understand the behaviour of ships like KVLCC2 and KCS in shallow waters. A major finding is the significant impact of underkeel clearance on ship performance, particularly in manoeuvres like zigzag tests. This research enhances the understanding of ship dynamics in shallow waters, offering valuable insights for navigation and design in such conditions.

The studies reviewed highlight the multifaceted challenges of navigating in shallow, restricted, and confined waterways. From the impact of environmental factors like mud layers and bank effects to the design considerations such as propeller direction and barge configurations, these papers underscore the need for a comprehensive approach to maritime navigation safety and efficiency. As shipping continues to evolve, understanding these complexities becomes ever more critical for the sustainable and safe operation of vessels in such specialized conditions.

2.1.2 Deep and Unrestricted Waterways

Environmental effects

Lu et al. (2023) assessed the manoeuvrability of a 7m KVLCC model numerically and experimentally. The tests presented by the authors were conducted under field conditions, and some random factors of the field environment were not considered into the mathematical model. This approach amplifies the idea, that the impacts of wind, wave and current should be integrated into the modular model to describe motion responses of different ship manoeuvrings in real sailing situations.

Yasukawa et al. (2022) investigated the influence of slight initial disturbances made by environmental factors, which occur immediately after the start of the stopping test, on the stopping performance by propeller reverse rotation. The authors additionally discussed the standard for acceptable initial disturbances. It was concluded that initial disturbances on track reach (RT) are closely related to the course stability of the ship. It is suggested that for analysed bulk carrier in course-unstable loading condition the absolute non-dimensional value of the initial yaw rate should be minimized, and the non-dimensional value of the initial lateral velocity component should be maintained at −0.02 to 0.02. In course-stable loading condition even if those values were exceeded the error in RT was minimal.

Testing procedures

Park et al. (2021b) presented a new method for testing of towing operation stability (see Figure 1). The authors introduced forced oscillation device changing frequency and amplitude. As an example, tugboat -FPSO configuration has been tested and results of towing- and course-stability have been checked. The authors investigated the influence of the length, trim condition and speed of the tug-barge set on the reaction of the towed FPSO.

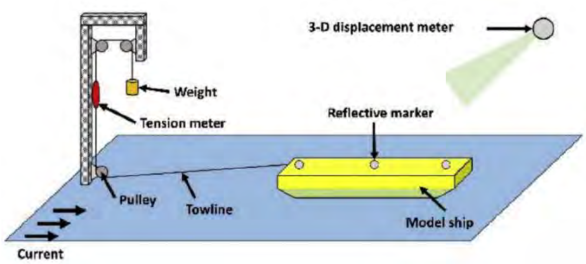

(a)

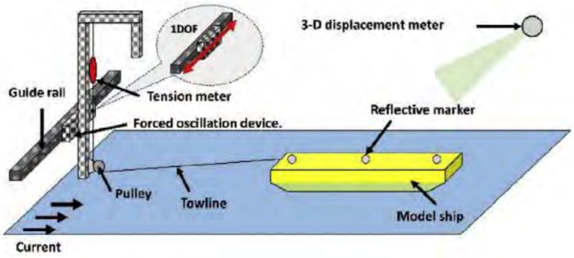

(b)

Figure 1. Conventional (a) vs. new (b) experimental method for towing testing.

Kitagawa et al. (2022) described a methodology for carrying out the free-running model tests with correction for skin friction between full scale and model scale. An Auxiliary Thruster System (ATS) was introduced to minimise the scale effect on rudder effectiveness induced by the propeller loading condition, measured results of ship motion and surface pressures. The authors calculated the skin friction correction as recommended by ITTC ’78 and used this value as the target thrust of the ATS, that consisted of an aerodynamic ducted fan, a loadcell and a PC for controlling the exact value.

Mathematical modelling

Kryvyi and Miyusov (2021) presented multivariate regression analysis of mathematical models of hydrodynamic forces and moments. The authors suggest a unified approach to the construction of models of hydrodynamic forces and moment, based on multivariate regression analysis, using Fisher's and Student's criteria.

Yasukawa et al. (2021) presented a new method for improving the formula for the longitudinal inflow velocity component to the rudder used in the MMG modelling method. The authors pointed out that the original MMG model is applicable to estimating the rudder force, including the hull-rudder interaction force component, when the absolute values of the hull drift angle are smaller than 45°. In the region where the absolute values of the hull drift are larger than 45°, the flow straightening factor is not constant, and the MMG model cannot be applied.

For improving the original formula for longitudinal inflow velocity component to the rudder, a new formula was proposed by the authors.

Ma et al. (2021a) presented research on uncertainty analysis of Planar Motion Mechanism PMM model tests. The authors performed randomness analysis, stationarity analysis, normality analysis, and statistical convergence of the acquired data to assess their quality. Additionally, the uncertainty analysis (UA) method for the PMM tests performed in the circulating water channel was also developed by the authors.

Sadati and Zeraatgar (2023) presented in their paper the tuning manoeuvre of the planning craft simulations carried out using 4+2DOF method in several operation modes such as semi-planning to semi-planning, planning to planning and planning to semi-planning. The hydrodynamic derivatives in the simulations were concluded from PMM tests in both the planning and semi-planning modes in a range of forward speeds.

Zhang et al. (2023) evaluated the manoeuvrability of a fast waterjet-propelled trimaran with three methods – CFD, EFD and MMG. The authors concluded that empirical hydrodynamic derivatives based MMG method produced the fastest results, but lacked accuracy in simulating a constant turning diameter, making it suitable for fast manoeuvring estimation and prediction during the design stage. Conversely, a direct force (moment)-based CFD model required more accurate input estimates to acquire acceptable simulated results. Meanwhile, a body force based CFD model considered more complex nonlinear impacts and was most similar to reality, achieving better agreement with the experimental results.

Nautical studies related manoeuvrability

Reichel (2021) presented the influence of propulsion-steering system on the position of pivot point on a large LNG carrier during standard manoeuvres. The author analysed two arrangements, i.e., twin-pod propulsion system and the conventional twin-propeller twin-rudder configuration. He pointed out that the pivot point for the same pod/rudder angles is much closer to midship for pod version than for ruder version.

Berg et al. (2021) presented manoeuvring analysis of a double-ended ferry based on CFD, PMM and full scale tests. An extremely important issue raised by the authors is that IMO standard manoeuvring tests are of little value for ship captains on double-ended ferries, and more data on low-speed manoeuvring is needed from safety of navigation point of view.

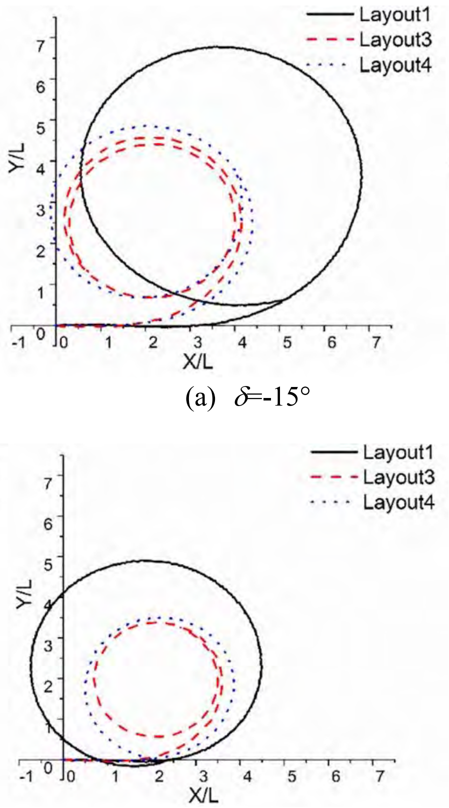

(a) δ=-15°

(b) δ=-25°

Figure 2. Turning trajectory with different layouts and rudder angles at F_r=0.353.

Jiang et al. (2022) investigated a self-propelled trimaran model powered by two waterjet impetus. The manoeuvrability of the trimaran is studied in self-propulsion navigation tests in a reservoir (open water). The turning and zig-zag manoeuvres with different layouts (i.e. side hull positions) and nozzle angles are carried out at various speeds. It is found that the position of the side hulls has an obvious influence on turning manoeuvres, as shown in Figure 2. A larger hull separation leads to a larger turning diameter. However, the effect of layout on zigzag manoeuvres is relatively weak.

Park et al. (2021a) investigated the course-keeping stability of a water-jet propelled planning boat through model- and full-scale experiments as well as model-scale CFD analysis. The results show that the flat and wide waterjet intake plane of the initially designed boat makes the course-keeping stability worse.

2.2 Numerical Simulations

2.2.1 Shallow, Restricted and Confined Waterways

The shallow, restricted and confined water definitions in the 28th Manoeuvring Committee are used in this report.

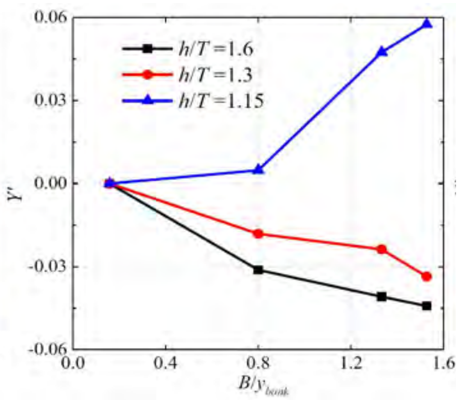

Figure 3. Non-dimensional sway force at different water depths for KCS at U = 0.73 m/s.

Liu et al. (2021) presented a CFD validation and analysis of ship-bank interaction for a model scale KRISO Container Ship (KCS) under extreme ship-bank distance conditions, water depth and ship speed. The predicted resistance and squat were compared with the model test data for depth to draft ratios of h/T = 1.3 and 1.6, and good agreement was achieved. However, the trim was over-predicted. It was found the sway force (Y') changes from attraction to repulsion force with an increase in the water depth, as seen from Figure 3. The magnitude of these parameters increases with a decrease in ship-bank distance (y_{bank}). Comparison of the results with and without free-surface modelling also indicated that the wave action is a key factor significantly influencing the hydrodynamic characteristic of the ship-bank interaction.

Delefortrie et al. (2022b) developed a mathematical model to predict the force and moment on a rudder behind the propeller of KCS applicable to the ship manoeuvring in shallow and confined water. The coefficients of the mathematical model for the rudder force and moment were driven from the captive model tests conducted at Flanders Hydraulics Research. The tests were performed in full four quadrant conditions and for a full drift and yaw range a ship may experience in a harbour. The predicted rudder force was compared against measurement for all captive test conditions and good agreement was achieved, as presented in Table 1. Enhancement in rudder torque prediction was recommended. The predicted rudder forces were also compared with the force measurement of a free-running model test and good agreement was found with slight discrepancy for the lateral force, as demonstrated in Figure 4.

Table 1. Comparison between measured and modelled rudder force.

Ukc (%)	Longitudinal force (N)	Lateral force (N)
100	$F_{X,mod} = 0.9485F_{X,meas} - 0.0217$ $R^2 = 0.9416$	$F_{Y,mod} = 0.9562F_{Y,meas} + 0.0171$ $R^2 = 0.9509$
50	$F_{X,mod} = 0.9340F_{X,meas} - 0.0372$ $R^2 = 0.9148$	$F_{Y,mod} = 0.9477F_{Y,meas} + 0.0022$ $R^2 = 0.9454$
20	$F_{X,mod} = 0.9430F_{X,meas} - 0.0288$ $R^2 = 0.9338$	$F_{Y,mod} = 0.9422F_{Y,meas} - 0.0097$ $R^2 = 0.9427$
10	$F_{X,mod} = 0.9066F_{X,meas} - 0.0421$ $R^2 = 0.9112$	$F_{Y,mod} = 0.9028F_{Y,meas} + 0.006$ $R^2 = 0.9127$

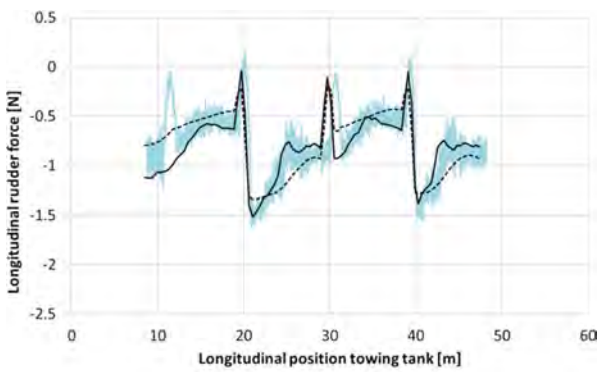

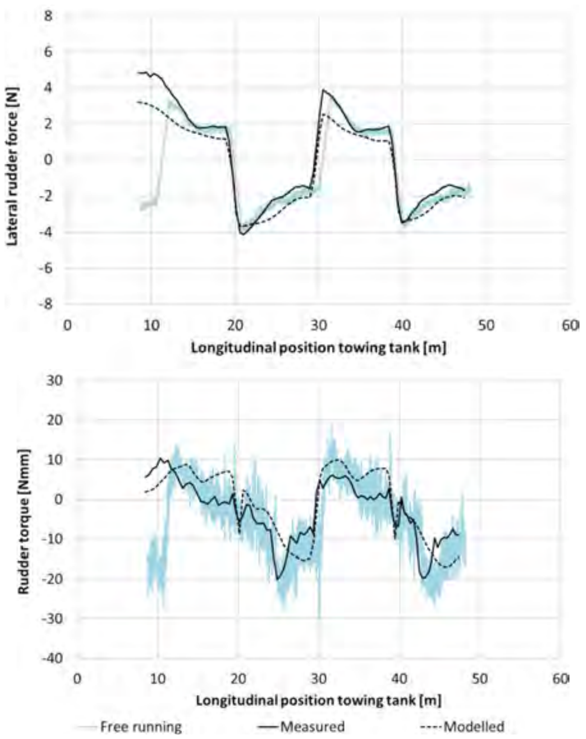

Figure 4. Comparison between modelled and measured rudder forces in a − 20/5 free-running tests, 50% under keel clearance (UKC).

The 6th International Conference on Ship Manoeuvring in Shallow and Confined Water (MASHON) was held in Glasgow, UK in 2022 and research in several shallow and confined water subjects was presented, as summarized below.

Most of the studies presented in the 6th MASHCON are based on CFD simulations. Zheng et al. (2022b) used STAR-CCM+ to investigate the unsteady hydrodynamic interaction of KCS parallel passing a moored Neo-Panamax container ship in port as a MASHCON benchmark case. The relative motions between the two ships were modelled with a dynamic overset mesh technique. For a UKC of 10%, similar trends between the CFD prediction and model test data were reported for hydrodynamic quantities and flow field details with some discrepancies at the early and late passing stages. Closer agreement between the two studies was found for a larger UKC of 50%. Yu et al. (2022) also performed viscous flow simulations of KCS passing Aframax tanker in shallow and confined water using an in-house CFD code. The spatial and temporal sensitivity analysis of the numerical approach for the stand-alone KCS showed convergence of the predicted heave and pitch motions to less than 5% relative difference to the model test. The predicted forces, motions and wave elevations during passing exhibited the same trends as the measured quantities. Kwon and Yeon (2022) used CFD to predict the ship-ship hydrodynamic interactions in a confined waterway. An overset gridding method was employed for movement of the passing ship, a KCS container ship, while the model was fixed in heave and pitch. The predicted forces and moments on the moored ships, a Neo-Panamax containership and an Aframax tanker were consistent with the MASHON 2022 benchmark data. The calculated dynamic pressure field and free surface elevation in the vicinity of the ships were also analysed, and it sheds light on the ship-ship interaction problem. It was shown that the pressure field generated by the Bernoulli effect around the passing ship influenced the moored ship, while the effect of moored ship on the passing ship was subtle. Yang and Moctar (2022) performed CFD simulations with a PMM of a KCS at a range of water depths to examine the shallow water effects on added mass and its frequency dependence. It was found that the hydrodynamic forces become highly non-linear when increasing the motion amplitude in shallow water (h/T = 1.2 and 1.5), while the effect of the motion amplitude was negligible in deep water. Frequency dependency of the yaw added mass coefficients in shallow water was also observed. For the PMM tests in shallow waters, small motion amplitudes at low frequencies were recommended. Kim et al. (2022a) performed CFD analysis of KCS free running manoeuvring in shallow waters with h/T = 1.2 – 4. Comparison of the predicted manoeuvre at a selected condition with model test data was satisfactory. It was shown that the standard turning circle parameters increase as the water depth decreases, with predicted transfer and tactical diameter being more than twice for h/T = 1.2 than those at deep water conditions.

Potential flow method, empirical formulas and system identification based method were also used to tackle the issues occurs in confined waterways. Liu et al. (2022b) used a 3D potential flow solver, called MHydro which is based on the Rankine source panel method to model a KCS passing a Neo Panamax containership for water depth to draft of 1.5. Due to the unsteady nature of the problem, the code automatically re-meshed the entire computational domain. A three-time-level scheme was proposed in their study to investigate the contribution of the unsteady terms on the ship-ship hydrodynamic interaction. A satisfactory agreement between the prediction and model test data was obtained for the forces and wave elevations, while a great discrepancy was observed for the yaw moment. In addition, keeping the unsteady terms in the free surface conditions improved the prediction of unsteadiness in forces and waves for the most part of the passing. Liu et al. (2022c) also employed MHydro to simulate a ship entering a lock and showed the importance of the unsteadiness introduced by the free surface in predicting the hydrodynamic forces and waves in a lock. The potential flow method was also used by Lindberg and Vilmann (2022) to predict the hydrodynamic effects of ships in shallow and confined waters. The predicted squat and bank effects with this model for KCS and KVLCC2 operated in shallow water were compared against experiments and a satisfactory comparison was achieved. Miyauchi et al. (2021) developed a system-based mathematical model suitable for a berthing manoeuvre. System identification (SI) method was adopted for optimizing system parameters which reduced the amount of model tests compared to the captive model test approach. The results of the mathematical model based on the SI optimization approach showed a better agreement with the free running model test than the captive model approach.

Following the 2008 and 2014 workshops on the Verification and Validation of Ship Manoeuvring Simulation Methods, the SIMMAN 2020 workshop was held in 2023. The objective of these workshops is to assess the current simulation methods for ship manoeuvring, aid code development, establish best practices and guide industry. Two test cases including KVLCC2 and KCS were in shallow water ($h/T = 1.2$) condition. A summary of the selected papers on this topic is given below.

Sakamoto (2023) performed RANS validation and analysis for KCS under static drift and rudder configurations. The differences in hydrodynamic force prediction observed between false and true bottom condition indicated the importance of replicating the tank bottom in simulation for validation purpose. Hoydonck (2023) performed CFD simulations of KVLCC2 in shallow water under static drift and steady turn (Case 2.1) and predicted drag and lateral forces and yaw moment. A reasonably linear variation of the lateral force and yaw moment with the drift angle at low drift angle ($\beta \leq 6°$) was observed. The lateral force was higher for the wall resolved grid compared to the wall functions grid for $6° \leq \beta \leq 10°$. Pressure field around the hull in relation with the lateral force under the steady turn conditions was examined. Sensitivity of the predictions to the grid resolution was also investigated.

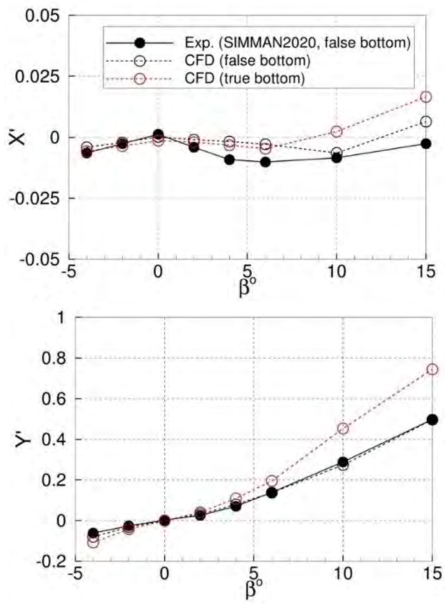

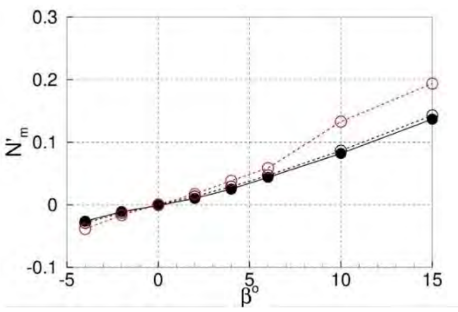

Figure 5. Experimental and computational results of surge force, sway force, and yaw moment acting on the KCS under static drift in shallow water (h/T = 1.2) with false bottom, the experimental data with true bottom.

False bottom problem, which has been highlighted in The 29th ITTC Manoeuvring Committee (2021) has been systematically studied by Sakamoto et al. (2023). An in-house viscous flow solver, NAGISA, was used to investigate the effect of a false bottom on a KCS model in shallow water (h/T = 1.2) under static drift and static rudder conditions. Figure 5 compares the predicted forces and yaw moment and model test under static drift conditions. The predicted loads with a false bottom correlate the measured quantities with an identical bottom configuration. However, the predicted hydrodynamic coefficients of the true bottom configuration deviate from those with the false bottom configuration at moderate to large drift angles. The study showed that even a gap size of 10% of the KCS length used for the false bottom was not sufficient to represent a true bottom. The forces and moments were not affected by the bottom configuration under the static rudder test. However, 7 – 10 % differences in the hull-rudder coefficients were observed between the results of the two bottom configurations. The authors extended this analysis to a pure yaw motion and found that the true bottom generated a smaller 1st harmonic amplitude of the total yaw moment than the false bottom. Significant differences were also observed for the linear hydrodynamic coefficients of the two bottom configurations. A local flow analysis provided insight into potential contributors to these differences. Asymmetric patterns of pressure distribution with respect to the centreline was observed on the tank bottom with a larger magnitude for the true bottom. Integration of bottom pressure quantifies the required mass for a false bottom unit, which can be helpful for design of a false bottom. Clear differences in the unsteady vortical structures during the yaw motion were also observed between the two tank bottoms, which could explain the discrepancies in the predicted hydrodynamic coefficients.

2.2.2 Deep and Unrestricted Waterways

Numerical simulations of ship manoeuvring in deep and unrestricted water typically involve solving the six-degree-of-freedom manoeuvring equation based on hydrodynamic coefficients. Chame and Tannuri (2023) adopted an open-source code OpenFOAM and conducted static drift tests on the model-scale bare hull of the KVLCC2. The predicted cross-flow drag coefficient and resistance force coefficient are all in good agreement with those from the literatures. The friction resistance coefficient showed a remarkable difference between model-scale and full-scale Reynolds numbers, as expected. The discrepancy between numerical and experimental of Y_v is 1.3% and 3.1% for model-scale and full-scale Reynolds numbers respectively. However, scale effects have a negligible effect on N_v.

Zhu and Kim (2023) adopted a CFD method to simulate the oblique towing test (OTT) and circular motion test (CMT) in deep water conditions. The simulated results show highly nonlinear behaviour at high rate of turns. In CFD numerical setups, more refined boundary meshes are required to capture the boundary flow.

Lu et al. (2022) proposed an integrated CFD and empirical manoeuvring model to predict the manoeuvrability of a twin-propeller twin-rudder (TPTR) inland vessels. This model was validated against free-running model test data of a 64TEU TPTR inland container. By comparing their simulation results to the experiments, it shows that applied CFD methods can help to increase the modelling accuracy, and the integrated manoeuvring model can roughly fit main characteristics of different motion parameters during manoeuvring motions.

There are more applications of CFD methods to directly simulate the self-propelled manoeuvring motions of ships. Propeller modelling is one of the key elements for analysis of hull-propeller-rudder interactions. Two major techniques, namely the direct or actual propeller (AP) method and the body force model, have been widely used by researchers in ship hydrodynamic community.

Oud and Toxopeus (2022) proposed a solution based on a single grid setup with consistent boundary conditions and incorporating a body force wake damping zone to accurate computation of hydrodynamic loads on ships during steady yaw manoeuvres. Their method could solve challenges when a ship encounters its own wake when rotating (see Figure 6), leading to an effective, fast, and accurate method to compute hydrodynamic loads of a ship in steady yaw manoeuvres.

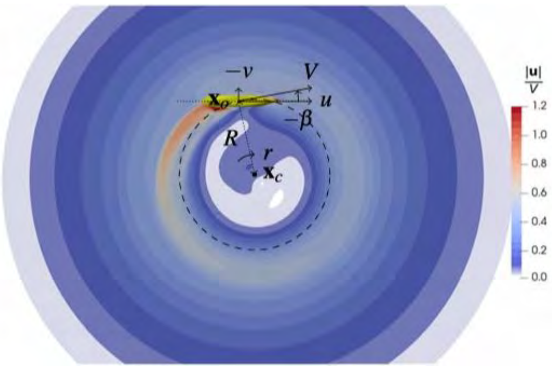

Figure 6. Velocity contours resulting from a steady computation of a rotational manoeuvre with drift in shallow water.

Aram and Mucha (2023) conducted turning circle simulation of the ONRT model with rudder angles of 25° and 35° and 20° zig-zag manoeuvre at F_r = 0.2. They utilized two distinct propeller models: a body force model rooted in open-water propeller testing and a discretized propeller model. The predicted manoeuvring characteristics were compared against the model test data. The actual propeller (AP) model showed a closer agreement to the experiments compared to the virtual disk (VD) model. Although all propeller models offered an excellent agreement to the model test for the time history of motions and velocities in the transient phase of the turning manoeuvre, the VD models deviated more from the experiment in the steady turn phase compared to the AP model, as shown in Figure 7. Their findings revealed that the absence of propeller side force in the body force model contributes significantly to its inferior accuracy when compared to the discretized propeller model. However, AP model is about 36 times more expense than VD model in terms of computational cost.

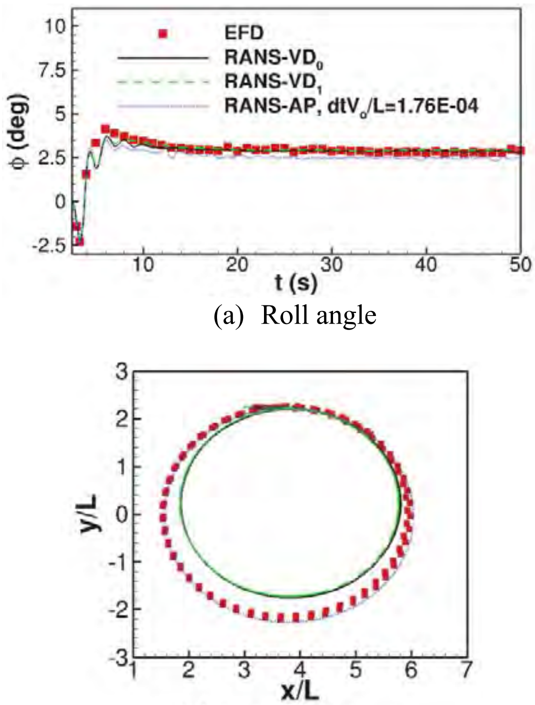

(a) Roll angle

(b) Trajectory

Figure 7. Time history of ship manoeuvring characteristics in port turn with 25° rudder angle.

It is important to note that recently there are more studies focusing on the application of intelligent methods, such as Neural Network, to predict the hydrodynamic characteristics. Support vector machine (SVM) based on a grey box model is one of the most commonly used methods. Based on the MMG model, Mei and Shi

(2023) proposed a 4-DOF grey-box model to predict ship manoeuvring motions. The results show that the fidelity of the model is high when the disturbance level is low and decreases with the increase of the disturbance level. Compared with black-box model, the grey-box model can reflect the physics of ship manoeuvring motions, and it is convenient to observe the changes of specific parameters under different disturbances. It should be noted that this grey-box model only involves one-time identification modelling. It cannot be applied to real-time modelling of ship motion when ship parameters are subject to change, for instance, under different loading conditions.

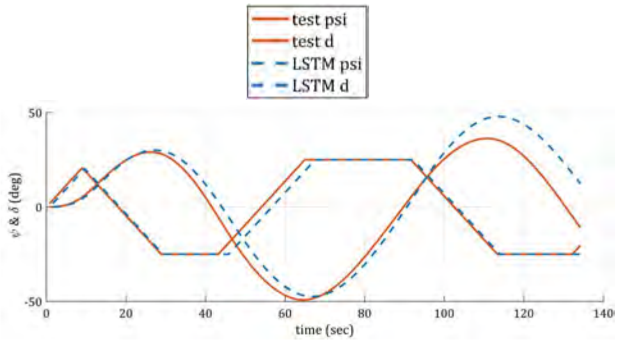

Figure 8. Predicted result of 10°/5° zig-zag test using LSTM deep neural network.

Another widely used method is the neural network method. Jiang et al. (2022) proposed a novel system identification scheme based on long–short-term-memory (LSTM) deep neural network to obtain the multi-input multi-output (MIMO) model of ship manoeuvre motions. As shown in Figure 8, the comparison between the simulated and predicted results demonstrates that the LSTM neural network is capable of identifying the mathematical model of ship manoeuvring motion. In particular, the robustness to noise of the LSTM model is validated by learning the model of manoeuvring motion using the training data artificially contaminated with Gauss white noise of different levels. The results show that the proposed identification modelling method has promising anti-noise performance. It should be noted only artificially contaminated data from the simulated manoeuvres are used to train the LSTM. For such data-based method, real data from model tests or even full-scale trials are urgently needed.

Jeon et al. (2022a) proposed a 4-DoF dynamics model to predict the manoeuvring motion of a warship in both intact and damaged conditions. The asymmetric manoeuvring characteristics of starboard and port turning motions under the damaged condition were successfully captured by their model, as shown in Figure 9. However, it is very challenging to address the simultaneous drifting phenomenon. Their method relies on captive model test results, and it cannot solve the multicollinearity caused by high correlation between motion variables. If there are no captive model test results, it is recommended to first estimate the hydrodynamic derivatives using empirical formulas and CFD simulations, and then perform system identification.

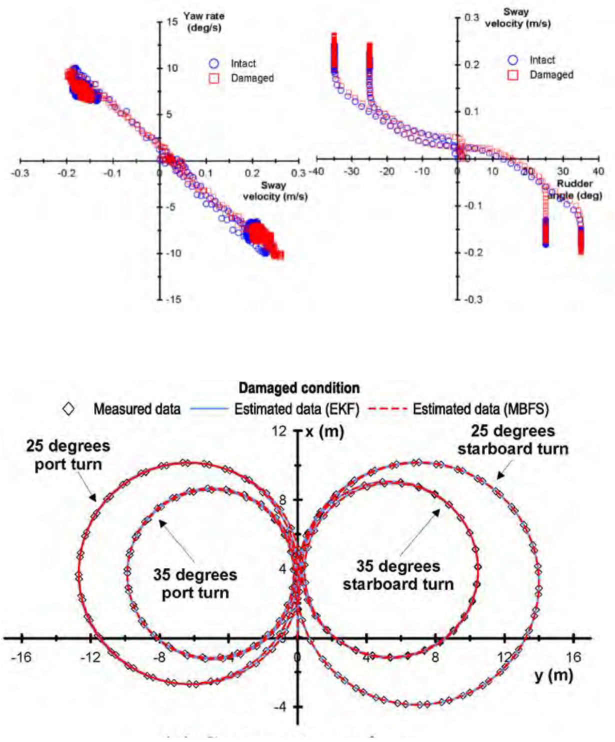

Figure 9. Measured and estimated trajectories of a warship under damaged conditions in a 25° turning motion.

Wakita et al. (2022) proposed a new system identification method to predict low-speed manoeuvres by using RNN and free running model tests. They compared two RNN models and found the prediction accuracy of the RNN that ignores the memory before a certain time was better than the "standard" RNN. To reduce the adverse effect of the noise included in the measurement data, a loss function was used, which has been proved to significantly improve the NN's prediction accuracy. It should be noted that the prediction accuracy of their method is strongly depended on the dataset, in particular the amount of data and types of manoeuvres in the data set. RNN is also used by Hao et al. (2022) to predict the ship manoeuvring motion of a KCS.

Based on full-scale trial data, Meng et al. (2022) developed a parameter identification scheme by using a Support Vector Regression (SVR) and a Modified Grey Wolf Optimizer (MGWO) to identify the response mathematical model and 4 DOF nonlinear whole-ship mathematical model of vessel YUKUN. Their prediction of ship motion state show that the MGWO algorithm has strong search and optimization ability. In the case that the reference values obtained by SVR are not accurate, MGWO algorithm can be used to identify accurate parameters of the mathematical model of ship manoeuvring motions.

Apart from CFD and data-based methods, mathematical models still play an important role in ship manoeuvring prediction. Barrera et al. (2021) developed a mathematical formulation to predict the actuation of vector tugs during docking, steering, and braking manoeuvres. The results show the proposed model can improve the realism of vector tug towing force prediction and positioning during maritime simulators manoeuvres. However, the model does not take into consideration of thruster-to-thruster interactions. As a result, it imposes an error of about 30% on the towing force prediction.

Daidola (2022) investigated the effects of hull roughness on ship manoeuvring characteristics. The hydrodynamic derivatives in ship manoeuvring motion equations are modified to incorporate roughness of the hull and rudder. By calculating turning motions of single screw cargo ships, it is found that the turning radius increases with time. After 25 years, the turning radius of a range of vessel sizes is in the range of 2.5–4.6% over which would be predicted for a smooth model,

Cura Hochbaum et al. (2022) proposed a mathematical model to predict the manoeuvrability of planning vessels in calm water considering all six degrees of freedom. All hydrodynamic coefficients of the used mathematical model were obtained from RANS simulations. A key advantage of their method is the ability to predict manoeuvres in vanishing CPU time once all coefficients have been determined. This allows for predicting new manoeuvres or easily repeat one with changed parameters, as well as to analyse the stability of chosen motion modes.

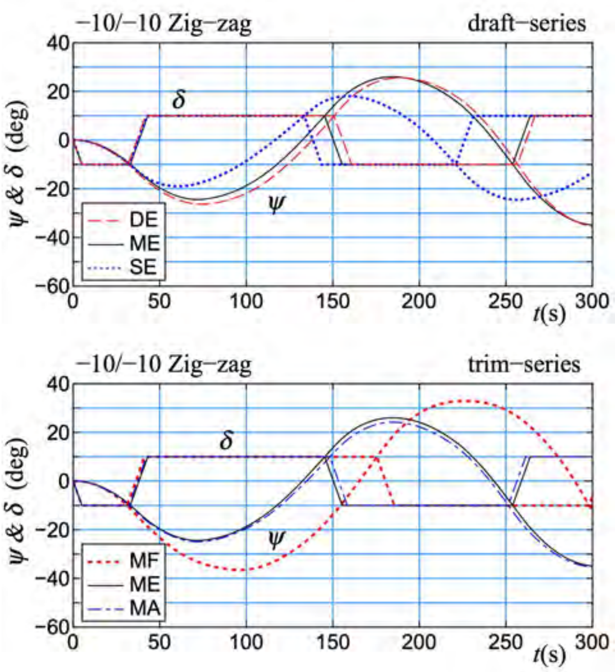

Figure 10. Time histories of ψ and δ in zig-zag manoeuvres under different loading conditions. ME: middle even; MF: middle fore-trim; MA: middle aft-trim; SE: shallow even; DE: deep even.

The MMG model is used by Yasukawa et al. (2023) to investigate how changes in the loading conditions affect ship manoeuvring. Five loading conditions with different displacements and trims were set in the vicinity of the full load condition for a container ship. It is found when the aft trim is attached to the ship, the course stability is improved, and the overshoot angle in the zig-zag manoeuvre is reduced. On the other hand, when the draft is deeper or when the bow trim is attached, the turning performance is improved, as shown in Figure 10, but the course stability deteriorates, and the overshoot angle often does not meet the IMO manoeuvrability criteria. It was concluded that the course stability of the container ship is significantly influenced by the loading condition.

3. BENCHMARK DATA

The main development in the field of benchmark data for manoeuvring prediction in the recent years has been connected to SIMMAN2020 concerning both captive and free running data in captive and free running mode in both calm deep water, calm shallow water and in waves. At the recent SIMMAN conference the focus was placed on the three hulls: KVLCC2, KCS and ONRT.

Besides SIMMAN, captive shallow water benchmark data have also been published for the 6th MASHCON, with focus on the effects of passing ships on moored ships.

3.1 SIMMAN2020

SIMMAN2020 was held in July 2023 in Seoul, South Korea, with the objective to obtain, assess and discuss the state of art in manoeuvring prediction techniques. The workshop was made as a follow up and continuation of the SIMMAN2014 and SIMMAN2008 workshops and like the past events, the purpose is still to benchmark the capabilities of manoeuvring prediction methods through comparisons with towing tank results.

Although the workshop was held in 2023, all submissions to the workshop were created in 2019 or earlier, with the latest submissions in January 2020. Due to the worldwide pandemic, the SIMMAN2020 workshop, which was planned for April 2020, was postponed to 2023. The delay turned out to influence the data analysis and the reporting and thereby changing the way in which the workshop was going to be organised. In 2021 the SIMMAN committee decided to issue the result as triple volume books, based on the results of SIMMAN2020 (Quadvlieg et al., 2023, 2024), instead of just a conference with presentations. Since all results were generated in 2019, the workshop was still called SIMMAN2020, as it reflects the state-of-the-art in 2020 and not in 2023. If submissions were allowed to be redone in 2023, due to increased insights, progresses in code development, increase of computer power, and increase of user experience, etc., the results might have been different.

The SIMMAN2020 test cases are a tanker, a container ship, and a surface combatant hull form like SIMMAN2008 and SIMMAN2014. The tanker and the container ships are still represented by the KVLCC2 tanker and the KCS container ship, whereas the 5415M surface combatant has been replaced by the ONR Tumble home (ONRT). The ONRT is a well-established surface combatant hull form like the 5415M and used in past CFD workshops and NATO-AVT. The KVLCC2 is kept as a reference ship due to the low Froude number and the high GM, which simplifies the problem as both the free surface and heel motion may be neglected. The KCS is kept as a reference ship because of the relatively strong heel-to-yaw coupling affecting the manoeuvring characteristics of the ship. The ship is tested at a very low GM (0.6m in full scale), which makes the ship a particularly interesting case when it comes to 4DOF motions. The ONR Tumblehome model 5613 (ONRT) is a preliminary design of a modern surface combatant and was introduced instead of 5415M to include new test cases for the participants. The benchmark data sets of the ONRT are all new model tests and includes both captive tests and free running model tests (FRMT).

For both the KCS and the ONRT the FRMT tests were carried out in calm water as well as regular waves. The full overview of all test cases in seen in Table 2.

Table 2 Overview of test cases.

		Case 1 KVLCC2-deep	**Case 2 KVLCC2-shallow**	**Case 3 KCS-deep**	**Case 4 KCS-shallow**	**Case 5 ONRT**
		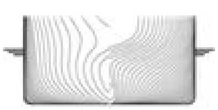	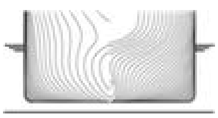	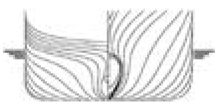	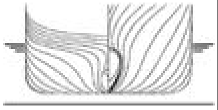	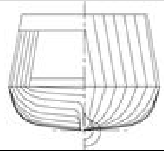
Calm water	Captive forces and moments	Case 1-1 1-1-1: pure drift 1-1-2: drift with yaw EXP by HMRI	Case 2-1 2-1-1: pure drift 2-1-2: yaw with drift EXP by BSHC	Case 3-1 3-1-1: pure drift 3-1-2: drift with yaw EXP by JMU	Case 4-1 4-1-1: pure drift 4-1-2: yaw with drift EXP by KRISO	Case 5-1 5-1-1: pure drift EXP by SNU
Calm water	Trajecto-ries	Case 1-2 1-2-2: 20/20 ZZ (SB) 1-2-3: 35 TC (PS) EXP by MARIN	Case 2-2 2-2-2: 20/5 ZZ (PS) 2-2-3: 35 TC (PS) EXP by FHR/MARIN	Case 3-2 3-2-2: 20/20 ZZ (PS) 3-2-3: 10/10 ZZ (PS) 3-2-4: 35 TC (PS) 3-2-5: 20/20 ZZ (SB) EXP by MARIN	Case 4-2 4-2-2: 20/5 ZZ (PS) 4-2-3: 35 TC (PS) EXP by MARIN	Case 5-2 5-2-2: 20/20 ZZ (SB) 5-2-3: 35 TC (PS) EXP by IIHR
Waves	Trajecto-ries			Case 3-3 3-3-1: 35 TC (SB) calm w 3-3-2: 35 TC (SB) waves EXP by HU		Case 5-3 5-3-2: 35 TC (PS) waves EXP by IIHR

SIMMAN2020 worked on two paths similar to SIMMAN2014:

- Captive forces and moments, where the focus is prediction of forces and moments for selected and well-defined cases using the force reconstruction method.

- Trajectories, where focus is prediction of trajectories of well-defined manoeuvres, which also includes turning circles in regular waves.

Based on the experience from SIMMAN2014 the following changes were introduced for SIMMAN2020 compared to SIMMAN2014 (and SIMMAN2008).

SIMMAN2020 used the force reconstruction as a measure for the quality of force and moment predictions. I.e. the submissions by the participant were not compared to individual tested point, but to an entire set of captive tests, which allows to make a simplified mathematical model. Previous SIMMAN workshops focused on a very selected point (such as only 1 drift angle), but the capabilities for predicting forces and moments have improved so much since the first SIMMAN workshop, that a range of drift angles and yaw rates are easily prescribed, which allowed for this different approach compared to previous workshops. The methodology to make this comparison was designed and made prior to the SIMMAN2020 workshop. The cases for the forces and moments were simplified as much as possible (only drift angles and yaw rate, no rudder angles, no RPM changes) to prevent misunderstandings and limit the uncertainties from the benchmark test cases. The total number of cases was minimized to increase the number of submissions per test case, i.e. only deep water and h/T = 1.2 was included, without considering intermediate water depths. A second measure to increase the number of submissions per test case was to apply a staircase approach for the test cases. It was only possible to make a submission for the complicated case if a submission is also made for the simple case. The comparisons for the free running model tests were partly blind in the sense that the FRMT data in calm water that was re-measured after SIMMAN2014 along with the data in waves was not provided to the participants prior to the workshop.

3.1.1 Prediction of forces and moments

Forces and moments are submitted for specific combinations of drift angle β and non-dimensional rotational velocity r'. All cases are defined with a rudder angle of zero. This means that the submissions are insufficient so make a simulation model, but the data is enough to make a decent fit of the hull forces with the rudder at zero. Three of the four cases have an acting propeller (case 1-1, 2-1 and 4-1), and one case is without propeller (case 3-1).

To make a base model for the comparison, a set of experiments was used, as obtained from one of the model basins around the world. Through these experimental points, a mathematical model is fitted. This model has the following shape for all cases:

$$X' = X'_0 \cdot u'|u'| + X'_{vv} \cdot v'^2 + X'_{vvvv} \cdot v'^4 + X'_{rr} \cdot r'^2 + X'_{vr} \cdot v'r'$$

$$Y' = Y'_v \cdot v' + Y'_{v|v|} \cdot v'|v'| + Y'_r \cdot r' + Y'_{r|r|} \cdot r'|r'| + Y'_{vvr} \cdot v'^2 r' + Y'_{vrr} \cdot v' r'^2$$

$$K' = K'_v \cdot v' + K'_{v|v|} \cdot v'|v'| + K'_r \cdot r' + K'_{r|r|} \cdot r'|r'| + K'_{vvr} \cdot v'^2 r' + K'_{vrr} \cdot v' r'^2$$

$$N' = N'_v \cdot v' + N'_{v|v|} \cdot v'|v'| + N'_r \cdot r' + N'_{r|r|} \cdot r'|r'| + N'_{vvr} \cdot v'^2 r' + N'_{vrr} \cdot v' r'^2$$

The values of these coefficients X'_0 through N'_{vrr} were determined by a least squared method and the quality of the fit was determined by the R^2 method.

An example of a fit of the experimental value, together with the obtained values for the coefficients is shown in Figure 11. The figure shows:

- the individual experimental data points (blue dots).
- the fit through the data points as determined using the least square fitting (blue drawn line).
- the light blue shaded area around the line indicates the 2 x standard deviations above and below the line.
- the values of the coefficients that describe this fit.
- the value of R^2.
- the standard deviation between the fit and the points.

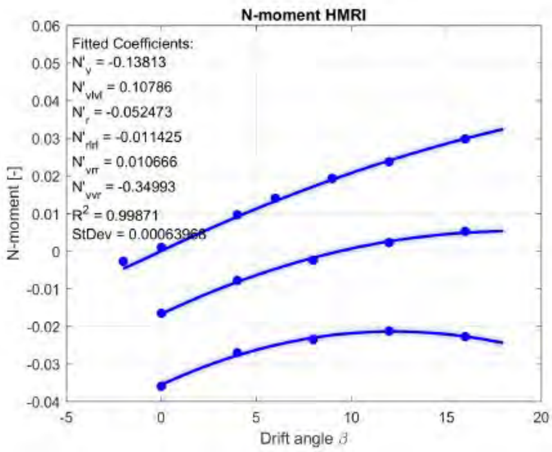

Figure 11. Uncertainty of the experiment in deep water with the KVLCC2.

Similar fit of the mathematical model was done for all the submissions. Just like for the experiments, it is possible to determine the R^2 for the fit of the submissions, which represents the quality of the fit.

The presently selected approach (the force reconstruction) is a new development engineered while performing the analysis for SIMMAN2020. The time needed to engineer the methodology was kindly provided by the delays caused by worldwide pandemic. The method is that:

– From the individual forces and moments for given drift angles and rotation rates a fit is created.
– This fit is compared against a fit from the experiments on a point-by-point basis.
– This is then summarised in a joint error per series.

For all cases, it was observed that the pure drift cases were well captured by the majority of CFD submissions, both in deep and shallow water. The average submission error $E\%D$ was 6.5% in deep water and 10.1% in shallow water. The submissions revealed a need for further improvements and investigations regarding rotation in especially shallow water, with an average error $E\%D$ of 16.2% in deep water and 26.2% in shallow water for combined yaw with drift or combined drift with yaw. For CFD submissions, it was unclear whether a distinction could be seen between free-to-heave-and-sink versus fully-captive, double body versus free surface, the choice of code, turbulence models, amount of grid cells, domain size and the different ways of modelling propellers.

Although the method of force reconstruction may be improved further, it is suggested in future work to gather experience with the present approach, as it appears to give a better overview of the capabilities than the approach used in the previous SIMMANs (2008 and 2014) which was based on individual data points. Furthermore, it is recommended to design one case for the next SIMMAN, which would focus on the prediction of flow separation during a manoeuvre, which can hopefully be compared to flow field data of separated flow. This might shed light on the recommended CFD settings to predict flow separation and hopefully achieve a better prediction accuracy for high drift angles and yaw rates. A much more thorough description of the validation approach and examination of the captive results is available in the final proceedings of SIMMAN2020 (Quadvlieg et al., 2024).

3.1.2 Prediction of trajectories in calm water and in waves

For the trajectory part of SIMMAN2020, it was chosen to compare data reduction and key characteristics, but not trajectories. For calm water manoeuvres in deep and shallow water, and for manoeuvres in waves, a set of key characteristics was defined and used. For all manoeuvres, it remains of interest to look at time traces of the velocities and the positions but to use the key characteristics to quantify the prediction errors.

Calm and deep water. For the calm water test cases, the focus on key characteristics and not the trajectories themselves proved to provide good insight into the capabilities to predict trajectories. The intention of the analysis was to obtain insight in:

1) A subgroup analysis, which resulted in the assessment of the capabilities of the different simulation methods also concerning the performance in deep water versus shallow water and calm water versus waves.
2) Status, quality, and suitability of the experiments.
3) Assessment of different hull forms.
4) Assessment of different manoeuvres.
5) Assessment of the data reduction and analysis procedures.
6) Assessment of effects CFD modelling: degrees of freedom, turbulence modelling, propeller models, free surface/double body flow, handling of wall functions etc.

In SIMMAN2014 the approach of considering the scatter in the results, alongside the prediction error, were introduced, i.e., the standard deviation σ of the submitted values S_i and errors in % of the mean value and experimental benchmark data D, respectively. The error averages $\bar{E}$ and standard deviations σ_E were also assessed using absolute value, which was found to provide a good assessment of prediction capability. Therefore, the same mind setting was continued in SIMMAN2020.

The error averages are interesting, as a small value of $\bar{E}$ indicates that the average of all submissions is close to the experiments. The spreading in the prediction error, which should also be small, is indicated by two variables in the SIMMAN2020 analysis: the standard deviation of all errors σ_E and the average of the absolute value of all errors $\overline{|E|}$. The advantage of the characteristic $\overline{|E|}$, is that it combines the average error and the standard deviation in one. $\overline{|E|} > \bar{E}$ will always apply, so the value of $\overline{|E|}$ will immediately reveal the quality of a (sub) group of predictions.

In SIMMAN2014 only the KVLCC2 had enough submissions to draw any conclusions, i.e. the KVLCC2 was selected to review the progress of the calm water manoeuvres between 2014 and 2020. The results of SIMMAN2008 were too scattered to make any clear error definition, and therefore these results are not included in the present review. To make a fair comparison to SIMMAN2014 (Quadvlieg et al., 2014), the values of advance AD and tactical diameter TD have been used, as well as the values for the first and second overshoot angle. The other derived characteristics are not considered, as they were not part of the analysis in 2014. The summary of the overall error for KVLCC2 from 2020 and 2014 is given in Table 3.

Table 3. Comparison of the prediction error for KVLCC2 in deep water.

	SIMMAN2020	SIMMAN2014
Zigzag error	16 %	27 %
Turning circle error	7 %	6 %
Overall	11 %	16 %

The comparison shows that the zigzag errors are reduced by about almost 40% (from 27% to 16%), whereas the turning circle errors are similar. I.e. overall, this shows that the average prediction error has reduced from 2014 to 2020 (based on the KVLCC2).

Looking at all the hulls for SIMMAN2020, the conclusions for the overall average were seen to be the same as for each hull form. The empirical methods have about 2 x larger $\overline{|E\%D|}$ and $\overline{\sigma_{|E\%D|}}$ than those from the whole ship models, modular mathematical models and CFD, where the latter three all have similar capability.

Calm and shallow water. For the KVLCC2 and the KCS, manoeuvres were asked in calm and shallow water at *h/T*=1.2 for four cases: a zigzag test and a 35 turning circle manoeuvre for the two ships. The average submission error $\overline{|E\%D|}$ and the standard deviation of the error $\overline{\sigma_{|E\%D|}}$ per method was evaluated by using a similar method in the deep and calm water test cases.

For the experimental reference data, the uncertainty $U_D\%D$ was seen to be more than twice larger than that in deep water. The prediction errors $\overline{|E\%D|}$ were seen to be nearly 4 times larger than those in deep water, and the standard deviation $\overline{\sigma_{|E\%D|}}$ more than 6 times larger.

The number of submissions for the shallow water test cases is much lower than that for the deep water cases (25 in shallow water versus 111 in deep water). The reduction of the amount of test cases in shallow water compared to SIMMAN2014 (from 42 to 4) led to more submissions per case, but still, the number of submissions were insufficient to make a meaningful subgroup analysis. Looking at trends though, the subgroup analysis for the shallow water cases was similar to those for the deep water cases: the empirical methods have about 2 x larger $\overline{|E\%D|}$ and $\overline{\sigma_{|E\%D|}}$ than those from the whole ship models, modular mathematical models and CFD, where the latter three all have similar capability. The number of submissions has increased from 2014 towards 2020, but given the criticality of manoeuvring in shallow water, this topic should deserve more attention.

Waves. Besides calm water test cases, new test cases in waves were introduced for SIMMAN2020.

Turning circles in regular waves were carried out with both the KCS and the ONRT. The turning circle manoeuvre was simulated for at least 3 full turns, i.e., the models turn at least 1080 degrees with regards to the original heading. The analysis of the prediction in waves was divided into three aspects:

1) The drift-away characteristics due to the 2nd order wave forces.

2) The impact of the wave on the manoeuvring characteristics: the rate of turn, drift angle and roll angle are depending on the wave heading direction and consequently, there is a variation in these parameters as function of the local angle wave heading.

3) The prediction of wave frequent motions (the 1st order motions) in surge, sway, heave, roll, pitch and yaw.

For each of the three aspects new key characteristics were derived.

The drift-away characteristics are evaluated based on the drift distance H_D and the drift direction μ_D.

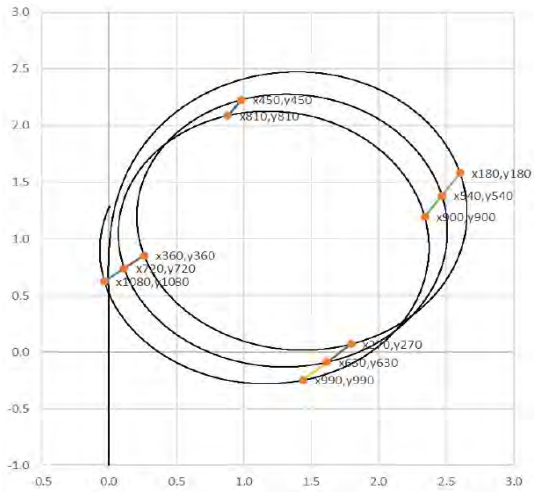

Figure 12. The drift-away characteristics.

The drift distance is calculated by the following two steps:

1) The drift distance of the individual points defined as the drift distance during 1 turn from 180° to 540°and up to 720° to 1080° (see Figure 12):

$$H_{D540-180} = \sqrt{(x_{540} - x_{180})^2 + (y_{540} - y_{180})^2}$$
$$\dots$$
$$H_{D1080-720} = \sqrt{(x_{1080} - x_{720})^2 + (y_{1080} - y_{720})^2}$$

2) The average drift distance H_D defined by:

$$H_D = average(H_{D540-180}, H_{D630-270}, H_{D720-360}, H_{D810-450}, H_{D900-540}, H_{D990-630}, H_{D1080-720})$$

The drift direction is calculated by the following two steps:

1) The drift direction of the individual points defined as the drift direction during 1 turn from 180° to 540°and up to 720° to 1080°:

$$\mu_{D540-180} = atan2(x_{540} - x_{180}, y_{540} - y_{180})$$
$$\dots$$
$$\mu_{D1080-720} = atan2(x_{1080} - x_{720}, y_{1080} - y_{720})$$

2) The average drift direction μ_D defined as:

$$\mu_D = average(\mu_{D540-180}, \mu_{D630-270}, \mu_{D720-360}, \mu_{D810-450}, \mu_{D900-540}, \mu_{D990-630}, \mu_{D1080-720})$$

In waves the speed of the ship will change depending on the wave direction. This is different from the calm water cases where the ship will turn with the same velocity at every sector of a steady turn. I.e. it is of interest to plot the speed, and other parameters to see the change of the values in each of the sectors as defined in Figure 13.

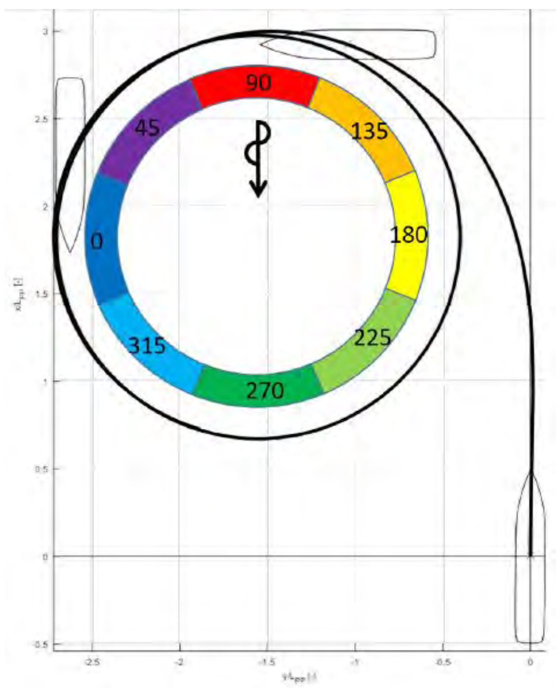

Figure 13. Sectors and colours used to describe the turning circles in waves.

The parameters of interest when evaluating the impact of the waves on the manoeuvring characteristics are the average speed loss V/V_0, the average non-dimensional rate of turn r', the average drift angle β, and the average roll angle ϕ and how they change in waves compared to the corresponding calm water values.

The average values are determined for every single sector of the circle, e.g.:

r'_{270}, $(V/V_0)_{270}$, β_{270} and μ_{270} are found by averaging between heading 247.5° and 292.5°, etc.

The change in waves is then found by averaging per sector per turn, i.e.:

$$r'_{w0} = \frac{average(r'_{180}, r'_{540}, r'_{900})}{r'_C}$$

Similar for r'_{w45} to r'_{w315}, with $w180$ representing head sea following the standard coordinate system of seakeeping. An example for the rate of turn is seen in Figure 14.

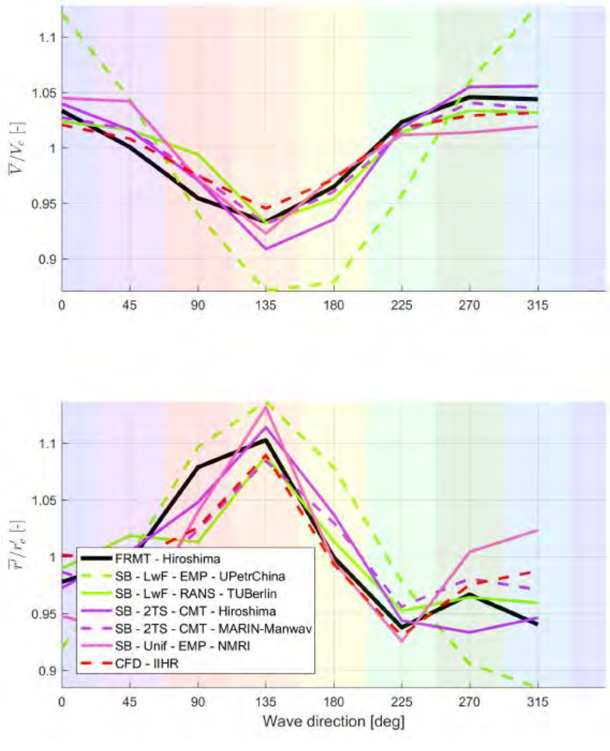

Figure 14. Example of change of rate in turn in waves.

The impact factor is then defined as the highest difference minus the lowest difference, e.g.:

$$\frac{r'_{w135} - r'_{w225}}{r'_C}$$

The same is repeated for V/V_0, β, and ϕ.

In addition to these values the turning ability in general were also analysed characterised by:

- Additional needed thrust, rpm_w/rpm_C
- Average nondimensional rate of turn (for 2 turns), r'_w
- Average speed loss, $\left(\frac{V}{V_0}\right)_w / \frac{V_C}{V_0}$
- Average drift angle, β_w/β_C

In the analysis of the wave frequent motions, only the heave, pitch and roll motion are analysed. Because the ship is moving in regular waves, and the speed is variable, the encounter frequency changes with the ship velocity and the instantaneous wave direction.

The analysis is therefore carried out for each sector in the turn (see Figure 13), by determining the standard deviation of the motion over the period in time where the wave direction is within each sector respectively.

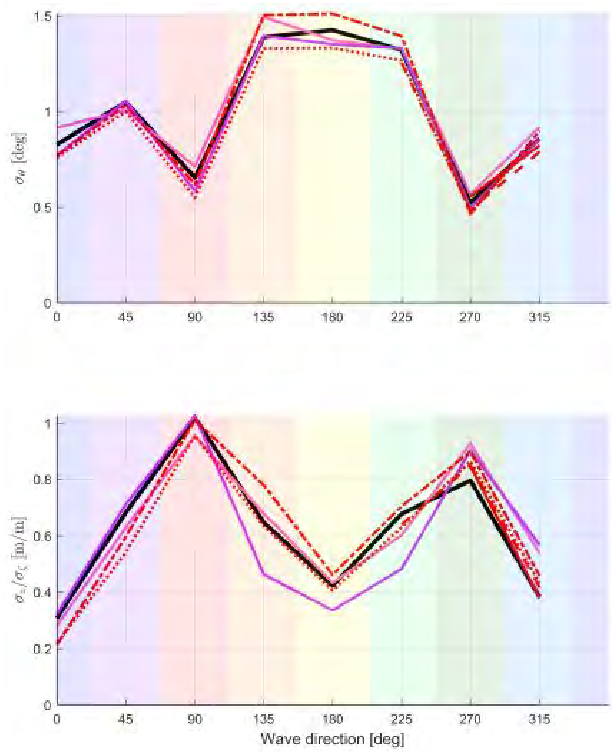

Figure 15. Example of the wave frequent motions per sector.

The values of the standard deviation of the heave motions will be divided by the standard deviation of the wave height σ_ζ, to obtain a non-dimensional value σ_z/σ_ζ. Besides the standard deviates for heave, roll and pitch, also the average heel angle $\bar{\phi}$ and the range of heel angles $\phi_{max} - \phi_{min}$ within each sector were evaluated for each wave sector. An example of the wave frequent motion parameters plotted against the heading of the waves are shown in Figure 15.

The results of the turning circles in waves are comparable to those for calm water in the sense that the number of submissions is similar to those of the other individual deep water trajectory test cases, and the U_D, $\overline{|E\%D|}$ and $\overline{\sigma_{|E\%D|}}$ values are like those for calm water. Thus, similar conclusions can be made concerning the uncertainties for waves vs. calm water manoeuvres, although the errors are somewhat larger, i.e., 17.5%D vs. 14.1%D respectively.

For code development, it would be good to have available insight in the forces on a ship while performing manoeuvring motions. For another ship, the SR108, such experiments were reported by Yasukawa and Faizul (2006). It is therefore recommended to the international community to perform similar experiments for KVLCC2, KCS or ONRT.

Considering the number of papers and global (academic) attention for manoeuvring in waves, the amount of 10 submissions at SIMMAN2020 is quite small and not in agreement with the general amount of academic attention.

The detailed evaluation of all the derived key parameters, the description of the validation approach and the examination of the trajectory results are available in the final proceedings of SIMMAN2020 (Quadvlieg et al., 2023).

3.1.3 Overall conclusions and recommendations

In general, a good progress was seen in the prediction capability. The predictions errors defined in 2020 were smaller than the prediction errors in 2014, though it was only properly statistically documented for the deep water cases.

The amount of test cases has decreased significantly from about 84 trajectory cases in SIMMAN2008, 66 cases in SIMMAN2014 to 14 trajectory cases in 2020. The decreasing of the amount of test cases in SIMMAN has led to more focus and sound conclusions.

A quantitative increase of submissions using time domain CFD simulations has increased throughout the years of SIMMAN, but still the present amount of free running CFD submissions is insufficient to give guidance regarding preferred turbulence models, wall functions, grid size, grid refinement techniques, etc. Future test cases ought to consider this aspect as well.

It is recommended to keep KVLCC2, KCS and ONRT. There is no need to change this as there are plenty of developments to be dealt with for these ships. Unless there is a ship for which full scale data will become available, it will be beneficial to stay with these three unrestricted ships. It is however recommended to include the propeller thrust and the rudder forces in the analysis.

The developments of analyses as initiated in this edition of SIMMAN are considered worthwhile to keep. The proposed key characteristics seem manageable and provide a good insight in the capabilities if the simulations. Likewise, it is recommended to keep the present error determination for captive forces for consistency and to gain experience with the method.

It is recommended to promote the research in shallow water. At the SIMMAN2020 workshop it was seen that less submissions were made for shallow water, and that both the experimental error and the prediction errors were larger than for the deep water cases.

3.2 UV, Inland Navigation, Model-Scale Vessels

Van Zwijnsvoorde et al. (2022) presented findings of a study that is part of the 6th MASHCON conference, focusing on port manoeuvres and passing ship effects on moored ships. These interactions are crucial as they involve large magnitude forces and long period excitations that can affect a ship's mooring system and potentially lead to unsafe situations.

The research is conducted under the PESCA (Passing Effects in Shallow and Confined Areas) project, where captive model tests were executed at FHR's towing tank for manoeuvres in confined waters in cooperation with UGent. The tests involved the KCS as the passing ship, and a Neo-Panamax container ship (C0P) and an Aframax tanker (T0Y) as moored ships. The Aframax tanker was moored in two configurations: along the tank wall (quay configuration) and connected to a measurement frame in the tank (jetty configuration), which represents open water mooring. This study provides data for understanding the dynamics of ship interaction in confined and shallow waters, particularly in high blockage areas. The results, scaled down to 1:80, offer valuable insights for the validation and verification of various research methodologies in this field.

4. AUTONOMOUS, NOVEL DEVICE AND CLEAN FUEL

Maritime autonomous surface ships (MASS) are a growing area of interest, with significant ongoing research and development. With high levels of autonomy, it can reduce operational costs, improve safety, and increase efficiency. Motivated by these advantages, many companies have incorporated artificial intelligence (AI) and autonomy technologies into their business operations and developed their first generation of MASS prototypes. The most widely known protypes include:

1) Yara Birkeland (see Figure 16 (a)) designed by Norwegian companies Yara and Kongsberg Maritime. It is an all-electric autonomous container ship, which was put into commercial operation in Porsgrunn in 2022.

2) Mayflower Autonomous Ship (see Figure 16 (b)), developed by ProMare with support from IBM. In 2022, it crossed the Atlantic Ocean from Plymouth UK, arrived in Plymouth, Massachusetts.

3) Soleil, developed by Nippon Foundation, Mitsubishi Shipbuilding, and Shin Nihonkai Ferry. This very large vehicle-carrying ferry (223 meters long) successfully completed an autonomous 240-kilometer return voyage from Fukuoka to the Iyonada sea.

4) USNS Apalachicola (EPF 13), developed by Austal. EPFs are designed to operate in shallow waterways and are capable of a wide range of activities. it has been delivered to US Navy in 2023 after several successful sea trials to assess its autonomous capabilities.

(a) Yara Birkeland

(b) Mayflower Autonomous Ship

Figure 16. MASS prototypes.

More MASS prototypes are under development. More importantly, the clean fuel technologies are integrated into autonomous ships. It is clear that the maritime shipping is heading towards autonomy and zero-emission era.

The published research papers on MASS also witness a significant increase over the past decade. Most of these works are focused on developing methods/algorithms for path planning/tracking that can reduce the risk of collisions, groundings, and stranding accidents at sea, as well as costs and time expenditure. Vagale et al. (2021a, 2021b) conducted a critical review of path planning and collision avoidance for autonomous surface vehicles. It was found that the artificial intelligence is an enabling technology for autonomous surface vehicles, with methods such as evolutionary algorithms, artificial potential fields, fast marching methods, and many others becoming increasingly popular for solving problems such as path planning and collision avoidance. However, there is no unified way to evaluate the performance of different algorithms. Real-world field tests are needed to evaluate the actual performance of the developed algorithms in various scenarios.

It is a very challenging issue to standardize the sea trial procedure for MASS. For traditional surface ships, the procedures for tank testing or sea trials are well established. The manoeuvrability of a ship, which is mainly determined by its hydrodynamic performance, can be evaluated and compared in a fair manner by conducting standard manoeuvring tests, regardless of ship types and sizes. However, when it refers to the MASS, its autonomous performance is not only determined by the ship's hydrodynamics, but also by its control system that consists of three main modules: Guidance, Navigation and Control (GNC). To evaluate the effectiveness of the control system, the testing of autonomous ships may need to be conducted in specific test areas with both land-based and on-board technological infrastructure that can be used for navigation, communication, and monitoring. Over the past decade, several countries, including UK, Norway, Finland, Belgium, and the USA, have developed specific testing areas for autonomous ships. There are also some existing guidelines for MASS trials, including IMO's Interim Guidelines for MASS (International Maritime Organization, 2019), the EU Operational Guidelines for Trials of (Trials of MASS, 2020) UK Industry Conduct Principles and Code of Practice for (Maritime UK, 2023) , etc. However, there are no standard tests proposed for autonomy, and types of tests between the sites may differ significantly. As pointed by Bellingmo et al. (2022), plans and results from autonomous tests are not unified and shared. It is hard to compare results from different tests. It is important to standardize and document autonomous tests to accelerate the technology and regulatory development.

As a ITTC technical committee, Manoeuvring Committee seeks to evaluate the importance of MASS trials and feasibility of conducting standard tests. Some key questions should be considered before recommendations are provided:

1) How will the existing procedures/guideline for conventional ships be used for MASS tests?
2) How to define the autonomy capacity/ ability?
3) What type of standard tests to evaluate each ability defined in 2)?
4) How to perform the tests?
5) What are the results to be documented from standard tests?
6) How can these testing results be served as inputs to develop the regulations by maritime authorities?

The autonomous shipping sector is still at an early stage. To answer the above questions, it requires to consult with different stakeholders, including maritime authorities, infrastructure owners, service providers, classification, clusters, and research and education stakeholders. This will be one of the terms of reference of the 31st ITTC.

4.1 Course Planning, Following and Tracking

This subject and its closely related topics, including berthing, formation control, and obstacle avoidance (as detailed in section 4.2), have seen a substantial volume of literature published over the last decade. Importantly, the quality of these articles varies considerably, with most of them lacking essential experimental validations. Notably, only the most significant contributions in the field are considered in this report. It should be emphasized that special consideration is deserved by the topic of AI assistant autonomy.

Course planning and path optimization are fundamental research topics in autonomous ship's navigation. Wu et al. (2021) proposed a multi-scale visibility graph method for long-voyage route planning of autonomous ships, addressing the issues of slow planning and poor route accuracy. The method involved extracting obstacle data from electronic charts, establishing multi-scale visibility graph models, and using a local planning window approach to reduce complexity and search time. The results showed that the proposed method could greatly reduce the complexity of visibility graph models and shorten the search time, improving the efficiency and accuracy of ship route planning.

Hinostroza et al. (2021) presented experimental results of the cooperative operation of two autonomous surface vehicles (ASVs) navigating in a complex marine environment. The ASVs were equipped with algorithms for motion planning, path-following, and motion control, and the experiments were conducted to validate the developed. Li et al. (2022) presented a dynamic path planning method for unmanned ships in a multi-object environment, integrating ship manoeuvrability, COLREGS, and good seamanship to ensure safe navigation. The proposed method utilized the multi-layer Morphin adaptive search tree algorithm to build an environment model, calculate collision avoidance ranges, and optimize the ship's trajectory. Through a case study and comparison with traditional artificial potential field models, the method demonstrated its applicability and potential in autonomous navigation for unmanned ships. Krell et al. (2022) presented a novel approach to path planning for ASVs using Particle Swarm Optimization (PSO) and Visibility Graphs. The goal was to generate energy-efficient routes based on water current forecasts and to incorporate reward-based planning to increase the scientific return of the mission. Ma et al. (2022b) presented a new coverage path planning algorithm for unmanned surface mapping vehicles (USMVs) to improve the efficiency and accuracy of underwater topographic mapping. The algorithm overcame the limitations of local optimization and incorporated task decomposition and map dynamic updating to achieve significant improvements in path length, number of turns, unit number, and coverage. The effectiveness of the algorithm was validated through simulations and mapping experiments. Zhang et al. (2022c) proposed a time-optimal path planning algorithm based on the MMG manoeuvring model and spatial reformulation of dynamic model. The path planning is implemented by Model Predictive Control (MPC). Extend Kalman Filter is used to minimise real-time disturbances.

Path Following and Trajectory Tracking are key performance criteria for ship manoeuvring Choe and Furukawa (2019) introduced an automatic track keeping algorithm consisting of a waypoint switching system and a rudder control system, as shown in Figure 17. The effectiveness of the algorithm was verified by the fact that the ship can closely follow the desired track under realistic environmental conditions.

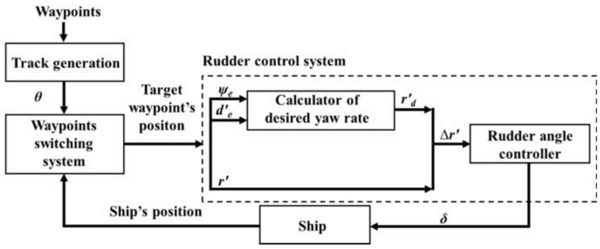

Figure 17. Block diagram of a track keeping algorithm.

Huang et al. (2021b) proposed an observer-based motion control system for an approach ship in a process of underway replenishment, addressing the challenge of maintaining a certain distance between the guide ship and the approach ship. The control strategy utilized a leader-follower approach, an extended state observer, and the command filter backstepping method to achieve trajectory tracking without velocity measurements. Simulation results demonstrated the effectiveness of the proposed method. Nie et al. (2021) presented a finite-time output feedback path following control strategy for underactuated marine surface vehicles (MSVs) with unknown velocity, dynamics, and external disturbances. The strategy utilized a finite-time extended state observer (FTESO) to accurately observe the unknown velocity and disturbances and constructed finite-time output feedback controllers to achieve precise path tracking performance. Simulation results demonstrated the effectiveness of the proposed strategy. Min and Zhang (2021) proposed a concise robust track-keeping control strategy for ships using a multi-technique improved LOS guidance system, which included a robust course-keeping controller and a nonlinear feedback technique. The strategy addressed the limitations of parameterized LOS guidance and enhanced the track-keeping effect through the introduction of three techniques. Simulation results demonstrated the superiority of the proposed strategy in both dynamic and static performance, making it significant for enhancing ship's autonomous navigation.

Zheng et al. (2022) proposed a soft actor-critic based control strategy for unmanned surface vessels (USVs) to achieve path tracking under wind and wave disturbances. The authors utilized a three-degree-of-freedom manipulative modelling group (MMG) model to represent the USV's dynamics and designed a linear active disturbance rejection controller (LADRC) combined with SAC algorithm for adaptive control (see Figure 18). The effectiveness of the proposed method was validated through simulation experiments.

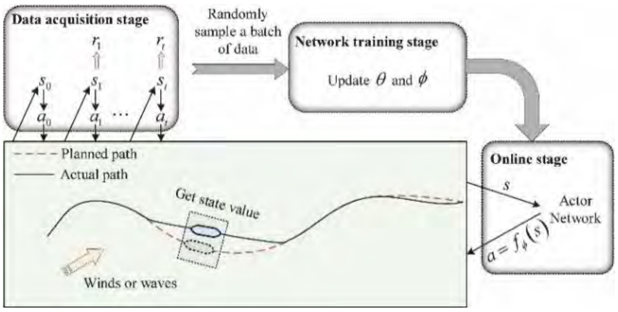

Figure 18. Schematic diagram of process of USV path tracking LADRC controller based on SAC optimization.

Qu et al. (2021) addressed the path-following control problem of USVs with unknown dynamics and unmeasured velocities. The main contributions of this work included the design of a finite-time velocity observer (FVO) to estimate velocities, the proposal of a heading-surge (HS) guidance scheme, and the use of a wavelet neural network (WNN) and adaptive techniques to accurately estimate unknown dynamics. Zhang et al. (2022b) proposed a novel robust adaptive fault-tolerant control algorithm for USVs using a multiplied event-triggered mechanism. The algorithm addressed challenges such as gain uncertainty, actuator faults, and limited communication resources, and was validated through simulations and physical experiments. Chen et al. (2021) introduced a new tracking controller for ship manoeuvring in shallow or confined water and compared it with an existing model-based tracking controller. The performance of the new controller was evaluated through simulation studies, demonstrating advantages such as improved speed control and reduced computational cost. Wang et al. (2022b) proposed an Antenna Mutation Beetle Swarm Predictive (AMBS-P) algorithm for path-following of underactuated cargo ships with unknown dynamics, using data gathered during operation to improve the model and path-following performance.

The path-following control of a ship by pushing using a single autonomous tugboat (see Figure 19) is studied by Choi (2023); Sawada et al. (2021a). The contact between the ship and tugboat is assumed to be a point contact, and the contact point does not slip. The simulation results show that the proposed control method causes the ship to follow the given straight-line paths correctly without slipping at the contact point.

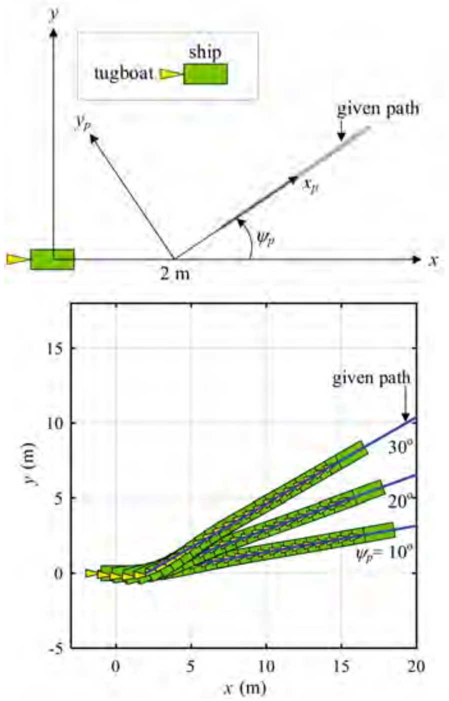

Figure 19. Simulation results of path-following of a ship pushed by a tugboat at different path angles.

Experimental tests were conducted by He et al. (2023) to validate their proposed model predictive controller (MPC) for surface ships' path following. It is concluded that the MPC could achieve a high tracking accuracy, smooth track transition, insensitive parameter setting and strong robustness in the presence of inherent model uncertainty, despite the simplifications made for practicality. Kim et al. (2023a) investigated the path following performance of a ship operating at low forward speeds in adverse weather conditions based on CFD modelling. It is found that increasing the propulsive power could achieve a better path following performance, while the impact of the propulsion power on path following in quartering waves is less important. Zhang et al. (2024a) proposed a manoeuvring model under waves for autonomous ships. Second-order wave loads are introduced to MMG model the simulate the manoeuvring operation with wave load and a turning motion of ship manoeuvring is validated compared with experimental test. Two control strategies were proposed to track the planned path with an MPC control algorithm.

4.2 Berthing, Formation Control and Obstacle Avoidance

Automatic Berthing is a crucial technical challenge that involves advanced technology in autonomous ship's manoeuvring.

Sawada et al. (2023) proposed the 2 DoF controller for automatic berthing under wind disturbances based on the path following control algorithm originally developed in Sawada et al. (2021a). The authors implemented this algorithm in a programmable logic controller (PLC) and conducted performance verification by installing it on an experimental ship (see Figure 20). After analysing the impact of wind disturbances on path following, the newly developed control algorithm for automatic berthing demonstrated high performance even under disturbances, as confirmed through validation on the experimental ship.

Figure 20. Experimental Ship "Shinpo".

Maki et al. (2021) proposed an automatic method to generate take-off and landing pier paths. Many merchant ships equipped with fixed-pitch propellers do not engage in manoeuvres that involve repeatedly reversing propeller during berthing operation. Therefore, the proposed algorithm limited the number of times of switching to once. An optimization was performed through covariance matrix adaption evolution strategy (CMA-ES). The proposed method enabled the acquisition of a more realistic take-off/landing path.

A novel ASV-centric Berthing assistance system (BAS) is proposed by Wang et al. (2024a) for the real-time calculation of navigable regions and idle berths during the berthing process. Applying a 3D-LiDAR, this method provides:

1) Localisation - estimating precise vessel position data through a simultaneous localisation and mapping algorithm with LiDAR and RTK data).

2) Details of navigable region - segmenting point clouds based on horizontal emission angles and identifies the nearest points within each segment. By employing a fitting algorithm, multiple lines are fitted, and those are selected to establish the berth line (Figure 21).

3) Idle berth information - determined based on the nearest point cloud passed by the fitted berth line.

4) Berthing state parameters (berthing distance, berthing speed, approaching angle and yaw rate)

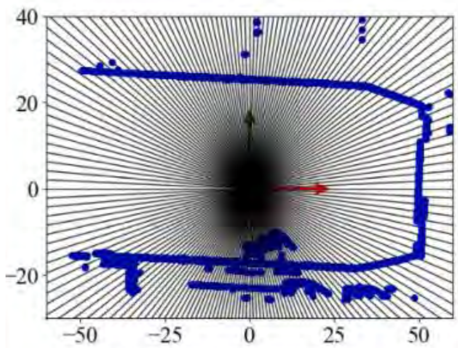

Figure 21. Point cloud segmentation map.

Formation Control is a significant challenge for technological development of autonomous ships, which requires complex manoeuvring operation.

Huang et al. (2021b) proposed a leader-follower motion control strategy to realize the synchronized control of two ships engaged in underway replenishment operation (UNREP). It was based on the command filtered adaptive backstepping approach combined with a novel extended-state observers to design the motion controller of the follower ship including model uncertainties and external disturbances with hydrodynamic interactions and effects of the highline cable. Simulations were performed on two scaled model ships to demonstrate the effectiveness of the proposed motion control strategy and the results showed the follower ship precisely tracks the desired trajectory and the relative positioning between the leader-follower ships were maintained near expectations, which guaranteed the safety of the UNREP operation.

Tan et al. (2021) proposed a hybrid behaviour-based (HB) method to achieve the coordination control of multiple USVs in the dynamic environment. Kalman filter algorithm is incorporated into the HB method to predict states of other ships based on their previous AIS information and to filter the signal noise. The objective of this paper was to achieve the rendezvous issue, formation keeping and obstacle avoidance for multiple USVs at the same time by considering the model uncertainty and the feature of the AIS broadcasting mechanism. Three numerical simulations were performed to validate the effectiveness of the HB method and results showed that the multiple USVs maintained a relatively stable formation while following the desired path sailing to the goal without colliding with each other, static obstacle or other moving ships.

Zhang et al. (2021a) also proposed a formation control system of USVs. This study employed event-triggered robust neural control, in which state variables and control inputs were updated when reaching certain threshold values. The proposed system is characterized by its capability to reduce the communication load between the controller and the actuator. The validity of the system was also demonstrated through extensive simulations considering disturbances (Figure 22).

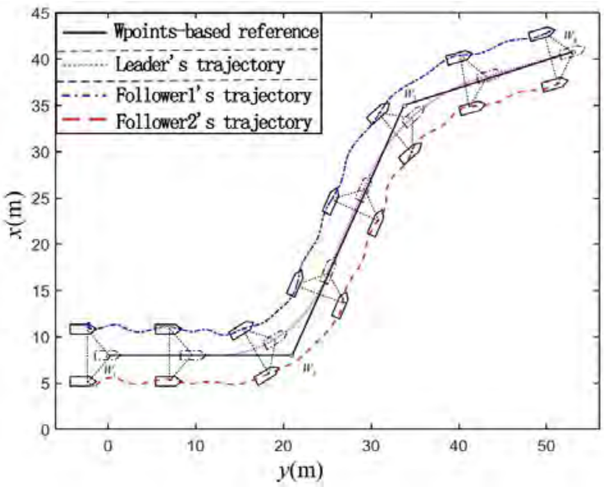

Figure 22. Comparison of the formation trajectory.

Obstacle Avoidance is key technology for ensuring the safety of autonomous ships. In collision avoidance manoeuvres, compliance with COLREG is a fundamental premise, but how to incorporate this into avoidance algorithm is a highly important aspect in the technological development of this field.

Hagen et al. (2023) proposed a method for representing the COLREG steering and sailing rules with concise mathematical expressions and conducting quantitative safety evaluations. Their findings may become crucial components in the development of this field.

Sawada et al. (2021b) proposed a method for the automatic collision avoidance based on deep reinforcement learning (DRL) approach. The proposed DRL was established by implementing a reward function, which considers efficient avoiding and the COLREG. Risk assessments were performed with setting the obstacle zone defined by speed and distance of own ship and other ships. The proposed method was successfully validated through the scenario sets of the Imazu problem.

Lyu et al. (2024) proposed a unique method applying environmental potential field modelling to express static obstacles combined with a dynamic obstacle modelling method for target ships considering COLREGs. The first-order Nomoto model was adopted to consider dynamic response of ships to input rudder angle in their simulations. Though frequent and unnecessary steerage and fluctuated trajectories are observed in simulation studies, it was shown that reasonable paths were obtained to avoid collision with static obstacles and target ships in various scenarios.

Wang et al. (2023) proposed a collision avoidance method for unmanned surface vehicles when navigating restricted waters. In global path planning phase, a genetic algorithm was applied to pursue the path series with the least energy consumption and the shortest distance, with the fitness function designed to favour the exploration of as straight a path as possible. In local path planning phase, obstacle avoidance was conducted using dynamic window approach applying a simplified COLREG. Simulations for several scenarios involving changes in velocity demonstrated that the proposed algorithm exhibited high performance. As another example of research considering COLREG and energy efficiency (Seo et al., 2023).

Wang et al. (2021a) proposed an improved genetic algorithm to solve the problem of multiple USVs collaborative collision avoidance. The authors prepared a multiple USVs model of motion and sensors, established encounter scenarios and formulated corresponding collision avoidance strategies (Figure 23) and calculated the motion parameters and risk of collision to determine whether to take avoidance measures. Furthermore, the authors designed simulation cases to verify the effectiveness of the proposed collision avoidance planning with and without communication. The results showed that the proposed method enabled to plan the current best path of collision avoidance for multiple USVs in complex environment and had good stability and smooth trajectories. Compared with the conventional genetic algorithm, the improved algorithm effectively reduced the number of iterations, running time, and standard deviation, and improved the success rate.

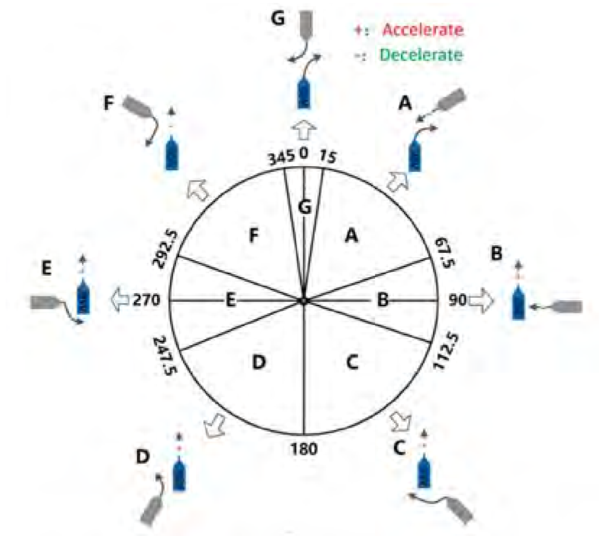

Figure 23. Schematic diagram of multiple USVs encounter scenarios.

Wang et al. (2021b) proposed a model to detect other vessels that might obstruct a ship's course. Considering scenarios involving multiple vessels, the authors combined a two-step approach: first, analysing the traffic situation and classifying cases based on relative motion, followed by inferring the operational intentions of the other vessels. The first step involves evaluating the traffic situation by multiplying the collision risk matrix and encounter situation matrix between each pair of vessels. The second step infers the intentions of each vessel from the traffic situation, incorporating fuzzy logic methods. The authors demonstrated the method by using real operational data.

Yuan et al. (2021) proposed a dynamic risk-informed collision awareness approach for real-time operating conditions to show the safe navigable space and the collision risk caused by current velocity, course, position of encountered obstacles. It was established by modifying NLVO method. The improved method called Uncertainty Non-Linear Velocity Obstacles (UNLVO) that enables to take the dynamic and uncertain characteristics of ship motion patterns into consideration and make real-time risk visualization. Simulations on multi-ship encounter scenarios were thoroughly conducted to validate the method. Compared with DCPA and TCPA, UNLVO provided more accurate predictions in expressing collision risk, and generated a uniform and acceptable risk evaluation.

Jia et al. (2023) proposed a RAGAN (Risk Aware Generative Adversarial Network) model to predict multi-ship's trajectories in encountering and avoiding situations. The trajectory prediction by RAGAN is derived from analysing encounter situations and collision risks among traffic ships based on AIS data and estimating the subsequent vessel behaviour. It is expected that RAGAN enhances situational awareness and provides valuable insights for decision-making in maritime operations.

Wang et al. (2024b) addressed the problem of automatically generating simulation scenarios to validate collision avoidance algorithms in ship navigation issues. In the generation process, real AIS data is incorporated, and the following steps are followed:

1) Analyse encounter situations after handling anomalies or missing data;
2) Evaluate importance based on both occurrence frequency and severity;
3) Generate simulation scenarios deemed important after excluding those with low severity;

Creating scenarios to validate collision avoidance algorithms is laborious, so this kind of studies is expected to be useful in the future.

4.3 Novel Device and Clean Fuel Technology

4.3.1 Novel Devices

Generation of greenhouse gases, CO2 and other toxic substances that are proven to contribute to the climate change, have been rising continuously in the last few decades. A 2010 report by the Office of the European Union indicated that the ship operations (Jaramillo, 2016) contribute to 3 – 5 % of CO2 emissions. Adverse effects of climate change on human and wildlife have urged international organizations to take actions towards reducing the emissions of the toxic gases. Among them is the International Maritime Organization (IMO), which has set requirements for ships contracted from 2013 to be 10% more efficient by 2015, 20% more efficient by 2020 and 30% more efficient from 2025. To meet this target, potential applicability of various methods such as energy saving devices and clean fuel technology have been investigated in the recent years. In this section, the effect of adapting some of the low emission technologies and novel devices on the ship manoeuvrability will be discussed.

Energy Saving Devices (ESDs). Stark et al. (2022) categorized the energy saving devices to five groups based on their locations on ships as shown in Figure 24: hull resistance reduction measures, propeller/hub modifications, propeller flow conditioning devices, renewable energy-assisted propulsion, and manoeuvring energy-saving devices.

Figure 24. Applicability of Energy Saving Devices based on their location on the vessel.

Hull Resistance Reduction Measures. The hull resistance could consume a significant percentage of fuel. Therefore, the hydrodynamic community has been examining various techniques to reduce the hull resistance. One of the methods for lowering the fuel consumption is to attach a fixed hydrofoil called Hull Vane (HV) below the waterline and to the transom of a vessel. HV was originally invented by Peter Van Oossanen in 1992, first patented in 2002 and has been widely investigated for various ship types with reported fuel reduction between 3 to 10% for merchant ships. Hou et al. (2020) generated the lift by the foil to reduces the pitching motion and consequently wave resistance, corrects trim, reduces the stern wake generation, and generates additional thrust. Despite potential benefits of HV on the fuel saving, it can cause adverse effects on manoeuvrability of ships. Full scale sea trials on a 55 m Fast Supply Intervention Vessel, Karina, retrofitted with a HV showed a reduction in engine power requirement by 15%. However, Uithof et al. (2014) indicated the manoeuvrability tests turning circle was slightly increased which was caused by an increase in the directional stability by the struts used to connect the HV to the hull.

Propeller/Hub Modifications. Energy saving of marine vessels can also be achieved through geometry modifications of the propeller and hub. Various methods have been investigated to improve propeller performance from the power requirement standpoint. Contracted and Loaded Tip (CLT) propeller is a novel propeller design, where the blade tip is modified to act as a winglet and reduce the interactions between flow on the pressure and suction side of the blade. A survey study by (Gennaro and Gonzalez-Adalid, 2012) on the CLT propeller application to 280 ships of different types indicated the following improvements: 5-8% higher efficiency which results in fuel savings, lower emissions and greater range, reduction in cavitation and tip vortex and consequently lower noise and vibrations, greater thrust and better manoeuvrability.

Hub modifications have shown to be an effective way to save energy, but direct effect of this modification on the ship manoeuvring performance has not been reported yet.

Propeller Flow Conditioning Devices (PFCDs). PFCDs are used slightly upstream of the propellers to adjust the propeller inflow with the purpose of improving the propeller performance. Several PFCDs have been examined and fuel saving between 5 to 12% have been reported. Among these devices is the pre-swirl duct, where Sasaki and Aono (1997) investigated and indicated 5% power savings based on the sea trials, as well as reduction in the hull vibrations and enhancement in the manoeuvring characteristics. In another effort, Kishimoto et al. (2016) performed a series of tank tests on a Japan Bulk Carrier (JBC) with two different model scales to examine the effect of a stern duct shown in Figure 25 on the propulsion efficiency. The study showed significant improvement in propulsion efficiency with no adverse effects on the manoeuvring performance.

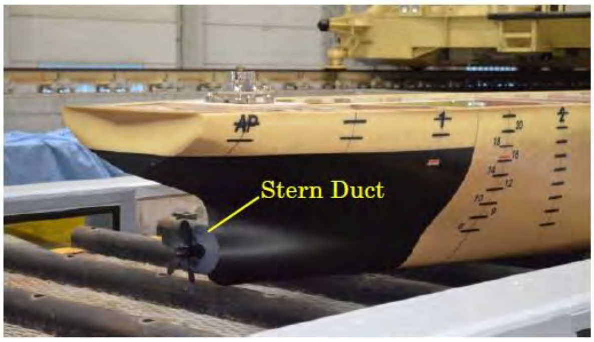

Figure 25. Stern duct on Japan Bulk Carrier.

Renewable Energy Assisted Propulsion. Clean energies such as wind and solar power have gained attention in the recent years as potential alternatives to the conventional energy sources. Despite significant advantage of these energy resources for reducing fuel consumption, their potential benefits for enhancing manoeuvring performance of marine vessels have not been reported in the public domain.

Manoeuvring Energy Saving Devices. The rudder not only serves as a steering and course keeping device, but also plays an important role in recovering the energy of the propeller wake. Therefore, proper design of rudders can reduce the power requirement for propulsion system. Three types of rudders including twisted rudder, gate rudder, and Hebel rudder are discussed in this section and each aims to reduce the energy expenditure.

1) Twisted Rudders

Rudders operate behind the slipstream of propellers and can experience large inflow angles varying along the rudder span. Large inflow angle typically causes the cavitation and consequently erosion of the rudder surface, which increases maintenance cost, rudder drag, lift in the case of massive flow separation on the suction side caused by cavitation, and introduces hull vibration and noise. The concept of twisted rudders based on rotation of rudder cross sections along the span was originally introduced by. Shen et al. (1997) and is aimed at elimination or reduction in rudder cavitation. Their experimental study in the U.S. Navy Large Cavitation Cannel (LCC) showed a wider cavitation inception envelope for the twisted rudder compared to the non-twisted rudder. However, the lift slopes of the twisted and non-twisted rudders were close, which indicates that the effectiveness of the turning manoeuvre is compatible between the two designs.

The X-Twisted rudder was originally designed by Hyundai Heavy Industries, where the leading edge of the rudder is continuously twisted along the span. Ahn et al. (2012) compared the hydrodynamic characteristics of an X-Twisted rudder (Figure 26) and a semi-balanced rudder. The manoeuvring model tests showed overall improvement in manoeuvrability of a TEU class container carrier with the X-Twisted rudder and in particular a well-balanced manoeuvre between the port and starboard.

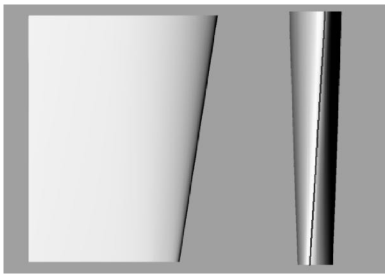

Figure 26. Drawing of X-Twisted rudder.

Calcagni et al. (2014) performed CFD comparative analysis of untwisted and twisted rudders on a single screw tanker operated at constant speed and at a range of rudder angles between 0 to 20 degrees. Computational results were also compared against experimental data. The predicted side force and yaw moment produced by untwisted and twisted rudders were comparable, which indicated that the manoeuvring performance of the ship was not affected by changing the rudder design. However, the twisted rudder reduced the suction pressure peak occurring on the rudder surface, and as a result, the cavitation was mitigated.

Sukas et al. (2021) examined the effect of a twisted rudder on the manoeuvring performance of a model scale Duisburg Test Case (DTC) hull. Both system-based and direct CFD methods were adopted in this study. Numerical results showed that the twisted rudder generated significant asymmetry in the flow, where the starboard turning with twisted rudder was close to turning with a normal rudder. Meanwhile, a significant reduction in steady turning diameter was reported for the port turn. Part of the reported asymmetry was caused by the rotational direction of the propeller. In general, the manoeuvring ability of the ship seemed better to port side than the starboard turning.

2) Gate Rudders

Figure 27. Gate rudder system of Shigenobu.

Figure 27 shows a gate rudder, where unlike the traditional designs, the two rudders are positioned astride of the propeller. The gate rudder was initially designed and patented by Kuribayashi in Japan in 2012. In 2020, Wartsila licensed the technology for marketing and development, by Sasaki et al. (2018). The European Union (EU) granted a team of researchers at the University of Strathclyde in 2020 under the Horizon 2020 Research and Innovation Framework Program to demonstrate the retrofit of the system for short sea shipping operations, explore the technology for oceangoing shipping operations, and evaluate it for fuel savings and manoeuvrability improvement of commercial ships.

One of the unique features of the gate rudder is its ability to act as a duct and increase the propeller thrust, which can remarkably reduce the energy consumptions and emissions of the ships particularly within coastal and port areas. The independent movement of the two rudders offers a more flexible steering and sideway movements compared to the conventional designs. The rudders can be retrofitted to the existing ships, as well as integrated to other fuel saving devices. Compared to the traditional rudder systems, gate rudders are in general quieter, reduce hull wake, and can reduce the propeller damage by the environment.

The gate rudder for the first time was tested on a 2400 GT container ship called “Shigenobu” in 2017 in Japan. Fukazawa et al. (2018) compared it to her sister ship “Sakura” equipped with the conventional rudders, a trial report indicated 14% energy savings with the gate rudder system in calm water. Sasaki et al. (2019) performed evaluation of two ships in rough weather in the northeast coast of Japan showed a higher reduction of 30% in fuel consumption with the gate rudder system.

The sudden or significant speed loss introduces a large turning rate and change in the ship direction, which poses adverse effects on the ship stability and safety of operation. Recent investigation on the turning capability showed that the gate rudder offers remarkably safe turning ability without excessive speed loss. The speed of a gate rudder ship at the same turning rate and the same tactical diameter is 20-30% greater than a ship with conventional rudder.

Joint sea trial of Sakura and Shigenobu conducted in following quartering wave and wind indicated that the gate rudder produced significant damping effect on the ship motions during their running period on the same track. The yawing and rolling amplitudes of Shigenobu were about half of Sakura14. The joint sea trial was also conducted for crabbing mode and pivot turn. By the combination of two rudder angles, 55° and 110°, Shigenobu proved a superiority in berthing using a pivot turn and a crabbing in the extremely narrow port.

3) Hebel Rudders

Dereszewski et al. (2021) presented a new type of rudder called Hebel rudder shown in Figure 28. The blade is divided into two parallel parts and the general idea is to use the accelerated flow between the blades to generate additional steering force.

Figure 28. Hebel rudder.

The Hebel rudder has been tested in full scale on a small trawler and the manoeuvring test results were compared with those carried out with standard NACA profile. The results showed much better turning ability of the tested trawler with the Hebel rudder than with a standard rudder, especially for small rudder deflections. However, the authors didn't mention the overall test conditions. Following the ITTC procedures, more tests may be required to draw a more general conclusion regarding the performance of the proposed rudder.

4.3.2 Clean Fuel Technology

Along with development of the energy saving devices, the shipping industry has been investigating the technology readiness level and potential adoption of the zero-emission technology such as ammonia, hydrogen, and batteries to reduce the production of greenhouse gases. One of the existing hurdles with clean fuel technology is the higher cost of its production compared to traditional fuel. Nuclear power is one of the zero-emission technologies. However, the significant cost required for preparing the infrastructure has made it less attractive for commercial shipping. Another challenge for transition to clean fuel is the dependence of the technology to the type of vessel, travel distance and cargo choice. For example, Sims et al. (2014) show that batteries are an environmentally friendly choice in cases powered by renewable energy sources such as wind or solar but it can only be employed for driving light vessels over a short distance. Green ammonia is another zero-emission technology with no carbon content but it can release NOx during the use which is highly toxic.

Green hydrogen, which can be produced from renewable energy sources such as wind, is one of the strongest candidates for the clean shipping in the future. One of the current challenges with this technology is the storage space requirement due to the low energy density, as well as higher production cost relative to traditional fuel. There are safety concerns with the fuel as well, since it is highly flammable and could be explosive, and difficult to detect leaks due to it being colourless and odourless. Despite existing challenges, a few projects have demonstrated the viability of hydrogen fuel propulsion systems for maritime application. Hydroville was the first passenger shuttle certified in 2017 to operate with hydrogen fuel on a hybrid hydrogen-diesel engine. The FLAGSHIP project was co-funded by the European Union (EU) is deploying two commercially operated hydrogen fuel cell vessels in 2023. The demo vessels include a new build in France (Zulu) and a retrofit in Netherland (FPS Waal). Zulu operates on compressed hydrogen produced from electrolysis. The propulsion system for FPS Waal consists of PEM fuel cells, battery packs, an electric motor and hydrogen storage with the total power ~ 1.2 MW. HyShip is another EU funded project which is in the process of building a cargo vessel for commercial operation equipped with liquid hydrogen, a 1 MWh battery pack and 3 MW proton exchange membrane fuel cells. With the EU support, DFDS, a Danish company plans to build a large ferry designed for 1,800 passengers in collaboration with external partners. The ferry named Europa (Europa Seaways) is powered by electricity from a hydrogen fuel cell, where the green hydrogen will be produced by a projected offshore wind energy-powered electrolyser plant.

The main limitation of fuel cells is an adverse effect of transient loads on their lifetime and performance. Unsteady loads occur in various conditions such as ship manoeuvring, propeller cavitation, and ship operation in strong winds and high sea states. Further investigation into the problem and pursuing potential solutions for propulsion system such as power management systems and combination of fuel cells with batteries are recommended. Despite growing investment in fuel cells, the impact of these technologies on ships' manoeuvrability is not well studied. The current studies are mainly focused on propulsion. One of the suggested topics for the future investigation would be to determine the minimum propulsion power requirement supplied by the clean fuels to maintain the manoeuvrability of ships in adverse conditions.

5. MANOEUVRING IN WAVES

5.1 Experimental

Free running model tests in waves. Free running model tests allow a more realistic simulation of a ship's behaviour in waves. The model is not constrained or artificially guided, enabling it to respond freely to wave-induced motions, providing insights into the actual performance of the ship in dynamic sea conditions. The results obtained from the free running model tests serve as valuable validation data for computer simulation models.

Stern et al. (2022) performed the experimental and the numerical turning circles test in waves. They found the physics of turning circles in waves can be best explained using inverse dynamics: wave induced motions (mainly, pitch and heave) result in oscillating X and Y forces (mainly, added resistance X_H/X_w, and side forces Y_H/Y_w), which produce the oscillating u, v, drift angle (hull vortices), and propeller and rudder loads; all of which combine as the time mean and unsteady responses, and wave drift direction and distance.

Suzuki et al. (2023) investigated the rudder effectiveness and the engine limits effects in short waves by conducting course-keeping manoeuvres in regular waves. Duct-fan-type auxiliary thruster was used to allow various rudder effective conditions. They found that the rudder effectiveness for the full-scale ship and (smaller) engine outputs increase the time-averaged values of the ship speed reduction and the drift angle from head to beam waves. This implies that the full-scale ship is more susceptible to waves than the model-scale ship. The difference in the rudder effectiveness affects the time-averaged rudder angle (i.e. check helm), although definite wavelength-independent trends are not observed.

Captive model tests in waves. Captive model tests in waves have been performed to investigate the forces and moment induced by waves. In case of static straight or oblique tests, in which the incident wave direction is fixed, both the first and the second order wave forces can be obtained by fitting and averaging.

Suzuki et al. (2023) investigated the effects of the steady wave force variations generated by oblique motions. Oblique tests in regular short waves with various combination of towing speed and drift angles were performed to measure the steady wave forces. They observed that the steady wave forces in short waves are affected by not only the ship advancing speed but also the oblique motion. The steady wave sway forces at a positive drift angle becomes smaller than those at zero drift angle, and the steady wave yaw moment increases in the negative direction when the drift angle increases under such wave conditions.

5.2 Numerical

Mean wave force methods. Oladele et al. (2023) developed an integrated time-domain seakeeping and manoeuvring model for the self-propelled ONR Tumblehome vessel in waves. Memory effects due to radiated waves and incident wave forces are incorporated into a 4DOF (surge/sway/yaw/roll) lumped-parameter model for manoeuvring in calm water to simulate the manoeuvring of the ship in waves. The proposed combined manoeuvring/ seakeeping model is validated against available experimental results on the self-propelled ONRT model using zigzag tests in head and following waves.

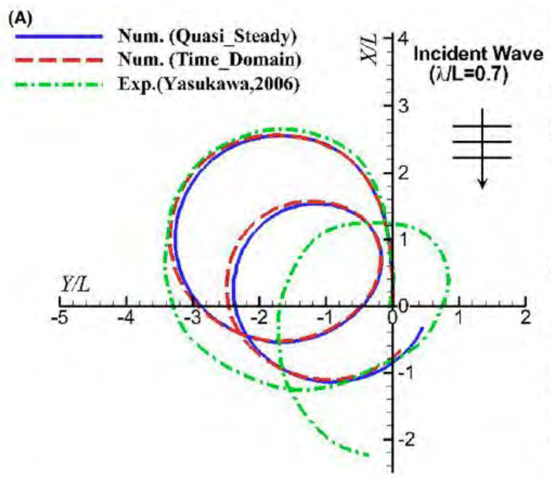

Figure 29. Results of the port side 35 turning manoeuvres of a S-175 model in regular waves of *l/L*=0.7, χ = 180°.

Zhang et al. (2022d) added wave drift loads obtained from the potential flow theory to the MMG model to account for the wave effects on ship manoeuvring. Two numerical methods were proposed to handle the coupled manoeuvring and seakeeping problem, a time domain approach and a quasi-steady method. A time-domain seakeeping computation was conducted that parallels to the manoeuvring simulation for the time domain approach. For the quasi-steady method, the wave drift loads were evaluated using a frequency domain method. The free turning of a S-175 container ship in regular waves were validated with experimental data. The results of the quasi-steady method and the time domain approach show good agreements (see Figure 29).

Two-time scale methods. Zhang et al. (2022a) proposed numerical simulation of ship manoeuvrability in irregular wave based on Taylor Expansion Boundary Element Method (TEBEM) with two-time scale model. The added resistance in wave was calculated first and followed by the free turning trajectory of KVLCC2 with different sea states. The comparison with available model test results shows good agreement (see Figure 30).

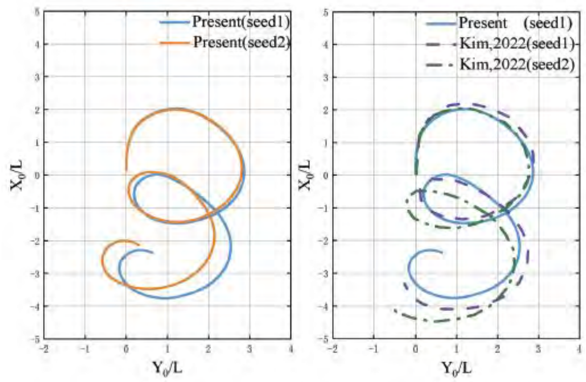

Figure 30. +35° turns with 5.54 RPS sea state 6.

Ma et al. (2022a) compared the two-time-scale method and the unified method on manoeuvrability in waves. The turning circle, heading angle and roll motion of a S-175 container ship in regular waves obtained from the two methods were compared with experiments. It was concluded that the two-time-scale method and the unified method can predict the ship turning circle and motions satisfactorily even though there are some differences between the simulated results and the experimental ones in short wavelength conditions.

TEMPEST is a time-domain potential-flow code developed at NSWCCD to predict the ship manoeuvring in waves using blended method as reported by Aram and Wundrow (2022). Manoeuvring forces due to linear circulatory lift are modelled by a low-aspect ratio wing theory and are parameterized by user supplied calm-water stability derivatives. Sectional coefficients account for nonlinear cross-flow drag induced manoeuvring forces. The TEMPEST results are validated against model data and high fidelity free-running simulations (Star-CCM+ setup with overset grids and actuator disk) for turning circle manoeuvres in calm water and regular waves for the ONRT. The rudder inflow condition calculated from captive double-body simulations does not accurately account for hull-propeller-rudder interactions, which apparently influences the prediction of manoeuvring characteristics by TEMPEST.

Hybrid numerical framework. White et al. (2022) proposed a hybrid numerical framework for simulation of ship manoeuvring in waves. A combination of CFD and a linear time-domain boundary element method, and a propeller-force model are developed for efficient computation of the total hydrodynamic forces. This approach is distinguished from previous two-time-scale approaches in that the manoeuvring forces are computed from a viscous DB RANS computation rather than a mathematical manoeuvring model. It demonstrates that the hybrid method offers an efficiency gain by at least a factor of 10 using a VOF method with free-surface capturing. The comparable accuracy and reduced computational expense highlight the hybrid method as an attractive option for prediction of ship manoeuvring performance in waves.

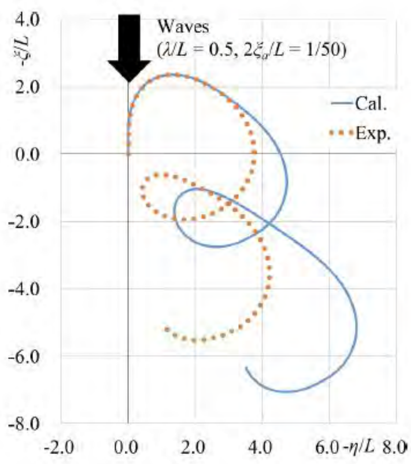

Figure 31. Comparison of 35° turning trajectories in regular waves for KVLCC1 ($\lambda/L = 0.5$, $2\zeta a/L = 1/50$).

Unified methods. Suzuki et al. (2021) proposed a modified unified method to directly solve 6-DOF ship motions, without separating the motions according to frequency. To validate the proposed method, free-running model tests for KVLCC1 and KCS hull have been conducted. Comparisons for the regular waves ($\lambda/L = 0.5$, $2\zeta a/L = 1/50$) for KVLCC1 show that the drifting directions of the estimated trajectories roughly agree with those of the FRMTs (Figure 31); however, the proposed mathematical model overestimates the drifting distance in wavelengths. The modified unified method can estimate the manoeuvring characteristics (e.g., mean ship speed, drift angle, and check helm) for course-keeping manoeuvres and turning trajectories, as well as 6-DOF ship motions induced by waves.

Paramesh and Suresh (2021) applied a unified seakeeping and manoeuvring model with a PID controller for path following of a KVLCC2 tanker in regular waves. The second order wave mean drift forces are calculated based on Salvesen's method and the wave exciting forces/moments and the restoring forces in the vertical planes are calculated for the exact wetted surface area. Through a set of pre-defined way-points using LOS algorithm, the largest cross track error of 0.78L is observed for port and starboard turn. This deviation is mainly due to the large drift force in sway and yaw when the ship is in oblique sea condition.

Yao et al. (2021) proposed the pure low-frequency and pure high-frequency ship motion equations in regular waves for ship manoeuvring prediction in waves. These motion equations, in which the inertia forces due to two coupled high-frequency motions were derived, were the modified versions of the traditional motion equations, e.g. the equations solved in the two-time scale methods. The predicted results based on the solution of the pure low-frequency ship motion equations reached a very high accuracy (see Figure 32).

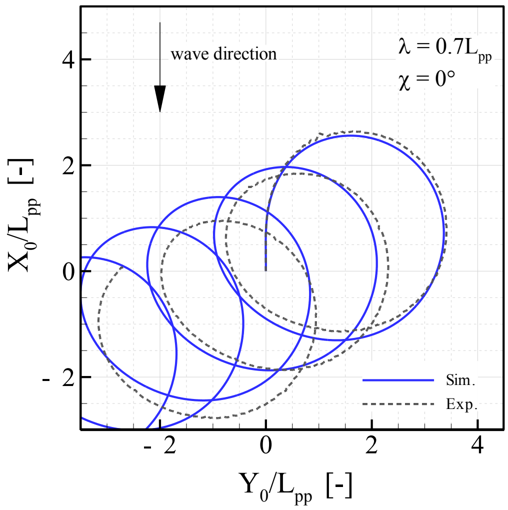

Figure 32. Comparison of the experimental turning trajectory with the precited one based on the solution of the pure low-frequency ship motion equations for S-175 in regular waves.

CFD based direct simulation methods. Ma et al. (2021b) performed the planar motion mechanism (PMM) tests on a containership S175 in regular waves systematically using CFD method for the first time. The hydrodynamic derivatives in waves of the target model are obtained by simulations in following waves or the surf-riding condition. The overset grid combined with Euler overlay method are useful and efficient. It is shown that wave effect on the hydrodynamic derivatives is significant.

5.3 Minimum Power Requirement

Overview. Since the introduction of the Energy Efficiency Design Index (EEDI), there was a concern that one of the most effective ways of reducing EEDI is simply by choosing a smaller main engine or main propulsion motor. However, it is required to keep sufficient propulsion power for operations in adverse weather conditions. At MEPC.232(65) (2013), Interim Guidelines for determining minimum propulsion power to maintain the manoeuvrability of ships in adverse conditions were developed to avoid construction of extremely under-powered ships. At MEPC 71/INF.28 (2017), it was agreed to extend the application period of the Interim Guidelines towards phase 2 of EEDI regulation. The application date of Phase 3 is approaching, and finalisation of the Guidelines was the urgent matter. At MEPC.1/Circ.850/Rev.3 (2021), amendments to Guidelines for determining minimum propulsion power to maintain the manoeuvrability of ships in adverse conditions were adopted. The amendments include changes to the definition of adverse weather conditions, new default values for thrust deduction factor and wake fraction, and two newly recommended semi-empirical methods for estimating the added resistance in waves in the new “minimum power assessment” method. MEPC 76 also agreed to further consider the concept of shaft/engine power limitation as measures to comply with both EEDI and minimum propulsion power requirements at MEPC 77.

Major amendments. The amendments are detailed in MEPC76/5/1 (2021). The major revisions include the following aspects:

1) Revised definition of adverse conditions (wave and wind conditions) which is now harsher, as seen from Table 4.

Table 4. Comparison of definition of adverse sea conditions.

	Existing	Revised
Wind speed [m/s]	15.7~19.0	19.0~22.6
Hs [m]	4.0~4.5	4.5~6.0

2) The “Simplified Assessment” method in 2013 Interim Guidelines is replaced by a new “Minimum Power Assessment” method, which examines the “maximum total resistance in the longitudinal ship direction over wind and wave directions from head to 30 degrees off-bow”.
3) The navigational speed of the ship for assessment is defined to 2 knots.
4) Default conservative estimates of the thrust deduction factor t and wake fraction w are changed to t = 0.1 and w = 0.15, respectively. This change of t will lead to significant change of the required thrust. And apparently, the resultant hull efficiency η_H will also change.

5) Several practical methods recommended for the prediction of added resistance in waves to facilitate the assessment.
6) Introduction of added rudder resistance due to manoeuvring in seaway.

With the amendments referring to higher sea states and lower ship speed, the added resistance in waves will practically dominate the prediction of the required power in adverse condition. Liu et al. (2022b) reviewed the revised Guidelines and found an inconsistency in the recommended methods for the added resistance prediction on typical tankers and bulk carriers. The proposed simple formula in the Guidelines is too simple, as it uses only the main ship particulars L, B and d in the calculation. Hence, for ships with the same main dimensions, but of different hull forms, the method will always lead to the same values and, it gives very low values for larger ship sizes. They also found that, due to the revision of the default thrust, deduction factor t, the required thrust has been decreased, which finally leads to a relaxed/reduced torque and power requirement.

Mao and Zhan (2022) developed a manoeuvring-seakeeping unified model of ship motions in waves to simulate the course-keeping manoeuvres of KVLCC2. The course-keeping ability in different wave directions with different autopilot parameters, as well as a MCR limit of engine, were discussed. The level-3 comprehensive assessment of minimum propulsion power (MPP) was compared with the level-1 and level-2 results according to MPP Guidelines. It was found that the level-2 simplified assessment is not enough to simulate the safe manoeuvrability of ships. The level-3 assessment by time-domain method should be adopted for the course-keeping ability simulation of ships in adverse conditions.

Sui et al. (2022) investigated the influence of propeller pitch and the PTO/PTI on ship propulsion and manoeuvring performance in adverse sea condition through simulation. The engine could more easily exceed the thermal loading limit at high propeller pitches and overspeed at low pitches. A shaft generator, PTO, will narrow the ship thrust/velocity envelope and reduce the operational safety at adverse weather condition. On the other hand, PTI extends the ship thrust envelope and results in better operational safety of both the engine and ship.

6. UNDERWATER VEHICHLES

6.1 Manoeuvring Hydrodynamics of UV

<u>Numerical Methods.</u> CFD tools have been widely used for self-propelled simulations of underwater vehicles' (UV) manoeuvring motion. There are a lot of works about a standard submarine model Joubert BB2. Carrica et al. (2021a) presented a study of a 10/10 vertical zigzag manoeuvre of the generic submarine Joubert BB2. Its manoeuvring characteristics, such as depth, pitch, pitch rate, vertical drift, vertical velocity, absolute velocity, and propeller thrust and torque coefficients were analysed at 6, 10 and 15 knots. The results show the overshoots in pitch and depth increase with the UV speed, and the velocity decreases rapidly, but the dimensionless pitch rate is only mildly affected. The average thrust and torque coefficients decrease as the speed increases, but the amplitude of the fluctuations increases.

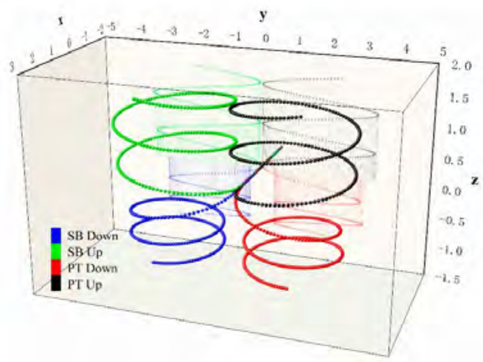

Figure 33. 3D trajectories for the space spiral manoeuvres.

Han et al. (2021) focused on analysing Joubert BB2's turning capabilities during both ascending and descending motions. Their analysis encompassed both steady turning manoeuvres and complex space spiral manoeuvres, as shown in Figure 33. The findings reveal that the turning motion significantly impacts the submarine's depth and pitch attitude, with a notable "stern heavier" phenomenon observed post steering. Notably, underwater turning can serve dual purposes for a submarine: reducing braking speed and limiting dangerous depths.

Skejic and Faltinsen (2022) predicted the manoeuvring behaviour of Joubert BB2 with particularly focusing on its sail design configuration in the horizontal plane under authentic seaway conditions. They employed a pre-selected Tabain's wind wave energy spectrum to describe the irregular wave field at specified geographical locations. Their simulations examined the submerged submarine's manoeuvring behaviour in a deep-water seaway as it executed turning circle (see Figure 34) and zig-zag manoeuvres at pre-determined periscope depths. Furthermore, this study introduces a novel 3 DOF combined manoeuvring and seakeeping two-time scale model, built upon a modular concept, to enhance the accuracy and comprehensiveness of the predictions.

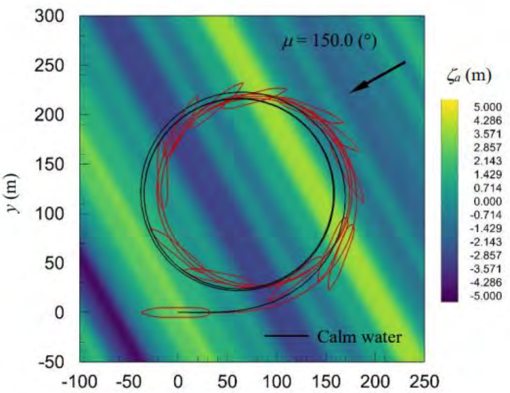

Figure 34. 20° port turning circular manoeuvre of Joubert BB2 at an approach speed of 10 knots.

Carrica et al. (2021b) conducted an extensive study involving a 20-degree turning manoeuvre, controlled vertically through the stern planes, as well as a 20/20 zig-zag manoeuvre, where both the sail and stern planes were vertically controlled, as shown in Figure 35. Both manoeuvres were executed at a standard speed of 10 knots. Additionally, a 20-degree rise manoeuvre was performed with horizontal control at 12 knots. The findings indicate that computational fluid dynamics accurately predicts the motions and speeds of the submarine under free-sailing conditions. However, replicating controller commands proved to be challenging. Notably, the computational results for the rise manoeuvre with surfacing closely aligned with experimental data, encompassing even the crash-back manoeuvre designed to halt the submarine's motion.

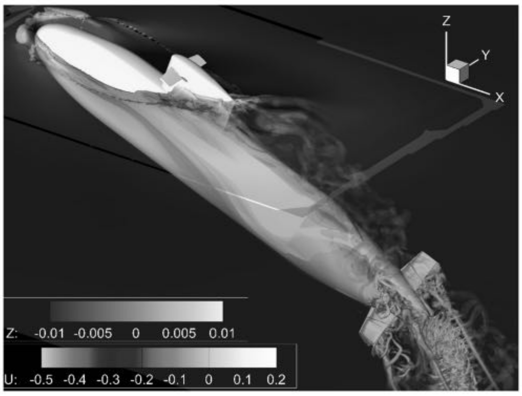

Figure 35. A submarine manoeuvres at a large pitch angle after breaking the surface. Vortical structures are shown as isosurfaces of Q = 3000 coloured with axial velocity.

Jeon et al. (2022b) predicted the dynamic characteristics of an X-rudder submarine. The near surface manoeuvres were analysed, and the jamming cases of control planes were discussed. The prediction results show the X-rudder submarine can execute standard manoeuvres when only one control plane is functional.

Kim et al. (2022b) investigated capability of a coefficient-based model to predict the stern dipping of a submarine during a turning motion. A simplified method was introduced to examine the influence of sail's position on stern dipping. It was found that the out-of-plane loads were very large when the sail was located further aft along the hull.

Arslan and Kefeli (2022) conducted 3-DoF numerical simulations a SUV, focusing on the changes in cavitator's pitch deflection, angle of attack, control surface angle, and pitch rates. The simulation results demonstrated that hydrodynamic analyses of vehicles exhibiting supercavitation can be accurately conducted under both cruising and manoeuvring conditions, and the hydrodynamic characteristics of an SUV can be thoroughly examined using validated CFD analysis models.

Doyle et al. (2022) employed RANS CFD methods to calculate the forces and moments arising from the presence of the sail. Their findings revealed the generation of normal forces and pitching moments was attributed to the interaction between the sail vortex system and the flow along the hull. It is also found that while the in-plane forces and moments were accurately predicted, the out-of-plane force and moment were significantly overestimated at high angles of drift.

Amini Foroushani and Sabzpooshani (2021) proposed a method to estimate the variation of hydrodynamic coefficients of UVs with low Reynolds number. They conducted rotational arm tests on a standard UV model, DARPA SUBOFF, to simulate the rotational linear damping hydrodynamic coefficients. Numerical results are used for deriving proper functions to estimate hydrodynamic coefficients. It was concluded that it is more appropriate to use fitted functions instead of constant values especially at low Reynolds numbers.

Experimental Methods. Zhang et al. (2021) carried out the tests by a drag method to obtain different inflow rates with 0° attack angle under different gliding speeds at 0.25 m/s, 0.5 m/s, 0.75 m/s, 1 m/s, and 1.25 m/s. The results showed the theoretical values were in good agreement with the experimental values, and the error was controlled at about 5%.

Khan et al. (2022) conducted wind tunnel tests to meticulously investigate the distribution of surface pressure over the SUBOFF hull form at elevated angles of incidence. The data collected from this comprehensive study will serve as a valuable adjunct to computational and experimental research on turbulent flows over submerged bodies, encompassing a broad spectrum of angles of incidence.

Wei et al. (2022) developed a numerical prediction method for the emergency ascent of a submarine with flow holes in calm water based on a RANS method, which was then validated by physical tests, as shown in Figure 36. The ascent motion was shown to be influenced by buoyancies, longitudinal and vertical positions of the centre of gravity, and diving depths.

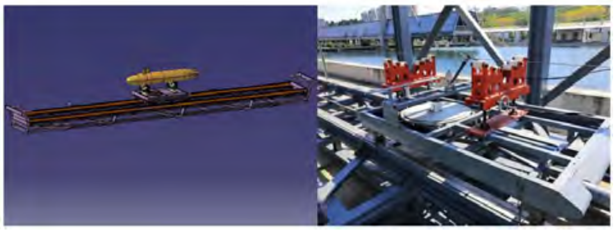

Figure 36. Underwater trailer.

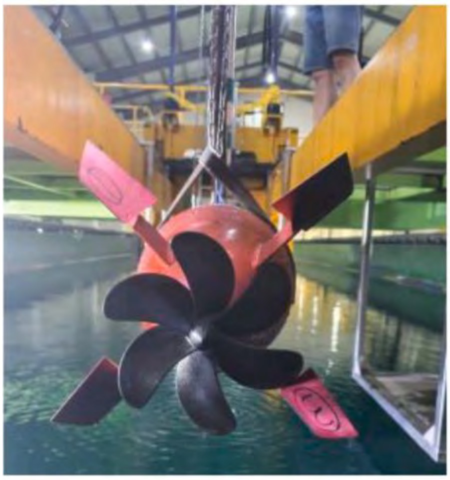

Figure 37. Snapshot of the effective elevator angle $\delta s = 40°$.

Kim et al. (2023a) carried out a series of captive model tests of the BB2 model with a scale ratio of 35.1, as shown in Figure 37. Combination tests including a horizontal static drift with rudder test and pure yaw with rudder were performed in the model basin at Pusan National University, and a mathematical model was constructed based on hydrodynamic coefficients obtained from captive tests. The key parameters, including the tactical diameter and transfer, are well predicted by using this mathematical model. However, the initial rate of turning shows significant discrepancy against the free-running model experiment due to the estimation error of the added mass in the sway or yaw motions.

Novel technology. It is noteworthy that some novel model-free approaches have been recently implemented to predict the hydrodynamic characteristics of underwater vehicles. Mai et al. (2023) developed a novel empirical formula for the hydrodynamic derivatives of a submarine using multiple regression analysis. They derived estimation formulae through based on CFD simulations, and then applied it to calculate the hydrodynamic derivatives of BB2 and a 2,000 tons submarine. Good agreement indicates that the established empirical formulae can be extended to submarines in general at the designing phase.

Thurman and Somero (2022) employed machine learning algorithms to establish prediction models for force and moment coefficients of axisymmetric bodies of revolution. They conducted a uniform experimental design encompassing 50 design points across five factors. A comprehensive test dataset was created to ensure that the prediction models were not overfitted to the training data and could accurately predict arbitrary geometries and inflow conditions within the experimental design region. This approach allows for a thorough assessment of the impact of varying geometric parameters on each force and moment coefficient.

6.2 UV control

The control system of an underwater vehicle is the key technology and the main indicator for measuring the performance of an UV. In case of the control of UVs, robustness and reliability are the most emphasized aspects.

The purpose of those research of the control of UV can be categorized into the following:

- to design a controller of a single underwater vehicle (Borlaug et al., 2021; Chen et al., 2022; Herman, 2021; Huang et al., 2021a), (Ma et al., 2023; Tran et al., 2021; Wang et al., 2022a; Zhang et al., 2021b; Zhang et al., 2024b; Zhang et al., 2024c; Zhu et al., 2024);
- to design a control system of a heterogeneous multiple autonomous vehicles including UVs (Sato et al., 2023; Weng et al., 2022; Xia et al., 2021);
- to investigate robust and reliable controller design operating under error factors like model uncertainties, under-actuations, and unknown environmental disturbances (Borlaug et al., 2021; Chen et al., 2022; Huang et al., 2021a; Tran et al., 2021; Wang et al., 2022a; Xia et al., 2021; Zhang et al., 2021b; Zhang et al., 2024b; Zhang et al., 2024c; Zhu et al., 2024);
- to design a controller of a multi-articulated, non-streamline shaped underwater robot (Borlaug et al., 2021);

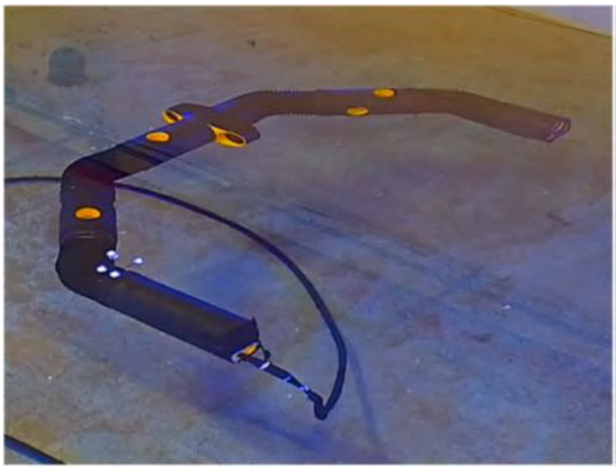

Figure 38. The Eelume vehicle with reflective markers attached at the base.

Borlaug et al. (2021) presented a trajectory tracking method for an articulated intervention autonomous underwater vehicle (AIAUV), as seen from Figure 38. For coping with hydrodynamic and hydrostatic parameter uncertainties, uncertain thruster characteristics, unknown disturbances, and unmodelled dynamic effects, super-twisting algorithm with adaptive gains and a generalized super-twisting algorithm were adopted for trajectory tracking of the position and orientation. A higher-order sliding mode observer was used for estimating the linear and angular velocities, for the case that velocity measurements were not available. To verify the algorithm applicability, comprehensive simulations and experiments were conducted.

Chen et al. (2022) investigated the fixed-time trajectory tracking problem of a small autonomous underwater vehicle (AUV) in the Trans-Atlantic Geotraverse (TAG) active mound with ocean current, unknown disturbances, model uncertainties, actuator faults, and input saturations. A high-order adaptive extended state observer, a continuous fixed-time sliding mode manifold, and an adaptive fault-tolerant trajectory tracking control law with an auxiliary dynamic system were used. The designed algorithm was verified through numerical simulations over the virtually generated topography of the TAG mound.

Herman (2021) presented a preliminary UV trajectory controller design method. The controller, which is applicable for fully actuated vehicles, contains the system dynamics in the control gains. Two examples of numerical simulations of underwater vehicle model were provided to suggest the effectiveness of the approach.

Huang et al. (2021a) dealt with the adaptive trajectory tracking control problem for an underactuated UV, to cope with unmodeled hydrodynamics, ocean disturbances and input quantization. The command filter-based backstepping design and minimum learning parameter algorithm were used for the controller design to avoid the adverse effect of explosion of complexity and computational complexity inherent in neural network. A mapping function was applied to transform the constrained control problem into the unconstrained one. Numerical simulations were conducted to verify advantage and effectiveness of the designed controller.

Ma et al. (2023) dealt with the position keeping process of an UV concept, subsea shuttle tanker (SST) for the offloading process. A linear quadratic regulator was designed for station-keeping in stochastic current. Numerical simulations were conducted to show that the designed control system could keep position during offloading process.

Tran et al. (2021) presented a study of depth controller design of a hybrid torpedo type AUV in the presence of model uncertainty and propeller torque’s effect. They suggested a nonlinear disturbance observer (NDO) to deal with the linearization errors and uncertain components in the depth-plane model. The backstepping technique was adopted to design a depth controller. To verify the effectiveness, feasibility, and stability of the designed controller, numerical simulations were carried out by changing 20~30% of model parameter.

Wang et al. (2022a) presented heading control of an AUV by using the robust sliding mode control method. Control parameters were tuned by an automatic tuning method through a continuous hybrid model-based and model-free reinforcement learning method based on the deterministic policy gradient. To demonstrate the robustness and effectiveness of their approach, numerical simulations and sea trials were presented.

Zhang et al. (2021b) proposed an approach-angle-based three-dimensional path-following control scheme for an underactuated AUV with unknown actuator saturation and environmental disturbance. A path-following error dynamic model was derived based on the principle of relative motion which was followed by the design of approach-angle-based guidance law. A control law was designed based on the Lyapunov theory, backstepping technique, and fuzzy logic system approximation method. Numerical simulations, including straight path following and spatial helix path following, were presented to verify the effectiveness and robustness of the proposed control scheme.

Zhang et al. (2024b) addressed the issue of learning from suboptimal demonstrations and suggested a model-free reinforcement learning method. They integrated a recurrent neural network into the policy network, based on a soft actor-critic, to capture the relationship between states and actions. Simulations with two reference trajectories were suggested for validation.

Zhang et al. (2024c) investigated a rotation-matrix-based finite-time trajectory tracking problem for AUVs in the presence of output constraints, input quantization, and uncertainties. To satisfy the finite-time stability of AUV tracking control and the output constraints imposed by introducing the new attitude error vector, a finite-time command-filtered backstepping controller was proposed based on the asymmetrical time-varying barrier Lyapunov function, and a second-order auxiliary dynamic system was proposed to estimate the negative effects of input quantization errors. An adaptive finite-time disturbance observer was also developed to estimate the lumped uncertainties without prior information on the bounds of the uncertainties. Through numerical simulations, they argued the effectiveness of the control scheme.

Zhu et al. (2024) proposed an adaptive sliding mode tracking control method with a nonlinear disturbance observer to solve the trajectory tracking problem of the underwater vehicle-manipulator system (UVMS) in the presence of large dynamic uncertainties and severe external disturbances. They employed an adaptive control law, an improved fractional-order sliding mode, and a nonlinear disturbance observer to achieve tracking performance of the UVMS. Tracking accuracy, system stability, and interference attenuation under the application of external disturbances were suggested through numerical simulations and experiments.

Sato et al. (2023) presented a basic formation control system that enables various AUV control with minimal software and hardware modifications to autonomous surface vehicle (ASV) and AUVs, for controlling a group of heterogeneous AUVs with different design concepts when operating multiple AUVs simultaneously. Designed control system was successfully tested in actual sea conditions. Four AUVs and one ASV from different manufacturers were used in the sea trials. The basic formation control system kept all AUVs within acoustic communication range and successfully acquired seafloor topographic data. The tests demonstrated the capability of basic formation control with heterogeneously navigated AUVs.

Weng et al. (2022) proposed a method for maintaining the relative position and orientation between AUVs, for establishing a line-of-sight underwater communication link to realize high data rate optical communication in ocean exploration. The policy that could suppress external disturbances and optimize the link establishment efficiency was searched using a reinforcement learning algorithm. To evaluate the performance of the proposed method, a hovering AUV was used to conduct the link establishment experiments. The reinforcement learning policy trained in a simulation environment, then the policy was tested in real sea environments. Based on field experiment results, the performance of the link establishment policy was evaluated.

Xia et al. (2021) dealt with three-dimensional (3-D) formation control of multiple underactuated AUVs with a multi-time-scale structure under uncertain nonlinearities and environmental disturbances. A double-layer independent position-velocity fixed topology was adopted to overcome the drawback of narrow bandwidth of underwater communication. An extended high-gain observer was used to cope with uncertain nonlinearities and environmental disturbances. An integral sliding mode controller was used for formation control of multiple AUVs. Numerical simulations were presented to verify the control performance.

7. PROCEDURES

7.1 General and Minor Changes

The MC reviewed the procedures and guidelines under its responsibility and made updates to the following six procedures and guidelines:

- 7.5-02-06-02 Captive Model Test Procedure.
- 7.5-02-06-03 Validation of Manoeuvring Simulation Models.
- 7.5-02-06-05 Uncertainty Analysis for Free Running Model Tests.
- 7.5-02-06-06 Benchmark Data for Validation of Manoeuvring Predictions.
- 7.5-04-02-02 UV Full Scale Manoeuvring Trials.

The MC made minor changes to the following procedures:

- 7.5-02-06-04 Uncertainty Analysis for Manoeuvring Predictions based on Captive Manoeuvring Tests. Minor English corrections were carried out.
- 7.5-02-06-07 Captive Model Test for Underwater Vehicles. Minor changes were made for the implementation of steady straight-line tests.
- 7.5-03-04-01 Guideline on Use of RANS Tools for Manoeuvring Prediction. Minor updates of the list of nomenclature, and minor English corrections were carried out.
- 7.5-03-04-02 Validation and Verification of RANS Solutions in the prediction of Manoeuvring Capabilities. Some minor changes were made for format, gramma, etc.
- 7.5-04-02-01 Full Scale Manoeuvring Trials. Some minor changes are made for format, gramma. Minor English corrections were carried out.

The procedures of manoeuvring in waves are implemented into two existing procedures:

- 7.5-02-06-01 Free Running Model Tests.
- 7.5-02-06-02 Captive Model Test.

7.2 Uncertainty Analysis for Free Running Model Tests

The purpose of the guideline 7.5-02-06-05 ‘Uncertainty Analysis for Free Running Model Tests’ is to provide guidance for ITTC members to perform UA of a model scale free running model test following the ITTC Procedures 7.5-02-06-01, ‘Free running model tests’.

The guideline outlines the factors that should be considered in conducting free running model tests, focusing on elements that may impact the test results’ uncertainty. It also discusses the basic approach to quantifying uncertainty in tests results.

No newer material dealing with UA was found with respect to free running model tests. Thus, 30th ITTC MC made some cosmetic corrections and added ‘List of Symbols’ to the guideline in accordance with 30th QSG’s instructions.

7.3 Captive Model Test Procedure

A major change has been introduced to procedure 7.5-02-06-02 ‘Captive Model Test”. This procedure has been updated with testing details in waves, such as wave parameters, waiting time, loading conditions, etc.

Some minor changes on alternative steering devices have been introduced to define the suggested operational parameters of these devices for captive model testing. Furthermore, a list of necessary documentation on alternative devices used during the tests is proposed.

Additional information on hexapods and on movable bottom have been introduced to the procedure. Finally, the list of symbols has been updated according to the ITTC Symbols List

7.4 Guideline for Manoeuvring in Waves

The aim of the guideline “Manoeuvring in waves” is to addresses the necessary steps and documentation for the manoeuvring model tests in waves, including captive and free-running model tests.

One of the tasks given to MC was to survey two guidelines for manoeuvring in waves submitted by the Specialist Committee on Manoeuvring in Waves (SC-MW) of 29th ITTC, and to make draft guidelines for manoeuvring in waves based on the given references.

After surveying the reference guidelines, the 30th ITTC MC found that there are many similarities between the guideline for manoeuvring in waves and the guideline for manoeuvring in calm sea condition. Therefore, the 30th ITTC MC and AC agreed to merge the guidelines for manoeuvring in waves, which were originally prepared by the Specialist Committee on Manoeuvring in Waves (SC-MW) of 29th ITTC, with the guidelines for manoeuvring in calm condition.

Merging of two guidelines was conducted based on the following conditions:

- Use simple and effective representation for merging.
- Keep the original meanings.
- Procedures should be described as precisely as possible.
- Separate descriptions should be added for the parameters that are used only in waves tests.

The merged guidelines have been reviewed by the 30th ITTC Seakeeping Committee (SC) and 30th ITTC AC to incorporate any revision requests.

7.5 Guideline for UV

In the 29th ITTC, two new guidelines were proposed for captive model test and full-scale manoeuvring trials for underwater vehicles. in this ITTC, MC continues to work towards the completion of these two guidelines.

Minor changes have been made to 7.5-02-06-07 Captive Model Test for Underwater Vehicles, including the implementation of steady straight-line tests. Compared to surface ships, the Froude number is less important for underwater vehicles. The scaling effects for conducting UV captive tests are discussed and included in the update guideline, and the non-depersonalization of hydrodynamic derivatives is removed.

Major changes have been made to UV Full Scale Manoeuvring Trials (7.5-04-02-02). MC decided to make this guideline focused on unmanned UVs. It is very challenging to include the manned UVs, e.g. submarines, into this procedure. There are very limited literatures available on submarine full scale tests. The information on full scale test procedure is very sensitive. Each country may have its own procedure. It will be challenging to propose a standard testing procedure for submarines without collaborations among different nations and institutions. Even though we propose standard trials for submarines, these procedures are less likely to be applied by these countries/institutions.

The current guideline is focused on AUVs and ROVs. Their performance is determined by both hydrodynamics and autonomy system. It is noted that the 2021 version focuses too much on the control tests, which are hard to be standardized. Even in ITTC 7.5-04-02-01, full scale manoeuvring trials, the procedures are proposed for standard manoeuvring tests for surface ships, and no intension was made there to test the autonomy. Therefore, in this guideline, MC proposes to focus on standard manoeuvring trials, leaving the autonomy and control system tests for future tasks. The tests for autonomy are replaced by 8 standard manoeuvring trials. MC also defines the following 11 manoeuvrability for AUVs and ROVs:

1. horizontal inherent dynamic stability
2. vertical inherent dynamic stability
3. course-keeping ability
4. depth-keeping ability
5. course-changing ability
6. depth-changing ability

7. yaw checking ability
8. pitch checking ability
9. turning ability in horizontal plane
10. horizontal stopping ability
11. vertical stopping ability.

To evaluate the above 11 manoeuvrability, 8 standard tests are recommended as following:

Table 5. Standard manoeuvring tests for AUVs and ROVs.

Type of Tests		Manoeuvrability to be checked
1	Turning Circle Test	9
2	Zig-zag Test	5,6,7,8
3	Spiral Test	1,3
4	Pull-out Test	1,2
5	Stopping Test	10,11
6	Stopping Inertia Test	10,11
7	Thruster Test	5,6,7,8,9
8	Crabbing Test	5,6

The executions of the above 8 manoeuvres are updated accordingly in 7.5-04-02-02.

8. CONCLUSIONS

Experimental tests. MC has reviewed the literatures regarding the development of new methods, trends, and challenges in experimental hydrodynamics. Although more attention is put in manoeuvrability in waves, some issues on calm water manoeuvring tests are still to be solved. One of the issues is the correction of manoeuvring model test results with consideration of environmental factors. Especially the influence of wind should be considered as an important factor. Other yet unsolved topics include the scale effect in manoeuvring model tests. This is however extremely challenging due to lack of sufficient full scale data.

Low-speed manoeuvre is another challenging topic which has attracted many attentions. It is usually accompanied with the shallow and narrow water problem. This topic is extremely important in case of developing navigational simulators, in which the ship behaviour in muddy areas and ship-to-ship interactions are two focused areas. Model test data on ship-bottom, ship-bank and ship-ship problems have been well documented in literatures over the last few years.

Uncertainty analyses of experimental tests, especially captive model tests, is also a challenging topic in manoeuvring tests. New UA methods have been proposed, for instance in SIMMAN2020 workshop. They need to be carefully reviewed and assessed before they can be implemented into general procedures.

Numerical manoeuvring simulations. There is a growing interest in applying high-fidelity numerical approaches such as CFD for manoeuvring predictions. The majority of CFD studies have employed RANS as a practical turbulence modelling approach, providing reasonable accuracy. However, free-running manoeuvring perdition remains a computational challenge and is currently infeasible for application at the design phase and not practical for evaluating ship manoeuvring performance. Consequently, high-fidelity computations have primarily been used for captive model manoeuvring predictions to inform reduced order manoeuvring models.

Benchmarking the numerical models continues to be an active area of research. The uncertainty in the numerical predictions is generally greater in shallow and restricted water than deep, unconfined water, Future efforts should focus on improving numerical models to reduce uncertainty, leveraging CFD to deepen our understanding of the underlying flow physics in ship manoeuvring, and utilizing this knowledge to enhance reduced-order manoeuvring models. Application of ML&AI technologies should be considered for improving the models.

Benchmark data. The SIMMAN 2020 workshop has given a large amount of new valuable benchmark data for validation. Besides additional and updated data for the KVLCC2 and the

KCS, the workshop introduced the surface combatant ONRT as a replacement for the 5415M. The benchmark data sets of the ONRT were all new and included both captive tests and free running model tests. Besides the calm water data in deep and shallow water, free running model tests (e.g. turning circles) in regular waves were also introduced for both the KCS and the ONRT.

The overall results from the workshop showed a good progress in the prediction capability. The prediction errors defined in 2020 were smaller than those in 2014, though it was only properly statistically documented for the deep-water cases. The amount of time domain CFD simulations submissions increases significantly compared to past workshops, though it is still an insufficient amount to give sound guidance and recommendations.

Based on the outcome of SIMMAN2020, it is recommended to keep the focus on KVLCC2, KCS and ONRT for future workshops unless a ship with open full scale data becomes available and to include propeller thrust and rudder forces in analysis, which were not considered in SIMMAN2020. It is also recommended to promote research in shallow water as the errors in general were larger than those in deep water cases.

In parallel with SIMMAN, a limited set of benchmark data has also been released in connection with the 6th MASHCON. The dataset contained captive shallow water benchmark data with focus on the effects of a passing ship (KCS) on two different moored ships (a Neo-Panamax container ship (C0P) and an Aframax tanker (T0Y)).

Autonomous, novel device and clean fuel. The number of the published paper on autonomous ships increases rapidly over the past decades. There are numerous methods/algorithms developed for ship path planning/following/tracking, collision avoidance, formation control, and berthing manoeuvres. Most of these works are mainly focused on simulations without sufficient validations of their proposed control algorithms. There are no widely accepted benchmark autonomous ship model or manoeuvring scenarios to compare the performance of the control strategy. Efforts are required to put forward benchmark models and standardize the testing scenarios to accelerate the technology and regulatory development for autonomous ships.

Zero-carbon shipping is another hot topic in maritime community. There are many zero-emission technologies, such as ammonia, hydrogen, and batteries, being proposed and validated by the shipping companies and research institutes to reduce the production of greenhouse gases. Novel devices, such as wind assist devices, novel rudders, have been proposed to reduce ship resistance, hence saving energy. Most of these studies are focused on propulsion. The impact of these technologies on ship manoeuvring are not well understood.

Manoeuvring in waves. There is no new PMM test in wave results published in this period. Only a few oblique towing tests in waves were available. The steady drift in regular waves for steady wave forces have been conducted in Actual Sea Model Basin for KVLCC1, under three wave frequencies with different drift angles and speeds. A series of steady drift tests in oblique waves to measure surge and sway wave drift forces and yaw drift moment acting on KVLCC2 have been performed in KRISO. On the other hand, several free-running model tests (FRMT) in wave are available during this term (the 30th) of ITTC. Trajectories of self-propelled ship with 35 degree turning circle for KCS and ONRT have been published in SIMMAN2020. Zig-zag model tests were performed on an unmanned wave glider.

In numerical simulation of manoeuvring in wave, mean wave force method is still attractive due to its simplicity. Two-time scale methods and Unified methods have been widely used to predict the manoeuvrability of ships in waves.

Direct CFD simulations of ship manoeuvring in waves continue to draw broad attention. Self-propulsion and turning circle motions in waves can be simulated using an overset method. However, due to the high computational cost and longer simulation time, direct CFD manoeuvring simulations in irregular waves are still changeling. A new combination of CFD, a linear time-domain boundary element method, and a propeller-force model are developed for efficient computation of the total hydrodynamic force. Another new direction for manoeuvring in wave is data-driven hybrid machine learning architectures to improve knowledge and forecasting capabilities for ships operating in waves.

Underwater vehicles. There have been a large number of publications on underwater vehicles during this term (the 30th) of ITTC, which include the studies on hydrodynamic design, interaction between UV and environment, appendages, path following, trajectory tracking, station keeping etc. Discussions are highlighted on UVs' hydrodynamic performance, flow field and control algorithms. However, the manoeuvrability of UVs is not clearly defined, and the manoeuvres presented in these studies are very scattered. Not like surface ships, the mathematical model of UVs' 3D manoeuvring motion has not been well established and progressed over the past few decades. The existing model is very complicated due to the cross-coupling terms in hydrodynamic derivatives, which largely hindered the application of this model in UV community. It also hinders the development of captive model test technologies for UVs, particularly for those with asymmetrical geometry in horizontal plane. Although CFD technology has been widely used to predict the hydrodynamic forces and simulate the free running manoeuvring motions of UVs, there is very limited benchmark data to validate and verify the CFD predictions. There is an urgent demand from UV community to put tother some joint efforts to benchmark UV models and test procedures.

Procedures. The MC reviewed the procedures and guidelines under its responsibility. A symbol list is added to all the procedures and guidelines. Major updates and improvements were made to:

- 7.5-02-06-03 Validation of Manoeuvring Simulation Models
- 7.5-03-04-02 Validation and Verification of RANS Solutions in the Prediction of Manoeuvring Capabilities
- 7.5-04-02-02 UV Full Scale Manoeuvring Trials

No new procedures and guidelines are developed in this term. However, the guidelines developed by the 29th ITTC specialist committee on manoeuvring in waves are merged to the following to general procedures:

- 7.5-02-06-01 Free Running Model Tests
- 7.5-02-06-02 Captive Model Test

9. RECOMMENDATIONS

The 30th ITTC Manoeuvring Committee recommends the following:

Update procedure 7.5-02-06-02 Captive Model Test with regards to hexapod tests.

Review the uncertainty analysis by SIMMAN 2020. If needed, procedure 7.5-02-06-04 Uncertainty Analysis for Manoeuvring Predictions based on Captive Manoeuvring Tests, will be updated to incorporate the outcome of SIMMAN 2020.

Update procedure 7.5-03-04-01 Guideline on Use of RANS Tools for Manoeuvring Prediction, update the numerical simulation procedure for calm water, add the guideline for simulations in waves, replace the example on simulation based on derivatives (calm water), add an example of direct manoeuvring simulation in waves.

Update procedure 7.5-03-04-02 Validation and Verification of RANS Solutions in the Prediction of Manoeuvring Capabilities, evaluate the feasibility of adding an example of manoeuvring in waves.

Update 7.5-02-06-03 Validation of Manoeuvring Simulation Models, reflecting the outcome of SIMMAN and any other new developments.

Liaise with the authorities/organizations/associations on marine autonomous, evaluate the feasibility to propose standard manoeuvring trials for MASS.

Collect benchmark data for surface and underwater vehicles include these benchmark data in 7.5-02-06-06 Benchmark Data for Validation of Manoeuvring Predictions.

Liaise with Full-Scale Ship Performance Committee, review and collect benchmark data for full-scale manoeuvring tests.

Review the guidelines for low-speed manoeuvring tests and full-scale manoeuvring trials, if needed, update 7.5-02-06-01 Free Running Model Tests and 7.5-04-02-01 Full Scale Manoeuvring Trials by implementing the low-speed tests and/or bow thruster test procedures.

Investigate the novel propulsion/steering technologies, e.g. wind-assisted propulsion devices, and evaluate their impacts on ship manoeuvrability.

Survey the AI and data-based technology and their application to ship manoeuvring.

Keep updated on the ongoing discussions regarding amendments to the IMO Manoeuvring Standard and investigate the effects on tank tests and simulations.

The Manoeuvring Committee recommends to the Full Conference to adopt the updates to the procedures and the newly created guidelines.

10. REFERENCES

Ahn, K., Choi, G.-H., Son, D.-I., Rhee, K.-P., 2012, "Hydrodynamic Characteristics of X-Twisted Rudder for Large Container Carriers." , International Journal of Naval Architecture and Ocean Engineering , Vol. 4, pp. 322–334.

Amini Foroushani, J., Sabzpooshani, M., 2021, "An Approach for the Estimation of Hydrodynamic Coefficients of an Underwater Vehicle in Off-Design Velocities." , Journal of Marine Science and Technology , Vol. 26, pp. 368–381.

Aram, S., Mucha, P., 2023, "Computational Fluid Dynamics Analysis of Different Propeller Models for a Ship Maneuvering in Calm Water." , Ocean Engineering , Vol. 276, pp. 114226.

Aram, S., Wundrow, D., 2022, "Application of Blended-Method Computation and CFD to Ship Maneuvering Prediction," in: 34th Symposium on Naval Hydrodynamics (SNH34). Washington, DC, USA.

Arslan, S., Kefeli, S., 2022, "Modeling of Supercavitation Phenomenon for Underwater Vehicles in Cruise and Maneuvering Conditions," in: 34th Symposium on Naval Hydrodynamics (SNH34). Washington, DC, USA.

Barrera, R.D., Schiaveto Neto, L.A., Vieira, D.P., Mesquita, E.S., Tannuri, E.A., 2021, "Azimuth Stern Drive (ASD) Vector Tugs Positioning and Towing Force Prediction during Docking, Steering and Braking Maneuvers." , Applied Ocean Research , Vol. 110, pp. 102611.

Bellingmo, P.R., Fjørtoft, K., Jørgensen, U., Kvam, P.E., Bratbergsengen, I.L., Gisbert, J.V.P., 2022, "The Importance of Documenting Autonomous Tests." , Journal of Physics: Conference Series , Vol. 2311, pp. 012019.

Berg, T.E., Selvik, Ø., Steinsvik, K., Leinebø, D., 2021, "Manoeuvring Study – Norwegian Double-Ended Ferry." , TransNav, the International Journal on Marine Navigation and Safety of Sea Transportation , Vol. 15, pp. 63–69.

Borlaug, I.-L.G., Pettersen, K.Y., Gravdahl, J.T., 2021, "Comparison of Two Second-Order Sliding Mode Control Algorithms for an Articulated Intervention AUV: Theory and Experimental Results." , Ocean Engineering , Vol. 222, pp. 108480.

Böttner, C.-U., Kondziella, B., 2022, "Passing Ship Effect In Shallow And Confined Waters, A Systematic Model Test Study Of Moored Containership At Quay," in: 6th Conference on Ship Manoeuvring in Shallow and Confined Water (MASHCON 2022). Glasgow, UK, pp. 10–18.

Calcagni, D., Bellotto, F., Broglia, R., Salvatore, F., Bensow, R.E., 2014, "Comparative Analysis of the Hydrodynamic Performance of Untwisted and Twisted Rudders Using a Hybrid RANSE/BEM Model," in: 24th International Ocean and Polar Engineering Conference (ISOPE 2014). Busan, Korea.

Carrica, P.M., Kerkvliet, M., Quadvlieg, F., Martin, J.E., 2021a, "CFD Simulations and Experiments of a Submarine in Turn, Zigzag, and Surfacing Maneuvers." , Journal of Ship Research , Vol. 65, pp. 293–308.

Carrica, P.M., Kim, Y., Martin, J.E., 2021b, "Vertical Zigzag Maneuver of a Generic Submarine." , Ocean Engineering , Vol. 219, pp. 108386.

Chame, M.E.F., Tannuri, E.A., 2023, "Scale Effects in Ship Maneuvering Prediction Based on CFD Hydrodynamic Coefficients of KVLCC2," in: 3rd Workshop on Verification and Validation of Ship Manoeuvring Simulation Methods (SIMMAN 2020). Incheon, South Korea, pp. 50–55.

Chen, C., Verwilligen, J., Mansuy, M., Eloot, K., Lataire, E., Delefortrie, G., 2021, "Tracking Controller for Ship Manoeuvring in a Shallow or Confined Fairway: Design, Comparison and Application." , Applied Ocean Research , Vol. 115, pp. 102823.

Chen, G., Sheng, M., Wan, L., Liu, Y., Zhang, Z., Xu, Y., 2022, "Tracking Control for Small Autonomous Underwater Vehicles in the Trans-Atlantic Geotraverse Hydrothermal Field Based on the Modeling Trajectory." , Applied Ocean Research , Vol. 127, pp. 103281.

Choe, B., Furukawa, Y., 2019, "Automatic Track Keeping to Realize the Realistic Operation of a Ship." , International Journal of Fuzzy Logic and Intelligent Systems , Vol. 19, pp. 172–182.

Choi, J.-K., 2023, "Path-Following Control of a Ship by Pushing Using a Single Autonomous Tugboat." , Journal of Marine Science and Technology , Vol. 28, pp. 649–657.

Cura Hochbaum, A., Blum, B., Uharek, S., 2022, "A Novel 3+3 DOF Method for Manoeuvring Prediction of Planing Boats," in: 34th Symposium on Naval Hydrodynamics (SNH34). Washington, DC, USA.

Daidola, J.C., 2022, "Effects of Hull and Control Surface Roughness on Ship Maneuvering." , Journal of Ship Research , Vol. 66, pp. 15–24.

Delefortrie, G., Eloot, K., Van Hoydonck, W., 2023, "EFD Based Submissions for the Shallow Water Cases of Simman 2020," in: 3rd Workshop on Verification and Validation of Ship Manoeuvring Simulation Methods (SIMMAN 2020). Incheon, South Korea, pp. 19–29.

Delefortrie, G., Sotelo, M., Boucetta, D., 2022a, "Practical Squat Assessment for a Ship Manoeuvring in Muddy Environments." , Applied Ocean Research , Vol. 123, pp. 103181.

Delefortrie, G., Van Hoydonck, W., Eloot, K., 2022b, "Forces and Torque Acting on a Rudder While Manoeuvring." , Journal of Marine Science and Technology , Vol. 27, pp. 383–407.

Delefortrie, G., Villagomez, J., Verwilligen, J., 2022c, "Maneuvring Behavior of Push Convoys in Different Barge Configurations." , Journal of Ship Research , Vol. 66, pp. 231–249.

Dereszewski, P., Hebel, W., Dereszewski, M., Dymarski, P., 2021, "Investigation of Heading and Manoeuvring Properties of Stern Trawler B-280 with Hebel Type

Rudder Blade," in: 22nd International Symposium on Hydrodynamics in Ship Design, Safety, Manoeuvring and Operation (HYDRONAV 2020). Sopot and Iława, Poland.

Doyle, R., Farooq, A., Carson, M., Jeans, T., Holloway, G., Raval, S., 2022, "Numerical Study on the Circulatory Forces Generated by Submarine Hull and Sail Interactions," in: 34th Symposium on Naval Hydrodynamics (SNH34). Washington, DC, USA.

Esferra, R., Bernardino, J.C., de Oliveira Bezerra, R., Pion, L.M., 2021, "Simulation in Reduced Scale Hydraulic Models of the Mooring System of Ships Docked Under the Effect of the Passage of Other Vessels (Passing Ship)." , TransNav, the International Journal on Marine Navigation and Safety of Sea Transportation , Vol. 15, pp. 845–852.

Europa Seaways, n.d., "Partnership Aims to Develop Hydrogen Ferry for Oslo-Copenhagen."

Fukazawa, M., Turkmen, S., Marino, A., Sasaki, N., 2018, "Full-Scale GATE RUDDER Performance Obtained from Voyage Data," in: 3rd International Meeting on Progress in Propeller Cavitation and Its Consequences: Experimental and Computational Methods for Predictions. Istanbul, Turkey, pp. 71–76.

Gennaro, G., Gonzalez-Adalid, J., 2012, "Improving the Propulsion Efficiency by Means of Contracted and Loaded Tip (CLT ®) Propellers."

Hachiya, Y., Sano, M., Okuda, R., Furukawa, Y., Yasukawa, H., 2022, "False Bottom Effect on the Hydrodynamic Forces Acting on a Ship Hull During an Oblique Towing Test and Countermeasures," in: 6th Conference on Ship Manoeuvring in Shallow and Confined Water (MASHCON 2022). Glasgow, UK, pp. 58–71.

Hagen, I.B., Vassbotn, O., Skogvold, M., Johansen, T.A., Brekke, E.F., 2023, "Safety and COLREG Evaluation for Marine Collision Avoidance Algorithms." , Ocean Engineering , Vol. 288, pp. 115991.

Han, K., Cheng, X., Liu, Z., Huang, C., Chang, H., Yao, J., Tan, K., 2021, "Six-DOF CFD Simulations of Underwater Vehicle Operating Underwater Turning Maneuvers." , Journal of Marine Science and Engineering , Vol. 9, pp. 1451.

Hao, L., Han, Y., Shi, C., Pan, Z., 2022, "Recurrent Neural Networks for Nonparametric Modeling of Ship Maneuvering Motion." , International Journal of Naval Architecture and Ocean Engineering , Vol. 14, pp. 100436.

He, H., Van Zwijnsvoorde, T., Lataire, E., Delefortrie, G., 2023, "Model Predictive Controller for Path Following Ships Validated by Experimental Model Tests." , Ocean Engineering , Vol. 288, pp. 115971.

Herman, P., 2021, "Preliminary Design of the Control Needed to Achieve Underwater Vehicle Trajectories." , Journal of Marine Science and Technology , Vol. 26, pp. 986–998.

Hinostroza, M.A., Xu, H., Guedes Soares, C., 2021, "Experimental Results of the Cooperative Operation of Autonomous Surface Vehicles Navigating in Complex Marine Environment." , Ocean Engineering , Vol. 219, pp. 108256.

Hou, H., Krajewski, M., Ilter, Y.K., Day, S., Atlar, M., Shi, W., 2020, "An Experimental Investigation of the Impact of Retrofitting an Underwater Stern Foil on the Resistance and Motion." , Ocean Engineering , Vol. 205, pp. 107290.

Hoydonck, W.V., D.G., E.K., 2023, "Prediction of Hydrodynamic Forces on KVLCC," in: 3rd Workshop on Verification and Validation of Ship Manoeuvring Simulation Methods (SIMMAN 2020). Incheon, South Korea.

Huang, B., Zhou, B., Zhang, S., Zhu, C., 2021a, "Adaptive Prescribed Performance Tracking Control for Underactuated Autonomous Underwater Vehicles with Input Quantization." , Ocean Engineering , Vol. 221, pp. 108549.

Huang, Y., Hu, Y., Wu, J., Zeng, C., 2021b, "Observer-Based Motion Control System for the Approach Ship with Propeller and Rudder in the Process of Underway Replenishment." , Ocean Engineering , Vol. 222, pp. 108586.

International Martime Organization, 2019, "Interim Guidelines for Mass Trials."

Jaramillo, S.E., 2016, "Optimization of Twisted Rudder (With Bulb and Hub Cap)" (Master Thesis). University of Rostock, Germany, Rostock, Mecklenburg-Vorpommern, Germany.

Jeon, M., Yoon, H.K., Park, J., Rhee, S.H., Seo, J., 2022a, "Identification of 4-DoF Maneuvering Mathematical Models for a Combatant in Intact and Damaged Conditions." , International Journal of Naval Architecture and Ocean Engineering , Vol. 14, pp. 100480.

Jeon, M., Yoon, H.K., Park, J., You, Y., 2022b, "Analysis of Maneuverability of X-Rudder Submarine Considering Environmental Disturbance and Jamming Situations." , Applied Ocean Research , Vol. 121, pp. 103079.

Jia, C., Ma, J., Yang, X., Lv, X., 2023, "RA-GAN: A Generative Adversarial Network for Risk-Aware Trajectory Prediction in Multi-Ship Encounter Situations." , Ocean Engineering , Vol. 289, pp. 116188.

Jiang, Y., Hou, X.-R., Wang, X.-G., Wang, Z.-H., Yang, Z.-L., Zou, Z.-J., 2022, "Identification Modeling and Prediction of Ship Maneuvering Motion Based on LSTM Deep Neural Network." , Journal of Marine Science and Technology , Vol. 27, pp. 125–137.

Khan, Md.K., Korulla, M., Nagarajan, V., Sha, O.P., 2022, "Surface Pressure Measurements on a Generic Submarine Hull Form at High Angles of Incidence." , Journal of Marine Science and Technology , Vol. 27, pp. 677–694.

Kim, D., Tezdogan, T., Incecik, A., 2022a, "Hydrodynamic Analysis of Ship Manoeuvrability in Shallow Water Using High-Fidelity URANS Computations." , Applied Ocean Research , Vol. 123, pp. 103176.

Kim, D., Yim, J., Song, S., Park, J.-B., Kim, J., Yu, Y., Elsherbiny, K., Tezdogan, T., 2023a, "Path-Following Control Problem for Maritime Autonomous Surface Ships (MASS) in Adverse Weather Conditions at Low Speeds." , Ocean Engineering , Vol. 287, pp. 115860.

Kim, D.-H., Kim, Y., Baek, H.-M., Choi, Y.-M., Kim, Y.J., Park, H., Yoon, H.K., Shin, J.-H., Lee, J., Chae, E.J., Shin, Y., Kim, E.S., 2023b, "Experimental Study of the Hydrodynamic Maneuvering Coefficients for a BB2 Generic Submarine Using the Planar Motion Mechanism." , Ocean Engineering , Vol. 271, pp. 113428.

Kim, H., Renilson, M.R., Ranmuthugala, D., Binns, J., 2022b, "Prediction of the Stern Dipping Tendency of a Submarine in a Turn," in: 34th Symposium on Naval Hydrodynamics (SNH34). Washington, DC, USA.

Kishimoto, T., Ikeda, T., Sawata, T., Matsumura, N., 2016, "Maneuvering Characteristics of a Bulk Carrier with an Energy Saving Device," in: 15th Asia Navigation Conference (ANC 2016). Yeosu, Korea.

Kitagawa, Y., Tsukada, Y., Ohashi, K., 2022, "On Measurement of Hydrodynamic Pressures on Hull and Rudder Surface in Free-Running Model Test," in: 15th International Symposium on Practical Design of Ships and Other Floating Structures (PRADS 2022). Dubrovnik, Croatia.

Krell, E., King, S.A., Garcia Carrillo, L.R., 2022, "Autonomous Surface Vehicle Energy-Efficient and Reward-Based Path Planning Using Particle Swarm Optimization and Visibility Graphs." , Applied Ocean Research , Vol. 122, pp. 103125.

Kryvyi, O., Miyusov, M., 2021, "Construction and Analysis of Mathematical Models of Hydrodynamic Forces and Moment on the Ship's Hull Using Multivariate Regression Analysis." , TransNav, the International Journal on Marine Navigation and Safety of Sea Transportation , Vol. 15, pp. 853–864.

Kwon, C., Yeon, S., 2022, "A Study on the Numerical Captive Model Tests for Ships in Shallow and Confined Waters Using CFD: Comparative Study for PESCA (Passing Effects in Shallow and Confined Areas) Project," in: 6th Conference on Ship Manoeuvring in Shallow and Confined Water (MASHCON 2022). Glasgow, UK, pp. 119–127.

Ley, J., Broß, H., Kämmerling, E., 2022, "Experimental Investigation of Passing Ship Effects on Moored Ships in a Canal Port," in: 6th Conference on Ship Manoeuvring in Shallow and Confined Water (MASHCON 2022). Glasgow, UK, pp. 128–138.

Li, M., Mou, J., He, Y., Zhang, X., Xie, Q., Chen, P., 2022, "Dynamic Trajectory Planning for Unmanned Ship under Multi-Object Environment." , Journal of Marine Science and Technology , Vol. 27, pp. 173–185.

Lindberg, O., Vilmann, O., 2022, "Accurate and Efficient Simulation Tools for Squat Prediction and Hydrodynamic Interaction Effects," in: 6th Conference on Ship Manoeuvring in Shallow and Confined Water (MASHCON 2022). Glasgow, UK, pp. 139–150.

Liu, H., Ma, N., Gu, X., 2021, "CFD Prediction of Ship-Bank Interaction for KCS under Extreme Conditions." , Journal of Marine Science and Technology , Vol. 26, pp. 1062–1077.

Liu, S., Papanikolaou, A., Shang, B., 2022a, "Regulating the Safe Navigation of Energy-Efficient Ships: A Critical Review of the Finalized IMO Guidelines for Assessing the Minimum Propulsion Power of Ships in Adverse Conditions." , Ocean Engineering , Vol. 249, pp. 111011.

Liu, Y.-H., Yuan, Z.-M., Chen, M.-L., 2022b, "Time Domain Simulation of Passing Ship Effects in Shallow and Confined Waterways," in: 6th Conference on Ship Manoeuvring in Shallow and Confined Water (MASHCON 2022). Glasgow, UK, pp. 162–173.

Liu, Y.-H., Yuan, Z.-M., Chen, M.-L., Liu, H.-R., 2022c, "Unsteady Hydrodynamics of Ships Entering a Lock," in: 6th Conference on Ship Manoeuvring in Shallow and Confined Water (MASHCON 2022). Glasgow, UK, pp. 151–161.

Lu, S., Cheng, X., Liu, J., Li, S., 2023, "Experimental and Numerical Study on Free-Running Tests of a 7m KVLCC2 Model," in: 3rd Workshop on Verification and Validation of Ship Manoeuvring Simulation Methods (SIMMAN 2020). Incheon, South Korea, pp. 30–36.

Lu, S., Cheng, X., Liu, J., Li, S., Yasukawa, H., 2022, "Maneuvering Modeling of a Twin-Propeller Twin-Rudder Inland Container Vessel Based on Integrated CFD and Empirical Methods." , Applied Ocean Research , Vol. 126, pp. 103261.

Lyu, H., Liu, W., Guo, S., Tan, G., Fu, C., Sun, X., Zhao, Y., Zhang, L., Yin, Y., 2024, "Autonomous Collision Avoidance Method for MASSs Based on Precise Potential Field Modelling and COLREGs Constraints in Complex Sailing Environments." , Ocean Engineering , Vol. 292, pp. 116530.

Ma, C., Ma, N., Gu, X., 2022a, "A Contrastive Study of Two-Time Scaled Method and Unified Method in Maneuverability-in-Waves," in: 41th International Conference on Ocean, Offshore and Arctic Engineering (OMAE2022). American Society of Mechanical Engineers, Hamburg, Germany.

Ma, C., Ma, N., Gu, X., 2021a, "Benchmark Study and Uncertainty Assessment of Planar Motion Mechanism Tests on KVLCC2 in a Circulating Water Channel," in: 40th International Conference on Ocean, Offshore and Arctic Engineering (OMAE2021). American Society of Mechanical Engineers.

Ma, C., Ma, N., Gu, X., Feng, P., 2021b, "Numerical Study on Hydrodynamic Forces and Course Stability of a Ship in Surf-Riding Condition Based on Planar Motion Mechanism Tests." , Journal of Offshore Mechanics and Arctic Engineering , Vol. 143.

Ma, Y., Xing, Y., Sui, D., 2023, "Trajectory Envelope of a Subsea Shuttle Tanker Hovering in Stochastic Ocean Current—Model Development and Tuning." , Journal of Offshore Mechanics and Arctic Engineering , Vol. 145.

Ma, Y., Zhao, Y., Li, Z., Yan, X., Bi, H., Królczyk, G., 2022b, "A New Coverage Path Planning Algorithm for Unmanned Surface Mapping Vehicle Based on A-Star Based Searching." , Applied Ocean Research , Vol. 123, pp. 103163.

Mai, T.L., Jeon, M., Vo, A.K., Yoon, H.K., Kim, S., Lee, J., 2023, "Establishment of Empirical Formulae for Hydrodynamic Derivatives of Submarine Considering Design Parameters." , International Journal of Naval Architecture and Ocean Engineering , Vol. 15, pp. 100537.

Maki, A., Akimoto, Y., Naoya, U., 2021, "Application of Optimal Control Theory Based on the Evolution Strategy (CMA-ES) to Automatic Berthing (Part: 2)." , Journal of Marine Science and Technology , Vol. 26, pp. 835–845.

Mao, X., Zhan, X., 2022, "Course-Keeping Ability and Minimum Propulsion Power Assessment in Adverse Weather Conditions Using a Manoeuvring-Seakeeping Unified Model," in: 15th International Symposium on Practical Design of Ships and Other Floating Structures (PRADS 2022). Dubrovnik, Croatia.

Maritime UK, 2023, "Maritime Autonomous Surface Ships (MASS) UK Industry Conduct Principles and Code of Practice 2023 (V7)."

Mehr, J.A., Javanmardi, M., Tham, S.W., Yin, Y., 2022, "Experimental Investigation on the Effect of Water Depth on Roll Natural Period and Damping Coefficient of Large Commercial Ships in Shallow Water Regions," in: 6th Conference on Ship Manoeuvring in Shallow and Confined Water (MASHCON 2022). Glasgow, UK, pp. 174–184.

Mei, B., Shi, G., 2023, "A Novel Grey Box Manoeuvring Model for Free Running Model and Full-Scale Ship Based on System Identification," in: 3rd Workshop on Verification and Validation of Ship Manoeuvring Simulation Methods (SIMMAN 2020). Incheon, South Korea, pp. 194–198.

Meng, Y., Zhang, X., Zhu, J., 2022, "Parameter Identification of Ship Motion Mathematical Model Based on Full-Scale Trial Data." , International Journal of Naval Architecture and Ocean Engineering , Vol. 14, pp. 100437.

MEPC 71/INF.28, 2017, "Draft Revised Guidelines for Determining Minimum Propulsion Power to Maintain the Manoeuvrability of Ships in Adverse Conditions."

MEPC.1/Circ.850/Rev.3, 2021, "Guidelines for Determining Minimum Propulsion Power to Maintain the Manoeuvrability of Ships in Adverse Conditions."

MEPC76/5/1, 2021, "Report of the Correspondence Group on Air Pollution and Energy Efficiency."

MEPC.232(65), 2013, "2013 Interim Guidelines for Determining Minimum Propulsion Power to Maintain the Manoeuvrability of Ships in Adverse Conditions."

Min, B., Zhang, X., 2021, "Concise Robust Fuzzy Nonlinear Feedback Track Keeping Control for Ships Using Multi-Technique Improved LOS Guidance." , Ocean Engineering , Vol. 224, pp. 108734.

Miyauchi, Y., Maki, A., Umeda, N., Rachman, D.M., Akimoto, Y., 2021, "System

Parameter Exploration of Ship Maneuvering Model for Automatic Docking / Berthing Using CMA-ES." , Journal of Marine Science and Technology , Vol. 27, pp. 1065–1083.

Nie, J., Wang, H., Lu, X., Lin, X., Sheng, C., Zhang, Z., Song, S., 2021, "Finite-Time Output Feedback Path Following Control of Underactuated MSV Based on FTESO." , Ocean Engineering , Vol. 224, pp. 108660.

Okuda, R., Yasukawa, H., Sano, M., Hirata, N., Yoshimura, Y., Furukawa, Y., Matsuda, A., 2022, "Maneuvering Simulations of Twin-Propeller and Twin-Rudder Ship in Shallow Water Using Equivalent Single Rudder Model." , Journal of Marine Science and Technology , Vol. 27, pp. 948–970.

Oladele, O., Lambert, W., Brizzolara, S., 2023, "A Combined Maneuvering and Seakeeping Model for the ONR Tumblehome," in: 42nd International Conference on Ocean, Offshore and Arctic Engineering (OMAE 2023). American Society of Mechanical Engineers, Melbourne, Australia.

Oud, G., Toxopeus, S., 2022, "A Technique for Efficient Computation of Steady Yaw Manoeuvres Using CFD." , International Shipbuilding Progress , Vol. 69, pp. 3–24.

Paramesh, S., Suresh, R., 2021, "A Unified Seakeeping and Manoeuvring Model with a PID Controller for Path Following of a KVLCC2 Tanker in Regular Waves." , Applied Ocean Research , Vol. 116, pp. 102860.

Park, K., Kim, D.J., Kim, S.Y., Seo, J., Suh, I., Rhee, S.H., 2021a, "Effect of Waterjet Intake Plane Shape on Course-Keeping Stability of a Planing Boat." , International Journal of Naval Architecture and Ocean Engineering , Vol. 13, pp. 585–598.

Park, S.H., Lee, S.J., Lee, S., 2021b, "Experimental Investigation of Towing- and Course-Stability of a FPSO Towed by a Tug-Boat with Lateral Motion." , International Journal of Naval Architecture and Ocean Engineering , Vol. 13, pp. 12–23.

Qu, X., Liang, X., Hou, Y., Li, Y., Zhang, R., 2021, "Path-Following Control of Unmanned Surface Vehicles with Unknown Dynamics and Unmeasured Velocities." , Journal of Marine Science and Technology , Vol. 26, pp. 395–407.

Quadvlieg, F., Stern, F., Kim, Y.-G., Flensborg-Otzen, J., Yasukawa, H., Wang, W., Han, Y., 2024, "Analysis of Submissions for Forces and Moments in Captive Conditions," in: Final Workshop Proceedings, Volume II, SIMMAN 2020. Songdo, South Korea.

Quadvlieg, F., Stern, F., Kim, Y.-G., Flensborg-Otzen, J., Yasukawa, H., Wang, W., Han, Y., 2023, "Analysis of Trajectory Submissions," in: Final Workshop Proceedings, Volume III, SIMMAN 2020. Songdo, South Korea.

Reichel, M., 2021, "Influence of Propulsion-Steering System on the Position of Pivot Point on a Large LNG Carrier during Standard Manoeuvres," in: 22nd International Symposium on Hydrodynamics in Ship Design, Safety, Manoeuvring and Operation, Online.

Sadati, K., Zeraatgar, H., 2023, "Simulation of Turning Maneuver Using the 4+2DOF Method in Planing and Semi-Planing Modes." , Ocean Engineering , Vol. 287, pp. 115763.

Sakamoto, N., 2023, "Overset RaNS Study of the Effect of Tank Bottom Condition for KCS under Static Drift/Rudder Configurations in Shallow Water," in: 3rd Workshop on Verification and Validation of Ship Manoeuvring Simulation Methods (SIMMAN 2020). Incheon, South Korea, pp. 66–71.

Sakamoto, N., Ohashi, K., Kobayashi, H., Hino, T., 2023, "Overset RaNS Simulations and Validations for the Effect of False Bottom to the KCS under Static

Drift and Static Rudder in Shallow Water.” , Journal of Marine Science and Technology , Vol. 28, pp. 248–269.

Sasaki, N., Aono, T., 1997, “Energy saving device SLID; Sho energy sochi SLID no kaihatsu.” , Sumitomo Jukikai Giho , Vol. 45.

Sasaki, N., Kuribayashi, S., Atlar, M., Steam Co, K., 2018, “Gate Rudder,” in: 3rd International Symposium on Naval Architecture and Maritime (INT-NAM 2018). Istanbul, Turkey, pp. 24–25.

Sasaki, N., Kuribayshi, S., Steamship Co, K., 2019, “Full Scale Performance of Gate Rudder.” London, UK.

Sato, T., Kim, K., Sasano, M., Okamoto, A., Inaba, S., Kondo, S., Matsumoto, H., Murashima, T., Fujiwara, T., Osawa, H., 2023, “Sea Trials of Multiple Heterogenous Cruising AUVs and ASV With Basic Formation Control,” in: 42nd International Conference on Ocean, Offshore and Arctic Engineering (OMAE 2023). American Society of Mechanical Engineers, Melbourne, Australia.

Sawada, R., Hirata, K., Kitagawa, Y., 2023, “Automatic Berthing Control under Wind Disturbances and Its Implementation in an Embedded System.” , Journal of Marine Science and Technology , Vol. 28, pp. 452–470.

Sawada, R., Hirata, K., Kitagawa, Y., Saito, E., Ueno, M., Tanizawa, K., Fukuto, J., 2021a, “Path Following Algorithm Application to Automatic Berthing Control.” , Journal of Marine Science and Technology , Vol. 26, pp. 541–554.

Sawada, R., Sato, K., Majima, T., 2021b, “Automatic Ship Collision Avoidance Using Deep Reinforcement Learning with LSTM in Continuous Action Spaces.” , Journal of Marine Science and Technology , Vol. 26, pp. 509–524.

Seo, C., Noh, Y., Abebe, M., Kang, Y.-J., Park, S., Kwon, C., 2023, “Ship Collision Avoidance Route Planning Using CRI-Based A∗ Algorithm.” , International Journal of Naval Architecture and Ocean Engineering , Vol. 15, pp. 100551.

Shen, Y.T., Jiang, C.W., Remmers, K.D., 1997, “A Twisted Rudder for Reduced Cavitation.” , Journal of Ship Research , Vol. 41, pp. 260–272.

Simonsen, C.D., Stern, F., Quadvlieg, F., Flensborg Otzen, J., 2014, “SIMMAN 2014 Workshop on Verification and Validation of Ship Manoeuvering Simulation Methods Copenhagen Workshop Proceedings.” Copenhagen December.

Sims, R., Schaeffer, R., Creutzig, F., Núnez, C.X., Agosto, D.M., Dimitriu, D., Figueroa Meza, M.J., Fulton, L., Kobayashi, S., Lah, O., 2014, “Transport Climate Change: Mitigation of Climate Change, Assessment Report of the Intergovernmental Panel on Climate Change.” Cambridge, UK; New York, NY, USA.

Skejic, R., Faltinsen, O.M., 2022, “Maneuvering of Submarines at Periscope Depths in a Seaway,” in: 15th International Symposium on Practical Design of Ships and Other Floating Structures (PRADS 2022). Dubrovnik, Croatia.

Stark, C., Xu, Y., Zhang, M., Yuan, Z., Tao, L., Shi, W., 2022, “Study on Applicability of Energy-Saving Devices to Hydrogen Fuel Cell-Powered Ships.” , Journal of Marine Science and Engineering , Vol. 10, pp. 388.

Stern, F., Sanada, Y., Park, S., Wang, Z., Yasukawa, H., Diez, M., Quadvlieg, F., Bedos, A., 2022, “Experimental and CFD Study of KCS Turning Circles in Waves,” in: 34th Symposium on Naval Hydrodynamics (SNH34). Washington, DC, USA.

Sui, C., de Vos, P., Hopman, H., Visser, K., Stapersma, D., Ding, Y., 2022, “Effects of Adverse Sea Conditions on Propulsion and Manoeuvring Performance of Low-Powered Ocean-Going Cargo Ship.” , Ocean Engineering , Vol. 254, pp. 111348.

Sukas, O.F., Kinaci, O.K., Bal, S., 2021, "Asymmetric Ship Maneuvering Due to Twisted Rudder Using System-Based and Direct CFD Approaches." , Applied Ocean Research , Vol. 108, pp. 102529.

Suzuki, R., Tsukada, Y., Ueno, M., 2023, "Effects of Steady Wave Forces on Course-Keeping Manoeuvres of Full- and Model-Scale Ships Moving Obliquely in Short Waves." , Ship Technology Research , Vol. 70, pp. 190–208.

Suzuki, R., Ueno, M., Tsukada, Y., 2021, "Numerical Simulation of 6-Degrees-of-Freedom Motions for a Manoeuvring Ship in Regular Waves." , Applied Ocean Research , Vol. 113, pp. 102732.

Tan, G., Zhuang, J., Zou, J., Wan, L., 2021, "Coordination Control for Multiple Unmanned Surface Vehicles Using Hybrid Behavior-Based Method." , Ocean Engineering , Vol. 232, pp. 109147.

The 29th ITTC Manoeuvring Committee, 2021, "The Manoeuvring Committee - Final Report and Recommendations to the 29th ITTC."

Thurman, C.S., Somero, J.R., 2022, "Hydrodynamic Characterization of Bodies of Revolution through Statistical-Empirical Prediction Modeling Using Machine Learning." , Journal of Ship Research , Vol. 66, pp. 182–191.

Tran, H.N., Nhut Pham, T.N., Choi, S.H., 2021, "Robust Depth Control of a Hybrid Autonomous Underwater Vehicle with Propeller Torque's Effect and Model Uncertainty." , Ocean Engineering , Vol. 220, pp. 108257.

Trials of MASS, 2020, "EMSA and European Commission 2020 EU Operational Guidelines for Trials of Maritime Autonomous Surface Ships (MASS)."

Uithof, K., Van Oossanen, P., Moerke, N., Van Oossanen, P.G., Zaaijer, K.S., 2014, "An Update on the Development of the Hull Vane," in: 9th International Conference on High-Performance Marine Vehicles (HIPER). Athens, Greece.

Vagale, A., Bye, R.T., Oucheikh, R., Osen, O.L., Fossen, T.I., 2021a, "Path Planning and Collision Avoidance for Autonomous Surface Vehicles II: A Comparative Study of Algorithms." , Journal of Marine Science and Technology , Vol. 26, pp. 1307–1323.

Vagale, A., Oucheikh, R., Bye, R.T., Osen, O.L., Fossen, T.I., 2021b, "Path Planning and Collision Avoidance for Autonomous Surface Vehicles I: A Review." , Journal of Marine Science and Technology , Vol. 26, pp. 1292–1306.

Van Zwijnsvoorde, T., Delefortrie, G., Lataire, E., 2022, "Passing Ship Effects in Shallow and Confined Water: Open Model Test Data for Validation Purposes," in: 66th Conference on Ship Manoeuvring in Shallow and Confined Water (MASHCON 2022). Glasgow, UK, pp. 254–283.

Verwilligen, J., Lataire, E., Ruiz, M.T., Eloot, K., 2022, "Evaluation of Bank Effects on a Bulk Carrier in a Confined Channel Based on Towing Tank Tests and Full-Scale Measurement," in: 6th Conference on Ship Manoeuvring in Shallow and Confined Water (MASHCON 2022). Glasgow, UK, pp. 284–298.

Wakita, K., Maki, A., Umeda, N., Miyauchi, Y., Shimoji, T., Rachman, D.M., Akimoto, Y., 2022, "On Neural Network Identification for Low-Speed Ship Maneuvering Model." , Journal of Marine Science and Technology , Vol. 27, pp. 772–785.

Wang, D., Shen, Y., Wan, J., Sha, Q., Li, G., Chen, G., He, B., 2022a, "Sliding Mode Heading Control for AUV Based on Continuous Hybrid Model-Free and Model-Based Reinforcement Learning." , Applied Ocean Research , Vol. 118, pp. 102960.

Wang, H., Fu, Z., Zhou, J., Fu, M., Ruan, L., 2021a, "Cooperative Collision Avoidance for Unmanned Surface Vehicles Based on Improved Genetic Algorithm." , Ocean Engineering , Vol. 222, pp. 108612.

Wang, H., Yin, Y., Jing, Q., Cao, Z., Shao, Z., Guo, D., 2024a, "Berthing Assistance System for Autonomous Surface Vehicles Based on 3D LiDAR." , Ocean Engineering , Vol. 291, pp. 116444.

Wang, J., Li, S., Li, B., Zhao, C., Cui, Y., 2023, "An Energy-Efficient Hierarchical Algorithm of Dynamic Obstacle Avoidance for Unmanned Surface Vehicle." , International Journal of Naval Architecture and Ocean Engineering , Vol. 15, pp. 100528.

Wang, L., Li, S., Liu, J., Wu, Q., 2022b, "Data-Driven Model Identification and Predictive Control for Path-Following of Underactuated Ships with Unknown Dynamics." , International Journal of Naval Architecture and Ocean Engineering , Vol. 14, pp. 100445.

Wang, S., Zhang, Y., Zheng, Y., 2021b, "Multi-Ship Encounter Situation Adaptive Understanding by Individual Navigation Intention Inference." , Ocean Engineering , Vol. 237, pp. 109612.

Wang, W., Huang, L., Liu, K., Zhou, Y., Yuan, Z., Xin, X., Wu, X., 2024b, "Ship Encounter Scenario Generation for Collision Avoidance Algorithm Testing Based on AIS Data." , Ocean Engineering , Vol. 291, pp. 116436.

Wei, K., Gao, X., Liu, D., Wei, F., Luo, P., 2022, "Numerical Calculation of Six Degree of Freedom Floating Motion of Submarine with Flow Holes." , Journal of Marine Science and Technology , Vol. 27, pp. 916–934.

Weng, Y., Matsuda, T., Sekimori, Y., Pajarinen, J., Peters, J., Maki, T., 2022, "Establishment of Line-of-Sight Optical Links between Autonomous Underwater Vehicles: Field Experiment and Performance Validation." , Applied Ocean Research , Vol. 129, pp. 103385.

White, P.F., Piro, D.J., Knight, B.G., Maki, K.J., 2022, "A Hybrid Numerical Framework for Simulation of Ships Maneuvering in Waves." , Journal of Ship Research , Vol. 66, pp. 159–171.

Wicaksono, A., Hashimoto, N., Takahashi, T., 2021, "Representation of Small Passenger Ferry Maneuvering Motions by Practical Modular Model." , International Journal of Naval Architecture and Ocean Engineering , Vol. 13, pp. 57–64.

Wu, G., Atilla, I., Tahsin, T., Terziev, M., Wang, L., 2021, "Long-Voyage Route Planning Method Based on Multi-Scale Visibility Graph for Autonomous Ships." , Ocean Engineering , Vol. 219, pp. 108242.

Xia, G., Zhang, Y., Zhang, W., Chen, X., Yang, H., 2021, "Multi-Time-Scale 3-D Coordinated Formation Control for Multi-Underactuated AUV with Uncertainties: Design and Stability Analysis Using Singular Perturbation Methods." , Ocean Engineering , Vol. 230, pp. 109053.

Yang, Y., Moctar, O. el, 2022, "Effects of Shallow Water on Added Mass," in: 6th Conference on Ship Manoeuvring in Shallow and Confined Water (MASHCON 2022). Glasgow, UK, pp. 299–309.

Yao, J., Liu, Z., Song, X., Su, Y., 2021, "Pure Low-Frequency and Pure High-Frequency Ship Motion Equations in Regular Waves." , Ocean Engineering , Vol. 233, pp. 109152.

Yasukawa, H., Faizul, A.A., 2006, "Experimental Study on Wave-Induced Motions and Steady Drift Forces of an Obliquely Moving Ship." , Journal of the Japan Society of Naval Architects and Ocean Engineers , Vol. 3, pp. 133–138.

Yasukawa, H., Fujiwara, R., Hirata, N., Tanaka, S., Matsuda, A., 2022, "Influence of Initial Disturbances on Ship Stopping Performance by Propeller Reverse Rotation." , Journal of Marine Science and Technology , Vol. 27, pp. 740–758.

Yasukawa, H., Himaya, A.N., Hirata, N., Matsuda, A., 2023, "Simulation Study of the Effect of Loading Condition Changes on the Maneuverability of a Container Ship." , Journal of Marine Science and Technology , Vol. 28, pp. 98–116.

Yasukawa, H., Ishikawa, T., Yoshimura, Y., 2021, "Investigation on the Rudder Force of a Ship in Large Drifting Conditions with the MMG Model." , Journal of Marine Science and Technology , Vol. 26, pp. 1078–1095.

Yu, J., Liu, L., Zhang, Z., Yao, C., Feng, D., Wang, X., 2022, "Numerical Investigation of Passing Ship Effects in Shallow and Confined Water Using Ship-HUST Code," in: 6th Conference on Ship Manoeuvring in Shallow and Confined Water (MASHCON 2022). pp. 310–318.

Yuan, X., Zhang, D., Zhang, J., Zhang, M., Guedes Soares, C., 2021, "A Novel Real-Time Collision Risk Awareness Method Based on Velocity Obstacle Considering Uncertainties in Ship Dynamics." , Ocean Engineering , Vol. 220, pp. 108436.

Zhang, G., Chen, J., Duan, W., 2022a, "Numerical Simulation of Ship Maneuverability in Irregular Waves Based on TEBEM Method," in: 14th International Conference on Hydrodynamics (ICHD 2022). Wuxi, China, pp. 64–72.

Zhang, G., Chu, S., Huang, J., Zhang, W., 2022b, "Robust Adaptive Fault-Tolerant Control for Unmanned Surface Vehicle via the Multiplied Event-Triggered Mechanism." , Ocean Engineering , Vol. 249, pp. 110755.

Zhang, G., Yu, W., Li, J., Zhang, X., 2021a, "A Novel Event-Triggered Robust Neural Formation Control for USVs with the Optimized Leader–Follower Structure." , Ocean Engineering , Vol. 235, pp. 109390.

Zhang, J., Guo, Z., Zhang, Q., Shang, Y., Zhang, L., 2023, "Turning and Zigzag Maneuverability Investigations on a Waterjet-Propelled Trimaran in Calm and Wavy Water Using a Direct CFD Approach." , Ocean Engineering , Vol. 286, pp. 115511.

Zhang, J., Xiang, X., Lapierre, L., Zhang, Q., Li, W., 2021b, "Approach-Angle-Based Three-Dimensional Indirect Adaptive Fuzzy Path Following of under-Actuated AUV with Input Saturation." , Applied Ocean Research , Vol. 107, pp. 102486.

Zhang, M., Hao, S., Wu, D., Chen, M.-L., Yuan, Z.-M., 2022c, "Time-Optimal Obstacle Avoidance of Autonomous Ship Based on Nonlinear Model Predictive Control." , Ocean Engineering , Vol. 266, pp. 112591.

Zhang, M., Kim, D., Tezdogan, T., Yuan, Z.-M., 2024a, "Time-Optimal Control of Ship Manoeuvring under Wave Loads." , Ocean Engineering , Vol. 293, pp. 116627.

Zhang, W., Cheng, J., Li, X., He, G., 2022d, "Comparative Study on Predicting Ship Maneuvering in Waves Using a Quasi-Steady Method and a Time Domain Approach." , Journal of Ship Research , Vol. 66, pp. 204–218.

Zhang, Y., Zhang, T., Li, Y., Zhuang, Y., 2024b, "Tracking Control of AUV via Novel Soft Actor-Critic and Suboptimal Demonstrations." , Ocean Engineering , Vol. 293, pp. 116540.

Zhang, Y., Zhang, Z., Quan, Z., Liu, G., 2021c, "Hydrodynamic Performance and Calculation of Lift–Drag Ratio on Underwater Glider." , Journal of Marine Science and Technology , Vol. 26, pp. 16–23.

Zhang, Z., Xu, Y., Wan, L., Chen, G., Cao, Y., 2024c, "Rotation Matrix-Based Finite-Time Trajectory Tracking Control of AUV with Output Constraints and Input Quantization." , Ocean Engineering , Vol. 293, pp. 116570.

Zheng, Y., Tao, J., Sun, Q., Sun, H., Chen, Z., Sun, M., Xie, G., 2022a, "Soft Actor–Critic Based Active Disturbance Rejection Path Following Control for Unmanned Surface Vessel under Wind and Wave Disturbances." , Ocean Engineering , Vol. 247, pp. 110631.

Zheng, Z.-Q., Zou, L., Zou, Z.-J., 2022b, "A Numerical Investigation on the Ship-Ship Interaction Between a Passing Ship and a Moored Ship in Restricted Waterways," in: 6th Conference on Ship

Manoeuvring in Shallow and Confined Water (MASHCON 2022). Glasgow, UK, pp. 344–355.

Zhu, Q., Shang, H., Lu, X., Chen, Y., 2024, "Adaptive Sliding Mode Tracking Control of Underwater Vehicle-Manipulator Systems Considering Dynamic Disturbance." , Ocean Engineering , Vol. 291, pp. 116300.

Zhu, Z., Kim, Y., 2023, "CFD Analysis of Oblique Towing Test and Circular Motion Test for KCS Model," in: 3rd Workshop on Verification and Validation of Ship Manoeuvring Simulation Methods (SIMMAN 2020). Incheon, South Korea, pp. 88–92.

ITTC2024
30TH INTERNATIONAL TOWING TANK CONFERENCE
22–27 SEPTEMBER 2024 | HOBART TASMANIA AUSTRALIA

REPORT OF THE SEAKEEPING COMMITTEE

SEAKEEPING COMMITTEE

1. INTRODUCTION

1.1 Membership and meetings

The Committee appointed by the 29th ITTC consisted of the following members:

- Frederik Gerhardt (Chairman), RISE, Gothenburg, Sweden;
- Ole Andreas Hermundstad (Secretary), SINTEF Ocean, Trondheim, Norway;
- Benjamin Bouscasse, École Centrale de Nantes (ECN), Nantes, France;
- Kay Domke, Schiffbau Versuchsanstalt Potsdam (SVA), Potsdam, Germany;
- WenYang Duan, Harbin Engineering University (HEU), Harbin, China;
- Bertrand Malas, École Centrale de Nantes (ECN), Nantes, France;
- Munehiko Minoura, Osaka University, Osaka, Japan;
- Bo Woo Nam, Seoul National University, Seoul, Korea;
- Yulin Pan, University of Michigan, Ann Arbor, USA;
- Antonio Souto-Iglesias, Universidad Politécnica de Madrid (UPM), Madrid, Spain.

Two in-person meetings were held:

- SSPA Maritime Center, Gothenburg, Sweden, June 2023
- Escuela Técnica Superior de Ingenieros Navales (ETSIN), Madrid, January 2024

In addition, 12 video teleconferences were held in the time-period of November 2021 to June 2024.

1.2 Terms of Reference given by the 29th ITTC

The Seakeeping Committee is primarily concerned with the behaviour of ships underway in waves. The Ocean Engineering Committee covers moored and dynamically positioned ships. For the 30th ITTC, the modelling and simulation of waves, wind and current is the primary responsibility of the Specialist Committee on Modelling of Environmental Conditions, with the cooperation of the Ocean Engineering, the Seakeeping and the Stability in Waves Committees.

1. Update the state-of-the-art for predicting the behaviour of ships in waves, emphasizing developments since the 2021 ITTC Conference. The committee report should include sections on:
   - the potential impact of new technological developments on the ITTC new experiment techniques and extrapolation methods
   - new benchmark data

- the practical applications of numerical simulation to seakeeping predictions and correlation to full scale
- the need for R&D for improving methods of model experiments, numerical modelling and full-scale measurements.

2. Review ITTC Recommended Procedures relevant to seakeeping procedures, and
   - identify any requirements for changes in the light of current practice, and, if approved by the Advisory Council, update them
   - identify the need for new procedures and outline the purpose and contents of these.
3. Create a new guideline on verification and validation of the CFD methods for seakeeping analysis. For example, finite-volume-based methods and particle methods which solve RANS and LES, for seakeeping procedures, collaborating with the Specialist Committee on Combined CFD/EFD Methods and taking existing procedures for verification and validation of CFD methods into account.
4. Investigate the functionality of Procedure 7.5-02-07-02.8, Calculation of the Weather Factor *fw*, when applied to ships smaller than 150 m in length, and provide any method to improve the current procedure for small ships.
5. Investigate if there is any practical problem in the application of MEPC.1/Circ.850/ Rev.2 for minimum power requirement, and develop a new ITTC guideline, if needed.
6. Develop a guideline for wind loads for ships, collaborating with the committees related to this issue, particularly the Ocean Engineering Committee, the SC on Renewable Ocean Energy, Manoeuvring Committee and the Full-Scale Performance Committee.
7. Organize a benchmark experimental campaign, including the added resistance measurement in oblique seas and different loading conditions, and the characterization of the uncertainty in the measurement of added resistance.
8. Survey the state of the art for the acquisition and analysis in on-board and/or real-time seakeeping data, and investigate the need of ITTC activities, including future issues related to autonomous vessels.
9. Collaborate with Manoeuvring Committee for the development of guidelines related to manoeuvring in waves.

2. STATE OF THE ART

2.1 New Experimental Facilities

2.1.1 Boldrewood Towing Tank, Southampton

The University of Southampton Boldrewood Towing Tank became fully operational in February 2022, as reported by Malas et al. (2024). The tank, which is used for teaching, research and commercial activities, is 138 m long, 6 m wide and 3.5 m deep and equipped with a 12 paddle HR Wallingford wavemaker capable of generating regular and irregular waves with a maximum height of 0.70 m and a significant wave height of 0.37 m respectively. It also has the capability of generating oblique waves and to run in active absorption mode.

The tank carriage is driven by two winches and two cables located at both ends of the facility and is capable of speeds up to 10 m/s and 8 m/s in the East/West and West/East directions respectively.

The tank is also equipped with a parabolic end beach for waves absorption and an automatic side beach that can be deployed within seconds after pressing the on/off button on the side of the tank or on the carriage. The side beach is left deployed for calm water experiments and is deployed and retracted between seakeeping runs to reduce the waiting time and therefore increase the facility productivity.

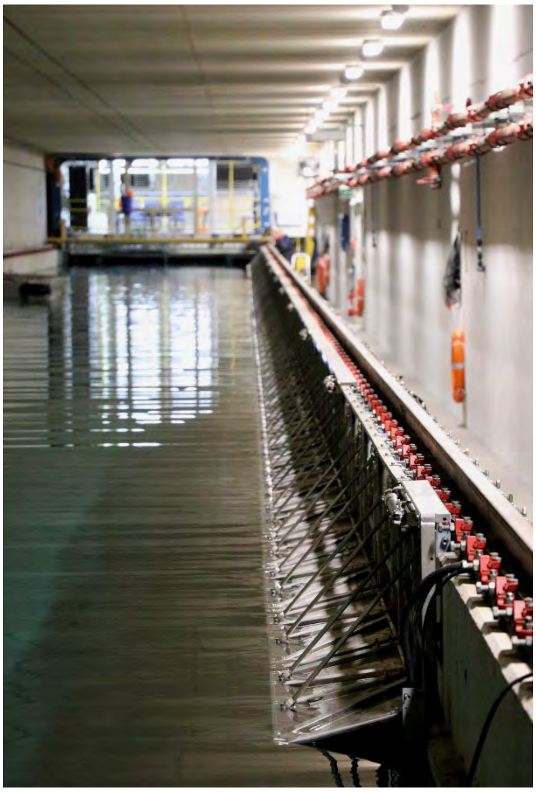

Figure 1: View of the deployed automatic side beach at Boldrewood towing tank (Malas et al. 2024).

The facility is also equipped with an underwater 500 kg lifting platform located at 10 m from the wavemaker. This can be used for static moored experiments where the quality of waves is best and available experimental time is optimum.

2.1.2 Coastal and Ocean Basin (COB), Ostend

The basin, part of the Flanders Maritime Laboratory in Ostend, and with ties to Ghent University, was fully commissioned in 2023. The facility is 30x30 m, with a variable water depth ranging from 0 to 1. 4 m. A 4 m deep central pit is also present. The facility is equipped with a 20x20 m Van Halteren L-shaped piston wavemaker capable of generating waves up to 0.55 m in multiple directions. On the opposite sides are located rock-based absorption beaches. A current generation system is also scheduled to be installed, with a speed up to 0.4 m/s.

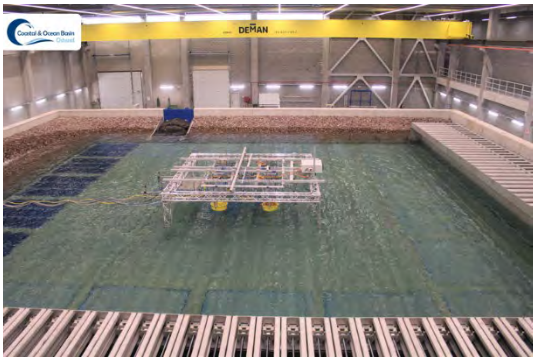

Figure 2: View of the COB (https://www.ugent.be/ea/civil-engineering/en/research/coastal-bridges-roads/coastal-engineering/cob-ugent/wecfarm-1).

2.1.3 Technology Centre for Offshore and Marine (TCOMS), Singapore

The TCOMS large ocean basin was open in July 2022. The basin is 60x48 m with a depth of 12 m and a 10 m diameter central pit reaching a depth of 50 m. The facility is equipped with 180 flaps L-shaped Edinburgh Design wavemaker on two sides, capable of generating waves up to 1.0 m. On the other sides are located deployable absorption beaches. An X/Y instrumented carriage is also present. This carriage can reach speeds up to 2 m/s and 4 m/s in the longitudinal and transverse directions respectively. A current generation system can produce six layers of inflow with maximum near surface current of 0.5 m/s and has the capability to produce variable current profiles such as uniform and shear currents. The water depth of the basin can be varied from 0 to 12 m, as required based on the test set-up to cater to deep-water or shallow-water studies, by adjusting the elevation of the movable floor.

Figure 3: View of the TCOMS ocean basin (https://news.nus.edu.sg/tcoms-opens-ocean-basin-facility/).

2.1.4 Virginia Tech Towing Tank

The Virginia Tech towing tank was commissioned in the 1960s. The facility is 30 m long, 1.8 m wide and 2.7 m deep. As reported by Gilbert et al. (2023), the original Kempf and Remmers carriage was recently replaced by a modern one supplied by Edinburgh Design with the support of Donald L. Blount Associates. The new carriage is driven by electric motors and belts and is capable of a maximum speed of 7.0 m/s (compared to the original 3.0 m/s).

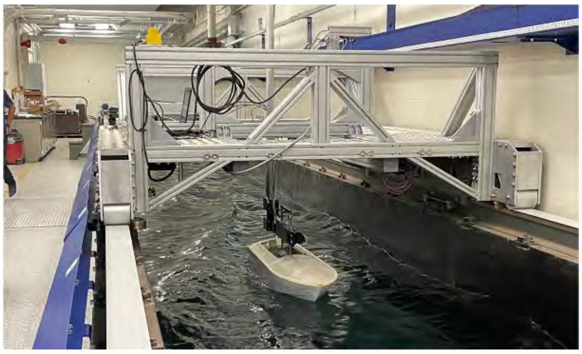

Figure 4: View of the new towing carriage at Virginia Tech (Gilbert et al. 2023).

Comparative resistance experiments were performed against past experiments and showed that measured resistance, heave and pitch are higher than previous results. Investigations are ongoing.

A Vertical Planar Motion Mechanism (VPMM) is planned to be installed allowing to perform controlled slamming as well as vertical motions manoeuvring experiments. The facility wavemaker is also anticipated to be replaced in the coming years.

2.1.5 CSSRC Seakeeping and Manoeuvrability Basin

The new Seakeeping and Manoeuvring Basin (SMB) at CSSRC was opened in late 2021, Figure 5. With dimensions of 170×47×6 m (length × width × water depth), it is typically used for manoeuvring and seakeeping tests. The carriage spanning the basin can move in the X direction at a maximum speed of 5.0 m/s and in the Y direction at a maximum speed of 4.0 m/s. The basin is equipped with flap-type wave makers along two adjacent sides and adjustable wave-absorbing beaches along the two opposite sides. Regular waves can be generated with periods ranging from 0.5 to 5.0 seconds and a maximum wave height of 0.58 m, while irregular waves can reach a significant wave height of 0.45 m.

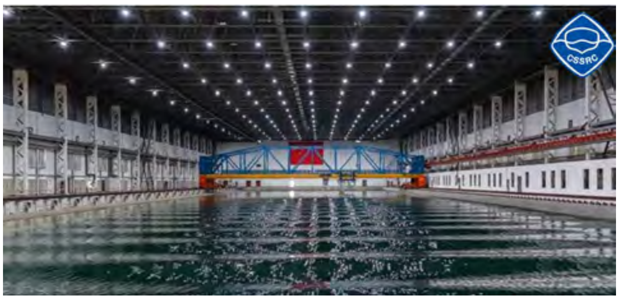

Figure 5: V The new Seakeeping and Manoeuvring Basin at CSSRC (Photo: CSSRC).

2.2 Experimental Techniques

2.2.1 Measurement of roll motion

Subramaniam et al. (2021) investigated trapped deck water and its effect on the roll dynamics of an offshore supply vessel by free-running model tests. The test setup combines measurements with pressure sensors and of motions by an optical fibre gyroscope. Additionally, cameras were used to monitor the deck water motion. The pressure sensor and camera setup is shown in Figure 6. Roll damping is evaluated by determining the phase difference between the ship roll and the deck water motion. Therefore, frequency-domain analysis is best suited for irregular wave situations, where the spectra of the signals from the gyroscope and the pressure sensors are compared to identify the phase relationship between peaks in the spectrum. The analysis of the ship roll and deck water motion points to damping within the operational speed range in regular as well as irregular waves. Furthermore, the investigations show that at higher Froude numbers the positive damping effect is reduced.

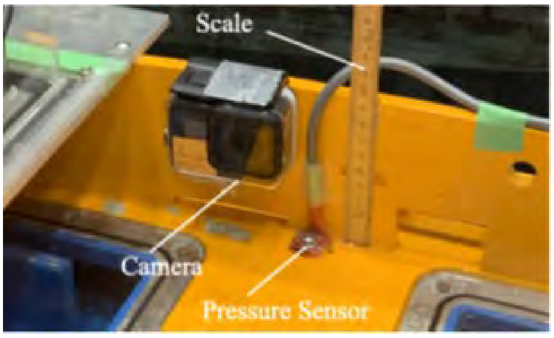

Figure 6: Arrangement of the pressure sensor and camera (Subramaniam et al. 2021).

Wang et al. (2023d) investigated the sloshing effect at model scale tests by a large LNG carrier model outfitted with three partially filled prismatic tanks. They analysed sloshing behaviour and model motions for different equal filling levels as well as different filling levels inside the tanks at different exciting wave periods. The roll, pitch and heave motions were measured by an attitude and heading reference system with 50 Hz and an error tolerance of 0.04° in normal temperature. It is pointed out that using different tank fillings at the same time will lead to a strong reduction in roll amplitude especially at the roll natural period of the ship motion. This effect is caused by one more natural period of sloshing inside the tanks.

For investigating extremes on a floating hinged raft wave energy converter Jin et al. (2022) used the application of short design waves. A 1:50 scale two-body hinged raft wave energy converter model was built. The test setup is presented in Figure 7. The main objective of measuring the relative hinge angle was demonstrating the application of short design wave on the floating structure. This was measured with a rotary sensor. The aim was to investigate four types of short design waves experimentally. They pointed out that response conditioned design waves have a good performance for generating extremes on a floating structure and that the setup used is suitable for further investigations.

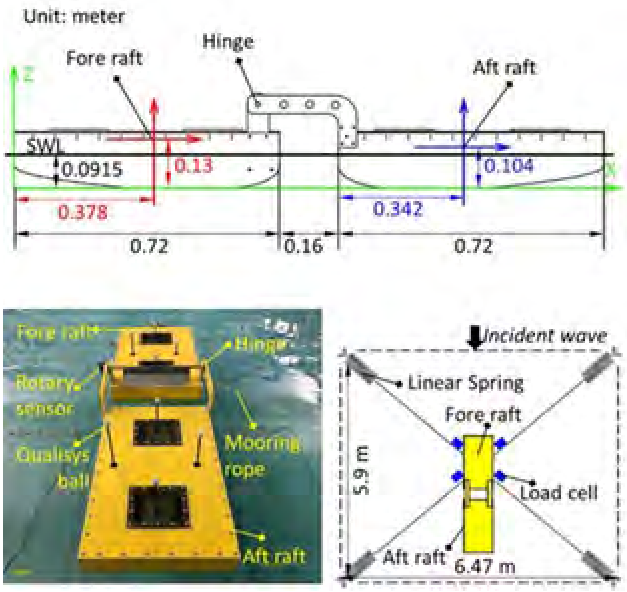

Figure 7: Test setup and arrangement for investigations on a wave energy converter (Jin et al. (2022).

2.2.2 Instrumentation, measurement technologies and machine learning support

Suzuki et al. (2023) developed a method for measuring and analysing the spatial pressure distribution over the ship-hull surface using many Fibre Bragg Grating (FBG) pressure sensors to obtain experimental data on the details of the flow induced by the ship disturbance. In their work they analysed the improvements installed in version 7 of the sensor, which are increase of rigidity of the ring frame, the installation of a stainless steel-frame on the diaphragm and the adoption of the glass soldering method at both ends of the optical fibres in the pressure sensitive part. FBG is a diffraction grating embedded into a fibre core that reflects a particular wavelength of light. The reflected wavelength is called the Bragg wavelength. Deformation resulting from pressure leads to spacing between the reflectors and so the Bragg wavelength changes, too. The amount of change in this Bragg wavelength is used to estimate the pressure. The principle of FBG and of the FBG pressure sensor is shown in Figure 8. The authors have shown that version 7 of the FBG pressure sensors was significantly improved in respect to temperature interference effects compared to version 6. Furthermore, they showed that the effect of temperature interference depends on the material of the ship model and recommend material with low thermal conductivity. It was also pointed out that the measurement accuracy of steady pressures is not as good as that of the strain-type pressure sensor due to the sensor thickness.

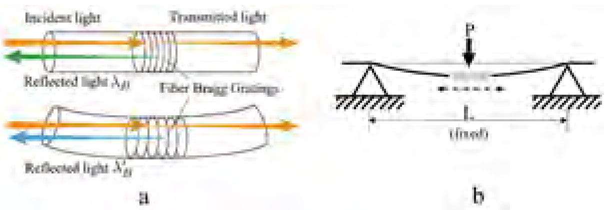

Figure 8: Schematic representation of a) Principle of FBG, b) Principle of the FBG pressure sensor used by Suzuki et al. (2023).

Ma et al. (2023) measured and illustrated the wet deck slamming for a SWATH cross-section model using PIV and pressure measurements. The instrumentation with a sampling frequency of 20 kHz at overall 15 positions and 3 different kind of pressure sensors regarding the measurement range as well as 1 kHz PIV measurement with adjustable camera exposure time was used. The measurement was started by a trigger impulse-based release of the model, which was held by a steel truss attachment at the model and an electromagnet. The analysis of three initial water-entry velocities focused on the fluid field, slamming pressure, and air cushion effect during the wet deck slamming.

For the investigation of turning circles in waves, Stern et al. (2022) analysed CFD and experimental data. For a detailed comparison of the investigated tuning circles, they introduced a transformation which uses the wave drift distance H_D and direction μ_D. This leads to a collapse of the trajectories onto a single circle.

The application of Machine Learning (ML) and Artificial Intelligence (AI) techniques has recently become a contentious issue. Current publications show promising application possibilities and only hint at the extent to which their influence will increase in the upcoming years.

Nielsen et al. (2023) used ML-based methods to explore and determine the relation between waves and wave-induced ship responses entirely through data. This method was compared to an experimental physics-based data evaluation. The advantage of the ML-method is that transfer functions are not needed, and all associated uncertainties are thus removed. On the other hand, the data input values need to be as good as possible which requires very high-quality sensors. The authors present a good correlation between ML and physics-based method. Furthermore, they show that ML-based methods have wide and large potential but the complexity of the system being considered makes the use of ML delicate, and the generalisation of the results must be made with care. As part of the problem, the quality of ship telemetry data is low. A fallback framework is recommended from the actual point of view.

2.2.3 Hydroelastic ship models and structural loads

Kim et al. (2023b) investigated the influence of mooring lines at an experimental setup with a 9-segmented model in -120° oblique regular waves without forward speed. Experiments with and without a mooring system under the same wave condition were conducted; see Figure 9. They qualitatively confirmed that the mooring system's restoring moment correlates with the asymmetric horizontal bending moment and average yaw movement change.

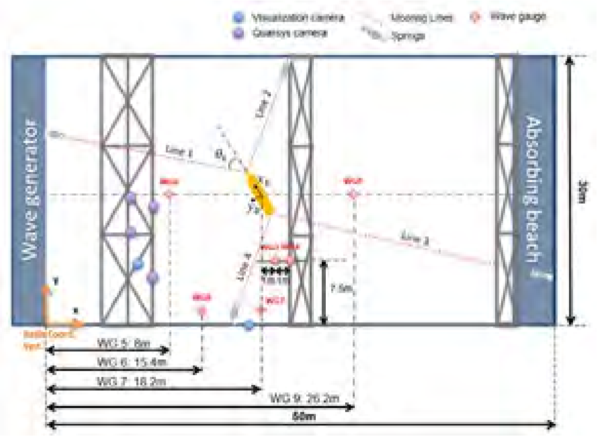

Figure 9: Experimental setup for segmented model tests with mooring lines used by Kim et al. (2023b).

Tang et al. (2022) used a segmented model with the backbone of an ultra large container ship over 300 m. They presented the design and calibration procedure of the segmented ship model with a variable cross-section backbone beam. They introduced the application and the conversion from the signals of strain to the bending moments by calibration. With the setup they investigated the transfer function of vertical bending moments at different Froude numbers and wave headings as well as analysing phase differences between wave frequency and high-order harmonics in extreme waves.

2.3 Numerical Methods

The research of recent years numerical methods on ship seakeeping can be divided into three aspects. The potential flow numerical method, viscous flow numerical method and potential flow viscous flow coupled numerical method.

2.3.1 The Potential flow numerical method

2.3.1.1 Linear free surface potential flow BEM method

The boundary element method (BEM) based on the potential flow theory is the main computational method to linear free surface ship seakeeping problem.

Chen et al. (2021a) proposed a three-dimensional unsteady potential flow numerical method to solve the seakeeping of ships in waves. The flow field is divided into inner and outer regions by artificial matching surface. The inner domain includes the wet body surface, the matching surface and the free surface of the inner region near ship; The outer region includes matching surface, outer region free surface and far field boundary. Using impulse response function, the boundary integral equation of the inner and outer domains is established and solved by Taylor expansion boundary element method (TEBEM). The hydrodynamic coefficients of different ships at different forward speeds are calculated, and the accuracy of the numerical results is verified by the experimental data. TEBEM method has also been used to study propeller propulsion performance in waves. Duan et al. (2022a) proposed a fast and effective calculation method for predicting ship speed and power in head waves based on TEBEM.

Song et al. (2022) developed a 3D time-domain desingularized Rankine panel (DRP) method based on near-field and mid field theories to calculate the wave added resistance of ships in regular waves. By comparing with experimental data, it is shown that the numerical method can accurately calculate the ship wave added resistance.

Li et al. (2023b) established a numerical model of multi-ship hydrodynamic interaction in waves based on the Rankine source element method in the time domain. He et al. (2023) proposed a set of boundary integral methods for wave diffraction-radiation problems applicable to offshore structures or ships sailing in regular waves. It can effectively calculate the influence coefficients in the Rankine source and Fourier component.

Zhang et al. (2023c) established a three-dimensional frequency domain seakeeping calculation model based on Rankine surface element method and calculated the wave drift force and moment acting on a ship with forward speed. Chen et al. (2022) proposed a numerical simulation method for the hydroelastic response of very large floating structures (VLFS) in focused waves. The modal expansion method is used to decouple the fluid-structure coupling problem. The high order boundary element method for the fluid dynamics problem is solved in the frequency domain and a finite element model is used for the structural analysis.

Lu et al. (2023) proposed a time-domain hydroelastic analysis method considering the asymmetric slamming on ships and adopted the three-dimensional Rankine surface element method to solve the problem of ship seakeeping, and the modified Logvinovich model (MLM) is used to calculate the asymmetric slam load of a 21000 TEU container ship.

2.3.1.2 Nonlinear potential flow numerical method

When the incident wave is highly nonlinear, it is necessary to develop the corresponding nonlinear potential flow calculation method to calculate the motion response more accurately.

Tang et al. (2021b) calculated the motion characteristics of container ships in irregular waves based on the fully nonlinear time-domain potential flow theory. Lin et al. (2021) established a fully nonlinear potential flow (FNPF) numerical model to simulate nonlinear water wave interaction problems. Wang et al. (2021a) simulated irregular sea waves with different breaking strength based on the FNPF program. Irannezhad et al. (2022) calculated ship motion response and resistance based on FNPF. The ship motion characteristics near resonant frequencies in waves are studied.

Liang et al. (2023) established a two-dimensional fully nonlinear numerical wave tank based on the higher-order boundary element method. The second order harmonic displacement of large-scale elastic plate near the second order natural frequency is calculated. Zhang et al. (2023b) developed a fully nonlinear potential flow theory based on the Rankine source method to calculate the motion response and wave added resistance of ships. By calculating the radiation, diffraction and motion responses of Wigley hull and S-175 container ship, it is shown that the fully nonlinear method can better predict the peak of ship motion response and wave added resistance.

In the calculation of potential flow problem, the singularity at the corner of the body surface will lead to the wrong pressure integral. In nonlinear potential flow problems, the singularity occurs at corner points for the higher order derivatives. Qian and Teng (2023) proposed a coupling method combining scaled boundary finite element method (SBFEM) and finite element method (FEM) to solve this problem. SBFEM can provide an accurate and effective direct pressure integral for second-order wave forces.

Hanssen and Greco (2021) propose a fully nonlinear numerical method based on potential flow theory to study the two-dimensional interaction between water waves and body. The velocity potential and its time derivatives are calculated by solving Laplace equation with Harmonic Polynomial Cell (HPC) method. At the same time, it uses the immersion boundary method to simulate moving boundaries. The method is verified and analysed for wave propagation, forced heave motion of semi-submersible cylinders, and stationary and free-moving floating bodies in beam waves.

Xu et al. (2023b) developed a fully nonlinear potential flow solver based on high order finite difference to calculate nonlinear wave loads on ocean structures. All boundary conditions were treated by immersion boundary method. The nonlinear wave load on a cylinder with forced heave motion on the water surface is analysed.

Takami et al. (2023) combined the HOS (High-Order Spectral) method with the first-order Reliability method (FORM) and applied it to the prediction of the linear and nonlinear wave response of ships in nonlinear waves. Chen et al. (2023a) used a HOS method coupled with a fully nonlinear hydrodynamic solver (HOS-FNL) to simulate the interaction between waves and structures in nonlinear waves.

Shi and Zhu (2023) proposed a nonlinear time-domain simulation method. In this method, the overlapping grid method is used to track the ship motion. The hydrodynamic characteristics of Wigley and Series 60 sailing at different speeds were calculated. Zhang et al. (2024) studied the motion response and wave loads on semi-submersible platforms under different wave steepness by using a fully nonlinear potential flow calculation method.

2.3.2 The viscous flow numerical method

2.3.2.1 Free surface flow algorithm

For the seakeeping problem, how to accurately and effectively capture the water-gas interface with a large density ratio, especially the interaction between strong nonlinear waves and ships involves complex physical phenomena such as wave slamming and breaking, and droplet splashing, are the difficulty of viscous flow numerical method research problem.

Li et al. (2022a) used the hybrid method of THINC/QQ-SF and HRIC to capture the details of wave breaking around a forward speed ship. This method can calculate ship resistance with less numerical dissipation.

Ferro et al. (2022) developed a solver (MarineFOAM) that combines the VOF method with the Ghost Cell method to deal with the discontinuity of the free surface. It is shown that this method can be used for larger Courant number in numerical simulation, while avoiding the free surface oscillation.

Chatzimarkou et al. (2022) proposed the coupled Level-set and VOF method (CLSVOF). The VOF method is used to track and reconstruct the free surface, which guarantees the conservation of mass. At the same time, Level Set function is used to calculate the geometric parameters (normal vector, curvature, etc.) of the free surface, so that the surface tension can be calculated accurately. The free surface turbulence damping (FSTD) boundary conditions are added to limit the overprediction of turbulence near the free surface. Simulations of wave breaking are in good agreement with experimental results. Chen and Chen (2023) improved CLSVOF to solve the problem of non-uniform interface on the boundary. It is shown that the improved method can better simulate the green water and droplets splashing phenomena.

Meshless methods are based on Lagrange description, which is very suitable for dealing with large deformation problems. The movement of particles along with the interface makes it possible to automatically track the multiphase interface. The advantage is that it can accurately capture the droplet phenomenon caused by breaking waves. Zhong et al. (2023) show that an SPH method can accurately calculate the hydrodynamic characteristics of a ship hull and can better track droplet splash details. Salis et al. (2024) studied the dynamic interaction between focused waves and mooring and structural based on a three-dimensional SPH method coupled with multi-body solvers.

To improve computational efficiency of the SPH method, Liu et al. (2023a) proposed a coupling algorithm based on SPH and finite difference. Through the calculation domain decomposition, the near field adopts SPH method to simulate the flow with severe deformation of the free surface, while the far field adopts the finite difference method to reduce the calculation load of SPH and increase its calculation efficiency. The Euler solution and Lagrange solution are coupled to each other by interpolating in the near and far field overlapping region. The algorithm has good accuracy, convergence and applicability. Di Mascio et al. (2021) conducted a three-dimensional simulation based on the coupling of SPH and finite volume method, for ship's bow waves breaking.

Zhang et al. (2021c) developed an ISPH_QSFDI solver based on the second order semi-analytic finite difference interpolation scheme (QSFDI) to discrete Laplacian operator and applied it to the simulation of wave propagation and wave impact on structures. The results show that ISPH_QSFDI is more accurate and requires less computation time compared to alternative schemes but at slower convergence. Zhang et al. (2023a) combined convolutional neural network (CNN) with ISPH method to calculate fluid pressure without solving Poisson equation. Through the parameter training, the calculation results show that the solver can maintain high calculation accuracy with large particle number.

Chen et al. (2024) proposed an adaptive SPH algorithm based on multi-GPU acceleration. Through a series of optimization algorithms, the computational efficiency of SPH method in multi-GPU parallel computing is improved.

2.3.2.2 Fluid structure interaction

Ship hydroelasticity simulation by coupling the viscous flow numerical algorithm with the finite element analysis method is the typical fluid structure interaction problem in seakeeping research.

Jiao et al. (2021a, 2021b) and Wei et al. (2023) proposed a CFD and FEA two-way coupling numerical method for calculating the nonlinear hydroelasticity response of ships sailing in waves. The external fluid pressure derived from the CFD simulation is used to calculate the structural response in the FEA structure solver, while the structural deformation is transferred to the CFD solver to deform the mesh. By calculating the hydrodynamic characteristics of the container ship S175, it is shown that the coupling method can accurately simulate seakeeping and hydroelasticity characteristics.

2.3.3 Potential flow and viscous flow coupled numerical method

The advantage of the potential flow method is that the calculation speed is fast. However, the effect of fluid viscosity is ignored in the potential flow formulation, so the computational accuracy for seakeeping problem is limited. The viscous flow numerical method can simulate the real flow field environment considering viscosity, and the calculation accuracy is high. But the computing speed is slow.

Therefore, the potential flow and viscous flow coupled numerical method has been developed in recent years. The coupling of potential flow and viscous flow algorithm expands the engineering application range of potential flow algorithm, saves more computing resources and speeds up the calculation compared with viscous flow algorithm.

Li et al. (2021) investigated SWENSE (Spectral Wave Explicit Navier-Stokes Equations) method which was coupled with HOS method through wave velocity decomposition in OpenFOAM and applied to the numerical simulation of wave-structure interaction. Zhang et al. (2021d) used SWENSE method to study the wave added resistance and seakeeping of KVLCC2. The calculation results show that this method can predict the wave added resistance and seakeeping of ships in irregular waves. Yu et al. (2023b) developed a new solver, HUST-SWENSE, which uses dynamic structure grid superposition technology to deal with four-DoF motion of ship. The motion of surge, heave, roll and pitch of KCS ship in regular oblique waves are numerically simulated.

Zhuang and Wan (2021) proposed a method by coupling the potential flow HOS method with the viscous flow solvers naoe-FOAM-SJTU. The parameters of nonlinear wave propagation are studied, and the wave response of an LNG ship is solved. Also based on the coupling of HOS and SPH, Xie et al. (2023) proposed a new algorithm for solving the strong nonlinear wave-structure interaction. This method combines the advantages of the HOS method to generate nonlinear waves and the SPH method to solve strong nonlinear free surface problems. The accuracy of the coupling method is verified by comparing the numerical simulation and experimental results of regular and irregular waves. The results show that the coupling method can effectively improve the calculation efficiency and greatly reduce the numerical dissipation.

Lu et al. (2022a) developed a fully nonlinear near-far-field coupling solver for the wave-body interaction problem. The GPU-based HOS solver is used to simulate the wide range of far-field wave propagation and its interaction with the flow field, while the incompressible flow field solver based on OpenFOAM are used in the near-field to solve the nonlinear wave load and motion response of the hull. The calculation accuracy and reliability of the solver are verified by the simulation of ship seakeeping problem.

Saincher and Sriram (2022) propose a new one-way coupling solver by combining a three-dimensional fully nonlinear potential flow solver with a viscous flow CFD solver, and apply it to solving the interaction between a focused wave and a fixed and moving cylinder. Based on the one-way coupling method, Dempwolff et al. (2024) developed a new potential-viscous flow coupling solver. The shallow-water-equation (SWE) solver REEF3D::SFLOW was coupled with the RANS viscous flow CFD solver REEF3D::CFD, and its calculation accuracy was verified.

Zhao et al. (2022) proposed a new velocity decomposition method (VDM) where the potential flow velocity is calculated by solving the Laplace equation without considering the influence of the free surface, while the remaining non-potential flow velocity is determined by OpenFOAM for the complementary Navier-Stokes equation. Zhong et al. (2022) developed a potential-viscos flow two-way coupling algorithm solver based on the open-source software package OceanWave 3D through the region decomposition method. By simulating different types of wave propagation, the validity of the coupling process in bidirectional data transmission is proved, and the accuracy and computational efficiency of the model are verified.

2.4 Rarely Occurring Events

Rarely occurring events for ships can generally be divided into three categories: (1) slamming, with the hull (bow, bottom or stern) of the vessel impacting onto the wave surface, (2) green water events, where a mass of water flows onto the deck, possibly impacting on the superstructure or cargo and (3) emergence events of propellers or other equipment, sometimes associated with ventilation. Other rarely occurring events, related to dynamic stability are the topic of the Stability in Waves Committee and not included here.

2.4.1 Water entry

Water impact problems of wedge type shapes are often considered as a basic model for bow and stern slamming or flat plates for bottom slamming or green water impact problems. Studies can be experimental, looking into two- or three-dimensional impacts at model scale, or numerical, with methods ranging from semi-empirical and analytical, incompressible (potential flow and Euler methods) to fully compressible and two-phase CFD approaches.

2.4.1.1 Experimental

Subramaniam et al. (2021) investigated trapped deck water and its effect on the roll dynamics of an offshore supply vessel by free-running model experiments. They measured the water pressure and observed the water motions on deck by camera. The presence of roll damping is evaluated by determining the phase difference between the ship roll and the deck water motion. The analysis of the ship roll and deck water motion points to damping within the operational speed range in regular as well as in irregular waves. Furthermore, the investigations show that at higher Froud numbers the positive damping effect is reduced. For astern wave conditions a positive damping effect of deck water motion was observed.

Hasheminasab et al. (2022) investigated the effect of adding a spray rail on a catamaran section model with a centre bow on the slamming pressures recorded during water entry, Figure 10. Pressure transducers were placed at three locations on the model and three water entry speeds were considered. The results show that the addition of the spray rail provides a 60% reduction in peak acceleration and 70% reduction in peak pressure. The effects of air entrapment are also discussed.

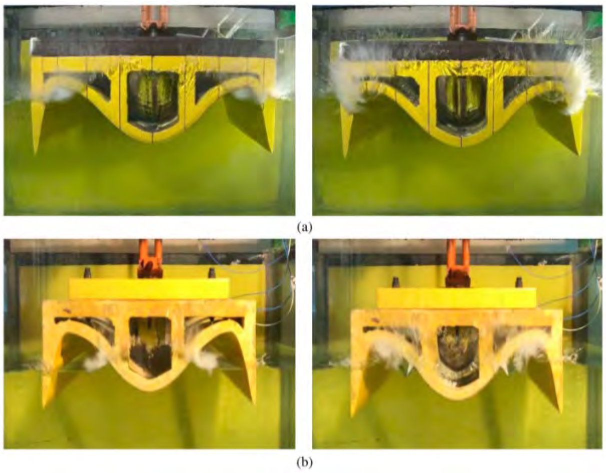

Figure 10: Effect of a spray rail on the water entry of a catamaran section model with a centre bow from Hasheminasab et al. (2022).

Liu et al. (2023b), Figure 11, developed a novel fluid–structure interaction (FSI) scheme based on the immersed boundary method to numerically investigate the high—speed water entry of different projectiles. This method allows to suppress the non-physical force oscillation and also uses a quaternion-based six degrees of freedom motion system to describe rigid body motions. Using analytical solutions, experimental data and literature data, the accuracy and robustness of the FSI scheme were validated. Different nose shapes were investigated, and the tail slamming phenomenon was extensively discussed.

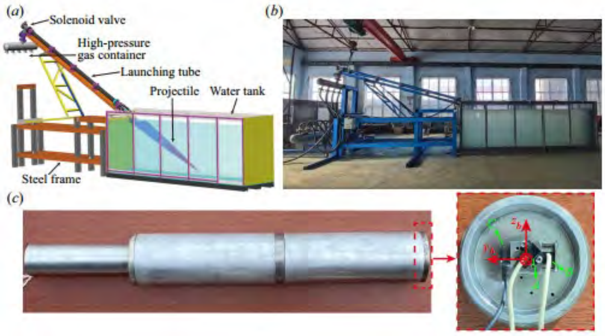

Figure 11: Experimental setup (Liu et al. 2023b).

An experimental study performed by Jain et al. (2022), Figure 12, investigated wedge and cone impacts into water across a wide range of velocities, precisely controlled using a linear motor. Pressure transducers placed on the impactors recorded pressure data, revealing under-pressure prior to peak pressure upon impact, likely due to hydrodynamic factors. Comparisons with various theoretical models showed that the Zhao & Faltinsen model aligns closest with measured pressure peaks. Theoretical treatments assumed 2-D flows for wedges and axisymmetric flows for cones, a method validated by comparing predicted pressure ratios to experimental results. Air cushioning prior to impact, causing water surface deflection, was examined, with results indicating the entrapment of air layers depends on the gradient of the deformed liquid surface compared to the impactor. In these slamming impacts, surface deformation due to inertial effects precedes viscous effects, which may lead to air bubble entrapment.

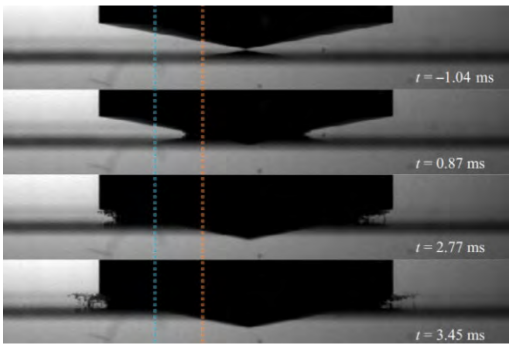

Figure 12: Early stages of a cone entering water (Jain et al. 2022).

Wang et al. (2022a) led an experimental study of the impact of three aluminium plates with different thicknesses and a pitch angle of 10° on a quiescent water surface, Figure 13. The impacts occurred with a combination of constant horizontal and vertical velocity. By varying the Froude number, the velocity normal to the free surface, the plate stiffness ratio (R_D) and the plate submergence time and by measuring the force normal to the plate surface, the moment of the plate's surface, the moment arm about the plate's trailing edge, the spray root position and shape and the plate's out-of-plane deflection along the centreline, they created a wide range of impact conditions. These impacts ranged from cases at small R_D in which the plate's deflection was less than a millimetre to impacts at large R_D in which the plate deflection was as large as 50 mm.

The authors analysed the results of 24 impact conditions for each of the three plates to identify the dynamic effect of the various dimensionless ratios on the results, namely Froude number, plate stiffness ratio and plate submergence time ratio.

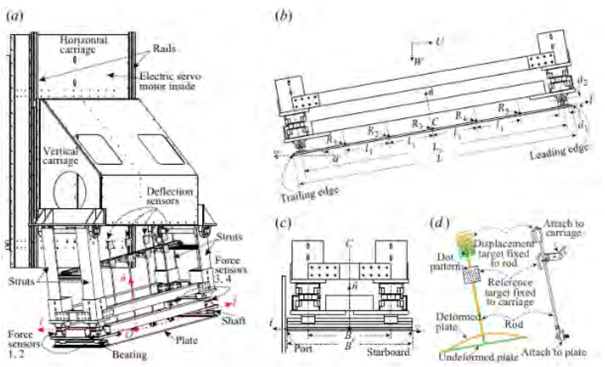

Figure 13: Experimental setup (Wang et al. 2022a).

2.4.1.2 Numerical

Liu et al. (2022a) numerically investigated green water and slamming loads of a ship advancing in freak waves. The authors separated their investigations in two steps: first the modelling of the wave and second the numerical simulation of green water on an FPSO and the motion of KCS were conducted. The representative stages of waves on deck are shown in Figure 14. The observation of the motion showed that the dominant factors of first and second green water events were different. The initial green water event was primarily driven by wave motion, while the second was predominantly influenced by the motion of the ship. The relation between heave and pitch motion and the largest ship position of the freaking waves were analysed, which showed that the maximum movement appeared in the second green water. Regarding the slamming pressures, the authors found that the wave slamming area was mainly located in the connection area between the deck and the superstructure midship.

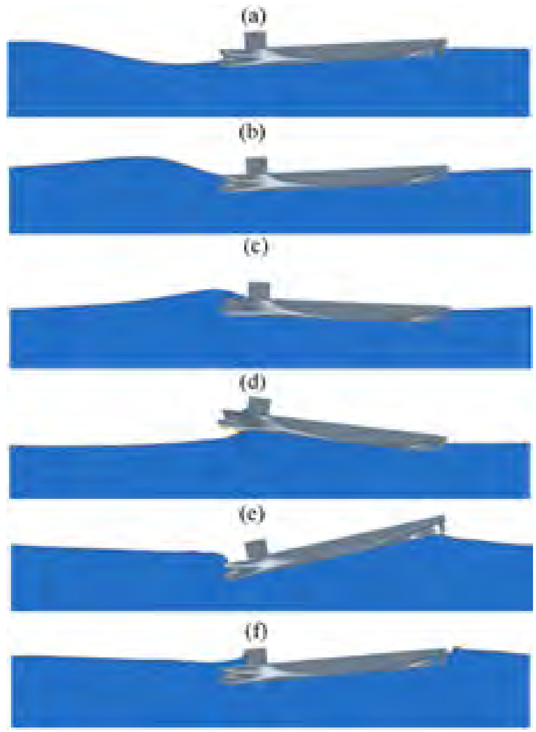

Figure 14: Representative stages of waves on deck presented by Liu et al. (2022a).

Molaemi et al. (2023) investigated the generic two-dimensional impacts on vertical cylinders on a non-flat water surface, Figure 15. This was done through physical experiments with impact on a stranding wave for both crest and trough impact. They found the wave load relative to the flat impact to be smaller for crests and larger for troughs. On a trough impact noticeable air entrapment takes place which results in a slamming coefficient up to Cs = 30. For crest impacts it can be as low as 2.5. A second finding is that the crest slamming coefficient increases with the relative wavelength λ/D and decreases with the relative amplitude A/D. The authors explain this relationship by the ratio between the local instantaneous water surface curvature at the point and moment of impact and the cylinder curvature, which becomes closer to one for shorter wavelengths and higher amplitudes. Consequently, the wetted length grows at a faster rate at the initial impact time.

The authors successfully reproduced their findings in numerical simulations and analytical extensions of the von Kármán and Wagner methods. These numerical results were used to demonstrate how entrapment of air pockets can lead to oscillatory slamming loads with sub-atmospheric pressures. The numerical simulations enabled the extension of the results from the physical experiment to short wavelengths. In these conditions, impact on subsequent crests during the entry can lead to multiple slamming peaks and formation of multiple air pockets.

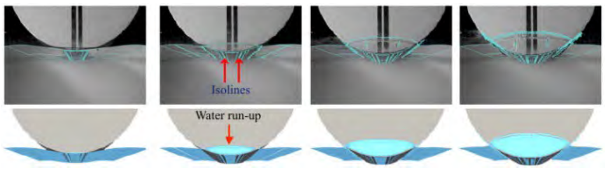

Figure 15: Comparison between experimental and numerical results (Molaemi et al. 2023).

2.4.2 Slamming

Slamming assessments are focused on quantifying the occurrence rates of bow slamming and stern slamming, as well as quantifying the magnitude of the impact loads.

Silva et al. (2023) investigated the slamming effects of FPSO platforms. They analysed standard mooring balcony structures numerically as well as experimentally. Furthermore, an analysis of the modification by various wedge type and fender type protection configurations of the aft mooring balconies as well as a perforated balcony were investigated, too. Using a diffraction model for identification of the most critical waves and a simplified CFD model the maximum expected vertical slamming loads were identified. With these specifications the model tests were performed and analysed. Figure 16 shows the experimentally evaluated absolute maximum loads for different balcony configurations for one test setup. The authors lined out that the results indicate that wedge type and cylindrical (fender type) structures beneath the balcony may reduce the extreme loads up to 50% and the perforated balcony structure may reduce the magnitude of slamming forces up to 80%.

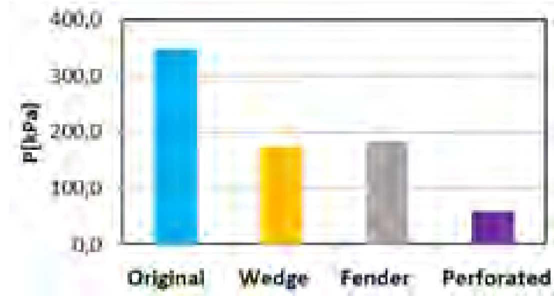

Figure 16: Results of Silva et al. (2023) for the investigation of absolute maximum loads for different balcony configurations for test setup H_s = 4.11m, T_p = 9s, Balcony airgap 3.03m.

A “double slamming” phenomenon at trimaran connecting bridge was studied by Tang et al. (2021a) at falling body experiments at seven heights. The "first slamming" is caused by the jet of the main hull into the water and the "second slamming" is generated when the cross structure enters the water. The relationship between the distribution of the slamming pressures and the velocity was analysed by the authors. Their intention was to provide the theoretical basis for the load prediction and structural design of the cross bridge of trimarans. With a falling frame experimental setup and 10 installed pressure sensors on the trimaran cross section in a scale of 1:100 the authors investigate the pressure pulses. Additionally, they observed the tests by video with a framerate of 1000 fps. Therefore, the authors were able to uncover a general understanding of the trimaran slamming events e.g. a rising jet caused by the first slamming event and its water entry speed coupled behaviour.

Chen and Wu (2021) carried out model experiments of wave load and slamming pressure for an example ship with a bottom sonar opening. Experiments with multiple speeds, wave heights and wave directions were carried out to measure the motion of the ship model, vertical and horizontal bending moments of the hull beam, torque, bow slamming pressure and bottom pressure at the large opening area. The test ship model was designed under the premise that the model is similar to the real ship in terms of geometrical shape, motion and power. Figure 17 shows the model with bow opening used in the tests. Among other things, they figured out that due to the hull slamming phenomenon, high frequency flutter signals in the vertical bending moment resulted in obvious nonlinear characteristics of the vertical bending moment. Slamming pressure increased with navigation speed. The authors also pointed out that the sonar opening had some effect on the bow vertical acceleration. The bow vertical acceleration decreased when the sonar opening was closed.

Figure 17: Model and bow opening used in the investigations of Chen and Wu (2021).

Wang et al. (2022b) numerically investigated slamming events by simplifying the ship as a wedge. With the wedge-shaped body they analysed the law and mechanism of the slamming pressures for different entering speeds as well as inclining angles of the wedge. The authors show that the slamming load changes first with the increase of the inclination angle, and that the peak value of slamming load increases with the increase of the inclination angle of the wedges, while the decreasing speed of slamming load slows down with the decrease of the inclination angle of the wedges. Furthermore, they figured out that with increasing initial speed, the peak value of the torque increases, too, and the time until the peak value is reached becomes shorter. The higher the initial velocity, the faster the slamming load reaches the peak value, and the higher the peak value. Something similar was carried out both numerically and experimentally by Liu et al. (2021a) with a steel wedge with stiffened panels and a deadrise angle of 45°. Their focus was on the comparison of the peak pressure, duration time and stress responses on the wedge structure. The authors found a good agreement between simulations and experiments.

Antolik et al. (2023) provided experimental and theoretical treatment of a simplified hydroelastic problem involving the water entry of a 2 DoF (one axial elastic mode) impactor with a hemispherical nose, Figure 18. The impactor nose and body are coupled with a set of compliant flexure springs in order to achieve a system that closely approximates a simple harmonic oscillator. Comparisons between the experimental results and reduced-order models are presented and show that the latter can be used for early-stage design work.

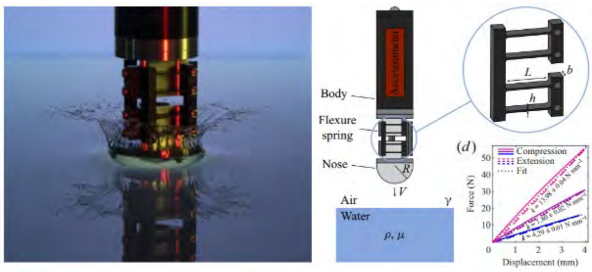

Figure 18: View of the flexible impactor used by Antolik et al. (2023).

Acharya et al. (2023) investigated bottom slamming with one-way and two-way coupled methods to estimate peak pressure at any point in the longitudinal axis. The results showed the trends are similar for both coupling methods with steady differences. One-way coupling can be helpful to estimate peak pressure although it does not capture the detail of spatial distribution of pressure at high forward speed (Fn > 0.2). The authors also developed an empirical formulation at forward speed to estimate peak pressure for the S175 hull. This formulation fails to predict peak pressure correctly for Fn < 0.2 but performs as well as the DNV's for Fn = 0.275.

Wu et al. (2021) conducted a numerical and experimental study of the slamming problem for a trimaran hull to validate the modified MPS (Moving Particle Semi-implicit) method developed by one of the authors, Figure 19. This numerical method is for a 2D fluid structure with free surface, thus the model used in the 20 drop-tests is an extrusion of the trimaran hull cross section. The authors achieved a convergence of the MPS method and a good agreement with the experimental results in time history, where the difference of peak magnitude and its occurrence time is within the allowable error range. The MPS method also simulates correctly the change of free surface during entry, the overturning and breaking of free surface and splash at different stages. These results show that the modified MPS method can simulate these complex fluid dynamics, but it does not take into account the impact of air whose effect is obvious when it becomes trapped at the inner side of the root of the exterior hulls.

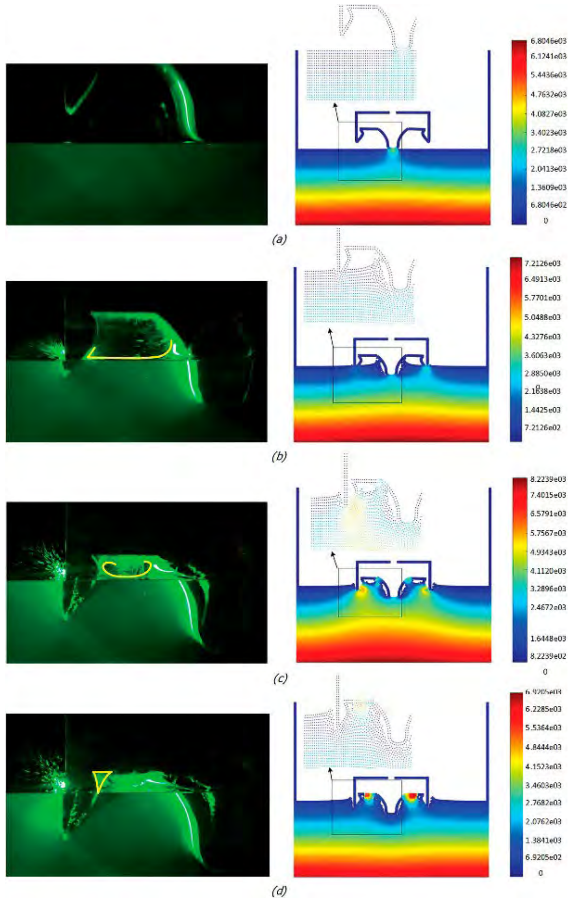

Figure 19: Comparison between pressure contours from numerical simulation and free surface profiles (Wu et al. 2021).

2.4.3 Green water

Park and Nam (2023) analysed green water events numerically by using an artificial neural network (ANN). They predicted the peak values of relative wave motion and the occurrence of green water events. The authors applied two ANN models for their investigations. The so-called T-ANN model is based on the time series of the incident wave and linear relative wave motion (RWM) calculation as input, and the F-ANN model which uses local parameters from the incident wave and linear RWM calculation rather than directly using the time series. For the input data model, test data of the KFPSO were used. Both models predicted the peak values of RWM with good accuracy, shown in Figure 20 for a location close to the bow. The authors found that the ANN models significantly improved the prediction performance for relative wave motions compared to the linear calculations. Furthermore, it is shown that the ANN model based on the time series was more accurate than the feature-based ANN model.

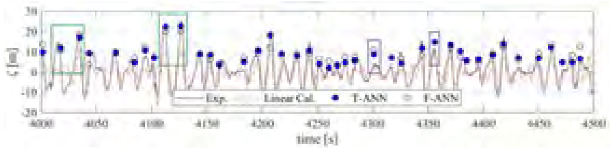

Figure 20: ANN predicted results at a location close to the bow for test time series by Park and Nam (2023).

Van Essen et al. (2021) compare different numerical screening indicators for green water loads on a containership with experiments. Their idea of 'screening' is to use lower-fidelity numerical methods to identify the occurrence of extreme load events such as slamming or green water at the basis of indicators. A good indicator has a significant correlation with the design load but is easier to calculate. Based on this first analysis, a high-fidelity tool is then used to determine the loads during these events. Their study with this technique in comparison with experiments shows that the peaks and steepness of the relative wave elevation around the bow serve as effective indicators of green water loads, alongside the undisturbed wave crests at the bow. Fine mesh CFD simulations were conducted for the identified events using a selected indicator as a reference. The outcome yielded a green water load distribution remarkably similar to that observed in the experimental data. Furthermore, the authors show that this screening method could massively reduce the required high-fidelity modelling time.

Liao et al. (2021) developed a 3D hybrid Eulerian–Lagrangian method for simulating green water on the deck. Two benchmark cases, green water on a fixed simplified FPSO model and green water on a ship model, were used to perform comparisons and validate the proposed method. It was found that the green water behaviour on deck, Figure 21, is well captured by the new method. Pressure values are mostly in good agreement with the experimental results (although underestimated) for most pressure gauges, but the impact pressure peak value differs considerably. Further work will focus on improving the peak pressure value prediction and CPU time optimisation.

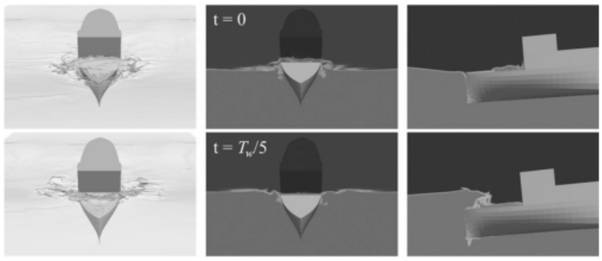

Figure 21: Green water behaviour captured by the method proposed by Liao et al. (2021).

Zhang et al. (2021a) numerically investigated the pressure induced by green water events from freak waves on the deck and superstructure of a typical simplified ship, Figure 22. They used a 3D numerical wave tank and the Peregrin breather solution model to generate freak waves. They found this model, previously validated under regular wave conditions, able to give reasonable results to investigate qualitatively the process and characteristics of green water events from freak waves. The authors characterised six different stages of said events and inferred the most dangerous areas on deck and on superstructure.

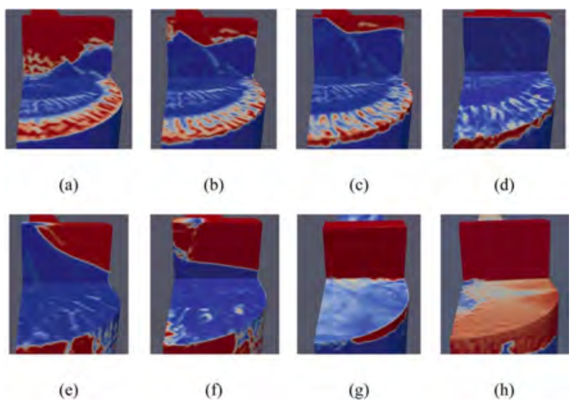

Figure 22: Stages of green water motion after arriving at superstructure, Zhang et al. (2021a).

2.5 Sloshing

Sloshing in ship tanks with liquid cargo is still a problem to which significant research has been dedicated in this last ITTC term. This can be attributed to an increased interest for the ship transportation of liquified natural gas LNG, in turn connected to supply constraints due to the Russian invasion of Ukraine and to the use of natural gas as a transitional fuel towards the path of reduced emissions. More recently, additional interest can be a consequence of the growth in research on transportation of liquid hydrogen LH2 in cryogenic conditions; using hydrogen as an energy vector has emerged as an alternative to reduce greenhouse emissions.

In this context, studies have been carried out using experimental and numerical simulations, but also, in recent times, machine learning based models. The studies refer, among other things, to the prediction of sloshing impact loads and boil-off rates, to a better understanding of free-surface dynamics, to assessing the influence of sloshing on the coupled dynamics of ships when transporting liquid cargo, to the investigation of sloshing reduction devices, and to modelling fluid-structure interaction (FSI) in sloshing related problems. A short but interesting review paper in the period was written by Zheng et al. (2021a).

As for sloshing impact loads, Ahn et al. (2023) conducted a large series of joint industrial experiments using six-degree-of-freedom irregular sloshing tests. The case study was a tank from a real 174K LNG Carrier, scaled 1/50. They focused on impacts on the upper part of the tank (Figure 23, Figure 24). In this paper they provided an assessment of sloshing loads based on a comparison of short- and long-term approaches distinguished by the guidelines of various classification societies. Their key findings indicated that the different analysis procedures of the international classification societies lead to different sloshing loads for the same cargo hold design of the LNGC. Another of their key findings is that using the long-term approach was more than twice as conservative as the short-term one.

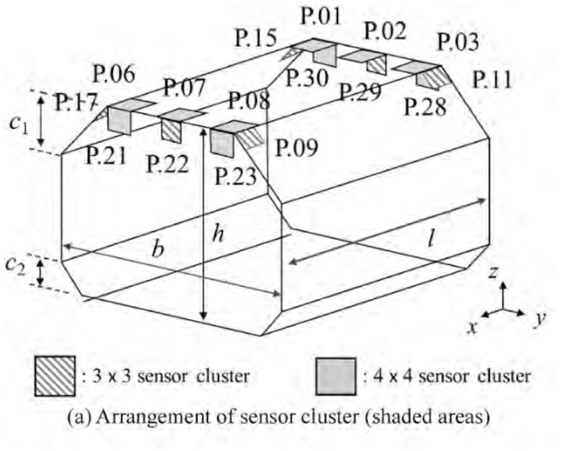

Figure 23: Arrangement of sensor clusters (Ahn et al. 2023).

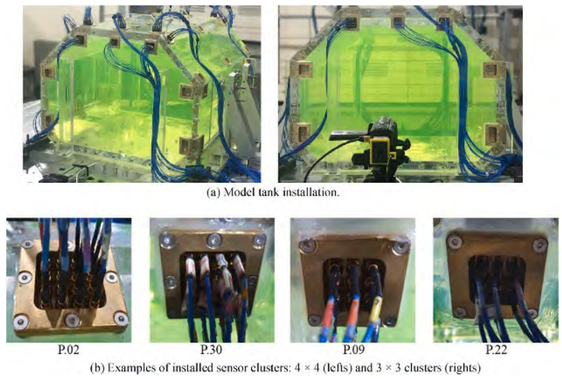

Figure 24: Model tank installation and cluster of sensors (Ahn et al. 2023).

Also, Ahn et al. (2021) developed a neural network to predict extreme sloshing loads, with good agreement for validation cases. Later, Ahn (2023) used genetic programming (GP) to predict sloshing impact loads. Although the scope of the research was limited, promising results were obtained, suggesting this technique can be used in the future to save experimental work.

As for free-surface dynamics, the interesting topic of turbulence modelling when conducting sloshing flow simulations with RANS solvers was investigated by Mahfoze et al. (2022). They arrived at the conclusion that excessive dissipation was induced by such types of models. Damping through sloshing has been the target of investigations in this period, with a focus on that induced in vertical motions (Martinez-Carrascal and Gonzalez-Gutierrez, 2021). Remmerswaal and Veldman (2022) tried to provide evidence linking the variability of sloshing loads to free-surface physics. To this aim, they looked into how the physics can be simulated, discussing the influence of capillarity, the onset of instabilities and a number of numerical details in their VOF based scheme.

Regarding the transportation of cryogenic hydrogen, Liu et al. (2022c) investigated sloshing in these cases. They report that heat transfer is enhanced when the first sloshing mode is excited, finding in these conditions the largest forces and moments but also the largest fluid pressure drops due to these heat transfer effects. Also in this context, Smith et al. (2022) presented an approach for estimating fuel boil-off behaviour in cryogenic energy carrier ships, such as future liquid hydrogen (LH2) carriers. Their results indicate that an LH2 ship with the same tank volume and glass wool insulation thickness as a conventional LNG carrier stores 40% of the fuel energy and is characterized by a boil-off rate nine times higher and twice as sensitive to sloshing. Their results indicate that LH2 carriers will necessitate significant redesigns if LNG carrier standards are desired.

As for coupled dynamics, Koo et al. (2021) carried out time-domain simulations, including coupled sloshing loads, of the offloading of an FLNG on an LNGC. They used their own time-domain solver and were able to document the influence of the tank filling level on the roll response (Figure 25) Along this line, Lyu et al. (2022) modelled ship motion-sloshing interaction with forward speed in oblique waves. They did this study considering a 138000 m^3 LNG carrier. They paid particular attention to beam seas, for which, the derivation of a roll damping model was of particular relevance.

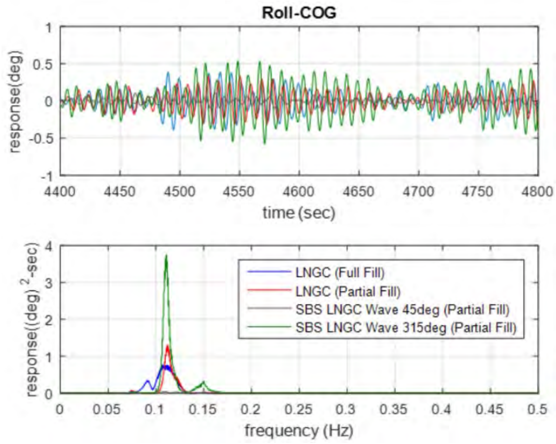

Figure 25: Comparisons of LNGC Roll Responses for offloading Operational Sea State (Koo et al.2021).

The influence of sloshing on the onset of parametric roll was studied numerically by Liu et al. (2022b). They used an in-house CFD solver (Figure 26). They showed sloshing could significantly decrease the natural roll frequency of the ship model, which led to a lower speed range where the parametric roll occurred compared with the model without sloshing.

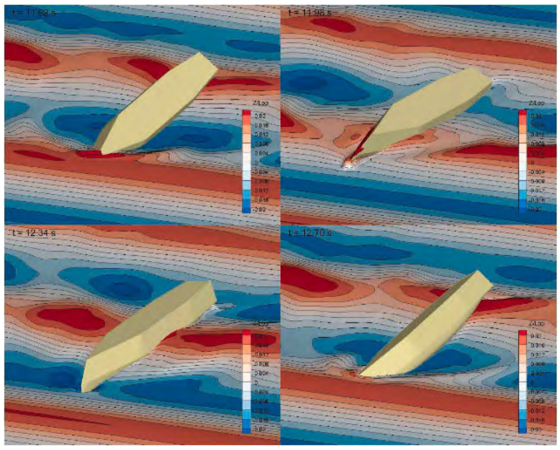

Figure 26: Snapshots of CFD simulation of coupled sloshing motions and parametric roll (Liu et al., 2022b).

Also, regarding coupled dynamics, Igbadumhe et al. (2023) carried out experiments with an FPSO comparing the inclusion of a tank partially filled with liquid to using an equivalent “frozen” mass (Figure 27). They studied beam sea conditions and found that in some frequencies the influence of the sloshing loads could significantly change the roll angle (Figure 28).

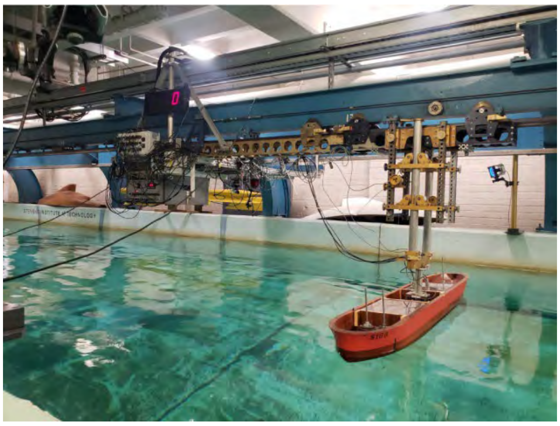

Figure 27: Coupled sloshing experiments (Igbadumhe et al. 2023).

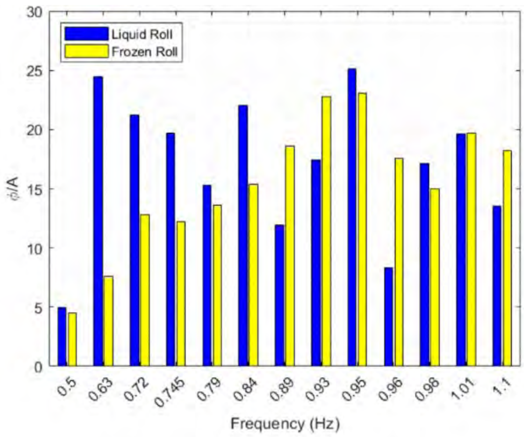

(a) Loading condition 2 FPSO roll response amplitude for each excitation frequency for both liquid and frozen condition

Figure 28: Roll response in coupled sloshing experiment (Igbadumhe et al. 2023).

Finally, Faltinsen and Timokha (2021) adapted their multimodal theory to model the coupling between resonant sloshing and the lateral motions in a 2D rectangular tank.

Related to coupled dynamics but with a different angle, Zheng et al. (2021b) conducted an experimental investigation on the effect of sloshing on ship added resistance in head waves. They used a scale model of a relatively small (23603 m^3) LNG carrier. They found (see Figure 29) that sloshing could help reducing added resistance due to its favourable influence in reducing ship motions. A combined numerical-experimental study dealing with this same topic was carried out by Zhu et al. (2021).

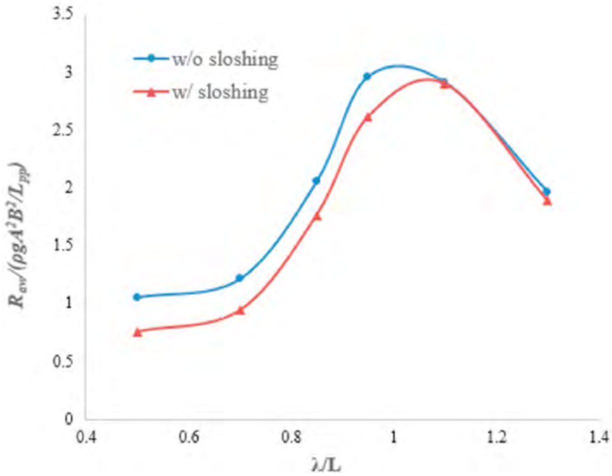

Figure 29: Comparisons of added resistance in waves with and without sloshing, (Zheng et al, 2021b).

A last relevant reference in this period for couple dynamics is an experimental and numerical investigation of the hydrodynamic response of an aquaculture vessel by Tao et al. (2023). Their case study consists of a 258 m long vessel with 83000 m^3 aquaculture tanks (Figure 30). They showed that the double-row tank arrangement scheme adopted by their vessel could reduce the coupling effect of sloshing and hull motion effectively.

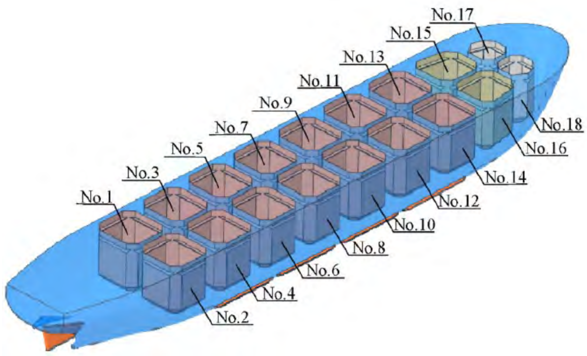

Figure 30: Layout of the aquaculture vessel by Tao et al. (2023).

As for FSI problems Wang et al. (2021b) modelled the influence of hydroelastic effects in a tank transporting LNG. Adina CFD, Adina Structures and coupled FSI ADINA solver were used for modelling. They found the average pressure in the elastic tank to be smaller than for the rigid tank.

As for sloshing reduction devices Barabadi et al. (2023) proposed to use floating foams to reduce the intensity of sloshing inside tanks. They demonstrate the sloshing reduction by using a combined experimental and numerical approach. Also to reduce sloshing, Ma et al. (2021) used vertical baffles. They modelled the flow with a Lattice-Boltzman scheme (Figure 31) and assessed the efficiency of the baffle arrangement by linking the pressure field with the viscous dissipation.

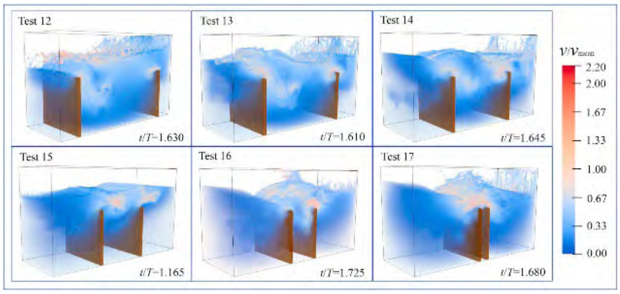

Figure 31: 3D snapshots of sloshing modelling with baffles by Ma et al. (2021).

2.6 Hydroelasticity

2.6.1 Experimental study on container ships using a backbone model

A segmented model with a backbone is extremely useful for experimentally investigating the hydroelastic response of ships. Tian et al. (2022) produced two different scaled backbone models to collect benchmark model test data for a 20000 TEU container ship of about 400 m in length and summarized their findings for producing accurate backbone models by comparing them with modal analysis of 3D FEM models. Zhang et al. (2022) conducted experiments on wave loads and hydrodynamic response to head-on and oblique waves using a model with a variable cross-section backbone (10000 TEU container ship). The results indicate that hull stiffness has little effect on the frequency of slamming, but that wave loads due to slamming become more severe as stiffness decreases. Tang et al. (2022) similarly used a model with a variable cross-section backbone to systematically analyse nonlinear bending moments from experimental data, Figure 32. The effects of Froude number, wave direction, and wave height, asymmetry of the hogging and sagging moments, and phase differences between wave frequency and higher harmonics in extreme waves were investigated.

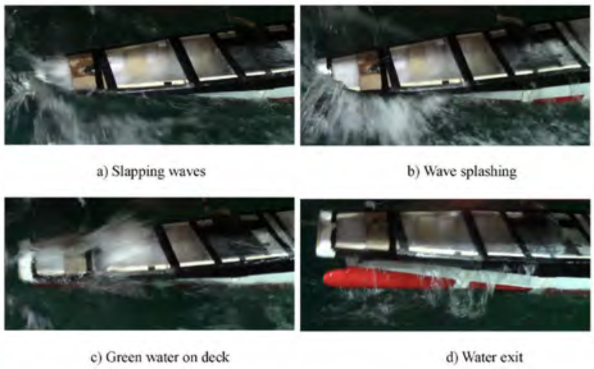

Figure 32: Image records of the model in extreme waves by Tang et al. (2022).

Ahn and Jung (2022) made comparisons by design wave conditions and by towing tests and numerical calculations for the final strength evaluation, including the increase in elastic response level due to whipping of the very large ore carrier (VLOC). The design wave conditions are equivalent design wave (EDW) and equivalent design sea state (EDS), where EDW is determined from the long-term analysis results and EDS is determined by the maximum contribution to the 10^{-8} exceedance probability of the vertical bending moment (VBM) in each sea state of the actual sea route. The towing tests were conducted on a segmented model with backbone support, and numerical calculations were performed under the same conditions using the nonlinear time-domain hydroelastic analysis program WISH-FLEX. As a result, the load effect from EDW was evaluated to be greater than that from EDS in both experimental and numerical calculations, and the load effect from experiments was evaluated to be greater than that from numerical calculations. Kim et al. (2023b) experimentally investigated the wave motion and loading of a container ship model without forward speed in oblique regular waves to determine the nonlinear effects of wave steepness on the vertical bending moment (VBM) and horizontal bending moment (HBM) near the centre of the hull, as well as on the 6-

DoF motion, Figure 33. The results show that as the wave steepness increases, the higher harmonic components including slamming phenomena increase. It was also qualitatively confirmed that the restoring moment of the mooring system correlates with the asymmetric HBM and the change in mean yaw motion.

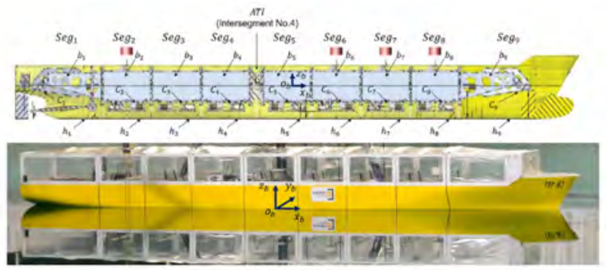

Figure 33: 9-segmented 6750-TEU containership model and load sensor location by Kim et al. (2023b).

2.6.2 Experimental and numerical analysis of sloshing

Sloshing loads in LNG tanks are complex phenomena that depend on the density ratio of gas and liquid, the phase transition of the fluid, and the elastic response of the tank wall. Lee et al. (2022a) studied the effects of the density ratio of gas and liquid in the tank and the phase transition of the fluid on the sloshing phenomenon. They measured the sloshing impact pressure on the wall and characterized it in terms of maximum impact pressure, pressure rise time, and pressure impulse area. These data may be useful for LNG tank design. Using the experimental sloshing loads, Park et al. (2022) performed direct dynamic structural analysis under different sloshing impact loading patterns to investigate the hydroelastic effects and dynamic response of a membrane-type cargo containment system (CCS). The results, Figure 34, show that the level and frequency of the dynamic structural response may be lower than previously estimated due to the additional mass and damping effects of the LNG considering the fluid domain.

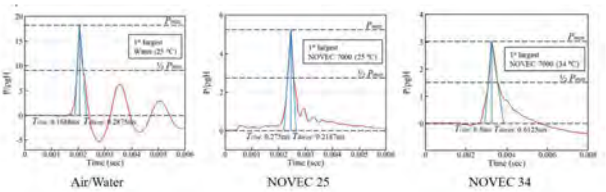

Figure 34: Pressure signal for the air/water and NOVEC 7000 (20%H Filling, $\omega/\omega_0 = 1.27$ by Park et al. (2022).

2.6.3 Numerical study of hydroelasticity

The recent trend toward larger hulls has the potential to make hulls relatively elastic. For such problems, Wei and Tezdogan (2022) proposed a fluid-structure interaction coupling scheme using the preCICE library communicating with the fluid solver OpenFOAM and the structural solver calculiX. Its effectiveness was demonstrated by comparing the hydroelastic behaviour of a container ship moving forward in regular waves. Tavakoli et al. (2023b) analysed the water surface impact of a 2D object using the fluid-structure interaction of finite volume method (FVM) incorporated in OpenFOAM and showed that the impact load is reduced by elastic motion. Kim et al. (2023a) extended the modal method to time-domain hydrodynamic analysis of floating bodies, Figure 35. Three numerical schemes were considered for wave force calculations: the case of deflection force only, the case of 6-DoF radiation force + deflection force, and the case of elastic degree of freedom radiation + deflection force, and their accuracy and efficiency were systematically compared.

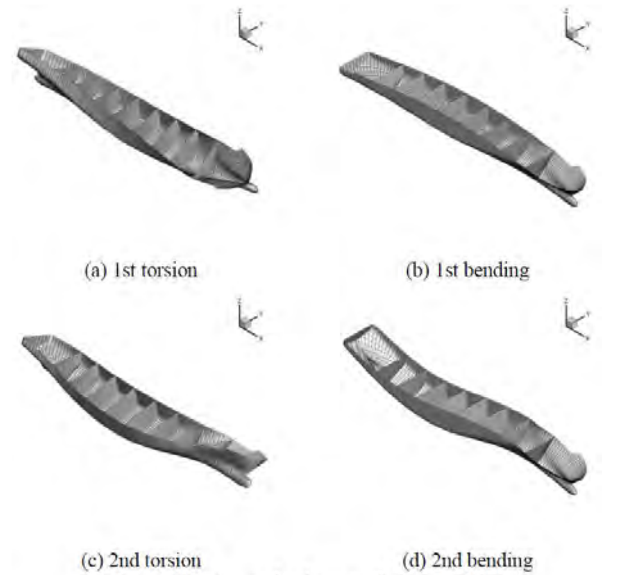

Figure 35: Elastic mode shapes of sample ship by Kim et al. (2023a).

Park and Lee (2022, 2023) proposed a method to perform hydroelastic analysis under various conditions on a single mesh model by non-matching meshing between finite element and boundary element methods. Wang et al. (2022c, 2023a) used Taylor Expansion Boundary Element Method (TEBEM) generalized to elastic modes to calculate the vertical motion, heaving motion, and vertical bending moment of a container ship moving forward in head waves. Nonlinear effects become more pronounced as the forward speed increases. Vertical hydroelastic response is currently focused, and horizontal, torsional, and coupled bending and torsion are neglected in this study. On the other hand, Riesner et al. (2021) proposed a time-domain numerical method to predict higher-order springing by coupling horizontal, torsional, and bending and twisting to account for forward velocity. The structural dynamics adopted a beam element approach, and the hydrodynamic solver considered nonlinearities induced by wetting surface changes due to incident waves. The vertical bending, horizontal bending, and torsional moments at the centre of the hull induced by sprigging were shown to compare favourably with experimental measurements. Pal et al. (2022) developed a semi-empirical reduced order model (ROM) based on coupled CFD-FEM analysis and experimental results. It accounts for the effects of springing and whipping at different probability levels when calculating the extreme value distribution of the VBM, as well as the effects of continuous bow and stern slamming. This method provides real-time ship loading prediction without the expensive computational cost of coupled CFD-FEM. Lu et al. (2023a) proposed a 3-D nonlinear time-domain hydrodynamic analysis method for ship wave loads considering asymmetric slamming and solved the seakeeping problem by combining modal analysis and 3-D Rankine panel method for 3-D finite element models. The results show that asymmetric slamming has a significant effect on the horizontal torsional whipping response of the hull when the wave encounter frequency coincides with the natural frequency. Vijith and Rajendran (2023) proposed a nonlinear time-domain numerical solution method by combining a seakeeping solver based on potential flow theory and a structural solver based on Timoshenko beam theory. The solver captures the effects of higher-order springing and whipping in vertical bending and identifies whipping effects due to slamming. In most cases, the numerical results are shown to be in good agreement with experimental results, Figure 36.

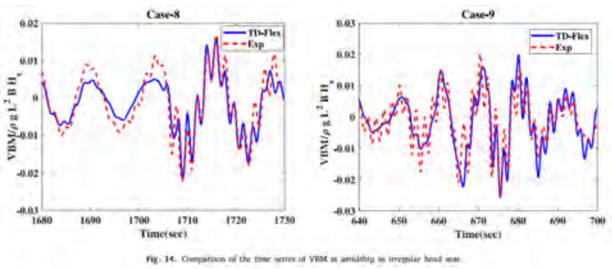

Figure 36: Comparison of the time series of VBM at amidship in irregular head seas by Vijith and Rajendran (2023).

In this study, Wei et al. (2023) applied a fluid-structure coupled interaction framework to model the interaction between flooding and the wave field in the damaged tank of a moving forward ship in OpenFOAM and analyse the structural deformation in MBDyn. The results are useful for assessing the safety of damaged vessels and determining whether they suffer secondary damage due to hydrodynamic elastic response.

2.6.4 Numerical analysis of water surface impact

Hosseinzadeh et al. (2021) numerically investigated the water surface impact of a two-dimensional symmetric elastic wedge due to free-fall motion using a two-way coupling approach between finite volume and finite element methods. Coupling methods for two-dimensional symmetric elastic wedge sections under various conditions are presented. It is observed that the importance of hydroelasticity increases with decreasing slope angle and increasing impact velocity. Feng et al. (2021) proposed an efficient fluid-structure interaction (FSI) coupling between the boundary element method (fluid part) and the mode superposition method (structural part) to study the hydroelastic slamming of wedge cross sections, Figure 37. Results showed that the maximum response of the structure was underestimated, and a time difference effect was found between the results of the separated and coupled solutions.

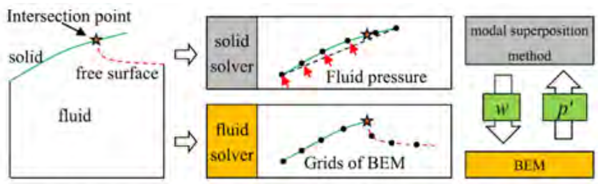

Figure 37: Partitioned solution of solid solver (modal superposition method) and fluid solver (BEM) by Feng et al. (2021).

2.6.5 Theoretical analysis of hydroelasticity

The theoretical-analytical approach clarifies and develops the physical principles and mechanisms of hydrodynamic elasticity. Hong et al. (2021) used Legendre polynomials and Chebyshev polynomials, which are mathematically orthogonal but do not satisfy the free end boundary conditions, to represent the mode function of a uniform Timoshenko beam, Figure 38. The mode superpositions represent the hydroelastic forces on the ship and the resulting bending deflection of the ship in waves. In combination with the Rankine panel method, the hydrodynamic forces for the modes were calculated. Since the Eulerian beam model tends to overestimate the natural frequencies of elastic motion in the high elastic modes, there is an advantage in using Timoshenko beams that account for deformation due to shear forces. As the number of modes increases, the total deflection of the ship is found to converge, and the results obtained using the Legendre polynomials and Chebyshev polynomials are in almost perfect agreement with those obtained using the dry eigen modes of the Timoshenko beam over a wide wave frequency range. The Legendre polynomials were shown to be concise, common, and can be used with the weighted residual method, indicating that they are expected to be versatile enough to be applied to a wide range of engineering problems.

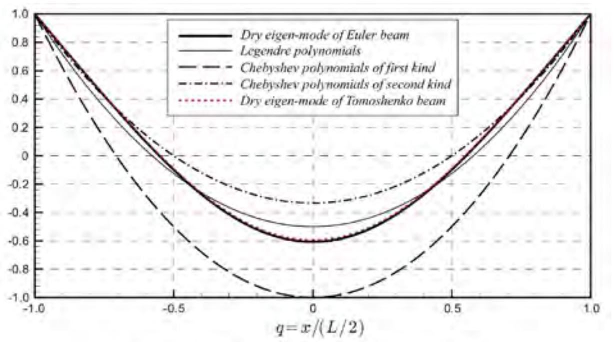

Figure 38: The first elastic mode shapes (j = 7) of mode functions used by Hong et al. (2021).

Jagite et al. (2021) analysed the hydroelastic response of a number of container ships. The dynamic ultimate strength of reinforced panels was investigated, and realistic loading scenarios were derived. They also developed a new strain rate sensitivity model. Korobkin and Khabakhpasheva (2022) addressed a three-dimensional unsteady problem of a rigid body impacting a floating plate with a viscoelastic layer on its surface. The reaction forces of the viscoelastic layer are determined by a nonlinear, one-dimensional Winkler-Kelvin-Voigt model. The plate deflections are described using the normal modes method, and the added mass matrix of the plate is calculated analytically. Plate deflections are calculated for various positions of the impact. Spinosa and Iafrati (2022) treated a water surface impact on a rectangular flat plate. A simplified quasi-static model based on modal expansion for the structural response and a self-similar solution for the hydrodynamic problem was used. The inertial contribution was found to be small, justifying the use of a quasi-static approach. Tavakoli et al. (2023b) theoretically proved that the pressure acting on an elastic body can be predicted using a simple equation that uses momentum exchange. They presented a new methodology for analysing the hydroelastic response of a flat plate to water immersion using the momentum transferred to the solid immediately after impact, Figure 39. Although the paper is limited to flat plates, it could lead to practical methods for FSI problems in ships and offshore structures.

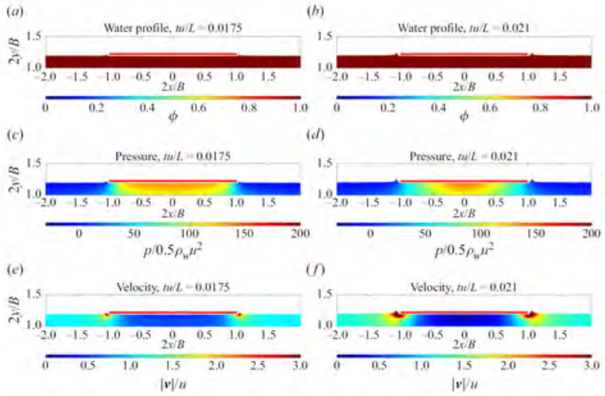

Figure 39: Snapshots showing the fluid motion around an elastic plate entering water. The plate thickness is not to scale by Tavakoli et al. (2023b).

2.7 Added Resistance in Waves and Power Requirements

2.7.1.1 Semi-empirical Formula for Added Resistance in Waves

In the ship design stage, it is necessary to consider the added resistance in the operational environment to accurately estimate the ship's performance. While model test or direct 3-D numerical computations ensure accurate and reliable results, they obviously require high costs with extensive times, as well as detailed information of ship hull design. With the accumulation of more model test data, new semi-empirical formulae have been developed for the rapid estimation of added resistance in the early design stage, applicable not only to head sea but also to various wave headings. Moreover, to address the limitation of applicability to novel hull shapes or unconventional vessels with extreme dimensions, revised empirical formula have also been proposed recently.

Mittendorf et al. (2022) proposed a data-driven methodology for the parameter calibration of a semi-empirical approach for estimating added resistance in arbitrary wave headings, taking into account uncertainty quantification. They endeavoured to refine the semi-empirical formulation by Liu and Papanikolaou (2020), optimizing the parameter vector with respect to two datasets for both full and slender ships, comprising 25 different ships and approximately 1100 data points obtained from publicly available model tests. The validity of the proposed method was confirmed through comparison with experimental data and established prediction methods, indicating satisfactory accuracy of the mean estimate and reliability of the adapted semi-empirical formulation, Figure 40. They noted that calibrating the semi-empirical definition resulted in a performance increase of around 9%, significantly reducing parameter uncertainty.

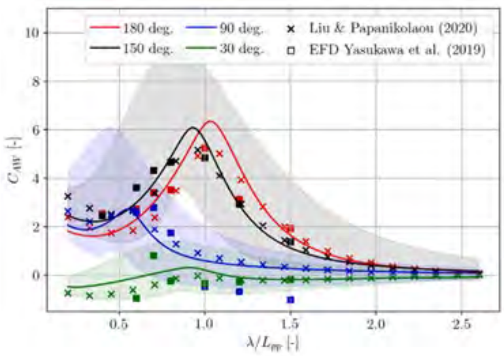

Figure 40: Comparison of added resistances between experimental data and semi-empirical formulae with uncertainty estimates (Mittendorf et al., 2022).

Liu and Papanikolaou (2023) enhanced the semi-empirical SNNM (SHOPERA-NTUA-NTU-MARIC) method by combining numerical experiments for the consideration of ships with extreme dimensional ratios, where experimental data are limited. They introduced the parameter L/B into the SNNM method based on large-scale numerical calculations using a potential-flow-theory-based 3D panel code NEWDRIFT+. The improved SNNM formula was validated against an experimental database comprising 131 data points from 11 ships with extreme dimensional ratios of various types. The validation study demonstrated a higher correlation coefficient and smaller mean percentage error compared to the original formula, indicating a significant enhancement in the prediction of added resistance in waves for various types of ships with extreme dimensional ratios

Mittendorf et al. (2023) provide statistical analyses of mean added resistance estimations in actual wave conditions based on in-service data from a fleet comprising more than 200 container vessels. The prediction data resulting from an indirect calculation of added resistance, utilizing shaft power measurements and empirical estimates of the remaining resistance components, were presented alongside comparisons with theoretical estimates. In this study, the calculation of the theoretical added resistance has been carried out by using a semi-empirical formula proposed by Mittendorf et al. (2022) for the added resistance transfer function and then applying the spectral method for long- and short-crested irregular waves. The comparison reveals a bias in bow oblique waves and higher sea states of the spectral estimates, as well as a large variance of the empirically derived predictions, particularly evident in beam-to-following waves. The authors addressed that added resistance is generally difficult to predict in actual conditions due to the substantial associated uncertainties, particularly in short and oblique waves.

Kim et al. (2022) proposed a new estimation method by combining two existing semi-empirical methods, CTH and L&P methods, which have high accuracy and availability against arbitrary wave headings. The new combined method was validated by full-scale measurements of a general cargo ship and a containership. They reported that the combined method showed good overall performance in estimating added resistance in the range of high wave height, resonance frequency, arbitrary wave headings, and low ship speed.

Lee and Kim (2023) developed an empirical-asymptotic approach (SNNM-SNU formula) for the added resistance of ships at arbitrary speed and headings by combining the SNU formula for short waves and the SNNM formula for long waves. They validated the developed method through a series of comparative studies, demonstrating that the proposed method shows a good agreement with experiments and exhibits strong capabilities in estimating added-resistance in the high-frequency region for oblique waves.

2.7.2 Data-driven Model for Estimation of Added Resistance in Waves

The feasibility of a data-driven model utilizing deep learning techniques to estimate added resistance in waves has recently been studied with the aim of improving accuracy compared to existing semi-empirical formula. The data-driven model has typically been constructed based on deep neural networks using extensive experimental data. Additionally, attempts to integrate data-driven and physics-based models have been observed, showing some corrective effects on the physics-based model.

Duan et al. (2022b) introduced a method based on deep feedforward neural networks (DFNs) for predicting the added resistance of ships in head waves. They utilized a dataset comprising 25 different ships, including 10 vessels with experimental data from published studies and 15 ships with calculation data obtained through a potential flow solver. They reported that the DFN model with multiple hidden layers exhibited higher prediction accuracy for added resistance compared to single hidden layer models. Furthermore, they observed significant improvements in prediction accuracy when additional information such as pitch radius of gyration and bow entrance angle was included in the DFN model input. The study demonstrated that the prediction accuracy of the developed DFN model is better than that of the semi-empirical formula, suggesting the feasibility of its practical application for predicting added resistance in head waves.

Yang et al. (2022) proposed a data-driven and physics-based symbiotic model (DPSM) for predicting the added resistance of ships in head waves, Figure 41. The 2D strip method was employed to construct a physics-based model, providing physics-based information and constraints, while the data-driven module was developed based on a fully connected neural network structure and radial basis function. The authors demonstrated that the DPSM results closely align with experimental data, exhibiting a noticeable adaptive correction effect on the outcomes of its embedded physics-based model. Furthermore, they showed that the DPSM achieves superior generalization ability compared to fully data-driven models by leveraging the strengths of both the physics-based and data-driven approaches.

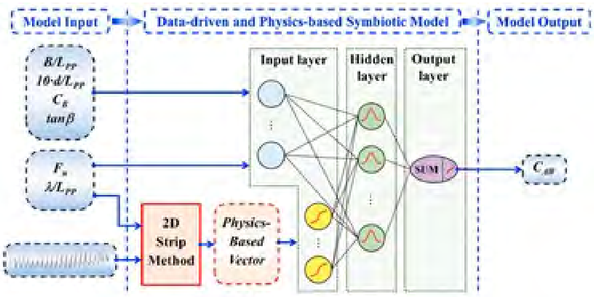

Figure 41: Combined method with data-driven and physics-based models for predicting the added resistance of ships in waves (Yang et al. 2022).

Cepowski et al. (2023) developed artificial neural network (ANN) models to predict added resistance using basic design parameters of ships. The experimental data, measured from 19 ship models representing a wide range of diverse vessels, was used to train the ANNs. The added resistance was predicted by calculating the algebraic mean of the results obtained from five ANNs using different segregated data. The authors asserted that this ensemble of artificial neural networks ensure more reliable and accurate estimates than using an individual ANN.

2.7.3 Experimental Studies on Added Resistance in Waves

Model tests have been used as high-fidelity methods to predict or validate the added resistance of ships in waves, especially focusing on irregular waves or quartering waves. Additionally, some experimental studies have been carried out to understand more about the physics related to added resistance in waves, such as the sloshing effects on added resistance.

Kim et al. (2021) estimated the motions and added resistance of an LNG carrier with twin skegs through experimental investigations under various wave heading angles. They reported that the added resistance due to waves is significant in bow quartering seas and not negligible even in following and stern-quartering seas. Additionally, they discussed the uncertainty in the model test, indicating that the error level is larger in shorter wave lengths. For validation, a series of numerical computations were carried out using the potential-flow-based Rankine panel method (WISH) and RANS-based CFD method (STAR-CCM+). They found that the added resistance estimated by numerical methods followed the trends observed in the experiment but could be scatted at a wide range of wave lengths and heading angles, Figure 42.

Zhu et al. (2021) conducted an experimental and numerical investigation on the sloshing effects on the added resistance of ships in waves, Figure 43. They utilized a modified Wigley hull equipped with two inner tanks in the model test to observe the hydrodynamic responses under head wave conditions. Numerical computations were performed based on the three-dimensional Rankine panel method for both seakeeping and internal sloshing flow using linear potential flow theory. They found good agreement between experimental data and numerical results, both with and without sloshing effects. Additionally, they reported that when the wave encounter frequency approaches the tank's natural frequency, a strong coupling effect at medium filling tanks can restrain ship motion responses as well as added resistance. Zheng et al. (2021b) also carried out a model test for an LNG carrier with a single prismatic tank to study the effect of sloshing on ship motion and added resistance in waves. They found that sloshing inside the tank alters the ship's motion, particularly reducing surge the most, and it modifies the added resistance under the specific conditions.

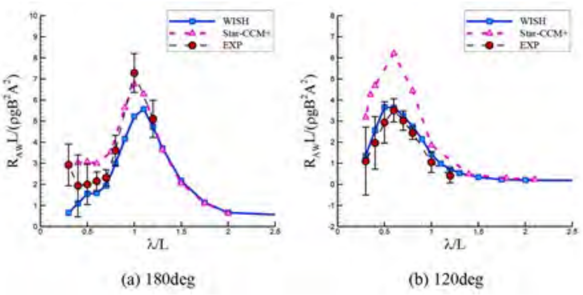

Figure 42: Comparison of added resistances from experiment and numerical computations (Kim et al. 2021).

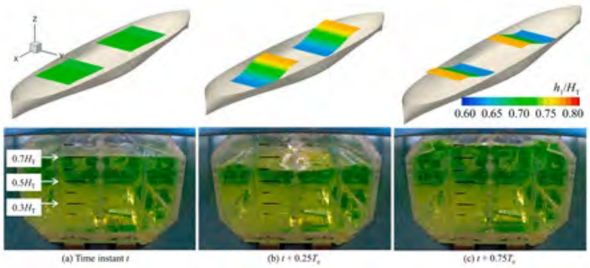

Figure 43: Snapshots of inner sloshing development (Zhu et al. 2021).

Yasukawa and Enui (2021) studied the effect of the pitch moment of inertia on the added resistance in waves using model tests and strip-method-based calculations for an S175 container ship. Their findings indicate a reduction of approximately 30% in added resistance when the pitch radius of gyration is decreased from 0.27L to 0.23L. Furthermore, they observed that this effect is notably pronounced in bow waves but insignificant in beam and following waves.

Yu et al. (2022) assessed ship resistance and propulsion performance for an 1800 TEU container ship through model tests in regular head waves and spectral method in irregular waves. They demonstrated that the added propeller revolution, thrust, and torque in waves exhibit a linear increase as the added resistance does to balance an overloaded propeller. They observed that the added delivered power in waves originates not only from added resistance but also from decreased propulsive efficiency.

Park et al. (2023) conducted a design optimization of the hull form and appendage of a 6500 DWT tanker to reduce added resistance, considering in-service navigation condition. In this study, the added resistance was firstly evaluated based on regular-wave CFD simulations, followed by the use of the spectral method to calculate the added resistance in irregular waves. A series of model tests was also performed to validate the improvements of the optimal hull form over the original design. The optimized hull featured a bow hull form with a sharper entrance and increased length between perpendiculars, along with a stern hull form with a V-shaped section to reduce viscous pressure resistance. The results show that the daily fuel oil consumption and CO_2 emissions for the optimal hull form under in-service conditions can be reduced by 14.8%.

2.7.4 Numerical Studies on Added Resistance in Waves

Various levels of numerical methods can be applied to directly evaluate the added resistance acting on ships in waves. Recently, CFD methods have been widely used to predict the added resistance in regular waves, with considering various wave heading effects or nonlinear effects, but they still require significant computational times, especially in the case of irregular waves. Time-domain numerical methods based on potential flow models have also been used to predict the added resistance in both regular and irregular waves with relatively short computational times.

Jawa and Minoura (2023) proposed a novel probabilistic method to address the nonlinearities of added resistance concerning wave height in short-term sea conditions. Their approach incorporates a correction function, Figure 44, for the nonlinearity of added resistance, where the relative ratio of nonlinearity is derived from CFD calculation results. The proposed nonlinear PDF method enables the prediction of added resistance in irregular waves while accounting for the nonlinearity with respect to wave height.

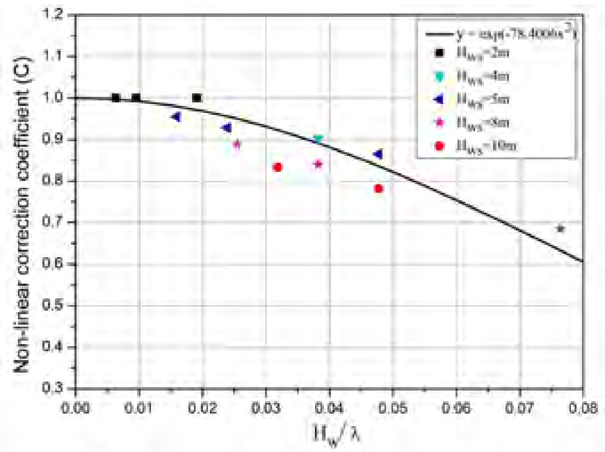

Figure 44: Non-linear effect correction function with respect to wave steepness (Jawa and Minoura 2023).

Yu et al. (2023b) predicted the motion responses and added resistance for the surge-free KCS model in head and oblique regular waves using a hybrid approach of potential and viscous flows based on the functional decomposition model SWENSE (Spectral Wave Explicit Navier-Stokes Equations). In the SWENSE method, the total physical field is decomposed into the incident wave field, where the linear wave model with the Wheeler stretching method is used, and the complementary field. They presented that surge motion has a significant impact on the seakeeping performance of the ship in astern seas, especially regarding added resistance. They also explained that the nonlinear added resistance is mainly caused by the nonlinear features of the incident, radiation and diffraction wave systems.

Dogrul et al. (2021) conducted a numerical investigation on the motions and added resistance of the Delft catamaran 372 in regular head waves using unsteady RANS CFD simulations. They showed that the interference factor varies with wave frequency, where the interference factor of total resistance in head waves oscillates around that of the calm water due to the pitch motion.

Lee et al. (2021a) carried out a series of CFD analyses for ship performance in regular waves. They employed the body-force propeller method of the virtual disk model to represent the effect of the propeller and reduce the computational time. The self-propulsion factors and power predicted by CFD were compared with results obtained using the load variation method.

Coslovich et al. (2021) developed an unsteady fully nonlinear boundary element method to calculate the ship motion and added resistance for the KVLCC2 hull in regular head waves at design speed. This study utilized an adaptive grid refinement scheme and a Mixed Eulerian-Lagrangian (MEL) approach based on potential flow model. They introduced the nonlinear decomposition for the free surface elevation and the velocity potential. It was found that generally good agreements can be observed for heave and pitch motion and added resistance compared to experimental data, especially for long waves.

Li et al. (2022b) conducted optimizing the dynamic trim of a 300000 DWT VLCC, considering both wind and wave loads. They introduced the Taylor Expansion Boundary Element Method (TEBEM) for calculating added resistance in both regular and irregular waves. They demonstrated that dynamic trim optimization was performed, resulting in a recorded fuel saving potential of approximately 0.04%.

2.8 CFD Applications

CFD applications are wide, and this section cannot be exhaustive. The degree of maturity of CFD is very high in some topics. As an example, Park et al. (2023) extended the scope of the design process to the performance of a ship in the in-service condition, with an emphasis on the added resistance due to waves. In their study, hull and fins are optimized thanks to Star-CCM+ simulations.

Added resistance and added power is indeed a very hot topic for CFD applications. Complex incoming waves are considered as oblique or cross waves. Other topics with nonlinear physics are also commonly tackled with CFD, such as roll damping, sloshing, high-speed vessels, and impacts.

A large portion of the studies is conducted with finite-volume implicit RANSE solvers, in particular with solvers built from the open-source platform OpenFOAM, and with the commercial Simcenter STAR-CCM+. There are still in-house solvers that are state of the art and very competitive on complex problems.

CFD is largely used for impact flow computation as slamming or other rarely occurring events, and the reader can refer to the specific sections.

2.8.1 Added resistance

Kobayashi et al. (2021) present a detailed guideline to compute motions and added resistance with an application on the Duisburg Test Case and the Japan Bulk Carrier. The results are obtained with an in-house solver with overset capabilities.

Lee et al. (2022b) compute the motion and added resistance on the KVLCC2 under various regular and irregular waves conditions with STAR-CCM+. The effect of the wave steepness is shown.

The consideration of the wave steepness in evaluating the added resistance is also the subject of Jawa and Minoura (2023). They compare several Fine Marine computations in regular and irregular waves to experiments.

Li et al. (2022c) also conduct simulations in irregular sea on the DTMB 5512 destroyer model with an in-house viscous overset code.

Islam and Soares (2022) using OpenFOAM also simulate the KCS in head regular waves.

Zhang et al. (2021d) use a functional SWENSE decomposition to simulate the KVLCC2 in waves with a finite difference in-house code. A similar work on the KCS is performed with another finite difference in-house code in Yu et al. (2023b).

Cho et al. (2023) study the added resistance and motion of a SVLCC in bow quartering waves using a soft spring system. They present the differences in results obtained when removing the mooring lines and restricting three DoF’s. The solver is STAR-CCM+.

CFD is also used for smaller size ships, Zheng et al. (2023b) study with STAR-CCM+ the performance of a tugboat in waves.

Sun et al. (2023) study with an OpenFOAM solver the impact of the moonpool configuration on motions and added resistance.

2.8.2 Added power

Lee et al. (2021b) provide some methodology to use a virtual disk in a self-propelled simulation done with STAR-CCM+.

Yu et al. (2023a) compare the results obtained using several body-forces propeller models, and a discretized propeller for a KCS advancing in waves. The simulations are performed with an in-house RANS solver. They discuss the applicability conditions of the propeller models.

Wang et al. (2023b) also compared the results of a KCS in waves by doing OpenFOAM simulations with an actual discretized propeller and with a body force model. The solver is an in-house OpenFOAM package with overset capabilities, Figure 45.

Figure 45: Vortical structures around ship hull. Above: actual propeller. Below: body force propeller, (Wang et al. 2023b).

Htay et al. (2021) also used a body-force model in CFD Ship-IOWA to assess the effectiveness of a Rudder Bulb Fins System.

Bi-directional waves are simulated with STAR-CCM+ to study the seakeeping behaviour of an S175 by Huang et al. (2021a). Green water and slamming are discussed.

A similar work is presented by Lu et al. (2022b), where the influence of cross waves in DTMB5415 motions is proposed.

A body-force propeller model developed in an in-house OpenFOAM package is tested in bow quartering seas in Wang et al. (2022d). The results are shown to be reasonable, and the difficulty associated with the oblique seas are discussed. Other wave directions are tested with the same solver in Wang et al. (2023c). Motions and added resistance are presented.

Sanada et al. (2022) assess the accuracy of CFD in estimating the added power in head and oblique seas for the KCS. An uncertainty analysis is conducted on both numerical and experimental results. They concluded that both EFD and CFD are fit for ship design use.

2.8.3 Sloshing and coupled motions with liquid tanks

Liu et al. (2022b) conduct a complex simulation, reproducing a parametric roll condition on the ONR Tumblehome carrying a liquid tank. They use an in-house overset RANSE solver.

Huang et al. (2021b) also investigate coupled motions with an in-house finite difference RANSE code and in Tao et al. (2023) for the vessel carrying aquaculture tanks. STAR-CCM+ is used with overset.

2.8.4 Roll motion

Duan et al. (2023) used Star-CCM+ to predict the roll damping and the excessive acceleration of a ship with moonpool.

Li et al. (2023c) simulate with an in-house URANS solver the extreme roll motion of the ONR Tumblehome in beam sea.

Still on the same ONR Tumblehome, Wu et al. (2022) reproduce the parametric roll happening in head waves, with an in-house overset RANSE code, Figure 46.

Figure 46: Body-fitted mesh used in the overset solver, Wu et al. (2022).

Koop et al. (2021) present modelling practices dedicated to decay calculations. The practices were verified during the Reproducible CFD JIP.

Decay calculations are also the object of Spyrou and Papadakis (2021), with an in-house URANSE solver.

Zhang et al. (2021e) reproduce Ikeda's forced roll experiment with a high-order fractional step finite volume solver. They compute the 2D coefficients and discuss the flow pattern and the effect of separation.

2.9 Seakeeping of High Speed Marine Vehicles

High-speed craft operating in waves are subject to significant and frequent slamming impacts. These do not only affect structural integrity but also human performance and safety. Consequently, research on the seakeeping of High-Speed Marine Vehicles (HSMV) seems to focus on three main areas:

1. Experimental and numerical predictions of motions and loads

2. Novel predictive methods for motions and loads (e.g. by machine learning)

3. Ride Control Systems (RCS) to improve passenger comfort and to actively reduce slamming and the resulting structural loads.

Over the past three years the most investigated types of HSMV were wave-piercing catamarans and trimarans.

2.9.1 Experimental and numerical investigations

A number of experimental and numerical studies on seakeeping of HSMV has been published over the last three years. Research focused on numerical solutions clearly dominates and experimental investigations were mainly conducted to validate the numerical studies. Numerical methods applied for the seakeeping of high-speed craft need to cope with highly nonlinear behaviour due to the large variations in wetted surface and impacts. This results in the adoption of nonlinear time domain methods. Besides the more traditional inviscid methods, CFD methods are becoming more and more popular.

Mai et al. (2023) experimentally studied the wave induced motions and loads on a 1.5 m long catamaran model that was towed with a spring-setup. Tests in both, regular and irregular waves were conducted in the wave basin of Changwon National University, Korea. The results obtained in regular waves consist of 6-DoF motions (response amplitude operator), wave-induced forces, and vertical acceleration. Results are compared with other catamarans and numerical methods to verify the accuracy of the experimental method. Results from tests in irregular waves, corresponding to sea states 2, 3, and 4, were used to directly obtain statistics of the motion responses of the catamaran. The motion responses in irregular waves are analysed by statistical analysis methods, based on motion times series and spectral analysis which employed the motion RAOs in regular waves and wave spectrum density. The motion response showed a good agreement between the spectral and statistical analysis methods.

Tavakoli et al. (2023a) presented a strongly coupled FSI numerical investigation of the water entry process of elastic hard-chine sections. A finite volume method (FVM) based flexible fluid-structure interaction (FFSI) based on the OpenFOAM CFD code was used to solve the multi-physics problem, Figure 47. Quantitative comparisons between experimental and computational results are also provided. Results show that the structural responses can attenuate the pressure acting on the hard-chine section for deadrise angles of 10, 20 and 30 degrees. For a section with a deadrise angle of 45 degrees, however, the pressure peaks at the keel, and is insensitive to elastic motions. It is concluded that the numerical results, presented in a non-dimensional format, may be useful for preliminary design purposes.

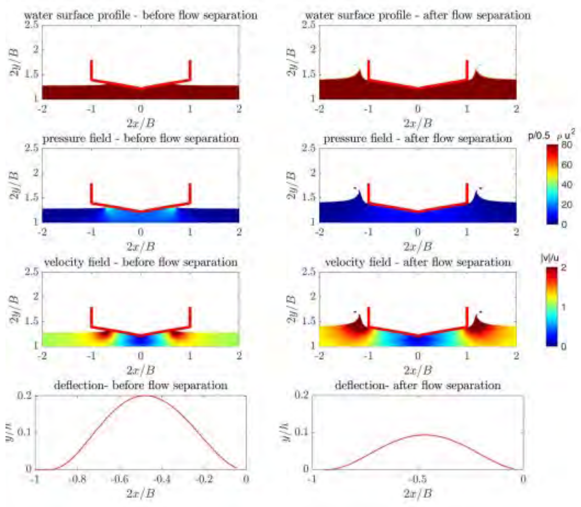

Figure 47: Fluid flow around a hard-chine section entering water at two different stages (Tavakoli et al. 2023).

Fu et al. (2021a, 2021b) studied the coupled roll-pitch motions of a trimaran in oblique stern wave conditions with the open source CFD code OpenFOAM. The numerical method is first validated against experimental data obtained in the towing tank of Harbin Engineering University and then used to study the motions of the vessel in waves. Results show i.e. that the rolling motion exhibits nonlinear characteristics.

Katayama et al. (2022) used the commercial CFD code STAR-CCM+ to calculate the flow field around different size prismatic planing surfaces and to investigate scale effects on their hydrodynamic forces. Their study highlights that, even in calm water, the accuracy of calculated frictional force is poor by appearance of Numerical Ventilation. In order to obtain more accurate results, the resolution of a partial mesh around the stagnation line needed to be increased and a surface tension model was considered.

Almallah et al. (2021) used the commercial CFD code STAR-CCM+ to study the global loads acting on the 98 m Wave Piercing Catamaran shown in Figure 50. A comparison to sea trial results indicated that full-scale CFD simulations combined with a rigid body dynamics formulation can be a reliable method to study motions and loads associated with high-speed vessels, Figure 48. The analysis was extended to oblique seas to investigate the torsional loads acting on the catamaran hull using CFD simulations by Almallah et al. (2022), Figure 49.

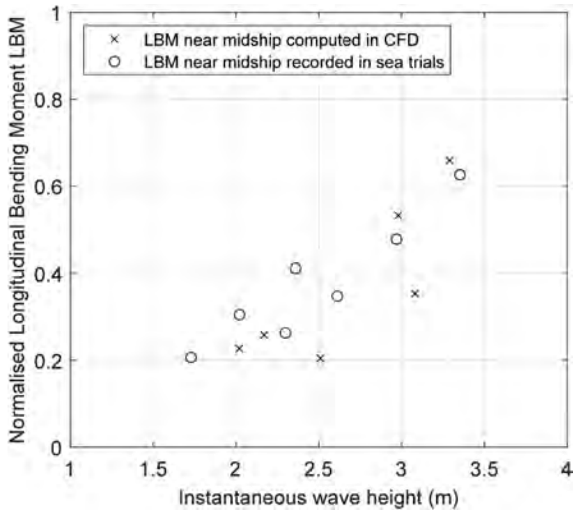

Figure 48: Slam longitudinal bending moment load as a function of instantaneous wave height prior to slam event (Almallah et al. 2021).

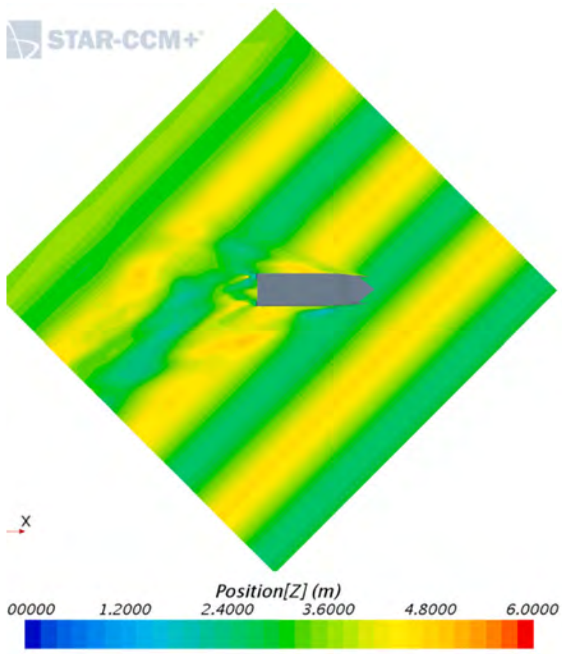

Figure 49: Water surface scene for verification of domain size in regular wave CFD in bow quartering seas at a speed of 20knots (Almallah et al. 2022).

Himabindu and Groper (2023), report on a Motion Assessment of Planing Craft in a Seaway (MAPCS) tool based on a nonlinear time-domain approach. The tool is compared against several other approaches based on experimental, empirical and classification societies' formulae and it is found that the MAPCS approach provides more realistic estimations compared to the other methods that were studied.

2.9.2 Statistical analysis and machine learning

A number of researchers have applied signal processing concepts and machine learning techniques to the seakeeping of HSMV.

Diez et al. (2022), for example, used a k-means data clustering approach to study what type of wave sequences cause different types of severe slamming. Using CFD results for the test case of an 8 ft generic prismatic planning hull (GPPH) the authors identify the number of clusters present in the data, and thereby the slamming types. For this they use two metrics, the within cluster sum of squares and the silhouette. In addition, the t-distributed stochastic neighbour embedding (t-SNE) is used to visualize data clusters in a reduced dimensionality space. The paper discusses how the proposed approach allows to investigate what type of wave sequences causes severe acceleration, pressure and strain peaks.

Marlantes and Maki (2022) applied a Long Short-Term Memory (LSTM) recurrent neural network (RNN) approach to the seakeeping problem of a planing craft. The method can make predictions of nonlinear ship motions in a range of wave conditions when trained on response data from only a single seaway. The method is formulated around the equations of motion in the time domain, but the equations are augmented with data-driven terms from the LSTM-RNN. The resulting hybrid governing equations are solved numerically. Predictions from the method are compared to nonlinear test data of 2-DoF motion of a GPPH at forward speed in head seas, with time histories given for both regular and irregular waves. The training data requirements to classify a specific seaway are investigated and quantified. Predictions over a range of significant wave heights and peak periods are performed using training data from only a single seaway to show the effectiveness of the method in generalizing across different environmental conditions.

Sebhatleb et al. (2023) used classical, response reconstruction by transmissibility functions to predict slamming and wave load responses of the wave-piercing catamaran in Figure 50. The transmissibility functions and matrix are first derived from a small portion of the available sea trial data and then tested under the same operating condition they were derived. Then a single transmissibility matrix is used to reconstruct responses for various sea states, vessel headings and speeds. The transmissibility matrix is also tested under sea states that were not included in its derivation ("unseen data"). Good agreement is achieved, particularly for larger loading events that would be of interest to structural designers.

Zheng et al. (2023a) analysed heave and pitch motions of a trimaran, both with a "direct" CFD calculation method and with an "indirect" method based on particle swarm optimization (PSO) and polynomial fitting methods, to identify transfer function parameters. To compare the direct and indirect methods, tank tests of the trimaran were performed. Results show that the direct and indirect methods are all effective for calculating the heave and pitch motions of a trimaran.

2.9.3 Ride Control Systems (RCS)

Controlling vessel motions using Ride Control Systems (RCS) to ensure smoother journeys is a widely adopted practice and continues to be of interest to the industry. Such systems regulate vessel motions, enhance passenger comfort, and reduce structural loads.

Zhang et al. (2021b) report on developing a robust anti-pitching controller for a high-speed multihull. They propose a decoupled anti-pitching controller composed of a proportional–

differential (PD) control term and an extended state observer (ESO)-based uncertainty compensation term. The stability of the closed-loop control system is first proven theoretically. The effectiveness of the algorithm is then verified by simulations and experiments in which the heave and pitch are reduced by 20–35 % and 40–50 %, respectively.

Lau et al. (2022) analysed the influence of an active T-foil on motions and passenger comfort for a large high-speed wave-piercing catamaran (WPC, Figure 50).

Figure 50: 98 m Incat Tasmania Hull 061 WPC and swift ride-control surface locations (Lau et al. 2022).

More specifically, the influence of a ride-control system on the heave and pitch response amplitude operator (RAO) of the full-scale high-speed catamaran was investigated using extensive sea trial data from the US Navy. The reduction in motion sickness incidence (MSI) was estimated to examine the effectiveness of the RCS in improving passenger comfort. With the existing control algorithm, the vertical accelerations were found to be best controlled by the active T-foil working together with the active stern tabs, while the pitch RAO was mainly mitigated by deploying only the stern tabs. About a 23% reduction was observed in the peak heave RAO with deployment of an active T-foil. The MSI can be reduced by up to 23% with respect to the cases with stern tabs only. The analysis was later extended to oblique wave directions (Lau et al. 2023b) and, in terms of MSI percentage reduction, the ability of T-foil in vessel motion control in oblique seas was found to be limited compared to the results in head seas.

Lau et al. (2023a) developed the Forcing Function Method (FFM), a CFD-based approach to efficiently evaluate the effectiveness of different Ride-Control System geometries. Their work encompasses two main components: a standalone T-foil analysis and an assessment of the influence of various RCS geometries on a Wave-Piercing Catamaran, Figure 51 by FFM. In the standalone T-foil study, the lift and drag forces were investigated with respect to the angle of attack and immersed depth. The results indicated that the T-foil lift coefficient diminished logarithmically by decreasing the immersed depth smaller than 1 chord length. They utilised the FFM to examine different RCS geometries on a 2.5 m WPC model operating at a speed of 2.89 m/s (Fr~0.6). The effectiveness of motion control is evaluated by measuring the changes in sinkage and trim over time after deflecting the FFM T-foil by ±15° in calm water. Through these CFD simulations, the impact of total planform area, number of T-foils, and longitudinal location of the T-foil were analysed. It was found that controllability of motion was a function of total planform area, regardless of the number of foils, and although moving the T-foil away from the bow reduces motion control in trim, it does not affect sinkage significantly.

Figure 51: Incat Tasmania 112 m wave piercing catamaran ‘Express 1’ and 2.5 m model in towing tank (Lau et al. 2023a).

Javanmard et al. (2023) report on a set of towing tank model tests in irregular waves to study the effectiveness of different control algorithms, including linear and nonlinear versions of the heave control, pitch control, and local control. The model was again a 2.5 m scaled model of a 112 m INCAT Tasmania high-speed catamaran. The RCS included a centre bow-fitted T-foil and two transom-mounted stern tabs, Figure 52.

Figure 52: 2.5 m model of Incat Tasmania 112 m WPC in the towing tank at Australian Maritime College. Location of the fitted T-foil (left) and stern tabs (right) operating as active RCS. Javanmard et al. (2023).

Ma and Zuh (2022) proposed an enhanced active disturbance rejection controller (ADRC) which compensates for the wave-induced heave and pitch motions of a fast trimaran. Controller parameters are optimized via a novel Levy flight-based ant colony algorithm (LACA). Numerical simulations and experiments under different sea conditions were conducted to validate the proposed method. Results showed the effectiveness of the proposed motion controller in improving the seakeeping performance of the trimaran.

Using the same trimaran ship model, Xu et al. (2023a) proposed a sliding mode predictive anti-pitching control considering appendages constraints. The control method combines the advantages of model predictive control and sliding mode control to both improve the strong robustness of the system and to ensure the optimization and the ability to handle constraints explicitly. The vertical motion model is established for multihulls with two types of appendages, T-foils and flaps, to achieve anti-pitching. According to the characteristics of the first-order autoregressive wave disturbance model, a low complexity disturbance observer is devised to estimate the wave disturbance force and moment online and combine the estimates with the prediction model to enhance the accuracy of the prediction. On this basis, a prediction model and an objective function are established with the sliding mode states as variables, and the sliding mode terminal stability constraint set is adopted to improve the stability of the closed-loop system. The effectiveness of the designed controller is verified by simulation and experiment, in which the multihull heave displacement is reduced by 52 % and the pitch angle is reduced by 58 %.

Li et al. (2023a) investigated the roll-pitch coupling of a trimaran in oblique head waves and how this can be attenuated by a T-foil RCS. They used fully nonlinear unsteady RANS simulations based on the finite volume method to study the motions of the vessel with and without RCS. Results show that lower forward speed and large wave steepness will lead to roughly coupled motion in oblique head waves and that nonlinear characteristics of ship motions were present during coupled motions. A T-foil RCS can significantly reduce the motion responses and have a positive effect on the coupled motion of the trimaran.

2.9.4 Design aspects

Marin-Lopez et al. (2021) and Paredes at al. (2022) describe the conceptual design of a small high-speed craft providing inter-island transportation in the Galápagos. An optimization procedure at conceptual design level was developed. First, time histories of vertical accelerations on an existing ferry were measured and analysed. Weighted acceleration signals are compared with those from well-known experimental tests and are also used to evaluate the index of motion sickness with ISO 2631 standard to determine the number of persons affected by craft motion. Then, an optimization procedure using feasible directions is implemented with a combination of resistance and CG acceleration of the vessel to be minimized. Both functions were evaluated using well-known empirical formulations. The results show that by increasing length and deadrise angle, and moving LCG forward, it is possible to reduce the acceleration by 20 % while obtaining a 4 % reduction in resistance.

3. PROCEDURES

As part of ToR 2 the committee was tasked to review the existing ITTC Recommended Procedures relevant to seakeeping and identify any requirements for changes in the light of current practice. After discussions with the Advisory Council the updates summarised in the next sections were made.

The Committee also added a list of suggested keywords and an abstract for DOI registration to each procedure.

Additionally abstracts and keywords for DOI registration were written for all procedures and submitted to the ITTC Secretary.

3.1 Seakeeping tests HSMV (7.5-02-05-04)

The procedure was updated with some minor editorial revisions. Furthermore, a reference that was not cited in the text was removed from the reference list.

3.2 Seasickness HSMV (7.5-02-05-04.1)

The procedure was updated by correcting erroneous references and pointing out that the underlying ISO standards are superseded. Nevertheless, the ITTC procedure (and the superseded ISO standard explained in it) are still valuable because it directly shows discomfort boundaries, whereas the newer standard uses the concept of “motion sickness dose value”, MSDV.

3.3 Structural loads HSMV (7.5-02-05-06)

The following changes have been done to procedure 7.5-02-05-06:

- Minor changes to the text in Section 1.
- Section 2 is renamed from “Test techniques and procedures” to “Model design and test techniques for HSMV”
- Section 2 has been restructured and now includes these subsections:
  - 2.1 Relevant HSMV procedures
  - 2.2 Loads and load effects
  - 2.3 Design of models for measurement of global load effects
  - 2.4 Local loads and load effects
- The order of the sections “Parameters” and “Validation” has been interchanged.
- The layout of the “Parameters” section has been changed from numbered to bulleted points.
- The list of parameters to be taken into account has been updated.

3.4 Seakeeping experiments (7.5-02-07-02.1)

Minor editing changes proposed.

3.5 Power prediction in irregular waves (7.5-02-07-02.2)

The following minor editorial revisions were applied:

- Some display errors in Table 1 - Summary of prediction methods - has been fixed.
- Uncited references have been removed.

3.6 Rarely occurring events (7.5-02-07-02.3)

Some minor editorial revisions were applied. In addition, the following changes were applied:

- Chp1: The reference to ITTC procedure 7.5-02-05-07 has been deleted as the - procedure was withdrawn
- Introduction of Section 2.4: The text was extended by recommendations to references for determination of statistical quantities. Respectively the reference list was extended.
- Section 2.5: An example with reference was added to study the severity of extreme conditions. Furthermore, a short paragraph about too high or too low events was deleted.
- Section 4.1: The parameter list was adapted to the ITTC standard

3.7 Validation of seakeeping computer codes (7.5-02-07-02.4)

This procedure has been deleted.

3.8 V&V of linear/weakly nonlinear computer codes (7.5-02-07-02.5)

The following changes have been done to procedure 7.5-02-07-02.5:

- Last line in Section 2.3, a dot is added to ITTC procedure 7.5-02-07-02.1.
- Last line in Section 2.4, Harmonic motions and loads. Is deleted. Because for time domain linear seakeeping simulations the assumption of Is not necessarily right.
- In Table 1 linear method, Impulse-Response-Function, is added.
- In Section 3.1 Geometry formula is corrected from KM+BM to KB+BM is equal to KG+GM
- In Section 5.7 Check cargo modelling is corrected.
- In reference, Ikeda Y, Himeno Y, Tanaka N.，1978，Prediction method for ship roll damping， Report No.00405 of Department of Naval Architecture, University of Osaka.is added

3.9 Global loads seakeeping (7.5-02-07-02.6)

Besides editorial revisions the following changes were applied:

- Section 2.1: The text was made more to the point and a paragraph about comparison of complexity in model construction was deleted. Another paragraph was rewritten to increase readability
- Section 2.2: A figure of different model types for global load tests was added.
- Section 2.4: The section was partly rewritten to condense the important information and increase the readability
- Section 2.8: The headline and content were supplemented with respect to towed model tests. Additionally, the first paragraph about the powering of the model was rewritten from the perspective of the current state of science.
- Section 2.9: Two paragraphs were rearranged with the images within this section and sensor recommendations were added.
- Section 2.10: The first section was supplemented by statements on the importance of decay tests and how to perform those tests.
- Section 3.1: In this section as well as at the reference list a reference was added.
- Section 4.1: The parameter list was completed and adapted to the ITTC standard.

3.10 Sloshing (7.5-02-07-02.7)

Minor editing changes proposed.

3.11 Calculation of weather factor - fw (7.5-02-07-02.8)

Procedure 7.5-02-07-02.8 was slightly modified with the following changes:

- The reference section has been updated.
- List of symbols and parameters has been updated and aligned with ITTC notation.
- A secondary axis has been added to Figure 2 to underline the issue of fw-waves and small vessels.
- Editorial changes have been made, including compliance with ITTC standard format of procedures (e.g., placing the “Parameters and Symbols” section at the end, not at the beginning)
- Section 4 has been re-named from “Recommended Practical Method” to “Example Practical Method” to underscore that the combinations shown in Table 3 are not mandatory.
- Table 3 has been modified to make it more practice oriented.

4. NEW GUIDELINE ON CFD FOR SEAKEEPING (TOR3)

Under ToR 3 the committee was asked to create a new guideline on verification and validation of the CFD methods for seakeeping analysis.

The task was approached through the following five steps:

1. Review of literature and existing procedures that could be relevant for this topic.
2. Identify key areas within the general topic of CFD methods for seakeeping analysis.
3. Contact Specialist Committee on Combined CFD/EFD and discuss what is their view on seakeeping and CFD.
4. Contact a number of prominent researchers in the field asking concrete questions regarding the need for ITTC guidelines on Seekeeping and CFD ("How to use" guidelines and V&V).
5. Elaborate recommendations regarding this topic.

Each step with details and discussions are presented in the next subsections.

4.1 Review of literature

Seakeeping analysis with CFD includes a number of diverse physical problems that are covered by the other procedures of the SKC, e.g:

- Rarely occurring events
- Global loads
- Motions
- Added resistance
- Sloshing
- Damage stability in waves
  Hydroelasticity in waves

The requirements for the CFD simulations would depend on the particular problem.

Literature on how to use and V&V for these topics is generally scarce, though several papers were published in the recent years.

For subjects such as maneuvering or resistance or self-propulsion, ITTC CFD "how to use" guidelines exist separated from V&V procedures. They indicate the requirements of the numerical models (turbulence, scheme order) and provide information on parametrization (domain size, time stepping, grid discretization).

The ToR mentions several types of CFD solvers, but the V&V approach is mostly used with mesh-based CFD solvers (except sloshing, where particle methods can be competitive).

4.2 Identify key areas

Wave generation and propagation are fundamental parts of seakeeping CFD simulations except uncoupled sloshing. CFD is much more dissipative than an actual test and the quality of the wave is by itself a problem that could require guidelines and V&V. This also introduces the question whether waves should be calibrated beforehand for a procedure on how to conduct a CFD seakeeping test. If the answer is positive, how should this calibration be carried out (on which mesh, …).

Other aspects that might need attention:

- How to obtain calm water resistance?
- How to introduce the waves in the domain?
- How to deal with velocity ramping?
- How to avoid residual transients, etc. ?
- Towing points, springs need to be specified.

About V&V, the generic V&V guidelines deal with a set of constant scalar outputs (calm water resistance, sinkage, trim, etc.). For seakeeping problems the outputs can be much more complex. What are the quantities that should be targeted by the V&V? Is it something like the 1^{st} harmonic of a series of quantities, or mean values as in added resistance problem, the maximum load during an impact, or even a transient time trace?

4.3 Contact Specialist Committee on Combined CFD/EFD

A dialogue was opened with the SC on Combined CFD/EFD Methods. However, not much momentum was gained with such dialogue.

4.4 Contact prominent researchers

A number of prominent researchers in the field were contacted following this interchange asking concrete questions regarding the need for ITTC guidelines on Seakeeping and CFD ("How to use" guidelines and V&V). Diverse answers were received from Prof. El Moctar, Prof. Maki, Dr. Koop and Dr. Vaz. Such answers have been useful to confirm that:

- the matter is relevant,
- there is no clear consensus on how to proceed, with many open questions along the aforementioned lines.
- therefore, it could be too early for a full V+V guideline
- a V&V procedure is important to be able to justify potential "How to use" guidelines (time stepping, mesh size).

4.5 Elaborate recommendations

Considering all what has been mentioned, our recommendation for the next term reduces to propose that ITTC should create a Specialist Committee on Seakeeping and CFD, with the following tentative ToRs:

- Follow the new literature on the topic.
- Assess whether the same structure as in manoeuvrability should be followed ("How to use" guidelines and V&V separated guidelines).
- Assess how to adapt such guidelines to the seakeeping particularities, e.g. whether to focus explicitly on particular matters such as average value of added resistance in waves, or whether to have a holistic approach, looking into the unsteady variables such as short-term statistics of resistance, motions, etc., or any other given events.
- Define the role of the quality of the input wave, and how to handle it in the V&V procedure. Should waves be calibrated first?
- Define how to obtain calm water resistance, necessary for the computation of the added resistance in waves.
- Define how to introduce the waves in the domain.
- Define how to deal with velocity ramping and how to avoid residual transients etc.
- Specify how towing points, springs should be defined.
- Decide whether to focus on conducting a wide comparison study by several groups to settle the matter before writing guidelines.
- Decide whether some use can be given to the experimental ITTC seakeeping benchmark carried out during the 2021-2024 term.
- Decide whether a practical approach should be developed as well to be able to get confidence in the results without having to go through a likely expensive V&V study.
- Define how to conduct V&V when coupling CFD solvers with structural solvers in springing or whipping problems.

5. FUNCTIONALITY OF FW-PROCEDURE FOR SMALL SHIPS (TOR4)

5.1 Background

As part of ToR 4 the committee was tasked to investigate the "functionality" of the fw-procedure (7.5-02-07-02.8) when applied to ships smaller than 150 m in length.

As a first step the history of this task has been tracked, and it became apparent that the issue is not about the prediction methods listed in procedure 7.5-02-07-02.8 but about in how far the wind and wave conditions defined by IMO are appropriate for small ships.

In the fw-context IMO currently specifies only one single “representative” sea condition, regardless of ship size, see Table 1 below.

Table 1: Representative sea conditions based on IMO (2012).

Significant wave height $H_{1/3W}$	3.0 m
Mean wind speed 10m above sea surface U_{10}:	12.6 m/s
Zero-up crossing period T_2	6.16 s

The corresponding long-crested wave energy spectrum from IMO (2012) is plotted in Figure 53. As illustrated by the secondary abscissa in the figure this spectrum contains a lot of energy in the wavelength region of around 100 metres. It can therefore be expected that ships of around 100 m length and below will severely pitch when encountering such waves. These motions, and the related accelerations might require a voluntary speed reduction by the ship’s master to avoid excessive motions and loads.

Consequently, the wave conditions are not “representative”/typical any longer.

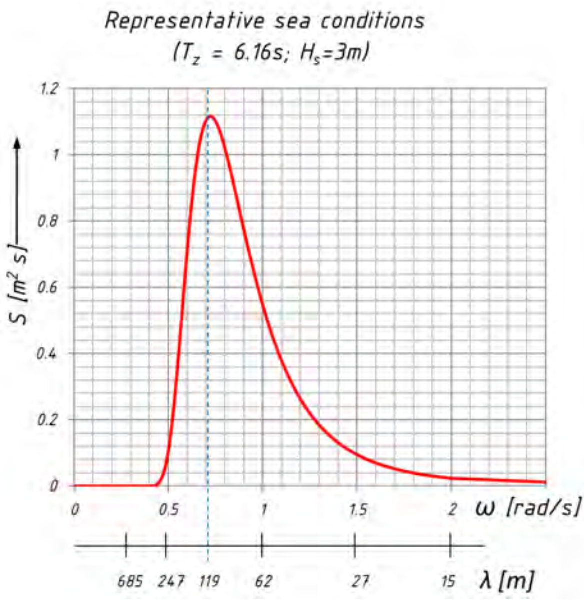

Figure 53: Wave energy spectrum *S(ω)*. Secondary x-axis shows length of regular deep-water wave with same frequency.

5.2 Available data for small ships in fw-waves

A literature search resulted in only one published value of the weather factor fw for a small ship. Gerhardt and Kjellberg (2017) conducted experiments for a 96-metre vessel in fw-wave conditions according to IMO (2012) (Table 2). For this ship we get fw=0.67. The corresponding ship speed at 75% MCR is about 9knots.

As part of their work the committee has located the original experimental dataset behind the Gerhardt and Kjellberg (2017) publication, re-evaluated the results, and compared motions and accelerations to criteria for voluntary speed reduction from the literature, Nordforsk (1987). Results are summarised in Figure 54.

Table 2: Main parameters of ship tested in fw-waves by Gerhardt and Kjellberg (2017).

Parameter	Value
Length, Lpp	96 m
Breadth, moulded	18 m
Draft forward (FP)	4.7 m

Parameter	Value
Draft aft (AP)	4.7 m
Block coeff.	0.74
Displacement	5900 m^3
GM	0.76 m
Radii of gyration, roll	0.33 B
pitch & yaw	0.23 Lpp

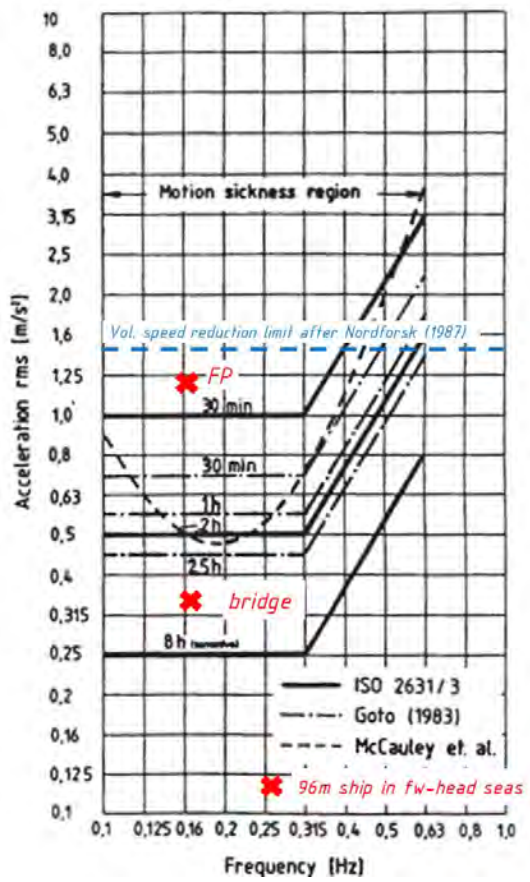

Figure 54: Severe discomfort boundaries with regard to vertical acceleration as a function of frequency for different exposure times (Nordforsk 1987). Also shown are seakeeping model test results for a 96 m ship (Gerhardt and Kjellberg 2017).

As Figure 54 shows, motion induced vertical accelerations will create some discomfort, particularly near the forward perpendicular but values are below, albeit close to, the limit for voluntary speed reductions from Nordforsk (1987), illustrated by the blue line in the figure.

The probability of green water on deck was also evaluated by the committee and found to be 0.06, slightly above the limiting value of 0.05 (events per 100 wave encounters) from Nordforsk (1987).

In summary it can be said that a voluntary speed reduction for small vessels appears to be relevant and should be investigated further. Future investigations should focus on ships smaller than 100 m, but still within the applicability of the EEDI.

5.3 Suggested changes to fw-procedure

As a result of the above investigation ITTC procedure 7.5-02-07-02.8 was slightly modified to further highlight the issue of voluntary speed reduction for small ships, see Section 3.11 above.

5.4 Suggested next steps

Since experimental data for small ships in fw-conditions is rare, it is recommended that the next Seakeeping Committee uses simulations to investigate the topic of 'voluntary' speed reduction for vessels smaller than 100 m in length, but still within the applicability of the EEDI. If required, such simulations can also be used to develop alternative, milder sea states for small ships.

6. NEW GUIDELINE ON MINIMUM POWER REQUIREMENT (TOR5)

Under ToR 5 the committee was asked to "investigate if there is any practical problem in the application of MEPC.1/Circ.850/ Rev.2 for minimum power requirement, and develop a new ITTC guideline, if needed."

6.1 Background

The introduction of the EEDI more than a decade ago, slow steaming, and the wish to reduce bunkering costs have resulted in a trend to install less powerful engines in ships. To avoid vessels becoming underpowered and thus unsafe, the International Maritime Organization

(IMO) has published a guideline regarding the "Minimum Propulsion Power to Maintain the Manoeuvrability of Ships in Adverse Conditions". IMO "Interim Guideline" MEPC.1/Circ.850/Rev.2 outlined the details of how to determine this "Minimum power".

Since July 2021 there is a Rev. 3 of this IMO circular. The most significant change from Rev.2 to Rev.3 is dropping the required speed for safe manoeuvring from in between 4 and 9 knots (depending on relative size of the rudder) to just 2 knots, while simultaneously prescribing slightly harsher weather conditions.

The work of the 30th ITTC Seakeeping Committee has focused on Rev. 3 as the latest version of the IMO circular.

6.2 New ITTC guideline

After discussions with the ITTC Advisory Council a new ITTC "Guideline on determining Minimum Propulsion Power to Maintain the Manoeuvrability of Ships in Adverse Conditions" has been drafted. This draft has been shared and discussed with the Manoeuvring and Full-Scale Ship Performance committees and their feedback has been incorporated.

The draft is mainly based on MEPC.1/Circ.850/Rev.3 but it gives additional explanations and fills in gaps where required. Additionally, the draft guideline contains an example that follows the calculation process step by step and works out minimum power for the KVLCC2 tanker. It is hoped that this case study helps with understanding the calculation process and provides useful benchmarking data. A shortened summary of this case study is reproduced in Section 6.4 below.

For space reasons the 19-page draft guideline is not reproduced here, but it is available from the ITTC Secretary.

6.3 Problems found in IMO Circ.850/Rev.3

The main issues that the committee found in IMO MEPC.1/Circ.850/Rev.3 are:

1. The IMO circular appears to be contradictory in the choice of peak wave periods.
2. The IMO circular gives "default conservative" estimates for thrust deduction factor and wake fraction. These values appear to be questionable.
3. It is unclear whether the IMO-suggested 3 % thrust increase to account for rudder action in waves is realistic.

The following subsections briefly explain the above three issues. More details can be found in the draft guideline available from the ITTC Secretary.

6.3.1 Peak wave periods

The IMO circular appears to be contradictory on what range of peak wave periods T_P should be used in the minimum power assessment (step 16 of the IMO assessment contradicts the T_P values listed under the spectrum definitions by IMO).

6.3.2 Choice of propulsive factors

The IMO circular states that: "calm-water resistance, self-propulsion factors and propeller open-water characteristics, are defined by the methods approved for EEDI verification" and also gives "default conservative" estimates for thrust deduction factor and wake fraction; t=0.1 and w=0.15 respectively.

These values for t and w are based on IMO submission MEPC 72/5/9 by China (Figure 55) and reflect results from one single set of self-propulsion model tests in the speed range of 2-7 knots. It is unclear how the challenges in conducting low speed model tests were addressed and what type of ship (full block or low block coefficient) the results represent.

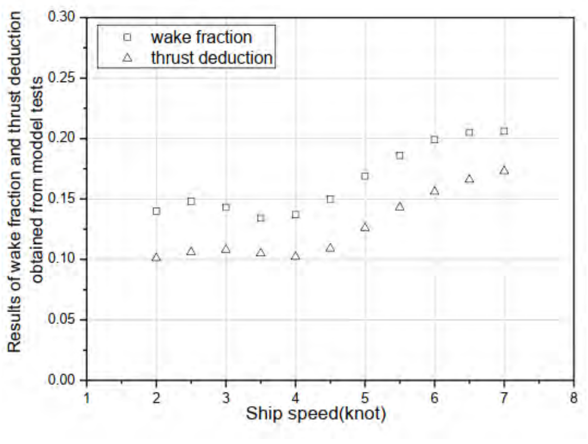

Figure 55: Wake fraction and thrust deduction factors at low speeds, from IMO submission MEPC 72/5/9.

As illustrated by the KVLCC2 case study in the next section, power predictions based on t=0.1 and w=0.15 are not necessarily conservative for a full-block ship. Particularly the choice of t=0.1 appears to be optimistic, compare top part of Figure 59.

More research on the behaviour of thrust deduction factor and wake fraction for different ships at low speeds is clearly needed before general recommendations about default values for t and w can be made. In addition to looking at w and t separately, such research should also evaluate the resulting hull efficiency η_h.

In the absence of more reliable data, the ITTC draft procedure now recommends relying on other methods approved for EEDI verification, i.e. ship specific model tests. In most cases, such model test results should already be available from the mandatory EEDI tests at standard speeds (i.e. 75 % MCR). Extrapolating wake, thrust deduction factor and relative rotative efficiency from these tests down to a speed of 2 knots appears to be preferable over the use of the generic IMO default values.

6.3.3 Rudder drag in waves

At this stage it is unclear whether the above 3 % value for added thrust due to rudder action is realistic. Further research in this area is required.

6.4 KVLCC2 case study

To investigate if there is “any practical problem in the application” of the IMO procedure this section contains a summary of a case study that follows MEPC.1/Circ.850/Rev.3 and the ITTC draft guideline step by step.

6.4.1 Benchmark case KVLCC2

Due to the availability of data and the usefulness as a benchmark case it was decided to use the KVLCC2 for such a case study.

Figure 56 shows a photograph of the 4.7 m long model used for the seakeeping tests related to the case study. A second, larger model was used to assess calm water performance in a towing tank.

Figure 56: KVLCC2 model used for study.

6.4.2 Adverse conditions

The environmental conditions in the IMO guideline are not defined by one single wave condition but by spectra with modal (peak) periods varying from 7 s to 15 s. As a result, not one but several predictions of minimum power need to be carried out. The highest power value calculated during this process determines the required engine MCR. For a large ship like the KVLCC2 (L_{pp}=320 m) three example spectra according to Table 1 are plotted in Figure 57.

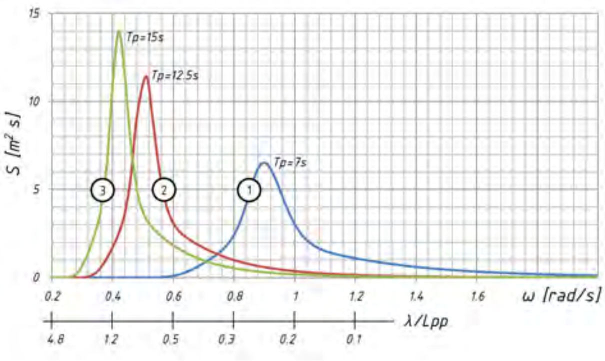

Figure 57: Example JONSWAP spectra. *Hs*=6 m and 3 different modal periods Tp. Secondary x-axis shows length of regular deep-water wave with same frequency, relative *Lpp*.

6.4.3 Resistance components

Figure 58 illustrates resistance components for the KVLCC2 sailing at 2 knots. As can be seen the calm water resistance is negligible compared to added wind and wave resistance. The total resistance for the three example spectra becomes:

R1=1060.2 kN

R2=1286.9 kN

R3=1089.8 kN

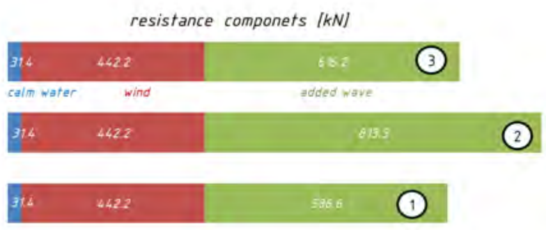

Figure 58: Comparison of resistance components for KVLCC2 at 2 knots.

The individual resistance components behind these numbers were determined as follows:

- Calm water resistance: Towing tank tests with a 7 m model
- Added wind resistance: Based on $X'_w = 1.1$
- Added wave resistance: Regular wave tests with the model from Figure 56.

6.4.4 Choice of propulsive factors

Based on the data presented in Figure 59 the following values for the propulsive factors were used in the case study: *t*=0.18 and *w*= 0.3 (blue lines in Figure 59). The figure also shows the IMO default values in red. A representative value for the relative rotative efficiency was also chosen based on tank tests results: η_R = 1.052.

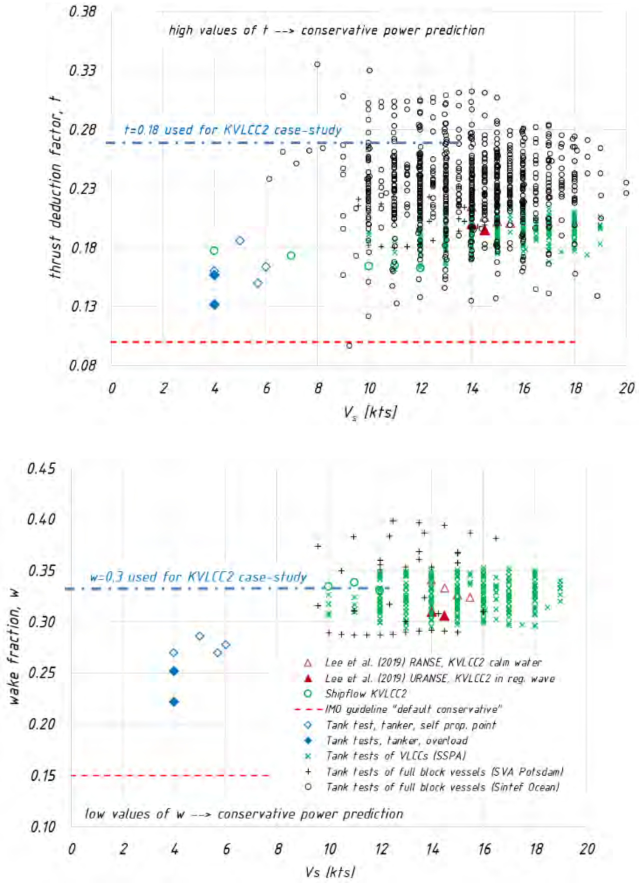

Figure 59: Wake and thrust deduction factors for tankers.

6.4.5 Calculation of required break power

Figure 60 shows results from the calculation of required power to maintain a speed of 2 knots in wind and waves.

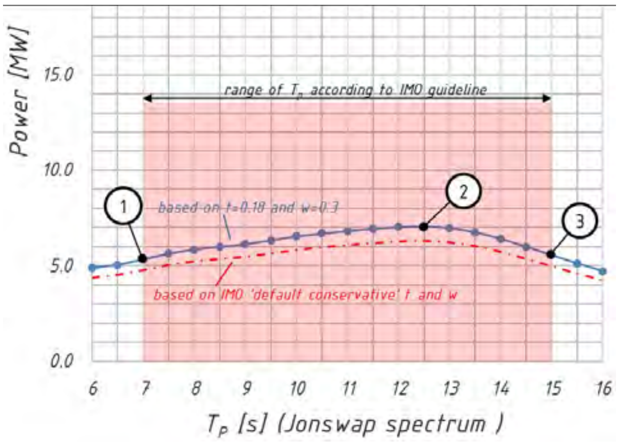

Figure 60: Required power to maintain a speed of 2 knots as function of modal period *Tp*.

The maximum required power and the corresponding *rpm* for the KVLCC2 correspond to point ② on the blue line in Figure 60:

$$P_B^{req} = 7.1\ MW \quad @\ 45.2rpm$$

The red line in Figure 60 represents power values based on the "default conservative" estimates of thrust deduction *t* and wake fraction *w*. As can be seen the IMO "default conservative" estimates produce power values that are not conservative.

6.4.6 Available break power

The above value of 7.1 MW is only the required shaft power to propel the ship at 2 knots. For combustion engines, torque and other limitations must be considered.

To determine the available brake power P_B^{av} of the installed engine, Figure 61 finally plots the operational points 1-3 (i.e. power/rpm combinations corresponding to wave spectra 1-3) into load diagrams for two engines.

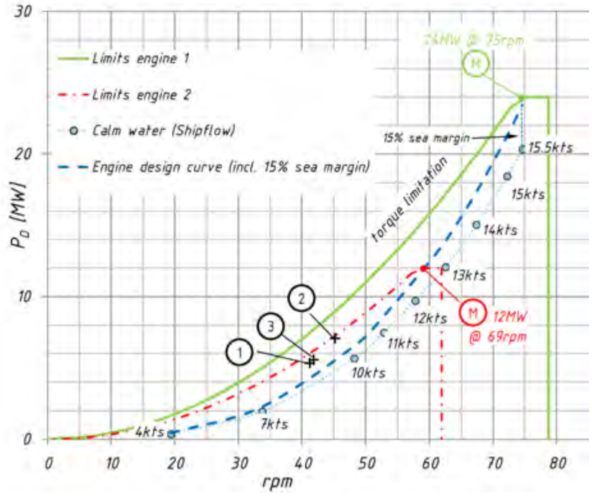

Figure 61: Engine load diagram.

Engine 1, with an MCR of 24 MW at an *rpm* of 75, is a typical VLCC-engine (green solid line). It can bring the KVLCC2 up to a design speed of 15.5 knots in calm water with a sea margin of 15 %. Engine 2 (red dash-dotted line) is much smaller (12 MW @ 69 *rpm*) and can be considered a "slow steaming" option. It will propel the ship at about 12.2 knots in calm water with the same sea margin as the larger engine.

It can be seen from the figure, that the larger engine will deal effortlessly with all the situations the KVLCC2 might encounter under the "IMO adverse conditions". This is because the operational points (①②③) end up below the torque limit line (solid, green curved line).

Engine 2 on the other hand will just be able to provide the required power for *Vs* = 2 knots. As illustrated in the figure at Point ② the available engine power equals the required power:

$$P_B^{av} = P_B^{req} = 7.1\ MW \ \ (\ @\ 45.2rpm)$$

For the KVLCC2 such an engine with an MCR of 12 MW is the minimum that can be installed while still complying with IMO minimum power requirements.

6.5 Suggested next steps

The ITTC "Guideline on determining Minimum Propulsion Power to Maintain the Manoeuvrability of Ships in Adverse Conditions" that was drafted by the 30th Seakeeping Committee is a technical interpretation of IMO MEPC.1/Circ.850/Rev.3. During the preparation of the guideline three issues became apparent, see Section 6.3 above. The next ITTC Seakeeping Committee should investigate these in detail and update/improve the draft guideline prepared by the 30th committee accordingly. For more details see Section 11.3 at the end of this report.

7. NEW GUIDELINE ON WIND LOADS FOR SHIPS (TOR6)

Under ToR 6 the SKC was asked to develop a guideline on wind loads for ships, collaborating with the committees related to this issue.

After review of the first progress report (dated August 2022), the SKC was asked by the Advisory Council (AC) to list and summarise the methods for estimating wind loads in ITTC procedures; see Table 3 and Table 4.

Table 3: Wind load prediction methods as recommended in various ITTC procedures.

ID #	Procedure	Generic Values	Dedicated WT	Dedicated CFD	Direct modelling (wind during experiment)	Datasets for typical ships	Generic regression method	Refers to ITTC 7.5-04-01-01.1
①	ITTC 7.5-02-03-01.4	✓	✓					
②	ITTC 7.5-02-03-01.5							✓
③	ITTC 7.5-02-07-02.8		✓	✓		✓	✓	✓
④	ITTC 7.5-02-07-03.6		✓					
⑤	ITTC 7.5-02-07-04.1		✓		✓			
⑥	ITTC 7.5-02-07-04.2				✓			
⑦	ITTC 7.5-02-07-04.4		✓	✓		✓	✓	
⑧	ITTC 7.5-03-02-05		Not applicable (guideline on how to do CFD)					
⑨	ITTC 7.5-04-01-01.1		✓	✓		✓	✓	
⑩	ISO 15016:2015		✓			✓	✓	

Table 4: Summary of wind related content.

ID #	Procedure	Summary of wind part
①	ITTC 7.5-02-03-01.4 78 Performance Prediction Method	Guideline mentions air drag coefficient of ship above waterline. Can be determined from wind tunnel tests. Value of 0.8 can be used as default value
②	ITTC 7.5-02-03-01.5 Predicting Powering Margins	Refers to ITTC 7.5-04-01-01.1: (and ISO 15016 which is very similar)
③	ITTC 7.5-02-07-02.8 Calculation of the Weather Factor fw for Decrease of Ship Speed in Wind and Waves	Section 3.5.2 says: *"This resistance component is calculated in accordance with ITTC Procedure 7.5-04-01-01.1: Preparation, Conduct and Analysis of Speed/Power Trials"* Wind force coefficient best found from WT tests. Alternatively: WT tests of similar ship, WT results from Blendermann, viscous flow CFD or Fujiwara
④	ITTC 7.5-02-07-03.6 Dynamic Positioning System Model Test Experiments	Text: "In general, the following model test program should be carried out for floating structures equipped with DP systems: Wind tunnel tests to determine wind resistance coefficients"
⑤	ITTC 7.5-02-07-04.1 Model tests on intact stability	Direct modelling of wind forces via fan-arrays or force coeff. From separate WT tests.
⑥	ITTC 7.5-02-07-04.2 Model tests on damaged stability in waves	"Model must be allowed to drift freely under influence of waves and wind" Direct modelling of wind forces via fan-arrays as one possible method, no other methods specified
⑦	ITTC 7.5-02-07-04.4 Simulation of Capsize Behaviour in Irregular Beam Seas	"Wind load coefficients in six degrees of freedom can be obtained from wind tunnel experiments and CFD, or from empirical methods based on non-dimensional wind tunnel data. Examples are Isherwood (1972), Blendermann, (1994) and Fujiwara (1998)
⑧	ITTC 7.5-03-02-05 Use of CFD methods to calculate wind resistance coefficient	Guideline on how to use CFD for prediction forces acting on above water parts of ships
⑨	ITTC 7.5-04-01-01.1: Preparation, Conduct and Analysis of Speed/Power Trials	For calculating the resistance increase due to wind one of the following methods are to be used. F.1. Wind resistance coefficients by wind tunnel test If wind resistance tests for the specific, or similar, vessel have been performed in a qualified wind tunnel, the wind resistance coefficients derived by these measurements shall be used to compute the wind resistance of the vessel in the trial condition. F.2. Wind resistance coefficients by CFD F.3. Data sets of wind resistance coefficients Guideline gives dataset for common ship types F.4. Regression formula by Fujiwara et al.
⑩	ISO 15016:2015: Guidelines for the assessment of speed and power performance by analysis of speed trial data	Annex C: Resistance increase due to wind C.2.1 Wind tunnel test C.2.2 Data set on the wind resistance coefficient C.2.3 Regression formula by Fujiwara et al.

It was found that many different methods are recommended in various procedures. It was found that the best and most recent recommendation on how to determine wind resistance was in Annex F of ITTC procedure 7.5-04-01-01.1 - Preparation, Conduct and Analysis of Speed/Power Trials.

The SKC made the following recommendations at the start of 2023 and in the second progress report (dated August 2023):

- Extend Appendix F of ITTC 7.5-04-01-01.1 so that it covers aerodynamic forces and moments in more degrees of freedom (minimum surge, sway, pitch and roll);
- Lift the hereby revised Appendix into a standalone procedure;

- Modify all procedures listed above: remove all recommendations about wind loads and refer to new procedure.

In October 2023, feedback from AC was received and the SKC was asked to develop a standalone wind load guideline based on Appendix F of 7.5-04-01-01.1

This was done at the start of 2024 and at the end of February, the draft document was circulated to other relevant committees for comments and when relevant, modified accordingly. A table of the modifications needed in other ITTC procedures was also produced and circulated for comments. The final version of this table will be handed over to the next committee via the ITTC secretary.

The work of the current SKC and the discussions with other committees have shown that there is a need to address a significant number of wind-related issues. Tasks could include:

- Include wind load coefficients for side force, yawing moment and roll moment in the new guideline on "Wind Loads on Ships";
- Improve this guideline, make it more comprehensive and turn it into an ITTC procedure;
- Survey state of the art in describing atmospheric boundary layer profiles (ABL) and natural turbulence spectra of the wind over the sea. Unify equations to describe ABL profiles across all ITTC procedures;
- Make recommendations how to measure wind speed and direction in the disturbed flow around a moving ship;
- Develop ITTC guidelines on wind tunnel testing of ships;
- Investigate the question whether Wind Tunnel Facilities working with ships, marine structures and wind propulsion technologies should be invited to join ITTC.

8. EXPERIMENTAL BENCHMARK ON ADDED RESISTANCE (TOR7)

In the 30th term the Seakeeping Committee has organised a world-wide benchmarking study on measuring added resistance in waves.

8.1 Background

Under ToR 7 the Committee was asked to "Organize a benchmark experimental campaign, including the added resistance measurement in oblique seas and different loading conditions, and the characterization of the uncertainty in the measurement of added resistance." To this end all ITTC members were invited to join a benchmark study.

8.2 Organisation of study

The study was prepared and organised by a working group consisting of nine members from the Seakeeping Committee (F. Gerhardt; M. Minoura; B. Bouscasse, BW Nam, K. Domke, A. Souto-Iglesias, W. Duan, Y. Pan, B. Malas). A series of initial discussions and industry interviews resulted in the following structure of the study.

8.2.1 Call for participation

All ITTC membership organisations were invited to participate in a benchmark campaign with the following format:

- Seakeeping tests with scale models of a VLCC/tanker (KVLCC2, Table 5)
- Tests in regular and irregular waves. Head and following seas as well as oblique wave directions.
- Choice of two KVLCC2 models that can be borrowed free of charge (Table 6). Alternatively, model built by participant.
- All steps from model preparation over testing procedures to measurement-evaluation to be documented and shared with ITTC.

- All experimental costs to be paid for by participants.
- ITTC to summarise results and share with all participants.
- Option to withdraw results before final publication.

Table 5: Main parameters of KVLCC2 as used in this benchmarking study (target values).

Ship particulars	Value
L_{pp} [m]	320.0
Beam, B [m]	58.0
Design draft, T [m]	20.8
Gyradius roll [m]	$0.40 \cdot B$
Gyradius pitch [m]	$0.25 \cdot L_{pp}$
Gyradius yaw [m]	$0.25 \cdot L_{pp}$
GM [m]	5.7
Displacement [m^3]	312 784
VCG	18.6

Table 6: Main particulars of available KVLCC2 models.

Ship particulars	SSPA/RISE	CEHIPAR
Scale	68	80
LPP [m]	4.706	4
Beam [m]	0.853	0.725
Draft [m]	0.306	0.26
Displacement	995 kg	611 kg
Weight (empty model)	250 kg	120 kg

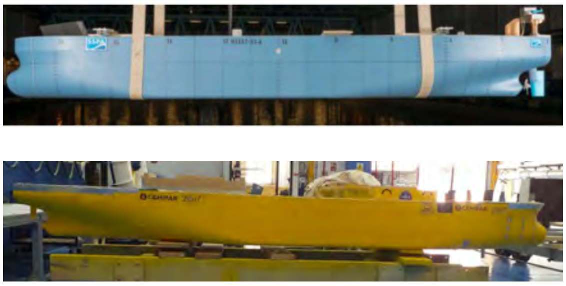

Figure 62: The two freely available models (SSPA/RISE top, CEHIPAR bottom).

The test program is summarised in Table 7 below. Participants could choose between three different levels of involvement:

- Towing tank: head and following seas only, time requirement about 5 days
- Seakeeping basin (light version): 3 wave directions, time requirement about 9 days
- Seakeeping basin (full version): 7 wave directions, time requirement about 22 days

8.2.2 Participating organisations

A total of sixteen ITTC member organisations answered the call and expressed general interest in the study. Of these, ten organisations were eventually able to conduct tests and submit results in time. In alphabetical order:

1. CSSRC
2. Gdansk University of Technology
3. Hanwha Ocean
4. IMABARI Ship Model Basin
5. KRISO
6. MARIN
7. Osaka University
8. RISE
9. Samsung model basin
10. SVA Potsdam

To preserve anonymity each of these organizations was assigned a random letter from A-J.

8.3 Test program and participation

The suggested test program from the call for participation is shown Table 7 below. Table 8 provides an overview of the facilities A-J and Table 9 finally summarises actual test programs as conducted in each of the ten facilities.

Table 7: Suggested test program from call for participation

Regular waves

Design draft, 15.5 knots

		H/λ		Wave direction: 180 (head)	150	120	90	60	30	0
				Nr. repeats						
λ/Lpp	0.2	4%	2%	4	4	4	4	4	4	4
	0.3	4%	2%	4	4	4	4	4	4	4
	0.4	4%	2%	3	3	3	3	3	3	3
	0.5	4%	2%	3	3	3	3	3	3	3
	0.6		2%	3	3	3	3	3	3	3
	0.7		1%	3	3	3	3	3	3	3
	0.8		1%	2	2	2	2	2	2	2
	0.9		1%	2	2	2	2	2	2	2
	1		1%	2	2	2	2	2	2	2
	1.1		1%	2	2	2	2	2	2	2
	1.2		1%	2	2	2	2	2	2	2
	1.3		1%	2	2	2	2	2	2	2
	1.4		1%	2	2	2	2	2	2	2
	1.6		1%	2	2	2	2	2	2	2
	2		1%	2	2	2	2	2	2	2

Nr runs		SSPA-example calc		
per dir.	52			
Tank	104	Tank		
Basin (light)	156	Basin (light)	7.8	days
Basin (full)	364	Basin (full)	18.2	days

Irregular long-crested waves

IMO min power (ToR #5)
MEPC.1/Circ.850/Rev.3
Vs=2kts
Jonswap Hs=6m
Tp= [7s, 7.5s...15s] 17 waves
short crested by spreading fct.
or 1.3*head wave Raw
minimum 17 runs in head waves

Nr runs		SSPA-example calc		
Tank	17	Tank		
Basin (light)	17	Basin (light)	1	days
Basin (full)	102	Basin (full)	6	days

Fw tests (ToR#4)
ITTC 7.5.-02....-2.8
Vs @ 75% MCR
ITTC spectrum Hs 3m
Tz=6.16s
short crested by cos^2 spreading fct.
or 1.0* head wave Raw
12 runs (6 long-crested wdir, 2 speeds)
min 2 runs (180deg, 1 speed above, 1 below 75% MCR)

Nr runs		SSPA-example calc		
per dir.	0			
Tank	2	Tank		
Basin (light)	2	Basin (light)	0.1	days
Basin (full)	12	Basin (full)	1	days

we need more than 100 waves for this project

Total, per draft

Nr runs		SSPA-example calc		
per dir.				
Tank	123	Tank	0	
Basin (light)	175	Basin (light)	9	days
Basin (full)	478	Basin (full)	25	days

Levels of involvement

Table 8: General information on facilities A-J and model data

	General info								
Participant	**Facility type**	**Wavemaker**	**Setup**	**Scale**	**Rudder present**	**Propeller present**	**turbulence stim.**	**Method of of determining model inertia**	**GM / incliantion test**
A	Tank	plunger type	towed with springs	68	yes	dummy hub	trip wire	same load plan as Participant G	yes
B	Basin	flap type	towed (free in roll heave pitch; springs in surge sway yaw)	58	yes	dummy hub when towed	2 trip wires	inertia measuring and adjustment platform	yes
C	Basin & Tank	segmented flap	1. free sailing surge retrained 2. soft mooring 3. Free sailing 4. towed (free in heave + pitch) 1-3 basin, 4. tank	68	yes	yes	trip wire	shaker table	yes
D	Basin	segmented flap	soft mooring with springs	58	no	no	studs	CAD modelling, swing testing	yes
E	Tank	segmented flap	Towed (2kts) & free sailing (15.5 kts)	68	yes	yes	studs	CAD modelling, inclining test, free decay test	yes
F	Basin	plunger type	towed with springs	98.6133	yes	no	studs	swinging in pitch	yes
G	Basin	flap type	soft mooring with springs	68	yes	dummy hub when towed	trip wire	swining in yaw and roll	yes
H	Tank	plunger type	soft mooring with springs	50	yes	dummy hub	studs	swing table	yes
I	Tank	flap type	towed	110	no	no	trip wire	swinging in pitch	yes
J	Tank								

Table 9: Test program in facilities A-J and information on data analysis

Participant	Test program					Min. Nr. of wave enc.		Data Analysis	
	wave calibrations prior to tests	regular waves, 15.5 knots	regular waves, 2 knots	minimum power 2 knots irreg. Waves	fw tests	Regular waves	Irregular waves	Regular waves	Irregular waves
A	yes	180 & 0 deg	x	180 deg, 17 periods	irregular waves, 180deg, 2 speeds	10	50		Statistical analysis, zero-up crossing from time histories, Significant values from counting zero-up
B	yes	180, 150,120, 90,60,30, 0 deg	180deg	180 deg, 11 periods	x	15	200	Fourier Analysis	
C	no	180, 150,120, deg	x	x	irregular waves, 180, 150, 120 deg, 1 speed	?	0.5h full scale time	Fourier Analysis	
D	yes	180, 150,120, deg	x	180 , 150deg, 12 periods	irregular waves, 180, 150, 120deg, 3 speeds	10	100	Fourier Analysis	Statistical analysis, zero-up crossing from time histories, Significant values from counting zero-up
E	yes	180deg	x	180,150,120 ,90,45,0 deg, up to 14 periods	irregular waves, 180deg, 3 speeds	10	150	Fourier Analysis	
F	yes	180, 150,120, 90,60,30, 0 deg	x	180 deg, 12 periods	irregular waves, 180, 150, 0deg, 2 speeds	10	100	Fourier Analysis	
G	yes	180, 150,120, 90,60,30, 0 deg	180, 150,120, 90,60, deg	x	x	10	100	Fourier Analysis	Statistical analysis, zero-up crossing from time histories, Significant values from counting zero-up
H	yes	180 & 0 deg	x	180 deg, 17 periods	irregular waves, 180deg, 3 speeds	10	200	Fourier Analysis	
I	yes	180deg	x	x	x	15	x	Fourier Analysis	
J									

8.4 Results

8.4.1 Achieved mass properties and metacentric heights

Achieved metacentric heights (GM-values) from the different participants are shown in Figure 63. As can be seen in most cases the deviation from the target value of 5.7 m is smaller than ±1.5% with many participants reporting values less than ±1%.

Figure 63: Deviation of achieved GM values from target value, participants A-J.

As Figure 64 and Figure 65 show, the deviations from the target volume displacement of 312784 m^3 and the target pitch gyradius of $0.25 \cdot L_{pp}$ and are even smaller.

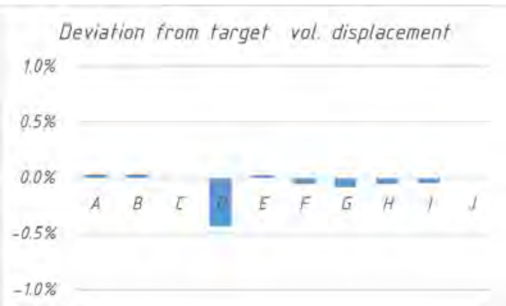

Figure 64: Deviation of achieved displacements from target value, participants A-J.

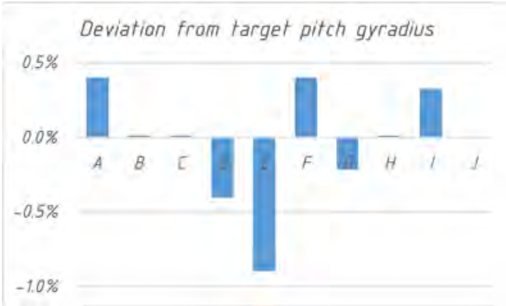

Figure 65: Deviation of achieved pitch gyradii from target value, participants A-J.

Figure 66 illustrates that most institutions do not put equally tight requirements on achieving the nominal yaw gyradius, deviations are up to 2%. As far as pure seakeeping tests are concerned this approach of focusing on the pitch inertia instead appears to be sensible.

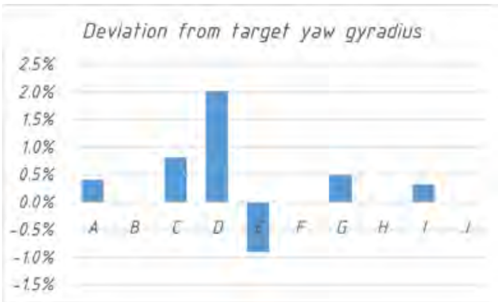

Figure 66: Deviation of achieved yaw gyradii from target value, participants A-J.

Only a few participants reported achieved values for roll gyradii. Values are summarised in Figure 67. Due to the model design and structural strength reasons, participant B chose 0.37 B as the roll inertia of the model This explains the large deviation of around 7%.

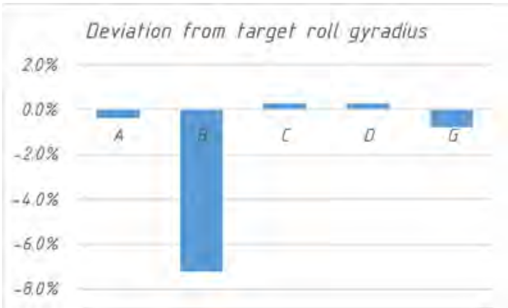

Figure 67: Deviation of achieved roll gyradii from target value, only relevant participants.

8.4.2 Repeatability of regular waves

Participants were asked to supply wave surface elevation measurements from repeatedly sending the same signal to the wavemaker and comparing measured results to the target values. Results for wavelength ratios of λ/L_{pp} = 0.3, 0.5, 1.1 and 2.0 are shown in Figure 68.

8.4.3 Regular wave tests at 15.5 knots

Figure 69 shows a comparison of the Quadratic Transfer Functions (QTF) in regular head seas as reported by the various participants.

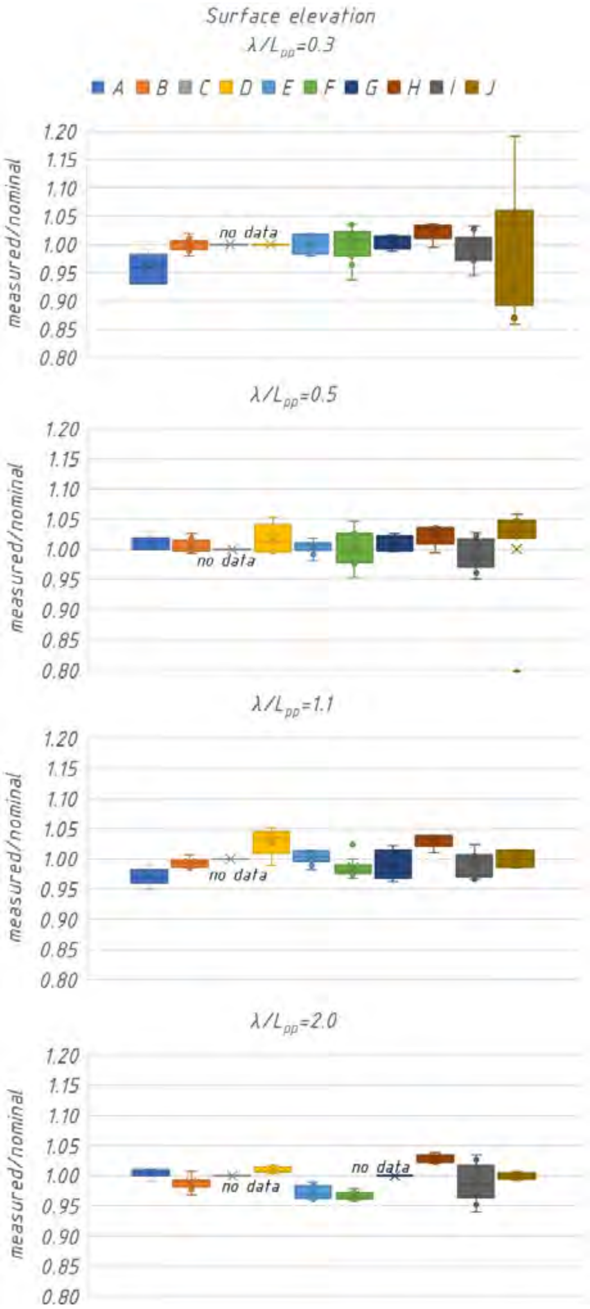

Figure 68: Comparison of measured and target surface elevations (“wave heights”) for 4 wavelength ratios.

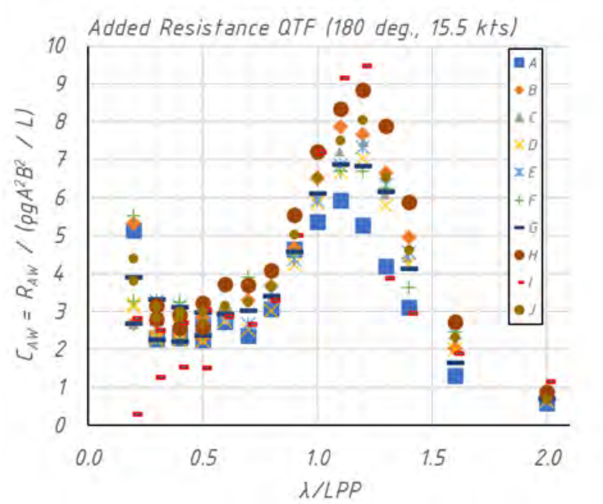

Figure 69: Added resistance coefficient QTF in head seas, comparison of results from all participants.

Figure 70 and Figure 71 show the corresponding Response Amplitude Operators (RAOs)

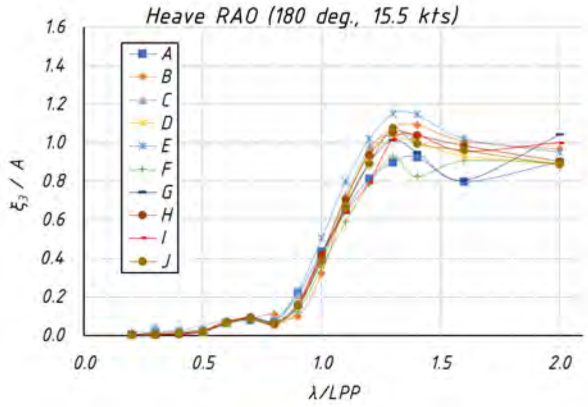

Figure 70: Heave RAO in head seas, comparison of results from all participants.

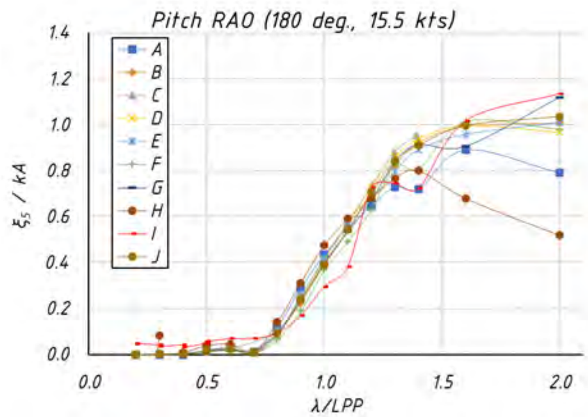

Figure 71: Pitch RAO in head seas, comparison of results from all participants.

Figure 72 to Figure 77 show comparisons of the added resistance coefficient QTFs for wave direction ranging from 150 degrees to following waves.

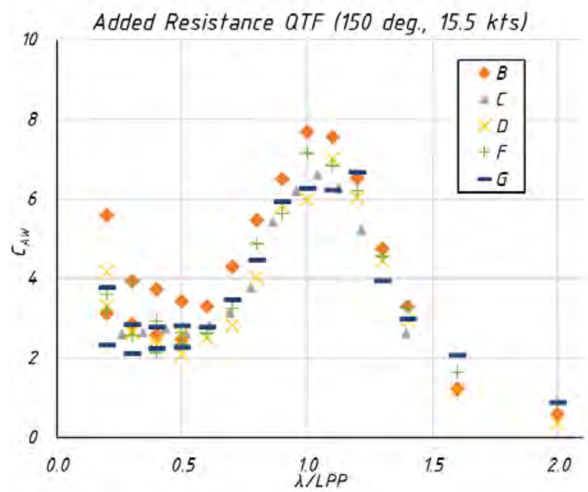

Figure 72: Added resistance QTF in 150 degree wave direction.

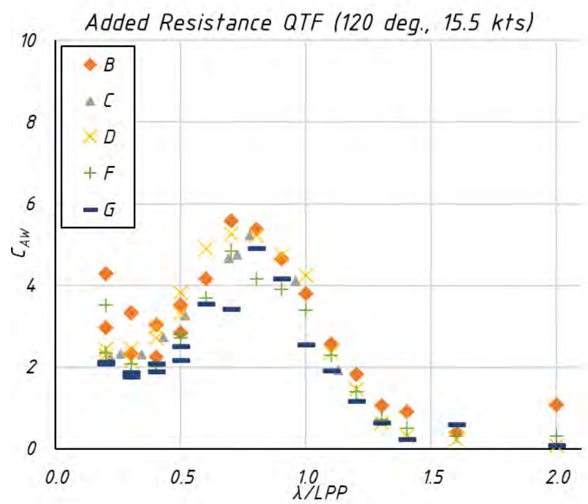

Figure 73: Added resistance QTF in 120 degree wave direction.

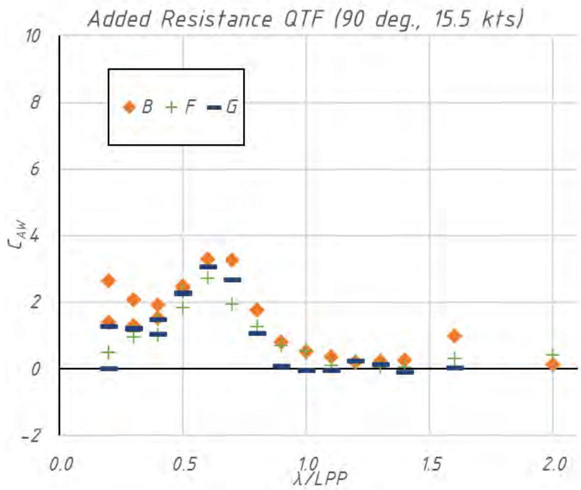

Figure 74: Added resistance QTF in beam waves.

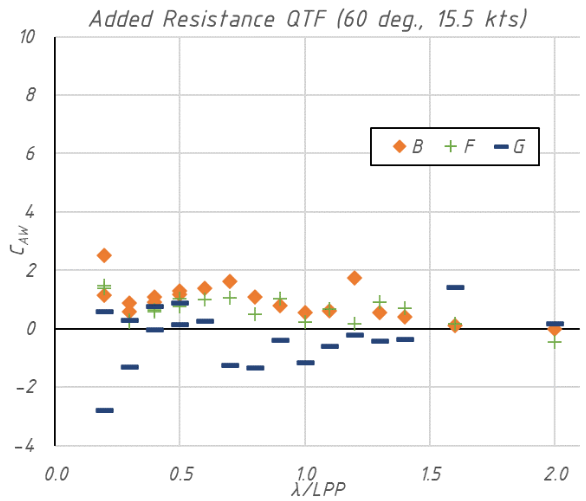

Figure 75: Added resistance QTF in 60 degree wave direction.

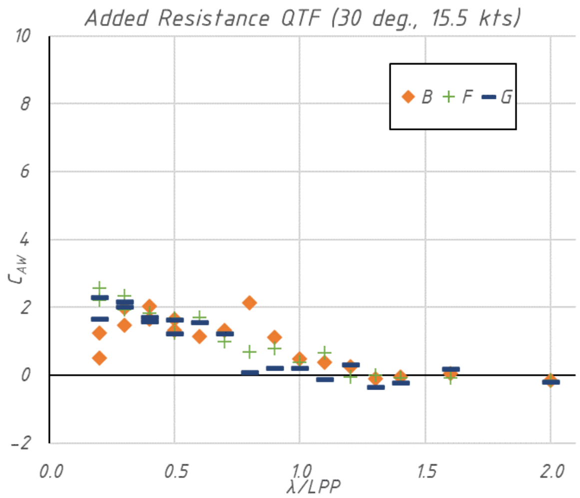

Figure 76: Added resistance QTF in 30 degree wave direction.

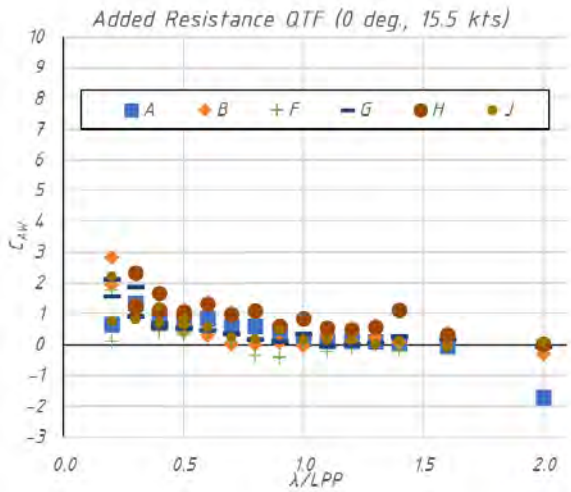

Figure 77: Added resistance QTF in following waves.

Participants B, F, and G conducted seakeeping tests in a basin and provided measured data for all wave directions. Their results are compared in the "radar plots" below, Figure 78 to Figure 81.

8.4.4 Irregular wave tests at 2 knots

In addition to the design speed tests in regular waves, tests in irregular waves were conducted at the very low speed prescribed in the IMO regulations on "minimum power".

IMO MEPC.1/Circ.850/ Rev.3 defines the "adverse conditions", under which the ship should be able to sustain the advance speed V_s by means of JONSWAP wave spectra with a range of peak (modal) periods varying from 7 s to 15 s. Before this background participants in the benchmarking study were asked to conduct irregular wave tests with the KVLCC2 sailing at 2 knots.

Participants A, D, E, F, H, and J submitted results for this part of benchmarking campaign, and these are compared in Figure 82. As illustrated in Table 8 all participants chose to use a towed model for these low-speeds tests.

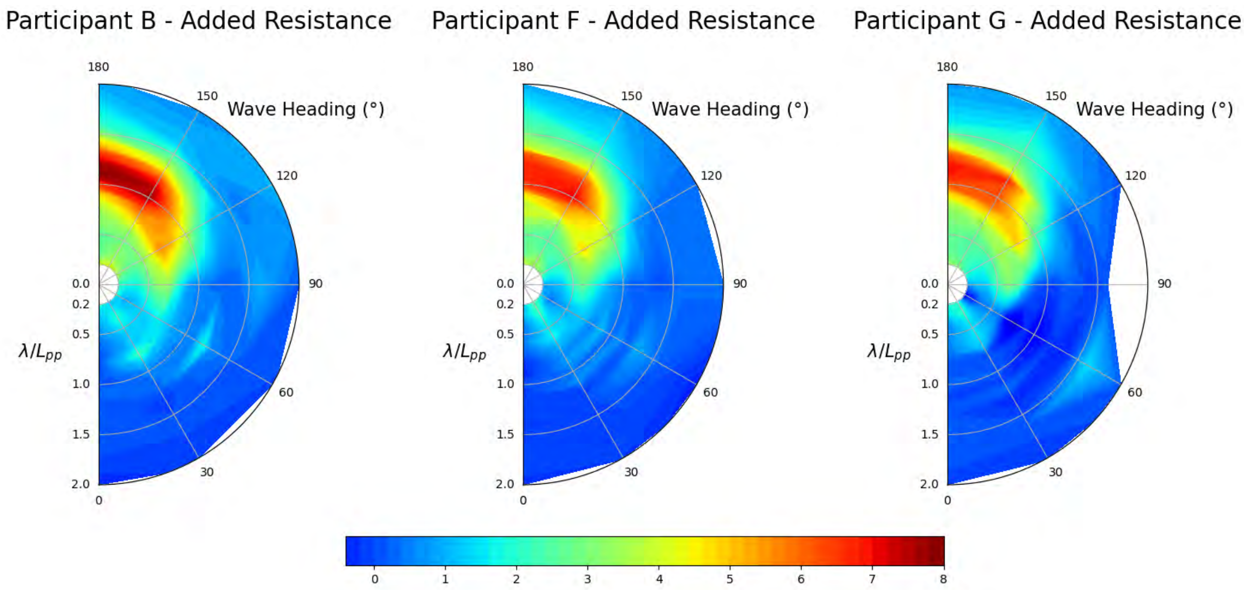

Figure 78: Added resistance coefficient QTF as function of wave direction, same non-dimensionalisation as Figure 69.

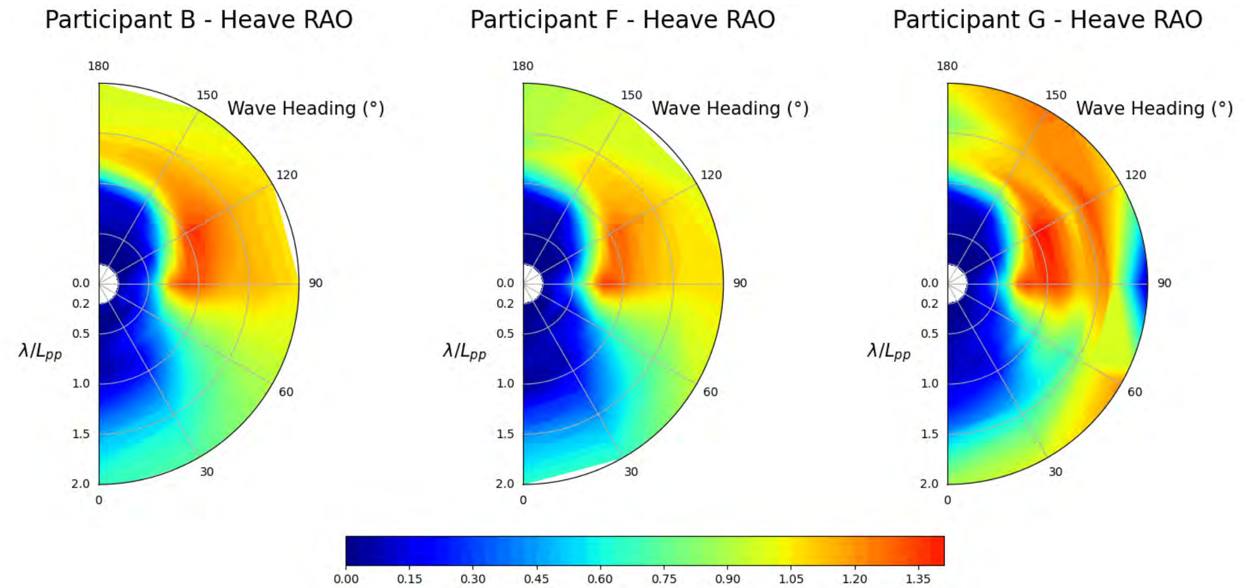

Figure 79: Heave RAO as function of wave direction, same non-dimensionalisation as Figure 70.

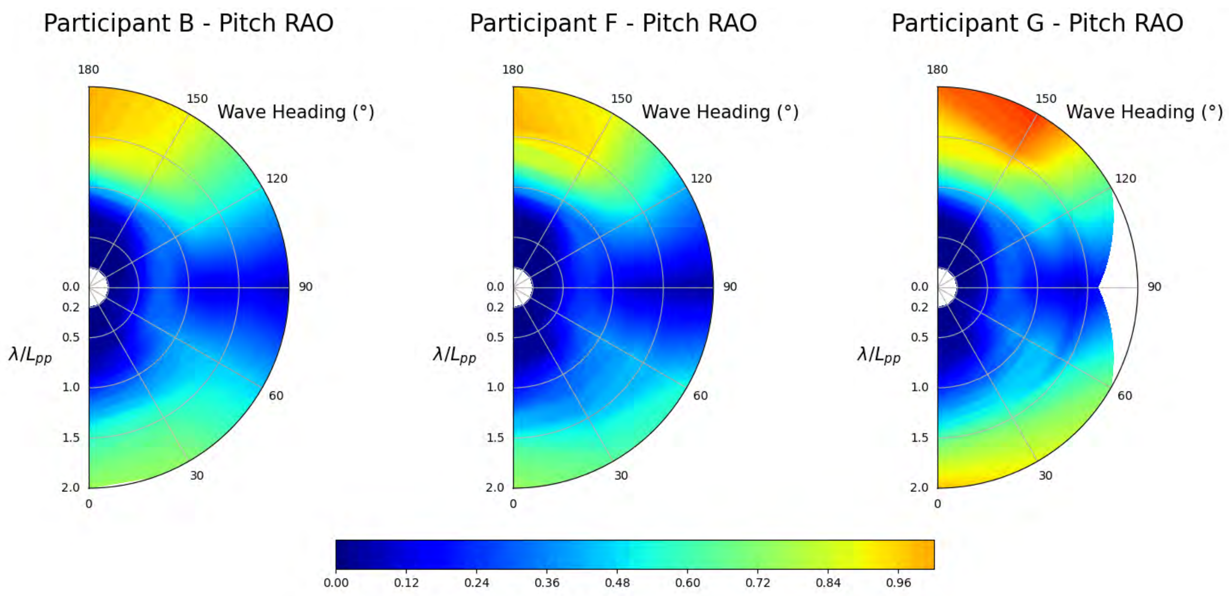

Figure 80: Pitch RAO as function of wave direction, same non-dimensionalisation as Figure 71.

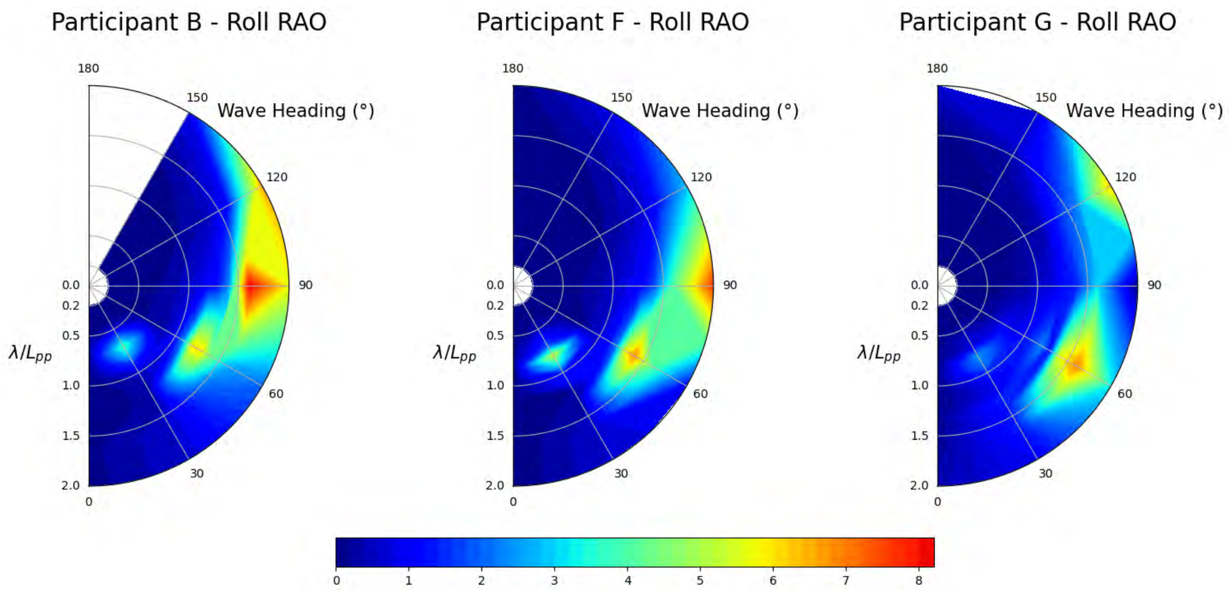

Figure 81: Roll RAO as function of wave direction, same non-dimensionalisation as Figure 71.

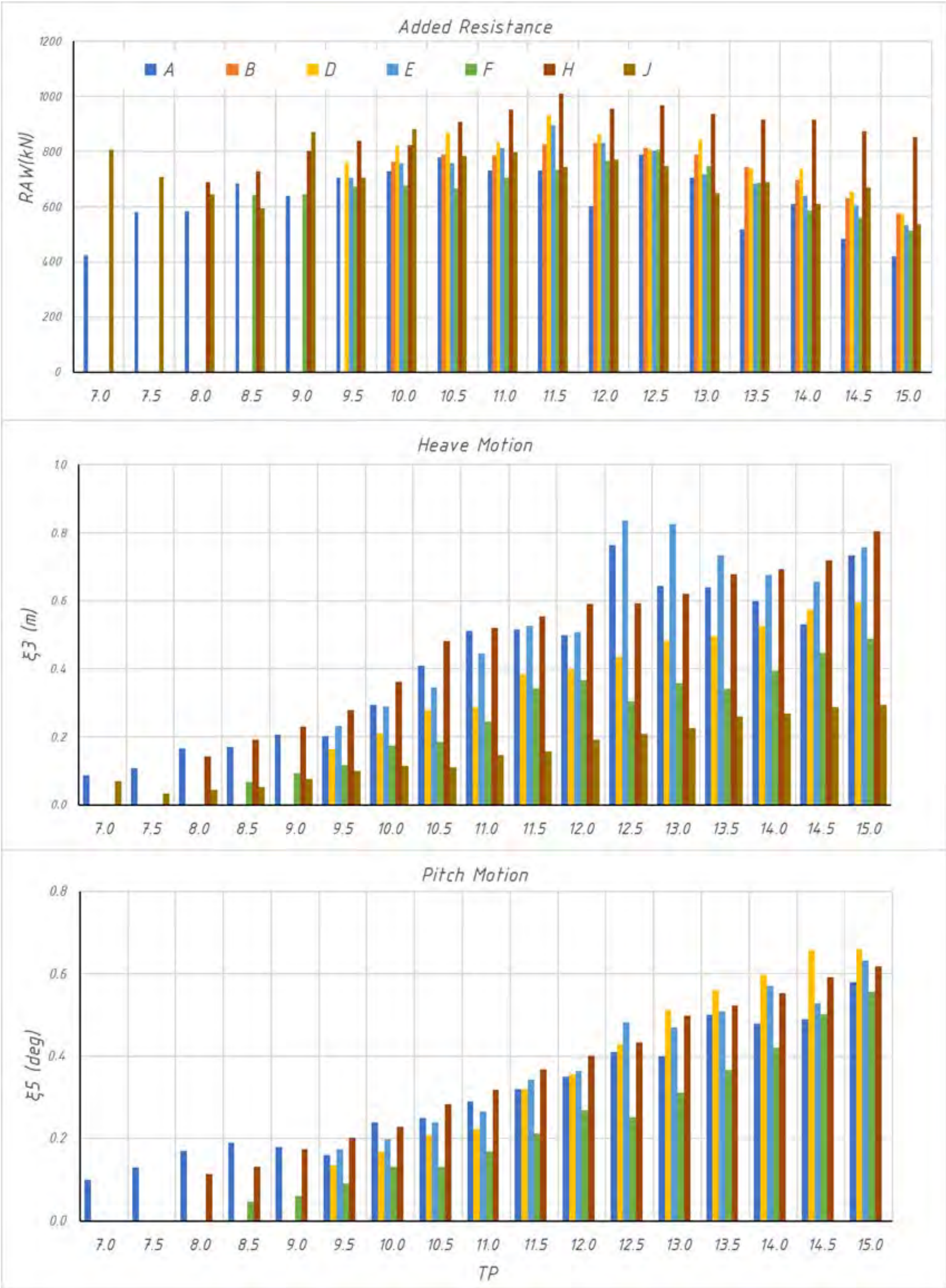

Figure 82: Tests in irregular head waves at 2 knots. Added resistance, heave and pitch motions (standard deviations) as function of peak period T_p. Values scaled to full-scale. Comparison of results from participants A, D, E, F, H and J.

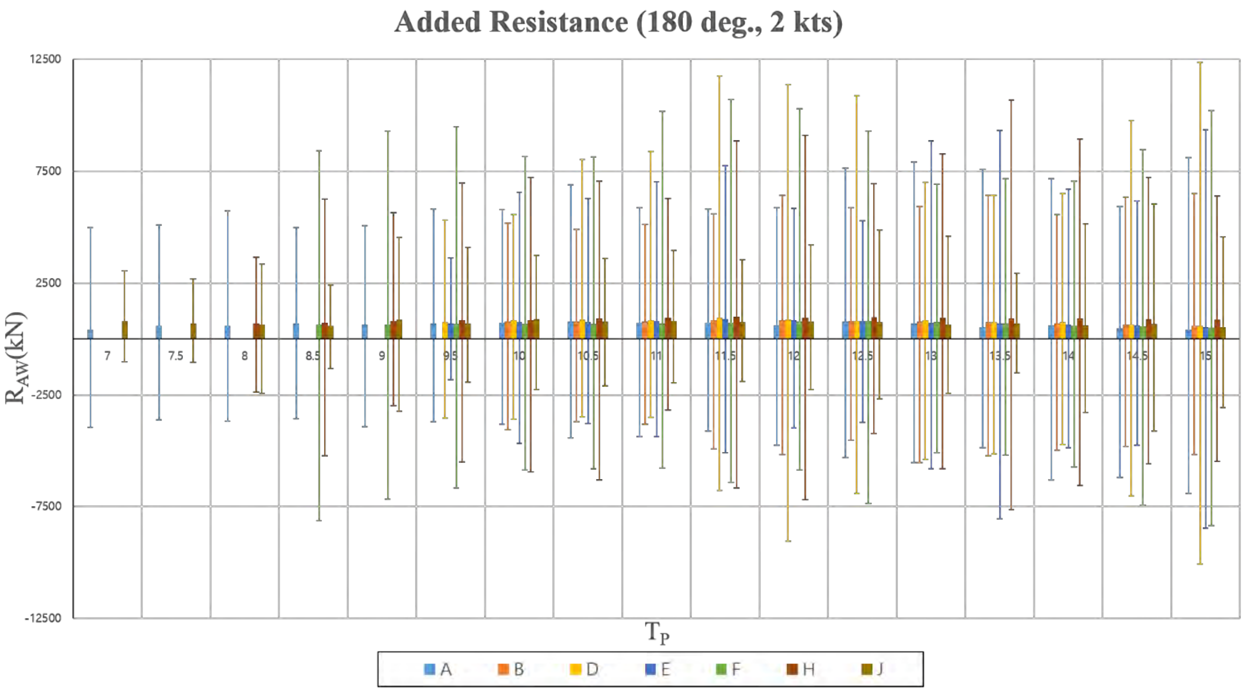

Figure 83: Comparison of mean, max and min values of added resistance recorded in irregular head waves at 2 knots. Mean values are these shown in top plot of Figure 82.

8.4.5 Tests in irregular fw-waves

Participants A, C, D, E, F, and H also submitted results from tests in irregular "f_w-waves" i.e. the sea state stipulated in IMO Circular MEPC.1/Circ.796 and explained in ITTC procedure 7.5-02-07-02.8.

Results are shown in Figure 84. Participant C (grey triangles) submitted results from tests with various towing and propulsion arrangements, these are labelled in the figure.

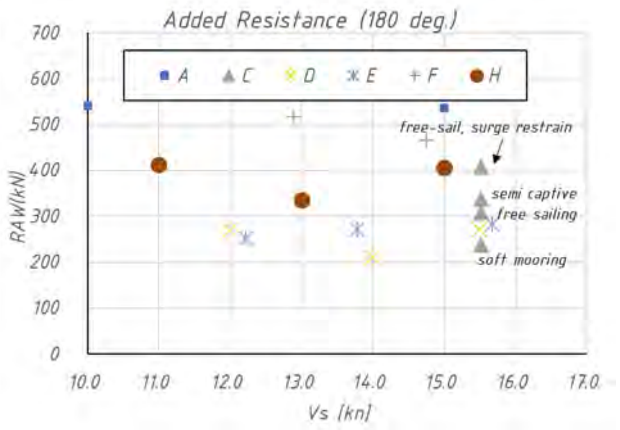

Figure 84: Tests in irregular head waves of *fw*-type i.e. significant wave height 3 m and zero-up crossing period 6.16 s.

8.5 Analysis of results

Below follows an attempt to analyse the submitted results and find some trends. For space reasons, the analysis focuses on the bulk of the submitted data i.e. the design speed tests in regular waves.

8.5.1 Regular wave tests at 15.5 kts

Figure 85 shows an idealised added resistance transfer function (QTF) and some main parameters describing it. Based on this the following parameters were analysed in more detail:

- Peak value
- Peak position
- "tail end" value

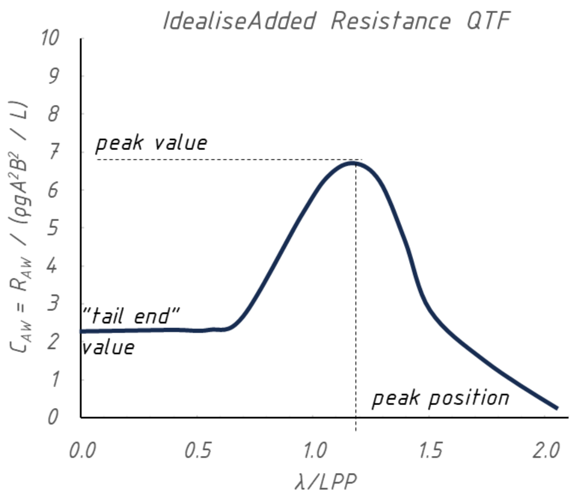

Figure 85: Idealised QTF and parameters describing it.

Figure 86 shows results from the analysis of the peak value. As can be seen, variation in head waves is larger than in oblique waves. This could partly be a result of the different sizes of the datasets, only 5 participants conducted tests in oblique waves.

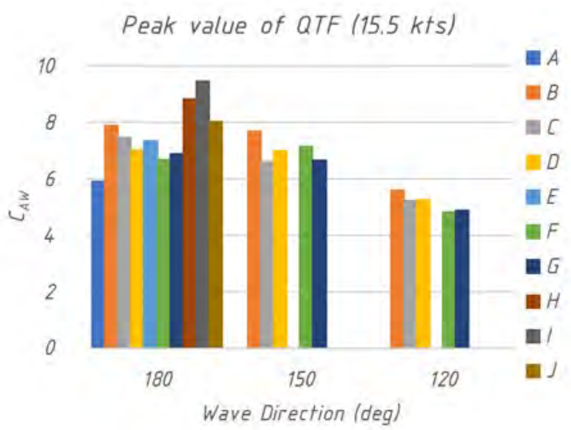

Figure 86: Analysis of QTF peak values reported by participants A to J.

As illustrated in Figure 87 the standard deviation of reported QTF peak values in head seas is about 13% (green corridor in Figure 87)

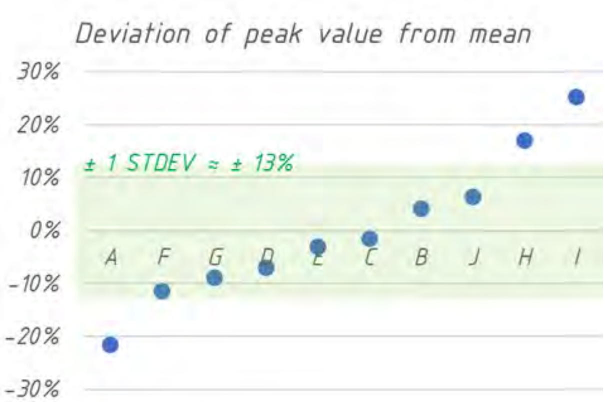

Figure 87: Deviation of head sea QTF peak values from mean.

The corresponding standard deviation for oblique waves becomes about 5% and 4% for wave directions of 150 and 120 degrees respectively.

Figure 88 looks at the variation in reported peak positions. As can be seen six of the ten participants predict the peak to occur at a wavelength ratio of λ/Lpp = 1.2 and four participants report peaks at 1.1. The situation is similar for oblique wave directions of 150 and 120 degrees.

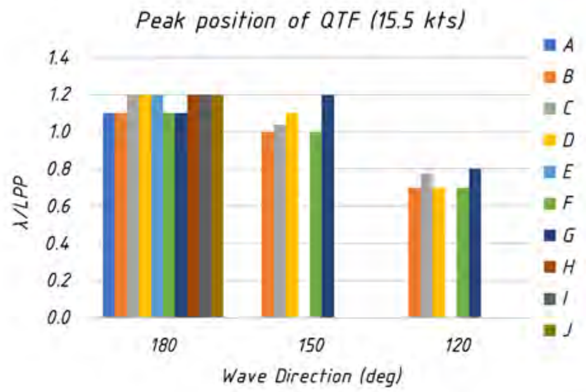

Figure 88: Analysis of QTF peak positions reported by participants A to J.

QTF behaviour at the short-wave "tail-end" is analysed in Figure 89 and Figure 90 for the two wavelength ratios of λ/L_{pp} = 0.5 and 0.2. As can be seen, the spreading increases with shorter wavelength.

The reason for this divergence is that such experiments are difficult to conduct. Added resistance, as the difference between time-averaged data from measurements in waves and calm water measurements, is very small and becomes sensitive to disturbances. The issue is illustrated further in Figure 91, where the individual repeat runs behind the data in Figure 89 and Figure 90 are plotted, and also analysed in terms of wave-steepness. As can be seen, the spreading from run to run increases significantly for λ/L_{pp} = 0.2.

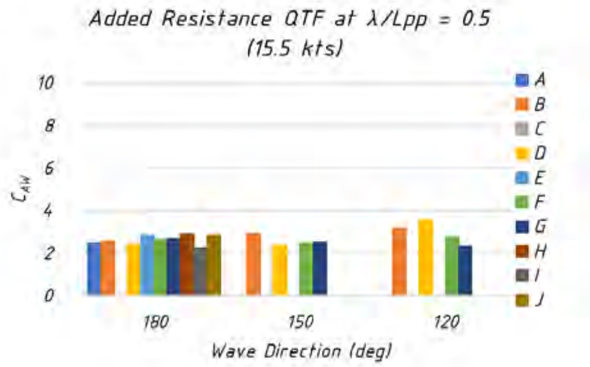

Figure 89: Analysis of QTF tail-end value in short waves (λ/L_{pp} = 0.5).

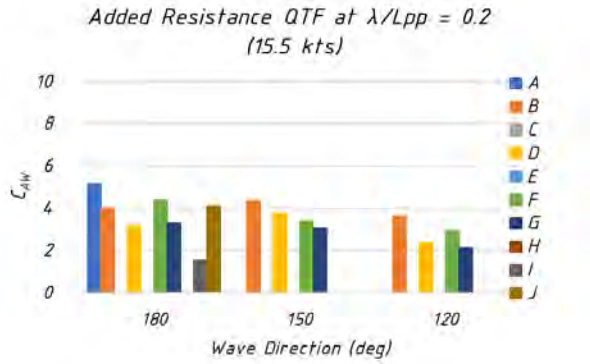

Figure 90: Analysis of QTF tail-end value in short waves (λ/L_{pp} = 0.2).

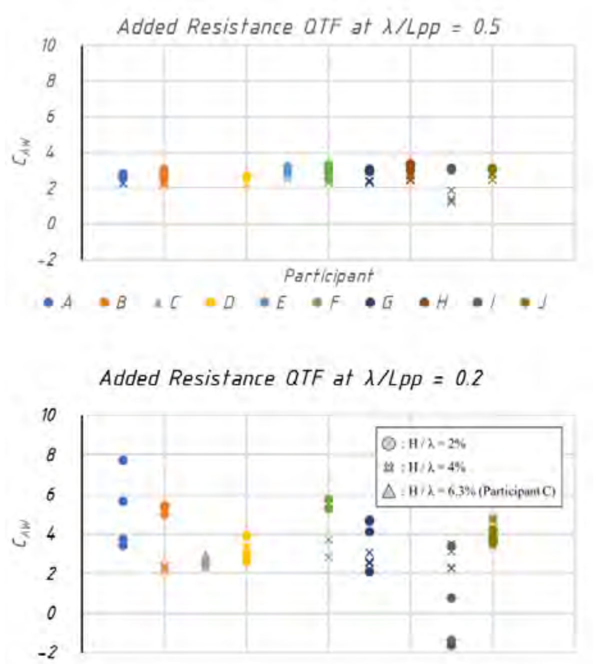

Figure 91: Analysis of QTF tail-end value in short waves. Variation with wave-steepness and in between repeat runs.

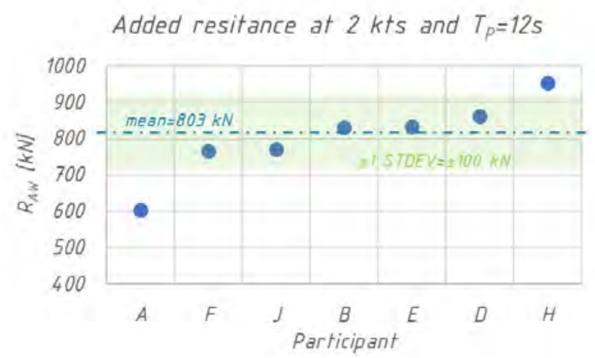

Figure 92: Analysis of added resistance spreading between participants. IMO minimum power conditions, ship speed 2 knots, T_P=12s.

8.5.2 Irregular wave tests at 2 kts

Figure 83 provides an impression of how challenging "IMO-minimum power" added resistance tests at low speeds are. As can be seen, the extreme values recorded during such tests are by about a factor of 10-20 larger than the mean value that one needs to extract.

The maximum value of the added resistance occurs at around a spectral peak period of around 12 s, compare Figure 82, top plot.

Figure 92 shows a more detailed analysis of submitted results at this peak period. As can be seen, the mean value across all participants is about 800 kN with a standard deviation of 100 kN, corresponding to 12 %.

8.5.3 Analysis by facility type, scale factor, and type of experimental setup

The Committee also attempted to analyse submissions in terms of the following parameters:

- Basin vs. tank tests
- Scale factor / model size
- Type of setup:

Results for the head sea added resistance QTF are illustrated in Figure 93 to Figure 95. These figures are identical to Figure 69 but highlight the above parameters.

Results obtained in basins seem to be more similar to each other than those measured in towing tanks, Figure 93.

No clear trends can be observed from the scale factor analysis in Figure 94. The two smallest models (scale 110 & 99.6) are at the extremes of the plot.

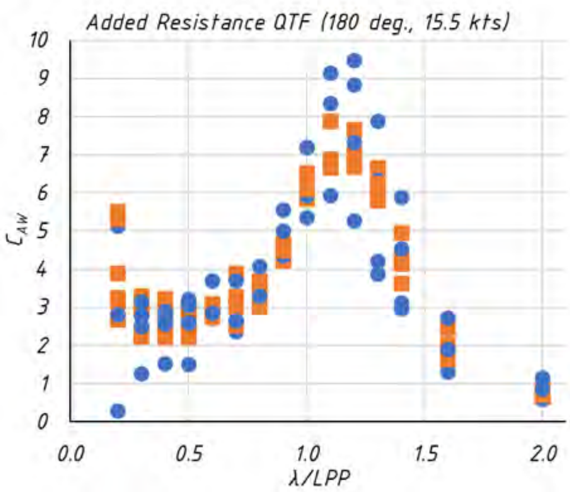

Figure 93: Head Sea QTF: Analysis by facility type.

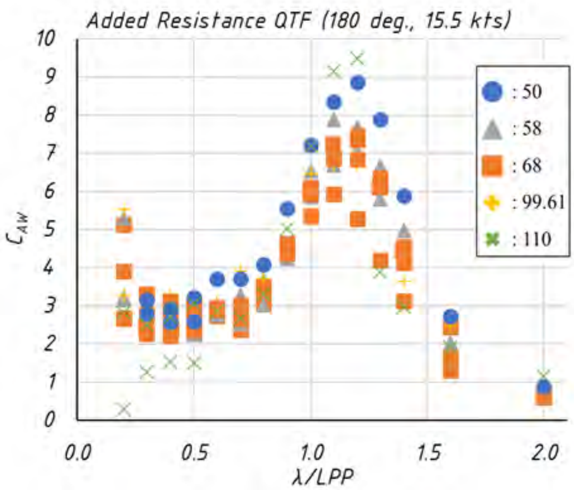

Figure 94: Head Sea QTF: Analysis by scale factor.

Figure 95, the analysis by type of setup, seems to show the trend that soft-mooring and free sailing tests are closer together than the group of results from towed tests.

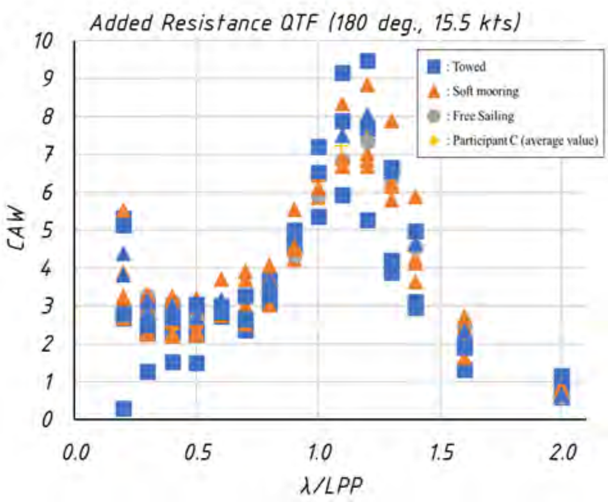

Figure 95: Head Sea QTF: Analysis by type of setup (participant C submitted data using a range of techniques, compare Table 8).

8.6 Conclusions

The following preliminary conclusions can be drawn from the above analysis:

<u>Added resistance Quadratic Transfer Function (QTF) at design speed and in regular waves:</u>

- Six of the ten participants predict the head sea QTF peak to occur at wavelength ratios of λ/L_{pp} = 1.2. The other four participants report the peak at λ /Lpp = 1.1.
- The mean value of the peak height in the head sea QTF becomes C_{AW}=7.6 with a standard deviation of around 13% around this value, depending on participant
- At about 5% and 4% the corresponding standard deviations for wave directions of 150 and 120 degrees are smaller.
- The short-wave “tail ends” of the QTFs are difficult to measure. For λ/L_{pp} <0.5 experimental spreading increases significantly.

Low speed testing under IMO minimum power conditions:

- These tests are challenging to conduct, and all participants used towed models for this, either with soft-mooring or spring arrangements.
- For the KVLCC2 the maximum value of the added resistance occurs at a spectral peak period of about 12 s.
- The mean value of all submitted results at this period is about 800 kN with a standard deviation of 12% across participants.

Other conclusions:

- There appears to be a (difficult to explain) trend that soft-mooring and free sailing tests are closer together than the group of results from towed tests.
- Results obtained in basins seem to be more similar to each other than those measured in towing tanks. This is also difficult to explain.
- There is quite a variation in wave repeatability between the participating organisations, particularly is short waves.

8.7 Suggested next steps/future work

The next ITTC Seakeeping Committee could extend/deepen the above analysis of the benchmarking results and make the collected data accessible online. Such an online "repository" should include the post-processed time-averaged data and possibly also the raw time histories of the measurements (some participating organisations have agreed to share the data).

9. ONBOARD/REALTIME SEAKEEPING DATA (TOR8)

Under ToR 8 the SKC was asked to survey the state of the art for the acquisition and analysis in on-board and/or real-time seakeeping data, and investigate the need of ITTC activities, including future issues related to autonomous vessels.

Literature on the topic has been reviewed and stakeholders considered relevant for this topic have been identified, and eventually meetings carried out (Signaled inside parentheses):

Classification Societies (CCSS)

- DNV (H.A. Tvete, Program Director, Maritime at DNV, Oslo. and Principal Researcher Bingjie Guo, 20220630)
- BV (J. Pancorbo - Principal Surveyor - Spain, 20220601)
- ABS (E. Alvarez - Principal Surveyor - Spain, 20220601)

Shipowners

- ElCano - Gas carriers (meeting with fleet-operations department, 20221013)
- Sicar - General Cargo (meeting with fleet-operations department, 20220910)

Weather routing code developers

- Ali - F. Cañavate - 20230405

Researchers on seakeeping codes and weather routing, ships as buoys, etc.

- Matt Collette, Assoc. Prof., University of Michigan NA&ME Dep. 20230404
- Munehiko Minoura (Osaka U.) 20230501
- Nielsen (DTU) 20230510

Other stakeholders

- Other ITTC committees
- Sea Trials group
- Wind assisted vessels owners/operators
- IMO ITTC representative.

Among the take-aways from these interviews are that the CCSS' rules on autonomous ships are function/goal oriented. They think having seakeeping data is important but at this stage it seems they do not think it is reasonable to set standards on how such data should be acquired. The focus of CCSS is on safety at the moment, not on performance. However, the quality of seakeeping data could have an impact on safety:

- Motions may affect maneuverability and hence increase the chance of collisions.
- If ship motions are large, maybe some sensors do not work.
- Capabilities to identify objects may be affected by the motions.
- Routing may be affected by seakeeping data. Since there are no people onboard, motion restrictions can be relaxed.

Further for CCSS, monitoring motions can be relevant to decide which systems to pay more attention to e.g. fatigue.

As for shipowners, having standards on how full-scale data is monitored, which weather routing providers can comply with, can be an added value for these stakeholders. Use of such weather routing applications is often requested by charterers.

As for weather routing code developers, it seems that measuring motions very accurately may not be very useful for weather routing unless the wave excitation is also accurately measured. The reason is that the motion estimation is obtained based on satellite data for the forecasting of the sea state. Since this is not very accurate, the expected accuracy of the motion estimations will not be very accurate either, and therefore, having very accurate actual motion measurements is not in principle necessary.

As for applications in which motion data are used for short term motion predictions (crane ships operations for wind turbines, maintenance ships for wind turbines, SpaceX autonomous ship for rocket landing, autonomous ships maneuverability in specific collision checks, etc.), the weather routing code developer we interviewed stated that having such a procedure can be interesting for these applications. In such a case, it could be interesting to have standards on location and precision of sensors.

As for researchers on seakeeping codes and weather routing, ships as buoy etc., they agreed that high-quality full-scale seakeeping data is important for the progress of their research and provided some ideas on minimum standards for e.g. sampling frequency, magnitudes to register, etc.

To summarize, it seems the topic is relevant, but it could be too early to elaborate procedures on "the acquisition and analysis in on-board and/or real-time seakeeping data, including future issues related to autonomous vessels".

If such a procedure were considered pertinent, its potential scope could include these items:

- Define precisely the load condition of the ship when data are taken.
- Minimum recording frequency.
- Register motions.
- Register vessel speed (GPS, relative to water).
- Register heading.
- Register sea state: directional spectrum.
- Register wind.
- Register current.
- Document how to deal with communication and integration of the dedicated sensors with other systems in the ship, including how to use the communication capabilities of the ship to transfer information to ground stations.
- Document onboard location of sensors.

10. GUIDELINES ON MANOEUVRING IN WAVES (TOR9)

The Seakeeping Committee (SKC) was tasked to collaborate with the Manoeuvring Committee regarding the development of guidelines related to manoeuvring in waves, ToR 8 of the Manoeuvring Committee (MC). As part of this work the MC has modified two procedures (7.5-02-06-02, "Captive Model tests" and 7.5-02-06-01, "Free Running Model tests") to also include guidance on manoeuvring in waves. During August 2023 the SKC thoroughly reviewed the changes and proposed some modifications.

11. CONCLUSIONS AND RECOMMENDATIONS

11.1 State of the art and research trends

The Committee has reviewed the State of the Art in the field of seakeeping by examining publications for the calendar years 2021-2023. Papers published in more than 35 of the most relevant journals and conferences were reviewed and summarised, resulting in the conclusions below.

A limited number of *new experimental facilities* have opened or became operational since 2021. These include a large ocean basin in Singapore, a towing tank in Southampton, United Kingdom and a shallow water towing tank and a coastal and ocean basin in Ostend, Belgium. In addition, a small towing tank was refurbished in Virginia, USA.

Special *experimental setups* are often used for investigations related to hydroelasticity with segmented models as well as for deck wetness. The focus here is on the use of sensitive, partly new developed sensors, but also on optical sensor technology. It has become standard practice to validate measurements and CFD results against each other to check the plausibility of revealed effects and minimise the uncertainties.

The application of Machine Learning (ML) and Artificial Intelligence (AI) techniques has recently become a contentious issue. Current publications show promising application possibilities and only hint at the extent to which their influence will increase in the upcoming years.

Research about numerical methods on seakeeping focus on the development of fully nonlinear potential flow algorithms and viscous flow methods on the treatment of free-surface wave breaking. Major progress on coupling different potential flow and viscous flow methods has been achieved. Looking for the coming research progress, the wave-body interaction in complex strong nonlinear ocean environments are major challenges for ship seakeeping numerical methods. The development of various coupling algorithms with different advantages may become a hot spot in numerical simulation research and development for ship seakeeping problems.

Green water, slamming and water entry have been extensively investigated by many institutions over the world, both numerically and experimentally. There has been a focus on the validation of CFD calculations as well as the development of more time efficient hybrid methods. The validation results are promising, but there is still work to be done to achieve high fidelity numerical predictions.

Regarding *sloshing*, significant research has focused three areas: comparing results from experiments with tanks of LNG carriers to the guidelines regarding sloshing loads proposed by classification societies. Such research indicates that different rules led to significant differences in such loads, signalling a future line of research. Also increased interest is being paid to sloshing while transporting liquid H2 in cryogenic conditions. This is motivated by perspectives on the use of hydrogen as an alternative fuel for the decarbonization of maritime and ground transportation. Such research indicates that sloshing leads to a substantial increase in the boil-off rates. Finally, substantial work has been carried out considering the coupled dynamics of sloshing and ship motions, a topic computationally expensive on which further research will likely be carried out during the next ITTC term.

Efforts on *hydroelasticity* problems were classified into five categories: experimental study using backbone segmented models, hydroelasticity on tank sloshing, water surface impacts, numerical study, and advanced theoretical study. Experiments using backbone segmented models have focused on oblique wave conditions, and future accumulation of experimental techniques and expansion of data is expected. Since backbone models are difficult to fabricate and handle, and the number of tanks in which they can be tested is limited, we believe that the widespread sharing of the results of leading groups will promote the development of numerical analysis techniques in the future. As for theoretical analysis, it is noteworthy that hydroelasticity was discussed based on the momentum exchange between fluid and flat plate. This could lead to practical methods for FSI problems in ships and offshore structures.

Research on the *added resistance* and speed-power predictions seems to focus on four main areas:

1. Development of new semi-empirical formulae with the accumulation of more model test data for the rapid estimation of added resistance, including various wave headings and hull shapes
2. Novel data-driven models utilizing deep learning techniques to estimate added resistance in waves
3. Various numerical methods, including potential-flow and CFD methods, to directly evaluate the added resistance acting on ships in waves
4. Model tests for the added resistance of ships in various wave conditions or with coupling effects

CFD is now a popular tool in seakeeping applications. Commercial SIMCENTER STAR-CCM+ and open-source OpenFOAM solvers are widely used in recent scientific productions, but other codes and in-house solvers, often based on Finite-Volume Method with overset capabilities, are also successful. Seakeeping CFD studies now commonly include uncertainty quantification and comparison to experimental results, and confidence in the calculations is expected to increase in the next years. Simulations of self-propelled sailing ships in complex wave systems exist but there is no widely used methodology to perform this kind of applications. This is expected to change in the next years.

Research on the seakeeping of *High-Speed Marine Vehicles* seems to focus on three main areas:

1. Experimental and numerical predictions of motions and loads
2. Novel predictive methods for motions and loads, including machine learning/ AI-based methods.
3. Ride Control Systems (RCS) to improve passenger comfort and to actively reduce slamming and the resulting structural loads.

Over the past years the most investigated types of high-speed marine vehicles were wave-piercing catamarans and trimarans.

11.2 Recommendations to the full conference

During the 30th term the procedures below have been updated with minor modifications. The Seakeeping Committee recommends to:

1. Adopt the updated procedure No. 7.5-02-07-02.1 (Seakeeping Experiments).

2. Adopt the updated procedure No. 7.5-02-07-02.2 (Prediction of Power Increase in Irregular Waves from Model Tests).

3. Adopt the updated procedure No. 7.5-02-07-02.3 (Experiments on Rarely Occurring Events).

4. Adopt the updated procedure No. 7.5-02-07-02.5 (Verification and Validation of Linear and Weakly Non-linear Seakeeping Computer Codes).

5. Adopt the updated procedure No. 7.5-02-07-02.6 (Global Loads Seakeeping Procedure).

6. Adopt the updated procedure No. 7.5-02-07- 02.7 (Sloshing Model Tests).

7. Adopt the updated procedure No. 7.5-02-07- 02.8 (Calculation of the Weather Factor fw for Decrease of Ship Speed in Wind and Waves).

8. Adopt the updated procedure for high-speed marine vehicles No. 7.5-02-05-04 (HSMV Seakeeping Tests).

9. Adopt the updated procedure for high-speed marine vehicles No. 7.5-02-05-04.1 (Excerpt of ISO2631, Seasickness and Fatigue).

10. Adopt the updated procedure for high-speed marine vehicles No. 7.5-02-05-06 (HSMV Structural Loads).

11.3 Proposals for future work

11.3.1 Benchmarking data for added resistance in oblique waves

The 31st Seakeeping Committee should make the recently collected data from the "benchmarking experimental campaign on added resistance" (ToR 7 for SKC of 30th ITTC) accessible online. This repository should include the post-processed time-averaged data and possibly also the raw time histories of the measurements (some participating organisations have agreed to share the data). Such an online repository of measured time series of motions and other signals would be very valuable for Verification and Validation of CFD calculations and other purposes.

11.3.2 Number of wave encounters required for model tests in irregular waves

ITTC procedure 7.5-02-07-02.1 (Seakeeping Experiments) recommends a total number of wave encounters of N=50 as a lower limit for seakeeping experiments and states that N=200 or above is considered "excellent practice". The next seakeeping committee should check "experimental convergence" of motion and added resistance values to back-up or refute this statement. Recent experience by several members of the 30th Seakeeping committee has indicated that the required number of wave encounters for convergence could be higher. Liaise with the Full-Scale Ship Performance Committee on the topic.

11.3.3 Weather factor fw for small ships

As pointed out in Section 8.2, experimental data for small ships in fw-conditions is rare. It is recommended that the next Seakeeping Committee uses simulations to investigate the topic of 'voluntary' speed reduction for vessels smaller than 100 m in length. If required, such simulations can also be used to develop alternative "milder" sea states for small ships.

11.3.4 Investigate special topics related to the drafted minimum power guideline

The ITTC "Guideline on determining Minimum Propulsion Power to Maintain the Manoeuvrability of Ships in Adverse Conditions" that was drafted by the 30th Seakeeping Committee is a technical interpretation of IMO MEPC.1/Circ.850/Rev.3. During the preparation of the guideline several issues with the IMO Circular became apparent. The 31st Seakeeping Committee should investigate these in detail and update/improve the draft procedure accordingly:

- The IMO guideline appears to be contradictory on what range of peak wave periods TP should be used in the minimum power assessment (step 16 of the IMO assessment contradicts the TP values listed under the spectrum definitions by IMO). Discuss and resolve this issue with IMO.
- The IMO circular gives "default conservative" estimates for thrust deduction factor and wake fraction. These values are based on a single source of information (MEPC 72-5-9

submission by China) and on difficult to conduct experiments for one single ship.

As illustrated by the work of the 30th Seakeeping Committee, power predictions based on the IMO default values are not necessarily conservative for a full-block ship.

The 31st Seakeeping Committee should continue to investigate this topic by e.g. collection of available data on the behaviour of propulsive factors of different types of ships at low speeds (ideally in waves). In this context hull efficiency, ηH, as a measure for the combined effect of wake fraction and thrust deduction, should also be considered.

The minimum power guideline developed by the 30th Seakeeping Committee should be updated with the findings from such a study.

- Investigate whether the IMO-suggested 3% thrust increase to account for rudder action in waves is realistic.

11.3.5 Wind loads

The work of the current SKC and discussions with other committees have shown that there is a need to address a significant number of issues related to wind loads on ships. The below list of tasks could either be distributed between existing committees or a new specialist committee could be installed:

- Include wind load coefficients for side force, yawing moment and roll moment in the new guideline on "Wind Loads on Ships".
- Improve this guideline, make it more comprehensive and turn it into an ITTC procedure
- Survey state of the art in describing atmospheric boundary layer profiles (ABL) and natural turbulence spectra of the wind over the sea. Unify equations to describe ABL profiles across all ITTC procedures.
- Make recommendations how to measure wind speed and direction in the disturbed flow around a moving ship.
- Develop ITTC guidelines on wind tunnel testing of ships.
- Investigate the question whether Wind Tunnel Facilities working with ships, marine structures and wind propulsion technologies should be invited to join ITTC.

The current committee drafted a wind loads guideline based on the Annex F of ITTC procedure 7.5-04-01-01.1 Preparation, Conduct and Analysis of Speed/Power Trials. This draft guideline, along with a list of suggested modifications to other ITTC procedures, will be passed to the next Committee.

11.3.6 Verification and Validation of CFD methods for seakeeping

Continue to create a guideline on Verification and Validation (V&V) of the CFD methods for seakeeping analysis, taking into account the findings and recommendations of the 30th Seakeeping Committee. Collaborate with the Specialist Committee on Combined CFD/EFD Methods and taking existing procedures for verification and validation of CFD methods into account.

The work of the current (30th) Seakeeping committee has shown that drafting a guideline for V&V of CFD methods for seakeeping is a substantial task involving many complex issues.

11.3.7 On-board and real time data collection

Continue to monitor the state of the art for the acquisition and analysis in on-board and/or real-time seakeeping data. Assess the implications on ITTC activities, including future issues related to autonomous vessels.

12. REFERENCES

Acharya, A., De Chowdhury, S., Peerali Paloth, F. and Datta, R., 2023, "Numerical investigation of bottom slamming using one and two way coupled methods of S175 hull", Applied Ocean Research.

Ahn, I-G. and Jung, B-H., 2022. "Hydroelastic Effect on the Ultimate Strength Assessment of Very Large Ore Carrier based on the Segmented Model Test", International Journal of Offshore and Polar Engineering, 3 (4), pp. 487-494.

Ahn Y. and Kim Y., 2021, "Data Mining in Sloshing Experiment Database and Application of Neural Network for Extreme Load Prediction," Marine Structures, 80, 103074.

Ahn Y., Lee J., Park T. , Kim Y., Kwon C. S. ,. Jung J. H, Gwan Choi M., and Kim S.-Y., 2023, "Long-term Approach for Assessment of Sloshing Loads in LNG Carrier, part I: Comparison of short- and long-term Approaches," Marine Structures, 89, 103381.

Ahn Y., 2023, "Sloshing Loads Estimation using a Genetic Programming", OMAE2023 Melbourne, Australia, OMAE2023-104632.

Almallah, I., Ali-Lavroff, J., Holloway, D. and Davis, M., 2021, "Slam Load Estimation for High-Speed Catamarans in Irregular Head Seas by Full-Scale Computational Fluid Dynamics", Ocean Engineering, 234, 109160.

Almallah, I., Ali-Lavroff, J., Holloway, D. and Davis, M., 2022. "Estimation of Torsional and Global Loads for a Wave-Piercing High-Speed Catamaran at Full-Scale in Irregular Bow Quartering Seas Using CFD Simulation", Ocean Engineering, 266, 113006.

Antolik, J. T., Belden, J. L., Speirs, N. B. and Harris, D. M., 2023, "Slamming forces during water entry of a simple harmonic oscillator", Journal of Fluid Mechanics, 974, A23.

Barabadi, S., Iranmanesh, A., Passandideh-Fard, M. and Barabadi, A., 2023, "A numerical study on mitigation of sloshing in a rectangular tank using floating foams", Ocean Engineering, 277, 114267.

Cepowski, T., 2023, "The use of a set of artificial neural networks to predict added resistance in head waves at the parametric ship design stage", Ocean Engineering, 281, 114744.

Chatzimarkou, E., Michailides, C. and Onoufriou, T., 2022. "Performance of a coupled level-set and volume-of-fluid method combined with free surface turbulence damping boundary condition for simulating wave breaking in OpenFOAM." Ocean Engineering 265, 112572.

Chen, B., Sun, S., Incecik, A., Hou, X. and Ren, H., 2023. "Investigation on wave-body interactions by a coupled High-Order Spectrum method with fully nonlinear Rankine source method". Ocean Engineering 288, 115941.

Chen, D., Feng, X., Hou, C. and Chen, J.-F., 2022. "A coupled frequency and time domain approach for hydroelastic analysis of very large floating structures under focused wave groups". Ocean Engineering 255, 111393.

Chen, D., Yao, X., Huang, D. and Huang, W., 2024. "A multi-resolution smoothed particle hydrodynamics with multi-GPUs acceleration for three-dimensional fluid-structure interaction problems". Ocean Engineering 296, 117017.

Chen, H.-C. and Chen, C.-R., 2023. "CFD Simulation of a container ship in random waves using a coupled level-set and volume of fluid method". Journal of Hydrodynamics 35 (2), 222-231.

Chen, J., Duan, W., Ma, S. and Li, J., 2021. "Time domain TEBEM method of ship motion in waves with forward speed by using impulse response function formulation". Ocean Engineering 227, 108617.

Chen, X. and Wu, Y., 2021, "Model Experimental Research of Wave and Slamming Load of Ship Hull with Bottom Sonar Opening", Proc. ISOPE Rhodes, Greece.

Cho, J. H., Lee, S. H., Oh, D., and Paik, K. J. (2023). "A numerical study on the added resistance and motion of a ship in bow quartering waves using a soft spring system". Ocean Engineering, 280, 114620.

Coslovich, F., Kjellberg, M., Ostberg and M., Janson C.E., 2021, "Added resistance, heave and pitch for the KVLCC2 tanker using a fully nonlinear unsteady potential flow boundary element method", Ocean Engineering, 229, 108935

Dempwolff, L.-C., Windt, C., Bihs, H., Melling, G., Holzwarth, I. and Goseberg, N., 2024. "Hydrodynamic coupling of multi-fidelity solvers in REEF3D with application to ship-induced wave modelling". Coastal Engineering 188, 104452.

Di Mascio, A., Marrone, S., Colagrossi, A., Chiron, L. and Le Touzé, D., 2021. "SPH–FV coupling algorithm for solving multi-scale three-dimensional free-surface flows". Applied Ocean Research 115, 102846.

Diez, M., Serani, A. and Stern, F., 2022, "A Data Clustering Approach to Identifying Slamming Types in Irregular Waves", Proc. 9th International Conference on Hydroelasticity in Marine Technology, Rome, Italy.

Dogrul, A., Kahramanoglu, E. and Cakici, F., 2021, "Numerical prediction of interference factor in motions and added resistance for Delft catamaran 372", Ocean Engineering, 223, 108687

Duan, W., Tang, S. and Chen, J., 2022a. "Power and speed prediction of KVLCC2 in head waves based on TEBEM." Ocean Engineering 249, 110811.

Duan, W., Yang, K., Huang, L., Jing, Y. and Ma, S., 2022b, "A DFN-based method for fast prediction of ships' added resistance in heading waves", Ocean Engineering, 245, 110484

Duan, F., Ma, N., Gu, X., and Zhou, Y., 2023. "An Improved Method for Predicting Roll Damping and Excessive Acceleration for a Ship With Moonpool Based on Computational Fluid Dynamics Method." Journal of Offshore Mechanics and Arctic Engineering, 145 (5), 051401.

van Essen, S.M., Monroy, C., Shen, Z., Helder, J., Kim, D.H., Seng, S. and Ge, Z., 2021. "Screening wave conditions for the occurrence of green water events on sailing ships", Ocean Engineering, 234, 109218.

Faltinsen, O.M. and Timokha, A.N., 2021. "Coupling between Resonant Sloshing and Lateral Motions of a two-dimensional Rectangular Tank", Journal of Fluid Mechanics, 916, p. A60.

Feng, S., Zhang, G., Wan, D., Jiang, S., Sun, Z. and Zong, Z., 2021. "On the treatment of hydroelastic slamming by coupling boundary element method and modal superposition method", Applied Ocean Research, 112, 102595.

Ferro, P., Landel, P., Pescheux, M. and Guillot, S., 2022. "Development of a free surface flow solver using the Ghost Fluid Method on OpenFOAM". Ocean Engineering 253, 111236.

Fu., Z., Li, Y., Gong, J. and Dai, K., 2021a. "Study on Pitch-Roll Coupled Motion Characteristics of Trimaran in Oblique Stern Wave", Proc ISOPE, Rhodes, Greece.

Fu, Z., Li, Y., Gong, J., Zhang, D. and Li, A., 2021b. "Effect of sailing directions on the coupled motion and stability of trimaran in waves", Ocean Engineering, 240, 109955.

Gerhardt F.C. and Kjellberg, M., 2017. "Determining the EEDI 'Weather Factor' fw" RINA, Influence of EEDI on Ship Design and Operation, London, UK.

Gilbert, C., Javaherian, M. J., Woolsey, C. and Shepheard, M., 2023, "Virginia tech advanced towing carriage", Journal of Engineering for the Maritime Environment, IMechE.

Hanssen, F.-C.W. and Greco, M., 2021. "A potential flow method combining immersed boundaries and overlapping grids: Formulation, validation and verification". Ocean Engineering 227, 108841.

Hasheminasab, H., Zeraatgar, H., Malekmohammadi, J. and Azizi, A., 2022. "Analysis of slamming loads on a catamaran section with a centre-bow appended by spray rail", Ships and Offshore Structures.

He, J., Yang, C.-J., Zhu, R.-C., Noblesse, F., 2023. "Alternative flow models, vector Green functions and boundary integral flow representations in ship and offshore hydrodynamics". Ocean Engineering 270, 113630.

Himabindu, A. and Groper, M., 2023. "Speed–Wave Height Operational Envelope for High-Speed Planing Craft in Seaways: Theoretical vs. Empirical Methods", Ship Technology Research, 70 (1): 46–55.

Hong, Y., Heo, K. and Kashiwagi, M., 2021. "Hydroelastic analysis of a ship with forward speed using orthogonal polynomials as mode functions of Timoshenko beam", Applied Ocean Research, 112, 102696.

Hosseinzadeh, S. and Tabri, K., 2021. "Hydroelastic effects of slamming impact Loads During free-Fall water entry", Ships and Offshore Structures,. 16, 68-84.

Htay, W. N., Magari, A., and Toda, Y., 2021. "A Study on the Performance of Rudder Bulb Fins System of KVLCC2 in Regular Head Waves". Proc. ISOPE.

Huang, S., Jiao, J., and Chen, C., 2021a. "CFD prediction of ship seakeeping behavior in bi-directional cross wave compared with in uni-directional regular wave". Applied Ocean Research, 107, 102426.

Huang, W., He, T., Yu, J., Wang, Q., and Wang, X., 2021b. "Direct CFD Simulation and Experimental Study on Coupled Motion Characteristics of Ship and Tank Sloshing in Waves". OMAE2021-63775.

Igbadumhe J.-F., Bonoli J., Dzielski J., and Fürth M., 2023. "Coupled FPSO Roll Motion Response and Tank Sloshing in a pair of two Row Cargo Tanks," Ocean Engineering, 278, 114273.

IMO, 2012, "Interim Guidelines for the Calculation of the Coefficient f_w for Decrease in Ship Speed in a Representative Sea Condition for Trial Use", IMO Circular MEPC.1/Circ.796.

Irannezhad, M., Eslamdoost, A., Kjellberg, M. and Bensow, R.E., 2022. "Investigation of ship responses in regular head waves through a Fully Nonlinear Potential Flow approach". Ocean Engineering 246, 110410.

Islam, H., and Soares, C. G., 2022. "Head Wave Simulation of a KRISO Container Ship Model Using OpenFOAM for the Assessment of Sea Margin". Journal of

Offshore Mechanics and Arctic Engineering, 144(3), 031902.

Jagite, G., Bigot, F., Derbanne, Q., Malenica, Š., Le Sourne, H. and Cartraud, P., 2021. "A parametric study on the dynamic ultimate strength of a stiffened panel subjected to wave- and whipping-induced stresses", Ships and Offshore Structures, 16 (9), 1025-1039.

Jain, U., Novaković, Bogaert, H. and van der Meer, D., 2022 "On wedge-slamming pressures", Journal of Fluid Mechanics, 934, A27.

Javanmard, E., Mehr, J., Ali-Lavroff, J., Holloway, D. and Davies, M. 2023. "An experimental investigation of the effect of ride control systems on the motions response of high-speed catamarans in irregular waves". Ocean Engineering, 281, 114899.

Jawa, S. and Minoura, M., 2023. "Validation of short-term prediction of added resistance in head seas considering wave steepness nonlinearity with probability density function method", Ocean Engineering, 278, 114353

Jiao, J., Huang, S., Tezdogan, T., Terziev, M. and Soares, C.G., 2021a. "Slamming and green water loads on a ship sailing in regular waves predicted by a coupled CFD–FEA approach". Ocean Engineering 241, 110107.

Jiao, J., Huang, S., Wang, S. and Soares, C.G., 2021b. "A CFD–FEA two-way coupling method for predicting ship wave loads and hydroelastic responses". Applied Ocean Research 117, 102919.

Jin, S., Tosdevin, T., Hann, M. and Greaves, D., 2022. "Experimental study on short design waves for extreme response of a floating hinged raft wave energy converter", 37th International Workshop on Water Waves and Floating Bodies, Giardini Naxos, Italy.

Katayama, T., Yamaguchi, K., Nanami, T., Umeda, J., Ozeki, S., Soga, M. and Watanabe, T., 2022, "Calculation of Hydrodynamics Forces Acting on Prismatic Planing Surface by CFD", Proc. PRADS, Dubrovnik, Croatia.

Kim, B.W., Kim, H-S., Lee. K., Hong, S.Y., 2023a. "Comparison of Wave Force Calculation Methods in Time Domain Hydro-elastic Analysis of Floating Body", Proc. ISOPE, pp. 19-23.

Kim, S., Bouscasse, B., Ducrozet, G., Delacroix, S., De Hauteclocque, G. and Ferrant, P., 2023b. "Experimental investigation on wave-induced bending moments of a 6,750-TEU containership in oblique waves", Ocean Engineering, 284, 115161.

Kim, T., Yoo, S. and Kim, H.J., 2021. "Estimation of added resistance of an LNG carrier in oblique waves", Ocean Engineering, 231, 109068.

Kim, Y.R., Esmailian, E. and Steen, S., 2022. "A meta-model for added resistance in waves", Ocean Engineering, 266, 112749

Kobayashi, H., Kume, K., Orihara, H., Ikebuchi, T., Aoki, I., Yoshida, R. and Mizokami, S., 2021. "Parametric study of added resistance and ship motion in head waves through RANS: Calculation guideline". Applied Ocean Research, 110, 102573.

Koo B., Auburtin E. and Kim H., 2021. "Sloshing Effects on FLNG and LNGC side-by-side Offloading", OMAE2021-63778.

Koop, A., Crepier, P., Loubeyre, S., Dobral, C., Yu, K., Xu, H. and Huang, J. 2021. "Development and Verification of Modeling Practice for CFD Decay Calculations to Obtain Roll Damping of FPSO". OMAE2021-62411.

Korobkin, A.A. and Khabakhpasheva, T.I., 2022. "Three-Dimensional Hydroelastic

Impact onto a Floating Circular Plate", Proc. 9th Int. Conference on Hydroelasticity in Marine Technology, pp.79-88.

Lau, C.Y., Ali-Lavroff, J., Holloway, D., Dashtimanesh, A. and Mehr, J., 2023a. "Ride-Control Systems Geometries on a High-Speed Catamaran Using a CFD Forcing Function Method", Proc. 13th Symp. on High Speed Marine Vehicles, Progress in Marine Science and Technology, IOS Press.

Lau, C.Y., Ali-Lavroff, J., Holloway, D., Mehr, J. and Thomas, G., 2023b. "Influence of an active T-foil on motions and passenger comfort of a wave-piercing catamaran based on sea trials in oblique seas", Proc. Institution of Mechanical Engineers, Part M: Journal of Engineering for the Maritime Environment, 237 (1), 83-95,

Lau, C.Y., Ali-Lavroff, J., Holloway, D., Shabani, B., Mehr, J. and Thomas, G., 2022. "Influence of an Active T-Foil on Motions and Passenger Comfort of a Large High-Speed Wave-Piercing Catamaran Based on Sea Trials", Journal of Marine Science and Technology, 27 (2).

Lee, J., Kim, Y., Ahn, Y., 2022a. Hydroelastic Responses of LNG CCS due to Sloshing Loads I: Hydrodynamic Impact due to Different Liquids and Gases, Proc. of 9th International Conference on Hydroelasticity in Marine Technology, pp. 63-70.

Lee, J., Kim, Y., Kim, B.S., Gerhardt, F., 2021a. "Comparative study on analysis methods for added resistance of four ships in head and oblique waves", Ocean Engineering, 236, 109552.

Lee, S. H., Paik, K. J., Hwang, H. S., Eom, M. J., and Kim, S. H., 2021b. "A study on ship performance in waves using a RANS solver, part 1: Comparison of power prediction methods in regular waves". Ocean Engineering, 227, 108900.

Lee, S. H., Paik, K. J., and Lee, J. H., 2022b. "A study on ship performance in waves using a RANS solver, part 2: Comparison of added resistance performance in various regular and irregular waves". Ocean Engineering, 263, 112174.

Lee, J. and Kim, Y., 2023. "Development of enhanced empirical-asymptotic approach for added resistance of ships in waves", Ocean Engineering, 280, 114762.

Li, A., Yan, F. and Zhang, Y., 2023a. "Influence of Wave Amplitude on the Characteristics of Coupled Motion of a Trimaran Equipped with T-Foil in Oblique Head Waves", Proc. ISOPE, Ottawa, Canada.

Li, C., Duan, W.-y. and Zhao, B.-b., 2022a. "Breaking wave simulations for a high-speed surface vessel with hybrid THINC and HRIC schemes". Applied Ocean Research 125, 103257.

Li, J., Duan, W., Chen, J., Ma, S. and Zhang, Y., 2022b. "A study on dynamic trim optimization of VLCC oil tanker in wind and waves", Ocean Engineering, 253, 111270.

Li, M., Pan, S., Cheng, Y., Yuan, Z.-M. and Tao, L., 2023b. "Time-domain numerical simulation for multi-ships moving in waves with forward speed". Ocean Engineering 290, 116325.

Li, Z., Bouscasse, B., Ducrozet, G., Gentaz, L., Le Touzé, D. and Ferrant, P., 2021. "Spectral wave explicit navier-stokes equations for wave-structure interactions using two-phase computational fluid dynamics solvers". Ocean Engineering 221, 108513.

Li, J., Liu, L., Zhang, Z., Wang, L., and Yao, X., 2022c. "Numerical Study on Vertical Motions of a Destroyer With Different Speeds in Extreme Seas". OMAE2022-78652.

Li, J., Chen, J., Yu, J., Liu, L., and Zhang, Z., 2023c. "CFD prediction for the extreme roll motion of ONR Tumblehome in beam waves". Proc. ISOPE.

Liang, S., Gou, Y. and Teng, B., 2023. "The nonlinear wave interaction with a two-dimensional large-scale floating elastic plate". Ocean Engineering 282, 115046.

Liao, K., Duan, W., Ma, Q., Ma, S. and Yang, J., 2021. "Numerical Simulation of Green Water on Deck with a Hybrid Eulerian-Lagrangian Method”", Journal of Ship Research.

Lin, Z., Qian, L., Bai, W., Ma, Z., Chen, H., Zhou, J.-G. and Gu, H., 2021. "A finite volume based fully nonlinear potential flow model for water wave problems". Applied Ocean Research 106, 102445.

Liu, D., Li, F. and Liang, X., 2022a. "Numerical study on green water and slamming loads of ship advancing in freaking wave". Ocean Engineering, 261, 111768.

Liu, H., Xiong, Y., Xu, H. and Gao, S., 2021a. "Experimental and Numerical Investigation of Slamming on Wedges with Different Stiffened Panels", Proc. ISOPE, Rhodes, Greece.

Liu, K., Liu, Y., Li, S., Chen, H., Chen, S., Arikawa, T. and Shi, Y., 2023a. "Coupling SPH with a mesh-based Eulerian approach for simulation of incompressible free-surface flows". Applied Ocean Research 138, 103673.

Liu, L., Feng D., Wang X., Zhang Z., Yu J., and Chen M., 2022b. "Numerical Study on the Effect of Sloshing on Ship Parametric Roll," Ocean Engineering, 247, 110612.

Liu, S. and Papanikolaou, A., 2020. "Regression analysis of experimental data for added resistance in waves of arbitrary heading and development of a semi-empirical formula". Ocean Engineering, 206.

Liu, S. and Papanikolaou, A., 2023. "Improvement of the prediction of the added resistance in waves of ships with extreme main dimensional ratios through numerical experiments", Ocean Engineering, 273, 113963.

Liu, W.-T., Zhang, A.-M., Miao, X.-H., Ming, F.-R. and Liu, Y.-L., 2023b. "Investigation of hydrodynamics of water impact and tail slamming of high-speed water entry with a novel immersed boundary method", Journal of Fluid Mechanics, 958, A42.

Liu Z., Yuan K., Liu Y., Andersson M., and Li Y., 2022c. "Fluid Sloshing Hydrodynamics in a Cryogenic Fuel Storage Tank under Different Order Natural Frequencies," Journal of Energy Storage, 52, 104830.

Lu, L., Ren, H., Li, H., Zou, J., Chen, S. and Liu, R., 2023a. "Numerical method for whipping response of ultra large container ships under asymmetric slamming in regular waves", Ocean Engineering, 287, 115830.

Lu, X., Dao, M.H. and Le, Q.T., 2022a. "A GPU-accelerated domain decomposition method for numerical analysis of nonlinear waves-current-structure interactions". Ocean Engineering 259, 111901.

Lu, Y., Shao, W., Gu, Z., Wu, C., and Li, C., 2022b. "Study on the influence of cross wave on ship motion characteristics based on computational fluid dynamics". Proc. ISOPE.

Lu, L., Ren, H., Li, H., Zou, J., Chen, S. and Liu, R., 2023b. "Numerical method for whipping response of ultra large container ships under asymmetric slamming in regular waves". Ocean Engineering, 287, 115830.

Lyu, W., el Moctar, O. and Schellin, T.E., 2022. "Ship motion-sloshing interaction with forward speed in oblique waves", Ocean Engineering, 250, 110999.

Ma C., Xiong C., and Ma G., 2021. "Numerical Study on Suppressing Violent Transient Sloshing with Single and Double Vertical Baffles", Ocean Engineering, 223, 108557.

Ma, S., Duan, W., Cao, Z., Liu, J., Zhang, M., Li, X. and Liu, D., 2023. "Experimental study on the drop test on wet deck slamming for a SWATH segment model", Ocean Engineering, 285, 115377.

Ma, Y. and Zhu, Q., 2022. "Fast Trimaran Anti-Longitudinal Motion Control System Based on Active Disturbance Rejection Control with Controller Tuning", Journal of Marine Science and Technology, 27 (2).

Mahfoze O.A., Liu W, Longshaw S.M., Skillen A. and Emerson D.R., 2022. "On the Efficiency of Turbulence Modelling for Sloshing", Applied Sciences. 12 (17):8851.

Mai, T.L., Vo A.K., Cho, A. and Yoon, H.K., 2023. "Experimental Study of Wave-Induced Motions and Loads on Catamaran in Regular and Irregular Waves", Proc. ISOPE, Ottawa, Canada.

Malas, B., Creasey, L., Buckland, D., and Turnock, S. R., 2024. "Design, Development and Commissioning of the Boldrewood Towing Tank – A decade of endeavour", Int. J. Maritime Engineering, RINA.

Marin-López, J.R., Villamarín, E., Mendoza, J., Paredes, R. and Datla, R., 2021. "Conceptual Design Recommendations to Improve Seakeeping of Small High-Speed Craft Providing Interisland Transportation in Galápagos", SNAME Int. Conf. Fast Sea Transportation (FAST), Providence, Rhode Island, USA,

Marlantes, K. and Maki, K., 2022. "A Neural-Corrector Method for Prediction of the Vertical Motions of a High-Speed Craft", Ocean Engineering, 262, 112300.

Martinez-Carrascal J. and Gonzalez-Gutierrez L., 2021. "Experimental Study of the Liquid Damping Effects on a SDOF Vertical Sloshing Tank," J. Fluids and Structures, 100, 103172.

Mittendorf, M., Nielsen, U.D., Bingham, H.B. and Liu, S., 2022. "Towards the uncertainty quantification of semi-empirical formulas applied to the added resistance of ships in waves of arbitrary heading", Ocean Engineering, 251, 111040.

Mittendorf, M., Nielsen, U.D., Bingham, H.B. and Dietz, J., 2023, "Assessment of added resistance estimates based on monitoring data from a fleet of container vessels", Ocean Engineering, 272, 113892

Molaemi, A. H., Bredmose, H., Ghadirian, A. and Kristiansen, T., 2023. "Cylinder water entry on a perturbed water surface", Journal of Fluid Mechanics, 965, A16.

Nielsen, U. D., Brodtkorb, A. H., Iseki, T., Jensen, J. J., Mittendorf, M., Mounet, R. E. G., Sørensen, A. J. and Takami, T., 2023. "Estimating Waves Through Measured Ship Responses", International Workshop on Water Waves and Floating Bodies.

Nordforsk, 1987, "Assesment of Ship Performance in a Seaway", The Nordic co-operative project: Seakeeping Performance of Ships, ISBN 87-982637-1-4.

Pal, S.K., Ono, T., Takami, T., Tatsumi, A. and Iijima, K., 2022. "Effect of springing and whipping on exceedance probability of vertical bending moment of a ship", Ocean Engineering 266, 112600.

Paredes, R., Gaona, A., Toala, A., Marín López, J., Datla, R., and Pratt, J., 2022. "Zero-Emission Small High-Speed Craft Conceptual Design using NSGA-II Algorithm for Galapagos Interisland Service", HIPER 2022, Cortona, Italy.

Park, C., Lee, J. and Kim, Y.. 2022. "Hydroelastic Responses of LNG CCS due to Sloshing Loads II: Structural Responses due to Different Impact Patterns", Proc 9th International Conference on Hydroelasticity in Marine Technology, pp. 71-78.

Park, H.J. and Nam, B.W., 2023. "Prediction of Green Water Events for FPSO in Irregular Waves using ANN Model", Int. Workshop on Water Waves and Floating Bodies.

Park, M. and Lee, P-S., 2022. "Non-matching Mesh Treatment in Hydro-elastic Analysis", Proc. 9th Int. Conference on Hydroelasticity in Marine Technology, pp. 359-365.

Park, M. and Lee, P-S., 2023. "Integrated hydrostatic and hydrodynamic analysis of flexible floating structures", Ocean Engineering, 288, 114945.

Park, Y., Hwangbo, S.M., Yu, J.W., Cho, Y., Lee, J.H. and Lee, I., 2023. "Development of a small-sized tanker with reduced greenhouse gas emission under in-service condition based on CFD simulation", Ocean Engineering, 286, 115588.

Qian, Y. and Teng, B., 2023. "A finite element-scaled boundary finite element coupled method for corner singularities in 2D second-order radiation problems". Ocean Engineering 281, 114910.

Remmerswaal, R.A., Veldman, A.E.P. Ronald A. R. and Arthur E. P. V., 2022. "On Simulating Variability of Sloshing Loads in LNG Tanks", OMAE2022-81105.

Riesner, M. and el Moctar, O., 2021. "A numerical method to compute global resonant vibrations of ships at forward speed in oblique waves", Applied Ocean Research, 108, 102520.

Saincher, S. and Sriram, V., 2022. "A three-dimensional hybrid fully nonlinear potential flow and Navier Stokes model for wave structure interactions". Ocean Engineering 266, 112770.

Salis, N., Hu, X., Luo, M., Reali and A., Manenti, S., 2024. "3D SPH analysis of focused waves interacting with a floating structure". Applied Ocean Research 144, 103885.

Sanada, Y., Kim, D. H., Sadat-Hosseini, H., Stern, F., Hossain, M. A., Wu, P. C., and Grigoropoulos, G., 2022. "Assessment of EFD and CFD capability for KRISO Container Ship added power in head and oblique waves". Ocean Engineering, 243, 110224.

Sebhatleb, G., Holloway, D. and Ali-Lavroff, J., 2023. "Slam and Wave Load Response Reconstruction in High Speed Catamarans Using Transmissibility on Full Scale Sea Trials", Ocean Engineering, 271, 113822.

Shi, K.-y. and Zhu, R.-c., 2023. "A fully nonlinear approach for efficient ship-wave simulation". Journal of Hydrodynamics 35 (6), 1027-1040.

Silva, D.F.C., Menezes, F.G.T., Schmidt, D. and Mello, P.C., 2023. "Slamming Effects on FPSO Balconies: Numerical and Experimental Analysis of Alternative Configurations for Impact Attenuation", OMAE2023-105066.

Smith J.R., Gkantonas S. and Mastorakos E., 2022. "Modelling of Boil-Off and Sloshing Relevant to Future Liquid Hydrogen Carriers". Energies. 15 (6):2046.

Song, X., Zhang, X. and Beck, R.F., 2022. “Numerical study on added resistance of ships based on time-domain desingularized-Rankine panel method”. Ocean Engineering 248, 110713.

Spinosa, E. and Iafrati, A., 2022. “Analysis of the Fluid-Structure Interaction during the Water Entry of a Flat Plate at High Horizontal Speed”, Proc. 9th Int. Conference on Hydroelasticity in Marine Technology.

Spyrou, I. T. and Papadakis, G., 2021. Numerical investigation on the effect of bilge keels in ship roll damping, Proc. 1st Int. Conference on the Stability and Safety of Ships and Ocean Vehicles, Glasgow, Scotland, UK. Proc. 1st Int. Conference on the Stability and Safety of Ships and Ocean Vehicles, Glasgow, Scotland, UK.

Stern, F., Sanada, Y., Park, S., Wang, Z., Yasukawa, H., Diez, M., Quadvlieg, F. and Bedos, A., 2022. “Experimental and CFD Study of KCS Turning Circles in Waves”, 34 th Symp. on Naval Hydrodynamics, Washington, DC, USA.

Subramaniam, S., Umeda, N., Matsuda, A. and Maki, A., 2021. “Experimental study on the water-on-deck effect for an offshore supply vessel running in regular and irregular stern quartering waves”, Proc. 1st Int. Conference on the Stability and Safety of Ships and Ocean Vehicles, Glasgow, Scotland, UK.

Sun, J. Y., Sun, S. L., Sun, S. Z., and Ren, H. L. 2023. “The impact of piston and sloshing motions on added resistance from moonpool configurations”. Ocean Engineering, 267, 113179.

Suzuki, K, Iwashita, H., Kashiwagi, M., Wakahara, M., Iida, T. and Minoura, M., 2023. “Temperature interference in improved FBG pressure sensor for towing tank test”, Journal of Marine Science and Technology, 28:351, 369.

Takami, T., Fujimoto, W., Houtani, H. and Matsui, S., 2023. “Combination of HOSM and FORM for extreme wave-induced response prediction of a ship in nonlinear waves”. Ocean Engineering 286, 115643.

Tao, Y., Zhu, R., Gu, J., Li, Z., Zhang, Z., and Xu, X. 2023. “Experimental and numerical investigation of the hydrodynamic response of an aquaculture vessel”. Ocean Engineering, 279, 114505.

Tang, S.Q., Zhang, Y., Sun, S.L. and Ren, H.L., 2021a. “Experimental Study on the Double-Slamming of a Trimaran Cross Section in Vertical Free Fall Motion”. Proc. ISOPE, Rhodes, Greece.

Tang, Y., Sun, S.-L. and Ren, H.-L., 2021b. “Numerical investigation on a container ship navigating in irregular waves by a fully nonlinear time domain method”. Ocean Engineering 223, 108705.

Tang, Y., Sun, S. L., Yang, R. S., Ren, H. L., Zhao, X. and Jiao, J. L., 2022. “Nonlinear bending moments of an ultra large container ship in extreme waves based on a segmented model test”, Ocean Engineering, 243, 110335.

Tao, Y., Zhu, R., Gu, J., Li, Z., Zhang, Z. and Xu, X., 2023, “Experimental and numerical investigation of the hydrodynamic response of an aquaculture vessel”, Ocean Engineering,. 279, 114505.

Tavakoli, S., Babanin, A., and Hirdaris, S., 2023a. “Hydroelastic Analysis of Hard Chine Sections Entering Water—Observations for Use in Preliminary Design Stage”, Journal of Offshore Mechanics and Arctic Engineering, 145 (5), 051901.

Tavakoli, S., Mikkola, T. and Hirdaris, S., 2023b. ”A fluid–solid momentum exchange method for the prediction of hydroelastic responses of flexible water entry problems”, J. Fluid Mech, 965, A19.

Tian C, Si H. L., Zhou Q. Y., Lu Y., Cheng X. M., Ye Y. L. and Wu Y. S., 2022. “Investigation on Modal Characteristics of Test Models of Ultra Large Containership for Hydroelastic Responses”, Proc. 9th International Conference on Hydroelasticity in Marine Technology, pp.29-40.

Vijith P.P. and Rajendran, S., 2023. “Hydroelastic effects on the vertical bending moment of a container ship in head and oblique seas”, Ocean Engineering, 285, 115385.

Wang, A., Pan Wong, K., Yu, M., Kiger, K. T. and Duncan, J. H., 2022a. "The controlled impact of elastic plates on a quiescent water surface", Journal of Fluid Mechanics, 939, A4.

Wang, G., Wu, Q., Chen, M., Xie, Y. and Yu, H., 2022b. “Investigation on the Slamming of Wedge-Shaped Body with Oblique Free Entry into Water” Proc. ISOPE, Shanghai, China.

Wang, H., Chen, J., Duan, W. and Shan, M, 2022c. “Time-domain TEBEM for Hydroelastic Responses of a Container Ship with Forward Speed”, Proc. PRADS, pp. 1884-1895.

Wang, H., Duan, W., Chen, J., Ma, S., 2023a. “A numerical method to compute flexible vertical responses of containerships in regular waves”, Ocean Engineering, 266, 112828.

Wang, J., Wang, W., and Wan, D. 2023b. “Study of Self-Propulsion Performance of a Single-Screw Ship in Waves Based on Improved Propeller Body Force Model”. Proc. ISOPE.

Wang, S., Kim, B., Zhu, Z., and Kim, Y. 2022d. “CFD Predictions on Ship Performance in Waves Using OpenFOAM Solver”. Proc. ISOPE.

Wang, S., Kim, B. S., Zhu, Z., Choi, J. H., and Kim, Y. 2023c. “OpenFOAM-Based Computation of Added Resistance in Head and Oblique Seas”. Proc. ISOPE.

Wang, W., Pákozdi, C., Kamath, A. and Bihs, H., 2021a. “A fully nonlinear potential flow wave modelling procedure for simulations of offshore sea states with various wave breaking scenarios”. Applied Ocean Research 117, 102898.

Wang, Y., Jiang, S. and Zhou, T., 2023d. “Experimental Investigation On Response Of Ship Rolling Motion Coupled With Liquid Sloshing”, OMAE2023-104423.

Wang Z., Jiang M., and Yu Y., 2021b, “Nonlinear Behaviours of Three-Dimensional Sloshing in the LNG Elastic Tank”, OMAE2021-61679.

Wei, Y., Incecik, A., Tezdogan, T., 2023. “A hydroelasticity analysis of a damaged ship based on a two-way coupled CFD-DMB method”. Ocean Engineering 274, 114075.

Wei, Y. and Tezdogan, T., 2022. “A Fluid-Structure Interaction Model on the Hydroelastic Analysis of a Container Ship Using preCICE”, OMAE2022-78131.

Wu, J., Sun, Z., Jiang, Y., Zhang, G. and Sun, T., 2021. "Experimental and numerical study of slamming problem for a trimaran hull", Ships and Offshore Structures, 16 (1), 46-53.

Wu, S., Liu, L., Wang, X., Chen, J., and Wang, L. 2022. “Study of wavelength effect on the parametric roll in head waves”. Proc. ISOPE.

Xie, C.-M., Yang, J.-C., Sun, P.-N., Lyu, H.-G., Yu, J. and Ye, Y.-L., 2023. “An accurate and efficient HOS-meshfree CFD coupling method for simulating strong nonlinear wave–body interactions". Ocean Engineering 287, 115889.

Xu, W., Zhang, J. and Zhong, M., 2023a. "A Sliding Mode Predictive Anti-Pitching Control for a High-Speed Multihull", Ocean Engineering 285, 115466.

Xu, Y., Bingham, H.B., Shao, Y., 2023b. "A high-order finite difference method with immersed-boundary treatment for fully-nonlinear wave–structure interaction". Applied Ocean Research 134, 103535.

Yang, K., Duan, W., Huang, L., Zhang, P., Ma, S., 2022. "A prediction method for ship added resistance based on symbiosis of data-driven and physics-based models", Ocean Engineering, 260, 112012.

Yasukawa, H. and Enui, K., 2021. "Effect of Pitch Moment of Inertia on Added Resistance of Container Ship in Waves", Journal of the Japan Society of Naval Architects and Ocean Engineers, 33.

Yu, J., Yao, C., Liu, L., Feng, D., and Wang, X., 2023a. "Application of virtual disk propulsion model for self-propelled surface ship in regular head wave". J. of Marine Science and Technology, 28(2), 471-495.

Yu, J., Yao, C., Wang, J., Liu, L., Dong, G., and Zhang, Z., 2023b. "Numerical study on motion responses and added resistance for surge-free KCS in head and oblique waves based on the functional decomposition method". Ocean Engineering, 285, 115300.

Yu, J.W., Kim, S.G., Jeong, W., Kim, Y.I., Choi, J.E. and Lee, I., 2022. "Prediction of resistance and propulsion performances using calm-water and resistance tests in regular heave waves of a 1,800 TEU container ship", Int. J. Naval Architecture and Ocean Engineering, 14, 100458

Zhang, H., Yuan, Y., Tang, W., Xue, H., Liu, J. and Qin, H., 2021a. "Numerical analysis on three-dimensional green water events induced by freak waves", Ships and Offshore Structures.

Zhang, J., Liu, Z., Dai, X. and Li G., 2021b. "Robust Decoupled Anti-Pitching Control of a High-Speed Multihull", Journal of Marine Science and Technology, 26 (4), 1112–25.

Zhang, N., Yan, S., Ma, Q. and Zheng, X., 2021c. "A QSFDI based Laplacian discretisation for modelling wave-structure interaction using ISPH". Applied Ocean Research 117, 102954.

Zhang, N., Yan, S., Ma, Q., Guo, X., Xie, Z. and Zheng, X., 2023a. "A CNN-supported Lagrangian ISPH model for free surface flow". Applied Ocean Research 136, 103587.

Zhang, Y., Reliquet, G., Bouscasse, B., Gentaz, L. and Le Touzé, D., 2021d. "Numerical investigation on the added resistance and seakeeping performance of KVLCC2 with the SWENSE method". Journal of Ship Research 65 (04), 362-379.

Zhang, X., Gu, X., and Ma, N., 2021e. "Comparative Study on Eddy Roll Damping with Experimental Results Using a High-order Fractional Step Finite Volume Solver". International Journal of Offshore and Polar Engineering, 31 (02), 199-209.

Zhang, X., Song, X. and Beck, R.F., 2023a. "Numerical investigations on seakeeping and added resistance in head waves based on nonlinear potential flow methods". Ocean Engineering 276, 114043.

Zhang, Z., Ma, N., Lin Y., Gu, X. and Shi, Q., 2022. "Experimental Study on Non-Linear Wave Loads of a Ship Model with Variable

Cross-section Backbone in Irregular Waves", Proc. ISOPE, pp. 2315-2322.

Zhang, Z., Yang, J., Zhang, H., Zou, Z. and Zhang, X., 2023b. "Numerical study on mean wave drift forces and moment of ships using Rankine panel method in frequency domain". Ocean Engineering 283, 114986.

Zhang, Z.-L., Sun, S.-L., Chen, B.-Y. and Ren, H.-L., 2024. "Numerical investigation of a semi-submersible platform interacting with steep waves using a fully nonlinear method". Ocean Engineering 294, 116755.

Zhao, J., Zhu, R. and Zhou, W., 2022. "Implementation of a velocity decomposition method coupled with volume-of-fluid method for simulating free-surface flows". Ocean Engineering 263, 112339.

Zheng, Jh., Xue, M.A. and Dou, P., 2021a. "A Review on Liquid Sloshing Hydrodynamics". J Hydrodynamics 33, 1089–1104.

Zheng, L., Liu, Z., Zeng, B., Meng, H. and Wang, X., 2023b. "Experimental and Numerical Study on Heave and Pitch Motion Calculation of a Trimaran", J. Marine Science and Technology, 28 (1):136–52.

Zheng, M., Ni, Y., Wu, C. and Jo, H., 2021b." Experimental investigation on effect of sloshing on ship added resistance in head waves", Ocean Engineering, 235, 109362.

Zheng, Y., Yiew, L., Jin, Y., Ravindra, K., and Magee, A. R., 2023c. "Experimental and numerical study on seakeeping performance of a benchmark ASD tug in head seas". Ocean Engineering, 272, 113800.

Zhong, S.-Y., Sun, P.-N., Peng, Y.-X., Liu, N.-N., Lyu, H.-G. and Huang, X.-T., 2023. "An SPH study of slamming and splashing at the bow of SYSU vessel". Ocean Engineering 269, 113581.

Zhong, W.-j., Wang, W.-t. and Wan, D.-c., 2022. "Coupling potential and viscous flow models with domain decomposition for wave propagations". J. Hydrodynamics 34 (5), 826-848.

Zhu, Z., Lee, J., Kim, Y., Lee, J. and Park, T., 2021, "Experimental measurement and numerical validation of sloshing effects on resistance increase in head waves". Ocean Engineering, 234.

Zhuang, Y. and Wan, D.-c., 2021. "Parametric study of a new HOS-CFD coupling method". Journal of Hydrodynamics 33, 43-54.

ITTC2024
30TH INTERNATIONAL TOWING TANK CONFERENCE
22–27 SEPTEMBER 2024 | HOBART TASMANIA AUSTRALIA

REPORT OF THE OCEAN ENGINEERING COMMITTEE

OCEAN ENGINEERING COMMITTEE

1. INTRODUCTION

1.1 Membership and Meetings

The members of the Ocean Engineering Committee of the 30th ITTC are:

- Prof. Longfei Xiao (Chair), Shanghai Jiao Tong University, China;
- Prof. Yasunori Nihei, Osaka Prefecture University, Japan;
- Dr. Nuno Fonseca, SINTEF Ocean, Norway;
- Prof. Narakorn Srinil, Newcastle University, United Kingdom;
- Dr. Nick Markov, Bulgarian Ship Hydrodynamics Centre, Bulgaria;
- Dr. Guillaume Ducrozet, École Centrale de Nantes, France;
- Dr. Hasanat Zaman, National Research Council of Canada, Canada;
- Prof. Kwang-Hyo Jung, Pusan National University, Korea;
- Dr. Pedro Mello, University of São Paulo, Brazil.

Two virtual committee meetings have been held during the work period:

- Virtual meeting, December 19th, 2022;
- Virtual meeting, January 16th, 2023.

1.2 Tasks based on the Recommendations of the 29th ITTC

The Ocean Engineering Committee covers moored and dynamically positioned ships and floating structures. For the 30th ITTC, the modelling and simulation of waves, wind and current is the primary responsibility of the Ocean Engineering Committee with the cooperation of the Seakeeping and the Stability in Waves Committees.

The recommendations for the work of the Ocean Engineering Committee as given by the 29th ITTC were as follows:

(1) Update the state-of-the-art for predicting the behaviour of bottom founded or stationary floating structures, including moored and dynamically positioned ships, emphasizing developments since the 2021 ITTC Conference. The committee report should include sections on:

a. the potential impact of new technological developments on the ITTC;

b. new experimental techniques and extrapolation methods;

c. new benchmark data;

d. the practical applications of computational methods for prediction and scaling;

e. the need for R&D for improving methods of model experiments, numerical modelling and full-scale measurements.

(2) Review ITTC Recommended Procedures relevant to ocean engineering, including CFD procedures, and

a. identify any requirements for changes in the light of current practice, and, if approved by the Advisory Council, update them;

b. identify the need for new procedures and outline the purpose and contents of these.

(3) Review and identify areas of concern in modelling and simulation of waves, wind and currents. In particular:

a. report on methods to generate extreme wave packets for studying responses to extreme waves in a towing tank. Examine the effects of wave breaking and statistics of occurrence on the wave spectrum, its spectral shape, extreme wave generation, and the role of wind-wave interaction on wave breaking occurrence;

b. investigate the influence of the vertical wind profile on the aerodynamic loads experienced by platforms and other offshore objects. Develop a standard vertical wind profile for model testing purposes and methods for modeling it both numerically and experimentally.

c. Continue work on using a small controllable fan to mimic forces developed during a floating offshore wind turbine test due to the turbine itself. Expand the work on Software-in-the-Loop (SiL) systems for modeling wind turbine loads to be used as a general tool to model many types of wind loads. For example, wind loads on a ship during a maneuvering in waves test. Liaise with the SC on Ocean Renewable Energy and the Seakeeping Committee.

d. Develop specifications for a benchmark test program for wind loads and their influence on the motions of floating structures. Compare wind loads developed using SiL to model the wind loads versus using fans to produce an actual model scale wind. Among other data, repeatability, and consistency between the methods and between different facilities should be reported. The benchmark study may also include CFD comparisons.

e. Report on state-of-the-art for wave-current interactions. In particular, the role played in terms of the generation of extreme waves.

(4) Review the state-of-the-art in offshore aquaculture systems since the 2021 report of the Ocean Engineering committee including large volume closed containment systems, extreme wave environments, and modelling of entire systems.

(5) The benchmark tests with the square cylinders are complete. However, it is recommended that, owing to the complicated wave-column interactions, more experimental and CFD studies should be considered for four-column cases with different configurations and more extreme waves such as focused waves. In addition, local wave impact loads on the columns are also critical and deserve further in-depth studies.

(6) The work on the CFD benchmark study of two-bodies in close proximity shall be continued. Smaller gaps need to be studied

and the procedure for 2-body model tests shall be updated based on the CFD benchmark study.

(7) Investigate extraction methods of nodules from the seabed. Develop a guideline for testing Nodule Mining Machines in a towing tank including their riser systems.

(8) Investigate testing methods to characterise the influence of changing bottom bathymetry and coastline for tankers at offloading terminals.

2. REVIEW OF STATE-OF-THE-ART

2.1 Bottom Founded Structures

Bottom founded structures are widely used as production or oil recovering platforms in shallow or moderate waters but have been also applied as offshore wind turbine supporting structures in recent years.

Zhang & Teng (2021) present the development of a time-domain nonlinear potential flow model based on the weak scatterer approximation using High-Order BEM to deal with the interaction of surface-piercing bodies and moderately steep waves. The main objective of their work is to provide an improved numerical model for computing higher-harmonic wave loads and ringing response of offshore wind turbine foundations. The numerical model is validated on the classical configuration of a vertical cylinder subjected to regular waves of different steepnesses. The wave runup profile around the cylinder as well as the higher-harmonic wave forces are studied and compared to different nonlinear wave models and experiments. Finally, the ringing response of a monopile in moderately steep focused waves is investigated for several wave conditions. The effects of peak frequency, input wave amplitude and damping ratio on the ringing response are discussed. The importance of including higher-harmonic components for an accurate estimate of the response, especially for large wave steepness and small damping ratio is demonstrated.

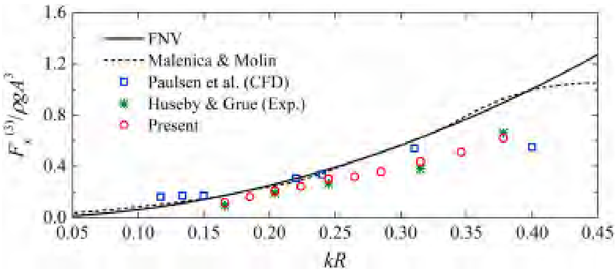

Figure 1: Amplitudes of the third-harmonic horizontal force on the vertical cylinder (Zhang & Teng, 2021)

Kim et al (2021) evaluates higher-order diffraction forces on vertical cylinders using a 3D fully nonlinear numerical wave tank (NWT). The NWT accurately determines hydrodynamic pressure using potential theory, the boundary element method, and a mixed Eulerian-Lagrangian (MEL) approach. In the fully nonlinear NWT simulation, all higher-order terms are produced simultaneously using a fast Fourier transformation (FFT). The results demonstrate an increased third-order sum-frequency force in shallow water long waves when compared to experiments and perturbation-based data. The incident waves are linear, Stokes 2nd and 3rd order waves. Results are compared for hydrodynamic pressure, and forces for different mono- and bichromatic waves on the cylinder surface for first-order, second-order mean-double, and third-order triple frequency waves altogether.

Suja-Thauvin et al. (2020) conducted model experiments of a monopile structure subjected to different severe irregular sea states, see Figure 2. The experimental model was designed to reproduce the first and second natural frequencies of the NREL 5MW reference wind turbine monopile. The paper compares the experimental results to four different hydrodynamical models of increasing complexity: i) Morison equation with second-order wave kinematics, ii) Morison equation with fully-nonlinear wave (FNL) kinematics, iii) model proposed by Kristiansen and Faltinsen, with FNL kinematics and iv) the model proposed by Rainey, with FNL kinematics. Those hydrodynamical loads are then used as input in a finite element solver. The Morison equation with second-order kinematics matched the main population of events well but underestimated the largest measured shear forces. The models using fully non-linear kinematics predicted the most extreme shear forces reasonably well, but they were not in general conservative. These three force models generally matched the main population of measured acceleration reasonably well, with underprediction, however, of the extreme accelerations. It was found that the models generally overpredicted the first mode acceleration but underpredicted the second mode acceleration for large response events. This was expected since no slamming load model is implemented in the current analysis.

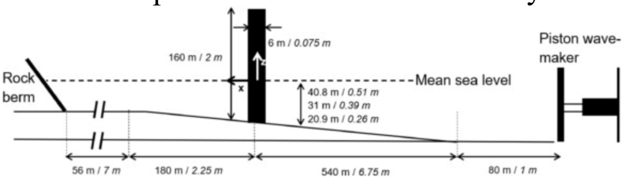

Figure 2: Experimental set-up (Suja-Thauvin et al., 2020)

Moghtadaei et al. (2022) utilized a RANS (Reynolds Average Navier-Stokes) model employing the volume of fluid (VOF) method to assess wave kinematics, shear forces, and moments arising from the interaction of near-breaking to weakly nonlinear waves with a bottom-seated cylindrical pile, representing a 5MW wind turbine. This comprehensive study incorporates both regular and irregular waves, with the latter adopting JONSWAP wave spectra. To address turbulence effects, a k-w model is employed. To validate the numerical model, relevant experiments are conducted. In these experiments, a load cell is integrated at the point where the cylinder meets the bottom of the wave basin, enabling the recording of time series data for shear force and bending moment resulting from wave loads induced by the incoming wave field. The findings reveal that inertia force dominates the shear force in all regular waves. For irregular waves, a larger KC number leads to the amplification of higher-order wave loads. The paper highlights that the nonlinearity of wave forces is a consequence of the interplay between inertia forces from nonlinear waves, diffraction, and associated turbulence.

The analysis of Vijoy et al. (2020) involves utilization of the two-dimensional small-amplitude water wave theory to study the interaction of gravity waves with a normally incident monochromatic wave when Bragg breakwaters are present. In this study, they investigated wave scattering caused by multiple submerged structures of various shapes, including rectangular, trapezoidal, semi-trapezoidal, triangular, semicircular, and quarter-circular configurations. The research returns reflection, transmission and energy loss coefficients. Additionally, the study examines the effects of structural width, thickness, barrier spacing, number of structures, and their specific shapes in the interaction processes.

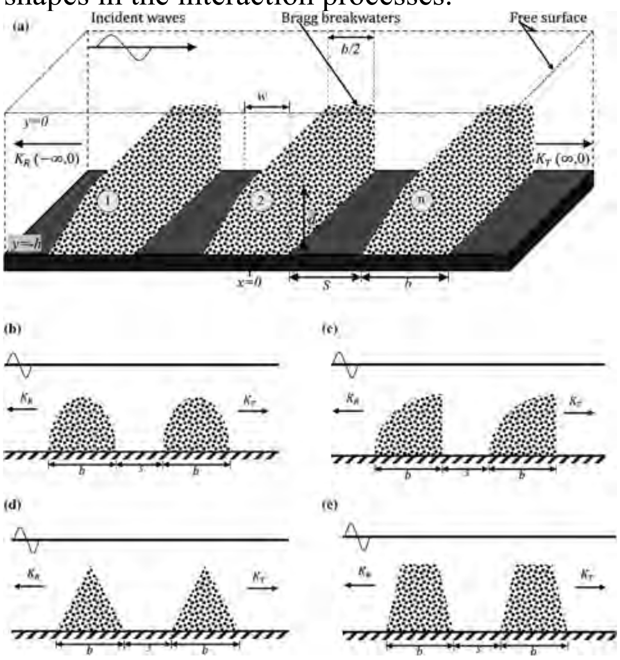

Figure 3: Schematic diagram of Bragg breakwaters having a) semi-trapezoidal, b) semicircular, c) quarter-circular, d) triangular, and e) trapezoidal configurations (Vijoy et al., 2020)

The comparison between impermeable and porous breakwaters clearly shows that the impermeable ones exhibit higher transmission coefficients. Due to the increased reflections, the trapezoidal and semi-trapezoidal shapes demonstrate lower transmission capabilities.

Multiple triangular structures damp waves minimally. As the breakwater number increases, Bragg's reflection sharpens and bandwidth decreases; quarter-circular shapes minimize this effect compared to others.

In their work, Mackay et al. (2021) introduce a boundary element method (BEM) model for analyzing wave forces on structures featuring both porous and solid surfaces. This model accommodates porous surfaces with linear or quadratic pressure-velocity relations. Notably, for quadratic pressure-velocity relationships, the model concurrently addresses the structure's combined motion response and wave forces. Moreover, the model encompasses solutions for diffraction and radiation scenarios as specific cases.

The credibility of their approach is evidenced by an analytical solution applied to a submerged vertical cylinder featuring a porous outer boundary. This arrangement operates under a linear pressure-velocity relation for excitation forces and the far-field drift force. Their technique effectively mitigates the impact of irregular frequencies on different forces. They investigated wave forces on a porous-solid truncated cylinder with a quadratic pressure system. The outer cylinder generally amplifies excitation force and added mass compared to no outer cylinder. Notably at low and high frequencies, where radiation damping is weak, porous surface dissipation notably boosts damping. This combined increase in added mass and damping reduces the resonant frequency and motion response amplitude.

Stansberg (2020) studies the impact loads on horizontal decks with a particular application to Gravity-Based Structures (GBS). To address this problem from the practical point of view, he proposes a simple a simple 2D analytical slamming model, based on the rise velocity from the incoming wave elevation. Based on previous GBS wave-in-deck experiments and despite a significant random scatter in the results (that increases with increasing velocities), reasonable correlation between measured deck impact loads (see Figure 4) and the underlying wave rise velocity is demonstrated, corroborating the idea underlying the simple model development. This is confirmed with the overall good comparison between the simple model and the experiments, especially regarding the fact that the model provides an approximate upper limit for the measured impact loads.

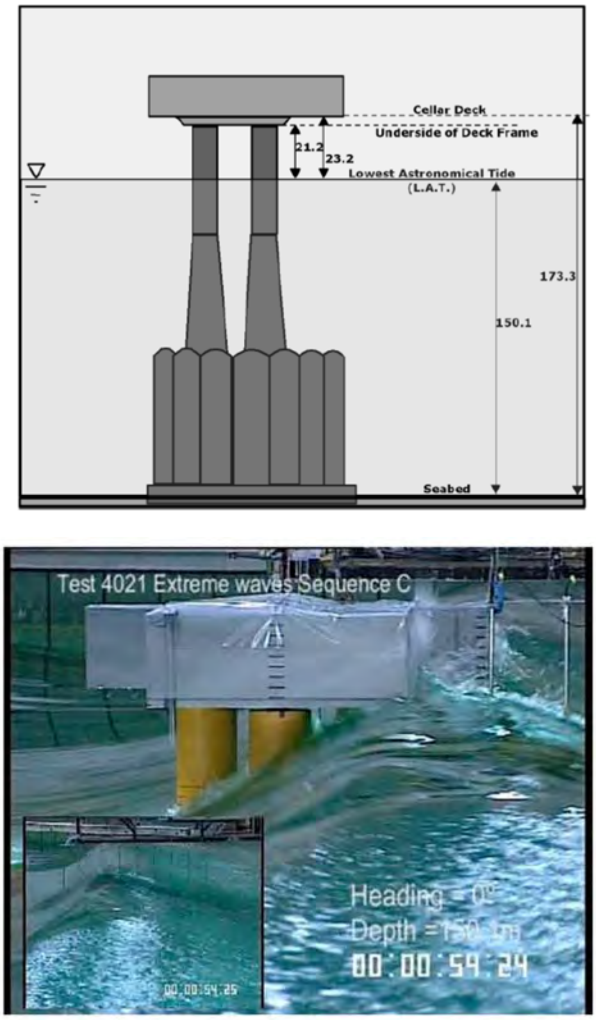

Figure 4: Experimental arrangement of the GBS (top) and picture of the wave impact on the GBS (bottom) (Stansberg, 2020)

Mackay et al. (2021) present a numerical and experimental study dealing with the interaction of waves with fixed and floating porous cylinders, see Figure 5. The paper focuses on wave forces on fixed porous cylinders with and without a solid inner cylinder and wave-induced motions of floating cylinder with and without a porous outer cylinder. The numerical model is based on Boundary Element Method (BEM) with a pressure drop proportional to the square of the velocity across porous surface. Its ability to accurately predict the nonlinear variation of the forces with wave amplitude or motion amplitude is demonstrated. The addition of a porous outer cylinder to a solid vertical cylinder increases the excitation force on the combined structure. However, it is shown that for low Keulegan Carpenter numbers, the damping coefficient for a porous cylinder is significantly higher than the viscous damping on a solid cylinder, which could be interesting for the damping of floating structures.

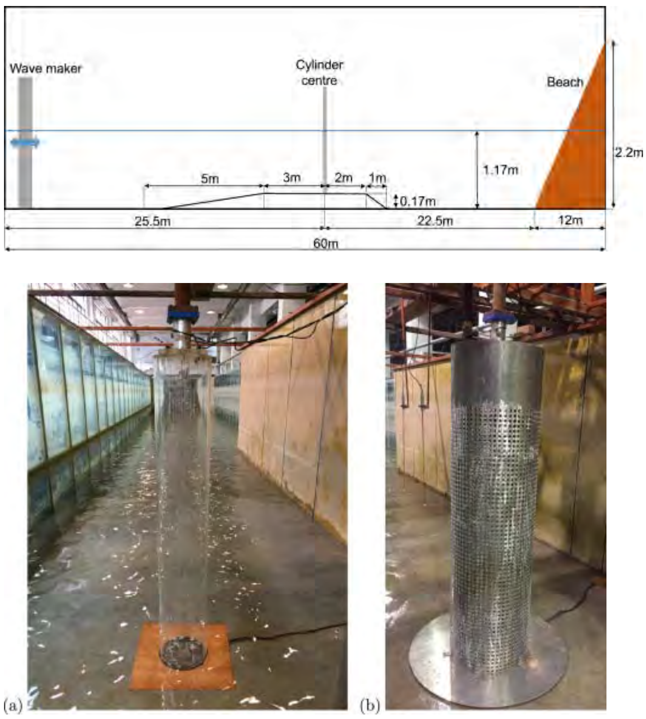

Figure 5: General experimental set-up (top) and picture of the solid cylinder (bottom left) and porous cylinder (bottom right) (Mackay et al., 2021)

Shi et al (2023) studied how the ice-breaking cones affect the nonlinear force and runup on the monopile in a focused wave group by a three-dimensional numerical. They used the commercial Star-CCM+ tool to integrate the VOF technique with the incompressible Navier-Stokes equations. A phase decomposition method through a 'Stokes-like' formulation was adopted to extract and investigate higher harmonics. In a viscous numerical wave tank, numerical simulations are run. They reported that comparing the installed ice-breaking cone to the uninstalled cone, the second harmonic coefficient typically rises by about 40%. They stated that an upward-downward-type ice-breaking cone increases the third harmonics, whereas an inverted-type ice-breaking cone exhibits the opposite behavior when compared with the uninstalled cone.They showed that the presence of two ice-breaking cone types raises wave loads. Contrary to monopiles, upward-downward cones boost wave load by about 6%, while inverted cones boost it by 1.5 to 3 times, depending on the wave's steepness and the amount of cone edge-induced breaking. They also compared the locations of the highest and lowest runup in the presence and absence of ice-breaking cones.

Li and Fuhrman (2022) used a coupled higher-order boundary element method (HOBEM) with FEM. A weak-scattering approach determined higher harmonic loads, while the linear Euler-Bernoulli beam model assessed structural ringing response. They reported that the peak force resulting from initial wave breaking can be accurately predicted without any turbulence model but for the prediction of the secondary force, a turbulence model is necessary as the process involves both turbulence production and flow separation behind the vertical pile. They observed that the Reynold stress–ω model is more accurate than a two-equation k–ω turbulence model for the prediction of the secondary load due to better prediction of flow separation points and vorticity.

In Zeng et al. (2021), the effects of breaking wave impact on a monopile-type offshore wind turbine installed at different locations at the edge of a 1:25 slope are investigated. The paper covers a numerical study that makes use of StarCCM+, a commercial CFD model using VoF method and solving Unsteady RANS equations. Dedicated experiments are also included, with the aim of validating the numerical results, see Figure 6. This is achieved through comparisons of the wave run-up around the monopile and of the forces induced by the waves. Accurate comparisons between experiments and simulations are reported, validating the CFM model that is used afterwards to investigate the wave breaking evolution and impact kinematics for different monopile locations.

Bachynski et al. (2020) report an experimental study dealing with flexible monopile subjected to a set of regular and irregular waves with different seeds, see Figure 7. Compared to the previous campaigns, the larger diameter, inclusion of several damping levels, and increased number of realizations and repetitions allow for drawing new conclusions. The importance of the steepness of the sea state is pointed out: the extreme accelerations, shear forces, and base bending moment tend to be larger for the highest steepness rather than the largest Hs. Furthermore, increasing the damping ratio tends to decrease the accelerations and bending moment for the main body of responses (Pexc > 0:01), but does not have a significant effect on the largest events. In addition, qualitative differences in the exceedance probability distribution of the nacelle acceleration and base shear were noted. Modal contributions to bending moment, shear force, and acceleration near first and second natural frequency are studied. It is found that the importance of the quasi-static response decreases for the largest events, while the importance of the responses at the second mode natural frequency tends to increase. Finally, the correlation between large nacelle accelerations and the wave breaking limits was not as clear as in previous tests

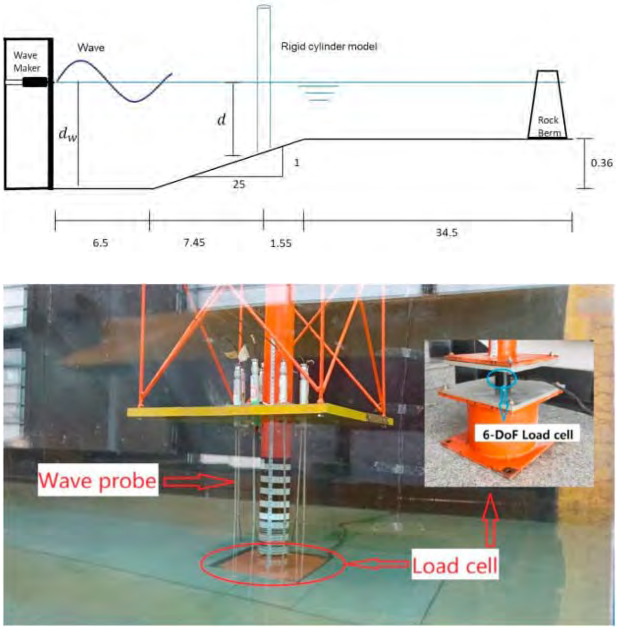

Figure 6: Sketch of the experimental set-up (top) and picture of the arrangement (bottom) (Zeng et al., 2021)

Leroy et al. (2021) present a hydro-elastic model that includes a non-linear hydrodynamic solver based on weak-scatterer approach, coupled to a structural solver based on flexible modes pre-computed from a FEM model. This new model is compared to a more conventional approach based on Morison solver for the hydrodynamic part. The application case studied in the paper is an offshore wind turbine on a monopile foundation. The numerical results are compared to experimental measurements made on a flexible 1/50 Froude-scaled model, which includes the wind turbine tower and an RNA mass and damper and which respects Froude-scaled modal frequencies, see Figure 7 and Bachynski et al. (2020). The load cases include a series of regular waves, with various steepnesses and periods that allowed to characterize the capabilities of the new model.

Teng and Liu (2023) describe an approach in which the incident and scattered wave components of the problem are isolated during computation. They proposed to evaluate the incident wave component using a spectral model. They utilized a coupled higher-order boundary element method (HOBEM) and finite element method (FEM) model based on a weak-scattering approximation for the solution of the scattered wave, where the fluid field would be predicted using HOBEM, and the resulted response would then be addressed using the FEM. To determine the structural ringing response for the monopile foundations of an offshore wind turbine, the linear Euler-Bernoulli beam model was used in their work. When compared to the pertinent published data, they found good agreement for wave elevations and loads. They claimed that the third-harmonic motion or ringing was most intense when the focal position was set at the center of the monopile and that the maximum positive and negative moments appeared when the focused position was on the downstream and upstream sides. The computational domain is shown in Figure 8.

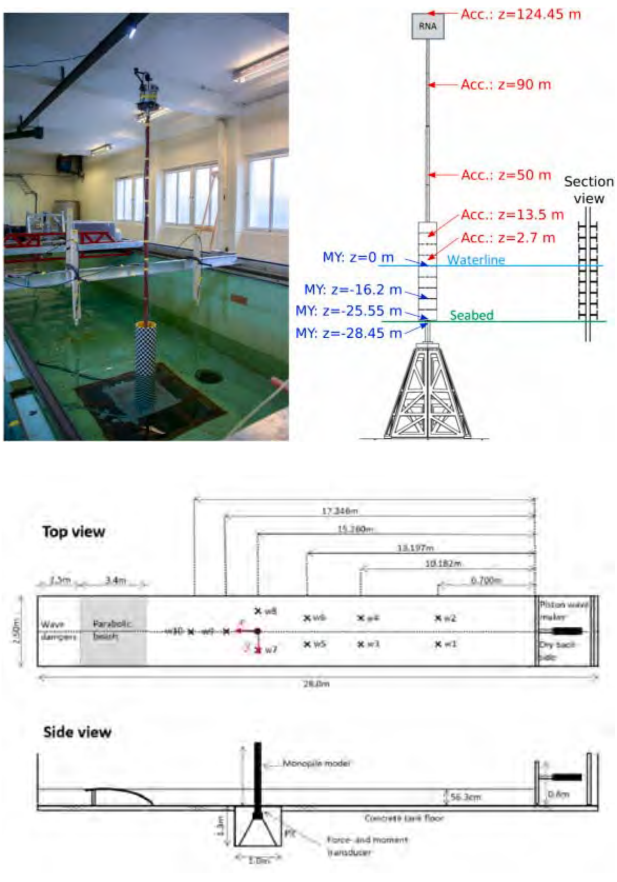

Figure 7: Picture and details of the experimental set-up (Bachynski et al., 2020))

In Jahani et al. (2022), a review of the most important concerns related to the structural dynamics of offshore wind turbines (OWTs) is presented. This details the importance of modal alignment in OWTs. Then, recent articles on aeroelasticity, hydroelasticity and vibrations of OWTs are reviewed. This is followed by a study on the interactions between OWTs and their support structures. Up to date in situ and lab-based experiments on structural dynamics of OWTs are reviewed. Finally, major topics that require further investigation on the structural dynamics of OWTs are outlined.

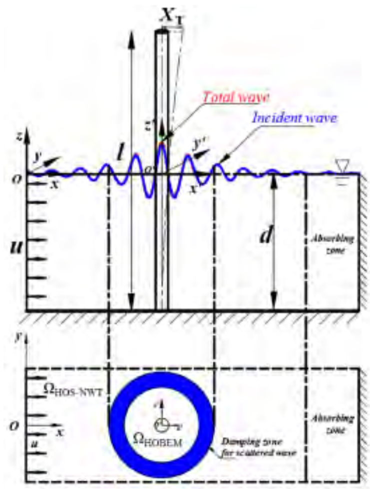

Figure 8: The computational domain (Teng and Liu, 2023)

2.2 Stationary Floating Moored Structures

Stationary floating structures addressed in this section include FPSOs, semisubmersibles, TLPs, spars, VLFS, FLNG, and their riser/mooring and dynamic positioning systems. Unless specified, this section is focused on platforms for oil and gas industry.

2.2.1 FPSOs

Park et al (2022) describe an experimental study about slamming at the FPSO bow. A set of pressure sensors installed in different heights and aside the center line map the pressure distribution of impact by different irregular waves response periods (10yr, 50yr, 100yr and 1000yr) and current. A treatment of pressure data was defined to discard wrong pressure peaks for rise time and decay time calculation. Pressure distribution was analyzed concluding that the location of maximum pressure changes to up with a tendency to wave crests increases. However, the maximum impact point was not occurred exact in each sensor's discrete location. The maximum and average pressure peak values were a tendency to move to up with wave heights, but the sensor needs to be allocated in the exact point to record it. For higher wave steepness the same behavior was observed when impact pressure increases. The tendency of higher-pressure peaks was associated with short pressure rise time. The current direction propagation associated with the wave at the same direction shift the wave steepness to lower values and reduce the severity of the impact peaks at the FPSO bow.

Chen et al (2021), presents a study based in OpenFOAM CFD to evaluate the runup around a FPSO shape vessel. In order to verify the CFD modelling, experimental tests in wave flume and wave diffraction analysis were carried out. A group of waves was executed in four phase shifts in frequency domain, focus on to generate a runup in the bow of the FPSO. The vessel was free to move by a soft mooring anchor at the flume sides. Wave probes attached to the model monitoring the runup of waves. It was used a separation method to extract the harmonics of the wave group of non-linear waves decomposition associated of Stokes perturbation expansion method. In the experimental and numerical data, the scattered waves from the bow of the vessel shows harmonics associated with the runup elevation. The vessel movement in wave presents predominantly linear behavior and the runups are mostly decomposed by low-harmonics and high-harmonics of the second harmonic of waves. The separation method described could be useful to predict the runups for others type of vessels and shapes in numerical and experimental tests with better results than linear theory models to predict runup and green water.

Zhang et al (2022), studied the green water in OpenFOAM simulating the events of impact in a bow of a hull. The hull presents a deck and a superstructure assembled over then. A Peregrine Breather solution of nonlinear Schrödinger equation (NLS) was used to generate a freak wave at the inlet boundary of numerical model. The freak wave was focus on the region of the bow of the hull. The wave created reach the bow generating a green water event of the type plugging dam break (PDB). A virtual mesh of virtual pressure probes mapping the pressure distribution on deck and a superstructure over the deck. The maximum pressure occurs close to the joint of the deck to the superstructure in the midship. Close to the superstructure the pressure presents two or three peaks due water drops in contact with the superstructure. The simulation in 2D and 3D were evaluated, and the second type is adequate for freak wave green water events simulation. The relationship between wave heights and periods of the freak waves was verified in the pressure impacts on the deck and superstructure during the green water occurrences. The parameter combination changes the characteristics of green water events and the pressure distribution.

The article of Fontes et al (2021), shows qualitative aspects of green water classification in relation of format of the events over the deck of a generic structure. An image-based technique analysis was applied to measure different aspects of the events occurrences during several regular waves realized in a wave flume experiment. The work classified the green water events in three types: dam break (DB), plugging dam break (PDB) and hammer fist (HF). The authors explore the characteristics of each type of green water such as: free board elevation, volume of water over deck, wave characteristic highlighting the steepness and in time event evolution. In the sequence article Fontes et al (2022), the applicability to modelling green water over de deck with analytical model considering terms of advection-diffusion equations solution of Navier-Stokes model, was investigated. The premise is to develop an analytical tool for estimating green water for project phase of vessels and offshore structures. An analytical convolution approach was investigated to describe in time evolution of single-valued water elevations of different types of green water events generated by incident wave trains impact to the bow of structure, particularly dam break, plunging dam break and hammer first described early. The convolution analytical model was compared to the experimental data captured by image-based technique for a single event and a sequence of events of green water propagating from the edge of the bow and so on over the deck in time domain. The results show an improvement due the traditional dam break theory. The decay tendency of water peak evolution in time were acceptable representation. However, the peaks of water propagation over the deck are over predicted in comparison of experimental data. The coefficients value needs to be investigated in future works to obtain better approximation related the deck characteristics in special the rugosity. Nonetheless the analytical model is useful to simulate the green water events in simplified way.

Lee et al (2022) perform an experiment to study the green water behaviour in wave flume in a captive FPSO bow simplified structure varying the flare angles of 45°, 60°, 75° and 90° (vertical bow). Regular waves hit the bow of the FPSO, and a camera record the water elevation and air bubbles trapped in the interface. The BIV (bubble image velocimeter) technique serve as to quantify the liquid velocity. The dam breaks phenomenon occurs over the deck structure and a set of five pressure gages record the pressure distribution at the surface during the events of green water. A comprehensive methodology analysis of pressure and BIV measurement was presented to modelling the dam break events and predict the pressure distribution and green water wave elevation.

Kwon et al (2023) realized an experimental and numerical study regarding the riser hand-over operation between an installation vessel and a FPSO. The study was realized with two model in the test in regular waves. Due the deep of the basin, the riser truncation was applied to modelling the similarity in the hand-over operation. The vessels hydrodynamic interaction observed was confirmed in the numerical simulation, highlighted in the heave and pitch motions affected in two wave headings. The numerical model with hydrodynamic interaction of vessels confirmed the transfer functions of the load behaviour in the riser, observed in the wave basin tests. Under lower load transfer percentage between 0 and 5%, cables snapping phenomenon occurs and increasing the load transfer up to 50%, vessels interactions increase and tension transfer function increase to 80-90% above initial values.

Ha et al (2024) use a FPSO model in experiments with irregular waves to study green water at the side walls and at the bow in oblique waves incidences. A set of 12 wave probes attached to the model measures de relative waves elevation over the deck. Cylindrical pillars over the deck were used to measure forces due green water events. Video cameras record the events of green water waves occurrences in a qualitative way. The results treated using correlation between motion and relative wave elevations shows some aspects important to explain the phenomenon. In highlight, there is a close correlation between heave motions and side walls green water. At the same way, pitch and roll motion are important to explain the bow green water.

2.2.2 Semi-submersibles

Semi-submersibles have attracted much more attention in the recent years due to their suitability in reducing wave-induced motions of the floating system. However, there are still various challenges related to damage mooring conditions. Size of mooring, columns, pontoon shape and airgap help in the mitigation of dynamic responses in waves and wind, but their effects need to be further investigated during damage occurrence. Artificial intelligence methods are being introduced in the global performance evaluation.

Yu et al. (2021) investigated parametric resonance of the deep draft semi-submersible under regular waves experimentally and numerically. The focus was on the occurrence of parametric resonance in damage mooring condition. Model tests with and without mooring chains were conducted in a wave flume. For a model with 12 mooring lines representing intact mooring, parametric resonance did not occur. Whereas for the model with four mooring chains, representing the damage mooring condition, parametric resonance occurred. It was observed that parametric resonance occurred when wave period is about the natural period of heave and half of the natural period of Pitch or Roll. Numerical simulations of the test conditions were conducted using a potential-theory based weakly nonlinear model. Parametric resonance was successfully reproduced numerically. It was found that the numerical model accurately predicted the parametric resonance amplitudes and periods except for the damage mooring cases.

These findings should be verified in a larger wave basin to evaluate potential distortions due to blockage effects caused by the nearby basin walls (Figure 9).

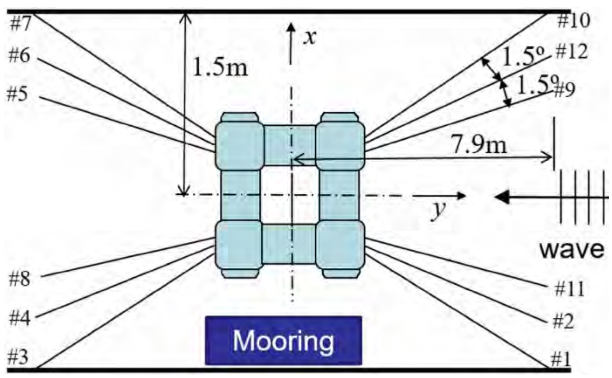

Figure 9: Model test setup with 12 mooring lines

The station-keeping system of offshore platforms is susceptible to complex metocean conditions. The failure of the mooring line is of concern due to uncertainty in the mooring lines behaviour and the potentially severe aftermath of an incident. Once the mooring line breakage occurs, the remaining mooring lines should provide sufficient tension to warrant the safety of the personnel and protection of the environment. Mao et al. (2022) proposed a deep neural networks (DNN) approach to predict the dynamic mooring line tension under one mooring line failure condition. First, the tension change of mooring lines induced by a mooring failure was investigated in two hydrodynamic models. The tensions of the mooring line with maximum sensitivity to failure was selected as the output objective. Second, two datasets of different hydrodynamic models were generated using the global response of the floating structures and their mooring tensions (Figure 10). Two DNN models were trained utilizing grid search to determine the optimal network structure. Finally, some case studies with different mooring arrangements and sea state conditions were employed to verify the feasibility and adaptability of two established DNN models and compare their accuracy.

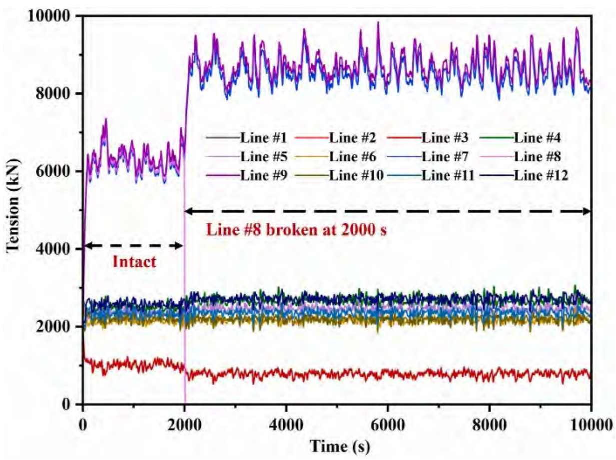

Figure 10: Time-domain analysis results

The results imply significantly increased sway and surge motions due to the mooring damage. Based on the study, it may be possible to combine in a practical way the input from GPS and the remaining intact mooring line tensions to monitor and control the mooring damage condition in real time.

Semi-submersible platforms can suffer slamming damage from extreme waves, making it crucial to improve their airgap performance. To address this issue, Liu et al. (2023) propose an innovative flare barrier that can be attached to the surface of a column at a certain height above the waterline, drawing on bow flares used in ship design. This study conducts a series of experiments to investigate the effectiveness of the flare barrier in mitigating wave run-up and motion response of a semi-submersible platform. The experiment simulates the wave field in 100-year irregular waves in headings 180° and 135°. Two different wave seeds are considered for each wave heading to reduce the transient effect. The results show that the flare barrier significantly mitigates wave run-up, especially at the height of the lowest edge of the barrier. Adding a flare barrier has no adverse effect on the surge, heave and pitch response. In heading 180°, it even has a slight mitigation effect on heave and pitch. The mitigation effect is also demonstrated in the power spectral analysis. Considering the wave run-up and motion response, a flare barrier is recommended to mitigate wave run-up on the column and improve the airgap performance under extreme waves.

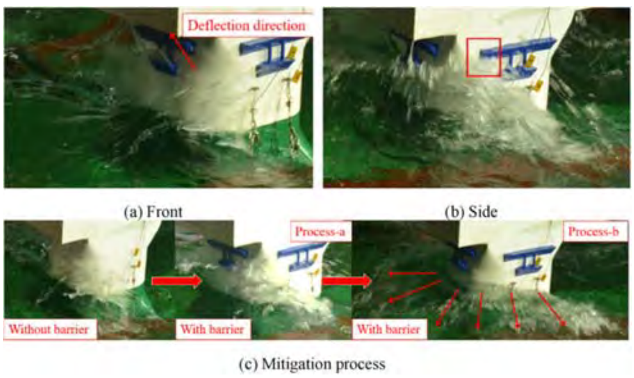

Figure 11: Flare barrier performance in 100-yr waves (Liu et al., 2023)

Additional model tests are recommended to validate the flare barrier design because two wave seeds may be insufficient to generate reliable wave run-up statistics.

Zhao et al. (2023) investigate the influence of mooring line disconnections on the response of a semi-submersible system (Figure 12) under regular waves and irregular waves. Two failure modes were performed and compared according to the disconnected positions of mooring lines: the top breakage and bottom unlatch. A numerical model of a fully coupled hull/mooring/riser system was created using in-house software to obtain the detailed behaviour of each component. The results indicated that the platform motion became a 4-period nonlinear response containing a super-harmonic motion when three moorings were unlatched. The disconnected moorings produced a large deformation due to the sliding of their anchor points. The riser tension exhibited robustness under mooring failure because of its low tension level and the robustness of the platform heave. Compared with bottom unlatch conditions, the platform under top breakage conditions showed larger-amplitude fluctuations and a slightly greater offset particularly when three moorings disconnected. The total mooring force during top breakage conditions would lose more fairlead tension at the failure time, thus inducing a lower mooring force to the platform.

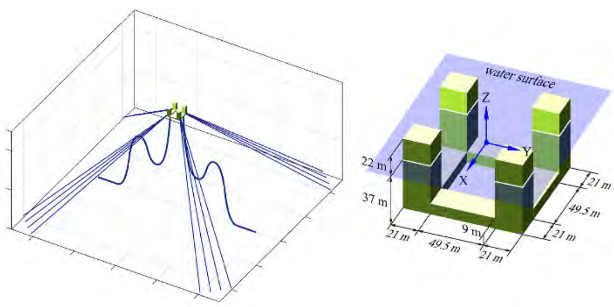

Figure 12: General view

Yeon et al (2022) investigated the wind loads on a semi-submersible rig using computational fluid dynamics. A maritime atmospheric boundary layer model for wind profile was implemented such that the wind profile shapes were retained throughout the computational domain.

Wind loads on the semi-submersible rig were calculated under the maritime atmospheric boundary layer and matched well with the results from the wind tunnel within a ±20% error. Among the topside structures, five structures, including the deck box (Figure 13), were selected and analyzed on the contribution to the wind load, particularly overturning moments, by decomposing the moments into drag and lift components. Overall, moments ignoring lift components tended to overestimate overturning moments by approximately 20% at maximum. The majority of the lift components originated from the deck box, which served as a lifting body owing to the accelerated streamlines between the waterline and the bottom of the deck box.

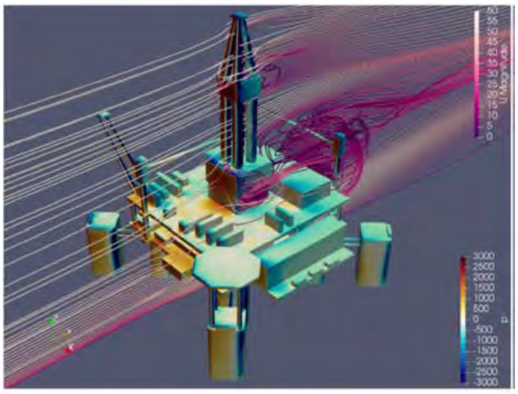

(a) top view

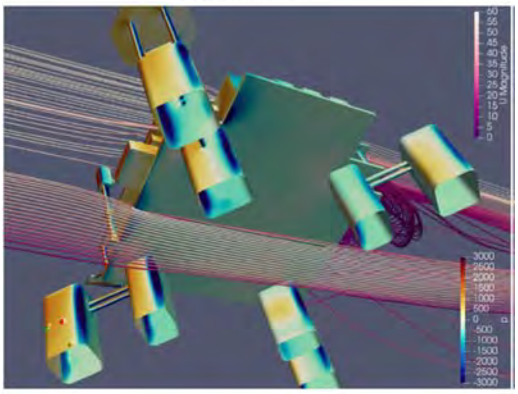

(b) bottom view

Figure 13: Streamlines around semi-submersible

The uncertainty level should be reduced to validate better the conclusions related to the lift effect on the overturning moment.

Jeon et al. (2023) analyzed a moored buoy's motions using a solver developed by coupling a computational fluid dynamics platform (OpenFOAM) with a lumped mass mooring line model (MoorDyn). The time-marching interface transferring the shared variables was developed to maximize the robustness and accuracy of the solver. The developed coupled solver was validated in waves using a moored cubic-shaped box model. Different mesh configurations, mesh generation techniques and mooring line discretization were considered in the numerical study. The cubic-shaped box moored with tensioned lines was simulated, and the results were compared with experimental results. The motion responses of a moored semi-submersible platform designed by the Korean Research Institute of Ship and Ocean Engineering (KRISO) were predicted numerically. The mooring line forces acting on the platform, the anchor, and the platform's motion performance were analyzed. Comparisons between the numerical results and experimental data were presented.

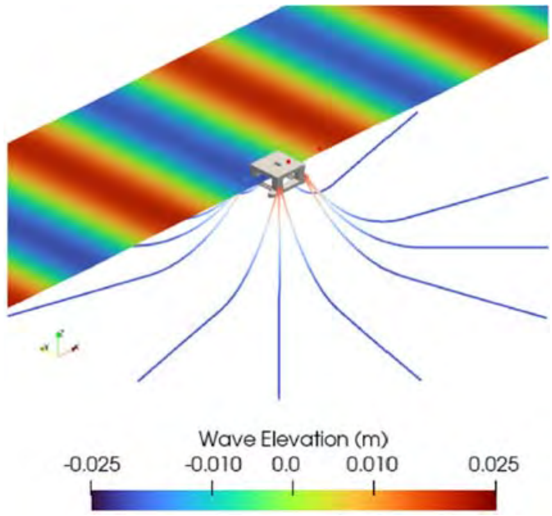

Figure 14: A snapshot of wave elevation around K-SEMI

Carmo et al. (2023) developed a slender-body approximation to evaluate the first- and second-order wave loads acting on a floating structure comprised of slender cylinders. It combines Rainey's equation, which can be seen as an extension of the inertial part of Morison's equation to include nonlinear terms, with

Pinkster's formulation for the low-frequency second-order loads on floating bodies. The objective is to obtain expressions that allow the evaluation of second-order wave loads considering the mean body position so that an Inverse Fast Fourier Transform algorithm can efficiently compute the second-order wave loads in realistic sea conditions directly in the time domain. Similarly to Morison's equation, this approach cannot model wave scattering and radiation effects, but this is acceptable if the diameters of the cylinders that compose the structure are small in the face of the length of the incoming waves. To verify the method, it was applied to the computation of the slow motions of a simplified semi-submersible FOWT model, first under the action of bichromatic waves and then in an irregular sea state. The results were compared with results from WAMIT, OpenFAST and experiments (Figure 15).

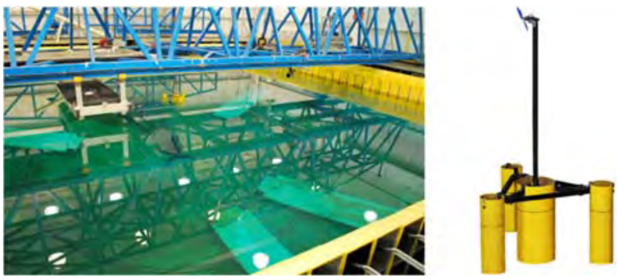

Figure 15: São Paulo wave basin (left) and the semi model

Under complex operating conditions of a semi-submersible platform, significant differences exist between the measured data in full-scale and the numerically simulated or experimental model-scale data. Yuan et al.'s (2023) study uses the measurement data collected during the operation of the semi-submersible ocean platform "Deepsea One" to train, validate, and test an artificial intelligence model, compensating for the lack of actual measurement data samples in previous studies. Their work provides a hybrid method for predicting mooring tension on semi-submersible maritime platforms based on VMD, error correction, and the convolutional neural network–long short-term memory (CNN-LSTM, Figure 16) and convolutional neural network–bidirectional long short-term memory (CNN-BiLSTM) models. The proposed hybrid prediction model was trained, validated, and tested using monitored mooring tension data acquired from the "Deepsea One" semi-submersible ocean platform in the South China Sea under different orientations and sea conditions.

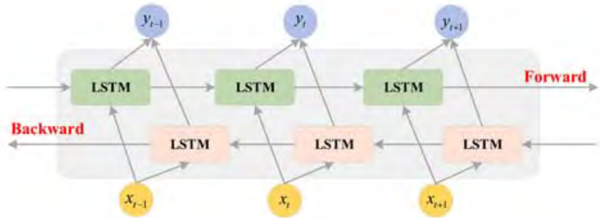

Figure 16: Structure of bidirectional long short-term memory neural network.

The results showed that the proposed hybrid prediction model for mooring tension on semi-submersible offshore platforms had lower values of the root mean square error, mean absolute error, and mean absolute percentage error and higher values of the coefficient of determination (R^2) than almost all of the other comparison models when predicting complex time series data of the actual monitored mooring tension. This indicated that the proposed hybrid prediction model had better precision and stability than other models. Furthermore, this method can be used to anticipate nonlinear, nonstationary time series data in different fields of maritime engineering.

2.2.3 TLPs

During the review period, TLPs behaviour has been investigated numerical and experimentally with special focus on responses under extreme and damage conditions. The experimental work related to vortex-induced motions also continues. An experimental investigation of the global performance responses of a TLP under different environmental conditions is presented by Jin et al. (2021). The TLP model included platform, tendons and risers (Figure 17). Regular and irregular waves, current, and a combination of irregular waves and current were generated during the tests. The influence of different headings on the motion responses in the in-line (IL) and cross-flow (CF) directions are presented. The motion spectra, wavelet transform, and motion trajectories were used to analyse the time histories. Statistical analysis of motion characteristics of TLP under different environmental conditions was presented and the governing for design heading pinpointed. With an increase of reduced velocity, the vortex-induced motion (VIM) of the platform first increased and then decreased, and multi-frequency time-varying coupling characteristics were presented in the cases of large reduced velocity. The VIM in this experiment were compared with towing tank were compared. In addition, the influence of free surface waves on the VIM has been illustrated through qualitative and quantitative analysis.

Figure 17: TLP tendons model

Cheng et al (2021) studied failure of tendons that might induce continuous failure and lead to the platform capping (Figure 18). The study modelled a typical TLP under tendon breakage. Time-domain analysis for a floating hull coupled with mooring lines was used to analyse the equilibrium position and amplitude of the steady-state response. The change laws of the balance positions of the motions and the reasons for the changes in the movement amplitudes were explored. By changing the wave parameters, the change rules of nonlinear motions and the damage caused by the change in the natural period were investigated.

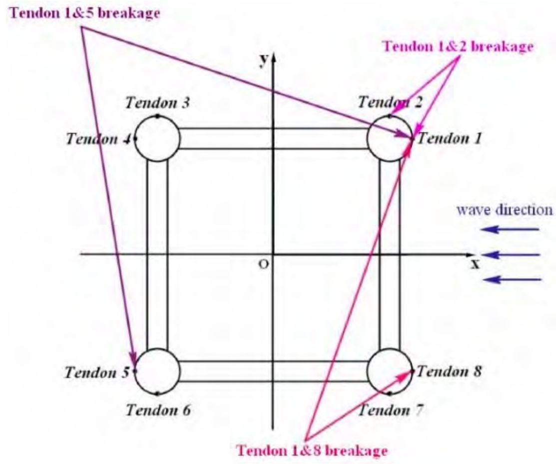

Figure 18: Schematic diagram of tendon failure modes

Zhi et al (2022) present an experimental study investigating the effect of draft, current heading and mooring stiffness on the Vortex-Induced Motion (VIM) responses of a Tension-Leg Platform (TLP) with four circular columns (Figure 19). The nominal transverse and yaw amplitudes and the corresponding spectra obtained by fast Fourier Transform (FFT) and continuous wavelet transform (CWT) are analysed to examine the characteristics of the motion responses. Four headings from 0° to 45° are adopted in the model test. The results show that the maximum response amplitude in both transverse and yaw directions is achieved at 0° current incidence. The maximum nominal amplitude decreases for the transverse response, and the lock-in range narrows as the current heading increases. The spectral analyses for the transverse and yaw motions at 0° current heading show that the dominant peak frequencies increase as the reduced velocity increases. It is observed that the low-frequency spectral peak of the in-line motion amplitude spectra increases as reduced velocity increases. A colour band or a ribbon concentrates stably around the frequency of $f<0.05$ in the wavelet analysis. It is primarily caused by the initial acceleration of the model in the towing tank. The absolute values of correlations between the spring tensions and the transverse motion of the platform are much larger than those between the spring tensions and the in-line or yaw motions. Moreover, it is found that the VIM trajectories of the TLP are primarily always along the direction perpendicular to the current heading.

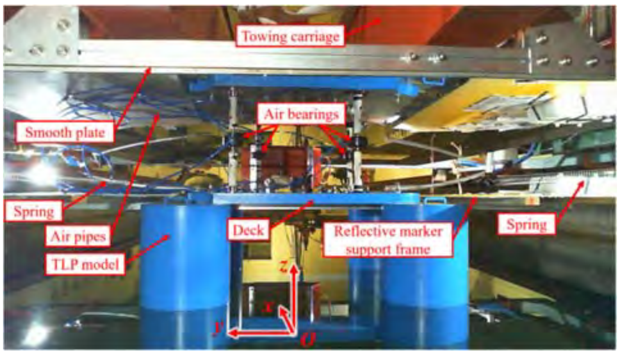

Figure 19: Experimental set-up in the towing tank

The experimental study conducted by Du et al (2023) investigated the dynamic response of a tension-leg platform (TLP) in complex flows, with the objective to improve the fatigue life of the mooring and riser systems. In this study, full-water-depth tendons and top-tension risers (TTRs) were modelled. Linear horizontal springs were installed instead of a mooring system used in other traditional models. Different types of shear flow with non-uniform distribution along the water depth were set to study the TLP response in heading 45° (Figure 20). Significant VIM and lock-in phenomena were observed, with the maximum amplitude occurring at *Vr = 7*. The response of the TLP when local flow accelerates around the columns and pontoons was discussed.

The reasons for the motion amplitude increase outside the lock-in region were clarified, and the mooring system's non-linear effect was demonstrated experimentally. To better understand the forces during the motion of TLP, the authors propose a method to reconstruct the fluid force, dividing it into two parts: the disturbing force and the radiation force.

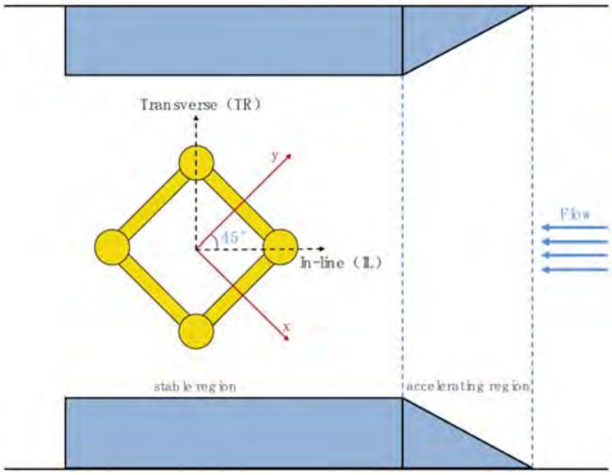

Figure 20: Arrangement of the model and the local flow velocity enhancement device

Kang et al. (2023) studied the nonlinear motion characteristics in the coupled behaviour of a Tension Leg Platform (TLP) combined with a Tender-assisted Drilling Unit. A time-domain numerical model was developed accounting for the nonlinear behaviour of mooring systems and the hydrodynamic interferences. Experiments were performed to validate the numerical model (Figure 21). Nonlinear motion characteristics of the steady-state response of the time-domain results were analysed using Poincaré mapping and fast Fourier transform.

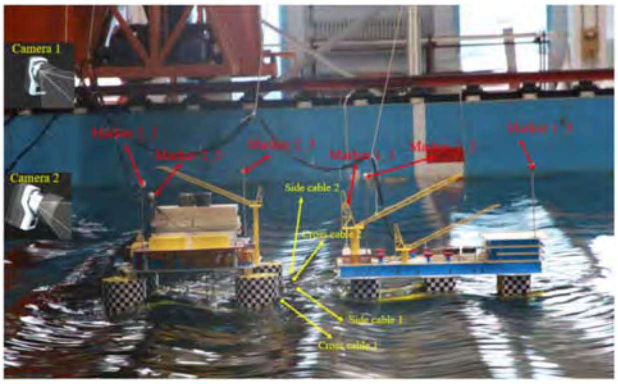

Figure 21: The experimental model of the coupled system

The study focused on investigating the motion response of the TLP in three degrees of freedom under coupled states. The surge motion consisted mainly of the wave frequency and half-wave frequency subharmonic components.

Meanwhile, the wave-frequency, subharmonic, and super-harmonic vibration components were observed in both heave and pitch motions. Three types of nonlinear regimes, namely chaos, transition, and multiple periodic, were identified in the heave and pitch motions under different wave conditions.

Investigating further how the vortex-induced motion would contribute to the coupled motion responses may be necessary. Also, would the designed hawser length be sufficient to keep their maximum tensions within practical limits?

During service life, a TLP is under potential damage caused by attendant vessel collisions. The influence of local dents on the maximum strength of TLP is a challenge in ocean engineering structures. Proper regulations outside the industrial practices are required to identify and rehabilitate the strength of these structures subjected to collision. Existing design methods require improvement to accurately predict the ultimate strength of TLPs subjected to accidental collision. Thus, it is imperative to develop viable approaches for predicting the residual ultimate strength of such structures.

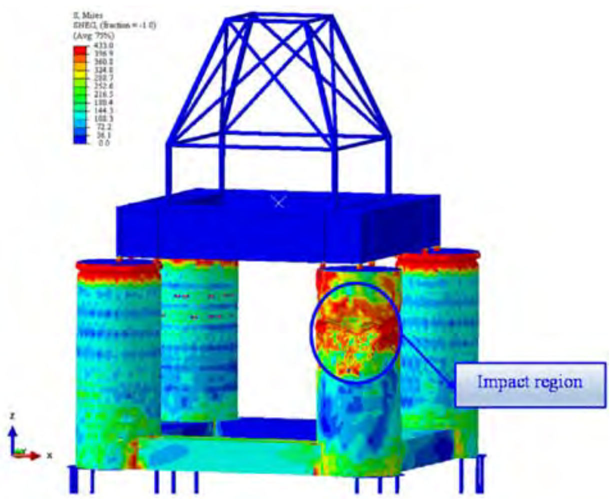

Figure 22: Deformed shape of a dented TLP column

This paper aims to establish practical modelling techniques and equations to predict the residual strength of dented TLPs subjected to combined axial compression and hydrostatic pressure.

The computational models proposed by Do et al. (2023) employ nonlinear finite element analyses (NFEA) considering the dynamic effects of materials properties such as strain rate and dynamic fracture strain. A series of NFEA of actual TLP with different collision scenarios and parameters were carried out using ABAQUS software (Figure 22). The empirical equations were provided through the database out of the NFEA results. The reliability of derived empirical formulations was compared with NFEA results, existing formulations, and test data.

2.2.4 Spars

Spar platform has become one of the most attractive floating platforms allowing top-tensioned riser operations thanks to its superior stability and low Heave motions in deep-water offshore sites. The focus of the listed below studies is on heave plate, strake performance, viscous drag and parametric resonance in relation to the spar motions.

Rao et al (2021) predict the hydrodynamic parameters of heave plates, namely, damping and added mass of the floater not only at its natural frequency, which can be obtained from free decay tests but also at other frequencies because the floater response is of interest over a wide range of amplitudes and frequencies. Forced oscillation tests in calm water can aid the investigation of these parameters at various motion frequencies and amplitudes. Heave damping and added mass of classic spar with heave plate were investigated in this study using experiments and numerical simulations of forced heave oscillation of a 1:100 scale model in calm water for various frequency-amplitude combinations. The least square method was used to determine the added mass and damping using three damping models, namely, linear, quadratic, and linear-plus-quadratic, and their applicability assessed. The effect of amplitude and frequency of oscillation on the parameters are discussed for various heave plate configurations with the aid of flow visualization from numerical simulations Figure 23. Added mass effect was examined using flow visualization of the fluid acceleration field. The scale effect on the parameters was also addressed.

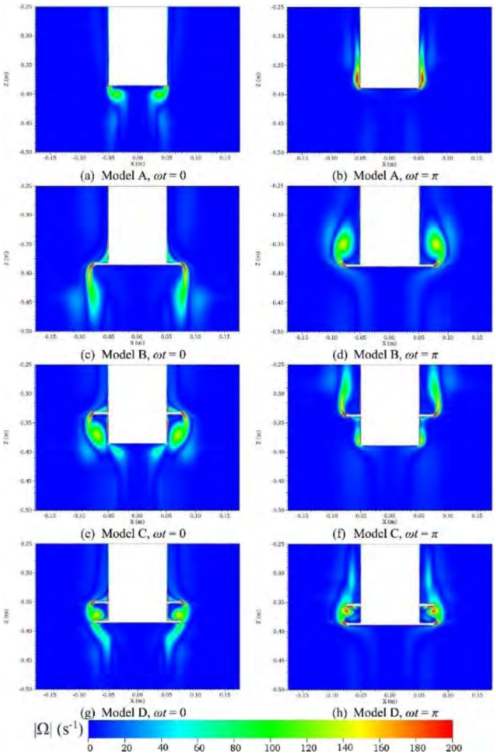

Figure 23: Vorticity magnitude contours around spar models

Kharazmi et al (2022) performed a numerical study aiming to reduce the Spar hull surge and sway response due to marine currents for various arrangements of strakes. The interaction of the marine current with a Spar model was numerically simulated. The results were compared with the VIM response of existing Spars with conventional strake design to validate the model. Different strake patterns and a conventional bare hull Spar equipped with strakes (base model, Figure 24) were used to model the VIM response of the platform. The results demonstrated the possibility of the Spar VIM response reduction due to improved design of the strakes. The best proposed configuration showed 58% suppression in sway motion and 9% in surge VIM response.

Figure 24: Bare model with strakes

Rao et al (2021) carried out experimental and numerical investigation on heave damping and added mass of a scaled model of spar with a variety of heave plate configurations (Figure 25) using free heave decay for a range of initial heave displacements. Applicability of the linear and quadratic damping models were assessed for all configurations. The effects of parameters such as heave plate diameter, location of heave plate above the keel, and spacing between two plates on damping and added were also studied. Flow fields obtained from numerical simulations were presented, and their implication on damping discussed.

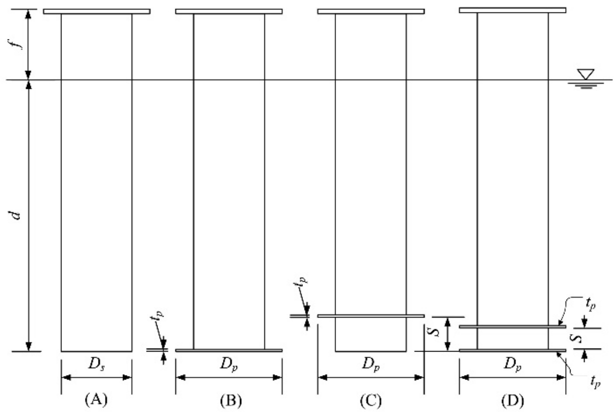

Figure 25: Experimental setup

Hegde and Nallayarasu (2023) investigated a classic spar and buoy form spar with a heave plate attached at the keel and near the free surface (Figure 26) for its effectiveness in reducing the overall response by conducting experimental studies in the wave basin and parametric studies using numerical simulations. The experimental investigations have been carried out using 1:100 scale models in the laboratory wave basin and compared with numerical simulations. It is observed that the buoy form spar with a heave plate attached near the free surface reduces peak heave motion response by about 75% and peak pitch response reduction by about 30% compared to classic spar without a heave plate. The motion response of the buoy form spar with different heave plate positions and diameters are compared, and the buoy form with heave plate near the free surface has been found to be effective in reducing the motion response considerably and hence recommended for use in practical design.

The findings should be confirmed in a lower than 1:100 model scale to reduce potential scaling distortions.

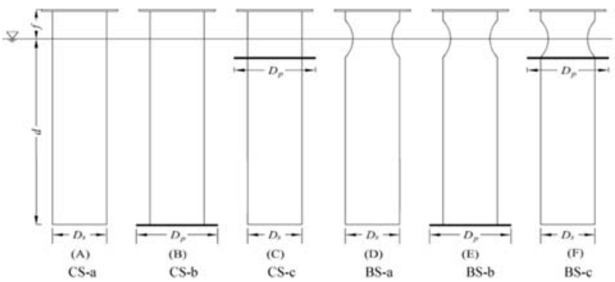

Figure 26: Experimental Setup

Wright et al (2022) proposed a novel method for the numerical–experimental fitting of non-constant drag damping to decay curves in still water, current and sinusoidal waves. The authors applied it to a moored advanced spar platform (Figure 27). The method involving a combined potential flow and Morison's equation model is used to calculate the drag coefficients and added mass from decay tests in still water, monochromatic sinusoidal waves and current flows. An inverse KC number drag coefficient relationship was observed for still water and wave cases. With increasing current flow velocity, the KC number drag coefficient tendency decays to a constant value equal to the steady state drag coefficient. A similar inverse KC number drag coefficient relationship is shown from the full-scale Fukushima FORWARD's floating substation. Discussions on the flow behaviour and recommendations on simulation techniques are given.

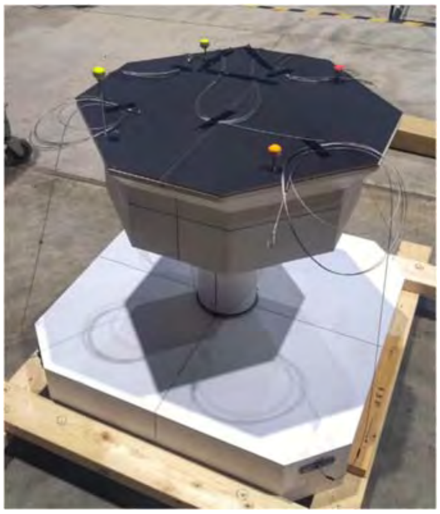

Figure 27: Advanced spar model

Parametric resonance is a phenomenon caused by time-varying changes in the parameters of a system which may result in undesirable motion responses and instability. Floating bodies like ships and spar buoys are prone to Mathieu instability mainly due to the instantaneous change of the metacentric height. With the fast-growing developments in Ocean Renewable Energy systems, spar buoys are commonly used for wave energy converters and floating wind turbines.

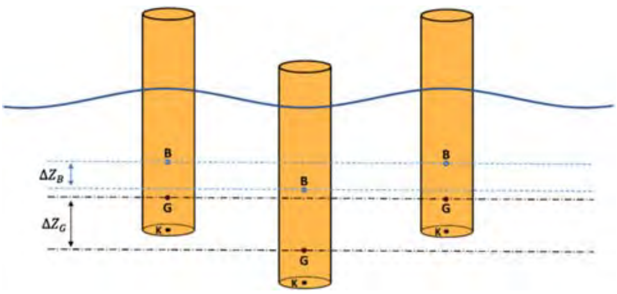

Figure 28: Vertical oscillations of center of buoyancy and center of gravity in heave motion

Undesirable, unstable motions resulting from the parametric resonance can be problematic as it may cause inefficiency in operations and structural risk integrity. Aziminia et al (2022) developed a new approach to investigate these nonlinear oscillations and analyse the conditions when parametric resonance occurs. The hydrodynamic loads are calculated using the linear approach, and the motion responses of the floating body coupled in heave, pitch and surge are determined (Figure 28). It is shown that the eigenvalues obtained from Floquet Theory can be used as indicators of stability under different wave conditions. This procedure can be practically used with little computational cost to determine factors affecting the equilibrium status of a system in regular waves.

Multi-body systems are becoming common in engineering practice, such as the catamaran float-over installation for a Spar platform, one of the most complex marine system designs (Figure 29). The gap resonance phenomenon occurs in the catamaran float-over system due to strong hydrodynamic interactions, inducing inaccuracy in evaluations of the hydrodynamic coefficients. To obtain reasonable hydrodynamic coefficients, Chen et al. (2023) first validated the damping lid method in AQWA, which provides viscous correction for the potential flow theory. Then, they applied it to the model in this study. It is found that the damping lid can deal with the gap resonance phenomenon. With the introduction of the damp lid method in the catamaran float-over system with $\alpha = 0.20$, the relative error between the frequency-domain and time-domain declined from 690% to 1.7%.

Based on the corrected frequency-domain results a time-domain model, considering various types of mechanical coupling components in the float-over system, including leg mating units (LMUs), deck support units (DSUs), steel-to-steel impacts on LMUs, lateral constrains of LMUs and DSUs, sway fenders, hawsers, and the mooring system. The first and last contact stages were simulated under different incident wave angles. It was observed that the relative motions in the quartering sea during the first contact stage are the largest. Furthermore, to reveal the coupling mechanism, different configurations of the barges and Spar are investigated for the first contact stage under irregular waves. It is found that the relative heave motions on the LMUs are larger when the deck and barges are rigidly connected to form a catamaran-barge.

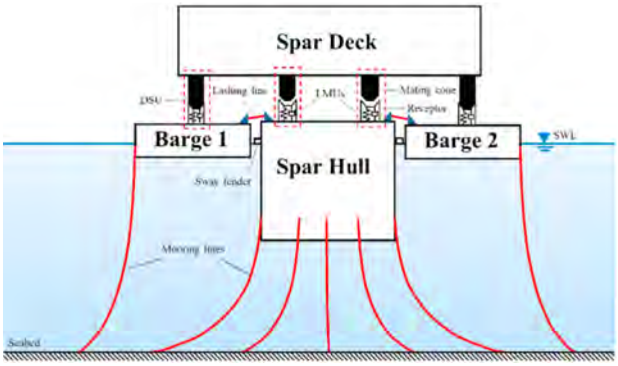

Figure 29: Front view of the catamaran float-over system

2.2.5 VLFS

Huang et al. (2023) predicted hydroelastic responses of a single module VLFS in extreme wave conditions using CFD-FEA coupling method. Freak waves, as a kind of strong nonlinear waves, have a great threat to the safety of Very Large Floating Structures (VLFS). Freak wave produces enormous wave height, which caused the hydroelastic responses on the VLFS to increase significantly. Nevertheless, due to the complexity of the highly nonlinear interactions between waves and VLFS, studies of wave-induced loads and the hydroelastic responses of VFLS in freak waves are rare. In this paper, a fluid-structure interaction technique that strongly connects the CFD and FEA solvers is proposed to evaluate the wave-induced loads and hydroelastic responses of a single module VLFS under freak wave circumstances. The result shows that the freak wave will lead to the global motion of VLFS being multiplied several times and largely increasing the instantaneous maximum vertical bending moment.

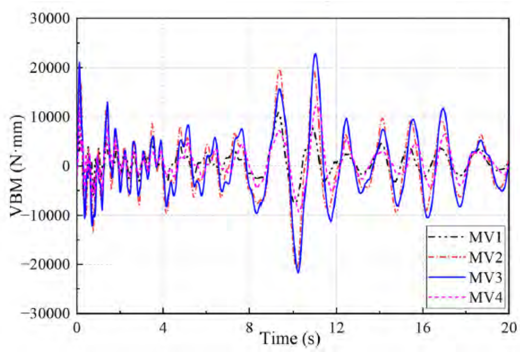

Figure 30: Time histories of VBM at different sections in freak waves

Yang et al. (2023) proposed boundary controller for floating beam system in irregular waves under one end pinned to reduce hydroelastic response. The structural stability is of great importance in research and development of VLFS. The structural stability is of great importance in research and development of VLFS. The vibration reduction on VLFS would not only prevent the structural fatigue but also improve the platform serviceability. Yang et al. investigate a boundary control method for a floating beam system with irregular waves in this paper. Through utilizing Lyapunov direct method, a boundary controller is proposed to reduce the hydroelastic response of the floating beam system restrained at its downstream end. The numerical simulation with experimental calibration is given to verify the effectiveness of the suggested control strategies on the floating beam system.

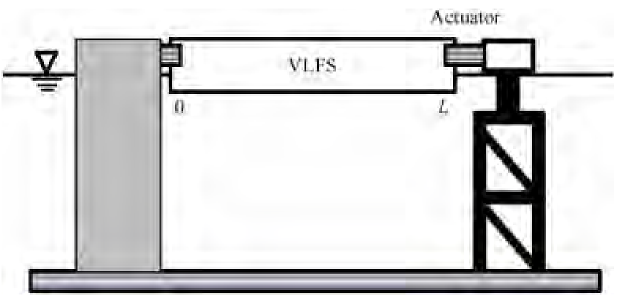

Figure 31: Very large-scale floating structure with one end pinned with mooring system

Jiang et al. (2023) reviewed advances in modeling hydrodynamics and hydroelasticity for very large floating structures. VLFSs have the potential to serve various functions such as maritime airports, logistic hubs, and even floating cities, thereby enhancing ocean utilization and management. This paper aims at providing a state-of-the-art review of the recent advancements and developments in the key technologies required for VLFSs, including a clear classification of their shapes, applications, connection systems, and mooring systems.

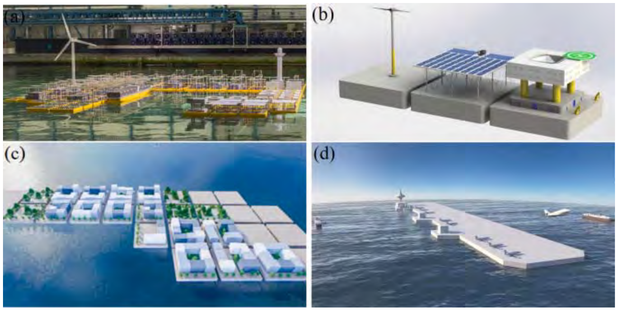

Figure 32: Examples of VLFSs for various applications: (a) logistics, (b) energy, (c) living, (d) others designed for specific tasks (the first three figures are from the Space@Sea project, and the fourth is adapted from the Mega-float) (Jiang et al., 2023)

Chen et. al. (2023) extended the discrete-module-finite-element (DMFE) method into the interconnected large floating flexible structures. DMFE method has been proposed and well-developed to analyze the hydroelasticity of floating flexible structures, in which the structure is discretized into several macro-submodules (for hydrodynamic analysis) and each of them is further discretized with finite element (for consideration of deformation). The DMFE method omits the determination of optimal modal combination, which is sometimes difficult for the mode superposition method in analyzing floating structures with complex geometric features and maintains greater computational efficiency over the direct method in analyzing floating structures with huge size. In this present paper, it is investigated in the framework of the DMFE method the hydroelasticity of interconnected floating structures.

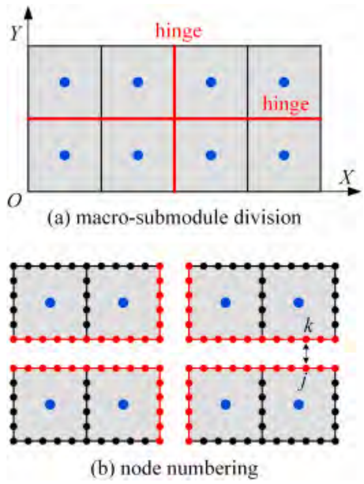

Figure 33: A schematic of a VLFS with two hinge connections. (a) Macrosubmodule division, a Y-axis-parallel hinge and a X-axis-parallel hinge; (b)reserved boundary nodes and lumped masses after elimination of inner nodes (Chen et. al., 2023)

Sakthivel et. Al. (2023) numerically investigated dynamic responses of serially connected truss pontoon-MOB. Very large floating structures (VLFS) are typically made up of several modules of offshore platforms, such as semi-submersibles, connected by mechanical connectors. The Truss Pontoon Mobile Offshore Base (TPMOB) is a new type of offshore platform based on the truss pontoon semi-submersible design. The design of the connectors is crucial for the functionality of the structure. The flexible connectors are modeled witha 3D source distribution method and the wave forces are estimated with 3D linear potential theory in this paper. The opensource finite element-based numerical model, HYDRAN-XR, is used to analyze the structural responses and connector forces in both regular and irregular wave conditions. The results indicate significant differences in responses between single and multi-module cases, especially in extreme waves. Loads on the connector change greatly for three- and five-module cases, with maximum values at specific wave angles.

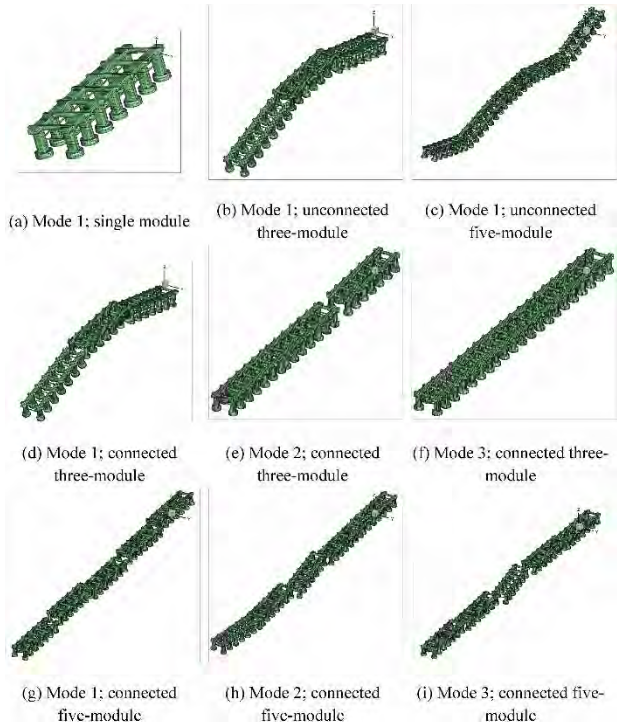

Figure 34: The dry mode shapes of a single module, multi-module are both unconnected and connected cases

Tay (2023) used Artificial neural network framework for prediction of hydroelastic response of very large floating structure. The response of a VLFS must take into consideration the elastic deformation of the structure (commonly termed hydroelastic response) under wave action. Conventionally, the hydroelastic response could be computed by using the coupled finite element-boundary element (FE-BE) method, where the mat-like structure is modelled using plate theory and the water modelled using the potential theory. To accelerate the computational time in predicting the hydroelastic response of the VLFS, a surrogate model trained using the feed-forward neural network is proposed in this paper. The hydroelastic responses under different wavelengths, structural stiffnesses and wave directions are first generated where these data are split into three groups for training, validation, and testing (prediction) purposes.

Huang et al. (2023) established a method to predict hydroelastic responses of a VLFS under waves and moving loads. A VLFS can be simplified as a multi-floating-body model connected by universal joints, and its elastic deformation can be reflected by the rotation of the joints. According to displacement and torsional angle equivalent of the elastic beam model and multi-floating-body model in static analysis, the equivalent rotation stiffness of universal joints can be determined. The proposed method is verified against the results obtained from relative references and 3D-hydroelasticity theory. Then, a VLFS under oblique regular waves and moving loads are further investigated.

Gusev et al. (2023) developed the numerical algorithms for shallow water models. The results are validated using potential flow model. A cutout in the body bottom increases the transmitted wave amplitude. The basin bottom irregularity has the most effect on the interaction when located directly under the body. The bottom protrusion located behind the structure may slightly decrease the wave force.

Liu et al. (2022) reports a novel hybrid modular floating structure (HMFS) system consisting of a certain number of outermost box-type modules and inner semi-sub modules. Semi-sub modules are connected with ball joints in both longitudinal and transverse directions. Box-type modules are connected with adjacent semi-sub modules with pitch hinges. Outermost box-type modules mainly function as wave energy converters (WECs) and breakwaters. Based on the rigid module and flexible connector (RMFC) method, the effects of different wave directions, longitudinal expansion, positions of modules and connectors on hydrodynamic responses of the HMFS system are emphatically investigated under typical sea conditions.

Rodrigues et al. (2022) presented an experience in designing and carrying out a model test campaign of a generic floating bridge. The tested model represents a truncated segment of a generic full straight bridge at a fjord crossing in Norway. Environmental conditions comprise combinations of regular and irregular waves, current and wind, including a spectral amplitude inhomogeneous condition realization. A novel approach for carrying out static pull-outs, decays, and inducing inhomogeneous wind conditions, is applied using winch actuators. A dataset of time series and selected video recordings is publicly shared for selected measurements and test runs. Recommendations for testing of floating bridges in a basin are given.

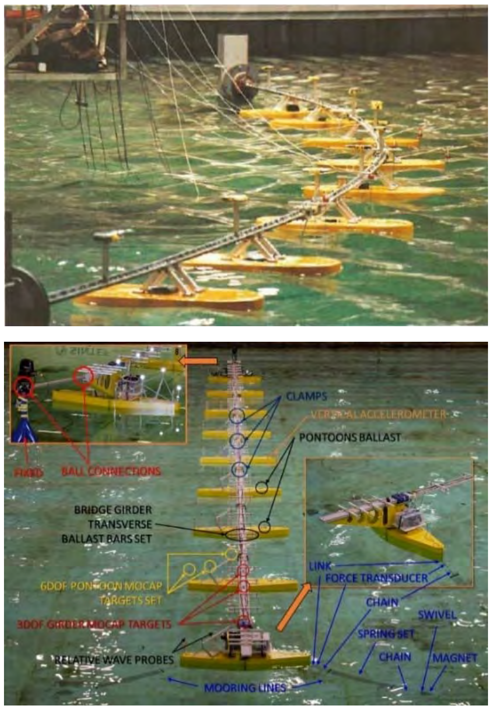

Figure 35 Hydroelastic bridge model and instrumentation (Rodrigues et al., 2022)

Zhang et al. (2022) proposed a cut-off scheme to model large arrays of modularized floating structures. The radiation interaction effects among multiple rectangular boxes are quantified. Some critical curves showing the optimal cut-off radius are depicted. Two cases are designed to examine the accuracy and efficiency of the proposed scheme.

Li et al. (2022) clarified hydrodynamic response of VLFS under typhoon-driven waves is clarified by numerical tank test. Jonswap spectral characteristic parameters could effectively simulate Typhoon Megi. An FMRC modeling method for VLFS satisfying longitudinal slope of airport runways is proposed. Mechanisms of energy conversion between Marine airport and environmental loads are revealed.

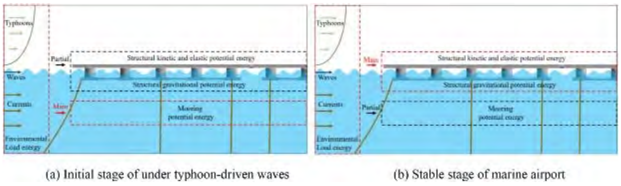

Figure 36 Energy transfer mechanisms of the marine airport under typhoon-driven waves (Li et al., 2022)

Zhang et al. (2022) reviewed an experimental and numerical investigations on continuous floating elastic structures with focus on models and methods. A new category of Very Flexible Floating Structures (VFFS) is introduced based on motion response characteristics. The applicability of hydroelastic theory to the newly envisaged VFFS is assessed.

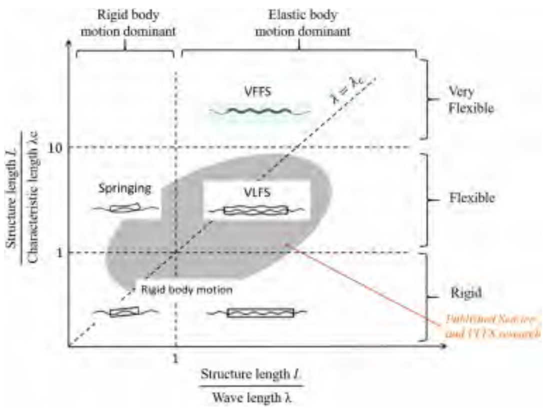

Figure 37 Mapping of global response of floating structures (Zhang et al., 2022)

Chen et al. (2022) constructed a numerical framework of one dimensional discrete-module-beam hydroelasticity method. Unsteady external excitations are categorized and corresponding dealing procedures are regulated. A hybrid integration-interpolation method is developed to calculate structural force response of a VLFS in time domain. Motion and internal force/moment responses of a VLFS in four engineering scenarios are given.

Sakthivel et al. (2022) investigated A novel-Truss Pontoon Mobile Offshore Base (TP-MOB) VLFS experimentally under regular wave conditions for different heading angles. Details of the fabrication of the 1:150 scaled model are presented. Responses of the model, namely vertical displacement besides roll and pitch motion are measured by sensors at three locations. Response Amplitude Operators (RAOs) are obtained, and these plots show the characteristic diminishing peaks of the elastic body responses within the wave excitation range, unlike the case of a barge. Results ascertained that the frequency response curve obtained is consistent with existing literature.

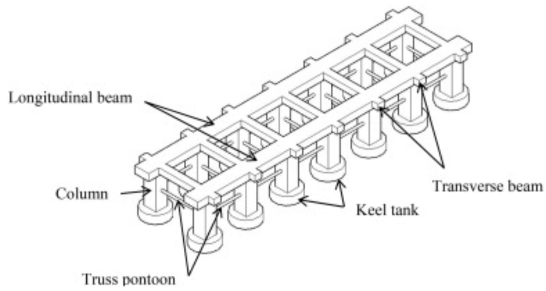

Figure 38 A schematic representation of TP-MOB in isometric view (Sakthivel et al., 2022)

Xu et al. (2022) analyzes nonlinear model for strong hydro-elastics of very large floating structures. The floating structure is modeled as a nonlinear Euler Bernoulli–von Kármán (EBVK) beam coupling with water beneath. A multi-time-scale perturbation method leads to hierarchic partial differential equations by introducing the wave steepness squared as the perturbation. Pontoon structures and LPOFPV are studied and compared.

Figure 39 Large-scale polymer offshore floating structure for photovoltaics (Xu et al., 2022)

Iijima et al. (2022) measured the waves propagating along a long thin plate floating at the water surface using digital image correlation (DIC) method. The effectiveness of the measurement by the DIC is shown. The tank test model is made of closed cell rubber foam. The material properties are measured by a static four-point-bending test and vibration test. The uncertanty with respect to the material properties is discussed. The measured results are compared with numerical simulation results based on linear potential theory. The overall agreement is found good in terms of wave length, response amplitude, and distribution. Nonlinearity of deflection waves on the floating plate, which is similar in some point to Stokes wave is identified for the first time by measurement.

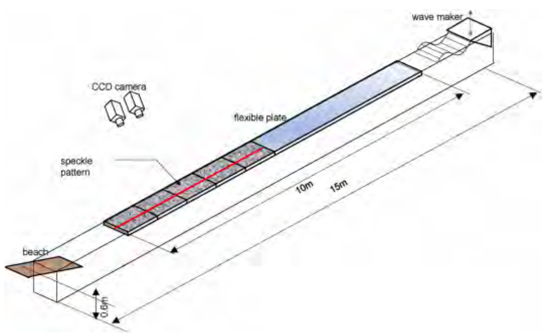

Figure 40 Schematic of a long thin plate model (Iijima et al., 2022)

Wang (2022) Performance of closed-form RAO solutions for Modular floating structures (MFS) benchmarked against smoothed particle hydrodynamics. Heave and roll damping ratio of 0.1 recommended for conservative assessment of MFS. Building slenderness and building/pontoon mass ratio on human comfort explored. Analytical procedure enables the preliminary design of MFS prior to CFD modeling.

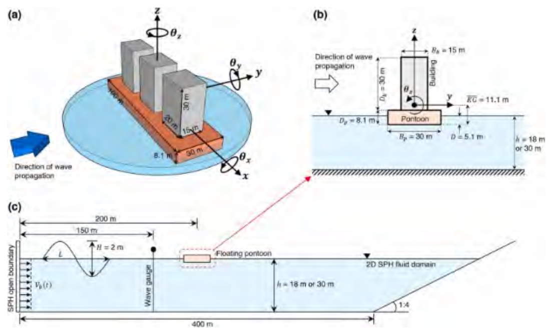

Figure 41 Module9000 MFS model for dynamic analysis (Wang, 2022)

Jiang et al. (2021) evaluated various structural systems for concrete floating modules and developed optimal structural solutions of modular units for engineering practice. Hydroelastic responses of VLFS with the hybrid BEM – FEM code are investigated. Preferable geometrical shapes and connection properties for VLFS are explored.

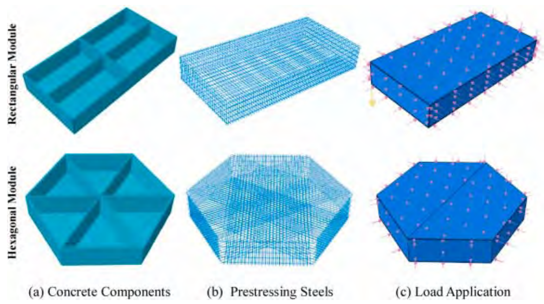

Figure 42 Finite element models of different floating modules (Jiang et al., 2021)

2.2.6 Other stationary floating structures

According to the IGU World LNG report (2022 edition), the global LNG fleet is relatively young due to the rapid increase in LNG trade over the past two decades. In other words, vessels under 20 years of age make up 90% of the active fleet with newer vessels. And in 2022, a total of 45 FSRUs make up 7% of the active global LNG fleet. It is necessary to study the hydrodynamic characteristics of the floating structure such as FLNG and FSRU for LNG utilization is continuously needed.

Figure 43: Global active LNG fleet and orderbook by delivery year and average capacity, 1991-2026

Kang et al. (2022) carried out a study focusing to develop and verify a one-side spread mooring system, an alternative spread mooring system to be applied to FLNG operated in West Africa. The mooring line analysis utilized various numerical analyses (Ariane8, OrcaFlex, WADAM, SIMA) in accordance with the ABS position mooring rules. The one-side mooring system was satisfied with ULS(Ultimate Limit State) and ALS (Accidental Limit State) requirements of ABS design criteria. Also, design offsets for both intact and damaged mooring condition were within the offset limit. The operability of side-by-side offloading was more than 99%, and thus safe offloading was expected during almost life time.

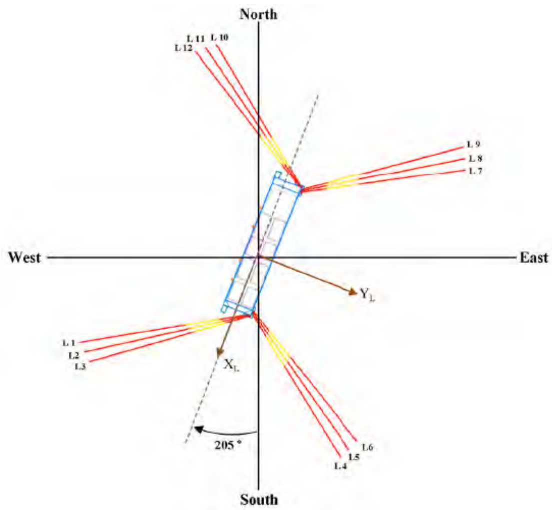

Figure 44: One-side mooring arrangement

Jung et al. (2022) presented the hydrodynamic characteristics of a rectangular structure that wave excitation force, damping coefficients, and 3-DOF motion response were experimentally studied in various wave and water depth conditions in a 2-D wave tank. The rectangular structure was installed in fixed and soft spring moored conditions in beam sea condition, and the experiment was performed in regular wave conditions of the range of wave period with varying the ratio of the water depths and draft. And the results were validated and compared to the simulations (HydroStar) based on potential theory. The results showed trends of added mass and damping coefficients getting larger at shallower water depth and emphasized that the water depth to draft ratio was less than 2.0. And, they suggested that viscous damping effect should be considered to find RAOs of roll and heave motions at less than 2.0 of the water depth to draft ratio.

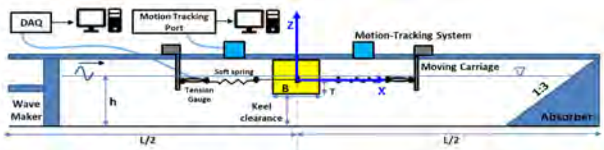

Figure 45: Experimental schematics of fixed structure in 2D wave tank

Nwafor J.C. (2022) carried out the nonlinear coupling of the gap resonance and the hydrodynamics of FLNG and LNG carrier in proximity for the offloading operation in side-by-side configuration was investigated numerically. The numerical analysis was conducted to understand how the variation in loading conditions and environmental factors affect the side-by-side offloading operation. The numerical results demonstrated that the LNG carrier had a larger vessel motion compared to the FLNG and the bow and aft lines were affected by relative sway while the spring lines were affected by surge, hence further improvements on the optimal hawser line arrangement needed to be further investigated for different loading conditions.

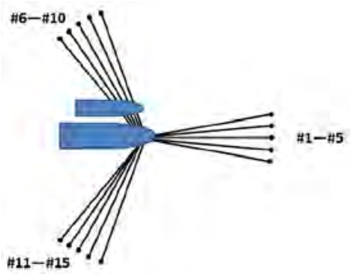

Figure 46: General arrangement of mooring system

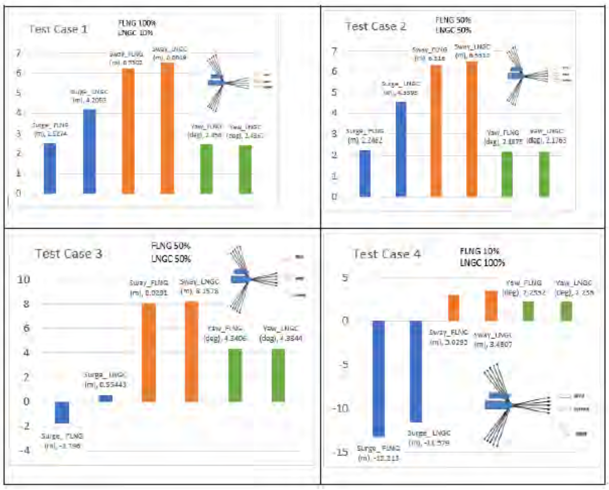

Figure 47: Comparison of Low frequency motion for FLNG and LNGC

Qi et al. (2021) conducted experiments to investigate the hydrodynamic performance of singly-moored FSRU and side-by-side moored FSRU-LNGC and assess the security of the quay-mooring system. The model tests were mainly divided into two parts including a quay-moored test of a single FSRU and a test of FSRU and LNG carrier moored side by side to the quay.

Figure 48: Model-set up for the quay mooring system (Whole system)

In singly-moored FSRU case, the loads of mooring lines and fenders (mooring system) were sensitvie to the wave direction and all the maximum loads on the mooring system was less than the break strength. However, during the test of FSRU and LNGC moored side by side condition, under all the beam sea condition, motions of the LNG carrier was larger than FSRU and the largest tension acting on the mooring line was larger than its break strength. Therefore, it was necessary to improve performance of the mooring system or to stop the operation work under worse sea conditions.

Rudan et al. (2021) presented the methodology for direct analysis of the mooring system of LNG carrier using finite element method. First, rule-based calculations were made first to obtain the properties of the mooring lines and fenders. Numerical analysis based on potential theory was conducted to solve the hydrodynamic coefficients such as added mass, damping, etc. Based on those results, commercial software (LS-Dyna) and numerical code (MCOL) used to perform the analysis of non-linear problem with the suggestion of a spring fender to simulate a rubber fender effect. The spring fender model could reduce the computing time, but its results differed from the analysis of rubber fender model. Forces along the ropes of the spring fender model were resulted into somewhat higher values than those of the rubber fender model. It showed that 'MCOL' could be useful tool for assessing ship hydrodynamic response in real time, within the highly non-linear explicit dynamics analysis. However, it was unstable in long-term simulations due to underlying theory was not coded correctly.

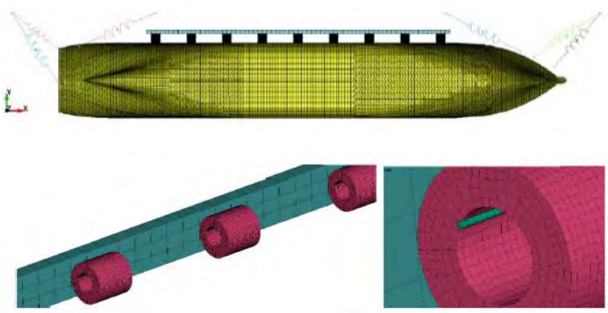

Figure 49: Moored ship and fenders FEM models

Shen et al. (2020) gave the results of a numerical study based on three-dimensional frequency domain potential flow theory of the effects of different spacings and different draft (different loading) on the resonance of the intermediate water body. During the ship to ship operation system of FSRU and LNG under the head sea condition, the value of the maximum resonance wave elevation, significantly, decreased with the increasing of the distance between the two ships, and the wave period corresponding to the maximum resonance wave elevation increased. In beam sea consition, the maximum resonance wave elevation increased with the increasing of the distance between the two ships, and the wave period corresponding to the maximum resonance wave elevation increased with the increasing of the distance between ships.

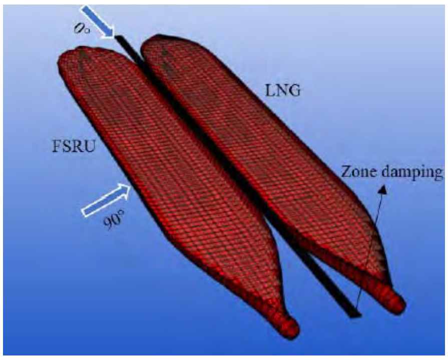

Figure 50: Ship to ship operation

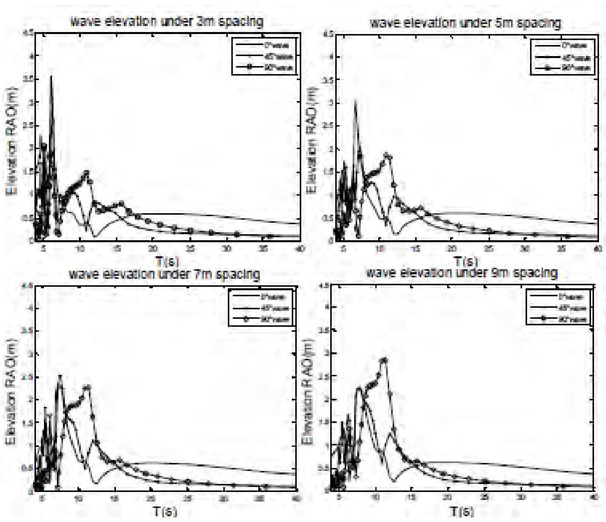

Figure 51: Wave surface elevation at different intervals

Teng et al. (2022) presented the hydrodynamic characteristics of floating structures using rectangular floating barge by numerical methods. Numerical analysis of the hydrodynamic coefficient and motion response of the barge were carried out using commercial software (WAMIT and STAR-CCM+). The six-water depth and three-bathymetry conditions were used in numerical analysis. From this study, the hydrodynamic coefficients such as the added mass, viscous damping, and current drag coefficients were found to be significantly affected by changes in shallower water depth. In addition, it was confirmed that both added mass and viscous drag coefficients were further increased at the steeper bottom slope when the water depth reduced.

2.3 Dynamically Positioned Floating Structures

Dynamic positioning (DP) is a computer-controlled system to automatically maintain the position of floating structures and heading by using its own propellers and thrusters. Position reference sensors, combined with wind sensors, motion sensors and gyrocompasses, provide information to the computer pertaining to the position of floating structure and the magnitude and direction of environmental forces affecting its position.

The computer program contains a mathematical model of the floating structure that includes information pertaining to the wind and current drag of the floating structure and the location of the thrusters. This knowledge, combined with the sensor information, allows the computer to calculate the required steering angle and thruster output for each thruster. This allows operations at sea where mooring or anchoring is not feasible due to deep water, congestion on the sea bottom (pipelines, templates) or other problems. Some of the most relevant recent works are described as follows:

Zhang et al. (2020) presented a novel robust neural event-triggered control algorithm to achieve the dynamic positioning operation of marine surface ships in the presence of actuator faults. In the algorithm, the model uncertainty and the "explosion of complexity" were addressed by fusion of the robust neural damping and dynamic surface control techniques. The gain related adaptive law was constructed to compensate the gain uncertainties and the unknown actuator faults, which improved the stability of the ship dynamic loop system. Furthermore, the event-triggered mechanism was introduced to reduce the communication load between the controller and actuator. For merits of the aforementioned design, the proposed algorithm was with the advantages of concise form and easy to be implemented in practical ocean engineering. Based on the Lyapunov theory, rigorous analysis was proved to guarantee the semi-global uniform ultimate boundedness (SGUUB) of the closed-loop system.

Conventional dynamic positioning (DP) systems on larger ships compensate primarily for slowly time-varying environmental forces. In doing so, Halvorsen et al. (2020) used wave filtering to prevent the DP from compensating for the first-order wave motions. This reduced wear and tear of the thruster and machinery systems. The overall control system architecture can be seen in Figure 52. In the case of smaller autonomous vessels, the oscillatory motion of the vessel in waves may be more significant, and the thrusters can be more dynamic. This motivated the use of DP to compensate for horizontal wave motions in certain operations. They studied the design of DP control and filtering algorithms that employ acceleration feedback, roll damping, wave motion prediction, and optimal tuning. Six control strategies were compared in the case study, which was a small autonomous surface vessel where the critical mode of operation was launch and recovery of an ROV through the wave zone.

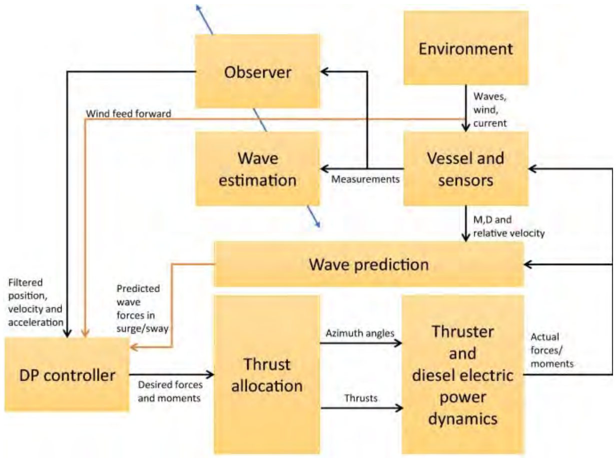

Figure 52: Block diagram of the control architecture. (Orange arrows are feed-forward terms and blue arrow indicates adapting gains.)

In Hosseinnajad et al. (2020), a new control system was proposed for dynamic positioning (DP) of marine vessels with unknown dynamics and subjected to external disturbances. The control system was composed of a substructure for wave filtering and state estimation together with a nonlinear PD-type controller. For wave filtering and state estimation, a cascade combination of a modified notch filter and an estimation stage was considered. In estimation stage, a modified extended-state observer (ESO) was proposed to estimate vessel velocities and unknown dynamics. The main advantage of the proposed method is its robustness to model uncertainties and external disturbances and it does not require prior knowledge of vessel model parameters. Besides, the stability of the cascade structure was analyzed and input to state stability (ISS) was guaranteed. Later on, a nonlinear PD-type controller with feedforward of filtered estimated dynamics was utilized. Detailed stability analyses were presented for the closed-loop DP control system and global uniform ultimate boundedness was proved using large scale systems method.

Martelli et al. (2020) aimed to present a novel approach to design a dynamic positioning system by using a dynamic model based-design approach. The proposed study has been performed to both develop and preliminarily test the control logic that should be implemented on a model scale vessel. Indeed, the proposed tool has been designed for a fully actuated tug vessel equipped with two azimuthal thrusters and one bow-thruster, emulated in behaviour with a dynamic simulator. Thanks to the model actuation, it was possible to design a unique, optimised allocation logic able to fulfil both open-loop and closed-loop commands, sufficiently proved and tuned before the installation onboard. Moreover, a thorough comparison between different design methods, static and dynamic performance evaluation has been carried out. Figure 53 shows the difference between a standard DP capability polar plot and the one obtained with the dynamic analysis. Two different operational modes were tested, and the results were presented: joystick and station keeping.

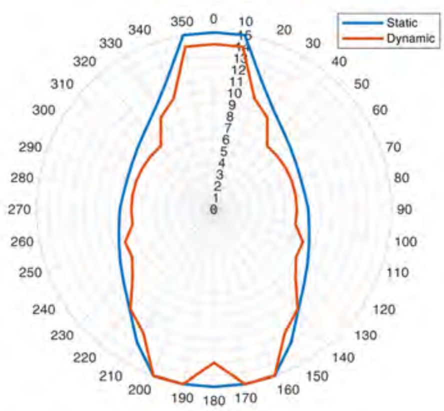

Figure 53: Comparison between static and "dynamic" DP capability plot.

It is possible to perform combined analysis of station keeping and seakeeping problems, determining seakeeping criteria for dynamic positioning (DP) due to ship motions, and use it as effective limiting environmental criteria for capability plots. In any case, even though seakeeping operational criteria are probably more restrictive than DP ones, it can be useful to investigate the effective operability of the DP system. For this purpose, Mauro et al. (2020) developed an enhanced and innovative procedure to establish the effective DP operability of an offshore vessel, by explicitly considering the vessel geographic operational area. The procedure has been tested on a pipe-lay vessel (PLV), as shown in Figure 54, and compared with the standard DP calculations, considering all the possible failures requested by regulations. Differences obtained from the comparison are significant and constitute a matter for further discussions.

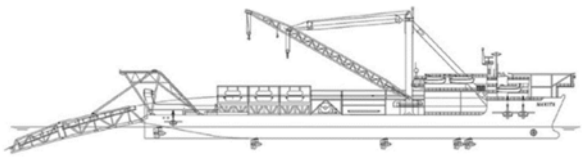

Figure 54: Generic PLV used as reference ship for the study.

It is nontrivial to tune the control parameters, and the station-keeping performance varies with environmental or loading conditions since the dynamics of the vessel were essentially nonlinear. In Xu et al. (2020), a fuzzy rule-based PID controller was evaluated, which took the estimated positioning error and low-frequency velocity as inputs, and outputs the time-varying PD control coefficients through fuzzy inference, while the integral control parameters were kept constant. The performance of the proposed controller was evaluated numerically through a time domain simulation of a dynamically positioned semi-submersible platform operating in variable environmental disturbances. Simulation results were compared with the conventional fixed gain PID controller, and the comparison results show that the proposed fuzzy PID controller can automatically tune the PD control coefficients according to the positioning accuracy and significantly improve the performance of the dynamic positioning system.

When considering the characteristics of a dynamic positioning (DP) vessel involving uncertain modelling and unknown disturbances, the vessel control problem becomes a mismatched nonlinear control issue. To resolve this issue, Hu et al. (2021)proposed a control method based on the sliding mode control (SMC) and the uncertainty and disturbance estimator (UDE). The total disturbance in the DP vessel was determined using the UDE, whereas the trajectory tracking function of the vessel was achieved via SMC. The effectiveness of the proposed control strategy was verified via simulations. The control system for the DP vessel is presented in Figure 55.

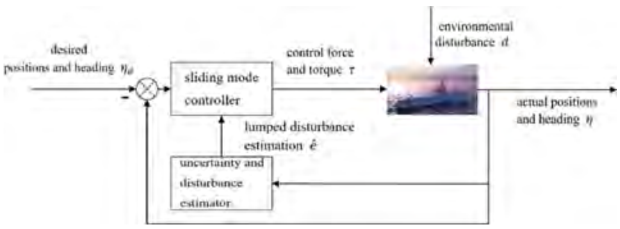

Figure 55: Schematic of the vessel tracking control system

In Liang et al. (2021), a robust adaptive neural networks control based on minimal–parameter-learning (MLP) was proposed for dynamic positioning (DP) of ships with unknown saturation, time delay, external disturbance and dynamic uncertainties. Through the velocities backstepping method, radial basis function (RBF) neural networks and robust adaptive control were incorporated to design a novel controller of which an appropriate Lyapunov-Krasovskii Function (LKF) was constructed to overcome the effect caused by time-delay. In additional, a robust adaptive compensate term was introduced to estimate the bound of the lumped disturbance including the unknown saturation, unknown external disturbance and the approximate error of neural networks control while the robustness of MLP was improved and the unknown saturation was compensated. The developed control law made the DP closed-loop system be uniformly ultimately stable which can be proved strictly through Lyapunov theory.

Zhang et al. (2021) presented a novel event-triggered cooperative dynamic positioning control algorithm for multiple marine surface ships in the presence of actuator faults. In this algorithm, the undirected interaction topology was employed to construct the communication networks among marine surface ships, and the assumption that the information of leader can be available to all followers was relaxed successfully. To avoid the unnecessary information transmission among ships, the event-triggered mechanism was incorporated in control design. And the strict positive lower bound on interevent interval was proved, which indicated no accumulation of triggering instants. Only two adaptive parameters were designed to estimate the actuator fault parameters online, they were updated when the event-triggered condition was violated and held otherwise. Considerable effort was made to guarantee the semi-global uniform ultimate bounded (SGUUB) stability by the extension of Lyapunov approach. Finally, numerical simulations were provided to verify the effectiveness and feasibility of the proposed algorithm. Under the interaction topology in Figure 56, the formation trajectories are shown in Figure 57 for three DP ships.

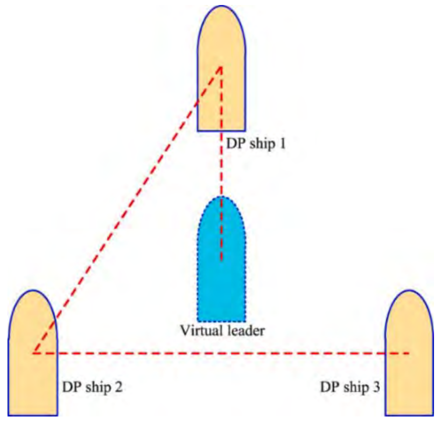

Figure 56: Interaction topology diagram among ships

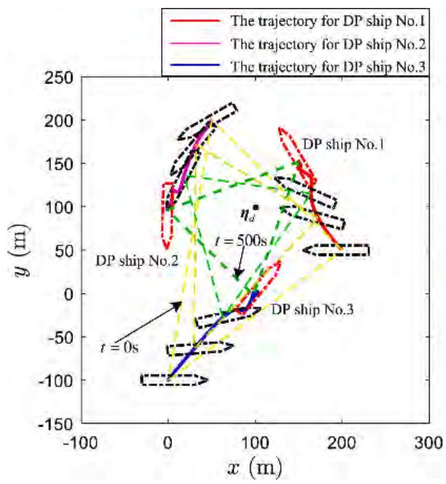

Figure 57: The formation trajectories for DP ships

Wang et al. (2021) investigated the trajectory tracking control problem of dynamic positioning ship subject to modeling uncertainties, environment disturbances, and unmeasurable velocity. A high-gain observer was constructed to estimate the unmeasurable velocity vector. Then, a special finite-time performance function was introduced to impose performance specifications in advance on the output tracking errors according to the mission requirements. Subsequently, through introducing error transformation functions, the tracking control problem with guaranteed transient performance was transformed to the output constrained control problem. In view of this, an asymmetric barrier Lyapunov function was designed to ensure that the transformed errors remain within specified ranges. By virtue of Lyapunov theory, it was shown that all the closed-loop signals were uniformly ultimately bounded and the tracking errors strictly comply with the prescribed performance envelops, despite the presence of modeling uncertainties, environmental disturbances and unmeasurable velocity. The simulation results of proposed controller are provided in Figure 58.

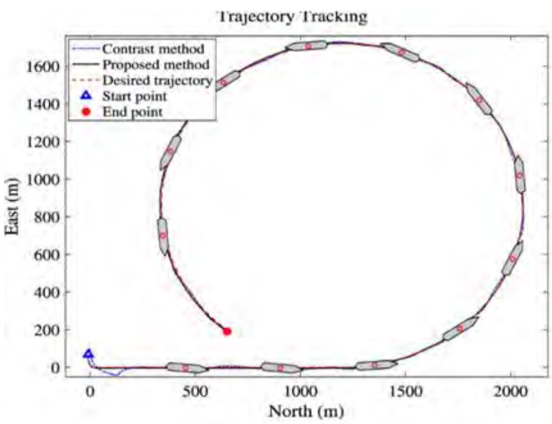

Figure 58: Time response of the trajectory tracking with proposed method and contrast method

A Dynamic Positioning (DP) system enables vessels and rigs to accurately maintain a predetermined position and heading or track, the role of the DP operator (DPO) was considered to monitor and keep the vessel in position. In Hogenboom et al. (2021), Applied cognitive task analysis (ACTA) was performed to analyze how the different operational settings influence the role and decision-making of the DPO. Recommendations for the improvement of safety, the design of the DP system, training and set-up of DP operations were formulated in this research.

In the “DP in Ice” Project, the authors conducted two extensive physical model test programs to generate a dataset on the managed ice- DP vessel interactions. One of the ice basin testing objectives was to generate a comprehensive dataset on the effects of managed ice-field characteristics on the thruster forces and moment encountered by DP-controlled vessels. The test case consisted of a vessel moving through a field of ice floes and brash ice, as shown in Figure 59. The test programs were executed at the ice basin of the NRC-OCRE using a non-proprietary DP system installed on two model vessels and a suite of sensors to acquire a dataset of ice-field and DP vessel interactions in various managed ice conditions. A series of physical modelling programs formed the basis of the empirical and numerical models developed in the “DP in Ice” program. Further details of the two test programs can be found in Islam et al. (2016), Wang et al. (2016), Islam et al. (2018), Islam et al. (2021), Islam et al. (2021a), Islam et al. (2022) and Islam et al. (2022a).

Figure 59: View of the ice basin and the model DP vessel

Islam et al. (2022) presented the methodologies and validations of a novel numerical model based on empirical-statistical techniques for predicting dynamically positioned (DP) vessels and ice-field interactions. The workflow for the development of the model is outlined in Figure 60. The authors developed multiple regression models for predicting the time-averaged and average peaks of thruster forces and yawing moment of the DP vessel due to managed ice actions. The model showed reasonable accuracy in predicting the effects of several ice-field parameters on the forces and moments of two DP-controlled vessels. Subsequently, integration of the model into a DP-in-ice validation platform was offered, which can simulate and optimize the performance of a DP-controlled vessel in ice-infested water.

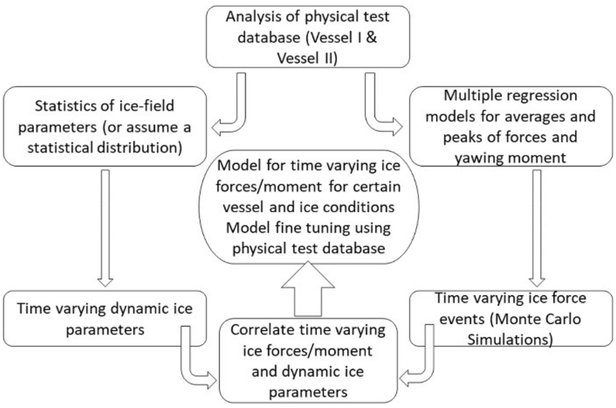

Figure 60: Flow chart of empirical-statistical modelling technique

Islam et al. (2022a) presented the tools, techniques and outcomes of a model testing program of a dynamically positioned (DP) Ice-1A classed Anchor Handling Tug Supply (AHTS) vessel called the “Magne Viking” in different managed ice environments. A total of 168 test runs were carried out in 7 ice sheets to evaluate the vessel's thruster forces and moment on the horizontal plane and the vessel's 6-DOF motions and accelerations. The time series and probability of exceedance plots of thruster forces and yawing moments were presented, along with the vessel's positioning relative to a set-point in various managed ice conditions. Overall, the study demonstrated the capability of the DP-controlled ship to maintain the station for most head-on tests and the oblique ice tests not exceeding 15°.

Li et al. (2022) presented a dedicated robust adaptive neural network control (RANNC) scheme for dynamic positioning (DP) of marine vessels with a prescribed performance under model uncertainties, external disturbances and input saturation. The command filter, RBFNN, auxiliary dynamic system (ADS), adaptive control and minimal learning parameter technique were adopted to design the RANNC scheme and guarantee the transient performance of DP vessel, as shown in Figure 61. The RANNC scheme was developed with the backstepping technique, and the method of command filter was introduced to avoid the “dimension disaster” problem. Moreover, minimal learning parameter technique was introduced to minimize the computational burden triggered by weight update of neural networks. Finally, comparison simulation results were provided to illustrate the performance of the proposed RANNC scheme.

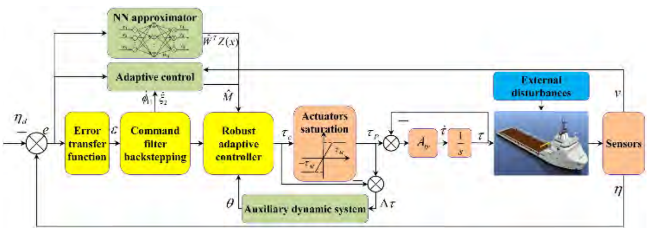

Figure 61: Control scheme of RANNC

Gustavo et al. (2022) discussed the application of the motions of a dynamically positioned platform supply vessel to perform inferences by means of a Bayesian method. The method was formulated considering a methodology for hyperparameter calibration based on an optimization process, and the definition of an iterative estimation scheme. Small-scale seakeeping tests in irregular waves were carried out with the model of a platform supply vessel (PSV) equipped with a dynamic positioning (DP) system, which was calibrated to be consistent with a typical real system. For evaluating any possible influence the DP responses might have had on the motion-based wave estimations, the same test conditions were also performed with the model moored by means of an equivalent soft-mooring configuration. Estimation results were obtained from the motions measured in the experiments, showing that wave parameters could be computed with good precision in both arrangements.

(Li 2022a) investigated the prescribed performance trajectory tracking control problem for dynamic positioning vessels in the presence of velocity constraints and thruster faults. By using a structurally simple error transformation, the issue of guaranteeing prescribed transient and steady state tracking performance was converted to a general state-constraint problem, which together with the velocity constraints form a trajectory tracking control problem with full-state constraint. Neural network and adaptive techniques were incorporated to construct a fault-tolerant trajectory tracking controller, which can not only estimate thruster faults, but also provide better robustness against model uncertainties and external disturbance. Finally, tracking control task for dynamic positioning systems was carried out to illustrate the merits of the proposed method. The simulation results are presented in Figure 62.

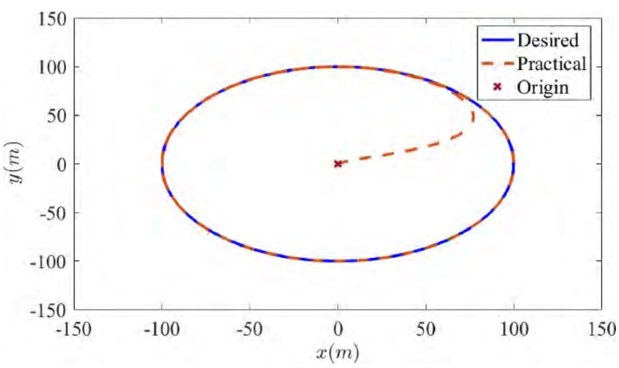

Figure 62: Simulation results of tracking the desired trajectory

Li et al. (2022b) studied the trajectory tracking control method for dynamic positioning vessels with state constraints and parameter uncertainties. A composite learning method was introduced to identify unknown parameters online. The structure of the control system was depicted in Figure 63. Regressor filtering together with dynamic regressor extension and mixing procedure were combined not only to relax the dependence of parameter estimation convergence process on the persistent excitation condition, but also to ensure the independence and flexibility of each parameter. Subsequently, a finite-time composite learning controller was designed based on asymmetric integral barrier Lyapunov functions, which guaranteed the asymmetric constraints on vessel states.

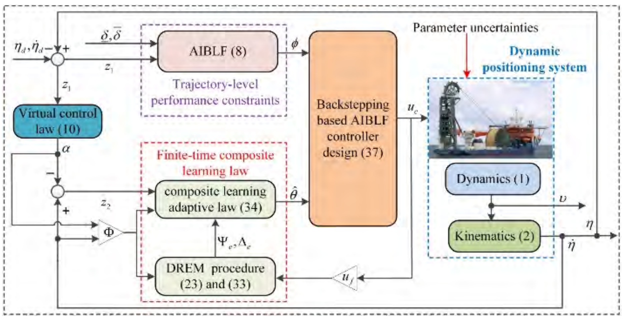

Figure 63: Block diagram of the control system

Martelli et al. (2022) presented the procedure for designing a Dynamic Positioning system and evaluating its performance using a dynamic approach. The proposed Time-domain Dynamic Positioning Capability Plots were obtained by a model-based design approach using a ship's dynamic simulator. The dynamic simulator was based on a fully actuated testing model. Indeed, the proposed tool has been designed on a tug vessel equipped with two azimuth thrusters and one bow-thruster. In particular, two force allocation logics for the station keeping manoeuvres have been developed; one is an optimised thrust allocation logic, the other is obtained with the primary goal to reduce as much as possible azimuth thrusters rotation. In Figure 64, the schematic system's view was reported. Eventually, the comparison between static capability plots and the capability plots obtained by several dynamic simulations has been provided, presented, and discussed.

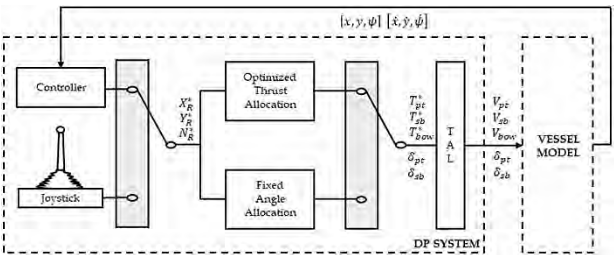

Figure 64: Dynamic positioning system structure

In Mauro et al. (2022), using known wind–waves joint distributions for the long-term environmental conditions further improved the scatter diagram approach, assessing the operability of a Dynamic Positioning system through a Quasi-Monte Carlo sampling of the joint distribution. Analysing the results of the Quasi-Monte Carlo process, it was possible to obtain a site-specific capability plot. The application of this novel method in the case of quasi-static calculations both to a reference supply vessel and a pipe-lay vessel showed the flexibility of the proposed approach for site-specific Dynamic Positioning capability predictions.

In Gopmandal et al. (2022), the ship dynamics with hydrodynamic parameter uncertainties was represented in an uncertain state-space descriptor form. Then, the design of feedback gains of 2-DOF PID controller for the uncertain descriptor plant was converted into a state feedback design for an augmented uncertain descriptor plant. the 2-DOF MIMO PID controller to be used was shown in Figure 65. Next, a linear matrix inequality-based condition was obtained to solve this state feedback problem in order to ensure a desired linear quadratic (LQ) performance, even in presence of uncertainties. Finally, to further improve the tracking performance, the feedforward gain of the 2-DOF PID controller was designed using H∞ approach. The DP performance of the proposed controller was tested for the considered ship model along with uncertainties, actuator constraints, and environmental disturbances. A comparison with the existing PID controllers was also carried out to show superiority of the proposed controller.

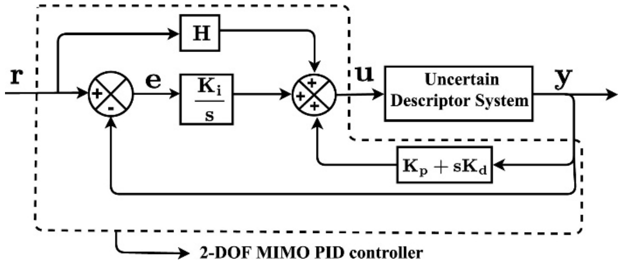

Figure 65: Feedback interconnection of the proposed controller and uncertain plant

Tang et al. (2022) proposed a robust control approach based on nonlinear model predictive control (NMPC) for dynamic positioning (DP) ships. An improved nonlinear disturbance observer (INDO) based on super-twisting control was constructed for disturbances estimation and attenuation. Furthermore, the NMPC optimization problem was formulated to reject the disturbances by combining the disturbance estimates into the prediction model. In light of this, a detailed time-iteration NMPC algorithm for DP ships was presented. Numerical simulations based on the INDO-based NMPC (INDO-NMPC) strategy under the scenario of trajectory tracking were performed to explore the robustness of DP system. Control architecture of DP system was given in Figure 66. Theoretical analysis and simulation results well proved the effectiveness and superiority of the proposed control law.

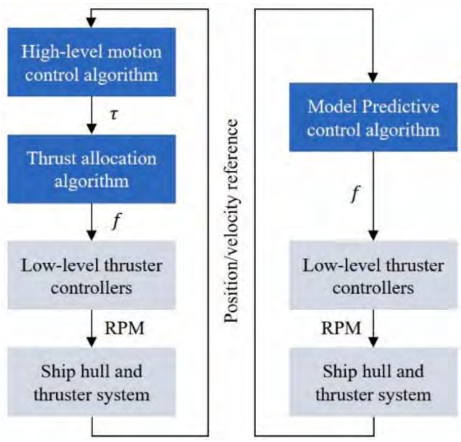

Figure 66: Control architecture of DP system (Left: INDO-NMPC-TA, Right: INDO-NMPC)

In order to establish the maximum environmental conditions in which a DP vessel can maintain its position and heading for a proposed thruster configuration, a DP capability analysis (DPCAP) must be carried out. The most crucial step in a DPCAP was to estimate the environmental loads due to the wind, current and waves in an accurate, consistent and efficient manner. In Aydin et al. (2022), semi-empirical methods and a RANS based analysis tool were compared in order to determine the reliability of such approaches for the purpose of early assessment of wind, wave and current loads. The main focus of this approach was to cross validate the semi-empirical and CFD based procedures so that the initial rough estimates on the loads could be refined accurately as well as to provide a comprehensive example of a reference work for the literature. Typical DP capability polar plots for an offshore supply vessel were presented to illustrate the application of the computational analysis procedure.

DNVGL-ST-111(DNVGL2021) Assessment of Station Keeping Capability of Dynamic Positioning Vessels, defines clear and consistent methodical requirements for DP station-keeping capability assessments. The standard also set requirements for the documentation of the calculations and for the presentation and verifiability of the results. It defined three different DP capability levels based on the Beaufort environmental scale, each requiring a specific assessment method. DP capability plots shall be generated for each level, and the result of the assessment was expressed as a DP capability number. In addition, the standard defined two DP capability assessment levels that allowed the inclusion of site-specific environmental data and external forces: Level 2-Site and Level 3-Site. The results of the site-specific analyses were presented by plots indicating the relevant wind speed limits for the given conditions.

3. REVIEW OF THE EXISTING PROCEDURES

The Committee reviewed and updated the following procedures and guidelines:

- 7.5-02-07-01.1 Laboratory Modelling of Multidirectional Irregular Wave Spectra;
- 7.5-02-07-01.2 Laboratory Modelling of Waves;
- 7.5-02-07-01.4 Confidence Intervals for Significant Wave;
- 7.5-02-07-01.5 Laboratory Modelling of Wind;
- 7.5-02-07-01.6 Laboratory Modelling of Currents;
- 7.5-02-07-03.1 Floating Offshore Platform Experiments;
- 7.5-02-07-03.2 Analysis Procedure for Model Tests in Regular Waves;
- 7.5-02-07-03.5 Passive Hybrid Model Tests of Floating Offshore Structures with Mooring Lines;
- 7.5-02-07-03.6 Dynamic Positioning System Model Test Experiments;
- 7.5-02-07-03.10 Guideline for VIV Testing;
- 7.5-02-07-03.11 Guideline for model tests of stationary multi-bodies operating in close proximity;
- 7.5-02-07-03.13 Guideline for VIM Testing;
- 7.5-02-07-03.14 Analysis Procedure of Model Tests in Irregular Waves.

- 7.5-02-07-03.16 Model Construction of Offshore Systems.

The objective of the review was to update the procedures/guidelines according to the current practices, and to provide references to understand and implement the techniques.

4. REVIEW AND IDENTIFY AREAS OF CONCERN IN MODELLING AND SIMULATION OF WAVES, WIND AND CURRENTS

4.1 Extreme Waves

The main objectives are: 1) to report the main recent literature findings regarding the methods to generate extreme wave packets for studying responses to extreme waves in a towing tank; 2) to examine the effects of wave breaking and statistics of occurrence on the wave spectrum, its spectral shape, extreme wave generation, and the role of wind-wave interaction on wave breaking occurrence. It takes as basis the previous work of Specialists Committee on Modelling Environmental Conditions (28th and 29th ITTC) and describe the new methodologies or questions that raised in this context.

4.1.1 Methods to generate extreme wave packets

SC on Modelling Environmental Conditions of the 28th ITTC listed the main methodologies for the deterministic generation of extreme waves. Different wave sequences may be used as extreme waves during experiments: i) Focusing waves, ii) Deterministic wave sequences embedded in an irregular sea state, iii) Wave tank realization of observed wave record or iv) Analytical extreme wave sequence such as breather-type solution (*e.g.* Peregrine breather). Specific method need to be set-up for the accurate generation of such deterministic wave sequences in a wave tank. This mostly rely on iterative correction of the phases (as well as amplitudes if necessary) to advocate the nonlinear effects.

For the 29th ITTC, this SC complement the methodologies, including improved phase-correction methods (Niu et al. (2020)), combined numerical and experimental procedures using non-linear wave models and Time-Reversal methodology (Ducrozet et al. (2020)).

Most of the recent works involving the generation of extreme wave events are based on the approaches described previously. The focus hereafter is on new methodologies.

Klein et al. (2023) study the effect of extreme waves on a LNG Carrier. In the context of extreme responses, they compare reference long-term irregular wave tests with different extreme wave sequences. This includes different analytical breather type solutions as well as the recreation of the measured at sea Draupner wave. By comparing the motions, vertical wave bending moment, green water column and slamming pressures it is concluded that the breather solutions are a powerful and efficient tool for the generation of design extreme waves of certain critical wave lengths for wave/structure investigations on different subjects.

Esandi et al. (2020) propose an experimental study on wave forces on a vertical cylinder due to spilling breaking and near-breaking wave groups. The extreme waves are generated as focused waves, which are corrected iteratively in amplitude and phase. One specificity of the method, that ensures a faster convergence is that the amplitude spectrum is measured near the wave generator and the phase spectrum is measured at the focus position.

Klein et al. (2021) introduce the use of envelope solitons as design waves for wave-structure interactions. They show that envelope soliton solutions can be used for generating tailored extreme design waves that causes extreme ship response. Then, they compare the impact of steep envelope solitons with results obtained in extreme waves such as Peregrine breather solution and the Draupner wave. The Peregrine breather is seen as more appropriate for design questions associated with the highest possible waves and wave breaking (e.g. green water on deck, local loads at the bow or other structures as well as air-gap investigations). Other design questions, where steep wave events are relevant but wave breaking not, may be better investigated by the envelope soliton due to the very short duration of such steep wave group.

Houtani et al. (2022) present a numerical and experimental study of modulated wave trains. It is found that the phases of all the spectral wave components of the nonlinearly evolving modulated wave trains coincided at the peak of the modulation. This phase convergence process contributes to the crest enhancement of modulated wave trains beyond the solution of the cubic Non-Linear Schrödinger Equation. In addition, it is demonstrated that the free-wave spectral broadening energizes the bound-wave production at high wavenumbers. The bound wave components can contribute more than a quarter of the maximum crest height at an initial wave steepness of 0.115.

Ma et al. (2022) introduce an additional correction step to the Time-Reversal methodology in order to account for possible inaccuracies associated to wave generation or to non-conservative phenomena during wave propagation. This step consists in a classical correction of amplitude and phase between measured and target elevation. The proposed methodology is successfully validated on the experimental reproduction of four different wave profiles extracted from measurements at sea. The authors then analyze the physics of the formation of those extreme waves with wavelet-based bicoherence.

Wang et al. (2020) investigate the generation of extreme waves as a result of the focusing of two wave groups with different peak frequencies. This particular mechanism has been observed during the formation of rogue waves and may be a candidate to generate representative extreme wave profiles. Phase shifts and amplitude changes are observed during the propagation as a result of third-order non-linearity.

Kim et al. (2022) present a novel methodology for the generation of the so-called Equivalent Design Wave (EDW). This paper focus on wave-only problem, the EDW being defined as the most probable wave with a crest amplitude corresponding to a given probability of occurrence. The novelty in the construction of the EDW comes from the use of a High-Order Spectral Numerical Wave Tank (HOS-NWT) together with an optimization algorithm based on First-Order Reliability Method (FORM). As a result, the methodology provide a wavemaker motion able to generate this extreme wave. The approach has been validated with dedicated experiments that compared the Monte-Carlo irregular time series and the EDW results. The geometrical similarity between the measured EDW wave signal and the corresponding irregular wave signals measured in a given sea state was reviewed. It confirmed that the FORM-based EDW generates a comparable wave profile.

Xu et al. (2021) numerically investigate the effects of amplitude distribution of wave components on focusing wave generation, including the focusing wave crest elevation and the focusing position. Wave amplitude spectra with three types of variation across the frequency range are constructed. It is expected that the findings will help for amplitude spectra type selection or construction for efficiently generating tailored focusing waves (or extreme waves) in physical or numerical wave tank.

4.1.2 Effects of wave breaking and wind-wave interaction

SC on Modelling Environmental Conditions of the 28th ITTC provides a brief overview of the effect of wave breaking on statistics. It covers some numerical high-fidelity CFD as well as some experimental works. Effect of wind on wave breaking is not addressed. A more detailed review on the effect of breaking on spectral content is provided in the work of the SC for the 29th ITTC. The referenced works cover different type of wave conditions:

- Irregular sea states in experiments and high-fidelity CFD: reduction of energy in the high-frequency range
- Modulational instability: experimental and numerical simulations indicating the down shifting consecutive to the breaking
- Two uni-directional wave field interacting locally with an angle (X-arrangement): severity of breaking increase with the angle between the two components

Up to the 29th ITTC, research on the effect of wind-wave interaction on wave breaking occurrence was mostly limited to the study of localized events (focusing wave, modulational instability) with and without wind to identify the effect on the breaking occurrence. Numerical and experimental works have been reported on this topic.

In Craciunescu and Christou (2020) an experimental study on wave breaking energy dissipation in focused waves is presented. An accurate two-camera set-up is used to evaluate the local wave geometry during breaking process and define breaking characteristics. Those measurements are used to propose a new parametrization of an existing wave breaking model that is used in nonlinear wave models.

Eeltink et al. (2022) present a blended machine learning framework in which a physics-based nonlinear evolution model for deep-water, non-breaking waves and a recurrent neural network are combined to predict the evolution of breaking waves. Wave tank measurements are used for training data and as reference data for comparisons. The proposed framework gives accurate predictions of breaking events and their effects on wave propagation. This might be a first step toward the use of such procedure to characterize the effect of breaking on wave field characteristics.

As part of the JIP ‘Reproducible CFD Modeling Practices for Offshore Applications’, experiments on unidirectional breaking sea conditions have been conducted and serves as basis to the benchmark of potential-based numerical wave tanks (Fouques et al. (2021)) as well as CFD based NWT (Bouscasse et al. (2021)). The probability of exceedance of wave crests as well as elevation rise velocity are reported for qualified wave spectrum (i.e. following accurately the target wave spectrum despite the wave breaking). Same wave spectrum is generated in two different experimental facilities and at different scales in Canard et al. (2022).

In Khait et al. (2022), the energy dissipation associated to wave breaking is simulated with a coupled potential and high-fidelity CFD solver. Main purpose of the study is to decompose the energy dissipation into a potential part and a non-potential part, representing the effect of vertical structures. For breaking waves, there is a strong non-potential motion triggered by breaking wave and that persists in the flow for dozens of wave periods.

Lee and Monty (2020) studied the statistical properties and development of wave fields with different wind forcings in a unidirectional configuration. If breaking waves are not studied specifically, it is observed that when waves develop under the competing effects of wind forcing and nonlinear wave interaction, wind–wave interaction due to wind forcing dominates the growth mechanism over the wave–wave interaction. The exceedance probability of wave crests is found to depend on wind speed most obviously for the lowest probability (largest) waves, where a deviation from empirical second-order models is clearly evident. At lower wind speed, the Forristall distribution underestimates the probability of occurrence of the high amplitude waves, yet overpredicts at high wind speeds. This overprediction is mainly because, at the high wind speeds, the growth of extreme waves is limited by the wave breaking mechanism as the local wave steepness increases with wind speed.

4.2 Vertical Wind Profiles

Vertical profile of horizontal wind (shortened to wind profile) refers to the horizontal wind vector as a function of height. Due to the surface influence wind speed in boundary layer can change significantly from the surface values. The exact shape of the wind profile depends on surface roughness and atmospheric stability. Wind direction is approximately constant near the surface and begins to change only in the Ekman layer above. For this reason, wind profile near the surface usually refers to simply wind speed as a function of height.

The standard vertical wind profile offers a choice of mean wind velocity profiles. The velocity profiles determine the mean velocity at each height for the length of the numerical and experimental simulation. For velocity profiles that use a reference height and wind speed, the standard uses the inputs z_r and u_r as the reference point and velocity to calculate the mean velocity at other vertical heights.

(1) Power-Law Wind Profile

The power-law mean velocity profile uses the input parameter α to calculate the average wind speed at height z using the equation:

$$u_z = u_r\left(\frac{z}{z_r}\right)^{\alpha}$$

where u_z is the wind speed (in metres per second) at height z (in metres), and u_r is the known wind speed at a reference height z_r. The exponent (α) is an empirically derived coefficient that varies dependent upon the stability of the atmosphere. For neutral stability conditions, α is approximately 1/7, or 0.143. The value of 1/7 for α is commonly assumed to be constant in wind resource assessments, because the differences between the two levels are not usually so great as to introduce substantial errors into the estimates (usually < 50 m). However, when a constant exponent is used, it does not account for the roughness of the surface, the displacement of calm winds from the surface due to the presence of obstacles (i.e., zero-plane displacement), or the stability of the atmosphere. In places where trees or structures impede the near-surface wind, the use of a constant 1/7 exponent may yield quite erroneous estimates, and the log wind profile is preferred. Even under neutral stability conditions, an exponent of 0.11 is more appropriate over open water (e.g., for offshore wind farms), than 0.143, which is more applicable over open land surfaces.

When the wind speed is strong enough, the relationship between the roughness length z_0 and power law exponent α can be given as follows (Nakajima et al, 2020):

$$\alpha = 0.24 + 0.096(\log z_0) + 0.016(\log z_0)^2$$

The power law is often used in wind power assessments where wind speeds at the height of a turbine (>50 m) must be estimated from near surface wind observations (~10 m), or where wind speed data at various heights must be adjusted to a standard height prior to use. Wind profiles are generated and used in a number of atmospheric pollution dispersion models.

The wind profile of the atmospheric boundary layer (surface to around 2000 meters) is generally logarithmic in nature and is best approximated using the log wind profile equation that accounts for surface roughness and atmospheric stability. The relationships between surface power and wind are often used as an alternative to logarithmic wind features when surface roughness or stability information is not available.

Estimates of wind power density are presented as wind class, ranging from 1 to 7. The speeds are average wind speeds over the course of a year, although the frequency distribution of wind speed can provide different power densities for the same average wind speed.

Table 1 Wind power density presented as wind class

Class	10 m (33 ft)		30 m (98 ft)		50 m (164 ft)	
	Wind power density (W/m²)	Speed m/s (mph)	Wind power density (W/m²)	Speed m/s (mph)	Wind power density (W/m²)	Speed m/s (mph)
1	0 - 100	0 - 4.4 (0 - 9.8)	0 - 160	0 - 5.1 (0 - 11.4)	0 - 200	0 - 5.6 (0 - 12.5)
2	100 - 150	4.4 - 5.1 (9.8 - 11.5)	160 - 240	5.1 - 5.9 (11.4 - 13.2)	200 - 300	5.6 - 6.4 (12.5 - 14.3)
3	150 - 200	5.1 - 5.6 (11.5 - 12.5)	240 - 320	5.9 - 6.5 (13.2 - 14.6)	300 - 400	6.4 - 7.0 (14.3 - 15.7)
4	200 - 250	5.6 - 6.0 (12.5 - 13.4)	320 - 400	6.5 - 7.0 (14.6 - 15.7)	400 - 500	7.0 - 7.5 (15.7 - 16.8)
5	250 - 300	6.0 - 6.4 (13.4 - 14.3)	400 - 480	7.0 - 7.4 (15.7 - 16.6)	500 - 600	7.5 - 8.0 (16.8 - 17.9)
6	300 - 400	6.4 - 7.0 (14.3 - 15.7)	480 - 640	7.4 - 8.2 (16.6 - 18.3)	600 - 800	8.0 - 8.8 (17.9 - 19.7)
7	400 - 1000	7.0 - 9.4 (15.7 - 21.1)	640 - 1600	8.2 - 11.0 (18.3 - 24.7)	800 - 2000	8.8 - 11.9 (19.7 - 26.6)

(2) Logarithmic Wind Profile

The logarithmic profile of wind speeds is generally limited to the lowest 100 m of the atmosphere (i.e., the surface layer of the atmospheric boundary layer). The rest of the atmosphere is composed of the remaining part of the planetary boundary layer (up to around 1000 m) and the troposphere or free atmosphere. In the free atmosphere, geostrophic wind relationships should be used. The equation to estimate the mean wind speed (u_z) at height (z) above the ground is:

$$u_z = \frac{u_*}{\kappa}\left[\ln\left(\frac{z-d}{z_0}\right) + \psi(z, z_0, L)\right] (+Coriolis\ force\ term)$$

where u_* is the friction velocity, κ is the Von Kármán constant (~0.41), d is the zero plane displacement, z_0 is the surface roughness, and ψ is a stability term where L is the Obukhov length from Monin-Obukhov similarity theory. The equation above can be modified to include the Coriolis force-related parameter, $34.5\ fz/u_*$ for a somewhat improved wind profile. Here $f = 2\omega \sin\phi$; where ω is the angular velocity of the earth in rad/s and ϕ is the latitude.

As per DNV(2010), the stability function ψ is zero under neutral atmospheric condition, positive under unstable condition, and negative under stable atmospheric conditions. Ref: DNV(2010): [DNV-RP-C205: Environmental Conditions and Environmental Loads -(October 2010- Recommended Practice]

The general form of the stability function for an unstable atmospheric condition is as follows according to DNV (2010):

$$\begin{aligned}\psi = 2\ln[1 + (1 - 19.3\, z/L)^{0.25}] \\ + \ln[1 + (1 - 19.3\, z/L)^{0.5}] \\ - 2\tan^{-1}[(1 - 19.3\, z/L)^{0.25}]\end{aligned}$$

Under neutral stability conditions, $z/L = 0$ and ψ drops out and the equation is simplified to,

$$u_z = \frac{u_*}{\kappa}\left[\ln\left(\frac{z-d}{z_0}\right)\right]$$

Zero-plane displacement d is the height in meters above the ground at which zero wind speed is achieved as a result of flow obstacles such as trees or buildings. It clarification needed can be approximated as 2/3 to 3/4 of the average height of the obstacles. For example, if estimating winds over a forest canopy of height 30 m, the zero-plane displacement could be estimated as d = 20 m.

Roughness length z_0 is a corrective measure to account for the effect of the roughness of a surface on wind flow. That is, the value of the roughness length depends on the terrain. The exact value is subjective and references indicate a range of values, making it difficult to give definitive values. In most cases, references present a tabular format with the value of z_0 given for certain terrain descriptions. For example, for very flat terrain (snow, desert) the roughness length may be in the range 0.001 to 0.005 m. Similarly, for open terrain (grassland) the typical range is 0.01-0.05 m. For cropland,

and brush/forest the ranges are 0.1-0.25 m and 0.5-1.0 m respectively. When estimating wind loads on structures the terrains may be described as suburban or dense urban, for which the ranges are typically 0.1-0.5 m and 1-5 m respectively.

In order to estimate the mean wind speed at one height (z_2) based on that at another (z_1), the formula would be rearranged,

$$u(z_2) = u(z_1)\frac{\ln((z_2 - d)/z_0)}{\ln((z_1 - d)/z_0)}$$

where $u(z_1)$ is the mean wind speed at height z_1.

Log wind profiles are generated and used in many atmospheric pollution dispersion models. The log wind profile is generally considered to be a more reliable estimator of mean wind speed than the wind profile power law in the lowest 10–20 m of the planetary boundary layer. Between 20 m and 100 m both methods can produce reasonable predictions of mean wind speed in neutral atmospheric conditions. From 100 m to near the top of the atmospheric boundary layer the power law produces more accurate predictions of mean wind speed (assuming neutral atmospheric conditions). The neutral atmospheric stability assumption discussed above is reasonable when the hourly mean wind speed at a height of 10 m exceeds 10 m/s where turbulent mixing overpowers atmospheric instability.

(3) IEC Wind Profile

The IEC wind profile was the wind-speed profile available for wind turbine. This profile uses the power-law wind profile for the wind speeds at heights on the rotor disk and the logarithmic profile for heights not on the rotor disk. For example, if u_r is specified at a z_r below the rotor disk, the logarithmic profile is used to calculate the mean wind speed at hub height. Then the power-law profile would be used with the hub height wind speed to calculate winds across the rotor disk. This profile could cause a discontinuity in the wind profile at the bottom of the rotor disk.

(4) Low-Level Jet Wind Profile

The low-level jet wind profile is derived from Lamar Low-Level Jet Project (LLLJP) 10-minute SODAR measurements and is available with only the Great Plains Low-Level Jet Model spectral model. The Great Plains model is based on measurements from a 120-m tower and from an acoustic wind profiler (SODAR [sonic detection and ranging]) obtained during the Lamar Low Level Jet Project in southeastern Colorado. The tower included three-axis sonic anemometers at 54 m, 67 m, 85 m, and 116 m above the ground; cup anemometers and direction vanes located at 3, 52, and 113 m; and temperature measurements obtained at 3 m, 52 m, 83 m, and 113 m. The SODAR provided measurements of wind speed and direction at 10-m vertical increments from 20 m to 500 m. The spectra and spatial coherence parameters defined in this model are based on 20-Hz time-series data collected at the sonic anemometers.

The Great Plains Low-Level Jet Model defines vertical profiles of shear velocity. This profile type is unique because it generates both wind-speed and wind-direction profiles. The low-level jet wind-speed profile is defined using Chebyshev polynomials,

$$u_z = \sum_{n=0}^{10} c_n \cdot T_n(z)$$

where z is the height above ground, u_z is the mean wind speed at height z, $T_n(z)$ is the n^{th} order Chebyshev polynomial, and c_n is a Chebyshev coefficient. The Chebyshev coefficients are derived from LLLJP data and are a linear combination of the jet wind speed (u_{ZJetMax}), gradient Richardson number (RICH) and u_*

$$c_n = C_{1,n}u_{\mathrm{ZJetMax}} + C_{2,n}\mathrm{RICH} + C_{3,n}u_* + C_{4,n}$$

The coefficients, $C_{i,n}$ =1, 2, 3, 4, are determined by the input parameter *ZJetMax*. The low-level jet wind-direction profile, like the wind-speed profile, is a Chebyshev polynomial with coefficients derived from the same parameters in the LLLJP data.

(5) API Wind Profile

The API wind profile is based on 1-hr mean wind speed at 10 m above sea level, it is defined by the equation

$$u_z = u_r(1 + 0.0573\sqrt{1 + 0.15u_r})\ln z/z_r$$

Where z is the height, u_z is the mean wind speed at height z, u_r is the one-hour mean wind speed, and z_r is 10 meters.

(6) Gust wind profile

Gust wind is a sudden, brief increase in speed of the wind. In contrast with the boundary layer winds, the gust winds are nonstationary due to their transient characteristics. Therefore, the stationary wind model typically used in boundary layer winds may not be valid for gust winds which may be described in terms of time-varying parameters.

The vertical profile of gust winds is critical in evaluating the wind effects on structures, however, very limited full-scale data along the height is available to identify and reliably establish a description of the vertical profile. From a practical viewpoint, the worst scenario for wind loads on structures may be the highest wind speed which occurs at about one downdraft jet diameter from its point of impact. Note that several analytical models have been proposed for vertical profile of gust winds. Although there are some discrepancies among models, especially a profile over z_{max}, all models moderately fit well with a limited full-scale data. Thus, without loss of generality, the following model is utilized due to its simplicity:

$$u_z = 1.354 \cdot V_{max}[e^{-0.22(z/z_{max})} - e^{-2.75(z/z_{max})}]$$

where V_{max} is maximum horizontal wind speed, z_{max} is the height where V_{max} occurs.

The vertical profile model of a downburst describes a short time averaged maximum mean wind speed at a height, which may be treated as a gust profile as used in the boundary layer wind case. Since z_{max} and V_{max} in the model are unknown, it is necessary to establish a criterion to relate the velocity profile in a gust wind and a boundary layer for design considerations. Two criteria are considered: (i) gust wind speed at 10 m height, is set equal to the boundary layer gust speed at 10 m; (ii) the maximum gust wind speed (V_{max}) is equal to gust speed at the gradient height in boundary layer winds. One may conveniently introduce additional criterion that may better reflect the data or may meet other site-specific requirements when it becomes available in the future.

(7) User-Defined Velocity Profiles

For user-defined velocity profiles, the standard linearly interpolates the input velocity profiles. The profiles are calculated from the mean values of the input time series. The profiles are extrapolated by using a nearest-neighbor approach: the profiles are constant at heights above or below the heights where the input profiles are defined.

4.3 STATE-OF-THE-ART IN HYBRID TESTING – SOFTWARE-IN-THE-LOOP TESTS FOR MODELLING WIND FORCES

The state-of-the-art in hybrid testing of offshore wind turbines are reviewed, to continue work on using a small controllable fan to mimic forces developed during a floating offshore wind turbine test due to the turbine itself, and to expand the work on Software-in-the-Loop (SiL) systems for modeling wind turbine loads to be used as a general tool to model many types of wind loads.

4.3.1 Development of hybrid testing methods for floating wind turbines

Conventional full physical model tests of floating wind turbines (FWTs) typically utilize Froude scaling to preserve gravitational wave loads. However, this approach results in a lower Reynolds number, causing the aerodynamic loads to be out of scale. Additionally, model tests of FWTs require adjusting the blade pitch angle and generator torque to accurately simulate the coupling effects. Nevertheless, designing a specialized apparatus to effectively mimic the control system’s performance in the prototype poses a significant challenge (Yu et al., 2017).

To overcome these challenges, particularly the scaling conflict, researchers have employed various methodologies for testing FWTs. One approach is the use of static cables to replicate steady wind forces. Another method involves the utilization of a drag disk at the top of the tower to approximate the thrust force. In Robertson’s research, Froude-scaled rotors with increased wind speed were employed to match the correct thrust force. Redesigned rotors, which perform identically to the full-scale rotor at a lower Reynolds number, were also utilized to accurately generate the rotor’s aerodynamic loads. Hybrid testing is another technique that combines physical testing and real-time numerical simulation. An actuation system enables the coupling between the simulated wind turbine and the physical floater, either in a wave basin or, conversely, in a wind tunnel.

The concept of real-time hybrid model experiments was initially introduced in civil engineering. Originally, this method was used to study the dynamic responses of large buildings subjected to seismic forces. In 1992, Nakashima et al. (1992) proposed a real-time hybrid model experimental method that utilized the same loading rate as a real earthquake to obtain the actual response of the test components. Over time, this idea expanded and found application in offshore engineering experiments. In hybrid tests, a physical part of the model is replaced by an actuator connected to a numerical tool. This approach can be implemented in wind tunnels or wave basins. By using the hybrid approach, FWTs can be tested under combined wind and wave conditions without the need for a wind generation system. The actuators take the place of the rotors and generate the required aerodynamic loads.

Compared to the conventional full physical testing method, the hybrid model testing approach offers several advantages, which can be summarized as follows (Otter et al., 2022):

- ***Cost-effectiveness***: Hybrid testing can be more cost-effective since it replaces certain physical components with actuators and numerical tools, reducing the need for expensive full-scale physical models.

- ***Flexibility***: The hybrid approach allows for greater flexibility in testing various scenarios and conditions. It can simulate different wind and wave conditions, providing a more comprehensive understanding of the system's behavior.

- ***Time efficiency***: Hybrid testing can significantly reduce the testing time compared to full physical testing. The use of numerical tools enables faster simulations and real-time responses, allowing for quicker data analysis and decision-making.

- ***Scalability***: Hybrid models can be easily scaled up or down, making it possible to test different sizes of FWTs without the need for separate physical models for each size.

- ***Control system emulation***: The hybrid approach enables more accurate emulation of the control system's performance in the prototype. This is achieved by integrating the physical floater with the simulated wind turbine using actuators, resulting in more realistic and reliable results.

However, the hybrid model testing approach also presents certain challenges, which can be summarized as follows (Otter et al., 2022):

- ***Complexity***: Hybrid testing involves the integration of physical and numerical components, which can be technically complex and require advanced expertise in both areas. Designing and implementing the actuation system and ensuring its synchronization with the numerical simulation can be challenging.

- ***Validation***: Validating the accuracy and reliability of the numerical tools used in the hybrid model can be difficult. Ensuring that the numerical simulations accurately represent the behavior of the physical system requires thorough validation and calibration.

- ***Uncertainty***: There may be uncertainties associated with the numerical models used in the hybrid approach, such as the accuracy of the numerical algorithms or the assumptions made in the simulations. These uncertainties can affect the reliability of the test results.

- ***Hardware constraints***: The physical components used in the hybrid model, such as actuators, may have limitations in terms of their load capacity, response time, or other hardware constraints. These limitations can impact the fidelity and realism of hybrid testing.

The advantages and disadvantages of full physical testing and hybrid testing are further summarized in Table 2:

Table 2: The comparison of pros and cons of the full physical method and hybrid method (Otter et al. 2022)

Full physical modeling	
Advantage	• Models aerodynamic thrust, torque, and gyroscopic moment • Captures aerodynamic damping • Turbine control can be applied
Disadvantage	• Requires expensive and bulky wind generation equipment • Difficult to generate high-quality laminar steady wind • Difficult to generate stochastic wind with good repeatability • Requires a unique turbine model for each turbine design and scale • Rotor often requires the aid of an electric motor to reach the correct TSR
Hybrid modeling	
Advantage	• Depending on the number of actuators it is possible to emulate thrust, torque, and gyroscopic moment with good repeatability • Capture aerodynamic damping • Turbine control can be applied • Stochastic wind loads can be implemented without great difficulty • Versatile, can be used for any type of turbine or scale • Requires less space and is considerably cheaper than a wind generation system
Disadvantage	• System latency • Multiple actuators required to emulate all aerodynamic loads add complexity and uncertainty • Phenomena not simulated with the numerical model will not be captured during testing

4.3.2 Types of actuators used in the hybrid testing method

The following recaps the hybrid testing campaigns of FWTs and highlights the advantages of each actuation system employed in these tests.

（1）Propeller actuators

In terms of actuators, researchers commonly use propellers and ducted fans in hybrid testing. One widely applied actuator is the single propeller actuator with SIL, which has been used in various campaigns. For example, at the Kelvin Hydrodynamics Laboratory (KHL) at the University of Strathclyde, a 1:36.67 scale model of the Iberdrola TLP was tested using this actuator (Oguz et al., 2020). However, it should be noted that the single fan actuator is designed to replicate the thrust force only, and does not emulate other aerodynamic loads and gyroscopic moments. Therefore, efforts have been made to develop multi-actuator systems that are capable of reproducing the full aerodynamic tensor.

At the Instituto Hidraulica Cantabria (IHC), an actuator consisting of six drone propellers was developed and utilized in the testing of the TELWIND FWT (Urbán et al., 2020). The propellers were carefully calibrated and tuned to account for the aerodynamic effects resulting from their proximity. The results of these tests were promising, showing only minor deviations compared to the expected load values. Another actuator, developed and calibrated by Hmedi et al. (2022), utilized three propellers to replicate both thrust and aerodynamic moments. While this system performed well overall, it struggled to accurately emulate the high-frequency components of the loads. Additionally, a multi-propeller system was also employed to test a vertical-axis wind turbine (Kanner et al., 2016).

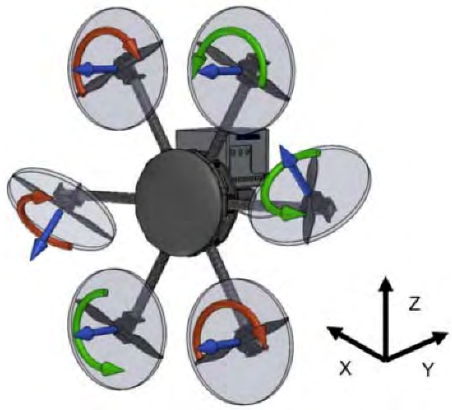

(a) CAD View

(b) Model tests view

Figure 67: The (a) CAD view and (b) Model tests view of multi-fan employed in the hybrid testing of TELWIND FWT (Urbán et al., 2020)

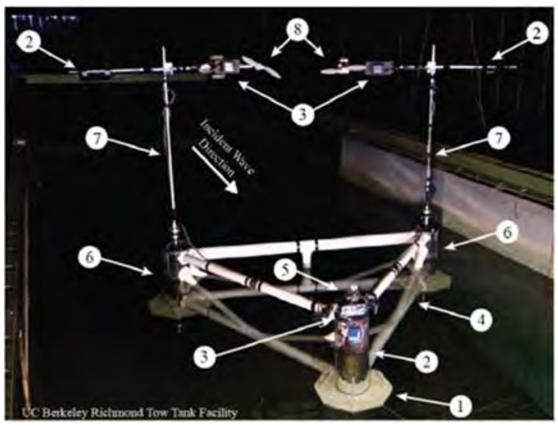

(a) Main components of hybrid testing MIST platform

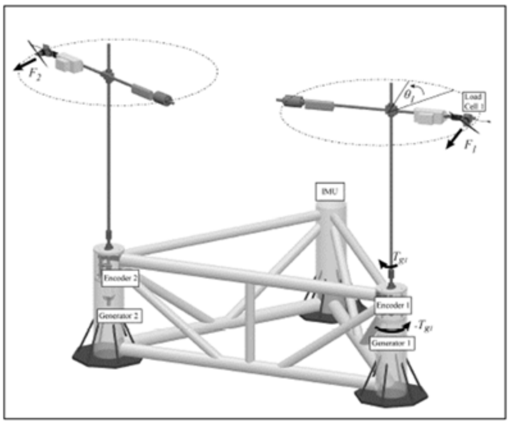

(b) Schematic of sensors and actuators on the MIST platform

Figure 68: The presence of the details of the hybrid testing of a vertical axis floating wind turbine in the UC Berkeley physical-model testing facility (Kanner et al., 2016)

（2）Cable winch actuators

Cable winches have also been employed as actuators in hybrid testing. In the early testing campaigns, static lines or cables were utilized to replicate the static thrust obtained from the thrust curve of the specific turbine being tested. These campaigns encompassed various types of tests, such as decay, regular, and irregular wave tests. Additionally, regular wave tests were conducted with a constant thrust force applied at the top of the tower through the use of cables. However, it is important to note that these cable winches solely focused on reproducing the thrust force and did not take into consideration other aerodynamic loads and interactions, such as turbulent wind, aerodynamic damping, controller effects, and gyroscopic moments.

Indeed, using cable winches as actuators in hybrid testing offers simplicity and efficiency, as it involves a straightforward mechanical system with cables applying static tensions at the top of the tower. However, this method has limitations in terms of control and variability, as it can only replicate static loads. Furthermore, relying solely on the wind turbine's thrust curve does not account for the platform's response when calculating aerodynamic loads. Additionally, gyroscopic effects cannot be emulated using this technique. Moreover, it is important to note that this method only emulates the thrust force and neglects other components of aerodynamic loads.

To overcome the limitations of the static cable method, a significant improvement involves applying tensions instantaneously to the model in real-time, based on the load simulation. This approach is similar to the Software-In-the-Loop (SIL) system with propeller actuators, but instead of using propellers, cable winches are utilized to apply the loads calculated by the numerical tool. By implementing this method, the limitations of static loads and neglecting other aerodynamic load components can be addressed, allowing for a more dynamic and accurate representation of the wind turbine's behavior during testing.

The first real-time hybrid system utilizing cable winches was developed at SINTEF in Norway. This system involves six cables that are connected to a square frame at the hub height of the wind turbine. Researchers at SINTEF (Bachynski et al., 2016) referred to this approach as ReaTHM testing and employed it to test the NOWITECH model, which incorporates the NREL 5 MW wind turbine. This innovative system allows for dynamic and real-time load application, enabling more accurate and comprehensive testing of wind turbine models.

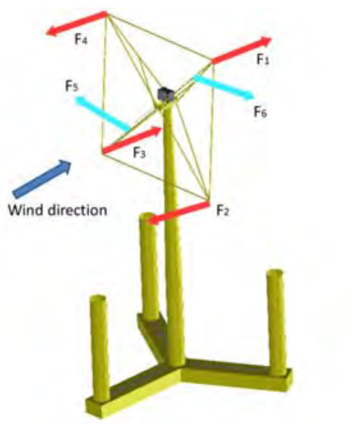

(a) The physical substructure

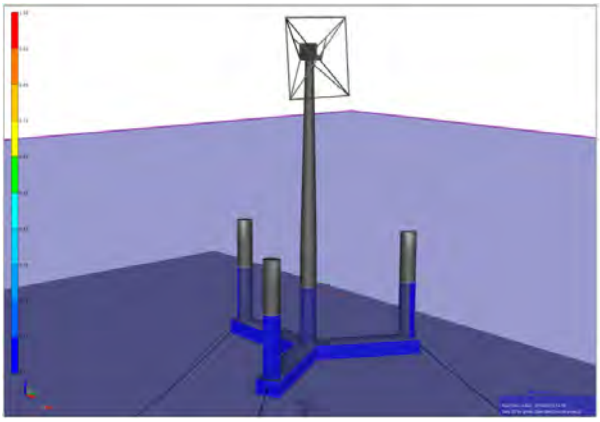

(b) The FWT modeled in SIMA with a frame for the hybrid testing method

Figure 69: The presence of the details of the hybrid testing in the SINTEF in Norway (Bachynski et al., 2016)

Antonutti's research work also utilized a hybrid system with cables similar to the one used at SINTEF (Antonutti et al., 2020). The model tested in Antonutti's research was a semi-submersible platform with the Haliade 6 MW wind turbine. The system consisted of five cables that allowed for the actuation of the surge, pitch, and yaw degrees of freedom (DOFs). The results of the study demonstrated a successful correlation between the experimental and numerical models, indicating the effectiveness of this hybrid testing approach in accurately capturing the behavior of the wind turbine system.

(a) Floating wind turbine model tested at MARIN

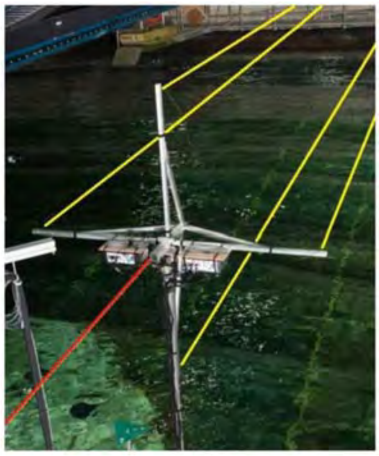

(b) Turbine superstructure with winch lines highlighted

Figure 70: The presence of the details of the hybrid testing of a 6 MW semi-submersible FWT in the MARIN (Antonutti et al., 2020).

（3）Wind tunnel tests

Indeed, hybrid tests with cables and propellers are often conducted in wave basins to study the hydrodynamics of the tested platform. In these tests, the actuators emulate the aerodynamic loads instead of subjecting a scaled rotor to a wind flow. This approach allows for a comprehensive analysis of the platform's behavior in a controlled environment. Another type of hybrid testing takes place in wind tunnels and focuses on studying aerodynamic loads, wakes, and interactions of the wind turbine. In this case, instead of calculating the aerodynamic loads, the motions of the FWT model are simulated using a numerical tool. The physical model, including a physical rotor, is placed in the wind tunnel, and the motions of the FWT are replicated using actuators. This method enables researchers to study the dynamic response of the wind turbine and its interactions with the surrounding flow, providing valuable insights into its aerodynamic performance.

In the study conducted by Schliffke et al. (2020), wind tunnel tests were performed to investigate the influence of surge motion on wake characteristics. The tested model used in this study was the FLOATGEN barge, which supported a 2 MW wind turbine. Instead of using a scaled rotor, a porous disc concept was adopted. The surge displacement of the model was controlled by a linear motor, which was operated using the manufacturer's software. During the tests, a nearly constant delay was observed between the assigned and emulated motion. However, since the focus of the study was on investigating the influence of surge motion on wakes and not on motion dynamics, this delay was considered insignificant. Importantly, the delay remained consistent regardless of the imposed frequency and amplitude of the motion. Furthermore, hybrid tests in wind tunnels were also conducted to examine the impact of pitch motion on the wakes of the FWT. Additionally, the effect of wake interactions on the FWT was investigated in these tests. These studies were carried out by Rockel et al. (2020, 2021), providing valuable insights into the complex dynamics of wakes and their interactions with the FWT.

(a) Photography of experimental facility and scaled wind turbines

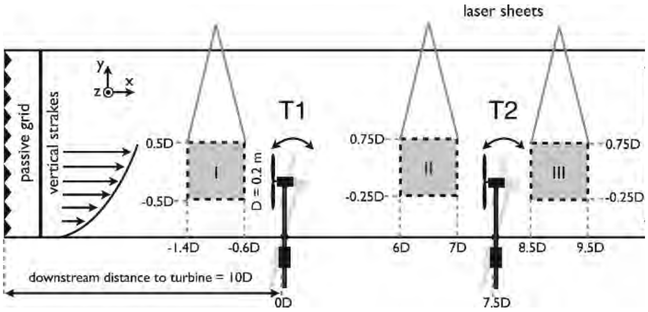

(b) Wind tunnel setup with two model turbines

Figure 71: Details of hybrid wind tunnel testing of two scaled wind turbines (Rockel et al., 2021).

4.3.3 Recent advances and applications of hybrid model tests

Wen et al. (2022) have developed a Multi-drive Aerodynamic Loading Simulator (MALS) that utilizes individually-controlled UAV propellers as actuators. The MALS was designed to generate desired aerodynamic thrust accurately for both steady and unsteady cases. Extensive performance evaluation tests were conducted to assess the capabilities of the MALS. Figure 72 illustrates the procedures used to calculate the target rotor thrust and generate the control command for the MALS. These procedures ensure that the desired aerodynamic thrust is achieved with satisfactory accuracy. To investigate the coupling dynamics of a FWT system, a hybrid model test system was constructed using the proposed MALS. This system allows for the examination of the interactions and dynamics of the FWT system. For comparison and validation purposes, a typical FWT model test system with a physical wind turbine was also constructed. This system serves as a benchmark to assess the performance of the MALS in integrated FWT model tests, as shown in Figure 73.

Overall, the work by Wen et al. (2022) highlights the development and evaluation of the MALS as a versatile tool for studying the aerodynamic characteristics and coupling dynamics of FWT systems.

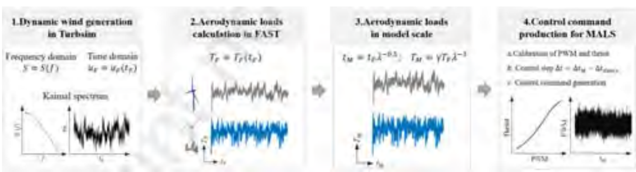

Figure 72: Procedure to produce the control command of MALS for complex aerodynamic loads (Wen et al., 2022).

Figure 73: The presence of a full physical model and hybrid model in the experiment (Wen et al., 2022)

Sun et al. (2022) have proposed a real-time hybrid simulation (RTHS) framework for studying the structural performance of floating offshore wind turbines (FOWTs) under wind-wave loading. The framework, as shown in Figure 74 and Figure 75, combines numerical modeling and physical testing. In the RTHS framework, the blades, nacelle, and tower of the FOWT are numerically modeled, while the floating platform is physically tested in real-time using an actuation system in a laboratory setting. The numerical and physical substructures communicate at the tower-floater interface, enabling the simulation of the FOWT's behavior under wind-wave loading conditions. To evaluate the feasibility of the proposed framework, a 5 MW spar-type FOWT at a scale of 1:50 was simulated. A sensitivity analysis was conducted to quantify the errors caused by delays and noises in the system. The results indicated that the delays in the sensors and actuators had a more significant influence on the performance of the RTHS framework compared to the noises.

Overall, the work by Sun et al. (2022) demonstrates the potential of the RTHS framework for studying the structural performance of FOWTs under wind-wave loading conditions. The findings highlight the importance of minimizing delays in sensors and actuators to improve the accuracy and reliability of the simulation results.

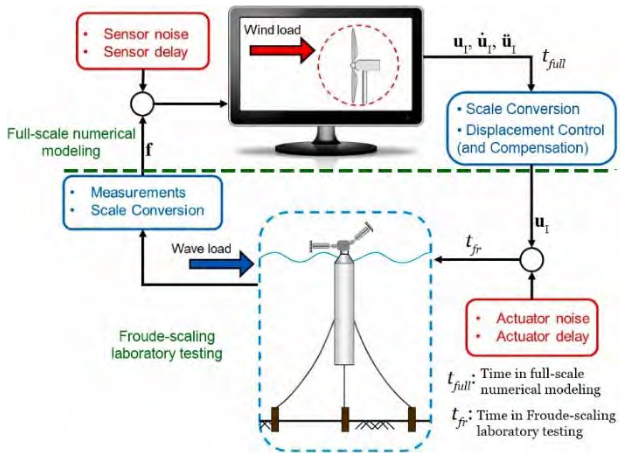

Figure 74: Block diagram of the proposed RTHS framework (Sun et al., 2022)

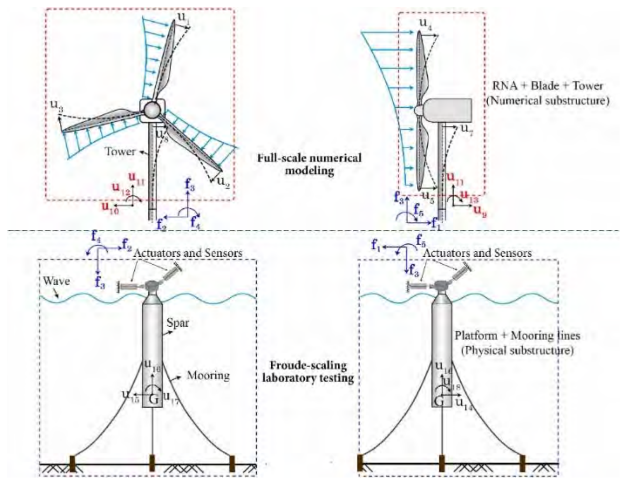

Figure 75: Schematic model for RTHS of spar-type FOWTs (Sun et al., 2022)

To further enhance the capabilities of the real-time hybrid simulation (RTHS) method, a distributed RTHS (dRTHS) approach was proposed, developed, and validated in Sadraddin's doctoral research (2022). This approach (see Figure 76) utilizes geographically distributed wind tunnels and wave tanks that are interconnected through network communications to conduct large-to-full-scale FWT experiments. The dRTHS method takes advantage of the availability of multiple testing facilities located in different geographical locations. By leveraging network communications, these facilities can be connected to create a distributed testing environment. This allows for the simulation of FWT experiments at larger scales, up to full-scale, by combining the capabilities and resources of multiple wind tunnels and wave tanks.

Sadraddin's research focused on the development and validation of the dRTHS approach. The findings demonstrated the feasibility and effectiveness of using distributed testing facilities for conducting FWT experiments. This approach opens up new possibilities for studying the behavior and performance of FWT systems at larger scales, which can provide valuable insights for the design and optimization of offshore wind energy systems.

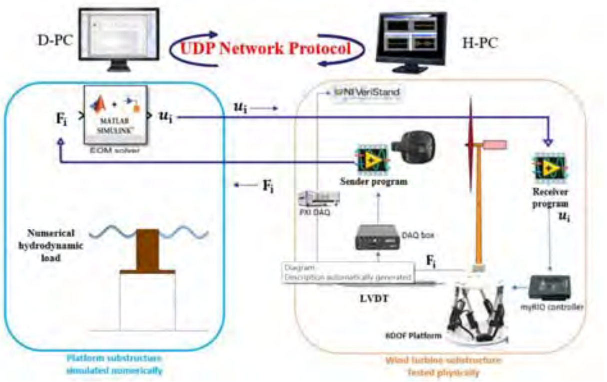

Figure 76: Experimental setup with software (Sadraddin, 2022)

Ha et al. (2023) have proposed a real-time hybrid method for the performance evaluation of a 10 MW class floating offshore wind turbine. In this experimental technique, six duct fans, as shown in Figure 77, were attached at the tower top of the wind turbine to actuate the real-time hybrid method. Figure 78 illustrates the loop of the real-time hybrid method for the 10 MW floating wind turbine. In the model test, the platform motions were measured using Qualisys, and the converted nacelle velocities were used as the relative wind velocities in each direction. Numerical simulations were conducted based on the calculated relative wind velocities and input wind velocity. The duct fans in the model test were operated based on the thrust and yaw moment of the nacelle obtained from the numerical simulation. To validate the model test technique, the experimental results were directly compared with the fully coupled analysis results. Additionally, repetitive tests were performed to investigate the repeatability of the model test technique. From the experimental results, it was observed that the model test technique performed well and exhibited good repeatability. The comparison with the fully coupled analysis results demonstrated the effectiveness and accuracy of the proposed real-time hybrid method for evaluating the performance of the 10 MW floating wind turbine.

Overall, the work by Ha et al. (2023) achieves the successful implementation of the real-time hybrid method using duct fans for performance evaluation of a 10 MW class floating offshore wind turbine. The experimental results validate the model test technique and highlight its repeatability, providing valuable insights for the design and assessment of large-scale wind energy systems.

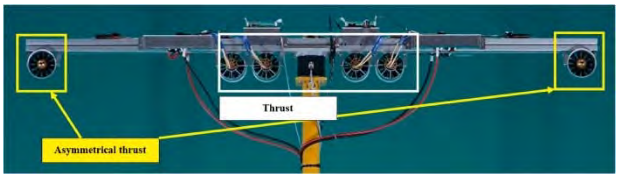

Figure 77: Configuration of the duct fans (Ha et al., 2023)

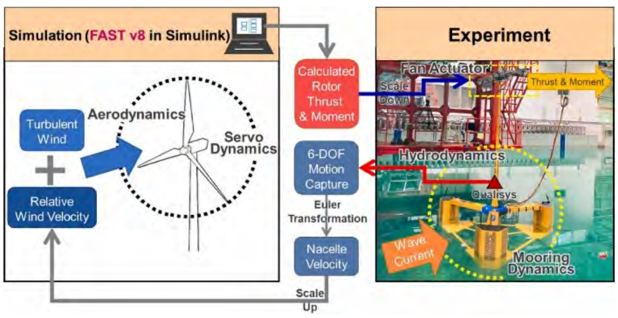

Figure 78: Loop of real-time hybrid method for 10 MW FOWT (Ha et al., 2023)

Wang et al. (2022) conducted a series of tank tests using a scaled spar-type floating offshore wind turbine and employed an AI-based software-in-the-loop hybrid testing method. The tests were carried out in different scenarios, including wave-only cases, wind-only cases, and combined wind-wave cases, to investigate the influence of wave frequency and wind speed on the platform motions. In addition to the tank tests, numerical simulations were also performed to compare the results with the experimental data. It was observed that the numerical calculations generally aligned with the testing results, indicating the accuracy and reliability of the numerical models. Figure 79 illustrates the AI-based real-time hybrid model testing rig developed by Jiang (2020). The tower of the wind turbine is equipped with a fan that generates a real-time thrust force based on Froude's law of similarity. This fan is driven and controlled by a prediction algorithm, which considers the real-time platform motions (such as surge, surge velocity, pitch, pitch velocity, and wind speed) measured by an optical capture system. Thus, the entire experimental procedure of this rig can be viewed as a loop, where the prediction algorithm and real-time measurements drive the fan to provide an equivalent real-time thrust force.

The research allows for the integration of numerical simulations and physical testing, providing a comprehensive and accurate evaluation of the platform motions of floating offshore wind turbines. This approach contributes to the understanding of the effects of wave frequency and wind speed on the performance of such wind turbines.

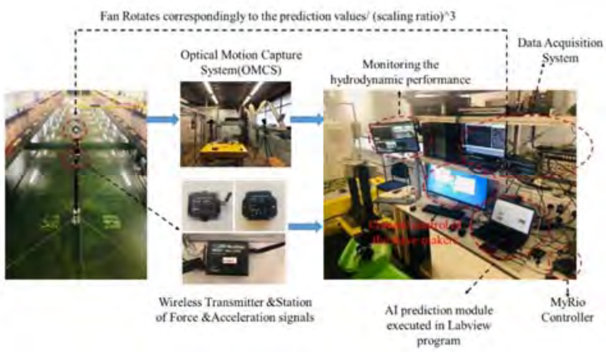

Figure 79: AI-based real-time hybrid model testing rig (Wang et al., 2022)

Yu et al. (2022) conducted a hybrid test campaign for a floating offshore wind turbine (FOWT) at a scale of 1:36. Figure 80 illustrates the setup used in the campaign. Instead of using a scaled physical turbine model, a multi-fan system was employed to create equivalent aerodynamic thrust forces. The aerodynamic loads of the turbine were defined and generated using a hardware-in-the-loop (HIL) system developed at IH Cantabria. The HIL system involved the multi-fan system, which accurately replicated the rotor aerodynamics. Figure 81 shows a block diagram of the HIL system and the integration of the state observer. This allowed for precise control and simulation of the aerodynamic forces acting on the FOWT. Various tests were conducted as part of the campaign to identify and calibrate the FOWT system. These tests included regular waves, irregular waves, and turbulent winds. The dynamic responses of the FOWT system were measured and compared with numerically reproduced results. The comparison showed a good agreement between the experimental and numerical data.

The hybrid test campaign carried out by Yu et al. (2022) demonstrates the effectiveness of using a multi-fan system and HIL technology to simulate the aerodynamic forces on a floating offshore wind turbine. The tests conducted in different wave and wind conditions provide valuable insights into the performance and behavior of FOWTs. The agreement between the experimental and numerical results further validates the accuracy and reliability of the hybrid testing approach.

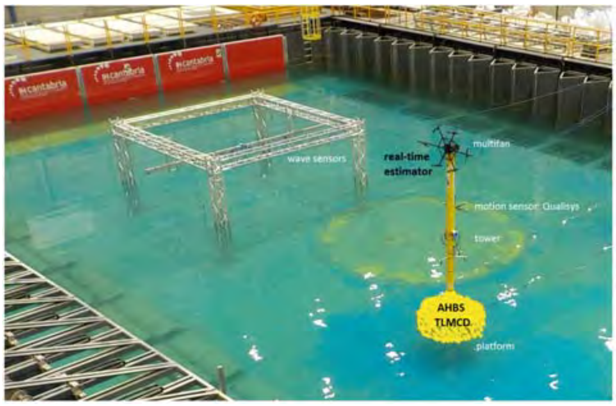

Figure 80: Setup of the wave tank hybrid tests (Yu et al., 2022)

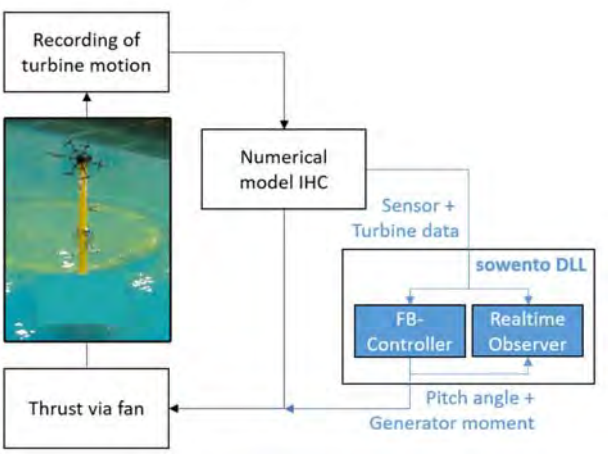

Figure 81: HIL system and the integration of the state observer (Yu et al., 2022)

Vittori et al. (2022) conducted a wave tank test campaign to evaluate a 1/49 scaled SATH 10 MW floating platform. Figure 82 illustrates the setup used in the campaign. To incorporate the wind turbine thrust and in-plane rotor moments, a software-in-the-loop (SIL) hybrid method was employed, as depicted in Figure 83. The experimental results obtained from the wave tank tests were compared with a numerical model developed in OpenFAST for the floating wind turbine. The aim was to validate the numerical model against the physical testing data. In this test campaign, an actuator with four propellers was utilized to introduce rotor loading. Each propeller was powered by a commercial brushless motor typically used in drones. An electronic speed controller (ESC) controlled the motor, which was supplied with power from an industrial AC-DC power supply. The rotational speed of each motor, and consequently the force generated by the propeller, was controlled using a pulse width modulation (PWM) signal. This signal was generated with the LabVIEW control software, utilizing servo libraries for Arduino.

The use of the SIL hybrid method in combination with the wave tank tests allowed for the inclusion of the wind turbine thrust and in-plane rotor moments in the experimental setup. By comparing the experimental results with the numerical model, the study aimed to assess the accuracy and reliability of the numerical modeling approach. The actuator system with propellers provided a means to replicate the rotor loading in the wave tank tests.

The work conducted by Vittori et al. (2022) demonstrates the successful implementation of the SiL hybrid method and the utilization of an actuator system with propellers for wave tank testing of a floating wind turbine. The comparison between the experimental and numerical results contributes to the validation and improvement of numerical models for floating wind turbines.

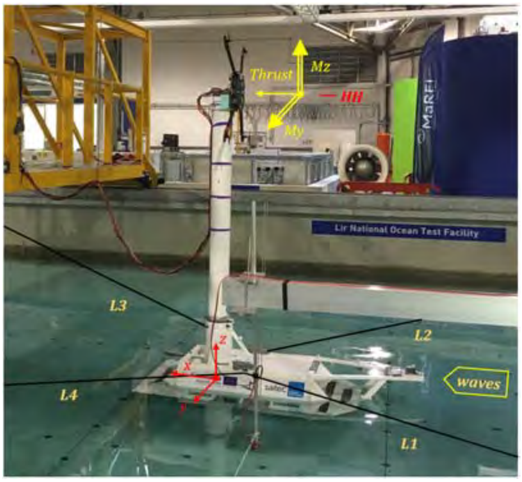

Figure 82: Setup of the wave tank hybrid test (Vittori et al., 2022)

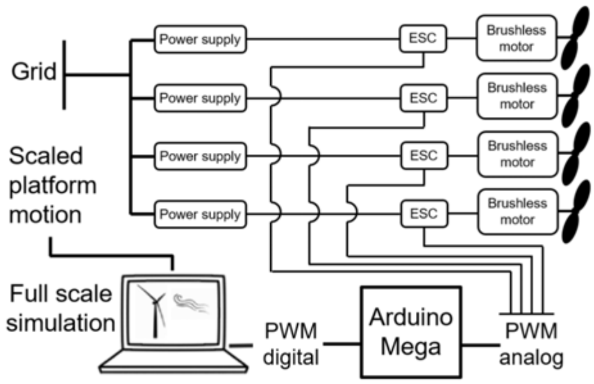

Figure 83: SIL control diagram (Vittori et al., 2020)

Thys et al. (2021) conducted model tests using a scaled model of the INO WINDMOOR 12 MW floating wind turbine in the Ocean Basin at SINTEF Ocean. Real-time hybrid model testing was employed, as depicted in Figure 84, to model the wind turbine rotor and aerodynamic loads. In this study, the physical subsystem consisted of a Froude-scaled floating substructure, tower, and mooring lines. The numerical subsystem utilized a modified version of FAST, a widely-used software for wind turbine simulation, which ran in real-time. The numerical model incorporated measured positions, velocities, and accelerations of the RNA (Rotor-Nacelle Assembly) from the model tests. The simulations provided outputs such as the aerodynamic loads on the tower, the aerodynamic loads on the rotor, and the mass-related rotor loads, including gyroscopic effects. These simulated loads were applied at the top of the tower on the model using a cable-driven parallel robot (CDPR). The real-time hybrid model testing approach employed by Thys et al. allowed for the integration of physical and numerical subsystems to accurately replicate the behavior and loads of the floating wind turbine. The use of the CDPR facilitated the application of the simulated loads on the model.

The model tests conducted in this study provide valuable insights into the performance and behavior of the INO WINDMOOR 12 MW floating wind turbine. The combination of real-time simulation and physical testing enables a comprehensive understanding of the aerodynamic loads and response of the turbine system.

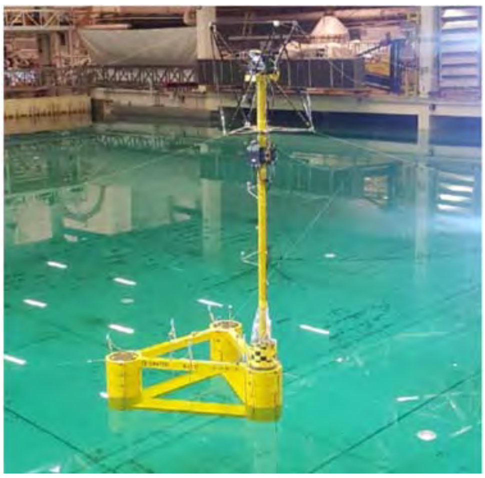

Figure 84: The layout of the hybrid model tests at a scale of 1:40 (Thys et al., 2021)

Cinello et al. (2022) introduced a real-time hybrid modeling technique that combined real-time numerical simulations with basin model tests. The technique was applied to a floating offshore wind turbine, and the study aimed to compare different modeling assumptions and experimental setups. Figure 85 depicts the basin model test setup used in the study. To emulate the thrust load in real-time, the real-time hybrid modeling technique was employed, as illustrated in Figure 86. Initially, basin tests were conducted using a single fan and a numerical model of the turbine with rigid blades. These tests served as a baseline. In the second set of tests, improvements were made. On the experimental side, a dual-rotating fans system was implemented. On the software side, the influence of blade flexibility was incorporated into the numerical model. By incorporating these enhancements, the study aimed to investigate the impact of blade flexibility on the performance of the floating offshore wind turbine. This allowed for a more accurate representation of the turbine behavior in the real-time hybrid modeling approach.

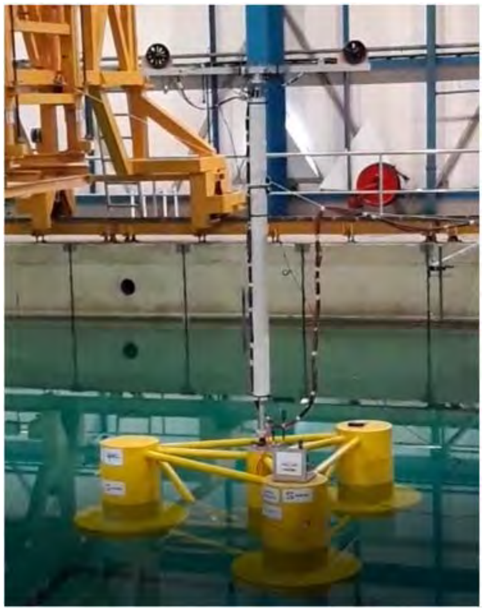

Figure 85: Model in the BGO FIRST basin (Cinello et al., 2022)

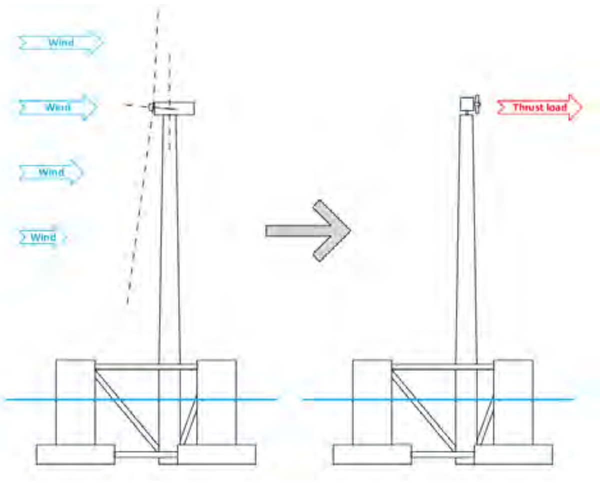

Figure 86: Thrust load emulation (Cinello et al., 2022)

Somoano et al. (2021) analyzed the accuracy of a large-scale experimental testing procedure in an ocean basin facility using real-time hybrid model testing (ReaTHM) techniques. Figure 87 illustrates the ReaTHM setup employed in the study. The analysis was based on a scaled concept for a 15 MW floating offshore wind turbine (FOWT) supported by a concrete semi-submersible platform known as ActiveFloat. This concept was developed within the framework of the COREWIND project. The real-time hybrid model used in the study included a multi-fan system located at the aero-rotor interface. This system allowed for the generation of aerodynamic loads, helping to mitigate the limitations typically associated with scaled models. By utilizing the ReaTHM techniques, Somoano et al. aimed to assess the accuracy of the experimental testing procedure for large-scale floating offshore wind turbines. The analysis focused on the performance and behavior of the scaled concept, specifically the interaction between the FOWT and the concrete semi-submersible platform.

The study by Somoano et al. (2021) provides valuable insights into the accuracy and limitations of large-scale experimental testing procedures for floating offshore wind turbines. The use of real-time hybrid model testing techniques, combined with the multi-fan system, enhances the understanding of the performance and behavior of these systems, ultimately supporting the development and optimization of floating offshore wind turbine technologies.

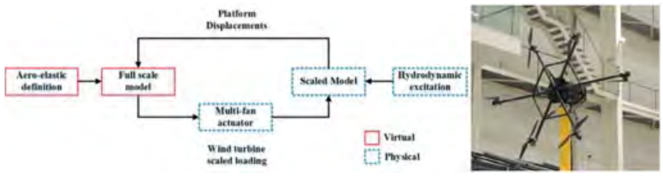

Figure 87: HIL scheme implementation and an overview of the multi-fan actuator system (Somoano et al., 2021)

Ransley et al. (2022) presented a real-time hybrid testing strategy that employed a feedback loop to emulate the aerodynamic forces acting on a floating offshore wind turbine (FOWT) system. The strategy was applied to a 70th-scale IEA Wind 15 MW reference wind turbine mounted on a version of the VolturnUS-S platform, as depicted in Figure 88. Unlike other similar methods, which directly simulate the aerodynamic loads using an aerodynamic code running in parallel with the experiment, this strategy utilized a surrogate model trained on numerical model data calculated in advance. This approach allowed for the inclusion of high-fidelity numerical model data or even physical data in the aerodynamic emulation, without the need for real-time simulation. By employing the feedback loop, which consisted of an onboard fan and a control algorithm, the strategy enabled the emulation of accurate aerodynamic forces on the FOWT system. The surrogate model, trained on pre-calculated numerical model data, facilitated improved loading predictions in the experiments.

This real-time hybrid testing strategy presented by Ransley et al. (2022) offers a novel approach to emulating aerodynamic forces in FOWT systems. By incorporating a surrogate model trained on numerical model data, the strategy allows for more accurate loading predictions without the need for real-time simulation. This approach has the potential to enhance the accuracy and reliability of experimental testing for FOWT systems and support the development and optimization of these technologies.

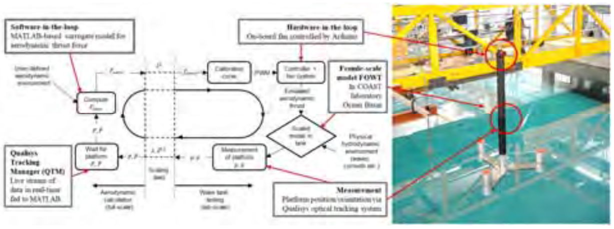

Figure 88: Real-time hybrid testing workflow and layout of hybrid model tests (Ransley et al., 2022)

4.3.4 Comments and recommendations

Indeed, both propeller systems and cable actuators have been used successfully to replicate the thrust force in hybrid testing. However, there are some challenges associated with using propellers to reproduce the aerodynamic moment, as highlighted by Otter et al. (2020). It can be difficult to accurately consider the propellers' torque in the force allocation process, as pointed out by Hmedi et al. (2020). On the other hand, cable actuators are capable of reproducing moments effectively. However, controlling the cables can be more complex compared to propellers. Additionally, the cable's frame requires a larger space on the top of the tower, unlike propellers, which occupy smaller space. It is worth noting that the pretension of the cables can slightly affect the results of free decay tests, as mentioned by Sauder et al. (2016). In contrast, conducting free decay tests with propeller actuators turned off is simpler. These considerations highlight the trade-offs and challenges associated with choosing between propeller systems and cable actuators in hybrid testing, depending on the specific objectives and constraints of the study.

Propellers, due to their high rotational speed, can introduce unwanted vibrations to the model being tested. In contrast, cables tend to induce fewer vibrations, making them a more desirable choice in terms of minimizing vibrations in hybrid testing setups. Another important consideration when using propellers is the temperature of the active emulator. It is crucial to monitor and control the temperature to avoid overheating and potential damage to the propeller's electrical motor or demagnetization. In multi-actuator systems with propellers, it is essential to take into account the interaction between the propellers when tuning them. The wakes generated by adjacent propellers can modify the air inflow of other propellers, leading to changes in their performance. This wake interaction effect can result in performance variations of up to 10%, as highlighted by Urbán et al. (2020). These factors emphasize the need for careful attention to vibration control, temperature management, and wake interactions when using propellers in hybrid testing setups. Alternatively, cable actuators can provide a smoother and less problematic solution in terms of vibrations and temperature management.

The selection of hybrid testing in a wind tunnel or a wave basin depends on the specific phenomena being investigated. If the primary focus is on studying wakes and the interaction between turbines, hybrid testing in wind tunnels is more appropriate. Wind tunnels allow for the replication of wind conditions and the observation of wake behavior and turbine interactions. On the other hand, if the objective is to study hydrodynamics, such as the behavior of floating platforms, hybrid testing with propellers or cables in wave basins is preferred. Wave basins provide a controlled environment for studying the effects of waves and water on the platform's performance. When thrust loading is the dominant load being considered in the tests, a single propeller or a ducted fan is recommended. These setups accurately replicate the thrust forces experienced by the platform. For analyses that require the consideration of aerodynamic and gyroscopic moments, a multi-cable winch system is more suitable. This system allows for the emulation of these moments and provides a comprehensive analysis of the platform’s behavior.

In summary, the selection of the appropriate hybrid testing setup depends on the specific phenomena being studied, the dominant load being considered, and the desired analysis objectives.

4.4 Benchmark Test Program for Cyber-Physical Hydrodynamic Testing Involving Wind Loads

The specifications for a benchmark test program for wind loads and their influence on the motions of floating structures are developed as follows. It aims to compare the wind loads developed using SiL to model the wind loads versus using fans to produce an actual model scale wind. Among other data, repeatability, and consistency between the methods and between different facilities should be reported if the test is carried out by voluntary participants within the 31st ITTC at different facilities following the specifications. The benchmark study may also include CFD comparisons.

(1) Background

A major issue related to hydrodynamic testing complex structures exposed to wind is the Froude-Reynolds scaling conflict, which prevents accurate modelling of aerodynamic loads in hydrodynamic laboratories. This issue concerns particularly floating wind turbines (Martin et al., 2015) or sail-assisted propulsion of ships.

Cyber-physical testing is a method that alleviates this issue by combining numerical simulations with experimental testing in real time (Azcona et al., 2014; Sauder et al., 2016). A physical model located in a hydrodynamic laboratory interacts in real-time with a simulator computing the wind loads. An actuator applies these loads on the physical model. Motions are recorded and fed back to the simulator, creating a closed-loop system.

The actuator can take the form of an individual winch, a cable-driven parallel robot (several winches acting in parallel on the floater), a single fan, or a multi-rotor platform.

The wind load simulator can be based on a set of wind coefficients (relevant for e.g. topside), or a more complex numerical model such as lifting line (for sail-assisted propulsion) or blade element momentum theory (for floating wind turbines).

(2) Test objectives

The present benchmark aims at assessing and ensuring the quality of cyber-physical testing of floating structures subjected to wind loads that are generated numerically and applied with actuators. The benchmark targets the hardware and low-level software components of the laboratory setup.

The benchmark will employ a floating wind turbine model, but for simplicity, the wind loads will be considerably simplified compared to realistic rotor loads.

Important remark #1: The present benchmark does not address the *validity of the numerical model* used to generate the wind loads as it is strongly application-dependent.

Important remark #2: Purely *physical* solutions to apply wind loads, that rely on laboratory-fixed fans generating a wind field are not part of the scope of the present benchmark,

(3) Physical model

The open floating wind turbine design INO WINDMOOR 12MW , fully described in (Souza et al., 2021), is used as an object for benchmark. This report is available online and contains a full description of the model properties.

Main particulars for the floater are repeated here for convenience:

- Column diameter (m) 15.0
- Column height (m) 31.0
- Column Center-Center distance (m) 61.0
- Draught (m): 15.5
- Deck height above waterline (m): 15.5
- Pontoon width x height (m) 10.0 x 4.0

- Deck beam width (m) 3.5
- Deck beam height (m) 3.5
- Mass floater (t) 11974.0
- Total mass (t) 14176.0

See (Souza et al., 2021) for a complete definition of the floater and tower dimensions and inertia.

Figure 89: Open INO WINDMOOR 12MW concept. Courtesy Inocean.

A scale of 1:40 should preferably be employed for the model. Only full-scale values are provided in the following.

Water depth should preferably be 150m. If not feasible, at least 75 m which will ensure deep water wave kinematics.

The platform shall be moored as indicated in the report with a horizontal mooring attached to the column top and suspended over the water surface (as to generate a minimum amount of damping). The restoring from the mooring shall be 102.0 kN/m, 98.3 kN/m and 5204 kNm/deg in surge, sway and yaw respectively.

Nautral periods targets are 97.3s 98.0s, 16.3s, for the surge, sway and heave motions, and 29.5s, 31.4s, and 88.0s for the roll pitch and yaw motions.

Unless otherwise mentioned, loads generated by the actuator shall be applied at the location of the tower top, that is 125.7m above water line (i.e. 110.20m over deck).

(4) Coordinate systems

Notations consistent with (Souza et al., 2021) are used. The XYplane of the, Earth-fixed coordinate system coincides with the mean water level, and the Z-axis is positive upwards. A *local* coordinate system is also defined. Its origin is at mean water level and over the platform's horizontal geometric center is also defined. This system is fixed to the body and translates/rotates along with the body.

Loads to be applied by the actuators are provided in the *local* coordinate system.

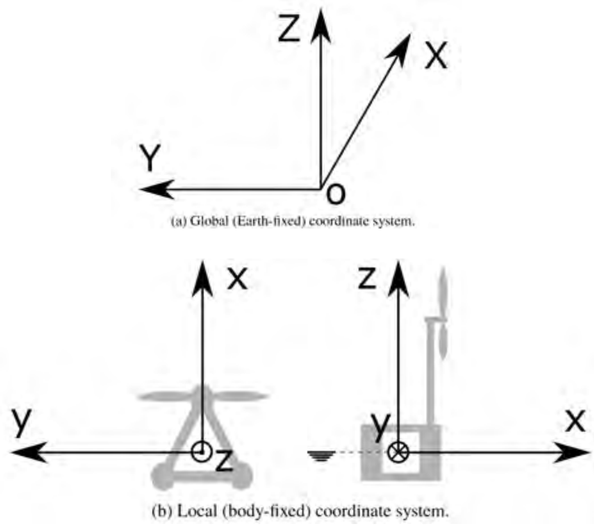

Figure 90: Global and local coordinate systems

(5) Waves

Waves propagate in the negative X-direction.

For the purpose of the benchmark, a wave that follows a JONSWAP spectrum with Hs=6.19m Tp=12.0s gamma=1.23, shall be calibrated. An example of wave spectrum / time series is provided as an electronic appendix to the present document. The wave shall last at least one hour at full-scale.

The calibration point shall be the equilibrium position of the model in the basin when no external loads are applied.

(6) Wind load model

Three reference wind spectra / velocity time series are provided as an electronic appendix to the present document. They correspond to uniform but time-varying turbulent wind with mean velocities 8 m/s, 11.5 m/s and 25 m/s at a height of 131.7m (slightly above tower top), Kaimal spectrum, with turbulence intensity of 0.166, 0.133 and 0.106, respectively.

The wave and wind realizations shall be synchronized such that they start at the same time and do not drift with respect to each other.

Depending on the case, wind will propagate either in the negative X- direction, or with 45 degrees offset from that direction such that it has a positive mean Y-velocity component.

The relative wind velocity at tower top and in the local coordinate system Ur=(Ur,1,Ur,2,Ur,3) (3 components) shall be computed at all times. It is the vector difference between the (undisturbed) incoming wind and the tower top velocity (estimated by the laboratory).

The modulus of the relative wind velocity, and its direction in the plane orthogonal to the tower are defined by Uw = |Ur| and hangle = atan2(Ur,2,Ur,1)

The relative velocity shall be combined with the thrust curve provided below to compute the thrust generated at tower top.

The surge load shall be F1=Thrust * cos(hangle)

The sway load shall be F2=Thrust * sin(hangle)

The heave load shall be null F3=0

We recall that these loads are given in the local coordinate system.

A positive moment *about the tower top* should be applied based on the torque curve provided in the figure above.

Roll moment M4 = Torque (positive)

Pitch moment shall be null M5 = 0

Yaw moment shall be null M6 = 0

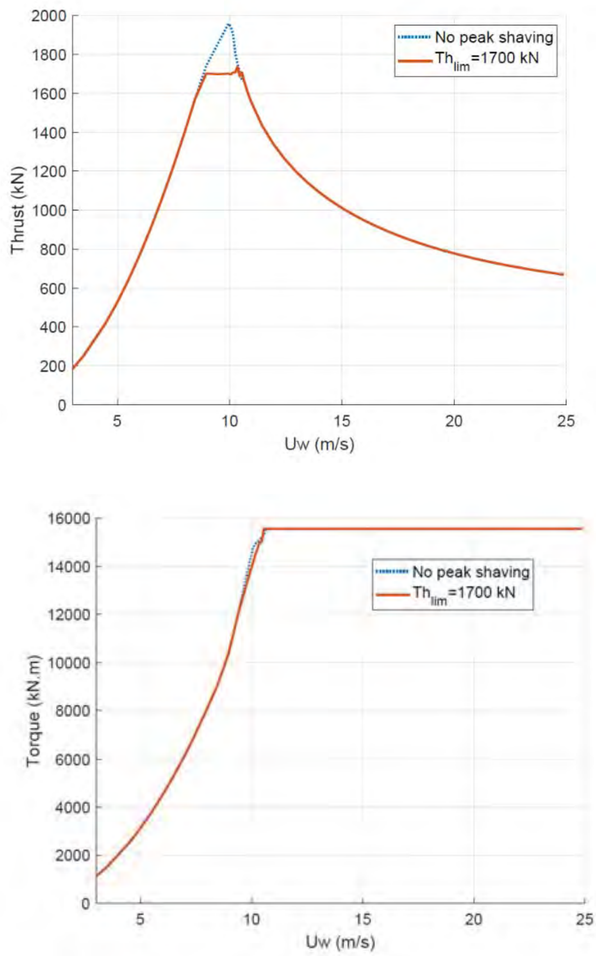

Figure 91: Wind loads vs relative wind velocity

(7) Instrumentation and data acquisition

The following quantities shall be recorded for all the tests, at the minimum sampling frequency given between parentheses (model scale):

- 6 degrees of freedom motions of floater (100 Hz.)
- 3-components accelerations at tower top (200Hz)
- Wind velocity, computed relative velocity, and 6 components of the computed loads to be applied to the model (200Hz).
- 6 component of the loads actually applied from the actuator to the model (200Hz), including those not controlled by the actuator.
- Wave elevation in the basin at calibration point, and at another location kept constant during calibration and testing (100Hz)

No filtering shall be applied except anti-aliasing filter.

(8) Test matrix

The following tests shall be conducted by order of priority.

Wave calibration/documentation (1 test)

Prior to placing the model in the basin, the wave described above shall be calibrated.

Excursion and decay tests (6+6 tests)

Actuator shall be deactivated.

Excursion tests (up to 30m surge/sway and 30deg yaw offset) shall be performed to verify the stiffnesses provided above.

Decay tests shall be performed to ensure that natural periods match the targets above. Initial offsets shall be at least 10m for surge and sway, at least 6 degrees for roll/pitch, and 10 degrees for yaw.

Chirp tests in calm water (2 tests)

Chirp tests consist of applying a constant amplitude load centered on 0 N, at an increasing frequency ranging from range [0, 1 Hz] full scale (that is about [0, 6.5Hz] at scale 1:40). The duration of the chirp shall be at least 100s.

Two load directions should be tested, first surge, then sway. They will induce a pitch and roll moment about tower base, respectively.

The load actually applied by the actuators should be measured and compared to the desired load.

Free decay with actuators activated in "zero-load" mode. (6 tests)

This test is not relevant for e.g. fan- or multi-rotor-based actuators as deactivating the actuator will have the same effect as activating them with zero load.

This benchmark consists in free decay tests, where the actuator shall be activated while applying zero net load on the floater.

The initial conditions for the decays shall be as close as possible to the ones performed without actuator connected. This force shall be suddenly removed, triggering a free decay.

Motions time series, natural periods and damping ratios for the excited degrees of freedom should be compared to the free decays performed without actuator.

Free decay in pitch with constant wind velocity (3 tests)

Free decay tests in pitch shall be performed in three *constant* wind velocities 8m/s, 11.5m/s and 25m/s. At least 5 degrees of additional pitch as an initial condition

Wave only tests (1 test)

Actuators shall be deactivated. The model shall be exposed to the calibrated wave.

Wave tests with actuators activated in "zero-load" mode (1 test)

This test is not relevant for e.g. fan- or multi-rotor-based actuators as deactivating the actuator will have the same effect as activating it with zero load.

In this benchmark test, the actuator is bound to apply zero load, but this time the motions of the floater are triggered by the wave.

Motions time series measured during these tests should be compared to these measured during a test involving the same wave.

Wind only tests – aligned conditions (3 tests)

The model shall be exposed to the turbulent winds with velocities 8m/s, 11.5m/s and 25m/s.

Wave tests with constant thrust force (2 tests)

The model shall be exposed to the wave, and the actuators should generate a constant thrust force of 1600kN, first along the surge direction. Then the test shall be repeated with the thrust force acting along the sway direction.

The load actually applied by the actuators should be measured and compared to the desired load.

Wind and wave tests – aligned conditions (3 tests)

The model shall be exposed to the wave and to the turbulent winds with velocities 8m/s, 11.5m/s and 25m/s. Wind and wave directions are colinear.

Wind/Wave tests – misaligned conditions (3 tests)

The model shall be exposed to the wave and to the turbulent winds with velocities 8m/s, 11.5m/s and 25m/s. Wind direction makes a 45 degrees angle with the wave.

Wind tests with large changes of wind direction (1 tests)

The model shall be exposed to turbulent wind with mean velocity of 11.5m/s. The *wind direction* (*not* force direction) shall be varied as the following function of time: windDir = 90deg * abs(sin(2*pi/120 * t)) such that the wind rotates by a quadrant in a minute at full scale.

Wind tests with additional yaw moment (1 test)

The model shall be exposed to turbulent wind with mean velocity 11.5m/s and direction 0 degrees. However an additional positive yaw moment shall be applied equal to the (time varying) thrust force x 20m.

(9) Data analysis

A short memo including pictures should summarize the test setup. The actuator system should be described. It should be in particular stated how many load components are controlled.

Results shall be reported at full-scale, using Froude scaling. The scaling of loads shall include the ratio between the specific weights of sea water and fresh water in the basin ($\gamma_w \approx 1.025$).

4.5 State-of-the-art for Wave-Current Interactions

SC on Modelling Environmental Conditions of the 28th ITTC presents mostly a review of current generation in experiments with only few studies related to wave-current interactions. For the 29th ITTC, the issues associated with an accurate and reliable measurement of current in the field are pointed out. A set of model scale experiments coupled to the corresponding nonlinear simulations analyze the effect of current on extreme wave occurrence (Toffoli et al. (2019)). The effect of current on breather-type solutions is also studied experimentally (constant current) and numerically with a linear shear.

Ducrozet et al. (2021) discuss the dynamics of unidirectional random wave fields that propagate against an opposing current through laboratory experiments and direct numerical simulations of the Euler equations solved with a high-order spectral method. Both approaches demonstrate that the presence of a negative horizontal velocity gradient increases the probability of the occurrence of extreme and rogue waves in the course of their propagation with the emergence of a rapid transition from weakly to strongly non-Gaussian properties. Numerical simulations capture quantitatively well the statistical properties of laboratory observations and substantiate that underlying physics are associated to quasiresonant nonlinear interactions triggered by the background current.

Zhou et al. (2024) investigate numerically the impact of uniform currents on nonlinear characteristics of double-wave-group focusing. The analysis was carried out by a fully nonlinear numerical wave–current model established based on the high-order spectral method. Different current speeds covering strongly opposing current, weekly opposing current as well as following current were considered. Seastates with sea-swell energy equivalent are selected to study the influence of uniform current on focused double wave group. Among other interesting conclusions, the study reveals that, for bimodal waves, the asymmetries of the wave crest and that of the wave envelop influenced by the currents are not synchronous, unlike the case of unimodal waves.

Nguyen et al. (2020) describe the design of a recirculating wave-current flume as well as the methods used to obtain such design, taking into consideration the different constraints in the project.

Zheng et al. (2023) study numerically the statistics of weakly nonlinear waves on currents with strong vertical shear. A unidirectional irregular sea state following JONSWAP spectrum is studied with different vertical current profiles. It is found that that opposing vertical shear leads to increased wave height and skewness while a following shear has opposite effects. This supports the need to account for shear current in wave modelling.

Regarding the importance of including shearing current in wave-current interaction analysis, Soffer et al. (2023) discuss the effects of shearing current on the estimation of wave direction from data collected by measurement devices such as buoys, pressure gauges and acoustic Doppler current profilers. The authors numerically generated data for a predefined spread and then processed the data based on potential irrotational flow theory (i.e. not accounting for the rotational shearing current). The analysis shows significant errors in estimation of wave directional spread. An approach is proposed for estimating the directional spectrum accounting for wave-shearing current interaction.

Ellingsen et al. (2024) studied the evolution and kinematics of dispersive focusing of a waves' group atop a shearing current, considering linear theory. They derived analytical approximate relations assuming long crested linear waves and different current profiles (e.g., current varying with depth linearly and exponentially etc.) with arbitrary angles between them. The analysis shows that while the shear current has modest effect on the evolution of the wave group's envelop, it affects the individual crests and troughs rising and falling inside the group. They show that shearing currents change wave kinematics significantly and highlight the importance of considering current profiles in maritime operations.

Wang et al. (2021) present a numerical study on the properties of extreme waves in directional seas subjected to current in different directions. For the waves with strong nonlinearity, the nonlinear wave-current interactions have significant impacts on the wave statistics and spectral properties. Main elements are: i) enhancement of the tail of the wave crest probability of exceedance and kurtosis with a maximum effect at 135°, ii) broadening of the spectra for angles larger than 110° iii) large asymmetry in vertical and horizontal direction induced by the current and iv) at fix incident angle, effect is more pronounced for steeper wave conditions.

Zhang et al. (2023) conducted an experimental study of propagating unidirectional irregular waves with following current over a varying seabed resembling coastal areas with ambient currents. The results show that an accelerating following current can increase the freak wave occurrence. In the experiment, the incident irregular waves were generated following the JONSWAP spectrum. The current was uniform in the vertical direction but due to the presence of a submerged trapezoidal bar, the current speed was varied in the horizontal direction. The results indicate that a following current entering a shallow-water area can increase the probability of freak waves. The effect is related to non-equilibrium dynamics induced by inhomogeneity of the seabed and current field, while the modulation instability is considered to be insignificant.

For nearshore areas, a review of the state of research in the interaction of waves and currents is provided in Zhang et al. (2022). In this field, the concern is more associated to turbulent currents with possible applications to sediment transport or dispersion of pollutants. The review proposes an overview of experimental and numerical investigations with a synopsis of advantages and limitations of previous studies.

5. STATE-OF-THE-ART IN OFFSHORE AQUACULTURE SYSTEMS

The state-of-the-art in offshore aquaculture systems was reviewed based on the articles since the 2021 report of the Ocean Engineering committee including large volume closed containment systems, extreme wave environments, and modelling of entire systems.

Aquatic products are one of the main sources of food in the world. According to a survey reported by the Food and Agriculture Organization (FAO, 2018), aquaculture production has increased significantly in the past few decades.

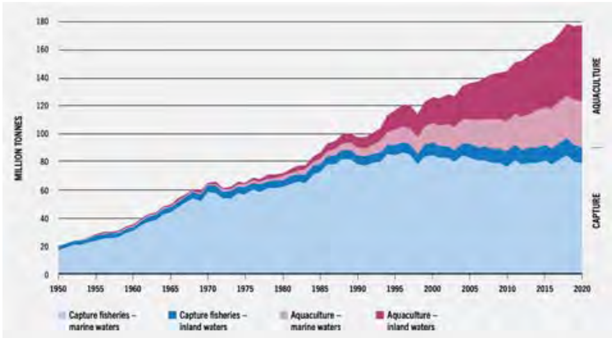

Figure 92: World capture fisheries and aquaculture production (FAO, 2022).

Although most of the aquaculture products are still farmed inland, the portion of marine and coastal cultured seafood has increased rapidly (FAO, 2018). With the expansion of the nearshore fisheries, conflicts have appeared in some aspects such as shipping, tourism, and recreation (Tidwell et al. 2012; Shainee et al., 2013;). Marine fish farming should move towards offshore regions to pursue more space and better water quality.

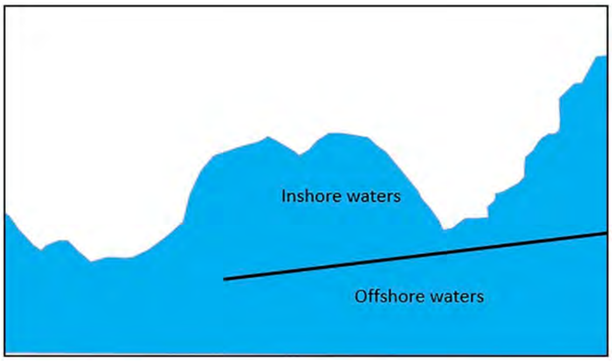

Figure 93: Definition of offshore waters according to Spanish law (Chu et al., 2020).

According to Chu et al. (2020), the definition of offshore fish farming should involve:

(i) unsheltered waters outside a straight line joining two major capes or promontories, at least about 3 km distance from the shoreline but still within the Exclusive Economic Zone (EEZ).

(ii) water depth that is larger than 50 m or larger than 3 times the cage height and no less than 15 m between the cage bottom and the seabed.

(iii) current speed ranging from 0.1 m/s to 1 m/s.

(iv) wave height exceeding 3m.

There is a variety of studies concerning the classifications or design analyses of offshore aquaculture systems. Relevant reviews can be found in Chu et al. (2023), Morro et al. (2021), and Fan et al. (2023). In the following, several dominant types of offshore aquaculture systems will be presented with examples emphasizing their advantages and disadvantages. The challenges and considerations for design and operation are also summarized concisely.

5.1 Classification

Offshore fish farms can be categorized based on their structural materials (rigid or flexible), shapes (spar, column, ship-shaped), or operating floating forms (floating, semi-submersible, and submersed). There have been some attempts at fish cage classifications by researchers or by the maritime communities (DNV, 2017; ABS, 2018; Chu et al., 2020). In this section, several representative types of offshore aquaculture systems are classified and presented with examples. A rigorous review of the classification can be referred to Chu et al. (2023).

5.1.1 Flexible cage system

Flexible cages are assembled mostly with floatable flexible elements. They were first invented in the 1970s and have been widely used in nearshore regions. Their buoyancy is mainly provided by floating pipes made of high-density polyethylene (HDPE). A series of brackets are applied to hold the pipes together to suspend the fish net (Cardia et al., 2016).

Typical examples of floating flexible cages are PolarCirkel (Figure 94 (a)), a plastic cage concept invented in Norway in 1974 using circular cages with circumferences of 60m to 240m, and Triton (Figure 94 (b)), developed by FusionMarine covering open sizes up to a circumference of 180 m.

(a) PolarCirkel fish cage

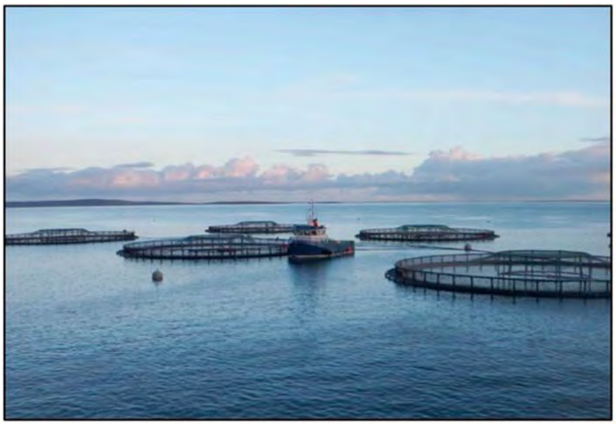

(b) FusionMarine fish cage

Figure 94: Typical examples of floating flexible cages

This kind of cage usually has a high resilience to wave forces (Zhang et al., 2022). The applied HDPE material can dissipate the wave energy and reduce surface wave forces by structural deformation. Besides, the material is easily-formed and has a high resistance to rotting and biofouling at a relatively low cost.

The cages are usually constructed inland and the towing and installation procedure is convenient.

The main problem of the floating flexible cages is that they might have severe deformations under very harsh waves or current actions, as shown in Figure 95. This limits their application in offshore regions with stronger wave energy. Apart from that, the feeding systems are usually difficult to be placed due to the waves, and large service vessels are thus necessary for the flexible cages.

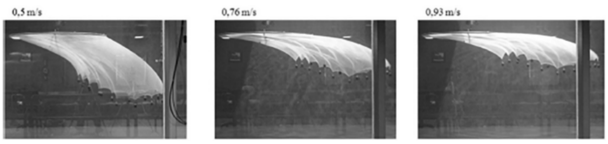

Figure 95: Deformation of flexible net cages subjected to high flow velocity (Moe-Føre et al., 2016)

One way to adapt flexible cages to deep seas is by utilizing a semi-submersible structure. The semi-submersible flexible cages are characterized by the capability to submerge during harsh weather to avoid the high-energy surface waves. Relevant examples can be shown in Figure 96, the Refa tension leg cage (TLC) concept, in which the buoyancy frame is held in place by mooring lines attached to the seabed.

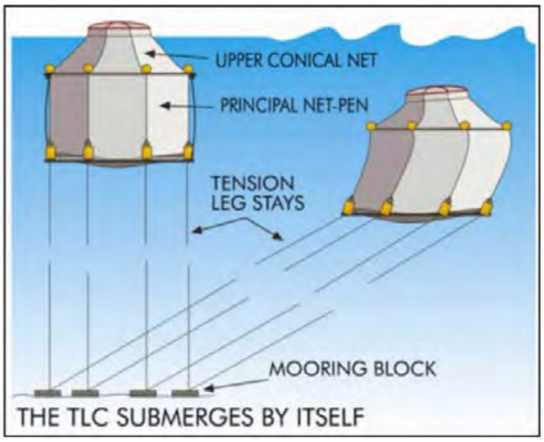

Figure 96: Semi-submersible flexible cage concept: Refa tension leg cage (TLC)

The concept can survive in very hazardous weather conditions. However, there are also concerns that a long period of submergence may affect the fish's welfare. Besides, it needs a sub-surface feeding system and the tension leg mooring systems might be difficult to be installed, especially on the soft seabed.

5.1.2 Ship-shaped cage system

Ship-shaped cage system belongs to the floating rigid cages and has been widely developed in recent years (Ma et al., 2023; Pang et al., 2023). A relevant example is shown in Figure 97. Instead of attempting to dissipate wave energy, this concept withstands waves by rigid structural components usually made of steel.

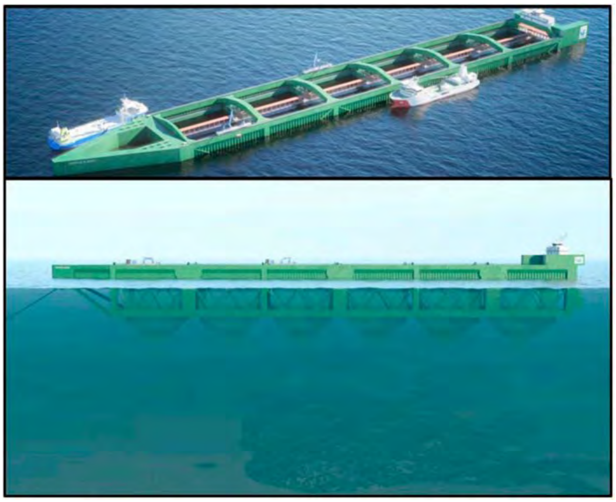

Figure 97: Ship-shaped farm Havfarm

Owing to their vessel-like shape, the cage system can be integrated with various operational and management infrastructures. Their transportation is especially convenient with enough fuel loaded. In addition, the construction and repair operation can be easily conducted in a conventional shipyard (Scott and Muir, 2000).

On the flip side, rigid cages might require large and heavy structures, which can be expensive and difficult to install. In operation status, the vessel-shape cage should be moored to be held in a settled station for the fish's well-being, which may not be easy due to their large mass.

5.1.3 Semi-submersible rigid cage system

Semi-submersible rigid cage has a similar structure to the traditional platforms utilized in the oil and gas industry. As shown in Figure 98, the cage is usually designed with a large-space rigid framework to restrict movement or volume change under external loads (Liu et al., 2021). The rigid framework makes it possible for the ballast adjustment and thus changes the draft under harsh weather.

(a) Shenlan 1

(b)Shenlan 2

Figure 98: Semi-submersible rigid cage (a) Shenlan 1 and (b) Shenlan 2

The semi-submersible rigid cage may provide the longest service life as has been validated by other traditional platforms. The rigid structure allows the installation of infrastructures, such as feeding systems, harvest cranes, and surveillance systems. Moreover, the cages can keep fish in a relatively stable place, where the volume of space is also maintained.

The disadvantage of such cages is that they requires extremely high capital costs. The structure should be rigorously analyzed during the design procedure to ensure safety in offshore operations. The towing and installation might also be difficult and regular maintenance should be planned in advance.

5.1.4 Submerged cage system

For a submerged cage system, the primary mode for normal operation is in a submerged position (Scott and Muir, 2000). Studies were carried out to investigate the health condition of salmon at long-period submerged positions (Dempster et al., 2008). Examples of submerged rigid cage designs are AquaPod (Figure 99a) and NSENGI sinking fish cages (Figure 99b).

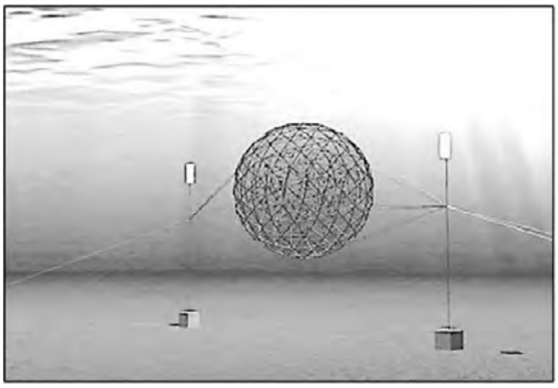

(a) AquaPod cage

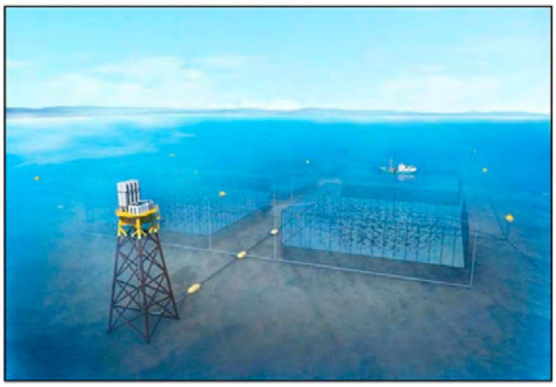

(b) NSENGI Sinking fish cage

Figure 99: Submerged cage system (a) AquaPod cage and (b) NSENGI Sinking fish cage

Submerged cages have the best responses to avoid strong surface waves and the effects of storms. The structural components can thus be less strong, which can save the capital costs significantly. The length of moored lines can also be reduced or even replaced by locating the cages on the seabed.

Their disadvantages are also distinct. Since the cages are normally submerged, regular operation and maintenance might be difficult to be performed due to the lack of visibility. Besides, if they are located near the seabed, the transportation of waste might be hindered, affecting the welfare of the fish.

5.1.5 Closed containment tank system

The closed containment tank system concept was developed to control the water quality (oxygen, temperature, and salinity) and the production process in the 1990s (Beveridge, 2004). An example of a floating closed containment tank is the egg-shaped fish farm developed by Hauge Aqua (Figure 100). The water quality and volume can be controlled, ensuring stable oxygen levels.

Figure 100: Closed egg-shaped fish tank developed by Hauge Aqua

The concept has the potential of achieving the best production rate because it can guarantee optimized physical parameters for fish welfare. By dividing the internal layers with external environments, the organic wastes and problems of predators are solved thoroughly.

The cost of optimized water quality is that the tank system requires an additional power supply system when it is deployed in offshore regions. In addition, the system might incur significant construction and equipment costs for monitoring and intervention. Another problem is that sloshing might occur and injure the fish inside (Cui et al., 2022).

5.2 General Design Considerations

Offshore fish farms are usually deployed at exposed sites with better water quality, larger spaces, and more energetic environments. The structures face several challenges that have not been recognized or considered thoroughly in previous studies. A general summarization would help provide confidence for the decision-making of fish farmers.

In the following some general design considerations for offshore fish farm systems are presented, relevant reviews can be referred to Chu et al. (2020), Zhang et al. (2023), and Fan et al. (2023).

5.2.1 Water depth and sea bed

Water depth has a direct influence on the capital cost of mooring systems. The cost for installation and maintenance increases proportionally with the length of mooring lines and is thus close related to the water depth. On the other hand, a smaller water depth might induce difficulties in the transportation of feed pellets and feces, which is harmful to the health of fish (Cardia et al., 2016). Therefore, the water depth is recommended to be over three times the cage height and to have at least 15 m between the cage bottom and the seabed (Chu et al., 2020).

The properties of the seabed in particular affect the anchor of the mooring system. A detailed seabed analysis should be performed to determine a suitable anchor method for the deployment of other submarine fiber optic cables, lines, or pipelines. A large water depth might induce challenges for the survey of seabed conditions.

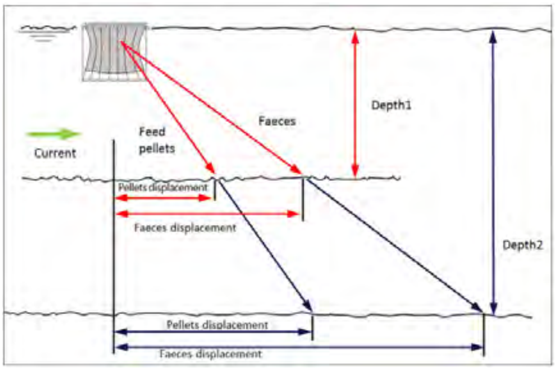

Figure 101: Influence of water depth on transportation of feed pellets and feces for fish cages (Cardia et al., 2016)

5.2.2 Wave action and storm incident

The wave energy in offshore sites can be stronger and more harmful to not only the structures but also the fish. The continuous severe wave actions can also hinder the regular operation of fish farmers.

One possible approach to control the wave actions is to employ breakwater systems (Dai et al., 2018). The systems were regularly used in coastal regions with their bottom fixed on the seabed. In offshore regions, floating breakwaters are more feasible but would require more techniques for their design and installation.

Another short-term strategy is to submerge the fish cages in very bad weather such as storms or typhoons. The submergence can help avoid the impacts of strong surface waves and guarantee oxygen in harsh weather. It also entails more efforts for the design and monitoring of the fish cages and requires consideration for the prediction of the sea state.

5.2.3 Current speed

Current speed is essential for fish farms because it ensures the replenishment of oxygen and the transportation of wastes. With moderate current flows, the fishes can swim in a similar natural status as in wild seas. However, a harsh current flow might cause extremely dangerous conditions for fish and structures.

The horizontal drag forces acting on the cages and mooring lines increase with the current speed, which can induce large deformations of the net and reduce the space and volume. The current speed inner the cages is reduced when using nets with high solidity, but it requires more strengthening for the cage design. (Moe-Føre et al., 2016).

5.2.4 Fish welfare

Fish farms are different from traditional offshore structures because they should ensure fish welfare. The welfare usually includes water temperature, salinity, dissolved oxygen, PH, turbidity and etc. (Pillay et al., 2004). The best water quality is species-dependent and should be considered before the structural design.

Moreover, to guarantee a healthy, abundant, and clean environment, infrastructures are required for routine operation and regular maintenance. Owing to the long distance away from land, water-based infrastructures should be developed and validated in practice to reduce the reliance on land-based supporting facilities (Chu et al., 2020).

5.3 Recent Challenges & Developments

Wang, H. et al. (2023) performed a series of physical experiments to investigate the hydrodynamic interaction between nets and the cylindrical supporting structure for some typical offshore aquacultural structures. The drag and lift forces of only the cylinder, only nets and combined cylinder-net structures under uniform inflow are measured and analyzed systematically. Results in this paper can be used to improve the design of fish farms and other relevant offshore structures by revealing the influence of the interaction between the cylinder and nets on their hydrodynamic characteristics, which is often ignored in present hybrid numerical models (by combining the potential flow theory, Morison and screen models).

Nasyrlayev et al. (2023) investigated the tensions on anchor lines of different arrangements of salmon fish cages under various environmental conditions, including strong currents and waves, by the FEM based AquaSim program. Three orientations (i.e., 2x2, 1x4 and 2x4 multi-cage fish farm), each with two sinker tube weights, were simulated for both current and current and wave loads and varying angles of attack. Through an extensive sensitivity analysis, the study provides insights into the range of possible mooring line loads for different configurations that could be valuable for the design and optimization of aquaculture mooring lines.

Cheng et al. (2021) investigated the effects of mooring line breakage on respectively a single-cage and a 1×4 multi-cage fish farm by conducting time-domain simulations using the program FhSim. Based on the simulations, a method is further developed to predict the maximum tension increment within the remaining mooring lines. The results indicate that structural collapses and fish escapes might occur with the breakages. Recommendations are proposed to improve the mooring design and monitor to prevent fish escapes.

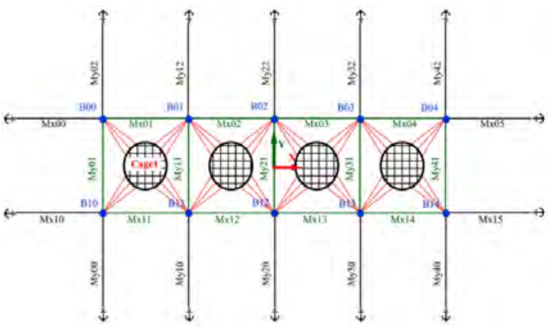

Figure 102: Top view of the 1 × 4 multi-cage fish farm (Cheng et al., 2021)

Cheng et al. (2022a) developed an open-source numerical library for the structural analyses of gravity-type fish cages under the toolbox Code_Aster. The library was then applied for time-domain simulations of gravity fish cages with various commonly-used physical parameters including depths, weights, collar circumferences, and current velocities. The study is valuable for structural optimization. Moreover, the toolbox Code_Aster is coupled with OpenFOAM by Cheng et al. (2022b) for the fluid-structure interaction analysis of submerged nets. The algorithm could handle the wake effects of thin, flexible, and highly permeable structures with complex geometries. The coupled method has been validated with published experiments for both fixed and flexible nets.

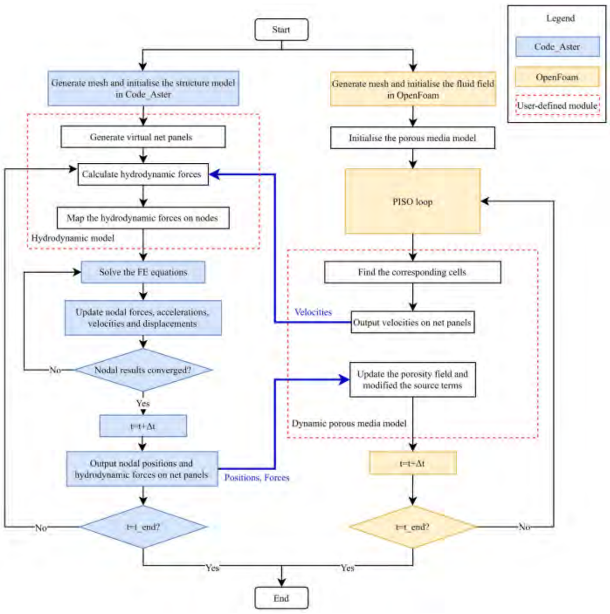

Figure 103: Flow chart of the coupled algorithm (Cheng et al., 2022b)

Sim et al. (2021) investigated the influences of multi-cage interactions on the response of the fish farm. The time-domain simulation program FhSim is employed to model the mooring tensions, drag force, and cultivation volume of each cage in a full-scale 4 × 2 multi-cage fish farm. It is found that the wake effects can overestimate the total drag force of the eight cages and underestimate the total cultivation volume, indicating that wake effects can be significant for a multiple-cage system.

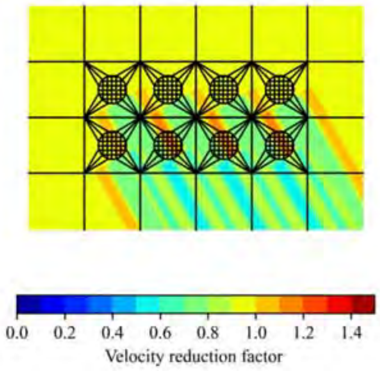

Figure 104: Flow field around the fish farm for illustration of cage-to-cage wake effects (Sim et al., 2021)

Ma et al. (2021) developed a semi-analytical model for the wave field description around a single gravity-type cylindrical open fish net cage. The fish cage net is modeled as a flexible porous membrane while the net chamber is modeled by the transverse vibration equation of strings. The velocity potential is expanded in the form of the Fourier–Bessel series based on the small-amplitude wave theory. The model was employed to investigate the effects of several important design parameters on hydrodynamic actions of the net cage by parametric studies (Ma et al., 2022a). It is concluded that increasing the net porosity and flexibility can alleviate the hydrodynamic actions and wave scattering.

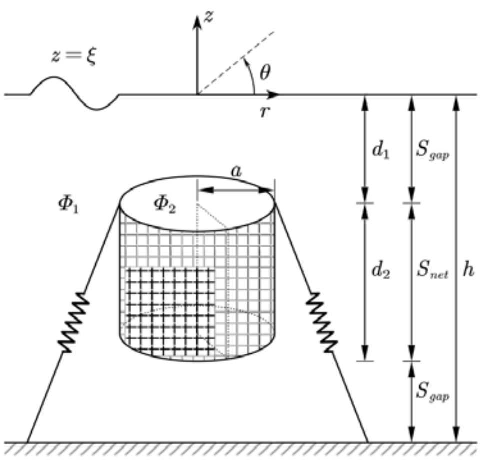

Figure 105: Side view of a cylindrical net cage submerged in a finite water depth (Ma et al., 2021)

The developed semi-analytical method was expanded by Ma et al. (2022b) to investigate the dynamic responses of an array of submersible flexible fish cages. The solution is expanded as a series of eigenfunctions in the local coordinate system of each cage based on the potential flow theory. The mean wave drift effect was also explored. It was found that the first-order wave force could vanish at a certain ratio of cage diameter to wavelength. These studies provide a benchmark for understanding the hydroelastic characteristics of multi-cage systems.

Zhao et al. (2021) analyzed the flow patterns inside and around a semi-submersible aquaculture platform by developing a method combining porous media and rigid walls. The fish nets and other mainframes are modeled by porous media and rigid wall conditions, respectively. The model was verified by experiments and the results indicate that fish nets play a vital role in the attenuation of flow velocity. In addition, the risk of resonance is found to increase when the frequency of the vortex shedding is close to the natural frequency of the structure.

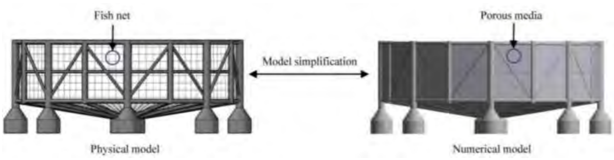

Figure 106: Model simplification of the semi-submersible aquaculture platform (Zhao et al., 2021)

Yu et al. (2023) presents an experimental and numerical study on hydrodynamic forces and mooring performance of an aquaculture platform with a regular hexagonal prism shape. The analysis was performed for both the operation draft as well as for the typhoon survival draft when the platform is fully submerged and sitting on the seabed. A spread mooring system with a hybrid mooring line composition, containing steel chain and fibre rope in each line, was designed and its performance was assessed.

Figure 107: Physical model of the floating aquaculture platform in operational (left) and extreme bottom-sitting (right) conditions (Yu et al. 2023)

Slagstad et al. (2023) proposed a simplified analytical model for the fatigue life prediction of aquaculture nets. The axial force is first estimated in the ropes supporting the fishnet, for which the hydrodynamic loads are calculated using a screen model. The results from the simplified calculations are compared to numerical simulations performed in RIFLEX. It is concluded that the simplified method is extremely efficient with acceptable accuracy. The model is of interest for the preliminary design of fish nets.

In a follow up work, Slagstad et al. (2024) further developed the model described in the previous paragraph and presented a simplified force response calculation for circular aquaculture nets in waves and current conditions. The basis for the method is a quasi-static solution calculated using the principle of virtual displacements. In the analysis they considered a cylindrical net connected to a steel frame inspired by fish farm facilities located in harsh environments such as Ocean farm 1. The method provides fast and simple estimates of the forces with good accuracy which is suitable for the design or optimization process.

Zhao et al. (2022a) performed an experiment study on a multi-body floating aquaculture platform to investigate the influences of coastal topography. In the experiment, the wave slamming of the net cage is captured and the wave breaking inside the cage becomes more evident if the incident wavelength is close to the width of the cage. It is concluded that the low-frequency component of the surge motion of the cage increases significantly under the influence of the sloping seabed while the vertical motions change slightly.

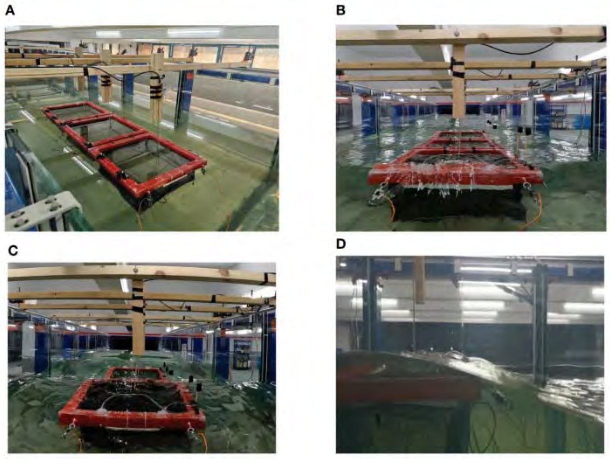

Figure 108: Physical model of the floating aquaculture platform: (A) model in the calm water, (B) wave slamming of the net cage, (C) wave reflection inside the cage, (D) completely submerged net cage (Zhao et al., 2022a)

Another experiment study was carried out by Zhao et al. (2022b) to verify a digital twin model for rapid detection of damage to a fixed panel. The model is developed based on the artificial neural network where the wave parameters and rope tensions are used as input while the intact and damaged states of the fishing net are considered as outputs. The model accuracy was ensured regarding different wave-current directions. Moreover, the model can accurately detect net damage when sea conditions and sensor data are not included in the training.

Miao et al. (2021) proposed a hybrid numerical method for the hydrodynamic performances of a semi-submersible offshore fish farm. The three-dimension dimensional potential theory, Morison's equation, and the screen model are employed respectively for the large pontoon, the frame system, and the net system. The method is validated against the experiment with good agreement. The developed codes were then used to investigate the effects of some key parameters on the motion responses, such as draft, wave height, and net solidity ratio.

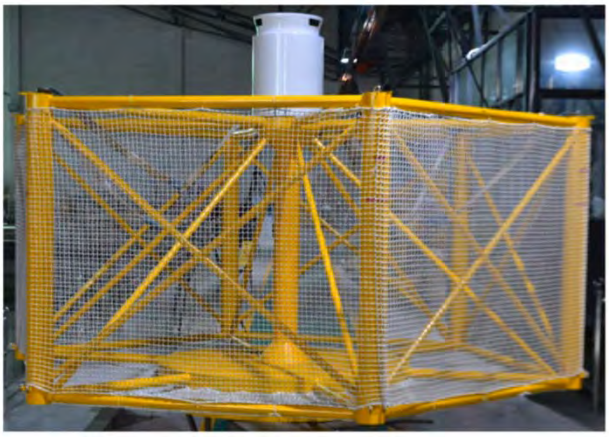

Figure 109: Physical model of the semi-submersible fish farm (Miao et al., 2021)

Wang et al. (2022) investigated the loads on a vessel-shaped fish cage based on the potential theory. The global hydrodynamic responses of the floating body are first calculated by the state-space method. Based on the time-domain simulations, velocity transfer functions are obtained and then their effects on the forces of the nets and steel frames are calculated by Morison equations. The internal loads of the main steel structures are calculated by employing a quasi-static method. The method was expanded to consider irregular load effects by Wang et al. (2023) and it is found that the diffraction and radiation waves make a significant difference in the twine tension and connector load effect.

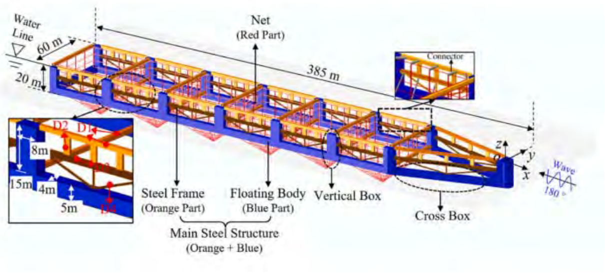

Figure 110: Model of the vessel-shaped fish cage (Wang et al., 2023)

The semi-submersible aquaculture platform "Pu Sheng 1" is the first marine breeding equipment in South China. The platform is equipped with photovoltaic power generation equipment, utilizing clean energy and ensuring its green and environmentally friendly operation. (Ding et al. 2023) conducted a numerical study of the hydrodynamic performance of this semi-submersible aquaculture platform with fully coupled analysis in OrcaFlex.

Figure 111: Semi-submersible aquaculture platform "Penghu" (Ding et al. 2023)

Shen et al. (2022) conducted a comparative analysis between a closed cage (CC) and a semi-closed/open-bottom cage (OC) to examine the similarities and differences of the hydrodynamic behaviors under wave actions. Experimental results show that the two cages have similar performance in surge motion, ovalizing deformations, interior wave elevation, and mean drift loads in shorter waves, which also indicates that the linear potential flow solver WAMIT can provide a reasonable prediction for OC in shorter waves. In addition, survival conditions are also considered for both cages where the platform freeboard is identified as the most critical parameter. The study provides a valuable reference for the experimental analyses of closed cages.

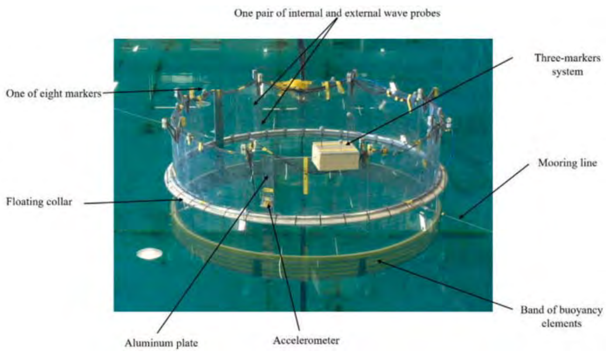

(a) Open-bottom cage

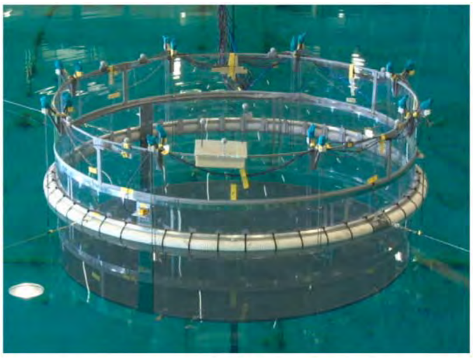

(b) Closed cage

Figure 112: Physical model for the (a) open-bottom cage and (b) closed cage (Shen et al., 2022)

Another experimental study was conducted by Wiegerink et al. (2023) focusing on the inner water surface of the floating closed fish tank. The study developed a slosh suppression block for mitigating sloshing in floating closed containment fish tanks. Different designs of suppression blocks are tested to investigate their effectiveness in mitigating sloshing considering the state of the internal fluid for fish well-being. Results show that slosh suppression blocks can effectively reduce the overall sloshing amplitudes, which makes it possible for deploying closed containment systems in offshore fish farming sites with higher energy.

Figure 113: Concept of a slosh suppression block applied to a cylindrical floating closed fish tank system (Wiegerink et al., 2023)

Dong et al. (2021a) experimentally measured the drag force, cage deformation, and flow field inside and around a scaled net cage model with different bottom weights in a flume tank. The cage is originally used to farm the Pacific bluefin tuna in Japan. A complex fluid – structure interaction is observed owing to the significant deformation of the flexible net cage. Later, a full-scale test involving a sea trial at a silver salmon farm site is conducted by Dong et al. (2021b), the drag force values of the full-scale net cage are lower than the converted values by model-scale experiments.

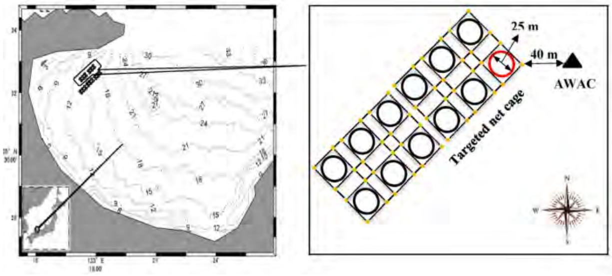

Figure 114: Layouts of the full-scale fish farm site for silver salmon (Dong et al., 2021b)

Chu et al. (2022) established a frequency-domain approach for motion analyses of an integrated offshore fish cage and wind turbine (named COSPAR). The frequency-domain analyses are first performed by ANSYS AQWA to obtain response amplitude operators (RAOs) for motions and mooring tension. Wind thrust was estimated by using a linearization method and incorporated in AQWA for the integrated analysis. The model is validated and it is concluded that COSPAR can provide a stable working platform for offshore fish farms subjected to wind, wave, and current loads. The pitch angles are also acceptable for wind turbine operation.

Figure 115: Integrated COSPAR fish cage and wind turbine (Chu et al., 2022)

Figure 116 shows an illustration of the FOWT-SFFC concept which combines a conic steel fish cage and a multi-megawatt wind turbine (Lei et al. 2024). OrcaFlex was used to perform a time domain analysis of the system responses to wind and waves and the results compared with model test data to calibrate the numerical model.

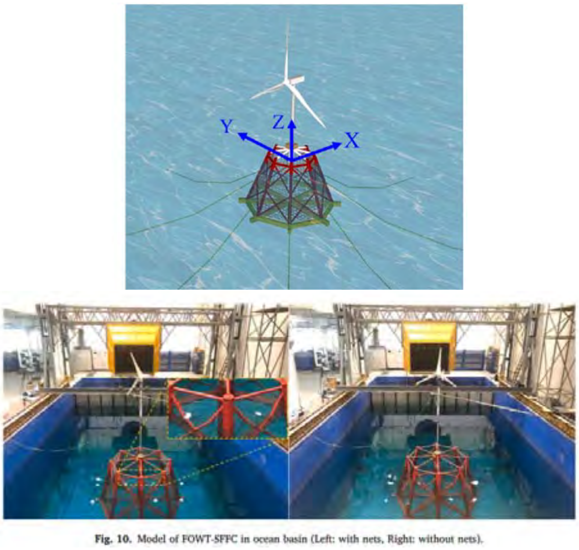

Figure 116: Top: FOWT-SFFC concept, bottom figure: model test setup with (left) and without nets (right) (Lei et al. 2024)

Another integrated concept was proposed by Li et al. (2023) using a jacket-supported wind turbine, named JOWT-SC. The depth of the closed cage can be changed to adapt to various waters and prevent fish from escaping. Time-domain simulations are conducted by the software SACS and the dynamic responses are compared with and without the fish cage. The results demonstrate that the aquaculture steel cage significantly influences the dynamic responses of the integrated JOWT-SC and the pile-foundation shear responses are more sensitive to the wave frequency.

One more integrated concept with fixed foundation was studied by Tu et al. (2023). The authors propose a design scheme for a multi-pile-support offshore wind turbine foundation integrated with an aquaculture net cage. The hydrodynamic analysis of the combined structure was performed to study the effect of the net on hydrodynamic loads on the foundation of the wind turbine. The analysis shows that the hydrodynamic loads on the structure increases while the natural frequency remained largely unaffected.

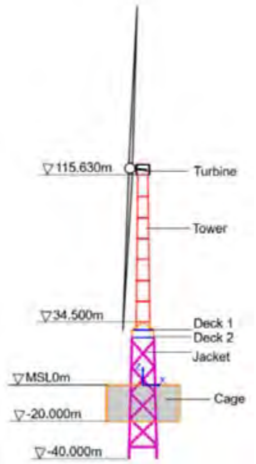

Figure 117: Design concept of the integrated JOWT-SC structure (Li et al., 2023)

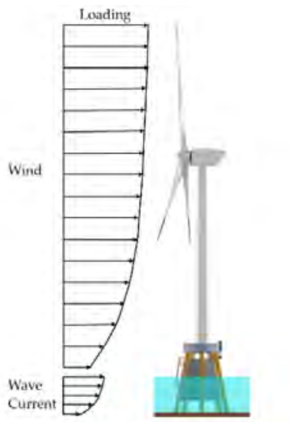

Figure 118: Model of an integrated offshore wind turbine with an aquaculture net cage (Tu et al. 2023)

Liu et al. (2022) investigated the feasibility of the idea to integrate an open ocean aquaculture ship with a NREL 5 MW wind turbine. A fully coupled analysis was performed with the turbine aerodynamic loads and responses calculation in FAST and hydrodynamic calculations in AQWA. Figure 119 shows the schematic sketch of the concept, where the internal turret mooring system installed at the bow aligns the wind turbine with the wind direction.

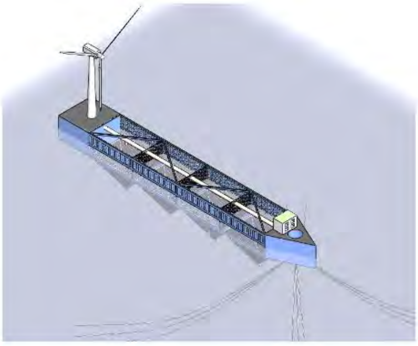

Figure 119: Integrate an open ocean aquaculture ship with a NREL 5 MW wind turbine (Liu et al. 2022)

Zheng et al. (2021) conducted a feasibility study of the wind-solar-aquaculture concept (WSA) that combines multi vertical-axis wind turbines (VAWTs) and solar panels with a steel fishing cage as the supporting substructure. A simulation package is developed to couple with WAMIT, OrcaFlex and validated against ANASYS under combined wind-wave actions. The results show that aerodynamic loads have greater influences on platform surge and pitch motions, tower bending moments and mooring tensions. The responses are further analyzed in the frequency domain to identify contributions from various environmental loads.

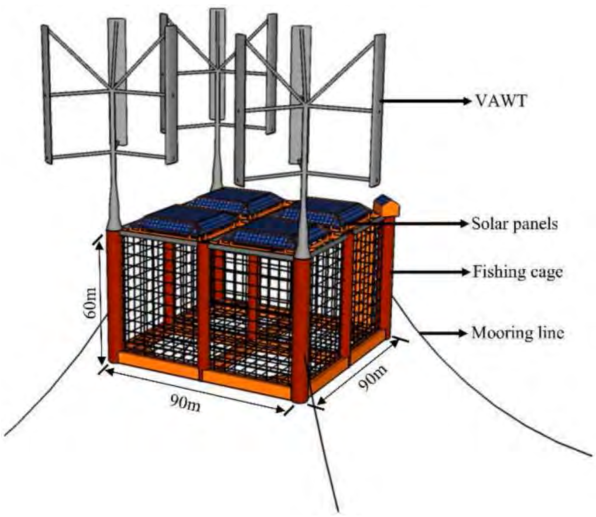

Figure 120: Concept of the wind-solar-aquaculture (WSA) system (Zheng et al., 2021)

6. EXTENDED EXPERIMENTAL WAVE RUN-UP BENCHMARK STUDIES --- FOUR SQUARED VERTICAL CYLINDERS

More experimental studies were conducted for four-column cases with more extreme waves such as focused waves, due to the complicated wave-column interactions. In addition, local wave impact loads on the columns are also critical and further in-depth studies were completed.

6.1 Experimental Program for Four-Squared-Cylinder System

The extended experiments for wave run-ups on fixed four-squared-cylinder systems with different configurations and extreme waves such as focused waves were carried out by SKLOE (State Key Laboratory of Ocean Engineering) of Shanghai Jiao Tong University. The benchmark data are summarized in the following sections.

A series of model tests on a fixed four-squared-cylinder array with focused waves were conducted in a wave tank at the State Key Laboratory of Ocean Engineering (SKLOE), Shanghai Jiao Tong University. As shown in Figure 121, the total length, width and depth of the wave tank were 300, 16 and 7.5 m, respectively. Multi-flap wavemakers were installed at one end of the tank to generate different types of waves, which were defined as the for wave-generation origin ($X = 0\,m$). A right-handed coordinate system O-XYZ used in this test is also depicted in Figure 121. The coordinate origin was set to the still-water level. The positive X-axis points towards the incident wave direction, and the direction of the Z-axis is vertically upward. Additionally, wave-absorbing beaches were installed to effectively eliminate reflected waves. One configuration of fixed four-truncated-square-cylinder system is considered, in which the half column breadth $a = 8$ m and the column spacing $b = 34$ m, respectively. The fillet radius of all columns is 3 m, the height of all columns is 60 m, and the constant draft is 20 m. The model scales are 1:50.

The column array was made of fibre reinforced plastic (FRP), which offers the advantages of lower density and adequate strength. The overall appearance of the physical model is displayed in Figure 122. During the test, the column array was installed on the external frame, with the upstream surface of the front column at 15 m ($X = 15\,m$) from the wavemakers.

There is a total of 35 different focused waves, as shown in Table 3, where A denotes the amplitude of focused wave, T is the spectral peak period, γ is the peak enhancement factor, T_f is the focus time point, x is the focus position, Δx is the forward distance of the focus position. The focused wave steepness was defined as H/λ, where λ and H are the length and height of a Stokes wave whose period is equal to the spectral peak period T. For a focused wave of given T and H/λ, the linear amplitude sum A was set equal to the crest elevation of the corresponding Stokes wave of period T and height H. The periods of wave components were uniformly ranged from 0.2s to 2.8s. The focus position of FW1 is at the front face of the front column. Based on original focused wave, other focused waves are obtained by shifting the focus position forward by a distance of Δx. In this way, waves with different degrees of breaking are obtained. Model tests were conducted by SKLOE for fixed four-squared-cylinder systems of two different wave direction as 0° and 45° (F1 series for 0° wave direction, F2 series for 45° wave direction, as shown in Table 4).

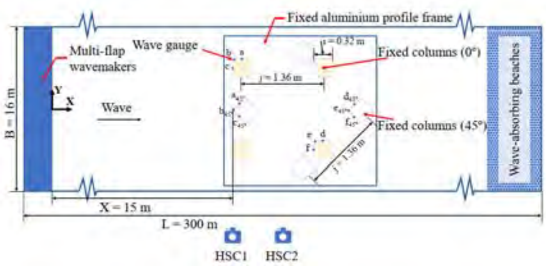

(a) Top view

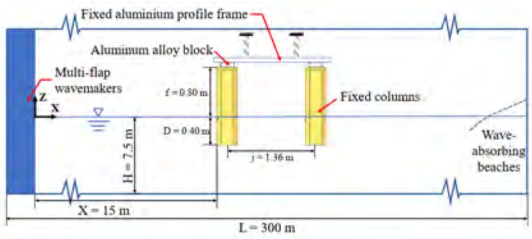

(b) Side view

Figure 121: Schematic of the experimental setup in the wave tank

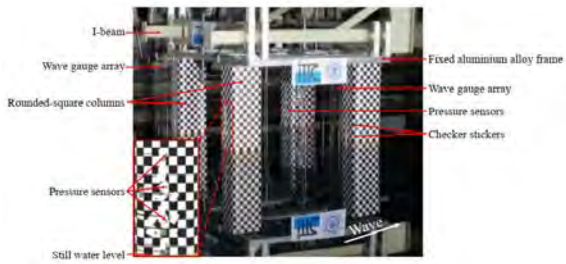

Figure 122: Overall appearance of physical model

Table 3: Environment matrix (focused waves)

Wave No.	Scale: 1:50						
	A (m)	T (s)	γ	T_f (s)	x m	Δx m	H/λ
FW1	0.3	2.4	2.5	40	15	0.00	0.07
FW2	0.27	2.3	2.5	40	15	0.00	0.07
FW3	0.25	2.2	2.5	40	15	0.00	0.07
FW4	0.235	2.0	2.5	40	15	0.00	0.08
FW5	0.21	2.0	2.5	40	15	0.00	0.07
FW6	0.21	2.0	2.5	40	15	-0.40	0.07
FW7	0.21	2.0	2.5	40	15	-0.20	0.07
FW8	0.21	2.0	2.5	40	15	0.32	0.07
FW9	0.21	2.0	2.5	40	15	1.36	0.07
FW10	0.21	2.0	2.5	40	15	1.68	0.07
FW11	0.19	2.0	3.3	40	15	0.00	0.06
FW12	0.16	2.0	3.3	40	15	0.00	0.05
FW13	0.16	1.5	2.5	40	15	0.00	0.09
FW14	0.14	1.5	2.5	40	15	0.00	0.08
FW15	0.12	1.5	2.5	40	15	0.00	0.07
FW16	0.12	1.5	2.5	40	15	-0.40	0.07
FW17	0.12	1.5	2.5	40	15	-0.20	0.07
FW18	0.12	1.5	2.5	40	15	0.32	0.07
FW19	0.12	1.5	2.5	40	15	1.36	0.07
FW20	0.12	1.5	2.5	40	15	1.68	0.07
FW21	0.11	1.5	3.3	40	15	0.00	0.06
FW22	0.09	1.5	3.3	40	15	0.00	0.05
FW23	0.11	1.2	2.5	40	15	0.00	0.10
FW24	0.1	1.2	2.5	40	15	0.00	0.09
FW25	0.09	1.2	2.5	40	15	0.00	0.08
FW26	0.08	1.2	2.5	40	15	0.00	0.07
FW27	0.08	1.2	2.5	40	15	-0.40	0.07
FW28	0.08	1.2	2.5	40	15	-0.20	0.07
FW29	0.08	1.2	2.5	40	15	0.32	0.07
FW30	0.08	1.2	2.5	40	15	1.36	0.07
FW31	0.08	1.2	2.5	40	15	1.68	0.07
FW32	0.07	1.2	3.3	40	15	0.00	0.06

FW33	0.06	1.2	3.3	40	15	0.00	0.05
FW34	0.055	1.0	2.5	40	15	0.00	0.07
FW35	0.035	0.8	2.5	40	15	0.00	0.07

Table 4: Test matrix

Wave No.	Case No. (Dir. 0°)	Case No. (Dir. 45°)
FW1	101	201
FW2	102	202
FW3	103	203
FW4	104	204
FW5	105	205
FW6	106	
FW7	107	
FW8	108	
FW9	109	
FW10	110	
FW11	111	211
FW12	112	212
FW13	113	213
FW14	114	214
FW15	115	215
FW16	116	
FW17	117	
FW18	118	
FW19	119	
FW20	120	
FW21	121	221
FW22	122	222
FW23	123	223
FW24	124	224
FW25	125	225
FW26	126	226
FW27	127	
FW28	128	
FW29	129	
FW30	130	
FW31	131	
FW32	132	232
FW33	133	233
FW34	134	234
FW35	135	235

The locations of wave probes are shown in Figure 123. The coordinates of wave probes are given in Table 5.

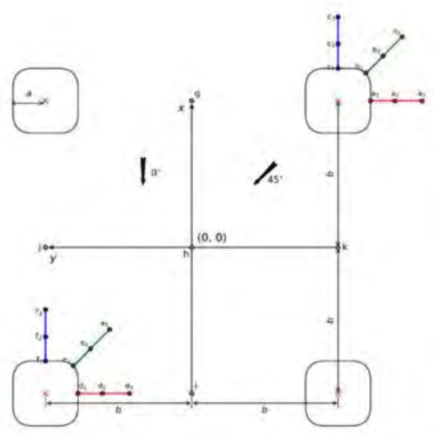

Figure 123: Locations of wave probes

Table 5: Coordinates of wave probes

Scale: 1:50		
	x (m)	y (m)
a_1	0.6800	-0.8400
a_2	0.6800	-0.9300
a_3	0.6800	-1.0300
b_1	0.8224	-0.8224
b_2	0.8861	-0.8861
b_3	0.9568	-0.9568
c_1	0.8400	-0.6800
c_2	0.9300	-0.6800
c_3	1.0300	-0.6800
d_1	-0.6800	0.5200
d_2	-0.6800	0.4300
d_3	-0.6800	0.3300
e_1	-0.5376	0.5376
e_2	-0.4739	0.4739
e_3	-0.4032	0.4032
f_1	-0.5200	0.6800
f_2	-0.4300	0.6800
f_3	-0.3300	0.6800
g	0.6800	0.0000
h	0.0000	0.0000
i	-0.6800	0.0000
j	0.0000	0.6800
k	0.0000	-0.6800

To measure the local wave impact pressure, the four-square-vertical-cylinders are covered by 31 miniature pressure sensors, as shown in Figure 124. The locations of all pressure sensors are summarized in Table 6.

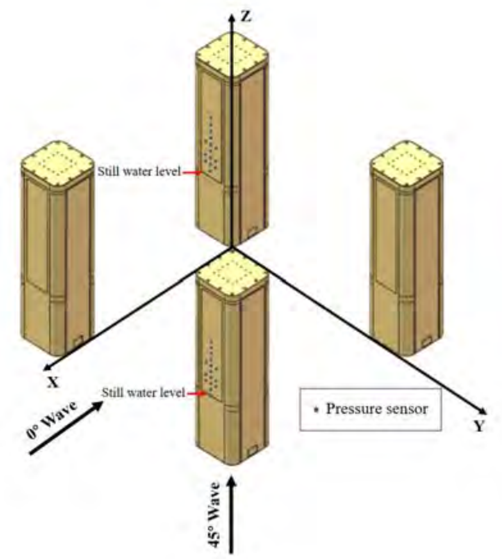

Figure 124: Pressure sensor location

Table 6: Coordinates of thirty-one (31) pressure sensors

Sensor No.	Scale: 1:50			
	Unit	X	Y	Z
Slam001	mm	840.00	680.00	0.00
Slam002	mm	840.00	680.00	50.00
Slam003	mm	840.00	630.00	100.00
Slam004	mm	840.00	680.00	100.00
Slam005	mm	840.00	730.00	100.00
Slam006	mm	840.00	630.00	150.00
Slam007	mm	840.00	680.00	150.00
Slam008	mm	840.00	730.00	150.00
Slam009	mm	840.00	680.00	200.00
Slam010	mm	840.00	630.00	250.00
Slam011	mm	840.00	680.00	250.00
Slam012	mm	840.00	730.00	250.00
Slam013	mm	840.00	680.00	300.00
Slam014	mm	840.00	680.00	350.00
Slam015	mm	840.00	680.00	400.00
Slam016	mm	840.00	680.00	450.00
Slam018	mm	-520.00	-680.00	50.00
Slam019	mm	-520.00	-730.00	100.00
Slam020	mm	-520.00	-680.00	100.00
Slam021	mm	-520.00	-630.00	100.00
Slam022	mm	-520.00	-730.00	150.00
Slam023	mm	-520.00	-680.00	150.00
Slam024	mm	-520.00	-630.00	150.00
Slam025	mm	-520.00	-680.00	200.00
Slam026	mm	-520.00	-730.00	250.00
Slam027	mm	-520.00	-680.00	250.00
Slam028	mm	-520.00	-630.00	250.00
Slam029	mm	-520.00	-680.00	300.00
Slam030	mm	-520.00	-680.00	350.00
Slam031	mm	-520.00	-680.00	400.00
Slam032	mm	-520.00	-680.00	450.00

The sampling rate was 100 Hz for wave probes. For the impact pressure, a high-speed measurement system of a sampling rate of 20 kHz was used. The 100 Hz and 20 kHz measurements were synchronized and the recordings were started simultaneously. The wave calibration should be performed prior to placing the model in the basin. The effective record duration of each focus wave test shall be twice than the focus time T_f.

In the benchmark studies, the max results of following measured items were compared at various wave periods, focus positions and wave steepness in terms of H/λ:

1) Wave elevations at 23 wave probe locations.

2) Wave impact pressure at 31 pressure sensor locations.

6.2 Wave Run-up Characteristics in Focused Waves

6.2.1 Wave run-up height at 0°

For the wave direction of 0°, Figure 125-Figure 128 depict the maximum values of wave run-up ratios at six locations (a_1, b_1, c_1, d_1, e_1, f_1) for the fixed four-square-column array at various wave steepness, spectral peak periods, and focus positions, respectively. In the figures, y denotes the lateral position from the column center, and D represents the column width. The maximum wave run-up height η_{max} is normalized by the incident focused wave amplitude (A). The vertical dotted line represents the wave probes, and the blue area represents the front projection of the column.

For the front column, the peak value is observed at the central location (c_1), while the lowest value is found at the shoulder (a_1). Figure 125 shows that for waves of relatively small steepness (H/λ=0.05), the maximum wave run-up ratio is significantly smaller (~1.2 to 1.6) than that of larger waves with steeper steepness. As illustrated in Figure 128(a), the reason of this phenomenon is that the process of wave run-up is primarily manifested by the gentle uplift of the local water as the focused wave crest approaches and passes through the column. Due to the relatively gentle steepness of the focused wave, only minor diffraction and disturbance occur during the interaction between the wave and the front column, without any significant phenomena taking place. As the steepness of the focused waves increases (H/λ =0.06), a more pronounced wave upwelling can be observed during the wave-column interaction as depicted in Figure 128(b). And the ratio of wave run-up height has reached to 1.6-1.8. When the incident wave steepness continues to increase (H/λ=0.07), more obvious wave upwelling occurs on the surface of front column as shown in Figure 128 (c). As a result, the wave run-up ratio is significantly increased (~1.6 to 2.2). And there is no breaking and water jet in the whole process. For the focused waves with larger wave steepness (H/λ =0.08), the waves near breaking or break precisely at the focal point, a water jet can be generated by the uprush flow, as shown in Figure 128 (d), and hence increases the run-up ratio significantly (~1.8 to 2.8). Especially for T=2.0s, the wave run-up ratio at steepness of 0.08 increases significantly. In general, the effect of wave steepness is more pronounced for long waves compared to short waves.

Figure 126 illustrates that when the wave steepness is relatively low (H/λ=0.05~0.06), there is a declining trend in the wave run-up ratio with increasing wave period, although the differences are minor. This is because, when the wavelength is significantly larger than the column width, the nonlinear wave-column interaction diminishes as the wave period increases. Especially for H/λ=0.06, Figure 127 shows that the wave run-up ratio is almost consistent at all spectral peak periods. However, for higher wave steepness values (H/λ=0.07~0.08), changes in the spectral peak period leads to significant variations in wave run-ups. When the wave steepness is 0.08 and the spectral peak period is 2.0s, the maximum wave run-up ratio reaches 2.79, emphasizing the significant impact of wave steepness on long waves, as mentioned earlier.

For the rear column, the positive peak value of the wave run-up height almost appears at the center (f_1), and appears at the filet point (e_1) in a minority of cases. It is noteworthy that the difference in wave run-up ratios between locations f_1 and e_1 is not significant, which indicating that the interference between the columns has a significant effect on the rear column, and the design of the upper deck structure at the rounded corner is also important. Due to the dissipation of wave energy, the maximum wave run-up ratio for the rear column is lower than that of the front column.

Figure 127 demonstrates that the focus position has a substantial influence on the wave run-up ratio. For the front column, the wave run-up ratio is maximized when the focus position is situated behind the rear surface of the front column. Although the focusing position is on the rear surface, the incident waves have already begun to go up on the front surface. Due to the obstruction of the column, the wave is compelled to persistently run-up, leading to a significantly greater run-up ratio compared to those under other focus positions. Conversely, for the rear column, the wave run-up ratio attains its maximum value when the focus position is located at the front surface of the rear column. This is because even though the focusing position is on the rear column, a portion of the wave energy dissipates as it passes through the front column.

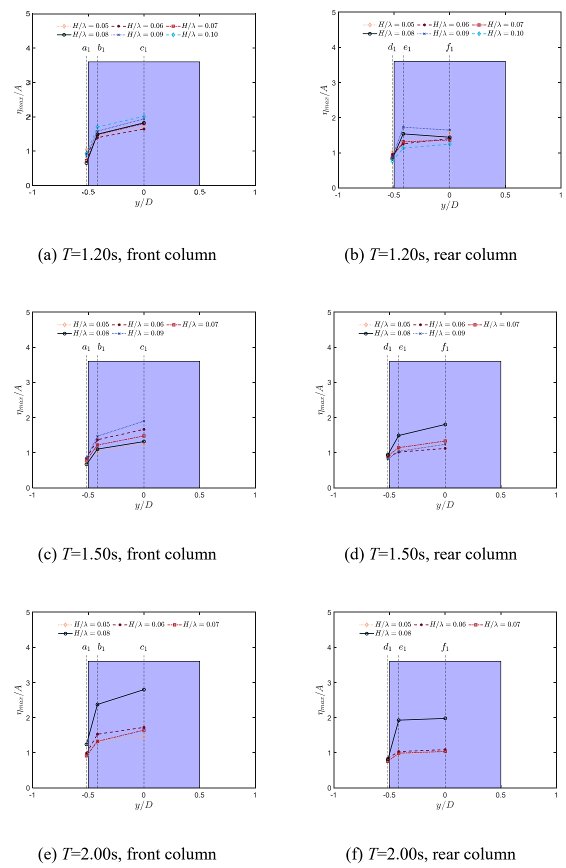

(a) T=1.20s, front column (b) T=1.20s, rear column

(c) T=1.50s, front column (d) T=1.50s, rear column

(e) T=2.00s, front column (f) T=2.00s, rear column

Figure 125: Maximum wave run-up ratios at various wave steepness (heading 0°)

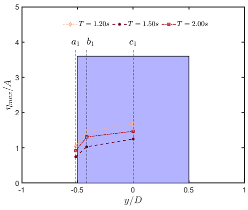

(a) H/λ=0.05, front column

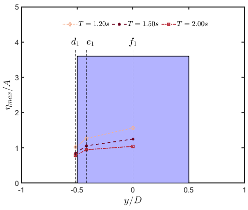

(b) H/λ=0.05, rear column

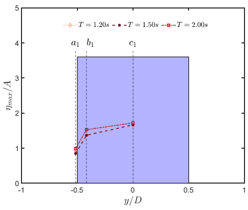

(c) H/λ=0.06, front column

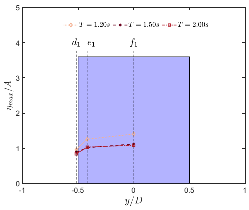

(d) H/λ=0.06, rear column

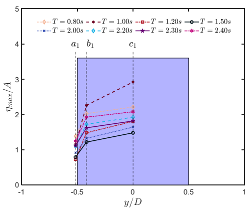

(e) H/λ=0.07, front column

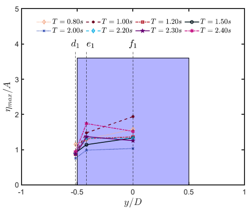

(f) H/λ=0.07, rear column

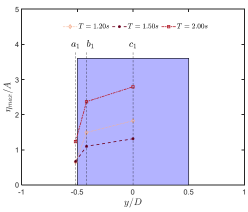

(g) H/λ=0.08, front column

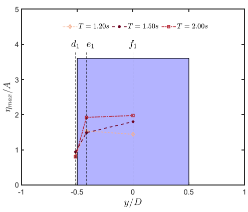

(h) H/λ=0.08, rear column

Figure 126: Maximum wave run-up ratios at various wave periods (heading 0°)

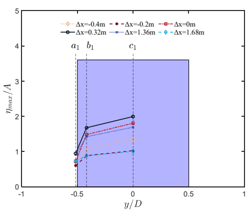

(a) T=1.20s, front column

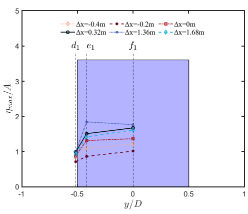

(b) T=1.20s, rear column

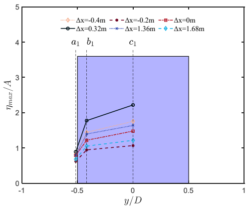

(c) T=1.50s, front column

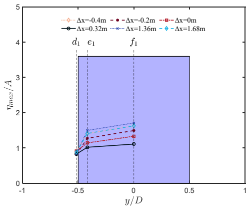

(d) T=1.50s, rear column

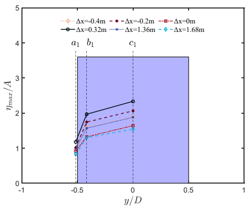

(e) T=2.00s, front column

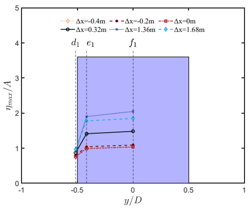

(f) T=2.00s, rear column

Figure 127: Maximum wave run-up ratios at various focus positions (heading 0°, H/λ=0.07)

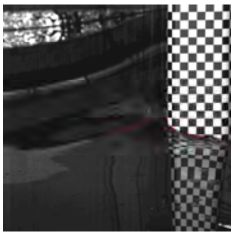

(a) H/λ=0.05, T=2.0s

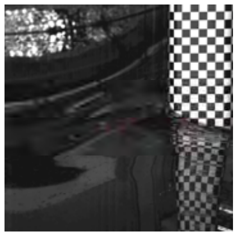

(b) H/λ=0.06, T=2.0s

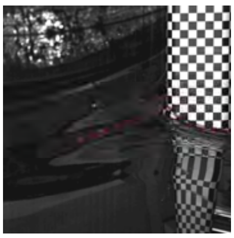

(c) H/λ=0.07, T=2.0s

(d) H/λ=0.08, T=2.0s

Figure 128: The wave run-up along the surface of the front column.

6.2.2 Wave run-up height at 45°

For the wave direction of 45°, Figure 129 and Figure 130 show the maximum wave run-up ratios at 6 locations $(a_1, b_1, c_1, d_1, e_1, f_1)$ represented by y/D_1, where y denotes the distance along the diagonal to the column center, D_1 is column diagonal width.

For both the front and rear columns, the maximum wave run-up ratio occurs at the rounded corner (b_1 and e_1).

For the front column, the conclusion is the same as that of the 0° wave direction. When the focused wave steepness is small (H/λ=0.05), the maximum ratio of the wave run up is significantly smaller than that of other large wave steepness. As the steepness of the wave increases gradually, so does the maximum ratio of wave run-up. It's also attributed to varying degrees of interaction between the wave and the local water in front of the column.

For the rear column, due to the dissipation of wave energy, the wave run up ratio at the surface is significantly lower than that of the front column. By comparing the results at probes c_1 and f_1 in Figure 129, it illustrates that the wave steepness variation has a different effect on the wave run-up ratio at the center of the front and rear columns. This may be attributed to the complex wave interactions among the columns. In addition, the highest wave run up ratio point shifts from the front of the column to the rounded corner, indicating that the wave interference among the columns has a significant effect on the rear column, and the design of the upper deck structure at the rounded corner is also important.

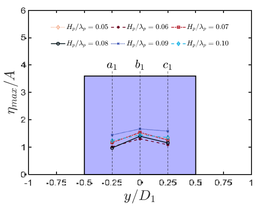

(a) T=1.20s, front column

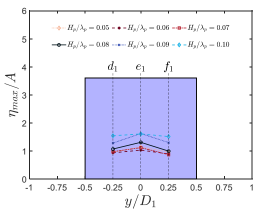

(b) T=1.20s, rear column

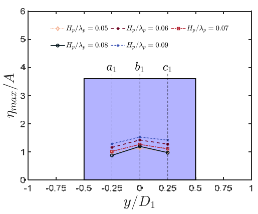

(c) T=1.50s, front column

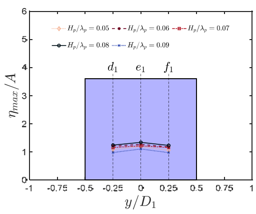

(d) T=1.50s, rear column

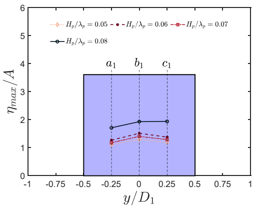

(e) T=2.00s, front column

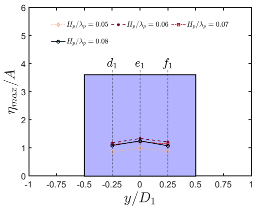

(f) T=2.00s, rear column

Figure 129: Maximum wave run-up ratios at various wave steepness (heading 45°)

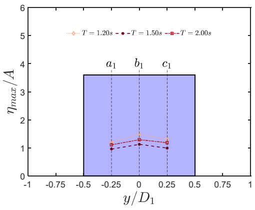

(a) H/λ=0.05, front column

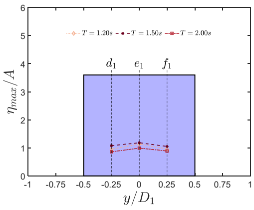

(b) H/λ=0.05, rear column

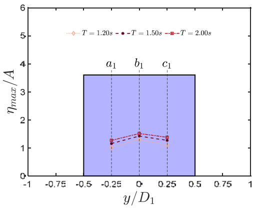

(c) H/λ=0.06, front column

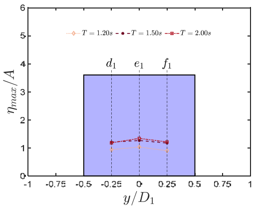

(d) H/λ=0.06, rear column

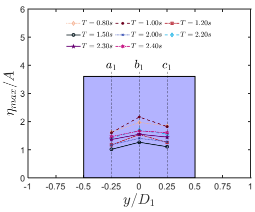

(e) H/λ=0.07, front column

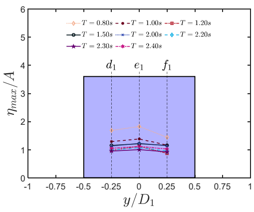

(f) H/λ=0.07, rear column

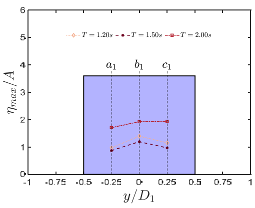

(g) H/λ=0.08, front column

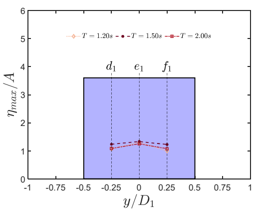

(h) H/λ=0.08, rear column

Figure 130: Maximum wave run-up ratios at various wave periods (heading 45°)

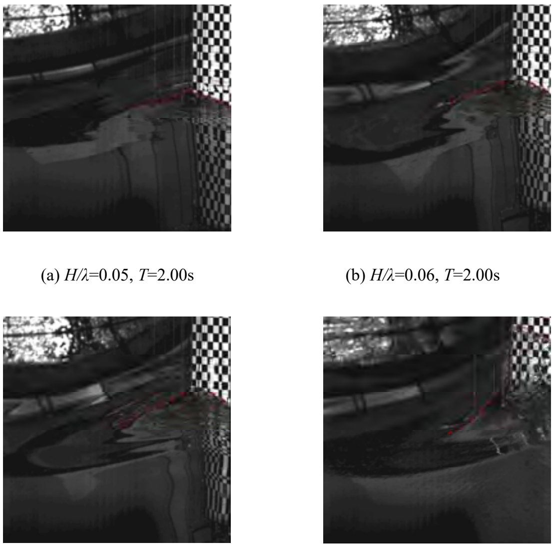

(a) H/λ=0.05, T=2.00s (b) H/λ=0.06, T=2.00s

(c) H/λ=0.07, T=2.00s (d) H/λ=0.08, T=2.00s

Figure 131: Snapshots of visual observations during the focused wave acting on the front column (heading 45°)

6.2.3 Wave run-ups around fixed four squared cylinders

Figure 132 show the max value of wave elevations at 18 locations (a_1~a_3, b_1~b_3, c_1~c_3, d_1~d_3, e_1~e_3, f_1~f_3) for fixed four-squared-cylinder systems of each case with 0° wave heading direction. In the figure, x means the distance from wave probe to the column surface, D means the column width. Figure 133 shows the max values for each case with 45º wave direction.

From these images, it can be observed that under varying wave steepness, spectral peak periods, and focus positions, the wave run-up evolution follows a consistent pattern: the closer the waves are to the column surface, the more pronounced the wave run-up becomes, with the maximum run-up occurring near the column surface. Furthermore, the steeper the focused wave, the more pronounced the wave run-up evolves with x/D, resulting in stronger wave run-up phenomenon. However, for the rear column, the wave run-up evolution with x/D is much gentler, and the run-up phenomenon only intensifies under short wave period and large wave steepness.

Figure 132 illustrates that for the front column, when the spectral peak period is smaller (T= 1.20s, T = 1.50s), and the focus position is near the column surface, the wave run-up evolves more steeply with x/D. Conversely, when the focus position is near the surface of the rear column, the evolution is nearly flat. This is because, with constant wave steepness, a shorter wave period results in lower wave energy. Consequently, when the focus position is near the rear column, the wave energy has reduced at the front column, leading to a less noticeable wave run-up phenomenon. Conversely, when the focus position is near the front column, the wave energy is concentrated in its vicinity, amplifying the wave run-up phenomenon. With a larger period, the wave energy increases. Therefore, even with the focus position near the rear column, a notable wave run-up phenomenon is observed at the front column, reflected in a steeper evolution. However, for the rear column, due to the wave energy dissipation, even with a larger period, there won't be a significantly pronounced climbing phenomenon.

Figure 133 illustrates the wave run-up evolutions at 18 locations (a_1~a_3, b_1~b_3, c_1~c_3, d_1~d_3, e_1~e_3, f_1~f_3) for fixed four-squared-cylinder systems of each case with 45°. It can be observed that the wave run-up evolution follows a pattern similar to that observed at 0°.

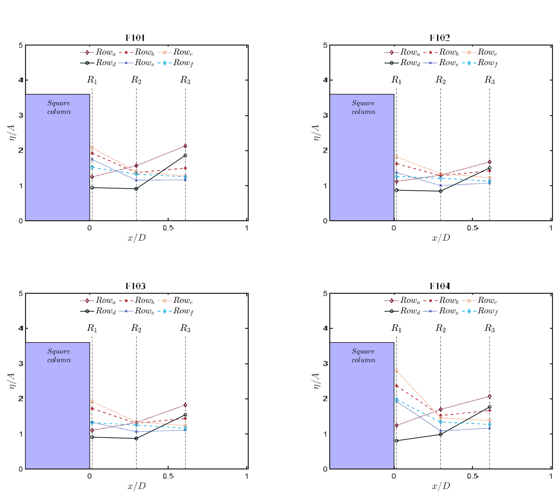

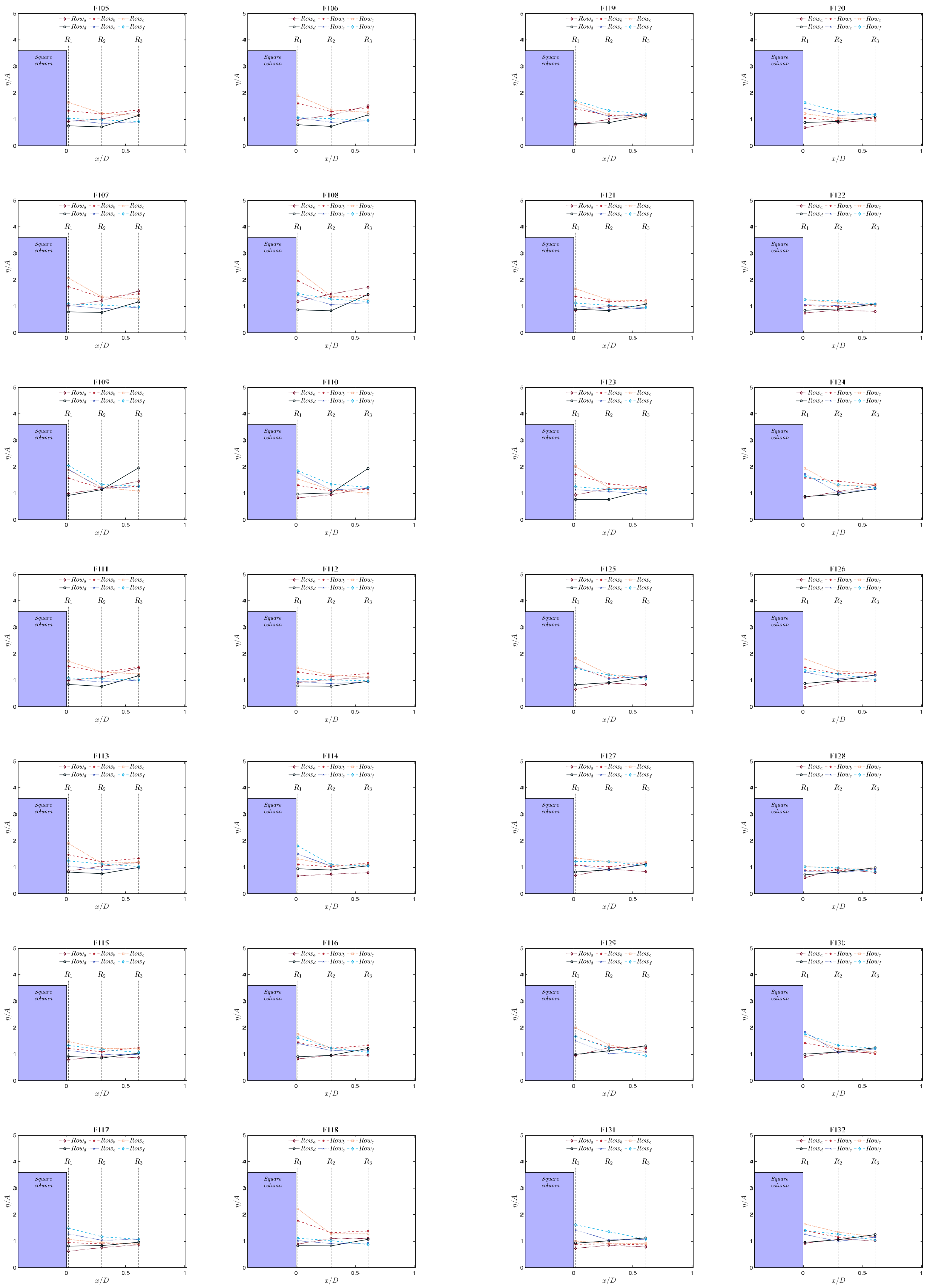
F105
F106
F119
F120
F107
F108
F121
F122
F109
F110
F123
F124
F111
F112
F125
F126
F113
F114
F127
F128
F115
F116
F129
F130
F117
F118
F131
F132
Square column
η/A
x/D
R_1 R_2 R_3
Row_a Row_b Row_c Row_d Row_e Row_f

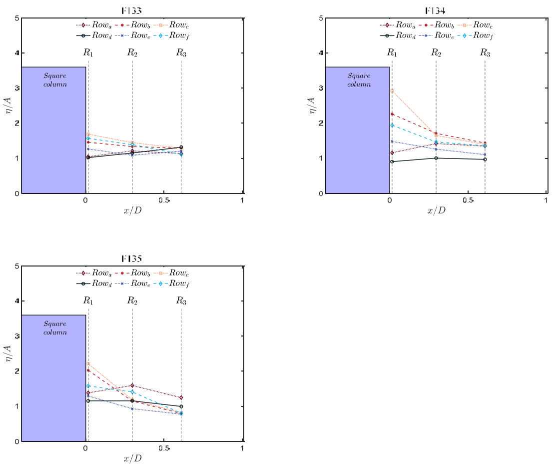

Figure 132: Wave run-up evolution in front of columns (heading 0°)

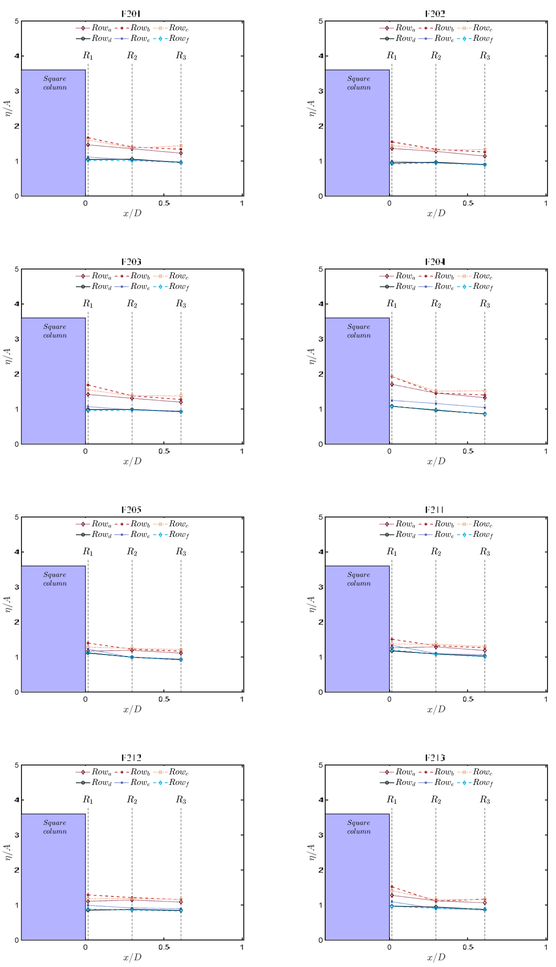

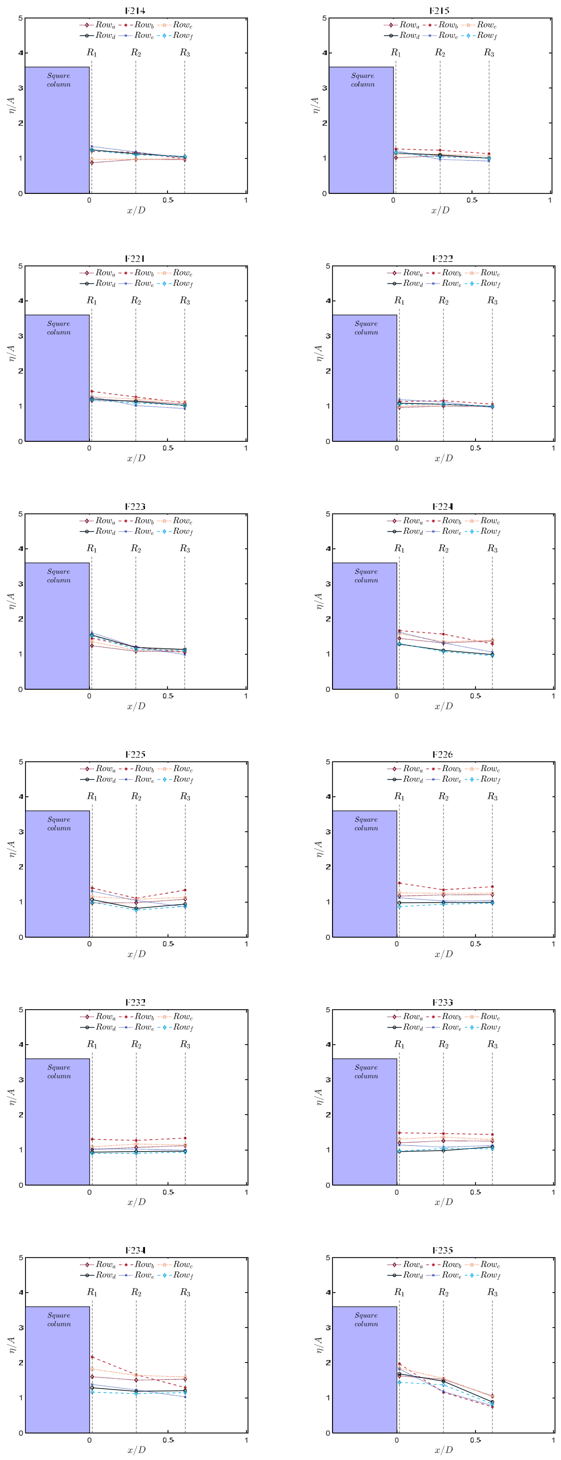

Figure 133: Wave run-up evolution in front of columns (heading 45°)

6.3 Wave Impact Pressures in Focused Waves

6.3.1 Load separation

Before load separation, the wavelet denoising method is employed to eliminate noise interference in the wave impact measurements. Figure 134 and Figure 135 present the denoise wave pressure P_{total} on fixed four-squared-cylinder systems, measured by the pressure sensor in case F101 and F201. P_{total} consists of quasi-static wave pressure P_{qs} and wave impact pressure P_{imp} in a wave impact event. Since this study aims to investigate local wave impact loads on the columns, it is crucial to separate the quasi-static component P_{qs} from the P_{total}.

A robust locally weighted LOESS smoother is applied to estimate the quasi-static wave pressure. The smoothing method is realized by local regression using weighted linear least squares and a second-degree polynomial model. The fitted data outside five mean absolute residuals are assigned zero weight in the procedure.

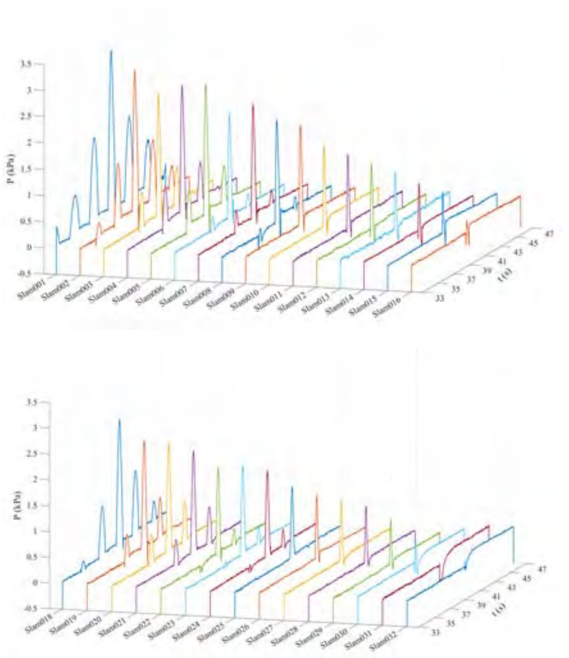

Figure 134: Wave pressure time histories for all pressure sensors for case F101

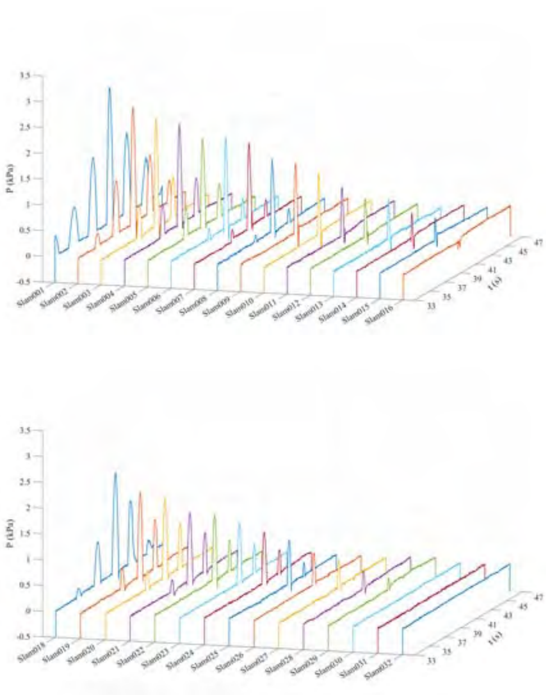

Figure 135: Wave pressure time histories for all pressure sensors for case F201

The wave impact pressure P_{imp} equals the total wave pressure minus the quasi-static part, as shown in Figure 136. The wave impact pressure increases rapidly with a strong nonlinearity. Then, the pressure decreases and a negative valley appears. This is because the entrapped air pocket occurs in wave impact, as illustrated in Figure 137. The air pocket, serving as a cushion between wave and structure during the impact, induces a negative pressure when the liquid separates from the structure's surface. In addition, the wave impact has a relatively long duration due to the air pocket.

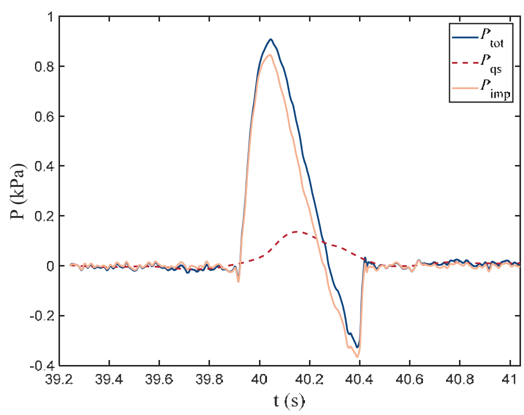

Figure 136: Example of the separation of different load components (Slam012 in case F103)

Figure 137: Snapshot of the wave impact instant on the front column for case F103 (the dashed red line denotes the incident wave profile)

6.3.2 Effects of wave periods

Figure 138 and Figure 139 display the spatial distribution of wave impact pressure peaks on the surface measurement points with different height (0~45 cm) at various wave periods with 0° and 45° wave direction, respectively. In the figure, 0 cm represents the still water level.

Figure 138 and Figure 139 illustrates that wave impact pressure increases first and then decreases with the height increasing. According to the nonlinear dispersion relation of waves, the wave height increases with an increase in the period for a given wave steepness. It is not difficult to understand that the wave impact pressure induced by focused waves tends to be distributed over a broader spatial range, as the wave period increases from 0.8 to 2.4 s. For the largest wave period ($T_p = 2.4$ s), the wave impact pressure is generally larger than that of the other focused waves, revealing that a large wave period remarkably increases the wave impact pressure.

In this subsection, the focus position was located at the front surface of the front column. Therefore, wave impact events are mainly dominated by the front column, called fore-column dominating wave impacts, in which the impact pressure of the rear column was notably lower than that of the front column, regardless of the variations in the incident wave period. In this study, the elementary loading processes (ELPs) primarily consisted of ELP2, which is the most common process used in engineering applications. ELP2 is characterised by the run-up (or downward) of the wave along the structure, inducing hydrodynamic loads due to the rapid upwelling jet parallel to the surface of the column, as depicted in Figure 140(a). After the wave passes through the front column, the partial energy of the wave dissipates because of the upwelling jet and wave breaking (Figure 140(b)), causing a lower wave run-up around the rear column. Consequently, the amplitude and spatial range of the impact pressure in the rear column were substantially smaller than those in the front column.

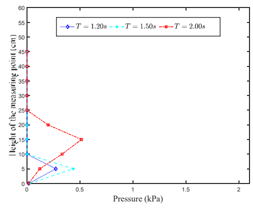

(a) H/λ=0.05, front column

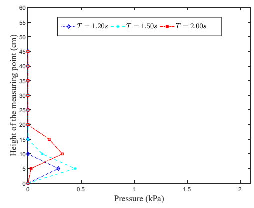

(b) H/λ=0.05, rear column

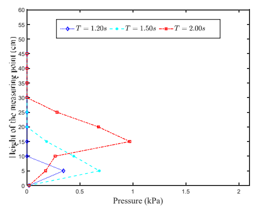

(c) H/λ=0.06, front column

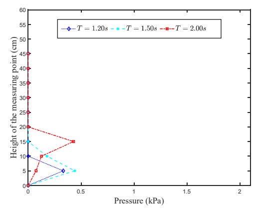

(d) H/λ=0.06, rear column

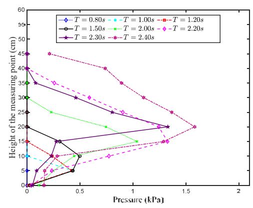

(e) H/λ=0.07, front column

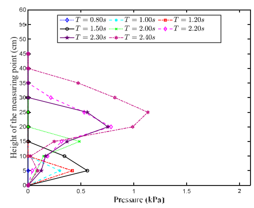

(f) H/λ=0.07, rear column

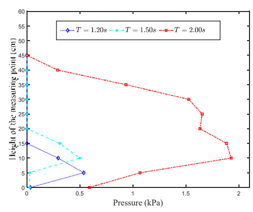

(g) H/λ=0.08, front column

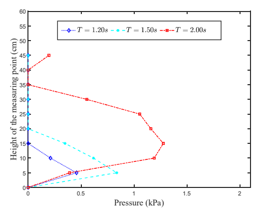

(h) H/λ=0.08, rear column

Figure 138: Spatial distributions of wave impact pressure at different wave periods (heading 0°)

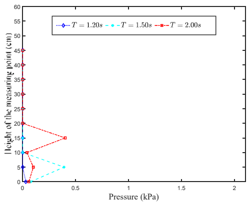

(a) H/λ=0.05, front column

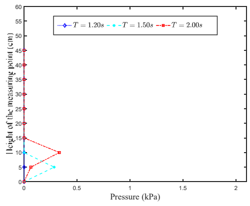

(b) H/λ=0.05, rear column

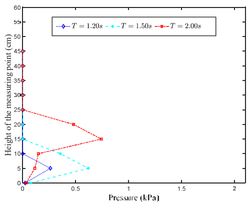

(c) H/λ=0.06, front column

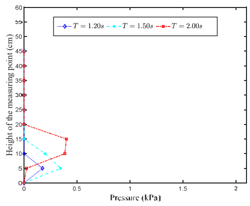

(d) H/λ=0.06, rear column

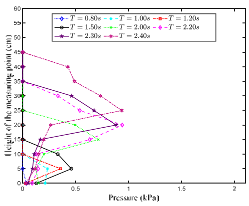

(e) H/λ=0.07, front column

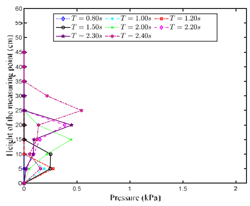

(f) H/λ=0.07, rear column

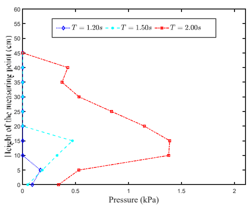

(g) H/λ=0.08, front column

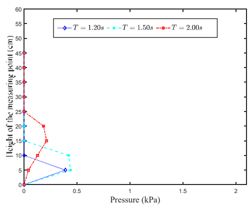

(h) H/λ=0.08, rear column

Figure 139: Spatial distributions of wave impact pressure at different wave periods (heading 45°)

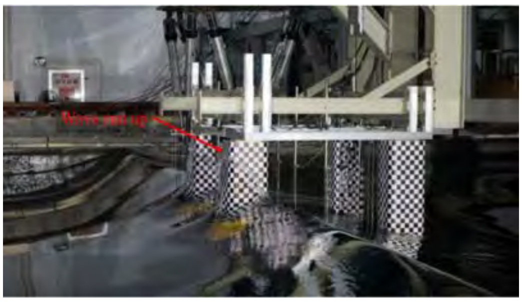

(a) Severe wave run-up in the front column

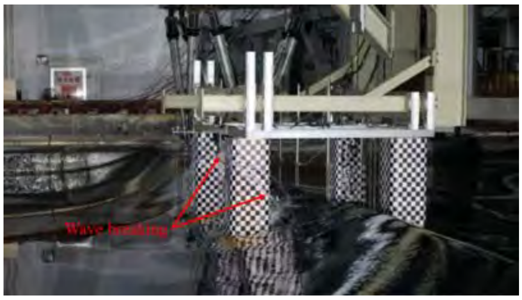

(b) Obvious wave breaking after passing through the front column

Figure 140: Wave propagation snapshots as the main crest acts on the front column

6.3.3 Effects of wave steepness

In addition to the spectral peak period, the wave pressure on the rounded-square column is significantly influenced by the shape of the incoming focused wave. Wave steepness is a key parameter for characterising the shape and stability of waves.

Figure 141 and Figure 142 present the spatial distribution of wave impact pressure peaks on the surface measurement points with different height (0~45 cm) at various wave steepness (0.05, 0.06, 0.07, 0.08, 0.09, 0.10) with 0° and 45° wave direction, respectively. Generally, the wave impact caused by large steepness wave (such as $H/\lambda = 0.10$) is more severe than that caused by small steepness wave. The volume of water impacting the column increased with the wave steepness in the wave-propagation direction, causing a greater transfer of kinetic energy to the column. Comparing Figure 141(a) with (c), it is evident that the steep wave with short wave periods can also induce large impact pressure, such as focused wave FW23 ($T = 1.20s,\ H/\lambda = 0.09$). This partially illustrates that the wave steepness has a considerable effect on the wave impact pressure spatial distribution.

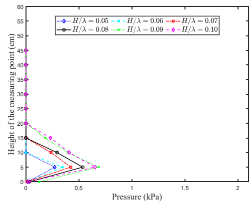

(a) T=1.20s, front column

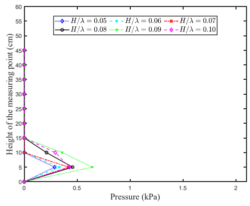

(b) T=1.20s, rear column

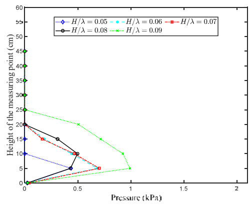

(c) T=1.50s, front column

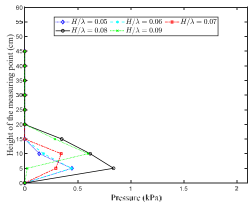

(d) T=1.50s, rear column

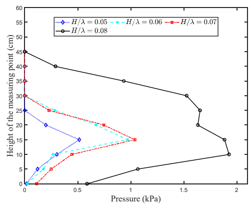

(e) T=2.00s, front column

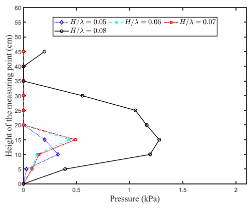

(f) T=2.00s, rear column

Figure 141: Spatial distributions of wave impact pressure at different wave steepness (heading 0°)

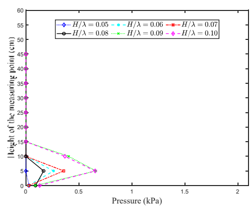

(a) T=1.20s, front column

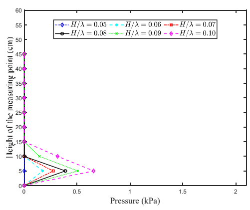

(b) T=1.20s, rear column

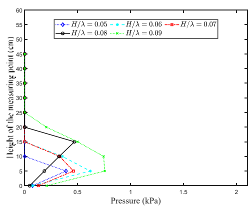

(c) T=1.50s, front column

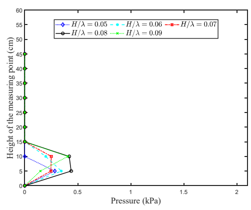

(d) T=1.50s, rear column

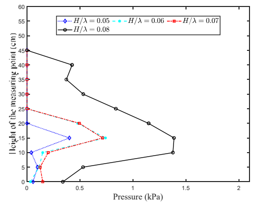

(e) T=2.00s, front column

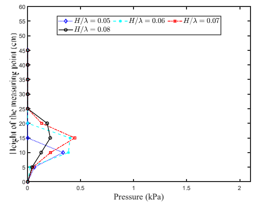

(f) T=2.00s, rear column

Figure 142: Spatial distributions of wave impact pressure at different wave steepness (heading 45°)

6.3.4 Effects of focus positions

The focus position is a crucial parameter of the focused wave that directly affects the processes of waves impacting the structure by influencing the wave energy aggregation and wave run-up capacity.

Figure 143 shows the spatial distribution of wave impact pressure peaks on the surface measurement points with different height (0~45 cm) at various focus positions with 0° wave heading direction. The front column suffers the greatest impact when the focus position is located on the rear surface of the front column (ΔX = 0.32 m), while in rear column when the focus position is set on the front surface of the rear column (ΔX = 1.36 m). Combined with Figure 127(e) and (f), this result can be explained by the variations in the wave run-up height for different focus positions. For the front column, the maximum wave run-up ratio is observed in front column at focused waves with ΔX = 0.32 m. Although the focus position is on the rear surface, the wave has already started to move upwards on the front surface and is forced to persistently run-up by the obstruction of the column, resulting in a notably greater run-up height compared with other focus positions. For the rear column, the wave run-up ratio reaches its maximum under the focused waves with ΔX = 1.36 m. Due to the disturbance of front column, the wave run-up decreases markedly when the wave focus position is ΔX = 1.68 m, smaller than the test for ΔX = 1.36 m. This further demonstrates that the wave impact pressure is closely associated with the wave run-up along the structure, as mentioned in the previous section. Therefore, adding appropriate structures to suppress the wave run-up height is an effective method for mitigating the wave impact load on columns.

Previous studies have primarily focused on wave impact events with a focus position around the front column, and little research has been conducted on wave impact pressure with a focus position at the rear column. In this study, when the focus position was $\Delta X = 1.36$ m, the spatial distributions of peak pressure exhibit evident different features, especially at an impact position height of 35 cm. As illustrated in Figure 144, the total wave pressure is primarily composed of the impact pressure with a few quasi-static wave pressure. It is speculated that this instantaneous large impact was caused by accelerated water jets or wave amplification due to interference with the front and rear columns. The duration of this phenomenon was remarkably short, aligning with the typical characteristics of the impact induced by splashing.

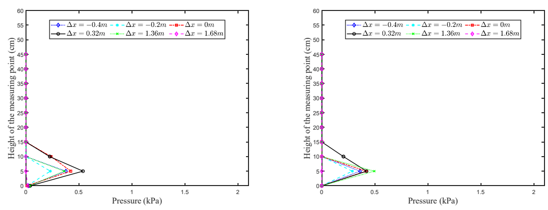

(a) T=1.20s, front column (b) T=1.20s, rear column

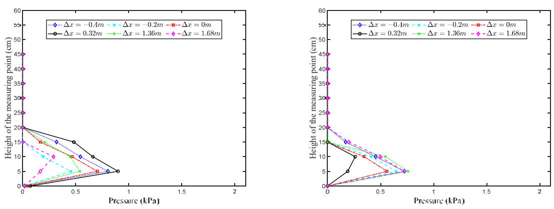

(c) T=1.50s, front column (d) T=1.50s, rear column

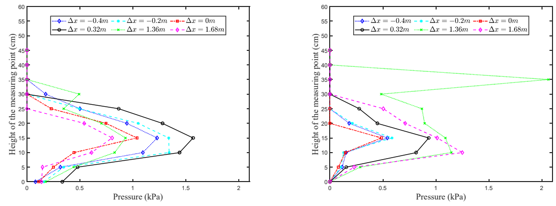

(e) T=2.00s, front column (f) T=2.00s, rear column

Figure 143: The spatial distribution of wave impact pressure peaks on the surface measurement points with different height at various focus positions (heading 0°, $H/\lambda = 0.07$)

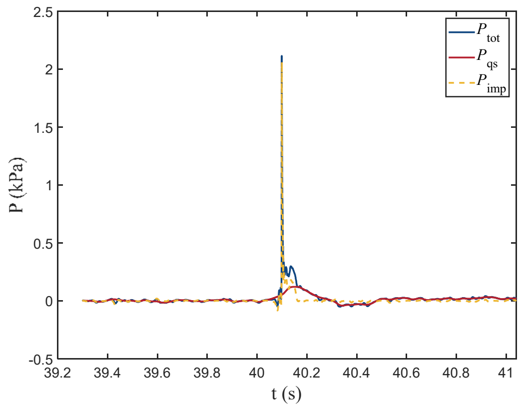

Figure 144: Wave pressure time histories for Slam030 (measuring point height: 35cm) for case F109

7. CFD BENCHMARK STUDY ON TWO-BODY INTERACTIONS IN CLOSE PROXIMITY

7.1 Literature Review on Recent Studies of Two-body Interactions

In decades, numerous studies were conducted to understand the interactions between two ships by experimental and numerical methods for various cases of ship-ship operating conditions. The studies could be classified into 4 sub-groups based on the operating conditions (Zhou et al., 2023), as shown in Figure 146. In this task, the literature on ship-ship interaction with rectangular boxes and the case of lightering, including the studies for simplified models in a static condition, were considered to focus on gap resonance, which means violent water column oscillations in the gap of the structures when incident wave frequency is close to the natural frequency of the oscillating fluid mass.

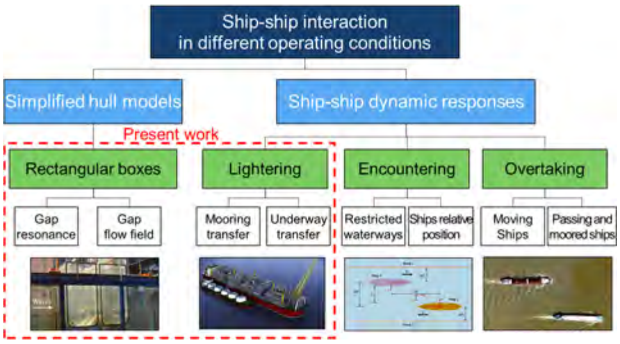

Figure 145. Classification of studies for two-body interaction

7.1.1 Experimental studies on two-body interactions

To be used as benchmark data for numerical methods, the experimental studies in early stages were conducted in 2-D with simplified structures. Tan et al. (2019) investigated the effect of the geometry of structures in gap resonance between the structures under regular wave conditions with suggestions of a modified potential flow model with a damping mechanism to estimate the phenomenon. The experimental results showed that the resonant amplitude and frequency could increase when the shape of the structure changed from sharp to round corners.

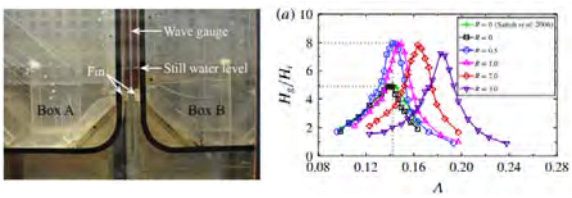

Figure 146: Experimental setup and results of Tan et al. (2019)

Ning et al. (2018) performed a series of experiments to study the gap resonance with various draft of the structures, showing that the wave frequency decreased with a higher draft for both structures, and the water height increased with the higher draft of the lee-side structure.

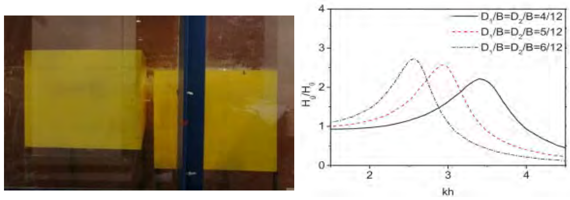

Figure 147: Experimental setup and results of Ning et al. (2018)

There also have been some 3-D experiments with ship-type structures. Xu et al. (2014) investigated the hydrodynamic performances of two identical structures to study the effect of gap distance. In the results, single and multi-peaks were observed at resonance and shorter periods, respectively, and some discrepancies were found in the resonance period between the cases of motion-limited and free structures.

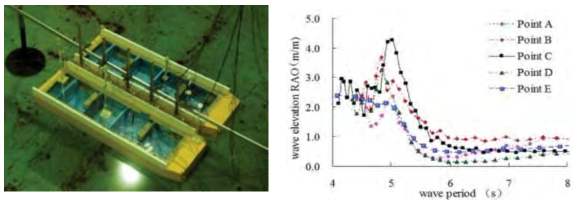

Figure 148: Experimental setup and Results of Xu et al. (2014)

Jin et al. (2018) studied the wave responses in the gap with structural interactions of FLNG and LNG varying those lateral spacings. The paper observed that the resonance happened when incident wave frequency approached to the natural frequency of the fluid between the two ships, and the reduction of the gap distance made greater exaggeration of the responses shifting to a higher frequency levels.

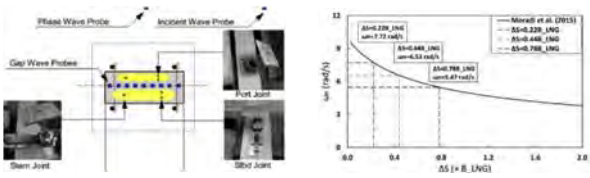

Figure 149: Experimental setup and results of Jin et al. (2018)

Zhao et al. (2018) performed a series of experiments on the two-body interactions in 3-D, measuring the resonance RAO in the gap, and showed that the RAO agreed well with a numerical model suggested by Molin et al. (2021) with a linear viscous damping results from Stokes oscillatory laminar boundary layers.

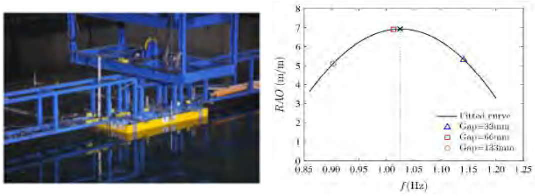

Figure 150: Experimental setup and results of Zhao et al. (2018)

Zhang et al. (2019) also conducted experiments to study the motions and wave field between the barges and showed that the barge motion and the wave elevation in the gap generally increased with the reduction of the gap distance.

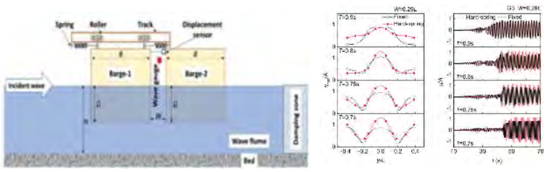

Figure 151: Experimental setup and results of Zhang et al. (2019)

Chua et al. (2018) performed a series of model tests for the two-body interactions to investigate the free surface response in the gap between two barges in irregular waves. The study was extended to study the effect of the structural bilge geometry (Chua et al., 2019) and cases with liquid sloshing effect (Liang et al., 2022).

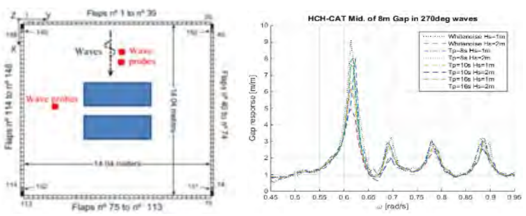

Figure 152: Experimental setup and results of Chua et al. (2018)

To provide experimental benchmark data f for the two-body interactions, a series of experiments have been carried out by ITTC 27 and 28th Ocean Engineering Committee in four phases below (Qiu et al., 2019),

- 1st phase: Model test with simplified identical ships in the towing tank of Memorial University (MUN), measuring wave elevations and motions for three different gaps between the structures (Zhou et al., 2015).

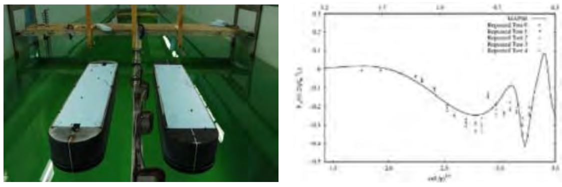

Figure 153: Experimental setup and results in MUN (Zhou et al., 2015)

- 2nd phase: Experiments in 1st phase were extended to measure drift forces, and the same experiments were conducted in the wave basin of Ecole Centrale de Nantes (ECN, 2016).

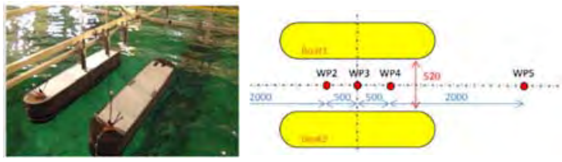

Figure 154: Experimental setup and results in ECN (ECN, 2016)

- 3rd phase: Same experiments were carried out in the wave basin of LabOceano at Rio de Janeiro, Brazil with the same models.

- 4th phase: Large models were tested in the wave basin of Ecole Centrale de Nantes to investigate the scale effect.

7.1.2 Numerical studies on two-body interactions

Due to the limitations and difficulties of experiments to implement and measure complex physical phenomena, many studies used numerical methods to investigate the two-body interactions. In the early days to study the phenomena, most of the numerical studies tried to simulate the two-body interaction using potential methods, which require relatively less computational load than CFD. However, the studies showed that the resonant RAO can be overestimated with the potential method due to its characteristics not to consider the viscous effect (Li and Zhang, 2016), most studies with potential methods focused to suggest an artificial resistance coefficient to simulate the two-body interaction with higher accuracy.

In recent, the CFD method is widely used to consider the viscous effect in the simulation of two-body interaction. For the simulations in 2-D, Moradi et al. (2016) simulated the two-body interaction using OpenFOAM to study the effect of the geometry on the resonant water height. The study investigated the grid dependency in the gap and showed that curved edges could make a significant increase in the resonant water height.

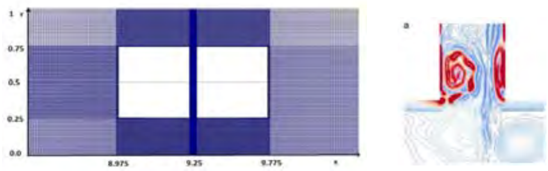

Figure 155: Simulation setup and results of Moradi et al. (2016)

Zhang et al. (2019) also simulated the phenomena using OpenFOAM and showed the best accuracy for the gap resonance water height with Laminar flow.

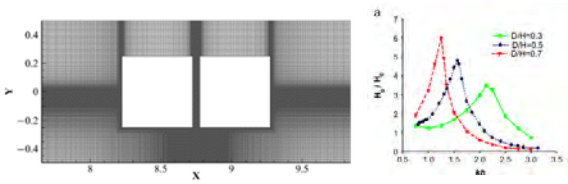

Figure 156: Experimental setup and results of Zhang et al. (2019)

In 3-D simulation study, Zhou et al. (2018) tried to apply artificial damping-lid methods in the simulation and showed that the incident wave directions have a significant influence on the phenomena, especially with the oblique wave because it made more violent motions of the structures.

Wang et al. (2019) also performed the simulation with OpenFOAM with a series of grid dependency tests and showed that the cell height for normal to wall in the gap is the most important parameter in the simulation of two-body interactions.

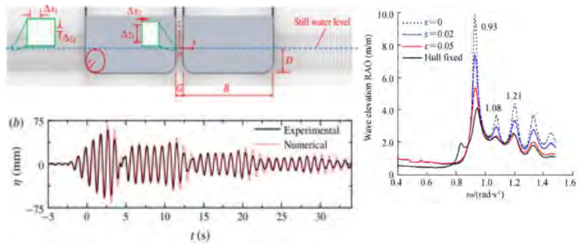

Figure 157: Experimental setup and results of Wang et al. (2019) and Zhou et al. (2018)

The two-body interaction is a phenomenon that is complex and can be affected by various parameters, such as incident wave period, height, and direction, gap distance, and properties of structures like mass, draft, motion characteristics, and so on. Numerous studies have been conducted to study the complex hydrodynamic features of the two-body interactions, but it still requires more studies to understand the physical characteristics of the phenomena. Especially, due to the limitations in experiments, the numerical methods seem more reasonable, using the CFD method to consider the viscous effect, and it is needed to study the parameters in the CFD simulations with those effects in the results for the two-body interactions.

7.2 Experiments to Validate the CFD Benchmark Study

To validate the CFD benchmark study on two-body interactions with focusing on gap surface elevation, the model tests of single barge and two identical rectangular barges were performed in the 2-D wave tank of Pusan National University.

7.2.1 Experiment of single-body motion

a. Experimental setup

The experiment was carried out for the motions of a rectangular barges ($C_M = 1$) in a 2-D wave tank. Table 7 shows the main dimensions of the barges and the wave tank. The soft spring system was designed so that the natural periods of the motions were not affected by the mooring system, especially for sway and roll motions. Free decay tests were performed in the conditions with and without the soft spring and natural period of the roll motion was recorded and checked and both conditions showing almost similar roll natural periods.

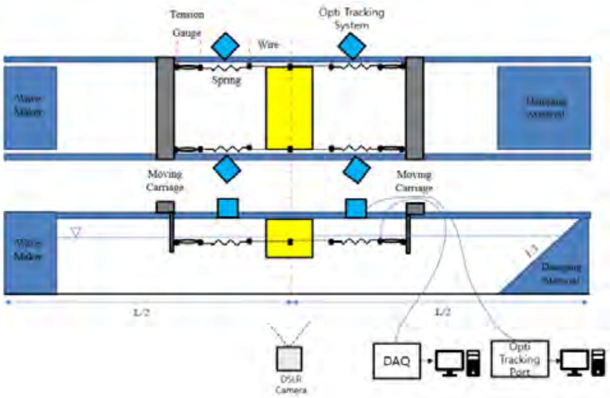

Figure 158: Experiment setup for single body motions

For motion measurements, the Opti-Track motion tracking system was used. The system was able to track the model motions in 6DOF. In this experiment, only sway, heave and roll were measured. The camera system was set up at 100 Hz sampling frequency. All the measurement systems and wave maker were synchronized.

Table 7: Main dimensions of the wave tank and models

Wave tank	Length	30 m
	Breath	0.6 m
	Depth	1.0 m
Barge	Length (L)	0.595 m
	Breath (B)	0.30 m
	Depth (D)	0.25 m
	Draft (T)	0.12 m
	VCG	0.08 m
	K_{xx}	0.35B
	T_{roll}	1.17 s
	T_{heave}	0.95 s

b. Experimental conditions

The incident wave periods are presented in Table 8, the wave height was kept as 1 cm. All the incoming waves are considered as linear wave cases.

Table 8. Incident wave conditions for single-body motions

Wave period (s)	0.80, 0.90, 0.95, 1.00, 1.05, 1.10, 1.15, 1.20, 1.25, 1.30, 1.40

c. Experimental results

Figure 159 shows the time series of the roll free decay experiment.

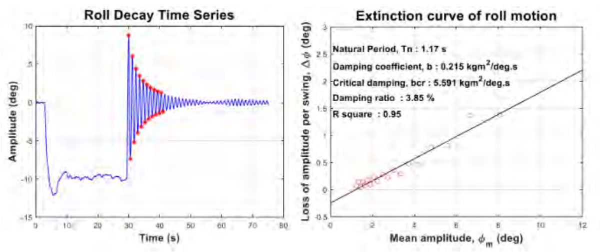

Figure 159: Time series of roll free decay test and the extinction curve

The motion response from experiment were compared with the first order motion response from linear hydrodynamic analysis with additional damping correction calculated by Ansys Aqwa software. The results show a good agreement between the measured motions and the numerical calculations.

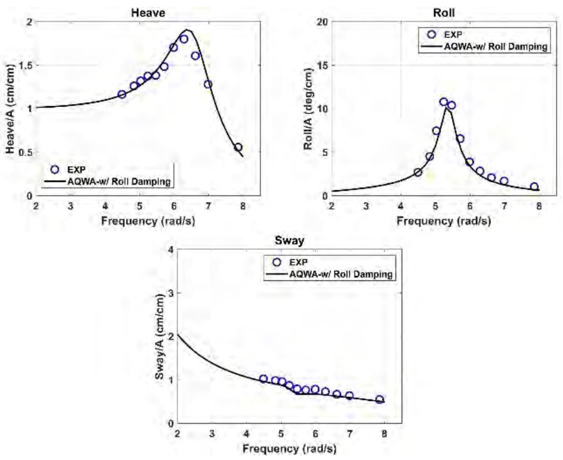

Figure 160: Motion responses of single body motion in regular waves.

7.2.2 Experiment of two-body interactions

a. Experimental setup

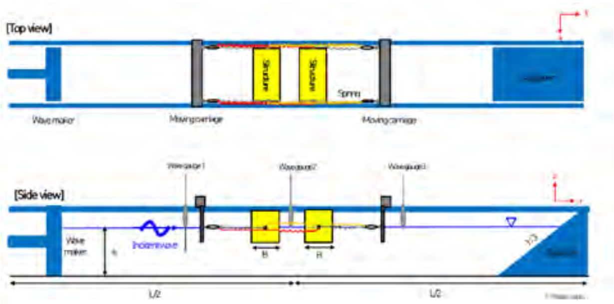

Figure 161: Experimental setup in 2-D wave tank

The experiment was carried out for the motions of two identical rectangular barges in the same 2-D wave tank in PNU. Each barge was moored by four soft mooring lines, which were connected to the VCG of the model. The stiffness of each spring is 1.0 N/m.

Three wave gauges were used to measure the wave elevations at upstream, downstream locations and at the gap with sampling frequency of 100 Hz. The Opti-Track motion tracking system was used to measure the motions of the barges.

7.2.3 Experimental conditions

The incident wave periods and frequencies are presented in Table 9, the wave height was kept as 2 cm. The experiment was performed in beam seas. To study the two-body interactions with small gap, the gap width was set at 7.0 cm (0.23B).

Table 9. Incident wave conditions for two-body

Condition No.	Wave period (s)	Wavelength (m)	Wave frequency (rad/s)
1	0.8	1.0	7.85
2	0.9	1.26	6.98
3	1.0	1.56	6.28
4	1.1	1.87	5.71
5	1.2	2.2	5.24
6	1.3	2.54	4.83
7	1.4	2.88	4.49

7.2.4 Experimental results

Figure 162 shows the motion RAOs of the two barges. In high frequency range (> 6 rad/s), the heave RAOs of barge 2 are larger than those of barge 1, the opposite observation is shown in low frequency range.

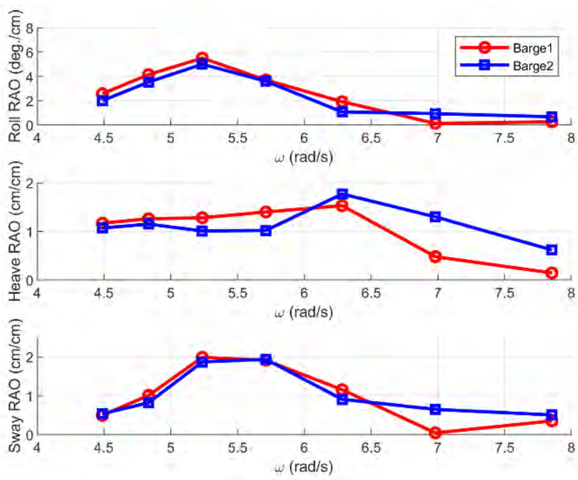

Figure 162: Motion RAOs of the two barges

Figure 163 presents the wave elevations measured at the gap (WG2). The time series of wave elevation reveals a stronger second-order effect for incident wave conditions with a period similar to the natural roll period of the barges (1.17 s).

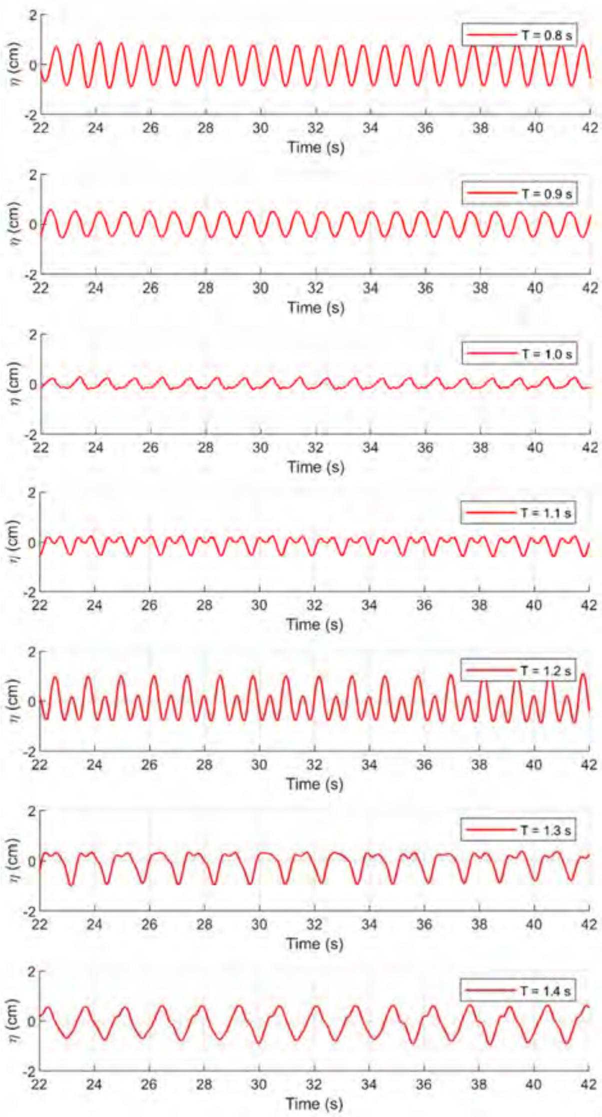

Figure 163: Wave elevation measured at WG2

The FFT results of the measured wave elevations at WG2 are shown in Figure 164. The second-order resonance occurs at the incident wave frequency similar to the roll natural frequency of the barge and the second-order effect reduces for small or high incident wave frequencies.

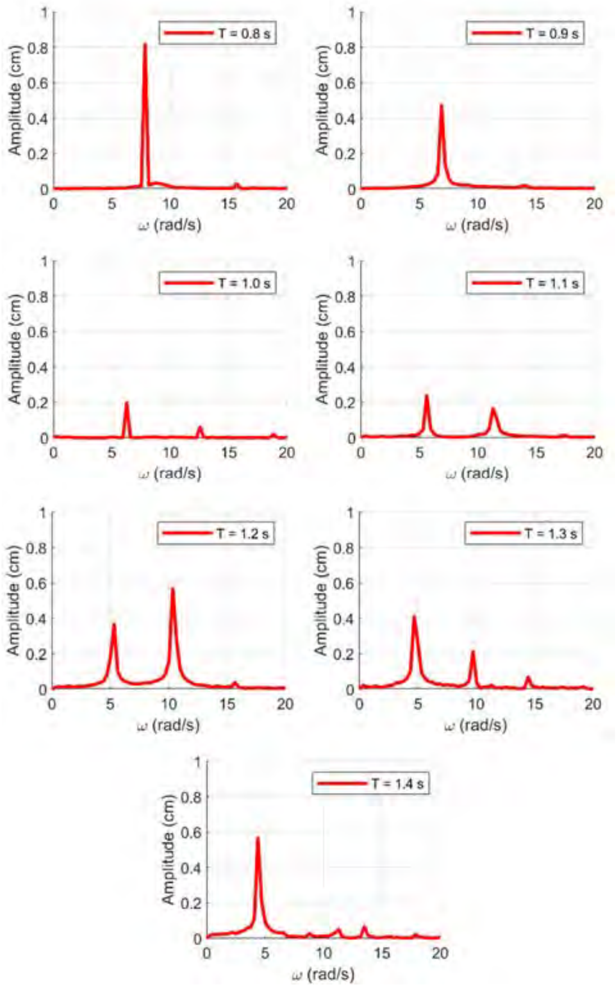

Figure 164: FFT results of the wave elevation measured at WG2

7.3 CFD Benchmark Study on Two-body Interaction

A test procedure was suggested for the CFD benchmark study on two-body interaction, with test parameters to be investigated in each step as

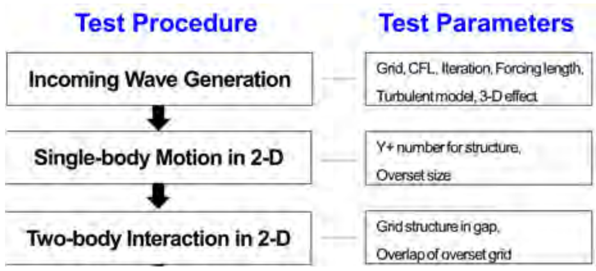

Figure 165: Test procedure and parameters to be studied for the CFD benchmark study on two-body

shown in Figure 165. The procedure was set to include the whole parameters that may have influenced on the results, and each parameter were studied at each step with that dependency and uncertainty tests.

7.3.1 Incoming wave generation (numerical wave tank setup)

As the first step, incoming wave generation, which is the main factor for the structure's motion, was conducted with the setup of the numerical wave tank. The test parameters to be studied and each number of cases are listed below,

- Grid and CFL condition (5 cases)
- Iteration number (5 cases)
- Wave reflection (5 cases for forcing length, 2 cases for w/ and w/o grid damping)
- Turbulent model (5 cases)
- 3-D effect (5 cases)

For the validation of the wave generation in the CFD simulation, the theoretical wave elevation and water particle velocity profiles were compared to simulate not only the wave shape but also the flow kinematics of the incoming wave.

7.3.2 single-body motion in 2-D

Uncertainty studies for single-body motion simulations were carried out in 2-D to investigate the parameters related to the structure's motion in CFD for the targets below,

- Implementation of viscous effect: Y+ number (5 cases for viscous sub-layer (1, 5), buffer layer (30), and outer layer (100, 200))
- Size of overset grid (5 cases)

The validation was performed with the experiments of single body motion as described in section 6.2, that provided the results of the free decay test, roll, heave and sway RAO under regular waves for a rectangular box in 2-D.

7.3.3 Two-body interaction in 2-D

The CFD will be performed in 2-D conditions, to study the feasibility of the methodologies for two-body motion analysis with less calculation loads than 3-D with investigation on the sensitivity of the wave elevation in the gap that is one of the main purposes of this study. The parameters to be studied in this step are listed below,

- Feasibility study of two-body overset grid system (for overlap of two overset grids).
- Grid system in the gap between two bodies.

In this study, the validation will be conducted with the experimental results of two body interactions mentioned in section 6.2.

7.4 Computational setup for simulation

In this study, commercial software of STAR-CCM+ was used to simulate the two-body interaction in CFD. The general numerical methods are listed below,

- Software: STAR-CCM+ V13.06
- Discretization scheme: Finite Volume Method (FVM)
- Density: Incompressible Flow
- Pressure and velocity field: Segregated SIMPLE method
- Unsteady: Unsteady with dynamic time step (based on CFL number)

Specific numerical schemes are followed below,

- Convection term: 2nd order Upwind
- Temporal term: 2nd order Euler implicit
- Conserved: Mass, momentum, kinetic energy
- Linearization: Newton
- Iterative: Direct matrix inversion
- Pre-conditioning/acceleration: Under relaxation

The simulation was performed using Intel Xeon E5-2690 with 212 processors with MPI paralleling method.

7.5 Simulation Results

7.5.1 Incoming wave generation

As the first step of the CFD benchmark study, a series of uncertainty tests were performed for an accurate simulation of incoming wave generation. Figure 166 shows the computational domain for the uncertainty test of wave generation. The domain has a length of 18m in 2-D, and boundary conditions of velocity inlet and pressure outlet at inlet and outlet planes, respectively, and symmetry for the top and bottom. The grid system was generated with hexahedral mesh in Cartesian coordinates.

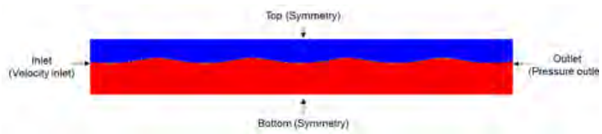

Figure 166: Computational domain for uncertainty test of incoming wave generation

The uncertainty tests for the incoming wave generation were processed following the verification and validation methodology suggested by Stern et al. (2001) and ITTC (2007) for the parameters of the grid, CFL, number of iterations, wave reflection, and turbulent model to determine the proper value with an estimation of the error of the spatial and temporal discretization.

The uncertainty test requires at least three solutions, i.e., between medium-fine $\varepsilon_{i,21} = S_{i,2} - S_{i,1}$ and coarse-medium $\varepsilon_{i,32} = S_{i,3} - S_{i,2}$, to define the convergence ratio R_i as below,

$$R_i = \varepsilon_{i,21}/\varepsilon_{i,32}$$

In the study, five solutions were used for higher accuracy of the uncertainty test. When the ratio was from 0 to 1, the uncertainty was obtained using the method of Richardson Extrapolation using below equations,

$$p_i = \frac{ln\left|\varepsilon_{i,32}/\varepsilon_{i,21}\right|}{ln(r_i)}$$

$$C = \frac{r_i^{p_i} - 1}{r_i^{p_{i,est}} - 1}$$

where p_i is the order of accuracy, C is correction factor, and r is the refinement ratio. Then, the uncertainty U) and corrected uncertainty (U_C) can be calculated using the equations below,

$$U_i = \left|C\,\frac{\varepsilon_{i,21}}{r_i^{p_i}-1}\right| + \left|(1-C)\,\frac{\varepsilon_{i,21}}{r_i^{p_i}-1}\right|$$

$$U_{i_C} = \left|(1-C)\,\frac{\varepsilon_{i,21}}{r_i^{p_i} - 1}\right|$$

Table 10 and Table 11 show the simulation cases and uncertainty test results for the grid setup for the wave generation. The tests were performed with the refinement ratio of $\sqrt{2}$, and five cases were simulated from very coarse to very fine. The results of incoming wave height showed monotonic convergence for the coarse-medium-fine cases with an uncertainty of 0.005% as shown in Figure 167.

Table 10: Simulation cases for grid uncertainty test

	Very coarse	Coarse	Medium	Fine	Very fine
Cell length (m)	0.06	0.042426	0.03	0.021213	0.015
Cell height (m)	0.008	0.005657	0.004	0.002828	0.002
No. of cells in length	68	96	135	191	271
No. of cells in height	17	24	34	48	68
Result (Wave height, m)	0.13397	0.13429	0.13437	0.13449	0.13440

Table 11: Uncertainty test results for grid setup

Case	1-2-3	2-3-4	3-4-5	1-3-5
R (Convergence Ratio)	4.19	0.614	-1.31	13.3
P (Order of Accuracy)		1.41		
C (Correction Factor)		0.630		
U_G(Uncertainty)		0.012%	0.006	
$U_{G,C}$ (Corrected Uncertainty)		0.005%		

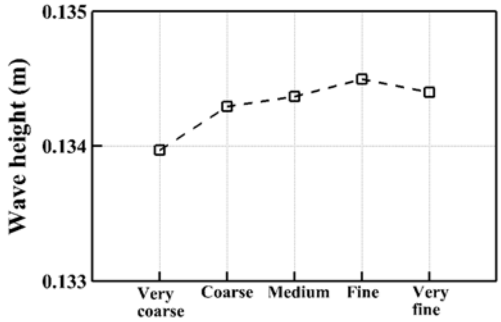

Figure 167: Uncertainty test results for various grid size

Table 12 and Table 13 show the simulation cases and uncertainty test results for the CFL number for the wave generation. The tests were performed with the refinement ratio of $\sqrt{2}$,, and five cases were simulated from 1.0 to 0.25. The results of incoming wave height showed monotonic convergence for the coarse-medium-fine cases with an uncertainty of 0.009% as shown in Figure 168.

Table 12: Simulation cases for CFL uncertainty test

	Very coarse	Coarse	Medium	Fine	Very fine
CFL Number	1.0	0.71	0.50	0.35	0.25
T/Δt	459	647	918	1312	1837
Result (Wave height, m)	0.13453	0.13441	0.13438	0.13433	0.13435

Table 13: Uncertainty test results for CFL number

Case	1-2-3	2-3-4	3-4-5	1-3-5
R (Convergence Ratio)	3.43	0.778	-2.25	6.20
P (Order of Accuracy)		0.725		
C (Correction Factor)		0.286		
U_G(Uncertainty)		0.001%	0.002	
$U_{G,C}$ (Corrected Uncertainty)		0.009%		

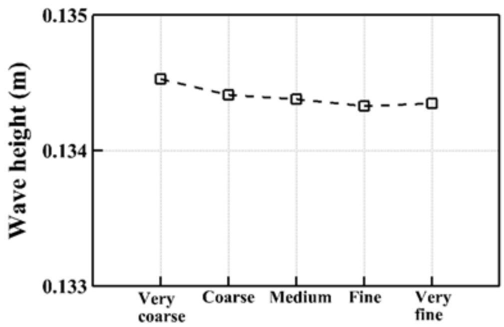

Figure 168: Uncertainty test results for various CFL number

In this study, the forcing method (Siemens, 2023) was applied to avoid wave reflection in the numerical wave tank. The forcing method is to damp the source term in the transport equation as below.

$$q_{\emptyset} = -\gamma\rho(\emptyset - \emptyset^*)$$

where γ is the forcing coefficient,ρ is the fluid density, $\emptyset$ is the current solution of the transport, and $\emptyset^*$ is the value towards which the solution is forced. To determine the forcing lengths in the simulation domain, the reflection coefficients were calculated for various forcing length from 1 wavelength to 4 times of the wavelength with a refinement ratio of $\sqrt{2}$ as shown in Table 14. The reflection coefficient was obtained using the method suggested by Goda and Suzuki (1976) to estimate the incoming and reflected wave heights using two-point methods.

Table 14: Uncertainty test results for wave reflection

	Very short	Short	Medium	Long	Very long
Forcing Length	2.03	2.87	4.06	5.74	8.12
Result (Reflection Coff.)	7.26%	3.68%	1.47%	5.90%	Diverged

The results showed the lowest reflection coefficient of 1.47% when the forcing length was 4.06m, which corresponds to double of incoming wavelength.

The turbulent model for the wave generation was also tested with 5 different models as listed below,

- Laminar
- 1-equation model: Spalart-Allamas (SA)
- 2-equation model: $k - \varepsilon$, $k - \omega$
- 7-equation model: Reynolds Stress Model (RSM)

Figure 169 shows the comparison of incoming wave elevations for each turbulent model. The wave shapes were almost similar for all of the turbulent models, and the wave heights were also similar as shown in Figure 170. In this study, the turbulent model of $k - \omega$ was applied for the simulation considering the simulation of the structure's motion (Kim et al., 2020).

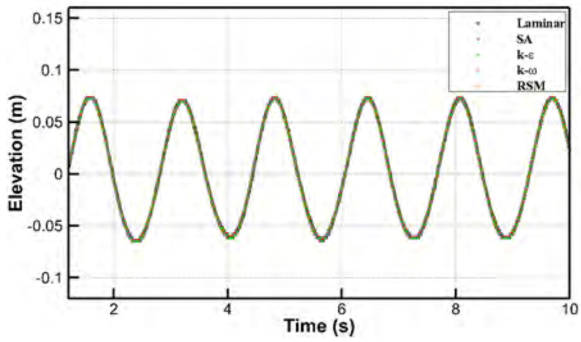

Figure 169: Comparison of wave elevation for various turbulent model

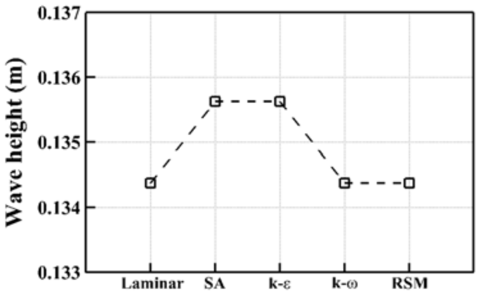

Figure 170: Comparison of wave height for various turbulent model

Figure 171 and Figure 172 show the final wave elevation and water particle velocity profiles in comparison with the theoretical value of Stokes' 3rd order wave theory. The wave elevation and water particle velocity profile agreed well with the theoretical values using the parameters determined by the uncertainty tests for the grid, CFL, iteration, wave reflection, and turbulent model.

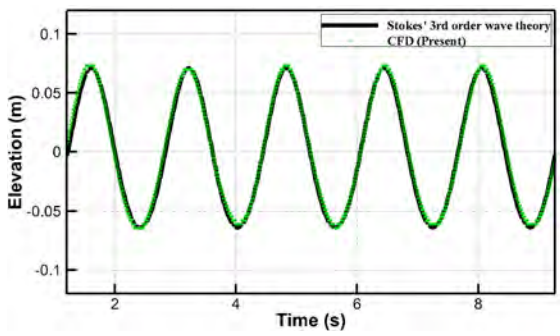

Figure 171: Wave elevation in comparison with theoretical results of Stokes' 3rd order wave theory

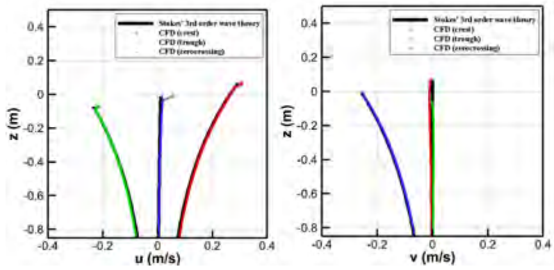

Figure 172: Water particle velocity profile in comparison with theoretical results of Stokes' 3rd order wave theory

7.5.2 Single-body motion in 2-D

In this section, the roll motion analysis was performed for a simplified structure in 2-D to study the parameters related to the motions, Y+ number, and size of the overset grid. A series of simulations was performed with the experimental study of Kim et al. (2020) with the experimental condition as shown in Figure 173.

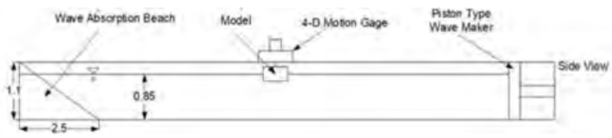

Figure 173: Experimental condition in Kim et al. (2020)

To study the viscous effect in the structure's motion, the parametric test was carried out for the free decay test with various Y+ numbers in the normal direction of the structure's wall. Table 15 shows the Y+ number used in the study corresponding to each structure in the turbulent boundary layer. The free decay test was performed with its initial angle of 22°, with a fixed overset grid size of 0.60m X 0.33m.

Table 15: Uncertainty test condition and results for Y+ number

	Viscous sub-layer 1	Viscous sub-layer 2	Buffer layer	Outer layer 1	Outer layer 2
Y+ number	1	5	30	100	200
1st cell height (mm)	0.0008	0.0044	0.0263	0.0878	0.1756
Total num. of grid	0.232 M	0.231 M	0.229 M	0.228 M	0.227 M
Mean roll period (s) [Exp. 0.500s]	**0.506**	**0.501**	**0.502**	**0.512**	**0.504**
Extinction slope [Exp: 0.493]	**0.429**	**0.485**	**0.484**	**0.498**	**0.486**

The results of the parametric test were shown in Figure 174 and Figure 175 as time history and extinction curve for the free decay tests. It was found that the natural roll period was varied with the different Y+ numbers, and it corresponded to the slope in the extinction curve. The smallest error with the experiments was shown with the Y+ number of 5 corresponding to the viscous sub-layer.

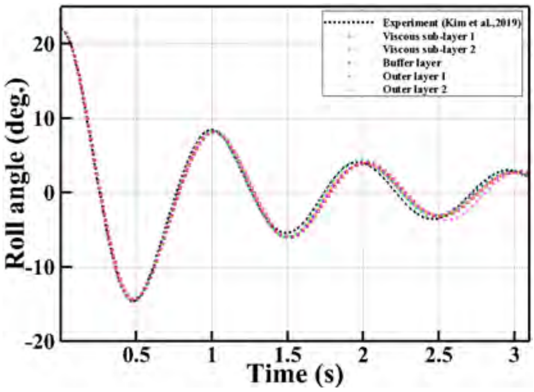

Figure 174: Time history of free decay test for various Y+ number

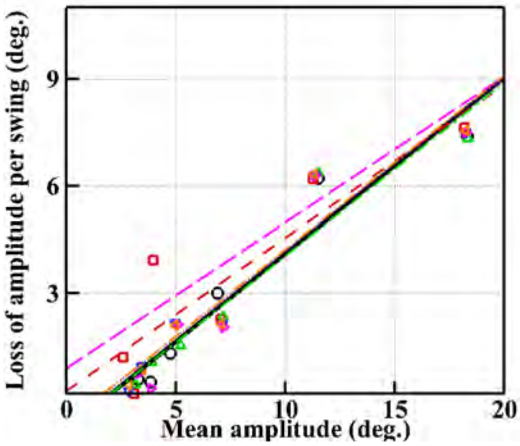

Figure 175: Time history of free decay test for various Y+ number

Table 16: Uncertainty test condition and results for overset size

	Very small	Small	Medium	Large	Very Large
Breadth (m, ratio to B)	0.30 (1.5)	0.42 ($1.5\sqrt{2}$)	0.60 (3)	0.85 ($3\sqrt{2}$)	1.20 (6)
Draft (m, ratio to d)	0.11 (1.5)	0.15 ($1.5\sqrt{2}$)	0.21 (3)	0.30 ($3\sqrt{2}$)	0.42 (6)
Freeboard (m, ratio to F)	0.08 (1)	0.11 ($\sqrt{2}$)	0.16 (2)	0.23 ($2\sqrt{2}$)	0.32 (2)
Total num. of grid	Failed	0.210 M	0.231 M	0.253 M	0.276 M
Mean diff. of peak angle(°)	-	0.296	0.336	0.181	1.438
Mean roll period (s) (Exp. 0.500s)	-	0.503	0.502	0.506	0.496

The parametric test was also performed to determine the proper size for the overset grid. The size was varied from very small to very large with the refinement ratio of $\sqrt{2}$, as shown in Table 16, and the results for the time history and extinction curve for the free decay tests are shown in Figure 176 and Figure 177, respectively. Unlike the variation of Y+ number, it was found that the amplitude of the roll angle was changed for the different overset grid size and showed the best agreement with the small size of the overset grid.

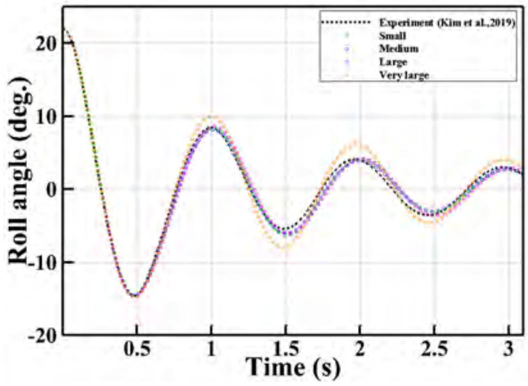

Figure 176: Time history of free decay test for various overset grid size

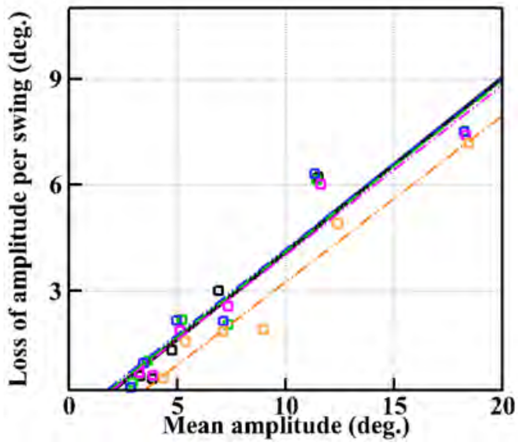

Figure 177: Time history of free decay test for various overset grid size

Using the Y+ number and overset grid size determined in the parametric tests, the simulation will be performed for the motions of the rectangular barge under regular waves and validated with the experimental results provided in section 6.2.

After the simulations of single body motions, the simulations for the two-body interactions in section 6.2 will be performed following the test procedure in Figure 165, and the results will be included in the next report.

8. EXTRACTION METHODS OF NODULES FROM THE SEABED

Deep-sea mining technology has been gradually developed since the 1960s to alleviate the contradiction between the supply of and demand for land-based mineral resources (Simon-Lledó et al. (2019)). The most commonly used deep-sea mining system consists of mother ship, hydraulic lifting pipe and seabed mining vehicle, which is proposed by OMI, as shown in Figure 178 (Hong et al. (2010)). Among the three parts, the seabed mining vehicle fulfils the function of extracting nodules from the seabed. At present, methods of nodule extraction mainly include mechanical, hydraulic and hybrid hydraulic-mechanical types.

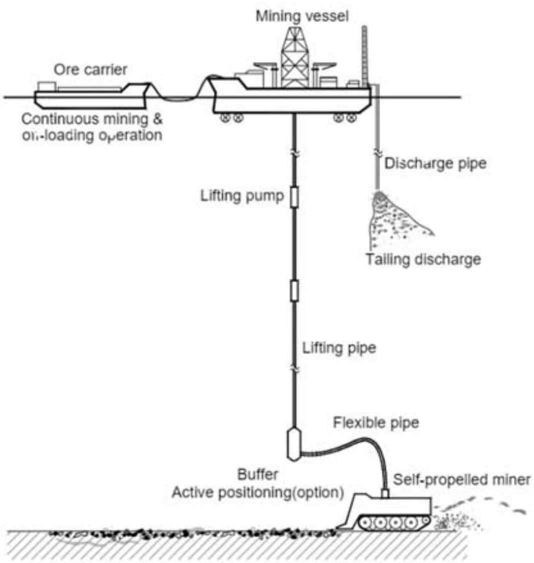

Figure 178: Typical deep-sea mining system (Hong et al. (2010))

The studies on nodule extraction methods are mainly focused on two aspects (Boetius et al. (2018)): (1) high collection efficiency, to collect as many nodules as possible with the same energy consumption, and (2) low environmental disturbance, to disturb and damage the seabed sediment and the native ecological environment as little as possible. Relevant scholars and institutions have conducted research on different nodule extraction methods by means of numerical calculations, model experiments and in situ experiments.

8.1 Mechanical Nodule Extraction Methods

Mechanical nodule extraction methods undercuts the seabed with a rake-like front to dislocate the nodules, and then lifts the nodules through a steep incline belt conveyor (Cho et al. (2019)). OMCO's nodule extraction facility used a rotary chain tooth structure to collect nodules and transport them to the seafloor mining vehicle (Welling et al. (1981)). Combined comb shovels have been used in India to collect nodules from the seafloor and deliver them to a rotating chain plate during sea trials (Deepak et al. (2007)).

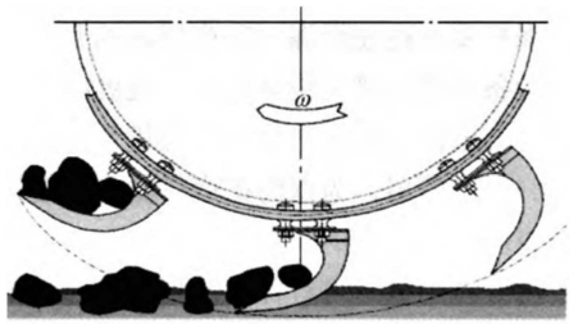

Figure 179: OMCO's nodule extraction facility (Welling et al. (1981))

The mechanical nodule collector developed by IKS is mounted on a cable to keep it at a certain distance from the ground (Handschuh et al. (2001)). The other end is connected to the lower conveyor drum shaft. The frame consists mainly of profiled metal plates assembled with a comb grid structure. The tooth-like front of the structure undercuts the seabed to allow for smooth displacement of the manganese nodules. In addition, a mechanically driven mobile comb structure moves through the gaps of the frame structure. In this way, the nodules are lifted and moved onto the belt conveyor. In order to clean the nodules before discharging them onto the conveyor belt, a vibrator is mounted on the basic frame. The two comb-like structures clean each other of sediment residue by relative motion. The nodules are then lifted from the picker or loader unit by the steeply inclined belt conveyor and conveyed to the crusher before entering the piston pump inlet.

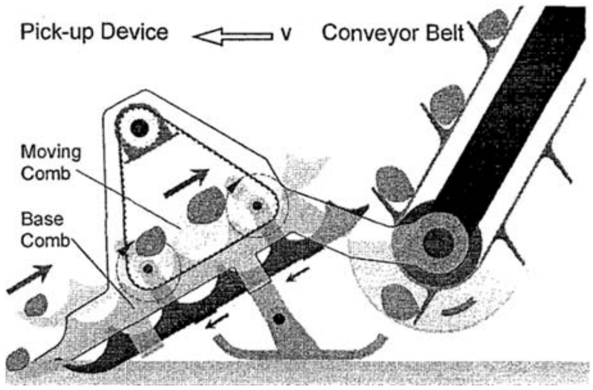

Figure 180: Concept of IKS's mechanical nodule collector (Handschuh et al. (2001))

However, the results of many experiments show that, although the collection efficiency of the mechanical nodule extraction methods is relatively high, the moving parts in the structure are easy to be damaged. The nodules are easy to be trapped in the moving parts, so the requirements of long-time and continuous work cannot be satisfied. Moreover, the mechanical method will dig up a large amount of sediment while extracting the nodules, which is more destructive to the environment. As a result, mechanical nodule extraction methods are less frequently used in existing sea trial equipment.

8.2 Hydraulic Nodule Extraction Methods

The hydraulic methods use water currents to separate and move nodules that are deposited on the surface of the seabed, and capture manganese nodules with hydrodynamic low-pressure action (Jia et al. (2022)). The mechanism is relatively simple and durable. However, due to the eddy current effect, the hydraulic methods have a lower collection efficiency and higher energy consumption compared to the mechanical methods. According to the characteristics of the flow field structure, the typical hydraulic nodule extraction methods can be divided into three types: suck-up-based method, Coandă-effect-based method, and double-jet hydraulic method.

8.2.1 Suck-up-based method

The principle of suck-up-based method is similar to a vacuum cleaner, generally using axial vane pumps to absorb the nodules. The flow field formed by the suction current drives the nodules to move. In the OMA DEEPSEA MINER II sea trials in 1977-1978, the suck-up-based method collected about 500 tons of nodules continuously in a single day, basically achieving the expected collection results. The performance was generally acceptable in terms of reliability, but it was also found to have high energy consumption and low hydraulic efficiency (Kaufman et al. (1985)).

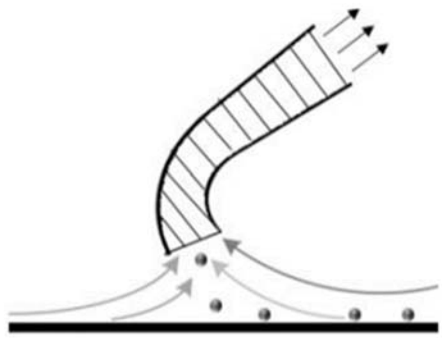

Figure 181: Principle of the suck-up-based method (Kaufman et al. (1985))

Xiong et al. (2018) abstracted the physical model of the flow of spheres inside a vertical pipe from the suck-up-based method. A numerical model of solid-liquid two-phase flow with a large particle was established based on the coupled Resolved CFD-DEM method, and the effect of particle size on its motion characteristics and flow field structure inside the pipe was investigated. The force analysis of single spherical particles in the fluid provided the equations of motion of the particles and revealed the relationship of each parameter in the equations. The results showed that the flow field velocity is large in the middle of the vertical pipe and small near the pipe wall, and both the settling velocity and floating velocity of the particles increase with the increase of particle size.

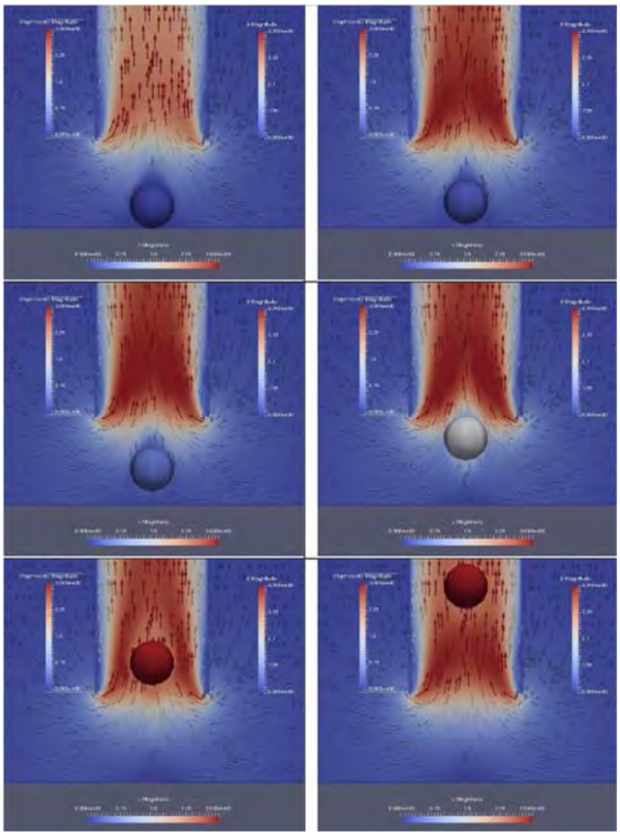

Figure 182: Numerical simulation diagram by Xiong et al. (2018)

Zhao et al. (2018) set up a model test system and tested 253 cases, and established an empirical model for the prediction of collection performance by studying the vertical force characteristics and vertical initial motion characteristics of the particles in suction flow field. The study revealed the effects of the parameters of the particle size, round tube size, and height of the collector head off the bottom on the vertical force characteristics and vertical initial motion characteristics of the particles. The results showed that the vertical suction force coefficient decreases exponentially with the ratio of bottom clearance to diameter of the particle, increases linearly with the ratio of diameter of the suction pipe to diameter of the particle, and is almost unaffected by the Reynolds number (Re). In addition, a new experimental phenomenon in which vortex could help strengthen the suction force was observed.

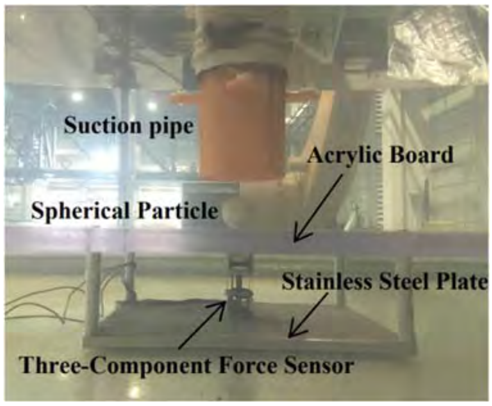

Figure 183: The experimental system by Zhao et al. (2018)

Based on the principle that the vertical axis vortex can induce particle initiation, Zhao et al. (2021) proposed a new concept of using spiral flow to collect nodules. Five types of tests (fixed suction, moving suction, suction flow field, sediment-water mixture, and vertical incipient motion tests) were conducted to investigate the similarities and differences in the collection performance of pick-up devices with and without spiral deflectors. In addition, the study measured velocity vectors and velocity distributions using the particle image velocimetry (PIV) system to reveal suction flow field characteristics. The results proved that the pick-up device using the spiral flow principle can realize enhanced suction forces on the nodules, an increased h' for a certain v, as well as a significantly increased occurrence probability of the circular motion of nodules.

Furthermore, Liu et al. (2023) designed a new type of sucker-shaped hydraulic nodule pick-up device equipped with four tangential jet nozzles. The study investigated the characteristics of flow field velocity distribution, the nodule initiation trajectory and collection rate under three different collecting flow models of low, medium, and high swirling strength. The results showed that the nodules are affected by the vertical axis vortex, which produces an obvious circular motion when moving vertically in the high swirling strength, and are lifted near the center region of the collecting head. When the nodule collection rate exceeds 90%, the necessity of collecting flow reduces as the swirling strength rises.

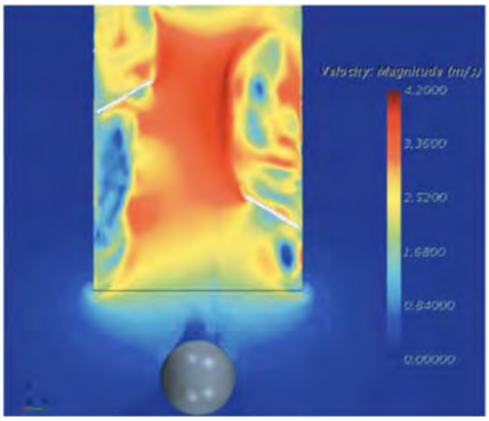

Figure 184: Velocity distribution in spiral flow (Zhao et al. (2021))

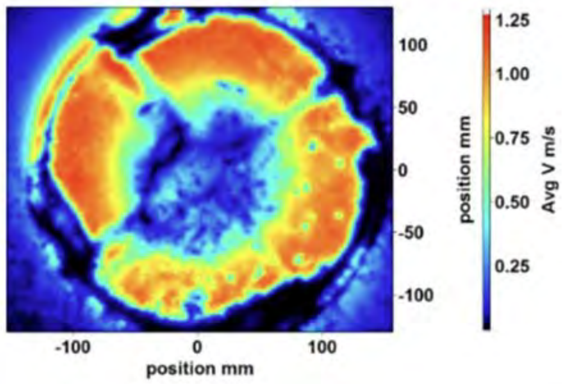

Figure 185: Numerical simulation diagram by Liu et al. (2023)

8.2.2 Coandă-effect-based method

The Coandă-effect-based method creates a flow structure with low pressure near the wall and high pressure at the far wall. The nodules are lifted by the vertical pressure difference. In 1997, the manganese nodule collection test in Japan verified that the collection efficiency of the attached-wall jet type technology could reach a maximum of 87% (Yamada et al. (1998)).

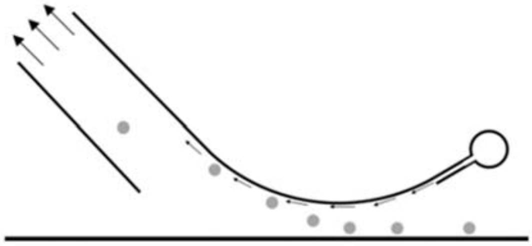

Figure 186: Principle of the Coandă-effect-based method (Kim et al. (2019))

Rodman et al. (1989) simulated two-dimensional straight and curved wall jet flows by axial jetting on a cylinder, and showed that integral momentum analysis was able to accurately predict the effect of curvature on the mean flow in both two-dimensional and annular attached-wall jets, and that the transverse curvature of the upstream portion of the jet had a smaller effect on the mean flow and the turbulent shear stress.

Lim et al. (2015) investigated the distribution of flow velocity and streamlines and the change of turbulent kinetic energy in the flow field during the operation of the collector by numerical calculation. The results showed that the operation flow rate and the behavior of polymetallic nodule would largely affect the characteristics of the flow field of the attached-wall jet. The outflow discharge effect reaches to about 2~3 times of the collecting device in the back while the front flow field of device was slightly affected by the outflow discharge, and the degree of influence is also dependent on the travel speed of the collector. Additionally, averaged turbulent kinetic energy is up to 7.5 times higher than that of other areas where flow is not influenced by the device while its variation in vertical and side directions is rather limited near the collecting device.

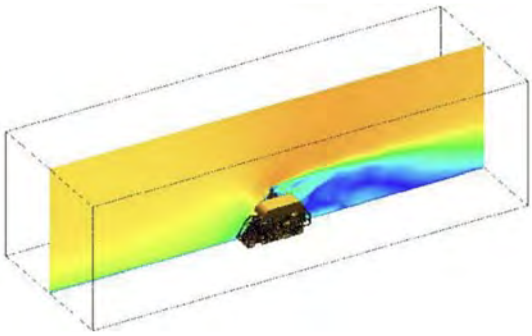

Figure 187: Velocity distribution in numerical simulation by Lim et al. (2015)

Lee et al. (2012) synthesized numerical simulations and physical experiments to study the collection effect of the Coandă-effect-based method, and proposed an optimized design for the mining machine using the multidisciplinary design optimization (MDO) method. Cho et al. (2019) simulated the collection process of nodules through model experiments, and designed optimization of deep-seabed pilot miner system with coupled relations between constraints. The study considered the influence of variables such as nozzle structure, collector plate radius, and flow rate on the collection effect, and investigated the coupling relationship among the sub-systems. The total power consumption of the collector after the final optimized design was reduced by about 14.1% compared with that of a general collector.

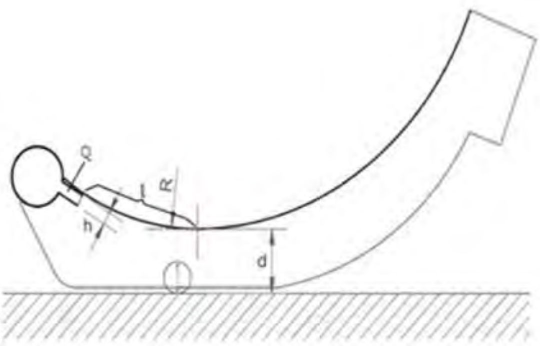

Figure 188: Design variables of collector part of pilot mining robot system by Cho et al. (2019)

Jia et al. (2023) carried out a simplified model of jets on the surface of a logarithmic spiral, and studied the lift ability of the reduced form of a Coandă-effect-based collector model. It is found that the Coandă effect on the logarithmic spiral becomes stronger with higher jet exit velocity, larger local curvature, and non-dimensional jet slot height. The growth rate, which represents the width of the main jet flow, went up in proportion to the downstream distance. The lift capability of jet flow in logarithmical spiral of x/R = 1 is significantly better than that of x/R = 2/3.

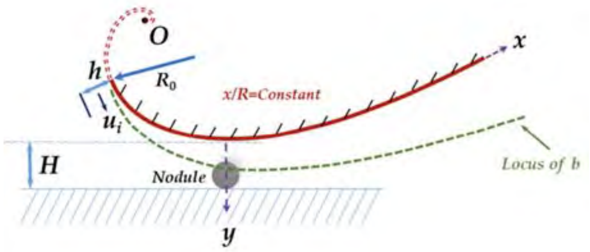

Figure 189: Schematic diagram of a turbulent jet flow over logarithmic spiral wall surface by Jia et al. (2023)

8.2.3 Double-jet hydraulic method

The double-jet hydraulic method uses two rows of opposite nozzles to spray water jets diagonally to the seabed. Water jets intersecting in the intermediate area lift the surrounding nodules into the conveying tube. The OMI sea trials in 1978 used high-pressure water jets to blow nodules up from the seafloor and collect them on the mining vehicle (McFarlane et al. (2008)). The results demonstrated that the hydraulic extraction method had a higher collection efficiency compared to the mechanical method.

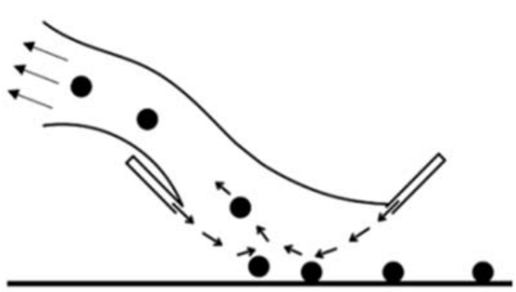

Figure 190: Principle of the double-jet hydraulic method (Handschuh et al. (2001))

Hong et al. (1999) built a double-jet hydraulic nodule extractor consisting of jet pipes and baffles and carried out experiments in a two-dimensional flume. The effects of parameters such as the jet flow rate, the moving speed of the collecting head, the bottom clearance, and the position and shape of the baffles on the collection rate of the collecting head and the fluctuation of the bottom pressure were investigated, and the relationship between the characteristics of the bottom pressure distribution and the pick-up efficiency was revealed. The results showed that the most dominant factor governing the pick-up performance is the water-jet power. To increase the water-jets power it requires enormous energy supply, whereas a good design of baffle plates saves cost with operation. In addition, the function of the rear water-jets is predominant, so enforcement of the rear water-jet by using larger nozzles can improve the pick-up performance at high tow speeds.

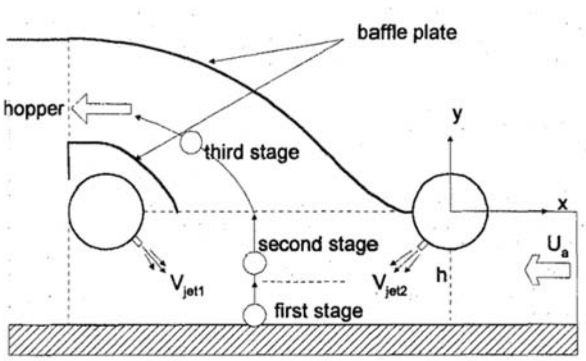

Figure 191: Schematic illustration of nodule lifting process (Hong et al. (1999))

Yang et al. (2003) studied the influence of the shape, size, and mutual position of the baffleplates, jet angle and size of the conveying pipe on the collection effect and power consumption of the double-jet hydraulic method. The results showed that the distance between two rows of the jets should be between 500 and 550 mm, and it will be the best nodules' catching for the heights of two rows of the jets to vary between 90 and 190mm. Additionally, when the distance between the upper and lower walls of the conveying pipe is about 1.3-1.5 times the maximum diameter of the nodule particles, the collection rate of polymetallic nodules is most effective.

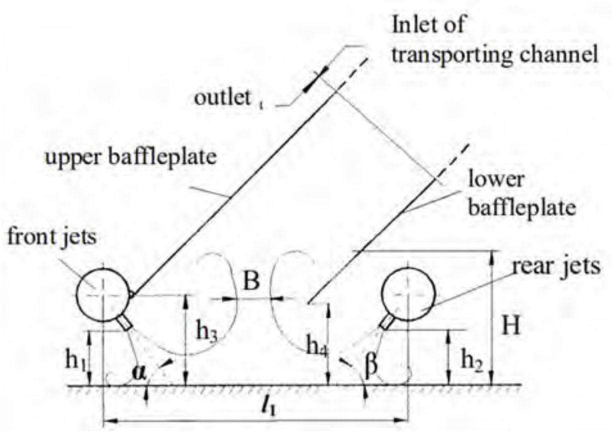

Figure 192: Mechanism of capturing of pick-up device by Yang et al. (2003)

Liu et al. (2023) studied the three-dimensional flow structure near the double-jet hydraulic collector based on numerical simulation, and analyzed the effects of jet flow speed and nodule size on the local flow field, bed shear stress and nodule collecting energy efficiency. The results showed that the bed shear stress increased rapidly from the hysteresis point to the inner side and reached the maximum value near the middle of the two hysteresis points. The maximum bed shear stress increased linearly with the increase of the jet flow speed. The maximum bed shear stress increased by 197.93% when the jet flow speed increased from 6 m/s to 11 m/s. The effective area of incipient motion of nodules and collecting energy efficiency decreased with the increase of nodule diameter, and nodule of smaller size were easier to be stripped and initiated. In addition, the effective area increased exponentially with the increase of jet flow speed. considering the combined influence on both the collecting productivity and the energy efficiency, it is recommended that the flow rate of the collector head jet should be 8-9 m/s.

Some scholars have also conducted a comprehensive comparative study of the above three hydraulic nodule extraction methods. Yue et al. (2021) used numerical simulation to compare these three hydraulic methods in terms of both nodule collection performance and the degree of environmental disturbance, and investigated the effects of flow rate and tow speed on collection rate. The suck-up-based method was found to have the smallest flow field disturbance and require the largest flow rate under the same operating conditions. The double-jet hydraulic method has a significant advantage in terms of collection rate, but has large seafloor disturbances. The Coandă-effect-based method is able to maintain a high collection rate while reducing the disturbance to the sediment, and has greater research value and development prospects.

8.3 Hybrid Hydraulic-Mechanical Methods

The hybrid hydraulic-mechanical pick-up device generally uses a pair of water jets to lift the nodules. These nodules are moved through a baffle plate to a mechanical conveyor, which transports them inside the collector by using a fin scraper. Hybrid pick-up devices have been intensively studied and applied to pilot mining robots because of their environmental friendliness and reliability.

The Korean research team designed a hybrid hydraulic-mechanical pick-up collector as shown in the Figure 193 (Kim et al. (2019)), where the nodules are blown up by high-pressure water from nozzles, channeled through a baffle, and then carried up the collector on a rotating chain plate with a scraper. For this device, Kim et al. (2019) used reliability-based design optimization (RBDO) to improve the reliability of the collection efficiency under environmental uncertainties. A computational model based on the Coandă effect was firstly developed for predicting the collection efficiency of pick-up devices. Next, RBDO based on the Akaike information criterion method was employed to design the pick-up device by using this model. The results showed that the proposed design method significantly improved the design of the pilot mining robot pick-up device.

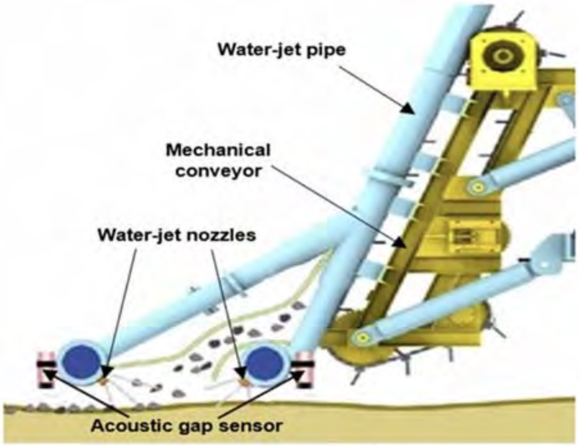

Figure 193: Hybrid hydraulic-mechanical pick-up collector designed by Korea (Kim et al., 2019)

9. TESTING METHODS TO CHARACTERISE THE INFLUENCE OF CHANGING BOTTOM BATHYMETRY AND COASTLINE FOR TANKERS AT OFFLOADING TERMINALS

9.1 Introduction

Ships play a crucial role in global trade as a key component of maritime transportation. They can be categorized into various types based on their specific functions, including commercial vessels, service vessels, and warships. Among these, commercial vessels encompass tankers, which are specifically designed for transporting cargo, as shown in Figure 194 (Ghosh *et al.*, 2015). When conducting a generic, high-level risk assessment for tankers, the research ultimately concluded that the major risk factors associated with tanker transportation originate from five general accident categories: collision, grounding, contact, fire and explosion, and incidents occurring during tanker loading and unloading at terminals (Yeo *et al.*, 2016).

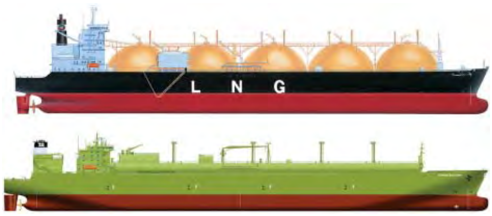

Figure 194: Main types of LNG carriers: moss spherical tankers (top) and membrane tankers (bottom)(Vanem *et al.*, 2008)

In maritime transportation, tanker offloading operations at terminals are of paramount importance (Vanem *et al.*, 2008). Bottom bathymetry and coastline constitute vital environmental factors that influence the operational conditions and safety of tanker offloading terminals. The adequacy of bottom bathymetry is a critical factor in ensuring safe berthing and unloading of tankers, while changes in the coastline may impact port sedimentation and navigation channels, thereby affecting the safety and efficiency of tanker berthing and operations. By conducting a thorough assessment and continuous monitoring of these factors, a better understanding and proactive response to potential changes and challenges can be achieved, thereby ensuring the smooth and safe conduct of tanker offloading processes.

9.2 Physical Model Testing Methods

There have been numerous studies focused on investigating operational challenges during tanker offloading processes resulting from a series of environmental changes using physical model testing methods.

9.2.1 Testing methods focusing on coastline

The proximity of tankers anchored near a breakwater, such as those utilizing berth "A" terminal, highlights the notable impact of the coastline. Creating a scaled model that models both the tanker and the breakwater is a feasible approach. The Hydraulics Laboratory at the Faculty of Engineering - University of Porto (FEUP) conducted physical model tests to study the behavior of moored ships at berth "A" terminal (Santos *et al.*, 2008). A properly calibrated physical model has the potential to provide valuable insights into the effectiveness of potential interventions at the berth "A" oil terminal. As part of a newly approved research project in Portugal, the findings from these physical model tests will be supplemented by motion measurements taken on the prototype (at the berth "A" oil terminal) as well as numerical simulations.

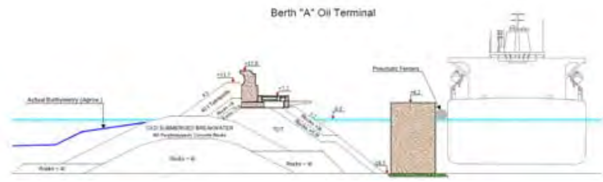

(a)

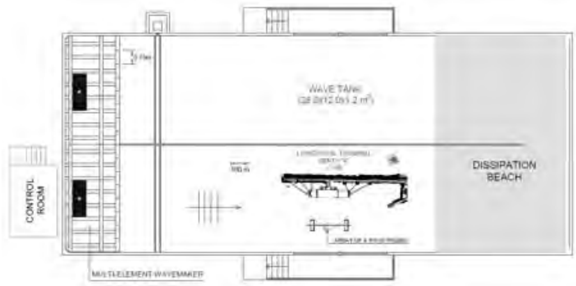

(b)

Figure 195: Model testing of tankers at berth "A" oil terminal: (a) Front view and (b) Top view (Santos *et al.*, 2008)

To investigate the influence of breakwater on the wave field near tanker, 2D physical model is feasible. Following the model tests above, the 2D physical model tests were conducted using both regular and irregular waves. The primary objective of these tests was to juxtapose the current operational conditions with ten diverse proposed alternatives, focusing on variables such as the amount of water overtopping the studied breakwater cross section and the stability of the armor layer blocks.

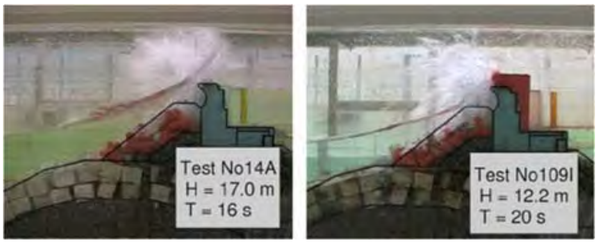

Figure 196: Samples of images taken from the video record of the tests (Santos *et al.*, 2008)

In addition, if the nature coastline should be modelled, movable bed physical model as shown in Figure 197 is feasible. The model was constructed in the wave tank of the hydraulics laboratory of FEUP, in order to reproduce a small stretch of the Portuguese northwest coast, undergoing an erosion situation, having been defined based on typical conditions (hydrodynamic and sedimentary).

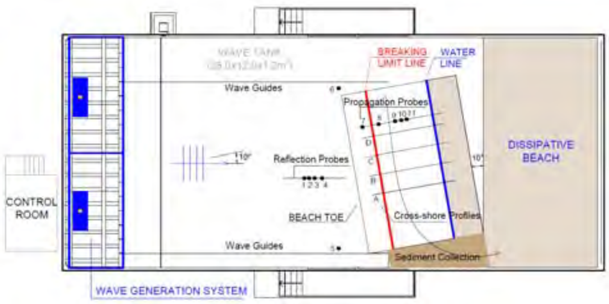

(a)

(b)

Figure 197: 3D movable bed physical model: (a) Top view and (b) Physical model

9.2.2 Testing methods focusing on changing bottom bathymetry

The inadequacy of state-of-the-art methods to accurately predict the slow-drift motion of moored structures in changing bottom bathymetry and coastline has been demonstrated (Liu *et al.*, 2023). This deficiency arises from the fact that not only do the second-order long waves fail to achieve the amplitudes predicted by the flat bottom model, but their phases are also altered in relation to the short wave envelopes. While these phenomena have long been recognized in coastal engineering (Battjes *et al.*, 2004), the full implications of the phase modification on the Quadratic Transfer Functions may not have been fully grasped.

An experimental campaign was conducted to study the slow-drift motion of a rectangular barge moored at different positions along an inclined beach, across water depths ranging from 54 cm to 21 cm. Utilizing the shoaling model for the barge tests led to notably improved concordance between numerical and experimental results for its slow-drift sway motion (Liu *et al.*, 2011).

Figure 198: Barge model undergoing irregular wave tests at the shallowest position (Liu *et al.*, 2011)

Similar testing method was also used to investigate the linear and quadratic damping coefficients over variable bathymetry (Wang *et al.*, 2022). An artificial steel-made bottom is installed on the basin bottom modeling the varying seafloor. The seafloor consists of two sloping angles. A 4.5 m-long and 22.5 m-wide plate is installed first to form a 2 deg sloping seafloor. A 1 m-long plate is utilized as the second 7 deg sloping seabed. The module is deployed at 3 m away from the origin of the long plate. The water depth changes from 60.47 cm to 33.11 cm. This multi-slope seafloor is modeled based on the underwater environment of the practical operating location.

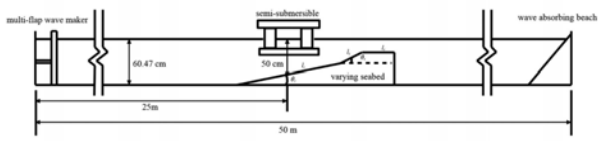

(a)

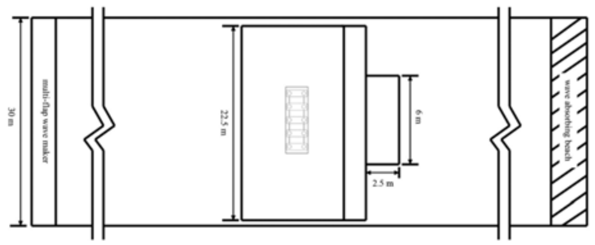

(b)

Figure 199: (a) Side view and (b) Top view of basin bottom modeling the varying sea floor (Wang *et al.*, 2022)

9.3 Field Measurements and Data Collection

From the perspective of investigating the influence of changing bottom bathymetry and coastline on tankers at offloading terminals, there are also studies that have utilized field trials as a method of data collection for model tests.

In the context of investigating the impact of changing bottom bathymetry and coastline on tankers at offloading terminals, six distinct methodologies were examined for characterizing the initial surf zone and nearshore bottom boundary conditions at both Narrabeen and Duck (Turner *et al.*, 2016). These methodologies encompass three "representative" bathymetries, which were developed using abundant historical survey data from both locations, as well as two "synthetic" bathymetries derived from equilibrium beach profile theory (Matheen *et al.*, 2021).

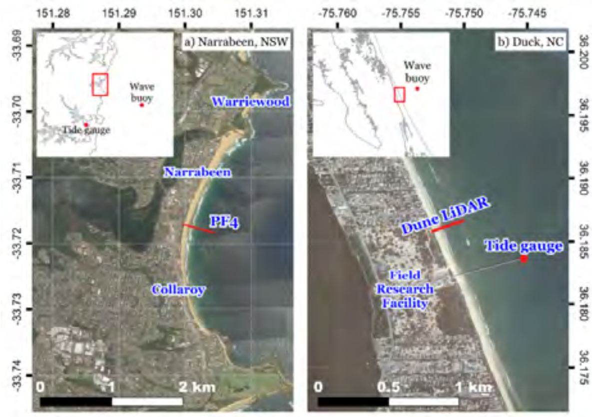

(a) (b)

Figure 200: (a) Narrabeen and (b) Duck study sites used in the study (Turner *et al.*, 2016)

As an example, considering the case of a pre-storm surveyed bathymetry, which is designed to represent the most optimal scenario. In this approach, an in-situ survey is conducted shortly before each individual storm, serving as the initial bottom boundary condition for XBeach modeling. At Narrabeen, these pre-storm surveys of the surf zone and nearshore areas were performed using a single-beam echo sounder mounted on a jet-ski (Turner *et al.*, 2016). Meanwhile, at Duck, the pre-storm bathymetry was derived by combining approximate monthly surveys of the surf zone and nearshore areas with an available regional dataset (Young *et al.*, 2018). This process also yielded a seamless bathymetry extending up to the offshore model boundary.

During the months of July and August in 1976, the research vessel R/V KARLUK conducted a series of soundings across the entrance channel of Prudhoe Bay and in the vicinity of the newly constructed causeway to the west of the channel. Additionally, a smaller boat was utilized to collect data by running lines between Stump Island and the causeway. This collected data was then juxtaposed with the detailed coastal outlines and nearshore bathymetry provided by the U.S. Coast and Geodetic Survey's smooth sheet (7857) and 1970 U.S. Geological Survey orthophotos. This comparison allowed for the identification of qualitative changes in bathymetry and coastal configurations. Ultimately, this assessment established a foundational point from which to evaluate both natural alterations and human-induced changes that have occurred since 1950 (Barnes *et al.*, 1977).

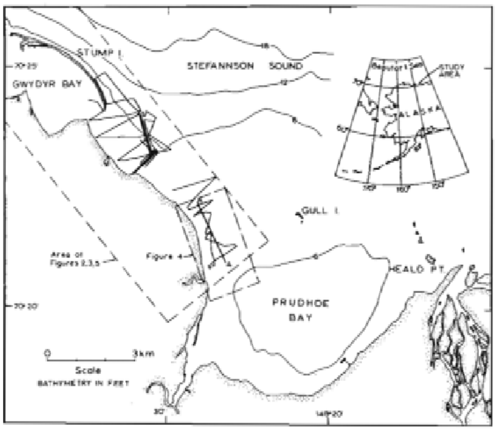

Figure 201: a series of sounding lines (Barnes *et al.*, 1977)

10. CONCLUSIONS & RECOMMENDATIONS

10.1 State-of-the-art Reviews on Bottom Founded and Floating Offshore Structures

In the present ITTC period (2021-2024), the review has allowed the identification of some issues of concern associated with bottom-founded structures and stationary floating structures, including FPSOs, Semi-submersibles, TLPs, Spars, VLFS, FLNGs, FSRUs, and their riser/mooring and dynamic positioning systems. Artificial intelligence methods are being introduced in the global performance evaluation of the floating platforms. The hydrodynamic behavior has been investigated numerically and experimentally, focusing on responses under extreme and damage conditions. The experimental work related to vortex-induced motions also continues. The focus of the spar studies is on heave plate, strake performance, viscous drag and parametric resonance in relation to the floater motions.

10.2 Review of the Existing Procedures

The Committee has reviewed and updated fourteen (14) procedures and guidelines. In general, minor revisions have been made. The detailed comments from the Advisory Committee have also been incorporated.

Concerning the existing procedures and guidelines, the Ocean Engineering Committee would like to make the following recommendations to the 30th ITTC:

- Adopt the updated guideline: 7.5-02-07-01.1 Laboratory Modelling of Multidirectional Irregular Wave Spectra;
- Adopt the updated guideline: 7.5-02-07-01.2 Laboratory Modelling of Waves;
- Adopt the updated procedure: 7.5-02-07-01.4 Confidence Intervals for Significant Wave;
- Adopt the updated guideline: 7.5-02-07-01.5 Laboratory Modelling of Wind;
- Adopt the updated guideline: 7.5-02-07-01.6 Laboratory Modelling of Currents;
- Adopt the updated procedure: 7.5-02-07-03.1 Floating Offshore Platform Experiments;
- Adopt the updated procedure: 7.5-02-07-03.2 Analysis Procedure for Model Tests in Regular Waves;
- Adopt the updated procedure: 7.5-02-07-03.5 Passive Hybrid Model

Tests of Floating Offshore Structures with Mooring Lines;

- Adopt the updated procedure: 7.5-02-07-03.6 Dynamic Positioning System Model Test Experiments;
- Adopt the updated guideline: 7.5-02-07-03.10 Guideline for VIV Testing;
- Adopt the updated guideline: 7.5-02-07-03.11 Guideline for model tests of stationary multi-bodies operating in close proximity;
- Adopt the updated guideline: 7.5-02-07-03.13 Guideline for VIM Testing;
- Adopt the updated procedure: 7.5-02-07-03.14 Analysis Procedure of Model Tests in Irregular Waves.
- Adopt the updated guideline: 7.5-02-07-03.16 Model Construction of Offshore Systems.

10.3 Review and Identify Areas of Concern in Modelling and Simulation of Waves, Wind and Currents

The recent literature findings regarding the modelling of extreme waves are reported. Most of the recent works involving the generation of extreme wave events are based on the approaches described previously. Some new methodologies are focused on within the report, such as using the envelope soliton solutions for generating tailored extreme design waves, a High-Order Spectral NWT with an optimization algorithm based on First-Order Reliability Method (FORM). The effects of wave breaking and statistics of occurrence on the wave spectrum, and the role of wind-wave interaction on wave breaking occurrence are examined by review of recent numerical and experimental works.

The state-of-the-art reviews for wave-current interactions are reported. The studies focused on the impact of uniform currents, opposing and following vertical shear currents on the extreme and rogue waves, unidirectional and directional irregular waves.

The exact shape of the wind profile depends on surface roughness and atmospheric stability. The influence of the vertical wind profile is significant on the aerodynamic loads experienced by platforms. Some standard vertical wind profiles for model testing purposes are reported, such as Power-Law Wind Profile, Logarithmic Wind Profile, IEC Wind Profile, Low-Level Jet Wind Profile and API Wind Profile.

Both propeller systems and cable actuators have been used successfully to replicate the thrust force in hybrid model testing. However, there are some challenges associated with using propellers to reproduce the aerodynamic moment and controlling the cables with more complexity. The selection of hybrid testing in a wind tunnel or a wave basin depends on the specific phenomena being investigated. Wind tunnels allow for the replication of wind conditions and the observation of wake behavior and turbine interactions. Wave basins provide a controlled environment for studying the effects of waves and water on the platform's performance. A single propeller or a ducted fan can accurately replicate the thrust forces. For analyses that require the consideration of aerodynamic and gyroscopic moments, a multi-cable winch system is more suitable for the emulation of these moments and provides a comprehensive analysis of the platform’s behavior.

The software in the loop (SIL) system used in the hybrid testing is still under development and there are some issues with regard to repeatability and experimental methodology which require further refinement.

10.4 State-of-the-art in Offshore Aquaculture Systems

Offshore aquaculture systems continue to attract attention, with particular focus on larger floating structures. A variety of studies concern the classifications or design analyses of offshore aquaculture systems. Close containment tank systems have been proposed to avoid the effects of sea lice on fish. Hydrodynamic interactions among the main floating structure, mooring system, and the fishing nets continue to be a major concern, especially under harsh environmental conditions. Several dominant types of offshore aquaculture systems, including flexible cage system, ship-shaped cage system, semi-submersible rigid cage system, submerged cage system and closed containment tank system, are presented with examples emphasizing their advantages and disadvantages. The general considerations, recent challenges and developments for design and operation are also summarized concisely.

10.5 Extend Experimental Wave Run-up Benchmark Tests (Four Squared Vertical Cylinders)

As an extension of the benchmark tests of wave run-ups on four squared vertical cylinders conducted during the 29th ITTC, the present benchmark tests were conducted to measure the wave run-ups and local wave impact loads on fixed four squared cylinders under focused waves. Through systematic analyses, including variations in wave period, steepness and incidence angle, the spatial distribution and vertical variations of wave run-ups and wave impact loads are revealed and the dependence on the wave parameters is examined. A set of benchmark data and results were provided for validating related numerical simulations. Owing to the complicated wave-column interactions, CFD studies are recommended in consideration of four-square-column cases with different configurations and extreme waves.

10.6 CFD Benchmark Study on Two-body Interactions, Focusing on Gap Surface Elevation

The CFD benchmark study for two-body interactions in close proximity is now on going and the interim conclusions can be summarized as below.

- To study the two-body interactions with small gap (0.23B), experiments of two-body motion in beam sea were carried out in 2-D wave tank.
- The experimental results of two-body motions show that the second-order resonance occurs at the incident wave frequency similar to the roll natural frequency of the barge and the second-order effect reduces for small or high incident wave frequencies.

Further CFD benchmark studies on two-bodies in close proximity need to be continued and validated with the experimental results. Experimental benchmark studies are needed for two-body interaction problem with small gaps and resultantly to update the procedure for two-body model test. The final conclusions will be made when the model test and CFD studies with smaller gaps are carried out.

10.7 Extraction Methods of Nodules from the Seabed

In geneal, breakthroughs have been made in some separate technical areas of deep-sea mining, and more and more nodule extraction methods are being proposed. However, the sea trials that have been conducted so far are only individual partial subsystem tests, with limited sea trial time and performance verification. The high productivity, reliability and environmental requirements of commercial deep-sea mining have brought new challenges and opportunities to the development of deep-sea polymetallic nodule mining technologies.

It is also urgent to improve the ability to intelligently sense and recognize the abundance of nodules on the seafloor during the collection process, and to realize the intelligent evaluation and decision-making adjustments of the relevant parameters in order to improve the collection efficiency.

10.8 Testing Methods to Characterise the Influence of Changing Bottom Bathymetry

The impact of changing bottom bathymetry and coastline on tankers at offloading terminals was investigated through a comprehensive analysis of various testing methods. It allowed for an improved understanding of factors such as the water volume overtopping the breakwater cross section and the impacts of water depths. Furthermore, the results of the field measurements and data collection efforts complemented the findings from the physical model tests. This integrated approach enabled a comprehensive assessment of the operational conditions at the tanker offloading terminal. The obtained insights have implications for both safety and efficiency considerations in tanker offloading operations.

In light of these findings, it is recommended that ongoing research in this area continues to employ a combination of physical model testing and field measurements. This multi-faceted approach will contribute to a more accurate understanding of the complex interactions between changing bottom bathymetry, coastline alterations, and their impact on the operational performance of oil terminals.

10.9 New Guideline for Testing Nodule Mining Machines in a Towing Tank

The Ocean Engineering Committee would like to make the following recommendation to the 30th ITTC:

- Adopt the new guideline: 7.5-02-07-03.17 Testing Nodule Mining Machines in a towing tank.

11. REFERENCES

ABS, 2020. Guide for Building and Classing, Aquaculture Installations; American Bureau of Shipping: Houston, TX, USA.

Antonutti, R., Poirier, J. C., Gueydon, S., 2020. Coupled testing of floating wind turbines in waves and wind using winches and software-in-the-loop. In Offshore Technology Conference (p. D021S019R001). OTC. https://doi.org/10.4043/30555-MS

Aydın, Ç., Ünal, U. O., Sarıöz, K., 2022. Computation of environmental loads towards an accurate dynamic positioning capability analysis. Ocean Engineering, 243, 110201. https://doi.org/10.1016/j.oceaneng.2021.110201

Azcona, J., Bouchotrouch, F., González, M., Garciandía, J., Munduate, X., Kelberlau, F., Nygaard, T. A., 2014. Aerodynamic thrust modelling in wave tank tests of offshore floating wind turbines using a ducted fan. In Journal of Physics: Conference Series (Vol. 524, No. 1, p. 012089). IOP Publishing. doi:10.1088/1742-6596/524/1/012089

Aziminia, M. M., Abazari, A., Behzad, M., Hayatdavoodi, M., 2022. Stability analysis of parametric resonance in spar-buoy based on Floquet theory. Ocean Engineering, 266, 113090. https://doi.org/10.1016/j.oceaneng.2022.113090

Bachynski, E. E., Thys, M., Dadmarzi, F. H., 2020. Observations from hydrodynamic testing of a flexible, large-diameter monopile in irregular waves. In Journal of Physics: Conference Series (Vol. 1669, No. 1, p. 012028). IOP Publishing. doi:10.1088/1742-6596/1669/1/012028

Bachynski, E. E., Thys, M., Sauder, T., Chabaud, V., Sæther, L. O., 2016. Real-time hybrid model testing of a braceless semi-submersible wind turbine: Part II—Experimental results. In International Conference on Offshore Mechanics and Arctic Engineering (Vol. 49972, p. V006T09A040). American Society of Mechanical Engineers. https://doi.org/10.1115/OMAE2016-54437

Battjes, J. A., Bakkenes, H. J., Janssen, T. T., van Dongeren, A. R., 2004. Shoaling of subharmonic gravity waves. Journal of Geophysical Research: Oceans, 109(C2). https://doi.org/10.1029/2003JC001863

Boetius, A., Haeckel, M., 2018. Mind the seafloor. Science, 359(6371), 34-36. doi: 10.1126/science.aap7301

Bouscasse, B., Califano, A., Choi, Y. M., Haihua, X., Kim, J. W., Kim, Y. J., Lee, S. H., Lim, H., Park, D. M., Peric, M., Shen, Z., Yeon, S. M., 2021. Qualification criteria and the verification of numerical waves: Part 2: CFD-based numerical wave tank. In International Conference on Offshore Mechanics and Arctic Engineering (Vol. 85116, p. V001T01A007). American Society of Mechanical Engineers. https://doi.org/10.1115/OMAE2021-63710

Canard, M., Ducrozet, G., Bouscasse, B., 2022. Experimental reproduction of an extreme sea state in two wave tanks at various generation scales. In OCEANS 2022-Chennai (pp. 1-6). IEEE. doi:10.1109/OCEANSChennai45887.2022.9775216

Cardia, F., Lovatelli, A. (2015). Aquaculture operations in floating.

Carmo, L. H., Simos, A. N., de Mello, P. C., 2023. A second-order slender-body approach for computing wave induced forces with application to a simplified semi-submersible FOWT model. Ocean Engineering, 285, 115410. https://doi.org/10.1016/j.oceaneng.2023.115410

Chacon-Torres, A., Ross, L. G., Beveridge, M. C., 1988. The effects of fish behaviour on dye dispersion and water exchange in small net cages. Aquaculture, 73(1-4), 283-293. https://doi.org/10.1016/0044-8486(88)90062-2

Chen, L. F., Taylor, P. H., Ning, D. Z., Cong, P. W., Wolgamot, H., Draper, S., Cheng, L., 2021. Extreme runup events around a ship-shaped floating production, storage and offloading vessel in transient wave groups. Journal of Fluid Mechanics, 911, A40. https://doi.org/10.1017/jfm.2020.1072

Chen, M., Ouyang, M., Li, T., Zou, M., Ye, J., Tian, X., 2023. Numerical modelling of a catamaran float-over deck installation for a spar platform with complex hydrodynamic interactions and mechanical couplings. Ocean Engineering, 287, 115905. https://doi.org/10.1016/j.oceaneng.2023.115905

Chen, Y., Zhang, X., Shen, K., Ren, X., 2023. Extension of the discrete-module-finite-element method into the interconnected large floating flexible structures. Ocean Engineering, 269, 113549. https://doi.org/10.1016/j.oceaneng.2022.113549

Chen, Y., Zhang, Y., Tian, X., Guo, X., Li, X., Zhang, X., 2022. A numerical framework for hydroelastic analysis of a flexible floating structure under unsteady external excitations: Motion and internal force/moment. Ocean Engineering, 253, 111288. https://doi.org/10.1016/j.oceaneng.2022.111288

Cheng, H., Li, L., Ong, M. C., Aarsæther, K. G., Sim, J., 2021. Effects of mooring line breakage on dynamic responses of grid moored fish farms under pure current conditions. Ocean Engineering, 237, 109638. https://doi.org/10.1016/j.oceaneng.2021.109638

Cheng, H., Li, L., Ong, M. C., 2022. Comparative study of five commonly used gravity type fish cages under pure current conditions. Ocean Engineering, 250, 110977. https://doi.org/10.1016/j.oceaneng.2022.110977

Cheng, H., Ong, M. C., Li, L., Chen, H., 2022. Development of a coupling algorithm for fluid-structure interaction analysis of submerged aquaculture nets. Ocean Engineering, 243, 110208. https://doi.org/10.1016/j.oceaneng.2021.110208

Cheng, S., Yu, Y., Yu, J., Wu, J., Li, Z., Huang, Z., 2021. Mechanistic research on the complex motion response of a TLP under tendon breakage. Ocean Engineering, 240, 109984. https://doi.org/10.1016/j.oceaneng.2021.109984

Cho, S. G., Park, S., Oh, J., Min, C., Kim, H., Hong, S., Jang, J., Lee, T. H., 2019. Design optimization of deep-seabed pilot miner system with coupled relations between constraints. Journal of Terramechanics, 83, 25-34. https://doi.org/10.1016/j.jterra.2019.01.003

Chu, Y. I., Wang, C. M., Park, J. C., Lader, P. F., 2020. Review of cage and containment tank designs for offshore fish farming. Aquaculture, 519, 734928. https://doi.org/10.1016/j.aquaculture.2020.734928

Chu, Y. I., Wang, C. M., Zhang, H., 2022. A frequency domain approach for analyzing motion responses of integrated offshore fish cage and wind turbine under wind and wave actions. Aquacultural Engineering, 97, 102241. https://doi.org/10.1016/j.aquaeng.2022.102241

Chu, Y. I., Wang, C. M., Zhang, H., Abdussamie, N., Karampour, H., Jeng, D. S., Baumeister, J., Aland, P. A., 2023. Offshore fish farms: a review of standards and guidelines for design and analysis. Journal of Marine Science and Engineering, 11(4), 762. https://doi.org/10.3390/jmse11040762

Chua, K. H., de Mello, P. C., Nishimoto, K., Choo, Y. S., 2019. Model experiments of floating side-by-side barges. In International Conference on Offshore Mechanics and Arctic Engineering (Vol. 58882, p. V009T12A008). American Society of Mechanical Engineers. https://doi.org/10.1115/OMAE2019-95238

Cinello, A., Pétrié, F., Rousse, B., Le Cunff, C., 2022. On the Real Time Hybrid Modelling of Floating Offshore Wind Turbine Using Ducted Fan (s). In International Conference on Offshore Mechanics and Arctic Engineering (Vol. 85932, p. V008T09A024). American Society of Mechanical Engineers. https://doi.org/10.1115/OMAE2022-78985

Craciunescu, C. C., Christou, M., 2020. Wave breaking energy dissipation in long-crested focused wave groups based on JONSWAP spectra. Applied Ocean Research, 99, 102144. https://doi.org/10.1016/j.apor.2020.102144

Cui, M., Li, Z., Zhang, C., Guo, X., 2022. Statistical investigation into the flow field of closed aquaculture tanks aboard a platform under periodic oscillation. Ocean Engineering, 248, 110677. https://doi.org/10.1016/j.oceaneng.2022.110677

Dai, J., Wang, C. M., Utsunomiya, T., Duan, W., 2018. Review of recent research and developments on floating breakwaters. Ocean Engineering, 158, 132-151. https://doi.org/10.1016/j.oceaneng.2018.03.083

Deepak, C. R., Ramji, S., Ramesh, N. R., Babu, S. M., Abraham, R., Shajahan, M. A., Atmanand, M. A., 2007. Development and testing of underwater mining systems for long term operations using flexible riser concept. In ISOPE Ocean Mining and Gas Hydrates Symposium (pp. ISOPE-M). ISOPE.

Dempster, T., Juell, J. E., Fosseidengen, J. E., Fredheim, A., Lader, P., 2008. Behaviour and growth of Atlantic salmon (Salmo salar L.) subjected to short-term submergence in commercial scale sea-cages. Aquaculture, 276(1-4), 103-111. https://doi.org/10.1016/j.aquaculture.2008.01.018

Ding, W. W., Jiang, J. Q., Yue, W. Z., Li, Y. Z., Wang, W. S., Sheng, S. W., Chen, M., 2023. Numerical Study on Hydrodynamic Performance of a New Semi-Submersible Aquaculture Platform. Applied Sciences, 13(23), 12652. https://doi.org/10.3390/app132312652

DNV, 2017. DNV-RU-OU-0503: Offshore Fish Farming Units and Installations.

DNVGL, 2021. DNV-ST-0111: A station-keeping capability standard for better benchmarking of dynamic positioning vessels. Technical Report. DNVGL.

Do, Q. T., Ghanbari-Ghazijahani, T., Prabowo, A. R., 2023. Developing empirical formulations to predict residual strength and damages in tension-leg platform hulls after a collision. Ocean Engineering, 286, 115668. https://doi.org/10.1016/j.oceaneng.2023.115668

Dong, S., You, X., Hu, F., 2021. Experimental investigation on the fluid–structure interaction of a flexible net cage used to farm Pacific bluefin tuna (Thunnus orientalis). Ocean Engineering, 226, 108872. https://doi.org/10.1016/j.oceaneng.2021.108872

Dong, S., Park, S. G., Kitazawa, D., Zhou, J., Yoshida, T., Li, Q., 2021. Model tests and full-scale sea trials for drag force and deformation of a marine aquaculture net cage. Ocean Engineering, 240, 109941. https://doi.org/10.1016/j.oceaneng.2021.109941

Du, Z., Yang, J., Xu, W., Yang, Y., Li, X., Feng, J., 2023. An experimental investigation on flow-induced motion and fluid force of a tension leg platform in complex flows. Ocean Engineering, 281, 114790. https://doi.org/10.1016/j.oceaneng.2023.114790

Ducrozet, G., Abdolahpour, M., Nelli, F., Toffoli, A., 2021. Predicting the occurrence of rogue waves in the presence of opposing currents with a high-order spectral method. Physical Review Fluids, 6(6), 064803. https://doi.org/10.1103/PhysRevFluids.6.064803

Ducrozet, G., Bonnefoy, F., Mori, N., Fink, M., Chabchoub, A., 2020. Experimental reconstruction of extreme sea waves by time reversal principle. Journal of Fluid Mechanics, 884, A20. https://doi.org/10.1017/jfm.2019.939

Ecole Centrale de Nantes, 2016. Experimental investigations of the interactions between two FPSO in waves, Experimental report for ITTC 27th benchmark study.

Eeltink, D., Branger, H., Luneau, C., He, Y., Chabchoub, A., Kasparian, J., van den Bremer, T. S., Sapsis, T. P., 2022. Nonlinear wave evolution with data-driven breaking. Nature communications, 13(1), 2343. https://doi.org/10.1038/s41467-022-30025-z

Ellingsen, S. Å., Zheng, Z., Abid, M., Kharif, C., Li, Y., 2024. Dispersive wave focusing on a shear current: Part 1—Linear approximations. Water Waves, 1-45. https://doi.org/10.1007/s42286-024-00085-3

Esandi, J. M., Buldakov, E., Simons, R., Stagonas, D., 2020. An experimental study on wave forces on a vertical cylinder due to spilling breaking and near-breaking wave groups. Coastal Engineering, 162, 103778. https://doi.org/10.1016/j.coastaleng.2020.103778

Fan, Z. Q., Liang, Y. H., Yun-Peng, Z., 2023. Review of the research on the hydrodynamics of fishing cage nets. Ocean Engineering, 276, 114192. https://doi.org/10.1016/j.oceaneng.2023.114192

FAO (Food and Agriculture Organization), 2022. The State of World Fisheries and

Aquaculture 2022, Towards blue transformation.
Fontes, J. V., Hernández, I. D., Mendoza, E., Silva, R., Brandão da Silva, E., Rocha de Sousa, M., Gonzaga, J., Kamezaki, R. S., Torres, L., Esperança, P. T., 2021. On the evolution of different types of green water events. Water, 13(9), 1148. https://doi.org/10.3390/w13091148
Fontes, J. V., Mendoza, E., Silva, R., Hernández, I. D., González-Olvera, M. A., Torres, L., 2022. On the Evolution of Different Types of Green Water Events—Part II: Applicability of a Convolution Approach. Water, 14(4), 510. https://doi.org/10.3390/w14040510
Fornshell, G., Hinshaw, J., Tidwell, J. H., 2012. Flow-through raceways. Aquaculture production systems, 173-190. doi:10.1002/9781118250105
Fouques, S., Croonenborghs, E., Koop, A., Lim, H. J., Kim, J., Zhao, B., Canard, M., Ducrozet, G., Bouscasse, B., Wang, W., Bihs, H., 2021. Qualification Criteria for the Verification of Numerical Waves–Part 1: Potential-Based Numerical Wave Tank (PNWT). In International Conference on Offshore Mechanics and Arctic Engineering (Vol. 85116, p. V001T01A011). American Society of Mechanical Engineers. https://doi.org/10.1115/OMAE2021-63884
Geological Survey (US), Barnes, P. W., 1977. Bathymetric and shoreline changes, northwestern Prudhoe Bay, Alaska. US Geological Survey.
Ghosh, M. K., Kumar, L., Roy, C., 2015. Monitoring the coastline change of Hatiya Island in Bangladesh using remote sensing techniques. ISPRS Journal of Photogrammetry and Remote Sensing, 101, 137-144. https://doi.org/10.1016/j.isprsjprs.2014.12.009
Gopmandal, F., Ghosh, A., Kumar, A., 2022. LQ optimal robust multivariable PID control for dynamic positioning of ships with norm-bounded parametric uncertainties. Ocean Engineering, 266, 113054. https://doi.org/10.1016/j.oceaneng.2022.113054
Gusev, O. I., Khakimzyanov, G. S., Skiba, V. S., Chubarov, L. B., 2023. Shallow water modeling of wave–structure interaction over irregular bottom. Ocean Engineering, 267, 113284. https://doi.org/10.1016/j.oceaneng.2022.113284
Ha, Y. J., Ahn, H., Park, S., Park, J. Y., Kim, K. H., 2023. Development of hybrid model test technique for performance evaluation of a 10 MW class floating offshore wind turbine considering asymmetrical thrust. Ocean Engineering, 272, 113783. https://doi.org/10.1016/j.oceaneng.2023.113783
Halvorsen, H. S., Øveraas, H., Landstad, O., Smines, V., Fossen, T. I., Johansen, T. A., 2021. Wave motion compensation in dynamic positioning of small autonomous vessels. Journal of Marine Science and Technology, 26, 693-712. https://doi.org/10.1007/s00773-020-00765-y
Handschuh, R., Grebe, H., Panthel, J., Schulte, E., Wenzlawski, B., Schwarz, W., Atmanand, M.A., Keyamani, R., Shajahan, M.A., Deepak, C.R., Ravindran, M., 2001. Innovative deep ocean mining concept based on flexible riser and self-propelled mining machines. In ISOPE Ocean Mining and Gas Hydrates Symposium (pp. ISOPE-M). ISOPE.
Hegde, P., Nallayarasu, S., 2023. Hydrodynamic response of buoy form spar with heave plate near the free surface validated with experiments. Ocean Engineering, 269, 113580. https://doi.org/10.1016/j.oceaneng.2022.113580
Hmedi, M., 2020. Development of a wind turbine emulator for the experimental testing of a floating offshore wind turbine in a wave tank. Ecole Central Nantes.

Hmedi, M., Uzunoglu, E., Soares, C. G., Medina-Manuel, A., Mas-Soler, J., Abad-Gibert, V., Souto-Iglesias, A., Vittori, F., Pires, O., Azcona, J., 2022. Experimental analysis of a free-float capable tension leg platform with a 10 MW turbine. Trends in Renewable Energies Offshore, 549-557.

Hogenboom, S., Vinnem, J. E., Utne, I. B., Kongsvik, T., 2021. Risk-based decision-making support model for offshore dynamic positioning operations. Safety science, 140, 105280. https://doi.org/10.1016/j.ssci.2021.105280

Hong, S., Choi, J. S., Kim, J. H., Yang, C. K., 1999. Experimental study on hydraulic performance of hybrid pick-up device of manganese nodule collector. In ISOPE Ocean Mining and Gas Hydrates Symposium (pp. ISOPE-M). ISOPE.

Hong, S., Kimg, H. W., Choi, J. S., Yeu, T. K., Park, S. J., Lee, C. H., Yoon, S. M., 2010. A self-propelled deep-seabed miner and lessons from shallow water tests. In International Conference on Offshore Mechanics and Arctic Engineering (Vol. 49118, pp. 75-86).

Hosseinnajad, A., Loueipour, M., 2020. Dynamic positioning system design for a marine vessel with unknown dynamics subject to external disturbances including wave effect. China Ocean Engineering, 34(5), 651-663. https://doi.org/10.1007/s13344-020-0058-9,

Houtani, H., Sawada, H., Waseda, T., 2022. Phase convergence and crest enhancement of modulated wave trains. Fluids, 7(8), 275. https://doi.org/10.3390/fluids7080275

Hu, C., Wu, D., Liao, Y., Hu, X., 2021. Sliding mode control unified with the uncertainty and disturbance estimator for dynamically positioned vessels subjected to uncertainties and unknown disturbances. Applied Ocean Research, 109, 102564. https://doi.org/10.1016/j.apor.2021.102564

Huang, H., Chen, X. J., Liu, J. Y., Ji, S., 2022. A method to predict hydroelastic responses of VLFS under waves and moving loads. Ocean engineering, 247, 110399. https://doi.org/10.1016/j.oceaneng.2021.110399

Huang, S., Hu, Z., Chen, C., 2023. Application of CFD–FEA coupling to predict hydroelastic responses of a single module VLFS in extreme wave conditions. Ocean Engineering, 280, 114754. https://doi.org/10.1016/j.oceaneng.2023.114754

Iijima, K., Ma, C., Pambela, A. R., Maeda, T., 2022. DIC measurement of deflection waves travelling along a thin flexural plate floating at water surface. Ocean Engineering, 266, 113079. https://doi.org/10.1016/j.oceaneng.2022.113079

Islam, M., Lau, M., Brown, J., Gash, R., Pearson, W., Mills, J., 2022. Investigation of the effects of managed ice field characteristics on a dynamic positioning AHTS vessel using physical modelling techniques. Ocean Engineering, 246, 110485. https://doi.org/10.1016/j.oceaneng.2021.110485

Islam, M., Mills, J., Gash, R., Pearson, W., 2022. Modelling of Dynamically Positioned vessels and managed ice-field interactions using multiple regression techniques. Ocean Engineering, 243, 110248. https://doi.org/10.1016/j.oceaneng.2021.110248

Islam, M., Mills, J., Gash, R., Pearson, W., 2022. Modelling of Dynamically Positioned vessels and managed ice-field interactions using multiple regression techniques. Ocean Engineering, 243, 110248. https://doi.org/10.1016/j.oceaneng.2021.110248

Islam, M., Wang, J., Gash, R., Pearson, W., Mills, J., 2021. Physical model testing I for investigating the effects of managed ice-field characteristics on a dynamic positioning vessel. Cold Regions Science and Technology, 192, 103376.

https://doi.org/10.1016/j.coldregions.2021.103376

Islam, M., Wang, J., Mills, J., Sayeed, T., Gash, B., Lau, M., Millan, D., Millan, J., 2016. Dp in ice environment-improving safety and efficiency of arctic operations. In OTC Arctic Technology Conference (pp. OTC-27349). OTC. https://doi.org/10.4043/27349-MS

Islam, S., Wang, J., Brown, J., Lau, M., Gash, R., Millan, D., Ocean, J. M., 2018. Physical model testing for supporting ice force model development of DP vessels in managed ice. In OTC Arctic Technology Conference (p. D023S009R005). OTC. https://doi.org/10.4043/29157-MS

ITTC, 2017. Uncertainty Analysis in CFD Verification and Validation Methodology and Procedures.

Jahani, K., Langlois, R. G., Afagh, F. F., 2022. Structural dynamics of offshore Wind Turbines: A review. Ocean Engineering, 251, 111136. https://doi.org/10.1016/j.oceaneng.2022.111136

Jeon, W., Park, S., Cho, S., 2023, Moored motion prediction of a semi-submersible offshore platform in waves using an OpenFOAM and MoorDyn coupled solver, International Journal of Naval Architecture and Ocean Engineering, Volume 15, 2023, 100544, ISSN 2092-6782, https://doi.org/10.1016/j.ijnaoe.2023.100544.

Jia, H., Yang, J., Su, X., Wang, Y., Wu, K., 2023. Flow characteristics and hydraulic lift of coandă effect-based pick-up method for polymetallic nodule. Coatings, 13(2), 271. https://doi.org/10.3390/coatings13020271

Jia, H., Yang, J., Su, X., Xia, Q., Wu, K.. 2022. Theoretical prediction on hydraulic lift of a coandă effect-based mining collector for manganese nodule. Energies, 15(17), 6345. https://doi.org/10.3390/en15176345

Jiang, C., Xu, P., Bai, X., Zhao, Z., el Moctar, O., Zhang, G., 2023. A review of advances in modeling hydrodynamics and hydroelasticity for very large floating structures. Ocean Engineering, 285, 115319. https://doi.org/10.1016/j.oceaneng.2023.115319

Jiang, D., Tan, K. H., Dai, J., Ang, K. K., Nguyen, H. P., 2021. Behavior of concrete modular multi-purpose floating structures. Ocean Engineering, 229, 108971. https://doi.org/10.1016/j.oceaneng.2021.108971

Jiang, X., 2020. Software-in-the-loop applications for improved physical model tests of ocean renewable energy devices using artificial intelligence. doi: 10.48730/vkf6-vh23

Jin, R., Jiang, Y., Shen, W., Zhang, H., Geng, B., 2021. Coupled dynamic response of a tension leg platform system under waves and flow at different heading angles: An experimental study. Applied Ocean Research, 115, 102848. https://doi.org/10.1016/j.apor.2021.102848

Jin, Y., Chai, S., Duffy, J., Chin, C., Bose, N., 2018. URANS predictions on the hydrodynamic interaction of a conceptual FLNG-LNG offloading system in regular waves. Ocean Engineering, 153, 363-386. https://doi.org/10.1016/j.oceaneng.2018.01.102

Jung, K.H, Park, S.B., Park, H., Mohamed, A.H., Kim, H.S. 2022, Hydrodynamic Characteristics of Rectangular Structure in Various Water Depth, 15th International Symposium on Practical Design of Ships and Other Floating Structures PRADS 2022.

Kang, D., Kim, T., Lim, J., Yoo, D., 2022. One Side Spread Mooring System Applied for Floating LNG in West Africa. In Offshore Technology Conference (p. D011S011R007). OTC. https://doi.org/10.4043/32067-MS

Kang, Z., Chang, R., Meng, W., 2023. Mechanistic research on the complex motion response of a TLP in a tender-assisted drilling state. Ocean Engineering, 288, 115935.

https://doi.org/10.1016/j.oceaneng.2023.115935
Kanner S, Yeung R W, Koukina E., 2016. Hybrid testing of model-scale floating wind turbines using autonomous actuation and control//OCEANS MTS/IEEE Monterey. IEEE, 1-6.
Kaufman, R., Latimer, J. P., Tolefson, D. C., Senni, S., 1985. The Design and Operation of a Pacific Ocean Deep-Ocean Mining Test Ship: R/V Deepsea Minner 2. In Offshore Technology Conference (pp. OTC-4901). OTC. https://doi.org/10.4043/4901-MS
Khait, A., Ma, Z., Qian, L., Bai, W., Lin, Z., 2022. Energy Dissipation and Nonpotential Effects in Wave Breaking. International Journal of Offshore and Polar Engineering, 32(01), 87-96. https://doi.org/10.17736/ijope.2022.ak43
Kharazmi, R., Ketabdari, M. J., 2022. Numerical modeling to develop strake design of Spar platform for Vortex-Induced motions suppression. Ocean Engineering, 250, 111060. https://doi.org/10.1016/j.oceaneng.2022.111060
Kim J., Lim, H.J., 2019. JIP on Reproducible CFD Modeling Practices for Offshore Applications. NWT Preparation Workgroup Year 1 Report, Rev. H., TechnipFMC.
Kim, M., Jung, K. H., Park, S. B., Lee, G. N., Duong, T. T., Suh, S. B., Park, I. R., 2020. Experimental and numerical estimation on roll damping and pressure on a 2-D rectangular structure in free roll decay test. Ocean Engineering, 196, 106801. https://doi.org/10.1016/j.oceaneng.2019.106801
Kim, S., Bouscasse, B., Ducrozet, G., Canard, M., De Hauteclocque, G., Housseine, C. O., Ferrant, P., 2022. Numerical and experimental study of a FORM-based design wave applying the HOS-NWT nonlinear wave solver. Ocean Engineering, 263, 112287. https://doi.org/10.1016/j.oceaneng.2022.112228
Kim, S., Cho, S. G., Lee, M., Kim, J., Lee, T. H., Park, S., Hong, S., Kim, H., Min, C., Choi, J., Ko, Y., Chi, S. B., 2019. Reliability-based design optimization of a pick-up device of a manganese nodule pilot mining robot using the Coandă effect. Journal of Mechanical Science and Technology, 33, 3665-3672. doi: 10.1007/s12206-019-0707-1
Klein, M., Clauss, G. F., Hoffmann, N., 2021. Introducing envelope soliton solutions for wave–structure investigations. Ocean engineering, 234, 109271. https://doi.org/10.1016/j.oceaneng.2021.109271
Klein, M., Wang, S., Clauss, G., Guedes Soares, C., 2023. Experimental study on the effect of extreme waves on a LNG carrier. Journal of marine science and application, 22(1), 52-74. https://doi.org/10.1007/s11804-023-00321-1
Kung, A., Svobodova, K., Lèbre, E., Valenta, R., Kemp, D., Owen, J. R., 2021. Governing deep sea mining in the face of uncertainty. Journal of Environmental Management, 279, 111593. https://doi.org/10.1016/j.jenvman.2020.111593
Lee, J. H., Monty, J. P., 2020. On the interaction between wind stress and waves: Wave growth and statistical properties of large waves. Journal of Physical Oceanography, 50(2), 383-397. https://doi.org/10.1175/JPO-D-19-0112.1
Lee, M., Cho, S. G., Choi, J. S., Kim, H. W., Hong, S., Lee, T. H., 2012. Metamodel‐Based Multidisciplinary Design Optimization of a Deep‐Sea Manganese Nodules Test Miner. Journal of Applied Mathematics, 2012(1), 326954. https://doi.org/10.1155/2012/326954
Lei, Y., Li, W., Zheng, X. Y., Zheng, H., Gao, S., Zhao, S., 2024. A floating system integrating a wind turbine with a steel fish

farming cage: experimental validation of the hydrodynamic model. Marine Structures, 93, 103525. https://doi.org/10.1016/j.marstruc.2023.103525
Leroy, V., Bachynski-Polić, E. E., Babarit, A., Ferrant, P., Gilloteaux, J. C., 2021. A weak-scatterer potential flow theory-based model for the hydroelastic analysis of offshore wind turbine substructures. Ocean Engineering, 238, 109702. https://doi.org/10.1016/j.oceaneng.2021.109702
Li, J., Xiang, X., Yang, S., 2022. Robust adaptive neural network control for dynamic positioning of marine vessels with prescribed performance under model uncertainties and input saturation. Neurocomputing, 484, 1-12. https://doi.org/10.1016/j.neucom.2021.03.136
Li, M. Y., Xie, W. B., Wang, Y. L., Hu, X., 2022. Prescribed performance trajectory tracking fault-tolerant control for dynamic positioning vessels under velocity constraints. Applied Mathematics and Computation, 431, 127348. https://doi.org/10.1016/j.amc.2022.127348
Li, M. Y., Xu, J., Xie, W. B., Wang, H. B., 2022. Finite-time composite learning control for trajectory tracking of dynamic positioning vessels. Ocean Engineering, 262, 112288. https://doi.org/10.1016/j.oceaneng.2022.112288
Li, N., Shi, W., Han, X., Li, X., Verma, A. S., Liu, C., 2023. Dynamic analysis of an integrated offshore structure comprising a jacket-supported offshore wind turbine and aquaculture steel cage. Ocean Engineering, 274, 114059. https://doi.org/10.1016/j.oceaneng.2023.114059
Li, W., Ke, S., Chen, J., Zhu, T., Ren, H., 2022. Hydrodynamic response and energy analysis in a very large floating structure supporting a marine airport under typhoon-driven waves. Ocean Engineering, 266, 112987. https://doi.org/10.1016/j.oceaneng.2022.112987
Li, Y., Zhang, C., 2016. Analysis of wave resonance in gap between two heaving barges. Ocean Engineering, 117, 210-220. https://doi.org/10.1016/j.oceaneng.2016.03.042
Liang, H., Chua, K. H., Wang, H. C., & Choo, Y. S., Chua, K. H., de Mello, P., Malta, E., Vieira, D., Watai, R., Ruggeri, F., Taylor, R. E., Nishimoto, K., Choo, Y. S., 2018. Irregular seas model experiments on side-by-side barges. In ISOPE International Ocean and Polar Engineering Conference (pp. ISOPE-I). ISOPE.
Liang, H., Liu, X., Chua, K. H., de Mello, P. C., Choo, Y. S., 2022. Wave actions on side-by-side barges with sloshing effects: fixed–free arrangement. Flow, 2, E20. https://doi.org/10.1017/flo.2022.14
Liang, K., Lin, X., Chen, Y., Liu, Y., Liu, Z., Ma, Z., Zhang, W., 2021. Robust adaptive neural networks control for dynamic positioning of ships with unknown saturation and time-delay. Applied Ocean Research, 110, 102609. https://doi.org/10.1016/j.apor.2021.102609
Lim, S. J., Kim, J. W., Jung, S. T., Cho, H. Y., Lee, S. H., 2015. Deep seawater flow characteristics around the manganese nodule collecting device. Procedia Engineering, 116, 544-551. https://doi.org/10.1016/j.proeng.2015.08.324
Liu, H., Chen, M., Han, Z., Zhou, H., Li, L., 2022. Feasibility study of a novel open ocean aquaculture ship integrating with a wind turbine and an internal turret mooring system. Journal of Marine Science and Engineering, 10(11), 1729. https://doi.org/10.3390/jmse10111729
Liu, H. F., Bi, C. W., Xu, Z., Zhao, Y. P., 2021. Hydrodynamic assessment of a semi-submersible aquaculture platform in uniform fluid environment. Ocean Engineering, 237, 109656.

https://doi.org/10.1016/j.oceaneng.2021.109656

Liu, J., Liu, M., Xiao, L., Wei, H., Li, X., 2023. Experimental study on the effect of flare barriers on wave run-up and motion response of a semi-submersible platform. Ocean Engineering, 281, 114998. https://doi.org/10.1016/j.oceaneng.2023.114998

Liu, J., Xu, D., Ji, C., Xia, J., Ran, Q., 2023. Numerical investigations on the flow structures around the hydraulic mining header of deep-sea polymetallic nodule collectors. The Ocean Engineering, 41: 123-136.

Liu, Y., Ren, N., Ou, J., 2022. Hydrodynamic analysis of a hybrid modular floating structure system under different wave directions. Applied Ocean Research, 126, 103264. https://doi.org/10.1016/j.apor.2022.103264

Liu, Y. N., Molin, B., Kimmoun, O., Remy, F., Rouault, M. C., 2011. Experimental and numerical study of the effect of variable bathymetry on the slow-drift wave response of floating bodies. Applied Ocean Research, 33(3), 199-207. https://doi.org/10.1016/j.apor.2011.02.004

Liu, Y., Yao, Y., Liao, Z., Li, S., Zhang, C., Zou, Q., 2023. Fully nonlinear investigation on energy transfer between long waves and short-wave groups over a reef. Coastal Engineering, 179, 104240. https://doi.org/10.1016/j.coastaleng.2022.104240

Liu, Z., Zhao, G., Xiao, L., 2023. Experimental study of submarine nodules collection method based on the hydrodynamic characteristics of vertical axis vortex. The Ocean Engineering: 1-10.

Ma, C., Zhao, Y. P., Bi, C. W., 2022. Numerical study on hydrodynamic responses of a single-point moored vessel-shaped floating aquaculture platform in waves. Aquacultural Engineering, 96, 102216. https://doi.org/10.1016/j.aquaeng.2021.102216

Ma, M., Zhang, H., Jeng, D. S., Wang, C. M., 2021. A semi-analytical model for studying hydroelastic behaviour of a cylindrical net cage under wave action. Journal of Marine Science and Engineering, 9(12), 1445. https://doi.org/10.3390/jmse9121445

Ma, M., Zhang, H., Jeng, D. S., Wang, C. M., 2022. Hydroelastic interactions between waves and an array of submersible flexible fish cages. Ocean Engineering, 266, 113035. https://doi.org/10.1016/j.oceaneng.2022.113035

Ma, M., Zhang, H., Jeng, D. S., Wang, C. M., 2022. Analytical solutions of hydroelastic interactions between waves and submerged open-net fish cage modeled as a porous cylindrical thin shell. Physics of Fluids, 34(1). https://doi.org/10.1063/5.0076659

Ma, Y., Tai, B., Dong, G., Fu, R., Perlin, M., 2022. An experiment on reconstruction and analyses of in-situ measured freak waves. Ocean Engineering, 244, 110312. https://doi.org/10.1016/j.oceaneng.2021.110312

Mackay, E., Shi, W., Qiao, D., Gabl, R., Davey, T., Ning, D., Johanning, L., 2021. Numerical and experimental modelling of wave interaction with fixed and floating porous cylinders. Ocean Engineering, 242, 110118. https://doi.org/10.1016/j.oceaneng.2021.110118

Mao, Y., Wang, T., Duan, M., 2022. A DNN-based approach to predict dynamic mooring tensions for semi-submersible platform under a mooring line failure condition. Ocean Engineering, 266, 112767. https://doi.org/10.1016/j.oceaneng.2022.112767

Martelli, M., Faggioni, N., Donnarumma, S., 2020. A novel model based-design approach for a dynamic positioning system. In Conference Proceedings of iSCSS. https://doi.org/10.24868/issn.2631-8741.2020.002

Martelli, M., Faggioni, N., Donnarumma, S., 2022. A time-domain methodology to assess the dynamic positioning performances. Ocean Engineering, 247, 110668. https://doi.org/10.1016/j.oceaneng.2022.110668

Martin, S., Day, S., Gilmour, C. B., 2015. Rotor scaling methodologies for small scale testing of floating wind turbine systems. In International Conference on Offshore Mechanics and Arctic Engineering (Vol. 56574, p. V009T09A045). American Society of Mechanical Engineers. https://doi.org/10.1115/OMAE2015-41599

Matheen, N., Harley, M. D., Turner, I. L., Splinter, K. D., Simmons, J. A., Thran, M. C., 2021. Bathymetric data requirements for operational coastal erosion forecasting using XBeach. Journal of Marine Science and Engineering, 9(10), 1053. https://doi.org/10.3390/jmse9101053

Mauro, F., Nabergoj, R., 2022. A probabilistic approach for Dynamic Positioning capability and operability predictions. Ocean Engineering, 262, 112250. https://doi.org/10.1016/j.oceaneng.2022.112250

Mauro, F., Prpić-Oršić, J., 2020. Determination of a DP operability index for an offshore vessel in early design stage. Ocean engineering, 195, 106764. https://doi.org/10.1016/j.oceaneng.2019.106764

McFarlane, J., Brockett, T., Huizingh, J. P., 2008. Analysis of Mining Technologies Developed in the 1970s and 1980s. Kingston: International Seabed Authority.

Miao, Y. J., Ding, J., Tian, C., Chen, X. J., Fan, Y. L., 2021. Experimental and numerical study of a semi-submersible offshore fish farm under waves. Ocean Engineering, 225, 108794. https://doi.org/10.1016/j.oceaneng.2021.108794

Moe-Føre, H., Lader, P. F., Lien, E., Hopperstad, O. S., 2016. Structural response of high solidity net cage models in uniform flow. Journal of Fluids and Structures, 65, 180-195. https://doi.org/10.1016/j.jfluidstructs.2016.05.013

Moradi, N., Zhou, T., Cheng, L., 2016. Two-dimensional numerical study on the effect of water depth on resonance behaviour of the fluid trapped between two side-by-side bodies. Applied Ocean Research, 58, 218-231. https://doi.org/10.1016/j.apor.2016.03.018

Morro, B., Davidson, K., Adams, T. P., Falconer, L., Holloway, M., Dale, A., Aleynik, D., Thies, P. R., Khalid, F., Hardwick, J., Smith, H., Giollibrand, P. A., Rey‐Planellas, S., 2022. Offshore aquaculture of finfish: Big expectations at sea. Reviews in Aquaculture, 14(2), 791-815. https://doi.org/10.1111/raq.12625

Nakashima, M., Kato, H., Takaoka, E., 1992. Development of real‐time pseudo dynamic testing. Earthquake engineering & structural dynamics, 21(1), 79-92. https://doi.org/10.1002/eqe.4290210106

Nasyrlayev, N., Dyson, A. P., Kefayati, G., Tolooiyan, A., 2023. Modelling the response of offshore aquaculture fish pens to environmental loads in high-energy regions. Applied Ocean Research, 135, 103541. https://doi.org/10.1016/j.apor.2023.103541

Nguyen, N., Davis, J., Alshuwaykh, A., Sharman, K. T., 2020. Design, Analysis, and Development of a Wave-Current Laboratory. In International Conference on Offshore Mechanics and Arctic Engineering (Vol. 84379, p. V06AT06A019). American Society of Mechanical Engineers. https://doi.org/10.1115/OMAE2020-19253

Ning, D., Zhu, Y., Zhang, C., Zhao, M., 2018. Experimental and numerical study on wave response at the gap between two barges of different draughts. Applied Ocean Research, 77, 14-25. https://doi.org/10.1016/j.apor.2018.05.010

Niu, X., Ma, X., Ma, Y., Dong, G., 2020. Controlled extreme wave generation using an improved focusing method. Applied Ocean Research, 95, 102017. https://doi.org/10.1016/j.apor.2019.102017
Nwafor, J. C., 2022. Numerical Investigation on Coupling Dynamic Performance of FLNG and LNG Carriers. In ISOPE International Ocean and Polar Engineering Conference (pp. ISOPE-I). ISOPE.
Oguz, E., Clelland, D., Day, A. H., Incecik, A., López, J. A., Sánchez, G., Almeria, G. G., 2018. Experimental and numerical analysis of a TLP floating offshore wind turbine. Ocean Engineering, 147, 591-605. https://doi.org/10.1016/j.oceaneng.2017.10.052
Otter, A., Murphy, J., Pakrashi, V., Robertson, A., Desmond, C., 2022. A review of modelling techniques for floating offshore wind turbines. Wind Energy, 25(5), 831-857. https://doi.org/10.1002/we.2701
Otter, A., Murphy, J., Desmond, C. J., 2020. Emulating aerodynamic forces and moments for hybrid testing of floating wind turbine models. In Journal of Physics: Conference Series (Vol. 1618, No. 3, p. 032022). IOP Publishing. doi: 10.1088/1742-6596/1618/3/032022
Pang, G., Zhang, S., Liu, H., Zhu, S., Yuan, T., Li, G., Han, X., Huang, X., 2023. Hydrodynamic response analysis for a new semi-submersible vessel-shaped fish farm platform based on numerical simulation. Frontiers in Marine Science, 10, 1135757. https://doi.org/10.3389/fmars.2023.1135757
Park, D. M., Kwon, Y. J., Nam, H. S., Nam, B. W., Lee, K., 2022. An experimental study of wave impact pressure on an FPSO bow under head sea conditions. Ocean Engineering, 249, 110993. https://doi.org/10.1016/j.oceaneng.2022.110993
Pillay, T. V. R., 2008. Aquaculture and the Environment. John Wiley & Sons.
Qi, K., Zhao, Y., LIU, L., Gan, S., Luo, X., Tian, X., 2021. Experimental Investigation on the Hydrodynamic Performance of Quay-moored FSRU and LNG Carrier, Journal of Ship Mechanics, 25(6).
Qiu, W., Meng, W., Peng, H., Li, J., Rousset, J. M., Rodríguez, C. A., 2019. Benchmark data and comprehensive uncertainty analysis of two-body interaction model tests in a towing tank. Ocean Engineering, 171, 663-676. https://doi.org/10.1016/j.oceaneng.2018.11.057
Ransley, E. J., Brown, S. A., Edwards, E. C., Tosdevin, T., Monk, K., Reynolds, A. M., Greaves, D., Hann, M. R., 2023. Real-time hybrid testing of a floating offshore wind turbine using a surrogate-based aerodynamic emulator. ASME Open Journal of Engineering, 2. https://doi.org/10.1115/1.4056963
Rao, M. J., Nallayarasu, S., Bhattacharyya, S., 2021. CFD approach to heave damping of spar with heave plates with experimental validation. Applied Ocean Research, 108, 102517. https://doi.org/10.1016/j.apor.2020.102517
Rao, M. J., Nallayarasu, S., Bhattacharyya, S., 2021. Numerical and experimental studies of heave damping and added mass of spar with heave plates using forced oscillation. Applied Ocean Research, 111, 102667. https://doi.org/10.1016/j.apor.2021.102667
Rockel, S., Camp, E., Schmidt, J., Peinke, J., Cal, R. B., Hölling, M., 2014. Experimental study on influence of pitch motion on the wake of a floating wind turbine model. Energies, 7(4), 1954-1985. https://doi.org/10.3390/en7041954
Rockel, S., Peinke, J., Hölling, M., Cal, R. B., 2016. Wake to wake interaction of floating wind turbine models in free pitch motion: An eddy viscosity and mixing length approach. Renewable Energy, 85, 666-676. https://doi.org/10.1016/j.renene.2015.07.012
Rodman, L. C., Wood, N. J., Roberts, L., 1989. Experimental investigation of straight and curved annular wall jets. AIAA journal,

27(8), 1059-1067. https://doi.org/10.2514/3.10221
Rodrigues, J. M., Viuff, T., Økland, O. D., 2022. Model tests of a hydroelastic truncated floating bridge. Applied Ocean Research, 125, 103247. https://doi.org/10.1016/j.apor.2022.103247
Rosa-Santos, P., Veloso-Gomes, F., Taveira-Pinto, F., Brógueira-Dias, E., Guedes-Lopes, H., 2008. Improving operational conditions at Leixões oil terminal–Portugal. In Proc. of the 7th International Conference on Coastal and Port Engineering in Developing Countries (COPEDEC VII), Dubai, United Arab Emirates, February (pp. 24-28).
Rudan, S., Karačić, J., Ćatipović, I., 2021. Non-linear response of a moored LNG ship subjected to regular waves. Ships and Offshore Structures, 16(sup1), 44-57. https://doi.org/10.1080/17445302.2021.1907064
Sadraddin, H. L., 2022. Developing Distributed Real-Time Hybrid Simulation for Dynamic Response Evaluation of Floating Wind Turbine. Western Michigan University.
Sakthivel, S., Kumar, N., Poguluri, S. K., 2023. Dynamic responses of serially connected truss pontoon-MOB–A numerical investigation. Ocean Engineering, 277, 114209. https://doi.org/10.1016/j.oceaneng.2023.114209
Sakthivel, S., Rajamanickam, P. S., 2022. Hydroelastic responses of a Truss Pontoon Mobile Offshore Base–An experimental investigation. Ocean Engineering, 259, 111889. https://doi.org/10.1016/j.oceaneng.2022.111889
Sauder, T., Chabaud, V., Thys, M., Bachynski, E. E., Sæther, L. O., 2016. Real-time hybrid model testing of a braceless semi-submersible wind turbine: Part I—The hybrid approach. In International conference on offshore mechanics and arctic engineering (Vol. 49972, p. V006T09A039). American Society of Mechanical Engineers. https://doi.org/10.1115/OMAE2016-54435
Sayed, M., Islam, S., Watson, D., Kubat, I., Gash, R., Wright, B., 2017. DP Drillship Stationkeeping in Ice-Comparison between Numerical Simulations and Ice Basin Tests. In ISOPE International Ocean and Polar Engineering Conference (pp. ISOPE-I). ISOPE.
Schliffke, B., Aubrun, S., Conan, B., 2020. Wind tunnel study of a “floating” wind turbine’s wake in an atmospheric boundary layer with imposed characteristic surge motion. In Journal of Physics: Conference Series (Vol. 1618, No. 6, p. 062015). IOP Publishing. doi:10.1088/1742-6596/1618/6/062015
Scott, D. C. B., Muir, J. F., 2000. Offshore cage systems: A practical overview. Option Mediterraneennes-International Centre for Advanced Mediterranean Agronomic Studies, 79-89.
Shainee, M., Leira, B. J., Ellingsen, H., Fredheim, A., 2012. An optimum design concept for offshore cage culture. In International Conference on Offshore Mechanics and Arctic Engineering (Vol. 44946, pp. 85-93). American Society of Mechanical Engineers. https://doi.org/10.1115/OMAE2012-83601
Shen, W., Chen, H., Jiang, Y., Gao, F., 2020. Analysis of resonance characteristics of FSRU and LNG ship under side by side operation. In ISOPE Pacific/Asia Offshore Mechanics Symposium (pp. ISOPE-P). ISOPE.
Shen, Y., Firoozkoohi, R., Greco, M., Faltinsen, O. M., 2022. Comparative investigation: Closed versus semi-closed vertical cylinder-shaped fish cage in waves. Ocean Engineering, 245, 110397. https://doi.org/10.1016/j.oceaneng.2021.110397
Silva de Souza, C. E., Berthelsen, P. A., Eliassen, L., Bachynski, E. E., Engebretsen, E., Haslum, H., 2021. Definition of the INO WINDMOOR 12 MW base case floating wind turbine.

Sim, J., Cheng, H., Aarsæther, K. G., Li, L., Ong, M. C., 2021. Numerical investigation on the cage-to-cage wake effect: a case study of a 4× 2 cage array. Journal of Offshore Mechanics and Arctic Engineering, 143(5), 051301. https://doi.org/10.1115/1.4049831

Simon-Lledó, E., Bett, B. J., Huvenne, V. A., Schoening, T., Benoist, N. M., Jeffreys, R. M., Durden, J. M., Jones, D. O., 2019. Megafaunal variation in the abyssal landscape of the Clarion Clipperton Zone. Progress in oceanography, 170, 119-133. https://doi.org/10.1016/j.pocean.2018.11.003

Slagstad, M., Amdahl, J., Yu, Z., 2024. A simplified force response calculation of circular pre-tensioned aquaculture nets in waves and current. Ocean Engineering, 294, 116825. https://doi.org/10.1016/j.oceaneng.2024.116825

Slagstad, M., Yu, Z., Amdahl, J., 2023. A simplified approach for fatigue life prediction of aquaculture nets under waves and currents. Ocean Engineering, 272, 113859. https://doi.org/10.1016/j.oceaneng.2023.113859

Soffer, R., Kit, E., Toledo, Y., 2023. Method of directional spectrum estimation accounting for the ambient shearing currents. Physical Review Fluids, 8(6), L062801. https://doi.org/10.1103/PhysRevFluids.8.L062801

Somoano, M., Battistella, T., Fernández-Ruano, S., Guanche, R., 2021. Uncertainties assessment in real-time hybrid model for ocean basin testing of a floating offshore wind turbine. In Journal of Physics: Conference Series (Vol. 2018, No. 1, p. 012036). IOP Publishing. doi:10.1088/1742-6596/2018/1/012036

Stansberg C.T., 2020. Wave Front Steepness and Influence on Horizontal Deck Impact Loads. Journal of Marine Science and Engineering, 8(5):314. https://doi.org/10.3390/jmse8050314

Stern, F., Wilson, R. V., Coleman, H. W., Paterson, E. G., 2001. Comprehensive approach to verification and validation of CFD simulations—part 1: methodology and procedures. J. Fluids Eng., 123(4), 793-802. https://doi.org/10.1115/1.1412235

Suja, L., Bachynski, E. E., Pierella, F., Borg, M., Krokstad, J. R., Bredmose, H., 2020. Critical assessment of hydrodynamic load models for a monopile structure in finite water depth. https://doi.org/10.1016/j.marstruc.2020.102743

Sun, C., Song, W., Jahangiri, V., 2022. A real-time hybrid simulation framework for floating offshore wind turbines. Ocean Engineering, 265, 112529. https://doi.org/10.1016/j.oceaneng.2022.112529

Tan, L., Lu, L., Tang, G. Q., Cheng, L., Chen, X. B., 2019. A viscous damping model for piston mode resonance. Journal of Fluid Mechanics, 871, 510-533. https://doi.org/10.1017/jfm.2019.302

Tang, L., Wang, L., Wang, Y., Zhang, Y., 2022. An enhanced trajectory tracking control of the dynamic positioning ship based on nonlinear model predictive control and disturbance observer. Ocean Engineering, 265, 112482. https://doi.org/10.1016/j.oceaneng.2022.112482

Tay, Z. Y., 2023. Artificial neural network framework for prediction of hydroelastic response of very large floating structure. Applied Ocean Research, 139, 103701. https://doi.org/10.1016/j.apor.2023.103701

Teng, Y., Tan, J. H., 2022. CFD-Based Simulations of Hydrodynamic Behaviors of a Floating Barge Near Shore. In Offshore Technology Conference Asia (p. D021S003R005). OTC. https://doi.org/10.4043/31480-MS

Thys, M., Fontanella, A., Taruffi, F., Belloli, M., Berthelsen, P. A., 2019. Hybrid model tests for floating offshore wind turbines. In International Conference on Offshore

Mechanics and Arctic Engineering (Vol. 59353, p. V001T01A023). American Society of Mechanical Engineers. https://doi.org/10.1115/IOWTC2019-7575

Thys, M., Souza, C., Sauder, T., Fonseca, N., Berthelsen, P. A., Engebretsen, E., Haslum, H., 2021. Experimental investigation of the coupling between aero-and hydrodynamical loads on a 12 mw semi-submersible floating wind turbine. In International Conference on Offshore Mechanics and Arctic Engineering (Vol. 85192, p. V009T09A030). American Society of Mechanical Engineers. https://doi.org/10.1115/OMAE2021-62980

Toffoli, A., Ducrozet, G., Waseda, T., Onorato, M., Abdolahpour, M., Nelli, F., 2019. Ocean currents trigger rogue waves. In ISOPE International Ocean and Polar Engineering Conference (pp. ISOPE-I). ISOPE.

Tu, Z., Zhang, C., Liu, H., Zhu, R., 2023. Hydrodynamic analysis of a multi-pile-supported offshore wind turbine integrated with an aquaculture cage. Journal of Marine Science and Engineering, 11(9), 1830. https://doi.org/10.3390/jmse11091830

Turner, I. L., Harley, M. D., Short, A. D., Simmons, J. A., Bracs, M. A., Phillips, M. S., Splinter, K. D., 2016. A multi-decade dataset of monthly beach profile surveys and inshore wave forcing at Narrabeen, Australia. Scientific data, 3(1), 1-13. doi: 10.1038/sdata.2016.24

Urbán, A. M., Guanche, R., 2019. Wind turbine aerodynamics scale-modeling for floating offshore wind platform testing. Journal of Wind Engineering and Industrial Aerodynamics, 186, 49-57. https://doi.org/10.1016/j.jweia.2018.12.021

Vanem, E., Antao, P., Østvik, I., de Comas, F. D. C., 2008. Analysing the risk of LNG carrier operations. Reliability Engineering & System Safety, 93(9), 1328-1344. https://doi.org/10.1016/j.ress.2007.07.007

Veloso-Gomes, F., Taveira-Pinto, F., Rosa-Santos, P., Brógueira-Dias, E., Guedes-Lopes, H., 2005. Berthing characteristics and the behaviour of the oil terminal of Leixões Harbour, Portugal. WIT transactions on the built environment, 79. doi: 10.2495/MH050451

Vittori, F., Azcona, J., Eguinoa, I., Pires, O., Rodríguez, A., Morató, Á., Garrido, C., Desmond, C., 2022. Model tests of a 10 MW semi-submersible floating wind turbine under waves and wind using hybrid method to integrate the rotor thrust and moments. Wind Energy Science, 7(5), 2149-2161. https://doi.org/10.5194/wes-7-2149-2022, 2022.

Vittori, F., Pires, O., Azcona, J., Uzunoglu, E., Soares, C. G., Rodríguez, R. Z., Souto-Iglesias, A., 2020. Hybrid scaled testing of a 10MW TLP floating wind turbine using the SiL method to integrate the rotor thrust and moments. In Developments in Renewable Energies Offshore (pp. 417-423). CRC Press.

Wang, B., Liang, X., Jiang, X., 2022. Experimental and Numerical Investigation on the Dynamic Response of Platform for a Spar-Type Floating Wind Turbine Under Aerodynamic and Hydrodynamic Forces. In International Conference on Offshore Mechanics and Arctic Engineering (Vol. 85932, p. V008T09A062). American Society of Mechanical Engineers. https://doi.org/10.1115/OMAE2022-81290

Wang, H., Wolgamot, H. A., Draper, S., Zhao, W., Taylor, P. H., Cheng, L., 2019. Resolving wave and laminar boundary layer scales for gap resonance problems. Journal of Fluid Mechanics, 866, 759-775. https://doi.org/10.1017/jfm.2019.115

Wang, H., Zhang, X., Zhang, X., Li, X., Tian, X., Shen, Y., Song, W., 2023. Experimental investigations on hydrodynamic interactions between the cylinder and nets of a typical offshore aquacultural structure in steady current. Marine Structures, 88, 103367.

https://doi.org/10.1016/j.marstruc.2022.103367
Wang, J., Ma, Q., Yan, S., 2021. On extreme waves in directional seas with presence of oblique current. Applied Ocean Research, 112, 102586. https://doi.org/10.1016/j.apor.2021.102586
Wang, J., Sayeed, T., Millan, D., Gash, R., Islam, M., Millan, J., 2016. Ice model tests for dynamic positioning vessel in managed ice. In OTC Arctic Technology Conference (pp. OTC-27430). OTC. https://doi.org/10.4043/27430-MS
Wang, L., Li, J. X., Liu, S. X., Fan, Y. P., 2020. Experimental and numerical studies on the focused waves generated by double wave groups. Frontiers in Energy Research, 8, 133. https://doi.org/10.3389/fenrg.2020.00133
Wang, S., 2022. Analytical solutions for the dynamic analysis of a modular floating structure for urban expansion. Ocean Engineering, 266, 112878. https://doi.org/10.1016/j.oceaneng.2022.112878
Wang, Y., Fu, S., Xu, Y., Li, S., Moan, T., 2022. Loads on a vessel-shaped fish cage steel structures, nets and connectors considering the effects of diffraction and radiation waves. Marine Structures, 86, 103301. https://doi.org/10.1016/j.marstruc.2022.103301
Wang, Y., Fu, S., Xu, Y., Cheng, T., Li, S., Moan, T., Fu, Q., Liu, F., 2023. Load effects on vessel-shaped fish cage steel structures, nets and connectors considering the effects of diffraction and radiation waves under irregular waves. Marine Structures, 91, 103468. https://doi.org/10.1016/j.marstruc.2023.103468
Wang, Y., Tang, Z., Wang, L., Wang, X., 2022. Linear and quadratic damping coefficients of a single module of a very large floating structure over variable bathymetry: physical and numerical free-decay experiments. Journal of Ocean Engineering and Science, 7(6), 607-618. https://doi.org/10.1016/j.joes.2021.10.011
Wang, Y., Wang, H., Li, M., Wang, D., Fu, M., 2021. Adaptive fuzzy controller design for dynamic positioning ship integrating prescribed performance. Ocean Engineering, 219, 107956. https://doi.org/10.1016/j.oceaneng.2020.107956
Welling, C. G., 1981. An advanced design deep sea mining system. In Offshore Technology Conference (pp. OTC-4094). OTC. https://doi.org/10.4043/4094-MS
Wen, B., Liang, Z., Zhang, H., Fan, K., Wang, Y., Li, D., Tian, X., Peng, Z., 2023. A multi-drive aerodynamic load simulator for floating wind turbine model tests: Development, test and application. Ocean Engineering, 286, 115579. https://doi.org/10.1016/j.oceaneng.2023.115579
Wiegerink, J. J., Baldock, T. E., Callaghan, D. P., Wang, C. M., 2023. Experimental study on hydrodynamic response of a floating rigid fish tank model with slosh suppression blocks. Ocean Engineering, 273, 113772. https://doi.org/10.1016/j.oceaneng.2023.113772
Wright, C. S., Yoshimoto, H., Wada, R., Takagi, K., 2022. Surge slow drift viscous drag damping of an advanced spar: A numerical–experimental method for variable damping rates. Ocean Engineering, 266, 112696. https://doi.org/10.1016/j.oceaneng.2022.112696
Xiong, H., Chen, Y., Yang, N., Xiao, J., Li, L., 2018. Numerical study on settling and floating movements of a sphere particle flowing in a vertical pipe. In ISOPE International Ocean and Polar Engineering Conference (pp. ISOPE-I). ISOPE.
Xu, G., Zhou, Y., Yan, S., Zhang, N., 2022. Numerical investigation of wave amplitude spectra effects on focusing wave generation. Ocean Engineering, 265, 112550.

https://doi.org/10.1016/j.oceaneng.2022.112550
Xu, P., Wellens, P. R., 2022. Theoretical analysis of nonlinear fluid–structure interaction between large-scale polymer offshore floating photovoltaics and waves. Ocean Engineering, 249, 110829. https://doi.org/10.1016/j.oceaneng.2022.110829
Xu, S., Wang, X., Yang, J., Wang, L., 2020. A fuzzy rule-based PID controller for dynamic positioning of vessels in variable environmental disturbances. Journal of Marine Science and Technology, 25, 914-924. https://doi.org/10.1007/s00773-019-00689-2
Xu, X., Yang, J. M., Li, X., Xu, L., 2014. Hydrodynamic performance study of two side-by-side barges. Ships and Offshore Structures, 9(5), 475-488. https://doi.org/10.1080/17445302.2014.889368
Yamada, H., Yamazaki, T., 1998. Japan's ocean test of the nodule mining system. In ISOPE International Ocean and Polar Engineering Conference (pp. ISOPE-I). ISOPE.
Yang, J. S., Yang, J. L., Wang, B., 2023. Boundary control for floating beam system in irregular waves under one end pinned to reduce hydroelastic response. Ocean Engineering, 270, 113586. https://doi.org/10.1016/j.oceaneng.2022.113586
Yang, N., Tang, H., 2003. Several considerations of the design of the hydraulic pick-up device. In ISOPE Ocean Mining and Gas Hydrates Symposium (pp. ISOPE-M). ISOPE.
Yeo, C., Bhandari, J., Abbassi, R., Garaniya, V., Chai, S., Shomali, B., 2016. Dynamic risk analysis of offloading process in floating liquefied natural gas (FLNG) platform using Bayesian Network. Journal of Loss Prevention in the Process Industries, 41, 259-269. https://doi.org/10.1016/j.jlp.2016.04.002
Young, D. L., Bak, A. S., Forte, M. F., 2018. Initialization and setup of the Coastal Model Test Bed: integrated bathymetry. http://dx.doi.org/10.21079/11681/30023
Yu, J., Cheng, X., Fan, Y., Ni, X., Chen, Y., Ye, Y., 2023. Mooring design of offshore aquaculture platform and its dynamic performance. Ocean Engineering, 275, 114146. https://doi.org/10.1016/j.oceaneng.2023.114146
Yu, L., Li, C., Wang, S., 2022. Model tests and numerical simulations on the parametric resonance of the deep draft semi-submersible under regular waves. Ocean Engineering, 243, 110273. https://doi.org/10.1016/j.oceaneng.2021.110273
Yu, W., Lemmer, F., Bredmose, H., Borg, M., Pegalajar-Jurado, A., Mikkelsen, R. F., Stoklund Larsen, T., Fjelstrup, T., Lomholt, A. K., Boehm, L., Schlipf, D., Azcona, Armendariz, J., Cheng, P. W., 2017. The triple spar campaign: Implementation and test of a blade pitch controller on a scaled floating wind turbine model. Energy Procedia, 137, 323-338. https://doi.org/10.1016/j.egypro.2017.10.357
Yu, W., Lemmer, F., Lehmann, K., Cheng, P. W., de Guzmán, S., Moreu, J., Battistella, T., 2022. Model test and validation of the CROWN floating offshore wind turbine. In International Conference on Offshore Mechanics and Arctic Engineering (Vol. 85932, p. V008T09A059). American Society of Mechanical Engineers. https://doi.org/10.1115/OMAE2022-81065
Yuan, L., Chen, Y., Zan, Y., Zhong, S., Jiang, M., Sun, Y., 2023. A novel hybrid approach to mooring tension prediction for semi-submersible offshore platforms. Ocean Engineering, 287, 115776. https://doi.org/10.1016/j.oceaneng.2023.115776
Yue, Z., Zhao, G., Xiao, L., Liu, M., 2021. Comparative study on collection performance of three nodule collection

methods in seawater and sediment-seawater mixture. Applied Ocean Research, 110, 102606. https://doi.org/10.1016/j.apor.2021.102606
Zeng, X., Shi, W., Michailides, C., Zhang, S., Li, X., 2021. Numerical and experimental investigation of breaking wave forces on a monopile-type offshore wind turbine. Renewable energy, 175, 501-519. https://doi.org/10.1016/j.renene.2021.05.009
Zhang, D., Yuan, Z. M., Du, J., Li, H., 2022. Hydrodynamic modelling of large arrays of modularized floating structures with independent oscillations. Applied Ocean Research, 129, 103371. https://doi.org/10.1016/j.apor.2022.103371
Zhang, G., Yao, M., Xu, J., Zhang, W., 2020. Robust neural event-triggered control for dynamic positioning ships with actuator faults. Ocean Engineering, 207, 107292. https://doi.org/10.1016/j.oceaneng.2020.107292
Zhang, G., Yao, M., Zhang, W., Zhang, W., 2021. Event-triggered distributed adaptive cooperative control for multiple dynamic positioning ships with actuator faults. Ocean Engineering, 242, 110124. https://doi.org/10.1016/j.oceaneng.2021.110124
Zhang, H., Gui, F., 2023. The application and research of new digital technology in marine aquaculture. Journal of Marine Science and Engineering, 11(2), 401. https://doi.org/10.3390/jmse11020401
Zhang, H., Liu, S., Ong, M. C., Zhu, R., 2019. CFD Simulations of the propagation of free-surface waves past two side-by-side fixed squares with a narrow gap. Energies, 12(14), 2669. https://doi.org/10.3390/en12142669
Zhang, H., Tang, W., Yuan, Y., Xue, H., Qin, H., 2022. The three-dimensional green-water event study on a fixed simplified wall-sided ship under freak waves. Ocean Engineering, 251, 111096. https://doi.org/10.1016/j.oceaneng.2022.111096
Zhang, J., Ma, Y., Tan, T., Dong, G., Benoit, M., 2023. Enhanced extreme wave statistics of irregular waves due to accelerating following current over a submerged bar. Journal of Fluid Mechanics, 954, A50. https://doi.org/10.1017/jfm.2022.1022
Zhang, M., Schreier, S., 2022. Review of wave interaction with continuous flexible floating structures. Ocean Engineering, 264, 112404. https://doi.org/10.1016/j.oceaneng.2022.112404
Zhang, X., Simons, R., Zheng, J., Zhang, C., 2022. A review of the state of research on wave-current interaction in nearshore areas. Ocean Engineering, 243, 110202. https://doi.org/10.1016/j.oceaneng.2021.110202
Zhang, Y., Feng, L., Zhang, L., Wang, L., Dong, S., Gao, Q., Hu, X., Li, J., 2024. A study of tension and deformation of flexible net under the action of current. Ships and Offshore Structures, 19(1), 27-44. https://doi.org/10.1080/17445302.2022.2140532
Zhang, Y., Teng, B., 2021. A nonlinear potential flow model for higher-harmonic wave loads and ringing response of a monopile. Ocean Engineering, 222, 108574. https://doi.org/10.1016/j.oceaneng.2021.108574
Zhao, G., Xiao, L., Peng, T., Zhang, M., 2018. Experimental research on hydraulic collecting spherical particles in deep sea mining. Energies, 11(8), 1938. https://doi.org/10.3390/en11081938
Zhao, G., Xiao, L., Yue, Z., Liu, M., Peng, T., Zhao, W., 2021. Performance characteristics of nodule pick-up device based on spiral flow principle for deep-sea hydraulic collection. Ocean Engineering, 226, 108818. https://doi.org/10.1016/j.oceaneng.2021.108818

Zhao, M., Yu, Y., Li, Z., Liu, C., Pang, H., 2023. Effect of bottom unlatch and top breakage mooring lines on the dynamic behavior of a semisubmersible platform system. Ocean Engineering, 276, 114182. https://doi.org/10.1016/j.oceaneng.2023.114182

Zhao, W., Taylor, P. H., Wolgamot, H. A., Taylor, R. E., 2018. Linear viscous damping in random wave excited gap resonance at laboratory scale—NewWave analysis and reciprocity. Journal of Fluids and Structures, 80, 59-76. https://doi.org/10.1016/j.jfluidstructs.2018.03.002

Zhao, Y., Xie, S., Ma, C., 2022. Experimental investigations on the hydrodynamics of a multi-body floating aquaculture platform exposed to sloping seabed environment. Frontiers in Marine Science, 9, 1049769. https://doi.org/10.3389/fmars.2022.1049769

Zhao, Y. P., Lian, L., Bi, C. W., Xu, Z., 2022. Digital twin for rapid damage detection of a fixed net panel in the sea. Computers and Electronics in Agriculture, 200, 107247. https://doi.org/10.1016/j.compag.2022.107247

Zhao, Y. P., Liu, H. F., Bi, C. W., Cui, Y., Guan, C. T., 2021. Numerical study on the flow field inside and around a semi-submersible aquaculture platform. Applied Ocean Research, 115, 102824. https://doi.org/10.1016/j.apor.2021.102824

Zheng, X. Y., Zheng, H. D., Lei, Y., Chen, H., 2021. Nonlinear stochastic responses of a newly developed floating wind-solar-aquaculture system. Ocean Engineering, 241, 110055. https://doi.org/10.1016/j.oceaneng.2021.110055

Zheng, Z., Li, Y., Ellingsen, S. Å., 2023. Statistics of weakly nonlinear waves on currents with strong vertical shear. Physical Review Fluids, 8(1), 014801. https://doi.org/10.1103/PhysRevFluids.8.014801

Zhi, P., Pei, H., Zhang, X., Xu, N., Yang, J., You, Y., 2022. Experimental studies on the effects of draft condition, current heading and mooring stiffness on vortex-induced motions of a Tension-Leg Platform. Ocean Engineering, 266, 112882. https://doi.org/10.1016/j.oceaneng.2022.112882

Zhou, B., Ding, K., Huang, J., Wang, L., Guo, J., Tang, T., 2024. Influence of uniform currents on nonlinear characteristics of double-wave-group focusing. Physics of Fluids, 36(3). https://doi.org/10.1063/5.0190701

Zhou, J., Ren, J., Bai, W., 2023. Survey on hydrodynamic analysis of ship–ship interaction during the past decade. Ocean Engineering, 278, 114361. https://doi.org/10.1016/j.oceaneng.2023.114361

Zhou, K., Hu, Z., Zhao, D., 2018. Time-domain analysis of the relative motions between side-by-side FLNG and LNGC under oblique waves. Journal of Marine Science and Application, 17, 519-530. https://doi.org/10.1007/s11804-018-0038-0

Zhou, Q., Liu, M., Peng, H., Qiu, W., 2015. Experimental studies of hydrodynamic interaction of two bodies in waves. In International Conference on Offshore Mechanics and Arctic Engineering (Vol. 56598, p. V011T12A011). American Society of Mechanical Engineers. https://doi.org/10.1115/OMAE2015-41304

ITTC2024

30TH INTERNATIONAL TOWING TANK CONFERENCE
22–27 SEPTEMBER 2024 | HOBART TASMANIA AUSTRALIA

REPORT OF THE STABILITY IN WAVES COMMITTEE

STABILITY IN WAVES COMMITTEE

1. INTRODUCTION

Membership and Meetings

The members of the Stability in Waves Committee of the 30th ITTC are:

- Dr. V. Belenky, (Chairman)
  Carderock Division, Naval Surface Warfare Centre (NSWCCD), USA
- Mr. J.-F. Leguen, (Secretary)
  DGA Hydrodynamics, France
- Dr. T. Kim
  Samsung Heavy Industries, South Korea
- Mr. A. Matsuda
  Japan Fisheries Research and Education Agency, Japan
- Dr. S. Bu
  China Ship Scientific Research Center (CSSRC), China
- Dr. Y. Liu
  Marine Design & Research Institute of China (MARIC), China
- Prof. E. Boulougouris
  University of Strathclyde, United Kingdom.
- Dr. C. Rodríguez
  Laboratory of Ocean Technology, Brazil.

Stability in Waves committee face to face meetings have been held during the work period:

- The first kindly hosted by Prof. P. Krata at University of Gdansk, Poland, the 15th September 2022, just after ISSW 2022.
- The second at Strathclyde University, Glasgow, UK, from the 30th May to the 1st June 2023.
- An opportunity meeting during the 19th International Ship Stability Workshop held in Istanbul in September 2023.
- The last face-to-face meeting at Carderock Division, Naval Surface Warfare Centre (NSWCCD), USA from 26th to 28th February.

A series of video meeting (more than 10) was also organized, regularly approximately every two months.

1.2 Tasks

The recommendations for the work of the Stability in Waves Committee as given by the 29th ITTC were as follows:

1. Update the state-of-the-art for predicting the behavior of bottom founded or stationary floating structures, including moored and dynamically positioned ships, emphasizing developments since the 2021 ITTC Conference. The committee report should include sections on:
   A) the potential impact of new technological developments on the ITTC
   B) new experimental techniques
   C) new benchmark data

- D) the practical applications of computational methods to prediction
- E) the need for R&D for improving methods of model experiments, numerical modelling.

2. Review ITTC Recommended Procedures relevant to stability, including CFD procedures, and
   - A) identify any requirements for changes in the light of current practice, and, if approved by the Advisory Council, update them,
   - B) identify the need for new procedures and outline the purpose and contents of these.
3. Update ITTC Procedure 7.5-02-01-08, Single Significant Amplitude and Confidence Intervals for Stochastic Processes when new information becomes available.
4. Develop new ITTC recommended procedures in support of direct stability assessment within 2nd generation IMO intact stability criteria:
   - A) Avoiding self-repeating effect in time-domain numerical simulation of ship motions,
   - B) Procedure of Estimation of Frequency of Random Events by Direct Counting,
   - C) Statistical Validation of Extrapolation Methods for Time Domain Numerical Simulation of Ship Motions.
5. Develop a new procedure, Computational procedure for instantaneous GZ curve during time-domain numerical simulation in irregular waves.
6. Investigate the current state of the art on flooding dynamics of damaged ship in waves, including EFD and CFD.
7. Continue the identification of benchmark data for validation of stability-in-waves predictions.

For the 30th ITTC, the modelling and simulation of waves, wind and current is the primary responsibility of the Ocean Engineering Committee with the cooperation of the Seakeeping and the Stability in Waves Committees.

2. STATE OF THE ART (TOR 1)

2.1 Potential impact of new technological developments on the ITTC (TOR 1 A)

Leveraging the combined strengths of neural networks and a spectrum of machine learning techniques, ship motion prediction has entered a new era of precision and adaptability. These sophisticated AI methodologies—encompassing artificial neural networks, support vector machines, and decision tree, etc.—excel in dissecting and learning from the vast and complex datasets related to maritime environments and vessel behaviors. They not only provide nuanced insights into ship movements across varying sea states but also enhance safety protocols and operational efficiencies through their ability to dynamically adapt and refine predictions based on continuous data ingestion. In the modern seafaring landscape, the integration of AI surpasses traditional prediction models, providing a robust and precise toolkit for navigating the complex challenges of maritime operations.

Pickering et al. (2022) addressed a computational framework by combining output-weighted training schemes in Bayesian experimental design (BED) with an ensemble of deep neural operators (DNOs) (Figure 1). This model-agnostic framework pairs a BED scheme that actively selects data for quantifying extreme events with an ensemble of deep neural operators that approximate infinite-dimensional nonlinear operators. It is concluded that it is scalable artificial intelligence (AI)-assisted experimental infrastructure that can efficiently discover and forecast extreme events.

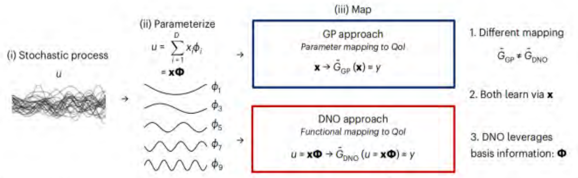

Figure 1: DNOs leverage functional information for mapping to the quantity of interest (QoI) (Pickering et al. 2022)

Zhou et al. (2023) propose a "grey box" algorithm consisting of a deep learning network and parametric roll equation to provide the parametric roll simulations, which can accurately recognize the time histories induced large-amplitude parametric roll of the C11 container ship.

Li et al. (2023a) used the Power-activation Feed-forward Neural Network (PFN) to achieve real-time prediction of the ship's parametric roll motion. The theoretical rationality of real-time prediction based on the ship's rolling motion time series data is verified. Results show that the simplified PFN model has advantages in real-time prediction of parametric roll motion due to its time-varying weight adjustment methods, with the safer mapping mode, higher accuracy, and shorter computing time.

González et al. (2023a) investigated the deployment of a ANN model for real-time forecasting parametric roll in ships, with an emphasis on its use for stability guidance on small to medium-sized fishing boats.

Louvros et al. (2023) introduced a methodology that integrates Machine Learning (ML) and Case-Based Reasoning (CBR), using pre-built databases for real-time analysis of damage scenarios. The approach can be easily applied, relying on straightforward inputs like crew observations and effectively managing prediction uncertainties, particularly in survival predictions. The authors argue that the outputs are consistent, and informative, encouraging further exploration of Machine Learning for dynamic damage stability assessments. Its accuracy depends on the range of pre-calculated scenarios, offering a robust alternative to conventional approximations. The methodology was demonstrated in the H2020 SafePASS project as part of a decision-support methodology during flooding incidents.

Mauro et al. (2023a) developed a surrogate model to enhance real-time onboard risk assessment for ship collisions, utilizing SHARP software's Super-Element methods for efficient scenario generation. This model, validated with over 4,400 damage scenarios, identified forest tree models as the most accurate approach, though simpler multiple linear regression models are also effective at the initial stage. Enhancing the model's accuracy involves increasing the variety of simulated collisions rather than just the number of experiments. Initially, multiple linear regression is advisable due to its simplicity and the uncertainty in direct damage calculations. As more data becomes available, a shift to forest tree models is recommended, with neural networks needing more extensive data to be effective. The developed methodology is an integral part of the real-time flooding risk evaluations proposed by Vassalos et al. (2023).

2.2 New experimental techniques (TOR 1 B)

Model testing is an effective means for investigating the GZ curve in the wave. CSSRC (Gu et al., 2014) constructed a partially restrained model test equipment for the GZ curve in waves, see Figure **2**.

The setup, shown in Figure **2** consists of five main components:

1. A pedestal with four locking jaws to secure the equipment to the towing carriage.
2. A guide rail bracket, a linear guide rail pair, a displacement sensor using a guide wire, heaving rod and a block.
3. Three diverging combination sensors that use rods to measure the surge force, sway force, and yaw moment. The measurement is done by a strain gauge.
4. A mechanism for measuring pitch, roll motions with potentiometers; roll moment is measured with a double flange torque sensor. The mechanism locks a model with a given roll angle.
5. A system for balancing the weight of the second and third components, which includes a pulley block, a vertical guide road and a counterweight.

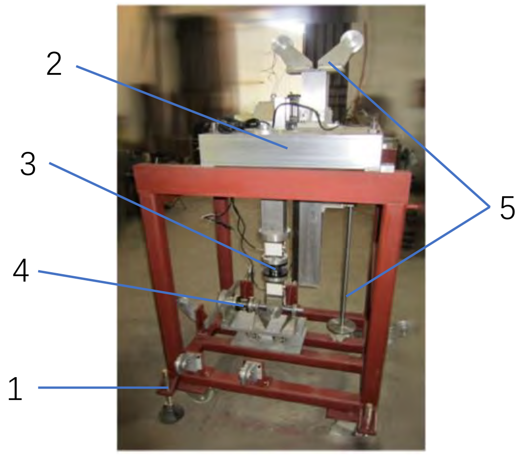

Figure 2: Equipment for GZ curve in waves (Lu et al., 2017)

Surge, sway and yaw motions are restrained, heave and pitch motions are free. Roll motion can be free or restrained depending on the test setup. Roll, pitch, and heave can be measured simultaneously. When roll is fixed at a given angle, the roll moment and the sway force are measured simultaneously, and the restoring moment can be recovered.

Examples of an experimental setup are shown in Figure 3 and Figure 4, from the model test at CSSRC's seakeeping basin with models of C11-class container carrier and ONRTH configurations respectively.

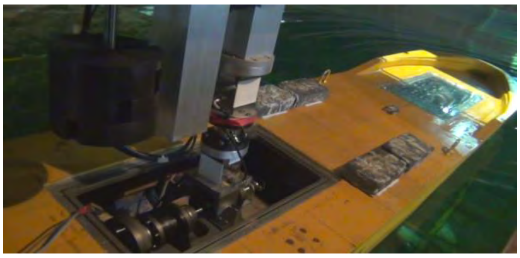

Figure 3: Ship model of C11 Containership in partially restrained experiment (Bu et al. 2019)

Figure 4: Ship model of ONR tumblehome hull in partially restrained experiment (Bu et al. 2021)

2.3 New benchmark Data (TOR 1 C)

The new benchmark on damaged ship stability is described below, see also in Section 8.

Ruponen et al. (2021, 2022, 2022a) present an international benchmark study on simulation of flooding and motions of damaged vessels that was conducted within the EU Horizon 2020 project FLARE, using new dedicated model tests as a reference. The benchmark was divided into three separate parts, each concentrating on specific phenomena:

- Part A: flooding fundamentals, with captive models and simplified geometries
- Part B: transient and progressive flooding of a cruise ship
- Part C: transient and gradual flooding of a ROPAX ship

In total, 11 organizations provided results to some parts of the benchmark:

- Brookes Bell (BROO)
- DNV
- HSVA
- MARIN
- University of Strathclyde, Maritime Safe-ty Research Center (MSRC)
- NAPA
- China Ship Scientific Research Center (CSSRC), China
- Korea Research Institute of Ships & Ocean Engineering (KRISO), Republic of Korea
- University of Applied Science Kiel (UAK), Germany
- University of Naples “Federico II” (UNINA), Italy
- University of Trieste (UNITS), Italy

Part A of the benchmark study (flooding fundamentals) studied three different flooding scenarios. Figure 5 depicts up-flooding in a box model with two compartments and down-flooding in the same box model with different openings. The time history of water levels in sensors

23 and 27 were measured. The third case considers extensive progressive flooding along a typical deck layout of a cruise ship, including a long central service corridor (see Figure 6) and the water levels were recorded at various locations on the deck, see Figure 7.

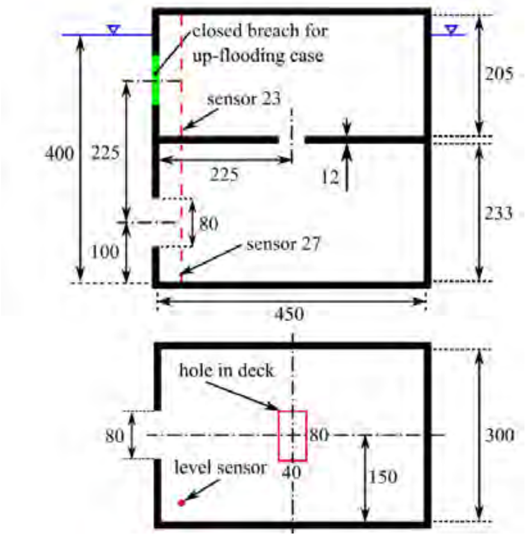

Figure 5: Box model arrangement and dimensions for the up-flooding case (Ruponen et al. 2021)

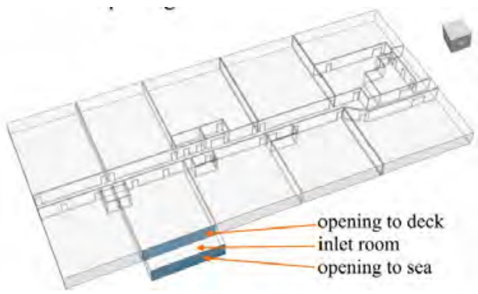

Figure 6: Arrangement for deck flooding case (Ruponen et al. 2021)

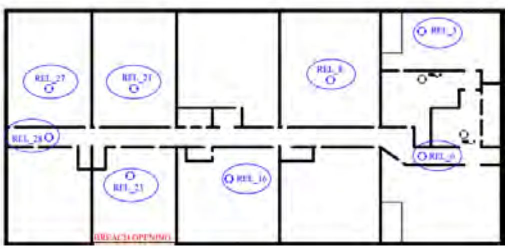

Figure 7: Locations of selected water level sensors (Ruponen et al. 2021)

Part B investigated an unbuilt large cruise ship design (about 95,900 GT) provided by Chantiers de l'Atlantique. Table 1 lists the main dimensions. As seen in Figure 8, the hull of the model extends vertically over 8 decks with floodable compartments positioned on 6 lower decks. The hatched rooms were filled with foam and thus not floodable, and the red squares mark the selected water level sensors, red "×" symbols denote holes in the deck and thick red lines mark the large breach.

In total, the model contains 60 floodable rooms bounded by bulkheads and decks. The rooms are connected by 82 internal openings in the bulkheads and 11 openings in the decks.

Model tests were performed at MARIN using a 1:60 scale model, see Figure 9. The flooding progression and ship motions were measured in three separate test cases: Transient flooding in calm water; Transient and progressive flooding in irregular beam seas; Up-flooding in calm water with smaller breach size.

Table 1: Main dimensions of the studied cruise ship and the applied initial intact condition in model tests. (Ruponen et. al., 2022)

	Full scale	Model scale
Length over all	About 300 m	About 5.0 m
Length between perpendiculars	270.00 m	4.5 m
Breadth	35.20 m	0.587 m
Draught (in tests)	8.20 m	0.137 m
Trim (in tests)	0.00 m	0.000 m
Height of bulkhead deck form base line	11.00 m	0.183 m
Gross tonnage	95 900	-
Metacentric height (in tests)	2.36 m	0.0393 m
Radius of inertia for roll	13.904 m	0.2317 m

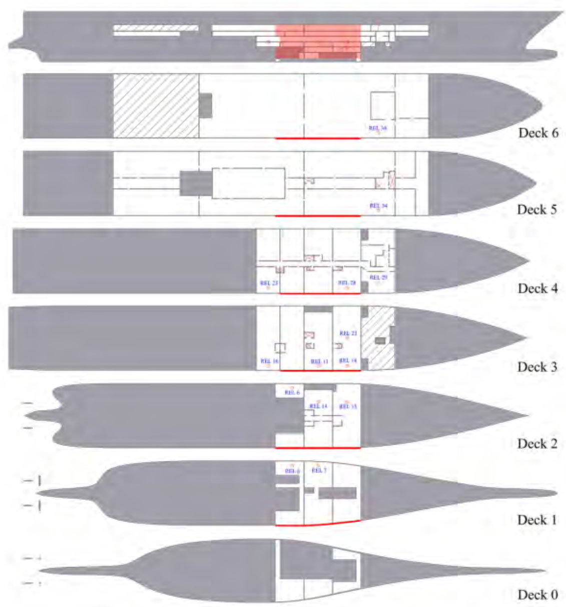

Figure 8: Arrangement of the ship model

Figure 9: Model of the cruise ship, courtesy of MARIN (Ruponen et. al., 2022)

Before the test, a magnetic cover sheet sealed the breach, see Figure 10. The coversheet was pulled upwards with a winch at zero time. In the model scale, the speed was about 2.5 m/s. As a result, the breach opened quickly- in less than 4 seconds at full scale. A nominal capsize limit of 40◦ was used in the tests. With a roll angle of positive to the breach side (starboard) and a pitch (trim) angle of positive towards the bow, all results are presented in full scale.

In the model tests, the model`s six degrees of freedom motion and the water levels in various locations within the flooded compartments were measured. As seen in Figure 11, the floodable compartments were vented using large air pipes on the leeward (intact) side. In this respect, the effects of air compression were considered small, and consequently full ventilation was assumed by most participants. Air pressures inside the model were not measured, so this assumption cannot be confirmed.

Figure 10: Breach opening and the magnetic cover (photo courtesy of MARIN)

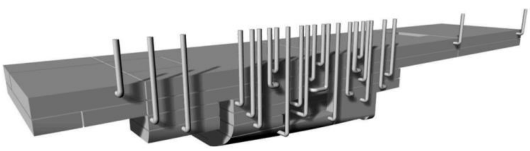

Figure 11: Rendering of the 3D model of the compartment and ventilation pipes (courtesy of MARIN)

Part C investigated an unbuilt ROPAX design that Meyer Turku provided, weighing roughly 28,500 GT. At HSVA, tests were conducted using a 1:28 scale model. Table 2 lists the ship's main parameters in both full and model scales.

Figure 12 and Figure 13 illustrate how the floodable compartments are arranged. The compartments are not internally connected to each other. The impact of a two-compartment collision is examined. There is a casing on the port side of the centerline on the vehicle deck, having an impact on the accumulation of water on the deck in waves. All damaged compartments were ventilated through ventilation pipes in the compartment corners.

Three test cases were investigated separately: Transient flooding in calm water with two different initial metacentric height (GM) values and a third one with slower opening time for the breach; Transient flooding in waves with two small variations in the initial steady heel angle; Gradual flooding of the vehicle deck in waves in two different sea states.

Table 2: Main dimensions of the studied ropax vessel

	Full scale	Model scale
Length over all	About 162 m	About 5.8 m
Length between perpendiculars	146.72 m	5.24 m
Breadth	28.0 m	1.00 m
Draught	6.1 m	0.218 m
Height of ro-ro deck from baseline	9.2 m	0.329 m
Height of tank top from baseline	1.5 m	0.054 m
Gross tonnage	28 500	-

All the tests were conducted for a freely drifting model. For the tests in waves, bow and stern lines were occasionally used to correct the model orientation back to beam seas condition. For practical reasons, the roll angle of 36◦ was used as the nominal limit for capsizing, and the test was interrupted when the roll angle exceeded this limit.

The model was equipped with instruments to measure the 6 Degrees-of-Freedom motions, the relative wave elevations at several positions on and below the main vehicle deck. Four video cameras were used to record the tests, two outside cameras focusing on the ship motions, one recording the water elevation in the compartment R1 below the main vehicle deck, and one showing water ingress to the vehicle deck (room R3).

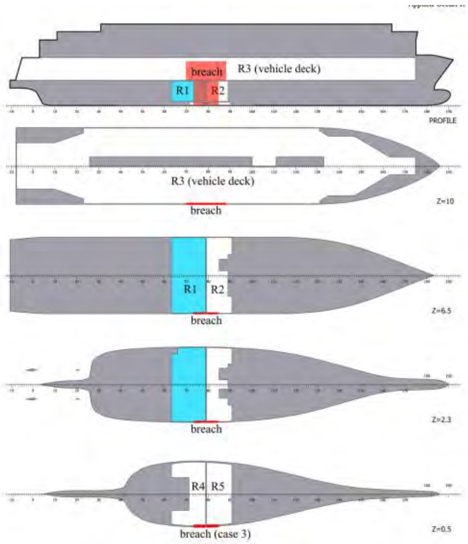

Figure 12: Breach and floodable compartments of the ropax model

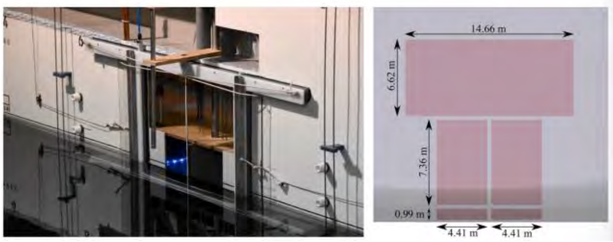

Figure 13: Breach opening mechanism for the transient flooding tests and full-scale dimensions of the breach

For transient flooding cases, the volume of water and its centroid in the blue compartment R1 were analyzed by HSVA based on the six water level sensors in the compartment. These sensors were located transversally, and therefore, the analysis is based on the assumption of two dimensional water surface.

2.4 The practical applications of computational methods for prediction and scaling (TOR 1 D)

2.4.1 Deck immersion

The false-negative inconsistency issue in the vulnerability criteria of stability under dead ship condition for low freeboard ships is examined by Munakata et al. in 2021. According to the model experiments, the deck immersion, which raises roll damping and lowers the effective wave slope coefficient, is mostly to blame for the inconsistency. These consequences were not taken into account by the level 2 vulnerability criteria that is in use to-day. According to the author, roll damping and the effective wave slope coefficient can be estimated using the model experiment. In the event that the experiment is impractical, an alternative method could be to calculate the effective wave slope coefficient using the non-linear strip theory and roll damping using Rakhmanin's empirical formula.

Subramaniam et al (2021) experimental investigate the effect of trapped deck water on the roll dynamics of one low weather deck offshore supply vessel (OSV) in both regular and irregular stern quartering waves. The study found that there is an increase in the roll angle due to the reduction of the positive damping effect at a higher Froude number. At very severe sea states, the possibility of large roll angles occurring at low Froude number exists, due to excessive static moment caused by the trapped water, see figure 14 and figure 15.

Figure 14: Movement of deck water due to ship roll with a phase lag for one of the irregular wave trial, Froude number 0.3 with open openings

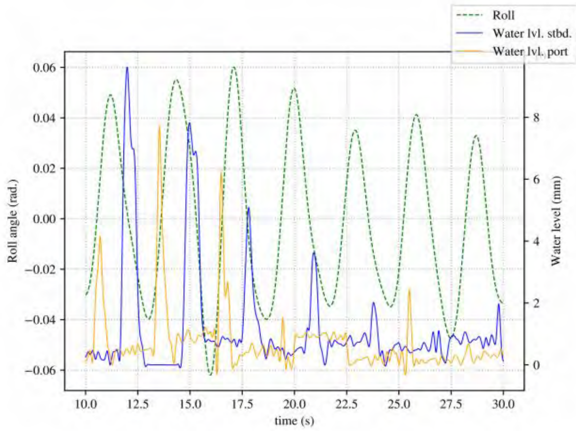

Figure 15: Time history of ship roll and deck water motion, Froude number 0.31

Masamoto et al. (2023) described experiments where trapped water on the deck affects the transverse stability of purse seiners running in stern quartering seas. The influence of trapped water on the deck is quantitatively evaluated by conducting a phase difference analysis of the measured trapped water on the deck motion and the time series of the ship model's rolling motion.

2.4.2 Sloshing

Sloshing impact loads are not usually relevant to stability in waves. Sloshing is here only considered as a factor, influencing on the dynamics of the vessel as a whole.

Liu et al., (2022a) performed the numerical simulations of the parametric roll of a ship coupled with liquid sloshing. Wu et al. (2021) introduced two improvements to the original Moving Particle Simulations MPS. Then the improved MPS was applied to solving two-dimensional liquid tank sloshing problems, and studied the coupled motion of swaying and rolling motion with different loading rates, which is aiming to provide some reference for further study on the influence of the sloshing impact loads on the motion of real ships.

Igbadumhe et al. (2022) carried out a series of roll decay tests for a FPSO model with a pair of two-row prismatic tanks. The results show that an increase in liquid cargo, the location of cargo load, and the geometry of the cargo tank affect the damping of the vessel. Interaction between sloshing and and ship motions at forward speed was considered by Lyu et al (2022).

2.4.3 Fundamentals

Hori published many papers recently, and a good summarised in 2021 (Hori, 2021). It is a proof that the centre of buoyancy is equal to the centre of pressure. Even if it was commonly used and verify in many studies, the proof was not really written as a demonstration before. An elegant proof was proposing by Hori for arbitrary shape of floating body applying Gauss's theorem and solve the undetermined solution of the equilibrium by solving it in a non-equilibrium position and go to the equilibrium at its limit, see Figure 16. Similar subject was considered by Spyrou (2022).

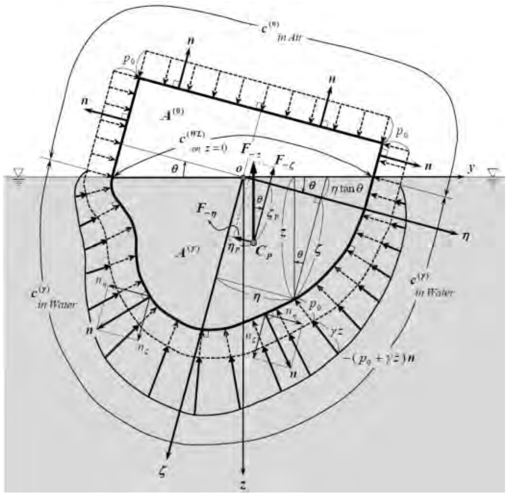

Figure 16: Hydrostatic pressure and centre of pressure acting on the inclined floating body with arbitrary form from Hori, 2021

2.4.4 GZ curve

Bu et al (2021) focused on the accurate prediction of roll restoring arm in waves. The investigations showed that the conventional FK assumption in which GZ_{RD} (GZ curve computed with diffraction and radiation) is ignored can be employed for the calculation of roll restoring arm of zero speed in different wave directions, because GZ_{RD} is negligible at zero speed. Considering that there is no obvious improvement on the prediction accuracy in following waves with forward speed even though GZ_{RD} is taken into account, the FK assumption can also be used.

Zhou et al. (2022a) aimed to study the Parametric Roll characteristic of ships with extended low weather deck, and carried out an experimental investigation and numerical comparison. The effect of highly nonlinear water-on-deck phenomena caused by ORV's extended low weather deck on Parametric Roll response is specially investigated. Regarding numerical simulation of ORV's parametric roll, the effects of assessment accuracies of GZ curves in waves and roll damping coefficients are analysed.

2.4.5 Motion in random waves

Evaluation of the probability of rare events, such as occurrence of maximum reactions over ship design life, from direct numerical simulations requires significant computational time.

For the "operational limitation" introduced by the framework of SGISC in MSC.1/Circ. 1627, the standard environmental conditions are substituted by specific environmental conditions, and this substitution generally has an impact on the calculation parameters of the criteria. Bulian and Francescutto (2021) developed a rational simple procedure for the limitation of information when the level 1 vulnerability are used for dead ship condition.

Due to significant nonlinearity of hydrostatic and Froude-Krylov forces, probability distribution of roll motion can significantly deviate from Gaussian distribution. To find the shape of this non-Gaussian distribution, Maki (2017) proposed to consider neglect self-dependence in expiation and describe as white noise. The distribution of response then can be found by solution of Fokker-Plank-Kolmogorov (FPK) equation. The resting distribution then can be scaled with outcome of numerical simulation.

For the prediction of the joint probability density function (PDF) of roll angle and rate, Maki et al. (2021) validated the method by comparing them with the Monte Carlo when the wave period is close to the natural roll period.

Katayama et al. (2023) looks into a way to derive a suitable non-Gaussian distribution for a short-term stability assessment. Maki et al (2022) describes application of this technique to roll angular accelerations. FPK equation is solved numerically with PDF line integral method. The results are compared with an outcome of Monte-Carlo simulation.

Maruyama (2022b) used the stochastic averaging method using Hamiltonian proposed by Maki et al. (2023) and the PDF of roll amplitude and Hamiltonian are derived from the equations of roll motion.

Zhou et al. (2023a) presented a novel extreme statistics strategy for predicting extreme values of ship parametric rolling motions based on limited model test observations. The synthetic moment method to estimate the distribution of extreme ship rolling motions, incorporating Hermite transformation to address the skewness and kurtosis in the data was used. This step helps in accurately representing the statistical properties of parametric roll. The Markov chain model is applied for correction, enhancing the precision of extreme value predictions from limited observations by considering the temporal sequence of rolling motions. By applying this strategy to the C11 container ship model, the study successfully predicts extreme rolling angles from minimal data, demonstrating the method's superiority over traditional approaches in small sample scenarios.

Rajaraman and Hariharan (2023) explored the steady-state ship rolling motion in random beam seas with nonlinear damping and restoring moments mathematically by using Hermite wavelets.

Chai et al. (2022) studied excessive roll motion for the cases of the dead ship condition and the parametric rolling. Two different methods, i.e. the traditional Gumbel method and the average conditional exceedance rate (ACER) method are applied in order to predict the extreme values of the stochastic process.

Glotzer et al. (2023) provided an important update on constructing confidence interval for mean and variance estimates for ship motions in irregular waves. Ship motions are characterized with self-dependence, strongly affecting the width of confidence intervals. The cited reference proposes to account for this self-dependence with an estimate of long-run variance and its square. The approach has been extended for the case of an ensemble with several independent records. Additionally an alternative algorithm of "self-normalization" is proposed. The information from the cited reference was use to update ITTC recommended procedure 7.5-02-01-08 as required by TOR 3. See details in section 4 of this Report.

Li et al. (2023) simulated the extreme roll motion of ONRH by using an in-house CFD solver in irregular beam waves without for-ward speed. Coupled roll-pitch-heave (3-DOF) and coupled sway-roll-pitch-heave (4-DOF) were considered to understand the impact of sway motion on ship stability. The results indi-cated that roll motion amplitude under 3-DOF conditions is significantly larger than under 4-DOF, with CFD predictions closely aligning with experimental findings, highlighting the importance of including sway in stability anal-yses under extreme conditions.

2.4.6 Second Generation Intact Stability Criteria (SGISC)

Umeda and Francescutto (2023) describe current status of the IMO SGISC, just prior finalization of the Explanatory Notes to the Interim , Guidelines of the Second Generation Intact Stability Criteria by IMO in April 2023 with MSC.1/Circ.1652 referred further simple as "the Explanatory Notes" . There are five stability failure modes considered: dead ship condition, excessive acceleration, pure loss of stability, parametric roll resonance and surf-riding / broaching-to. The Interim Guidance on the criteria was issued by IMO in 2020 as MSC.1/Circ. 1627. The criteria have tiered structure, where the first tiers are intended to detect possible vulnerability to stability failures, while the third tier is focused on application of state-of-the art numerical simulation techniques, referred as Direct Stability Assessment (DSA). As directed by the Term of References, the ITTC contributions to the DSA is addressed in sections 3, 5 and 9.

Peters et al. (2023) considers the relation between the second generation intact stability criteria and achieved safety level of a vessel, satisfying these criteria, emphasizing the connection with new approaches being promoted by IMO such as Goal Based Standards and Formal Safety Assessment.

Schrøter et al. (2023) describes systematic evaluation of the vulnerability criteria to obtain GM limit curves and identifies inconsistency between the levels of the criteria. The inconsistencies between the level 1 and 2 for dead ship condition and pure loss of stability is also studied in Peters and Belenky (2023), considering the relation of the former with the current IMO Intact Stability Code (IMO 2008). It was concluded that some inconsistency between level 1 and 2 of vulnerability criteria is unavailable. The level 1 vulnerability criterion is similar to weather criterion, which cannot be given a unique probabilistic interpretation, while level 2 vulnerability criteria is probabilistic.

Umeda et al. (2023c) considers inconsistency in vulnerability criteria for pure loss of stability encountered with offshore supply vessels, having an extended low deck. The reason of inconsistency is that the deck is likely to be flooded at large roll angles. Large extent of the deck means that the green water changes dynamics of roll motion beyond what was included in the vulnerability criteria. The described model tests do confirm that the water of the deck is a source of inconsistency.

Peters et al (2023a) gives a scientific background for the level 2 vulnerability criterion for surf-riding. This criterion is a good example of using Nonlinear Dynamics for practical calculation. The detection of dangerous surf-riding situation is based on Melnikov analysis, determining the speed setting leading to surf-riding at all initial condition at a given wave.

Shigunov (2023) considered specification for DSA focusing on the Poisson process, which is the main probabilistic model, relating probability of stability failure with time of exposure. As a result, complete probabilistic characterization of stability in wave can be done through rate of failures. General basis of use of Poisson process for stability regulations is described in Chapter 1 of Belenky and Sevastianov (2007). A brief description of application Poisson process for stability in waves can be found in Section 2 of IMO document SDC-8/INF.2, submitted by ITTC and prepared by 29th ITTC Stability in Waves Committee.

Wandji et al. (2024) provide mathematical basis for three methods of direct counting, described in the Explanatory Notes, including a formal analysis of bias and variance of estimators. Benchmarking of three estimators and their confidence interval is carried out using synthetic data, following Poisson process that also can be found in Shigunov et al. (2022). Wandji et al (2023) carry out this benchmarking on ship motion data, produced by numerical simulation.

Reed (2023) considers a formal process of Verification, Validation and Accreditation (VV&A) of numerical tools for simulation of ship motions, if such tool is to be applied for DSA. A formal VV&A process is essential for uniform application of DSA.

Umeda et al. (2023a) describes a comparison between numerical simulation and model test for dead ship condition and pure loss of stability. Special attention was paid to wind generation. Validation of numerical tools for pure loss of stability and parametric roll was addressed in Umeda et al. (2023b).

Francescutto (2023) examines a history of stability criteria, describing how this matter was developed starting from purely empirical approach of Rahola (1939) towards development of the weather criterion, forming the current International Intact Stability Code (IMO 2008), being the first generation intact stability criteria.

Weems et al. (2023a) considers application of fast volume-based simulation tool for direct stability assessment. Comparison with well-established, engineering-level potential flow/ hybrid simulation tool LAMP (Large Amplitude Motion Program, Shin et al. 2003) is provided.

Peters and Belenky (2021) suggested a methodology for the comparison of the alternatives with current criteria and its relevance to operational experience using pure loss of stability as an example. This was in response to comments regarding the testing and trial use of the SGISC.

Petacco (2021) investigated the sensitivity of ship stability performance in waves to geometric variation by means of a simulation-based design framework. A method developed in-house, combining the subdivision surface and free-form deformation approaches, has been used to create the whole set of design alternatives. The generated design configurations have been assessed analysing the results derived from application of the first- and the second-level SGISC vulnerability criteria for both the selected stability failure modes. To strengthen the correlation behaviours, the design space has then been further explored by using 10k design configurations exploiting the capabilities of a surrogate model–based approximation, relying on a Gaussian process formulation.

2.4.7 Surf-riding and Broaching-to

Umeda (1990) suggested a critical wave approach for the stability failure risk of broaching associated with sur-riding in both irregular following waves and stern quartering waves (Umeda et al. 2007). Matsubara et al. (2021) used a free-running model experiment and numerical simulation to validate the approach in irregular waves with both short and long crested waves.

Ma et al. (2021) studied the influence of hydrodynamic derivative on surf-riding using CFD method. The authors compared the course stability with hydrodynamic derivative in waves and also in clam water.

Tigkas and Spyrou (2023) focused on the surge dynamics of a ship operating in long following waves. A quite robust irregular version of hybrid surging was identified. The mathematical model includes three DoF (surge-pitch-heave) and it accounts for hydrodynamic memory effects.

Gong et al. (2022) applied a hybrid method coupling potential flow method and viscous flow method to simulate the autopilot trimaran in stern waves, aiming to study the process of being captured by waves and the surf-riding characteristics of the trimaran.

Feng et al (2023) focused on the level 2 surf-riding/broaching vulnerability criterion and proposes complements to the assessment procedures regarding two important issues. One is that the current procedure is only applicable to ships using propellers. The second issue is addressed through the proposal of a practical method to estimate the wave surge force correction factor based on the ratio between the first order wave surge force and its FK component.

Yu et al (2022) simulated surf-riding and broaching in irregular waves by using a previously developed 6-DOF numerical model. The surf-riding / high run is defined as exceedance of the instantaneous wave celerity. The approach identified “likely broaching” as 10 degree yaw deviation. Dependence on wave heading and speed has been studied. It is found that the ship capsizes after experiencing a relatively long duration of high run, which suggests correlation between capsizing and high run. High run in irregular wave is proved to be a good representation of surf-riding.

Liu et al. (2022b) investigated the capsizing behaviour of a free-running ONR Tumblehome model in stern quartering seas by an unsteady Reynolds-averaged Navier-Stokes (URANS) solver coupled with dynamic overset grid approach.

Spyrou et al. (2023) describes two calculation techniques to estimate probability of surf-riding in irregular waves. The first technique identifies points in the phase space where all the longitudinal forces are equal (pseudo-equilibria). As these points do move with acceleration they cannot be a solution of the equations of motion. The second technique detects “high-runs” – increases of the forward speed above the predetermined threshold. The values, estimated with both techniques, are compared.

Spyrou et al. (2023a) looks in the fundamentals of surf-riding in irregular waves, examining how the surge response changes when wave excitation goes from monochromatic to bichromatic and following with the further frequency increase. The surf-riding phenomenon goes through a qualitative transformation with addition just one more frequency, including a possibility of chaotic response.

Belenky et al. (2023) consider application of split-time method for estimation of probability of surf-riding in irregular waves. The metric of likelihood of surf-riding is computed by perturbation of the dynamical system in its phase space towards the pseudo-equilibria until the surf-riding response is observed. The latter is defined as an exceedance of the instantaneous wave celerity.

Belenky et al. (2023a) attempts to extend the split-time method for estimation of probability of broaching-to preceded by surf-riding. Similar to surf-riding, the metric of likelihood is computed as a perturbation in phase space towards a “dangerous” point. The latter is defined as an origin of significant deviation from the commanded course; it is searched numerically in the vicinity of pseudo-equilibrium.

2.4.8 Parametric roll

In order to reduce the risk of roll resonance incidents for sailing ships, Koop et al. (2021) developed a new operational method to identify the critical sea states by evaluating 2D wave spectra using radial basis function in on-board warning systems, see Figure 17.

Luthy et al (2021) extend the energy method to non-linear GZ for the prediction of parametric roll, see Figure 18.

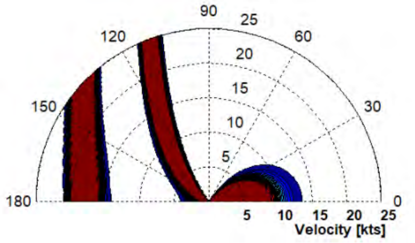

Figure 17: Polar diagram of critical combinations of sailing speed and incident wave angle for the C11 containership using the proposed basis functions. (Koop, 2021).

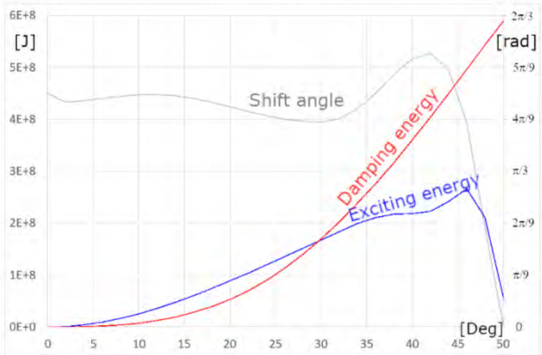

Figure 18: Damping and exciting energies and fitted, from Luthy et al (2021).

Luthy et al. (2022) introduced a method to calculate the steady state roll amplitude on monochromatic longitudinal wave when the encounter period is twice the natural roll period, which is the parametric roll condition. He extended this method to the speed of any ship, aiming to propose an alternative method for single degree of freedom simulation in the head sea, see Figure 19**Error! Reference source not found.**. It identifies the most conservative spreading angle for equivalent sets of waves, with a polar-plot summary of maximum roll angle.

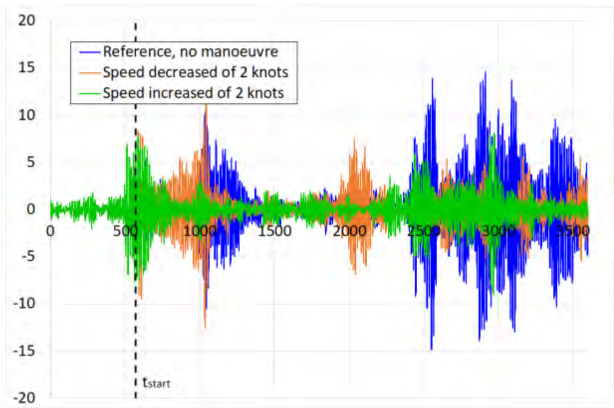

Figure 19: Effect of speed modification on the roll motion (Luthy et al., 2022).

Uchida et al. (2022) simplified the estimation of fundamental parametric rolling in longitudinal waves. An averaging method applied to an uncoupled roll model is used to estimate the amplitude of fundamental parametric rolling. A harmonic balance method is utilized to estimate the occurrence of fundamental rolling.

González et al. (2023a) presented a study of using neural network for predicting parametric roll. The neural network was trained with numerical simulation data and the compared to a model test results.

Liu et al. (2021) presented a computational fluid dynamics (CFD) prediction of a full-scale ship parametric roll in a regular head wave.

Jiang Y. et al. (2023) proposed a method of predicting the stability zone and checked by numerical simulation based on computational fluid dynamics. The relationship between the outrigger position and the potential risk of the parametric roll was analysed by the obtained stability zones. It was found that the decrease in the outrigger displacement ratio and the increase in the clearance can significantly raise the risk of parametric roll of a trimaran.

Wu et al. (2022) present a numerical investigation for the wavelength effect on the parametric roll in head waves. The computational fluid dynamics (CFD) simulations are carried out for a model-scale ONR Tumblehome to predict the heave, roll, and pitch motions as the parametric roll occurs. An in-house unsteady Reynolds-averaged Navier–Stokes (URANS) solver coupled with a dynamic overset grid approach is applied to the numerical simulations, along with the systematic verification and validation studies based on the experimental data from INSEAN model tests.

Yang (2023) conducted an extensive numerical study on the possibility of parametric rolling of a containership based on Mathieu instability. It reveals the coincidence and difference between the analysis results at each level of numerical analysis by presenting the analysis results obtained based on different numerical models pertaining to the possibility of the parametric rolling of the target containership. Li J. et al., (2023) applied an in-house CFD (computational fluid dynamics) solver and conducted the URANS (unsteady Reynolds-averaged Navier–Stokes) simulations to predict the roll motion of ONR Tumblehome in irregular beam waves without forward speed. The results show that the amplitude of ship roll motion under 3-DOF condition is significantly larger than that under 4-DOF condition.

Liu et al. (2022c) established a single-degree-of-freedom rolling equation under parametric excitation. Based on strip theory, the righting arm is calculated by numerical simulation with different roll angles, wave heights, and phase angles of the wave position. As a result, conditions for applicability of the stochastic averaging method of energy envelope for practical engineering problems are given. The follow-on studies are described in Liu et al. (2023, 2023a).

Zhou et al. (2022) constructed a 6-DOF three-dimensional weakly nonlinear time-domain model based on the IRF (Impulse Response Function) method to predict ship parametric roll in head waves.

A number of examples of the operational restrictions imposed on the parametric rolling failure model are provided by Hashimoto and Furusho (2021). They examined the effects of season, area, and route restrictions on the susceptibility to parametric rolling stability failure.

2.4.9 Following and stern quartering waves

Bonci et al. (2022), investigated the dynamics of capsize of a frigate, sailing in stern quartering waves, with nonlinear time-domain simulations. Using FREDYN from CRNAV, a numerical sensitivity study was conducted for the modelling of the dynamic linear and nonlinear maneuvering forces acting on the ship hull, and the effects of maneuvering forces on ship capsize was also examined, see Figure 20.

Zeng et al. (2023) carried out the CFD computation that simulates the pure loss of stability of a fully appended ONRTH in following waves. Forces and moments on individual appendages including propellers, rudders, and bilge keels are analyzed, see Figure 21.

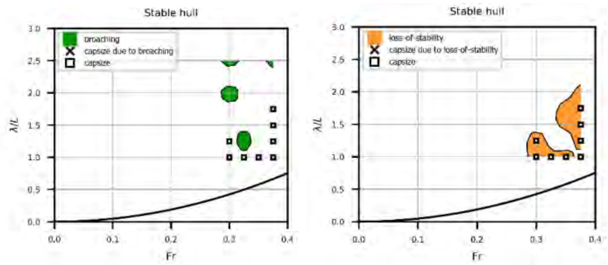

Figure 20: Broaching-to and pure loss of stability region. Wave heading: 30deg; wave steepness 0.067 (Bonci, 2022)

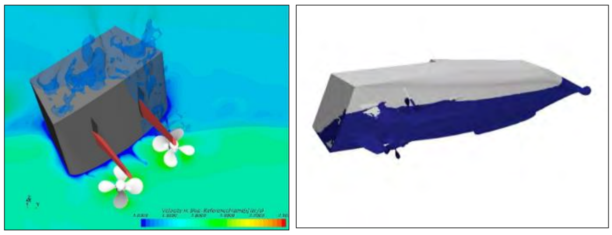
Figure 21: Flow field and wetted surface of the large rolling ONR tumblehome in following waves (Zeng et al. 2023)

Lu and Gu (2023) studied the 6-DoF coupled mathematical models for surf-riding/broaching and pure loss of stability in stern quartering waves. Rudder exposure and wave-particle velocity are considered for ship broaching, and the wave-excited surging force with instantaneous wet hull also shows an important role on predicting the pure loss of stability, see Figure 22figure 22.

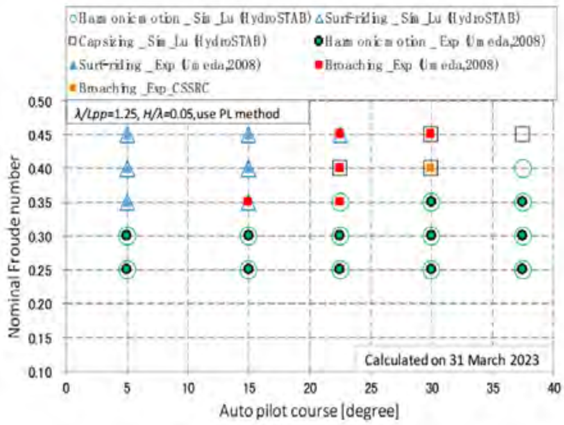

Figure 22: Ship motion modes with and without considering rudder exposure and wave particle velocity (Lu and Gu, 2023).

Based on the numerical study combined with the accident of the bulk carrier, Lu et al. (2021) observed synchronous rolling with yaw motions in stern quartering waves, see Figure 23.

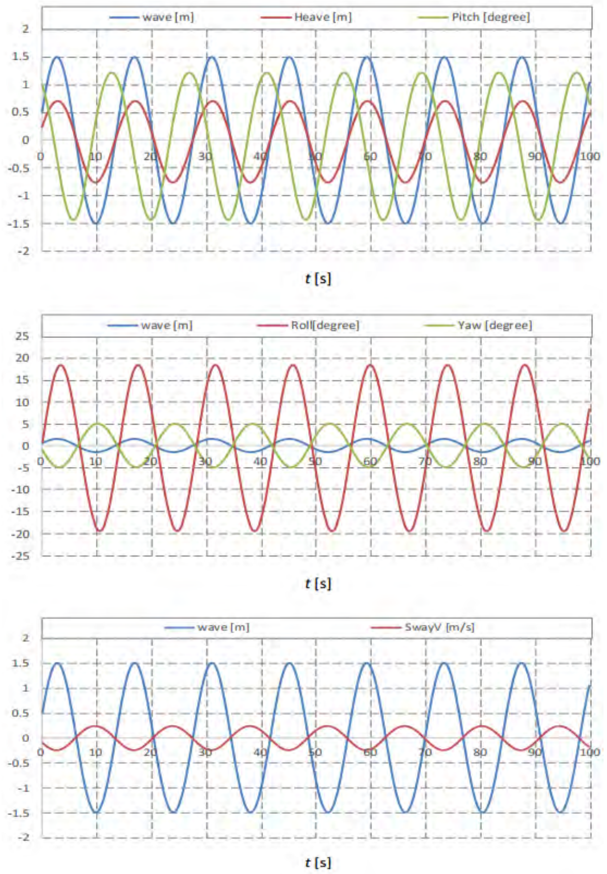

Figure 23: The time-domain simulation of ship motions with H=3m, λ/Lpp=1.20, heading angle=40 degrees, Fn=0.10, and Yaw=5 degrees.

2.4.10 Damage stability of ships in waves

Vassalos et al. (2023a) consider possible measures for improvement of survivability of Ro/Ro passenger ships after damage. The motivation came from the recent IMO decision to increase subdivision index and made it applicable to the existing fleet. Vulnerability screening is proposed as one of the risk mitigation options.

Bulian et al. (2023) considers additional aspects, not currently accounted for in damage stability regulation such as bottom grounding and side grounding or contacts. Monte-Carlo simulation is used to generate damage information based on a given distribution of the position and extent of those damages; the approach is referred to as “non-zonal”.

Atzampos et al. (2023) focuses on survivability-in-waves of cruise vessels after damage. Flooding of cruise ships bears very heavy consequences; despite those vessels do not have an open deck. A new formula was proposed for the s-factor, based on numerical simulation with cruise ships of different sizes. Another objective was finding a significant wave height where a cruise ship retains sufficient stability after damage.

2.4.11 Numerical tools

Weems and Belenky (2023) describe theoretical background and recent advances of fast volume-based numerical tool. The tool is built around the body-nonlinear formulation for hydrostatic and Froude-Krylov forces. Fast calculations are achieved with transition from surface to volume integral and decrease of necessary evaluation of irregular wave (Weems and Wundrow, 2013, Weems and Belenky, 2015). Approximation of diffraction and radiation forces (Kim et al 2023) recently has been added to the tool.

2.4.12 Roll damping

Katayama et al (2021) experimentally investigate the characteristic of roll damping for two types of hull (PCC and LNGC) with shallower draft and higher center of gravity compared to the ships, which existed when Ikeda's method was developed. The authors also verified the modified Ikeda's method, which has some modifications related to the effects of the draught and height of the center of gravity. In Figure 24, a comparison of the bilge keel associated damping between Ikeda's method and modified method is shown.

To improve the roll motion prediction of a particular ship, Zhang et al. (2023a) made an investigation of roll damping model form and its coefficients calculation methods based on benchmark roll decay data, see Figure 25. They concluded that all roll angle, angular roll velocity, and angular roll acceleration should be considered in damping model determination. Damping models with angle and angular velocity as independent variables are proposed. A model formulation procedure is developed based on the Prony-SS method (Hu et al. 2013) from which approximate analytical expressions of roll decay data are obtained, and roll damping formula can be determined by multivariate function fitting. The Fig shows one of the formulation results of roll damping moment normalized by the total roll moment of inertia. The results performance well in roll motion prediction.

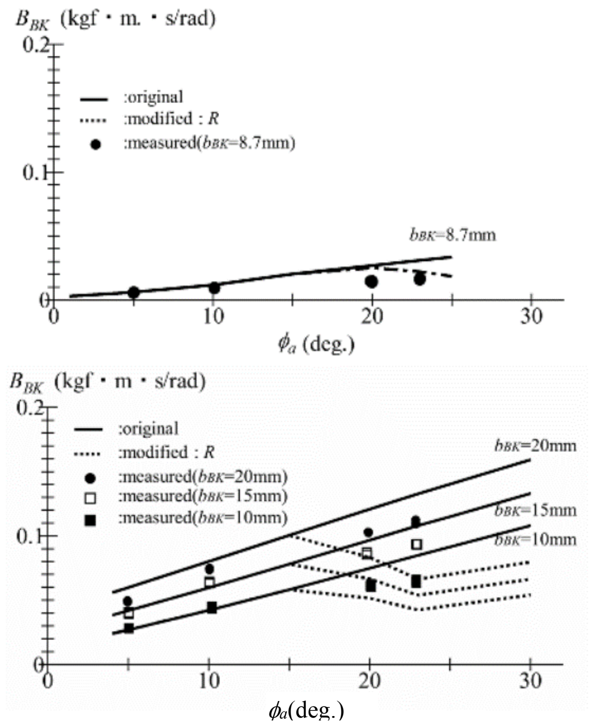

Figure 24: Comparison of bilge keel damping coef., B_{BK}, among measured, Ikeda`s original method and Katayama's modified method. (upper: PCC and T=1.96s, lower: LNGC at T=2.19s).

Katayama et al. (2022a) corrected a typographical error of Ikeda's formula of the eddy-making component for naked hull. They investigated a modified method that considers the effects of shallow draught.

Katayama and Yoshida (2023) investigated the effects of free surface on normal force component of bilge-keel component by using CFD computation (Figure 26). A new coefficient is applied to correct the drag coefficient of bilge keel, which improves the Ikeda's method for roll damping, see Figure 27.

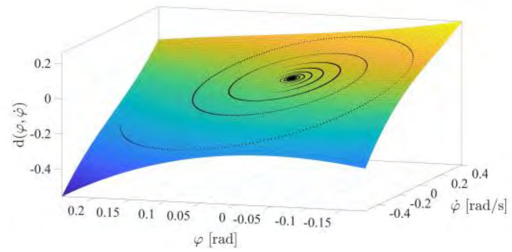

Figure 25: Normalized roll damping moment with angular roll velocity and angle, Zhang et al. (2023a).

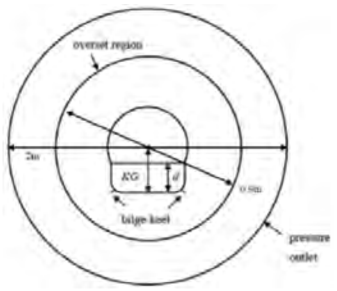

Figure 26: Computational domain and 2D model (Katayama et al., 2023)

Rudaković and Bačkalov (2023) considered roll damping for inland vessels with very full form and shallow draft (beam to draft ratio is over 4). Conventional semi-empirical methods may not be applicable to these vessels. In particular eddy making component or roll damping was a problem for cases with block coefficient more than 0.84. Correction to simplified Ikeda's method is proposed.

Rodríguez et al. (2022) showed the high dependency on roll damping coefficients by investigating the numerical simulations of VLCC roll responses in waves. Three different groups of roll damping coefficients were involved, which were obtained from roll decay tests, calibration of experimental roll responses in waves, and Ikeda's method, respectively (Figure 28).

Chen et al. (2023) investigated the roll natural period and damping coefficients in finite depth condition by using CFD computations. Water-depth effect has shown a strong influence on the roll behavior and ship hydrodynamic responses, see Figure 29.

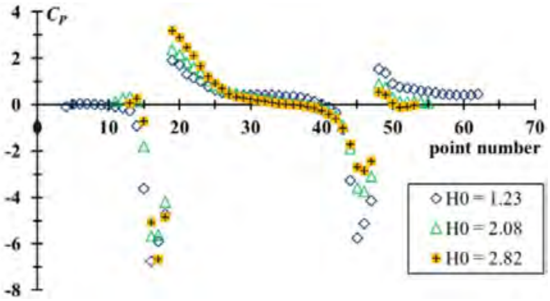

Figure 27: Distributions of hull pressure coefficient Cp for different water depths. (Katayama and Yoshida, 2023)

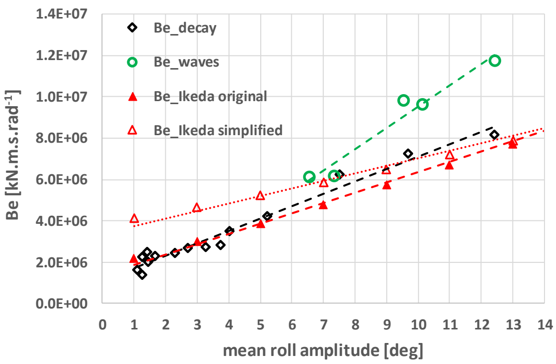

Figure 28: Linearized roll damping coefficients from decay tests, regular waves tests and Ikeda's original and simpli-fied predictions for the resonant roll period (Rodríguez et al., 2022).

Aram et al. (2023) developed a roll damping model for seakeeping codes through a series of CFD simulations with forced and free roll motions. The coefficients of damping model were obtained through an optimization procedure to minimize the difference between the hydrodynamic forces calculated by CFD and potential codes under prescribed roll motions.

Luthy et al. (2021) suggested an iterative optimization procedure to identified roll damping coefficient using the seakeeping tools used for roll analysis in irregular waves. The main advantage is to avoid double counting of some components.

Wassermann and Abdel-Maksoud (2023) describe CFD application for predicting bilge keel contribution into roll damping. The setup is based on ellipsoid with two normal-to-surface plates to model bilge keels. The cited reference also include an investigation on skin friction component.

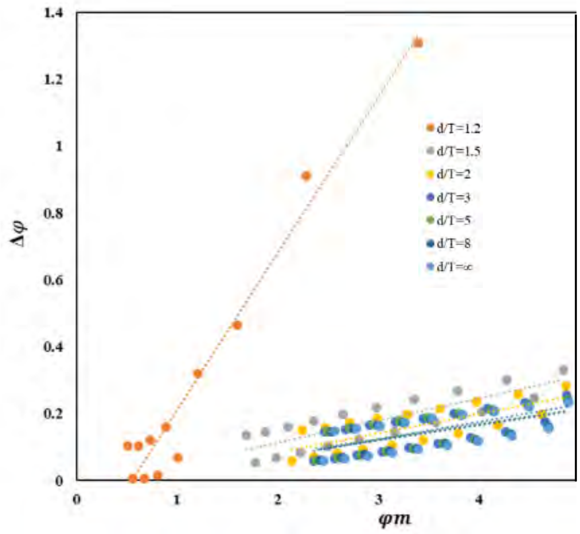

Figure 29: Curves of roll extinction of different depth to draft ratios (Chen et al. 2023)

Umeda et al. (2023) also look into the bilge keel component with CFD with a particular emphasis on roll motions in irregular seas. Certain type of memory effect was found, influencing evolution of the vortices.

Cichowicz and Vassalos (2023) offer a different perspective on roll damping. A study starts from a roll damping model test, aimed to determine hydrodynamic reaction and proceeds with derivation of roll/sway equations. Both intact and damage cases are considered.

Zhang et al. (2023) used a method of equivalent roll damping to study the parametric rolling of the KCS container ship. This method converts the nonlinear roll damping calculated by CFD into linear roll damping. Then the parametric rolling of the KCS container ship in regular waves is predicted based on the Rankine panel method.

2.4.13 High speed turn

Hinz et al. (2022) applied a 6-DoF ship dynamic model to predict the instantaneous maximum and quasi-static angle of heel developing during the ship steady turning maneuver.

2.4.14 Extrapolation Methods

Extrapolation is essentially a prediction beyond the range of data available. The statistical extrapolation is an essential technique for probabilistic assessment of stability in waves as most of engineering-level numerical simulation tools for ship motion are too slow to observe stability failure directly.

Reed (2023a) discusses interpretation of the results of numerical simulation, looking into linear and nonlinear dynamical systems. Extreme response of linear dynamical system is completely defined by its standard deviation. However, characterization of extreme response of nonlinear dynamical system will require handling rare events and fall into category of extrapolation methods. Statistical extrapolation method may be classified into three groups:

- Methods based on extreme value theory;
- Methods based on consideration critical wave groups (or single waves) and wave episodes;
- Methods based on extrapolation over environmental conditions.

The extreme value theory states that the largest number in a dataset of independent points follows a limit distribution – Generalized Extreme Value (GEV) distribution independently of underlying distribution. This leads to a conclusion that a tail of any distribution can be approximated with Generalized Pareto distribution (GPD).

While sounds very promising, practical application of GPD encounters a number of difficulties. Pipiras (2020), Anastopoulos and Spyrou (2023) have studied and summarized these difficulties. One of them is that the type of the distribution tail (heavy/exponential/light), approximated with GPD, is defined by a shape parameter, estimated from the data. Thus, the shape parameter estimate is a subject for statistical uncertainty. This uncertainty can make the tail too light, leading to appearance of a right bound in a random location of the tail. If this bound is below the target of extrapolation, the GPD-based method fails to deliver a result. Additionally, Anastopoulos and Spyrou (2023) note difficulty of comparison of the GPD outcome with Monte-Carlo and critical wave group results.

The practical way to resolve this problem is to determine the type of the tail, based on physical consideration. It was found in Belenky et al. (2019a) that the tail of distribution of roll peaks is heavy due to known phenomenon of "hanging roll". Campbell et al (2023) modeled heavy tail with Pareto distribution with the Envelope Peak-over-Threshold (EPOT) method. Originally, EPOT used GPD, but due to the reasons above, the reliability of application was low, while uncertainty of extrapolated estimate was high. Introduction of Pareto distribution decreases the uncertainty by several orders of magnitude, reflecting how physical information can inform a statistical model and shrink confidence interval.

Campbell et al. (2023a) describe statistical validation of EPOT using large validation dataset generated by the fast volume-based method, see (Weems and Belenky 2023). The validation dataset was 1.9 million hours long, included 82 extrapolation targets; there was only one sea state but 8 headings. The subject ship was ONRTH (Bishop et al. 2005). Validation of EPOT with Pareto tail was not successful for oblique seas (heading 135 deg), but performed well for all other considered headings (15 to 90 deg). EPOT with GPD had reasonable performance for all headings, but was not as reliable as Pareto for stern and beam seas headings.

Belenky et al. (2024) describes application of split-time method (MPM) for estimation of capsizing probability. The essence of the split-time method is to separate a complex problem of capsizing into two less complex problems: non-rare and rare. The non-rare problem is an up-crossing of an intermediate level that can be observed during a reasonable duration of numerical simulation. The rare problem is determining conditions for capsizing after upcrossing. These capsizing conditions are determined by perturbing the roll rate at the instant of upcrossing until a capsizing is observed. The amount of perturbation, needed for capsize, serves as a metric of capsizing likelihood at the instant of upcrossing. Repeating the calculation for a number of crossing creates a dataset that can be extrapolated. Physical consideration suggested the exponential tail for the metric, however GPD was also used for comparison. Similar to EPOT, application of physics-informed statistical model lead to significant decrease of uncertainty. The cited paper reviews almost 3 decades of development and examines different numerical and statistical aspects of the method, including perturbation algorithm and quantification of uncertainty.

Weems et al. (2023) describe statistical validation of the split-time method (MPM) of capsizing probability. A fast volume-based method (Weems and Belenky 2023) was used to generate a validation dataset of 4.8 million hours of roll motions in 14 different sea states; 872 capsizing cases were observed. Small subset of this data was used to estimate probability of capsizing and compare with the "true" value, observed from the validation dataset. Both exponential and GPD tails were tested; as expected, performance of the split-time method with exponential tail was significantly better.

Positive outcome of validation of EPOT and split-time methods (MPM) justified inclusion both methods in IMO Explanatory Notes and ITTC recommended procedure 7.5-02-07-04.6 by 29th ITTC. An update to this procedure is described in subsection 3.1 of this Report.

Critical wave group approach is based on two ideas. The first that large waves do appear in groups, which are hydrodynamically related. That means, the neighbourhood of a large wave is almost deterministic, despite waves, in general, being random. This manifests the Quasi-Determinism principle, see Boccotti (2000, 2014). The second idea is that only certain groups can cause significant dynamic response that brings the word "critical" into the name of the approach. Themelis and Spyrou (2007) proposed to consider a seaway as a sequence of critical waves groups, separated by benign waves. Then, ship response only needs to be evaluated in the critical wave groups.

Anastopoulos and Spyrou (2023a) provide an update on the development of the critical wave group method. The critical wave groups cause significant motion response; as this response is expected to be nonlinear, it strongly depends on initial condition upon encountering the group. The cited reference discusses possible simplification for finding these initial conditions. The second simplification, proposed is on determination of characteristics of what wave group is critical. The idea is that a ship is likely to produce significant response in resonant conditions, so the wave groups with period close to natural period are likely to be critical for the failure modes where the resonance is important.

The wave groups are relatively short. That creates an opportunity to apply high-fidelity methods to evaluate a response to the group. That include a model test (Anastopoulos et al. 2016; Bassler et al. 2019) and more recently CFD (see Silva and Maki 2021). Both model test and CFD, however, do require physically realizable initial conditions at the wave group encounter. The latter reference describe initial condition handling method, suitable for CFD, where a deterministic wave group is embedded into previously simulated ship response. Having in mind high computational cost of ship response simulation with CFD (Silva et al. 2022; Silva and Maki 2022a, 2023, 2023a; Silva 2023), utilize a Long Short Term Memory (LSTM) neural network to reproduce needed ship response. Architecture and training of LSTM is developed by Xu et al (2021) as well as Silva and Maki (2022).

The wave episode approach differs from a wave group approach. A wave sequence in the former does not have to maintain hydrodynamic relation; it is just a wave set likely to cause significant ship response. This was the objective of the Design Load generator, where the wave episode was created by manipulating random phase shift in Longuet-Higgins model of irregular waves (Alford and Troesch 2009). The method searches for combinations of the phases that lead to an expected roll response (Kim and Troesch, 2013, 2019).

Edwards et al. (2021) proposed improvements to the method with an equivalent linear dynamical system that has the same zero-crossing period as the system of interest.

Another way to apply wave episode approach was proposed by Mohamad and Sapsis (2018) employed adaptive sampling, based on Bayesian approach. The results of initial calculations are approximated with Gaussian process regression, taken as “prior knowledge”. Then the conditions for the next calculation can be chosen to minimize the uncertainty — this is “a posteriori knowledge.” The problem of initial conditions is considered by Guth and Sapsis (2022) with a “stochastic prelude” approach to capture the transitional behavior.

Reed (2021) proposed the identification of extreme response with a fast reduced-order numerical model of ship motions in waves. The approach seems to be promising with development of tunable fast volume-based simulation tool (Weems and Belenky, 2023) that can be informed or tuned with higher fidelity simulation (Kim et al. 2023).

The idea of extrapolation over environmental conditions (currently over significant wave height only) is also straightforward. Numerical simulations are performed in several high sea states, where stability failure is observable and then extrapolated towards lower sea state, where observation of the failure is not possible due to computational costs (Tonguć and Söding 1986). The method was included in both in the Interim Guidelines for the SGISC and the Explanatory Notes. Shigunov (2023a) provides detailed description of the method with particular emphasis on quantification of uncertainty. Two criteria for validation of the proposed technique are considered. The cited reference also describes construction of confidence interval for extrapolated failure rate. Other aspects related to application of this method are considered in Shigunov (2023b).

Anastopoulos and Spyrou (2022, 2023b) have presented a formal argument on the equivalency between the extrapolation over the wave heights and the critical wave group method. Moreover, they have proposed and evaluated two improved formulae for extrapolation which retain the simple character of the original. The extrapolation over the wave height has been included in the proposed revision of ITTC recommended procedure 7.5-02-07-04.6 and is described in subsection 3.1 of this Report.

Shigunov (2023) reviewed statistical extrapolation method to reduce the required computational time and considers in detail the extrapolation of failure rate over significant wave height. Application of these criteria shows that the extrapolation of failure rate over significant wave height does not satisfy the proposed criteria with the sample size 20 and satisfies with the sample size 200.

2.4.15 Development of Operational Guidance

Some types of the stability failures in waves are more efficient to prevent during the operation rather than at the design stage. Parametric roll is a good example, as excluding parametric roll by the altering the lines may lead to a very energy inefficient ship. That is a reason why more attention is paid to calculation methods suited for development of operational guidance. Operational guidance and operational limitations are included in the SGISC and reflected in Interim Guidelines and Explanatory Notes.

Shigunov (2023a) focused on harmonized treatment of design and operation as an efficient way to provide the required safety level. The cited reference discussed criteria and standards as well as if operational measures can always be an acceptable way to ensure safety. Examples of application of operational measures were included.

Hashimoto et al. (2023) described a case study for the development of operational limitations concerning parametric roll. The limitations are based on significant wave height and are meant to be used as an aid for course selection.

Efficient application of operational guidance can be facilitated by real-time wave measurement. It is the focus of Yano et al. (2023), where a utilization of sensors is discussed, including wave radar, combined with measurements of roll motions with a gyroscope.

Levine et al. (2021, 2022, 2024) describe a method for development of adaptive operational guidance, expected to be suitable for autonomous as well as crewed vessels. The idea is to use fast volume-based simulation tool (Weems and Belenky, 2023) to generate operational guidance on-board as soon as the next weather forecast becomes available. To improve accuracy of prediction LSTM neural network, trained with an engineering level potential flow code is applied to the simulation outcome.

Among all ships, fishing vessels are the most vulnerable to stability failure. Not only being relatively small, compared to ocean waves, fishing vessels sometimes perform dangerous operation at sea and frequently change their loading conditions. Caamaño et al. (2023) compares two techniques for real time monitoring of natural frequency of a stern trawler, operating in irregular waves. The described system is capable to alert the crew if stability of a vessel becomes unacceptable.

González et al. (2023) describe an algorithm of GM monitoring using spectral analysis of the roll motions.

Howard et al. (2022) introduced a machine learning method to improve prediction of ship seakeeping statistics in rough, bimodal seas. A data-adaptive model was used to evaluate predicted ship motions in unidirectional waves with a bimodal spectrum. Data-adaptive LSTM neural networks were investigated as part of a multi-fidelity approach incorporating Large Amplitude Motion Program (LAMP), and a reduced-order model known as SimpleCode. LSTM networks were trained and tested with 3-DoF LAMP simulations as a target, and 3-DoF (heave, roll and pitch) Simple-Code simulations. LSTM networks were shown to improve the fidelity of SimpleCode seakeeping predictions relative to LAMP, while retaining the computational efficiency of a reduced-order model. Then the research group (Edwards et al., 2023) extended the LAMP and SimpleCode simulations with generation of 6-DoF motions, which provided improved accuracy as compared to previous simpler 3-DoF simulations.

2.4.16 Accident Investigation

Taguchi et al (2023) describe an experimental investigation of stability accidents with two Japanese fishing vessels with the objective to clarify the reason for the accidents. The first vessel, a purse seiner has capsized while anchored at sea after encountering two large waves. The second vessel, a stern trawler has capsized while sailing in head seas. Both cases involved flooding of a deck and internal spaces.

2.4.17 Neural networks

González et al. (2023a) explored the implementation of an Artificial Neural Networks (ANN) based system for real-time prediction of parametric roll in ships, focusing on its application in onboard stability guidance for small and medium-sized fishing vessels. The research utilized a 1.5 DoF nonlinear mathematical roll model to train the ANNs, aiming to provide a cost-effective alternative to extensive towing tank tests for system training. The ANN model demonstrated good performance in predicting parametric roll under specific conditions compared with the test data, highlighting the potential of machine learning approaches in enhancing maritime safety by enabling early detection and corrective actions against stability threats.

Silva and Maki (2022) proposed the CWG-CFD-LSTM framework, which combines the critical wave groups method (CWG), computational fluid dynamics (CFD), and LSTM neural networks to develop computationally efficient surrogate models. The CWG-CFD-LSTM framework can predict the 6-DoF temporal response of the vessel and recover the extreme statistics. Two modelling approaches are considered. A general model approach where one model is trained with all the speeds and headings and an ensemble model approach where multiple models are trained, each responsible for a single speed and heading combination. The developed neural network models with the general approach are capable of accurately representing the temporal response of the free-running DTMB 5415 in extreme waves and also recovering the extreme statistics of roll for different speeds and headings.

2.4.18 Direct Stability Assessment (DSA)

Wandji (2023) describes an analysis of several statistical estimates, relevant for stability assessment, such as mean-crossing rate, time to first event, time between events, maximum value over an interval, etc., to the results of numerical simulations of ship motions in waves. The focus was on the influence of nonlinearity, so the analysis was exercised on linear and nonlinear samples, the volume of which was quite large. Pearson chi-square test was utilized for more formal determination if the difference between the obtained results is significant. The results from seven sea states were close between three methods, but showed that failure rate and confidence intervals could be slightly different at higher sea conditions. Since the tests were made in ideal conditions or in beam waves, further study is necessary to use the data from various sea conditions.

Shigunov et al. (2022), Wandji et al. (2023, 2024) carried out a benchmark study for the three direct counting methods using the data which comply with Poisson processes assumptions and the true rate of events is known. As a result, all three approaches were able to correctly estimate the failure rate. The estimate of confidence intervals was considered to be correct when a percentage of successes was close to the accepted confidence probability.

Matsubara et al. (2023) utilized the critical wave method in a validation study for broaching and in long-crested and short-crested irregular waves. The examined critical wave method provided conservative estimates of the probability of a large heel due to broaching, with a much shorter computational time.

Weems et al. (2023a) further developed the multi-fidelity code, which employs the seaway-dependent diffraction and radiation coefficients to the hydrodynamic forces. They found the developed code has a limitation when compared with potential-flow simulation. Further study will be made to overcome the limitation.

2.4.19 Multihulls

It should be noted that SGISC have not been tried on multihulls. Papers related to multihulls can be found in other chapters of the reports.

2.5 The need for R&D for improving methods of model experiments and numerical modelling (TOR 1 E)

The book titled "Contemporary Ideas on Ship Stability – From Dynamics to Criteria" has been published by Springer (Spyrou K., Belenky V., Katayama T., Bačkalov I., Francescutto A., editors) as a part of their series "Fluids Mechanics and Application" (ISBN 978-3-031-16328-9). The book summarizes advancement in the field with selected papers from international stability workshops from 2013 through 2019; these selected papers were extended and updated to reflect state-of-the-art. It is the third book in the

Springer series focused on stability, following Neves et al. (2011) and Belenky et al. (2019). The first book, summarizing advances in stability field was published by Elsevier (Vassalos et al. 2000). Chapters of the book are given a brief review in the appropriate section of this report. The book opens with a comprehensive overview by the editor-in-chief Spyrou (2023), where contents of each of the 42 chapters is described within context of the state-of-the-art.

A virtual special issue of Ocean Engineering "Extreme Stochastic Dynamics of Ships" was published 2022-24. Publication of this special issue was inspired by long-term research program "A Probabilistic Procedure for Evaluating the Dynamic Stability and Capsizing of Naval Vessels" run by the US Office of Naval Research. Most important results of this program were published in the special issue along with other papers focused on extreme ship motions. Totally, the special issue contains 17 full-length research papers, relevant to this committee. A list of the papers at this special issue is available at https://www.sciencedirect.com/special-issue/100R65G877Z

The dynamic stability of ships is quite complicated due to the stochastic seaway, and thus stochastic approach is generally necessary. Since evaluating the stochastic response typically requires many simulations, R&D objecting to reduce the computation times has been one of the important issues.

Anastopoulos and Spyrou (2022, 2023b) used the stochastic wave group theory in order to extrapolate the significant wave height. They checked capsize of a ship in mild seas using the critical wave group. The analysis showed higher accuracy if the spectrum was narrow enough. The key finding is that IMO's current "extrapolation over wave height" formula is rather empirical since the theoretical background does not coincide with the suggested formula. Although the study only focused on the dead ship condition, their findings about reliability of IMO's current criteria need to be considered.

Wandji (2022) applied two extrapolation techniques to dynamic stability events: extrapolation using a fitted distribution and extrapolation over wave height. They have seen that these extrapolation methods are derived in closed form for linear processes and can be used successfully with some assumptions for nonlinear processes.

Silva and Maki (2022) suggested combining the critical wave groups method, CFD, and LSTM neural networks in order to develop computationally efficient surrogate models and to recover the extreme statistics. When sufficient training data are prepared, both the general model and the ensemble model are comparable. Their further work would be focused on developing generalized condition-agnostic frameworks for evaluating extreme events.

Silva and Maki (2023a) extended the critical wave group method to a free-running model. The extreme events were observed using the natural initial condition methodology of embedding deterministic wave groups into random irregular wave trains. The necessity of further study is stated which performs the statistical validation by combining the critical wave groups method with a numerical hydrodynamic simulation tool.

Maruyama et al. (2022, 2022a) applied linear filter and moment equations to the parametric rolling of ships in irregular waves. The probability density function were approximated using the coefficients obtained from moment equations, which showed reasonable agreement with those from Monte Carlo simulation. Maki et al., (2023) used the stochastic approach to the various kinds of ship hydrodynamics, such as wind and wave generation, stability of parametric rolling, method of moment equation and maneuvering stability. Since the various theories are available for stochastic processes, further study will be focused on finding the appropriate theory for each hydrodynamic problem.

Explanatory Notes of SGISC currently employ three direct-counting procedures. These approaches are based on the estimation of failure rate from sample data using exponential distribution, statistical frequency of failures and binomial distribution.

Brown and Pipiras (2023) consider the uncertainty of an extreme value estimated from the dataset, comprised from the sources of different fidelity, e.g. model test and numerical simulation, or potential flow simulations and ordinary differential equation, i.e. multifidelity approach. The proposed method is based on multi-dimensional extreme value distribution.

Hydrodynamic prediction coded based on potential flow or RANS have matured, but are still too expensive to directly apply to many extreme response problems. Weems et al. (2022) pointed out that the formulation of two general principles could be applied to the development of reduced-order models: schematization of hydrostatic and FK forces; and reducing dimensionality of the space of random parameters through regression or/and active sampling. In addition, uncertainty quantification is an important tool to check the confidence of reduced order models.

Lu and Gu (2023) introduced a unified mathematical model in order to simulate the surf-riding/broaching and pure loss of stability in stern quartering waves. Their model was able to predict the surf-riding/broaching and pure loss of stability in stern quartering waves when rudder exposure and wave-excited surging force are properly taken into account. As a future work, they found the necessity to identify the several parameters in the equations.

Dostal et al. (2023) considers the first passage problem for nonlinear ship dynamics. The first passage problem is about finding a distribution of time to reach a certain (usually large) value. The solution of this problem is not trivial if self-dependence of the excitation is preserved. The proposed approach is based on roll energy of the ship that can be expressed explicitly. The paper also incorporates an expansion of Grim effective wave for the case of short-crested seas.

Matsuda et al. (2023) presents experimental study to find out if a typical design of Japanese and European fishing vessels make a difference in vulnerability to several capsizing scenarios. It was reported that while the European design is less vulnerable to usual instability, a dangerous subharmonic roll behavior has been detected for this design.

Koromila et al. (2023) describes experiments on cargo liquefaction with “shaking table”. The liquefaction of a mass cargo is major risk factor for stability of bulk carriers. The objective of the study is to gain insight on transformation of wet granular cargo during liquefaction. The tested materials were sand and olive pomace with different moisture contents.

Rodríguez et al. (2023) studies behavior of mono-column structures in regular and irregular waves with a model experiment. Parametric resonance was observed in roll and pitch, caused by energy transfer between different degrees of freedom. It was also found that the mooring system configuration has significant influence on possibility of dynamic stability failure.

van Walree and Thomas (2023) compare results of numerical simulation and experimental study on dynamics of a rigid-hull inflatable boat (RHIB) in heavy seas. The objective is to see if existing simulation tools can handle a body of such unconventional form and, if positive, what are the limitations. In the other navy-related work, van Walree and Sgarioto (2023) consider landing craft motions as well as impact loads and water ingress in heavy seas. Numerical simulations are compared with experimental results.

Kim et al. (2023) considers a regression-based approximation of diffraction and radiation forces to be used in reduced-order models of ship motion. The regression is performed on a series of runs of a potential flow simulation tool: motions without wave for radiation and wave without motion for diffraction.

Tsoumpelis and Spyrou (2023) examine the self-repeating effect in the Longuett-Higgins model of irregular wave from the time series perspective. An algorithm for capturing repeating portions of the time series is proposed. The cited reference also contains important insights into the mechanism of self-repeating effect, explaining why the repetitions usually are not exact even at uniform frequency discretization and the condition for exact repetition. The self-repeating effect is also addressed by Umeda et al. (2023b).

Glotzer et al. (2024) provides mathematically rigorous consideration of dynamical systems with piecewise linear restoring force, deriving distributions of critical response (leading to capsizing). A Duffing oscillator is also examined. The cited reference is essentially a theoretical background for the split-time method (Belenky et al. 2024), included in ITTC recommended procedure 7.5-02-07-04.6.

Yu et al. (2023) adopted the time-domain method to study and analyzed the occurrence of non-linear harmonic rolling phenomenon of ultra-large container ship and subsequent motion behaviors.

3. REVIEW ITTC RECOMMENDED PROCEDURES (TOR 2)

Review ITTC Recommended Procedures relevant to ocean engineering, including CFD procedures.

3.1 Requirements and update (TOR 2 A)

Identify any requirements for changes in the light of current practice, and, if approved by the Advisory Council, update them.

Procedure 7.5-02-01-01 (Guide to the Expression of Uncertainty in Experimental Hydrodynamics) was reviewed and no change is proposed by the committee.

Procedure 7.5-02-01-07 (Guideline to Practical Implementation of Uncertainty Analysis) was reviewed and no change is proposed by the committee.

Procedure 7.5-02-07-02.3 (Experiments on Rarely Occurring Events) was reviewed and no change is proposed by the committee.

Procedure 7.5-02-01-08 (Significant Amplitude and Confidence Intervals for Stochastic Processes) was reviewed, and the committee proposes to update the evaluation of variance of the mean and variance estimate, using new information recently published by Glotzer et al. (2023).

Procedure 7.5-02-05-07 (Dynamic Instability Tests) was reviewed and found no changes necessary at this moment.

Procedure 7.5-03-01-01 (Uncertainty Analysis in CFD Verification and Validation, methodology and Procedures) was reviewed and no change is proposed by the committee.

Procedure 7.5-03-02-03 (Practical Guidelines for ship CFD application) was reviewed and no change is proposed by the committee.

Procedure 7.5-02-07-04.1 (Model Tests on Intact Stability) was reviewed. Three references are being added to the procedure. For instance, if wind forces need to be included in the model tests, the projected areas need to be corrected (Umeda et al., 2023). Furthermore, as shown by Hashimoto et al. (2019), roll decay tests performed carefully by hand can be sufficiently accurate. Finally, standard uncertainty analysis can be applied to all measured basic quantities and motions. Capsizing could be a different situation due to the extreme phenomenon involved. However, a properly designed experimental system is reproducible for strongly nonlinear phenomena as reported in Matsuda et al. (2016).

Procedure 7.5-02-07-04.2 (Model Tests on Damage Stability in Waves) was reviewed and no change is proposed by the committee.

Procedure 7.5-02-07-04.3 (predicting the Occurrence and Magnitude of Parametric Rolling) was reviewed, and the committee updated it with the most recent references, primarily from publications of the SGISC, i.e. Interim Guidelines MSC.1/Circ.1627, Explanatory Notes as well as recently issued documents of classification societies: BV (2019) and ClassNK (2023).

Procedure 7.5-02-07-04.4 (Simulation of Capsize Behaviour of Damaged Ships in Irregular Beam Seas) was reviewed and the latest international benchmark study on simulation of flooding and motions of damaged vessels was added, Ruponen et al. (2022, 2022a). New sections on real time flooding risk evaluation and machine learning/Artificial Intelligence methodologies have been added.

Procedure 7.5-02-07-04.5 (Estimation of Roll Damping) was reviewed and some equations were updated. Ikeda's formulae were review following recent work from Katayama et al. (2021, 2022, 2022a, 2023) as already mentioned in paragraph 2.4.12.

Procedure 7.5-02-07-04.6 (Extrapolation for Direct Stability Assessment in Waves) was reviewed and updated. The original procedure described the application of envelope peak-over-threshold (EPOT) for estimation of rate of roll motions failures when none of these failures were observed in the output of numerical simulation and the split-time / motion perturbation method (MPM) to estimate rate of capsizing events.

Direct Stability Assessment (DSA) as a part of the SGISC is described in section 3 of the Interim Guidelines, whereas stability failure is defined as exceedance of 40° in the paragraph 3.2.1.1 of MSC.1/Circ.1627. Provision of application of EPOT and MPM extrapolation procedures is included in subsection 3.5.5.4 of MSC.1/Circ.1627. Description of these procedures can be found in sections 5.3 through 5.5 of Appendix 4 of the Explanatory Notes.

Description of DSA in the Interim Guidelines and Explanatory Notes includes several extrapolation methods, not covered in the procedure 7.5-02-07-04.6: extrapolation over wave height, critical wave method and linear superposition method for excessive accelerations. Publication of the Explanatory Notes in 2023 creates a background for relevant ITTC recommended procedures to be updated.

To harmonize the procedure 7.5-02-07-04.6 with the Interim Guidelines and Explanatory Notes, the Committee proposes the following updates:

- Amend the description of MPM for extrapolation for stability failure as defined in the Interim Guidelines, i.e. for exceedance of large roll angle
- Add the description of extrapolation over wave height
- Add an example where all three methods are applied to the same input data
- Update the references with recently published IMO documents and relevant technical papers.

Procedure 7.5-02-07-04.7 (Inclining Tests) was reviewed and updated. More detailed description of wind effects and uncertainty analysis have been added. Procedure was update, including some effect of wind gust. The effect of wind fluctuations during an IT were investigated from Leguen et al (2023). For a given accuracy chosen by the surveyor, a maximum value of the mean wind is calculated. In the other direction, estimation of uncertainty of KG can be estimated by taking into account gust wind velocity measurement, see Figure 30.

Figure 30: Heel measurement during an IT (3 hours), with gust wind effect visible, from Leguen et al (2023).

Procedure 7.5-02-01-09 (Avoiding Self-Repeating Effect in Time-Domain Numerical Simulation of Ship Motions) was submitted. The new procedure formulates a process for verification of absence of self-repetition effect and statistical validity of irregular waves and ship motions in a numerical simulation. More detailed descriptions of the changes are summarized in section 5.1 of this report.

Procedure 7.5-02-07-04.8 (Computational procedure for instantaneous GZ curve during time-domain numerical simulation in irregular waves) was submitted. The procedure describes the role that the instantaneous GZ curve and some calculation examples are included. It is the objective of TOR 4-A, detailed descriptions of this procedure are summarized in section 5.1 of this report.

Procedure 7.5-02-01-10 (Estimation of Frequency of Random Events) was submitted. The procedure addresses post processing of numerical simulation of roll motions or lateral accelerations. The draft procedure covers three methods of the rate estimations, and these methods offer different ways of addressing the independence of stability failures – the critical requirement of the Poisson model. It is the objective of TOR 4-B, detailed descriptions of this procedure are summarized in section 5.2 of this report.

Procedure 7.5-02-01-11 (Statistical Validation of Extrapolation Methods for Time Domain Numerical Simulation of Ship Motions) was submitted. This procedure describes the process for the validation of extrapolation methods used for direct stability assessment for the stability failure modes described in section 3.5.6 MSC.1/Circ. 1627. It is the objective of TOR 4-C, detailed descriptions of this procedure are summarized in section 0 this report.

3.2 Identify new procedures (TOR 2 B)

The Interim Guidelines on the Second Generation Intact Stability Criteria (MSC.1/Circ.1627) include provision for direct stability assessment (DSA). The intention of DSA is to "employ latest technology while being sufficiently practical to be uniformly accepted and applied using currently available infrastructure" (paragraph 3.1.3 of the Interim Guidelines). As ITTC members are a vital part of this infrastructure, developing ITTC recommended procedures, detailing and enhancing the Explanatory Notes to the Interim Guidelines (MSC.1/Circ.1652) is appropriate and beneficial for ITTC as well as Maritime Community in whole. ITTC has already developed 4 procedures in support of DSA, while another 4 procedures are cited in the Interim Guidelines and Explanatory Notes; three other ITTC-recommended procedures may be relevant for DSA, as described in IMO document SDC 10/INF.7.

The Stability in Waves Committee, in fulfilment of the item 2B of the Terms of References, identifies the following two procedures to be developed in support of Direct Stability Assessment within the framework of the second generation intact stability criteria.

3.2.1 Evaluation of Dynamical Characteristics of a Ship

The Interim Guidelines includes requirements for qualitative validation (section 3.4.2). The Explanatory Notes contains examples for several items, listed in the Interim Guidelines, specifically:

1. Backbone curve (section 3.4.2 and 2.1 of Appendix 4),
2. Response curve (section 2.2 of Appendix 4),
3. Change of stability in waves (section 2.3 of Appendix 4),
4. Principal parametric roll resonance (section 2.4 of Appendix 4).

While items 3 and 4 are already covered by ITTC recommended procedures 7.5-02-07-04.8 and 7.5-02-07-04.3, respectively, development of ITTC procedure(s) for items 1 and 2 is needed.

Other qualitative validation requirements, included in section 3.4.2 of the Interim Guidelines, but not reflected in the Explanatory Notes are:

5. Surf-riding equilibrium,
6. Heel during turn,
7. Turn in calm water,
8. Straight captive run in stern quartering waves,
9. Heel caused by drift and wind.

A detail step-by-step procedure, covering items 1, 2 and 5 through 9, will help with the qualitative validation of ship motion time-domain simulation software for trial application of the second generation intact stability criteria.

The new procedure is to include description of seven aspects of quantitative validation as indicated above. Each of these techniques may be outlined as follows:

- Objective and scope of application,
- Data requirements and preparation,
- Processing and post-processing,
- Analysis and adjudication of results.

The development effort is expected to be moderate to large.

3.2.2 Extrapolation Methods, not Covered by ITTC Recommended Procedures

A stability failure of an intact ship is a rare event even in high sea states. Therefore, there is a motivation to estimate the probability of stability failure from a limited sample of time histories that does not necessarily include observations of these stability failures. This objective can be achieved by application of a statistical extrapolation. Section 3.5.5 of the Interim Guidelines contains general provisions for application statistical extrapolation methods.

Paragraph 3.5.5.1 requires that a statistical extrapolation method has to be successfully validated in order to be applied for direct stability assessment. Details on statistical validation of specific extrapolation methods are available in sections 5.1.2 and 5.4.4 of Appendix 4 to the Explanatory Notes. Statistical validation of extrapolation is covered by ITTC Recommended Procedure 7.5-02-01-11.

The Interim Guidelines mentions four extrapolation methods:

1. Extrapolation over wave height in section 3.5.5.3,
2. Envelope peak-over-threshold (EPOT) in paragraph 3.5.5.4.1.1,
3. Split-time/motion perturbation method (MPM) in paragraph 3.5.5.4.1.2,
4. Critical wave method in in paragraph 3.5.5.4.1.3.

Additionally, section 5.6 of the Appendix 4 to the Explanatory Notes contains a description of

5. Linear superposition method for excessive accelerations failure mode.

The extrapolation methods 1, 2, and 3 are described in details in ITTC Recommended Procedure 7.5-02-07-04.6. This procedure originally was approved by 29th ITTC and with the description of extrapolation method 2 and 3 only. The revision 01 is presented to 30th ITTC includes method 1 as well. The next logical step would be developing procedures for application of statistical extrapolation methods 4 and 5.

It is proposed that the step-by-step descriptions of these extrapolation methods to follow the structure of 7.5-02-07-04.6, in particular:

- Data requirement;
- Data preparation;
- Statistical processing;
- Assessment of uncertainty.

It may make sense to include description of these two methods into revision 02 of ITTC Recommended Procedure 7.5-02-07-04.6. However, as the effort is expected to be moderate to large, it should be treated as a new development.

Some part of the proposed work need strong relationships with other ITTC committees, as manoeuvring committee for points 6 and 7 of the first suggested procedures. The propose contain with be consolidated in a fewer ITTC procedures.

4. UPDATE ITTC PROCEDURE 7.5-02-01-08, (TOR 3)

Item 3 of the Terms of References for the Stability in Waves Committee contains a task to update ITTC Procedure 7.5-02-01-08, titled “Single Significant Amplitude and Confidence

Intervals for Stochastic Processes” when new information becomes available. The new information became available (Glotzer et al., 2023) and the procedure was updated for the evaluation of variance of the mean and variance estimate.

The objective of the procedure 7.5-02-01-08 is to formulate the process for characterizing the uncertainty for data resulting from a stochastic process, such as ship motion data collected at either numerical simulation, model test or full scale trials.

A particular issue to be addressed is equation (4.1) (which appeared as equation (9) of the Revision 00 of the procedure). It defines the number of points of an estimate of auto-covariance function to be used when calculating variances of estimates of mean and variance of a stochastic process:

$$0.5\sqrt{N} \leq M \leq 2\sqrt{N}, \tag{4.1}$$

where N is the total number of points in a record, while M is a number of points of the autocovariance function estimate.

Essentially setting M meant to “cut” the autocovariance estimate where the self-dependence is still meaningful and to remove “statistical noise”. An error causing this statistical noise is inevitable when estimating autocovariance function from time series. It is caused by natural decrease of available data when time lag increases. Manifestation of this error can be seen in Figure 31. As the mean value of this error is zero, averaging of the autocovariance estimate over several records quickly remove this noise, see Figure 32.

Equation (4.1) was based on Priestley (1981); Kiefer and Vogelsgang (2002); Brockwell and Davis (2006); and Sun (2014) as well as Crowson (1963, 1963a). However, practical application of this equation for long time histories with relatively small time increments, resulted in visually unreasonable choice of the cutoff point M.

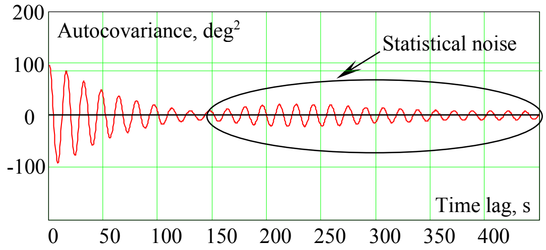

Figure 31: Autocovariance function (first 7.5 min) estimated on a single 30 min record

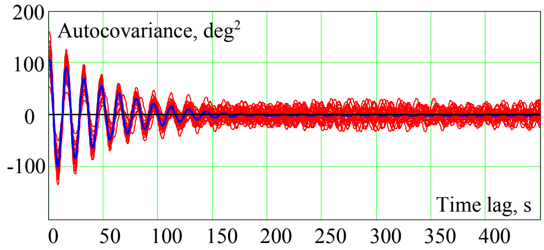

Figure 32: Estimate of autocovariance function averaged over several records (blue). Record estimates are shown in red.

To resolve the issue an optimization scheme by Lu and Park (2019) was considered. However, it was found that the approximate time to reach independence, found with an envelope of the autocovariance estimate, see Figure 33, produced similar results.

The approximate time to reach independence or decorrelation time is found when an envelope of the autocorrelation function estimate (autocovariance normalized by its first term) crosses the level of significance (paragraph 3.7.18 of Annex 4 to the Explanatory Notes, suggests using the value of auto-correlation of 0.05 to determine the limits of valid duration of a record). If the envelope never reaches the level of significance, the decorrelation time is ad hoc determined with the “minimum of the envelope”. This minimum is found as an average between the first local minimum and the lowest point of the envelope observed. More details are available from Glotzer et al. (2023).

Besides the resolution for the cut-off point, there were several other updates to the procedure. It was restructured to make it easier to understand and apply. The procedure has three major sections:

- Uncertainty of mean and variance estimate of a time series,
- Uncertainty of single significant amplitude,
- Construction of confidence interval.

The two first major sections are focused on assessment of uncertainty of statistical estimates in terms of their variance. As all the considered statistical estimates (i.e. mean, variance and single significant amplitude) are assumed normally distributed, their variance characterizes their distribution completely. As these estimates are unbiased or their bias is small, they equal to its own mean values. Once the distribution of an estimate is characterized, confidence interval is ready to be constructed. The third major section is focused on the confidence interval.

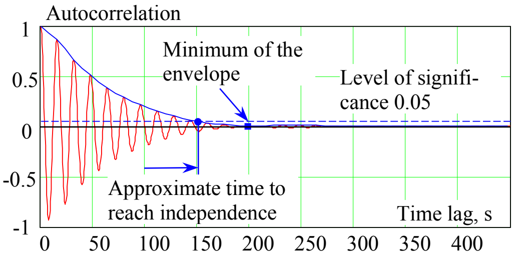

Figure 33: Determination of approximate time to reach independence.

Additionally, the procedure includes a new technique for construction of confidence interval, based on self-normalization algorithm. This technique is simple to implement as it does not require explicit account for autocorrelation of the data. Descriptions and comparisons are available from Pipiras et al. (2018) and Glotzer et al. (2023).

5. NEW ITTC PROCEDURES (TOR 4)

The Item 4 of the Terms of References directs the Stability in Waves Committee to develop new ITTC recommended procedures in support of direct stability assessment within 2nd generation IMO intact stability criteria. As it was already mentioned earlier in this Report, the Interim Guidelines on the Second Generation Intact Stability Criteria in MSC.1/Circ. 1627 includes a provision for application of direct stability assessment (DSA). The ultimate intention of DSA is to use the latest numerical simulation technology to ensure both exiting and future fleet has sufficient stability in waves. Application of these new technologies are especially important for unconventional vessels where design and operation experience is either insufficient or does not exist. ITTC member-organizations have an important role in support the innovation in maritime filed by providing DSA services.

ITTC-recommended procedures in support of direct stability assessment are meant to complement the Explanatory Notes for the Interim Guidelines. The ITTC procedures are specifically geared towards capabilities and skill sets, available to ITTC member-organizations that are expected to participate in trial application of the DSA.

Another benefit of ITTC involvement is an ability of prompt response. The ITTC-recommended procedures may be updated at each Conference i.e., every three years. That is a perfect opportunity for documenting DSA application experience. These updates may serve as a compliment to the submissions to IMO Subcommittee on Design and Construction (SDC) under the agenda item “any other business”.

In fulfilment of the Task 4 of the Terms of References, the Stability in Waves Committee has developed three draft procedures:

A) Avoiding self-repeating effect in time-domain numerical simulation of ships motions (QSG suggested number 7.5-02-01-09)
B) Estimation of Frequency of Random Events by Direct Counting (QSG suggested number 7.5-02-01-10)
C) Statistical Validation of Extrapolation Methods for Time Domain Numerical Simulation of Ship Motions (QSG suggested number 7.5-02-01-11)

More information on these procedures is available below.

5.1 Avoiding self-repeating effect in time-domain numerical simulation of ships motions (TOR 4 A)

The new procedure is made to formulate a process for verification of absence of self-repetition effect and statistical validity of irregular waves in a numerical simulation. The procedure targets on providing specific guidelines to check the self-repeating effect in the direct stability assessment defined in section 3.3.2.1 of Interim Guidelines and in section 3.3.2.1 of Explanatory Notes.

The superposition of N regular wave components is commonly used to construct time series of irregular wave elevations, ζ_W:

$$\zeta_W(t) = \sum_{i=1}^{N} A_i \cos(\omega_i t + \varphi_i) \qquad (4.2)$$

φ_i is i-th phase shift component, and it is uniformly distributed in [0, 2π]. The i-th component of wave amplitude, Ai, is determined from the segment of wave spectrum, $S(\omega_i)$, and selected wave frequency interval, $\Delta\omega_i$, and also directional probability if short-crested sea is assumed. The directional probability distribution function $D(\mu_i)$ for discretized heading angle μ_i has various form, and they can be found in ITTC Guideline 7.5-02 07-01.1.

For the purposes of detection of the self-repeating effect in wave model, the autocorrelation function r needs to be calculated from the spectrum using the same frequency discretization (constant $\Delta\omega_i$) as being planned to use for wave elevation reconstruction for ship motion simulations. The numerical integration has to be carried out with rectangles:

$$r(\tau_j) = V^{-1} \sum_{i=1}^{N} S(\omega_i) \cos(\omega_i \tau_j) \qquad (4.3)$$

S is e the spectrum, V is the variance of wave elevations respectively. The auto-correlation function r is the normalized version of auto-covariance function.

If the self-repeating effect does not present in the wave elevation time series of duration $T{=}\tau_{max}$ the auto-correlation function is "clean", and does not show any increase after initial decay, as shown in Figure 34. If the self-repeating effect is present, its appearance may be different depending on the frequency discretization. If the frequencies distributed uniformly, i.e. frequency increment $\Delta\omega_i$ is constant, the presence of self-repeating effect is observed as "spikes" in the auto-correlation plot as shown in Figure 35. If a non-uniformed frequency distribution is applied (i.e. the frequency increment $\Delta\omega_i$ varies), the presence of the self-repeating effect is observed as a series of increasing oscillations, as like in the Figure 36.

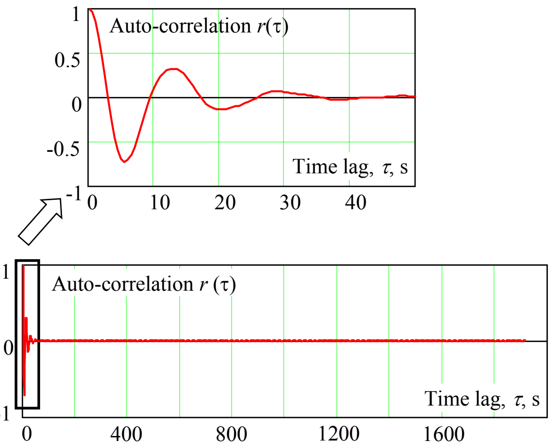

Figure 34: Auto-correlation function in absence of self-repeating effect.

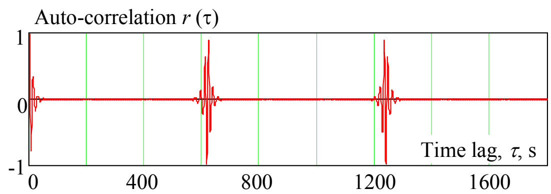

Figure 35: Auto-correlation function showing presence of self-repeating effect for uniformed discretization or constant frequency increment

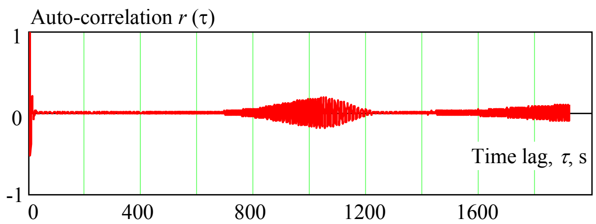

Figure 36: Auto-correlation function showing presence of self-repeating effect for non-uniformed discretization or variable frequency increment

Due to its nature the self-repeating effect will revel itself sooner or later. If the frequencies are selected uniformly, the beginning of the "spike" of the auto-correlation function limits valid duration of a record. For the case of non-uniformed frequency distribution, an envelope of auto-correlation function is useful to find when the of signal starts to increase. The envelope is constructed by connecting absolute values of the peaks of auto-correlation function. Paragraph 3.7.18 of Annex 4 to the Explanatory Notes suggests using the value of auto-correlation of 0.05 to determine limits valid duration of a record.

If the auto-correlation function begins to increase outside of this interval, then the model shows dependence where the real stochastic process should not have it. This limitation of validity is the essence of self-repeating effect leading to partial self-repetition of the constructed wave elevation time series (Belenky, 2011; Tsoumpelis and Spyrou 2023).

The reason of the self-repeating effect is rooted in an oscillatory nature of the integrand $s(\omega_i)\cos(\omega_i \tau)$. The appendix A of the developed procedure explains the nature of the self-repeating effect.

5.2 Procedure of Estimation of Frequency of Random Events by Direct Counting (TOR 4 B)

Item 4 of the Terms of References for the Stability in Waves Committee contains a task to develop new ITTC recommended procedures in support of direct stability assessment (DSA) with the SGISC. In particular, the task calls for devotement of the procedure for Estimation of Frequency of Random Events by Direct Counting.

The DSA is intended to employ the latest technology in time-domain numerical simulation of ship motion. The output of the time-domain simulation is a time series, from which stability failures are detected and counted. The developed procedure of Estimation of Frequency of Random Events by Direct Counting provides a detailed guidance for these calculations.

There are three approaches to DSA, described in the Interim Guidelines: full probabilistic assessment (section 3.5.3.2 of the Interim Guidelines), assessment in design situation using probabilistic criteria (section 3.5.3.3 of the Interim Guidelines), and assessment in design situation using deterministic criteria (section 3.5.3.4 of the Interim Guidelines). The direct counting is applicable to the first two approaches to DSA as the output of the assessment in design situation using deterministic criteria is deterministic, as its name suggests.

The probabilistic criterion, used for DSA, considers time of exposure i.e. accounts for dependence between time spent at severe see conditions and probability of stability failure. Poisson flow of random events is used as a mathematic apparatus to relate the probability and the time of exposure. The Poisson flow application allows computing probability of at least one failure P during any given time interval T as:

$$P = 1 - \exp(-rT) \qquad (5.1)$$

where r is rate of failure that is used as a probabilistic criterion in DSA. It is essentially a probability of stability failure per unit of time. Theoretical background on relationship between the time and the probability through application of the Poisson flow is available from section 2 of SDC-8/INF.2 (IMO, 2021).

One of the principle requirements for application of Poisson flow is that the random events must be independent. At the same time, due to self-dependence of ship motions, large roll angles or large values of lateral accelerations do appear in groups, referred in statistics as “clusters”. In order to use the Poisson flow, only one event per cluster can be counted, thus clusters need to be identified and each cluster needs to be substituted by a single event. This process is commonly referred as “declusterization”.

The Explanatory Notes provides three different techniques for direct counting in Section 3 of Appendix 4 to MSC. 1/Circ.1652 (IMO 2023).

These three techniques differ on their approach to declusterization, using:

- Exponential distribution of the time before the first event occurs; a simulation runs before the first failure occurs, time before-the-first event is recorded and averaged; the reciprocal of the average time before the event is used as an estimate of rate of failures;
- Estimation of probability of failure over the duration of a simulation record; the rate of failures is estimated from the equation above;
- Binomial distribution of the number of independent failures encountered; declusterization is performed with decorrelation time using an estimate of autocorrelation function, following section 3.8 of Appendix 4 to the Explanatory Notes as well as the ITTC recommended procedure 7.5-02-01-08.

Benchmarking of all three techniques have shown statistically identical results (Shigunov et al. 2022; Wandji et al. 2023). Thus, the choice on, which technique to use, depends on which one fits better to simulation technology, used at a particular organization. The developed recommended procedure contains step-by-step guidance on all three techniques as well as on constructing confidence interval for the estimates. An example of application of all three techniques is included for the same ship configuration, demonstrating equivalency of all the techniques. The test configuration is ITTC-A1 (Umeda et al. 2000), 150 m long containership.

Theoretical background of all three techniques, including formal study of properties of the estimators is available from Wandji et al. (2024). The IMO sub-committee on Ship Design and Construction (SDC) has been informed on the development of this recommended procedure by the way of an information paper SDC 10/INF.7 submitted by ITTC: (IMO 2023).

Statistical Validation of Extrapolation Methods for Time Domain Numerical Simulation of Ship Motions (TOR 4 C)

Procedure of Estimation of Frequency of Random Events by Direct Counting.

Procedure 7.5-02-01-11 Statistical Validation of Extrapolation Methods for Time Domain Numerical Simulation of Ship Motions (TOR 4 C).

The purpose of the procedure was to describe a process for the validation of extrapolation methods used for direct stability assessment for the stability failure modes described in section 3.5.6 MSC.1/Circ. 1627. The validation is considered successful if an extrapolation method (including those described in the ITTC Recommended Procedure 7.5-02-07-04.6) captures a “true” value. The percentage of these “successes” should be about accepted confidence probability.

The formulation of the procedure and the acceptance criteria for validation are based on the work of Smith (2019), i.e., the three-tier validation: single extrapolation, single condition and multiple conditions. The validation of the extrapolation is assessed by means of the confidence intervals of the “true” and the “extrapolated estimate. For the tier 1 validation, a single extrapolation is considered as a Bernoulli trial where success (overlap of confidence intervals) is attributed 1.0 and failure (no overlap of the confidence intervals) is given 0.0. The second tier (validation of a single condition with, for instance, 50 extrapolations) is computed through binomial quantiles, where 0.88 was suggested as the standard for passing rate (as in the IMO Interim Guidelines). Finally, the tier 3 validation (multiple conditions), which should account for different ship speeds, relative wave headings and sea states, accepts/rejects an extrapolation method or define limitations for it, for a particular specific intended use. For the tier 3 validation, an assumption allowance is suggested to be introduced in the lower limit of the tier 2 criterion. Based on data from Campbell et al. (2023), a numerical example of partial validation of EPOT extrapolation method has been provided in the appendix A of the procedure.

6. NEW PROCEDURE FOR INSTANTANEOUS GZ (TOR 5)

Historical Background

The roll righting arm (GZ) curve in waves is an important factor in the evolution of ship`s changing stability in waves. For more than a century, naval architects have been aware of the phenomenon of transverse stability change in longitudinal waves (Pollard and Dudebout, 1892). Methods for calculating the change in stability in waves are not considered as a new development by any means. Paulling (1961) proposed a quasi-static approach for accounting for pressure changes while a wave passes a ship. Boroday (1967) developed a method for theoretically predicting the statistical characteristics of restoring moment in irregular waves, taking into account Froude-Krylov pressures

The roll restoring moment is made up of two parts. The nonlinear Froude-Krylov component (GZ_{FK}) is calculated by integrating the wave pressure all the way to the wave surface. The other component is the hydrodynamic effects caused by the radiation and diffraction component (GZ_{RD}).

It is widely agreed that the Froude–Krylov assumption can explain the wave influence on roll restoring moment when assessing roll restoring arm variation in waves. However, a study Hashimoto and Umeda (2004), that include captive model experiments, show that Froude–Krylov assumption may overestimate the magnitude of GZ curve. An accuracy of the instantaneous GZ may be critical for predicting roll response (Vidic-Perunovic and Jensen, 2009). Thus, it make sense to develop more detailed and realistic mathematical model for predicting roll restoring moment.

So far, no consensus has been reached about the contribution of GZ_{RD}. This issue is still unresolved and requires additional experimental and numerical research. In terms of the consequences of GZ_{RD}, certain studies have shown that when the dynamic component is considered, prediction accuracy improves (Umeda et al., 2005; Hashimoto et al., 2007; Lu, et al., 2017). The computation of roll restoring arm variation in these studies is based on a strip theory under the linear and nonlinear assumption of GZ_{RD} with reference to roll angles. The roll restoring moment is particularly crucial when the rolling angle is relatively big at high incident wave steepness, according to a number of research done in the past, using the CFD approach (Sadat-Hosseini et al. 2010; Ma et al., 2018).

The CFD approach, however, makes it exceedingly challenging to discriminate between the effects of various components. The rules of roll restoring moment fluctuation in waves was investigated using a three-dimensional hybrid time domain panel method by Bu et al. (2019, 2019a). By taking into account the radiation and diffraction moments based on the body-exact condition, the nonlinear characteristics of roll restoring arm are studied for varied constant heeling angle, wave amplitudes and ship forward speeds. The results of the studies demonstrate that, particularly at high speeds, the component brought on by radiation and diffraction moments may be important in head or oblique waves. It was also found that the time history of *GZ* curve clearly exhibits the multi-frequency superposition phenomena. Just twice as often as the first resonance frequency, the second peak mostly results from nonlinear radiation and diffraction moment.

Hashimoto and Umeda (2004) found that the lift effect generated by a heeled hull due to asymmetry may have an influence on roll restoring in high speed. Cited research has been performed for a fishing vessel. Studies by Hashimoto and Umeda (2010), Gu et al. (2014), studying influence of different combinations of degrees of freedom, concluded that at least the coupled heave-roll-pitch model should be used for calculations of GZ curve in waves. Belenky and Weems (2008) describe calculation of variation of GZ curve during time-domain simulation with Large Amplitude Motion Program (LAMP, see Shin et al. 2003). That calculations were preformed with 3 DoF (heave-roll-pitch) and included diffraction and radiation forces computed over average waterplane.

Physical Background and Motivation

For ships with significant variation of a shape of the waterplane (such as flared bow or transom and buttock-flow stern), the change of GZ in waves can be particularly noticeable. The waterplane area has a substantial effect on ship stability, which is well known from ship hydrostatic. When the waterplane area is reduced, so is the GZ curve (see Figure 37). The change of stability in waves, is the physical basis for the stability failure modes parametric rolling and pure loss of stability, see, e.g. Appendix 1 of Explanatory Notes.

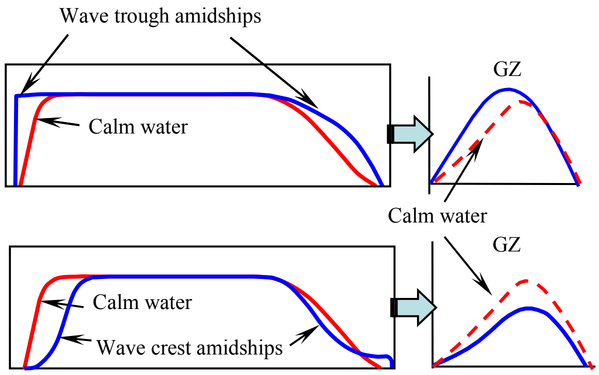

Figure 37: Stability, represented by righting level curves, corresponding to waterplane changed with the midship located on the wave trough (top) and the wave crest (bottom) (Appendix 1 of MSC.1/Circ.1652)

Large roll excursions may be better understood if evolution of the shape of the instantaneous GZ curve in irregular waves is known. Example of application of this analysis can be found in Spyrou et al (2014).

Calculation Procedure

In general, stability in waves is evaluated in the same way as it is done in calm seas. A vessel is rotated (heeled) about its longitudinal axis; the pressure on the hull surface is integrated to get the restoring forces and moments acting on the ship. The uncompensated moment relative to the longitudinal axis is used to derive a restoring arm that represents the value of the GZ curve for the rotation (heel) angle.

Most of commercially available hydrostatic programs are capable to compute the restoring arm as a quasi-static wave-pass problem, so only the variation in the Froude-Krylov and hydrostatic forces is evaluated. To perform the complete analysis similar to described above, actual dynamics of the ship in wave needs to be considered: i.e. the ship's hydrodynamic forces (including radiation, diffraction, influence of forward speed, appendages, etc. need to be included. However, Belenky and Weems (2008) have assumed these hydrodynamic forces do not to change with heel angle.

In the righting arm calculation, the heel rotation disturbs the ship's static or dynamic equilibrium in pitch and heave – in other words, the heave force and pitch moment also change. These changes may influence roll moment and need to be excluded. To exclude the pitch and heave influence, balancing is performed relative to instantaneous forces and moments acting on the ship. This is a direct result of application of the d'Alambert principle, as the instantaneous attitude in waves is a result of action of inertia forces and moments.

It makes sense to perform the instantaneous curve calculation in irregular waves in conjunction with time-domain numerical simulation for a preselected interval of time. The calculation also can be incorporated into a post-processing routine. The main steps of the calculations are listed below:

1. The ship is heeled through a range of angles relative to its instantaneous position.
2. At each heel angle, forces and moments acting on the ship are computed for the heeled position.
3. The ship's heave position and pitch angle, expressed relative to a global coordinate

system, are iteratively adjusted until the dynamic equilibrium in these degrees of freedom is achieved

4. The net roll moment defines the instantaneous GZ value corresponding to current heel angle.

The calculation procedure is detailed in the draft ITTC recommended procedure “Computational procedure for instantaneous GZ curve during time-domain numerical simulation in irregular wave”.

Belenky and Weems (2008) describe a technique for checking self-consistency of calculation. A simulation is set when a ship is placed on a wave and sails with the celerity of this wave and heeled by an external moment. Angle of heel is recorded and compared to the value from the GZ curve computed for this wave. This process can verify the values of the GZ curve in wave before the maximum, as the equilibrium above the maximum of GZ curve is unstable. A similar procedure is used in section 2.3 of Appendix 4 of Explanatory Notes for qualitative validation of mathematical model of ship motions in waves.

7. DAMAGED SHIP IN WAVES (TOR 6)

Investigate the current state of the art on flooding dynamics of damaged ship in waves, including EFD and CFD.

Mauro et al. (2021) proposed three methods to identify the critical scenarios for the assessment of damaged passenger ships. The first method is based on preliminary static calculations, the second on the energy absorbed by the ship during an impact, the third on a purely dynamic approach. The authors compared their differences based on two sample passenger ships, showing their respective advantages and disadvantages.

Zhang et al. (2021) introduces a method using AIS data to estimate collision frequencies and scenarios for use in ship damage stability, Figure 38.

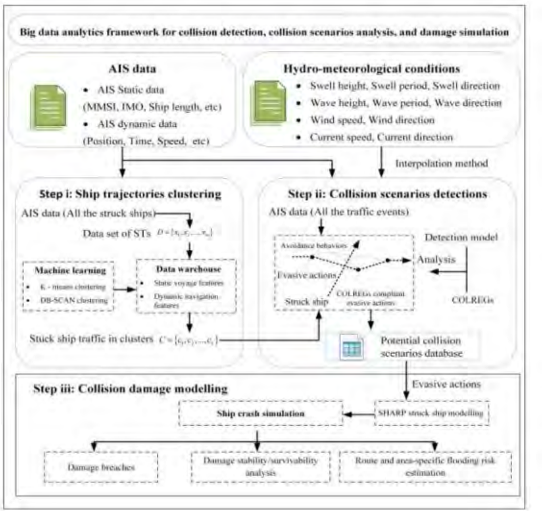

Figure 38: A framework for collision risk estimation using big data analysis

Vassalos, et al. (2021) presents the new developments in the H2020 FLARE project, especially the quantitative risk models pertaining to ship flooding. They also proposed a new risk-based method for the direct assessment of flooding risk estimation using numerical tools with support from datasets. Efforts has been made to build more suitable model for cruise ships than current high level risk models, Figure 39.

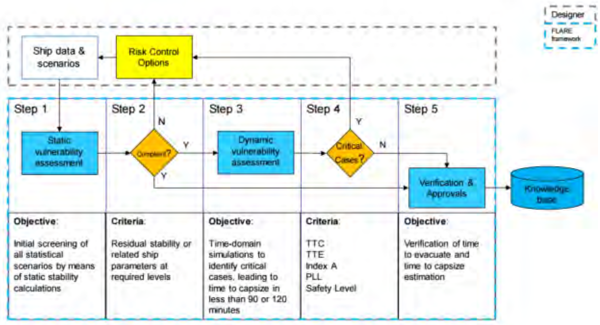

Figure 39: H2020 FLARE framework for direct flooding risk estimation

Krüger et al. (2021) extend the Monte Carlo principle for the computation of ship damage stability over the whole ship design process, with a focus on how to obtain the missing information through a sort of reverse engineering method and how the identified problems can be solved numerically. Traditionally, Monte Carlo simulation was used in the early stages of ship design.

van‘t Veer, et al. (2021) proposed a new flooding model for ship internal flooding. It has two modes of operation: one that uses the traditional steady Bernoulli equation and the other that includes a flow-averaged momentum term in each floodable region.

Bu et al. (2021) describe a viscous and potential prediction method for damaged ship motion. The method combines floodwater and motion in waves, see Figure 40 for the definition of the two domains. The three-dimension time domain potential method is coupled with CFD method. The described method can significantly improve computational efficiency while ensuring computational accuracy. Results are compared to the ITTC benchmark and to full CFD calculations.

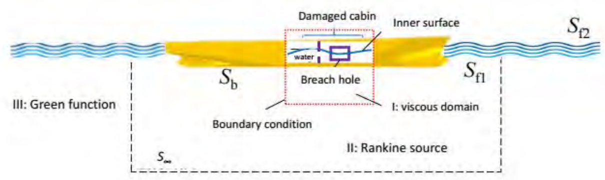

Figure 40: Diagram for the filed domains in the prediction method, from Bu et al. 2021a.

Valanto and Schumacher (2021) investigate the roll damping of intact ship with varying draughts and heeling angles to study the effect of the ship floating position on these coefficients. Then further study the roll damping of damages ship with different damaged cases was conducted. They studied the influence of the roll amplitude, installed bilge keels and ship speed on the roll damping behavior of the intact vessel. They also studied the influence of different floating condition, raking damage and collision damage on roll damping of the damaged vessel. From their first test simulation of damaged cases, they found that the transient flooding in calm water with a damage rapidly opening at the ship side, the use of draught and heel dependent roll damping coefficients can led to better results than using constant roll damping coefficients. However, the situation in a gradual flooding case in irregular beam seas is complicated, and the internal flooding models should be improved. The roll excitation is generated by a gyroscopic machine using gyroscopic controlled by a dedicated software, see Figure 41.

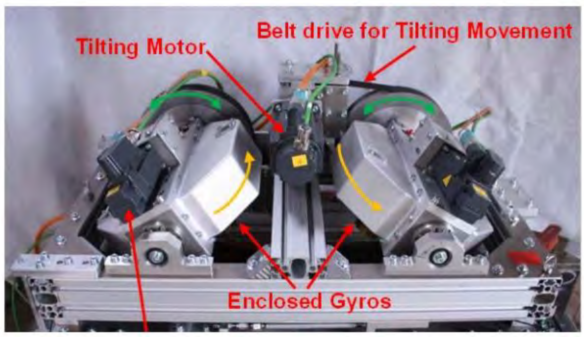

Figure 41: Gyroscopic roll excitation machine.

Predicting the motion responses of a damaged ship under various incoming waves is important. Vidić and Bačkalov (2022) investigated the present intact and damage stability requirements intended for Large Inland Passenger Ships, LIPS. They offer a critical analysis of the present stability regulations, highlight the need for a global harmonization of regulations, and probe into the hierarchy of the stability requirements for LIPS.

Hu et al. (2021) investigated the seakeeping performance of a DTMB 5415 model by focusing on its roll motion under beam wave condition, aiming to analyze the damaged ship motion performance under this rarely studied condition.

Bu et al. (2023, 2023a) investigated the motion and flooding process of a damaged passenger ship in regular and irregular beam waves experimentally and numerically at zero forward speed.

Pineau et al. (2022) present a numerical tool based on analytical formulations for rapid assessment of damage in ship grounding accidents. Through a step-by-step solution, the ship resistant force is assessed by the super-element method and transferred to a 6-DoF external dynamics solver, which updates the global ship motion by taking into account the action of hydrodynamic forces.

Dong et al. (2023) simulated the free-running turning maneuvers of a surface combatant with a damaged bow compartment numerically using an in-house unsteady RANS solver, coupled with the dynamic overset approach. Liu et al. (2022) predicted extreme roll motions with large amplitudes, induced by the pure loss of stability, for a benchmark combatant ONRTH running in stern quartering waves by CFD simulations. It is observed that ship capsizing occurs coupled with a rapid increase of yaw angle.

To assess the survivability of damaged ships, Kawamura and Hino (2023) developed a numerical method to simulate the motion of a floating body with partially filled tanks. The present method couples MPS and the Finite Volume Method (FVM), which are developed at the National Maritime Research Institute of Japan, by using peer-to-peer file exchange to retain the advantages of each discretization technique. The computational results are encouraging in that the Response Amplitude Operators (RAOs) of sway and roll motion show good agreement with the data measured in incident regular waves with various wave lengths.

Gao and Tian (2021) investigated the roll phenomena of a damaged ship in head waves using CFD. A series of head wave scenarios where the frigate was in a damaged condition and in an intact condition were simulated to highlight the main factors that affected the ship loads and motion response.

Pertaining to s-factor, according to SOLAS, a hybrid two-level framework for the stability of damaged ships was proposed (Mauro et al., 2023): Level-1 assessment based on static damage stability simulation and Level-2 assessment based on dynamic flooding simulation. The p-factor in SOLAS is calculated based on the dedicated marginal distribution functions of breaches in collision damage, which is commonly referred to as "zonal" approach. In order to calculate the p-factor of different damage types, the "non-zonal" approach is proposed (Krüger and Aschenberg 2021; Bulian et al. 2023). Duan et al. (2023) proposed an improved method within probabilistic framework for the survivability assessment of damaged ships in waves. To calculate s-factor, a fast dynamic numerical model to compute the motion of damaged ships under design sea states is put forward. Additionally, the p-factor is calculated based on the "non-zonal" approach.

Focused on the probability of occurrence of a certain breach, Vassalos et al. (2022) explained associated probabilistic content as p-factor, including pertinent assumptions and limitations. For a better understanding, a detailed statistical analysis on new damage breach distributions for passenger ships was undertaken according to the new database developed in the project H2020 FLARE. During the probabilistic damage stability calculation, concerning characteristics are illustrated, such as derivations of the breach distributions, sampling methods for numerical simulation, crash-worthiness considerations, and so on.

Aimed at enhancement of ship safety pertaining to flooding risk, Bae et al. (2023) suggested a quantitative risk assessment methodology (Figure 42), with the application of crashworthy structural designs as Risk Control Options (RCOs). The method provides equivalent damage stability criteria to the current SOLAS regulations within the IMO framework in a cost-effective way, which consist of seven steps. The first step is to calculate the damage stability of the target ship using standard damage stability analysis according to current SOLAS 2020, and select one or two high-risk zones for RCO application. The next step involves conducting ship collision simulations for the target vulnerable zone. The third step involves the implementation of alternative design arrangements as RCOs, to the target zones identified in the first step. After completing Step 3, the cumulative transverse breach distribution function of the target zone can be adjusted to obtain the corresponding PDF, after which the damage stability can be recalculated. The subsequent step involves conducting a cost-benefit analysis to determine the optimal RCO solution, utilizing the Gross Cost of Averting a Fatality (GCAF).

Based on above 6 steps, the final decision will be made after thorough discussion.

When evaluating ship damage stability, almost all pertinent parameters are calculated to extreme accuracy, except permeable volume and its distribution. Over the years, some generalized approximations have been adopted for principal ship spaces without differentiating between ship types. To demonstrate the impact of such approximations, Vassalos et al. (2022a) selected several passenger ships and undertook a sensitivity analysis addressing the main ship spaces and their contribution to permeable volume. Damage stability calculations (A-Index) are conducted to provide indicative measures on the impact of permeability. As a general remark, permeable volume plays a vital role in either case as it affects dramatically the slope of change of the A-Index to changes of permeability.

Figure 42: Overall methodology for quantitative risk assessment

Vassalos et al. (2022a) conducted a study about influence of life-cycle damage stability requirements on the internal ship layout, emergency response. Taking constraints and conflicting requirements into consideration, a framework of optimal configuration is presented, related to design, operation, and emergency response on a large passenger ship.

Take the existing failure probability calculation method on intact ship stability provided by IMO for reference, the application of the direct stability procedure and the direct counting method is investigated (Bu et al., 2023a), for calculating failure rate of damaged ships. Four methods are used to obtain failure rate in different sea states: a piecewise linear method on the GZ curve; a probabilistic method with first stability failure occur; a probabilistic method with fixed specified exposure time; and a deterministic method. All of them have a certain range of application for calculating the capsizing probability of damaged ships.

Forensic level flooding analysis is traditionally rooted in accident investigation. Nowadays, a great deal of process has been made, with more contemporary examples including the work conducted in Karolius et al., (2020), Vassalos et al., (2021) and Valanto, (2023). Paterson et al. (2023) developed a clear and rational methodology for conducting flooding forensic analysis, which is consisted of 9 distinct stages as shown in Figure 43. A transient capsize scenario and a progressive flooding loss scenario are selected as examples for elaboration.

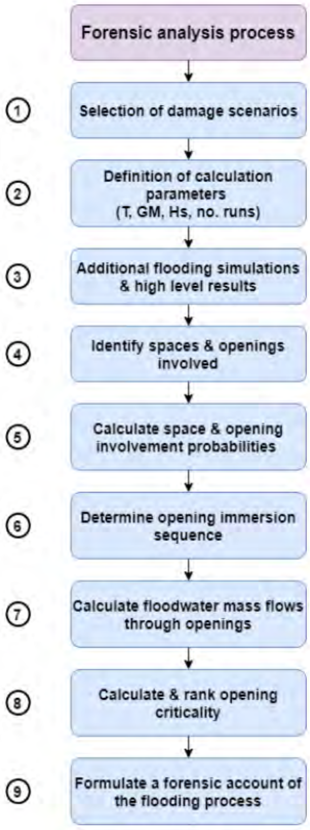

Figure 43: Process of forensic analysis

Bu et al. (2022, 2023, 2023a) adopted the experimental method to investigate motion and internal water height of a damaged passenger ship, which is compared with that under the intact state. The time history of the ship motion in regular and irregular beam waves are presented.

With the adoption of the self-designed electrically operated valve (Figure 44), the size of the opening can be controlled. The flooding into the side-damaged opening increased the period of ship's roll and the roll amplitude increased with increasing wave steepness in both ship states. Under testing damaged conditions, the roll amplitude of the damaged ship is smaller than that of the intact one. More nonlinear effects throughout the flooding process, as well as unsteady effects in irregular waves, should be added to improve the accuracy of the numerical method.

Figure 44: Self-designed electrically operated valve for control-ling the opening's size

ML/AI tools have started to be used in the damage stability area. Examples can be found in Section 2.1 of this report (Louvros et al. 2023; Mauro et al. 2023a; Vassalos et al. 2023a).

Lee et al. (2023, 2023a) describe work of 27th ITTC Stability in Wave Committee on handling inertia of floodwater. Three cases were identified in (Lee et al. 2023): water entering a ship, partially and fully flooded compartment. Approach to account for inertia of floodwater is different for each case. Lee et al. (2023) considers influence of trapped air in flooded compartment, comparing with a case of the vented compartment.

8. BENCHMARK (TOR 7)

The collection of benchmark data has always been a very important work of ITTC. This year, the members of ITTC SiW mainly collected benchmark data in the following aspects. The first one is about the GZ curve in wave for intact ship provided by the CSSRC. The test cases include mainly the change of the GZ curve in different wave conditions under a fixed heel angle for a container ship. The second one is about damage stability. H2020 FLARE presents an international benchmark study on flooding and motions of damaged ROPAX and cruised vessels. The 2023 ITTC procedure 7.5-02-07-04.4 "Simulation of Capsize Behaviour of Damaged Ships in Irregular Beam Seas" introduce the pertinent details. The dataset is located at the shipstab website: shipstab.org/index.php/news/98-added-flare-benchmark-study-damaged-cruise-ship).

Kapsenberg et al. (2020) describes benchmarking of numerical simulation tools for parametric roll, including comparison to a model test in irregular waves. The difference was actually not very much, considering how large roll motions were.

Marine casualties can give some good benchmark data for evaluation of stability tools if they can reproduce or estimate the risk of the realistic cases described. Example of complete documents came from EMSA but many countries have also interesting data and document. EMSA document gave the list of national investigative bodies in EU (see appendix 6 of EMSA 2023). National investigative bodies usually make available very detailed information about marine casualties in their geographical areas. Also many papers, particularly in ISSW, STAB and STAB&S conferences, describe some disasters with scientific point of view, for example, for one event as in Taguchi and Kuroda (2018), or analyzed for a type of ship as Mughadar-Palliparambil et al. (2021) for passenger ships.

9. ITTC LIAISON

SiW committee addressed the question put forward by SKC on wind loads. SiW committee emphasized that transverse loads for stability purposes must be considered alongside the longitudinal force (as mentioned in the proposed procedure focused on resistance evaluation). It was also noticed that the influence of heel angle on loads should be present.

10. IMO LIAISON

Per a request from ITTC secretary, the committee has prepared an information paper for the 10th session of IMO subcommittee on ship design and construction on ITTC support of the trial application of direct stability assessment within the second generation intact stability criteria. Following proper review and approval from ITTC governing bodies the paper has been submitted to SDC-10 under agenda item 16 “Any other business” identified as SDC 10/INF.7. The document gives a brief review of relevant ITTC recommended procedures, noting the status: existing, being updated or development-in-progress.

11. CONCLUSIONS

Technical conclusion

(1) A survey of literature has been conducted, including books, journals and proceedings of international conferences.

(2) The highlight of the reporting period is publication by IMO of the Explanatory Notes for the Interim Guidelines on the Second Generation Intact Stability Criteria with MSC.1/Circ. 1652 in April 2023. The Interim Guidelines was published in December 2020 (MSC.1/Circ. 1627). Direct stability assessment (DSA) is the most innovative part of the Second Generation Intact Stability Criteria (SGISC), where most advanced numerical simulation technology are being applied. As the trials of the SGISC has began, ITTC member-organizations may be interested in providing the DSA as one of their services.

(3) In support of the trail application of DSA, the committee has updated the ITTC recommended procedure 7.5-02-07-04.6 "Extrapolation for Direct Stability Assessment in Waves” one extrapolation over wave height in addition to already described Envelope Peak over Threshold (EPOT) and split-time /motion perturbation methods (MPM). The committee has tested all three method by running them with same input data, obtaining statistically identical output, favorably compared with a “true” values, estimated from a larger dataset.

(4) The committee has developed three more procedures, specifically aimed to aid the member- organizations in application of DSA: “Avoiding Self-Repeating Effect in Time-Domain Numerical Simulation of Ship Motions”, “Estimation of Frequency of Random Events”, and “Statistical Validation

of Extrapolation Methods for Time Domain Numerical Simulation of Ship Motions". The committee believes that those procedures are compliant with IMO Interim Guidelines can be also useful to general numerical simulation work.

(5) Another highlight of the reporting period was publication of the book "Contemporary Ideas on Ship Stability – from Dynamics to Criteria" by Springer in 2023. The book has 43 chapters, covering the entire development in the field of stability in waves over last 10 years, including an extended summary /overview of these chapters. The book is themed over the technical background of the SGISC, but contains all other topics too. The committee has reviewed the book, reporting the result is in Section 2.

(6) One more highlight of the reporting period is the publication of virtual special issue of Ocean Engineering "Extreme Stochastic Dynamics of Ships". Publication of this special issue was inspired by long-term research program "A Probabilistic Procedure for Evaluating the Dynamic Stability and Capsizing of Naval Vessels" run by the US Office of Naval Research. Most important results of this program were published in the special issue along with other papers focused on extreme ship motions. Totally, the special issue contains 17 full-length research papers, relevant to this committee. Review of these papers by the committee can be found in Section 2.

(7) One of the papers of the Special Issue contained the information that was necessary for updating the ITTC recommended procedure 7.5-02-01-08 Single Significant Amplitude and Confidence Intervals for Stochastic Processes. The information concerned account for self-dependence of a stochastic process constructing confidence interval. In fulfilment of Task 3 of the Terms of References, the committee has updated the procedure.

12. FINAL REPORT AND RECOMMENDATIONS TO THE 30TH ITTC

The 30th ITTC Stability in Waves Committee recommends the following:

- Adopt the updated ITTC Recommended Procedure 7.5-02-01-08 "Single Significant Amplitude and Confidence Intervals for Stochastic Processes".
- Adopt the updated ITTC Recommended Procedure 7.5-02-07-04.1 "Model Tests on Intact Stability"
- Adopt the updated ITTC Recommended Procedure 7.5-02-07-04.3 "Predicting the Occurrence and Magnitude of Parametric Rolling".
- Adopt the updated ITTC Recommended Procedure 7.5-02-07-04.4 "Simulation of Capsize Behaviour of Damaged Ships in Irregular Beam Seas".
- Adopt the updated ITTC Recommended Procedure 7.5-02-07-04.5 "Estimation of Roll Damping".
- Adopt the updated ITTC Recommended Procedure 7.5-02-07-04.6 "Extrapolation for Direct Stability Assessment in Waves"
- Adopt the new ITTC Recommended Procedure "Avoiding self-repeating effect in time-domain numerical simulation of ship motions", QSG suggested number is 7.5-02-01-09.
- Adopt the new ITTC Recommended Procedure "Estimation of Frequency of Random Events by Direct Counting", QSG suggested number is 7.5-02-01-10.
- Adopt the new ITTC Recommended Procedure "Statistical Validation of Extrapolation Methods for Time Domain Numerical Simulation of Ship Motions", QSG suggested number is 7.5-02-01-11.
- Adopt the new ITTC Recommended Procedure "Computational Procedure for Instantaneous GZ Curve during Time-domain Numerical Simulation in Irregular Waves", QSG suggested number is 7.5-02-07-04.8.

- Develop a new ITTC Recommended Procedure “Evaluation of Dynamical Characteristics of a Ship” to support application of Direct Stability Assessment within the framework of the Second-Generation Intact Stability Criteria (IMO, 2020).
- Further update ITTC Recommended Procedure 7.5-02-07-04.6 “Extrapolation for Direct Stability Assessment in Waves” to include two more extrapolation methods: Critical Wave Method and Linear Superposition Method, as described in the Explanatory Notes to the Second-Generation Intact Stability Criteria (IMO, 2023).

13. REFERENCES AND NOMENCLATURE

References

Alford, L. K. and Troesch, A. W. (2009). Generating Extreme Ship Responses using Non-Uniform Phase Distributions. *Ocean Eng.*, Vol. 36. pp. 641-649.

Anastopoulos, P. A., Spyrou, K. J., Bassler, C. and Belenky, V. (2016). Towards an Improved Critical Wave Groups Method for the Probabilistic Assessment of Large Ship Motions in Irregular Sea. *Probabilistic Eng. Mech.* Vol. 44, pp 18-27.

Anastopoulos, P. A. and Spyrou, K. J. (2022). Extrapolation over Significant Wave Height with the Aid of Stochastic Wave Groups Theory. *Proc. 18th ISSW*, Gdansk, Poland.

Anastopoulos, P. A. and Spyrou, K. (2023). Effectiveness of the Generalized Pareto Distribution for Characterizing ship Tendency for Capsize, in *Contemporary Ideas on Ship Stability – From Dynamics to Criteria*, Spyrou, K. et al., eds., Springer, pp. 245-263.

Anastopoulos, P. A. and Spyrou, K. (2023a). An Efficient Formulation of the Critical Wave Groups Method for the Assessment of Ship Stability in Beam Seas, in *Contemporary Ideas on Ship Stability – From Dynamics to Criteria*, Spyrou, K. et al. eds., Springer, pp. 157-174.

Anastopoulos, P. A. and Spyrou, K. J. (2023b). Extrapolation of Ship Capsize Probability over Significant Wave Height: Foundation on Wave Groups Theory. *Ocean Eng.*, Vol. 281, 114766.

Aram, S., Weems, K. M. and Belenky, V. (2023). Towards the uncertainty quantification of a roll damping model. *Proc. 19th ISSW*, Istanbul, Turkey.

Atzampos, G., Vassalos, D., Cichowicz, J., Paterson, D. and Boulougouris, E. (2023). Cruise Ship Survivability in Waves, in *Contemporary Ideas on Ship Stability – From Dynamics to Criteria*, Spyrou K et al. eds., Springer, pp. 589-606.

Bae, H., Vassalos, D., Paterson, D. and Mauro, F., (2023). Ship damage stability enhancement through crashworthiness. *Proc. 19th ISSW*, Istanbul, Turkey, pp. 63-76.

Bassler, C. C., Dipper, M. J. and Melendez, M., (2019). Experimental Ship Dynamic Stability Assessment Using Wave Groups, in *Contemporary Ideas on Ship Stability. Risk of Capsizing*, Belenky, V., et al., eds., Springer, pp. 507-520.

Belenky, V. L. and Sevastianov, N. B. (2007). Stability and Safety of Ships: Risk of Capsizing. 2nd edition SNAME, Jersey City.

Belenky, V. and Weems, K. M. (2008). Probabilistic Qualities of Stability Change in Waves. *Proc. 10th ISSW*, Daejeon, Korea.

Belenky, V. (2011). On Self-Repeating Effect in Reconstruction of Irregular Waves. in *Contemporary Ideas on Ship Stability and Capsizing in Waves*, Neves, M.A.S. et al., eds., Springer, pp. 589-598.

Belenky, V., Spyrou, K., van Walree, F., Neves, M. A. S., and Umeda, N. eds. (2019). Contemporary Ideas on Ship Stability. Risk of Capsizing, Springer, Series Fluid Mechanics and Its Application Vol. 119 ISBN 978-3-030-00514-6.

Belenky, V., Glotzer, D., Pipiras, V. and Sapsis, T. (2019a). Distribution Tail Structure and Extreme Value Analysis of Constrained Piecewise Linear Oscillators. *Probabilistic Eng. Mech.,* Vol. 57, pp 1-13.

Belenky, V., Weems, K. M., Sapsis T., and Pipiras, V. (2021). Influence of Deck Submergence Events on Extreme Properties of Wave-Induced Vertical Bending Moment. *Proc. 1st STAB&S*, Glasgow, Scotland, UK.

Belenky, V., Spyrou, K., and Weems, K. M. (2023). Critical Distance on a Phase Plane as a Metric for the Likelihood of Surf-Riding in Irregular Waves, in *Contemporary Ideas on Ship Stability – From Dynamics to Criteria*, Spyrou, K. et al. eds., Springer, pp 413-434.

Belenky, V., Weems, K. M, Spyrou, K., Pipiras, V. and Sapsis T. (2023a). Modeling Broaching-to and Capsizing with Extreme Value Theory, in *Contemporary Ideas on Ship Stability – From Dynamics to Criteria*, Spyrou, K. et al. eds., Springer, pp 435-457.

Belenky, V., Weems, K., Lin, W. M., Pipiras, V. and Sapsis, T. (2024). Estimation of Probability of Capsizing with Split-Time Method. *Ocean Eng.*, Vol. 292, 116452.

Bishop, R. C., Belknap, W., Turner, C., Simon, B., and Kim, J. H. (2005). Parametric Investigation on the Influence of GM, Roll Damping, and Above-Water Form on the Roll Response of Model 5613. Hydromechanics Department Report, Naval Surface Warfare Center Carderock Division, West Bethesda, Maryland, USA, NSWCCD-50-TR-2005/027.

Boccotti, P. (2000). Wave Mechanics for Ocean Engineering. Elsevier Science, Oxford, ISBN 9780080543727 496 p.

Boccotti, P. (2014). Wave Mechanics and Wave Loads on Marine Structures. Butterworth-Heinemann, Elsevier, doi.org/10.1016/C2013-0-13663-X, 344 p.

Bonci, M. (2022). Ship Capsize Dynamics: a Numerical Sensitivity Study. *Proc. 18th ISSW*, Gdańsk, Poland.

Boroday, I. K. (1967). Statistical Characteristics of Stability and the Probability of Capsizal of a Ship running on any Course in Irregular Seas. Documents of the USSR Expert of the IMCO, Working Group on Stability of Fishing Vessels, London.

Brockwell, P. J. and Davis, R. A. (2006). Time Series: Theory and Methods. Springer, 2nd edition.

Brown, B. and Pipiras, V. (2023). On Extending Multifidelity Uncertainty Quantification Methods from Non-Rare to Rare Problems. in *Contemporary Ideas on Ship Stability – From Dynamics* to Criteria, Spyrou, K. et al. eds., Springer, pp. 175-186.

Bu, S. X., Gu, M., and Abdel-Maksoud, M. (2019). Study on Roll Restoring Arm Variation using a Three-dimensional Hybrid Panel Method, *J. of Ship Research* Vol. 63, No. 2, pp. 94-107.

Bu, S. X., Gu, M., Lu, J. and Abdel-Maksoud, M. (2019a). Effects of Radiation and Diffraction Forces on the Prediction of Parametric Roll, *Ocean Eng.* Vol. 175, pp 262-272.

Bu, S. X., Lu, J. and Gu, M. (2021). Study on the Effects of Radiation and Diffraction Forces on Roll Restoring Arm with Flared and Tumblehome Vessels. *Ocean Eng.* Vol. 239, 109777.

Bu, S., Gu, M. and Lu, J. (2021a). Unified Viscous and Potential Prediction Method of Damaged Ship Motion coupled with Floodater in Regular Waves, *Proc. 1st STAB&S*, Glasgow, Scotland, UK.

Bu, S., Gu, M., Zhan, J. and Zhang P. J. (2022a). Experimental Investigation on one Damaged Passenger Ship in Regular and Irregular Beam Waves. *Proc. 18th ISSW,* Gdańsk, Poland, pp. 87-93.

Bu, S., Gu, M., Yang, C. and Zhang, P. J. (2023). Investigation on the Capsizing Probability of Damaged Ship in Irregular Seaway. *Proc. 19th ISSW*, Istanbul, Turkey, pp. 87-94.

Bu, S., Zhang, P., Liu, H., Shi, Y., and Gu, M. (2023a). Researches on the Motion and Flooding Process of a Damaged Passenger Ship in Regular and Irregular Beam Waves. *Ocean Eng.* Vol. 281, 114927.

Bulian, G., and Francescutto, A. (2021). An Approach for the Implementation of Operational Limitations in the Level 1 Vulnerability Criterion for the Dead Ship Condition. *Proc. 1st STAB&S*, Glasgow, Scotland, UK.

Bulian, G., Cardinale, M., Dafermos, G., Eliopoulou, E., Francescutto, A., Hamann, R., Lindroth, D., Luhmann, H., Ruponen, P. and Zaraphonitis, G. (2023). A Framework for Probabilistic Damage Stability Assessment of Passenger Ships Considering Collision, Grounding and Contact accidents, in *Contemporary Ideas on Ship Stability – From Dynamics to Criteria*, Spyrou, K. et al., eds., Springer, pp. 565-587.

Bureau Veritas (2019). Parametric Roll Assessment, Rule Note NR 667 DT R00 E

Caamaño, L. S., González, M. M. Galeazzi, R., Nielsen, U. D. and Casás, V. D. (2023). Application of Real-Time Estimation Techniques for Stability Monitoring of Fishing Vessels, in *Contemporary Ideas on Ship Stability – From Dynamics to Criteria*, Spyrou, K. et al. eds., pp. 351-365.

Campbell, B., Belenky, V., Pipiras, V., Sapsis, T. and Weems, K. (2023). Estimation of Probability of Large Roll Angle with Envelope Peaks over Threshold Method. *Ocean Eng.*, Vol. 290, 116296.

Campbell, B., Weems, K., Belenky, V., Pipiras, V. and Sapsis, T. (2023a). Envelope Peaks over Threshold (EPOT) Application and Verification, in *Contemporary Ideas on Ship Stability – From Dynamics to Criteria*, Spyrou, K. et al., Springer, pp. 265-289.

Chai, W., He, L., Leira, B. J., Sinsabvarodom, C., and Feng, P. (2022). Short-Term Analysis of Ship Capsizing Probability in Random Seas. *Proc. 41st OMAE*, Hamburg, Germany

Chen, J., Li, J., Yu, J., Liu, L. and Zhang, Z. (2023). Numerical study on the effect of water-depth on roll natural period and damping coefficient of DTC in shallow water regions. *Proc. 33rd ISOPE*, Ottawa, Canada.

Cichowicz, J. and Vassalos, D. (2023). A Pragmatic Approach to Roll Damping, in *Contemporary Ideas on Ship Stability – From Dynamics to Criteria*, Spyrou, K. et al., Springer, pp. 509-526.

ClassNK (2023). Guidelines on Preventive Measures against Parametric Rolling (Edition 1.0).

Crowson, H. L. (1963). An Error Analysis in the Digital Computation of the Autocorrelation Function. *AIAA J.,* Vol. 1, No 2, pp. 488–489.

Crowson, H. L. (1963a). Generalization of the Note 'An Error Analysis in the Digital Computation of the Autocorrelation Function'. *AIAA J.,* Vol. 1, No 8, pp. 1968–1969.

Dong, K., Yu, J., Liu, L., Zhang D. and Wang, X. (2023). An Investigation into the Effects of Damaged Compartment on Turning Maneuvers using the Free-running CFD Method. *Ocean Eng.,* Vol. 271, 113718.

Dostal, L., Hollm, M. and Maki, A. (2023). First Passage Times for Nonlinear Ship Dynamics using Gaussian Random Fields and Effective Waves. *Ocean Eng.*, Vol. 281, 114751.

Duan, J. W., Ma, N., Shi, Q. Q., Gu, X. C. and Li, X. (2023). An Improved Method for Dynamic Assessment of Survivability of Damaged Ships in Waves. *Proc. 19th ISSW*, Istanbul, Turkey.

Edwards, S. J., Troesch, A. W. and Collette, M. (2021). Estimating Extreme Characteristics of Stochastic Non-linear Systems. *Ocean Eng.* Vol. 233, 109042.

Edwards, S. J., Levine, M. and Harler, J. (2023). An Improved Method for Operational Guidance in Bimodal Seas. *Proc. 19th ISSW*, Istanbul, Turkey.

EMSA, (2023). Annual Overview of Marine Casualties and Incidents.

Feng, P., Cai, Y., Zhou, Y., Fan, S., and Ma, N. (2023). Complements to Level 2 Surf-riding/Broaching Vulnerability Criterion Regarding Waterjet Propelled Ships and Wave Surge Force Correction. *Ocean Eng.* Vol. 272, 113843.

Francescutto, A. (2023). Rahola Criterion and the Development of the Intact Stability Code. in *Contemporary Ideas on Ship Stability – From Dynamics to Criteria*, Spyrou, K. et al. eds., pp. 131-140.

Gao, Z. and Tian, X. (2021). Numerical Study on the Wave-Induced Roll Motion of a Damaged Ship in Head Seas. *Applied Ocean Research*, Vol. 114, 102805.

Glotzer, D., Pipiras, V., Belenky, V., Weems, K. and Levine, M. (2023). Statistical Inference for Mean and Variance of Oscillatory Processes. *Ocean Eng.*, Vol. 289, 116215.

Glotzer, D., Pipiras, V., Belenky, V., Weems, K., and Sapsis, T. P. (2024). Distributions and Extreme Value Analysis of Critical Response Rate and Split-time Metric in Nonlinear Random Oscillators. *Ocean Eng.* Vol. 292, 116538.

Gong, J., Li, Y., Yan, S. and Ma, Q. (2022). Numerical Simulation of Turn and Zigzag Maneuvers of Trimaran in Calm water and Waves by a Hybrid Method. *Ocean Eng.* Vol. 253, 111239.

González, M. M., Bulian, G., Caamaño, L. S., García,, S .A. and Casás V. D. (2023). Real-time Estimation of Natural Roll Frequency for the Stability Guidance of Fishing Vessels. in *Contemporary Ideas on Ship Stability – From Dynamics to Criteria*, Spyrou, K. et al. eds., Springer, pp. 367-383.

González, M. M., Casás, V. D., Peña, F. L. and Pérez Rojas, L. (2023a). On the Application of Artificial Neural Networks for the Real Time Prediction of Parametric Roll Resonance. in *Contemporary Ideas on Ship Stability – From Dynamics to Criteria*, Spyrou K. et al. eds., Springer pp. 335-349.

Gu, M., Lu, J. and Wang, T. H. (2014). Experimental and Numerical Study on Roll Restoring Variation using the C11 Containership. *Proc. 14th ISSW*, Kuala Lumpur, Malaysia.

Guth, S. and Sapsis, T. P. (2022). Wave Episode based Gaussian Process Regression for Extreme Event Statistics in Ship Dynamics: Between the Scylla of Karhunen-Loève Convergence and the Charybdis of Transient Features. *Ocean Eng.*, Vol. 266, 112633.

Hashimoto, H. and Umeda, N. (2004). Nonlinear Analysis of Parametric Rolling in Longitudinal and Quartering Seas with Realistic Modelling of Roll-restoring Moment. *J. Marine Sci. and Tech.*, Vol. 9, No 3, pp. 117–126.

Hashimoto, H., Umeda, N. and Sakamoto, G. (2007). Head-sea Parametric Rolling of a Car Carrier. *Proc. 9th ISSW*, Hamburg, Germany.

Hashimoto, H. and Umeda, N. (2010). A Study on Quantitative Prediction of Parametric roll in Regular Waves. *Proc. 11th ISSW*, Wageningen, the Netherlands.

Hashimoto, H., Omura, T., Matsuda, A., Yoneda, S., Stern, H., and Tahara, Y. (2019). "Several remarks on EFD and CFD for ship roll decay", *Ocean Eng.*, Vol. 186, pp. 371-382

Hashimoto, H. and Furusho, K. (2021).Application of Operational Limitations to the Parametric Rolling Failure Mode. *Proc. 1st STAB&S*, Glasgow, Scotland, UK

Hashimoto, H., Taniguchi, Y. and Fujii, M. (2023). A Case Study on Operational Measures for Avoiding Parametric Rolling. in *Contemporary Ideas on Ship Stability – From Dynamics to Criteria*, Spyrou, K. et al. eds., Springer, pp. 307-321.

Hinz, T., Krata, P., Malinowska, K., Montewka, J. and Matusiak, J. (2022). Evaluation of Stability Criteria Limiting the Angle of Heel due to Turning, in the Light of Ship Motion Simulation Results. *Proc. 18th ISSW,* Gdańsk, Poland.

Hori, T. (2021). Proof that the Center of Buoyancy is Equal to the Center of Pressure by Means of the Surface Integral of Hydrostatic Pressure acting on the Inclined Ship. *Bulletin of the Nagasaki Institute of Applied Science*, Vol. 61, No. 2, pp. 135-154.

Howard, D., Edwards, S. J., Levine, M. D., Sapsis, T., Weems, K., and Pipiras, V. (2022). A Method for Operational Guidance in Bimodal Seas. *Proc. 18th ISSW*, Gdańsk, Poland.

Hu, S. L. J., Yang, W. L., and Li, H. J. (2013). Signal Decomposition and Reconstruction Using Complex Exponential Models. *Mech. Syst. Signal Process*. Vol. 40, No 2, pp. 421–438.

Hu, L., Wu, H., Yuan, Z., Li, W., and Wang, X. (2021). Roll Motion Response Analysis of Damaged Ships in Beam Waves. *Ocean Eng.* Vol. 227, 108558.

Hu, S., and Zhou, L. (2023). Stochastic Hopf Bifurcation and Random Chaos of the Ship Rolling Dynamic System in Random Longitudinal Wave Induced by GWN. *Ocean Eng.* 286, 115572.

Igbadumhe, J. F., Sallam, O., Bonoli, J., Dzielskim, J. and Fürth, M. (2022). Equivalent Linear Roll Damping of a FPSO Coupled with Liquid Sloshing in a Pair of Two-row Tanks. *Ocean Eng.*, Vol. 255, 111162.

IMO International Code on Intact Stability. London, 2008.

IMO MSC.1/Circ.1627, Interim Guidelines on the Second Generation Intact Stability Criteria, London, December 2020.

IMO MSC. 1/Circ.1652, Explanatory Notes for Interim Guidelines on the Second Generation Intact Stability Criteria, London, April 2023

IMO SDC 8/INF.2 Physical Background and Mathematical Models for Stability Failures of the Second Generation Intact Stability Criteria. Submitted by ITTC, London 2021.

IMO SDC 10/INF.7 ITTC Support of the Trial Application of Direct Stability Assessment within the Second Generation Intact Stability Criteria, Submitted by ITTC, London, 2023.

Jiang, Y., Wang, M., Bai, J., Sun, Y., and Li, J. (2023). Effects of Outrigger Configuration on Trimaran Stability in Longitudinal Waves. *Ocean Eng.*, Vol. 280, 114500.

Kapsenberg, G., Wandji, C., Duz, B. and Kim, S. (2020). A Comparison of Numerical Simulations and Model Experiments on Parametric Roll in Irregular Seas. *J. of Marine Sci. and Eng.*, Vol 8, 474.

Karolius, K., Chichowicz, J. and Vassalos, D. (2020). Risk-based, Sensor-fused Detection of Flooding Casualties for Emergency Response. *Ships and Offshore Structures*, Vol. 16, No. 5, pp. 1-30.

Katayama, T., Kankaku, M., Yildiz, B., Sugimoto, K. and Fukumoto, Y. (2021). Characteristics of Roll Damping of Pure Car Carrier and Liquefied Natural Gas Carrier and Applicability of Ikeda`s Method with Some Modifications. *Proc. 1st STAB&S*, Glasgow, Scotland, UK.

Katayama, T., Yoshida, N., Yamamoto, Y. (2022). Effects of Free Surface on Normal Force Component of Bilge Keel Roll Damping and Improvement of Ikeda's Method. *Proc. 18th ISSW*, Gdańsk, Poland.

Katayama, T., Yoshida, N., Yamamoto, Y., Kashiwagi, M., and Ikeda Y. (2022a). Correction of Eddy Making Component of Ikeda's Method and its Modification for Shallow Draught Effects. *Proc. 18th ISSW*, Gdańsk, Poland.

Katayama, T., and Yoshida, N. (2023). Effects of Half Breadth to Draught Ratio on Pressure Distribution on Hull caused by Bilge Keels. *Proc. 19th ISSW*, Istanbul, Turkey.

Katayama, T., Kankaku, M., Maki, A., Sugimoto, K. and Fukumoto, Y. (2023a). Study on Short-Term Prediction of Roll in Beam Sea, in *Contemporary Ideas on Ship Stability – From Dynamics to Criteria*, Spyrou, K. et al. eds., Springer, pp. 133-156.

Kawamura, K and Hino, T. (2023). Development of a Coupled Method of Finite Volume and Particle Methods Based on Peer-to-Peer File Exchange. *Proc. 33rd ISOPE*, Ottawa, Canada.

Kiefer, N. M. and Vogelsang, T. J. (2002). Heteroskedasticity Autocorrelation Robust Testing using Bandwidth Equal to Sample Size. *Econometric Theory*, Vol. 18, No. 6, pp. 1350–1366.

Kim, D. H. and Troesch, A. W. (2013). Statistical Estimation of Extreme Roll Responses in Short Crested Irregular Head Seas. *Tr. SNAME*, Vol. 121.

Kim, D. H. and Troesch, A. W., (2019). Stochastic Wave Inputs for Extreme Roll in Near Head Seas, in *Contemporary Ideas on Ship Stability. Risk of Capsizing*, Belenky, V. et al. eds., Springer, pp. 393-405.

Kim, M., Pipiras, V., Reed, A. M. and Weems, K. (2023). Calibration of Low-fidelity Ship Motion Codes through Regressions of High-fidelity Forces. *Ocean Eng.*, Vol. 290, 116321.

Koop, O. R., Renac, L., de Haas. J., Onassis. J. (2021). Parametric Roll Excited by Low Wave Heights: a New Method to Avoid Critical Sea States Based on 2D Spectra. *Proc. 1st STAB&S*, Glasgow, Scotland, UK.

Koromila, I. A., Spandonidis, C. C. and Spyrou, K. J. (2023). Liquefaction of Sand and Olive Pomace Cargo and its Effect on the Stability of a Bulk-carrier, in *Contemporary Ideas on Ship Stability – From Dynamics to Criteria*, Spyrou K. et al. eds., Springer, pp. 679-690.

Krüger, S. and Aschenberg, K. (2021). Adding Damaged Zones to a Nonzonal Damage Stability Approach. *Proc. 1st STAB&S*, Glasgow, Scotland, UK.

Lee, G. J., van Walree, F., Reed, A. M., Peters, A., Gualeni, P., Katayama, T. and Duan, W. Y. (2023). The Inertia Contributions due to Floodwater Mass, in *Contemporary Ideas on Ship Stability – From Dynamics to Criteria*, Spyrou K. et al. eds., Springer, pp. 545-554.

Lee, G. J., van Walree, F., Reed, A. M., Peters, A., Gualeni, P., Katayama, T. and Duan, W. Y. (2023). Air Pressure Scale Effects during Damage Model Tests, in *Contemporary Ideas on Ship Stability – From Dynamics to Criteria*, Spyrou, K. eds., Springer, pp. 555-564.

Leguen, J.-F., Billard, J.-Y. and Grinnaert, F. (2023). Errors Induced by Wind Fluctuations during Inclining Test in Waves. *Proc. 19th ISSW*, Istanbul, Turkey, pp. 127-132.

Levine, M., Belenky V. and Weems, K. (2021). Method for Automated Safe Seakeeping Guidance. *Proc. 1st STAB&S*, Glasgow, Scotland, UK.

Levine, M. D., Edwards, S. J., Howard, D., Sapsis T., Weems K., Pipiras V. and Belenky, V. (2022). Data-Adaptive Autonomous Seakeeping. *Proc. 34th Symp. Naval Hydrodynamics*, Washington D.C., USA.

Levine, M. D., Edwards, S. J., Howard, D., Sapsis, T., Weems, K., and Pipiras, V. (2024). Multi-Fidelity Data-Adaptive Autonomous Seakeeping. *Ocean Eng*. Vol. 292, 116322.

Li, J., Chen, J., Yu, J., Liu, L., and Zhang, Z. (2023). CFD Prediction for the Extreme Roll Motion of ONR Tumblehome in Beam Waves. *Proc. 33rd ISOPE*, Ottawa, Canada.

Li, X., Ma, N., Shi, Q. and Gu, X. (2023a). Real-Time Prediction of Parametric Roll Motion Based on Power-Activation Feed-Forward Neural Network Using Measured Data from Model Experiments. *Proc. 33rd ISOPE*, Ottawa, Canada.

Liu, L., Chen M., Wang, X., Zhang, Z., Yu J., and Feng, D. (2021). CFD prediction of Full-scale Ship Parametric Roll in Head Wave. *Ocean Eng.* Vol. 233, 109180.

Liu, L., Feng, D., Wang, X., Zhang, Z., Yu, J., and Chen, M. (2022). Study on Extreme Roll Event with Capsizing Induced by Pure Loss of Stability for the Free-running ONR Tumblehome. *Ocean Eng.* Vol. 257, 111656.

Liu, L., Feng, D., Wang, X., Zhang, Z., Yu, J., and Chen, M. (2022a). Numerical Study on the Effect of Sloshing on Ship Parametric Roll. *Ocean Eng.* Vol. 247, 110612.

Liu, L., Yao, C., Feng, D., Wang, X., Yu, J. and Chen M. (2022b). Numerical Study of the Interaction between the Pure Loss of Stability, Surf-riding, and Broaching on Ship Capsizing. *Ocean Eng.* Vol. 266, 112868.

Liu, Y., Liu, L., Dostal, L., and Lu, J. (2022c). The Applicability of Stochastic Averaging Method to Solve the Ship Rolling Response Excited by Narrow-band Waves. *Ocean Eng.* Vol. 251, 111109.

Liu, Y., Liu, L., Maki, A., Lu, J., and Dostal, L. (2023). The Improvement of Stochastic Averaging Method to Solve the Ship Rolling Response Excited by Narrow-band Waves. *Ocean Eng.* Vol. 281, 114737.

Liu, Y., Liu, L., Maki, A., Bu, S. and Dostal, L. (2023a). Research on Second Level of Vulnerability Criteria of Parametric Rolling with Stochastic Stability Theory. *Ocean Eng.* Vol. 284, 115043.

Louvros, P., Stefanidis, F., Boulougouris, E., Komianos, A. and Vassalos, D. (2023). Machine Learning and Case-Based Reasoning for Real-Time Onboard Prediction of the Survivability of Ships. *J. of Marine Sci. and Eng.* Vol. 11, No 5, 890.

Lu, J., Gu, M., and Umeda, N. (2017). Experimental and Numerical Study on Several Crucial Elements for Predicting Parametric Roll in Regular Head Seas *J of Marine Sci. and Tech.*, Vol. 22, No 1, pp. 25-37.

Lu, J., Gu, M., Wang, T., Bu, S., Zeng, K. and Chu, J. (2021). Study on a New Stability Failure Model in Stern Quartering Waves. *Proc. 1st STAB&S*, Glasgow, Scotland, UK.

Lu, J. and Gu, M. (2023). A Unified Mathematical Model for Direct Stability Assessments of Surf-riding/Broaching and Pure Loss of Stability in Stern Quartering Waves. *Proc. 19th ISSW*, Istanbul, Turkey.

Lu, Y., and Park, J. Y. (2019). Estimation of Longrun Variance of Continuous Time Stochastic Process using Discrete Sample. *J. Econometrics* Vol. 210, pp. 236–267.

Luthy, V., Grinnaer, F. and Billard, J.-Y. (2021). Computation of Parametric Roll Amplitude using Energy Method Considering Non-linear GZ in Resonance Condition. *Proc. 1st STAB&S*, Glasgow, Scotland, UK

Luthy, V., Grinnaert, F., Billard, J.-Y., Delhaye, T., Claudel, R. and Leguen, J.-F. (2021). An Iterative Method to Estimate Damping Coefficients from Roll Decay Time Series. *Proc. 1st STAB&S*, Glasgow, Scotland, UK.

Luthy, V., Grinnaert, F. and Billard, J.-Y. (2022). Computation of Parametric Roll Amplitude using Energy Method Considering Non-linear Transverse Stability. *Ocean Eng.* Vol. 263, 112416.

Luthy, V., Grinnaert, F. and Billard, J.-Y. (2022). Identification of a Conservative Spreading Angle to Realize Operational Roll Polar Plots. *Proc. 18th ISSW*, Gdańsk, Poland.

Lyu W., el Moctar, O. and Schellin, T. E. (2022). Ship Motion-Sloshing Interaction with Forward Speed in Oblique Waves. *Ocean Eng.*, Vol. 250, 110999.

Ma, C., Ma, N., Gu, X. and Duan, J. (2021). Course Stability Assessment of a Ship on Surf-riding Conditions using the Computed Hydrodynamics Derivative by CFD. *Proc. 1st STAB&S*, Glasgow, Scotland, UK.

Ma, S., Ge, W. P., Ertekin, R. C., He, Q., and Duan, W. Y. (2018). Experimental and numerical investigations of ship parametric rolling in regular head waves. *China Ocean Eng.*, Vol. 32, No 4, pp. 431-442.

Maki, A. (2017). Estimation Method of the Capsizing Probability in Irregular Beam Seas using Non-Gaussian Probability Density Function. *J. of Marine Sci. and Tech.*, Vol. 22, No 2, pp. 351–360.

Maki, A., Dostal, L., Maruyama, Y., Sakai, M. and Umeda, N. (2021). New Aspects of Stochastic Evaluation of Random Roll Motion of Ship, *Proc. 1st STAB&S*, Glasgow, Scotland, UK.

Maki, A., Dostal, L. Maruyama, Y., Sasa, K., Sakai, M. and Umeda, N. (2022). Enhanced Estimation Method and Approximation method of the PDF of Roll Angular Acceleration and Jerk in Beam Seas. *Ocean Eng.*, Vol. 264, 112159.

Maki, A., Maruyama, Y., Sakai, M., and Dostal, L. (2023). Recent Results on Wind and Wave Generation, Stability of Parametric Rolling, Method of Moment Equation and Maneuvering Stability for Ship Dynamics in Irregular Seas. *Proc. 19th ISSW*, Istanbul, Turkey, pp. 133-140.

Maruyama, Y., Maki, A., and Umeda, N. (2022). Application of Linear Filter and Moment Equation for Parametric Rolling in Irregular Longitudinal Waves. *J. of Marine Sci. and Tech.*, Vol. 27, pp. 1252-1267.

Maruyama, Y., Maki A., and Dostal, L. (2022a). Stochastic Assessment Using Moment Equation Method for Parametric Rolling of Ships in Random Seaways. *Proc. 18th ISSW*, Gdańsk, Poland.

Maruyama, Y., Maki, A., Dostal, L., and Umeda, N. (2022b). Improved Stochastic Averaging Method using Hamiltonian for Parametric Rolling in Irregular Longitudinal Waves. *J. of Marine Sci. and Tech.,* Vol. 27, No 1, pp. 186-202.

Masamoto, S., Umeda, N., Subramaniam, S., and Matsuda, A. (2023). Experimental Study of the Water on Deck Effects on the Transverse Stability of a Fishing Vessel Running in Stern Quartering Seas. *Ocean Eng.*, Vol. 289, 116289.

Matsubara, K., Umeda, N. and Matsuda, A. (2021). Probabilistic Estimation of the Large Heel due to Broaching Associated with Surf-riding for a Ship in Short-crested Irregular Waves and its Experimental Validation, *Proc. 1st STAB&S*, Glasgow, Scotland, UK.

Matsubara, K., Umeda, N., and Matsuda, A. (2023). Probabilistic Estimation of the Large Heel due to Broaching Associated with Surf-riding for a Ship in Short-crested Irregular Waves and its Experimental Validation. *Ocean Eng.*, Vol. 269, 113540.

Matsuda, A., Hashimoto, H., Terada, D. and Taniguchi, Y. (2016). Validation of Free running Model Experiments in Heavy Seas, *Proc. of 3rd Intl. Conf. on Violent Flows (VF-2016)*, Osaka, Japan.

Matsuda, A., Terada, D. and Hashimoto H. (2023). Characteristics of Capsizing Phenomena of Fishing Vessels in *Contemporary Ideas on Ship Stability – From Dynamics to Criteria*, Spyrou, K., et al. eds., Springer, pp. 643-658.

Mauro, F., Paterson, M., Michalec, R., Boulougouris, E. and Vassalos, D. (2021). Damage Stability of Passenger Ships: Smart Methods to Identify Critical Scenarios, *Proc. 1st STAB&S*, Glasgow, Scotland, UK.

Mauro, D., Vassalos, D., Paterson, D. and Boulougouris, E. (2023). Evolution of Ship Dam-age Stability Assessment—Transitioning Designers to Direct Numerical Simulations. *Ocean Eng.* Vol. 268, 113387.

Mauro, F., Conti, F. and Vassalos, D. (2023a). Damage Surrogate Models for Real-time Flooding Risk Assessment of Passenger Ship. *Ocean Eng.* Vol. 285, Part 2, 115493.

Mohamad M. A. and Sapsis, T. (2018). Sequential Sampling Strategy for Extreme Event Statistics in Nonlinear Dynamical Systems. *Proc. Natl. Acad. of Sciences of United States of America* PNAS Vol. 115, 11138-43.

Mughadar-Palliparambil, M. A., Vassalos, D. and Boulougouris, E. (2021). Development of Collision and Grounding Accident Database for Large Passenger Ships. *Proc. 1st STAB&S*, Glasgow, Scotland, UK.

Munakata, S., Takagaki, K., Umeda, N., Koike, H., Maki, A., Manabe, K. and Matsuda, A. (2021). An Investigation into False-negative Cases for Low Freeboard Ships in Vulnerability Criteria of Dead Ship Stability. *Proc. 1st STAB&S*, Glasgow, Scotland, UK.

Neves M.A.S., Belenky V., de Kat J. O., Spyrou K. and N. Umeda, eds. (2011). Contemporary Ideas on Ship Stability and Capsizing in Waves, Springer Series Fluid Mechanics and its Application Vol. 97, ISBN 978-94-007-1481-6.

Paterson, D., Mauro, F. and Vassalos, D. (2023). Ship Vulnerability Assessment by Forensic Investigation of Critical Damage Scenarios. *Proc. 19th ISSW*, Istanbul, Turkey, pp. 47-62.

Paulling, J. R. (1961). The transverse stability of a ship in a longitudinal seaway. *J. of Ship Research*, Vol. 4, No 4, pp. 37-49.

Pollard, J. and Dudebout, A. (1892). Théorie du Navire, Vol. 3.

Petacco N., Vernengo, G., Villa, D., Coppedé, A., and Gualeni, P. (2021). Influence of Systematic Hull Shape Variations on Ship Stability Performances in Waves, *J. of Ship Research*, Vol. 65, No 3, pp. 243-256.

Peters, W. and Belenky V. (2021). An alternative Vulnerability Criteria: An Example Presentation Format for Pure Loss of Stability. *Proc. 1st STAB&S*, Glasgow, Scotland, UK.

Peters, W. and Belenky, V. (2023). On Regulatory Consistency of Criteria for Dead Ship Condition and Pure Loss of Stability, in *Contemporary Ideas on Ship Stability – From Dynamics to Criteria*, Spyrou, K. et al., eds., Springer, pp. 73-92.

Peters, W., Belenky, V and Spyrou, K. (2023). Safety Level of the IMO Second Generation Intact Stability Criteria, in *Contemporary Ideas on Ship Stability – From Dynamics to Criteria*, Spyrou K. et al., eds., Springer pp. 35-57.

Peters W., Belenky V. and Spyrou, K. (2023a). Regulatory use of Nonlinear Dynamics: an Overview, in *Contemporary Ideas on Ship Stability – From Dynamics to Criteria*, Spyrou K. et al., eds., Springer, pp. 113-127.

Pickering, E., Guth, S., Karniadakis, G. E. and Sapsis, T. P. (2022). Discovering and Forecasting Extreme Events via Active Learning in Neural Operators. *Nature Comp. Sci.* Vol. 2, No 12, pp. 823-833.

Pineau, J.-P., Conti, F, Le Sourne, H, and Looten, T. (2022). A Fast Simulation Tool for Ship Grounding Damage Analysis. *Ocean Eng.* Vol. 262, 112248.

Pipiras, V., Glotzer, D., Belenky, V., Levine, M. and Weems, K. (2018). On Confidence Intervals of Mean and Variance Estimates of Ship Motions. *Proc. 13th STAB*, Kobe, Japan.

Pipiras, V. (2020). Pitfalls of Data-driven Peaks-over-Threshold Analysis: Perspectives from Extreme Ship Motions. *Probabilistic Eng. Mech.*, Vol. 60, 103053.

Priestley, M. B. (1981). Spectral Analysis and Time Series. Volume 1, Academic Press.

Rahola, J. (1939). The Judging of the Stability of Ships and the Determination of the Minimum Amount of Stability—Especially Considering the Vessels Navigating Finnish Waters. Doctoral thesis, Helsinki, https://aaltodoc.aalto.fi/handle/123456789/15149.

Rajaraman, R. and Hariharan, G. (2023). Estimation of Roll Damping Parameters using Hermite Wavelets: An Operational Matrix of Derivative Approach. *Ocean Eng.,* Vol. 283, 115031.

Reed, A. M. (2021). Predicting Extreme Loads and the Processes for Predicting Them Efficiently, *Proc. 1st STAB&S*, Glasgow, Scotland, UK.

Reed, A. M. (2023). Verification, Validation and Accreditation in the Context of the IMO Second Generation Intact Stability Criteria and the Role of Specific Intended Uses in this Process", in *Contemporary Ideas on Ship Stability – From Dynamics to Criteria*, Spyrou K. et al., eds., Springer, pp. 211-223.

Reed, A.M. (2023a). Interpretation of Results of Numerical Simulation, in *Contemporary Ideas on Ship Stability – From Dynamics to Criteria*, Spyrou, K. et al., eds., Springer, pp. 291-303.

Rodríguez, C.A., Ramos, I. S., Esperanca, P. T. T. and Oliveira, M. C. (2022). Assessment of Damping and Nonlinearities on the Roll Responses of a VLCC in Waves without Forward Speed. *Proc. 18th ISSW*, Gdańsk, Poland, pp. 33-42.

Rodríguez, C. A., Polo J. C. F. and Neves, M. A. S. (2023). Experimental and Numerical Investigation on Parametrically-Excited Motions of a Mono-column Platform in Waves. in *Contemporary Ideas on Ship Stability – From Dynamics to Criteria*, Spyrou, K. et al., eds., Springer, pp. 693-709.

Rudaković, S. and Bačkalov, I. (2023). On Application of Standard Methods for Roll Damping Prediction to Ships with High Block Coefficient, in *Contemporary Ideas on Ship Stability – From Dynamics to Criteria*, Spyrou, K et al., eds., Springer, pp. 483-508.

Ruponen, P., van Basten Batenburg, R., Bandringa, H., Braidotti, L., Bu, S., Dankowski, H., Lee, G.J., Mauro, F., Murphy, A., Rosano, G., Ruth, E., Tompuri, M., Valanto, P. and van't Veer, R. (2021). Benchmark Study on Simulation of Flooding Progression. *Proc. 1st STAB&S*, Glasgow, Scotland, UK.

Ruponen, P., van Basten Batenburg, R., van't Veer, R., Braidotti, L., Bu, S., Dankowski¸ H., Lee, G. J., Mauro, F., Ruth, E. and Tompuri, M. (2022). International Benchmark Study on Numerical Simulation of Flooding and Motions of a Damaged Cruise Ship, *Applied Ocean Research*, Vol. 129, 103403.

Ruponen, P., Valanto, P., Acanfora, M., Dankowski, H., Lee, G. J., Mauro, F., Murphy, A., Rosano, G. and van't Veer, R. (2022a). Results of an International Benchmark Study on Numerical Simulation of Flooding and Motions of a Damaged Ropax Ship, *Applied Ocean Research*, Vol. 123, 103153.

Sadat-Hosseini, H., Stern, F., Olivieri, A., Campana, E. F., Hashimoto, H., Umeda, N., Bulian, G. and Francescutto, A. (2010). Head-Wave Parametric Rolling of a Surface Combatant. *Ocean Eng.,* Vol. 37, pp. 859-878.

Schrøter, C., Lützen, M., Erichsen, H., Jensen, J. J., Kristensen, H. O., Lauridsen, P. H., Tunccan, O. and Baltsersen, J. P. (2023). Second Generation Intact Stability Criteria – Robustness and Consistency Analysis. in *Contemporary Ideas on Ship Stability – From Dynamics to Criteria*, Spyrou, K., et al., eds., Springer, pp. 59-71.

Shigunov, V., Wandji, C. W. and Belenky, V. (2022). Benchmarking of Direct Counting Approaches. *Proc. 18th ISSW*, Gdansk, Poland, pp. 167-175

Shigunov, V. (2023). Extrapolation of Failure Rate over Wave Height. *Ocean Eng.*, Vol. 272, 113801.

Shigunov, V. (2023a). Intact stability operational measures: Criteria, standards and examples. *Ocean Eng.*, Vol. 279, 114751.

Shigunov, V. (2023b). Simplifications in Direct Stability Assessment, in *Contemporary Ideas on Ship Stability – From Dynamics to Criteria*, Spyrou, K. et al., eds., Springer, pp. 93-112.

Shin, Y. S, Belenky, V., Lin, W. M., Weems, K. and Engle, A. H. (2003). Nonlinear Time Domain Simulation Technology for Seakeeping and Wave-load Analysis for Modern Ship Design. *SNAME Trans*. Vol. 111, pp. 557-578.

Silva, K. M. and Maki, K. J. (2021). Towards a Computational Fluid Dynamics Implementation of the Critical Wave Groups Method. *Ocean Eng.* Vol. 235, 109451.

Silva, K. M. and Maki, K. J. (2022). Data-Driven System Identification of 6-DOF Ship Motion in Waves with Neural Networks. *Applied Ocean Research*, Vol. 125, 103222.

Silva, K. M. and Maki, K. J. (2022a). Towards a Generalized Neural Network Approach for Identifying Critical Wave Groups. *Proc. 18th ISSW*, Gdańsk, Poland.

Silva, K. M., Knight, B. G. and Maki, K. J. (2022). Numerical Prediction of Extreme Roll of a Free-Running Ship with Computational Fluid Dynamics and Neural Networks. *Proc. 34th Symp. on Naval Hydrodynamics*, Washington D.C., USA.

Silva, K. (2023). A Computational Fluid Dynamics Driven Machine-Learning Framework for Observation and Quantification of Extreme Ship Responses (Ph.D. thesis). The University of Michigan, Ann Arbor, Michigan, USA.

Silva, K. M. and Maki, K. J. (2023). Implementation of Critical Wave Groups Method with Computational Fluid Dynamics and Neural Networks. *Ocean Eng.*, Vol. 292, 116468.

Silva, K. M., and Maki, K. J. (2023a). Considerations for a Free-running Implementation of the Critical Wave Groups Method. *Proc. 19th ISSW*, Istanbul, Turkey.

Smith, T. (2019). Validation Approach for Statistical Extrapolation, in *Contemporary Ideas on Ship Stability. Risk of Capsizing*, Belenky, V., et al. eds., Springer, pp. 573-589.

Spyrou, K. J., Belenky, V., Reed, A., Weems, K., Themelis, N. and Kontolefas, I. (2014). Split-Time Method for Pure Loss of Stability and Broaching-To. *Proc. 30th Symp. Naval Hydrodynamics,* Hobart, Tasmania, Australia.

Spyrou, K. J. (2022). The Stability of Floating Regular Solids. *Ocean Eng.*, Vol. 257, 111615.

Spyrou, K. J. (2023). Contemporary Ideas on Ship Stability: From Dynamics to Criteria—an Overview, in *Contemporary Ideas on Ship Stability – From Dynamics to Criteria*, Spyrou, K. et al., eds, Springer, pp. 3-27.

Spyrou K. J., Themelis N., and Kontolefas, I. (2023). Estimates of the Probability of Surf-riding in Irregular Seas. in *Contemporary Ideas on Ship Stability – From Dynamics to Criteria*, Spyrou, K. et al. eds., Springer, pp. 387-399.

Spyrou, K. J., Kontolefas, I. and Themelis, N. (2023a). Abnormal High Speed Ship Motions in Two-frequency and Multi-frequency Following Waves, in *Contemporary Ideas on Ship Stability – From Dynamics to Criteria*, Spyrou, K. et al., eds., Springer, pp. 401-412.

Subramaniam, S., Umeda, N., Matsuda, A. and Maki, A. (2021). Experimental Study on the Water-on-deck Effect for an Offshore Supply Vessel Running in Regular and Irregular Stern Quartering Waves, *Proc. 1st STAB&S*, Glasgow, Scotland, UK.

Sun, Y. (2014). Let's Fix it: Fixed-b Asymptotics versus Small-b Asymptotics in Heteroskedasticity and Autocorrelation Robust Inference. *J. Econometrics*, Vol. 178, pp. 659–677.

Taguchi, H. and Kuroda, T. (2018). An Investigation into the Capsizing Accident of a Purse Seiner in Hauling a Fishing Net. *Proc. 13th STAB*, Kobe, Japan.

Taguchi, H., Matsuda, A. and Shoji, K. (2023). Experimental Investigations into Accidents of Two Japanese Fishing Vessels, *in Contemporary Ideas on Ship Stability – From Dynamics to Criteria*, Spyrou K. et al., eds., Springer, pp. 661-675.

Themelis N. and Spyrou, K. J. (2007). Probabilistic Assessment of Ship Stability. *SNAME Trans.*, Vol. 115, pp. 181-206.

Tigkas, I. G. and Spyrou, K. (2023). Hybrid Surging and Surf-riding Motions of a Ship in Steep Bi-chromatic Following Seas. *Ocean Eng.*, Vol. 269, 113522.

Tsoumpelis, D. and Spyrou, K. J. (2023). Identification of Recurring Patterns and Repetitions in Time-series, with Application to Pseudo-stochastic Ship Rolling. *Ocean Eng.* Vol. 271, 113717.

Uchida, Y., Sakai, M., and Umeda, N. (2022). Methodology for Assessing Fundamental Parametric Roll other than the Principal Parametric Roll, *Proc. 18th ISSW*, Gdańsk, Poland.

Umeda J., Katayama T., Hashimoto H. and Yildiz, B. (2023). Study on Bilge Keel Component of Roll Damping for Non-Periodic Motion, in *Contemporary Ideas on Ship Stability – From Dynamics to Criteria*, Spyrou, K. et al., eds., Springer, pp. 475-492

Umeda, N. (1990). Probabilistic Study on Surf-Riding of a Ship in Irregular Following Seas. *Proc. 4th STAB*, Napoli, Italy.

Umeda, N., Munif, A. and Hashimoto, H. (2000). Numerical Prediction of Extreme Motions and Capsizing for Intact Ships in Following/ Quartering Seas. *Proc. 4th Osaka Colloq. on Seakeeping Perf. of Ships*, Osaka, Japan.

Umeda N., Hashimoto H., Sakamoto G. and Urano, S. (2005). Research on Estimation of Roll Restoring Variation in Waves. *Proc. Kansai Soc. of Naval Arch.*, Vol. 24, pp. 17-19.

Umeda N., Shuto M. and Maki, A. (2007). Theoretical Prediction of Broaching Probability for a Ship in Irregular Astern Seas. *Proc. 9th ISSW*, Hamburg, Germany.

Umeda, N. and Francescutto, A. (2023). The Second Generation Intact Stability Criteria - Achievements and Remaining Issues, in *Contemporary Ideas on Ship Stability – From Dynamics to Criteria*, Spyrou, K. et al., eds., Springer, pp. 21-34.

Umeda, N., Kawaida, D., Ito, Y., Tsutsumi, Y., Matsuda, A. and Terada, D. (2023a). Overview of Model Test Procedures for Stability under Dead Ship Condition and Pure Loss of Stability in Astern Waves. in *Contemporary Ideas on Ship Stability – From Dynamics to Criteria*, Spyrou, K. et al., eds., Springer, pp. 609-623.

Umeda, N., Maruyama, Y., Okamoto, S., Oka, A., Masamoto, S. and Matsuda, A. (2023b). Filling Gaps in Direct Stability Assessment Procedures, *Proc. 19th ISSW*, Istanbul, Turkey, pp. 193-200.

Umeda, N., Subramaniam, S., Always, A., Matsuda, A., Maki, A., Usada, S. and Terada, D. (2023c). Model Experiments of an Offshore Supply Vessel Running in Astern Waves. in *Contemporary Ideas on Ship Stability – From Dynamics to Criteria*, Spyrou, K. et al. eds., Springer, pp. 625-642.

Valanto, P. and Schumacher, A. (2021). On the Roll Damping of Intact and Damaged Ships. *Proc. 1st STAB&S*, Glasgow, Scotland, UK.

Valanto, P. (2023). On Boundary Conditions for Damage Openings in RoPax-Ship Survivability Computations. *J. of Marine Sci. and Eng.*, Vol. 11, No 3, 643.

Vassalos, D., Hamamoto, M., Papanikolaou, A. and Molyneux D., eds. (2000). Contemporary Ideas on Ship Stability Elsevier, ISBN 0-08-043652-8.

Vassalos, D., Mughadar-Palliparambil, M. A., Boulougouris, E., Paterson, D., Mauro, F., and Michalec, R. (2021). Flooding Risk Assessment for Passenger Ship, *Proc. 1st STAB&S*, Glasgow, Scotland, UK.

Vassalos, D. and Paterson, D. (2021). Towards Unsinkable Ships. *Ocean Eng.*, Vol. 232, 109096.

Vassalos, D., Mughadar-Palliparambil, M. A., Paterson, D. and Mauro, F. (2022). Evolution of p-Factors in Probabilistic Damage Stability Assessment of Passenger Ships. *Proc. 18th ISSW*, Gdańsk, Poland.

Vassalos, D., Atzampos, G., Paterson, D., Mauro, F. and Mughadar-Palliparambil, M. A. (2022a). The Vital Role of Permeable Volume in Damage Stability Assessment of Passenger Ships. *Proc. 18th ISSW*, Gdańsk, Poland.

Vassalos, D. Paterson, D. and Mauro, F. (2023). Real-time Flooding Risk Evaluation for ship-to-ship Collisions Based on First Principles. *Ocean Eng.* Vol. 281, 114847.

Vassalos D., Boulougouris E., Guarin L. and Jasionowski, A. (2023a). Regulatory, Design, Operational and Emergency Response Measures for Improving the Damage Survivability of Existing RoPax, in *Contemporary Ideas on Ship Stability – From Dynamics to Criteria*, Spyrou, K. et al., eds., Springer, pp. 529-544.

van‘t Veer R., van den Berg, J., Boonstra, S., van Basten Batenburg, R. and Bandringa, H. (2021). A Steady and Unsteady Internal Flooding Model Utilizing a Network and Graph Solver, *Proc. 1st STAB&S*, Glasgow, Scotland, UK.

Vidic-Perunovic, J. and Jensen, J. J. (2009). Parametric Roll due to Hull Instantaneous Volumetric Changes and Speed Variations. *Ocean Eng.* Vol. 36, No 12-13, pp. 891-899.

Vidić, M. and Bačkalov, I. (2022). An Analysis of Stability Requirements for Large Inland Passenger Ships. *Ocean Eng.* Vol. 261, 112148.

van Walree F. and Sgarioto, D. (2023). Impulsive Loads on, and Water Ingress in, a Landing Craft: Model Tests and Simulations, in *Contemporary Ideas on Ship Stability – From Dynamics to Criteria*, Spyrou, K. et al., eds., Springer, pp. 733-739.

van Walree F. and Thomas, W. L. (2023). Validation of Simulation Tools for a RHIB Operating in Heavy Seas. in *Contemporary Ideas on Ship Stability – From Dynamics to Criteria,* Spyrou, K. et al., eds., Springer, pp. 713-731.

Wandji, C. (2022). Application of Statistical Extrapolation Techniques to Dynamic Stability. *Proc. 18th ISSW*, Gdańsk, Poland.

Wandji, C., Shigunov, V. and Belenky, V. (2023). Testing and Benchmarking of Direct Counting Methods. *Proc. 19th ISSW*, Istanbul, Turkey.

Wandji, C. (2023). Review of Probabilistic Methods for Direct Dynamic Stability of Ships in Random Seaway, in *Contemporary Ideas on Ship Stability – From Dynamics to Criteria*, Spyrou, K. et al. eds., Springer, pp. 189-209.

Wandji C., Shigunov V., Pipiras V. and Belenky, V. (2024). Benchmarking of Direct Counting Approaches, *Ocean Eng.*, Vol. 296, 116649.

Wassermann S. and Abdel-Maksoud, M. (2023). Estimation of Force Coefficients for Bilge Keel and Skin Friction Roll Damping of Ships by CFD Simulations, in *Contemporary Ideas on Ship Stability – From Dynamics to Criteria*, Spyrou, K. et al., eds., Springer, pp. 461-474.

Weems K., and Wundrow, D. (2013). Hybrid Models for Fast Time-Domain Simulation of Stability Failures in Irregular Waves with Volume-Based Calculations for Froude-Krylov and Hydrostatic Force. *Proc. 13th ISSW*, Brest, France.

Weems K. and Belenky, V. (2015). Fast Time-Domain Simulation in Irregular Waves With Volume-Based Calculations for Froude-Krylov and Hydrostatic Force. *Proc. 12th, STAB*, Glasgow, UK.

Weems, K., Sapsis, T. and Pipiras, V. (2022). Development of Reduced Order Models for Hydrodynamic Responses. *Proc. 18th ISSW*, Gdańsk, Poland.

Weems, K., and Belenky, V. (2023). Volume-base Reduced-Order Model for ship motions. *Ocean Eng.* Vol. 289, 116214.

Weems, K., Belenky, V. Campbell, B. and Pipiras, V. (2023). Statistical Validation of the Split-Time Method with Volume-Based Numerical Simulation, in *Contemporary Ideas on Ship Stability – From Dynamics to Criteria*, Spyrou, K. et al. eds., Springer, pp. 225-243.

Weems K., Pipiras V. and Belenky, V. (2023a). Multifidelity Fast Code for Direct Stability Assessment. *Proc. 19th ISSW*, Istanbul, Turkey.

Wu, Q., Bai, S., Zhang, Z., Chen, M. and Xie, Y. (2021). Investigation on Sloshing in a Rectangular Tank based on an Improved MPS Method. *Proc. 31st ISOPE*, Rhodes, Greece.

Wu, S., Liu, L., Wang, X., Chen, J. and Wang, L. (2022). Study of Wavelength Effect on the Parametric Roll in Head Waves. *Proc. 32nd ISOPE*, Shanghai, China.

Xu, W., Maki, K. J. and Silva, K. M. (2021). A Data-Driven Model for Nonlinear Marine Dynamics. *Ocean Eng.* Vol. 236, 109469.

Yang, S. H. (2023). Numerical Study on the Parametric Rolling of Post-Panamax Class Containership based on Mathieu Instability. *Proc. 33rd ISOPE,* Ottawa, Canada.

Yano, T., Umeda, N., Hirayama, K. Baba, M. and Sakai, M. (2023). Wave Radar Application to the Simplified Parametric Roll Operational Guidance at Actual Sea. in *Contemporary Ideas on Ship Stability – From Dynamics to Criteria*, Spyrou, K. et al. eds., Springer, pp. 323-333.

Yu, L., Qu, D., Wang, S. and Ma, N. (2022). On the Probability Estimates of Broaching in Irregular Waves by Direct Counting on Intensive Repeated Simulations. *Ocean Eng.* Vol. 266, 112854.

Yu, Y., Zhu, R, Lu, Z, Shi, K and Huang, S. (2023). Investigation on Time-domain Simulation and Experiment of Harmonic Rolling of Ultra-large Container Ship in Waves. *Ocean Eng.* Vol. 268, 113388.

Zeng, K., Lu, J., Gu, M. and Chen, Y. (2023). A Comparative Analysis of CFD and the Potential Flow Method for the Pure Loss of Stability in Following Waves. *J. of Marine Sci. and Eng*. Vol. 11, 2135.

Zhang, M., Conti, F., Le Sourne, H., Vassalos, D., Kujala, K., Lindroth, D. and Hirdaris, S. (2021). On the Estimation of Collision Frequency and Generation of Collision Scenarios from AIS Big-data Analysis. *Proc. 1st STAB&S*, Glasgow, Scotland, UK.

Zhang, W., Liu, Y., Chen C., He Y., Tang Y., and Sun, J. J. (2023). Research on the Parametric Rolling of the KCS Container Ship. *J. of Marine Sci. and Tech.*, Vol. 28, No 3, pp. 675-688.

Zhang, D., Wang, W., Bu, S., and Liu, W. (2023a). Formulation of Ship Roll Damping Models from Free-decay Data. *Ocean Eng.* Vol. 280, 114658.

Zhou, H., Pan, L., Tian, X. and Zhu, R. (2022). Numerical Study on Inner Mechanism of Ship Parametric Roll in Head Waves. *Proc. 32nd ISOPE,* Shanghai, China.

Zhou, Y., Sun, Q. and Shi, X. (2022a). Experimental and Numerical Study on the Parametric Roll of an Offshore Research Vessel with Extended Low Weather Deck. *Ocean Eng.*, Vol. 262, 111914.

Zhou, X., Li, H., Huang, Y. and Yihua, L. (2023). Deep Learning Machine based Ship Parametric Rolling Simulation and Recognition Algorithms. *Ocean Eng.,* Vol. 276, 114137.

Zhou, X., Li H., Huang, Y. and Yihua, L. (2023a). New Extreme Statistics Strategy for the Extreme Value Predictions of Ship Parametric Rolling Motions through Limited Model Test Observations. *Ocean Eng.*, Vol. 276, 114138.

Nomenclature

AIS	Automatic Identification System
BR	Broaching-to
CFD	Computational Fluid Dynamics
CRNAV	Cooperative Research NAVies
CTO	Centrum Techniki Okrętowei - Maritime Advance Research Centre
Circ.	IMO Circular
DoF	Degree of Freedom
DSA	Direct Stability Assessment
EA	Excessive Acceleration
EFD	Experimental Fluid Dynamics (or model experiments)
EMSA	European Maritime Safety Agency
EPOT	Envelope Peaks over Threshold
EU	European Union
FORM	First Order Reliability Method
FTA	Fault Tree Analysis
FVM	Finite Volume method
GEV	Generalized Extreme Value
GCAF	Gross Cost of Averting a Fatality
GPD	Generalized Pareto Distribution
HERM	Harmonic Exciting Roll Motion
IMO	International Maritime Organization
IS Code	Intact Stability Code

ISOPE	International Society of Offshore and Polar Engineers and International Ocean and Polar Engineering Conference
ISSW	International Ship Stability Workshop
IT	Inclining Test
ITTC	International Towing Tank Conference
LIPS	Large Inland Passenger Ships
LNGC	Liquefied Natural Gas Carrier
LSTM	Long-Short Term Memory
MPM	Split-time/ Motion Perturbation Method
MPS	Moving Particle Simulations
MSC	IMO Maritime Safety Committee
NSC	Naval Ship Code, published by NATO as ANEP-77
OMAE	International Conference on Ocean Offshore & Arctic Engineering
ONR	US Office of Naval Research
ONRTH	ONR Tumblehome Hull form
ORV	Oceanographic Research Vessel
OMAE	International Conference on Offshore Mechanics and Artic Engineering
PCC	Pure Car Carrier
PL	Pure Loss of stability
POT	Peak-Over-Threshold method
QoI	Quantity of Interest
QSG	ITTC Quality System Group
RAO	Response Amplitude Operator
RANS	Reynolds Average Navier Stokes
RCO	Risk Control Options
RPS	Revolution per Second
RNG	Renormalization Group (related to CFD)
ROPAX	Roll on Roll off Passengers
SDC	IMO Sub-Committee on Ship Design and Construction
SKC	ITTC Seakeeping Committee
SGISC	Second Generation of Intact Stability Criteria of IMO
SOLAS	International Convention for the Safety of Life at Sea
SSA	Single Significant Amplitude
SST	Share Stress Transport (related to CFD)
STAB	International Conference on Stability of Ships and Ocean Vehicles
STAB&S	International Conference on Stability and Safety of Ships and Ocean Vehicles
TOR	Terms of Reference
TTC	Time to Capsize
TTE	Time available to Evacuate
VCG	Vertical Centre of Gravity
VLCC	Very Large Crude Oil Carrier
VOF	Volume of Fluid method

ITTC2024

30TH INTERNATIONAL TOWING TANK CONFERENCE
22–27 SEPTEMBER 2024 | HOBART TASMANIA AUSTRALIA

REPORT OF THE FULL-SCALE SHIP PERFORMANCE COMMITTEE

1. INTRODUCTION

1.1 Membership and Meetings

The members of the Full Scale Ship Performance Committee of the 30th ITTC are:

- Hideo Orihara (Chair)
  Japan Marine United Corporation (JMUC), Japan
- Sebastian Bielicki (Secretary)
  Maritime Advanced Research Centre (CTO), Poland
- Se-Myun Oh
  Samsung Heavy Industries (SHI), South Korea
- Gongzhen Xin
  China Ship Scientific Research Centre (CSSRC), China
- Gijs Struijk
  Maritime Research Institute Netherlands (MARIN), The Netherlands
- Giuliano Vernengo
  Università de Genova, Italy
- Stephen Minnich
  Naval Surface Warfare Center, Carderock Division (NSWCCD), United States of America
- Peiyuan Feng
  Marine Design and Research Institute of China (MARIC), China
- Mariko Kuroda
  National Maritime Research Institute (NMRI), Japan
- Seok-Ho Son
  Hyundai Heavy Industries (HHI), South Korea (until Dec. 2022 replaced by Min Woo Kim)
- Min Woo Kim
  Hyundai Heavy Industries (HHI), South Korea (from Jan. 2023)

Thirteen committee meetings have been held during the work period:

- First meeting, 6, December, 2021, Online. All members attended.
- Second meeting, 4, March, 2022, Online. All members except 2 members (Gijs Struijk from MARIN, Seok-Ho Son from HHI) attended.

- Third meeting, 16, May, 2022, On-line. All members except 5 members (Gijs Struijk from MARIN, Giuliano Vernengo from Genova University, Stephen Minnich from NSWCCD, Seok-Ho Son from HHI) attended.

- Fourth meeting, 13, July, 2022, On-line. All members except 3 members (Se-Myun Oh from SHI, Seok-Ho Son from HHI) attended.

- Fifth meeting, 4, November, 2022, On-line. All members except 6 members (Se-Myun Oh from SHI, Gongzheng Xin from CSSRC, Giuliano Vernengo from Genova University, Stephen Minnich from NSWCCD, Seok-Ho Son from HHI) attended.

- Sixth meeting, 8, February, 2023, On-line. All members except 3 members (Giuliano Vernengo from Genova University, Stephen Minnich from NSWCCD) attended.

- Seventh meeting, 28, April, 2023, On-line. All members except 3 members (Se-Myun Oh from SHI, Giuliano Vernengo from Genova University, Stephen Minnich from NSWCCD) attended.

- Eighth meeting, 31 May – 1 July, 2023, SVA Wien, Austria. All members attended.

- Nineth meeting, 13, July, 2023, On-line. All members except 3 members (Gijs Struijk from MARIN, Giuliano Vernengo from Genova University, Stephen Minnich from NSWCCD) attended.

- Tenth meeting, 20, October, 2023, On-line. All members except 5 members (Se-Myun Oh from SHI, Gijs Struijk from MARIN, Giuliano Vernengo from Genova University, Stephen Minnich from NSWCCD, Min-Woo Kim from HHI) attended.

- Eleventh meeting, 12, December, On-line. All members except 2 members (Giuliano Vernengo from Genova University, Gongzheng Xin from CSSRC) attended.

- Twelfth meeting, 15-17, January, 2024, JMUC Yokohama, Japan. All members except 1 member (Giuliano Vernengo from Genova University) attended.

- Thirteenth meeting, 30, April, On-line. All members except 2 members (Giuliano Vernengo from Genova Uni-versity, Gongzheng Xin from CSSRC) attended.

Figure 1: Full Scale Ship Performance committee photo with Prof. Strasser (8th meeting)

The AC representative to IMO Prof. Gerhard Strasser attended all the meetings in order to keep close eye on the progress of the procedures and guidelines and provide feedback from IMO/MEPC meetings.

1.2 Contact with ITTC committees

The 30th Full Scale Ship performance committee has coordinated and exchanged information with the CFD/EFD, Seakeeping, and SC on Wind Powered and Wind Assisted Ships on relevant issues.

1.2.1 Contact Seakeeping committee

The committee has contacted Seakeeping committee on the following aspects: Wind loads on ships which include revision or development of new procedure for wind loads based on Speed/Power trial procedure (R.P. 7.5-04-01-

01.1). Acquisition and analysis of onboard monitoring data.

On the issue of wind loads on ships, this committee agreed to conduct this work in collaboration with Seakeeping committee at the end of February 2023. This committee discussed this issue seriously in the eighth meeting held 31th May to 1st June 2023 and agreed that this committee should prepare the draft of a new stand-alone procedure developed based on Appendix F in 7.5-04-01-01.1 during the present term. On 5th June, AC Chair informed that SC on Wind Powered/Assisted Ships have already prepared a draft of a new stand-alone procedure developed based on Appendix F in 7.5-04-01-01.1. It is also suggested that all Chairs of technical committees concerned should contact the Chair of SC on Wind Powered/Assisted Ships in order to match possible different approaches. In their procedures they then should refer to that ITTC procedures. Responsible member of this committee to this task (S. Bielicki from CTO) contacted the Chair of SC on Wind Powered/Assisted Ships on this issue.

On the issue of acquisition and analysis of onboard monitoring data, This issue was seriously discussed this committee's Ninth meeting in July 2023. It is decided that Chair of this committee will take care of this task since he has wealth of technical experience concerning this issue. On-line meeting on this issue was held on Nov. 2nd, 2023. 3 SKC members (Antonio Souto-Iglesias, Munehiko Minoura and Yulin Pan) and FSSPC Chair attended. Chair of this committee introduced FSSPC's activity on the onboard monitoring issue using the TC's progress report of present term.

1.2.2 Contact SC on Wind Powered/Assisted Ships

The committee has contacted SC on Wind Powered/Assisted Ships on the following aspects: the review of new R.P. 7.5-04-01-02 for conduct and analysis of Speed/Power trials for wind assisted ships powered/assisted ships.

This committee reviewed the new R.P. and the comments was sent to the SC on 12 September 2023. The SC sent the response to this committee's comment on 27 November 2023. In the twelfth (physical) meeting, these responses were discussed, and additional comments were prepared and sent to the Chair of the SC on 13 February 2024.

1.2.3 Contact other committees

The committee has contacted Manoeuvring committee about: Investigate the manoeuvring aspect of design for Smart Ships and Unmanned Surface Vehicles. Identify the need for new or modified procedures of experiments and simulations to evaluate manoeuvring performance.

Concerning the wave correction in Speed/Power trial analysis, at the request of AC Chair, a Windows-Excel format spread sheet for SPAWAVE method with short-term estimation capability has distributed to the FSSPC members for the review of this method.

· AC WG3 Chair (Prof. Y.-H. Kim) have asked this committee to conduct the evaluation of his newly developed combined SNNM-SNU formula for wave correction in Speed/Power trials in the framework of this committee's TOR task 5 B). This formula combines both SNNM for longer wave range and SNU formula for shorter wave range. This evaluation task was conducted using a simplified Windows Excel-format file with GUI provided by Prof. Y.-H. Kim. 4 members of this committee participated. The outcome of this evaluation is described in this final report.

1.3 Contact with AC chairman about IMO and ISO issues

(1) The AC representative to IMO Prof. Gerhard Strasser, attended IMO MEPC 76 - 80 and reported on it during this term. Major outcome/comments related to fluid dynamic issues are as follows:

(2) Major outcome/comments from IMO MEPC 76 meeting:

- 2021 Guidelines on the method of calculation of the attained energy efficiency existing ship index (EEXI) adopted. Amendment to unified interpretation on the dates related to EEDI Phase 2 and 3 for new ships, as provided in Table 1 of MARPOL Annex VI, Chapter 4, Regulation 24.

(3) Major outcome/comments from IMO MEPC 77 meeting:

- Mainly discussion of level of ambition and revision of IMO GHG emission strategy.

(4) Major outcome/comments from IMO MEPC 78 meeting:

- New Guideline for exhaust gas cleaning systems. 2021 Guidance on treatment of innovative energy efficiency technologies for calculation and verification of the attended EEDI and EEXI.
- IMO has received informative submission from ITTC with overview on all procedures that have changed after the 29th ITTC:
  - 7.5-02-02-01 Resistance Tests
  - 7.5-02-02-04 Wave Profile Measurement and Wave Pattern Resistance Analysis
  - 7.5-02-03-01.1 Propulsion/ Bollard Pull Test
  - 7.5-02-03-01.4 1978 ITTC Performance Prediction Method
  - 7.5-02-03-01.7 Performance Prediction Method for Unequally Loaded, Multiple Propeller Vessels
  - 7.5-02-03-02.1 Open Water Test
  - 7.5-04-01-01.1 Preparation and Conduct and Analysis of Speed/Power Trials
  - 7.5-02-07-02.8 Calculation of the Weather Factor f_w for Decrease of Ship Speed in Waves

(5) Major outcome/comments from IMO MEPC 79 meeting:

- Amendments to the 2014 Guidelines on survey and certification of the energy efficiency design index (EEDI) (resolution MEPC.254(67) in Paragraphs 4.3.5, 4.3.6, and 4.3.8 as follows:

  Ship speed should be measured in accordance with ITTC Recommended Procedure 7.5-04-01-01.1 Speed Analysis of Speed/Power Trials (2017, 2021 or 2022 version, as may be applicable at the time of sea trials) or ISO 15016:2015…..
- Discussion on biofuels.

(6) Major outcome/comments from IMO MEPC 80 meeting:

- Interim guidance on the use of biofuels.
- Amendment to the 2021 guidelines on the shaft/engine power limitation system to comply with the EEXI requirements and use of a power reserve (Resolution MEPC.335(76)

(7) Cooperation with ISO.

- The ITTC representative to ISO Prof. Gerhard Strasser attended all 17 virtual meetings and contributed the ITTC achievements for the update of ISO 15016.
- Major outcomes are:
  - STAWAVE 2 was replaced by SNNM method.
  - Raven's method for correction of shallow water replaced Lackenby's method. Higher requirements on instrumentation for environment measurements.

1.4 Tasks

The recommendations for the work of the Full-Scale Ship Performance Committee as given by the 29th ITTC were as follows:

1. Update the state-of-the-art for investigation of full-scale ship performance, emphasizing developments since the 2021 ITTC Conference. The committee report should include sections on:

A) the potential impact of new technological developments on the ITTC

B) new measuring techniques

C) new benchmark data

D) the practical applications of numerical simulation to full-scale ship performance

E) the need for R&D for improving methods of full-scale measurements and numerical modelling.

2. Review ITTC Recommended Procedures relevant to full-scale performance, and

A) identify any requirements for changes in the light of current practice, and, if approved by the Advisory Council, update them,

B) identify the need for new procedures and outline the purpose and contents of these.

3. Address issues related to hull and propeller surface roughness such as:

A) Definition of roughness properties

B) Components of roughness

C) Measurement of roughness

D) Effects of roughness on in-service performance including filtering and analysis methods for evaluating hull and propeller performance separately

E) Roughness usage in performance prediction and cross effects with correlation

4. Provide technical support to ISO and IMO in further development of approaches to in-service performance monitoring (e.g. ISO19030.)

5. Address the following aspects of the analysis of speed/power sea trial results:

A) Initiate and conduct speed trials on commercial ships on deep and shallow water to further validate Raven method.

B) More validation of wave-added resistance method, in particular SNNM, covering all wave encounter angles based on a set of significant ship parameters including the short-term estimation of wave-added resistance in irregular waves.

C) Investigate the influence of drift, rudder action, short wave and wave height on wave added resistance.

D) Investigate the influence of water depth on the hull-propeller interaction (thrust deduction, relative rotative efficiency)

E) Explore and monitor new developments in instrumentation and measurement equipment relevant for sea trials and in service performance assessment (e.g. wind, waves, thrust, speed through water).

6. Develop and keep updated an inventory of the data bases as well as the companies, organisations or any other bodies collecting and processing data on the ship in-service performance of interest to ITTC.

7. Study accuracy of CFD for shallow water applications – cooperate with CFD/EFD Committee.

8. Update the speed/power sea trial procedures 7.5-04-01-01.1 where appropriate, in particular:

A) complement it by a procedure for the correction of yawing (caused by wind) and rudder angle

B) wind averaging method to correctly reflect the wind effect in double run (true wind vector in each run).

9. Support ISO in updating ISO15016 in compliance with 7.5-04-01-01.1

10. Update guideline for determination of model-ship correlation factors, including shallow water and draft dependency (in cooperation with AC Working Group)

11. Update guideline on CFD-based wind coefficient; in particular, re-assess database of wind resistance coefficients and update it according to the new procedure for non dimensionalising.

12. Continue to monitor the development of relevant techniques for ship energy saving and identify the needs to complement the present EEDI framework in response to the adoption of alternative fuels and the receptivity of innovative technologies. Consider, if necessary, a complementary metric to EEDI to represent power savings.

13. Collect full scale data obtained through relevant benchmark tests on the effect of energy saving methods (ESM). Use the full scale data for validating the effect of ESM. Develop a guideline to conduct in-service performance evaluation for ESM. Full-scale data showing the benefits of ALDR (Air Layer Drag Reduction) would be of particular interest.

14. As smart ship technology for cargo and passenger transportation is one of the emerging technologies in maritime industry:

A) Investigate the hydrodynamic aspect of design for Smart Ship and Unmanned Surface Vehicles

B) Explore the suitability of the traditional design spiral for the smart ship and USVs.

C) Identify the need for new or modified procedures of experiments and simulations to evaluate performance in this particular field

2. STATE OF THE ART

2.1 Potential impacts of new technological developments on the ITTC

With the rapid development of artificial intelligence (AI) technologies, the machine learning and big data analysis techniques are getting increasing attentions and have been proven effective for many applications. These techniques are also relevant and useful for the prediction, evaluation and optimization of full-scale ship performance. The most straight-forward and useful application of AI is probably to handle the huge volume of ship's operational data for performance evaluation. Rapidly advancing sensor and telemetry technology onboard ships has provided operators with an extensive database that can be used to improve the assessment of actual ship performance.

Gupta et al. (2022) used machine-learning (ML) methods to estimate the hydrodynamic performance of a ship using the onboard recorded in-service data. Three ML methods, NL-PCR, NL-PLSR and probabilistic ANN, are calibrated using the data from two sister ships. The calibrated models are used to extract the varying trend of the ship's hydrodynamic performance over time and predict the change in performance through several propeller and hull cleaning events. The probabilistic ANN model performs the best, but the results from NL-PCR and NL-PLSR are not far behind, indicating that it may be possible to use simple methods to solve such problems with the help of domain knowledge.

Gupta et al. (2023) also proposed a streamlined semi-automatic approach to processing the data, which can be used to prepare a dataset for ship performance analysis. Typical data processing steps like interpolating metocean data, deriving additional features, estimating resistance components, data cleaning, and outlier detection are arranged in the best possible manner not only to streamline the data processing but also to obtain reliable results. A semi-automatic implementation of the data processing framework, with limited user intervention, is used to process the datasets and present the example plots for various data processing steps.

Jabary et al. (2023) presented the development of selected data science and ML approaches based on synchronized and integrated operational data available from a Ship Operation Information Model (SOIM). The SOIM is configured in a database management system (DBMS) and considers comprehensive operational data at low/high-frequency of noon reports, AIS, weather, loading conditions and numerous onboard sensors measuring operating and motion parameters. The pre-processed operational data are subjected to correlation analyses in order to identify the main interdependencies between the different operational parameters and thus evaluate the most important factors affecting an operational condition. On the other hand, they are used together with the corresponding design data to implement assessments of ship operational indicators under specific operational conditions.

In recent years, the importance of evaluation of the ship added resistance in waves has increased, both from an economic and environmental protection point of view. A trend can be noted that more and more studies have focused on the modelling and evaluation of wave added resistance using machine learning techniques or based on the big data analysis of actual ship operational data.

Martić et al. (2021) applied an Artificial Neural Network to evaluate the added resistance in different sea states that the ship will encounter during navigation, the model can estimate the added resistance of container ships with sufficient accuracy, based on the ship characteristics, sailing speed, and the sea state.

Taskar and Andersen (2021) used the full-scale data of two ships to compare five different added resistance prediction methods. The effect of using separate wave spectra for wind waves and swell on performance prediction has also been explored. Ships have been simulated in the same weather conditions and propeller speed as in the case of full-scale ships using different methods for added resistance. The performance of these methods has been quantified by comparing speed and power predictions with the full-scale data. It was observed that three out of five methods were able to predict added resistance even in high waves. Even though these methods showed significantly different responses in the frequency domain, its effect on speed and power prediction was minor. Moreover, there was minor improvement in results by using separate wave spectra for wind waves and swell instead of single wave spectrum for combined wind waves and swell.

Mittendorf et al. (2022) implements machine learning methods for the prediction of the added-wave resistance of ships in head to beam wave conditions. The study is focused on non-linear regression algorithms including Random Forests, Extreme Gradient Boosting Machines and Multilayer Perceptron. The employed dataset is derived from results of three different potential flow methods covering a wide range of operational conditions and 18 hull forms in total. A hyperparameter study based on Bayesian optimization is conducted, and the validation of the final models for three case studies against numerical and experimental data shows satisfactory generalization in case of the neural network. The tree-based ensemble methods, on the other hand, are not able to generalize sufficiently from the given parameter discretization of the underlying dataset.

Kim et al. (2022) proposed a so-called meta model for predicting added resistance in waves by combining two existing methods. The results from the two methods are combined smoothly using a tangent hyperbolic function according to wavelengths and wave headings. The coefficients constituting the function are tuned to minimize mean squared error between predictions and model experiments. Finally, the meta model is verified by full-scale measurements of a general cargo ship and a container ship, and it seems to give good agreement with measurements in all analysis areas, compared to existing semi-empirical methods. Especially, it showed better performance in estimating added wave resistance at high waves, resonance frequencies, arbitrary waves, and low speeds.

Mittendorf et al. (2023) merges telemetry data of more than 200 in-service container vessels with ocean re-analysis data from ERA5. Theoretical estimates relying on spectral calculations of added resistance are made for both long- and short-crested waves and are based on a combination of a parametric expression for the wave spectrum and a semi-empirical formula for the added resistance transfer function. The theoretical estimates are compared to predictions from an indirect calculation of added resistance relying on shaft power measurements and empirical estimates of the remaining resistance components. Overall, the comparison reveals a bias in bow oblique waves and higher sea states of the spectral estimates as well as the large variance of the empirically derived predictions — particularly in beam-to-following waves. One of the study's main findings is that added resistance assessment based on in-service data is complex due to significant associated uncertainties.

Moving on to another machine learning application, short-term temporal predictions of ship responses given the current wave environment and ship state would enable enhanced decision-making onboard and reduce the overall risk during operations for both manned and unmanned vessels. However, the current state-of-the-art in numerical hydrodynamic simulation tools are too computationally expensive to be employed for real-time ship motion forecasting and the computationally efficient tools are too low fidelity to provide accurate responses. In this regard, machine learning techniques have the potential to provide fast and efficient predictions with levels of accuracy closer to the higher-fidelity tools.

Guo et al. (2022) extended a deep learning (DL) model to predict the heave and surge motions of a floating semi-submersible 20 to 50 seconds ahead with good accuracy with the help of the dropout technique.

D'Agostino et al. (2022) investigated the prediction capability of recurrent-type neural networks for real-time short-term prediction (nowcasting) of ship motions in high sea state. The performance of recurrent neural networks, long short-term memory, and gated recurrent units models are assessed and compared. All three methods provide promising and comparable results.

Silva and Maki (2022) developed a methodology with long short-term memory (LSTM) neural networks to represent the motions of a free running David Taylor Model Basin (DTMB) 5415 destroyer operating at 20 knots in Sea State 7 stern-quartering irregular seas. Case studies are performed for both course-keeping and turning circle scenarios. The neural network is able to predict the temporal response of the ship due to unseen waves accurately, which makes this methodology suitable for system identification and real-time ship motion forecasting.

Schirmann et al. (2022) applied ridge regression and neural network models for heave, pitch, and roll prediction using time-and-place specific, multidirectional wave model parameters as input. The performance benefits of providing these predictive models with computationally efficient, physics-based model predictions (PBMPs) of heave, pitch, and roll as additional inputs were examined. Data measured aboard an operational research vessel were used to train and test the data-driven models. The results of this study showed effective reduction of motion amplitude mean-squared error (MSE) values on multiple test datasets relative to the PBMPs alone. The results also showed that inclusion of PBMPs as input to the data-driven models was typically beneficial in terms of MSE reduction, stressing the importance of retaining physics-based information in data-driven models.

Zhang et al. (2023) presents a novel data-driven methodology to provide multi-step prediction of the ship's roll motion in high sea states. A hybrid neural network is proposed that combines long short-term memory (LSTM) and convolutional neural network (CNN) in parallel. The motivation is to extract the nonlinear dynamics characteristics and the hydrodynamic memory information through the advantage of CNN and LSTM, respectively. Taken a scaled KCS as the study object, the ship motions in sea state 7 irregular long crested waves are simulated and used for the validation. The results show that at least one period of roll motion can be accurately predicted by using the proposed method.

Gao et al. (2023) developed a reliable and efficient tool for real-time and accurate prediction of ship motion. A ship motion attitude prediction model based on the Adaptive Discrete Wavelet Transform Algorithm (ADWT) and the spacetime Residual Recurrent Neural Network (RRNN) with a time-varying structure is proposed. The model performance tests are conducted based on the simulation data of the ship motion of DTMB5415. Compared with other prediction models, the prediction accuracy of the ADWT-RRNN is the highest under all working conditions, its prediction accuracy and stability of it do not fluctuate significantly over a long prediction period. Hence, the more severe the sea states, the more pronounced the performance advantage is over other models.

2.2 New measuring techniques

Full scale ship performance analysis requires a large amount of reliable sea trail data as support. The data of full scale ship sea trail contains not only environmental parameters such as wind, wave and current, but also real ship performance parameters such as speed, main engine power, torque and so on. The methods and ways to obtain these real ship data have been introduced in the past ITTC regulations. With the development of test instruments, sensor technology, data processing and analysing technology, some new technologies for real ship sea trail have been developed and applied continuously.

- Wave

Hyeok-Geun Ki (2015) carried out full scale measurement of 14k TEU containership with the Wave Finder. That is automatic wave data measurement system which records encountered wave data, i.e., wind wave, swell and total wave data including wind data. As described in Fig1, a wave finder antenna and system were installed.

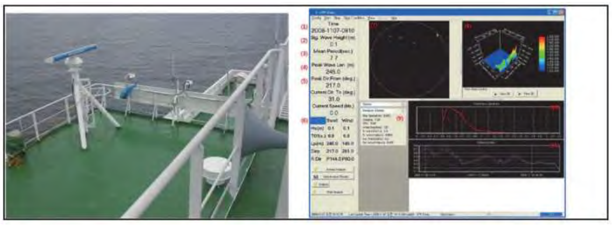

Figure 2 Wave Finder system and antenna

CSSRC developed binocular stereo vision measurement method for the measurement of encounter waves has been reviewed. This method is a type of direct wave measuring methods which is expected to be of higher accuracy compared to indirect wave measuring methods (e.g. wave radar, ship-motion based methods). Accuracy of the method has examined on a stationary offshore structure in China. Onboard tests in ship trials has been considered in China.

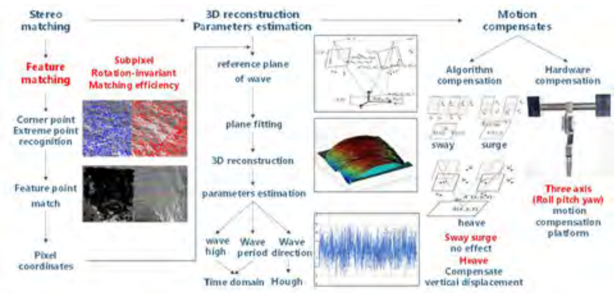

Figure 3 Wave observation technology based on binocular stereo vision.

- Flow field

A scale effect on flow field from model to ship scale has been a big concern for researchers in a ship industry for a long time. Yasuhiko Inukai (2019) presented a new measurement system, Multi-Layered Doppler Sonar (MLDS) was applied in full scale measurement of the flow. MLDS is a Doppler sonar capable of measuring relative water velocity at multiple arbitrary points along ultra-sonic beams. MLDS was installed on a 14,000 TEU container ship and full scale measurement was carried out.

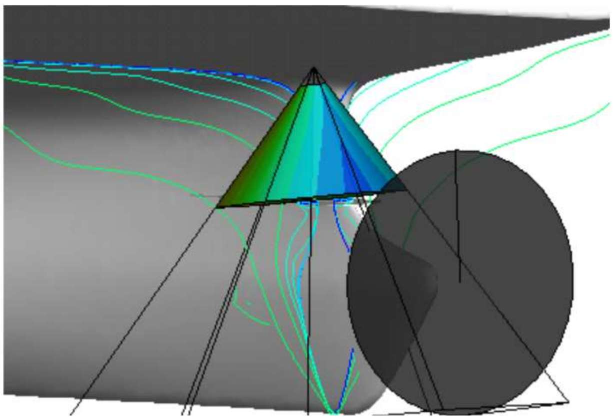

Figure 4 Measuring area by MLDS

Lina Nikolaidou (2021) measured on the characteristics of air lay regimes for a flat plat. Planar PIV was used upstream of the injector in a side-view configuration to characterize the incoming boundary layer. Images of the air layer regimes were acquired with a bottom up view with LaVisions Imager sCMOS CLHS camera. CSSRC (2024) used camara system that mounted on the bottom of ship to observe the shape and distribution of air layer generated by ALS for a “mid-scale” model ship.

- ESD

Pre-swirl ducts (PSDs) have been developed primarily from the viewpoint of improving propulsion efficiency. But little is known on how this affects a vessel’s overall manoeuvring qualities. To study the interaction of the different components of the propulsion system with the PSD, and to assess the maximum loads on the PSD models during manoeuvring. Steven Leonard（2024）carried out manoeuvring tests with a free-running model on a lake. The duct forces were measured throughout. The sensor was integrated into the hull, positioned below the shaft axis. The duct, fins and brackets were manufactured from a single piece and mounted directly on the sensor, having a cylindrical opening for the propeller shaft. The external fairing, in form of the ship contour, covers the sensor and the fins without contact.

Figure 5 Sensor for measurement of duct forces

- Resistance and propulsion

Youngjun You (2018) propose a new approach to predict and verify the actual RPM and engine power of an LNGC from full-scale measurement data. The sea route, speed over ground and environmental conditions obtained from the measured data. The results of the simulation are qualitatively reviewed by comparing the calculated time histories of the RPM and the power with the measured RPM and power. Finally, the power increment due to the environmental load is estimated by comparing the predicted power considering the environmental load with the predicted power, not considering the environmental load.

Ulrik D. Nielsen (2019) investigated a semi-empirical model used to estimate added-wave resistance on a ship sailing in waves. The model relies on measurements from a continuous monitoring system, and produces an estimate- the indirect measurement- of added-wave resistance, based on the difference between, on the one side, the measured power and, on the other side, a summation of theoretically calculated resistance contributions but neglecting the component because of seaway. The model has been applied to more than three months of full-scale data recorded on an in-service operating container ship.

Roughness of marine propellers can profoundly affect the efficiency of maritime transportation. Mohamed A. Mosaad（2024）aims to develop a graphical user interface (GUI) program using volumetric image processing (VIP) techniques to predict marine propeller roughness values.

R. Stigter (2024) aimed to investigate the relationship between cavitation inception and microbubble characteristics at full scale. Measurements were conducted on the research vessel Pelagia, operated by the Netherlands Oceanographic Institute (NIOZ), during a 6-day trial from the Bahamas to Curaçao. Cavitation inception and development were measured acoustically, using pressure sensors, and visually, using high and low-speed cameras. The concentration of microbubbles in the proximity of the propeller was monitored using Interferometric Particle Imaging (IPI). Two windows were manufactured in the hull of the ship. One window at portside, just above the propeller, to enable cavitation observations with the high and low-speed cameras. The other window was located at starboard, a few meter upstream from the starboard window. This window was used for the IPI setup, and made it possible to measure the microbubble content upstream of the propeller.

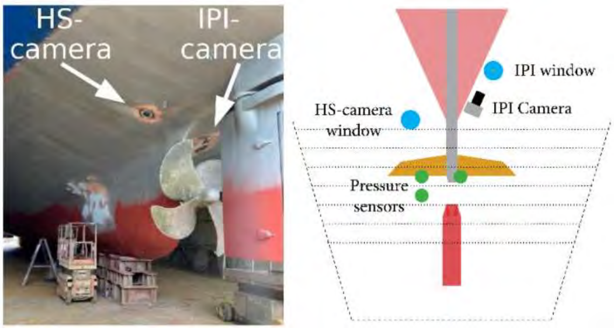

Figure 6 The positions of HScamera window and IPI camera window on the ship

Koruri Tamura (2024) carried out pressure fluctuations around the stern hull of 22,000 DWT chemical tanker were measured during the sea trial using FBG (Fiber Bragg Grating) pressure sensor that can be simply attached to the hull surface without extensive construction work. FBG pressure sensor with a total length of 15 mm, a width of 9 mm and a thickness of 0.7 mm was selected for the purpose of establishing a new method for performing the preparation and measurement efficiently in a short time. This sensor can be directly attached to the hull surface and has the advantage of eliminating the conventional drilling and complicated installation work.

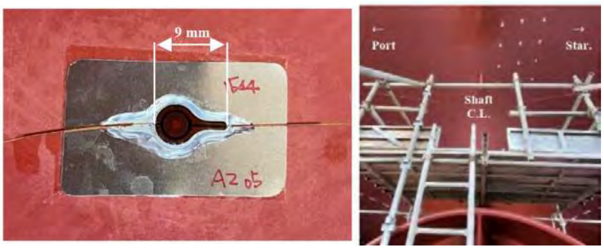

Figure 7 FBG pressure sensor and installed on the stern hull

- Ice environment

Ship operation and ice loading in floe ice fields have received considerable interest during recent years. For the prediction of ship resistance and transit speed in various ice conditions, ship performance in level ice, ridged ice and channel ice are evaluated based on full-scale measurement data of two ships by Fang Li (2018). In their works, Ice thickness in full-scale data was measured using multiple methods to minimize the uncertainty. The thickness of level ice was measured by a stereo camera system. The ridge profile was identified through measurement with an electromagnetic device. Visual observation was conducted for the description of encountered ice conditions. For a better estimation of ship net thrust through propulsive data, the net thrust model is revised in their method to take the effect of power and propeller pitch into consideration. Data acquisition is the most problematic for the investigation of channel ice.

Public data obtained from full-scale measurement covering comprehensively ship performance and ice loads under various ice thicknesses, concentrations and floe sizes are rare. The 2018/19 Antarctic voyage of the Polar Supply and Research Vessel (PSRV) S.A. Agulhas II gathered considerable data of the ship in floe ice fields under various thicknesses, concentrations, and floe sizes. Fang Li (2021) carried out statistical analysis to seek suitable probability distributions which adequately fit the measured ice load and therefore suitable to be used as parent distributions for long-term estimation. The ship is instrumented with shear strain gauges at the starboard side on a total of nine frames, including two at the bow, three at the bow shoulder and four at the stern shoulder. The ice conditions during the voyage are monitored via two sources. The first is visual observation, which are conducted by dedicated ice observers on the bridge, estimating ice concentration, floe size and thickness approximately every minute and summarizing the results in 10-min interval. In addition to that, an ice condition camera is installed on the ship to take photos of the ice condition constantly during the voyage. Hanyang Gong (2022) provides an approach to digitally measuring channel widths from drone videos. Full-scale tests of the Icebreaker (IB) Polaris in the Bay of Bothnia during 2021 were analysed the relation between measured channel widths and icebreaker's operations.

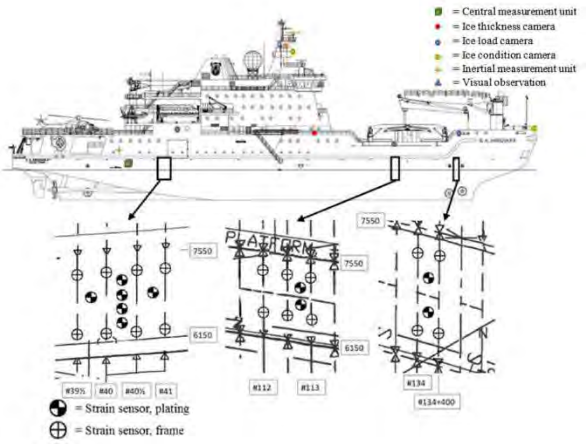

Figure 8 Instrumentation of S.A. Agulhas II.

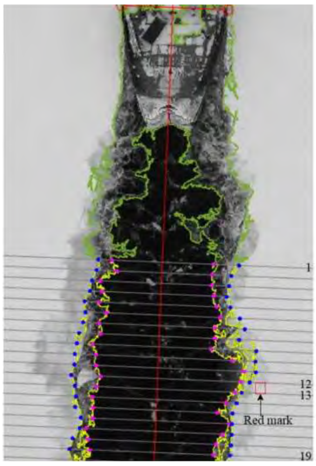

Figure 9 A scheme of the digital channel width measurement approach

2.3 New benchmark data

It is considered that MARIN's JoRes ship-scale test cases data to be published in December 2024 (Ponkratov 2023) are most relevant to meet this TOR task, in particular, due to its coverage of ship types, 3D configurations, ESDs, roughness measurements.

Therefore, it seems to be appropriate for us to recommend ITTC full conference to employ JoRes test cases as benchmark data for full-scale issues in ITTC activity. While the JoRes test cases will not available to the public by December 2024, it will not cause any trouble since next term activity will starts October 2024.

Survey to ITTC member organizations regarding the provision of their full-scale data to this TOR task was conducted. 1 organization (SVA Potsdam) has contributed full-scale speed/power trails results for 7 ships.

2.4 Practical application of numerical simulation to full-scale ship performance

Possibility of the use of full-scale CFD simulations in ship performance prediction has examined. It is found that the reliability of full-scale CFD simulation results have remined quite low compared to that of model-scale results mainly due to the lack of sufficient full-scale validation data, and that performance prediction based on full-scale CFD simulation results is not practically feasible at present.

3. REVIEW ITTC PROCEDURES

3.1 Requirements for Changes

3.1.1 Overview

The ITTC Recommended Procedure for the Preparation, Conduct and Analysis of Speed/Power Trials (7.5-04-01-01.1) was last updated to Revision 07 in 2022. This version was reviewed to determine whether any updates are required to reflect current practice. An editorial review was conducted first to address various grammatical and formatting issues and to identify any logical gaps in the procedures. The initial result of this effort is a proposed revision to RP 7.5-04-01-01.1. Additionally, a survey was conducted to evaluate the utilization of existing testing and analysis procedures and determine whether there are additional procedures that should be considered for adoption given current practice.

3.1.2 Editorial Review

In addition to basic grammatical and formatting updates, the editorial review identified issues with the 2022 version of RP 7.5-04-01-01.1 regarding missing definitions. These issues are identified here, but potential revisions to address them are recommended as future work of the Full-Scale Ship Performance Committee (FSSPC).

RP 7.5-04-01-01.1 does not provide definitive guidance as to when to transition from the approach phase into the trial run. The procedure recommends monitoring propulsion parameters to determine they have achieved steady state but it does not provide a concise definition of what that condition is. While this ambiguity in the procedure provides the performer flexibility, it also precludes any standardization in this regard and may introduce undesirable error. It is recommended, therefore, that a concise, numeric definition of “steady” be developed and implemented into a future revision of RP 7.5-04-01-01.1.

Next, the concept of the “speed component in the heading direction” is utilized in the process for analysing speed/power (S/P) trial data without a corresponding definition. This terminology implies the scalar projection of the velocity over ground, V_G, in the direction of the ship’s heading, ψ. A mathematical definition of this term should be provided in a future revision of RP 7.5-04-01-01.1.

Finally, it is noted that RP 7.5-04-01-01.1 does not provide any treatment as to the estimation of uncertainty from S/P trials data and corresponding analyses. ITTC General Guideline for Uncertainty Analysis in Resistance Tests (7.5-02-02-02) provides a starting point for some of the considerations of S/P trial uncertainty analysis. The corrections involved in the analysis of S/P trial data complicate a full and accurate estimation of the uncertainty due to its propagation through these various calculations. Nonetheless, S/P trial uncertainty estimates have been demonstrated with propagation through STAWAVE-2 corrections (Seo & Oh, 2021).

3.1.3 Survey

A questionnaire on the usage and sufficiency of RP 7.5-04-01-01.1 with regards to testing and analysis procedures was distributed to member and non-member organizations. A total of 18 responses were received with 11 (61%) indicating that the organization conducts S/P trials and 13 (72%) responding that the organization conducts analyses of S/P trials. The results are discussed here with regards to these two aspects.

Nearly all responses indicated that RP 7.5-04-01-01.1 (or ISO 15016:2015) is currently in practice. Most responses indicated that S/P trials are conducted on displacement monohulls and multihulls as well as high-speed monohulls. Trials on high-speed multihulls and naval or coast guard vessels are less frequent. Other vessel types that respondents indicated include offshore supply vessels, anchor handlers, service operation vessels, fishing boats, research vessels, icebreakers, and submarines.

Regarding the conduct of trials, majorities of responses indicated practice of ITTC recommended limits regarding wind (82%), significant wave height (82%), minimum water depth (73%), current speed change (64%), minimum run length (64%), and maximum steering angle (73%). Negative responses were limited to trials of non-EEDI vessels, use of proprietary limits which are more restrictive than those of RP 7.5-04-01-01.1, or practical limitations of the available test areas. Most respondents indicated that trials are typically aligned to either the wind or waves, whichever has the greater effect (64%). Some organizations are limited by the configuration of the available test areas. The Iterative method is most common amongst respondents (55%), while 18% indicated use the Mean of Means method and a further 18% indicated use of either of those methods.

Only 45% of responses indicated that all recommended primary parameters are measured during trials, with a common exception being bow acceleration. Some respondents indicated that additional parameters are measured beyond those of RP 7.5-04-01-01.1 with common responses including rudder or steering angle and angular rates and displacements. It is recommended that these parameters be considered for inclusion in Table 1 or 2 of RP 7.5-04-01-01.1. Data acquisition capabilities vary widely and are often proprietary in nature. A minority of respondents indicated that wave spectra are sometimes or always measured during trials (36%), but those organizations which measure waves tend to collect the directional spectra instead of the point spectra.

Responses regarding analysis practices indicated more variance relative to recommended procedures. Approximately equal preference was ascribed to each wind resistance correction technique of RP 7.5-04-01-01.1 (wind resistance coefficients derived from model tests, CFD estimates of wind resistance, wind resistance coefficients from standard data sets, and regression formulae). The most common wave resistance correction techniques are STAWAVE-2 and seakeeping model tests (46% each) while STAWAVE-1, SNNM, and the theoretical method are less common at 23-31%. Only 46% of respondents indicated application of shallow water corrections but most negative responses were due to satisfactory water depth at the available test areas. Corrections for water temperature and salinity (58%) and vessel displacement (69%) are in common practice. The analytic tools utilized by respondents were equally divided amongst STAIMO, Class NK PrimeShip-Green/ProSTA, and proprietary tools.

3.1.4 Conclusions

In summary, the survey results indicated that RP 7.5-04-01-01.1 is broadly in practice to guide the conduct of S/P trials amongst respondents. Considering current practice, it is recommended that rudder or steering angle and angular rates and displacements be added to the recommended parameters for measurement during S/P trials. More variability was found in the data analysis techniques and tools employed by respondents. The flexibility afforded by the choice of analytic corrections within RP 7.5-04-01-01.1 is apparently being leveraged. Finally, it is recommended that future revisions to RP 7.5-04-01-01.1 consider the inclusion of definitions of steady approach conditions and the concept of “speed component in the heading direction,” and the potential addition of analysis procedures to enable uncertainty estimation for S/P trials.

3.2 Need for new procedures

Air Lubrication technology reduces frictional resistance, comprising more than 60% of total resistance (ITTC, 2017), by introducing air bubbles between the ship's hull and seawater. Between 2010 and 2022, 68 papers have been published on air lubrication technologies, with interest notably increasing after 2018 due to stringent regulations targeting enhanced energy efficiency (EEDI requirements). Figure 10 (Tadris et al., 2023) depicts the distribution of these publications. Several full-scale air lubrication systems are now commercially available and according to ABS (ABS report, 2019) up to 2018 there were 23 ships equipped with ALS. Recently, the MSC ship owner company inquired more than 30 ships equipped in that ship, which will be built in 2022-2024.

Figure 10 Distribution of air lubrication technologies papers over the years.

Specialist Committee on Energy Saving Methods of 29th ITTC recognized the ALS testing techniques and extrapolation issues, and proposed guideline 7.5-02-02-03 concerning this topic. However, in light of new MEPC.1/Circ.896 guidance, where the reduction rate of ship propulsion power due to ALS is not clearly defined, the update of existing guideline should be considered. Especially for the EEDI draught, for which the reduction rate has status: estimated.

Regarding that fact, in accordance to terms of reference, proposed by FSSP committee the update of existing guideline 7.5-02-02-03 concerning determination of air lubrication system (ALS) scaling issue was proposed. This topic should be considered more precisely due to predicted by increasing share of the air lubrication technology applied in newly designed ships, which follow the IMO regulations towards the green shipping industry.

4. HULL AND PROPELLER SURFACE ROUGHNESS

4.1 General

Effect of hull and propeller surface roughness on ships performance has been thoroughly examined in the previous ITTC activities (e.g. ITTC(2011), ITTC(2014), ITTC(2017), ITTC (2021a)). As described in ITTC(2021a), it is well known that ship’s hull and propeller surface roughness have a significant influence on full-scale ship performance. Deterioration in performance can result in more than 10% increase in propulsive power after short time duration after delivery of newly built ships. Principal causes of surface roughness are normally surface coatings and biofoulings. Among them, effect of roughness due to surface coating have examined intensively in recent years compared to that of biofouling. Thus, emphasis has placed on the effect of roughness due to biofouling in the activity of this committee.

In the following roughness related aspects specified as this committee's tasks are described.

4.2 Definition of roughness

Definition of hull and propeller surface roughness is normally made using single roughness parameter height. As a roughness height parameter, Maximum surface roughness parameter *Rz* is employed which is equivalent to BMT roughness parameter in case of 50 mm evaluation length. On the other hand, other roughness shape parameter, in particular, it is well known that roughness wave length has noticeable influence on roughness effect. According to ITTC (2017), roughness effect is reduced when the roughness wave-length is sufficiently longer than the roughness height on coated surfaces. In addition to this, it is also known that the non-uniformity of roughness distribution is not normally considered in the evaluation of roughness effect while the non-uniformity has significant influence. For hydrodynamic evaluation of roughness effect, roughness function is employed. Roughness function ($\Delta U+$) is a downward velocity shift in logarithmic overlap region of the turbulent boundary layer. Roughness function is normally defined as function of roughness Reynolds number ($k+$) evaluated using roughness height parameter (k). Concerning roughness definition, relevant published literatures have investigated in the following.

Demirel et al (2017) evaluated roughness functions for arbitrary barnacle fouling by towing tests of flat plate with artificial roughness with varying height and coverage area. Corresponding roughness length scale k_G is derived so that roughness functions for various roughness conditions are converged to the single functions. k_G is calculated from the polynomial with roughness height (h) and percentage covering area (SC). In the towing tests, actual barnacles of differing sizes were scanned in 3-D in order to generate a CAD model of typical barnacle geometries. Balanus improvisus, an adult juvenile barnacle species, which can grow up to 10 mm in diameter and 5 mm in height (big sized barnacle model) was selected. The digital models of the barnacles were then printed in3-D using 3-D printing technology to generate artificial barnacles. From the towing tank test results the abovementioned single roughness function of k_G for arbitrary barnacle type roughness has derived. By using this roughness function, hydrodynamic evaluation can be conducted by theoretical or numerical calculations.

Song et al (2021a) investigated the effect of heterogeneous hull roughness on ship resistance. Towing tests were conducted in Kelvin Hydrodynamics Lab. at University of Strathclyde with a Wigley model of 3m length in both homogeneous and heterogeneous (1/4, ½ bow/aft rough) conditions. Bow-rough conditions showed larger resistance than aft-rough conditions as expected from the consideration of boundary layer thickness. Using roughness functions derived from the towing tests, new added resistance predations method for homogeneous roughness based on Granville's method is proposed.

Kawashima et al (2019) investigated on the effect of roughness shape parameter of painted surface on frictional resistance by measuring the frictional resistance of flat plates with painted rough surface of different wave length to wave height ratio in towing tests. Surface roughness of painted roughness flat plates are measured with a laser displacement meter, then roughness shape parameters are obtained. By analysing test results and roughness shape parameters, frictional drag coefficient estimation formula for arbitrary wavy rough surface is derived. The estimation formula is derived based on the following assumptions:

- the increase in frictional resistance due to roughness is the sum of the local profile drag of each roughness.
- The frictional resistance of the painted rough surface is the sum of the frictional resistance of the surface and the profile drag of the roughness.

- Resistance increase due to the roughness occurs in the region higher than the thickness of the viscous sublayer, and in the region under the viscous sub-layer there is no increase in resistance.

The derived frictional drag coefficient estimation formula for arbitrary wavy rough surface is defined as a function of following parameters: 1) Total effective front projected area of roughness. 2) flow velocity at the roughness height at the long. centre of plate., 3) average roughness height, 4) average roughness wavelength and 5) experimentally derived coefficient and constants. To show the availability of the newly derived formula, resistance increase ratio for the cases of ks = 150mm with a variety of ship's speeds and lengths were evaluated.

Mieno et al. (2021) investigated added resistance due to roughness of coated surface by rotating cylinder tests. Friction increase rate (*FIR*) due to roughness is examined by means of roughness steepness (*Rc/Rsm, Rc*: average roughness height, *Rsm*: average roughness wave length). By analysing test results and roughness parameters, following features of roughness resistance increase are confirmed:

- Roughness height smaller than a certain level (non-effective thickness $ds \sim k+=2\sim 4$) do not contribute to resistance increase.

- Simplified projected area of roughness in streamwise direction above ds (*CPA*) calculated with *Rc* and *Rsm* correlate strongly with *FIR* due to roughness is influenced by roughness steepness (*Rc/Rsm*).

From the above results, simple empirical formula for estimating *FIR* for arbitrary wavy rough surface is derived in which *FIR* is calculated with *Rc* and *Rsm*. The range of application is as: Rc/Rsm <1/12(=0.083), this implies that the derived empirical formula is not applicable to sand-grain type steeper roughness.

From the literature survey described above, following findings are obtained concerning the definition of roughness for use in full-scale performance evaluation:

- Formulae proposed by Demirel et al. (2017) for estimating roughness function with corresponding roughness height for arbitrary roughness pattern may be useful for application in CFD and other theoretical calculation.

- Formulae proposed by Kawashima et al. (2019), Mieno et al. (2021) for estimating added resistance due to roughness considering wavelength effects are quite simple and will be applicable in Seed/Power trial in the future after careful verification/ validation for conditions covering wide range of ship types.

- Introduction of the consideration of roughness wave length effects into the present Speed/Power trial analysis in which only roughness height is considered seems to be inevitable since it is shown in the literature that wavelength roughness height to wavelength ratio has significant effects on added resistance due to roughness.

- However, it should be very careful to implement new method/formulae into the ITTC Recommended Procedure (RP) to avoid deterioration of RP's validity and effectiveness, in particular intentional underestimation of roughness effects.

4.3 Components of roughness

As described in 4.1, main components of hull and propeller surface roughness are coating and biofouling. Concerning the biofouling, hydrodynamic drag penalties due to hard macrofouling is better understood than losses due to soft bio fouling. (e.g. slime, macroalgae, tunicates, hydroids) as mentioned in ITTC (2017). Since micro biofouling is most frequently encountered roughness in both speed/power trials and operations, those rough-ness components should be thoroughly addressed in the context of full-scale ship performance issue. Based on these considerations, relevant published literatures have investigated in the following.

Hunsucker et al (2019) studied performance of fouling control coatings by means of hydrodynamic testing. In this study, replicated samples of 5 commercially available coatings (3 fouling release types (FR, silicone based), 2 anti-fouling types (AF, silicone matrix with a biocide(AF1), ablative cooper (AF2))) were deployed at 2 sites (east coast of Florida, USA) for 4 months, then hydrodynamically tested up to a speed of 15m/s to determine the frictional drag increase. After that tests hard fouling adhesion testing was made. Both total coverage of fouling organisms and drag forces were compared before/after hydrodynamic tests. It is found that both coverage of fouling and drag vary significantly among test sites and coating materials. Also noted is that composition of organism's components differs significantly among test sites and that lower fouling with hard structure had a minimum removal at the top speed in hydrodynamic testing.

Yeginbayeva et al (2020) examined combined effects of roughness range of foul-release coating (FRC) and light biofouling (slime). Natural and laboratory biofilms are grown on FRC panels by exposing them in realistic fouling environment. Boundary layer velocity measurement and similarity-law scaling is used to predict the added resistance due to fouling. Following 2 dynamic biofilm growth methods simulating realistic fouling environment are employed:

1) In-field method: panels were placed on the strut arrangement under the moonpool plug of Newcastle University research catamaran vessel operate around port of Blyth (55oN,1oW). Tests were conducted 35% of 6 month period (Mar.-Sep.), research vessel speed 6-20kt. water temperature was 6^{o}C-14^{o}C.

2) Laboratory method: panels were placed in the closed-loop system. Inoculated with the culture extracted from the research vessel. flow speed 0.5m/s for the duration of 1 month and 2 weeks, water temperature was 19^{o}C – 21.5^{o}C.

4 types of coatings were tested in this study. Biofilm coverage area and mean peek-to-valley height (*Rt*) were measured after exposing them in realistic fouling environment. Then, skin friction coefficients is evaluated from moment-um thickness measured in the boundary layer velocity measurement conducted in Emerson Cavitation Tunnel of Newcastle University. Resistance increases for the tested coating ty-pes were compared for the case of KCS container ship using roughness functions evaluated by Granville's similarity-law method. The results showed that resistance increase due to biofilms can be 10% to 20% relative to clean conditions.

From the literature survey described above, following findings are obtained concerning the definition of roughness for use in full-scale performance evaluation:

- Biofouling on hull surface is significant and varied greatly depending on types of coating and environmental conditions encountered.

- Field tests of coating replica will be useful for the examination of anti-fouling performance of coating.

- Light biofouling (slime) has noticeable impact on hydrodynamic resistance with the increase in excess of 10% relative to clean surface condition.

- Coating materials and ambient environmental conditions have significant influence on increase in hydrodynamic resistance. Examination of these issues should be continued and conducted on a variety of ship types.

4.4 Measurement of roughness

Hull roughness impacts fuel consumption significantly. Accurate measurement of this roughness is essential for analysing the speed-power performance of a vessel. Understanding and managing surface roughness optimizes fuel efficiency and enhances overall performance, making it a critical aspect of performance monitoring in operation at sea.

Two different measuring systems, contact and non-contact type, were implemented to compare the results as shown in Figure 1.

- Contact Type - - Non-contract Type –

Figure 11 Hull roughness measurement system

As roughness increases, the difference in measurement results between the two measuring devices increases as shown in Figure 2. Above roughness 500 m, the difference and difference ratio are more than 100 m, 25%.

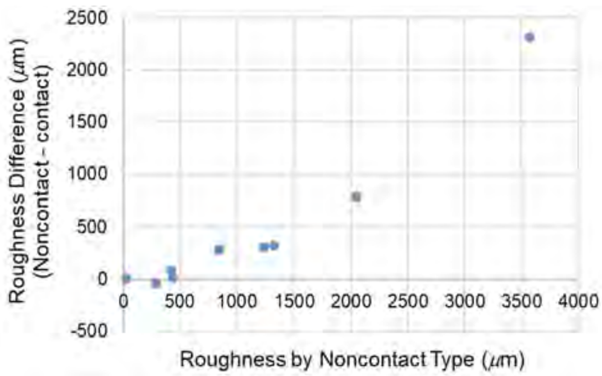

Figure 12 Comparison of roughness measurements

To verify the measurement results, the Laser-Doppler velocimetry (LDV) measurements were performed on a flat plate having roughness elements of various heights in Chungnam National University-Cavitation Tunnel (CNU-CT). Three flat plates with smooth and rough surface were used. The roughness of smooth is $k = 20$ m, and attached sandpapers are $k = 265$ and 1300 m from non-contract measurement system as shown in Figure 13.

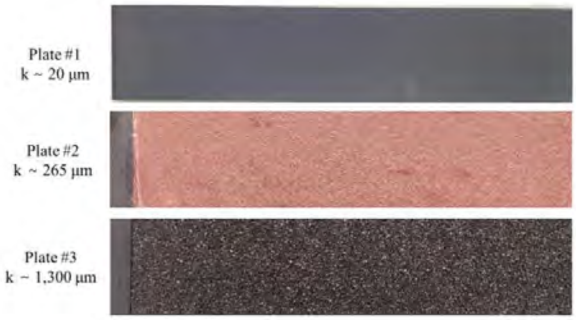

Figure 13 Three flat plates with smooth and rough surface

As shown in Figure 14, the velocity profile based on the roughness from non-contract system shows close agreement between the Schlichting equation's predictions and the LDV measurements.

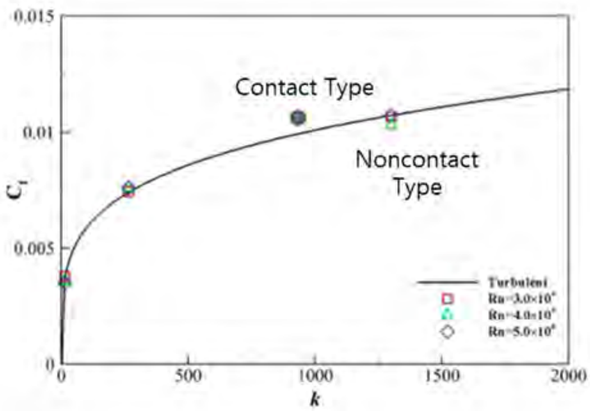

Figure 14 Calculated skin friction coefficient (Cf) along the roughness element, k.

Conclusions. From the LDV measurements of turbulent boundary layer velocity profiles on flat plates with different surface roughness, hull roughness over 500 m recommends to use non-contract type measurement system.

4.5 Effect of roughness on in-service performance

Effect of hull and propeller surface roughness on in-service performance have studied extensively using roughness functions derived from both CFD simulations and model experiments as reported in ITTC (2021) and IMO

(2022). Typical published works are reviewed in the following:

Song et al (2021b) conducted validation of similarity law scaling procedure for roughness effects by tank tests of a flat plate and a ship model in smooth and rough conditions. Roughness functions are derived from the flat plate test results. Total resistance of rough ship is predicted using the similarity-law scaled frictional resistance with 2D and 3D extrapolation method and compared with rough ship model results. It is shown that 3D extrapolation pre-dictions agree well with the measured rough model results.

Song et al (2020) simulated roughness effect of biofouling by URANS calculations for KCS and KVLCC2. Experimentally obtained roughness functions of barnacle fouling were employed in the wall-function of CFD software. The fouling effects on the resistance components, form factors, wake fractions and the flow characteristics were investigated from the simulations.

Song et al (2019) investigated the effects of biofouling on full-scale propeller performance using CFD. Simulations for the full-scale performance of KP505 propeller in open water, including the presence of marine biofouling. Experimentally obtained roughness functions of barnacle fouling (Demirel et al 2017) were employed in the wall-function of CFD. Rough-ness effect of barnacles of varying sizes and coverages on open water performance was predicted for advance coefficients ranging from 0.2 to 0.8.

IMO (2022) compiled and summarized all kinds of results relevant to the effect of biofouling on ship's performance found in the available scientific literature in the form of increase in GHG emissions from ships for different categories of biofouling. It is highlighted in the report that the inherent ability of biofilm sand slime to induce an effective roughness that is well in excess of what its physical appearance would traditionally suggest. For example, a layer of slime as thin as 0.5mm covering up to 50% of a hull surface could trigger an increase of GHG emissions in the range of 25 to 30%, depending on ship characteristics, its speed and other prevailing conditions. For more severe biofouling conditions, such as a light layer of small calcareous growth (barnacles or tubeworms), an average-length container ship could see an in-crease in GHG emissions of up to 60%, dependent on ship characteristics and speed. For the medium calcareous fouling surfaces, the in-crease in GHG emissions could be as high as 90%.

As described above, full-scale performance deterioration due to roughened hull and propeller surfaces have studied extensively using roughness functions derived from both CFD simulations and model experiments. However, as mentioned in IMO (2022), How-ever, estimating their impact of biofouling is not straightforward from such findings in the literature, as quantification is done using different ship performance parameters such as in-creased frictional resistance, effective power or shaft power. These parameters are not easy to understand from the perspective of non-specialists in ship hydrodynamics. In addition, validation of the predictions is decisively scare due to the non-availability of appropriate full-scale data. Therefore, rigorous validations of the full-scale predictions are indispensable for the development of practically reliable procedure for evaluating roughness effects on in-service performance.

4.6 Roughness usage in full-scale performance prediction

Roughness relates to fouling and aging effects on the full-scale performance prediction. In order to evaluate performance with these effects, ship performance throughout lifecycle in operation should be considered. Then, the evaluation of life cycle fuel consumption is considered as shown in Figure 15 (Sogihara, 2019).

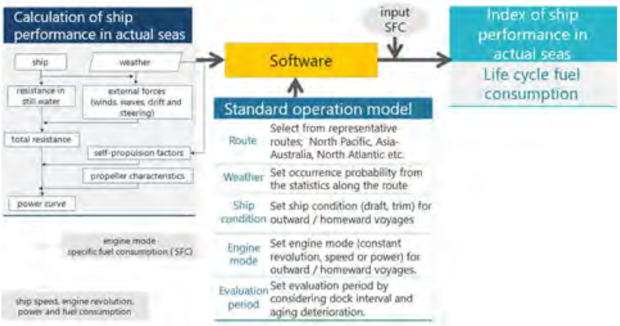

Figure 15 Concept of life cycle fuel consumption.

According to the concept shown in Figure 15, the life cycle fuel consumption is evaluated by combining the prediction of ship performance in actual seas (speed-power curve), which is estimated by following the flowchart shown in Figure 16 (Tsujimoto, 2018), and the standard operational model. (Kuroda, 2022)

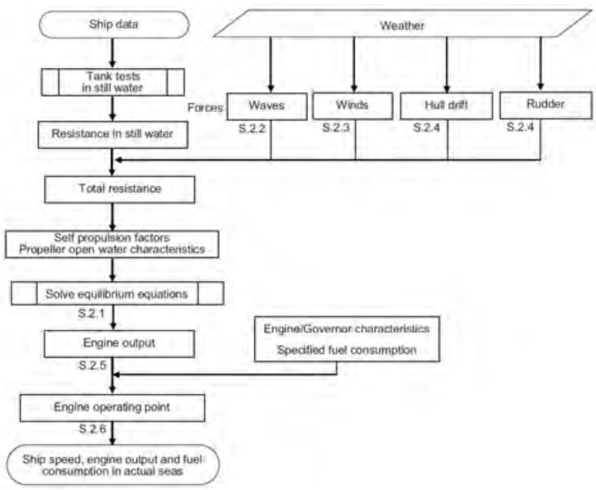

Figure 16 Flowchart for prediction of ship performance in actual seas.

In standard operational model, deterioration due to fouling and aging can be expressed as changes in hull resistance, propeller thrust and propeller torque as shown in following formulae. Here R_t is the hull resistance, T_p is the propeller thrust, Q_p is the propeller torque, t is the elapsed time, R_{t0}, T_{p0}, Q_{p0} are values at newly-built, p_{as} and p_{fs} are the deterioration ratios per year on hull resistance due to aging and fouling respectively, p_{fp} is the deterioration ratio per year on propeller efficiency, t_{ch} and t_{cp} are timings of cleaning for hull and propeller respectively.

$$R_t(t) = R_{t0}\{1 + p_{as}t + p_{fs}(t - t_{ch})\} \quad (1)$$

$$T_p(t) = (1 - a)T_{p0} \quad (2)$$

$$Q_p(t) = (1 + a)Q_{p0} \quad (3)$$

$$a = \frac{p_{fp}(t - t_{cp})}{2 - p_{fp}(t - t_{cp})} \quad (4)$$

Aging deterioration pas and fouling deterioration p_{fs} for hull resistance are expressed with the roughness parameter as shown in the following equation based on the Himeno's equation for the resistance coefficient due to roughness. (Himeno, 1983) Here, R_n is the Reynolds number, C_{T0} is the total hull resistance coeffeient, L is the ship length, and k_A is the apparent roughness height.

$$\left.\begin{matrix} p_{as} \\ p_{fs} \end{matrix}\right\} = \frac{1.8 \times 10^{-5} R_n^{0.55}}{C_{T0}L} \frac{dk_A}{dt} \quad (5)$$

Fouling deterioration pfs was set from the investigation results by Schultz(2007), and the life cycle fuel consumption is evaluated for the Cape-size bulker as shown in Figure 17. (Sogihara, 2022) Here p_{fs} was set as 2%(high-quality), 6.5%(middle), 11.0%(low quality) depending on quality of paint type, and pas was set as 0.3% based on the survey by Schultz(2007).

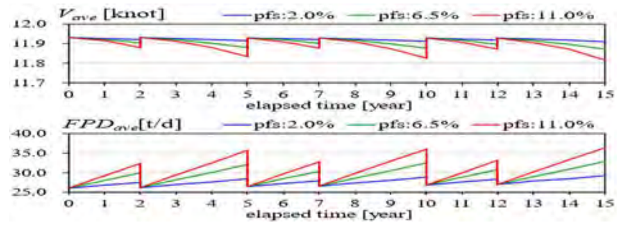

(a) Time variation of fuel consumption per day

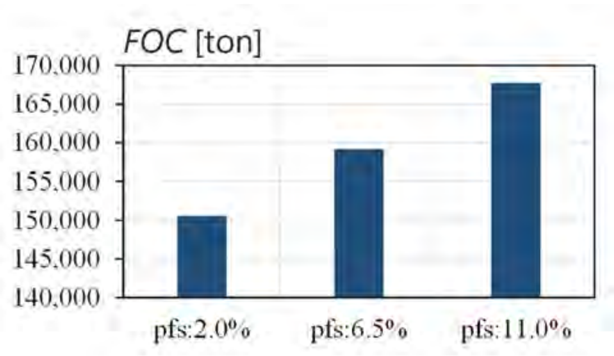

(b) Total fuel consumption in life cycle (15 years)

Figure 17 Results of fuel consumption

Performance prediction with roughness can be carried out with the relation between Roughness parameter and hull resistance. The aging effects can be considered with the change in resistance due to hull surface condition. Using the presented calculation model, aging effects on hull and propeller as well as fouling effect on hull can also be reflected in the performance prediction.

If analysed results for fouling and aging effects by onboard monitoring data for full-scale ships is obtained, a more realistic evaluation can be conducted.

5. SHALLOW WATER CORRECTION

5.1 General

The results of speed power trials are aimed to represent ideal conditions, including unrestricted deep water. In reality, the choice for practical trial locations may result in depths at which the ship's propulsion is influenced. In such case, a shallow water correction method is warranted to correct for these effects. Last term, a new shallow water correction method was introduced: the "Raven method". From that term, the need for further validation work was indicated. Within the current term, Raven's full report on the correction method was published and shared to the public. The committee reviewed the full report.

The 30th ITTC assigned the FSSPC with the following tasks:

Initiate and conduct speed trials on commercial ships on deep and shallow water to further validate Raven method)

Investigate the influence of water depth on the hull-propeller interaction (thrust deduction, relative rotative efficiency)

5.2 Validation

The committee members were invited to contribute to the validation of the method by conducting full-scale trials in shallow (and deep) waters. An emphasis was put on other parties than the developer of the method (MARIN), which has already provided validation within its publications. Organising such dedicated systematic trials on commercially operated ships has proven difficult, and no new results from trials were delivered or collected.

Propulsion factors

From literature review, including Raven's full report, it was concluded that the total propulsion efficiency is expected to remain relatively unaffected within the application range of the correction method. Raven's study on different ships showed the thrust deduction factor t increases for decreasing depth, but only for very shallow water (outside the method's application range). No clear trend was found within the application range. The wake fraction is more sensitive to shallow water effects within the application range, with (*1-w*) decreasing for decreasing depth. However, no usable approximation for all ship types is found yet. The changes in thrust deduction and wake fraction combined lead to a rise in hull efficiency. On the other hand, the propeller open water efficiency is expected to drop due to the increased resistance, (and thus higher propeller loading) and a reduced inflow speed (due to the increase of the wake fraction). This counteracts the rise in hull efficiency, leading to a small overall change in propulsive efficiency η_D .

Based on several test cases, it was concluded by Raven that assuming an unchanged propulsive efficiency η_D showed better merit. For the relative rotative efficiency no clear indication is found on the effect of shallow water. While large changes to the wake field may occur at very shallow water, the effect within the trial application range is expected to be minor.

5.3 Conclusion

For the last two terms, validation efforts by conducting dedicated series of trials have proven difficult to realize.

After review, is concluded appropriate to keep considering the propulsion effects unchanged within the application range of the shallow water correction method.

Based on the presently available validation results, it is recommended to keep the Raven method as the shallow water correction method in ITTC 2024 Procedure 7.5-04-01-01.1.

It is recommended to continue monitoring the research efforts in this field in the future.

6. WAVE CORRECTIONS

The mean value of wave added resistance in irregular waves is the end result to be actually used for the S/P trial analysis. Therefore, more validation of wave-added resistance methods, in particular SNNM, covering all wave encounter angles are carried out targeting the short-term estimation of wave-added resistance in irregular waves.

Additionally, following the request of AC, validation of the SNNM-SNU and SPAWAVE methods is conducted with the participation of 3 members of this committee. The wave added resistance responses in regular waves are validated against model test results.

6.1 Validation of SNNM method for the evaluation of wave added resistance in irregular waves

Validation setup. Validation of wave added resistance in irregular waves is not as straightforward as that in regular waves. To properly validate methods for the evaluation of mean wave added resistance in irregular waves, it is necessary to carefully setup the validation procedures.

The first and foremost issue is to determine the benchmark data. One obvious option is to use the model test result in irregular waves. However, it is unanimously agreed by this committee that such model results are scarce and the uncertainty of such tests can be very high. Therefore, it is deemed rational to apply the spectral analysis technique to the Quadratic Transfer Functions (QTFs) obtained from seakeeping model test, and use the short-term prediction result of mean wave added resistance as the benchmark. Moreover, due to limited available data, the evaluation is considered only for long-crest irregular waves, as according to equation (1).

$$R_{mean} = 2 \times \sum_{\omega_{min}}^{\omega_{max}} QTF(\omega) \cdot S_\eta(\omega) \cdot \Delta\omega \qquad (6)$$

The parameters in equation (1) will influence the end result of mean wave added resistance, which are listed and explained as follows:

- $QTF(\omega)$: quadratic transfer function of wave added resistance in regular waves corresponding to wave frequency ω;
- $S_\eta(\omega)$: wave energy spectrum;
- $\omega_{\min}$: lower limit of wave frequency for integration;
- $\omega_{\max}$: upper limit of wave frequency for integration;

- $\Delta\omega$: wave frequency interval for integration.

Considering that only a limited number of wave frequencies can be obtained through seakeeping model test, interpolation and extrapolation are necessary.

Three interpolation methods are compared, i.e., linear, spline, and a function approximation method provided by CTO Fowles and Cassiday (1986). Based on the model test result of a 20000TEU container vessel, these methods are compared as shown in Figure 1~3. As can be noticed, the spline and the function approximation methods may sometimes produce unrealistic wiggles. Therefore, linear interpolation of the QTF is preferred for robustness, and is adopted for the validation.

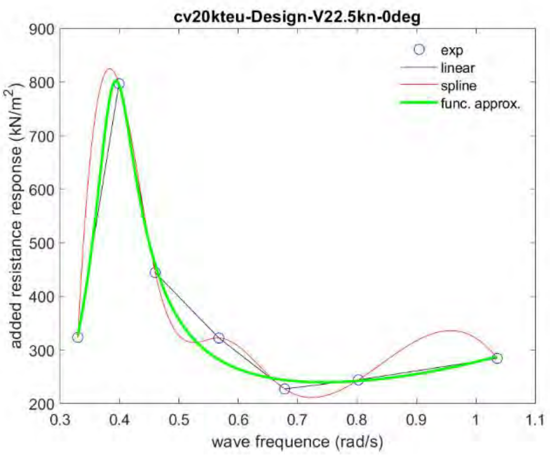

Figure 18 Comparison of interpolation methods (head wave case).

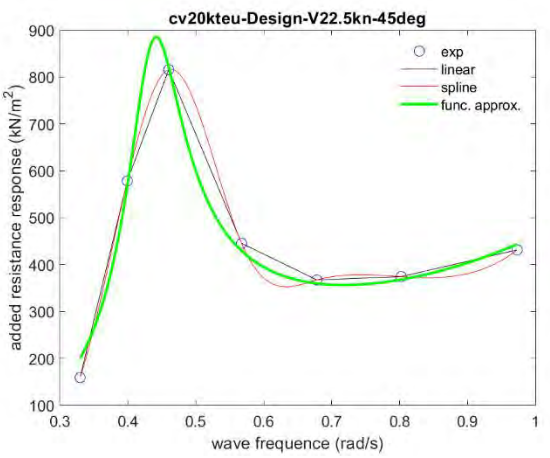

Figure 19 Comparison of interpolation methods (bow oblique wave case).

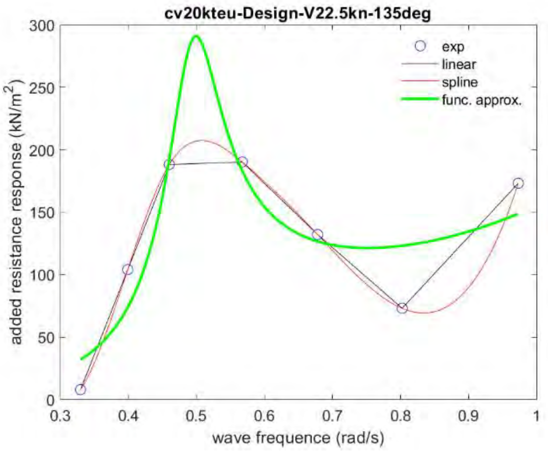

Figure 20 Comparison of interpolation methods (stern quartering wave case).

Extrapolation of the QTF in the long-wave (low wave frequency) range is manageable since it is both theoretically and experimentally proved that the wave added resistance responses will approach zero with the increase of wave length. In line with the linear interpolation method adopted for the validation, the QTF is considered to be linearly decrease to zero in the long-wave range, from the end data point to the upper limit.

Extrapolation of the QTF in the short-wave (high wave frequency) range is much more controversial, because there is no consensus on the trend of wave added resistance responses in the short-wave range. This is further due to the limited testing capacities and high uncertainties associated with the wave added resistance tests in short waves. To circumvent the problem, it is required that the model test data to be used as benchmark must contain at least one data point tested in the short regular waves, whose wave length to ship length ratio (λ/L) is smaller or equal to 0.5. If this requirement is met, then the QTF is extrapolated as constant in the short-wave range; otherwise, the set of model test data is discarded.

Moreover, it is also required that the set of model test data must contain at least 5 data points covering the range of λ/L from 0.5~2.0, with the peak response included to properly reflect the shape of the response spectrum.

Figure 21 is a demonstration of the treatment of the QTF for spectral analysis.

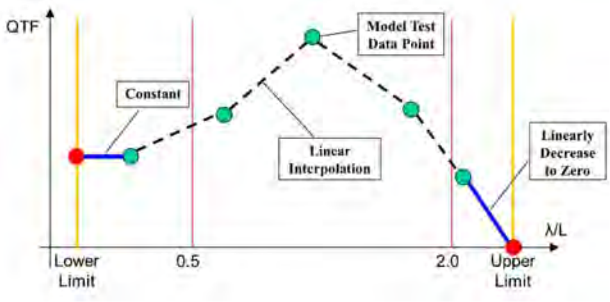

Figure 21 Treatment of QTF for spectral analysis.

Subsequently, the ITTC wave spectrum according to equation (2) is adopted for the validation, in consistent with the ITTC R.P. and the ISO15016 standard.

$$S_\eta(\omega) = 173\frac{H_S^2}{T_{01}^4\omega^5}\exp\left(-\frac{691}{T_{01}^4\omega^4}\right) \quad (7)$$

In equation (2), H_S is the significant wave height; T_{01} is related to the peak wave period T_P, i.e., $T_{01}=0.773T_P$.

In order to more comprehensively validate the performance of SNNM method in various sea conditions, four sea states are considered. Each sea state is the combination of one wave height with four likely wave peak periods, as listed in Table 1.

Table 1 Sea conditions for the validation

Sea State	SS2	SS3	SS4	SS5
H_S (m)	0.5	1.0	2.0	3.0
T_P (s)	6,7,8,9	7,8,9,10	8,9,10,11	9,10,11,12

Last but not least, computational-wise, the evaluation of equation (1) presents no challenge at all, so for our purpose, ω_{min} is set to be 0.01rad/s, ω_{max} is set to be 10rad/s, and $\Delta\omega$ is set to be 0.001rad/s to guarantee adequate spectrum coverage and integration accuracy.

Validation database. The same database adopted by the 29th ITTC Specialist Committee on Ships in Operation at Sea (SOS) is used for the current validation, containing the necessary input parameters of the sample ships for SNNM calculations and the seakeeping model test result of wave added resistance QTFs in regulars under various loading conditions, ship speeds and wave headings.

The sets of QTFs available from the database are checked according to the requirements specified in the validation setup section. Some cases are excluded either due to too few data points, or lack of certain input parameters. For cases involve repeated tests, the mean values are used for the spectral analysis.

In result, a total of 23 ships are included for the validation as listed in Table 2. The composition of ship types is shown in Figure 5.

Table 2 Validation database

No.	Ship	Organization	Condition	Vs (kn)	Heading (deg)
1	bulker	CSSRC	ballast	9	0, 45, 90, 135, 180
			scantling	9	0, 45, 90, 135, 180
			ballast	13	0, 45, 135, 180
			scantling	13	0, 45, 135, 180
			ballast	15	0, 45, 135, 180
			scantling	15	0, 45
2	KCS	CTO	design	12	180
			design	20	180
		MARIC	design	24	0, 45
3	cruise	HSVA	design	13	0
4	cruise		design	17	0
5	cruise		design	15	0, 30, 60, 90, 120
			design	21	0, 30, 60, 90, 120, 150, 180
6	cruise		design	15	0, 30, 60
			design	21	0, 30, 60
7	bulker	MARIC	design	13	0, 30, 60, 90, 120, 150, 180
8	bulker		design	10	0, 45, 90, 135, 180
9	KVL CC2		design	12	180
			design	15	0
10			design	14	0, 45, 90

	LNGC		design	20	0, 45, 90
11	S175		design	12	0, 30, 60, 90, 120, 150, 180
			design	20	0, 30, 60, 90, 120, 150, 180
12	bulker		design	8	0, 30, 150
13	tanker		design	10	0, 30, 60
			design	14	0, 30, 60
14	cruise	MARIN	design	12	0, 45, 90, 135, 180
15	ropax		design	22	0
			design	20	0
16	ropax		design	23	0, 45, 120
17	container		design	22	0, 45
			design	12	0
18	bulker	NMRI	ballast	17	0, 40
			laden	15	0, 40, 60
19	container		laden	21	0, 20, 40
20	pcc		laden	17	0, 60
			laden	21	0, 40
21	tanker		laden	18	0, 45
22	tanker	SAMSUNG	laden	10	0, 30, 60, 90, 120, 150, 180
			laden	15	0, 30, 60, 90, 120, 150, 180
23	LNGC		laden	13	0
			laden	20	0

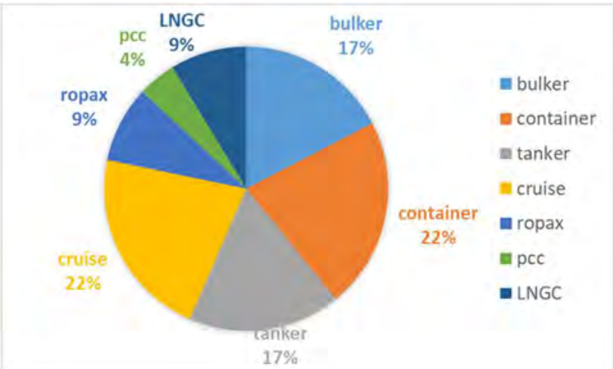

Figure 22 Composition of ship types.

<u>Validation result.</u> The spectral analysis of the QTFs under the sea conditions listed in Table 1 result to a total of 2144 data points. Calculations based on the SNNM method under the same conditions are performed.

The validation results are plotted in Figures 6~10, with data binned for various wave heading ranges. The correlation factors *R* between the benchmark and the SNNM method are listed in Table 3. The performance of SNNM is excellent in head to beam waves, but deteriorate in beam to following waves where the mean wave added resistances are small.

Table 3 Correlation factor

Wave heading range	Correlation factor
All wave headings	0.919
Head wave only	0.972
Head to bow oblique waves	0.946
Head to beam waves	0.931
Beam to following waves	0.713

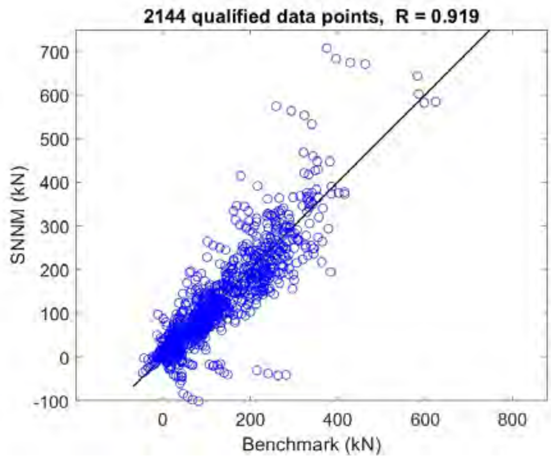

Figure 23 Validation result (all wave headings).

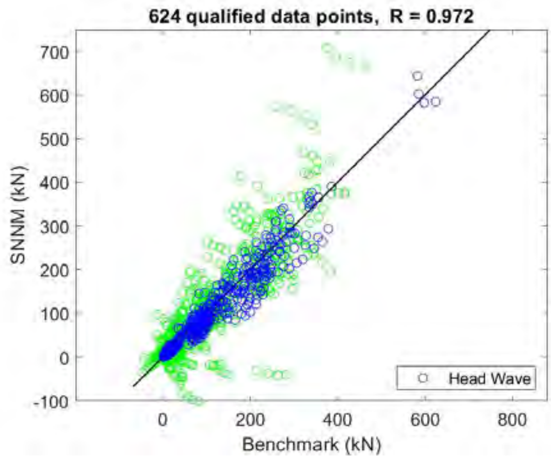

Figure 24 Validation result (head wave only)

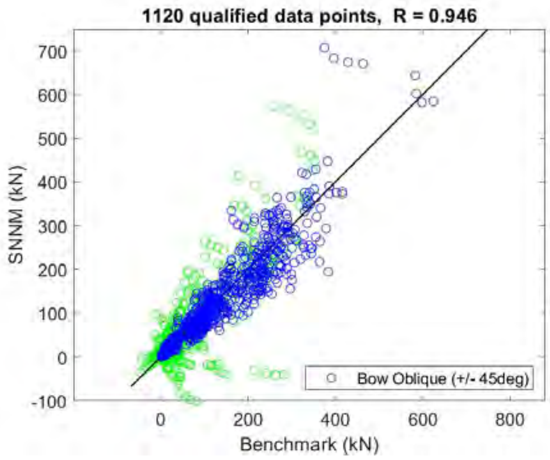

Figure 25 Validation result (head to bow oblique waves).

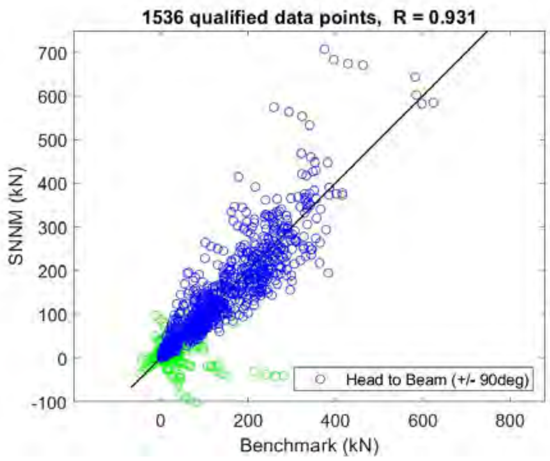

Figure 26 Validation result (head to beam waves).

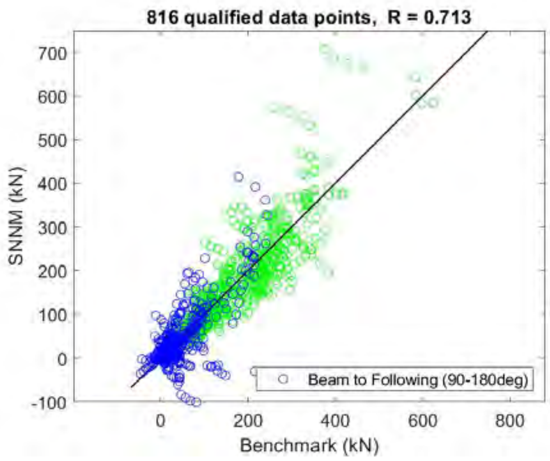

Figure 27 Validation result (beam to following waves).

6.2 Validation of various methods for the evaluation of wave added resistance in irregular waves using devoted dataset

Due to the lack of input parameters of the sample ships, the validation of methods other than the SNNM method is not feasible using the database in Section 6.1. For this reason, NMRI provided an in-house database and this committee performed the evaluation of wave added resistance in irregular waves based on 4 methods: STAWAVE-1, SNNM, NMRI and simple-NMRI (Kuroda, 2023). Among the methods, simple-NMRI is the latest and is introduced as follows.

Simple-NMRI method was proposed in order to solve the issue on the current simplified method: STAWAVE-1, that is, the effect of ship speed on added resistance in waves is not taken into account in STAWAVE-1. Because the speed trials are conducted at the different ship speed, the lack of the consideration of the ship speed is the critical matter and should be improved.

The update of the simplified method was considered based on the concepts for a simplified method:

- Easiness: calculate with a calculator,

- Simplicity: calculate with a small number of ship dimension,

and also based on the concepts for STAWAVE-1:

- Considering the component of the added resistance due to wave reflection in head waves which is primary in the short-waves,

- The same input as STAWAVE-1.

Simple-NMRI method applies the parameter expressing the effect of speed based on the NMRI method (theoretical method) in order to solve the problem for the current simplified method that the ship speed is not taken into account.

The outline of the method is described by the following formula. The details of the method and the validation results can be referred to the paper (Kuroda, 2023).

$$R_{AWL} = \frac{1}{16}\rho g H_S^2 B \frac{1.3(B/2)^2}{L_{BWL}^2 + (B/2)^2}(1 + C_{Ue}F_r) \quad (8)$$

$$C_{Ue} = \begin{cases} 10 & \text{for } \frac{L_{BWL}}{B} \leq 1.22 \\ 68 - 310\frac{1.3(B/2)^2}{L_{BWL}^2 + (B/2)^2} & \text{for } \frac{L_{BWL}}{B} > 1.22 \end{cases} \quad (9)$$

Where, R_{AWL} is the added resistance in long-crested irregular waves, ρ is the fluid density, g is the gravitational acceleration, H_S is the significant wave height, B is the ship breadth and L_{BWL} is the distance of the bow to 95% of the maximum breadth of the waterline, Fr is the Froude number.

Validation setup. The treatment of the QTFs obtained by seakeeping model test is the same as that elaborated in Section 3.1.

As for the wave conditions, the ITTC wave spectrum is also used, but only the significant wave height of 1m is considered, along with the wave peak periods varying from 6s to 12s at an interval of 1s.

Validation database. The sample ships included in the database provided by NMRI are listed in Table 4. Seakeeping model test results of the head wave case alone are considered for the validation.

Table 4 Validation database

No.	Ship	Condition	Vs (kn)
1	container	laden	21, 26
2	PCC	laden	16.8, 20.9
3	PXBC	laden	12.1, 14.9
4	VLCC	laden	13.3
5	JBC	laden	14.5
6	DTC	laden	16, 18
7	chemical tanker	laden	12.7
8	domestic cargo ship	laden	8.9

Validation result. The validation results are shown in Figure 28÷Figure 39. The correlation factors of the 4 methods against the benchmark are listed in Table 5. All methods have achieved a R value larger than 0.8. For the given data set, NMRI method is the most competitive.

Table 5 Correlation factor

Method	Correlation factor
STAWAVE-1	0.822
SNNM	0.887
NMRI	0.982
Simple-NMRI	0.897

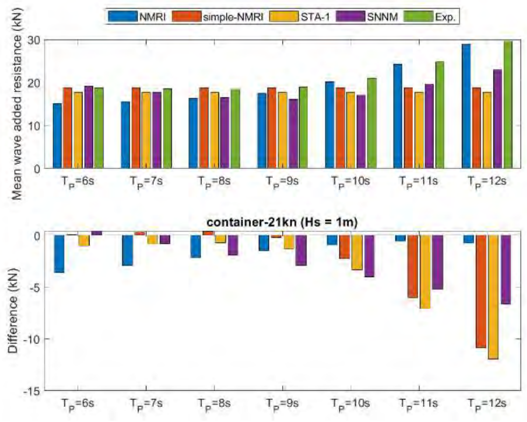

Figure 28 Validation result (container, 21kn).

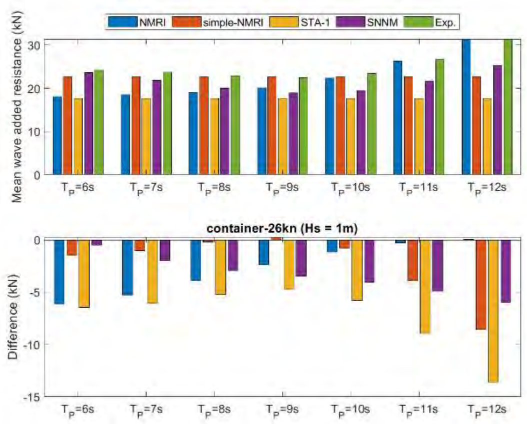

Figure 29 Validation result (container, 26kn)

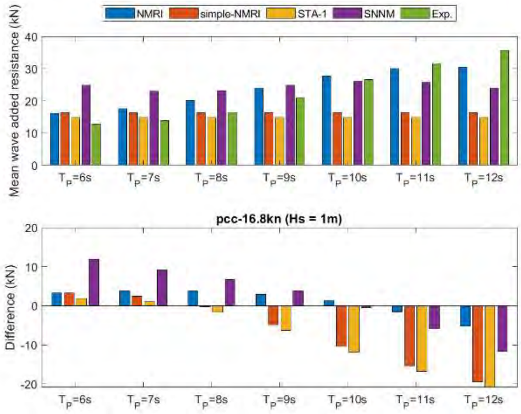

Figure 30 Validation result (PCC, 16.8kn).

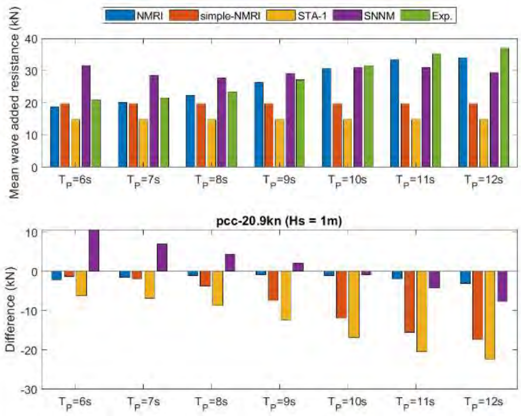

Figure 31 Validation result (PCC, 20.9kn).

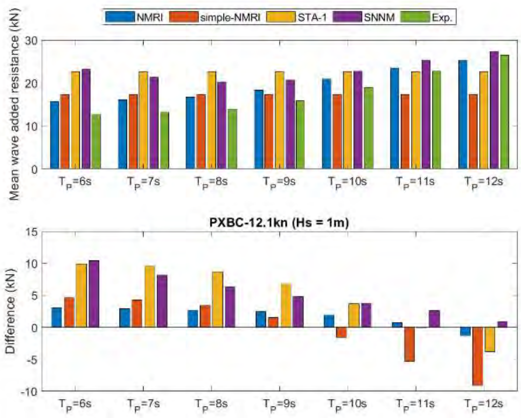

Figure 32 Validation result (PXBC, 12.1kn).

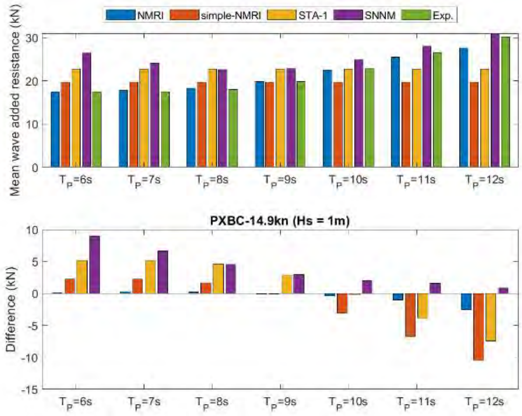

Figure 33 Validation result (PXBC, 14.9kn).

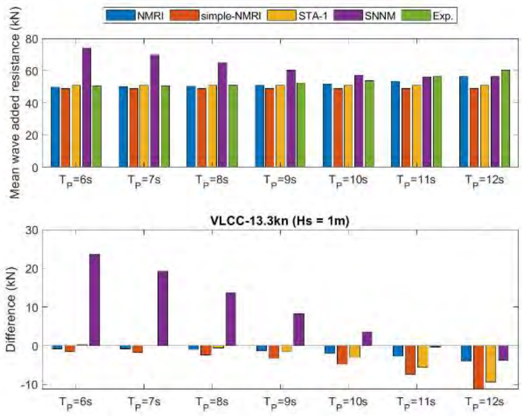

Figure 34 Validation result (VLCC, 13.3kn).

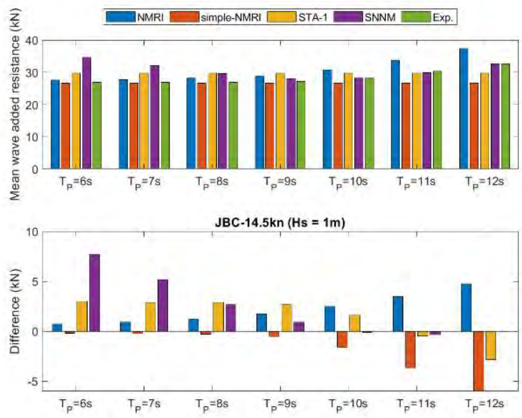

Figure 35 Validation result (JBC, 14.5kn).

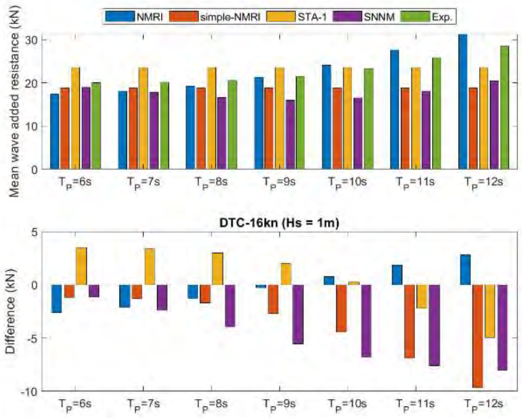

Figure 36. Validation result (DTC, 16kn).

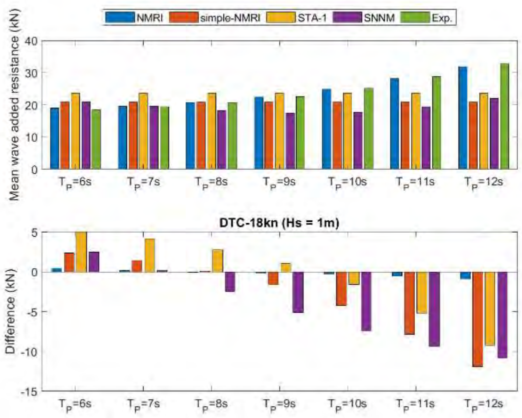

Figure 37 Validation result (DTC, 18kn).

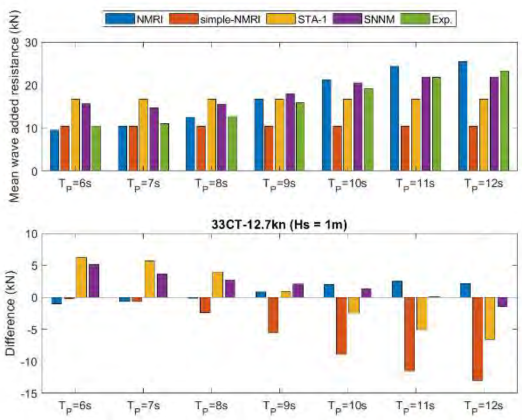

Figure 38. Validation result (chemical tanker, 12.7kn).

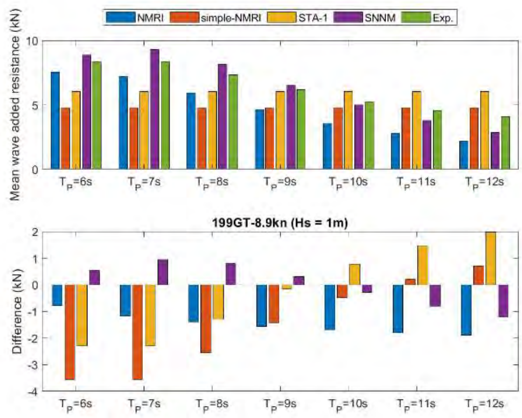

Figure 39 Validation result (domestic cargo ship, 8.9kn).

6.3 Comparison of calculated added waves resistance obtained from various methods in regular and irregular waves

To examine the capability of calculation methods for added wave resistance, comparisons have been made in terms of evaluation of added wave resistance in both regular and irregular waves. 3 methods including SNNM, SPAWAVE (Grin, 2022) and SNU methods (Lee & Kim, 2023) are used in this study.

The following 4 ship models are employed:

Model 1: Oil tanker
Model 2: Bulk carrier
Model 3: Ore carrier
Model 4: Container carrier

Added wave resistances in regular waves are calculated for the 4 ship models in fully loaded condition and compared with experimental data in Figure 40～Figure 43. 7 wave direction cases from head (180deg.) to following (0 deg.) with an interval of 30 degrees are examined. Added wave resistance is reduced to non-denationalized form (K_{AW}) with the square of double wave amplitude. It is noted that K_{AW} is equivalent to QTF for added wave resistance:

$$K_{AW} = \frac{R_{AW}}{4\rho g \zeta_a^2 (B^2/L)} \tag{10}$$

Where, R_{AW} is the added resistance in waves, ρ is the fluid density, g is the gravitational acceleration, ζ_a is the wave amplitude, B is the ship breadth and L is the ship length.

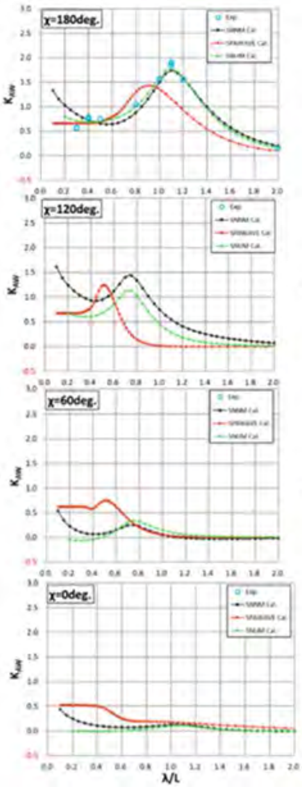

Figure 40 Comparison of added resistance in regular waves (Model 1 oil tanker).

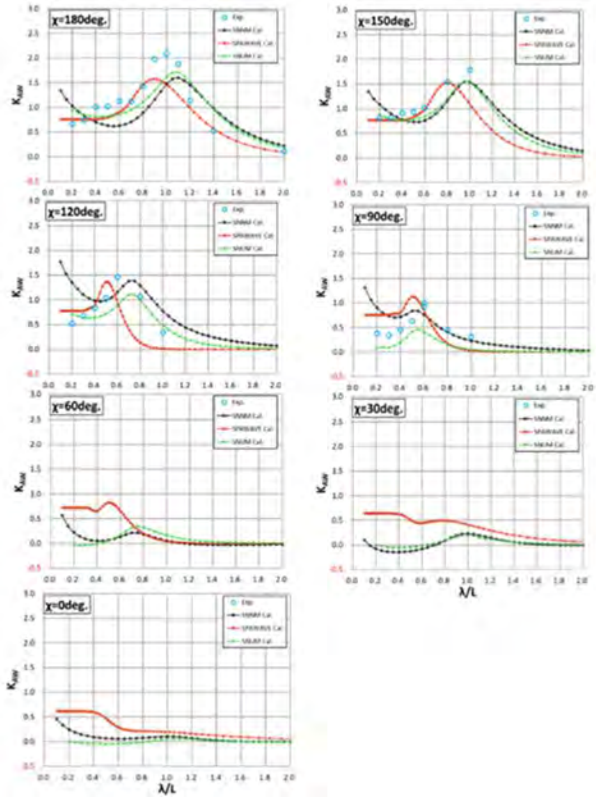

Figure 41 Comparison of added resistance in regular waves (Model 2 bulk carrier).

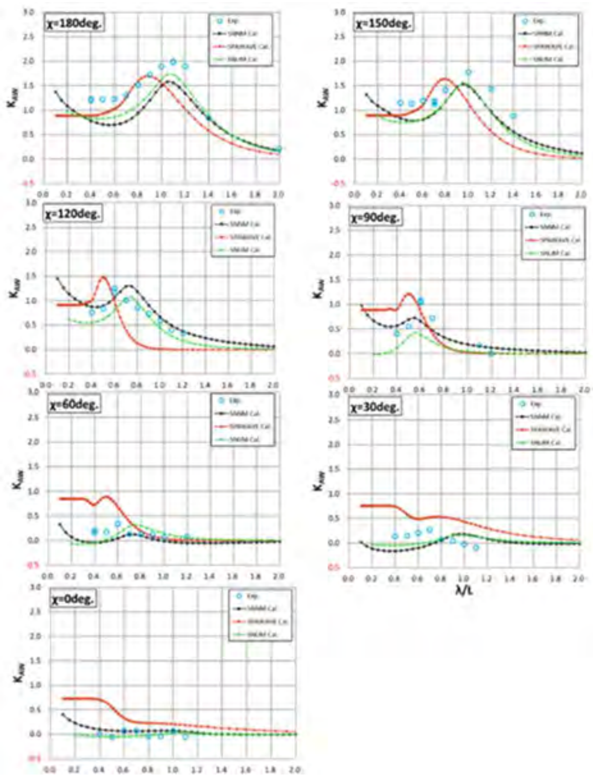

Figure 42 Comparison of added resistance in regular waves (Model 3 ore carrier)

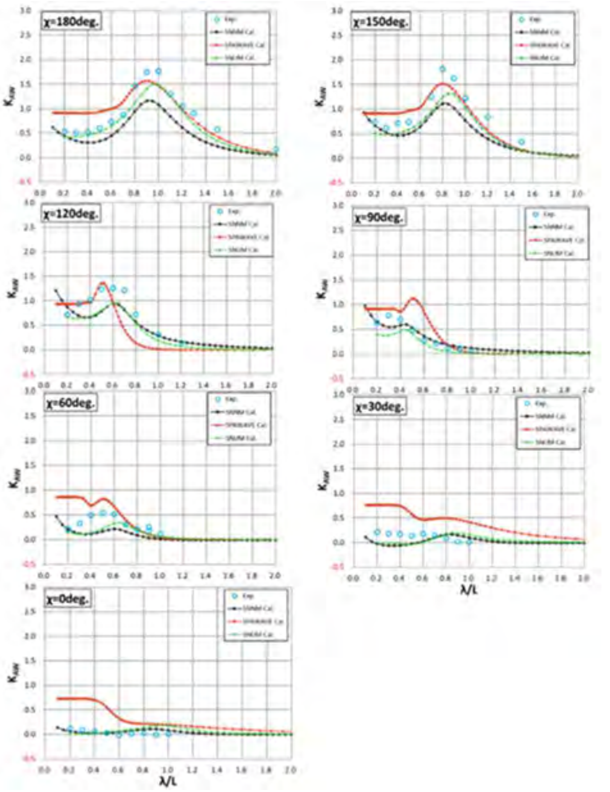

Figure 43 Comparison of added resistance in regular waves (Model 4 container carrier).

From the comparison of added wave resistances in regular waves, the following features can be observed among the calculation methods:

a) SNU method shows similar behaviour as SNNM method except for in shorter waves.

b) SPAWAVE method calculations are generally higher than the other 2 methods in shorter waves in beam to following directions.

c) SPAWAVE method tends to predict peak of added resistance in shorter waves than the other 2 methods.

Added wave resistances in long-crested irregular waves are calculated for the 4 ship models using QTFs shown in Figure 44÷Figure 47. In the calculation ITTC (1964) wave spectrum is employed. Mean Wave Period (Tm) range corresponding to BF scales from 1 to 12 (1.2s to 15.0s) are considered. Calculated data are compared with experimental ones in Figure 44÷Figure 47 at 7 wave direction cases from head (180deg.) to following (0 deg.) with an interval of 30 degrees. Mean added wave resistance in irregular waves are evaluated in the form normalized with the square of significant wave height.

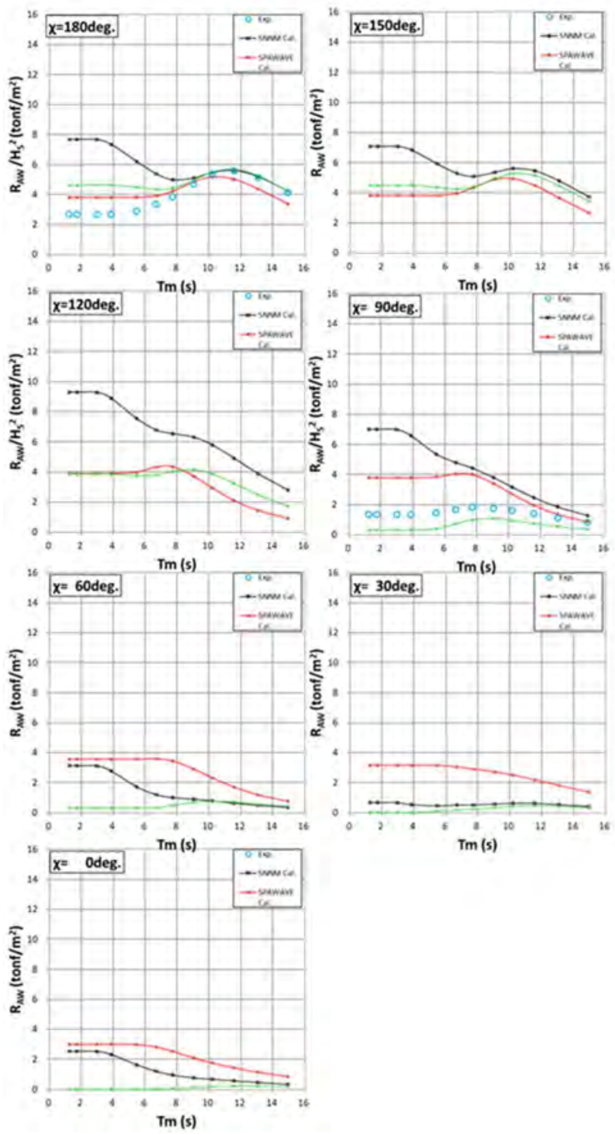

Figure 44 Comparison of added resistance in irregular waves (Model 1 oil tanker)

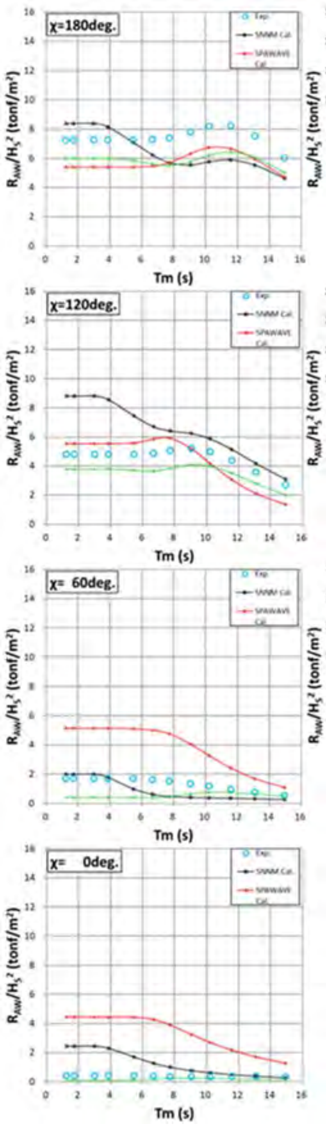

Figure 45 Comparison of added resistance in irregular waves (Model 2 bulk carrier).

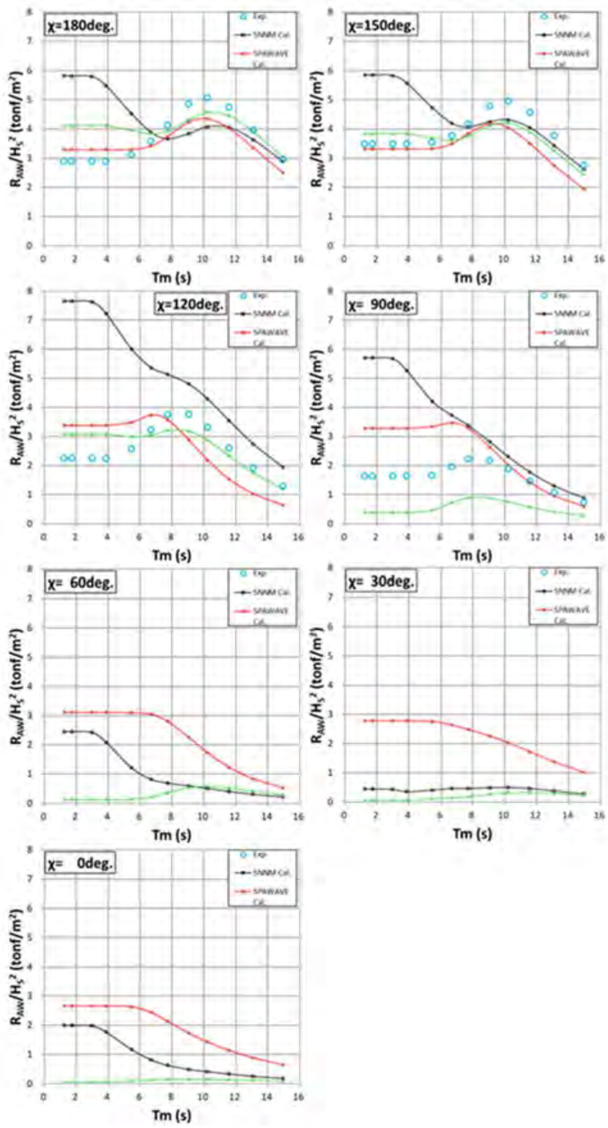

Figure 46 Comparison of added resistance in irregular waves (Model 3 ore carrier).

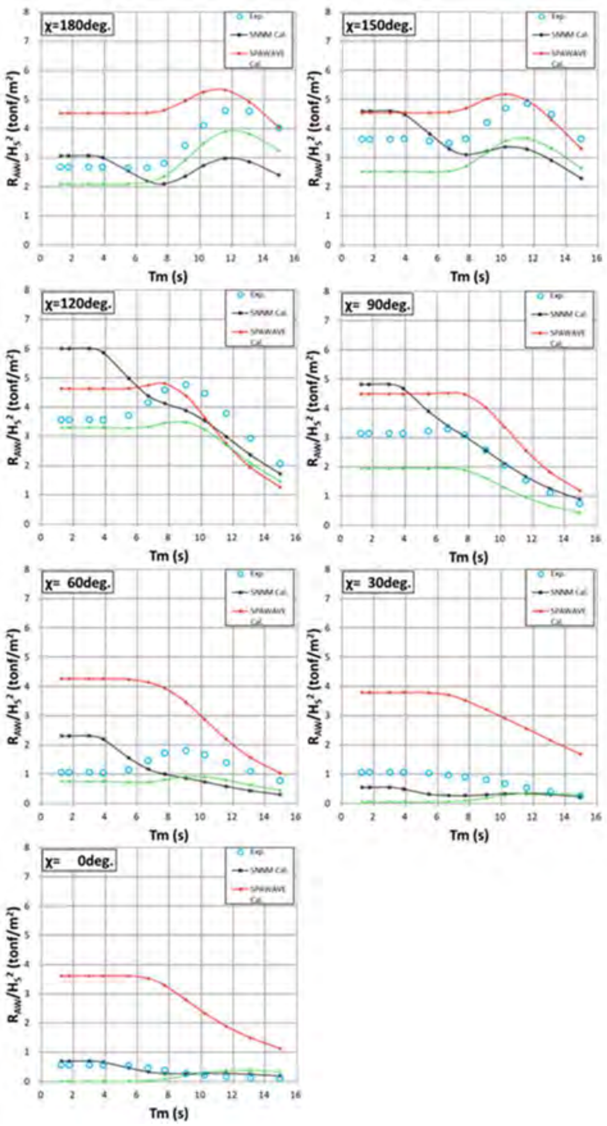

Figure 47 Comparison of added resistance in irregular waves (Model 4 container carrier).

As clearly shown in the comparisons above, there are significant variations among calculated added wave resistances, in particular, at shorter waves periods. Also noted is that agreement with the experimental data is not satisfactory. No general trends can be drawn from this comparison in terms of the capability of the calculation methods evaluated in this study. That is, difference between particular calculation methods and experimental data is quite variable depending on model cases. Since accuracy in calculated wave added resistance in shorter wave periods is indispensable to enhance the accuracy of Speed/Power trial results, further examination and refinement of methods for the capability of wave added resistance may be needed.

6.4 Validation of SNNM-SNU method

For SNNM-SNU method, the simplified method has been developed for the practicability, and it is denoted as SNNM-SNUs method (Lee & Kim, 2023). Here, SNNM-SNU method is used for the validation.

The published experimental data (Yokota and Kuroda et al. 2021, Yokota and Tsujimoto et al. 2021, Sasaki et al. 2009, Tsujimoto et al. 2018, Tsujimoto 2012, Tsujimoto et al. 2023) are used for the validation, which is data of the same ships shown in Table 4 in Section 6.2.

The validation results are shown in Figure 48. Here, K_{AW} is the coefficient of the added resistance in regular waves.

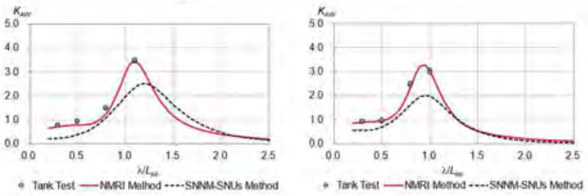

(a) container, 26kn(left: head waves, right bow waves(40 deg.)).

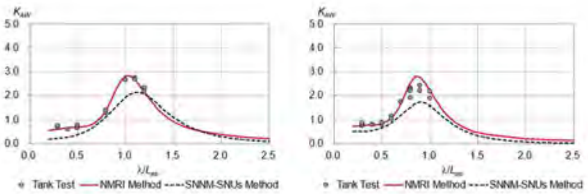

(b) container, 21kn(left: head waves, right bow waves(40 deg.)).

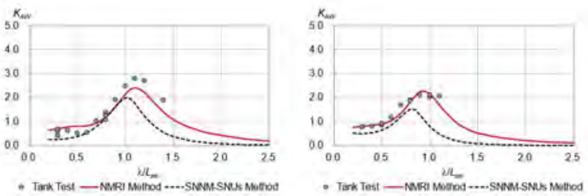

(c) PCC, 20.9kn (left: head waves, right bow waves(40 deg.)).

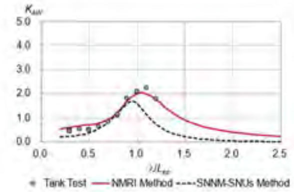

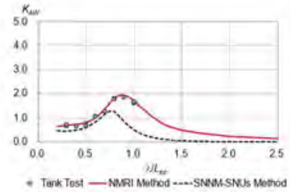

(d) PCC, 16.8kn (left: head waves, right bow waves(40 deg.)).

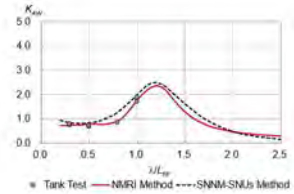

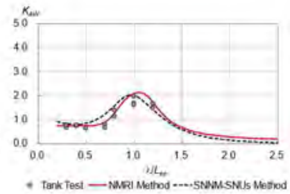

(e) PXBC, 14.9kn (left: head waves, right bow waves(40 deg.)).

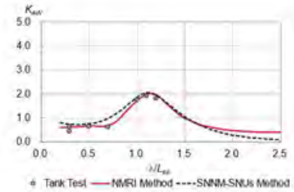

(f) PXBC, 12.1kn (head waves).

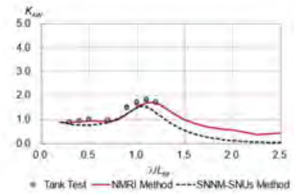

(g) VLCC, 13.3kn (head waves).

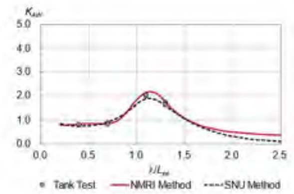

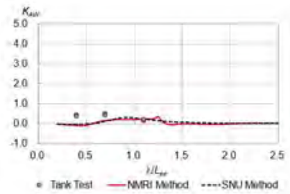

(h) JBC, 14.5kn (left: head waves, right: quartering waves(135 deg.)).

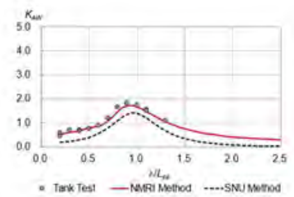

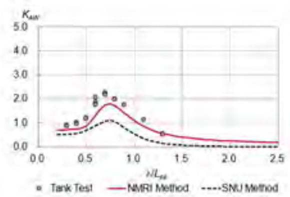

(left: head waves, right: bow waves(45 deg.))

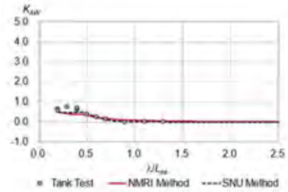

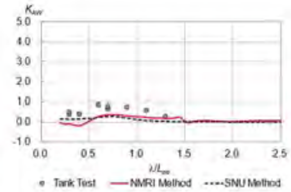

(left: beam waves, right: quartering waves(135 deg.))
(i) DTC, 18kn.

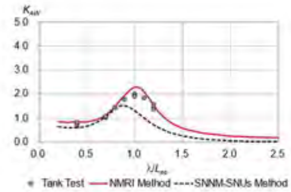

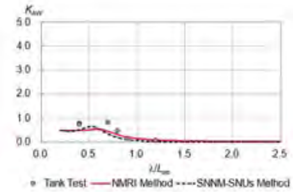

(left: bow waves(45 deg.), right: beam waves)

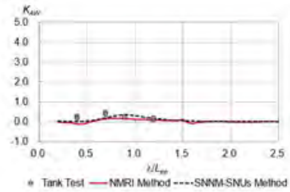

(quartering waves(135 deg.))
(j) chemical tanker, 12.7kn.

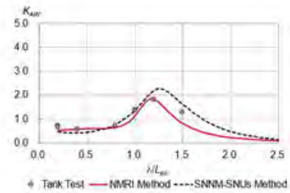

(k) domestic cargo, 8.9kn.

Figure 48 Validation result in regular waves for SNNM-SNUs

From the comparison between SNNM-SNUs method and tank test results, the followings are findings.

For fine ships: container ships and PCC, calculated results underestimate tank test results. For blunt ships: bulk carriers, tankers and general cargo, relation between calculated results and tank test results are different in each ship. These discrepancies have been found both in short waves where the contribution by SNUs is larger and in longer waves where the contribution by SNNM is larger. The cause is the effect of ship hull forms that cannot be considered just by representative ship parameters since calculated results by NMRI method are in good agreement with tank test results.

As the conclusions, there is no advantage to apply the SNNM-SNUs method as the recommended method since calculation accuracy of SNNM-SNUs is inferior to that of NMRI method.

6.5 Added resistance in short waves

The added resistance in short wave be-comes more important for the larger ship. However, due to the difficulties of generating very short waves in experimental tank, it is also difficult to validate the estimation method.

Here are shown the experimental results for very short waves in Actual Sea Model Ba-sin in NMRI and those from referred paper for the post-Panamax container ship (DTC) (Yokota, 2020).

Figure 49 shows the frequency response of the added resistance in regular waves and three types of interpolations. Case1 is the constant from λ/L =0.2 of EXP.1 (NMRI), case2 is monotonically increasing from λ/L=0.2 of EXP.2 (SHOPERA) and case3 is constant from λ/L =0.2 of EXP.2. Figure 50 shows the added resistance in long-crested irregular waves for three cases. It was found that the three types have difference only in very short waves for the frequency response, but when converted at irregular waves, there is a large difference. For example, at T=6.7s, the wave correction by case2 will be four times larger than that by case 1. It may lead unreasonable high-performance ship as a result of speed trial.

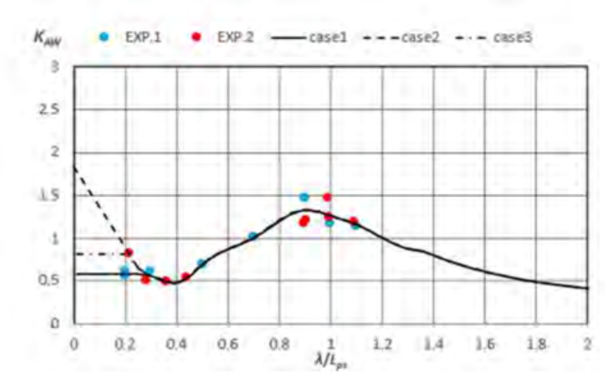

Figure 49 Three types of frequency response interpolated from experimental values.

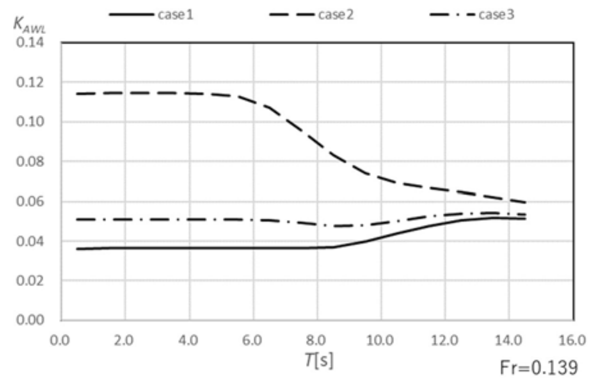

Figure 50 Added resistance in long-crested irregular waves (Fr 0.139).

The effect of the tendency of added resistance in very short waves is remarkable in irregular waves.

The effects of differences in test results in very short waves cannot be ignored, and highly accurate measurements are required.

For the validation in very short waves, quality assured data should be used and accumulated.

Until sufficient validation would be completed, it is recommended that the added resistance in short waves is treated as a constant value for the analysis of speed trial.

6.6 Wave height effect on the added resistance in waves

The added resistance in waves is expressed as proportional to the square of the wave height, and linear superposition with the wave spectrum is conventionally used for the evaluation in irregular waves. It has been reported that uncertainty of tank test is larger in smaller waves, and the added resistance divided by the square of wave height becomes small due to nonlinear effects in larger waves (e.g. Nakamura, 1975). However, the wave height effect has difficulty to treat on the linear superposition for the conventional spectrum method.

Figure 51 shows an example for the comparison between test results in long-crested irregular waves and predicted results with the wave frequency spectrum and the response function. (Yasukawa, 2020) It was found that the difference of added resistance in irregular waves was shown at the wave height of 5m.

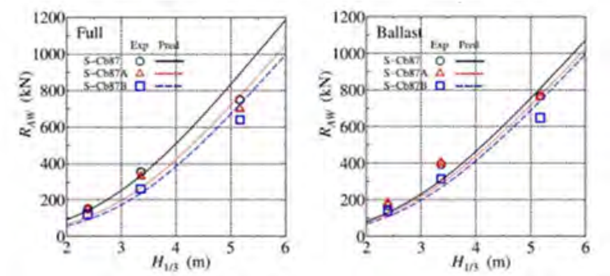

Figure 51 Comparison between test results in long-crested irregular waves and spectrum prediction.

On the other hand, In the guideline by ClassNK (Nippon Kaiji Kyokai, 2010), 3m is recommended for the experiment. Here, it is noted that for smaller ships, the wave height can be set to small: Length/100 in order to avoid nonlinear effects, and for larger ships, the wave height can be set to large: Length/100 in order to avoid large uncertainly.

The wave height effect is difficult to be included currently. Considering the wave height at the actual speed trial, the wave height effect can be negligible.

7. WIND CORRECTION

In full-scale ship performance evaluations by sea trials, the added resistance by wind has a significant impact. Considering this importance, accurate determination of wind speed and direction is essential. Ideally, undisturbed incident wind should be measured for accurate ship performance evaluation. However, the wind measurement method using an anemometer is susceptible to interference from the ship's structure. To address this, the Wind Averaging Method (WAM) was introduced, but its accuracy and potential side effects have not been thoroughly validated in actual sea environments. In this study, we examined the limitations of WAM in actual sea trial conditions and explored alternative approaches.

7.1 Problem of Wind Averaging Method in Actual Sea Trial Environments

Table 6 Power correction error due to WAM when wind velocity changes during double run

Incident true wind velocity	Wind velocity variation during double run					
	0%	+5%	+10%	+15%	+20%	+25%
10 m/s	0.0%	0.5%	0.9%	1.4%	1.8%	2.3%
8 m/s	0.0%	0.4%	0.8%	1.2%	1.6%	2.0%
6 m/s	0.0%	0.3%	0.7%	1.0%	1.3%	1.7%
4 m/s	0.0%	0.2%	0.5%	0.7%	1.0%	1.2%

Table 7 Power correction error due to WAM when wind direction changes during double run

Incident true wind velocity	Wind direction variation during double run				
	0°	+10 °	+20 °	+30 °	+40 °
10 m/s	0.0%	0.6%	1.9%	4.1%	6.5%
8 m/s	0.0%	0.3%	0.9%	2.2%	3.9%
6 m/s	0.0%	0.1%	0.5%	1.2%	2.2%
4 m/s	0.0%	0.1%	0.3%	0.7%	1.2%

It was confirmed that WAM can cause errors on ship's speed-powering performance evaluation in an environment where the wind changes during double run. Under the assumption that the wind measurement is accurate, if the incident true wind velocity and direction change during double run, the WAM itself generates error as shown in Table 6 and Table 7. The cases in which the error caused by the WAM due to the wind variation exceeds 0.5% and 1.0% of the total propulsion power are marked in orange and red respectively. For instance, errors due to WAM when over 1 m/s or 20 degrees change in actual true wind could significantly impact (over 1% in power) on performance evaluation.

In actual sea trial environments where wind speed and direction easily fluctuate, the WAM is likely to introduce significant errors during sea trials. Table 8 is the calculation results of the probability that the wind is stable (wind speed variation below 1 m/s and wind direction variation below 20 degrees) for 2 hours by analyses five years of data from the Korea Meteorological Administration (KMA)'s marine weather buoy located in the three sea areas surrounding the Korean Peninsula. The probability that such stable conditions occur is only 32% per year on average, with a particularly low probability during winter (around 12%). These findings highlight that WAM has a high possibility of causing performance evaluation errors exceeding 1% in typical sea trial situations. Therefore, the accurate wind measurement is crucial rather than compensating for disturbed wind using WAM.

Table 8 the probability of stable wind in Korean offshore

Location of buoy (Korea)		East sea (Ulsan)	West sea (Mokpo)	South sea (Jeju)	monthly average
Month	1	12%	33%	47%	31%
	2	12%	35%	31%	26%
	3	32%	40%	30%	34%
	4	24%	28%	44%	32%
	5	31%	32%	40%	34%
	6	37%	25%	24%	29%
	7	54%	36%	39%	43%
	8	48%	34%	41%	41%
	9	26%	41%	24%	30%
	10	25%	41%	28%	31%
	11	22%	37%	33%	31%
	12	12%	34%	25%	24%
average		28%	35%	34%	**32%**

7.2 Methods for Accurate Onboard Wind Speed Measurement

Two methods were investigated for accurate onboard wind speed measurement: LiDAR-based remote sensing and Computational Fluid Dynamics (CFD) simulations to determine optimal anemometer placement.

7.2.1 Remote wind measurement by using LiDAR

LiDAR appears to be a promising instrument that can remotely measure wind flow accurately, but its high cost and the need for continuous maintenance and large equipment for installation limit practical use. Additionally, its onboard installation may introduce the errors due to ship motion and vibrations, requiring further research for sea trial applications.

7.2.2 Validation of CFD-Identified Anemometer Locations

To address the practical limitations of LiDAR and avoid errors associated with WAM, Computational Fluid Dynamics (CFD) was employed to calculate the airflow around a ship and determine suitable locations for anemometer installation.

To establish criteria for identifying appropriate positions, we investigated errors of ship's performance estimation due to amount of wind distortion in 15K TEU container carriers where wind resistance is relatively significant. We aimed for power estimation errors due to wind distortion within 2%. As shown in Table 9 and Table 10, when wind disturbance by wind speed were within 10% and direction were within 10 degrees compared to inflow wind, the performance estimation error remained within 2%.

Table 9 Estimated propulsion power error due to 10% of wind velocity error in container carrier

Inflow wind velocity (m/s)	Inflow wind direction (deg.)						
	0	30	60	90	120	150	180
4	0.5%	0.5%	0.3%	0.0%	-0.2%	-0.2%	-0.2%
6	0.9%	0.9%	0.5%	0.1%	-0.1%	-0.3%	-0.2%
8	1.3%	1.3%	0.7%	0.3%	0.0%	-0.2%	-0.2%
10	1.8%	1.8%	1.0%	0.5%	0.0%	-0.1%	-0.1%

Table 10 Estimated propulsion power error due to 10 deg. of wind direction error in container carrier

Inflow wind velocity (m/s)	Inflow wind direction (deg.)						
	0	30	60	90	120	150	180
4	0.2%	-0.3%	-0.7%	-0.7%	-0.5%	-0.3%	0.2%
6	0.4%	-0.5%	-1.2%	-1.1%	-0.7%	-0.3%	0.2%
8	0.6%	-1.0%	-1.7%	-1.3%	-0.9%	-0.4%	0.1%
10	0.8%	-1.5%	-2.0%	-1.6%	-1.1%	-0.4%	0.1%

The CFD conditions used to calculate the airflow around the ship are summarized in Table 11 and Table 12. Calculations were performed for three ship types (LNG carriers, LPG carriers, and tankers). Incident wind is considered as relative wind to simulate the actual sea trial situation.

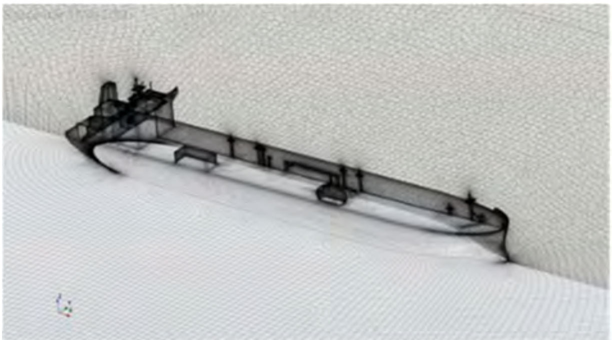

Figure 52 Example of CFD grid (LPG carrier)

Table 11 CFD calculation conditions

CFD Code/version	OpenFOAM v10
Solver	PimpleFoam
Fluid	Air, constant density
No. of cells	15~20 millions

Table 12 Incident wind condition for CFD calcualtion (V: velocity, D: direciton)

Ship type	LNGC		VLCC		LPGC		Container C.	
Ship V_{Ref}	18.0 knots		15.0 knots		16.0 knots		22.0 knots	
Wind V_{inflow}	8 m/s		8 m/s		8 m/s		8 m/s	
Inflow direction (deg.)	V	D	V	D	V	D	V	D
0	17.3	0	15.7	0	16.2	0	19.3	0
30	16.7	13.9	15.2	15.3	15.7	14.8	18.7	12.4
60	15	27.6	13.6	30.6	14.1	29.5	16.8	24.3
90	12.2	40.8	11.1	46	11.5	44.2	13.9	35.3
120	8.7	52.8	7.9	61.8	8.1	58.6	10.1	43.4
150	4.6	59.8	4.1	78.9	4.2	72	5.9	42.3
180	1.3	0	0.3	180	0.2	0	3.3	0

As shown in Figure 53 to Figure 58, the possibility of finding an appropriate location by CFD was confirmed. There were some anemometer positions where the disturbance of wind velocity and wind direction was calculated within 10% or 10 degrees respectively in cases of LNG carrier and tanker. However, for LPG carrier case, appropriate positions could not be determined by using CFD simulations. Therefore, some supplementary methods such as LiDAR or additional WAM usage may be necessary in this case. (These results are not representative of specific ship types because they are ones of example vessels)

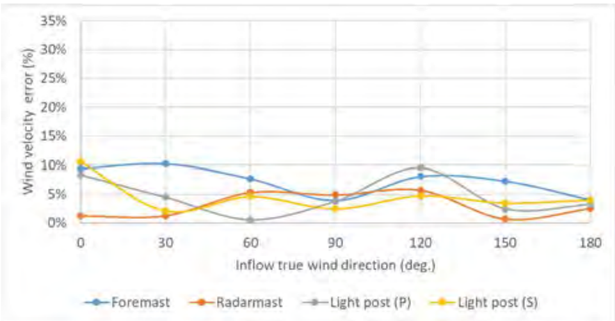

Figure 53 Wind velocity disturbance rate calculated by CFD for a LNG carrier

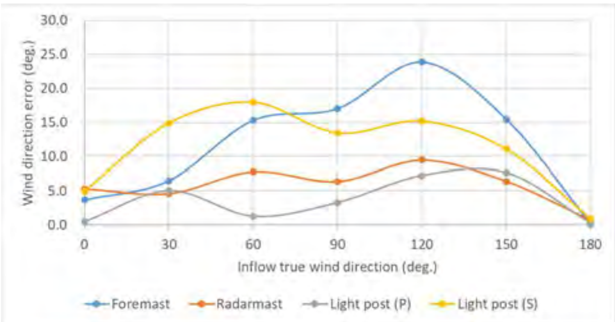

Figure 54 Wind direction disturbance calculated by CFD for a LNG carrier

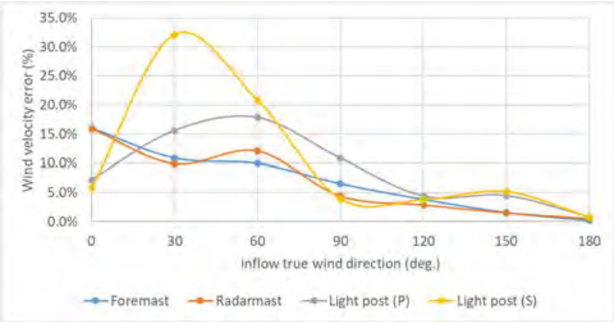

Figure 55 Wind velocity disturbance rate calculated by CFD for a LPG carrier

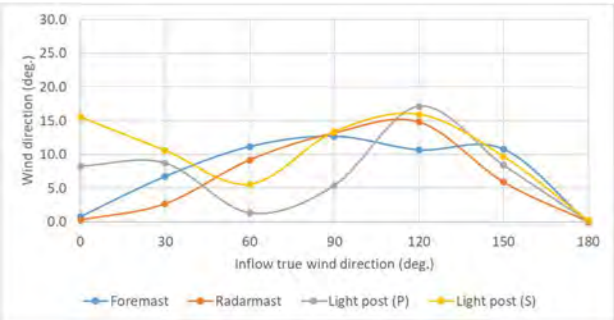

Figure 56 Wind direction disturbance calculated by CFD for a LPG carrier

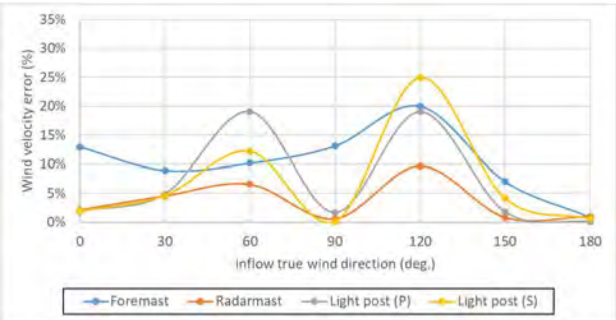

Figure 57 Wind velocity disturbance rate calculated by CFD for a Tanker

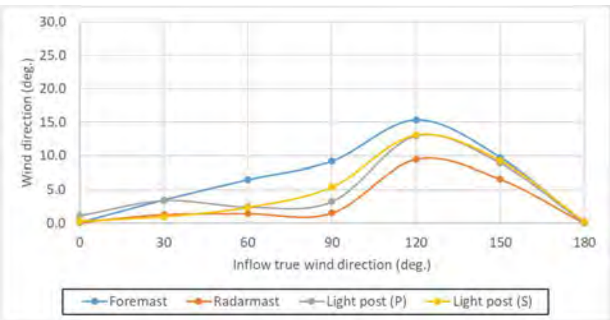

Figure 58 Wind direction disturbance calculated by CFD for a Tanker

Some anemometer positions where is evaluated by CFD were validated through onboard measurements during sea trials. The wind disturbance rate of radar mast, signal light post, and foremast was evaluated by CFD calculation, and measurements were performed at each location during speed trial of a LPG carrier and a container carrier. the wind measurement results obtained from anemometers at each location were compared to undisturbed wind measured by LiDAR. The comparison results were observed when the wind was stable and when the wind change was severe during sea trial.

As shown in Table 13, Figure 59, and Figure 60 below, it was confirmed that in a situation where the wind is stable during the speed trial of a LPG carrier, the measurement at Foremast where determined to be the best position by CFD can derive a more accurate wind than the case where measured wind is corrected by WAM at the onboard anemometer position (Signal post) where is being more disturbance.

Table 13 Absolute error rate at each anemometer position compared to Lidar measurement during speed trial

Run No.	Signal post (Onboard)	Radar mast	Foremast	WAM (Signal post)
1-1	16.3%	17.3%	7.8%	8.2%
1-2	2.0%	3.4%	0.6%	5.8%
2-1	27.5%	14.8%	12.7%	15.5%
2-2	0.4%	1.5%	3.0%	11.2%
3-1	17.1%	17.3%	9.3%	13.3%
3-2	0.2%	1.1%	2.1%	3.3%
Average	10.3%	8.3%	5.3%	8.9%
CFD results	9.9%	8.8%	2.3%	

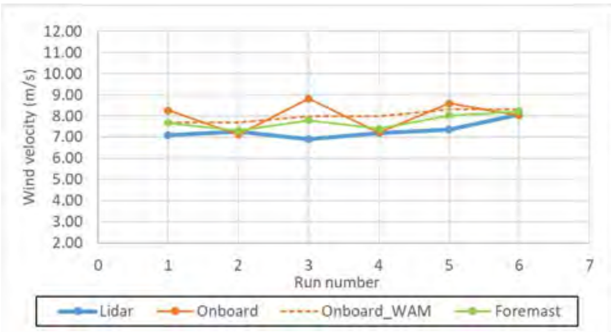

Figure 59 Wind velocity measurement results at each anemometer position during speed trial of a LPG carrier in stable wind

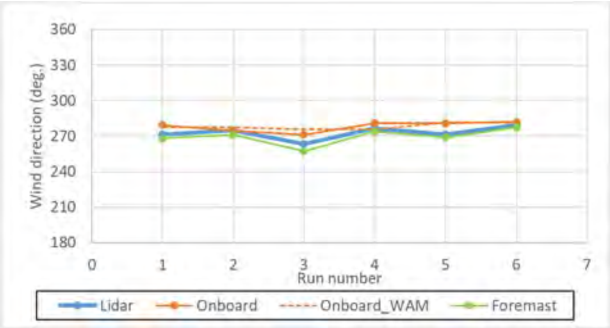

Figure 60 Wind direction measurement results at each anemometer position during speed trial of a LPG carrier in stable wind

As shown in Figure 61 and Figure 62, it was confirmed that even in the situation where the wind changes during speed trial, the measurement at Foremast, which was judged to be an appropriate position through CFD, can derive a more accurate wind than the case where measured wind is corrected by WAM at the onboard anemometer position (Radar mast) where is being more disturbance. In particular, when the wind dramatically changes during speed trial, the wind speed and wind direction corrected by WAM cannot even keep up with the actual wind trend measured by Lidar.

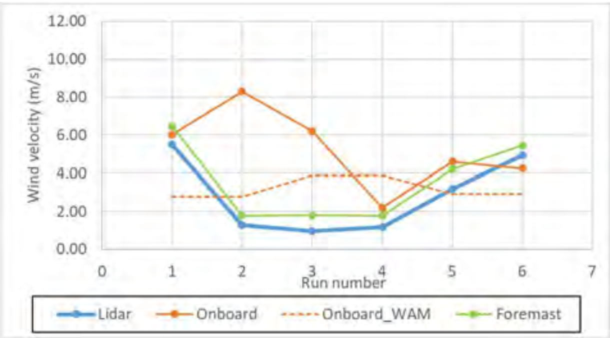

Figure 61 Wind velocity measurement results at each anemometer position during speed trial of a container carrier in unstable wind

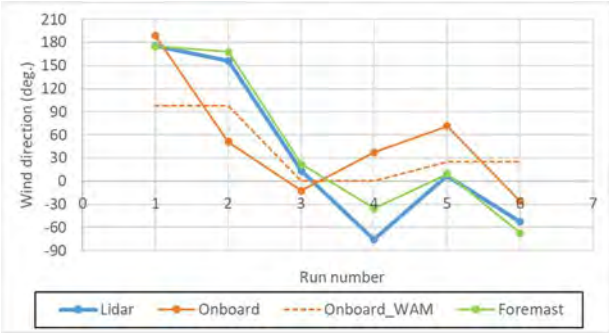

Figure 62 Wind direction measurement results at each anemometer position during speed trial of a container carrier in unstable wind

7.3 Conclusions

In the process of ship's performance evaluation, WAM could generate significant errors frequently, so it is important to make the accurate measurement rather than correcting the wind after disturbed measurement.

It was confirmed that remote wind measurement using LiDAR or the searching for an appropriate location for anemometer installation by CFD calculation were helpful for accurate wind measurement. LiDAR is a promising remote sensing technique for wind measurement but is necessary to have more practicality for sea trial. Also, the effects of ship motion or vibration on wind measurement by LiDAR should be assessed. It was confirmed that wind measurement with determination of appropriate anemometer location by using CFD calculation was effective to measure wind accurately and practically. It will be reviewed more to prepare standardized procedures.

It was confirmed that errors generated by WAM were increased when the wind velocity and direction change more during speed trial. Therefore, WAM should be applied only in an environment where the wind blows uniformly during double run in the speed trial.

8. YAW AND RUDDER ANGLE CORRECTIONS

8.1 Influence of yaw angle

As the influence of yaw angle, the effect due to drift is examined. First, the effect of the drift angle on the added resistance in waves can be considered as the change of inflow velocity as shown by the following equation.

$$\Delta R_{wave}(V,\beta) = \Delta R_{wave}(V\cos\beta) \qquad (11)$$

Additionally, the resistance due to drift is considered. Examples for experimental results of longitudinal force for wide range of the drift angle and for estimated results of speed-power curves are shown in Figure 63 and Figure 64 for a large container ship. (Kuroda, 2021) Here X_D' is the coefficient of longitudinal force due to drift expressed as the following equation, and X_D is the longitudinal force due to drift, ρ is the fluid density, L is the ship length, d is the draft and V is the ship speed.

$$X'_D = \frac{X_D}{0.5\rho L d V^2} \qquad (12)$$

In Figure 63, two types of estimation are also shown. The one by Kijima(1990) shows opposite tendency in small drift angle, and the other by Kijima's equation with lift-induced drug (Sogihara, 2010) shows a large discrepancy in large drift angle. From Figure 64, it is found that this discrepancy results in the effect on the power at low speed since the drift angle at low speed is larger than that at usual operational speed near design speed.

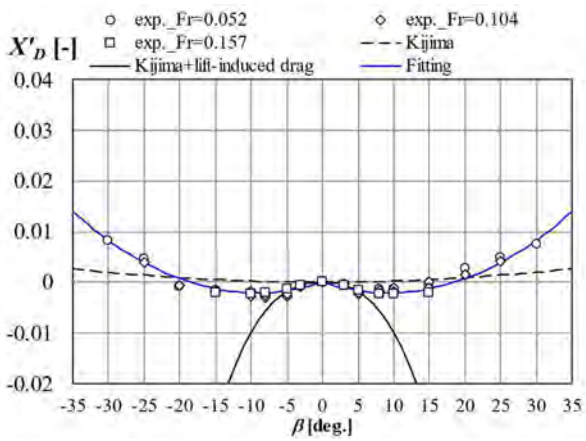

Figure 63 Longitudinal force due to drift for a large container ship.

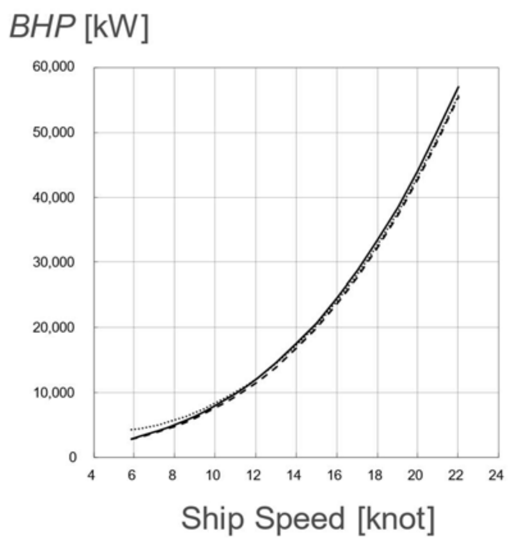

Figure 64 Speed power curve for a large container ship (Oblique weather conditions of Beaufort scale 6)

It was found that the resistance due to drift angle is larger at lower speed than the designed speed, and existing model may lead inaccurate estimation of power curve. However, the resistance due to drift is small at designed speed, and influence to speed trial analysis is limited. Therefore, on this stage, additional correction by the resistance due to drift is not needed.

8.2 Influence of rudder angle

In ITTC Recommended Procedures and Guidelines 7.5-04 01-01.1, conditions of speed trial are prescribed. According to the description, the rudder angles are assumed to be minimal (less than 5 degrees) in the speed trial. Therefore, the effect of rudder angle is expected to be limited.

For the quantitative investigation, contribution of rudder action to resistance components is investigated. (Kuroda, 2022, Sakurada, 2023) Here, hydrodynamic forces due to steering are estimated by following regression formulae. Parameters in the equations can be estimated by model tests or regression formulae by Kijima et al. (1990) They are the same expression as ISO15016(2002).

$$\Delta R'_{rud} = (1 - t_R) F_N{}' \sin\delta \tag{13}$$

$$F'_N = \frac{A_R}{Ld} f_\alpha U'^2_R \sin\alpha_R \tag{14}$$

$$f_\alpha = \frac{6.13\lambda_R}{2.25 + \lambda_R} \tag{15}$$

Where, t_R is the steering resistance deduction fraction, A_R is the projected rudder area, δ is the Rudder angle f_α is the rudder lift gradient coefficient, $U_R{}'$ is the non-dimensional resultant inflow velocity to the rudder, α_R is the effective inflow angle to the rudder, and λ_R is the aspect ratio of rudder.

As examples for calculated results, resistance components for PCC are shown in Figure 65. It indicates that the effect of steering is smaller than that of winds, waves and drift for lower speed and for designed speed.

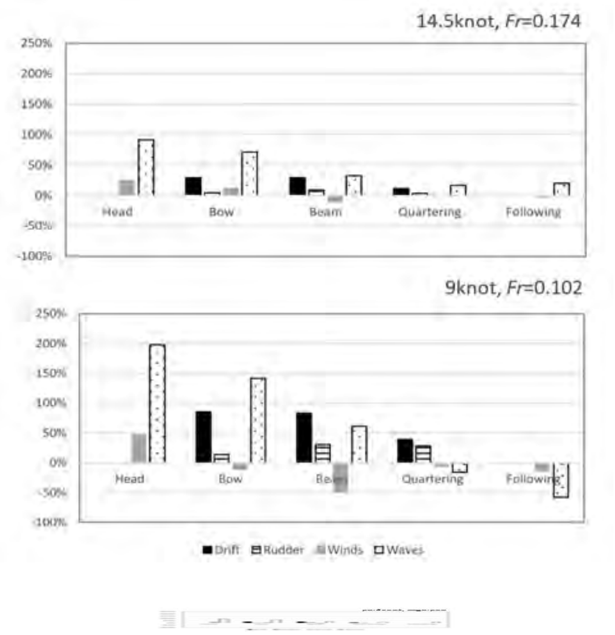

Figure 65 Resistance components for PCC (upper: 14.5 knot, lower: 9 knot)

The expression of the effect of rudder angle as the inclusion in the resistance due to drift has been proposed and is shown by the following empirical formulae.(eq.(16)-(18)) The formulae calculate the resistance due to drift by side wind. However, there are several issues such that the effect of waves is not considered, and that coefficients are not verified for the application.

$$\begin{aligned} R_{Drift} = \frac{\rho}{2} V^2 \Bigg(L^2 \bigg(0.00022 \frac{V}{u} \\ + 0.00466 \left(\frac{V}{u}\right)^2 \bigg) \\ + 0.5 S_{App} 0.0041 \delta_R \Bigg) \end{aligned} \tag{16}$$

$$Y_{Rudder} = 0.0372 \frac{\rho}{2} V^2 S_{App} \tag{17}$$

$$N_{Rudder} = 0.0372 \frac{L}{2} \frac{\rho}{2} V^2 S_{App} \tag{18}$$

Where, R_{Drift} is the resistance due to drift by the side wind, V/u is the ratio lateral/ longitudinal speed, S_{App} is the area of rudder, δ_R is the rudder angle, Y_{Rudder} is the rudder side force and N_{Rudder} is the rudder yawing moment.

As a conclusion, since the speed trials are assumed to be conducted in head winds and waves or following winds and waves as far as possible, and the rudder angles are assumed to be minimal (less than 5 degrees), the effect of steering is limited. Therefore, on this stage, additional correction by the resistance due to steering for correction is not needed.

8.3 Summary

Through investigations based on case studies with estimation and experimental results, it is concluded that additional corrections by the resistance due to drift and steering are not needed on this stage.

9. NEW DEVELOPMENTS IN INSTRUMENTATION AND MEASUREMENT EQUIPMENT RELEVANT FOR SEA TRIALS AND IN-SERVICE PERFORMANCE ASSESSMENT

Both the speed trials and in service performance, accurate measurement of environmental conditions and ship operational data such as wind, waves, and propeller thrust is crucial. These factors significantly impact the ship's performance and efficiency. Therefore, accurate and reliable on-board measurement of the wind and propeller thrust are essential for the evaluation of the ship’s speed power performance.

The full-scale measurements of the propeller thrust, torque, and revolution for a series of crude oil tankers were conducted during the speed trials. Two different measuring systems, strain gauge and optical type, were implemented to compare the performance of sensors as shown in Figure 66.

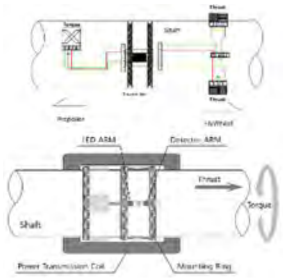

– strain gauges – – optical –

Figure 66 Schematic representation of strain gauges and optical measurement system

To verify the results of thrust measurement using electrical and optical sensors, the relation of revolution, torque and thrust are compared with model test results (Figure 67 and 68).

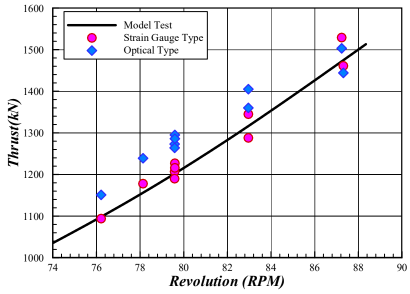

Figure 67 Comparison of thrust between speed trials and prediction results based on model test of crude oil tanker

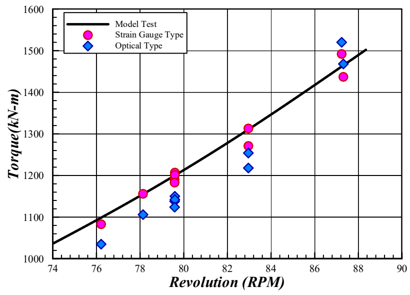

Figure 68 Comparison of torque between speed trials and prediction results based on model test of crude oil tanker

As an important index that decides the accuracy of the thrust measurement, the relation between propeller thrust and torque was investigated as shown in Figure 69.

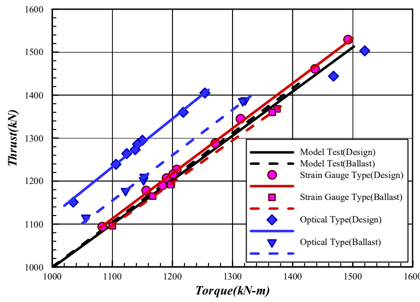

Figure 69 Comparison of thrust - torque of crude oil tankers

The results of thrust measurement at the same torque show approximately 10% difference from the model test results, mainly due to the stability of the zero value, which is found as a problem to be solved for the stable and reliable measurement of thrust.

The characteristics of wind speed and direction by LiDAR have been investigated for RV vessel, LNG carriers, and large container (Figure 70). As shown in Figure 71, true wind speed and direction based on the wind LiDAR measurements and empirical wind profiles were compared.

Figure 70 Wind LiDAR

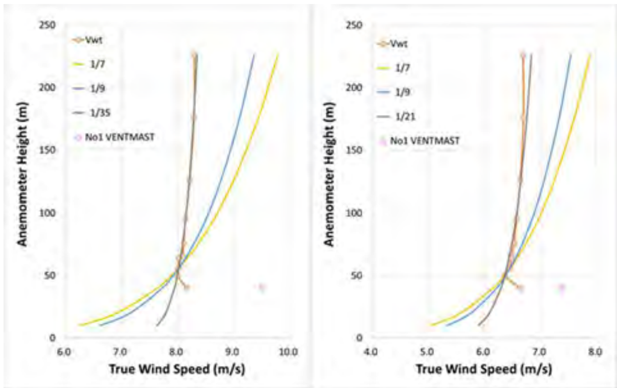

Figure 71 Comparison of Wind Profile for LNG Carrier

Conclusions. For explore and monitor new developments in instrumentation and measurement equipment relevant for sea trials and in-service performance assessment, propeller thrust measurement system and wind LiDAR have been investigated. The experience with the strain gauge and optical sensor shows that extensive effort is required to realize precise thrust measurement. For the further study, the long term stability of the thrust measurement needed. The wind LiDAR offers the advantage of high precision in measuring wind direction and speed under various environmental conditions. The discrepancies between traditional Wind Profiles and LiDAR measurement results have been investigated. Further research is needed to determine the cause of differences. .

10. UPDATE AN INVENTORY OF DATA BASES ON IN-SERVICE PERFORMANCE

It is considered that MARIN's JoRes ship-scale test cases data to be published in December 2024 (Ponkratov 2023) are most relevant to meet this TOR task, in particular, due to its coverage of features relevant to in-service performance issues, e.g., ship types, 3D configurations, ESDs, roughness measurements.

Therefore, it seems to be appropriate for us to recommend ITTC full conference to include JoRes test cases in data base for full-scale issues in ITTC activity. While the JoRes test cases will not available to the public by December 2024, it will not cause any trouble since next term activity will starts October 2024.

Survey to ITTC member organizations regarding the provision of their full-scale data to this TOR task was conducted. 1 organization (SVA Potsdam) has contributed full-scale speed/power trails results for 7 ships.

11. ACCURACY OF CFD FOR SHALLOW WATER APPLICATIONS

Accuracy of CFD for shallow water applications mainly concerning the shallow-water effect on propulsive performance has examined by the literature survey. Unfortunately, due to the scarcity of the published works, sufficient examination of the issue has not been conducted. In the following, results of literature survey conducted in this committee which are relevant to effect of shallow-water on self-propulsion factors are described.

Wang et al (2016) conducted the numerical prediction of ship self-propulsion in different shallow water conditions: H/T=2.0 and H/T=1.2(H : depth of water, T : draft of ship). The KRISO Container Ship (KCS) model is used in the simulations. Numerical computations are carried out by using a solver named naoe-FOAM-SJTU which is developed on the open source platform OpenFOAM and mainly composed of a dynamic overset grid module and a full 6DoF motion module with a hierarchy of bodies. A proportional-integral (PI) controller is applied to adjust the rotational speed of the propeller to achieve the desired ship speed. The simulated results, i.e. the rate of revolution of propeller n, propulsion coefficients, are compared to the experimental data provided by Flanders Hydraulics Research (FHR) in SIMMAN 2014. Good agreements between simulation results and experiment are demonstrated. It is concluded that the present approach is applicable for self-propulsive prediction in shallow water.

Cai et al. (2022) investigated the shallow-water effects on self-propulsion factors by numerical simulations. In this study, ship self-propulsion simulations were conducted by using STAR-CCM+, with both discretized propeller model and body force model. KVLCC2 hull form is employed. The results of the body force method show good agreement with the discretized propeller method in different water depths. In addition, it was shown that water depth influences the thrust deduction fraction and the wake fraction significantly. It is concluded that the calculation results can provide a basis for the optimization of ship with low speed and large block coefficient as well as for the propeller optimization in shallow water.

From the survey results described above, usefulness of CFD for the study of shallow-water effect on self-propulsion factors can be confirmed. However, validation of the CFD has not sufficient for the application to the evaluation of full-scale ship performance yet. Further validations, in particular, comparison with full-scale data may be indispensable and should be continued in the following ITTC terms.

12. TECHNICAL SUPPORT TO ISO AND IMO CONCERNING IN-SERVICE PERFORMANCE MONITORING

For this task, the initial intention of this committee's activity was directed to the contribution to the revision of ISO19030 for the measurement of changes in hull and propeller performance and defines a set of performance indicators for hull and propeller maintenance, repair and retrofit activities.

While ISO19030 has widely employed for the evaluation of in-service performance mainly in terms of performance of hull-surface coating system, its procedure seems to be not adequate from the ship hydrodynamic point of view and further modification may be necessary to be used as a technically reliable measure for in-service performance evaluation. Our main concern in the existing ISO19030 is in the lack of consideration of wave effect in analysing the on-board performance data, that is no correction for wave effect are applied, when reducing to the performance indicator. Due to the lack of the wave correction, the derived performance indicator which nominally intended to indicate the deterioration due to hull and propeller surface fouling is contaminated with the effect of wave during in-service navigation. Thus, this committee intended to contribute in the revision of ISO19030 by providing technical support concerning of introduction of wave correction procedure in on-board performance data analysis.

Despite above mentioned intention of this committee to provide technical support to the revision for enhancing accuracy of ISO19030, unfortunately from our point of view, the review for revision of ISO19030-2016 conducted in 2021 resulted in a major vote to leave ISO 19030:2016 unchanged. Thus, a new edition of ISO 19030 may not be published until 2029.

There is no activity in both ISO and IMO relevant to in-service performance monitoring during the present ITTC term. No activity in technical support to ISO and IMO concerning in-service activity.

13. SURPORT ISO IN UPDATING ISO15016 IN COMPLIANCE WITH RP7.5-04-01-01.1

This committee has closely followed the activities of ISO/TC 8/SC 6/WG 17 (WG for short hereafter) for revising ISO15016.

The 1st DIS voting of the ISO15016 revision was conducted from 25 September to 18 December 2023. In the voting, 72% of the participating members approved the DIS. However, 32% of all members disapproved the DIS, so the DIS was not approved. Technical comments submitted at DIS voting were reviewed, which included two specific proposals for amendment. One is that only the 3D ultrasonic anemometer system is allowed for wind measurement, and the other is that wave added resistance transfer functions derived from model tests/SNNM can only be used in combination with the in-situ measured wave spectrum. These two issues were eventually resolved and the 2nd DIS was approved.

This committee's members participating in the WG as experts tried strenuously to achieve harmonization of the revised ISO15016 with ITTC R.P. 7.5-04-01-01.1. However, full harmonization has not been achieved so far.

Besides several minor differences between the two documents, the most outstanding difference lies in the permissible methods for the evaluation of resistance increase due to waves, as shown in Table 14.

Table 14 Permissible wave correction methods

Method	ITTC R.P. 7.5-04-01-01.1	ISO15016 2nd DIS
Seakeeping model test	√	√
STAWAVE-1	√	√
STAWAVE-2	√	×
SNNM	√	√
NMRI	√	×

According to ITTC R.P. 7.5-04-01-01.1, five methods can be used for the evaluation of wave added resistance, including seakeeping model test, STAWAVE-1 (simplified correction method for ships with limited heave and pitch during the speed runs), STAWAVE-2 (empirical correction method with frequency response function for ships with heave and pitch during the speed runs), SNNM (semi-empirical method for predicting the added resistance of a ship advancing in waves of arbitrary directions) and NMRI (theoretical method with simplified tank tests in short waves or empirical formula). However, the STAWAVE-2 and the NMRI methods are not included in the 2nd DIS of ISO15016. Further work for harmonization should be continued.

14. UPDATE GUIDELINE FOR DETERMINATION OF MODEL- SHIP CORRELATION FACTORS

AC Working Group has been in principally responsible for this task and preparing the update. After receiving the report of AC Working Group, the Committee requested a proposal to forming a new guideline on model-ship parameters for full-scale power predictions. But their proposal was late for due date of last R&P submission, therefore, the Committee had no choice but to decide to postpone the preparation work for the new guideline to the next ITTC term. Since then, AC Working Group has drafted their own R&P and is currently in the process of collecting opinions from ITTC member organizations.

The main contents of the draft R&P for evaluating power ratio between drafts proposed by AC Working Group are as follows:

After the towing tank test of a given case, the facility predicts the extrapolated full-scale speed-power curves for trial and stipulated draught (EEDI draught and/or con-tract draught). The predicted power ratios are derived as

$$\Delta P_{PR} = P_{stipulated}/P_{trial} \tag{19}$$

To verify that the predicted power relations are reasonable, the model scale measurements and a few ship parameters are entered into a web-based software that AC Working Group has prepared. The output from the webpage is the Guideline power ratio:

$$\Delta P_{GL} = P_{stipulated}/P_{trial} \tag{20}$$

The fraction between the predicted and the guideline power ratios is derived as:

$$D = \Delta P_{GL}/\Delta P_{PR} - 1 \tag{21}$$

D expressed in % is the deviation when predicting the loaded draught curve, after that the trial model test curve would be shifted to the speed trial results.

The requirements of accepted test are:

- 10-15 cases are submitted to the Sample Collection (no more, no less)
- The median D of the Sample Collection should be within ±3%
- The absolute value of D should be within 5% for 90% of the cases in the Sample Collection
- The absolute value of D should be within 10% for 100% of the cases in the Sample Collection

15. UPDATE GUIDELINE ON CFD-BASED WIND COEFFICIENT

The update of the guideline on CFD-based wind coefficients was done by rearranging and simplifying the formulae for height average wind speeds V_{A1} and V_{A2}. The expanded new formulae are as follows:

$$V_{A1}^2 = \frac{V_{ref}^2}{2\alpha+1} \cdot \left(\frac{H_{BR}}{z_{ref}}\right)^{2\alpha} \tag{22}$$

$$V_{A2}^2 = \frac{V_{ref}^2}{2\alpha+1} \cdot \left(\frac{H_{L}}{z_{ref}}\right)^{2\alpha} \tag{23}$$

Above formulae were derived assuming the wind profile given by formulae:

$$V(z) = V_{ref} \cdot \left(\frac{z}{z_{ref}}\right)^{\alpha} \tag{24}$$

where:

α – wind profile exponent; 1/9 at the sea level
V_{ref} – reference velocity at reference level z_{ref}
z_{ref} – height of reference wind velocity; typically 10 m
The problem revolves around the dependence of wind resistance coefficients on the wind profile. The existing guidelines and databases do not adequately define the wind profile.

Taking the above into consideration, it is recommended to update the guideline on CFD-based wind coefficients by recalculating the existing database of wind resistance. The updated database should be used to provide a more accurate representation of wind resistance, taking into account the variations in wind profiles.

16. DEVELOPMENT OF RELEVANT TECHNIQUES FOR ENERGY SAVING AND THE NEEDS TO COMPLEMENT THE PRESENT EEDI FRAMEWORK

The shift towards low-carbon and zero-carbon fuels necessitates a reassessment of the EEDI framework to ensure it remains relevant and effective in promoting energy efficiency. Additionally, the integration of cutting-edge technologies in maritime design and operation requires new methods for evaluating their impact on energy efficiency. In cases where the EEDI alone may not adequately capture power savings, additional metrics may be needed to provide a more comprehensive assessment of energy efficiency improvements.

The IMO circular MEPC.1 / Circ.896 (14 Dec 2021) outlines methods for the calculation and verification of the attained EEDI, in line with various regulations of Annex VI to MARPOL. It addresses the combination of propulsion power (P_P) and reference speed (V_{ref}), integrating speed-power curves to reflect their combined effects. Additionally, it accounts for technologies that generate electricity (P_{AEff}), reducing the need for propulsion power.

According to the IMO circular the power reduction includes several categories. Category (A) involves adjusting the power curve by changing either P_P or V_{ref}. Category (B) focuses on reducing propulsion power at V_{ref} without generating electricity. Within this category, technologies usable anytime have an availability factor (f_{eff}) of 1.0 (category B-1), while those used under limited conditions have f_{eff} less than 1.0 (category B-2). Category (C) includes generating electricity to reduce propulsion power at V_{ref}. Technologies effective all the time have f_{eff} equal to 1.0 (category C-1), whereas those dependent on ambient conditions have f_{eff} less than 1.0 (category C-2).

Power reduction might be categorized into those that affect main engine power (A and B) and those that influence auxiliary power (C). Technologies that reduce friction, optimize hull and propeller design, or utilize energy-saving devices (ESDs) fall under Type (A). Hull air lubrication systems that can be switched on or off are categorized as Type (B-1). Wind assistance technologies like sails, Flettner rotors, and kites are classified as Type (B-2). Waste heat recovery systems that function continuously are categorized as Type (C-1), while photovoltaic cells that depend on environmental conditions fall under Type (C-2).

The air lubrication system (ALS) is becoming more popular in recent days; however, implementation in EEDI calculation needs a deeper look into the metrics used for sea-trial-derived power curve corrections. The auxiliary power requirement includes the energy consumed by running the air lubrication system itself. Performance measurement involves both calculated and measured data from full load and sea trials, both with ALS on and off. The total power reduction is given by formula:

$$P_{eff} = P_{effAL} - P_{AEeffAL} \frac{C_{FAE}}{C_{FME}} \frac{SF\ \ _{AE}}{SFC_{ME}} \tag{25}$$

where:

P_{effAL} – propulsion power reduction due to air lubrication

$P_{AEeffAL}$ – auxiliary power of running air lubrication

Further the power reduction due to air lubrication system is derived is calculated by:

$$P_{effAL(T)} = ADR_T \times P_P \tag{26}$$

where index (T) means draught, which might be trials draught, design or full load. It is obvious that during sea-trials the actual reduction rate (*ADR*) is derived directly from evaluated power curves (see Figure 72), however calculation of ADR for other draughts is based only on estimations. Thus there are several key challenges in the integration of ALS technology. Firstly, there is a lack of clear guidelines on how to estimate reduction rates using model tests, computational fluid dynamics (CFD), or empirical formulas. Secondly, there are no standardized procedures or recommendations for conducting sea trials with ALS. Additionally, there is no definitive evidence showing the proportional relationships between full load and sea trials load reduction rate scaling. Lastly, there is insufficient information on how sea state and weather conditions impact ALS performance.

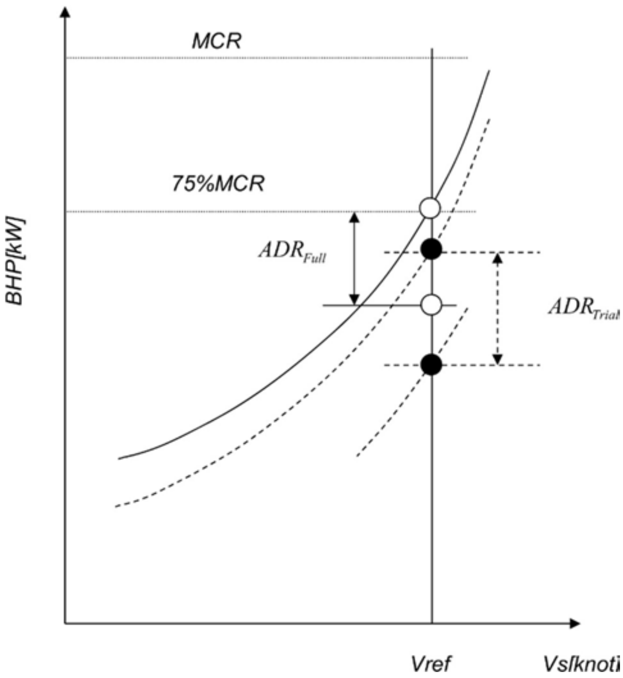

Figure 72 Definition of ADR from sea trials

Several areas need further research and standardization to improve the capability and reliability of ALS technologies. Clear estimation methods should be established to standardize ADR derivation for draughts other than those applied during sea trials. Standard procedures and recommendations for conducting sea trials with ALS need to be developed. Correlation studies are necessary to establish proportional relationships between different load conditions and reduction rates. Finally, investigating the influence of weather conditions on the performance of ALS and other innovative technologies is crucial.

17. FULL SCALE DATA ON THE EFFECT OF ENERGY SAVING METHODS

17.1 Overview

In the current context of carbon peak and carbon neutrality, the energy-saving and emission-reduction technologies that the ship industry is focusing on. Extensive theoretical research and practical ship applications have proven that these technologies are the potentially effective techniques for reducing the EEDI and EEXI of ships.

In order to improve the energy efficiency of operating ships, systematic energy efficiency solutions are often used today. These include the optimization of hull lines for actual sea conditions, the use of high-efficiency propellers, the selection of optimal hydrodynamic energy-saving devices (Pre-ESDs: PSV, WID, PSS; Post-ESDs: PBCF, Rudder Bulb, Rudder Fins and so on), and the adoption of revolutionary and innovative energy-saving technologies (ALDR, Wind Rotor, Wind Sail). There are multiple methods to evaluate the energy saving effect after the application of these technologies. Numerical simulations are usually used at the design stage to optimize the solution and forecast the energy saving effect. Laboratory model tests can also be used to assess the energy savings and to predict the energy efficiency level of the full scale ship. Both numerical simulations and model tests generally consider the relative comparison between applying energy-saving technologies and not using energy-saving technologies in still water. However, the real sea state environment, including wind, waves, and currents, will have an impact on the final energy efficiency, and there is also a scale effect between the model scale and the full scale, and all these factors need to be supported by sufficient sea trail data of full scale ship. Especially, the statistical data of long-term operation is more meaningful for evaluating the energy-saving effect after applying energy-saving technologies. Therefore, full scale data are very important for the prediction and evaluation of energy saving effect.

Table 15 Combination of energy saving technologies

OBJECT	TARGET	TECHNOLOGIES
HULL	DRAG REDUCTION	Hull lines optimization under still water and sea condition
		Trim optimization
		Upper building optimization for low wind resistance
		Surface drag reduction such as micro-bubble, low drag coat, etc.
ENGINE	EMISSION REDUCTIOIN	Power limitation
		Optimum working condition
		Low carbon fuel or no carbon fuel
PROPELLER	EFFICIENCY IMPROVING	Optimum match among stern, main engine and propeller
		Suitable Propulsion type
		High efficiency propeller
	ENERGY SAVING	Pre-ESDs (PSV, WID, PSS...)
		Post-ESDs (PBCF, Rudder Bulb, Rudder Fins...)

17.2 Hydrodynamic Energy Saving Technologies

Some energy-saving technologies whose basic principles are closely related to hydrodynamics, usually we call them hydrodynamic energy-saving technologies. The energy saving device pre-shroud-vanes (PSV or PSD) in front of the propeller, the high-efficiency propeller (HEP), and hub vortex absorbed fins (HVAF or PBCF) behind the propeller, etc. are all in this category. Different energy saving devices produce different energy saving benefits.

- **Pre-ESDs: PSV**

-Producing added thrust by accelerated ducts;
-Producing favourable pre-swirled inflow into propeller by inside vane and reducing rotational losses of slipstream;
-Helping to improve propeller efficiency by establishing a more uniform inflow into the propeller;
-Energy saving about 3%~8%;

- **Propeller Optimization: HEP**

-Optimum diameter for higher efficiency;
-Skewed blade for lower induced vibration;
-Using new profile for higher efficiency, better cavitation performance;
-Optimum radial pitch for higher efficiency, better cavitation performance;
-Specific skew at tip to vortex cavitation suppression;
-Wake adapted for optimum match with Hull;
-Theoretical design to Balance optimization on efficiency-vibration-cavitation;
-Energy saving about 3%~5%;

- **Post-ESDs: HVAF**

-Energy saving by installing behind propeller instead of Propeller Cap, to reduce the energy losses of hub vortex;
-Energy saving about 2%~5%;

17.3 Analysis Method Based on Sailing Records

Forecasting and evaluating the effect of energy saving methods can be done through model tests, including resistance and self-propulsion tests in towing tank, propeller hydrodynamic tests in cavitation tunnel, etc. These methods are used to compare with each other the propulsive efficiency of the whole ship with and without energy-saving devices, so as to forecast the performance of the full-scale ship and obtain the EEDI or EEXI index.

Another method is to obtain data such as loading capacity, speed, main engine power, fuel consumption and so on through the full scale ship sea trial or long-term monitoring. By comparing and analyzing the changes of these data with and without ESD with the same type of ships or sister ships, we can obtain the full scale energy saving effect.

However, full scale ship data are different from laboratory data, uncertain and subject to greater environmental interference. More systematic data are mainly analyzed and processed. For example, when utilizing full scale ship fuel consumption data for analysis, the effect of different loadings must be corrected.

The analysis is based on Admiralty Coefficient – C_m, i.e.,

$$C_m = \frac{\Delta^{2/3} \cdot V^3}{P_m} \tag{27}$$

Where, $\triangle$ is the displacement; V is the vessel speed; and P_m is the power of main engine.

Herein, the displacement and the power of main engine can be represented by the load capacity and the fuel oil consumption, respectively.

$$F.O.C_{\Delta correction} = \left(\frac{\Delta_{correction}}{\Delta_{actual}}\right)^{\frac{2}{3}} \times F.O.C_{actual} \tag{28}$$

$$F.O.C_{Vcorrection} = \left(\frac{V_{correctio}}{V_{actu}}\right)^{3} \times F.O.C_{\Delta correction} \tag{29}$$

Where,

$F.O.C_{\triangle correction}$: the fuel oil consumption after displacement correction;

$F.O.C_{actual}$: the fuel oil consumption before displacement correction;

$F.O.C_{Vcorrection}$: the fuel oil consumption after ship speed correction;

$\triangle_{correction}$: the displacement at the load condition after displacement correction;

$\triangle_{actual}$: the displacement at the load condition before displacement correction;

$V_{correction}$: the ship speed at the load condition after speed correction.

V_{actual}: the ship speed at the load condition before speed correction;

Based on this analysis method, the fuel oil consumption can be transformed into the same condition including the same vessel speed and same load capacity. Thus, the energy saving effect can be calculated by

$$EnergysavingEffect = \left(1 - \frac{F.O.C_{after}}{F.O.C_{befor}}\right) \times 100\% \tag{30}$$

Where,

$F.O.C_{after}$: the corrected fuel oil consumption after energy efficiency upgrade;

$F.O.C_{before}$: the corrected fuel oil consumption before energy efficiency upgrade.

According to the experiences, the data (with steaming time ⩾16 hours, the laden condition (drafts) close, and the rotation of ME close also before and after Energy Efficiency Upgrade are chosen as the sample data to analysis.

The actual fuel consumption depends not only on the technical status of the ship, but also on the sea condition (Removing the influence of sea state ⩾5) as well as hull fouling conditions (Basically the same). In order to even the influence of these conditions, it is necessary to collect more sailing data to get more accurate energy saving effect.

17.4 Some Full Scale Date about Energy Saving Effect of ESDs

In order to analyse the full-scale ship energy saving effect of ESDS, CSSRC collected some model test and full scale sail trail data through CMES-Tech (CSSC Shanghai Marine Energy Saving Technology Co., Ltd) to help the full scale analysis of the energy saving effect from 2021 to 2024.

- **HVAF or PBCF**

HVAF is a simple and commonly used energy saving device. Usually, the energy saving effect measured in the model test in the laboratory is only about 2%, while a large number of real ship application results show that the energy saving effect of the full scale is larger than that of the model scale. There were collected five cases full scale data about using HVAF (PBCF), and these cases can be compared with sister ships sea trail results. Some case has model test result.

Table 16 Full scale data with HVAF

No.	Ship	Sister Ship
Case1	27000DWT MPC	1
Case2	57000DWT B.C	1
Case3	75200DWT B.C	1
Case4	114,500DWT B.C	5
Case5	180,000DWT B.C	Long period record

Two 27000DWT MPC vessels, one is "PING AN" without HVAF and the other is "XIN FU" with HVAF, were carried out sea trail in Class 1 and Class 2 sea state respectively. Normally, the measured speeds under class 1~2 sea state can be uncorrected, and the ballast condition of these two ships is close to each other during the sea trial. The measurement and recording of the main engine shaft power during the sea trial can be used to derive the speed-power-revolution relationship of each ship. Comparative analysis of the data of the trial voyage of two vessels can be used to evaluate the energy-saving effect of HVAF. The result indicate that it can obtain about 4%~5% energy saving of HVAF.

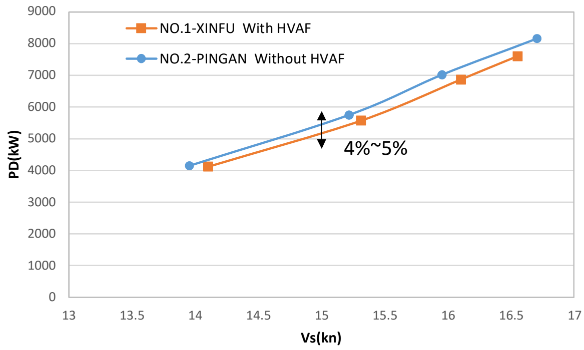

Figure 73 Energy saving effect of 27000DWT MPC with HVAF

Two sister vessels of 57000DWT bulk carrier, N276 is installed with conventional cap and N373 is installed with HVAF. N373 is moored in the harbour for a long time before the sea trial, and the hull has a lightly fouled. When analysing the data of the sea trail, if it directly compares the speed and power, the speed increased by 0.08 knots with HVAF under the same power, and consumed 167kW less power under the same speed. The energy saving effect is abt. 2.4%. If roughness correction is applied to the N373 vessel, the energy saving effect can be increased to 5%.

Table 17 Roughness effect for energy saving of HVAF

Design Draught	N276 Without HVAF	N373 With HVAF	△	Energy Save(%)	Corrected Roughness effect
7308kW	14.64kn	14.72kn	0.08kn	--	--
14.46kn	6927kW	6760kW	167kW	2.40%	~5%

HVAF for a 114,500DWT bulk carrier was designed and has been installed onto ship numbered as HN1164, and the sea trial was carried. According to the model test results, it can be seen that the efficiency of propeller with HVAF increased about 2.7% at design point ($J_0 \approx 0.43$), and the ship speed can be increased about 0.14kn at different drafts. Since there are five sea trial reports for five delivered sister ships of HN1164, the energy saving effect of HVAF can be analyzed based on the comparison between HN1164 and its sister ships. The sea trial drafts and environmental conditions of these ships are shown in Tab 18 and 19.

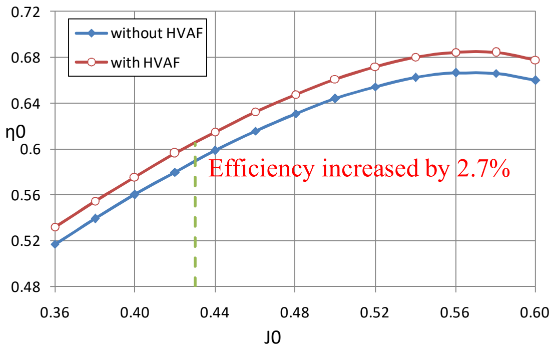

Figure 74 Open water efficiency of model test result with and without HVAF

Table 18 The sea trial drafts of HN1164 and its sister ships

Hull No.	Sea Trial Drafts			
	T_F (m)	T_M (m)	T_A (m)	Corresponding Disp. (tons)
HN1155	7.80	8.900	9.650	73959.30
HN1156	7.91	8.820	9.740	73975.20
HN1157	7.93	8.850	9.400	73674.06
HN1158	8.08	8.965	9.600	74877.80
HN1163	7.76	P 8.85/S 8.71	9.670	74634.00
HN1164	7.77	P 9.05/S 9.11	9.960	75583.80

Table 19 The environmental conditions of HN1164 and its sister ships

Hull No	Environmental Conditions				
	Geo-graphic Position	Wind Force	Wind Direc-tion	Sea Condi-tion	Depth
HN1155	East China Sea	4-5 Bft	NE	Douglas 3/4	Around 70m
HN1156	East China Sea	5 Bft	NW	Douglas 4	Around 70m
HN1157	East China Sea	3 Bft	SE	Douglas 2	Around 70m
HN1158	East China Sea	4 Bft	N	Douglas 3	Around 70m
HN1163	East China Sea	4-5 Bft	NE	Douglas 3	Around 70m
HN1164	East China Sea	2 Bft	SW	Douglas 1	Around 70m

With the correction of the wind, wave, tide, shallow water and still air condition of model test, the corrected results can be obtained as listed in Tab 20 without HVAF. From the results, it can be found that the displacement of each ship is different from the design condition. Thus, it is necessary to correct the displacement effect for each ship. According to ITTC Procedures and ISO 15016, the displacement effect can be corrected by Admiralty Coefficient Method. It is easy to find that the ship speed of each ship is quite different from each other, the difference between the highest one and the lowest one is about 0.456 knots. The averaged results of ship speed is 15.488 knots at service point.

Table 20 Ship speed of 114,500DWT bulk carrier without HVAF at service point

CSR with Sea Margin: P_D=MCR*0.85*0.985/1.15=11518kW						
Hull No.	T_F(m)	T_M(m)	T_A(m)	Displace-ment(t)	Vs (kn)	N(rpm)
Model Test	7.742	8.823	9.903	73716.36	15.080	98.27
HN1155	7.80	8.90	9.65	73959.30	15.670	98.58
HN1156	7.91	8.82	9.74	73975.20	15.214	99.73
HN1157	7.93	8.85	9.40	73674.06	15.678	100.58
HN1158	8.08	8.97	9.60	74877.80	15.349	99.45
HN1163	7.76	8.80	9.67	74634.00	15.411	99.44
Average	----	----	----	----	15.464	----

Table 21 Ship speed of 114,500DWT bulk carrier without HVAF after corrected for displacement

Hull No.	Model Test	HN1155	HN1156	HN1157	HN1158	HN1163	Average (Sea trials)
Vs (kn)	15.080	15.681	15.226	15.676	15.402	15.452	15.488

The HN1164 has been installed HVAF, and the sea trials has been carried. Passed through the wind and wave analysis, tide analysis and still air correction, the ship speed at service point before and after corrected displacement is shown in Tab 22. By analyzing the results, the ship speed with and without HVAF can be obtained. As for without correcting of displacement, the ship speed without HVAF is about 15.46kn, while it is about 15.60kn with HVAF. As for with correcting of displacement, the ship speed with and without HVAF is 15.69kn and 15.49kn, respectively. Consequently, the ship speed has been increased 0.14kn and 0.20kn before and after displacement correction, respectively. As a result, it can be concluded that energy saving effect of HVAF based on sea trial results is about 3% to 5%, better than the model test results.

Table 22 Ship speed of HN1164 with HVAF after corrected for displacement

CSR with Sea Margin: P_D=MCR*0.85*0.985/1.15=11518kW						
Hull No.	T_F(m)	T_M(m)	T_A(m)	Displacement(t)	Vs (kn)	N(rpm)
HN1164	7.700	9.100	9.960	75583.80	15.60	101.05
Displacement Correction						
HN1164	7.742	8.823	9.903	73716.36	15.69	----

Table 23 Ship speed prediction under heavy ballast draft before displacement correction

V_S(kn)	P_S (η_S=0.985) Unit: kW							ENERGY SAVING
	Without PBCF						With PBCF	
	HN1155	HN1156	HN1157	HN1158	HN1163	AVERAGE	HN1164	
14.5	8904.1	9779.6	8544.3	9682.0	9606.9	9303.4	8897.1	4.37%
15.0	10081.0	11091.9	9785.8	10870.5	10760.3	10517.9	10136.7	3.62%
15.5	11269.4	12467.4	11179.1	12068.2	11895.4	11775.9	11444.6	2.81%

Table 24 Ship speed prediction under heavy ballast draft after displacement correction

V_S(kn)	P_S (η_S=0.985) Unit: kW							ENERGY SAVING
	Without PBCF						With PBCF	
	HN1155	HN1156	HN1157	HN1158	HN1163	AVERAGE	HN1164	
14.5	8879.3	9750.9	8548.6	9567.2	9512.4	9251.7	8710.7	5.85%
15.0	10055.2	11060.5	9790.8	10743.9	10667.9	10463.7	9922.3	5.17%
15.5	11242.1	12433.6	11184.9	11943.6	11795.6	11720.0	11222.4	4.24%

The shipowner of 180,000DWT bulk carrier “DA YUAN” provided the data of full scale ship operation in one year period. Based on these data with and without HVAF, the energy saving can be analysed. Statistical analysis was performed by excluding data from days of sailing in rough sea conditions. Based on full scale operation record data, the HVAF can save fuel consumption about 10% both loaded and unloaded conditions.

Table 25 The record results in no load condition

Project	criterion: all record data		criterion: only include the data of MOD SEA and SLT SEA	
	Without HVAF	With HVAF	Without HVAF	With HVAF
Day.	86	54	56	36
Total voyage (mile)	23321	14736	15313	10456
Total time（h）	1919.5	1203.1	1248	841
Average speed (kn)	12.15	12.25	12.27	12.43
Total Fuel consumption（t）	2724.3	1579.5	1754.2	1117.9
24 hour AV. Fuel consumption（t/d）	34.06	31.51	33.7	31.902

Table 26 Comparison with 12kn Fuel consumption average

Project	criterion: all record data		criterion: only include the data of MOD SEA and SLT SEA	
	Without HVAF	With HVAF	Without HVAF	With HVAF
Average speed (kn)	12.15	12.25	12.27	12.43
24 hour AV. Fuel consumption（t/d）	34.06	31.51	33.7	31.902
At 12 kn speed condition 24 hour AV. Fuel consumption（t/d）	32.53	29.19	31.03	28.00
Energy saving (%)	10.26%		9.78%	

- **PSV or PSD**

PSV is increasingly used in many hydrodynamic energy saving devices. Its energy-saving effect is also very significant. It can be used alone or together with HVAP, rudder bulb (RB) and high-efficiency propeller, etc., thus pursuing higher energy-saving effects. There are some full scale data of cases with PSV.

Table 27 Full scale data with PSV

No.	Ship		ESDs
Case1	1100TEU	1	PSV
Case2	298,000DWT VLCC	1	PSV
Case3	325K DWT VLOC	1	PSV+HVAF

Case4	210K B.C	1	PSV+HVAF
Case5	57000DWT B.C	6	PSV+HVAF
Case6	175K B.C	1	PSV+HVAF
Case7	180,000DWT B.C	1	PSV+HVAF+ LR Coating
Case8	230,000DWT Ore CARRIER	1	PSV+HVAF+ RB+PM

Both the 1,100 TEU and 298,000 DWT VLCC are fitted with PSV energy saving devices. Forecasts of laboratory model test results show that the energy-saving effect of PSV on container ships is only about 3%, while PSV on VLCC can reach 5% to 7%. There are 11 voyages number and 22 groups data without PSV, and 9 voyages number and 18 groups data with PSV. According to the full scale voyage data of 1,100 TEU, the fuel consumption is decreased 1.4t every 24h, the energy saving is about 4.5% with PSV. For the VLCC, the energy saving effect by fuel consumption is about 9.6%. For the energy saving effect of these two ships with PSV, the full scale results show the same trend as the model tests.

Table 28 Energy saving effect of PSV at design draught for 1100 TEU by model test result prediction

Load Condition	Speed V_S (kn)	Delivered power with TM19226A P_{DT0} (kW)	with TM19226A&PSV-A P_{DT1} (kW)	with TM19226A&PSV-A Energy saving $1-P_{DT1}/P_{DT0}$	with TM19226A&PSV-B P_{DT2} (kW)	with TM19226A&PSV-B Energy saving $1-P_{DT2}/P_{DT0}$
Design draft	12.00	1840	1784	3.0%	1786	2.9%
	13.00	2227	2160	3.0%	2154	3.3%
	14.00	2666	2584	3.1%	2575	3.4%
	15.00	3206	3105	3.2%	3097	3.4%
	16.00	3892	3771	3.1%	3767	3.2%
	17.00	4789	4652	2.9%	4649	2.9%
	18.00	6073	5908	2.7%	5907	2.7%
	19.00	8024	7784	3.0%	7801	2.8%
	20.00	10954	10579	3.4%	10622	3.0%
	21.00	15240	14699	3.5%	14749	3.2%

Table 29 Energy saving effect of PSV at design draught for 298,000 DWT VLCC by model test result prediction

V_S(kn)	WITHOUT PSV P_{DT}(kW)	WITHOUT PSV N_T(rpm)	WITH PSV P_{DT}(kW)	WITH PSV N_T(rpm)	ENERGY SAVING EFFECT
11.5	7530	55.9	7008	54.0	6.93%
12.0	8522	58.4	7990	56.3	6.24%
12.5	9607	60.9	9042	58.7	5.88%
13.0	10774	63.3	10177	61.0	5.54%
13.5	12059	65.6	11370	63.2	5.71%
14.0	13500	68.1	12727	65.6	5.73%
14.5	15071	70.6	14178	68.0	5.93%
15.0	16834	73.2	15790	70.5	6.20%
15.5	18808	75.8	17541	73.0	6.74%
16.0	20997	78.6	19503	75.6	7.12%
16.5	23411	81.3	21630	78.2	7.61%
17.0	26042	84.0	23963	80.7	7.98%

Table 30 Fuel consumption for 1100 TEU with and without PSV

Proj.	Average speed (kn)	24 hour AV. Fuel consumption （t/d）	Average Loading	Corrected the same loading and speed of fuel consumption （design draft/14.5kn）
Without PSV	14.2kn	29.4t/24h	4582t	31.3t/24h
With PSV	14.5kn	29.1t/24h	3959t	29.9t/24h
Diff.	+0.3kn	-0.3t/24h	-623t	-1.4t/24h

Table 31 Fuel consumption for 298,000 DWT VLCC with and without PSV

Average data	Energy Efficiency Upgrade Before	Energy Efficiency Upgrade After	Remarks
F. O. C(13.00kn, T=20.0m) (tons/24hour)	75.09	67.91	PSV
$EnergysavingEffect = \left(1 - \frac{F.O.C_{ESDs}}{F.O.C_{NO\ ESDs}}\right) \times 100\%$	9.6%		

For the difference between the model test prediction results and the full scale sea trial results, both 325K DWT VLOC and 210K B.C give comparative results. The prediction result of ITTC method is lower than SINTEF Ocean method about 0.16kn，the sea trail result in the middle of the prediction results. The effect of input data of environments is significant，so environment parameter of the sea trail is very importance. The results of the full scale of these two ships with sea state corrections were closer to the model test prediction.

Table 32 The prediction results with different towing tank method for 325K DWT VLOC

CSR, 15%S.M		Prediction fullscale		
Condition	ESD	SINTEF Ocean method	ITTC method +prop. correction	Diff.
Ballast	PSV+HVAF	16.16kn 56.7rpm	16.00kn 56.9rpm	-0.16kn +0.2rpm

Table 33 The sea trial results with different input condition of environments for 325K DWT VLOC

CSR, 15%S.M		Sea trail results		
Condition	ESD	Input data（Wave 1.0m、tide 1.5m）	Input data（Wave 0.5m、tide 0.6m）	Diff.
Ballast	PSV+HVAF	16.12kn 57.2rpm	15.89kn 57.2rpm	-0.23kn +0.0rpm

Table 34 Model test prediction results & sea trail results for 210K B.C

		Vs(kn)	N(rpm)	LRM(%)
Design draft	Model	14.59	66.0	7.5%
	Sea trail	14.62	67.0	9.1%
Scantling draft	Model	14.05	65.7	7.1%
	Sea trail	14.08	66.8	8.8%

57000DWT B.C has six sister vessels with PSV and HVAF, four of which have good sea trail data. The unit energy consumption is significant effected by the loading. So the full scale ship energy saving value should be compared in the same loading condition. According to the full scale ship record results, the unit consumption of heavy fuel can be calculated for different voyage actual data and plotted the figure of “loading- unit consumption of heavy fuel”. From these results, using the unit consumption heavy fuel of the same loading condition, the energy saving is significant. The fuel consumption are decrease from 8% to 20%. The full scale sea trail result indicate that 175K DWT B.C also has 15.5% energy saving effect for fuel consumption with PSV and HVAF.

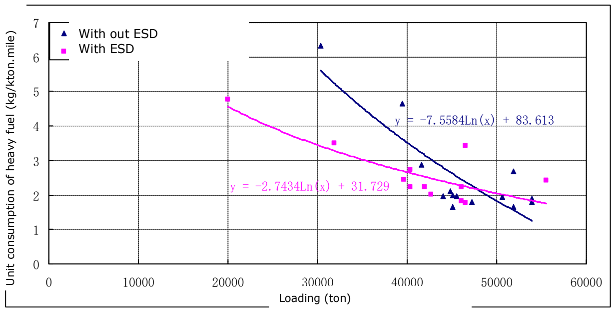

Figure 75 Loading- unit consumption of heavy fuel of “Pulan Sea”

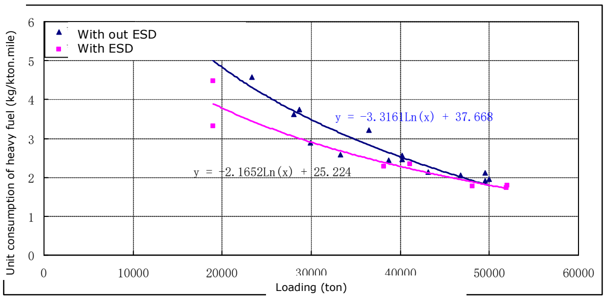

Figure 76 Loading- unit consumption of heavy fuel of “Daishan Sea”

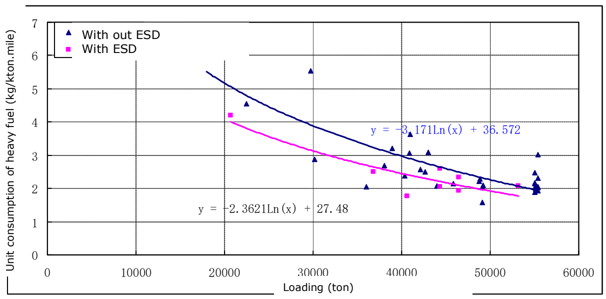

Figure 77 Loading- unit consumption of heavy fuel of “Hengshan Sea”

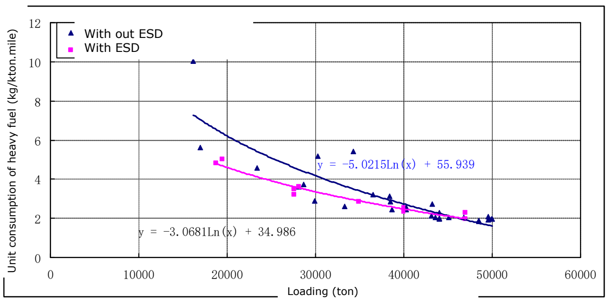

Figure 78 Loading- unit consumption of heavy fuel of “Changshan Sea”

Table 35 The fuel consumption compared with and without PSV + HVAF for 175K DWT B.C

	Without ESD	With ESD	Energy saving (%)
Total mileage recorder (mile)	46137	10834	/
Total time (h)	3834.9	796	
speed (kn)	12.03	13.61	
Total fuel consumption (T)	5467.50	1388.2	
Average day fuel consumption (T/day)	34.22	41.86	
Calculated 13kn Average day fuel consumption (T/day)	43.17	36.47	15.5%

It is common to ask whether repeated applications of energy-saving devices ahead and behind the propeller are in direct superposition energy saving effect to each other. The 180K DWT B.C could not meet the standard in the EEXI assessment, so PSV, HVAF and LR Coating were used. The model test results indicate that PSV and HVAF can increase efficiency 5.4% and 2.5%, respectively. LR Coating can saving energy 4%. Real ship data realistic combined fuel consumption assessment energy savings of 21.6%. The 230K DWT Ore Carrier used multiple energy-saving devices include PSV, Rudder Bulb and HVAF. The model test results show that the energy saving effect can obtain 9% and 10% at design and ballast condition. The full scale data give the same tendency on fuel consumption. The energy saving effect of ballast is slightly better than design draught.

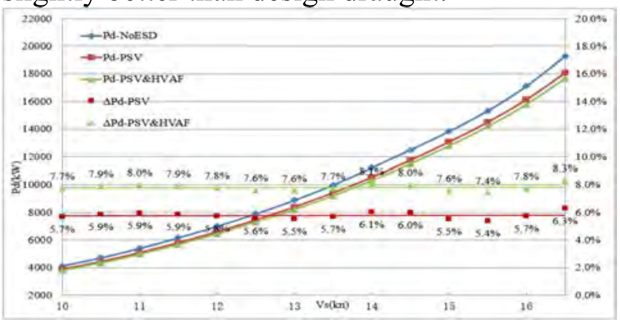

Figure 79 Model test verification the total energy saving effect of 180K DWT B.C

Table 36 The fuel consumption compared with and without ESDs for 180K DWT B.C

Average data	Energy Efficiency Upgrade		Remarks
	Before	After	
F. O. C(11.00kn, T=17.45m) (tons/24hour)	39.90	31.30	PSV+HVAF +LR Coating
$EnergysavingEffect = \left(1-\frac{F.O.C_{ESDs}}{F.O.C_{NO\ ESDs}}\right)\times 100\%$	21.6%		

Figure 80 Energy saving model test of 230K DWT Ore Carrier

Table 37 Model test results for 230K DWT Ore Carrier at design condition

without ESD			with PSV		with PSV + Rudder Bulb		with PSV + HVAF + Rudder Bulb	
Vessel Speed	Delivered Power	Rotational Speed	Power Difference	Energy Saving	Power Difference	Energy Saving	Power Difference	Energy Saving
Vs (kn)	PDT0 (KW)	N_{s0} (r/m)	P_{DT1}-P_{DT0} (KW)	ΔP_{DT1} (%)	P_{DT2}-P_{DT0} (KW)	ΔP_{DT2} (%)	P_{DT3}-P_{DT0} (KW)	ΔP_{DT3} (%)
11.0	6033	51.9	-274	4.5%	-343	5.7%	-513	8.5%
11.5	6916	54.2	-336	4.9%	-424	6.1%	-618	8.9%
12.0	7884	56.6	-404	5.1%	-511	6.5%	-732	9.3%
12.5	8940	58.9	-478	5.3%	-603	6.7%	-853	9.5%
13.0	10088	61.4	-550	5.4%	-695	6.9%	-977	9.7%
13.5	11328	63.8	-620	5.5%	-780	6.9%	-1097	9.7%
14.0	12667	66.3	-695	5.5%	-873	6.9%	-1227	9.7%
14.5	14108	68.8	-776	5.5%	-970	6.9%	-1365	9.7%
15.0	15701	71.3	-848	5.4%	-1056	6.7%	-1495	9.5%
15.5	17514	74.0	-880	5.0%	-1100	6.3%	-1592	9.1%
16.0	19582	76.7	-857	4.4%	-1081	5.5%	-1636	8.4%

Table 38 Model test results for 230K DWT Ore Carrier at ballast condition

without ESD			with PSV		with PSV + Rudder Bulb		with PSV + HVAF + Rudder Bulb	
Vessel Speed	Delivered Power	Rotational Speed	Power Difference	Energy Saving	Power Difference	Energy Saving	Power Difference	Energy Saving
Vs (kn)	PDT0 (KW)	N_{s0} (r/m)	P_{DT1}-P_{DT0} (KW)	ΔP_{DT1} (%)	P_{DT2}-P_{DT0} (KW)	ΔP_{DT2} (%)	P_{DT3}-P_{DT0} (KW)	ΔP_{DT3} (%)
11.0	4805	47.1	-324	-6.7%	-396	-8.2%	-528	-11.0%
11.5	5494	49.3	-352	-6.4%	-421	-7.7%	-573	-10.4%
12.0	6266	51.5	-390	-6.2%	-460	-7.3%	-635	-10.1%
12.5	7130	53.7	-443	-6.2%	-522	-7.3%	-720	-10.1%
13.0	8097	56.0	-515	-6.4%	-611	-7.5%	-835	-10.3%
13.5	9169	58.3	-604	-6.6%	-726	-7.9%	-980	-10.7%
14.0	10346	60.7	-695	-6.7%	-836	-8.1%	-1122	-10.8%
14.5	11627	63.2	-774	-6.7%	-920	-7.9%	-1241	-10.7%
15.0	13069	65.7	-869	-6.7%	-1024	-7.8%	-1385	-10.6%
15.5	14757	68.4	-1019	-6.9%	-1217	-8.2%	-1623	-11.0%
16.0	16633	71.1	-1164	-7.0%	-1417	-8.5%	-1874	-11.3%

Table 39 The fuel consumption compared with and without ESDs for 230K DWT Ore Carrier

Average data	Energy Efficiency Upgrade		Remarks
	Before	After	
F. O. C(13.00kn, Design draft) (tons/24hour)	65.36	55.51	Hull fouling is in good condition before Energy Efficiency Upgrade PSV+HVAF+RB+PM
$EnergysavingEffect = \left(1-\frac{F.O.C_{ESDs}}{F.O.C_{NO\ ESDs}}\right)\times 100\%$	15.1%		
F. O. C(10.50kn, Ballast draft) (tons/24hour)	33.00	27.43	
$EnergysavingEffect = \left(1-\frac{F.O.C_{ESDs}}{F.O.C_{NO\ ESDs}}\right)\times 100\%$	16.9%		

From the comparison of model test and real ship data from several ships regarding the use of energy saving devices, the energy saving effect of the full scale is usually higher than the results of the model test.

Table 40 Summary comparison of model tests and real ship data with ESDs

No.	Ship type	ESDs and HEP	Model test results	Real ship results
1	230k Ore Carrier	PSV, HVAF, RB,PM	9.7% at design draft 10.7% at ballast draft	15.1% at design draft 16.9% at ballast draft
2	57k Bulk Carrier	PSV, HVAF,PM	5.6% at scantling draft 6.6% at ballast draft	8.3% at scantling draft 16.5% at ballast draft
3	92.5k Bulk Carrier	PSV, HVAF,PM	6.6% at scantling draft 6.7% at ballast draft	11.1% at scantling draft 12.1% at ballast draft
4	53k Bulk Carrier	PSV, HVAF	6.2% at design draft	19.8% at design draft 23.9% at scantling draft
5	3300m3-LPG	HEP, HVAF	12.5% at design draft	about 10.0% at design draft
6	298k-VLCC	PSV	5.6% at scantling draft 5.9% at design draft 7.5% at ballast draft	about 9.5% at laden draft
7	298k-VLOC	PSV, HVAF, RB, LR	12.6% at scantling draft 12.4% at ballast draft	31.9% at scantling draft 36.9% at ballast draft
8	26k Bulk Carrier	HEP, HVAF	about 6.0% at design draft	10.8~11.8% at design draft
9	82k Bulk Carrier	PSV, LR	11.4% at scantling draft	13.9~27.5% at laden condition 14.9~19.7% at ballast condition
10	180k Bulk Carrier	PSV, HVAF, LR	11.1% at scantling draft	21.6% at laden condition

17.5 Innovative Energy-saving Technology

CMES-Tech company provided some full-scale data of the benefits of ALDR about their research works. The research on ALDR technology begins with a laboratory flat plate drag study to analyse the effect of air layer structure on drag reduction. Then, some test studies of the ship model are carried out in the towing tank to consider the effect of the hull line shape. After verifying the function and energy-saving effect of the ALDR system through a large-scale prototype vessel test on the lake. Finally, the energy-saving effect under different working conditions is analysed through the test on the full scale ship.

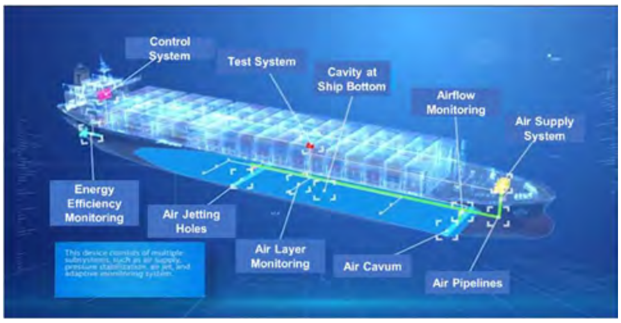

Figure 81 Air Layer Drag Reduction System (ALDR System，CMES-ALESS)

Table 41 Achieved technical index

Research Stage	Research object	Research Result
Principle Research	Flat plate model	Sigle side Friction resistance reduction was more than 60%.
Ship Model Research	Ship model	The typical drag reduction rate was about 50%.
Lake Test Research	100 ton class principle sample ship	① The typical net energy saving was about 18% within the applicable speed range; ② The net energy saving was more than 11% at designed condition.
Ship Utilization Research	Big flat plate model	The relative drag reduction rate was over 90% in the air layer covered zone.
Full Scale Ship Verification	432TEU Full scale ship	The net energy saving effect was more than 7%.
	334TEU Full scale ship	The net energy saving effect was more than 8%.

Designed and developed a 100 ton principle sample ship of the air resistance reduction principle. The application object is for 95,000 ton bulk carrier with a scaling ratio of 1:10. Within the applicable speed range, the typical energy-saving effect is 18%. Under the design draft and design speed, the energy-saving effect is more than 11%.

Figure 82 ALDR principle sample ship on lake

Table 42 Results of lake test results of ALDR

Ship Speed	Shaft Power-without ALDR	Shaft Power-with ALDR	Power of Air-jet	Net Energy Saving Effect
kn	kW	kW	kW	%
1.50	0.678	0.466	0.131	-11.95%
2.00	1.019	0.734	0.131	-15.11%
2.50	1.534	1.156	0.131	-16.10%
3.00	2.308	1.822	0.131	-15.38%
3.50	3.473	2.482	0.502	-14.08%
4.00	5.225	4.01	0.502	-13.65%
4.50	7.862	6.478	0.502	-11.22%
5.00	11.829	10.465	0.502	-7.29%
5.20	13.929	12.678	0.502	-5.38%

The ALDR system was applied to two real ships, 400 TEU and 334 TEU open container ship. The speed and shaft power obtained under the fixed engine speed N=390rpm and different air jet flow for 400TEU. The net energy-saving effect under the best air injection flow is 12.5%. For 334 TEU ship, the energy savings were tested at different speeds with optimal ventilation and obtain above 7%.

Figure 83 ALDR applied on 400TEU container ship

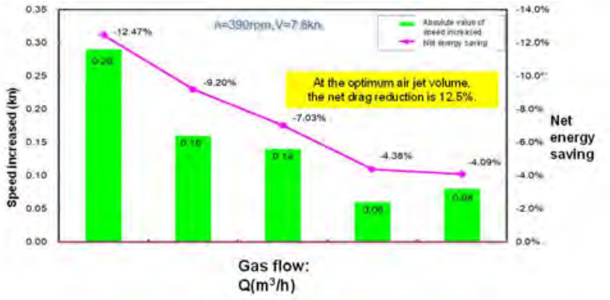

Figure 84 Speed and shaft power curve obtained under different jet volume for 400TEU

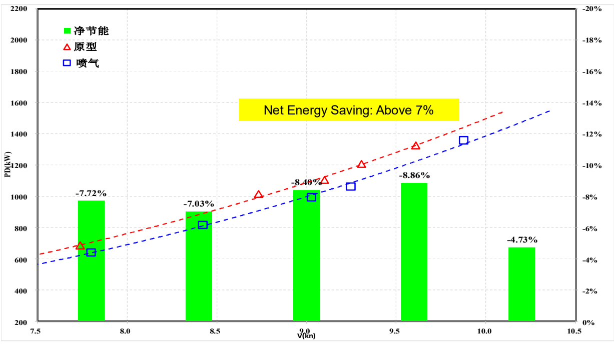

Figure 85 Full scale test result for 334TEU

Wind-assisted rotor, wind sail and seawing have been used on full scale ship. MEPC report indicate that the wind energy saving technique normally can obtain about 5%~20% energy saving. By statistical data of International Wind ship Association (IWA), there were 21 ships using the wind energy saving until third quarter of 2022. The data become to 49 ships to the end of 2023.

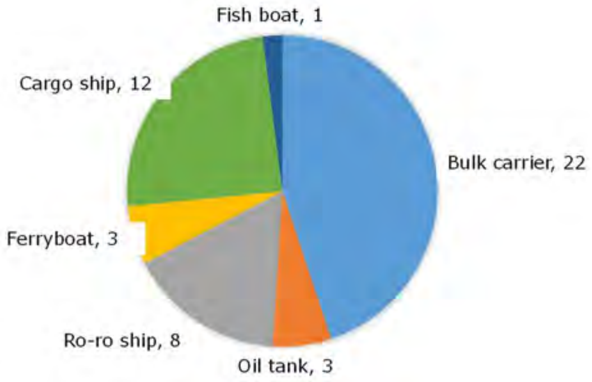

Figure 86 Using the wind energy saving ships

Figure 87 “E-Ship”-2010 and “Afros”-2018

In 2023, 45000DWT bulk carrier with four units wind-assisted rotor, the full scale sea trails have been finished at East sea of CHINA. The diameter of rotor is 2.9m and the total height is 21.6m. The max rotation speed of rotor is 280 r/min. The sea trail test content include the rotor with turn on and turn off condition. In ballast condition, wind speed is 12m/s, wind direction is 55°, the speed can be increased abt. 0.7kn. Converting into the same speed condition, the main power can be decreased more than 15%. In full load condition, wind speed is 22m/s, wind direction is 50°, the speed can be increased abt. 1.0kn. The main power can be saved abt. 30%.

Figure 88 Wind-assisted rotor of 45000 DWT B.C

Table 43 Sea trail results of 45000 DWT B.C with Wind-assisted rotor

NO.	Wind direction	Wind speed	Main Eng. Rotation speed	PD	Vs	ΔVs	Wind-assisted rotor	Rotor speed	Rotor consumed PD	Energy saving by speed increasing	Decreasing of shaft power	Consumed power	Net energy saving
	(°)	(m/s)	(r/min)	(kW)	kn	kn	ON/OFF	(r/min)	(kW)	%	%	%	%
1	56.7	11.7	95.1	3284	13.83	--	OFF	0	0.0				
	55.2	12.6	95.0	3208	14.71	0.74	ON	260	107.2	20.4%	2.3%	3.3%	19.4%
2	54.3	11.3	95.0	3261	13.97	--	OFF	0	0.0				
	52.5	11.7	95.1	3182	14.72	0.75	ON	208	62.2	17.0%	2.4%	1.9%	17.5%
3	47.7	11.3	95.0	3281	14.65	--	OFF	0	0.0				
	59.6	10.6	95.1	3178	15.36	0.70	ON	160	33.8	15.1%	3.1%	1.0%	17.2%
4	50.1	12.2	95.1	3318	14.69	--	OFF	0	0.0				
	51.6	12.3	95.1	3250	15.40	0.72	ON	160	36.2	15.2%	2.0%	1.1%	16.1%
5	53.5	11.3	95.0	3302	14.68	--	OFF	0	0.0				
	55.2	10.9	95.1	3185	14.96	0.31	ON	115	17.6	5.9%	3.5%	0.5%	8.9%

17.6 Scale Effect Research of ESDs

It is short of the model test and CFD calculation results, and compared with full scale data. Especially, it is difficult to obtain enough the full scale data when the shipyard makes the sea trial. In order to research the scale effect, the special test ship is necessary. But the full scale ship is too expensive. A mid-scale test ship can be used to do some research about the scale effect of energy saving technique. CSSRC carried out a project of "mid-scale" test ship. The "mid-scale" model tests on optimized hull lines, propeller. Model was equipped with reconfigurable ESD (pre-shroud vanes, hub vortex absorber, etc.). The particulars of the ship are L=55m, B =10m, *disp*.=1500t and speed 10knots at maximum. It can be equipped with propeller hub fins, replaceable: rudder, ESD, wind assisted rotor, air layer system. Geometry is close to VLCC under waterline. Stereo PIV measurement was carried out through the windows installed in the aft part. It is equipped with whole ship system, with the monitoring all the devices including ship route and speed optimization systems. SMART operating system was developed and ship was ready for remote control. Ship was launched 20/7/2023 and sea trials were carried out on September 2023. There were four combinations of installed ESD tested. The difference of the results between repeat tests was within the range of 1%. Turning circle tests were carried out and compared with model tests and simulation. The manoeuvring indices were compared and the influence of ESD on these indices was noticed. Further the smart operation system was tested in operation on fully remote vessel. Additional tests are planned to continue the study on the scale effect.

Figure 89 "Mid-scale" test ship

Figure 90 Carried out multiple exchange of ESDs on "Mid-scale" test ship

17.7 Conclusions

There are difficulties in comparing the effectiveness of ESD (Energy Saving Device) between model scale and full scale data due to environmental conditions during sea trials. Additionally, assessing the effectiveness of ESD in service is challenging due to uncontrolled differences in loading conditions between ships with ESD and ships without ESD.

Deep water towing tank test is the most commonly using and effective method to verify ship energy consumption. It has been verified by the actual ship operation that the hydrodynamic energy efficiency upgrade can improve the ship speed and save fuel for the main engine. It is proved that this model test is feasible.

For the operating ships, the combination of energy saving technologies such as Propeller Modification (PM), High Efficiency Propeller (HEP) and Energy Saving Devices (ESDs) can save energy consumption by more than 10%.

The energy-saving effect of real ship operation may be affected by sea conditions (such as wind, wave and current) and hull fouling conditions, and most of them are better than the results of model test.

It is necessary that more full-scale data of ALDR would be collected. Some detail influence factor should be analysed such as ship motion, wave and ship speed.

The wind-assisted rotor can obtain significant energy saving from the full scale sea trail results. It has bright future. But it is short of the model test and CFD calculation results, and compared with full scale data.

In the future, it is necessary for preparing a guideline on survey of energy saving methods for the performance of this systems in sea trials and operational conditions.

18. NEED FOR NEW PROCEDURES FOR EVALUATING SMART SHIP PERFORMANCE

18.1 Overview

Autonomous, unmanned, or smart ship technology holds promise in the commercial maritime industry due to potential improvements to safety and efficiency as well as reduced operating costs. Development of these technologies relies upon the ability to conduct tests and trials to validate predictions and demonstrate real-world performance. Existing ITTC trials procedures, notably RP 7.5-04-01-01.1, are agnostic to the method of vessel control, be it manned or unmanned. The question, therefore, is whether any gaps exist within ITTC trials procedures, unique to unmanned or autonomous ships, which are not already addressed through existing international regulatory policy.

18.2 IMO Maritime Autonomous Surface Ship (MASS) Code

In recognition of the unique safety and security issues associated with the trials of Maritime Autonomous Surface Ships (MASS), IMO issued Interim Guidelines for MASS Trials in MSC.1/Circ. 1604 (IMO, 2019). The Maritime Safety Committee (MSC) intends to adopt a non-mandatory, goal-based MASS Code to take effect in 2025. The non-compulsory code would serve as the basis for a mandatory, goal-based MASS Code expected to enter into force on 1 January 2028. The Interim Guidelines provide recommendations related to risk management, compliance, manning and qualification, human factors, infrastructure, and communications.

Regarding risk management, the Interim Guidelines address the specific risks to safety, security, and the environment. Risk identification and controls are recommended to reduce risks to acceptable levels. Contingency planning is suggested to mitigate the impacts of incidents or failures. Adequate notifications should be provided to outside parties who may be impacted by MASS trials and any associated incidents or failures. Finally, safety should be evaluated throughout trials and testing must be stopped when safety controls lose effectiveness.

Onboard or remote operation of the MASS vessel during trials should be only by qualified personnel. All personnel involved in the trials should be adequately qualified and familiar with MASS trial safety procedures. Trial planning should address the human-system interface as well the provision of adequate monitoring infrastructure to ensure that MASS trials can be conducted safely and securely.

Monitoring capabilities for all personnel should provide information regarding the performance of the vessel and the decision-making process for automated systems. Communication systems should support data and voice communications to ensure safe execution of testing and consideration of redundancy of these systems is recommended. Cyber security of the monitoring and communications systems, as well as other test infrastructure, should be considered as part of a holistic risk management process.

In summary, the Interim Guidelines for MASS Trials provide enhancements to the trial planning and execution processes to address the unique aspects of operation and testing of unmanned or autonomous vessels. The recommended guidance does not directly impact or change how S/P trials are conducted in accordance with RP 7.5-04-01-01.1.

18.3 International Network for Autonomous Ships (INAS)

The International Network for Autonomous Ships (INAS) was informally organized in 2017 as an outgrowth of the Norwegian Forum for Autonomous Ships (NFAS) (Rødseth, 2022a). The charter of the organization is to act as a forum for the retention and dissemination of information of common interest regarding unmanned, autonomous, and smart ships. SINTEF Ocean currently serves as the organization's secretariat. As of 2024, INAS is comprised of nearly 20 members or prospective members from Asia, Australia, Europe, and North America.

INAS maintains a listing of known autonomous ship test areas (Rødseth, 2022b). As of 2024, the autonomous ship test areas are in Belgium, Finland, Netherlands, Norway, the United Kingdom, and the United States. Additional test areas or research facilities that can support autonomous ship research are located in Germany and Italy.

In addition to consolidating information regarding autonomous ship test areas, INAS also maintains a repository of guidelines for MASS trials. These include various national policies, EU and IMO guidelines, as well as voluntary practices suggested by INAS itself. INAS and its progenitor, NFAS, currently serve as de facto coordinators of MASS testing guidance and policy in the absence of compulsory rules.

18.4 Conclusions

Trials of MASS vessels are typically focused on autonomous navigation and autonomous behaviours as these aspects set them apart from manned surface ships. While MASS trial procedures may incidentally coincide with the techniques utilized for S/P trials, this is expected to be the exception and rarely the purpose for MASS trials. IMO Interim Guidelines for MASS Trials do not fundamentally impact the test procedures or methodology utilized to conduct ship S/P trials. It is therefore recommended that FSSPC continue to monitor developments in IMO MASS policy, with compulsory rules expected to enter into force in 2028, as well the MASS testing guidance cultivated by INAS and NFAS.

19. CONCLUSIONS AND RECOMMENDATIONS TO THE 30TH ITTC

19.1 Main Conclusions

a) Task 1 A)
Literature survey has conducted on the application of data-driven approaches.
AI technologies can be useful and effective tools to analyze the huge volume of ship operational data and solve complicated problems such as validating the energy efficiency performance of ships, the modelling and prediction of wave added resistance of ships in the seaway, the on-line prediction of ship maneuvering behavior for collision avoidance, the monitoring of fouling and aging influence, etc.
It can be expected that there will be more and wider AI applications concerning full scale ship performance in the future.

b) Task 1 B)
Measuring techniques for waves in speed/power trials are reviewed through literature survey.

c) Task 1 C)
It is considered that MARIN's JoRes ship-scale test cases data to be published in December 2024 are most relevant to meet this

TOR task, in particular, thanks to its coverage of ship types, 3D configurations, ESDs, roughness measurements.

d) Task 1 D)
It is found that the reliability of full-scale CFD simulation results have remained quite low compared to that of model-scale results mainly due to the lack of sufficient full-scale validation data, and that performance prediction based on full-scale CFD simulation results is not practically feasible at present.

e) Task 2 A)
Survey on the requirements for changes in the light pf current practice has conducted through the questionnaire to ITTC member organizations for the revision of R.P. 7.5-01-01-01.1.

f) Task 2 B)
Needs for the new procedures for examining the full-scale effects of energy saving methods, hull/propeller surface roughness are identified.
Need for the revision of guideline for evaluating Air Lubrication System by introducing the modelling of system's parameters for air injection is identified.

g) Task 3 A)
Effect of roughness wave lengths have significant effect on added resistance due to roughness. This effect should be included in the full-scale ship performance predictions.
Non-uniformity of roughness distribution over wetter surface has significant effect on added resistance due to roughness. This effect should be included in the full-scale ship performance predictions.
Roughness height should preferably be treated in relation to the local thickness of viscous sublayer since the only part of roughness emerged from the viscous sublayer contribute in the added resistance.

h) Task 3 B)
Hydrodynamic properties of macro biofouling including newly coated surfaces have been clarified sufficiently. However, those of micro biofouling, in particular, slimes have not been fully elucidated. Since micro biofouling is most frequently encountered roughness in both speed/power trials and operations, those roughness components should be thoroughly addressed in the future.
Coating materials and ambient environmental conditions have significant influence on the growth of biofouling and resulting increase in hydrodynamic resistance. These issues should be thoroughly addressed in the future.

i) Task 3 C)
State of the art of the measurement of roughness has reviewed.
Comparison has made on the surface roughness measurements using both contact and non-contact type instruments.

j) Task 3 D)
Full-scale performance deterioration due to roughened hull and propeller surfaces have studied extensively using roughness functions derived from both CFD simulations and model experiments. However, validation of the predictions is decisively scare due to the non-availability of appropriate full-scale data.
Rigorous validations of the full-scale predictions are indispensable for the development of practically reliable procedure for evaluating roughness effects on in-service performance.

k) Task 3 E)
A prediction method developed in the Japanese cooperative research project (OCTARVIA) was reviewed. It is shown through case studies that the impact of roughness on propulsion performance can be assessed quantitatively if roughness can be expressed as an increase ratio in resistance or a deterioration rate of propulsion efficiency.

l) Task 4
The review for revision of ISO19030-2016 conducted in 2021 resulted in a major vote to leave ISO 19030:2016 unchanged. Thus, a new edition of ISO 19030 may not be published until 2029.

m) Task 5 A)
The committee members were invited to contribute to the validation of the method by conducting full-scale trials in shallow (and deep) waters. An emphasis was put on other parties than the developer of the method (MARIN), which has already provided validation within its publications. Organizing such dedicated systematic trials on commercially operated ships has proven difficult, and no new results from trials were delivered or collected.

n) Task 5 B)
The validation result of the SNNM method regarding the accuracy of its predicted mean wave added resistances in irregular waves based on a database comprised of 23 ships of various types shows that the Pearson correlation coefficient R=0.919 was achieved for all gathered data between the SNNM predictions and the benchmark data.
Further investigation based on binned wave headings shows that the SNNM method performs best in head waves (R=0.972), while its performance may be compromised in beam to following waves (R=0.713). It must be emphasized that the treatment of the extrapolation of wave added resistance QTFs in the very short-wave range plays an important role in the spectral analysis results. It is desirable to carry out further investigations concerning this issue.
Comparison of SNNM, SPAWAVE and SNU methods also reveal larger discrepancies in the short-wave period range. Moreover, the three methods have large discrepancies in stern quartering and following waves. SNU and SNNM methods are comparable except in the short waves range, while the SPAWAVE method tends to overpredict and shows larger deviations in short waves.
Another validation work using 8 ship types compared the wave added resistance QTFs obtained from the NMRI, SNNM-SNU methods and the experimental methods. The NMRI method shows very good agreement with input of more detailed hull-form data. This clearly implies that detailed hull form data is essential to improve the accuracy of added resistance predictions.

o) Task 5 C)
The resistance due to drift and rudder is small at designed speed, and influence to speed trial analysis is limited. On this stage, additional correction by the resistance due to drift and rudder is not needed.
Results of model tests with quality controlled carried showed that the tendency of added resistance in very short waves is almost constant. The effect of the tendency of added resistance in very short waves is remarkable in irregular waves. Until sufficient validation would be completed, it is recommended that the added resistance in short waves is treated as a constant value for the analysis of speed trial.
The wave height effect is difficult to be included in the conventional spectrum method. Considering the wave height at the actual speed trial, the wave height effect can be negligible.

p) Task 5 D)
From literature review, including Raven's full report, it was concluded that the total propulsion efficiency is expected to remain relatively unaffected within the application range of the correction method. Raven's study on different ships showed the thrust deduction factor t increases, but only for very shallow water (outside the method's application range). No clear trend was found within the application range. The wake fraction is more sensitive to shallow water effects within the application range, with (1-w) decreasing for shallower water.

However, no usable approximation for all ship types is found yet. The changes in thrust deduction and wake fraction combined lead to a rise in hull efficiency. On the other hand, the propeller open water efficiency is expected to drop due to the increased resistance, (and thus higher propeller loading) and a reduced inflow speed (due to the increase of the wake fraction). This counteracts the rise in hull efficiency, leading to a small overall change in propulsive efficiency ETA_D.
Based on several test cases, it was concluded by Raven that assuming an unchanged propulsive efficiency ETA_D showed better merit. For the relative rotative efficiency no clear indication is found on the effect of shallow water. While large changes to the wake field may occur at very shallow water, the effect within the trial application range is expected to be minor.
It is recommended to continue monitoring the research efforts in this field in the future.

q) Task 5 E)
Survey on new developments in measurements of wind and propeller thrust has examined has conducted.

r) Task 6
It is considered that MARIN's JoRes ship-scale test cases data to be published in December 2024 are most relevant to meet this TOR task in collecting and processing data on the ship in-service performance of interest to ITTC.
Survey to ITTC member organizations regarding the provision of their full-scale data to this TOR task was conducted. 1 organization (SVA Potsdam) has contributed full-scale speed/power trails results for 7 ships.

s) Task 7
Accuracy of CFD for shallow water applications mainly concerning the shallow-water effect on self-propulsion factors is examined by the literature. But, due to the scarcity of the published works, sufficient examination of the issue has not been conducted.

t) Task 8 A)
Based on the outcome from Task 5 C). It is decided that there is no need to update the procedure in this regard.

u) Task 8 B)
The Wind averaging method increases the uncertainty of ship's performance estimation in wind changing condition. Therefore, to directly derive wind speed and direction from each run, the utilize of Lidar or CFD pre-checking method to find proper anemometer positions could be used.

v) Task 9
The situation of ISO/TC 8/SC 6/WG 17 for revising ISO15016 has carefully followed, and some members have participated as experts in the WG so that ISO15016 can be updated in compliance with 7.5-04-01-01.1.
However, 1st DIS voting of the ISO15016 revision conducted from 25 September to 18 December 2023 resulted in the disapproval od 1st DIS.
Regarding the future schedule of the revision, it was reported that the TC 8/SC 6 Chairperson will choose from three options (2ndDIS, 2ndCD or Cancel) based on the discussions in the TC by March 12th and the Project Leader has to submit necessary materials to contribute to the TC 8/SC 6 Chairpersons ahead of the deadline of the revision.

w) Task 10
AC Working Group in principally responsible for this task and preparing the update. It is requested by AC that, after receiving proposal on the update from AC Working Group, FSSPC should prepare a new guideline on parameters for full-scale power predictions. But their work could not be conducted since AC Working Group has not provided their proposal to FSSPC. After that, AC Working Group submitted the proposal of a new guideline independently to AC

without the support of this committee due to the change of AC' policy.

x) Task 11
The guideline on CFD-based wind coefficient has revised according to the new procedure for non-dimensioning.

y) Task 12
Literature survey on the relevant techniques for ship energy saving has conducted.
A complementary metric to EEDI to represent power savings by Air Lubrication System (ALS) has examined, and issues for the future revision have clarified.

z) Task 13
Literature survey on full-scale data on the effect of energy saving methods (ESM) has conducted.
Data on the energy saving effects for a variety of ESMs have collected.

aa) Task 14 C)
State of the art of the procedures of experiments and simulations to evaluate performance of smart ship and unmanned surface vehicles has reviewed through literature survey.

19.2 Recommendations to the Full Conference

a) Adopt the revised Procedure 7.5-04-01-01: Preparation, Conduct and Analysis of Speed/Power Trials (2024)
b) Adopt the revised Guideline on the CFD-based Determination of Wind Resistance Coefficients (2024)

19.3 Recommendations for future work

1. To continue further works on update guideline for correlation factors

2. To employ outcomes from the JORES projects as benchmark data for study of full-scale performance

3. To focus on short waves issue and further investigation of QTF extrapolation method in short waves for the evaluation of added resistance

4. To conduct sensitivity study on influence of discrepancies in evaluation of added resistance on final corrections to the sea trials; study how it affects final speed-power curves

5. To carry out the comparison of validated methods on the larger set of ship types by using real ship parameters; It may be addressed to organisations not only performing model tests.

6. To consider possibility to make selection among the methods for wave correction in speed/power trials depending on the availability ship form data

7. To investigate cases when wind is sideways in head/following waves to find the necessity of correcting the issue of ship running with stable drift angles

8. To monitor and explore further measurement techniques applicable in speed/power trials and in-service monitoring: Lidar wind, thrust and wave spectra.

9. To conduct a validation of CFD based full-scale performance prediction method using full scale data

10. To perform CFD calculations for various ship types to determine the optimum anemometer position in speed/power trials.

11. To preform comparative study of influence of directional energy spreading on the wave correction in speed/power trials

12. To update database of wind resistance coefficients and validate them by using the new method included in the guideline on the use of CFD-based determination of wind resistance coefficient

13. To collect the full-scale data to evaluate the frictional resistance reduction by air lubrication system and validate correlation of actual reduction rate (ADR) and estimated reduction rate (EDR) to predict performance at full loading conditions

14. To evaluate the correlation line between the model scale and full scale friction resistance with working ALS by the CFD methods

15. To evaluate the model test procedure for flat plates (instead of method proposed in the guideline) at different Reynold numbers to find the correct α value extrapolation; standardize the injection pressure and flow rate scaling approach

16. To extend the sea trials procedure to include new metrics such as ADR and EDR, along with the methodology of measurements

17. To develop a guideline to conduct full scale performance evaluations for energy saving methods (ESM)

18. To continue monitoring the performance of energy saving devices (ESD) to collect more data to reduce the influence of weather conditions on their performances

19. To establish new committee for bio-fouling related roughness issues to cope with the fundamental issues elucidated by the committee.

20. To continue monitoring effect of roughness and analyse method for evaluating ship performance in service

21. To investigate the drift angle consideration in added wave resistance correction. And to develop definition of speed component in heading. Update procedure if necessary.

22. To develop formal definition of steady state ship's condition in speed/power trials. Update procedure if necessary.

20. REFERENCES

Air Lubrication Technology, ABS Report, April 1, 2019, https://ww2.eagle.org/content/dam/eagle/advisories-and-debriefs/Air%20Lubrication%20Technology.pdf

Cai, B. et al., 2022, "Numerical Simulation of Ship Model Self-propulsion in Shallow Water", 32th International Ocean and Polar Engineering Conference (ISOPE), Shanghai, China.

D'Agostino, D., Serani, A., Stern, F., Diez, M., 2022, "Time-series forecasting for ships manoeuvring in waves via recurrent-type neural networks", J. Ocean Eng. Mar. Energy.

Demirel, Y. K. et al., 2017, " Effect of barnacle fouling on ship resistance and powering", Biofouling, Vol.33, No.10.

Fowles, Grant R., and George L. Cassiday, 1986, Analytical Mechanics: Fifth Edition. 5th edition. Fort Worth, TX: Saunders.

Gao, N., Hu, A., Hou, L. and Chang, X., 2023, "Real-time ship motion prediction based on adaptive wavelet transform and dynamic neural network", Ocean Eng, 280, 114466.

Gong, H. and Matala, R. 2022, "A study of full-scale measurement of channel widening by IB Polaris", Proceedings of the Thirty-second International Ocean and Polar Engineering Conference Shanghai, China.

Grin, R., 2022, "SPAWAVE, an Empirical Method to Predict Wave Added Resistance in all Wave Directions", Proceedings of 14th International Marine Design Conference (IMDC 2022).

Guo, X., Zhang, X., Tian, X., Lu, W. and Li, X., 2022, "Probabilistic prediction of the heave motions of a semi-submersible by a deep learning model", Ocean Eng. 247, 110578.

Gupta, P., Rasheed, A. and Steen, S., 2022, "Ship performance monitoring using machine-learning", Ocean Eng, 254, 111094.

Gupta, P., Kim, Y.-R., Steen, S. and Rasheed, A., 2023, "Streamlined semi-automatic data processing framework for ship performance analysis", Int. J. Nav. Archit. Ocean Eng, 15, 100550.

Himeno, Y., 1983, "A study on Frictional Resistance of Painted Rough Surface", Journal of Kansai Society of Naval Architects, Vol. 191, pp.11-15. (in Japanese)

Hunsucker, K., Z. et al., 2019, "Using Hydrodynamic Testing to Assess the Performance of Fouling Control Coatings", Ocean Engineering, Vol.194.

IMO Maritime Safety Committee, 2019, "Interim Guidelines for MASS Trials," MSC.1/Circ. 1604, London.

IMO, 2021, " 2021 guidance on treatment of innovative energy efficiency technologies for calculation and verification of the attained EEDI and EEXI", MEPC.1/Circ.896, https://wwwcdn.imo.org/localresources/en/OurWork/Environment/Documents/Air%20pollution/MEPC.1-Circ.896.pdf

IMO, 2022, "Analysing the impact of marine biofouling on the energy efficiency of ships and the GHG abatement potential of biofouling management measures", GloFouling Partnerships Project Coodination Units. https://www.glofouing.imo.org/_files/ugd/34a7be_afd9d183df9a4526bd088007436c1079.pdf

Inukai, Y., 2019, "Full Scale Measurement of The Flow Field at The Stern by Using Multi Layered Doppler Sonar (MLDS)", Sixth International Symposium on Marine Propulsors smp'19, Rome, Italy.

ITTC, 2008, "Propulsion Committee Final Report", 25th ITTC Full Conference Proceedings, Fukuoka, Japan, 2014.

ITTC, 2011, "Specialist Committee on Surface Treatment Final Report", 26th ITTC Full Conference Proceedings, Rid de Janeiro, Brazil.

ITTC, 2014, "Resistance Committee Final Report", 27th ITTC Full Conference Proceedings, Copenhagen, Denmark.

ITTC, 2017, "Resistance Committee Final Report", 28th ITTC Full Conference Proceedings, Wuxi, China.

ITTC, 2021a, "Resistance and Propulsion Committee Final Report", 29th ITTC Full Conference Proceedings, Virtual.

ITTC, 2021b, " Specialist Committee on Ships in Operation at Sea Final Report", 29th ITTC Full Conference Proceedings, Virtual.

Jabary, W., Liu, C., Sprenger, F., Kleinsorge, L., Baumfalk, H., Kaster, M. and Mewes, S., 2023, "Development of machine learning approaches to enhance ship operational performance evaluation based on an integrated data model", Proceedings of the Thirty-Third International Ocean and Polar Engineering Conference, Ottawa, Canada.

Kawashima, H. et al., 2019, "Effect of Roughness Shape Parameter of Painted Surface on Frictional Resistance", Proc. PRADS 2019, Yokohama Japan.

Ki, H.-G., Park, S.-G. and Jang, I.-H., 2015, "Full scale measurement of 14k TEU containership", 7th Inter-national Conference on hydroelasticity in marine technology, Split, Croatia.

Kijima, K., Katsuno, T., Nakiri, Y. and Furukawa, Y., 1990, "On the manoeuvring performance of a ship with parameter of loading condition", Journal of the Society of Naval Architects of Japan, Vol. 168, pages 141-148.

Kim, Y.-R., Esmailian, E. and Steen, S., 2022, "A meta-model for added resistance in waves", Ocean Eng. 266, 112749.

Kuroda, M. and Sugimoto, Y., 2022, "Development of the Evaluation Method for Life Cycle Ship Performance", Journal of JASNAOE, Vol.34, pp 19-27.

Kuroda, M., Yokota, S., Tsujimoto M. and Fukasawa, R., 2022, "Effect of Hydrodynamic Forces due to Drift Motion on Ship performance in Actual Seas at Low Speed", Proceedings of PRADS2022, pp 257-266.

Kuroda, M. and Tsujimoto, M., 2023, "The Wave Correction Method for Speed Trial Analysis: Simple-NMRI method", Report of National Maritime Research Institute, Vol.23-1, pp 73-87.

Lee, J., Kim, Y-.H., 2023, "Development of enhanced empirical-asymptotic approach for added resistance of ships in waves", Appl. Ocean Res., 280, 114762.

Leonard, S., Lübke, L., 2024, "An Investigation into the Effect on Ship Manoeuvring of a Pre-Swirl Duct", Eighth International Symposium on Marine Propulsors smp'24, Berlin, Germany.

Li, F., Goerlandt, F., Kujala, P., Lehtiranta, J. and Lensu, M, 2018, "Evaluation of selected state-of-the-art methods for ship transit simulation in various ice conditions based on full-scale measurement", Cold Regions Science and Technology, 151 94-108.

Li, F.,Lu, L., Suominen, M. and Kujala, P, 2021, "Short-term statistics of ice loads on ship bow frames in floe ice fields: Full-scale measurements in the Antarctic ocean", Marine Structures, 80, 103049.

Martić, I., Degiuli, N., Majetić, D. and Farkas, A., 2021, "Artificial Neural Network Model for the Evaluation of Added Resistance of Container Ships in Head Waves", J. Mar. Sci. Eng., 9, 826.

Mieno, H. et al., 2021, "Experimantal investigation of added frictional resistance by paint rough surface using a rotating cylinder", Journal of Marine Science and technology, Vo.26 No.1.

Mittendorf, M., Nielsen, U.D. and Bingham, H.B., 2022, "Data-driven prediction of added-wave resistance on ships in oblique waves—A comparison between tree-based ensemble methods and artificial neural networks", Appl. Ocean Res., 118.

Mittendorf, M., Nielsen, U.D. and Bingham, H.B., Dietz, J., 2023, "Assessment of added resistance estimates based on monitoring data from a fleet of container vessels", Ocean Eng., 272, 113892.

Mosaad, M., A., and Hassan, H., M., 2024, "Volumetric Image Processing for Predicting Propeller Roughness Penalties", Eighth International Symposium on Marine Propulsors smp'24, Hurghada, Egypt.

Nakamura, S., Hosoda, R. and Naito, S., 1975, "Propulsive Performance of a Container Ship in Waves (3rd Report)", Journal of the Kansai Society of Naval Architects, Japan, Vol.158, pp.37-46.

Nielsen, U., D., Johannesen, J., R., Bingham, H., B., Blanke, M. and Joncquez, S., 2019, "Indirect Measurements of Added-wave Resistance On an In-service Container Ship", PRADS 2019.

Nikolaidou, L., Laskari, A., van Terwisga, T. and Poelma, C., 2021 "On the characteristics of air layer regimes", 11th International Symposium on Cavitation, Daejon, Korea.

Nippon Kaiji Kyokai (NK), 2010, "Guideline for the Technical Appraisal of Ship Performance in Actual Seas", Nippon Kaiji Kyokai (NK), Classification Notes, pp 1-27.

Oh., S.-M., Lee. D.-H., Kim. H.-J. and Ahn, A.-K., 2021. "Full-Scale Measurements of the Propeller Thrust during Speed Trials Using Electrical and Optical Sensors", Applied Sciences, 11(17), 8197.

Oh, S.-M., 2022. " Study on the Speed-Power Performance Assessment by Full Scale Measurements of the Propeller Thrust".

Ponkratov, D, 2023, "JoRes Joint Resraech Project – the largest global community developing benchmark for ship scale CFD", 25th Numerical Towing Tank Symposium, Ericeira, Portugal.

Seo, D.W. and Oh, J., 2021, "Uncertainty Analysis of Speed-Power Performance Based on Measured Raw Data in Sea Trials," International Journal of Naval Architecture and Ocean Engineering, Vol. 13, pp 396-404.

Rødseth, Ø.J., 2022, "Autonomous Ships Test Areas," https://www.autonomous-ship.org/testarea.html.

Rødseth, Ø.J., 2022, "International Network for Autonomous Ships," https://www.autonomous-ship.org/index.html.

Sakurada, A., Kuroda, M. and Tsujimoto, M., 2023, "Evaluation of Drift Force in Large Angles for PCC and Coastal Cargo Ship", Proceedings of 10th PAAMES and AMEC 2023.

Sasaki, N., Tsujimoto, M., Kuroda, M., Sogihara, N., Ichinose, Y., Usui, N., Ueno, M., Fujiwara, T., Hoshino, K., Kawanami, Y., Ohmatsu, S. and Shibata, K., 2009, "Development of Ship Performance Index (10 mode at Sea)", Report of NMRI, Vol.9-4, pp.219-264.

Schirmann, M.L., Collette, M.D. and Gose, J.W., 2022, "Data-driven models for vessel motion prediction and the benefits of physics-based information", Appl. Ocean Res., 120, 102916.

Schlichting, H. 1979. Boundary Layer Theory (7th ed.). McGraw-Hill.

Schultz, M., P,, 2007, "Effects of coating roughness and biofouling on ship resistance and powering", Biofouling, Vol. 23, pp.331-341.

Silva, K.M. and Maki, K.J., 2022, "Data-Driven system identification of 6-DoF ship motion in waves with neural networks", Appl. Ocean Res., 125, 103222.

Simanto, R. I. A., Hong, J. W., Ahn, B. K., and Jeong, S. W., 2023. "Experimental investigation on tip vortex cavity deformation and flow dynamics using high-speed imaging and laser Doppler velocimetry measurements". Physics of Fluids, 35(10).

Sogihara, N., Tsujimoto, M., Ichinose, Y., Minami, Y., Sasaki, N. and Takagi, K., 2010, "Performance Prediction of a Blunt Ship in Oblique Waves", Journal of Japan Society of Naval Architects and Ocean Engineers, Vol. 12, pages 9-15.

Sogihara, N., Yonezawa, T., Ishiguro T., Sugimoto, Y., Masuyama S., Mieno H., Shimada, M. and Matsubara, Y., 2019, "Introduction of OCTARVIA Project: Project for Ship Performance in Actual Seas", Proceedings of HullPIC2019, pp 12-21.

Sogihara, N., Kuroda, M. and Tsujimoto, M., 2022, "Lifecycle Assessment of Fuel Oil Consumption of a Ship in Service", Proceedings of HullPIC2022, pp 36-49.

Song, S. et al., 2019, " An Investigation into the Effects of Biofouling on Full-Scale Propeller

Performance using CFD ", 38th Int. Conf. Ocean, Offshore and Arctic Eng. (OMAE), Glasgow, UK.

Stigter, R., Birvalski, M., Schouten, R., van Rijsbergen, M.,X., van Terwisga, T., Westerweel, J., 2024, "An early assessment of the effect of water quality and sea-state on propeller cavitation inception of a full-scale vessel", 12th International Symposium on Cavitation.

Tadros, M., Ventura, M., Soares, C., G., 2023, "Review of current regulations, available technologies, and future trends in the green shipping industry", Ocean Engineering, Volume 280, 114670, ISSN 0029-8018

Tamura, K., Okada, Y., Okazaki, A., 2024, "Measurement of pressure fluctuation induced by propeller on actual ship using FBG pressure sensor", 12th International Symposium on Cavitation.

Taskar, B. and Andersen, P., 2021, "Comparison of added resistance methods using digital twin and full-scale data", Ocean Eng., 229, 108710.

Tsujimoto, M., 2012, "Validation for Estimation Methods of Added Resistance in Waves and Wind Resistance, Conference proceedings", The Japan Society of Naval Architects and Ocean Engineers, Vol.15, pp.175-178.

Tsujimoto, M., Matsuzawa, T., Sogihara, N., Hirayama, K., Sugimoto, Y., Hasegawa, K. and Yokokawa, K., 2018, "Advanced Weather Routing System for Ships in Actual Seas -Development and Validation by a Ship-", Proc. of 16th IAIN World Congress.

Tsujimoto, M. and Orihara H., 2018, "Performance prediction of full-scale ship and analysis by means of on-board monitoring (Part 1 ship performance prediction in actual seas)", Journal of Marine Science and Technology, Vol. 24, pp.16-33.

Tsujimoto, M., Yasukawa, H., Yamamoto, K. and Lee, Tae-il, 2023, "Validation of Added Resistance in Waves by Tank Tests and Sea Trial Data", Ship Technology Research (Shiffstechnik), Vol. 70, No. 1, pp.14-25.

Yasukawa, H. and Tsujimoto, M., 2020, "Impact of bow shape on added resistance of a full hull ship in head waves", Ship Technology Research (Shiffstechnik), Vol. 67, No. 3, pp.136-147.

Yokota, S., Kuroda, M., Fukasawa, R., Ohba, H. and Tsujimoto, M., 2020, "Detailed Study on the Behaviour of Ships in Very Short Waves", Proceedings of OMAE 2020.

Yokota, S., Kuroda, M., Fukasawa, R. and Tsujimoto, M., 2021, "Measurement and Estimation of Added Resistance in Waves at Low-speed", Proceedings of PAAMES/ AMEC 2021.

Yokota, S., Tsujimoto, M., Sakurada, A. and Kuroda, M., 2021, "A Practical Correction Method for Added Resistance in Oblique Waves Considering the Influence of Roll Motion", Journal of JASNAOE Vol. 34.

You, Y., Kim, J. and Seo, M.-G., 2018, "Prediction of an actual RPM and engine power of an LNGC based on full-scale measurement data", Ocean Engineering, 147 496-516.

Zhang, D., Zhou, X., Wang, Z.-H., Peng, Y. and Xie, S.-R., 2023, "A data driven method for multi-step prediction of ship roll motion in high sea states", Ocean Eng., 276, 114230.

ITTC2024

30TH INTERNATIONAL TOWING TANK CONFERENCE
22–27 SEPTEMBER 2024 | HOBART TASMANIA AUSTRALIA

REPORT OF THE SPECIALIST COMMITTEE ON WIND POWERED AND WIND ASSISTED SHIPS

1. INTRODUCTION

Wind assistance as a means to reduce fuel consumption of ships has gained an increased interest in the last few years. The number of companies providing wind propulsion technologies is increasing rapidly. In the coming decades the number of wind-powered ships is predicted to increase to 10 000+ ships according to UK Clean Maritime, Plan (2019) and Nelissen (2016). ITTC can play an important role in this development, especially regarding performance indicators, performance assessments and sea trials. Before this background, the 29th ITTC established the first Specialist Committee for Wind Powered and Wind Assisted Ships.

2. MEMBERSHIP AND MEETINGS

The members of the Specialist Committee on Wind Powered and Wind Assisted Ships Committee of the 30th ITTC are:

- Dr. Sofia Werner (Chair)
  RISE SSPA Maritime Centre,
  Sweden.
- Dr. David Trodden (Secretary)
  Newcastle University,
  United Kingdom.
- Dr. Anders Alterskjær
  SINTEF Ocean,
  Norway.
- Ir.Rogier Eggers,
  Maritime Research Institute Netherlands (MARIN),
  Netherlands.
- Dr. Yeongyu Kim,
  Korea Research Institute of Ships and Ocean Engineering (KRISO),
  South Korea.
- Dr. Yuling Gao,
  Shanghai Ship and Shipping Research Institute (SSSRI),
  China.
- Dr. Xinshu Zhang,
  Shanghai Jiao Tong University (SJTU),
  China
- Dr. Kenichi Kume
  National Maritime Research Institute (NMRI), Japan

5th committee meeting in Shanghai. From left: Rogier Eggers, Anders Alterskjær, Sofia Werner, Yuling Gao, Kenichi Kume and Xinshu Zhang

Five committee meetings have been held during the work period:

- The first meeting was held online on the 13th September 2021
- The second meeting was held online on the 18th & 19th January 2022
- The third meeting was hybrid held online and Trondheim, Norway on the 24th to 25th August 2022
- The fourth meeting was online on the 21st and 28th February 2023
- An intermediate meeting was online on the 17th November 2023
- The fifth meeting was hybrid held online and Shanghai, China from the 16th to 19th January 2024

3. TASKS

The recommendations for the work of the Wind Powered and Wind Assisted Ships Committee as given by the 29th ITTC were as the following Terms of Reference (ToR):

1. Review technologies for wind propulsion and wind assistance. Clarify the distinction between wind powered and wind assisted ships.

2. Review methods of ship model hydrodynamic tests, wind tunnel tests, CFD, ship dynamics simulations and routing relevant for predicting the performance and safety of wind powered and wind assisted ships at design stage with particular attention paid to higher side forces and drifting of the ship due to wind powering.

3. Review long-term statistics of winds and waves from the point of view of applicability for the evaluation of wind assisted ships at design stage.

4. Derive a guideline for predicting the fuel consumption of a wind propulsion ship on a route at design stage with the consideration of weather-routing effects.

5. Review safety and regulatory issues related to hydro/aero dynamic testing and evaluation and recommend measures to take at design stage.

6. Derive performance indicators for comparing the performance of wind propulsion at design stage.

7. Investigate the effect on propulsive factors due to reduced propeller load arising from the use of wind power. Identify the effects of wind propulsion on the propulsion system, e.g. pressure side cavitation occurrence. Liaise with Resistance and Propulsion Committee and SC on Cavitation and Noise.

8. Derive a modified procedure for full scale trial of wind propulsion ships. Liaise with Full Scale Performance Committee.

9. Cooperate with MEPC on the continuous development of the EEDI for wind propulsion ships. Liaise with Full Scale Ship Performance Committee.

10. Liaise with the Ocean Engineering Committee regarding their work on SiL and controllable fans to model wind loads.

4. STATE OF THE ART

This section describes the work done by the committee on tasks 1, 2, 3, 5, 7, 9 and 10 described in the previous “Tasks” Section 3.

The work done in the other tasks (4, 6, 8) can be found in the “Procedures” Section 5.

4.1 Review technologies for wind propulsion and wind assistance

The scope of this section is to briefly review the main technologies currently used in the production of power from wind for the use onboard ship. It serves as a reference for the ITTC Specialist Committee on Wind Powered and Wind Assisted Ships and defines a distinction between wind powered and wind assisted ships, which can be used to maintain consistency throughout other ToRs.

The technologies focus mainly on propulsion power, rather than power required for hotel loads etc.

There are seven predominant categories of wind propulsions systems (WPS), (International Windship Association, 2021):

1. Rotor Sails: Based on the "Magnus" effect. Commonly referred to as a Flettner rotor.

2. Kite Sails: Flown off the bow to assist propulsion, can be dynamic or passive.

3. Soft Sails: Traditional cloth and modern adaptations.

4. Hard Sails: Also referred to as wingsails. Have flaps to vary the camber for tacking.

5. Suction Sails: Non-rotating wing with boundary layer suction to increase maximum lift values

6. Turbines: Wind turbines used to generate electrical energy

7. Hull Form: Redesign of a ship's hullform to capture the wind force and generate thrust

The main disadvantages of all these technologies are that they cannot produce as much power as conventional prime movers, and that power levels cannot be guaranteed.

Table 1 summarises the maturity, costs, technical and operational aspects of sails, kites and rotor sails-

Table 1: Some aspects to consider when selecting a WPS (Gerhardt, Werner et al. 2021)

	Aspect	Flettner Rotors	Kite	Wingsails	Soft Sails	Suction Wing
Maturity	Proven Technology.	First tested in the 1920s. Most accepted + proven solution on the modern market.	Tested in a few commercial vessels.	Some experience from applications in the 1980s Yacht racing.	Long history of traditional sails.	Some experience of Turbosails. New technology being tested.
Commercial	System/Equipment Availability	Commercially available.	Commercially available.	Several concepts. Only a few off the shelf.	Available in large scale super yacht segment.	Available in small scale.
	CAPEX	High	Low	High	Medium	High
	OPEX	Low	High (wear and tear)	Low, medium if reefable	High (wear and tear)	Low
Technical	Retrofit off hire impact	Weeks	Days – Weeks	Weeks – Months	Weeks – Months	Hours (Containerised small-scale units)

	Deck space requirements	Open deck for optimal performance.	Deployed form a small mast near the bow.	Open deck for optimal performance.	Open deck for optimal performance. Removable container can be placed on cargo holds.	
	Operational wind directions	Optimal operation in 90° – 150°.	Broad reach to downwind. Risk that kite falls into the water in low wind speeds.	Efficient upwind, less efficient downwind.	Similar to wingsail but less efficient.	Similar to wingsail but less efficient.
	Sail Trimming	Only rpm can be adjusted.	Figure-eight pattern can be adjusted with windspeed.	Not many options to trim rigid wings. Twist impossible.	Can be trimmed in many ways.	Not many options to trim rigid wings. Twist impossible.
Operational	Cargo handling constraints	Foldable and movable solutions available on the market.	None.	Some concepts are foldable or collapsible to avoid constraints.	The rig implies constraints even with furlable and reefable sails.	Removable container available.
	Air draft	Largest available systems today 35m and tiltable.	No constraints when not sailing.	Often taller than rotor sails.	Often taller than rotor sails.	Containerised system 10.5 m.
	Risks imposed by adverse weather	Slender profile and robust design	Can be retrieved in storm	Required fast vaning response.	Reefable sails.	Small systems collapsible.
	Operational effects	Risk of reduced visibility. Gyroscopic roll stabilisation effect. Reverse rotation possible for improved manoeuvrability.	No contribution to heel. Cannot be used in areas with dense traffic.	Risk of reduced visibility.	Risk of reduced visibility.	Risk of reduced visibility.

4.1.1 Working Principles of Operation

To determine how a WPS generates a force, consider a fluid particle travelling at constant velocity along a curved streamline. The streamline is curved as it flows over the surface of the WPS. Because the particle is changing direction, there must exist a centripetal force acting normal to the direction of motion. Ignoring all other forces, this centripetal force can only be generated from pressure forces, i.e. the pressure on one side of the particle is greater than on the other. So, if a streamline is curved, there must be a pressure gradient across the streamline, with the pressure increasing in the direction away from the centre of curvature (Babinsky, 2003).

This analogy can be used to describe how a lift force is generated from a WPS.

To calculate the force produced from sails, provided the flow largely remains attached, inviscid codes have successfully been implemented since the 1960s (Milgram 1968). If the sails experience large regions of flow separation, then viscous flow solvers become necessary, increasing the time and resources necessary to complete the analysis.

All of these technologies work on the apparent wind velocity flowing over a WPS which produces lift. If the wind direction is not favourable, then the mechanism will produce more drag than lift, usually resulting in either a change in course or the cessation in use of the WPS.

4.1.2 Sails

This section will summarise the three main sail types, namely soft sails, wing sails (or rigid sails) and suction sails.

Generally, due to the nature of the structure being relatively tall, sails are more suited to vessels with low air draught.

4.1.3 Soft Sails

4.1.3.1 Background

Soft sails are usually manufactured from a flexible fabric, such as canvas or polyester. They are supported through various rigging configurations. The use of soft sails is a well-established and proven method of propelling water-borne vehicles, with evidence of their use dating back to 6000 B.C. (Carter 2012).

The sails generate thrust through different mechanisms depending on the apparent wind angle. When the vessel is on a broad reach or running before the wind, the sails no longer generate force from lift, but from drag, which is somewhat less efficient.

Greater lift coefficients can be obtained from using higher aspect ratio sails; however, this results in a relatively higher vertical centre of effort and consequently a greater heeling arm. To circumvent the higher heeling arm whilst retaining a high lift coefficient, many sails can be used. It is common to see three or perhaps four masts on commercial vessels, however little research has been conducted on sail interaction for many-masted vessels, as well as sails configured in rows, athwart ships.

Specialist rigs for large craft have been developed using modern materials and design methods (Thomas 2015), where the hullform and rig are designed together. One such rig is the DynaRig and resembles a traditional square rig. The masts are free-standing and able to rotate so as to adjust the sails' angle. The rig is able to be controlled by a single person. When fully deployed, there are no gaps between the sails, contributing to high efficiency, which is estimated to be twice that of a traditional square rig (Perkins, Dikstra et al. 2004).

Fore and aft rigs tend to have better upwind performance, whereas square rigged vessels generally have better downwind performance (Marchaj 1988).

4.1.3.2 Advantages and Disadvantages

Soft sails require no external power source to operate and can be easily reefed or furled and stowed due to their flexible nature. If designed correctly, spars and booms which support the sails can also be used as derricks for cargo handling.

Soft sails take up a large amount of deck space, meaning that consideration needs to be given in the design of the rigging to allow access to cargo hatches and docking.

4.1.3.3 Potential Energy Savings

The reduction potential is dependent on vessel size, segment, operation profile and trading areas. The likely reduction potential is estimated to be in the range of 1% to 10% on main engine fuel consumption (Glomeep 2019). However, given enough sail area, it is possible to propel the vessel using nothing other than the power from the sails.

4.1.3.4 Cost

Soft sails are relatively cheap to produce and can be manufactured in existing facilities. Operational costs of soft sails can be quite high, as extra, specialist crew is required to operate them and the rigging.

The price per mast (including installation) is expected to decrease dependent on how many masts are installed on board. Thus, the capital cost involved will range from \$170,000 to \$300,000 (USD) per mast installed (Glomeep 2019).

4.1.3.5 Commercial Adoption

The *Tres Hombres* is a successful example of a commercial cargo vessel, solely propelled by soft sails. It has been trading since 2007. Numerous commercial fishing vessels are operated solely by soft sails, especially in the middle and far East.

4.1.4 Wing Sails

4.1.4.1 Background

Wing sails, also known as hard sails, are rigid sails which operate in a similar way to their soft-sail counterparts. The main advantage of wing sail over traditional soft sails is that their camber can be varied, confer to Figure 1. This results in a sail that can be tuned more effectively to provide a greater lift to drag ratio than soft sails, greater efficiency, and more precise control. Wing sails can be constructed of metals, plastics with elements of fabric to reduce weight.

Figure 1: Top view of a rigid wing-sail from the Oceanbird concept (Oceanbird 2023).

4.1.4.2 Advantages and Disadvantages

Wing sails are usually operated on a rotating mast. This results in an optimum angle of attack over any apparent wind angle, and thus a greater efficiency compared to soft-sails is achieved.

Because of the rotating mast and variable camber, more precise control is available, making this technology more amenable to autonomous control. This in turn means that no extra crew are required for its operation.

Due to the rotating mast and sail, careful consideration needs to be given with regards to deck space and sail dimensions to ensure adequate clearance.

4.1.4.3 Potential Energy Savings

The Shin Aitoku Maru was fitted with a wing sail from NKK, an increase in power from the wing sails was measured between 5% and 10% when operated in the East China Sea.

The reduction potential is dependent on vessel size, segment, operation profile and trading areas. The likely reduction potential is estimated to be in the range of 1% to 10% on main engine fuel consumption (Glomeep 2019). However, given enough sail area, it is possible to propel the vessel using nothing other than the power from the sails.

4.1.4.4 Cost

Capital costs are larger for wingsails compared to soft sails.

The price per mast (including installation) is expected to decrease dependent on how many masts are installed on board. Thus, the capital cost involved will range from $170,000 to $300,000 (USD) per mast installed (Glomeep 2019).

4.1.4.5 Commercial Adoption

Commercial adoption of Wing Sails started to gain popularity in the late 1970s and early 1980s, where Japanese company NKK fitted a folding wingsail to the Shin Aitoku Maru and about 10 other vessels. The system successfully demonstrated fuel saving potential.

In 1986 Walker Wingsail Systems (WWS) plc built and sold an 8 tonne wingsail for use on MV Ashington. The WWS used a unique tandem arrangement of wingsails to allow for automatic feathering. In the Ashington's trading area, "usable wind" was restricted during the trial to approximately 30% of the total passage time. Average wind speeds were relatively low. There was also significant downtime due to necessary wingsail maintenance, and the vessel's fuel consumption results were not consistent. In summary, the wingsail produced thrust equivalent to 8% of normal engine load. At this time, there was a collapse of the world's oil prices which destroyed the economic use case, this and lack of investors ultimately lead to the demise of WWS plc (Cooke Associates 2023).

More recently the use of wing sails are becoming more popular, with the likes of Becker Marine Systems (Becker Marine Systems 2023) and OceanBird (Oceanbird 2023) investing in the wing sail concept.

4.1.5 Suction Sails

Suction Sails are a relatively new method for creating lift from wind, with the original Turbosail developed by Jacques Cousteau (Charrier, Constans et al. 2985). More recently the Ventifoil, which is based on the same principle, is currently being developed by (Econowind 2022).

Suction Sails operate on the same principle as conventional sails or aerofoils, generating lift from flow over the surface. However, Suction Sails have a relatively thick cross section with a moveable fin or flap (confer to Figure 2).

Such a thick profile would usually result in flow separation due to the adverse pressure gradient near the trailing edge and consequently a loss of lift. However, a fan provides suction to the leeward edge of the sail (through a mesh) which removes the retarded flow, leaving a thin, fast moving boundary layer which remains attached much further downstream and thereby producing relatively high lift coefficients.

Depending on which side of the ship the apparent wind is coming from, the flap can switch sides to cover the mesh on the windward side, thus enabling the Suction Sail to tack like a conventional sail.

Automatic control systems allow trimming and reefing of the Suction Sail through rotation of the 'mast' and variation of the suction strength respectively. This minimises additional training of crew. The Suction Sail can relatively easily be retrofitted, either by directly mounting on a reinforced deck, or deployed from a secured 40 foot shipping container, as on the Ventifoil system (Econowind 2022).

The lift of Suction Sails is comparatively very high but drag is also high and so the lift/drag ratio is limited. This leasd to restricted upwind performance, but high performance across and downwind on reaching courses.

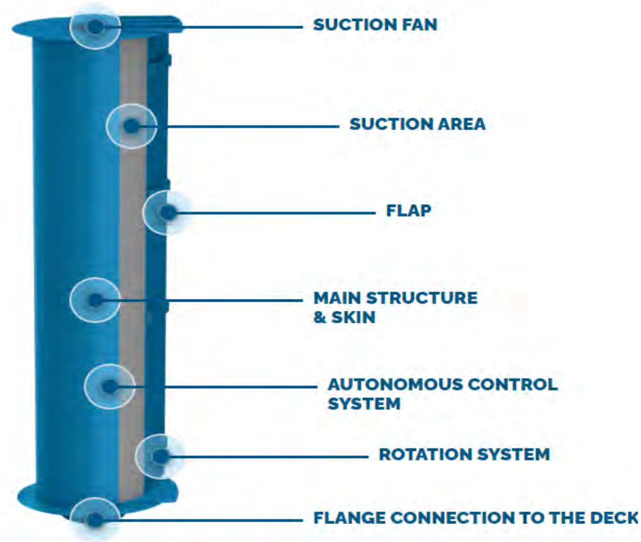

Figure 2: Main components of a suction sail (Bound4Blue 2022)

4.1.5.1 Advantages and Disadvantages

Some energy must be used to control the boundary layer separation; however this must be balanced with the extra lift that these WAP devices produce. Suction sails can be relatively easy to retrofit and can be versatile in their placement.

4.1.5.2 Potential Energy Savings

Boomsma Shipping retrofitted two Flatrack 11m suction wings from Econowind on the 6,446 DWT Frisian Sea and estimate a power saving of 10%.

4.1.5.3 Cost

There is insufficient data to make a meaningful analysis, however it is expected that both CAPEX and OPEX would be comparable to Rotor Sails, or perhaps a little more expensive from added complexity.

4.1.5.4 Commercial Adoption

As part of the EU Interrg WASP project, the 3,600 DWT general cargo vessel MV Ankie, made its first voyage with the two wings installed, sailing for Wagenborg from Delfzijl to Hamburg, onwards to Norway and back to Rotterdam. With this auxiliary propulsion, a proposed fuel saving of 1000 litres per day can be achieved. This installation is part of EU Interreg WASP project (Interreg North Sea Region 2021).

The 2300 DWT Tharis has also been retrofitted with two 9m x 3m TwinFoil retractable wingsails from Econowind in a similar Interreg WASP project.

4.1.6 Kites

A variety of WASP technologies are available on the market with each having its distinct characteristics. Kite propulsion has emerged as an attractive means to harness wind power in a way that yields environmental and financial benefits, which has been studied and installed on commercial ships. Kites offer significant advantages compared other WASP technologies and subject to some limitations at the same time. Some aspects such as maturity, operational potential of power saving etc. of this technology are reviewed.

4.1.6.1 Background

Although kites are believed to have existed since circa 500 BC, record of their use for propulsion only dates back to the 1820s. The concept of kite powered ships did not actually appear attractive at the time and was only brought back a few decades ago.

Kite is applied in naval transportation usually by two ways.

The kite is used to directly tow a ship, like a classical sail does. They provide thrust to ships with the lift generated by high altitude winds.

Another way is using a kite energy system, able to convert wind energy into electricity onboard, so that the ship propulsion can be obtained from the wind not only directly, through the towing forces exerted by the kite's lines, but also indirectly, through electric propellers. Electricity is supplied to the propellers, onboard auxiliaries like lights, pumps, etc. by a battery pack, and the batteries are recharged with the electric energy generated by the kite energy generator itself. This may not in the scope of wind-assisted propulsion options.

Kite propulsion has emerged as an attractive means to harness wind power in a way that yields environmental and financial benefits. Kite Systems (Figure 3) provide thrust to ships with the lift generated by high altitude winds. It can be seen in Figure 3 that the kite systems consist of three main components. These are a towing kite, a control system for automatic operation and a launch and recovery system. From 2006 to 2021, some commercial applications of towing kites were developed.

Figure 3: Towing kite - Airseaks L Line
https://airseas.com/

A distinction is made between static and dynamic flight for kites (Cadalen, Griffon et al. 2018). A static flight would be a much more passive system, where the kite acts primarily as a drag generating device, and thus only contributing to the ship's propulsion when sailing close to dead-downwind. Roughly speaking, the kite is able to pull the boat if the angle between the wind and the boat speed vector ranges from 0° (i.e. the boat moves downwind) to approximately 135° (i.e. 45° against the wind). Conversely, a dynamic flight would operate in an eight-shape pattern, with a very different kite design allowing lift. As such, a wider range of sailing angles can be achieved, and far greater performance attained. Typically, the dynamic mode can provide 13 to 30 times more force than the static flight (Paulig, Bungart and Specht 2013).

4.1.6.2 Advantages and disadvantages

The kite has significant practical advantages which make its commercial application attractive (Dadd 2013). Firstly, the ease of installation and ability to be fitted, or retrofitted, to virtually all ships. Secondly, Since the line tension acts through its tether at deck level, the heeling moment arm (between the centre of hydrodynamic and aerodynamic centres of effort) is reduced greatly compared to other conventional sailing rigs such as sails and rotors, thereby alleviating the significant stability concerns of the other methods. Thirdly, the towing kite may be mounted at the bow and does not require a large support structure such as a mast, so can be retrofitted without affecting the existing deck layout or operation. Kites can be retrieved in storm and there were no constrains when not sailing. Furthermore, additional performance benefit can be realised by raising the propulsive kites higher in the atmospheric boundary layer enabling exploitation of stronger winds at altitude. Lastly, kites have their own velocity in dynamic flight, which increases the apparent wind, and then the towing forces. The inflatable leading edge is another advantage, it shapes the kite and makes the launch easier.

There are practical disadvantages to the use of kites that must be avoided if they

are to continue successful use on shipping fleets. These difficulties arise primarily with launch and recovery reliability. In particular, excessive bow motions on many ships induce an undesirable vertical wind component that makes it very difficult to maintain steady line tension and this impairs the stability of the kite. Risk that kite falls into the water exists in low wind speeds. The consequences of a crash are uncertain; at the least it would cost the ship operators time to recover the fallen kite, and worse the kite would sustain significant damage and render the system unusable if there is no replacement kite.

For safety reasons the kite must fly sufficiently far from the sea and the line forces have to be contained, so to avoid line breaking and excessive roll moments on the boat speed. Kites cannot be used in areas with dense traffic.

4.1.6.3 Potential Energy Savings

Fuel saving predictions have been carried out in the literature by (Naaijen, Koster and Dallinga 2006), (Leloup, Roncin et al. 2016), and (Podeur, Merdrignac et al. 2016). The cost saving of the ship can be reduced from 10% to 35% considering the wind conditions by the virtue of the kite systems. At the optimal conditions, the amount of the cost saving reaches instantaneously about 50%. Actually, all cargo ships and newly built ships can be equipped by the kite systems.

Naaijen, Koster and Dallinga (2006) estimated the fuel saving potential of kite towing ships. As the estimation depends on the wind velocity, he showed the necessity to optimize the shipping route. His estimation of fuel saving can go up to 50% at Beaufort 7 using a kite of $500m^2$ attached to a $350m$ towing line for a 50,000 dwt (dead weight tonnage) tanker.

Leloup, Roncin et al. (2016), also implemented a procedure to predict the fuel saving potential by optimizing the elevation of the kite and the trajectory orientation and position (azimuth and elevation). The prediction are higher than Naaijen’s because Leloup introduced additionally the modeling of static flight in the optimization process, when Naaijen only took into account the dynamic flight. The kite can also switch between horizontal and vertical flight paths, which is useful for upwind conditions. Leloup predicted a fuel saving of about 10% for a 50,000 dwt tanker using a kite of $320m^2$ with a wind velocity of $10ms^{-1}$.

Kukner, Bulut and Halibese (2016) investigated wind-based propulsion for small craft and highlighted some further benefits of the towing kite approach.

Glomeep (2019) conclude that the reduction potential is dependent on vessel size, segment, operation profile and trading areas. The expected reduction potential is in the range of 1% to 5% on main engine fuel consumption.

Podeur, Merdrignac et al. (2016) performed fuel predictions on a 2200 TEU container ship towed by a kite of $800m^2$, over a 5-year period, a potential fuel economy of around 12% and 6.5% can be reached respectively at 16 and 19 knots on a North Atlantic crossing. Table 2 gives a review of fuel-saving performance of kites.

Table 2: Review of fuel-saving performance of kites

Study	Dimensions Area = $\boldsymbol{a}$, Rope Length = $\boldsymbol{l}$	Ship Type	Route	Fuel Saving Found
Naaijen, Koster and Dallinga (2006)	1 kite: $a = 500m^2, l = 150m$	50k dwt Tanker	N.A.	Up To 35%
	1 kite: $a = 500m^2, l = 350m$	50k dwt Tanker		Up To 50%
Naaijen, Koster and Dallinga (2006)	1 kite: $a = 500m^2, l = 350m$	50k dwt Tanker	N.A.	Up To 50%
Ran, Janson and Allenström (2013)	1 kite: $a = 640m^2, l = 600m$	73k dwt Tanker	N.A.	40%
Traut, Gilbert et al. (2014)	1kite: $a = 500m^2, l = 350m$	7k Dwt Roro	Dunkirk-Dover	3%
		8k dwt Product Tanker	London-Milford Haven	24%
		6k dwt Product Tanker	Varber-Gillingham	32%
		50k Dwt Bulk Carrier	Tubarao-Grimsby	6%
		30k dwt Container Ship	Yantian-Felixstowe	1%
Naaijen, Koster and Dallinga (2006)	1 kite: $a = 400m^2, l = 350m$	5k dwt Tanker	Worldwide Trades Of Each Ship Type According To AIS Data	9%–15%
		90k dwt Tanker		3%–4%
		7k dwt Bulk Carrier		9%–14%
		90k dwt Bulk Carrier		5%–9%
		1k TEU Container Ship		2%–4%
		5k TEU Container Ship		1%–2%
Leloup, Roncin et al. (2016)	1 kite: $a = 320m^2, l = 300m$	50k dwt Tanker	N.A.	10%–50%
Podeur, Merdrignac et al. (2016)	1kite: $a = 800m^2, l = 300m$	2200 TEU Container Ship	Le Havre - Halifax	12% at 16kn, 6.5% at 19kn

4.1.6.4 Cost

The main cost elements for the kite will be purchase, installation and operational expenses, and these are expected to increase with the size of the kite as shown in Table 3.

Table 3: Overview of size of kite and installation cost (Glomeep 2019)

Size of kite $[m^2]$	Power generated [kW]	Purchase cost [USD]
160	600	280 000
320	1 200	480 000
640	2 500	920 000
1 280	4 900	1 755 000
2 500	9 600	2 590 000
5 000	19 200	3 420 000

4.1.6.5 Commercial applications

Kite sails have been installed and tested in numerous commercial vessels. Ships can be retrofitted with kites in a few days or weeks. The CAPEX is relatively low, but the OPEX is high due to wear and tear (Gerhardt, Werner et al. 2021).

The French company Airseas has installed its first half-size automated Seawing kite to a cargo ship chartered by Airbus, and commence six months of trials from January, 2022. The full-size kite is estimated to save up to 20% of fuel burn and emissions.

The German company *SkySails* was one of the first to equip a cargo ship with a kite as an auxiliary propulsion device. In 2008, the company set up a prototype of kite propulsion system of $320m^2$ on a $132m$ ship (Erhard and Strauch 2012), (Fritz 2013).

In 2017, *SkySails* equipped the $35m$ catamaran Race For Water with a $40m^2$ ram air kite. The *Energy Observer* was launched in 2017, equipped with a Leading Edge Inflatable (LEI) kite from *Beyond the Sea*. Both types of kite have been deemed a success.

The *Airbus Group* has installed one $500m^2$ kite from *Airseas* on the Ro-Ro vessel *Ville de Bordeaux* in November 2020. Japanese ship owner *Kawasaki Kisen Kaisha (K Line))* installed one $1{,}000m^2$ kite on one capsize bulk carrier in 2021, and *Airseas* indicated that *K Line* would consider 50 possible installations conditional on a successful first delivery (Lloyd's List 2020), (Maritime Global News 2022).

The 210,000 dwt vessel will be built at Nihon Shipyard with delivery scheduled for the first half of 2024. In addition to LNG power to reduce emissions K Line will be installing an Airseas "Seawing" automated kite for wind propulsion (Hand 2021).

Table 4 provides further examples of commercial uptakes of kite technology.

Table 4: Some examples of the adoption of kite systems installed on merchant ships (Chou, Kosmas et al 2021)

Ship Name	Ship Type	DWT	Dimension of kite $[m^2]$	Ship Built Year	Installation Year
Michael A.	General Cargo	4884	160	1994	2008
BBC Skysails	General Cargo	9832	320	2008	2008

Theseus	General Cargo	3667	160	2009	2009
Aghia Marina	Bulk carrier	28522	320	1994	2012
Ville de Bordeaux	RoRo	5200	500	2004	2020

4.1.7 Rotor Sails

The Rotor Sail, commonly referred to as a Flettner rotor after its inventor Anton Flettner, is an electrically powered rotating cylindrical structure, with one end vertically installed on the deck.

4.1.7.1 Background

Referring to Figure 4, thrust is generated using the principle of the Magnus effect. This is caused by the wind encountering the spinning cylinder which, due to skin friction, pulls the air around to one side of the cylinder, creating a pressure difference across it. This results in a net force towards the low pressure side which, if the apparent wind is favourable, can be resolved into a thrust in the direction of the ship's travel.

If the ship changes tack, that is the apparent wind is now coming across the rotor on the other side, the direction of the rotation must be reversed to produce a thrust in the direction of travel, otherwise the force would be opposing the direction of travel.

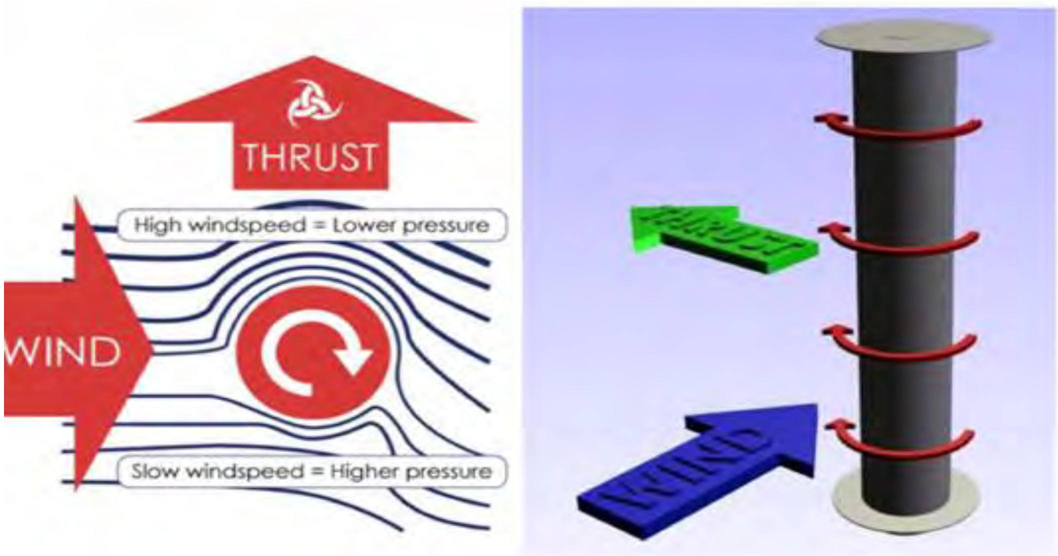

Figure 4: Magnus effect on rotating cylinder. (Source: http://www.norsepower.com/rotor-sail-solution/technology)

(Lu and Ringsberg 2020) studied the fuel saving performance of three wind-assisted ship propulsion technologies–the Flettner rotor, the DynaRig and a wingsail – for an Aframax Oil Tanker was simulated and compared on two actual voyages on two different routes. The results show that all three sail technologies contribute to fuel savings between 5.6% and 8.9%. The Flettner rotor contributed the most to fuel savings with the least sail area on the studied routes. Their parametric study of the Flettner rotor sail technology was presented to analyse the sensitivity in Flettner rotor dimensions, operations, and positioning of the rotor. The study was carried out on two ships on two routes. The results show that the Flettner rotor has a better performance for the smaller Handysize Bulk Carrier in comparison with the Aframax Oil Tanker, especially when the rotor is installed in the fore part of these two ships. Ship speed has a stronger effect on fuel savings compared to that of the rotor. However, the higher spinning speed and bigger sizes (keeping the same aspect ratio) of the rotor is not always positive to fuel savings. Therefore, it is necessary to select and operate the Flettner rotor according to its ship type, speed, voyage routes and corresponding weather conditions.

Seddiek and Ammar (2021) performed a case study, where one of the bulk carrier ships operating between Damietta port in Egypt and Dunkirk port in France has been investigated. The results showed the high influence of the interaction between ship course and wind speed and direction on the net output power of Flettner rotors.

4.1.7.2 Advantages and Disadvantages

Due to the vector of forces being generated, a rotor ship is able to sail closer to the wind than a conventional ship and the deck space required is relatively less than that of soft sails and wing sails.

4.1.7.3 Potential Energy Savings

Mittal and Kumar (2003), Craft, Iacovides et al. (2012) and Karabelas, Koumroglou et al. (2012) studied the aerodynamic performance of the Flettner rotor using computational fluid dynamics (CFD) simulations. Based on the CFD simulation results, Traut, Gilbert et al. (2014) proposed a performance model to simulate the power savings contributed by Flettner rotors. In their case study, a 5500 DWT cargo ship with three Flettner rotors (27 m in height and 4 m in diameter) installed onboard could save up to 50% of the power required by the main engine.

In 2015, two Norsepower rotors 18 m in height and 3 m in diameter were retrofitted on the 9700 DWT Ro-Ro Carrier M/V Estraden. It was confirmed by the company Norsepower and the ship owner that 5% fuel savings on yearly basis have been saved (confer to http://www.norsepower.com).

In another study, the classification society Lloyd's Register followed up the performance and handling test of the Integrated Greenwave MK1 Rotor assembly on a Panamax Bulk Carrier (Hirdaris and Cheng 2012). For a 1/85th scale model for a 182m waterline bulk carrier fitted with the Greenwave Flettner rotor, the performance and handling tests indicated that the Flettner rotor was capable to provide 50% of the required thrust in light winds and 100% of the required thrust in moderate winds.

Glomeep (2019) estimate the reduction potential of a Flettner motor as 3% to 15% on main engine fuel consumption depending on vessel size, segment, operation profile and trading areas. Some have reported reductions as high as 35%, but for a reduction potential in general, this is seen as high.

4.1.7.4 Cost

The range of cost for a Flettner rotor is \$400,000 to \$950,000 (USD) depending on the model (size) of the rotor. Size of a typical delivery with multiple rotor sails starts from \$1,000,000 to \$3,000,000 (USD) (Glomeep 2019).

4.1.7.5 Commercial Adoption

Flettner, with the aid of Betz, Ackeret and Prandtl, applied this concept to a marine vessel and created the first wind-powered ship called "Buckau" (Figure 5), which utilised the Flettner towers as the primary source of propulsive power. Flettner's attempts were considered not successful, because of inadequacies in overall operational performance and economics of the ship. One of the main reasons is that fossil fuels at the time were relatively cheaper. However, fossil fuels as a resource are limited and expensive. Recently, environmentally optimised solutions are being pursued and a renewed interest in this technology has been emerged recently.

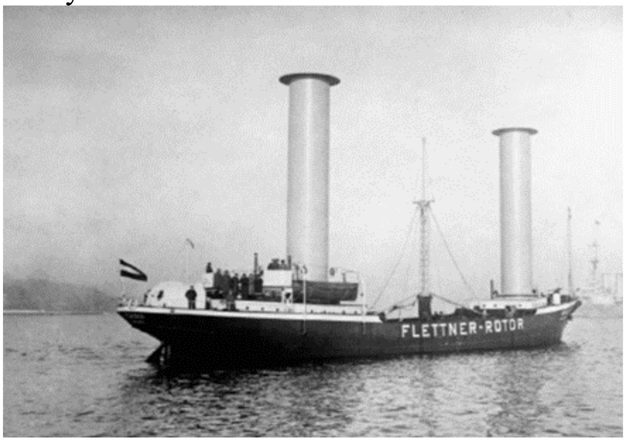

Figure 5: The Bukau, the first vehicle to be propelled by a Flettner rotor, photographed in 1924.

In 2008, the company ENERCON launched the first prototype vessel using this technology. The vessel ‘E-Ship 1’ is equipped with 4 Flettner towers, which are $27m$ in height and have a diameter of $4m$ each. The performance of the towers is controlled through the rotational speed of each individual tower and the study reports a maximum fuel consumption reduction of almost 25% (Morsy El Gohary 2013), (Schmidt, 2013).

4.1.8 Turbines

4.1.8.1 Background

Wind turbines can potentially be used in a number of ways. They can be coupled directly to a generator to produce electricity, or, on smaller vessels, they can be operated in autogyro mode or windmill mode, depending upon apparent wind direction. In the latter two cases, the turbine is attached to a propeller through some mechanism (mechanically, electrically or hydraulically) (Twidell 2021).

With the wind over the beam (i.e. on a reach), the turbine is used in autogyro mode, where no power is transmitted to the propeller and the turbine acts in the same manner as a conventional sail. When the vessel is sailing downwind, the apparent wind speed decreases with increasing ship speed. When the ship speed is greater than or equal to the wind speed, the apparent wind speed is zero (or negative), so the wind turbine cannot generate power or thrust in the autogyro mode. Windmill ships are thus limited to less than the wind speed when running before the wind, just as conventional sail driven vessels.

Generally, the force generated by the turbines alone is not sufficient to propel the vessel, unless the hullform has been specifically designed for reduced friction, such as multihulls or hydrofoils.

Research is still ongoing as to the most suitable design of rotor system. There are two main types, the Horizontal Axis Wind Turbine (HAWT), which tends to have a relatively higher centre of effort, and the Vertical Axis Wind Turbine (VAWT), such as the Savonius. The HAWT needs to yaw to find the correct position of the apparent wind direction, while the VAWT operates in all wind directions. The VAWT tends to be quieter than its HAWT counterpart as the blade tip-speed is lower.

4.1.8.2 Advantages and Disadvantages

Wind turbine propulsion systems are unique in that the device can provide propulsion in at all apparent wind angles, including directly into the wind. Performance is restricted, especially upwind, by the efficiency of transferring energy from wind to the water, wind turbine propulsion generally provides higher propulsive force than wingsails per turbine/sail area only when the ship speed is less than about half the wind speed (Blackford 1985). This implies that ship speeds should be slow, or the area of operation should have strong winds.

The engineering design of wind turbine systems is more complex compared to other WAP devices. Careful consideration needs to be given to the stability of the vessel, due to the large mas of rotating equipment required at height above deck, as well as dangers that this may impose to crew.

In order to operate efficiently in the typically slow speed through the water, the propeller must be large enough to generate more upwind thrust than the combined downwind force of the wind turbine and the air and water resistances of the ship structure itself. The design for this propeller may be different to the design of a propeller driven by the main engine, and thus may be an inefficient compromise.

Automatic control can easily be incorporated into the design of a wind turbine system.

4.1.8.3 Potential Energy Savings

Bøckmann and Steen (2011) conducted a fuel estimation analysis for a notional HAWT used as auxiliary propulsion for a $150\ m\ L_{WL}$ tanker, operated between Peterhead, UK and Bremerhaven, Germany. They concluded that using a pre-designed HWAT resulted in an energy saving of 24.4% and for an optimised wind turbine design, the energy saving was 33.1%.

Bøckmann and Steen (2011) also compared the energy savings from using an optimised HAWT to wingsails. In this comparison, the area of the wingsail was set equal to the wind turbine's rotor disc area and analysed on the same notional hullform. Using this method, this resulted in a fuel saving of 31.8%.

4.1.8.4 Cost

As there are no practical applications of the use of wind turbines being used for propulsive power generation, there is insufficient data to make an analysis.

4.1.8.5 Commercial Adoption

There are very few wind turbine driven vessels that have been built, and while some small craft and research vessels exist, there are no full-scale commercial ships existing using wind turbines for propulsive power generation. This is due to the disadvantages outlined above.

An early example of a wind turbine-powered vessel is the City of Ragusa, which was a converted lifeboat crewed by two men and a dog. They had the idea that the boat would be able to sail directly upwind without tacking by using the wind turbine to drive a propeller. The crossing was done East to West, into the wind and it took them 96 days to go from Liverpool, UK to Boston, USA (Anonymous 1870). There is some debate as to whether the turbine was actually utilised (Longyard 2005).

The Bois Rosé, produced by a French engineer Constantin was built in 1924 (Bose 2008). More recent examples include the Falcon, which was aimed at researching potential fuel savings for larger ships (Bose 2008).

Applications are most suited to slower speed vessels, or if used for electrical power generation, on vessels with a high electrical load.

4.1.9 Hull Form

Another interesting technology is that of the design of the hullform that can itself generate lift from the prevailing wind. Lade AS in Norway was established in 2010 and have been developing the project Vindskip (Lades AS 2023). Project Vindskip is a hybrid merchant vessel for sustainable sea transport.

The hull is shaped similar to a giant sail (Figure 6) and thus generates a forward thrust towards the apparent wind. This is Vindskip's Wind Power System. The ship is fitted with an LNG-electric propulsion system as well, the combination of the two forming a dynamic system that maintains a constant ship speed. Using computerized weighting of meteorological data, a computer program will calculate the best sailing route to exploit the available wind energy potential.

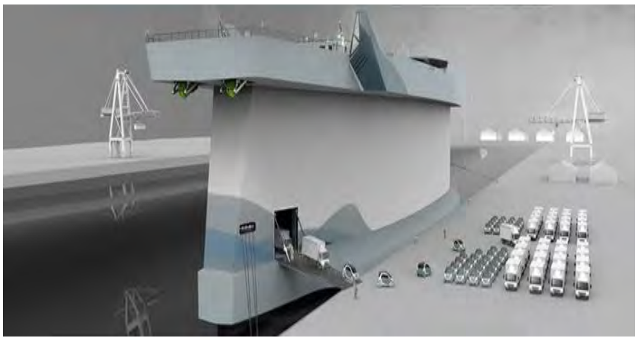

Figure 6: The Vindskip hybrid propulsion concept, *https://ladeas.no/*

Ship types that are particularly relevant to the Vindskip design are

- RoRo
- RoPax
- PCTC
- Passenger ships
- Container Ships

4.1.9.1 Advantages and Disadvantages

Because the hullform is shaped like a wing, air-draught may need to be increased in order to maintain cargo carrying capacity.

4.1.9.2 Potential Energy Savings

According to Lade AS the ship's design is estimated to cut fuel use by 60% and carbon emissions by up to 80% (Lades AS 2023).

4.1.9.3 Cost

There is no cost information available due to the concept not having been built yet. The more complex hullform shape may increase capital costs.

4.1.9.4 Commercial Adoption

The Vindskip is presently a concept design.

4.1.10 Conclusions

Section 4.1 has briefly reviewed the main technologies currently considered as the main source of power from wind for use onboard ship. This ToR can be used further in the ITTC Specialist Committee on Wind Powered and Wind Assisted Ships to maintain consistency.

4.2 Clarify the distinction between wind powered and wind assisted ships.

4.2.1 Introduction

The Committee was tasked to provide a distinction between wind powered and wind assisted ships. Possible usage scenarios for the distinction between wind powered and wind assisted ships could be general or specific. Specific use cases are normally associated with their own definitions. Indeed, the ToR calls for a distinction, rather than a definition.

The scope of the following commentary should therefore be for general use in initial design and vessel classification.

4.2.2 Rationale for the distinction

It is assumed that distinct definitions will be required for specific purposed, such as the application of rules and regulations of various kinds. However, since the scope of those applications differs, it is not wise to formulate one explicit definition that is valid for all purposes. Instead, each rule and regulation should include its own definition.

The distinction that the Committee propose is intended to be used when describing a type of ship in *general terms*. It is not an explicit definition that can be calculated for each ship. For example, if it is stipulated that a "Primary Wind Powered ship is powered by the wind for at least 90% of the time when full away on passage", then this becomes route and speed dependent, and requires definitions of calculation method to derive the percentage time. It would then chance its "status" if the route or speed is changed, which would be confusing.

The Committee propose the distinction given in Table 5.

Table 5: The SC proposal for distinction

Primary Wind Power	A Primary Wind Powered Ship is one which is designed to maintain service speed the majority of time using wind propulsion only.
Wind Assisted Ships	A Wind Assisted Ship is a motor ship which is adapted such that in favourable wind conditions, the propulsive power to maintain service speed is reduced from using wind powered technology.

During the work, the Committee has been in contact with the International Wind Ship Association (IWSA) regarding the distinction, since it would be favourable to have the same distinction throughout the industry. IWSA use currently the wording given in Table 6. It is noted by the Committee that IWSA's distinction describes the actual state of a ship in operation, where its status can change if it is operated on a different route or speed. ITTC's distinction seeks to categorise a vessel from its design and purpose.

Table 6: IWSA distinction (International Windship Association, 2024)

Primary Wind Power	Wind propulsion is the primary propulsion energy for that ship
Wind Assisted Ships	Wind propulsion system delivers on average less than 50% of the propulsive power to the ship at a given commercial speed

4.3 Review of methods for prediction of performance and safety of wind powered ships

Performance of ships with wind and wind-assisted propulsion in wind and waves is more complicated than ships with traditional propulsion. A lot of effort has been dedicated in the last few years to the study of predicting the performance of wind powered ships.

The following are the methods of ship model hydrodynamic tests, wind tunnel tests, CFD, ship dynamics simulations and routing relevant for predicting the performance and safety of wind powered and wind assisted ships at the design stage with particular attention paid to higher side forces and drifting of the ship due to wind powering.

4.3.1 Ship Performance prediction

Performance Prediction Programme (PPP) for WASP concepts couple the aerodynamic and hydrodynamic forces to obtain a solution for velocity under sail and ultimately power saving. The performance prediction fundamentally relies on achieving equilibrium for the degrees of freedom (DoFs) considered. Velocity prediction programs (VPPs) or Energy Prediction Programs (EPPs) or performance prediction programs (PPPs) for wind-assisted ships typically consider either: 3-DoF (surge, sway, roll), 4-DoF (surge, sway, roll, yaw), 6-DoF (surge, sway, roll, yaw, pitch , heave).

4.3.2 Performance Prediction Program

VPP was presented in (Tillig and Ringsberg, 2018; van der Kolk et al., 2019a; Viola et al., 2015). In (Viola et al., 2015; Lee et al., 2016), the aerodynamic interaction effects were evaluated using CFD computations, while the model in (van der Kolk et al., 2019a) was based on model tests. Typically, the hydrodynamics of a hull are based on empirical methods from maneuvering research, as in (Tillig and Ringsberg, 2018; Viola et al., 2015), or on CFD or model test results using standard series hulls (van der Kolk et al., 2019b; van der Kolk, 2016).

A 4-DoF ship performance prediction model called "ShipCLEAN" has been developed by Tillig and Ringsberg (2020), which includes aero-hydro coupling and a method for rpm control of Flettner rotors on a ship to maximize fuel savings. This ship performance prediction model based on analytical and empirical methods as well as on propeller and hull standard series. Thies et al. (2021) used the model ShipCLEAN in the example with a ferry operating on a short route in the Baltic Sea. Focus is put on evaluating the difference between 1-DoF and 4-DoF methods as well as the impact of aerodynamic interaction effects in between multiple sails.

Based on a generic energy systems model proposed by Tillig et al. (2017) and Tillig and Ringsberg (2019), the performance prediction model for ships at sea (ShipJOURNEY) is further developed by Ruihua Lu & Ringsberg (2019) which is a 4-DoF balance model. Ship profiles, voyage routes, operational conditions and sail technologies are the essential inputs and the voyage time and main engine fuel consumption are the major outputs (Figure 7).

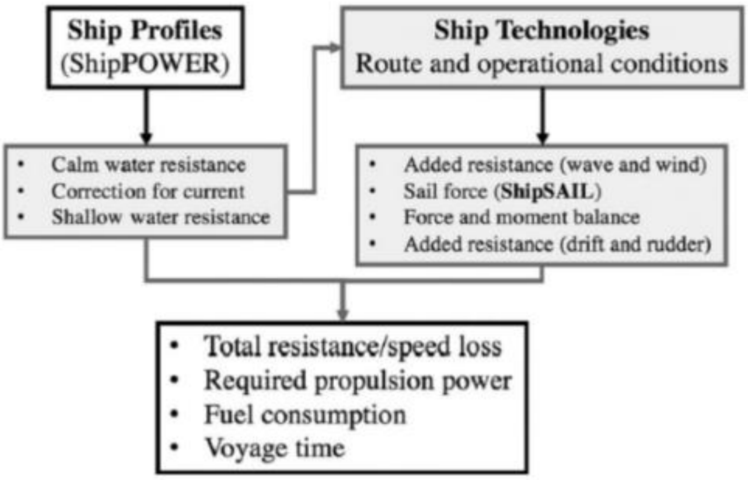

Figure 7. Schematic flowchart of Ship JOURNEY(Ruihua Lu & Ringsberg , 2019)

Reche-Vilanova et al. (2021) presented a 6-DoF PPP based on semi-empirical methods and a WAPS aerodynamic database created from published data on lift and drag coefficients which can predict the performance of any commercial ship with three possible different WAPS installed: rotor sails, rigid wing sails and DynaRigs. The tool was with only the ship main particulars and general dimensions as input data (Figure 8). The model did not take the sail-sail and sail-hull interaction effects on the aerodynamic performance.

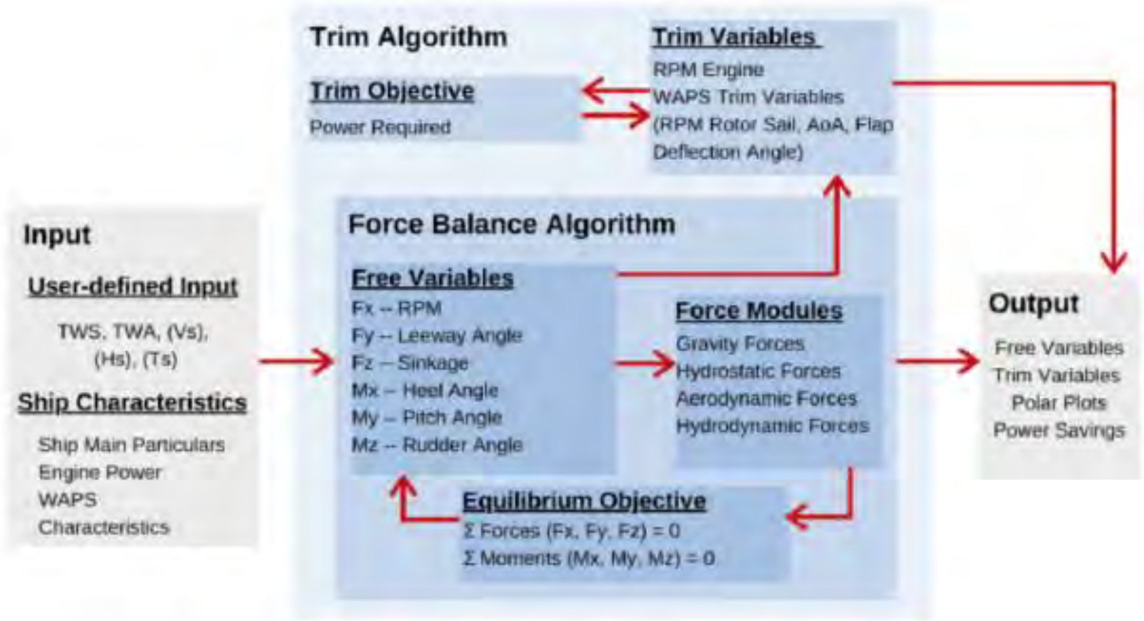

Figure 8. Outline of Performance Prediction Program (Reche-Vilanova et al., 2021)

Bataille et al. (2023) took the vessel ONRT as a reference study case to assess the wind-assisted vessel's performance on its operating route, based on the PERFO methodology (Figure 9) which contains two existing PPP tools: xWASP as an open-source solver is a 6 DoFs Dynamic VPP/PPP using semi-empirical formulations dedicated to WASP and SEECAT (Ship Energy Efficiency Calculation and Analysis Tool) with loads from CFD modelling is aiming at assessing the global efficiency of ships for realistic operational profiles and weather conditions and capable of modelling any kind of marine propulsion architecture.

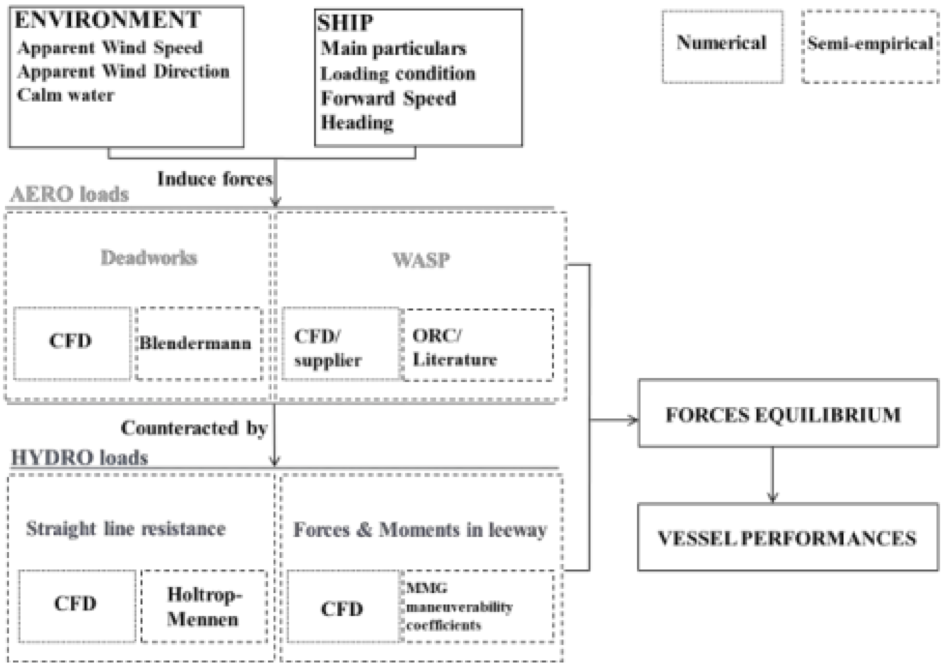

Figure 9. PERFO methodology (J Bataille et al. 2023)

Mason et al. (2021) described a performance prediction model developed by Bordogna et al. (2019, 2020) and van der Kolk et al. (2019, 2020, 2021). Specified lift and drag coefficients, scale effects, interaction effects between multiple Flettner rotors, as well as interaction effects between the Flettner rotors and the ship's deck are accounted for and the results were derived from the performance of dedicated wind tunnel experiments (Bordogna et al. 2019, 2020). The hydrodynamic and aerodynamic models combine to calculate the resulting force in the direction of motion of the ship that is required to achieve a given speed. For a range of wind speeds and wind angles, the forces are combined to calculate the main engine power, or brake power.

4.3.3 Route optimization method

Mason (2021), Paakkari (2022) and Dupuy et al. (2023) have highlighted the importance of weather routing for the performance of wind propulsion as it has been shown that the performance of wind propulsion can be as much as doubled when weather routing is utilized. On the other hand, different wind propulsion technologies have significantly different characteristics in terms of propulsion performance. Comparisons between different wind propulsion systems have been made by Sarsila (2022) and Maxime Dupuy et al. (2023) .

Mason et al. (2021) investigated the combined abatement fuel consumption potential of wind propulsion and voyage optimisation, alongside their subsequent interaction with speed reduction. The development and analysis of the ship routing model used the Voyage Optimisation for the International Decarbonisation of Ships routing model to calculate carbon savings from a Flettner rotor-assisted ship on the great circle route and optimised voyage route.

4.3.3.1 Safety prediction

There are several criteria and methods to evaluate the stability of sail-assisted ship as proposed by Classification Societies. Hussian (2021) used the recommended stability criteria on a sail assisted ship to do stability and structural analysis.

Van der kolk et al. (2019) presented the experimental results for the sailing performance of ships fitted with bilge keel appendages. Systematic variations in appendage height, length and position were tested, including several special cases (multiple bilge keels). The appendage typology has been shown to mitigate the strong "destabilizing" yaw moment that is characteristic of wind-assisted commercial vessels and to promote the non-linear sideforce component.

Wang et.al（2022）studied the dynamic stability under the combined wind and wave loads by using the spectral analysis method and the time domain analysis method with consideration of multiple wind spectrum, wave spectrum, and wave direction. The spectral analysis method did not consider the system nonlinearity, while the time domain analysis method considered the nonlinearity of the roll restoring stiffness.

Kite operation may enter resonance with ship roll or pitch natural period and dramatically impact the ship stability. Richard (2014) calculated the roll, pitch natural periods and kite structure behaviour with three different approaches. The results showed that for shorter tethers length, the risk of kite flight period entering resonance with the ship roll or heave period may appear and the kite flight trajectory may be adapted in order to prevent any risk of such phenomenon.

4.3.4 Hydrodynamic characteristics

4.3.4.1 Hybrid testing approach

In hybrid testing approach (cyber-physical approach), one part of the system is modeled physically, while the other part, whose behavior is assumed to be well described theoretically, is modeled numerically.

For sailing ships, generally, experimental methods of prediction seakeeping and manoeuvring can be grouped as captive tests and free sailing tests. With the various sub-categories shown in Figure 10.

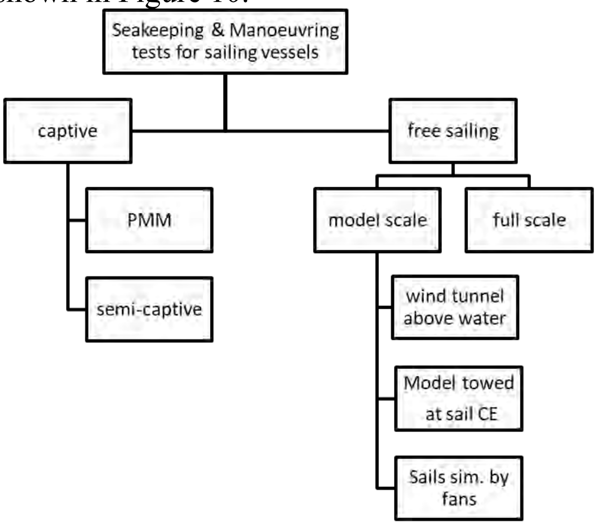

Figure 10. Alternatives for seakeeping and manoeuvring tests with sailing ships (F C Gerhardt et al. ， 2021)

The hybrid testing approach was used by F C Gerhardt et al. (2021) to investigate the seakeeping and manoeuvring properties of "Wind Powered Car Carrier" called Oceanbird , which is the "mirror image" of Hansen's RT-VPP: the sail forces are simulated (by fans) while the hull is tested in waves (Figure 11). The setup consists of the physical subsystem "hull" that is tested in the seakeeping basin and the numerical subsystem "sails" that is simulated by the two azimuth and rpm-controlled fans. As illustrated, strain gauges are used to measure the axial force of each fan. This allows determining the actual "sail" forces and moments.

Figure 11. Wave tests with a model of Oceanbird (the wing sails have been replaced by fans/airscrews) (F C Gerhardt et al. , 2021)

Sauder and Alterskjær (2022) used the cyber-physical approach to study a bulk carrier model (SOBC-1) retrofitted with four (virtual) Flettner rotor sails. The ship model was placed in the seakeeping carriage and the loads were applied on the frame through six thin wires visible as depicted in Figure 12. In the experiments, the ship model was running at self-propulsion, where propulsion was delivered from four numerically modelled Flettner rotors based on published CFD simulations results (De Marco et al. 2016), in addition to a single screw conventional propeller. The forces generated by the wind propulsors were applied to the model using a system of wires, connecting the model to actuators, providing forces in 5 degrees of freedom (except the heave force) according to prescribed wind conditions. Aerodynamic loads on the sails were computed in real-time based on the ship motions and on computational fluid dynamics results.

Figure 12. Model of SOBC-1 in the towing tank (left). Two of the six actuators mounted on the car-riage (right).(Sauder and Alterskjær , 2022)

4.3.4.2 Numerical methods

Bigi et al. (2018, 2020) proposed a numerical modelling associating the strip theory for the ship motion simulation and the zero-mass modelling for the kite force and motion simulation.

An extensive test matrix, adapted to assess the hull and appendages behaviour in a range of flow speeds and directions, was simulated in CFD to obtain the hydrodynamic forces and moments acting on the underwater part of the ship in Marimon et al (2020). Being a wind-assisted vessel, three different conditions were tested where the ship is propelled using only the propulsive power from the sails/wings, using only the propulsive power from the engine and a combination of the former two (50% sail, 50% power).

Kjellberg et al. (2022) developed a numerical method for predicting a ship's motions and loads in its rigid wing sails. The numerical method is based on an unsteady 3D fully nonlinear potential flow hydrodynamic model coupled with a hybrid 2D RANS/3D lifting-line aerodynamic model. Simulations in a seaway with short-crested irregular waves and corresponding wind conditions are conducted, resulting in time histories of the aerodynamic and inertial forces acting on the rig.

Fabio Pili et al. (2023) investigated the effect of Flettner rotors on the seakeeping of a catamaran, predicting the motions of the ship in the 6-DoFs. The rotors were modelled using a quasi-static approach and a linearized approach to analyze the effect of the rotor in pure roll motion in beam seas. The seakeeping model is based on regular waves. The aerodynamic interactions between the four rotors and variation of the hull wetted surface were neglected in this study.

4.3.5 Aerodynamic characteristics

4.3.5.1 Wind tunnel tests

Bordogna (2020) and Chen et al. (2023) experimentally investigated the aerodynamic performance of large-scale Flettner rotors for marine applications.Wind-tunnel experimental campaign on a single Flettner rotor and two analogous Flettner rotors for a range of different relative positions and velocity ratios (Figure 13 and Figure 14). In this series of tests, their lift and drag coefficients were measured and then compared to those of the single Flettner rotor to investigate the effects of the aerodynamic interaction.

Figure 13. The Delft Rotor and two Flettner rotors in Pol-ytechnic University of Milan wind tunnel (Bor-dogna, 2020)

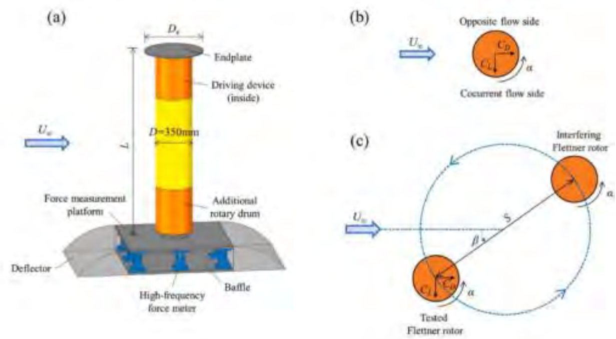

Figure 14. Experimental setup (a) tested model and meas-urement system, (b) single Flettner rotor, and (c) two Flettner rotors (Chen et al., 2023)

Aerodynamic interaction of two similar rigid sails exposed at apparent wind angles, the lift and drag forces, as well as the pressure measured on each sail, were compared with the results of measurements carried out on an analogous single sail in Bordogna (2020), shown in Figure 15. These results are eventually used to compare the performance, expressed in terms of driving and heeling force coefficients, of a "ship" equipped with one or two rigid sails. The number of sails employed and their gap distance are key parameters in the determination of the effects of the aerodynamic interaction on the performance of multiple sails.

Figure 15. Single sail model and two-sail arrangement mounted on the wind-tunnel turntable during the experiments (Bordogna 2020)

James et al. (2019) carried out Wind tunnel tests on a model of Actively Controlled Wing Sail. The data exhibits clear trends of increasing lift as injection momentum increases, with critical flow attachment points being identified at specific combinations of jet momentum coefficient and angle of attack.

A wind tunnel testing campaign was conducted to confirm the findings of the CFD optimisation study of the suction sail by A. Llopis Pascual, et al. (2023). The model consists of a main body and a span with interchangeable components: flap, porous plate, and winglets. The model was attached to a turntable, used to vary the angle of attack of the model.

4.3.6 Kite performances experiments

Wind tunnel testing of large deformable soft kites is in many cases practically not feasible. Johannes Oehler et al. (2019) reviewed experiments described in the literature to determine the lift-to-drag ratio of kites, and presented an experimental method for aerodynamic characterization of flexible membrane kites by in situ measurement of the relative flow, while performing complex flight maneuvers.

Experimental campaigns onshore by M. Behrel et al. (2018) and at sea by Kostia Roncin et al. (2020) were achieved to control and measure performances of small leading edge inflatable kite shown in Figure 16. Experiments set-up in M. Behrel et al. （2018） are a three-dimensional load cells to get kite force and kite position into the wind window. Kite is controlled using winches, and an autopilot performs repeatable 8-pattern trajectories. Experimental boat Kitelab (Kostia Roncin et al. 2020) experienced ten full days of measurements, keeping all parameters as fixed as possible. Various configurations of sailing were tested, using different kites, different lengths of tethers, different dagger boards, different points of sail and so various true wind angles. All these data were analysed using only average values for each run to get to an overview of the kiteboat performance.

Figure 16. Kite control and measurement device deployed on shore and picture of the Kitelab . (Kostia Roncin et al. 2020)

Cadalen et al. (2018) described experiments recorded by "Beyond The Sea" on the ground. The anchor point consists of a fixed manual steering device that allows for asymmetrical and symmetrical steering by acting on two handles at the end of the two steering lines. The traction line is connected to the ground as well, but is not used for control. On the wing, the measurements are made with an inertial measurement unit (IMU). On the steering device, each tether is connected to a load cell to measure the sustained force. Shaft encoders measure each line displacement. Additionally, an anemometer measures the wind speed and direction. The kite is then steered manually, via the two steering lines. The sensors measure the kite attitude, the tethers' force and their steering.

4.3.7 Kite force and motion simulation

In most wind conditions, compared to a static flight, a dynamic motion of a tethered wing with an eight-shaped pattern can provide sufficient force through traction to tow a ship.

4.3.7.1 Zero-mass model

The zero-mass kite modelling neglects the weights of the kite, the inertial forces and deformation of the tethers. The zero-mass model was established by Wellicome (1984) and is often used to estimate the kite performances. Under the assumptions of the zero mass model, Dadd et al. (2010, 2011, 2013) and Naaijen et al. (2006) calculated the kite velocity with an iterative algorithm. Dadd et al. (2010) used the zero-mass kite manoeuvring theory to predict kite line tension and other performance parameters. These results were compared with real kite trajectories that had been recorded using a purpose-specific kite dynamometer. Traut (2014) introduced a numerical performance model applying zero-mass model on a kite to predict wind-generated thrust and propulsive power which were computed as a function of local wind and ship velocity and linked with wind data along a set of five trade routes.

A kite flight modelling based on the zero-mass assumptions was rewritten by Leloup et al. (2014) in order to speed up the velocity and tether tension calculations along a flight path. The wind gradient and the ship velocity were integrated to the kite flight modelling.

C. Duport et Al. (2016) developed a 3D non-linear model based on the lifting line of Prandtl to be able to quickly estimate the traction that can provide a kite according to its trajectory. An iterative equilibrium procedure has been developed, based on zero-mass model assumptions. It allows the rapid calculation of aerodynamic forces for a wing with any laws for the dihedral angle, the twist, and the sweep angle, along the span; and for a general flight kinematic taking into account translation velocities and rotation rates.

4.3.7.2 Point mass model

A point mass model assumes that the kite mass is concentrated at a point and this entails the apparition of inertial forces and weight. It has been proposed in Fagiano (2009), Williams et al. (2008), Jehle and Schmehl (2014). Williams et al. (2008) used the point mass model of the kite to determine the optimal trajectory to maximize power generation while keeping low the efforts needed to control the kite. In order to obtain a sufficiently realistic model which can also be easily implemented in a controller, a point mass model was chosen by Baptiste (2018) and a transverse aerodynamic force nullifying the drift angle, as well as a slacking and hauling command have been taken into account. The steering lines are considered constant in length and non-deformable. Their effects on the wing dynamical behaviour are neglected .

Dadd et al. (2010) compared the results of the zero mass model with the point mass model , which showed that the mass of the kite and the tether can be neglected if the weight is small enough in comparison with aerodynamic forces.

Behrel et al. (2018) presented experimental results comparing zero mass and point mass modeling. Differences are about few percent. Actually, both modelings give the same results when their coefficients identification is consistent. If taking into account the mass can be important for control issue, this is clearly not the case for performance assessment.

4.3.8 CFD computations on other WPS

Karman D. (2016) investigated the flow around a Flettner-rotor without its end plate in 2D and 3D by CFD package. Several unsteady (LES and URANS) and steady (RANS) simulations were carried out and compared among several turbulence models. Two LES subgrid models: the Smagorinsky-Lilly and the Wall-

Adapting Local Eddy-Viscosity (WALE) were compared, also the analysis several RANS runs were carried out with the $\kappa - \varepsilon$, the $SST\ \kappa - \omega$ and the RSM stress$-\omega$.

De Marco et al. (2016) performed a parametric study with CFD aimed at establishing the drag and lift coefficients on various rotor sails geometries operating at various rotational speeds. Unsteady RANSE was solved using SST $\kappa - \omega$ turbulence model. Hybrid mesh approach, coupling unstructured and structured mesh, has been used for all the simulations.

A. Persson et al. (2019) presented CFD simulations on rotor sails and wing sails. The 3D lift and drag coefficients of the wing sail predicted by the different methods of Quasi-3D methods including Sectional Integration with 3D-correction (SILL), Non-linear Lifting Line algorithm (NL-LL) and 3D Sectional Integration Method (3D-SIM). They were compared with the 3D CFD simulations.

L. Jones et al. (2019) carried out a series of CFD simulations to evaluate the impact of parametric changes in Flettner rotor design, including the impact of multiple rotors operating in combination, and the influence of the ship induced flow field. Simulations were conducted using an unsteady Reynolds averaged Navier-Stokes based transient solver. Turbulence effects were accounted for using a $SST\ \kappa - \omega$ turbulence model, with the viscous sublayer modelled using wall functions.

James Cairns at.al (2019) carried out 2D CFD simulations on Actively Controlled Wing Sail using the Spalart-Allmaras model with rotation correction (SARC) and the $SST\ \kappa - \omega$ model with curvature correction (*SST-CC*). Good agreement was found when comparing simulation and experiment for low jet momentum coefficient, detached flow cases. However, certain simulation conditions exhibited a well-documented shortcoming of RANS-based turbulence models for circulation control flows and over-predicted surface pressures and lift coefficient for fully attached flow cases.

Will Hopes et al.(2021) carried out a CFD study on the performance of Suction Aerofoils choosing the RANS-based Shear Stress Transport (SST) turbulence model to determine values for the lift and drag coefficients over a range of angles of attack and suction levels. Supplementary studies also investigated the effects of introducing an endplate to reduce end vortices, and the effect of a ship side on the wind speed incident on the Suction Aerofoil.

4.3.8.1 Interaction effects

To improve the methods of performance prediction for wind-assisted propulsion, the importance of interaction effects in between the sails and between the sails and the hull, i.e., rudder angle and drift, was discussed in (Viola et al., 2015; van der Kolk et al., 2019b).

4.3.8.2 Aerodynamic interactions

Complex aerodynamic interaction effects of various wind-propulsion systems occur and that eventually have an impact on the amount of wind-generated thrust. Aerodynamical interactions are crucial to model to accurately predict the jaw moments and thus the necessary rudder angle and for reliable sail control. The results of studies from Bordogna (2020), Tillig and Ringsberg (2020) showed that in-between sails, potential flow interaction effects are predominant (Figure 17).

Wind tunnel tests interaction between two rotating cylinders were carried out by B Charrier (2021) to demonstrate the effect of the aspect ratio, the rotating endplates and the Reynolds number.

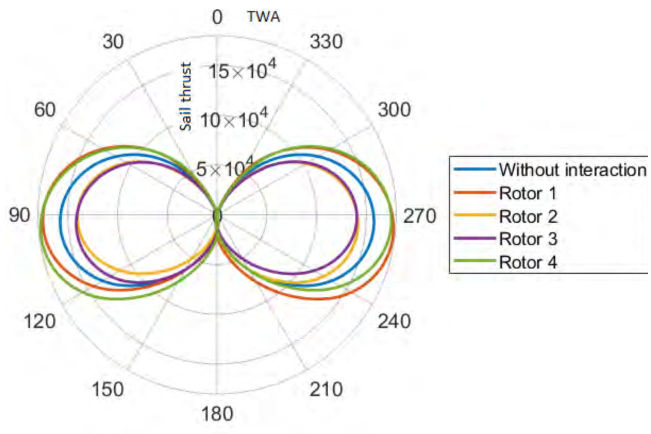

Figure 17. Effects of sail interaction (Tillig and Ringsberg, 2020)

An investigation into combination of the various aerodynamic interaction effects on the lift and drag was performed by Jones et al. (2019) on the interaction between multiple rotor sails, a block located at various positions relative to the rotor and the ship and superstructure. Garenaux et al. (2021) developed a numerical approach using steady full scale RANS simulations to estimate the effects of the interaction between the ship and its three Flettner rotors. Large interaction effects are found to depend on the apparent wind angle.

The Non-linear lifting line method described by Phillips (2000) was adapted for use for wind propulsors and implemented in the module of Wind Propulsor Interaction(wpi) by Schot and Garenaux(2023). The method can use a non-uniform wind profile which consists of an atmospheric boundary layer profile, ship speed and the disturbed wind from the ship and superstructure.

A. Llopis Pascual, et al. (2023) conducted CFD study to analyse the sail-to-sail interaction of two model eSAILS (suction sails) fitted at the stern of a ship. The images are aligned with the ship, where the bow is to the left and the wind is simulated at different apparent wind angle. A detailed analysis of these results allows to understand the influence each eSAIL has on the other and use that information to customise the control algorithm to maximise the performance of the systems for this specific installation.

4.3.8.3 Aero-hydrodynamic interactions

Integrated aero-hydrodynamic models in VPPs or PPPs for the prediction of performance of WPS usually include static VPPs and dynamic VPPs. Bigi et al. (2016) investigated the influence of the kite attachment point on the deck of a fishing vessel. A manoeuvring modelling limited to horizontal ship motions is implemented with a monolithic coupling approach between the ship and the kite. The water is supposed to be calm and the effect of the radiated waves on the ship motions was not taken into account. To consider drift and yaw effect on propulsion system, a MMG mathematical model-based simulation was carried out for different drift angles of motion of the ship considering hard sail-based wind loads in Hussain et al. (2021).

Steady-state VPPs are very efficient and fast , but it is not able to consider dynamic effects such as unsteady wave forces on the hull and the ship's motions in a seaway that the angles of attack of the sails fluctuate. Martin Kjellberg et al. (2023) used an unsteady 3D fully non-linear potential flow hydrodynamic model coupled with an efficient lifting-line aerodynamic model to investigate the differences in sailing performance of a vessel sailing in steady conditions to the performance when sailing in a seaway and gusty wind based on a spatio-temporal wind model. The analysis showed clearly that the unsteady wind model affected the predicted performance.

The motions of a ship towed by a kite are highly dynamic since a kite experiences a periodic dynamic flight. To perform a strong coupling between the kite and the ship, Bigi et al. (2020) applied a time domain method to assess the importance of taking into account the coupling between the kite and the ship motions. Seakeeping modelling is coupled with a zero-mass kite modelling assuming linear dependence of aerodynamic characteristics with respect to turning rate.

4.3.8.4 Fluid-structure interactions (FSI)

Fluid-Structure Interactions (FSI) is the interaction of the deformable structure with a surrounding flow. Such interactions are generally investigated numerically using the coupling of fluid simulation and structural simulation.

4.3.8.5 Numerical method

Breukels et al. (2011, 2013) carried out CFD simulation on a 2D aerofoil to compute its lift, drag and moment coefficients as a function of the angle of incidence, thickness and camber of the aerofoil. A model simulation was also compared with experimental data, tension in the four lines of various kites during a loop. Bosch et al. (2012, 2014) chose a complete finite element modelling of the wing. The canopy is modeled by triangular shell elements and the battens by beam elements. The fluid model is the same as the one used by Breukels (2011) and gives the forces distribution on the canopy as a function of the angle of incidence, thickness and camber of the section. .

Monolithic coupling to FSI problems where fluid and structure are solved simultaneously was used in Le Tallec & Mouro (2001). Monolithic coupling is more stable and more accurate than partitioned coupling (Michler et al. (2004)) but also more computationally expensive.

A fast and robust approach to model FSI for yacht sails is presented in Morvan et al. (2021). Specifically, interaction effects between the jib and the mainsail are taken into account in the flow model presented. The flow model is coupled with a structural finite element software, using shell elements for the modelling of sail membranes, beam stringers for battens modelling and a quasi-static resolution based on a dynamic backward Euler scheme.

4.3.8.6 Experimental method

The possibility of measuring a structural deflection under fluid load and the flow behaviour around the structure is particularly interesting with the rise of composite materials. A robust and repeatable experimental methodology will also provide researchers with a validation case for numerical FSI simulations.

A fully coupled FSI methodology was developed in a wind tunnel to assess the response of a PAC aerofoil in L. Marimon et al. (2017, 2018, 2020). Digital Image Correlation (DIC) and Particle Image Velocimetry (PIV) were used in-air to obtain high-speed full-field wing deformation and flow field velocity data in synchronous with forces and moments. Laura and Ivan (2021) carried out a detailed review of the experimental methods able to describe FSI events in an underwater dynamic environment. A feasibility study is carried out to understand the implications, limitations and advantages of being able to measure with full-field techniques in a towing tank.

4.3.9 Validation and Verification of CFD

Numerical methods are typically validated towards experimental results. In the case of performance predictions for wind assisted vessels, sail models can be validated by (or generated from) e.g. wind tunnel tests, hydrodynamic force models towards for instance PMM (Planar Motion Mechanism) tests, propeller and rudder models towards dedicated propulsor tests, and so on.

A modified version of the horseshoe vortex method to compute the velocity field behind a given wind-propulsion system were compared with numerical tools (CFD body force method and a standard RANS solver) as well as with experimental data obtained by means of dedicated wind tunnel tests in Bordogna (2016). Duport et al. (2016, 2019) developed a 3D non-linear model based on the lifting line of Prandtl for calculation of aerodynamic forces and this model has been verified by comparison with 3D RANSE simulations and produces satisfactory results in incidence and sideslip.

Duport et al. (2016) did estimation of the numerical accuracy of the RANSE simulations including the deviations, coming from the variations of the domain size, of the mesh and of the turbulence model. The numerical results were compared with experimental ones obtained in wind tunnel at the same Reynolds number.

ITTC procedure and guidelines and American Society of Mechanical Engineers (ASME) standard procedures are applied to verification and validation of RANS CFD simulations on hydrodynamics of wind-assisted ship propulsion in van der Kolk et al. (2016, 2017, 2019, 2020). The verification has been conducted with particular focus on the hydrodynamic sideforce, as a leading component of the hydromechanics of wind-assisted ships. Based on the results, the uncertainty procedure developed by Eça (2010), based on the Grid Convergence Index (GCI) of Roach (1997), was the most robust approach.

The RANS numerical set up has been extensively verified and validated using different experimental data including a twin rotor configuration by M Garenaux and J J A Schot (2021). A good correlation is found with experiments for both standalone rotor and twin-rotor configuration.

Kume et al. (2022) compared the results of RANS-based CFD calculations and wind tunnel tests of aerodynamic forces on a VLCC equipped with 4-Flettner rotors using model scale, indicating that CFD can be ued as a substitute for wind tunnel test. Eide et al. (2023) performed cyber-physical empirical model test of a wind-assisted cargo ship to validate a steady numerical simulation method which is a prediction program solving the motion of the vessel in three degrees of freedom (surge, sway and yaw).

N Abiven et al. (2023) demonstrated wind-powered cruise ship aerodynamic simulations, hydrodynamic simulations and correlations. Series of drift hydrodynamic numerical / experimental simulations and correlations to assess induced lateral drag and impact on ship hydrodynamic behaviour, in particular course stability and manoeuvrability have been developed and conducted.

R Azcueta and H Ward（2023） presented CFD simulation results of open water propeller, towing resistance at model and full scale and propulsion with the virtual disk and with rotating propeller approaches of a bulk carrier and the 6-DoF simulations of the full-scale vessel in motor-sailing conditions including the WASP devices which were validated by comparison to the test results. Numerical uncertainty analysis following the ITTC and IACS recommendations are described to verify the qualification of the CFD solution.

4.3.10 Conclusions

A review of the literature on the methods of ship model hydrodynamic tests, wind tunnel tests, CFD, ship dynamics simulations and routing relevant for predicting the performance and safety of wind powered and wind assisted ships has been undertaken. Verification and validation of numerical method including uncertainty analysis are commonly performed on hydrodynamics and aerodynamics.

The performance prediction methods show great promise in becoming a tool for designers and researchers for analysis and optimisation of wind propulsion device layout and operational parameters. To generate more accurate results for a specific ship with WPS, further investigation into the effects of drift angle on propulsion performance and resistance, routing simulations are needed for ship performance prediction of ship with wind and wind-assisted propulsion in wind and waves.

Detail developments of hybrid wind-propulsion ship for different ship applications with specific new features to address heel and drift during navigation and manoeuvring (e.g. development of anti-drift equipment and potential additional appendages), and corresponding ship design assessments and validations: stability, power management strategy, coupled aerodynamic / hydrodynamic CFD simulation and experimental tests at large scales on standard ship operation conditions (sailing, manoeuvring) as well as extreme cases (safety issues and rules) need to be investigated.

Sailing performance with an improved manoeuvring model and CFD simulations, simulations and hybrid model tests performed in waves, zig-zag manoeuvring model tests and time domain simulations, investigation into the effects of dynamic heel, trim and drift angle on the propeller wake are to be further studied.

4.4 Review long-term statistics of winds and waves from the point of view of applicability for the evaluation of wind assisted ships at design stage.

4.4.1 Introduction

Long-term statistics of winds are essential for the evaluation of wind assisted ships at the design stage. The Global Wind Probability Matrix is used to calculate the EEDI and EEXI for Wind Assisted Propulsion Systems, however the area of applicability is limited to the main global shipping routes as shown in Figure 18

Figure 18. The main global shipping network used for the wind chart (MEPC 62, 2011)

Inadequacies with this method may potentially arise when used outside of these routes. Werner et al. (2021) describes a methodology to analyse full scale speed trials on a wind-assisted hybrid ferry. The trial area is off Gedser, Falster, Denmark, outside of the main shipping routes depicted in the Global Weather Matrix. Wind statistics were obtained from the Global Wind Atlas (2022) and results are complimented with the wind statistics from the EEDI Global Weather matrix. As can be seen from Figure 19, the Global Wind Atlas predicts higher wind speeds for the actual sea area the ferry operates in, compared to the EEDI global weather matrix.

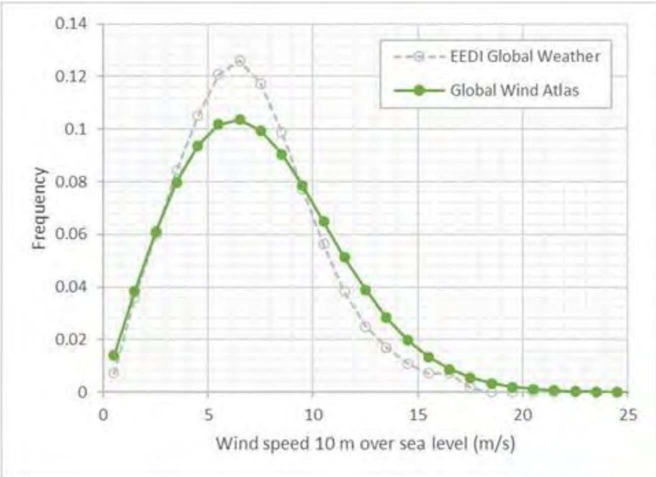

Figure 19. Wind speed distribution from Global Wind Atlas for ferry route, and the EEDI Glob-al Weather matrix (Werner et al., 2021)

Since global wind speed datasets are assembled from various sources of satellite and reanalysis data, the most-suitable dataset for a particular purpose is often unclear. The accuracy of global datasets differs depending on the ocean area. Due to their coarse resolution, reanalyses are known to fail to represent local climatic conditions adequately (Werner et al., 2021).

While global reanalysis data sets offer the advantage of conducting multi-country or global analyses without the need for country or region-specific climate data sources, their use for wind power simulation would benefit from a more granular spatial resolution (Staffell et al., 2016), as offered by regional reanalyses such as COSMO-REA (2019) which in more detail represents the local climatic conditions.

The great advantage of numerical models is their wide coverage on a high time and space resolution in a global scale, making it possible to produce long-term wind (and wave) climatologies without gaps.

4.4.2 Wind Models

To assess potential savings in power for wind assisted ships at the design stage, various data-sets incorporating different data assimilation models were selected for evaluation. Some data-sets are superseded by others but are included as many present-day methodologies still use them (Li et al., 2022). These climate models are summarised in the following sections, and in Table 7.

4.4.2.1 ERA-Interim

ERA-Interim dataset is provided by the European Centre for Medium-Range Weather Forecasts (ECMWF). It is a global atmospheric reanalysis from 1979, continuously updated in real time and replaces the previous ERA-40 reanalysis dataset. ERA-Interim is now obsolete and has been replaced by ERA-5.

4.4.2.2 ERA-5

ERA-5 dataset is provided by the European Centre for Medium-Range Weather Forecasts (ECMWF) and produced by the Copernicus Climate Change Service (C3S). It is a fifth-generation atmospheric reanalysis of the global climate covering the period from January 1940 to present, providing hourly estimates of a large number of atmospheric, land and oceanic climate variables. It is the most recent model out of the ones listed here.

4.4.2.3 NCEP – National Centre for Atmospheric Research (NCAR)

The National Centre for Atmospheric Research (NCAR), also known as R-1, is an atmospheric reanalysis produced by the National Centres for Environmental Prediction (NCEP). The time period spans from 1948 to the present.

4.4.2.4 NCEP – Department of Energy (DOE)

The Department of Energy (DOE), also known as R-2, is a climate model from the National Centers for Environmental Prediction (NCEP). It is based on the NCAR reanalysis but fixes some errors and uses updated parameterisations of physical processes.

4.4.2.5 NCEP – Climate Forecast System Reanalysis (CFSR)

The Climate Forecast System Reanalysis (CFSR) was developed by the National Centre for Environmental Prediction (NCEP) and spans the period from 1979 to 2017. It is a third-generation reanalysis product, superseding R-1 and R-2.

It is superior to previous NCEP reanalyses, having an improved model, including atmosphere-land-ocean-sea ice coupling, finer resolution and more advanced assimilation schemes.

There have been relatively few evaluations of CFSR so the performance is not well-known. Ocean-atmosphere interactions are not used directly. Rather the information is used for background information, meaning the actual reanalysis is uncoupled.

4.4.2.6 The Modern-Era Retrospective analysis for Research and Applications (MERRA)

The Modern-Era Retrospective analysis for Research and Applications (MERRA) is produced from the National Aeronautics and Space Administration (NASA). MERRA data span the period 1979 through February 2016. It is based on a version of the GEOS-5 atmospheric data assimilation system that was frozen in 2008. The MERRA dataset is superseded by MERRA-2.

4.4.2.7 The Modern-Era Retrospective analysis for Research and Applications Version 2 (MERRA-2)

The Modern-Era Retrospective analysis for Research and Applications, Version 2 (MERRA-2) is produced from the National Aeronautics and Space Administration (NASA). provides data beginning in 1980 to the present. It replaces the original MERRA dataset because of the advances made in the assimilation system.

4.4.2.8 The Cross-Calibrated Multi-Platform wind vector analysis (CCMP)

The Cross-Calibrated Multi-Platform (CCMP) is a gridded Level 4 (L4) product that provides vector wind over the world's oceans. It is produced by Remote Sensing Systems (RSS), (https://www.remss.com/). CCMP is a combination of ocean surface (10m) wind retrievals from multiple types of satellite microwave sensors and a background field from reanalysis. Data spans from 1987 to the present.

The reanalysis used in the latest version of CCMP (v3) is ERA-5.

The CCMP model generally performs poorly in rain and under high wind conditions (> 15m/s) and is not well suited for studies of global wind trends (CCMP, 2023).

4.4.2.9 JRA-55

The Japanese 55-year Reanalysis (JKA-55) dataset is provided by the Japan Meteorological Agency (JMA). The JMA carried out this second reanalysis project to address some of the shortcomings of the previous JRA-25 model, including the use of a much-improved data assimilation system. The analysis period covers the 55 years from 1958, when regular radiosonde observation began on a global basis.

The result of the JRA-55 project is the production of a high-quality homogeneous climate dataset covering the last half century.

4.4.3 Summary of Wind Models

A summary of the different wind models can be found in Table 7

Table 7. Summary of data sets used in analysis.

Data-set Name	Institution	Time Resolution (hours)	Spatial Resolution	Assimilation Method	Refs
CFSR	NCEP	1	0.3° × 0.3° (v1) 0.2° × 0.2° (v2)	3D-VAR	Saha et al. (2010)
NCAR	NCEP	6	1.875° × 1.875°	3D-VAR	Kalnay et al. (1996)
DOE	NCEP	6	1.875° × 1.904°	3D-VAR	Kanamitsu et al. (2002)
ERA-Interim	ECMWF	6	0.75° × 0.75°	4D-VAR	Dee et al. (2011)
ERA-5	ECMWF	1	0.1° × 0.1°	4D-VAR	Hersbach et al. (2020)
JRA-55	JMA	3	0.5625° × 0.5625°	4D-VAR	Kobayashi et al. (2015); Harada et al. (2016)
CCMP	RSS	6	0.25° × 0.25°	Scat/Rad	Atlas et al. (2023)
MERRA	NASA	6	0.5° × 0.66°	GEOS-5	Rienecker et al. (2011)
MERRA -2	NASA	1	0.5° × 0.625°	GEOS-5.12.4	Koster (2015)

4.4.4 Comparison of Wind Models for Reliability and Accuracy

The datasets outlined in the previous section are compared with a view to determining if there is an overall model which is most suitable for use in the applicability for the evaluation of wind assisted ships at design stage.

Suzuki et al. (2018) analysed the CCMP, NCEP/CFSR, NCEP-R1, NCEP-R2, ERA-Interim and JRA-55 global wind datasets and compared them to the measured wind speed from buoys. The data were analysed for the year, 2001 in which neither El Niño nor La Niña events occurred. The wind speed at 10m above sea surface was used. The wind speeds in the global dataset were converted to the smallest grids with 0.25°×0.25° through interpolation. To examine the validation, the wind speeds on a grid closest to the buoy location were used. 57 buoys were used, located in the Indian Ocean, Tropical Pacific, Tropical Pacific, Tropical Atlantic, North Pacific and Atlantic. The data from the buoys were converted to a value corresponding to 10m above sea level so as to correlate with the global wind speed datasets.

The Root Mean Square Errors (RMSE) for all datasets were calculated to investigate random errors of wind speed. Lower values indicate higher reliability. Results are shown in Table 8. The CCMP dataset is shown to be consistently the most reliable.

Table 8: RMSE of the wind speed of each datasets against the all buoy wind speed measurements

Data set	RMSE [m/s]	Data set	RMSE [m/s]
CCMP	1.05	NCEP/CFSR	1.53
NCEP-R1	2.16	ERA-Interim	1.42
NCEP-R2	2.46	JRA-55	1.64

The reliability of the datasets was also compared against buoy wind speed measurements for localised regions, as shown in Table 9

In all regions, the CCMP dataset is shown to be the most reliable. It can also be seen from the table that the lowest RMSE in Indian Ocean followed by Tropical Pacific, Tropical Atlantic, North Pacific, and North Atlantic.

Table 9: Reliability of datasets in localised regions.

Area	Data Set	RMSE [m/s]	Data Set	RMSE [m/s]
Indian Ocean	CCMP	0.89	NCEP/CFSR	1.32
	NCEP-R1	1.65	ERA-Interim	0.92
	NCEP-R2	2.08	JRA-55	1.29
Tropical Pacific	CCMP	0.99	NCEP/CFSR	1.54
	NCEP-R1	2.07	ERA-Interim	1.28
	NCEP-R2	2.20	JRA-55	1.57
Tropical Atlantic	CCMP	1.04	NCEP/CFSR	1.49
	NCEP-R1	1.86	ERA-Interim	1.22
	NCEP-R2	2.32	JRA-55	1.51
North Pacific	CCMP	1.23	NCEP/CFSR	1.45
	NCEP-R1	2.73	ERA-Interim	2.07
	NCEP-R2	3.41	JRA-55	2.07
North Atlantic	CCMP	1.52	NCEP/CFSR	1.73
	NCEP-R1	2.88	ERA-Interim	2.10
	NCEP-R2	3.73	JRA-55	2.07

Suzuki et al. (2018) concluded that the wind speed dataset in CCMP is the most accurate for any local ocean area. In the North Pacific and North Atlantic, all the tested datasets were inaccurate. All global wind speed values differ from the buoy wind speed measurements in low wind speed range. Distribution trends of all the global datasets are similar to that of the buoy's wind speed measurement. Compared to the buoy wind speed measurements, the NCEP-R1 and NCEP-R2 datasets show especially large dispersion and the CCMP dataset shows the smallest variation.

Gruber et al. (2022) conducted a study on the assessment of wind power simulation from bias-corrected MERRA-2 and ERA-5 reanalysis. They concluded that ERA-5 on average performs better than MERRA-2 in all regions, with ERA-5 showing approximately 0.05 higher correlations than MERRA-2 and 0.05 lower RMSEs in most regions. Only in New Zealand, MERRA-2 performs better on average than ERA-5.

Stefanakos (2021) studied several statistical features of the datasets are assessed, such as seasonal variability, quantiles of the probability distribution, monthly, annual and inter-annual variability, and several error metrics on two re-analysis products, ERA-5 and CFSR. The analysis was per-formed at both a global and regional scale. They conclude that the two datasets are in a very good agreement, with CFSR having little greater variability than ERA5.

Carvalho (2019) have made comparisons between NCEP-CFSR, ETA-Interim and JRA-55 and were analysed to evaluate the MERRA-2 model. Results showed that MERRA-2, CFSR, ERA-Interim and JRA-55 showed similar error metrics. All reanalyses showed a tendency to underestimate ocean surface winds, particularly in the tropics. MERRA-2 showed lower wind errors in the poles when compared to the other reanalyses.

4.4.5 Wave statistics

There are a number of approaches to obtain wave data. For instance, Fang and Lin (2013) used WAVEWATCH III to obtain the precise forecast of environmental factors along routes for ship route optimization. Eggers (2018) used wave scatter diagram to perform the route optimizations.

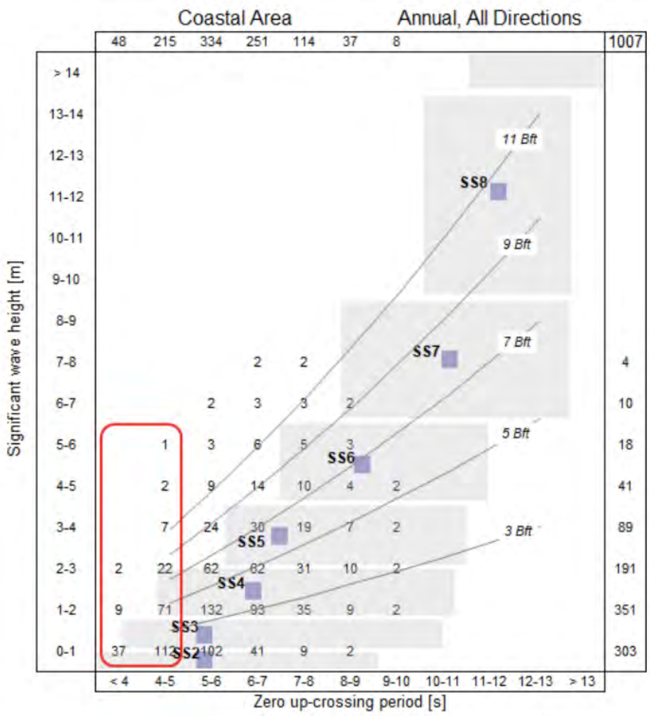

Figure 20. Typical wave scatter diagram (Egger, 2018), IACS wave scatter diagram.

Figure 20 Typical wave scatter diagram (Egger, 2018), IACS wave scatter diagram.

The IACS wave scatter diagram describes the wave data of the North Atlantic, covering the area as defined in the Global Wave Statistics (GWS) with more realistic considerations of the wave steepness. Short-term sea states are assumed to be statistically independent and hence uncorrelated in the standard procedure for the long-term response analysis (IACS, 2000). It should be noted that Bretschneider or two parameter Pierson-Moskowitz spectrum is recommended for the North Atlantic.

Global Wave Statistics (Figure 21) provides nearly worldwide coverage of wave climate in 104 sea areas, and an additional database providing smaller sea areas for the North European Continental Shelf. Based on 130 years of ship visual observations to provide a stable climatic average, the data has been quality enhanced by the well-established NMIMET process.

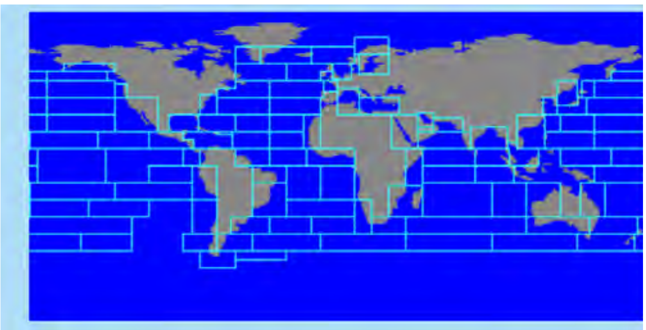

Figure 21. GWS plot

Bitner-Gregersen et al. (2013) investigated uncertainties in the Global Wave Statistics data and their effects on ship loads and responses, as well as on fatigue damage. They have concluded that the GWS should be used with care.

NMRI in Japan developed a system called Globus which can offer statistical results of global winds and waves, which are analysed by NMRI. The statistical data are based on the numerical weather prediction of 10 years, from 2006, calculated by Japan Meteorological Agency and these are composed of significant height, peak period and primary direction of waves, and mean speed and direction of winds in 2.5 degrees interval in space and 6 hours interval in time.

In terms of the wave forecast system, ECMWF was developed in Europe and Global Real Time Ocean Forecasting System (RTOFS) was developed by NOAA, US.

For the fatigue life prediction of ship structures, it is important to obtain both the long-term distribution and the time history of wave-induced loads. Gracia et al. (2019) compared two statistical wave models and validated them by a ship's actual encountered wave conditions. They found that Statistics of wave height and stresses generated from the two models agree well with that from hindcast and onboard measurements. They also concluded that the actual wave environments encountered by the ship differ significantly from the wave scatter diagram provided by class guidelines for ship fatigue design. Today's onboard wave radar sensor can provide rough approximation of a ship's encountered sea conditions, but the measured significant wave height may contain large errors in comparison with the hindcast wave data in particular at harsh sea environments.

Mikulić et al. (2021) studied the effect of spatial correlation of sea states on extreme wave loads of ships. By comparing the results using "uncorrelated scatter diagram" and "scatter diagram", they concluded that spatial correlation may considerably reduce extreme vertical wave bending moments.

4.4.5.1 Correlation between Wind and Wave Statistics

Sea surface wind speed and significant wave height follow a monotonical relationship under a growing sea up to the fully developed stage. This final stage is usually reached when the phase velocity corresponding to the dominant peak wave slightly exceeds the wind speed (Chen et al., 2002).

Wave forecasting models always employ the concept of a fully developed sea. For a given constant wind speed, if the upwind distance to the point of observation over which the wind has blown is larger than a certain distance and if the duration of the wind is longer that a certain time, then the wave height will be solely a function of wind speed (Sverdrup and Munk, 1947). Based on the statistics of wind speed and significant wave height of developed seas for a large enough fetch and a long enough duration, Pierson and Moskowitz (1964) found the significant wave height is positively related to the square of wind speed, i.e. $H_s = \alpha U^2$ (H_s is the significant wave height, U is the wind speed, α is a coefficient obtained by linear fitting). They reconciled the differences in wind speed at different heights and found $\alpha = 2.45 \times 10^{-2}$. Ewing and Laing (1987) found 33 examples of spectra for "nearly" fully developed seas by means of a study of the past winds at the measurement site and the wind pattern upwind of the measurement, and they proposed a third-order polynomial to describe the relation between the significant wave height and wind speed, i.e. $H_s = 10^{-3}(8.7U^2 + 0.728U^3)$. However, the Wave Model (WAM) found the relation $H_s = \alpha U^2$ applies to the lower wind speed, i.e. $0 < U < 7.5\ m/s$. To improve the accuracy of wave forecast in condition of larger wind speed, they adopted a third-order polynomial, i.e. $H_s = 10^{-3}(10U^2 + 0.81U^3)$ (Hasselmann et al., 1988).

Based on collocated wind speed and significant wave height measurements from simultaneous satellite scatterometer and altimeter sources, Chen et al. (2002) analyzed the global statistics of wind wave and swell, and plotted a scatter diagram of sea surface wind speed and significant wave height, which is shown in Figure 22. The three different lines are theoretical relations between wind speed and significant wave height for fully developed seas according to Hasselmann et al. (1988), Ewing and Laing (1987) and Pierson and Moskowitz (1964), respectively. Measurements lying below the curves are mostly from a growing sea, while those above the curves are probably swell dominated.

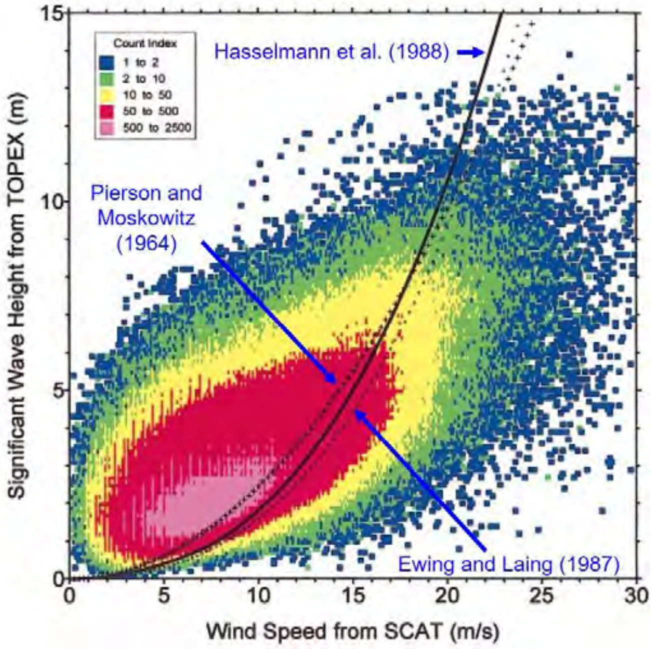

Figure 22. Scatter diagram of sea surface wind speed and significant wave height based on global wave data and wind data (Chen et al, 2002)

The wind speeds are extracted from QuikSCAT, and the significant wave heights are extracted from the TOPEX altimeter (Chen et al, 2002).

Because of the complexity of the wind wave-swell coupling, the assumption that the wave height is solely a function of wind speed in a fully developed sea is not suitable to the real sea state. Waves depend on both local and global wind conditions. It is not only the local wind that defines local waves, and wind from distant regions generates swells that may reach the target point (Ardhuin and Orfila, 2018).

Considering the complexity of the wind wave-swell coupling, Obakrim et al. (2023) developed a method to predict the significant wave height in wind seas and swells by including local and global predictors. Wind speed, duration, and the fetch are used as local predictors, while the zonal and meridional components of the wind data are used as global predictors. A regression-guided clustering method is used to constructed weather types, and the resulting clusters correspond to different wave systems (wind seas and swells). Then, in each weather type, a penalized linear regression model is fitted between the predictor and the significant wave height.

The extreme wind and wave storms can pose a threat to the safety of both marine structures. Based on the data from four meteorological (buoys and anemometers) stations of the National Data Buoy Center moored off the East Coast of the United States, Laface and Arena (2021) proposed a criterion to identify and associate wind and wave storm. An optimal threshold combination is achieved assuming both wind speed and significant wave height threshold as 1.5 time their respective averages. The wind speed is characterized by a higher variability with respect to the significant wave height. The significant wave height increases with the wind speed. However, the peak of the significant wave height does not always occur after that of the wind speed.

4.4.6 Conclusions and Recommendations

For the general purpose of the evaluation of wind assisted ships at design stage, it is recommended that the ERA-5 Reanalysis or CCMP product is used. However, if a shipping route is particularly localised, it may be beneficial to use a regional high-resolution reanalysis system such as COSMO-REA6 for Continental Europe, for increased accuracy and reliability. Regarding the wave scatter diagram, there is no special requirements for wind-assisted ships.

4.5 Review safety and regulatory issues related to hydro/aero dynamic testing and evaluation and recommend measures to take at design stage

4.5.1 Introduction

After discussion with the Advisory Council, it was understood that the main aim of this term of reference is to specify testing and evaluation methods. However, these methods of course need to address specific safety and regulatory issues as relevant for wind powered and wind assisted ships. Therefore, the present section begins with a review of safety (and operability) issues. Following that is a discussion of existing rules and regulations. Both of these sections describe scenarios and criteria that are to be satisfied. The final main section then discusses testing methods that may be used to simulate the scenarios and to evaluate compliance.

The scope of behaviour that is covered in the present section are those activities generally conducted by ITTC members, extended with aerodynamics. This means that the following topics are covered:

- Motions and accelerations
- Forces
- Energy and power as relevant to safety and rules & regulations.

Considering the focus is on safety, any rules & regulations on performance in steady conditions are not handled here. These are part of other Terms of Reference.

As will be seen in the following sections, rules and regulations on safety are at present not tailored for wind powered and wind assisted ships. Ships with modest assistance may operate with only small changes to their behaviour as a conventionally propelled ship. However, with more powering provided by the wind, ships start to behave differently. As of yet there are not much research results that give a general overview of the impact. Perhaps matching that, class societies have only provided guidelines, that also vary quite a lot from society to society. As a result, some assumptions are unavoidable to anticipate what kind of testing will be required going forward.

4.5.2 Potential safety and operability issues for wind powered and assisted ships

Potential safety and operability issues are discussed based on available literature. This is partially the same literature discussing testing and simulation methods as addressed in section 4. There is much to be said on the accuracy and practicality of these methods. However, that is discussed in section 4.5.6. For the purpose of the discussion here, the methods are deemed sufficiently accurate.

4.5.2.1 Course keeping

In principle one can think of two mechanisms for wind propulsion to affect course keeping ability:

1. Dynamic aerodynamic forces (wind gusts, changes in wind direction) that push the ship of course directly
2. Loss of steering capability from conventional actuators (rudders, thrusters, pod) due to a lower propeller thrust that reduces the flow along these actuators. This, combined with other external forces, specifically waves from the stern quarter, can lead to a decrease in course keeping performance. Part of the available rudder action is already committed to counter the (quasi-)steady sway forces and yaw moment from the wind propulsion system, thus, less margin may be available for countering unsteady forces from wind, waves and current.

Course changes directly through variable aerodynamic forces (mechanism 1) were tested and reported by Sauder and Alterskjær (2002). In a model test, a ship with three four Flettner rotors was exposed to wind gusts and variable wind directions. The model showed only marginal course changes and some modest rolling. The mentioned reason for the small course variation is the ship, which its large mass, that acts as a filter. The frequency of the excitation through the wind is much higher than the ship response. Inertia in heel is relatively less, which means that some rolling could still occur.

Eggers and Kisjes (2019) have illustrated mechanism 2. In substantial wind conditions (roughly 7 Beaufort) and a matching sea state from the stern quarter, four times increase of the yaw angle variation was observed for the coaster design that was tested with three Flettner rotors. The reference was the same ship in a very mild wind condition. Differently to mechanism 1, the excitation comes from the waves, and this excitation can have a substantial amplitude and relevant frequency in stern quartering seas, with a lower encounter frequency. In contrast, Gerhardt et al (2021) found in experiments that yaw oscillations were not substantially affected when testing a Car Carrier with three wing sails. The difference in conclusions may be attributed to the designs and test conditions. In the experiments by Eggers and Kisjes an existing ship model was taken without substantially changing it for wind propulsion, whereas the car carrier in the experiments by Gerhardt et al (Gerhardt et al. 2021) was a dedicated design. Also, wave heading was arguably more demanding in the coaster case. Based on this scarce data it can be concluded that wind propulsion could present a challenge for course keeping, but not necessarily always.

The discussed papers showed only a few ship designs and wind and sea conditions. Thus, the general applicability of the conclusions on more ship types and environmental conditions is not yet known.

4.5.2.2 Ability to keep speed in adverse bow (quartering) wind and waves

Keeping control in adverse bow (quartering) wind and waves is an important ability.

Whereas the main purpose of wind propulsion is to aid in the propulsion of the ships, there are two mechanisms in which wind propulsion may also lead to a decrease in performance in the conditions discussed here:

1. When wind propulsion systems cannot be fully reefed/lowered, then the windage of a ship can increase when sailing in unfavourable bow (quartering) wind. This adds to the overall resistance. Especially combined with a low/reduced capacity propeller and engine, ships could have trouble to remain under control. The speed of the ship could be reduced by too much.
2. Wind propulsion changes the equilibrium condition of the ship, in general affecting heel, leeway and rudder angle. These aspects could potentially impact the second order mean wave drift forces (which includes added resistance in waves). The hydrodynamic shape and inflow under water changes, which means that the general knowledge on added resistance in waves may need extension.

Heel, leeway and rudder angle may also directly by themselves lead to an increase in drag. However, it is considered that any smart design and control will make sure that this drag component is modest in relation to the thrust of the wind propulsion system. And if it is not, then the wind propulsion system may be depowered or disabled.

In most cases, wind, wind sea, and swell are assumed to be aligned in direction, i.e. they are “co-linear”. However, they don’t always need to be in equilibrium. Particularly swell does not full correlate with wind. If the sea or swell direction that provides the largest contribution to the second order mean drift forces has a considerable offset in direction compared to the wind direction, then there may be possibility for the wind propulsion to assist in the propulsion of the ship, thereby helping to maintain control in head waves. Although such a scenario may occur, it will likely be something that one can depend on. Nevertheless, it would be interesting to see this scenario elaborated in future research.

4.5.2.3 Heel, roll and stability

Heel (steady average value) and roll (dynamics) can affect the safety and comfort and result in loads on ship parts and cargo. This is already relevant for modest angles. However, ultimately too large roll may even lead to capsize. This is valid for all but one wind propulsion technology. Kites are an exception here: if the connection point on deck is relatively low, then the introduced roll moment is very low compared to other technologies and heel and roll effects are likely minimal.

Very generally it is found that wind propulsion:

1. Leads to an increased heel angle through the heeling moment directly introduced by the wind propulsion system
2. Can lead to increased roll motions due to dynamics in the wind propulsion systems, introduced e.g. through wind gusts
3. Can lead to decreased roll motions because of an increase in roll damping

Mechanism 1 is shown already in static VPP / PPP calculations for which there is a relatively large amount of data available in literature. The extent of heel depends on the vessel stability and the relative size and height of wind propulsion. Some new designs directly implement methods to limit heel. For instance, some projects are already using dedicated water ballast on board that can be pumped from side to side, so called “anti-heel tanks”. On few conditions, fin stabilisers are also used to provide a heel restoring moment.

Sauder and Alterskjaer (2022) show some test data where a wind spectrum leads to variable roll angles. In their tests the wind speed was variable. A variation in “quasi-static” roll due to variable wind is to be expected for any system (except kites if mounted low). However, on this aspect there is little literature.

Eggers and Kisjes (2019) showed the increased aerodynamic roll damping for Dynarigs and Flettner rotors. Especially with apparent wind from the bow quarter, roll motions lead to a strong variation of angle of attack, resulting in roll damping. When using relatively large devices compared to the ship, the aerodynamic roll damping may be similar in magnitude to the hydrodynamic damping and therefore its impact on roll motion is substantial. Devices that are not dependent on an angle of attack for their force magnitude, such as Flettner rotors still show increased roll damping due to the changing apparent wind speed, however with a smaller impact. If dynamic roll is much reduced then the acceptability of a non-zero (quasi) steady heel angle may be increased, though no research has been identified on this topic.

4.5.2.4 Manoeuvring in transit

Manoeuvring in transit has been studied by Vahs (2019), Gerhardt et al. (2021) and Eggers and Kisjes (2019), (2023) and Kisjes at al (2023). The general test case here are the manoeuvring criteria specified by IMO in resolution MSC 137(76) with the criteria further discussed in section 4.5.3.3.

The results for a coaster with a single Flettner rotor in 4 Beaufort wind presented by Vahs for the turning circle and crash stop easily comply with IMO criteria. Although the results for a ship without wind propulsion are not shown, the conclusion that wind propulsion had very small effect seems plausible.

The other publications, with a relatively larger contribution from wind propulsion, show an appreciable influence of sail propulsion on zig-zag overshoot angles. In Gerhardt et al. (2021) these are all increasing for the ship with wind propulsion, while the trend in Eggers and Kisjes varies. This may very well be case and wind condition specific. In the MHTC case presented by Eggers and Kisjes it was expected that the yaw moment that is introduced by increased or decreased heeling close to the wind may in fact stabilise the manoeuvre. When bearing away from the wind, the angle of attack and heeling moment increases. Heeling puts the thrust from the sails further outboard on the leeward side, generating a luffing moment, thus returning to the original course. The reverse happens when luffing to the wind. Such an affect may be irrelevant with little heel, other device types and other wind conditions. Eggers and Kisjes also show that there are also changes in the other derived characteristics from the zigzag manoeuvre. The MHTC tested by Eggers and Kisjes already had trouble to comply with the manoeuvring standards in IMO Resolution MSC 137(76) without wind propulsion. With some parameters deteriorating with wind propulsion, compliance could not be achieved. The MARIN Ferry case (Eggers and Kisjes, 2023) shows how manoeuvring is affected for ship that has a better “base” manoeuvring performance. Compliance is not exceeded. However, what is shown is the heel angle can increase substantially for a ship with a relatively low stability.

In the publications referred to, the control of the wind propulsion is not used to aid the manoeuvre. Some work underway suggests that controlling the wind propulsion to aid manoeuvring could help. The results likely vary per type of wind propulsion. E.g. it is known that some Flettner rotors have a slow response time to substantially change their rotation rate (or to stop), whereas other devices, that need to only slightly change their angle of attack, can respond rather fast. However, it is expected, that these specifications will prove to be important, the specifications of all devices can likely be changed in order to aid manoeuvring. Thus, this field of research is highly relevant. The possibilities to use wind propulsion to steer the ship should also be clearly identified in regulations, as discussed in section 4.5.3.

4.5.2.5 Manoeuvring in port or laying at anchor

It is assumed that wind propulsion is disabled when in port as far as possible. Wind propulsion devices that can be fully folded down or retracted should not lead to any change in manoeuvrability in port. However, devices that are still (partially) erect will lead to increased windage that will need to be dealt with. Likely, the capacity of on board thrusters or tugs needs to be increased if the (un)berthing still needs to happen at the same wind speeds.

Aside from a change in side force, the centre of effort of windage force may also be moved far forward in case of a wind propulsion system that is only fitted on the bow. This could introduce instabilities at anchor, potentially triggering fishtailing behaviour.

4.5.2.6 Structural loads

Wind propulsion devices and also their foundation on ships must be able to cope with the loads that they are subjected to. Loads originate from the aerodynamics. However, also ship motions, both as a rigid body and with deformations can yield loads due to structural inertia and added mass. In the specific case of Flettner rotors the loads are further increased due to precession load related to the rotation speed of the device. Devices could stop to work properly in case of excessive (elastic) deformation, It could fail on ultimate strength or fatigue. If a device fails then for modest assistance it is not likely to endanger the entire ship. However, in case of a ship where the majority of propulsion is from wind, the loss of one or more devices may be critical.

Limited literature gives few indications on the relevance of the topic. Eggers and Kisjes (2019) in their preparations identified that motion related loads on Flettner rotors may be in the same order of magnitude as the average aerodynamic loads, such that these should always be accounted for. However the loads are of course highly dependent on the encountered waves and motion response of the ship. Kjellberg (2022) performed an extensive analysis to estimate fatigue loads for wing sails.

4.5.2.7 Dead ship condition

In case a ship is sailing with wind propulsion, and loses all power due to a system malfunction (“dead ship” condition) , it may be more vulnerable than other ships. Unless there is a method onboard that readily disables the wind propulsion system, it will generally continue to exert forces on the ship. For small systems, this may not be problematic. However, for larger installations, the wind propulsion system may push the ship of course and potentially increase heeling moment when the angle of attack on sails or wings increases. Particularly combined with a demanding sea condition from the stern quarter, controllability of the vessel may be challenging. Nevertheless, no literature is published on this topic.

4.5.2.8 Loss of kites

A topic that is regularly raised is the potential loss of kites. If such a thing would happen, retrieving the kite from the sea or abandoning it would present an operational challenge and/or large cost in damage. One could also imagine the kite cable falling over the ship, damaging structures on deck. Such concern are sometimes raised in discussions within the wind propulsion community and stake holders, however no literature is available to illustrate whether this risk is real or can be practically avoided with autonomous control and proper safeguards in operations. Hence, the topic is not discussed further here.

4.5.3 Existing rules and regulations

This section is split in several sections. Statutory regulations are those that are established at IMO and should be enforced by flag and harbour states. Class rules are dealt with separately. IMO and class rules are effectively mandatory to be complied with. However, as already concluded in the previous sections there also aspects of ship behaviour with wind propulsion that are presently not associated with mandatory requirements. Nevertheless, owners may come up with criteria by themselves and later on new criteria may be considered for adoption at class or IMO. These are together discussed in the last section.

The rules and regulations discussed in this report is a selection that are relevant for hydrodynamic and aerodynamic testing and calculations at ITTC members. A larger number of rules and regulations are relevant for wind propulsion in shipping though these are not discussed here.

4.5.3.1 Statutory regulations (IMO)

4.5.3.2 Stability

IMO sets requirements on the GZ curve, down flooding angles and subdivision in the following documents:

- International Code on Intact Stability
- SOLAS II-1, Consolidated text of the International Convention for the Safety of Life at Sea
- MSC.429(98), Revised Explanatory Notes to the SOLAS Chapter II-1 Subdivision and Damage Stability Regulations
- SDC 7/WP.6 Finalization of Second Generation Intact Stability Criteria

Compliance to these criteria is checked generally by design offices using calculations. No tests or simulations are generally required. An exception is the severe wind and rolling criterion (weather criterion) as defined in the intact stability code, where this is often also tested in a basin.

4.5.3.3 Manoeuvring in transit

IMO MSC Resolution 137(76) (2002) specifies criteria that are to be verified with zig-zag, turning circle and crash stop tests. The purpose of these tests is to ascertain that ships have a satisfactory manoeuvring performance when sailing at speed. When following the rules to the letter, it is not relevant to ships with wind propulsion, because compliance needs to be demonstrated in a calm environment (with as little wind as possible). However, class societies are generally interpreting the rules such that all ships should be able to do evasive manoeuvres when in transit, including when sailing with wind propulsion. Though, interpretation amongst class societies varies on how to apply IMO Resolution 137(76) with wind propulsion.

4.5.3.4 Controllability in adverse conditions

4.5.3.5 Minimum Power Requirement

Ships equipped with a single diesel-direct propulsion line need to have a certain minimum power level on board to ascertain that they remain controllable in demanding wind and sea from the bow (quarter) as specified by IMO (2001). The requirement is evaluated in a tiered approach. In the simplest but most conservative method (assessment level 1), the required power is only dependent on deadweight and ship type, which does not consider whether a wind propulsion system is fitted. On the one hand this means that it does not require much effort at all to demonstrate compliance. However, It can be questioned whether the empirical relationships account properly for ships with wind propulsion. Assessment levels 2 and 3, require consideration of aerodynamic resistance. If potential increased windage with wind propulsion is properly accounted for, then the required engine power is automatically adjusted and any safety implications of fitting a wind propulsion system is properly accounted for in head wind and sea.

It is noted however, that the requirement is specified only for head wind. The requirement effectively assumes that being able to keep a head wind and sea heading is a requirement for safety. It may be argued that ships could be safe as well when adopting other headings in which conditions a wind propulsion could actually provide (part of) the ship propulsion. If this is indeed the case then the Minimum Power Requirement could be seen as conservative. However, that ships can generally be safe in a wind and wave heading where the wind propulsion can be used effectively is something that has not been demonstrated by research.

4.5.3.6 Safe Return to Port

The safe return to port requirement is defined in SOLAS [19] II-2 regulation 21 (Regulation 21 - Casualty threshold, safe return to port and safe areas), article 4, however specific guidance is given in explanatory notes MSC.1/Circ.1369 (2010). The requirement applies to passenger vessels of 120m in length or above. Such ships should have double engine rooms and/or propulsion rooms. In case one engine room or propulsion room is disabled and one of the propeller shafts or propulsion units becomes blocked, the ship should still be able to reach the nearest port while sailing through demanding wind and sea conditions. A minimum speed of 6 knots while heading into Beaufort 8 weather and corresponding sea conditions is recommended to show compliance. As this regulation accounts for windage in head wind, similarly like for the minimum propulsion requirement, any additional windage due to wind propulsion systems that cannot be completely retracted is to be accounted for. Therefore it is judged that the regulation does properly account for the impact of a wind propulsion system on performance in head wind.

A similar comment can be made as for the Minimum Power Requirement. If in the future it could be demonstrated that ships can be safe and reach port without needing to keep a minimum ship speed only in head wind and sea then, potentially, the wind propulsion system could help rather than only increase windage when it cannot fully be retracted.

4.5.4 Class rules

Class societies also commonly set requirements on the topics described above or they provide their own interpretations. However, in the overview here, focus is given on topics that are only addressed by class societies and not by IMO. Documents from the following class societies were considered to prepare the summary below: American Bureau of Shipping (2022) ,Bureau Veritas (2021), ClassNK (2023), Det Norske Veritas (2023), Lloyd's Register (2023a), (2023b). Except for DNV, the referenced documents concern dedicated rules for wind propulsion. Though the general rules from these organisations may also impact wind propulsion. In the cases of Class NK and Lloyd's Register the wind propulsion specific documents include only guidelines, e.g. they are not mandatory. The other referenced class societies have mandatory rules and regulations. In either case, guidelines or rules may not still cover all eventualities. Thus, custom processes may be required, such as Failure Mode and Effects Analysis (FMEA), Hazard Identification (HAZID) or Hazard and Operability Study (HAZOP). Using such procedures class may ascertain that a ship is safe, without having dedicated firm rules & regulations for a specific design feature.

4.5.4.1 Loads

Loads (and structural response) is a topic generally addressed by class. Although the elaboration is different per class, generally load cases are defined for:

- Wind load, by deriving the maximum wind load with the wind propulsion in operation and also when it's inactive
- Inertia loads (heel and ship motions)
- Green water loads

Subsequently it must be checked that the structure can cope with it considering various failure modes, including also fatigue. The rules & guidance generally includes methods to estimate the loads. However, it may be interesting to get this information from testing. Obtaining inertia loads for instance may be done using model tests. Testing methods have not been specified.

4.5.4.2 Machinery systems and control

So far in classification rules, wind propulsion has been purely treated as assistance in propulsion. The propeller propulsion is still there. Therefore the operability of wind propulsion is not a safety requirement. Redundancy to always have wind propulsion is not required. Nevertheless, the instrumentation of wind propulsion systems is subject to specific requirements. Nevertheless, the hydro- and aero dynamic testing doesn't seem to be directly relevant for these requirements.

4.5.5 Potential owner criteria or new formal regulations

It is identified that wind propulsion may trigger some behaviour that is undesirable but for which there are no accepted criteria. They have been identified already in section 4.5.3.2. In the feature we may see that either owners can up with their own criteria or that formalised criteria are developed.

4.5.5.1 Heel

Heel has an impact on stability. Although interpretation may be required, this is handled in the rules discussed in section 4.5.3.2. Heel may also have an effect on loads on the ship and cargo and this should also be accounted for, principally in class rules as discussed in 4.5.4.1.

But heel can have other impacts that are not covered by existing criteria. For instance, crew and passenger comfort may be decreased. Further specific systems on board may not function with large heel angles. We are considering here the (quasi-) steady heel. However, the impact is realised generally in combination with oscillatory heel due to waves.

We see in some publications that heel thresholds are used. Though, a clear rule or converged value, even for specific ship types, could not be identified. Though there are some (proposed) criteria for other applications that could give some reference:

- RINA (2012) proposed a maximum heel angle of 10 degrees for the steady part of a turning circle
- Dallinga and Bos (2010) derive a maximum "Effective Gravity Angle" (equivalent to heel in steady conditions) of 9 deg for naval staff and they suggest it should be about half for passengers that are not trained
- As identified also by Dallinga and Bos the ITTC (1999) suggested a maximum lateral acceleration of 0.8 m/s2 onboard high speed craft. This corresponds to about 4.6 deg of heel.

These references suggest a threshold in the range of about 5 to 10 deg. However, the higher side of that is really intended for trained crew and a temporary situation in a turning circle. They may therefore be judged as high. Although this report does not claim that it is well verified for the specific application of wind propulsion, a threshold maximum heel angle of 5 deg may be reasonable as a first reference. It is however expected that actual thresholds considered in projects will be adjusted to the specific ship type and operations. For instance, on a cruise ship, where untrained individuals are on board and comfort is paramount, a much lower threshold is expected.

4.5.5.2 Yaw and/or rudder angles

As discussed in section 4.5.2, wind propulsion may lead to larger yaw oscillations. At some point, controllability may be decreased as a result. Depending on control settings, the rudder gear needs to work harder, leading to more wear. It is not yet understood if and how problematic these changes in behaviour are, but it can be imagined that in the future owners will set criteria on the maximum variability of yaw and/or rudder angle.

4.5.5.3 Manoeuvring in port or laying at anchor

As discussed in section 4.5.2.5, due to increased windage, the maximum forces delivered by tug(s), tunnel thrusters and/or mooring equipment may need to be increased. How an owner will deal with this likely varies. In some cases the impact of increased windage may be well within the capabilities of the ship and port. Nevertheless, in other cases some increase cost may need to be anticipated. Operational cost for tugs of higher capacity or numbers or a larger investment in transverse tunnel thrusters.

A common indicator to describe how well ships can berth is the crabbing capability as for instance described by Ferrari et al (2018). The indicator is effectively the maximum wind speed that can be sustained at all wind angles when berthing. An example from Ferrari et al is shown in Figure 23. When an owner specifies that the same wind speed must be sustained for a ship with wind propulsion, then an increase in windage will be compensated for by specifying larger capacity tunnel thrusters (and/or tugs).

It is unknown to the owners how owners may specify criteria for increased anchor loads and yaw instability that could occur at anchor.

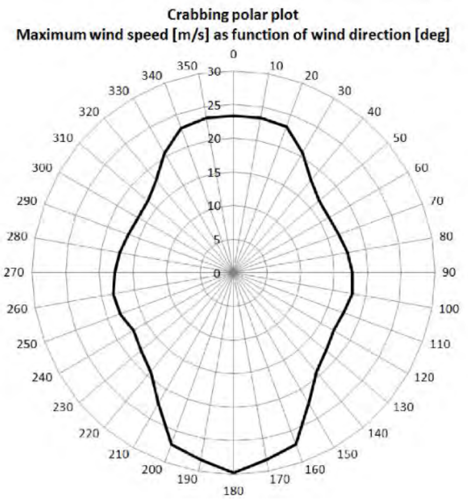

Figure 23: Crabbing capability plot from Ferrari et al (2018)

4.5.6 Testing and simulation methods

4.5.6.1 Simulations

4.5.6.2 Calculations on desktop and HPC

Whereas high fidelity simulations, at the level of CFD, have been shown for sailing yachts in waves, e.g. Mazas et al (2017) and Azcueta (2002), it is judged that this technology is not yet ready for a comprehensive analysis of safety and operability on its own. Assessing safety and operability requires a large amount of simulations with many degrees of freedom involved. The degrees of freedom do not only relate to motions of the vessel, but also the environment conditions, including several parameters for wind, wind sea, swell and potentially current. Long time traces are also required to derive statistics with sufficient certainty for seakeeping. The time (and cost) involved to resolving a full assessment is generally too high for running CFD. Nevertheless, these methods can be highly valuable for assessment of specific conditions. The simplified methods as discussed below are generally constrained to first order forces and motions strictly following a linear relation to wave height and second order forces a quadratic relationship, which are both simplifications. CFD does away with such assumptions.

For good reason, research on simulations has so far also focussed on simplified methods.

Kjellberg (2022) provides an extensive description of time domain simulations. In summary, the hydrodynamics is simulated in potential flow, with viscous corrections. The aerodynamics is simulated using a stripwise approach akin to lifting line. Whereas the principal objective was to verify fatigue loads in the rigs, the same calculation approach can deal with all kinds of manoeuvring and seakeeping scenarios. Hydrodynamic “manoeuvring” coefficients need to be prepared in advance as well as the stripwise aerodynamic forces.

Eggers and Kisjes (2023) and Kisjes and Eggers (2023) also documented manoeuvring simulations. For manoeuvring their approach is similar. It is based on pre-processed manoeuvring coefficients. The aerodynamics are implemented using coefficients just using the wind conditions at the centre of effort height of the rig(s). Although not documented in the publication, when modelling seakeeping, the MARIN methods rely on pre-processing to model wave excitation, radiation and damping using calculations in the frequency domain with a Boundary Element Method.

4.5.6.3 Bridge simulations

Vahs (2019) published on bridge simulations with wind propulsion. The Flettner rotor forces were accounted for in the simulations, although no detailed description is given on the methods. Manoeuvring simulations were conducted.

4.5.6.4 Model tests in wind tunnels

Quite some publications are available on wind tunnel tests with individual wind propulsion units up till complete ships with wind propulsion. However, no publications are known where the emphasis was on safety issues. The general focus is on steady forces as input to performance predictions. The data generally does allow to assess the loads against structural limits. However, as these are only the steady loads, it is likely not the full answer. It is known that tests have been conducted with dynamics, such as wind gusts, however these are not yet published.

For sailing yachts, experiments are known with some dynamics, such as by Fossati and Muggiasca (2011). They put a sailing yacht model with rigid sails on a set-up that culd make pitching motions. The methods used there could be used also for ships and systems deployed in merchant shipping.

4.5.6.5 Model tests in basins

Various approaches have been used to model wind propulsion in a model test basin with waves. It appears that modelling wind in the experiment itself is very challenging as described below. An approach where a simulation is running the loop (SiL) to calculate aerodynamic forces in real time seems to be preferred amongst several tests institutes. However, there are differences in the tools used to apply aerodynamic loads, e.g. winches versus wind fans. Relative advantages of one method over another are not yet clear. Details are described in the sections below.

4.5.6.6 A wind tunnel in the basin

Eggers and Kisjes (2019) fitted a (simplified) wind tunnel in a wave basin, to model both the aerodynamics and hydrodynamics experimentally. As also discussed by Gerhadt et al (2021), in such an approach it is impossible to satisfy similarity on Froude number and Reynolds number simultaneously. It has not yet been ascertained how important it is for the end result. In wind tunnels it is accepted practice to run wind tunnel experiments not at the Reynolds number of the actual application. However, assuming that some corrections are necessary, these are not trivial to apply. Moreover, the experiments by Eggers and Kisjes showed that on average the target wind conditions could be achieved in the centre of test section. However, there were deviations outside that centre. These could not be avoided with disturbances from the openings in the test section that were still required to run the tests. In order to create a better wind field throughout the test section, the section would need to be closed of further and likely more wind fans would need to be used. This would drive up the time (and cost) required for such experiments substantially. The method may have value in case the aerodynamic properties are not known and they are to be determined in the combined experiment itself. However, in general it appears to be more practical to apply aerodynamic forces using a numerical model using the methods described in sections 4.5.6.8 or 4.5.6.8. Nevertheless, experiments were done using the simplified wind tunnel, as shown in Figure 24. Results are discussed in section 4.5.2.1.

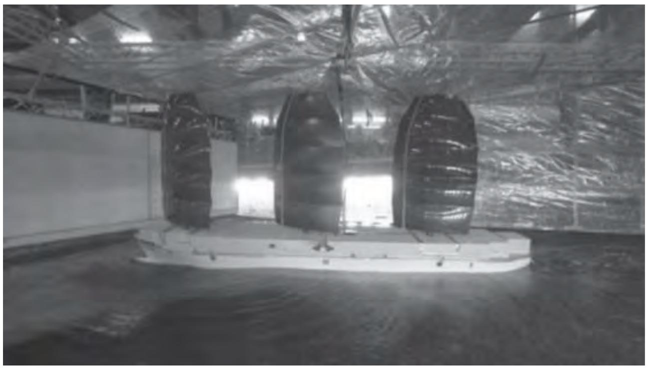

Figure 24: Coaster with Dynarigs in simplified wind tunnel in wave basin (Eggers and Kisjes, 2019)

4.5.6.7 Numerical aerodynamic loads applied using winches

Eggers (2018) demonstrated free running tests with winches on a sailing yacht. The same test set-up is in use for merchant ships with wind propulsion at MARIN. The aerodynamic loads are modelled dynamically in the (ship fixed) sway and surge directions using two winches. This is done using an adjustment in height of the winches on the carriage to an expected average heel angle per test. The connection point on the model is in the aerodynamic centre of effort. Assuming that this aerodynamic centre of effort remains constant throughout a test, the pitch moment and heeling moment are also modelled correctly. A third winch is used to correct for viscous scale effects, pulling strictly from the bow. The set-up is extendable with more winches, allowing more degrees of freedom to be modelled dynamically.

Sauder and Alterskjær (2022) have conducted experiments with a free running model using an advanced winch system named Cable-Driven Parallel Robots, essentially also a combination of multiple winches. Using 6 winches allows to dynamically apply forces in 5 degrees of freedom (only heave excluded). Assumptions on centre of effort are not necessary. Tests were run in calm water, but using a variation of wind conditions, including a spectrum. The tests showed that the target forces could be applied accurately.

4.5.6.8 Numerical aerodynamic loads applied using wind fans

Gauvain (2019) published on an unrestrained test set-up to apply aerodynamic loads for a yacht sailing in waves or manoeuvring. Although results are shown for a yacht as illustrated in, the set-up should also be suitable for merchant vessels. The set-up includes a mast with a single fan. With a possibility to rotate the fan on the mast manually, the proportion of surge and side force can be adjusted in between tests. It is not mentioned whether yaw moment can be varied, but this is assumed to be the case by moving the position of the mast in the model. A particular point of attention in the test set-up was to eliminate any connection to the carriage, thereby eliminating and unwanted influence from such connections.

Gerhardt et al (2021) published on manoeuvring and seakeeping tests with a wind powered car carrier. As opposed to using winches, air screws (fans) were used to impose aerodynamic loads. The set-up allowed to dynamically model forces in surge, sway and yaw moments. The publication discusses various options to apply aerodynamic loads and reflects on the impossibility to adhere to all scaling/similitude laws when real wind is used in the basin test. Viscous scale corrections are described in an accompanying paper by Giovanetti et al (2022).

4.5.6.9 Onboard trials and monitoring

A modest amount of publications is available on onboard trials an monitoring. However, also, on this topic, the emphasis is on (quasi-steady) performance measurements. No publications are known with an assessment concerning operability or safety.

4.5.7 Summary

The emphasis in research and projects directly for industry has mostly been on steady equilibrium conditions, which are directly relevant for performance, but are less relevant for operability and safety. This is evident both in regulations as well as methods to verify safety, operability and compliance.

There is a gap in regulations. These are presently dealt with for a large part within custom HAZID and HAZOP studies. As experience is gained with operation of ships with wind propulsion, it is expected that more rule or risk-based guidance will be specified.

New or existing assessment methods are trialled mainly in (subsidised) research studies. Some methods show good potential and it is expected that with their continued use, a convergence and refinement will be seen in the methods that are used.

4.6 Investigate the effect on propulsive factors due to reduced propeller load arising from the use of wind power.

The goal of this ToR is to investigate the effect on propulsive factors due to reduced propeller load arising from the use of wind power, identify the effects of wind propulsion on the propulsion system, e.g. pressure side cavitation occurrence and liaise with Resistance and Propulsion Committee and SC on Cavitation and Noise.

4.6.1 State of the art of effect on propulsive factors for wind propulsion ships

The research about effect on propulsive factors due to reduced propeller loading for wind propulsion ships has been few. Many researches have focused on propeller overloading due to added resistance by waves because of IMO regulations on EEDI (Energy Efficiency Design Index) and minimum propulsion power in adverse weather.

Propulsive factors like as wake fraction (w), thrust deduction factor (t) and propulsion efficiency (η_D) should be investigated for wind propulsion ships. Wind propulsion ship in steady state navigation has been in reduced propeller loading, drift angle, heel angle, wind and wave conditions.

Sauder & Alterskjaer(2022) carried out free running tests where real-time sail loads interact by Cable-Driven Parallel Robots. The target ship was SOBC-1(SINTEF Ocean Bulk Carrier-1, Lpp=190m), 4 rotor sails (height=35m, diameter=5m, top end plate diameter=6m), and all rotor sails are located on the ship's centreline. Figure 25 shows propulsive factors as a function of the true wind direction(TWD) and true wind speed(TWS). Vessel sails towards North. TWS = 10, 15, 20 m/s are represented in black, blue and red, respectively. The dashed black reference line represents values for the case without rotor sails at vessel speed 12.25 knots.

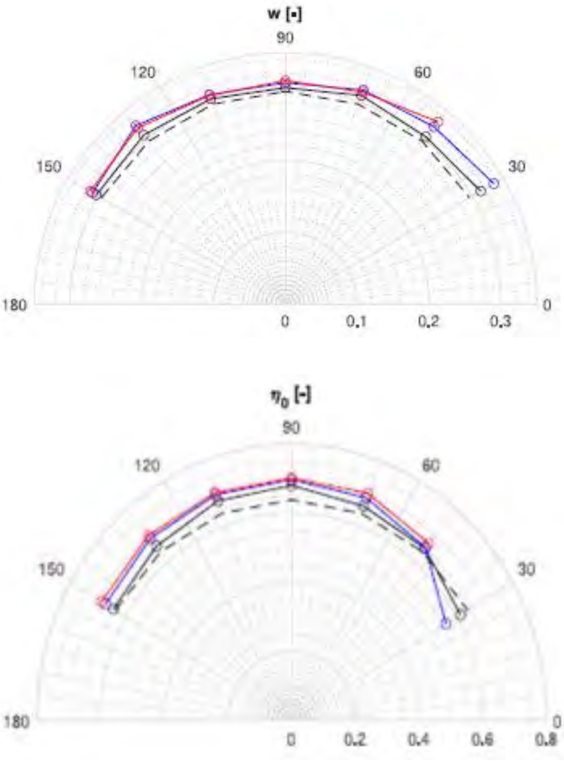

Figure 25. Propulsion parameters of model tests

Schot & Eggers(2019) studied on the effect of leeway(drift) angle on the propulsive factors by viscous flow calculation and captive model test. The predicted Taylor wake feaction(w_T) is compared with measured data for KVLCC2 in Figure 26.

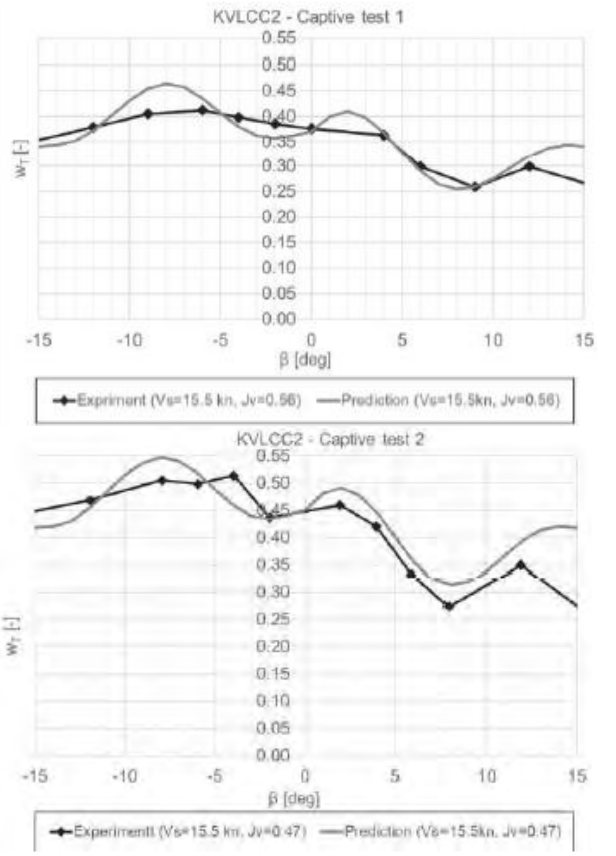

Figure 26. Comparison of the predicted wT and measured values for the two model tests campaigns on the KVLCC2

Yang et. al(2019) carried out CFD calculation for POW characteristics in oblique flows. Figure 27 shows the comparison results for Potsdam Propeller Test Case(PPTC).

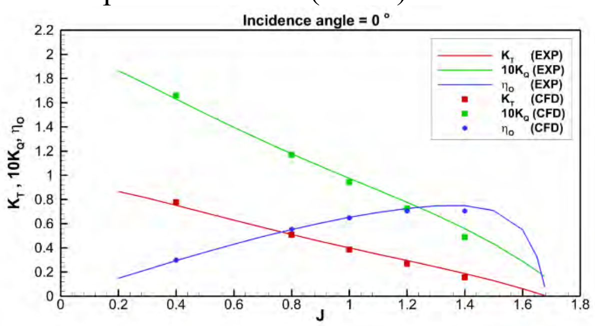

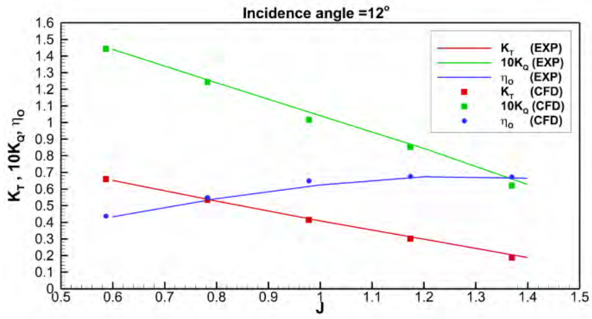

Figure 27. Comparison of POW curves for PPTC(Upper: incidence angle 0o, Lower: incidence angle 12°)

China(2018) proposed the thrust deduction factor and wake fraction at low speeds as t = 0.1 and w = 0.15 on IMO MEPC. (Figure 28)

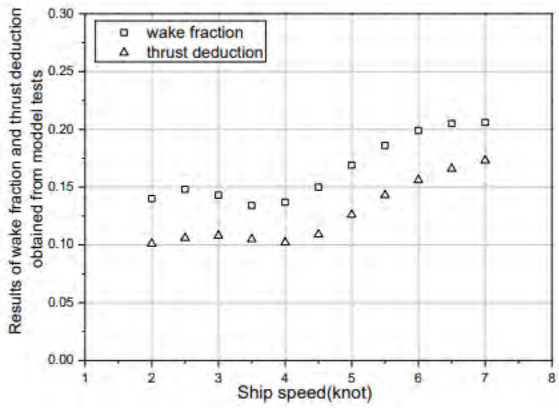

Figure 28. Model test results of wake fraction and thrust deduction at low speeds.

4.6.2 Modelling of propulsive factors for wind propulsion ships

With the steady state assumption the wind propulsion ship has drift (β) and heel angle. Manoeuvring mathematical model considers with drift angle for the modelling of wake fraction where POW test result is used to predict the wake fraction. POW test with drift angle can be carried out, but it is difficult to predict the inflow angle at the propeller position. However, the thrust deduction factor is kept constant value with the given speed for manoeuvring simulation. It is available to make a modelling of thrust deduction factor with drift angle.

Yasukawa & Yoshimura (2015) introduced the MMG mathematical model for manoeuvring simulation, and proposed several models for wake fraction with drift angle are as follows.

$$w_P/w_{P0} = \exp\left(-4\beta_P^2\right) \quad (1)$$

$$\frac{1-w_P}{1-w_{P0}} = 1 + C_1(\beta_P + C_2\beta_P|\beta_P|)^2 \quad (2)$$

$$\frac{1-w_P}{1-w_{P0}} = 1 + (1 - cos^2\beta_P)(1 - |\beta_P|) \quad (3)$$

$$\frac{1-w_P}{1-w_{P0}} = 1 + \{1 - \exp(-C_1|\beta_P|)\}(C_2 - 1) \quad (4)$$

$$\beta_P = \beta - x_P{}'r'$$

Where w_p is the wake fraction in manoeu-vring motion and wp_0 is the wake fraction in straight-line motion

In Figure 29 the analysis results of wake fac-tion with drift angles using Eq. (4) are shown.

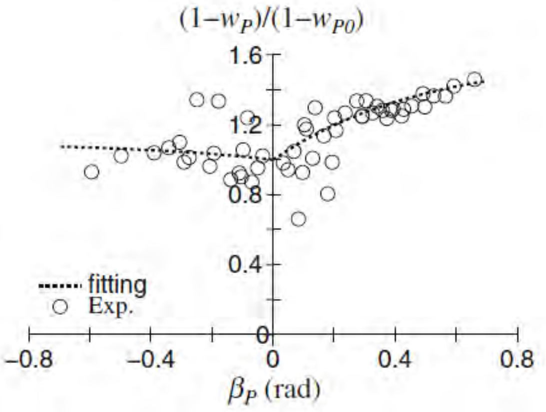

Figure 29. Analysis results of wake fraction in manoeu-vring motions for KVLCC2 model (Eq, (4))

4.6.3 Example of model test of effect on propulsive factors for wind propulsion ships

To investigate the propulsive factors in reduced propeller loading, model tests were carried out by Korea Research Institute of Ships and Ocean Engineering (KRISO). The Target ship is Ksupramax (KRISO Supramax class Bulk Carrier, Lpp=192m), and the test speed is 12 knots of real ship. The scale ratio of model ship is 26.087. Figure 30 shows the body plan and model ship of Ksupramax.

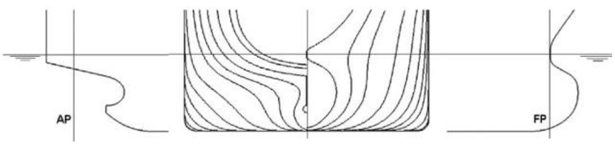

Figure 30: Body plan and model ship of Ksuparamx Bulk carrier

Two types of model test were carried out. One is load variation test, and the other is static drift test in reduced propeller loading condition. The wake fraction, thrust deduction factor and propulsive efficiency were analysed by ITTC Recommended Procedures and Guidelines 7.5-02-03-01.4. Wake fraction is obtained by thrust identity method and using POW data. Thrust deduction factor is obtained by using the measured thrust and resistance forces considering skin friction correction. Propulsive efficiency is obtained by using thrust deduction factor, measured propeller thrust force and torque.

4.6.3.1 Load variation test in reduced propeller loading

The loading conditions of load variation test on design draft condition is 50% ~ 130% of resistance force including skin friction correction, F_D. The photo of load variation test using self-propulsion test equipment is shown in Figure 31.

Figure 31: Photo of load variation test on design draft condition

The analysis results of propulsive factors are shown in Figure 32, Figure 33 and Figure 34.

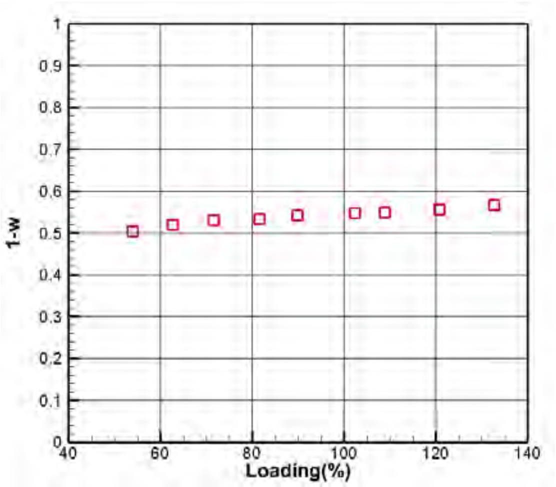

Figure 32: Analysis results of wake fraction with propeller loadings (design draft condition)

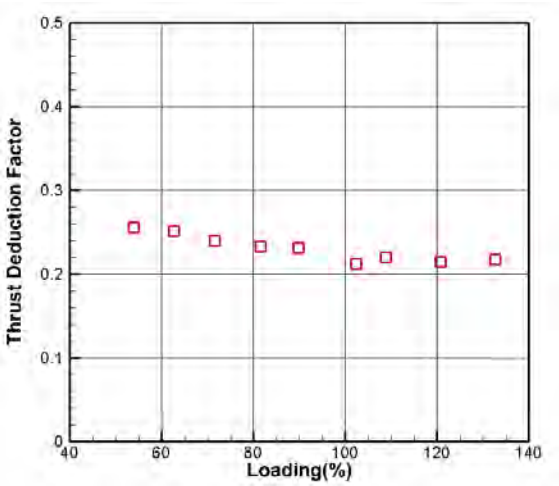

Figure 33: Analysis results of thrust deduction factor with propeller loadings (design draft condition)

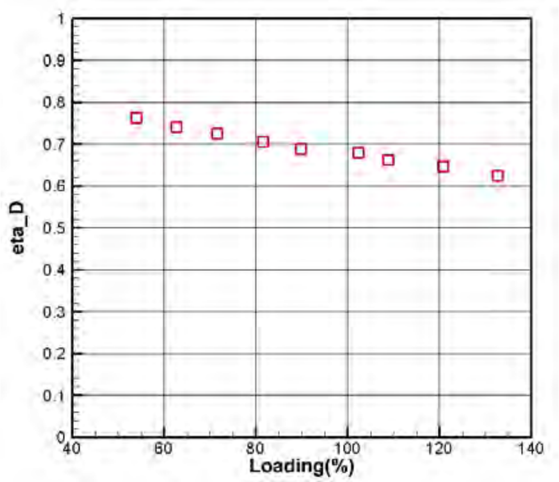

Figure 34: Analysis results of propulsive efficiency with propeller loadings (design draft condition)

4.6.3.2 Static drift test in reduced propeller loading

Static drift test in reduced propeller loading was carried out by planar motion mechanism (PMM) equipment of KRISO. Test speed of 12 knots of real ship on heavy ballast condition because of some problems of PMM system. The range of drift angles is -20° ~ + 20°, and propeller loading is at 60%, 80% and 100% of real ship's self propulsion point. Figure 35 shows the photo of static drift test.

Figure 35: Photo of static drift test on heavy ballast condition

Figure 36 to Figure 38 show the analysis results of wake fraction, thrust deduction factor and propulsive efficiency.

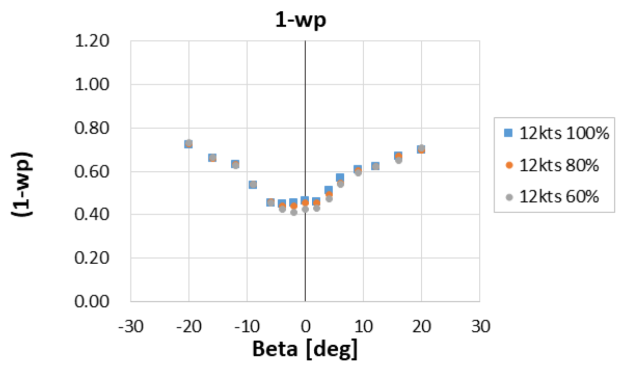

Figure 36: Analysis results of wake fraction with drift angles (heavy ballast condition)

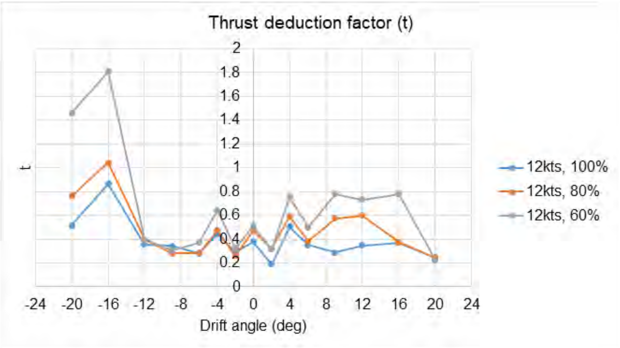

Figure 37: Analysis results of thrust deduction factor with drift angles (heavy ballast condition)

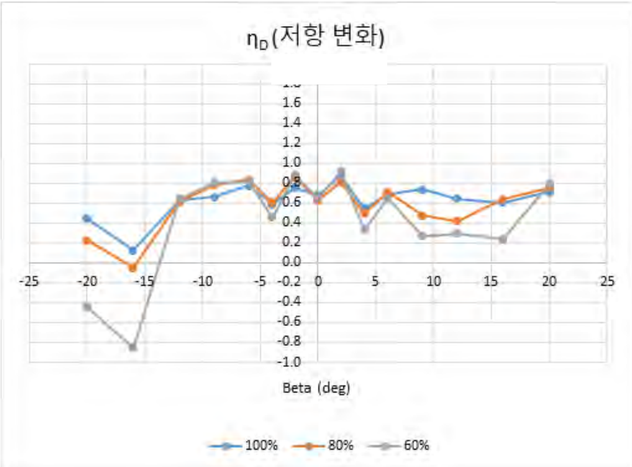

Figure 38: Analysis results of propulsive efficiency with drift angles (heavy ballast condition)

Wake fractions in several propeller loadings are fitted by Eq. (5), and the fitted result of 100% loading and manoeuvring coefficients are shown in Figure 39 and Table 10.

$$w_P/w_{P0} = \exp\left(-C_P v_P^2\right) \qquad (5)$$
$$v_P = v' + x_P{}'r'$$

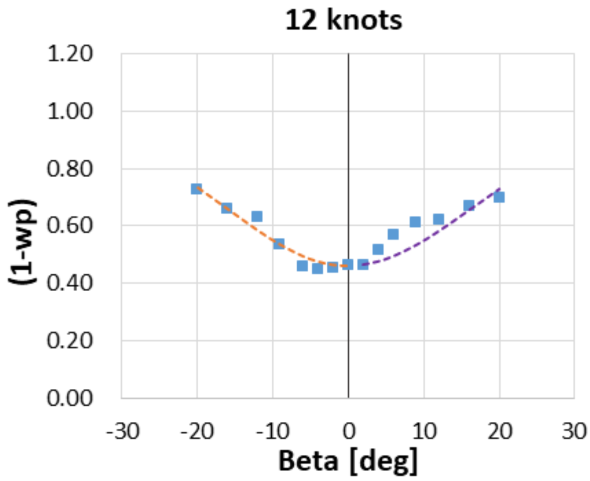

Figure 39: Fitted results of wake fraction by Eq. (5) (100% loading, 12 knots)

Table 10: Fitted results of wake fraction (Eq. (5))

	100% loading	80% loading	60% loading
C_P (for $+v_P$)	5.891	6.702	6.684
C_P (for $-v_P$)	6.019	6.236	6.989

The analysis of propulsive factors is proper, and the values of wake fraction are reasonable. But the values of thrust deduction factor and propulsive efficiency isn't acceptable. It is the reason that the measured propeller thrust and torque are appropriate values, but the X force measuring system of PMM of KRISO isn't appropriate to maintain the accuracy of X force. The X forces during static drift test in real ship's self-propulsion point are very small contrast to large capacity of X force gages because the X force measuring system of PMM should withstand the acceleration and deceleration forces during the tests. More accurate analysis of propulsive factors in manoeuvring motion, it is inevitable to use more accurate X force measuring system like as the clamp system for PMM.

Based on the experience reported above, the Committee recommends that for static drift test without accurate X force measurement system, the thrust deduction factor should be kept constant value obtained from self-propulsion test with given speed.

4.6.4 Liaise with other Committees

One of the goals of this ToR is to liaise with general committee on Resistance and Propulsion and specialist committee on Cavitation and Noise about the propulsive factors and reduced propeller loading.

The TOR 9 of the general committee on Resistance and Propulsion which is to update load variation test method in 7.5–02-03–01.4 "1978 ITTC Performance Prediction Method" taking into consideration a wider range of resistance and develop a new method if necessary, is related with this TOR. It is suggested that reduced propeller loading conditions (including 70%, 80% and 90% of resistance force) should be included in load variation test.

There is no related TOR of specialist committee on Cavitation and Noise. But it is necessary to investigate the pressure side cavitation occurrence, noise, vibration etc. in reduced propeller loading. The controllable pitch propeller (CPP) would be recommend to avoid the pressure side cavitation.

4.7 Cooperate with MEPC on the continuous development of the EEDI for wind propulsion ships. Liaise with Full Scale Ship Performance Committee

The Committee did not initiate action within this period to propose improvements to the Marine Environment Protection Committee (MEPC) in IMO. Until release of the ITTC guideline and procedure in September 2024, the only publicly available guideline for performance prediction for ships with wind propulsion is included in MEPC.1/Circ.896 as published in 2021. That guideline only serves to quantify the benefit of wind propulsion under EEDI and EEXI, which may justify that it does not necessarily need to achieve best accuracy. However, the Committee is of the opinion that there is substantial scope for improvement, even without increasing the effort for ship owners and their partners to follow the MEPC guideline. A submission for the 81th MEPC by IWSA and RINA (IMO, 2024, MEPC 81/INF.40), building on work by MARIN in the WiSP2 project illustrates how at present the specification of wind statistics does greatly influence the predicted savings. The submission illustrates that the benefit of the present specification can likely not be achieved in real operation. The submission also illustrates potential other methods to derive wind statics, which are more similar to what can be achieved in reality, without resorting the methods that were in place before 2021 (and that arguably disadvantaged wind propulsion). A follow-up specialist Committee, supported by R&D projects, may pick up this and other topics to deliver submissions to IMO's MEPC for adopting better guidance in MEPC.1/Circ.896.

4.8 Liaise with the Ocean Engineering Committee regarding their work on SiL and controllable fans to model wind loads.

We have unfortunately not been able to achieve any fruitful outcome in this task. We recommend that the next committee should focus more on sea keeping model test of wind powered ships in general.

5. PROCEDURES

This section describes the work done by the committee on tasks 4, 6 and 8 described in Section 3.

The work done in the other tasks (1, 2, 3, 5, 7, 9 and 10) can be found in “State of the Art” Section 4.

5.1 Proposed guidelines for performance predictions of wind assisted ships

The Specialist Committee for Wind Assisted and Wind Powered Ships under the 30th ITTC has prepared guidelines for prediction of power saving of wind propulsion technology. This section gives an outline of how the guideline is structured and how it connects to performance indicators.

In the process to derive common KPI's, several focus group meetings were held with industry stakeholder in cooperation with the International Wind Ship Association (IWSA) and the Interreg North Sea region project WASP. The proposed process was also presented at several international conferences in Europe and Korea (Werner 2022a, Werner 2022b). Furthermore, the Committee run several workshops with industry representatives, with the purpose to get feedback on the proposed method. The last workshop was held in February 2024, and the participants had received draft versions of the procedure beforehand. 18 organisations submitted in total 174 comments.

Some of the key pieces of feedback received from industry on the provisional version of the procedure document are listed below.

- The air density should as default have the value of 1.225 kg/m^3, equivalent to standard value for 15 deg, sea level.
- A standard value for power law exponent should be provided, but the user should in the end seek relevant documentation of the appropriate value for route to be studied.
- Uncertainty analysis and sensitivity analysis of all assumptions and models should be performed.
- Guidelines for route optimization should be further developed in future revisions

The proposed guideline is the first attempt to create a common ground and common terminology for expressing performance expectations of wind powered ships at design stage. It focuses on methodologies for predicting the power saving of a wind powered ship on a route at design stage, compared to the corresponding ship without wind propulsion. The guidelines give an overview of the type of methods that are suitable for the different stages of the ship design process, considering the balance of confidence level and computational cost. It is not the intention to provide detailed procedures. It is assumed that the organization conducting the predictions has relevant background knowledge and tools.

The guidelines are intended to be used by organizations conducting performance predictions for wind powered ships (e.g. consultants, yards, technology providers). They are also intended to be used indirectly by all stakeholders who need to discuss the resulting performance indicators (e.g. ship owners, operators, investors). By providing standard indicators that are linked to prediction procedures of varying confidence levels, the guidelines aim to provide a common terminology for all stakeholders.

The guidelines are mainly applicable to cargo vessels with wind assistance technology (moderate size of wind propulsion), although they can to some extent be applied to vessels with primary wind propulsion. Sailing yachts, racing boats or traditional sailing vessels are not in the scope.

The focus of the guidelines is the relative performance of wind assisted ships, i.e. the power saving relative to the same ship with conventional motor propulsion. The industry today still sees the conventional motorship as the benchmark which the business case for novel technologies relate to. However, this perspective may change in future versions. It is expected that the guidelines will be updated frequently the coming years as the knowledge and tools in the industry develops.

Deriving the expected fuel saving from a wind propulsion solution involves four principal steps:

1. Generating background data. (Towing tank tests, wind tunnel experiments, CFD simulations).
2. Generating models from the background data, which describes the sub-systems response to a changed of state. For example, describing the aerodynamic force of a sails in different wind angles.
3. Deriving steady state force equilibrium with Velocity Prediction Programs (VPPs) or Performance Pre-diction Programs (PPPs).

- Route studies, where the variation of environmental conditions that the vessel will meet on a route is combined with the static performance model to derive the expected average power or energy saving due to the wind propulsion.

Predictions of the power savings from wind propulsion systems are used at various stages of the design process, from initial assessments to final performance expectation. The guidelines are arranged into various levels of accuracy to meet the specific needs, requirements, and availability of data of each stage. The fidelity and the required efforts increase with increasing level. An overview is given in Table 11, the complete table is found in the guideline.

Table 11: Overview of methods for prediction of power sav-ing of wind propulsion technologies

	Level 0	Level I	Level II	Level III	Level IV
Applicability ->	**WPS rated power**	**Early idea**	**Early business case assessment**	**Business case & Performance expectation**	**Advanced Business case & Performance expectation**
Force balance	1DOF	1DOF	3-4DOF	4DOF	4 DOF (at least)
Aerodynamics	Specific	Generic	Low/Mid fidelity*)	High fidelity**)	High fidelity
Hydrodynamics		Generic	Low/Mid fidelity	High fidelity	High fidelity
Machinery interaction			Generic SFOC + limitations	Specific SFOC + limitations	Specific SFOC + limitations
Weather on the route		EEDI or intended route	Intended route	Intended route	Intended route or weather routing
					Optional effects: e.g. ship motions and varying wind energy management optimisation

*) Low/Mid fidelity methods can be for example high fidelity data or regression models from similar cases, or case specific lifting line methods

**) High fidelity refers to case specific CFD, model test or full-scale test.

5.2 Derive performance indicators for comparing the performance of wind propulsion at design stage.

The maritime wind propulsion industry is evolving rapidly, and many new wind propulsion technologies have emerged on the market. All these technologies have their specific strengths and weaknesses, which need to be assessed and quantified when selecting a WPT for a particular application. The wind propulsion community has, however, up to now not agreed on common key performance indicators (KPI). Some technologies are described using aerodynamic coefficients, others by e.g. expected fuel savings. Percentage saving figures are commonly used, but it is often unclear what is included in the comparison. This complicates comparing technologies, puts the level playing field at risk, and delays investment decisions.

Before this background the 29th ITTC Specialist Committee for Wind Assisted Ships co-operated with the Interreg North Sea region project WASP and the International Wind Ship Association (IWSA) to develop and propose KPIs for wind-assisted ships. As part of this effort, several focus group meetings were held during the autumn of 2022. These online workshops were open to all stakeholders from the wind propulsion community and aimed at sharing ideas and discussing implications of various KPI alternatives. Figure 40 summarises and groups the participants.

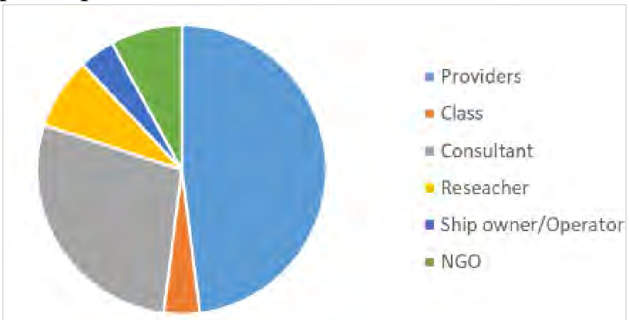

Figure 40: ITTC, IWSA and the WASP project hosted focus group meetings with the industry aiming for deriving harmonised KPIs. The participants affiliation business types are show the graph.

A summary of the considerations and recommendations from the Committee is given here. More details are given by Werner et.al (2023).

The industry focus groups indicated that the need from the industry can be summarised as:

- It would be helpful to have a set of agreed KPIs, especially for expressing ship specific fuel saving potential in the business case and procurement phase.
- KPIs that will be communicated to ship owners and operators should be tangible to their business.
- It would be useful if the KPIs reflect the prediction method used to derive the value.
- It would be useful to have a set of KPI definitions that is consistent and can accompany the ship design process from early concept stage to operation stage, gradually adding more and more complexity.

5.2.1 Recommended KPIs for Stand-alone wind propulsion units

Indicators in this category should describe the characteristics of wind propulsion units alone, without considering a ship. The Committee concluded the following recommendations:

- Nondimensional stand-alone coefficients are useful to understand the characteristics of a WPT but not directly the fuel saving potential. This is relevant for experts working with the design or assessment of wind powered ships. However, it should not be the first choice when communicating performance with community in general.
- There is no single nondimensional coefficient that describes all the important characteristics of a WPT. The best demonstration of the complete picture is a power coefficient curve over apparent wind angle.
- In the early concept phase, when scanning the market and shortlisting possible devices, it could be convenient to have easy, ship independent indicator of a unit size or its power. This could be achieved via a nominal or “rated” power derived in the same way as the “f_{eff}*P_{eff}” in MEPC.1/Circ.815 (2013)

$$Rated\ WPU\ Power_{10} =$$

$$\sum_{i,j}^{n,m} \left[\frac{F_x \cdot V_s}{\eta_D} - PTI\right]_{i,j} \text{ x } [\mathrm{W}_{i,j}] \tag{6}$$

where

$\mathrm{W}_{i,j}$ is the EEDI weather matrix (pre-2021)
η_D=0.7
F_x is the force matrix at the corresponding wind
V_s=10 knots

PTI is the power required by the wind propulsion unit (eg spinning a rotor)

Rated power values for other standard ship speeds (e.g. 15 and 20 knots) can be worked out in a similar way

This KPI is one way to describe a device while including the size. It is a theoretical number and gives an indication of a unit's theoretical potential. It should be understood that it this ignores the effects of aerodynamic side forces and that the propulsive efficiency, η_D may be different for a specific ship.

It is important that Standard conditions for nondimensional KPIs are defined by for example ITTC. That could be:

- Uniform/rectangular wind profile
- Area A defined as projected/planform area of WPT
- Standard air density of 1.225 kg/m3

5.2.2 Recommended KPIs for Performance expectation and business case input

The purpose of this type of indicators is to communicate a realistic expectation of the saving potential from a WPT. They are typically used as decision support for business cases, or for agreements between commercial stakeholders.

<u>Power saving, fuel saving, energy saving or CO_2 saving?</u>

The saving due to a WPT in absolute terms can be expressed either as power, fuel, energy, or CO_2 saving. While this choice will not affect the ranking between the WPTs for the same ship it can make a difference in how far a KPI resonates with different stakeholders of the shipping industry. Owners and operators tend to think in tonnes of bunker per day, engineers are more familiar power or energy-based numbers, lawmakers will mostly focus on CO_2 savings.

If we consider ships with conventional diesel engines and power saving for constant operational speeds, then there is an almost linear relation between the predicted power, fuel, and energy savings. This allows for an easy conversion between the savings expressions by simply post-processing route simulation results. For hybrid propulsion systems, and if routing and speed optimisation are included, the relation is not that so straight forward and must be modelled within in the voyage simulations. Some of the advantages and disadvantages of the various units for savings are summarised below. These points were raised during discussions with industry stakeholders.

5.2.3 Fuel saving

Definition: difference in fuel consumption between ship with WPT and without WPT for same route and speed.

Comments from industry focus group:

- Ship owners can relate to fuel (tons/day and kg/h).
- Tons/miles makes it easier to scale to different routes.
- Can be used in a transition period when HFO is still the standard in shipping.
- Need modelling of machinery efficiency, or stipulate fixed specific fuel oil consumption (SFOC).
- Not easy for hybrid propulsion systems.

5.2.4 Energy saving

Definition: difference in energy (=propulsion power x time on route) between ship with WPT and without WPT for same route and speed.

Comments from industry focus group:

- Using propulsion energy instead of fuel allows to leave out engine efficiency.
- For specific cases ship owners can translate to fuel themselves.

- More future proof considering future fuels.

5.2.5 CO_2 savings/ CO_2s avoided

Definition: difference in CO2 (=fuel x conversion factor) between ship with WPT and without WPT for same route and speed.

Comments from industry focus group:

- Parameter assessed in EEDI, CII and emission trading schemes like EU-ETS.
- Of interest to the wider society.

5.2.6 Power saving

Definition: difference in propulsion power between ship with WPT and without WPT for same route and speed.

Comments from industry focus group:

- Propulsion power is a measure that both yards, designers, ship owners and operators are familiar with.
- It does not require any modelling of engine efficiency or assumptions of fuels and hybrid propulsion.
- WPT providers do not always have information on the details of the propulsion system or engine efficiency. In this case the power makes for safe option for the saving prediction.

Considering these pro and cons, it appears that "power savings" are the most feasible way of expressing WPT performance and are also a concept that is familiar to owners and operators. However, nothing prevents showing them all in a prediction report.

5.2.7 Percentage

The percentage fuel saving is the most common KPI in communications around wind propulsion today.

The ship's propulsion power when employing the WPT is compared to the propulsion power when there is no WPT, for the same sea leg and same speed:

$$\Delta P\% = \frac{P_{no\,WPT} - P_{with\,WPT}}{P_{no\,WPT}} \quad (7)$$

One could think that a percentage saving is a clear KPI that can be used for comparison between different installations, since it is nondimensional. Very often, percentage saving claims are published without any further description of the specific cases. This is, however, a problematic approach.

The first issue is to *what* the savings have been related to, i.e. what number to have in the denominator. The calm water power, or power including sea margin, and should we use the fuel consumption for propulsion of the total fuel consumption including electric generation, harbour operation etc? That can change the KPI [%] by several %-units. Moreover, the percentage saving figure is very sensitive to ship speed. A higher ship speed gives much reduced %-saving. Thus, a percentage saving number, taken out if its context, may be misleading. A percentage number gives the false impression that it can be universally compared with other percentage saving predictions. For the reasons addressed here, many of the industry partners participating in the study are sceptical of using this KPI.

5.2.8 Power reduction

The performance of WPT could also be expressed as power reduction in kW, $\Delta P = P_{no\,WPT} - P_{with\,WPT}$. Several options for a standardised KPI related to ΔP were suggested by the industry partners involved in this study:

i. Max ΔP for TWS=10m/s (at the best wind direction)
ii. ΔP at a specified "design point" which could be for example TWS 10 m/s, TWA=60 deg
iii. ΔP at the most frequent weather

iv. ΔP on a given route, averaged over a year to include all season's weather
v. ΔP from the EEDI equation (pre or post 2021), but using weather statistics for an actual route

The advantage of option i) – iii) is that the prediction does not require any routing/voyage analysis tool. However, selecting one condition where ΔP is extracted can give large over or under predictions of the power reduction compared to the average saving on a route. The maximum ΔP gives also a misleading comparison between high lift versus high lift/drag devices. The same drawback is true for the option to derive ΔP at a specified "design point". Selecting the most frequent weather as the design point is completely misleading. The most frequent weather could well be head wind, where WPTs cannot even be employed. Figure 41 shows the comparison of three fictive wind propulsion technologies (WPT 1-3) fitted on the same ship, evaluated with the different suggested KPIs. The left most value is the Max ΔP for TWS=10m/s, which gives a very optimistic value compared to the result from the route analysis in the graph to the right. On the other hand, using the most frequent wind (third option in the left graph) gives over-pessimistic values (almost no saving). This shows that there is no way around using voyage simulations for deriving the power saving potential. The right graph shows the importance of conducting the analysis in the actual route, as the result is rather different for various routes.

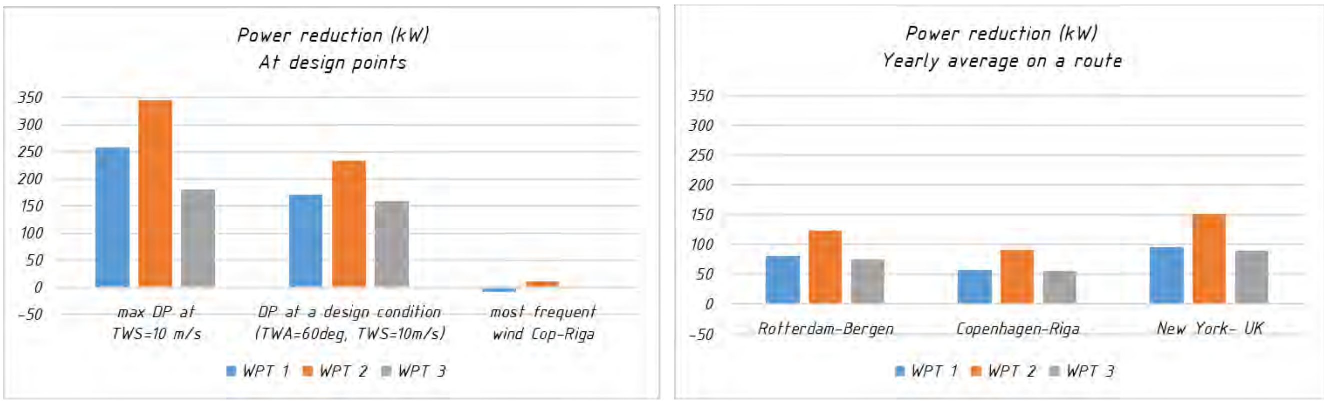

Figure 41: Example of how power saving can be computed in different ways, and different conditions, which results in different performance expectations. WPT 1, 2, 3 are fictive test cases.

5.2.9 Power Saving Potential (PSP)

No matter how accurate we try to model the power saving on a route, it is still a theoretical value. The real saving achieved in operation will depend on many practical aspects which cannot be foreseen in the predictions, such as maintenance time, changed route and speed, changed hull efficiency due to fouling, crew skill, function of the automated WPU control system, icing and wear. For this reason, it would be wise to denote the predicted ΔP the "Power Saving Potential". This will indicate that it is an ideal number derived under certain conditions. The PSP should be possible to verify during a short, controlled sea trial. After that, it is up to the owner, operator, and crew to use this potential in the best way.

5.2.9.1 Comparison of power saving

Some industry partners request that KPIs derived by different organisations should be truly comparable with each other also in terms of the derivation method. To ensure that all actors in the industry derive indicators that are truly comparable would require that some organisation could derive detailed procedures prescribing methods for CFD simulations and wind tunnel test. This is not a feasible solution. A true "apple to apple" comparison can only be achieved if the same simulation platform is used for the cases to be compared. However, we believe that it would be an improvement compared to today's situation if the industry agreed on a number of KPIs that are linked to certain levels of confidence. This is reflected in the proposed Guidelines for performance prediction, see section 5.1.

5.3 Derivation of a procedure for full scale trial of wind propulsion ships

5.3.1 Considerations before deriving a sea trial method for wind propulsion

Verifying the performance of wind propulsion solutions is essential for both shipowners and technology providers. Even without contractual obligations, such verification provides valuable confirmation for investments. Shipowners benefit from knowing the actual performance, while technology providers can use the data to enhance their designs and promote the technology. Additionally, accurate performance models are crucial for routing and performance monitoring software.

The Committee was tasked to suggest a method to verify the power saving from wind propulsion technology. After discussions with the industry, the current requirement for a verification method was identified:

- A method that verifies the saving from wind propulsion technology, not the absolute power. This is currently how WPT systems are sold, contracted, and also how it is treated in EEDI.
- A method that is commercially feasible for all yards and providers.
- A method that is transparent and possible to check by external verifiers.
- A method that does not require complex calculations or advanced equipment.

Various alternative strategies where discussed. Published full-scale campaigns for wind assisted ships have mainly been based on long-term monitoring data, such as for m/v Viking Grace Paakkari (2019) and for m/v Maersk Pelican Paakkari (2020). An advantage of this type of data is that it reflects the variety of weather conditions and operational profile that the ship encounters, as well as the real operability factors like idling time due to maintenance, weather routing, and crew skills. A challenge of using long-term monitoring data to detect even moderate power savings is the large scatter of such data, together with difficulties to find a comparable reference period with all other conditions except the wind propulsion installation unchanged. The main disadvantage is, however, the long period of time that such campaign requires. This is both costly and impractical in a commercial context and for EEDI verification.

Another alternative could be to measure the thrust forces from the wind propulsion devices directly. This requires, however, very complex measurement techniques that is now mature today. Moreover, with this method, the increased drift, increased rudder angle, and effect on the propeller are not taken into account.

The Committee suggests instead a process based on short sea trial runs, with the wind propulsion device turned on and off. The procedure is summarised in the next section.

5.3.2 Summary of recommended procedure

This section gives a summary of the new ITTC 7.5-04-01-02 Recommended Procedure Sea trials for assessing the power saving from wind assisted propulsion.

Like a conventional speed trial, the wind propulsion sea trial consists of a series of short runs. The main difference to a conventional sea trial is that the outcome is not the absolute value of the speed-power curve, but the power reduction due to the wind propulsion system. The effect of the wind propulsion system is extracted by comparing speed and power of single runs with and without wind propulsion for the same wind condition. The measured speed difference is converted to a power difference using the shape of the speed power curve and with some corrections for speed differences.

The minimum test program includes 5 wind conditions and can be conducted within one day. However, the scope can well be extended to include a larger number of conditions and can be conducted over a longer period during operation.

The signals to be measured are the same as for a normal speed-power sea trial: ship's speed, power, wind. In contrast to the normal procedures, the correction of current, which is usually done based on double runs, cannot be applied when wind propulsion is active. To overcome this, the speed is measured using the ship's log if the trial is conducted in a location which is known to be affected by tidal current. Since the purpose is to derive a speed difference, the relatively poor accuracy of the speed logs is acceptable.

The wind propulsion sea trial can be carried out at any wind conditions that gives sufficient driving force from the wind propulsion system, typically between Bf 4-7.

In the development of the procedures, the process was tested for five ships in the EU Interreg North Sea Region project WASP, and reported in Werner (2022).

Note that described procedure applies to ships with wind assisted propulsion, not primary wind powered ships.

The largest source of uncertainties probably originates from the measured wind. To minimise the uncertainty, it is recommended to use one, or even better, several, well calibrated, modern anemometers. However, it is unavoidable that the anemometers are disturbed by the superstructure, freeboard and WPS on the wind measurement. It is highly recommended if possible, to use a Lidar either to measure the wind at the trial, or to correct/calibrate the anemometer readings before the trial. CFD simulations can be used to find the most undisturbed position for the anemometer.

The uncertainty of wind propulsion sea trials is yet not fully investigated and document. It is recommended that the next Committee continue to improve the procedure and investigate the uncertainty.

5.3.3 How to apply the sea trial in contractual context

The wind propulsion sea trial verifies the power saving at one ship's speed, one wind speed, and a range of wind directions. It thus gives only spot check of the complete performance. To derive the total power saving potential for a given route or representative operational weather conditions, the sea trial needs to be combined with a performance prediction in the following manner:

1. The power saving is predicted according to ITTC 7.5-02-03-01.9 or for EEDI according to MEPC.1/Circ.896 sec 2.3 for all wind speeds, directions and relevant ship speeds.
2. The sea trial verifies the power saving for a limited number of wind conditions.
3. If the comparison between the predictions and the sea trial is satisfactory, the power saving for a given route or representative operational weather conditions can be calculated according to ITTC 7.5-02-03-01.9.
4. In case the comparison is not satisfactory, the provider of the prediction should give an updated prediction and a description of what has been modified. The changes should reflect all wind conditions in a reasonable way, not just the conditions tested in the sea trial.

The conventional motor-ship speed/power trial, which is conducted by shipyards before delivery of a new build ship, needs to be done in calm weather. It is very important to run the conventional speed/power trial as accurately as possible in calm weather. The introduction of wind propulsion systems should not be used as an excuse for performing the yard sea trial in heavier weather. Therefore, the wind propulsion sea trial needs to be done at a different occasion, when the wind conditions are suitable. If the wind condition is not suitable for wind propulsion sea trials at the time or location of delivery from a yard/retrofit site, it is suggested that the wind propulsion trial is conducted during service within an agreed period after delivery/installation.

The conventional speed/power trial procedure 7.5-04-01-01.1 do not need to be modified. In that trial, the ship is treated as a normal motor ship. This is the most useful and feasible way to treat wind assisted propulsion. If we in the future will build almost completely sailing vessels, there may be need for different approaches.

The proposed process was presented at several international conferences in Europe and Korea (Werner 2022a, Werner 2022b). The Committee also run several workshops with industry representatives, with the purpose to get feedback on the proposed method. The last workshop was held in February 2024, and the participants had received draft versions of the procedure beforehand. 18 organisations submitted in total 174 comments. Some of the key pieces of feedback received from industry on the provisional version of the procedure document are listed below.

- The instructions for the wind angle to be set during sea trial should be specific.
- The method of manoeuvring the ship during sea trial should be specified as either a constant heading or a constant course.
- It should be indicated how to determine whether a steady state is reached before measurement.
- The influence of errors in the electromagnetic logs for measuring ship speed on the results should be clarified.
- The acceptable difference in ship speed when a constant power condition is selected should be clarified.
- Clarify the rationale for the minimum wind speed conditions that are appropriate as sea trial conditions.
- Perform an uncertainty analysis and sensitivity analysis of all assumptions and models.

It is expected that the procedure will be updated ones more experience is gained. The uncertainty of the sea trial procedures, as well as the uncertainty of the performance predictions are still not well established. At current stage it is recommended to not yet use sea trials to confirm performance guarantees in a contractual context. However, it is strongly recommended to conduct sea trial of each wind propulsion installation to confirm the performance in a standardised manner.

6. CONCLUSIONS AND RECOMMENDATIONS TO THE 30TH ITTC

Wind propulsion for ships is a new area and it is developing quickly. Up to now, most wind installations are retro-fit ships with rather moderate wind assistance technology. A few ITTC members have been involved in research and commercial services related to wind propulsion, for example supporting ship owners with feasibility studies. The coming years, the interest in wind propulsion is expected to increase worldwide and there will likely be more new-built ships with very powerful wind installations. ITTC members can play an important role to support ship builders and ship designers in designing and assessing these new-built ships. Not only performance but also safety and regulation aspects will be important issues where ITTC members can contribute to the industry.

The 30th Specialist Committee on Wind Powered and Wind Assisted Ships has fulfilled all its TOR's except for one and produced two Procedures/Guidelines. Large efforts were spent on aligning these procedures and guidelines with the industry outside the ITTC. The development was presented at several public conferences and seminars. Several dedicated workshops were also held with technology providers, ship owners and designers.

The vast feed-back that the Committee received from the industry shows that there is a great interest in the coming procedures. Many stakeholders outside ITTC expressed their gratitude to our attempts. The young and developing industry seems to have lacked a common ground, and the new procedures fill a gap.

The Committee recommends to the full conference that the Specialist Committee is continued or even be turned into a permanent committee.

Producing two Procedures from scratch in a few years required large efforts. Although the procedures are complete, they can certainly be refined. More effort should be spent on scrutinizing every step and assumption. Thresholds and guides should be better motivated, and the uncertainty assessed.

The next committee should seek more closer cooperation with IMO, offering to assist with e.g. EEDI.

We also recommend wind tunnels to join ITTC and the SC.

The scope should be widened to include sea keeping and manoeuvring aspects. This is important when there will be very powerful wind powered ships being designed.

6.1 Future work

The Committee suggests the research community to study the following topics:

- Uncertainty analysis of sea trials for ships with wind assistance propulsion
- How to correct/calibrate anemometer with Lidar or CFD
- Sensitivity analysis of which wind statics is used in performance prediction on a route (source, year, duration)
- Effect of leeway and heel on propulsive efficiency determined with CFD. Validation and experience of different hull forms.
- Effect of leeway and heel on wave making and added resistance in waves
- Effect of reduced propeller flow on rudder
- The effect of wind propulsion on motions in waves, and conversely, the effects of motions on wind propulsion performance
- The effect of wind propulsion on manoeuvring
- The effect of control systems on performance, in relation to the actual wind experience by the WPU

7. REFERENCES

Abiven, N., Vautier, V., Cany, F., Fabre, J.B. and Rouxel-Duval, L. (2023). "Wind propulsion towards zero-emission cruise vessels". Wind Pro-pulsion ,16th – 17th February 2023, London, UK

American Bureau of Shipping, (2023). “Requirements for Wind Assisted Propulsion System Installation July 2022.”

Anonymous. (1870). "The City of Ragusa, two tons burden, now crossing the Atlantic". The Illustrated London News.

Ardhuin, F., Orfila, A., (2018), "Wind waves", New Frontiers in Operational Oceanography, Vol. 14, pp. 393-422.

Atlas, R., Hoffman, R., Ardizzone, J., Leidner, S., Jusem, J., Smith, D. and Gombos, D., (2011), “A cross-calibrated, multiplatform ocean surface wind velocity product for meteorological and oceanographic applications”, Bulletin of the American Meteorological Socie-ty, Vol. 92, pp. 157-174.

Azcueta, Rodrigo. (2002). “RANSE Simulations for Sailing Yachts Including Dynamic Sinkage & Trim and Unsteady Motions in Waves.” In High Performance Yacht Design Conference. Auckland, New Zealand: High Performance Yacht Design Conference.

Azcueta, R. and Ward, H. (2023). "Performance prediction of wind propulsion technologies via CFD" . Wind Propulsion ,16th – 17th February 2023,London, UK.

Babinsky, H. (2003). "How do wings work?" Physics Education 38(6).

Bureau Veritas. (2021). “Wind Propulsion Systems.”, NR 206 DT R01 E

Baptiste Cadalen, Fabien Griffon, Patrick Lanusse, Jocelyn Sabatier, Yves Parlier, (2018). "Modelling and control of a tethered kite in dynamic flight". Journal of Sailing Technology, Article 2018-03.© 2018, The Society of Naval Architects and Marine Engineers.

Bataille, J., Blayo, C. and Sergent, P. (2023). "Performance Methodology benchmark for wind assisted propulsion ship Performance estimation". International Conference on Wind Propulsion, 16-17 February 2023, London, UK.

Becker Marine Systems (2023). "Becker Marine Systems Joins Growing Wind Propulsion Family Of Technologies With Wingsail Project." from https://www.becker-marine-systems.com/news-media/beckers-wingsail-joins-growing-wind-propulsion-family.html.

Behrel, M.,Roncin, K., Leroux, J. Montel, F., Hascoët, R. (2018). "Application of phase averaging method for measuring kites performance: onshore results". Journal of Sailing Technology, The Society of Naval Architects and Marine Engineers, 2018, pp.2018-05. hal-01889988.

Blackford, B. (1985). "Optimal blade design for windmill boats and vehicles." Journal of ship research 29(02): 139-149.

Bigi, Nedeleg, Kostia Roncin, Jean-Baptiste Leroux, and Yves Parlier, (2020). "Ship Towed by Kite: Investigation of the Dynamic Coupling". Journal of Marine Science and Engineering 8, no. 7: 486. https://doi.org/10.3390/jmse8070486

Bitner-Gregersen, E. M., Eide, L. I., Hørte, T. (2013), “Ship and offshore structure design in climate change”, Springer.

Bøckmann, E. and S. Steen (2011). "Wind turbine propulsion of ships". Second international symposium on marine propulsors, Hamburg, Germany.

Bose, N. (2008). "Marine powering prediction and propulsors." The Society of Naval Architects and Marine Engineers, SNAME, ISBN: 0-939773-65-1.

Bound4Blue (2022). "eSAIL's Operational Principle}."https://bound4blue.com/esail/

Bordogna, G., Keuning, L., Huijsmans, R., Fossati, F. V., & Belloli, M. , (2016). "Validation of a simple aerodynamic model capable to pre-dict the interaction effects occuring between two generic wind propulsion systems". In R. H. M. Huijsmans (Ed.), Proceedings of the 12th Inter-national Conference on Hydrodynamics ICHD 2016

Bordogna, G. (2020). "Aerodynamics of wind-assisted ships: Interaction effects on the aerodynamic performance of multiple wind-propulsion systems". https://doi.org/10.4233/uuid:96eda9cd-3163-4c6b-9b9fe9fa329df071

Breukels, J., (2011). "An engineering methodology for kite design". Ph. D. Thesis, Delft Universityof Technology. URL: http://www.kitepower.eu/publications.html

Breukels, J., Schmehl, R., Ockels, W.J., (2013). "Aeroelastic Simulation of Flexible Membrane Wings based on Multibody System Dynamics". Airborne Wind Energy. U.Ahrens, M.Diehl, R.Schmehl(eds.), Springer, Heidelberg. doi: 10.1007/978-3-642-39965-7_16. http://www.kitepower.eu/publications.html

Cadalen, B., et al. (2018). "Modelling and control of a tethered kite in dynamic flight." Journal of Sailing Technology 3(01): 1--24.

Cairns, J., Vezza, M., Green, R., MacVicar, D. (2019). "Numerical and Experimental Comparison of Surface Pressures around a Scaled Ship Wind-Assisted Propulsion System".International Journal of Mechanical, Industrial and Aerospace Sciences.Vol:13, No:11, 2019.

Carter, R.A. (2012). "Watercraft." A companion to the archaeology of the ancient Near East: 347-372.

Carvalho, D., (2019), "An assessment of NASA's GMAO MERRA-2 reanalysis surface winds", Climate, Vol 32, pp. 8261-8281.

Charrier, B., et al. (1985). "Fondation Cousteau and windship propulsion 1980–1985 system Cousteau-Pechiney." Journal of wind engineering and industrial aerodynamics 20(1-3): 39-60.

Charrier, B. (2021). "Interactions between Two Flettner Rotors used for Wind Ship Assisted Propulsion". International Conference on Wind Propulsion, 15-16 September 2021, London, UK.

Chen, G., Chapron, B., Ezraty, R., Vandemark, D., (2002), "A global view of swell and wind sea climate in the ocean by satellite altimeter and scatterometer", Journal of Atmospheric and Oceanic Technology, Vol. 19, pp.1849-1859.

Chen W , Wang H , Liu X , (2023). "Experimental investigation of the aerodynamic performance of Flettner rotors for marine applications". Ocean engineering, 2023.

Chou, T. (2021). "A comeback of wind power in shipping: An economic and operational review on the wind-assisted ship propulsion technology." Sustainability 13(4): 1880.

ClassNK. (2023). "Guideline for Wind-Assisted Propulsion Systems for Ships (Edition 2.0).".

Climate Data Guide (2023), https://climatedataguide.ucar.edu/climate-data/ccmp-cross-calibrated-multi-platform-wind-vector-analysis (last accessed 20/04/2023)

Cooke Associates (2023). "Commercial History of the Walker Wing Sail." from http://www.cookeassociates.com/sports/commercial.php.

Craft, T.J. (2012). Back to the future: Flettner-Thom rotors for maritime propulsion?

Dadd, G. M. (2013). "Kite dynamics for ship propulsion." Engineering Environmental Science

Dallinga, R.P., and Bos, J.E., (2010). "Cruise Ship Seakeeping and Passenger Comfort." In HPAS. HPAS.

De Marco, A., Mancini, S., Pensa, C., Calise, G., DE luca, F., (2016). " Flettner rotor concept for marine applications: a systematic study" . Int. J. Rotating Machinery, 2016.

Dee, D., Uppala, S., Simmons, A., (2011), "The ERA-Interim reanalysis: configura-tion and performance of the data assimilation system", Quarterly Journal of the royal meteorological society, Vol. 137, pp. 553-597.

DNV. (2023). "Det Norske Veritas Rules and Standards.". https://rules.dnv.com/servicedocuments/dnvpm .

Duport, C., (2018) "Modeling with consideration of the fluid-structure interaction of the behavior under load of a kite for auxiliary traction of ships" (Doctoral dissertation, ENSTA Bretagne-École nationale supérieure de techniques avancées Bretagne).

Duport, Chloé & Leroux, J.-B & Roncin, Kostia & Jochum, C & Parlier, Yves. , (2016). "Comparison of 3d non-linear lifting line method calculations with 3D RANSE simulations and application to the prediction of the global load-ing on a cornering kite". Actes des 15èmes Journées del'Hydrodynamique. Available from http://website.ec-nantes.fr/actesjh/images/15JH/Articles/duport.pdf.

Duport, C., Leroux, J.B., Roncin, K., Jochum, C. and Parlier, Y. (2019). "Benchmarking of a 3D non-linear lifting line method against 3D RANSE simulations".. La Houille Blanche, (5-6), pp.70-73.

Dupuy, M., Letournel, L., Paakkari, V., Rongère, F.,Sarsila, S., Vuillermoz, L.(2023). "Weather Routing Benefit for Different Wind Propulsion Systems". The 6th International Conference on Innovation in High Performance Sailing Yachts and Wind-Assisted Ships, Lorient, France, May, 2023.

Dupuy, Maxime. (2023). "About the benefit of optimizing both speed and route in wind assisted ships multi-objective weather rout-ing". In: RINA Wind Propulsion Conference 2023.

Eça, V. Guilherme and M. Hoekstra, (2010). "Code Verification, Solution Verification, and Validation in RANS Solvers," Proceedings ASME Conference ence on Ocean, Offshore, and Arctic Engineering, 2010.

Econowind (2022). "Econology Powered by Wind." from https://www.econowind.nl/.

Eide, K.,Östman, A. and Alterskjær, A. (2023). "Validation of performance prediction program against cyberphysical model tests". Wind Pro-pulsion, 16th – 17th February 2023, London, UK

Eggers, R, and Kisjes, A.S.(2023) "WiSP2 Project on Wind Propulsion Performance Prediction Methods and Manoeuvring." In RINA Wind Propulsion Conference, 2023

Eggers, R. and Kisjes, A.S. (2019) "Seakeeping and Manoeuvring for Wind Assisted Ships," London, United Kingdom, 2019-10.

Eggers, R. (2018), "Prediction methods for team AkzoNobel in the Volvo Ocean Race and wind assisted ship propulsion for merchant vessels", Proceedings of the 25th international hiswa symposium on yacht design and yacht construction, Amsterdam.

Erhard, M. and H. Strauch (2012). "Control of towing kites for seagoing vessels." IEEE Transactions on Control Systems Technology 21(5): 1629--1640.

Ewing, J. A., Laing, A. K., (1987), "Directional spectra of seas near full development", Journal of Physical Oceanography, Vol. 17, pp. 1696-1706.

Fagiano, L. (2009) "Control of Tethered Airfoils for High–Altitude Wind Energy Generation". Ph.D. Thesis, Politecnico di Torino, Torino, Italy, 2009.

Fang, M., Lin, Y., (2013), "The optimization of ship weather-routing algorithm based on the composite influence of multi-dynamic elements", Applied Ocean Research, Vol. 43, pp. 184-194.

Ferrari, V., Kisjes, A. and Quadvlieg, F. (2018). "Quantifying the Uncertainty of the Crabbing Capability." In International Conference on Offshore Mechanics and Arctic Engineering, American Society of Mechanical Engineers.

Fossati, F. and Muggiasca, S. (2011) "Experimental Investigation of Sail Aerodynamic Behaviour in Dynamic Conditions." J. Sailboat Tech 2.

Fritz, F. (2013). Application of an automated kite system for ship propulsion and power generation. Airborne wind energy: 359--372.

Garenaux, M., Schot, J.J.A. (2021). "Flettner rotors performance and interaction effects on the marin hybrid transition coaster". International Conference on Wind Propulsion, 15-16 September 2021, London, UK.

Gauvain, E. (2019) “The un-restrained sailing yacht model tests–a new approach and technology appropriate to modern sailing yacht seakeeping,” 2019.

Gerhardt, F.C., Kjellberg, M., Wigren, I., Werner, S., Razola, M. “The Horns of the Trilemma: Seakeeping Model Tests for a Wind Powered Vessel,” 2021.

Gerhardt, F., Werner, S., Hörteborn, A., Lundbäck, O., Nisbet, J. and Olsson, T., (2021). HORSES FOR COURSES: HOW TO SELECT THE “RIGHT” WIND PROPULSION SYSTEM AND HOW TO MAKE THE BUSINESS CASE. In Wind Propulsion 2021 15-16 September 2021, Online Conference.

Gerhardt, F.C., Kjellberg, M., Wigren,I., Werner, S. (2021)."The horns of the trilemma: Sea-keeping model tests for a wind Powered vessel". International Conference on Wind Propulsion, 15-16 September 2021, London, UK.

Giovannetti, L.M., Gerhardt, F., Kjellberg, M., Alexandersson, M.and Werner, S. (2021). “The art of model testing: Using CFD to adapt traditional tank testing techniques to a new era of wind propelled shipping,” 2022.

Giovannetti, L.M., Banks, J., Turnock, S.R., and Boyd, S.W. (2017). "Uncertainty assessment of coupled Digital Image Correlation and Particle Image Velocimetry for fluid-structure interaction wind tunnel experiments". Journal of Fluids and Structures, vol. 68, pp. 125-140, 2017.

Giovannetti, L.M., Banks, J., Ledri, M., Turnock, S.R. and Boyd, S.W. (2018). "Toward the development of a hydrofoil tailored to passively reduce its lift response to fluid load". Ocean Engineering, vol. 167, pp. 1-10, 2018.

Giovannetti, L.M. (2020). "Appendages investigation and their effects on maneuvering coefficients for applications in wind assisted ships". Proceedings of 5th International Conference on Innovation in High Performance Sailing Yachts and Sail-Assisted Ship Propul-sion, Gothenburg, Sweden, June 2020.

Giovannetti, L.M. Charalampopoulos, O., Banks, J., Boyd S.W. and Turnock, S.R. (2020). "Developing fluid structure interaction experimental methodologies for dynamic foil measurements". Innov’sail 2020, Gothenburg, 2020.

Giovannetti, L.M., Olsson, F., Alexandersson, M., Werner, S. and Finnsgård, C., (2020), "The Effects of Hydrodynamic Forces on Maneuvrability Coefficients for Wind-Assisted Ships". In International Conference on Offshore Mechanics and Arctic Engineering (Vol. 84379, p. V06AT06A051). American Society of Mechanical Engineers.

Giovannetti, L.M., Stenius, I. (2021). "Review of undewater fluid-structure interaction measuring techniques". 7th High Performance Yacht Design Conference Auck-land, 11-12 March 2021.

Global Wind Atlas, (2022) https://globalwindatlas.info/ last accessed 16th August 2022

Glomeep (2019). "Global maritime energy efficiency partnerships." from https://glomeep.imo.org/. Last accessed 20th August 2022

Hand, M. (2021). "K Line orders LNG-powered bulker fitted with Airseas kite." from https://www.seatrade-maritime.com/shipyards/k-line-orders-lng-powered-bulker-fitted-airseas-kite.

Gracia, L., Wang, H., Mao, W. (2019), “Comparison of two statistical wave models for fatigue and fracture analysis of ship structures", Ocean Engineering, Vol. 187, 106161.

Gruber, K., Regner, P., Wehrle, S., Zeyringer, M., Schmidt, J., (2022), "Towards global validation of wind power simulations: A multi-country assessment of wind power simulation from MERRA-2 and ERA-5 reanalyses bias-corrected with the global wind atlas". Energy, Vol. 238.

Hans Ertel Zentrum für Wetterforschung, (2019), "COSMO regional reanalysis", https://reanalysis.meteo.uni-bonn.de.

Hasselmann, S., (1988), "The WAM model: A third generation ocean wave prediction model", Journal of Physical Ocean-ography, Vol. 18, pp. 1775-1810.

Harada, Y., Kamahori, H., Kobayashi, C., (2016), "The JRA-55 reanalysis: represen-tation of atmospheric circulation and climate variability", Journal of the Meteorological Soci-ety of Japan, Vol. 94, pp. 269-302.

Hersbach, H., Bell, B., Berrisford, P., (2020), "The ERA5 global reanalysis", 2020, Quarterly Journal of the royal meteorological society, Vol. 146, pp. 1999- 2049.

Hirdaris, S.E. and Cheng, F., (2012), June. The role of technology in green ship design (keynote address). In Proceedings of the 11th International Marine Design Conference (IMDC), 1: 21 (Vol. 40).

Hopes, W., Pearson, D., Buckingham, J. (2021). "A CFD Study on Wind Assisted Propulsion Technology for Commercial Shipping". RINA Wind Propulsion Conference, 2021, London, UK.

Kisjes, A., Eggers, R., and Bedos A., (2023). "Steering with Wind Propulsion." In Proceedings of the 19th International Ship Stability Workshop.

Kjellberg, M., Gerhardt, F., and Werner, S. (2022) "Sailing in Waves: A Numerical Method for Analysis of Seakeeping Performance and Dynamic Behavior of a Wind Powered Ship," 2022.

Kobayashi, S., Ota, Y., Harada, A., (2015), "The JRA-55 reanalysis: general specifications and basic characteristics", Journal of the Meteorological Society of Japan, Vol. 93, pp. 5-48.

IACS, (2000), "Standard wave data (north Atlantic scatter diagram)" Rec. No. 34.

International Windship Association (2021). "Technology and Design." from https://www.wind-ship.org/en/technology-design/.

International Maritime Organization. (2002). MSC Resolution 137(76) "Standards for Ship Manoeuvrability." Standards for Ship Manoeuvrability. International Maritime Organization (IMO).

International Maritime Organization. (2001). MEPC.1/Circ.850/Rev.3 "Guidelines for Determining Minimum Propulsion Power to Maintain the Manoeuvrability of Ships in Adverse Conditions." Standards for Ship Manoeuvrability. International Maritime Organization (IMO).

International Maritime Organization. (1974). "International Convention for the Safety of Life at Sea (SOLAS)."

International Maritime Organization. (2010). "Interim Explanatory Notes for the Assessment of Passenger Ship Systems' Capabilities after a Fire or Flooding Casualty." Standards for Ship Manoeuvrability.

International Maritime Organization. (2011), "Reduction of GHG emission from ships, global wind specification along the main global shipping routes to be applied in the EEDI

Calculation of Wind Propulsion Sys-tems”, IMO MEPC 62/INF. 34.

International Maritime Organization (2018) MEPC 72/5/9, 2 February 2018 , “Pro-posed amendments to the 2013 Interim Guidelines for determining minimum pro-pulsion power to maintain the manoeuvra-bility of ships in ad-verse conditions”, Sub-mitted by China.

International Windship Association (2024) Wind Propulsion_ Zero-Emissions Energyu So-lution for Shipping, Annex to MEPC 81/INF.39

Interreg North Sea Region (2021). "Come along on a wind-assist ride aboard Van Dam Shipping's MV Ankie and the newly installed ventifoil system from eConowind." from https://northsearegion.eu/wasp/news/come-along-on-a-wind-assist-ride-aboard-van-dam-shippings-mv-ankie-and-the-newly-installed-ventifoil-system-from-econowind/.

ITTC (2017) Recommended Procedures and Guide-lines 7.5-02-03-01.4, 2017, “1978 ITTC Performance Prediction Method”.

ITTC.(1999). “Testing and Extrapolation Methods High Speed Marine Vehicles Excerpt of ISO 2631, Seasickness and Fatigue - Recom-mended Procedures.” ITTC.

Jehle, C. and Schmehl, R., (2014). "Applied tracking control for kite power systems". Jour-nal of Guidance, Control, and Dynamics, Vol. 37, No. 4, p. 1211-1222.

Jones, L., Prince, M., Hudson, D., Cocks, J. (2019)."Predicted fuel-savings for a flettner ro-tor assisted tanker using computational fluid dy-nam-ics". Wind Propulsion, 15th -16th October 2019, London, UK.

Kalnay, E., Kanamitsu, M., Kistler, R., (1996), “The NCEP/NCAR 40-year reanaly-sis project”, Bulletin of the American Meteoro-log-ical Society, Vol. 77, pp. 437-472.

Kanamitsu, M., Ebisuzaki, W., Woollen, J., Yang, S., Hnilo, J., Fiorino, M., Potter, G., (2002), “NCEP-DOE AMIP-II reanalysis (R-2)”, Bulletin of the American Meteorological Socie-ty, pp. 1631-1643.

Karabelas, S. J., et al. (2012). "High Reyn-olds number turbulent flow past a rotating cylin-der." Applied mathematical modelling 36(1): 379--398.

Karman D. (2016). "Examination of high Reynolds number flow around a spinning cylin-der with different turbulence models" [J]. 2016.

Kjellberg, Martin, Gerhardt, Frederik, and Sofia Werner, (2022). "Sailing in Waves: A Nu-merical Method for Analysis of Seakeeping Per-formance and Dynamic Behavior of a Wind Powered Ship" . Paper presented at the SNAME 24th Chesapeake Sailing Yacht Symposium, Annapolis, Maryland, USA, June 2022.

Kjellberg, M., Gerhardt, F., Werner, S. (2023). "Sailing performance of wind-powered cargo vessel in unsteady conditions". The 6th In-ternational Conference on Innovation in High Performance Sailing Yachts and Wind-Assisted Ships, Lorient, France, May, 2023.

Koster, D., (2015), “Technical report series on global modelling and data assimilation, Vol-ume 43”, MERRA-2: Initial Evaluation of the Climate.

Kukner, A., S. Bulut and A. N. Halilbese (2016). "Renewable energy options and an as-sessment of wind-based propulsion systems for small crafts." Naval Academy Scientific Bulle-tin. \url http://dx. doi. org/10.21279/1454-864X-16-I2-006.

Kume K , Hamada T , Kobayashi H , (2022). "Evaluation of aerodynamic characteris-tics of a ship with flettner rotors by wind tunnel tests and RANS-based CFD"[J].Ocean engi-neering, 2022 (Jun.15):254.

Lades AS (2023). "About Lades AS." from https://ladeas.no/about-lade-as/. Last accessed August 2022.

Laface, M., Arena, F., (2021), "On correlation between wind and wave storms", Journal of Marine Science and Engineering, Vol. 9, 1426.

Lee, H., Jo, Y., Lee, D.J., Choi, S., (2016). "Surrogate model based design optimization of multiple wing sails considering flow interaction effects". Ocean Eng. 121, 422-436. https://doi.org/10.1016/j.oceaneng.2016.05.05

Leloup, R. (2016). "A continuous and analytical modeling for kites as auxiliary propulsion devoted to merchant ships, including fuel saving estimation." Renewable Energy 86: 483--496.

Li, X., Qin, X., Yang, J., Zhang, Y., (2022), "Evaluation of ERA5, ERA-Interim, JRA55 and MERRA2 reanalysis precipitation datasets over the Poyang Lake Basin in China", Interna-tional Journal of Climatology, Vol. 42, pp. 10435-10450.

Lloyd's List (2020). "From the News Desk: Will coronavirus accelerate the use of tech in shipping?". from https://lloydslist.maritimeintelligence.informa.com/LL1131917/From-the-News-Desk-Will-coronavirus-accelerate-the-use-of-tech-in-shipping.

Lloyd's Register. (2023a). "Guidance Notes for Flettner Rotor Approval.". https://r4s.oneocean.com/regulation/page/262879 .

Lloyd's Register. (2023b). "Guidance Notes for the Certification of Masts, Spars and Standing.". https://r4s.oneocean.com/regulation/page/258612 .

Llopis Pascual, A. Bailardi, G. Charrier, B. and Ferrer Desclaux, D. (2023). "Eerodynamic optimi-zation of the esail, bound4blue's suction sail for wind-assisted vessel propulsion". Interna-tional Conference on Wind Propulsion, 16th -17th February 2023, London, UK.

Longyard, W. H. (2005). "A Speck on the sea: Epic Voyages in the most improbable vessels."

Lu, R.,Ringsberg, R.W. (2019). "Ship energy performance study of three wind-assisted ship propulsion technologies including a parametric study of the Flettner rotor technolo-gy". Ships and Offshore Structures, DOI: 10.1080/17445302.2019.1612544

Lu, R. and J. W. Ringsberg (2020). "Ship energy performance study of three wind-assisted ship propulsion technologies including a parametric study of the Flettner rotor technology." Ships and Offshore structures 15(3): 249--258.

Marchaj, C. A. (1988). Aero-hydrodynamics of Sailing.

Maritime Global News (2022). "K Line Orders Airseas Kites for Three More Ships." from https://maritimeglobalnews.com/news/orders-aieseas-kites-three-ev3k1y.

Mason, J.C. (2021). "Quantifying voyage op-timisation with wind-assisted ship propulsion: a new climate mitigation strategy for shipping". In: Doctoral dissertation, The University of Manchester, (UK).

Mazas, L., Andrillon, Y., Letourneur, A., Kerdraon, P. and Verdier, G. (2017). "Comparison of Hydrodynamic Performances of an Imoca 60 with Straight or L-Shaped Daggerboard." INNOV'SAIL, 2017.

Mikulić, A., Katalinić, M., Ćorak, M., Parunov, J., (2020), "The effect of spatial correlation of sea states on predicted extreme significant wave heights along ship sailing routes", Marine Technology Engineering (in press).

Milgram, J. H. (1968). The aerodynamics of sails: 1397--1434.

Mittal, S. and B. Kumar (2003). "Flow past a rotating cylinder." Journal of fluid mechanics 476: 303--334.

Morsy El-Gohary, M. (2013). "Overview of past, present and future marine power plants." Journal of Marine Science and Application 12(2): 219--227.

Morvan, A. , Sacher, M. , Alain Nême, Leroux, J. B. , & Abiven, N., (2021). "Efficient jib-mainsail fluid-structure interaction modelling based on an extended lifting-line theory - valida-tions with semi-rigid sails experiments". The Royal Institution of Naval Architects.

Naaijen, P., V. Koster and R. P. Dallinga (2006). "On the power savings by an auxiliary kite propulsion system." International shipbuilding progress 53(4): 255--279.

Nelissen (2016), "Study on the analysis of mar-ket potentials and market barriers for wind propulsion technologies for ships", Delft, CE Delft

Obakrim, S., Ailliot, P., Monbet, V., Raillard, N., (2023), "Statistical modeling of the space–time relation between wind and significant wave height", Advances in Statistical Climatology, Meteorology and Oceanography, Vol. 9, pp. 67-81.

Oehler, Johannes and Schmehl, Roland, (2019). "Aerodynamic characterization of a soft kite by in situ flow measurement". Wind Energ. Sci., 4, 1–21, 2019 .

Oceanbird (2023). "Oceanbird Wing Sail." from https://www.theoceanbird.com.

Paakkari Ville; Wang, H; Stigler C, (2022). "Voyage optimization with wind propulsion Conference proceedings". In: RINA ICCAS 2022.

Paulig, X., M. Bungart and B. Specht (2013)."Conceptual design of textile kites considering overall system performance". Airborne wind energy: 547--562.

Perkins, T., (2004). "The maltese falcon: The realisation." 22nd International HISWA Symposium on Yacht Design and Yacht Construction: 1-30.

Persson, A., Li, D.Q., Olsson, F., Werner, S. and Dhome, U., (2019). Performance prediction of wind propulsion systems using 3D CFD and route simulation. In 6th International Conference on Computational Methods in Marine Engineering, MARINE 2015; Conference Date: 15 June 2015 Through 17 June 2015; (pp. 19-30). Royal Institution of Naval Architects.

Pierson, W. J., Moskowitz, L., (1964), "A proposed spectral form for fully developed wind seas based on the similarity theory of S. A. Kitaigorodskii", Journal of Geophysical Research, Vol. 69, pp. 5181-5190.

Pili, F., Babarit, A., Bonnefoy, F., Payne, G.S. (2023). "Numerical investigation of the seakeeping of a Flettner ro-tors-propelled catamaran in beam waves". The 6th International Conference on Innovation in High Performance Sailing Yachts and Wind-Assisted Ships, Lorient, France, May, 2023

Podeur, V. (2018). "Fuel economy assessment tool for auxiliary kite propulsion of merchant ship." La Houille Blanche 1(1): 5--7.

Podeur, V. (2016). "Simulation de voyage au long cours pour le calcul d'économies de carburant: application à la propulsion par cerfvolant."

Ran, H., C.E. Janson and B. Allenström (2013). "Auxiliary kite propulsion contribution to ship thrusti". International Conference on Offshore Mechanics and Arctic Engineering, American Society of Mechanical Engineers.

Reche-Vilanova, Martina & Hansen, Heikki & Bingham, Harry. (2021). "Performance Prediction Program for Wind-Assisted Cargo

Ships". Journal of Sailing Technology. 6. 91-117. 10.5957/jst/2021.6.1.91.

Reche-Vilanova M. et al., 2023. "Preliminary study on the propeller and engine performance variation with wind propulsion technologies". Wind Propulsion, 16th-17th February 2023, London, UK.

Rienecker, M., Suarez, M., Gelaro, R., (2011), "MERRA: NASA's Modern-Era Retrospective Analysis for Research and Applications", Journal of Climate, Vol. 24, pp. 3624-3648.

Roach, P.J., (1997). "Quantification of Uncer-tainty in Computational Fluid Dynamics". Ann. Rev. of Fluid Mechanics, vol. 29, pp. 123-160, 1997.

Roncin, K.; Behrel, M.; Iachkine, P.; Leroux, J.-B., (2020). "Benchmark Sea Trials on a 6-Meter Boat Powered by Kite". Appl. Sci. 2020, 10, 6148. https://doi.org/10.3390/app10186148

Royal Institution of Naval Architects, The, (2012). "Development of Amendments to the Criterion for Maximum Angle of Heel in Turns of the 2008 IS Code – Revised Proposal for Amending the 2008 IS Code', IMO SLF55/12," 2012.

Saha, S., Moorthi, S., Pan, H., (2010), "The NCEP climate forecast system reanalysis", Bulletin of the American Meteorological Socie-ty, Vol. 91, pp. 1015-1058.

Sauder, T., Alterskjær, S.A. (2022). "Hydrodynamic testing of wind-assisted cargo ships using a cyber–physical method". Ocean Engineering , Volume 243, Jan. 2022, https://doi.org/10.1016/j.oceaneng.2021.110206

Severi, S. (2022). "Comparison of achieved fuel savings on ships by different wind propulsiondevices using a 3-DoF resistance model". English. Master's thesis. Aalto Uni-versity. School of Engineering, p. 43. URL: http://urn.fi/URN:NBN:fi:aalto-202205223282

Schmidt, A. (2013). E-Ship 1-A Wind-Hybrid Commercial Cargo Ship.

Schot, J.J.A., Eggers, R., (2019), "The Effect of Leeway Angle on the Propeller Performance", Wind Propulsion(London, UK), pp 31 - 39.

Schot，J.J.A., Garenaux， M. (2023). "Modelling of aerodynamic interaction effects for wind propulsion applied in commer-cial shipping: Development of a non-linear lift-ing line method". The 6th International Confer-ence on Innovation in High Performance Sailing Yachts and Wind-Assisted Ships, Lorient, France, May, 2023.

Seddiek, I. S. and N. R. Ammar (2021). "Harnessing wind energy on merchant ships: case study Flettner rotors onboard bulk carriers." Environmental Science and Pollution Research 28(25): 32695--32707.

Staffell, I., Pfenninger, S., (2016), "Using bias-corrected reanalysis to simulate current and future wind power output", Energy, Vol. 114, 1224e39.

Stefanakos, C., (2021), "Global wind and wave climate based on two reanalysis data-bases: ECMWF ERA5 and NCEP CFSR", Journal of Marine Science and Engineering, Vol. 9, 990.

Sumon, Md Daluar Hussain and Osman, Amin.(2021). "A Comprehensive Analysis of the Stability and Powering Performances of a Hard Sail–Assisted Bulk Carrier". Journal of Marine Science and Application. 20. 426-445. 10.1007/s11804-021-00219-w

Suzuki, N., Konda, M., Kutsuwada, K., Utsunomiya, K., (2018), "Comparison of the accuracy of various global wind speed datasets obtained from satellites and reanalyses", Jour-nal of Advanced Marine Science and Technol-ogy Society, Vol. 24, pp. 31-37.

Sverdrup, H. U., Munk, W. H., (1947), "Wind seas and swell: Theory of relations for forecasting", U.S. Navy Hydrographic Office, Washington, DC.

Tillig F, Ringsberg JW, Mao W, Ramne B. (2017). "A generic energy systems model for efficient ship design and operation". IMechE, Part M, J EngMaritime Environ. 231(2):649–666. doi:10.1177/1475090216680672.

Tillig, F., Ringsberg, J.W., (2018). "A 4 DOF Simulation Model Developed for Fuel Con-sumption Prediction of Ships at Sea". Ships and Offshore Structures. https://doi.org/10.1080/17445302.2018.1559912.

Tillig, F., (2020). "Simulation model of a ship's energy performance and transportation costs". Doctoral thesis, Chalmers University of Technology, Sweden.

Tillig, F., Ringsberg, J.W., (2020). "Design, operation and analysis of wind-assisted cargo ships". Ocean Engineering, Volume211, 2020. https://doi.org/10.1016/j.oceaneng.2020.10760 3

Thomas, T. (2015). "The development of the high-tech DynaRig on sailing superyachts." from https://www.boatinternational.com/yachts/yacht-design/the-development-of-the-high-tech-dynarig-on-sailing-superyachts

Traut, M., et al. (2014). "Propulsive power contribution of a kite and a Flettner rotor on selected shipping routes." Applied Energy 113: 362--372.

Twidell, J. (2021). Renewable energy resources, Routledge.

UK GOVERNMENT (2019), Clean Maritime Plan 2019, Department for Transport, UK

Vahs, M. (2019) "Retrofitting of Flettner Rotors – Results from Sea Trials of the General Cargo Ship "Fehn Pollux"," London, United Kingdom, 2019-10.

van der Kolk, N., (2016a). "Hydrodynamics of wind-assisted ship propulsion: modeling of Hydrodynamic sideforce". In: 24th International HISWA Symposium on Yacht Design and Yacht Construction,14-15 Nov, Amsterdam.

van der Kolk, N., Keuning, J.A.., and Huijsmans, R.H.M. (2016b). "Hydrodynamics of wind-assisted ship propulsion verification and validation of RANS methodology". In Proceedings of the 12th International Conference on Hydrodynamics-ICHD 2016 [148]

van der Kolk, N., Keuning, L.A., and Huijsmans, R.H.M.. (2017). "Hydrodynamics of wind-assisted ship propulsion validation of RANS-CFD methodology". In P. Bot (Ed.), Proceed-ings of the 4th International Conference on In-novation in High Performance Sailing Yachts (INNOVSAIL 2017) (pp. 207-216). [796] Sailing YardResearch Foundation (SYRF).

van der Kolk, N.J., Bordogna, G., Mason, J.C.,Desprairies, P., Vrijdag, A. (2019a) "Case study: Windassisted ship propulsion performance prediction, routing, and economic modelling". RINA Conf.Power & Propulsion Alternatives for Ships, 2019.

van der Kolk, N.J., Keuning, J.A., Huijsmans, R.H.M., (2019b). "Part 1: experimental validation of a RANS-CFD methodology for the hydrodynamics of wind-assisted ships operating at leeway angles". Ocean Eng. 178.

van der Kolk,N.J., Keuning, J.A., and Huijsmans, R.H.M. (2020a). "Hydromechanics of wind-assisted ship propulsion verification of RANS methodology". Ocean Engineering Volume 201, 1 April 2020, 107024DOI: 10.1016/j.oceaneng.2020.107024AB van der Kolk, N.J., Akkerman, I., Keuning, J.A., Huijsmans, R.H.M., (2020b). "Part 2: simula-tion methodology and numerical uncertainty for RANS-CFD for the hydrodynamics of wind-assisted ships operating at leeway angles". Ocean Eng. 201.

van der Kolk, N.J., Akkerman, I., Keuning, J.A. (2021). "Low-aspect ratio appendages for wind-assisted ships". J Mar Sci Technol 26, 1126–1143(2021). https://doi.org/10.1007/s00773-020-00777-8

Viola, I.M., Sacher, M., Xu, J., Wang, F., (2015). "A numerical method for the design of ships with wind-assisted propulsion". Ocean Engineering, 105, pp.33-42, 2015.

Wang, Yonggong Liu, Yanshuo Li, Hongxia, (2022). "Stability Analysis of Airfoil Sail-Assisted Ship Under Combined Wind and Wave Load". Ship &Boat, DOI:10.19423/j.cnki.31-1561/u.2022.04.098.

Wellicome, J. F., and Wilkinson, S. , (1984). "Ship propulsive kites: an initial study". University of Southampton.

Werner, S., Nisbet, J., Hörteborn, A., Nielsen, R., (2021), “Speed trial verification for a wind assisted ship”, Proceedings of RINA International Conference on Wind Propulsion, London, UK.

Werner, S., Gerhardt, F., Santén, V., and Finnsgård, C., (2022a), “Wind Ship Research – How Science Can Support the Transition to Wind Powered Shipping,” Global Conference on Naval Architecture and Ocean Engineering, Changwon, Republic of Korea.

Werner, S., Nisbeth, J., Olsson, F. (2022b) "Speed trial methodology for wind assisted ships", 7th HullPIC Conf., Tullamore, pp.124-140, 2022.

Werner, S., Gerhardt, F., and Kontos, S., (2023) "Key Performance Indicators for Wind-Powered Ships", in the proceedings of RINA Wind Propulsion Conference 2023

Williams, P., Lansdorp, B. and Ruiterkamp R. (2008). "Modeling, simulation, and testing of surf kites for power generation". Proceedings of AIAA Modelling and Simulation Technologies Conference and Exhibit, Honolulu, Hawaii, USA.

Yang, K.K., Kim, Y.C., Kim, K.S., Kim, J., (2019). “RANS Analysis of Propeller Open Water Characteristics in Oblique Flow”, Proceedings of SNAK Autumn Conference (in Korean).

Yasukawa, H., Yoshimura, Y., (2015), “Intro-duction of MMG standard method for maneuvering predictions”, Journal of Marine Science and Technology, Vol. 20, pp 37 - 52.

ITTC2024

30TH INTERNATIONAL TOWING TANK CONFERENCE
22–27 SEPTEMBER 2024 | HOBART TASMANIA AUSTRALIA

REPORT OF THE SPECIALIST COMMITTEE ON COMBINED CFD AND EFD METHODS

Specialist COMMITTEE on Combined CFD and EFD Methods

1. INTRODUCTION

1.1. Membership and Meetings

The members of the Specialist Committee on Combined Computational Fluid Dynamics (CFD) and Experimental Fluid Dynamics (EFD) Methods of the 30th ITTC are:

- Prof. Kevin Maki (Chair)
  University of Michigan,
  Ann Arbor, Michigan,
  USA

- Dr. ir. Bram Starke (Secretary)
  MARIN,
  2, Haagsteeg, P.O. Box 28,
  6700 AA Wageningen,
  The Netherlands

- Jussi Martio
  VTT,
  Espoo,
  Finland

- Dr. Joseph Banks
  University of Southampton,
  Southampton
  United Kingdom

- Peter Horn
  Hamburg Ship Model Basin (HSVA),
  Bramfelder Str. 164,
  22305 Hamburg,
  Germany

- Dr. Riccardo Broglia[1]
  CNR-INM,
  Rome,
  Italy

- Prof. Diego Villa
  University of Genoa,
  Genoa,
  Italy

- Dr. Hyunse Yoon[2]
  University of Iowa,
  Iowa City, Iowa,
  USA

- Prof. Feng Zhao,
  China Ship Scientific Research Center (CSSRC),
  Wuxi, Jiangsu,
  China

[1] Replaced Stefano Zaghi in October 2022
[2] Originally appointed when working for DSME in Korea, and reappointed when he moved to University of Iowa in February 2023, to fill vacancy left by Marcelo Vitola from LabOceano in Brazil.

- Prof. Yichen Jiang,
  Dalian University of Technology,
  Dalian, Liaoning,
  China

- Dr. Eng. Shoji Shingo
  Shipbuilding Research Centre of Japan (SRC),
  Tokyo,
  Japan

- Dr. Stefano Zaghi[3]
  CNR-INM,
  Rome,
  Italy

- Marcelo Vitola[4]
  LabOceano,
  Brazil

Three in-person committee meetings have been held during the work period:

- The first was held in Ann Arbor, MI, May 10-12, 2022. The venue was the Michigan League, on the campus of the University of Michigan. There were six in-person participants, and four members joined the meeting virtually.

- The second meeting was held in Hamburg, Germany, April 18-20, 2023. The meeting was hosted at HSVA. There were 10 in-person participants, and one joined virtually.

- The third meeting was held in Tokyo, Japan, May 8-10, 2024. The meeting was hosted by SRC. There were ten committee in-person members, two in-person guests, and one virtual participant.

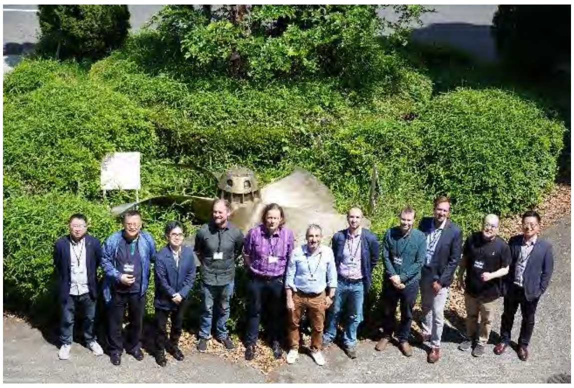

- The committee met many times virtually to prepare reports, prepare for the in-person meetings, and to discuss the progress of the work of the committee. There were approximately six virtual meetings per year.

2. TASKS

The recommendations for the work of the Specialist Committee on Combined CFD and EFD Methods as given by the 29th ITTC were as follows:

[3] Left his institute in May 2022, and resigned from committee. Was replaced by Riccardo Broglia.
[4] Was originally appointed to committee but left his institute before committee activities started. His vacancy was filled when Hyunse Yoon moved from Korea to USA.

1. Review and highlight good examples of combined methods, suggest and initiate new applications of combined methods, and co-ordinate and encourage each technical committee to perform detailed work on combined methods.

2. Co-ordinate and advise each technical committee to investigate and develop combined methods.

3. Monitor and review advances and challenges within full-scale and model scale CFD with special focus on speed/power predictions.

4. Review the outcome of ongoing CFD benchmark campaigns.

5. Encourage the establishment of open validation data for high Reynolds number flow cases for marine applications.

6. Review and study the performance of turbulence models and wall treatments at full scale. Monitor the development of new turbulence modelling approaches when they become available.

7. Monitor advances in the application of detailed flow measurements in the ITTC community.

8. Develop a standard process of performing a CFD benchmark study within ITTC.

9. Monitor how Verification and Validation is applied and reported in research publications and commercial work.

10. Continue to maintain and improve the existing Recommended Procedure 7.5-03-01-01, "Uncertainty Analysis in CFD, Verification and Validation Methodology and Procedures".

11. Monitor the use of the new Recommended Procedures 7.5-03-01-02 "Quality Assurance in CFD Ship Applications" and update it if needed.

12. Produce information material (articles, conferences, social media) directed towards stakeholders who receive and use the results hydrodynamic predictions. Explain state-of-the-art capability, and challenges of CFD versus EFD and Combined methods.

13. Update, as required, procedure 7.5-03-01-01, Uncertainty Analysis in CFD, Verification and Validation Methodology, and Procedure 7.5-03-01-02, Quality Assurance in CFD Ship Applications.

3. LIST OF ABBREVIATIONS:

ABL	Atmospheric Boundary Layer
AIAA	American Institute of Aeronautics and Astronautics
ASME	The American Society of Mechanical Engineers
AVT	Applied Vehicle Technology
BPG	Best Practical Guideline
CAD	Computer Aided Design
CF	Correction Factor
CSSRC	China Ship Scientific Research Center
DES	Detached Eddy Simulation
DIC	Digital Image Correlation
EEDI	Energy Efficiency Design Index
EEXI	Energy Efficiency Existing Ship Index
ESD	Energy Saving Device
FS	Factor of Safety
GCI	Grid Convergence Index
HVAF	Hub Vortex Absorbed Fins
HPC	High Performance Computing
IACS	Safer and Cleaner Shipping
IDDES	Improved Delayed Detached Eddy Simulation
JBC	Japanese Bulk Carrier
KCS	KRISO Container Ship
KRISO	Korea Research Institute of Ships & Ocean Engineering

LES	Large Eddy Simulation
LSR	Least Square Root
NDA	Non-Disclosure Agreement
PIV	Particle Image Velocimetry
PPTC	Potsdam Propeller Test Case
PSD	Pre-Swirl Duct
RANS	Reynolds-Averaged Navier-Stokes
Re	Reynolds number
RE	Richardson Extrapolation
RP	Recommended Procedures
SC	Specialist Committee
SRC	Shipbuilding Research Centre of Japan
STO	Science and Technology Organization
SVA	Schiffbau-Versuchsanstalt Potsdam
TKE	Turbulent Kinetic Energy
V&V	Verification and Validation
VVUA	Verification, Validation, and Uncertainty Assessment

4. UPDATES OF THE RECOMMENDED PROCEDURES

4.1. Background

Validation and Verification **(V&V)** in the field of maritime numerical fluid dynamics is a basic tool to assess the uncertainty of a calculation or simulation as well as to guarantee the accuracy and reliability of a result. There are generally two approaches to address these aspects described in two different ITTC procedures 7.5-03-01-01, "Uncertainty Analysis in CFD, Verification and Validation Methodology and Procedures" and 7.5-03-01-02 "Quality Assurance in CFD Ship Applications". The first one aims for a detailed mathematical look into the calculation or simulation itself, whereas the latter one addresses the accuracy of performed CFD calculations based on best practice guidelines on a statistical view.

TOR 9 addresses the application of the first procedure in commercial and academic work. In close connection to this, TOR 10 deals with the modification of this procedure. The usage of the second mentioned procedure is subject to TOR 11. Finally, TOR 13 requests the specialist group to update both procedures.

Focusing on the application of both procedures within commercial and scientific work, the ITTC specialist group has set up a survey among ITTC members to see if this procedure is used in their work. The following section represents the results of this survey, preceded by two sections of details on the update of both these mentioned procedures.

Following this, a final section summarizes the review and update of further ITTC guidelines and procedures reviewed by this committee.

4.2. Survey on V&V and Quality Assurance in CFD

The present committee prepared and distributed a questionnaire to ITTC members to share their vivid experiences and useful comments. The questionnaire was distributed to 102 member organizations, of which 42 organizations responded. These organizations comprised 20 research institutes, 13 universities, and 9 commercial companies. The regional composition is 4 Americas, 6 Central Europe, 5 North and West Asia, 5 Northern Europe, 11 Pacific Islands, 7 Southern Europe, and 4 South and East Asia of ITTC Geographical Area countries. Of these, two organizations submitted two separate responses, resulting in a total of 44 responses. Of these, 3 responses were deemed invalid, thus finally 41 valid responses were collected.

The survey is a two-part questionnaire consisting of Part A and Part B. Part A contains 11 questions (A1 ~ A11), and Part B contains 5 questions (B1 ~ B5). Questions A1 through A5 are related to TOR 9, A6 through A11 to TOR 10, and B1 through B5 to TOR 11. Here, each question statement is cited in italics and the responses are presented using a pie chart for each question. In the case of YES or NO response format, if the answer was non-explicit but the meaning was positive, it was classified as 'Affirmative,' whereas, it was classified as 'Negative' if the meaning was disagreeing. For each question, the responses were briefly discussed and the narrative responses, if any, were summarized. Finally, an overall summary and concluding remarks are given at the end.

Part A

The following questions (A1 – A5) are about CFD Verification and Validation in general.

A1. Did you ever prepare a V&V study for CFD simulation? If your answer to A1 is YES, how often do you prepare V&V studies and what kind of V&V methodology do you use? If possible, please let us know relevant reference(s) to the methodology. If your answer to A1 is NO, please let us know the reason (then, you may skip A2 through A5 and continue from there).

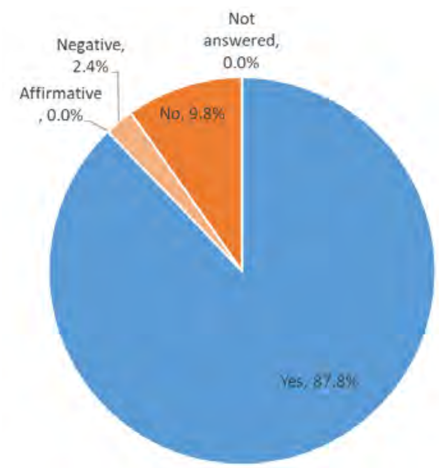

A vast majority (>85%) has ever carried out or have been involved in V&V studies and are mainly using the well-known procedures and papers which are relevant within this context (papers by the main authors, for example, Richardson (1911), Roache (1994), Eça and Hoekstra (2014), Stern et al. (2001), next to ITTC (2021), The American Society of Mechanical Engineers (ASME) (2009), American Institute of Aeronautics and Astronautics (AIAA) (1995) procedures). Those who replied "No" can be considered as pure experimental facilities or institutes who are planning to do V&V in near future.

A2. When you perform V&V studies, do you make it for a commercial CFD code, or do you use an in-house developed CFD code?

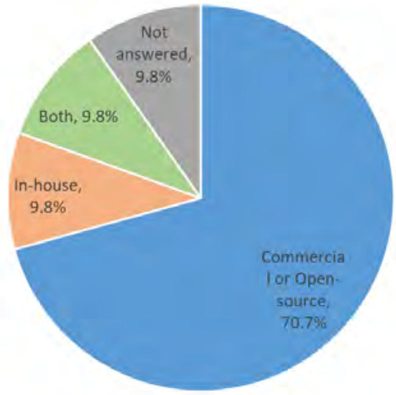

Commercial or Open-Source Codes are widely spread among the participants of this survey. About 70% of the respondents are using either Commercial or Open-Source Codes for V&V studies. Institutes only using in-house developed codes are 10% of the replies and another 10% of the replies using both In-house and Commercial/Open-source codes for their V&V studies. About 10% of the replies are without an answer. Specific CFD codes mentioned in the survey responses include OpenFOAM, STAR-CCM+, FINE/Marine, FINFLO, NEPTUNE, SURF, NAGISA, CFX, ReFRESCO, FreSCo+ and Fluent.

A3. Do you prepare V&V studies for CFD projects which can be considered as daily business in your organization?

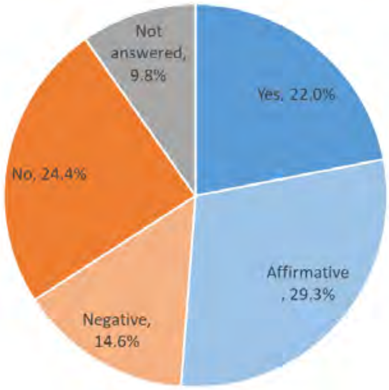

Half of the respondents replied "Yes", and the other half replied "No". Some rely on their developed best practices which are based on investigations which include V&V studies, so a V&V study is not necessary for everyday projects. Others do such a study for all daily projects although it is very time-consuming. Of course, the extent of such a V&V study can be very different. This result gives a good indication of the awareness for a V&V study: either they are done for a project, or the calculations are based on the settings verified with earlier V&V studies.

A4. Do you prepare V&V for new types of simulation cases or new ship types?

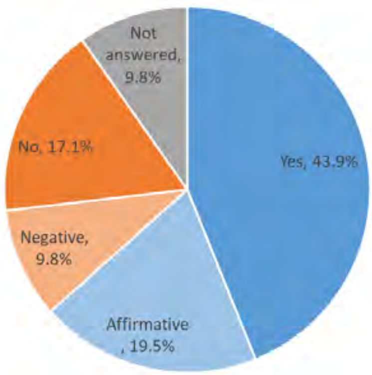

A majority (~65%) replied yes or gave a rather positive answer. Preparation of a new V&V study is then carried out when new ship types or simulation types must be calculated. It depends rather on the difference and the novelty of the new calculation case if a complete V&V study is carried out or not. So, there is no clear differentiation when a participant defines a new simulation as "new enough" or "very different to what was done before" that it is decided to carry out a complete V&V study.

A5. Do you perform Energy Efficiency Design Index (EEDI) / Energy Efficiency Existing Ship Index (EEXI) relevant CFD simulation in your organization and prepare a V&V study for this work as well?

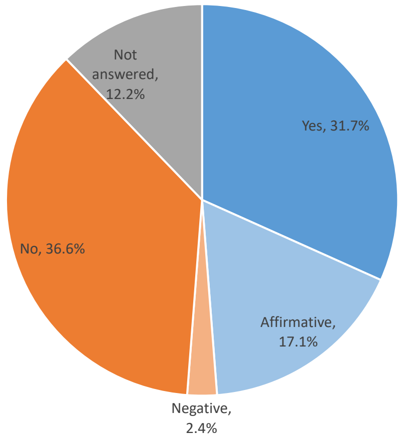

Unfortunately, the question is not posed perfectly as it covers two questions in one. The results cannot be used to distinguish between an answer "No, we do not carry out EEDI/EEXI calculation" and "We do not make a V&V Study for EEDI/EEXI calculation. Therefore, an evaluation can led to wrong conclusions.

Nonetheless, about 32% answered "Yes" indicating that they carry out CFD simulations for EEDI/EEXI and perform V&V studies for this. Some answered that they were going to prepare V&V for EEDI/EEXI in the future.

The following questions (A6 – A11) are about RP 7.5-03-01-01 "Uncertainty Analysis in CFD Verification and Validation, Methodology and Procedures."

A6. Do you use this procedure for your organization's activities?

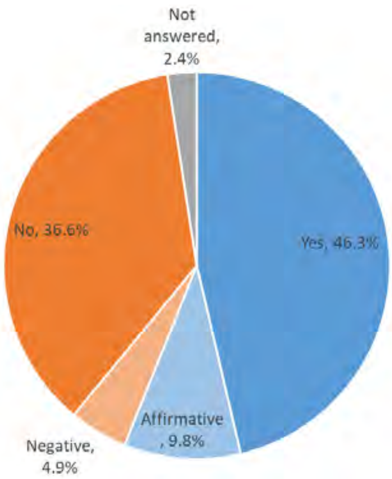

About 46% said they use this procedure, while about 37% said they do not. About 10% said they use it partially, and about 5% said they rarely use it or do not apply it to their daily tasks. In cases where they were partially used, they responded that they used definitions that were somewhat different from this procedure or that they mainly used ASME's procedures (ASME, 2009).

A7. Have you participated in benchmark studies where you have to prepare a verification study following this procedure? If your answer to A7 is YES, but you did not (or were not able to) submit your verification results, may we know what caused this?

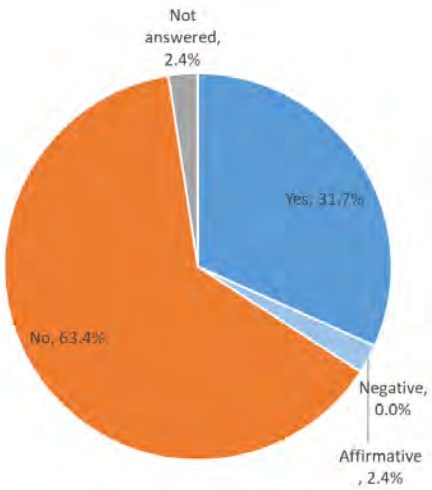

Approximately 32% responded that they had experience participating in benchmark studies requiring V&V, while 63% responded that they had no such experience. One respondent said they had not had this experience recently. Three respondents mentioned that they had participated in the Gothenburg 2010 Workshop (Larsson, 2014) and conducted this benchmark study. One respondent noted that they had participated in this benchmark study, but that creating similarity grids was very time-consuming and that a grid sensitivity study would have been more practical.

A8. Verification studies following the Richardson Extrapolation may not tend to be asymptotic in general. Do you think that other approaches are more suitable? If your answer to A8 is YES, please let us know other approaches that you think more suitable.

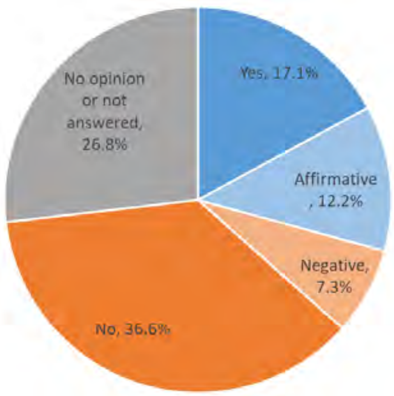

Approximately 17% responded that other approaches were more appropriate than the Richardson Extrapolation (RE) approach (Richardson, 1911), and another 12% agreed with this opinion. Many respondents expressed a preference for using the Least Square Root (LSR) method (Eça and Hoekstra, 2014), mentioning its advantages such as ease of application to unstructured grid systems, unsystematic grid refinement, and oscillatory convergence cases. Nevertheless, some respondents pointed out that the need for more than four grids is a disadvantage of the LSR method. Meanwhile, about 37% of respondents did not agree that a more appropriate approach is needed than the RE method, and another 7% answered that although the RE approach may have drawbacks but is still reliable. What is noteworthy is that about 27% of respondents had no opinion or not answered, citing reasons such as lack of knowledge or unfamiliarity with other possible approaches or methods that could replace the RE method.

A9. Do you follow the concept of the "Correction Factor" (item 4.3), the concept of "Factor of Safety" (item 4.4) or the concept of "Least Square Root Approach" (item 4.5) when you perform a verification analysis? Can you give an explanation?

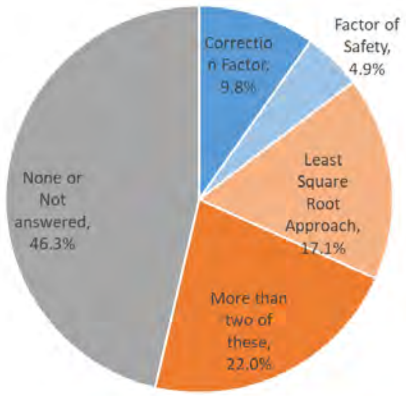

About 10% of respondents said they were using the Correction Factor (CF) approach, about 5% were using the Factor of Safety (FS) approach, and about 17% were using the LSR approach. Another 22% reported using two or more different methods. Among respondents who said they used CF or FS methods; some cited the simplicity and quick application of both methods as a reason for their choice. For respondents who answered that they use the LSR approach, the advantages mentioned in the previous question (i.e., easier application to unstructured grid systems, unsystematic grid refinement, and oscillatory convergence) were explained as reasons for choosing this method. Among the respondents who answered that they use two or more methods, some added that they apply the CF or FS method first because these are faster, and that they apply the LSR method if the condition of monotonic convergence required for RE is not met. Of the remaining 46% of respondents, about half said they did not use all three methods presented, and the other half did not respond.

A10. Do you see room for improvement of this procedure? Do you see this procedure as practical and applicable?

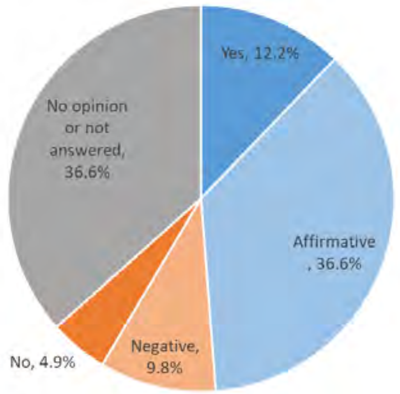

Approximately 12% said that the procedure needs improvement, and another 37% agreed. Most respondents said they believed the process was practical and applicable, but that there was still room for improvement. One of the most common improvements mentioned is the addition of as many examples as possible, allowing users to follow the procedures step by step. Respondents indicated that current procedures are generally described as too difficult to understand and therefore generally difficult to apply. Other respondents answered that the use of this procedure requires the creation and calculation of too many grid cases and that it is difficult to apply in practice even for systematic grid refinement.

A11. Do you have general remarks on the procedures of Validation and Verification studies and future fields of research?

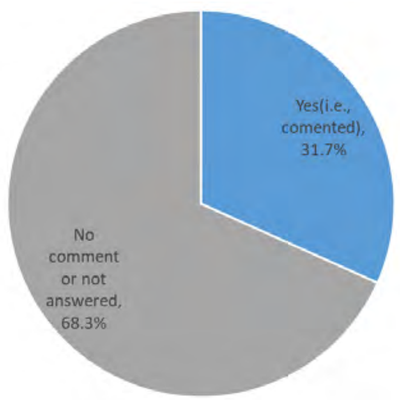

Approximately 32% left comments regarding this process and future improvements. While some say that this procedure was well designed and developed faithfully to the basic assumptions, there were several critical opinions, such as the ones below. While this procedure emphasizes grid studies, it has been suggested that the uncertainty analysis should include a variety of other error factors that affect the solution, such as resolution within the boundary layer and near-wall spacing. There was also criticism about the strict convergence conditions of the numerical solution that did not reflect reality. For example, even in cases where numerical solutions on different grids appear to be diverging or where large uncertainty is predicted, the difference between the coarsest grid and the finest grid solution can be less than 1-2%. Additionally, there are concerns that the systematic grid refinement process may have an undesirable effect on the convergence of numerical solutions. For example, when wall functions are used for turbulence prediction, they point out that wall boundary conditions can be affected if grid refinement is not done carefully enough. Although there are procedures that can improve the case of grid refinement involving the wall function, they may not be practical for typical applications. There is also criticism that this procedure is quite limited in its mention of uncertainty due to time discretization and that there is no recommendation for the prediction procedure. When the error or inaccuracy prediction procedure presented in this procedure is applied to a point variable, the convergence of the numerical solution is often not satisfied, and some argue that an integral-based procedure should be developed to prepare for such cases. Lastly, as an effort to improve the V&V procedures required for EEXI, which is a recent issue, some organizations expressed their willingness to participate in case a benchmark study was needed.

Part B

The following questions (B1 – B5) are about Quality Assurance in CFD Ship Applications

B1. Do you use RP7.5-03-01-02" Quality Assurance in CFD Ship Applications" for your organization's activities?

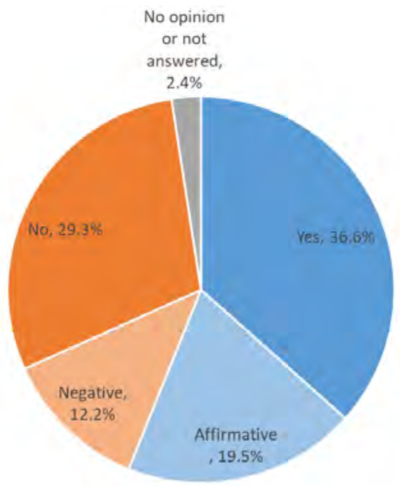

A majority (>63%) replied yes or affirmative answer. Here, affirmative comments are such as "using similar but not identical one" and "planning to use it." Negative comments are "will review later" and "now using the previous RP (2017 edition)". There were no comments from respondents who answered "No". So, it's unclear why they don't apply Quality Assurance in CFD in their activity. In any case, 36% of the respondents are using RP7.5-03-01-02 "Quality Assurance in CFD Ship Applications" itself and some organizations are using similar ones. It was confirmed that Quality Assurance in CFD is put to practical use.

B2. Do you use RP7.5-03-01-02" Quality Assurance in CFD Ship Applications" for your organization's activities? If your answer to B2 is YES, please let us know in what field did you use the RP, and to what kind of organization did you provide the results. If your answer to B2 is NO, could you please motivate why not?

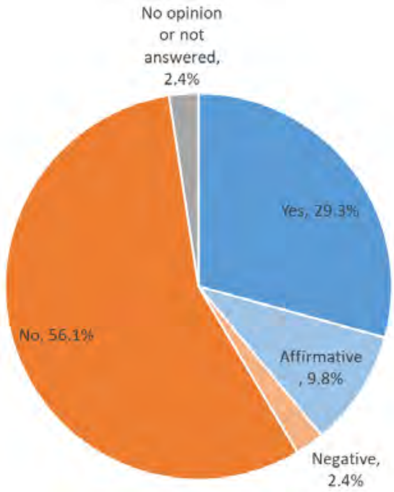

Procedures based on the Best Practical Guideline (BPG) were just included in this RP at the last conference, so it was found that the number of organizations strictly applying it was relatively small (34% of respondents). Despite the above, various cases of application were reported as follows. Application areas: Ship propulsive performance including EEXI related project and ship trim optimization, Ocean structure dynamics, Wake field, Propeller open water characteristics, Wind load for the superstructures. Providing to: Ship-owner, Design office, Class society, Academic application, Organization about ship hydrodynamic conference. Comments from respondents who answered "No" were such as "no opportunity", "not any serious problems", "Not required", "No needs from customers" and "Not necessary for educational purpose". Others commented that they are using similar or almost the same guidelines.

B3. Are you planning to provide CFD and EFD results using the Best Practical Guideline in accordance with RP7.5-03-01-02 in the near future? If your answer to B3 is YES, please let us know in what field you will use the RP and to what kind of organization you will provide the results.

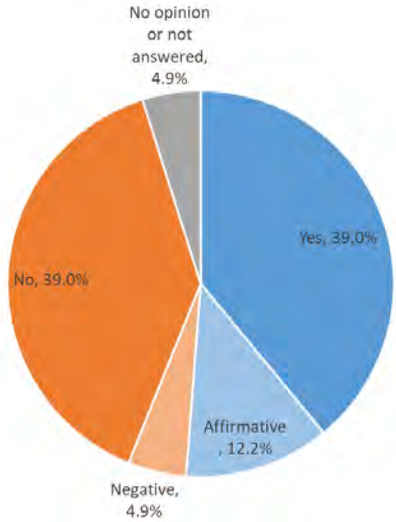

Related to question B.2, B.3 is the question regarding the future application of BPG. There are some relatively affirmative comments from several organizations such as "probably", "maybe" and "if required or mandatory". As a result, about half of the answers were yes or affirmative. Application areas, in addition to the answers in B.2, are: Nautical bottom effect, Ship seakeeping performance and Ship manoeuvrability performance. Shipbuilders will be added to the providing destination in the future. This indicates the utilize of BPG will expand more widely.

B4. Do you think there are any deficiencies in RP7.5-03-01-02? If your answer to B4 is YES, please describe them.

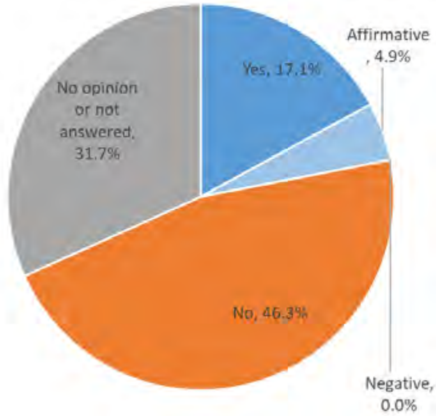

A vast majority (78%) has no opinion or opinion that there is no deficiency in this RP. On the other hand, a few organizations found deficiencies and pointed them out as follows. It is limited to steady simulations and its applications to unsteady/dynamic simulations are not clear. Following this RP would require a lot of computer resources. The current guideline is too concise and needs more detailed descriptions (Various turbulence models were introduced and some viewpoints for grid quality evaluation were described).

B5. Do you think there are any deficiencies in RP7.5-03-01-02? Do you need more detailed, standardized guidelines on how to present statistics for results preparation and delivery?

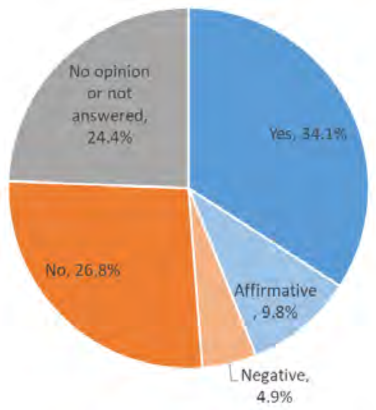

44% of the respondents requested that the guidelines should be improved in some way, and more than half of the respondents answered “No” or “No opinion”. Some of the comments, regardless of the respondent’s position, are as follows. We should try to concentrate on a handful of universal significant statistical parameters to concentrate/qualify as much as possible the reference standards. Not everyone has access to large databases of trials data, so statistics can be difficult to obtain. We hope to receive an additional description regarding sample size. The guideline has just been proposed and should be maintained for a while to gather information of the applicants. It would be better to provide more examples in the guidelines. It is important that the significance and effectiveness of V&V be widely recognized. In addition, it was pointed out that there are discrepancies in V&V studies due to selectable uncertainty analysis methods, and misunderstandings regarding the uncertainty of numerical simulations among non-experts.

Summary and Concluding Remarks. The organizations and institutes that responded to the questions are generally aware of the importance of conducting validation and verification studies for maritime applications. There is clearly sufficient experience in conducting V&V, as a large majority responded that they have already conducted such a study. It makes no difference whether a commercial or an open source CFD code is used: V&V studies are conducted for both types of flow solvers. It can be concluded from this that around half of the respondents see carrying out such studies as their day-to-day business, if the time permits. On the other hand, around two-fifths of the respondents are not able to carry out V&V studies on a day-to-day basis. It can be pointed out that a validation study is not carried out for all simulation tasks, but for new types of ships or calculations. This suggests that the distinction between when a simulation task is considered to be a new type of calculation or not (or whether a new type of ship is in focus) is not clearly defined and is left to the institute or organization to decide.

Most of the respondents indicated that they had experiences performing V&V for CFD, however, it is not encouraging to see that only slightly more than half said they were using RP 7.5-03-01-01. Additionally, the fact that only about one-third of the respondents had experience participating in a benchmark study that required V&V results using this procedure may be evidence that this procedure may not be used as actively as desired in the CFD community. Looking at the respondents' answers, one of the reasons is that the current procedure may be described as too difficult to be easily applied to real problems, and there are insufficient step-by-step examples to facilitate understanding. Among the three V&V approaches provided in this procedure, many respondents use the LSR method, which they say has the advantage of being relatively easy to apply to unstructured grids, less stringent on the requirements of systematic grid refinement, and practical application. It is also applicable to cases of oscillatory convergence that often occur. However, respondents also pointed out that the too large number of grids required for V&V approaches are inefficient in terms of time and computational cost for application to real-world problems, so some respondents preferred using CF or FS methods as these methods are faster in calculation and require fewer number of grids. Many respondents agreed that this process needs improvement, anticipating the above-mentioned difficulties resolved.

Through this survey, we could monitor the current use of the new RP 7.5-04-01-02 "Quality Assurance in CFD Ship Applications" accurately, and the future use of it was also found. More than half respondents are already using the RP 7.5-04-01-02 itself or something similar. It was confirmed that this RP and Quality Assurance in CFD are currently in practical use. The BPG is used by a small number of organizations, but various applications of it were reported, and the expansion of the use of BPG can be supposed from the comments of the questionnaire. Concerning deficiency in the RP 7.5-04-01-02, The vast majority either think that it has no deficiency or have no opinion about this. On the other hand, a few organizations found deficiencies in it and gave us their opinions. Those opinions will be helpful when this RP is revised.

4.3. Update of RP 7.5-03-01-01

RP 7.5-03-01-01 is updated based on the results of the survey discussed in the previous section. The introduced updates first limited the use of maybe too detailed formulas for deriving the variables related to uncertainty analysis as much as possible. Instead, the updated guide provides references to several published methods useful to conduct Verification, Validation, and Uncertainty Assessment (VVUA) as it relates to CFD for the ITTC, together with a current set of definitions of the different aspects of the field of VVUA.

The updated guide down-selects two different V&V methods, instead of the three methods provided in the old guide, which are the Correction Factor (CF) method, Factor of Safety (FS) method, and the Least-Square-Root (LSR) method. The CF and FS methods are replaced with the method of Stern et al. (Xing and Stern, 2010). The LSR method is retained but referred as the method by Eça and Hoekstra (Eça and Hoekstra, 2014). Step-by-step examples are provided by applying the two methods to practical problems, reflecting the demand raised from the survey outcomes discussed in the previous section.

This section first presents brief outlines of the two methods. Next, the two methods are compared to each other by using examples applying them to practical problems to show how both methods are equally suitable and the differences between them, with some aspects that users are to be careful about while using them. Lastly, future works are discussed.

<u>Common Background</u>. Both methods are based on the generalized Richardson Extrapolation (RE) and use an asymptotic expansion of the numerical solution S that depends on the step size h as

$$S = S_0 + \alpha h^p + o(h^p) \quad (1)$$

where, S_0 is the exact solution, α is an unknown constant, and p is the order of accuracy of the simulation. Then, the numerical discretization error is estimated as

$$\delta_{RE} = S - S_0 \quad (2)$$

<u>The Method by Stern et al.</u> This method solves Eq. (1) for the unknown p, with ignoring the higher order terms $o(h^p)$, by using a set of three different grids (a grid-triplet) that are refined systematically. For solutions, say, S_i, with i = 1, 2, and 3 representing the find, medium, and coarse grid, respectively, p is found to be

$$p = \frac{\ln(\varepsilon_{32}/\varepsilon_{21})}{\ln(r)} \tag{3}$$

where, $\varepsilon_{21} = S_2 - S_1$ and $\varepsilon_{32} = S_3 - S_2$ are the differences between different solutions, and $r = h_2/h_1 = h_3/h_1$ is the ratio of the systematic grid-refinement. The numerical error δ_{RE} per Eq. (2) can be written as

$$\delta_{RE} = \frac{\varepsilon_{21}}{r^p - 1} \tag{4}$$

The uncertainty is, then, estimated by multiplying the numerical error δ_{RE} with a factor of safety FS such as

$$U_{FS} = FS \cdot |\delta_{RE}| \tag{5}$$

Xing and Stern (2010) define a distance metric $P = p_{RE}/p_{th}$, where p_{RE} is the estimated (or the observed) order of accuracy calculated using Eq. (3) and p_{th} is the theoretical order of accuracy (e.g., 2 for a second-order solver), and derived FS as a function of P as

$$FS(P) = \begin{cases} 2.45 - 0.85P, & 0 < P \le 1 \\ 16.4P - 14.8, & P > 1 \end{cases} \tag{6}$$

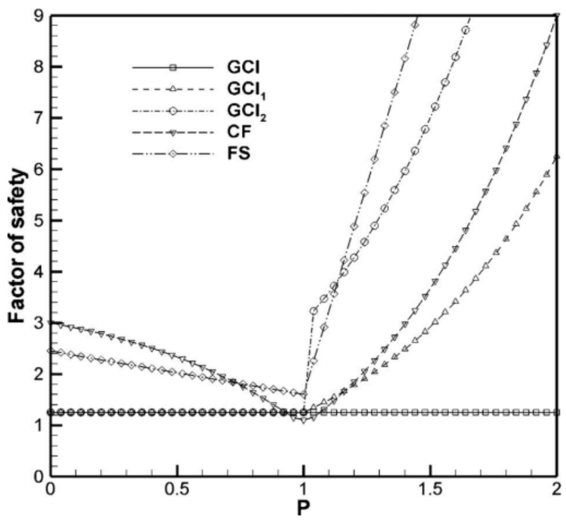

Figure 1. Factor of safety for different verification methods with p_{th} = 2 and r = 2 for the CF method (Xing and Stern, 2010).

Figure 1 shows the FS values over a range of P, with compared with other methods such as the Correction Factor (CF) method (Wilson et al., 2004) or the Grid Convergence Index (GCI, GCI1, GCI2) method (Roache, 1998). The authors state that the FS method is validated using statistical analysis of 25 samples with different sizes and argue that the FS method provides a reliability larger than 95%.

<u>The Method by Eça and Hoekstra</u>. This method determines ϕ_0, α, and p, by curve-fitting the solutions using the Least-Square-Root (LSR) method, again with the higher order terms ignored. Thus, this method requires at least four grids for the LSR process. Here, the symbol ϕ replaces the S in Eq. (1) to follow the authors' nomenclature.

For the uncertainty estimation, first a judgement is made for the quality of the data fit by using a data range parameter defined as

$$\Delta_\phi = \frac{(\phi_i)_{\max} - (\phi_i)_{\min}}{n_g - 1} \tag{7}$$

where n_g is the number of grids used for the curve-fitting. Then, the uncertainty is defined as

$$U_\phi(\phi_i) = \begin{cases} F_S \epsilon_\phi(\phi_i) + \sigma + |\phi_i - \phi_{\text{fit}}|, & \sigma < \Delta_\phi \\ 3\frac{\sigma}{\Delta_\phi}\left(\epsilon_\phi(\phi_i) + \sigma + |\phi_i - \phi_{\text{fit}}|\right), & \sigma \ge \Delta_\phi \end{cases} \tag{8}$$

Here, σ is the standard deviation of the fit. The safety factor F_S = 1.25 is used if the error estimation is considered reliable with $0.5 \le p < 2.1$ and if $\sigma < \Delta_\phi$, otherwise F_S = 3 is used. The error estimator ϵ_ϕ is selected among different choices of $\delta_{RE} = \alpha h_i^p$, $\delta_1 = \alpha h_i$, $\delta_2 = \alpha h_i^2$, or $\delta_{12} = \alpha_1 h_i + \alpha_2 h_i^2$, depending on the magnitude of the p value such that:

$$\epsilon_\phi = \begin{cases} \delta_{RE}, & 0.5 \le p \le 2 \\ \delta_1 \text{ or } \delta_2, & p > 2 \\ \delta_1, \delta_2, \text{or } \delta_{12}, & p < 0.5 \text{ or impossible} \end{cases} \tag{9}$$

For each case of Eq. (7), the error model that gives the smallest σ is chosen.

<u>Comparisons Between Two Methods</u>. Both methods use the asymptotic expansion Eq. (1) based on the generalized Richardson

Extrapolation and estimate the numerical discretization error such that $\delta \approx \alpha h^p$ as shown in Eq. (2). Thus, the convergence of δ as $h \to 0$ depends on p, or from Eq. (3), on the sign and magnitude of the convergence ratio,

$$R = \varepsilon_{21}/\varepsilon_{32} \tag{10}$$

Figure 2 illustrates four possible types of convergence based on R ranges and the corresponding error models used by the FS method. Figure 3 illustrates three different ranges of the observed order of accuracy p value and the corresponding error models used by the LSR method.

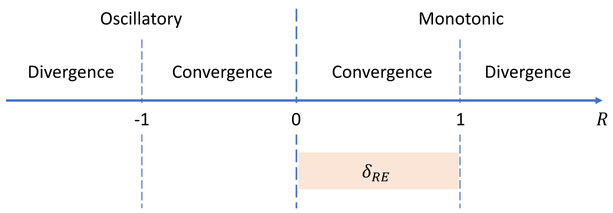

Figure 2. Convergence types based on the convergence ratio ***R*** and the corresponding error models used for the method of Stern et al. (the FS method).

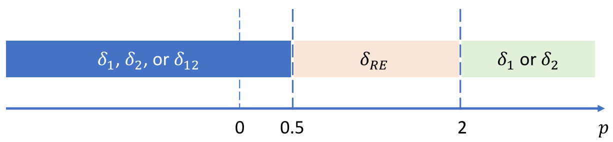

Figure 3. Different ranges of the observed order of accuracy ***p*** and the corresponding error models used for the method of Eça and Hoekstra (the LSR method).

The FS method is applicable only to the monotonic convergence type but is not applicable to all the other convergence types. This method uses the δ_{RE} in Eq. (4) as the error estimator. On the other hand, the LSR method directly uses the order of accuracy p value (instead of R) as a measure to select a proper error model from the choices listed in Eq. (9). Since the LSR method assumes that numerical simulations are of the 2nd-order or lower accuracy, thus limits the use of the error model δ_{RE} only to the cases of $0.5 \leq p \leq 2$. This p range corresponds to the case of $0.25 \leq P \leq 1$ in Eq. (6) of the FS method with $p_{th} = 2$. For $p > 2$, the LSR method again avoids using the δ_{RE} model since the order of accuracy is greater than the theoretical value of 2. Instead, the method introduces the δ_1 or δ_2 model to be used as an error estimator. Lastly, for $p < 0.5$, the LSR method introduces another error model δ_{12} that is a linear sum of δ_1 and δ_2, to allow a more flexible fitting of the possibly oscillatory data.

Table 1. Grid data and the simulation outcomes.

Grid, i	Total number of points	C_{FM} (e-3)	C_{TM} (e-3)
1	25,088,000	3.2148	4.0957
2	15,482,880	3.2116	4.0991
3	9,216,000	3.2075	4.1015
4	5,483,520	3.2021	4.1060
5	3,354,624	3.1945	4.1099

Table 2. Comparisons of VVUA results.

Var.	FS method (Grids 1, 3, 5)		LSR method (Grids 1~5)	
	CFM	CTM	CFM	CTM
p	1.69	1.12	1.72	0.72
δ_{RE}	-9.6e-3	1.3e-2	-9.3e-3	2.3e-2
$U(\%)$	0.5	0.6	0.4	0.7

An example is considered to compare the VVUA results by using the two different methods. Steady-state simulations are made for the model-scale frictional CFM and total CTM resistance coefficients of the Japanese Bulk Carrier (JBC) cargo ship by using a total of 5 different grids (Starke et al., 2024). Table 1 presents the grid data and the simulation outcomes, and Table 2 compares the VVUA results between the two methods. For the FS method, the grids 1, 3, and 5 are used, comprising a grid-triplet with a refinement ratio $r = \sqrt{2}$. The convergence ratio $R = \varepsilon_{31}/\varepsilon_{53}$ value is 0.57 for CFM and 0.67 for CTM, indicating monotonic convergence for both variables. For the LSR method, all five grids are used. The p value is 1.72 for CFM and 0.72 for CTM, thus $0.5 \leq p \leq 2$ for both variables and δ_{RE} is used as the error estimator ϵ_ϕ per Eq. (9). The resulting U values are comparable between the two methods with 0.4 ~ 0.5 % for CFM and 0.6 ~ 0.7 % for CTM.

Applications to practical problems such as high turbulent flows or complex geometries may be vulnerable to 'numerical noises' causing difficulties in achieving the so-called 'asymptotic range' required for a proper use of the RE approach. One of the criticisms of the FS method is that it can be sensitive to the spreads in the simulation results from grid sensitivity studies. An indication may be a higher value of the observed order of accuracy p far from the theoretical value, i.e., $P \gg 1$ in Figure 3. In this case, the large FS values may exceed such values that can be conceived as a typical 'safety factor'. As demonstrated from the above example, both methods, when the data exhibit monotonic convergence with the observed order of accuracy within expectations, provide practically equivalent error estimations. The FS method is simple to use and requires minimal computational resources among other methods. It can be a strategic approach first attempting to apply the FS method by using a grid-triplet. In case the convergence type of this data set is judged to be non-monotonic or non-converging, or the observed order of accuracy is out of the expectation, then one can proceed with using the LSR method. Nonetheless, it is noted there is criticism concerning the use of this method as it deals with even possibly diverging data without a good justification (Xing and Stern, 2015).

Future Updates. The present updates mainly focused on revisions for the verification process reflecting the user experience and suggestions for improvements learned through the survey. The major changes include a current set of definitions for VVUA, simplifying the mathematical derivations for a better readability, selecting the choices for different V&V approaches down from three to two, and providing step-by-step examples. Future updates should focus on revisions of the validation process with the most recent findings such as the N-version approach (Stern et al., 2017). Also, future updates should continue to adapt new verification processes providing better performance or demanding less computational resources.

Update of RP 7.5-03-01-02

Background. Based on the survey results, it was determined that there are no practical issues with this guideline, and a major update is not necessary. Therefore, we conducted a minor update, focusing on changes in terminology and the presentation of statistics.

Terminology correction. The term "total uncertainty" previously used is replaced with "statistics of comparison error". The reason for replacing the term is that in the previous uncertainty analysis, "total uncertainty" was defined as the combined value of the bias limits and the precision limits in EFD. However, in this guideline, "total uncertainty" was used with a different definition and meaning, which could lead to confusion.

The way to present the statistics of the comparison error. Due to insufficient detail in the guideline regarding how to present statistics of the comparison error, additional explanations have been included in this update.

4.4. Updates of other Procedures and Guides

The committee has also reviewed other guides per AC requests and made revisions/actions as summarized in Tab.3. (MC in table refers to the Manoeuvring Committee):

Table 3. Other guides per AC requests and made revisions/actions.

Number	Title	Actions
7.5-03-02-01	Uncertainty Analysis in CFD: Examples for Resistance and Flow	Minor changes
7.5-03-02-02	Benchmark Database for CFD Validation for Resistance and Propulsion	Database updated with new input
7.5-03-02-03	Practical Guidelines for Ship CFD Applications	No changes
7.5-03-02-04	Practical Guidelines for Ship Resistance CFD	Minor changes and corrections for inconsistencies in contents/chapters
7.5-03-03-01	Practical Guidelines for Ship Self Propulsion CFD	Minor changes
7.5-03-03-02	Practical Guidelines for RANS Calculation of Nominal Wakes	Minor changes

7.5-03-04-01	Guideline on Use of RANS Tools for Manoeuvring Prediction	Provided revision suggestions to MC
7.5-03-04-02	V&V of RANS Solutions in the Prediction of Manoeuvering Capabilities	Provided revision suggestions to MC

5. WAKE SCALING

The first SC on CFD and EFD Combined Methods identified a number of research topics within the area of combined EFD/CFD methods. These topics were ranked according to expected impact and possibility to improve with CFD. First in their ranking was the determination of the form factor, a subject they extensively studied and reported to the 2021 ITTC. Second in their ranking was the effective wake scaling and that subject has been studied by the present SC. CFD offers the possibility to compute wakes at either model or full-scale Reynolds number. Direct computation at full scale is attractive because it avoids extrapolation, but the primary drawback is the difficulty to estimate the quality of the solution since validation data is so sparse. Alternatively, it can be investigated if the assumptions underlying empirical methods, for instance the ITTC78 wake scaling formula, are confirmed by CFD computations. If so, it should increase confidence that CFD can be used as an alternative to the ITTC78 wake scaling formula, or that CFD can be used to improve the existing wake scaling formula.

If not, either the assumptions underlying the wake scaling formula are incorrect, or the CFD results are imperfect; that should then be further investigated. Here, the ITTC78 wake scaling formula and its components are shown as follows.

$$w_{TS} = (t + w_R) + \left(w_{TM} - (t + w_R)\right)\frac{(1+k)C_{FS} + \Delta C_F}{(1+k)C_{FM}} \quad (11)$$

Potential part: $(t + w_R)$

Viscous part: $\left(w_{TM} - (t + w_R)\right)\frac{C_{FS}}{C_{FM}}$

Roughness allowance part:

$$\left(w_{TM} - (t + w_R)\right)\frac{\Delta C_F}{(1+k)C_{FM}}$$

The first two parts consider the scale effects on the wake based on theoretical assumptions. The third part accounts for the influence of the surface roughness of an actual ship. All three parts are crucial for considering the full-scale wake, but to proceed cautiously in a step-by-step manner, we will limit our investigation here to the first two parts—the dominant factor in wake scaling—which are based on the respective works of Sasajima-Tanaka and Dickmann. Sasajima and Tanaka proposed that the nominal wake consists of a potential part and a viscous part; the potential part is the same for both the model and the ship, but the viscous part is subject to a scale effect. Dickmann proposed that the potential part of the wake fraction is proportional to the potential part of the thrust deduction. Detailed description of the full-scale wake formula can be found in RP 7.5-02-03-014.

- The three assumptions in the potential part and the viscous part of the ITTC78 wake scaling formula are:
- The potential part of the wake fraction is proportional to the potential part of the thrust deduction.
- The scale effect on the frictional part of the thrust deduction is small.
- The scale effect on the wake fraction is principally determined by a function of the scale effect on the friction coefficient.

To investigate if the validity of these assumptions is confirmed by CFD both model and full-scale CFD predictions have been made for 14 different ships, analysed by 9 different institutes and 7 different CFD codes. Potential wakes have been determined by replacing the viscous no-slip boundary condition at the hull by a free-slip boundary condition.

To maximize the number of cases that could be considered, the CFD set-up was simplified to double-body computations without the rudder, while surface-roughness effects for the full-scale ship were not taken into account. It was expected that such an approach would give a good first indication if the assumptions in the ITTC78 wake scaling formula are confirmed.

Figure 4 through Figure 6 give the CFD results that illustrate the three assumptions listed above. From these the following conclusions can be drawn:

- According to the CFD, the potential part of the wake fraction is indeed proportional to the potential part of the thrust deduction, with a (Pearson) correlation coefficient equal to r = 0.939.
- According to the CFD, the scale effect on the frictional part of the thrust deduction is not necessarily small. However, the frictional part is small compared to the potential part of the thrust deduction, it may not be an important assumption and thus may introduce a relatively small error in the extrapolation procedure.
- CFD does not at all support the assumption that the scale effect on the wake fraction is principally determined by a function of the scale effect on the friction coefficient: there is a large variation in predicted model-to-ship wake-fraction ratios between the various cases.

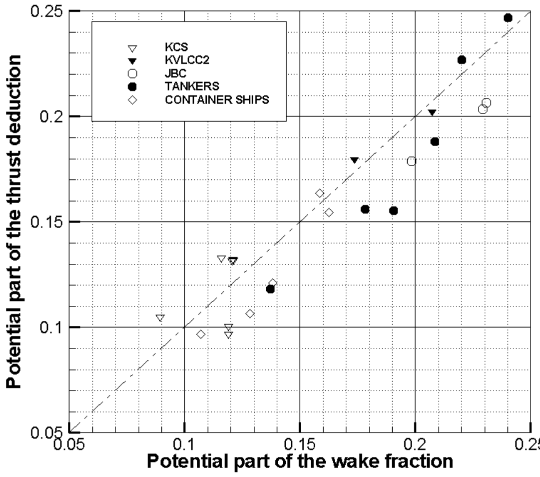

Figure 4. CFD predicted relation between the potential part of the nominal wake fraction and the potential part of the thrust deduction.

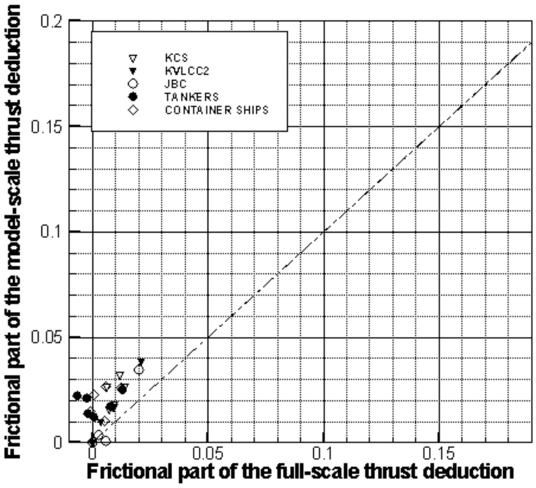

Figure 5. CFD predicted scale effect on the frictional part of the thrust deduction.

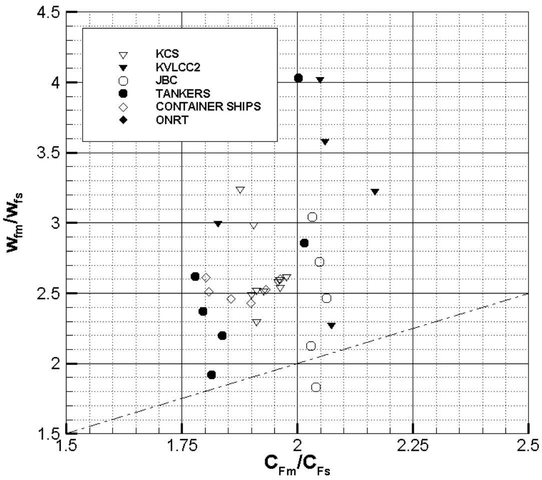

Figure 6. CFD predicted relation between the potential part of the nominal wake fraction and the potential part of the thrust deduction.

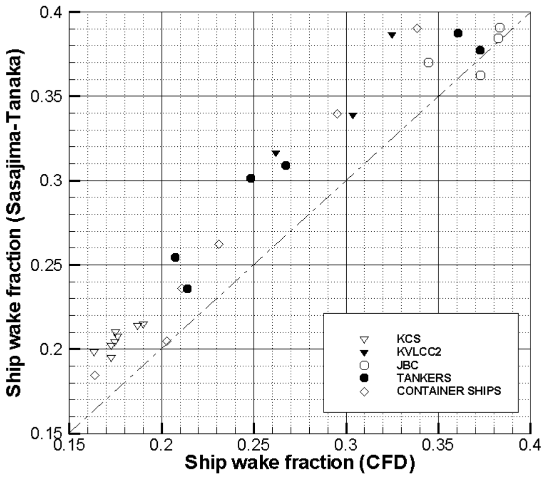

Figure 7. CFD-predicted nominal ship-wake fractions compared to the Sasajima-Tanaka method.

To investigate how the deviation from the three assumptions affects the prediction of the full-scale wake fraction, the CFD results have been used as input for the Sasajima-Tanaka method which targets nominal wake cases and the resulting full-scale nominal wake fractions have been compared to the nominal wake fractions coming directly from the full-scale CFD computations. In Figure 7 it can be seen that the full-scale CFD consistently predicts lower ship-wake fractions compared to the Sasajima-Tanaka method, with an almost constant vertical offset, except at higher wake fractions. The Pearson correlation coefficient evaluated for the data in this figure is r=0.976.

Contradictory to the Sasajima-Tanaka method, the ITTC78 wake scaling formula is based on the *effective* wake fraction rather than the *nominal* wake fraction. Additionally, the ITTC78 wake scaling formula includes the roughness allowance part. CFD propulsion computations have been performed for the same cases and the CFD predicted effective wake fractions have been compared to wake fractions determined with the ITTC78 wake scaling formula, using the corresponding model-scale CFD results as input. From Figure 8 it can be seen that this again results in lower wake fractions from the CFD compared to the extrapolation procedure with an almost constant vertical offset across the entire range of wake fractions without exception.

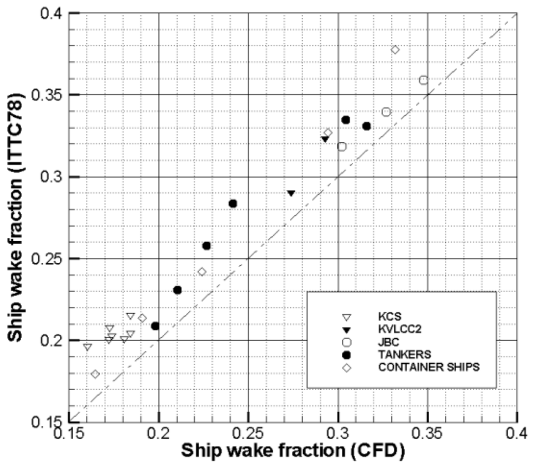

Figure 8. CFD-predicted effective ship-wake fractions compared to the ITTC78 wake scaling formula.

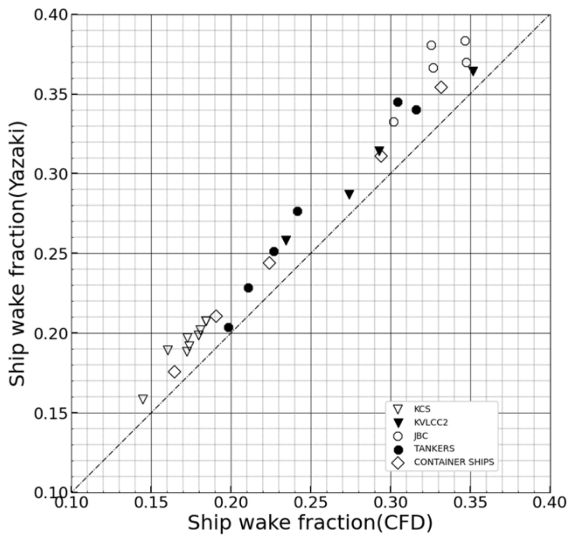

Figure 9. CFD-predicted effective ship-wake fractions compared to the Yazaki method.

And similar results are found when using the Yazaki method (1969), Fig. 9, which is based on correlation with trial data including roughness effect. It is concluded that there is a good correlation between the CFD predicted wake scaling and various empirical methods. Simplifications in the present CFD results will have some effect on the final wake scaling, and thus require further attention. Nevertheless, from this study the committee concludes that improvements in extrapolation procedures can be obtained, especially by replacing the assumed linear relation between the scale effect on the friction coefficient and the scale effect on the wake fraction with a CFD-based procedure.

Various combined EFD/CFD wake scaling procedures can be defined. For instance, replacing the friction ratio that is often taken from the ITTC57 line with a CFD predicted ratio between the wake fractions, or taking the ratio from the CFD predicted wake fractions to multiply the model-scale wake fraction that follows from, for instance, a wake survey:

$$w_{TS} = (t + w_{\mathrm{R}}) + \big(w_{TM} - (t + w_{\mathrm{R}})\big)\frac{w_{\mathrm{S}}^{CFD}}{w_{\mathrm{M}}^{CFD}} \quad (12)$$

$$w_{TS} = w_{TM}\frac{w_{\mathrm{S}}^{CFD}}{w_{\mathrm{M}}^{CFD}}$$

(13)

The committee recommends that a combined method for wake scaling be further analyzed, and any new method be evaluated using sea trial data.

6. OVERVIEW OF THE BENCHMARK CASES AND ONGOING CAMPAIGNS

This section deals with a comprehensive review of the benchmark campaigns relevant to CFD community which have been pursued in the last years in the naval hydrodynamic framework of interest for the ITTC reference community, with a particular focus on ship resistance and propulsion. This activity comes from a request of the previous committee, which considers the monitoring of the benchmark cases as a mandatory aspect to foster the growth of the trustworthiness of CFD calculations. Two Term of References (TORs) were assigned to the committee in the last ITTC conference (as reported in the introduction). The first one (TOR 4) focuses on the review of the outcomes of ongoing CFD benchmark campaigns, and support committees interested in organizing future benchmark activities. The second one (TOR 8) is focused on the definition of a standard procedure when a new benchmark case is planned.

6.1. Progress in the benchmark campaigns

To better understand the progress in the CFD capability in the marine research field, it is fundamental to monitor the evolution of the benchmark campaigns worldwide; therefore, within this section, the focus is on the analyses of the main outcomes arising from the latest CFD benchmark campaigns. Even if most of the sanitary problems concerning the SARS-CoV-2 (COVID-19) were generally overcome, this event reduced international cooperation in the last few years. Consequently, some of the planned international benchmark studies have been reduced in numbers and often postponed. One of the most emblematic examples is the Wageningen Workshop (which continues the Gothenburg and Tokyo Workshop series (Larsson, 2014 and Hino, 2020)), which was announced to be held in 2020 but has been postponed until 2025, so it is out of the scope of the present report.

Nevertheless, in the last four years, some benchmark campaigns have been monitored and found.

<u>JoRes Project.</u> The Joint Research (JoRes, 2024) project for "Development of an industry recognised benchmark for Ship Energy Efficiency Solutions" was a joint research project with more than 55 partners representing worldwide class societies, shipyards, research institutes, universities, propeller and Energy Saving Devices (ESDs) designers, CFD developers and CFD practitioners. The main objective of the project was the encouragement to establish ship full scale benchmark cases provided to the industry serving as a basis to validate the numerical results from CFD studies. Within the project time (2021 to 2024) two different vessels (a multi-purpose vessel and a tanker) have been investigated in several CFD workshops and results have been compared to the corresponding sea trial measurements. In addition to this, valuable CFD work of a flat plat benchmark case has been performed among the participant as well investigating details of different roughness models in full scale. Further full-scale data of four more vessels (ro-ro-ferry, cruise liner, tug and bulk carrier), suitable to serve as a benchmark case, have been collected within this project, but no CFD workshop has been made on this yet.

Considering the industrial nature of the project, most of the outcomes are still covered by a non-disclosure agreement (NDA); the consortium announced that the results will be shared and made available by the end of 2024.

The six different hull geometries, covering a wide range of worldwide ship types (multi-purpose-vessel, tanker, ro-ro ferry, cruise liner, tug and bulk carrier), some equipped with specific ESDs, have been collected. Valuable measurements at full scale (sea trials) were available for these geometries, whereas data at model scale were available only for some of them. In addition, to reduce the input data uncertainties, also some roughness measurements for the hull and propeller were provided and, for one case, full-scale flow measurements (PIV) were available of the inflow wake to the propeller at working conditions for a tanker. This quite rare data could be a valuable insight into a deeper understanding of effective wake at full scale and scale effects. The quality and variety of the data makes this activity very interesting; moreover, due to the well-known (strong) Reynolds number dependency on the ESDs performances, the availability of measurements at both model and full scale is deemed to deeply assess the CFD capability to predict the real efficiency of these devices. Considering the aim was to develop a full-scale benchmark case, also an uncertainty analysis on the sea trial measurements was reported, assessing an overall uncertainty level of about 4-6%. A first draft of the results was published on Ponkratov and Wheeler (2024). They report the evidence provided by one of the participants for a single test case, highlighting that the discrepancies for the predicted sea trials, with respect to the measurements, were about 4-6% for the shaft torque and power, and lower than 1% for the propeller revolution rate. This, as suggested by the authors, demonstrates that the actual CFD capabilities (even if with a not negligible computation effort: 40 million cells for about 100hours on 200 cores) are comparable with the sea trials.

The JoRes community established during this project will not end its collaborative work on analyzing full scale benchmark cases with CFD. Starting in 2024, CFD workshops will be organized by members of this consortium using the full-scale result data of the four vessels mentioned before (ro-ro-ferry, cruise liner, tug and bulk carrier).

<u>Open Workshop on Full Scale Resistance Prediction:</u> The Chalmers University of Technology has organized a freely available CFD benchmark campaign (workshop) in the second quarter of 2024, which has been shared among international research groups. The results will be available by the end of 2024. The workshop is focused on the assessment of CFD capabilities (blind test) in the estimation of full-scale resistance of an un-propelled ship advancing in calm water. The assessment will be pursued by comparing CFD submissions from different participants with full-scale experiments at varying speeds. The novelty of this activity with respect to the past, is the availability of full-scale experiments carried out without a propeller, therefore in towed conditions, so very close to resistance tests than self-propulsion trials. This will allow to focus the comparison on the resistance estimation without introducing any additional source of uncertainty coming from the presence of a propulsion system. The benchmark vessel is a 58m ship length (designed for a single screw-propeller) with a displacement of about 400 tons. The workshop is divided into three main stages, with mandatory and optional submissions. The first set of computations was performed at a fixed attitude in double-model (i.e. without free surface effects) using a mesh provided by the organizers. These simulations were used to compare the accuracy of different codes, setups, and schemes on a common grid. In the second set of computations, free surface effects were introduced; estimations were requested at different ship speeds. With the aim of focusing the comparison on the resistance (and its components) prediction, the computations were pursued at fixed (provided) sinkage and trim. Each participant has been requested to follow his own procedure and best practices, providing a comparison of the expected accuracy of these kinds of CFD simulations. Finally, the third sets were aimed at the analysis of the capabilities of the CFD predictions in estimating Reynolds number effects; to this aim, computations were requested for different scale factors for the reference speed. Even if this resistance benchmark campaign can provide very interesting data to assess the current CFD capability in the full-scale ship resistance prediction, the main outcomes cannot be reported here because their results will be shared only at the end of the 2024 year.

<u>Benchmark on Scale Effect for Open-water Propellers.</u> The liaison activities of this committee with the other technical groups within ITTC committees allows the creation of a new benchmark campaign. The ITTC Resistance and Propulsion Committee organized a benchmark activity devoted to assessing the impact of the model-to-full scale extrapolation on open-water propeller performances. The focus concerns the collection of CFD data useful to verify the accuracy of the actual ITTC extrapolation procedure and to collect relevant data suitable for possible improvement or to better assess its limits. The organizers adopt the well-known benchmark propellers provided by Schiffbau-

Versuchsanstalt Potsdam (SVA): the VP1304, named Potsdam Propeller Test Case (PPTC) for the SMP'11 Abdel-Maksoud (2011) and SMP'15 Workshops Kinnas (2015) and P1727, a controllable pitch and an unconventional tip rake propeller, respectively. The geometry of these propellers, already used in previous benchmark tests, was shared with the testing conditions at both model and full-scale. A matrix of CFD calculations at model and full scale was required at 5 advance coefficients fixing the propeller revolution rate (a single value at full scale and four values at model scale). All the participants were encouraged to adopt their best practices to perform the simulations and to collect their data following the proposed standard procedures. The results were collected by the end of March 2024, and the summary was shared during the ITTC 2024 conference after the drafting of the present report.

SIMMAN 2020. SIMMAN 2020 was the 3rd Workshop on Verification and Validation of Maneuvering Simulation Methods. The previous ones were organized in 2008 and 2014. Originally, the plan was to organize the workshop in 2019, but the project suffered from a four-year delay, due to the pandemic issues for COVID-19 (it was held in July 2022). The purpose of the workshop was to benchmark the capability of the ship manoeuvring simulators through comparisons with EFD results for different hull forms; namely, the three well-known ships widely used for several EFD and CFD benchmarks: the KRISO Container Ship (KCS), the KVLCC2 and the ONRT. The comparisons involved both free-running model tests and captive model tests. This benchmark study is noteworthy by the present committee because CFD-based methods were widely used to feed the systems-based model (virtual captive model tests) or to directly tackle the fluid dynamic problem (virtual free running tests). The workshop was organized by the Korea Research Institute of Ships & Ocean Engineering (KRISO) and The Society of Naval Architects of Korea and held in Incheon, Korea, in early June 2023. The workshop covers not only deep-water conditions but also shallow water ones up to a water depth to draught ratio of 1.2. For all the models, proper captive model tests were considered in shallow and deep water (except for ONRT, where only deep water was available), and, in the same conditions, experimental free model tests were performed. For the KCS and the ONRT, some trajectories were also recorded in wave (deep water) conditions. This latest data was the main novelty for this workshop with respect to the previous editions. Some main conclusions for the captive model tests are drawn from the workshop, see Quadvlieg et al. (2023a) and Quadvlieg et al. (2023b). EFD data are affected by a large scatter and some components cannot be compared among the measurements. The authors suggest improving the EFD measurements among all the institutions providing also an uncertainty quantification. The average error for the CFD-based predictions is generally lower than the empirical ones and the error goes from 6% for pure drift test growing for combined yaw and drift cases. The higher the value of the yaw rates, the larger the discrepancies will be (up to 20%). These conclusions are valid for both deep and shallow water conditions, but the shallow water presents slightly higher differences (10%). For the free running model tests, the main conclusions are that the scatter by CFD and empirical models is still comparable, and the discrepancies are significant, without being able to define which is the best practice for assessing a CFD prediction. The authors suggest further investigation in a new campaign.

NATO-AVT-STO. It is worth mentioning the activities that are pursued within the NATO Applied Vehicle Technology-Science and Technology Organization (AVT-STO). Several benchmark activities have been done and are currently ongoing concerning both physical studies and CFD/EFD assessments. Regarding maritime field, most of the activities have been focused on the assessment of the capabilities of CFD tools in predicting naval hydrodynamic related problems. However, the accesses to the results and the data collected are restricted to the NATO member states (with AUS and JAP in addition as extended opportunity partners), therefore, only few examples of activities are reported here. Activities focused on CFD and modelling assessment range from the analysis of turbulence and transition to turbulence model for CFD (Unsteady Reynolds-Averaged Navier-Stokes (RANS) based) simulations, such as the AVT-313 *"Incompressible Laminar-to-Turbulent Flow Transition Study"*. In these research activities, the assessment of the transition model for RANS code has been carried out on simplified geometries (such as flat plates and profiles) and at relatively low Reynolds numbers. In the AVT-301 team "*Flowfield Prediction for Manoeuvring Underwater Vehicles*", the capabilities of RANS based tools in the prediction of the flow field around complex geometries (the focus was a fully appended un-propelled submarine) have been assessed. The considered test cases concerned static manoeuvres of a submarine (straight ahead, static drift and steady turn), for which the flow field was characterized by largely separated flows, and a strong vortices/boundary layer interaction. Several submissions have been reported (with different solvers, different turbulent model, different computational meshes), allowing a comprehensive comparison between numerical predictions, including the influence of grid resolution and turbulence model on the estimation of local quantities and integral quantities. Ad-hoc experimental tests have been also conducted, providing a valuable data set for CFD benchmark. The conducted analysis highlighted a large discrepancy in the prediction of the flow field around the control surfaces (eventually stalled); this led to the need to deepen the analysis of CFD capabilities in the prediction of the flow around control surfaces at high Reynolds number (order of several Million) at large deflection angle (then eventually at stall conditions). This is the topic of the newer ongoing EFD/CFD benchmark study "*Assessment of numerical methods for complex flow over marine control surfaces*". Other benchmark studies in the marine hydrodynamic field have been focused on the flow field around surface vessels undergoing manoeuvres (both in calm water and in waves). For a complete view of these activities the interested reader can be referred to the public AVT-STO home page (https://www.sto.nato.int/).

Medium-scale Ship case. The Committee noted that China is planning to carry out flow field measurements on a medium-scale existing test ship. The ship was newly built in 2023 and it is mainly used for the validation of integrated energy-efficient propulsion systems, navigation technologies, and other new technologies. The main ship dimensions are: 55 meters in length, 10 meters in breadth, and 2.6 meters as design draught at 1500 tons in displacement (see figure 10). Currently, sea trials of self-propulsion and manoeuvring measurements have been carried out, but the data will be available only in the last part of 2024. In the first phase, the sea trials were conducted at four different propulsion conditions based on the ESD considered (see figure 11, i.e., without ESDs, with a Hub Vortex Absorbed Fins (HVAF), with a Pre-Swirl Duct (PSD), with a HSVF and a PSD. The self-propulsion tests were repeated three times without ESDs showing that the repeatability of the tests was about 1%. The manoeuvring tests, including turning circles and zig-zag, were conducted without ESDs, with a HVAF, and with a PSD. The novelty of this activity is the possibility of having consistent data without and with different energy-saving devices. In addition to the typical self-propulsion data, interesting 2D-3C PIV flow measurements of the inflow velocities to the propeller will be assessed. Unfortunately, due to the impact of COVID-19, the PIV measurement trial has been postponed to the second half of 2024, meaning these data are expected to be available in this committee's next term.

Figure 10. Overview of the medium-scale ship

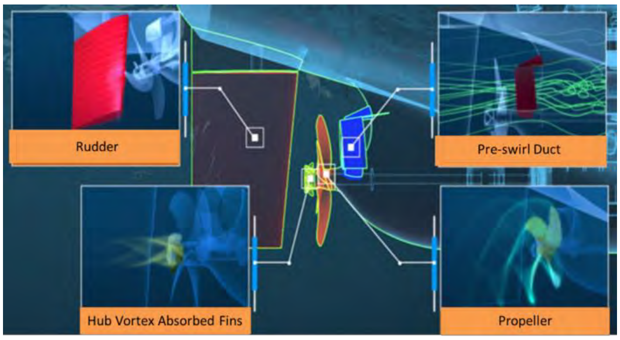

Figure 11. Propulsion system of the medium-scale ship

Future benchmark cases. The committee is also aware of some new benchmarks that will become available in the next years, but no detailed descriptions of them are currently available. Hereafter a not exhaustive list:

5. VTT (Finland) is working in the definition of a medium-size arctic ducted propeller-thruster case. The 'VTT Arctic Thruster' case involves model scale results in open water, full scale CFD including cavitation (OpenFOAM) and model scale CFD (OpenFOAM). The work has been conducted in the national MODPROP project funded by Business Finland. The thruster case will be published including the Computer Aided Design (CAD) model, open water experimental results together with the CFD tutorials.

6. SWOPP, organized by Rise (formerly SSPA) the project will provide a benchmark on wind assisted ships;

7. Wageningen 2025 CFD workshop (successor of Tokyo 2015 CFD workshop) is planned in summary 2025.

The committee recommends continuing to monitor the international scenario to be aware of additional data to be shared with the community.

6.2. Development of new benchmark cases

The second goal for this activity was the definition of a guideline (or a standard procedure) to generate a new benchmark case. Considering that the main interests of the marine engineer are in the ship resistance and performance predictions in general, they cover many different fluid-dynamic aspects, such as ship drag, self-propulsion, manoeuvring, seakeeping, and so on. All these classical marine problems are nowadays affordable by means of CFD tools as long as an adequate HPC infrastructure is available. Nevertheless, the key point to be able to trustfully tackle one of these kinds of simulations is the knowledge of reliable EFD similar data to compare with. This role is generally covered by the benchmark test cases. All the benchmarks share some general properties: they should be complete (all the data should be available) and well described in all their parts (all the data should be avoided by misleading). Apart from these general assumptions, each benchmark endeavour and experiment are unique, requiring proper ad-hoc procedures to be developed. For this reason, the present committee decided to avoid trying to standardize this process because the consequence could be an unused guideline or a too basic one. The only recommendations in this direction for a researcher who wants to assess a new benchmark can be sensitized in these simple questions:

- Did you completely describe how you performed the experiment?
- Did you provide all the data to reproduce it by other researchers?
- Did you report how you collect and analyses the results?
- Did you provide the level of accuracy of your input and output measurement?
- Are your data always available for the community?

These simple sentences can generally be a good way to guarantee that a benchmark test case can be used by the research community, particularly for CFD validation.

Nevertheless, in literature nowadays, considering that research institutes often test the same model more times (same geometry by different scholars or repeated tests with new equipment), similar (but not the same) data can be found from different sources. This often causes confusion and makes the collection of reference data a bottleneck in the CFD validation. For this reason, and in line with the previous conference proceedings, where the website was updated with the new “benchmark repository” section, the committee decided to collect all the sources of literature data (at the moment as references and links) in the ITTC survey repository, with the aim to share in a simpler and more effective way, all the nowadays available benchmark data (with a focus on the ship resistance and propulsion). This repository, which starts from the RP 7.5-03-02-02 material, collects 15 hull forms ranging from the historical ones (such as Wigley hull) to the most recent ones. The list collects systematically the ship name (or the used abbreviation), a short description of the vessel with the main characteristics, a list of links where the data can be downloaded and the references where the complete data was published. The Quality System Group, during last conferences, supported the idea to provide a structured space within the ITTC website fed by the community and under the supervision of the ITTC committees, to collect all the benchmark cases in all the marine field. The present committee agrees with this idea, but the activity was stopped by propriety issues. However, this repository, even if not still directly collects the data, can be considered a starting point for sharing data in this field, encouraging new researchers to compare and share their own data. This repository, if supported over the years, can encourage the naval hydrodynamic community to enlarge the database to be used to assess CFD capabilities and make the CFD predictions to be a more and more reliable tool for research and industrial activities.

Thanks to the contribution of the ITTC secretary, the committee uploaded and updated a webpage in the official ITTC site (https://ittc.info/benchmark-repository/ship-resistance-and-propulsion/). A new tab, named Ship resistance and propulsion, was added to the Benchmark Repository (previously under construction), as shown in Figure 12. In this page a link to a list of cases is reported (see Figure 13).

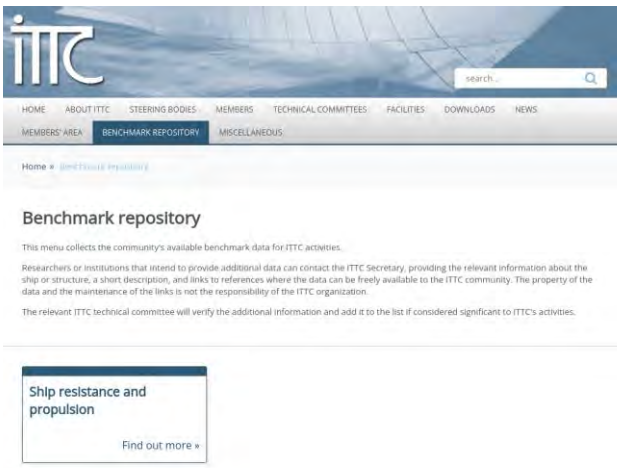

Figure 12. Example of the new ITTC webpages.

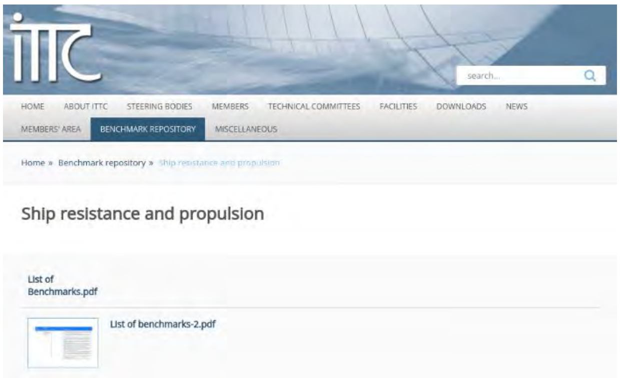

Figure 13. Example of the new ITTC report.

To further fosters the community to increase the available data with also more modern hull forms and propeller shapes, few lines are reported in the main pages, as follows: Researchers or institutions that intend to provide additional data can contact the ITTC Secretary, providing the relevant information about the ship or structure, a short description, and links to references where the data can be freely available to the ITTC community. The property of the data and the maintenance of the links is not under the responsibility of the ITTC organization. The relevant ITTC technical committee will verify the additional information and add it to the list if considered significant to ITTC's activities.

In light of this spirit, this committee suggests including in all the committees' TOR a request to check the correctness and the availability of the benchmark links and references in the list, updating when necessary. In addition, new committee members (each one with its own expertise) shall be involved in the verification part of the new community proposed cases.

7. LITERATURE REVIEW AND STATE OF THE ART

7.1. Advances, Accuracy and Challenges on Speed/Power Predictions

This section monitors and reviews the advances, accuracy and challenges within full-scale and model-scale CFD of maritime applications with special focus on speed/power pre-dictions.

The model-scale CFD methodology has been verified and validated for decades and reached an acceptable maturity level in terms of resistance, self-propulsion, and local flow predictions (Hino et al., 2020). However, the verification and validation effort for the full-scale CFD computations is relatively new and lagging behind mainly due to a lack of publicly available full-scale data. Lloyd's Register conducted a workshop on ship scale hydrodynamic computer simulation with a blind test case for full-scale numerical modelling validation in 2016. The results of the workshop offer valuable insights into the performance of various numerical modelling techniques. Upon closer analysis of the published results, it was found that the mean comparison error for the predicted power was 13% for all submissions, indicating a certain degree of variability in the accuracy of the models. Nevertheless, it is worth noting that three out of the twenty-seven participants achieved highly accurate results, with errors below 3% for all considered speeds. Andersson et al. (2022) conducted a CFD benchmark study comparing industrial state-of-the-art ship-scale CFD predictions of the power reduction through installation of a Pre-Swirl Duct (PSD), where the objective was to both obtain an indication on the reliability in this kind of prediction and to gain insight into how the computational procedure affects the results. The 10 participants conducted 22 different predictions of the power reduction through a PSD installation on KVLCC2. The predicted power reduction varies around zero, on average 0.4%, with a standard deviation of 1.6%-units, if not considering two predictions based on model-scale CFD and two outliers associated with large uncertainties in the results. However, since there were no sea trial results existing, only comparisons of the differences in computational methods were conducted. In addition, recent publications, such as Sasamoto et al. (2020), Sun et al. (2020), Orych et al. (2021), Schouten et al. (2022), and Mikulec and Piehl (2023), demonstrated good accuracy of predicting sea trial conditions with full-scale CFD. However, most of the full-scale validation studies in literature are performed on a ship with one or a limited number of sea trials. As discussed in Korkmaz et al. (2021), a large number of sea trials are required for full-scale validations since the uncertainty of each trial is large.

Korkmaz et al. (2023) conducted an extensive comparative study between full-scale CFD-based ship performance predictions and sea trial results, following procedures compliant with the Safer and Cleaner Shipping (IACS) recommendation for evaluating EEXI values using CFD simulations within the established EEXI framework (IACS, 2022). The full-scale CFD simulations were carried out in accordance with their Best Practice Guidelines (BPG) developed based on the ITTC RP for the quality assurance in CFD (2021). Statistics of comparison errors of the full-scale CFD results were presented for delivered power and propeller turning rates based on 59 sea trial results from 14 vessels. While the accuracy of the CFD predictions may not seem too impressive, the authors argue that a significant portion of the standard deviation is due to scatter among the sea trials.

Liefvendahl et al. (2023) presented statistics of the delivered power ratio between 29 full-scale sea trials conducted on 15 vessels and those predicted by CFD in their RISE/SSPA report. The special motivation behind the creation of the report was stated to demonstrate that the procedures used at RISE/SSPA fully comply with the recent IACS guidelines for evaluating EEXI with CFD (IACS, 2022), so the contents of the report followed the guidelines of IACS.

Ponkratov and Wheeler (2024) pointed out that the main challenge is associated with the fact that sea trials procedures (like ISO15016) were not developed for the purposes of CFD validation. The main objective of these procedures is to confirm contractual speed. As a result, these procedures do not require hull and propeller roughness measurements (which are important for CFD) and still rely on simplified methods (sea state assessment by the naked eye, visual observations of vessel draughts etc). Clearly to develop an accurate case for CFD validation stricter requirements for the ship scale measurements should be implemented.

These expectations led to organizing and executing a JoRes joint research project aiming to develop an industry-recognized benchmark for ship-scale CFD validation. As discussed in Ponkratov (2023), comprehensive ship scale measurements for six vessels were performed including actual hull and propeller roughness checks. The propeller roughness was measured and estimated to be 4 µm. All the detailed measurement values and postprocessing details will be publicly available within the JoRes project benchmark until December 2024. These are preliminary sea trial measurements of JoRes consortium as shown in Table 4, compared with the CFD simulations. Overall, the simulations matched the sea trial favorably. Despite all the effort to perform sea trials as accurately as possible, as discussed in Ponkratov and Strujik (2023) the sea trials uncertainty level for this case was 4-6%. The results can be considered to be validated as the CFD results are within this range.

Table 4. Percent comparison of CFD results to full-scale sea trial measurements

Percent Comparison of CFD Results to Sea Trial Measurements		
Metric	11.25 knots	13.34 knots
Propeller Rotation Rate	0.29%	0.66%
Torque	-5.75%	-4.64%
Shaft Power	-5.43%	-3.69%

7.2. Turbulence Models and Wall Treatments at Full Scale

This section reviews and studies the performance of turbulence models and wall treatments at full scale. The development of new turbulence modelling approaches and their performance for marine applications are also introduced. The section focuses on two main areas: turbulence models at full scale and wall treatments at full scale.

RANS Turbulence models at full scale. It was challenging to simultaneously satisfy both Froude number (Fr) and Reynolds number (Re) similarity, necessitating a choice between gravity similarity and viscosity similarity based on the specific research focus. However, full-scale simulation, unlike traditional scaled-down approaches, allows for the simultaneous fulfilment of both gravity and viscosity similarity requirements. It is crucial to select suitable turbulence models and boundary conditions in full-scale simulations.

The RANS method stands out for its high computational efficiency, acceptable precision, and well-established development, making it currently suitable for full-scale simulations of ships and marine structures. More than 90% of the full-scale simulations are done by RANS method. Many studies demonstrate the capability of full-scale RANS numerical simulations on determining ship performance, such as powering prediction (Song et al., 2020), seakeeping performance evaluation (Niklas & Pruszko, 2019), wake scaling (Can et al., 2020), and hull optimization (Seok et al., 2019). Precision of several percent is documented by comparison with full-scale trial for powering prediction (Korkmaz et al., 2023).

With respect to the validation of full-scale RANS simulations, Eça et al. (2023) assessed the effect of the Reynolds number on the performance of six different RANS turbulence models in the simulation of viscous flows at Re = 2 x10^6 (model scale,) and Re = 10^9 (full scale). It was found that discrepancies between solutions of the six selected turbulence models at model scale Reynolds number were significantly larger than those observed at full scale Re. This indicates that modelling error assessments (validation) performed at model scale Reynolds number cannot be extrapolated to full scale. Moreover, the small discrepancies obtained between the solutions of six turbulence models at full scale is encouraging. The ability to simulate full scale conditions, for which there is almost no experimental data available, is one of the biggest assets of CFD.

Detached Eddy Simulation (DES) Turbulence models at full scale. A small subset of researchers, driven by the demands of their studies, has adopted for more precise 'DES-type' turbulence models in full-scale simulations, with particular attention given to the Improved Delayed Detached Eddy Simulation (IDDES) method (Gritskevich et al., 2012). To accurately simulate the full-scale ship boundary layer, three turbulence modelling strategies suitable for simulating ship flows — k-ε, SST k-ω, and IDDES — were evaluated and compared with full-scale ship propeller torque data from the 138-meter general cargo ship MV Regal by Pena et al. (2020). Among the three different models, the IDDES replicated the sea trial measurements with the highest accuracy. Additionally, the study confirmed that the choice of turbulence strategy significantly influences the full-scale velocity field at the stern of the ship, especially in the wake and jet regions. In addition, the influence of hull roughness on the wake was investigated at real scale with and without propulsion by Kanninen et al. (2022). As simulations progressed, the differences in the wave patterns at the ship's stern between simulations using RANS and DES turbulence models became more pronounced. DES demonstrated better performance in addressing turbulence and wave breaking issues.

Besides the RANS and DES models, Large Eddy Simulation (LES) model is another option for full-scale simulations. While, due to the rapid reduction in turbulent scales with increasing Reynolds numbers, LES is currently not suitable for engineering applications at high Reynolds numbers.

Other turbulence modelling methods. There are developments in the modelling of laminar-turbulent transition, most noteworthy for the assessment of (scale effects on) propellers in open water and in behind conditions. Numerous studies have demonstrated the necessity of incorporating transition modelling in CFD to accurately determine propeller performance at model-scale, whereas full-scale simulations can successfully rely on two-equation turbulence models.

Kerkvliet et al. (2024) demonstrated that CFD, when employing the appropriate turbulence and transition models, can accurately predict propeller performance at model-scale, in scenarios involving partially laminar or fully turbulent boundary layers. The findings provide additional insights on improving extrapolation methods through CFD simulations, particularly when model-scale considerations prioritize the accurate development of turbulent boundary layers. A modelling method on laminar-turbulent transition was proposed based on Reynolds averaged Navier-Stokes solver (RANS) in combination with the k-ω SST turbulence and γ-Reθ transition model for a modern designed MARIN stock propeller. The predicted results by the method were compared to Experimental Fluid Dynamics (EFD) results, which involved propellers equipped with and without innovative turbulence stimulators, also known as turbulators. In addition to comparing performance characteristics, the boundary layer flows regimes were also examined using EFD paint test results. Furthermore, full-scale Reynolds numbers CFD simulations were conducted and compared to conventionally extrapolated EFD results. Excellent comparisons were achieved between EFD and CFD for model-scale Reynolds numbers, encompassing both uncontrolled and passively controlled boundary layers. A clear trend of Reynolds scaling was observed for propellers with a turbulent boundary layer at model-scale. This study enhances the understanding of boundary layer behavior in model and full-scale propellers. These insights are essential for improving model-test accuracy and to enhance the accuracy of full-scale performance predictions, with as end goal to design more efficient marine propulsion systems.

<u>Wall treatments at full scale.</u> There are significant activities and publications on simulating the effects of surface roughness for the wall treatment at full-scale. Roughness effects are one of the main challenges of the prediction of full-scale ship resistance using traditional model tests and extrapolation procedures.

Ohashi (2021) conducted a numerical study of roughness effects at an actual ship scale. In this study, Low-Reynolds number roughness models are developed, based on the two-equation turbulence model. Meanwhile, a wall function method to account for the roughness effect is also developed based on the assumption of local equilibrium. Both models are examined with respect to the computation of the 2D flat plate case at the actual ship scale. The resistance coefficients of the low-Reynolds number models increase with the roughness height similar to the value of the empirical formula. The resistance coefficients of the low-Reynolds number models increase with the roughness height similar to the value of the empirical formula. The wall function method also works properly with changing roughness height and Reynolds number. The uncertainties in the resistance coefficient of the wall function method reach larger values than those of the low-Reynolds number models at the Reynolds number 1.0×10^7 and the uncertainties become smaller at higher Reynolds numbers. Additionally, the distributions of the non-dimensional velocities u+ based on the non-dimensional heights y+ of the low-Reynolds number models and the wall function method are compared for changing the roughness height.

Moreover, both the roughness models and wall function method are applied to simulate the wake flow before the propeller plane of a ship at full scale. The simulated velocity contours are compared to the measured result obtained from the sea test of the actual ship. Both simulated results show good agreement with the measured data. The uncertainties in the total and pressure resistance coefficients of the wall function method are slightly smaller than those of the low-Reynolds number models. Consequently, the wall function method is a better method for full-scale simulations with the roughness effects.

Eça et al. (2022) simulated the flows around different geometries (flat plate, submarine and two ships) at full scale Reynolds numbers (10^8 to 10^9) with RANS solvers using the k-ω SST eddy-viscosity model. Roughness effects are included in the k and ω boundary conditions for values of the sand-grain roughness height covering hydraulically smooth and fully rough surfaces. The results show that with the proper scaling, the increase of the friction resistance coefficient with the sand-grain roughness height is equivalent for the four geometries tested. Conversion of average roughness height to sand-grain roughness is assessed by comparing CFD results with empirical correlations. Simulation results show the best agreement with the Townsin et al (1984). correlation with a small variation of the ratio between average roughness and sand-grain roughness heights.

Upcoming workshops, such as JoRes JIP and the Wageningen Workshop, should provide relevant information about accuracy and uncertainty of full scale and model scale ship predictions.

7.3. Advances in the Application of Detailed Flow Measurements

This section reviews the recent developments and applications of Particle Image Velocimetry (PIV) as a tool to provide detailed flow measurements for ship flows. This will focus on three main areas of recent activity: full scale, hydrodynamic and aerodynamics measurements.

Full scale measurements. The increased demand for full scale validation data for ship resistance and propulsion has led to a number of benchmark campaigns in this area (described in more detail in section 5). In particular the JoRes project has conducted full scale PIV measurements which will be published later in 2024. The PIV method used in this benchmark campaign is detailed by Birvalski et al (2023) where stereo PIV measurements are conducted in the wake of a full-scale sailing ship. They measured part of the propeller inflow area including the peak of the viscous wake using a novel PIV device called the ’FlowPike’. A range of different ship speeds and sailing conditions were assessed in order to help improve full-scale ship CFD simulations in the future. (add figure with measured wake?). Ponkratov & Wheeler (2024) provide a summary of the progress made in full-scale validation data since 2015 and compare their CFD simulations with the JoRes1 tanker full scale data.

There are also planned full-scale PIV measurements as part of the CSSRC full-scale benchmark campaign to be conducted later in 2024. This data along with model scale PIV measurements that have already been conducted should be available at some point in the future.

Hydrodynamics measurements. Since 2020 there have been a range of PIV measurement campaigns focused on Ship hydrodynamics.

Sun et al. (2020) used PIV to measure the flow velocities between the main and demi-hulls of a trimaran and compare this to CFD simulations. One demi-hull was made of a polycarbonate material with 90% light transmission rate and a refractive index 1.58 (close to that of water 1.33) to avoid occlusions from the demi-hull blocking the light source/camera view. A non-standard calibration was performed, and the optical distortions were mapped and corrected.

Wu et al (2020) used PIV to measure the wake flow field behind a Panamax Bulker ship model in a ballast condition and compared it to the design condition. The time-averaged velocity, turbulent fluctuations, turbulent kinetic energy (TKE), Reynolds stresses, and vorticity information were measured indicating a significant difference at the top of the propeller plane in ballast condition due to the proximity of the free surface.

Ortolani et al (2020) investigated propeller off-design conditions associated with a twin-screw vessel in straight ahead and drift angles of ±13◦ and ±27◦. In each condition the propeller inflow condition was measured using a boroscopic-based Stereo-PIV system and compared to the measured forces on individual propeller blades.

Bhushan et al (2021) conducted tomographic PIV measurements in a towing tank for the first time to measure vortical structures in the flow around the surface combatant 5512 with static drift angles of 0, 10° and 20°. The TPIV measurements provided detailed measurements for the progression of the vortical structures and associated mean and turbulent flow characteristics for ship flows. However, they had larger uncertainties near the hull (up to 17%), which limits analysis of the vortex onset characteristics. The authors followed this up with new experiments using four-dimensional particle tracking velocimetry (4DPTV) (Sanada et al., 2023). The same model was used with a static drift angle and a pure sway condition. A comparison between the TPIV and the 4DPTV setup is provided along with the advantages and disadvantages of each.

Deng et al. (2021) used a stereo PIV system in a towing tank to assess the flow field around the bow of a trimaran hull form with different bow configurations, including different bulbous bow designs and T-foils. Model tow speeds between 1.766 and 2.943 m/s were used.

She et al. (2021) conducted time resolved PIV measurements on the water entry of a typical 2D bulbous bow section taken from the KCS hull. Drop tests were conducted to investigate the free surface interactions and measure the induced flow velocities and estimate the surface pressure distribution based of pressure reconstruction.

Guo et al (2021a) investigated the flow field around the bow of a scientific research vessel using flow visualization methods (such as tufts) and stereo PIV at multiple planes. A 3-dimensional (3D) three-component (3C) space reconstruction of the time-averaged flow field around the bow was created. This method was then used in Guo et al (2021b) to characterize the trajectory of bubbles in the flow and compared this with the flow direction from a simple tuft visualization.

Jacobi and Nila (2021) conducted synchronised PIV and Digital Image Correlation (DIC) experiments in a towing tank for the first time to assess the fluid structure interactions of a flexible hydrofoil. This allowed the fluid flow field to be characterized at the same time as full-field structural deformations.

Jacobi et al (2022) characterized the flow velocity around the bow of a fast ship using stereo PIV at Froude numbers up to 0.8. The obtained velocity field is subsequently used for a volumetric description of the time-averaged hydrodynamic pressure field, with the pressure reconstruction conducted in OpenFOAM. A similar methodology is used by Jacobi (2023) to reconstruct the three-dimensional flow and pressure field from a total of 28 PIV measurement planes for a hydrofoil at angles of attack ranging from 0-12◦ in steps of 3◦

Savio et al (2024) evaluated the hydrodynamic performance of a flexible marine propeller in a cavitation tunnel. The fluid structure interaction was characterized using both stereo PIV and Stereo DIC measurements to measure both the propeller deformations and the flow field downstream of the propeller.

Aerodynamic measurements

Alongside the hydrodynamics measurement campaigns, there have been several studies conducted into the aerodynamics around ships.

Correia et al (2021) used PIV to characterize the impact of ship stack geometries on exhaust smoke dispersion in ports using wind tunnel experiments.

Setiawan et al (2022) used PIV experiments to investigate the impact of a simulated Atmospheric Boundary Layer (ABL) on the aerodynamic flow field over the flight deck of two different Naval vessels. The results showed that the ABL increased the turbulent fluctuations but reduced the length of the wake along the flightdeck centreline.

Hysa et al (2023) presented a multi-directional redundant 3D-PIV system for ship deck wind interactions. They investigated the need for redundant imaging and illumination directions with current results showing both the measurement domain and data interpretability benefit from redundancy in both areas.

Zhu et al (2024) used a high-speed, dual-plane, stereoscopic PIV system to measure the aerodynamic flow field around a simplified frigate geometry, with the aim of estimating various other planes in the flow field using a reduced order model.

Summary. The range of published experimental data using or developing PIV methods for ship-related flows indicates that this is an active area of research. This includes the development of new methods that will increase the range of validation data available in the future. Key examples include full-scale ship wake data, the use of tomographic PIV and Particle Tracking Velocimetry to characterize vortical structures, the use of near transparent hulls for reducing visual occlusions and the synchronized use of PIV and DIC to provide fluid-structure interaction data for flexible propellers and hydrofoils.

8. LIAISON WITH OTHER COMMITTEES

The specialist committee has initiated several contacts and liaisons with other committees, groups and people inside and outside the ITTC.

Contact to other chairman and chairwoman of ITTC committees: One of the tasks of TOR1 was to get in contact with other committees to get informed about newly established and used numerical methods in combination with experimental procedures. Furthermore, the contact should encourage the other committees to look explicitly for new combined EFD / CFD methods in their field of topic.

Contact was made and replies have been received from Full Scale Ship Performance Committee especially on details of shallow water correction for sea trial evaluation, the need of reliable full scale performance data and the details of full-scale flow field data. The Specialist Committee on Cavitation and Noise has been contacted with no further relevant update concerning upcoming new methods but existing applications for calculating self-propulsion points in model and full scale as well as for the design of wake-generating dummy models for experimental cavitation analysis. A good contact has been established with the Specialist Committee on Ice where noticeable methods are arising (not yet widely used) simulating ice movement, ice interaction (hull, propeller, ice) and ice breaking. Challenges are here to validate numerical results.

Our committee has been contacted by the Seakeeping Committee to answer their specific question on V&V methods for sea keeping and related unsteady RANS flows.

Review of procedures: For the review of procedures, the committee has been in contact with the manoeuvring committee of the ITTC.

Survey among ITTC members: For the tasks in TOR 9, 10 and 11 the specialist committee set up a survey and distributed it to all members of the ITTC. The focus was on the usage of validation and verification procedures of the ITTC within the context of numerical calculations. The feedback was very satisfying and could serve as a valuable basis for the committee to update the procedures relevant for the V&V (TOR 13). The results of the survey and the corresponding update of RPs are described in more detail in section Survey on V&V and Quality Assurance in CFD.

Review of IACS Recommendation No. 173: The specialist committee has been contacted by the IACS working group and requested to review their new, at that time unpublished, procedure IACS No. 173 “Guidelines on Numerical Calculations for the purpose of deriving the V_{ref}

in the framework of the EEXI Regulation" (IACS, 2022).

Driven by the IMO's focus on reducing emissions from ships and improving their energy efficiency, the IMO has recently introduced the Energy Efficiency Existing Ship Index (EEXI) for all existing ships, regardless of when they were built (IMO 2022a, 2022b). In the newly established framework of EEXI regulations targeting existing vessels, it becomes acceptable to evaluate propulsion performance of ships using only CFD simulations without towing tank testing.

The guidelines, IACS Recommendation No.173 (2022), require applicants for determining EEXI values based on CFD simulations to demonstrate their qualification in quality assurance for CFD simulations according to ITTC RP 7.5-03-01-02. The IACS recommendation presents a numerical calculation methodology, which involves three steps: demonstration of qualification, validation/calibration and calculation. Through these steps, procedures are presented to determine the vessel's reference speed (V_{ref}) required for calculating the EEXI value solely through CFD calculations.

The committee discussed referencing the IACS guideline No. 173 from the ITTC RP 7.5-03-01-02 as an exemplary guideline to produce CFD results based on correlation factors derived on model tests or sea trials. The committee abstained from recommending this, as the IACS guideline is a detailed recipe for the usage of CFD in a special context and references itself on the more generally described basic guidelines of the ITTC in this sense.

Contact to organizes of CFD benchmark campaigns: For the investigation of the description of the different benchmark campaigns (see section, overview of the benchmark cases and ongoing campaigns) the committee has multiple contact with other organizers of such campaigns. For example, the organizers of the JORES project (Jores, 2024) have been contacted by the committee for a discussion. The organizers of the upcoming Wageningen 2025 CFD workshop have been contacted as well. With the Resistance and Propulsion committee of the ITTC contact has been established to receive information on a specific benchmark campaign.

9. FINAL REPORT AND RECOMMENDATIONS TO THE 30TH ITTC

The 30th ITTC Combined EFD/CFD Specialist Committee has made the following conclusions and recommendations:

9.1. General Technical Conclusions

TOR1. The committee performed a literature survey about combined methods. We contacted other committee chairs via email and in person (when possible) to inquire about new combined methods, and to encourage them to consider developing new methods.

The committee considered the future work plan from the previous ITTC, and selected what it thought to be the best candidate to develop a new method, which is to study wake scaling. The committee embarked on a study that explored the assumptions in common wake-scaling formulae (ITTC 1978, Yazaki *replace with references*), and made detailed comparison of wake predictions at full and model scale for a range of ship type, with a variety of CFD codes.

TOR 2. The committee was in contact with the other technical committees to follow and encourage new combined methods. A survey was distributed to request information about current, new, planned, and desired combined methods.

TOR 3,4,5,6. There is an increase of full-scale (and model-scale) CFD applications appearing in the literature. There are notable examples in the recent literature of using turbulence models and wall treatments at full scale. Many studies demonstrate the capability of full-scale CFD numerical simulations on determining ship performance, such as powering prediction, seakeeping performance evaluation, wake scaling, and hull optimization. Precision of several percent is documented by comparison with full-scale trial for powering prediction.

There are significant activities and publications on simulating the effects of surface roughness at full-scale.

There are developments in the modelling of laminar-turbulent transition, most noteworthy for the assessment of (scale effects on) propellers in open water and in the behind condition.

Upcoming workshops, such as JoRES JIP and the Wageningen Workshop, should provide relevant information about accuracy and uncertainty of full scale and model scale ship predictions.

TOR 7. The range of published experimental data using or developing PIV methods for ship related flows indicates that this is an active area of research. This includes the development of new methods that will increase the range of validation data available in the future. Key examples include full-scale ship wake data, the use of tomographic PIV and Particle Tracking Velocimetry to characterise vortical structures, the use of near transparent hulls for reducing visual occlusions and the synchronised use of PIV and DIC to provide fluid-structure interaction data for flexible propellers and hydrofoils.

TOR 8. The committee decided to not develop a standard process for benchmark studies. The variety of studies is so great that a single process would have to be so general that it would not be useful for any particular study.

Instead, the committee worked with the ITTC Secretary to establish a single online location for benchmark studies to be represented on the ITTC website. The first version of collected benchmark cases for resistance and propulsion is online.

TOR 9. A literature study and a survey among members of the ITTC have been done on the use of V&V. More than 40 responses to the survey were received. Over 85% of the survey participants have carried out V&V studies. From the literature study, no relevant new methods for V&V, nor uncertainty assessment, have been found.

TOR 10. RP 7.5-03-01-01 has been substantially revised, including a new front section providing up-to-date definitions and objectives of CFD VVUA, down-selecting to two V&V methodologies, and step-by-step examples of the verification procedures. This update reflects the suggestions that were collected through the survey among ITTC members.

TOR 11. The committee conducted a survey to all ITTC members on the use of the Recommended Procedures 7.5-03-01-02 “Quality Assurance in CFD Ship Applications”. The results of the survey indicate that more than half of respondents are currently using the new RP 7.5-03-01-02, or something similar, for quality assurance.

A major revision has been deemed unnecessary at this time based on the survey results. Two minor updates have been made to the RP 7.5-03-01-02.

TOR 12. The members of the committee, together with several external collaborators, authored a paper in the 35th Symposium on Naval Hydrodynamics that presents results on the study of wake scaling. The paper analyses current wake extrapolation formulae and discusses how computations of ship wakes could be used in a future combined method. The paper also uses the new 7.5-03-01-01 procedure to assess uncertainty.

TOR 13. RP 7.5-03-01-01 and RP 7.5-03-01-02 have been updated according to feedback from the AC and the committee-distributed survey.

9.2. Recommendations

- The committee recommends that the list of future work proposals (including Appendix A, and those in Section xxx) be considered as a guide to continue the work on combined methods in the next ITTC.

- It is recommended that in the future a survey reviewing the use and desire for combined methods be distributed early in the committee work, and the feedback be incorporated in any plans to revise current and pioneer new combined methods.

- It is recommended that the benchmark repository on the ITTC website should be maintained and supported by the ITTC organization to guarantee the correctness and completeness of the information found therein.

- It is recommended to monitor the success of the ITTC benchmark repository and to periodically update it, if necessary. It is also recommended that each new committee consider expanding the list of benchmark cases in their respective fields.

- It is recommended to adopt the updated RP 7.5-03-01-01, and RP 7.5-03-01-02.

- The committee recommends collecting feedback on the usage of the interim version of RP 7.5-03-01-01, and to revise it based on the feedback. It is also recommended to include examples of validation in a subsequent update.

- It is recommended that RP 7.5-03-01-01 be extended for unsteady flows so that it can be used for seakeeping, manoeuvring in waves, and other unsteady problems.

10. REFERENCES

Abdel-Maksoud, M., 2011, “Proceedings of the workshop on cavitation and propeller performance”, The Second International Symposium on Marine Propulsors. SMP’11, Hamburg, Germany.

AIAA, 1995, “Guide for the verification and validation of computational fluid dynamics simulations”, American Institute of Aeronautics and Astronautics, AIAA-G-077-1998, Reston, VA.

Andersson, J., Shiri, A.A., Bensow, R.E., Yixing, J., Chengsheng, W., Gengyao, Q., Deng, G, Queutey, P., Xing-Kaedin, Y., Horn, P., Lücke, T., Kobayashi, H., Ohashi, K., Sakamoto N., Yang, F., Gao, Y., Windén, B., Meyerson, M.G., Maki, K.J., Turnock, S., Hudson, D., Banks, J., Terziev, M., Tezdogan, T., Vesting, F., Hino, T., Werner, S., 2022, “Ship-scale CFD benchmark study of a pre-swirl duct on KVLCC2 Numerical Ship Hydrodynamics”, Applied Ocean Research, Vol.123:103134.

ASME, 2009, “Standard for Verification and Validation in Computational Fluid Dynamics and Heat Transfer”, American Society of Mechanical Engineering, Standard No. ASME-V&V20.

Bhushan, S., Yoon, H. and Stern, F., 2021, “Detached eddy simulations and tomographic PIV measurements of flows over surface combatant 5415 at straight-ahead and static drift conditions”, Ocean engineering, Vol.238:109658.

Can, U., C. Delen, S. Bal, 2020, "Effective wake estimation of KCS hull at full-scale by GEOSIM method based on CFD", Ocean Engineering, Vol.218:108052.

Cavallo, P. A., and Sinha, N., 2007, “Error Quantification for Computational Aerodynamics Using an Error Transport Equation”, J. Aircr., Vol.44(6), pp. 1954-1963.

Cavallo P. A., Sinha, N., and O'Gara, M. R., 2008, "Viscous Error Transport Equation for Error Quantification of Turbulent Flows," 38th Fluid Dynamics Conference and Exhibition, Seattle, WA, Jun. 23-26, AIAA Paper No. 2008-3851, pp. 1-16.

Celik, I., and Hu, G. S., 2004, "Single Grid Error Estimation Using Error Transport Equation," ASME J. Fluids Eng., Vol.126(5), pp. 778-790.

Correia, L.P., Rafael, S., Sorte, S., Rodrigues, V., Borrego, C. and Monteiro, A., 2021, "High-Resolution Analysis of Wind Flow Behavior on Ship Stacks Configuration: A Portuguese Case Study", Atmosphere, Vol.12(3), p.303.

Deng, R., Wang, S., Luo, W. and Wu, T., 2021, "Experimental study on the influence of bulbous bow form on the velocity field around the bow of a trimaran using towed underwater 2D-3C SPIV", Journal of Marine Science and Engineering, Vol.9(8), p.905.

Eça, L. and Hoekstra, M., 2014, "A Procedure for the Estimation of the Numerical Uncertainty of CFD Calculations Based on Grid Refinement Studies", J. Comput. Phys., Vol.262(1), pp. 104-130.

Eça, L., Kerkvliet, M., Toxopeus, S.L., 2023, "Comparison of RANS Turbulence Models for the Simulation of Smooth Wall Boundary-Layers in Pressure Gradients at Moderate and High Reynolds Numbers", 10th Conference on Computational Methods in Marine Engineering, Madrid, Spain.

Eça, L., Starke, A.R., Kerkvliet, M., Raven, H.C., 2022, "On the contribution of roughness effects to the scaling of ship resistance", Journal of Ocean Engineering and Marine Energy, Vol.8, pp. 539-551.

Guo, C.Y., Kuai, Y.F., Wang, W., Han, Y., Xu, P. and Fan, Y.W., 2021a, "Experimental study on bow flow field of scientific research ship based on flow visualization", Ocean Engineering, Vol.235:109412.

Guo, C.Y., Xu, P., Wang, W., Han, Y., Kuai, Y.F. and Fan, Y.W., 2021b, "Experimental study on bubble sweep-down characteristics of research vessels", Ocean Engineering, Vol.228:108963.

Hino, T., Stern, F., Larsson, L., Visonneau, M., Hirata, N., and Kim, J., 2020, "Numerical Ship Hydrodynamics: An Assessment of the Tokyo 2015 Workshop", Springer International Publishing.

Hysa, I. , Tuinstra, M , Sciacchitano , A., and carano, F., 2023, "A multi-directional redundant 3D-PIV system for ship deck wind interactions", 15th International Symposium on Particle Image Velocimetry – ISPIV 2023, San Diego, California, USA.

IACS, 2022, "Guidelines on numerical calculations for the purpose of deriving the Vref in the framework of the EEXI regulation", IACS Rec., No. 173.

IMO, 2022a, "2022 guidelines on the method of calculation of the attained energy efficiency existing ship index (EEXI)", Annex 12: Resolution MEPC., 350(78).

IMO, 2022b, "2022 guidelines on survey and certification of the attained energy efficiency existing ship index (EEXI)", Annex 12: Resolution MEPC., 351(78).

ITTC, 1978, "Report of Performance Committee. In Proceedings of 15 ITTC", 15th International Towing Tank Conference, Hague, Netherlands, pp. 361-369.

ITTC – Recommended Procedures and Guidelines 7.5 – 03 – 02 – 02 Benchmark Database for CFD Validation for Resistance and Propulsion.

Jacobi, G. and Nila, A., 2021, “Simultaneous PIV and DIC Measurements in a Towing Tank Environment with a Flexible Hydrofoil”. In 14th International Symposium on Particle Image Velocimetry, Vol. 1, No. 1.

Jacobi, G., Thill, C.H. and Huijsmans, R.H.M., 2022, “Pressure reconstruction from PIV measurements in the bow region of a fast ship”, Ocean Engineering, Vol.252: 110318.

Jacobi, G., 2023, “Pressure reconstruction on a T-foil from underwater multi-plane stereo PIV measurements in a towing tank”, 15th International Symposium on Particle Image Velocimetry – ISPIV 2023. June 19–21, 2023, San Diego, California, USA.

JoRes Project, 2024, “Development of an industry recognised benchmark for Ship Energy Efficiency Solutions”, internet reference, https://jores.net/

Kanninen, P., P. Peltonen, V. Vuorinen, 2022, "Full-scale ship stern wave with the modelled and resolved turbulence including the hull roughness effect", Ocean Engineering, Vol.245: 110434.

Kerkvliet, M., Baltazar, J., Schuiling, B., Eça, L., 2024, “A numerical study on Model Propeller Performance Prediction Including Transitional and Passively Controlled Boundary Layer Considerations”, 8th Int. Symp. on Marine Propulsors, Berlin, Germany.

Kinnas, S.A., 2015, “Proceedings of the second workshop on cavitation and propeller performance”, The Fourth International Symposium on Marine Propulsors, SMP’15, Austin, Texas.

Korkmaz, K. B., Werner, S., Bensow, R., 2021, “Verification and validation of CFD based form factors as a combined CFD/EFD method”, Journal of Marine Science and Engineering, Vol.9(1), p.75.

Korkmaz, K., Kim, K., Liefvendahl, M., Werner, S., and Orych, M., 2023, “A Validation Study of Full-Scale CFD Simulation for Sea Trial Performance Prediction of Ships”, 10th Conference on Computational Methods in Marine Engineering, Madrid, Spain.

Kunihide, O., 2021, "Numerical study of roughness model effect including low Reynolds number model and wall function method at actual ship scale", Journal of Marine Science and Technology Vol.26, pp. 24-36.

Larsson, L., Stern, F., Visonneau, 2014, “Numerical Ship Hydrodynamics: An assessment of the Gothenburg 2010 Workshop”, Springer International Publishing.

Liefvendahl, M. and Finnsgard, C., 2024, “Ship power predictions with CFD in full scale”, SSPA/RISE Report, No: 2023:21, 2023.

M. Birvalski1, G. D. Struijk, D. Ponkratov., “Full-scale PIV measurements of the propeller inflow”, 15th International Symposium on Particle Image Velocimetry – ISPIV 2023, San Diego, California, USA.

Mikulec, M. and H. Piehl, 2023, "Verification and validation of CFD simulations with full-scale ship speed/power trial data", Brodogradnja, Vol.74(1), pp. 41-62.

Niklas, K. and H. Pruszko, 2019, "Full scale CFD seakeeping simulations for case study ship redesigned from V-shaped bulbous bow to X-bow hull form", Applied Ocean Research, Vol.89, pp. 188-201.

Ohashi, K., 2021, “Numerical study of roughness model effect including low Reynolds number model and wall function method at actual ship scale”, Journal of Marine Science and Technology, Vol.26, pp. 24-36.

Ortolani, F., Capone, A., Dubbioso, G., Pereira, F.A., Maiocchi, A. and Di Felice, F., 2020, “Propeller performance on a model ship in straight and steady drift motions from single blade loads and flow field measurements", Ocean Engineering, Vol.197: 106881.

Orych, M., Werner, S., and Larsson, L., 2021, "Validation of full-scale delivered power CFD simulations", Ocean Engineering, Vol.238: 109654.

Pena, B., E. Muk-Pavic, G. Thomas, P. Fitzsimmons, 2020, "An approach for the accurate investigation of full-scale ship boundary layers and wakes" Ocean Engineering, Vol.214: 107854.

Ponkratov, D., 2023, "JoRes Joint Research Project - the largest global community developing a benchmark for ship scale CFD", 25th Numerical Towing Tank Symposium, Portugal.

Ponkratov, D. and Wheeler, M., 2024, "Ship-Scale CFD Self-Propulsion validation – SMP'2024 vs SMP'2015", 8th International Symposium on Marine Propulsors, Berlin, Germany.

Ponkratov, D. and Struijk, G., 2023, "Quantifying the Uncertainty of High-Fidelity Speed/Power Trials", 8th Hull Performance and Insight conference HullPIC2023, Pontignano, Italy, pp. 28-30.

Quadvlieg, F.H.H.A., Flensborg-Otzen, L., Stern, F., Yasukawa, H., Kim, Y., Wentao, W., Yang, H. 2023a, "SIMMAN2020: Final Report before the workshop", Volume I; Captive conditions; Version 21 June 2023.

Quadvlieg, F.H.H.A., Flensborg-Otzen, L., Stern, F., Yasukawa, H., Kim, Y., Wentao, W., Yang, H. 2023b, "SIMMAN2020: Final Report before the workshop". Volume II; Trajectories; Version 16 June 2023.

Richardson, L. F., 1911, "IX. The approximate arithmetical solution by finite differences of physical problems involving differential equations, with an application to the stresses in a masonry dam", Philosophical Transactions of the Royal Society of London. Series A, Containing Papers of a Mathematical or Physical Character, 210(459-470), 307-357.

Roache, P., 1994, "Perspective: A Method for Uniform Reporting of Grid Refinement Studies," ASME J. Fluids Eng., Vol.116(3), pp. 405-413.

Roache, P. J., 1998, "Verification and Validation in Computational Science and Engineering", Albuquerque, NM: Hermosa, Vol. 895, p. 895.

Sakamoto, N., Kobayashi, H, Ohashi, K., Kawanami, Y., Winden, B. and Kamiirisa, H., 2020, "An overset RaNS prediction and validation of full scale stern wake for 1,600TEU container ship and 63,000 DWT bulk carrier with an energy saving device", Applied Ocean Research, Vol.105: 102417.

Savio, L., Jenssen, Y., Henry, P.Y. and Franzosi, G., 2024, "Experimental investigation on the flow and deformation fields of an elastic propeller". 8th International Symposium on Marine Propulsors, Norwegian University of Science and Technology, Department of Marine Technology, pp. 747-752.

Sanada, Y., Starman, Z., Bhushan, S. and Stern, F., 2023, "Four-dimensional particle tracking velocimetry measurements of unsteady three-dimensional vortex onset and progression for 5415 straight ahead, static drift, and pure sway", Physics of Fluids, 35(10).

Schouten, D. R., Drouet, A., Birvalski, M., and Morand, L., 2022, "Full Scale CFD Validation Using Ship Performance and Wave Pattern Measurements of a Mega Cruise Ship", American Society of Mechanical Engineers, Volume 7: CFD and FSI, page V007T08A041.

Sidi, A., 1997, "A Complete Convergence and Stability Theory for a Generalized Richardson Extrapolation Process," SIAM J. Numer. Anal., Vol. 34, No. 5, pp. 1761-1778.

Stern, F., Wilson, R. V., Coleman, H., and Paterson, E., 2001, "Comprehensive approach to verification and validation of CFD simulations – Part 1: Methodology and procedures," Journal of Fluids Engineering, Vol.123, pp. 793-802.

Stern, F., Diez, M., Satat-Hosseini, H., Yoon, H., and Quadvlieg, F., 2017, "Statistical Approach for Computational Fluid Dynamics State-of-the-Art Assessment: N-Version Verification and Validation," J. Verif. Valid. Uncert., 2(3): 031004.

Schouten, D. R., Drouet, A., Birvalski, M., and Morand, L., 2022, "Full Scale CFD Validation Using Ship Performance and Wave Pattern Measurements of a Mega Cruise Ship", International Conference on Offshore Mechanics and Arctic Engineering, ASME, Vol.85925.

Setiawan, H., Philip, J. and Monty, J.P., 2022, "Turbulence characteristics of the ship airwake with two different topside arrangements and inflow conditions", Ocean Engineering, Vol.260: 111931.

Seok, W., G. H. Kim, J. Seo, S. H. Rhee, 2019, "Application of the design of experiments and computational fluid dynamics to bow design improvement", Journal of Marine Science and Engineering, Vol.7(7), p. 226.

She, W., Zhou, G., Guo, C., Wu, T. and Song, K., 2021, "Experimental investigation on the water entry of a bulbous bow based on TR-PIV", Ocean Engineering, Vol.229, p. 108977.

Song, S., Y. K. Demirel, M. Atlar, S. Dai, S. Day, O. Turan, 2020, "Validation of the CFD approach for modelling roughness effect on ship resistance", Ocean Engineering, Vol.200: 107029.

Sun, C., Guo, C., Wang, C., Wang, L. and Lin, J., 2020, "Numerical and experimental study of flow field between the main hull and demi-hull of a trimaran", Journal of Marine Science and Engineering, Vol.8(12), p. 975.

Sun, W., Hu, Q., Hu, S., Su, J., Xu, J., Wei, J., Huang, G., 2020, "Numerical Analysis of Full-Scale Ship Self-Propulsion Performance with Direct Comparison to Statistical Sea Trail Results". Journal of Marine Science and Engineering, Vol.8(1):24.

Townsin RL, Medhurst JS, Hamlin NA and Sedat BS, 1984, "Progress in calculating the resistance of ships with homogeneous or distributed roughness", NECIES Centenary Conference in Marine Propulsion, Newcastle upon Tyne, United Kingdom.

Wilson, R., Stern, F., Coleman, H., and Paterson, E., 2001, "Comprehensive Approach to Verification and Validation of CFD Simulations-Part2: Application for RANS Simulation of a Cargo/Container Ship," ASME J. Fluids Eng., Vol. 123, Dec. 2001.

Wu, T., Luo, W., Jiang, D., Deng, R. and Li, Y., 2020, "Stereo particle image velocimetry measurements of the wake fields behind a Panamax bulker ship model under the ballast condition", Journal of Marine Science and Engineering, Vol.8(6), p.397.

Xing, T. and Stern, F., 2010, "Factors of safety for Richardson extrapolation", J. Fluids Eng. 132:6.

Xing, T. and Stern, T. 2015, Comments on "A procedure for the estimation of the numerical uncertainty of CFD calculations based on grid refinement studies", Journal of Computational Physics, Vol.301, pp. 484-486.

Yazaki, A., 1969, "A diagram to estimate the wake fraction for an actual ship from model tank test", Proceedings of the 12th International Towing Tank Conference, Rome, Italy.

Zhu, N., Zhang, Z., Gnanamanickam, E.P. and Leishman, J.G., 2024, "Estimation of 3D ship airwakes using dual-plane PIV", Experiments in Fluids, Vol.65(1), p.11.

Appendix A

The Combined EFD/CFD Specialist Committee proposes the following topics for future work.

The 7.5-03-01-01 guide has been substantially updated, and it is proposed to continue to promote its adoption, while gathering feedback about its use for its further refinement. There is a need to update other guides that rely on the 01-01 guide to reflect the changes in the 01-01 guide itself.

Currently there is not a guide for VV&UA for transient flows, and this is necessary for CFD to be used for seakeeping computations. It is proposed that in the future the 01-01 guide is expanded for transient flows, or that a new guide is developed for CFD in seakeeping.

The SC on Combined EFD/CFD in the 29th ITTC formed a list of issues affecting scaling and performance prediction. We reprint the list here and use it to make updated suggestions for future work. The list is ordered with the highest priority first:

1. Roughness allowance. Currently there are many researchers using CFD to understand roughness allowances. The next committee could gather the new information available and incorporate it into ITTC procedures and guides.

2. Finite-depth and restricted-water effects for full scale operation.

3. Propeller open water scaling (transition modelling at model scale). This work should consider both conventional and unconventional propellers, including azimuthing thrusters.

4. Flow separation and vortices shed the vessel

5. Energy saving devices

6. Transom drag

7. Wave resistance

8. Appendage resistance

9. Hull friction estimation using alternative friction or correlation line

Work that has already been initialized, but can benefit from further attention:

10. Nominal and effective wake scaling. This topic was studied by the SC on EFD/CFD in the 30th ITTC, and while progress was made towards understanding scaling of wakes, this topic could be continued in the future to develop a new technique to determine the full-scale wake fraction.

11. Form factor determination. This topic was studied by the SC on EFD/CFD in the 29th ITTC.

ITTC2024

30TH INTERNATIONAL TOWING TANK CONFERENCE
22–27 SEPTEMBER 2024 | HOBART TASMANIA AUSTRALIA

REPORT OF THE SPECIALIST COMMITTEE ON CAVITATION AND NOISE

This report summarizes the work of the Specialist Committee on Cavitation and Noise of the 30th International Towing Tank Conference.

1. INTRODUCTION

1.1 Membership and Meetings

The members of the Specialist Committee on Cavitation and Noise of the 30th ITTC are:

- Dr. **Romuald Boucheron** (Chair)
  DGA Hydrodynamics, FRANCE
- Dr. **Francisco Alves Pereira** (Secretary)
  CNR-INM, ITALY
- Dr. **Djahida BOUCETTA**
  GHENT University, BELGIUM
- Mr. **Crispin FETHERSTONHAUGH**
  QinetiQ, UNITED KINGDOM
- Dr. **Przemyslaw KROL**
  (up to 2023)
  CTO, POLAND
  replaced by
- Dr. **Jan HALLANDER** (since 2023)
  SSPA Maritime Center, SWEDEN
- Dr. **Thad MICHAEL**
  NSWC Carderock Division,
  UNITED STATES
- Dr. **Yezhen PANG**
  CSSRC, CHINA
- Dr. **Cheolsoo PARK**
  KRISO, KOREA
- Mr. **Kei SATO**
  Mitsubishi Heavy Industries, JAPAN
- Mr. **Ville VIITANEN**
  VTT, FINLAND

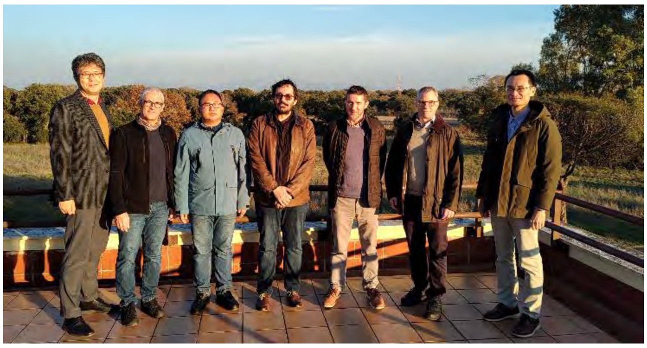

Figure 1: Photograph of the Specialist Committee on Cavitation and Noise at its 3rd in-person meeting in Roma.

The committee held four face-to-face meetings during the work period at the following locations:

- Val-de-Reuil, France at DGA Hydrodynamics on June 15-16, 2022.
- Daejeon, South Korea at KRISO on May 23-25, 2023
- Roma, Italy at CNR-INM on January 30 to February 1st, 2024.
- Wuxi, China at CSSRC on April 23-24, 2024.

Video conferences were held on January 12 and 13, 2022; December 13-14, 2022; November 28-29, 2023, July 15, 2024.

1.2 Recommendations of the 29th ITTC

The recommendations for the work of the Cavitation and Noise Specialist Committee as given by the 29th ITTC were as follows:

1. Review and update the current guidelines on model and full scale noise measurement and review and update the existing procedures on cavitation; provide recommendations for new guidelines / procedures, if any.

2. Review the state of the art on cavitation model testing (cavitation appearance, hull pressure fluctuation, thrust break down, cavitation erosion) with a focus on ways to reproduce the scaling effects on ship wakes. Conduct an Uncertainty Analysis on the full-scale prediction of all the cavitation parameters (cavitation appearance, hull pressure fluctuation, thrust break down, cavitation erosion).

3. Review the current CFD methods for cavitation extent and hull pressure fluctuation prediction and especially on the use of a dummy model (defined by using CFD calculation) on propellers / pods / other types. Liaise with the Specialist Committee on CFD/EFD Combined methods. Provide recommendation for a new guideline on how to proceed for the dummy model definition.

4. Review the currently available CFD benchmark data, including the on-going projects, such as JORES, and investigate the feasibility to establish an ITTC benchmark database.

5. Review new measurement techniques used for cavitation model testing and full-scale trials (optical measurement for blade cavity extent, fluctuating forces on blades…).

6. Organize the proposed round-robin test case as recommended in the 29th Noise committee.

7. Monitor and investigate specific aspects of model-scale noise measurements including reverberation, tip vortex scaling, water quality and the effect on uncertainty.

8. Review any open literature dealing with the respective contributions of the hull vibrations and of the propeller in the ship radiated noise at full scale (frequency line and broad band spectrum) and investigate ways of assessing those contributions

9. Continue monitoring progress on shipping noise measurement procedures for shallow water and regulations as developed by ISO, classification societies and regulatory agencies.

10. Continue monitoring progress on ship noise prediction by computational methods with emphasis on the prediction of cavitation noise using CFD methods and methods such as data driven models and machine learning techniques, and noise propagation modelling, especially for shallow waters

2. STATE OF THE ART

The assessment of underwater radiated noise (URN) and/or cavitation phenomena from vessels now plays a central role in ship design. Cavitation consequences (noise, erosion, thrust break-down, etc.) are well-known but still difficult to predict at the full scale accurately. Many different phenomena have to be taken into account in such studies (hydrodynamics, acoustics, vibrations, mass transfer, water quality, etc.).

In section 3, this report reviews the procedures and guidelines that have been updated with a focus on the main changes. Section 4 is dedicated to the extensive review of the literature and recent studies dealing with cavitation (§4.1), noise (§4.2) and vibrations (§4.3). Numerical and experimental aspects are presented.

<u>IMO background</u>

The IMO (International Organization for Standardization) started to pay attention to the adverse effects of ship underwater noise on marine life in 2005. In 2007, the United States proposed to study the impact of shipping noise on marine life at MEPC 57 (Marine Environment Protection Committee). In 2014, IMO issued the first edition of “Guidelines for The Reduction of Underwater Noise from Commercial Shipping to Address Adverse Impacts on Marine Life” (MEPC.1/Circ 883). In 2019, Australia and other countries proposed to review the first edition of the guidelines at MEPC 75, their research survey shows that there is no indication that these guidelines have had any impact. In June 2021, IMO agreed to further study the underwater noise from ships, and MEPC 76 agreed to review and update the first edition of the guidelines. The SDC 8 (Sub-Committee on Ship Design and Construction) Underwater Noise Communication Group submitted a guideline to MEPC 80 for review, which was approved in July 2023 as MEPC.1/Circ 906. The purpose of these Guidelines is to provide an overview of approaches applicable to designers, shipbuilders and ship operators to reduce the URN of any given ship; and assist relevant stakeholders in establishing mechanisms and programmes through which noise reduction efforts can be realized. Meanwhile the MEPC.1/Circ 906 is approved to provide additional information and guidance to operators transiting Inuit Nunaat and the Arctic.

SDC approved convening an Expert Workshop on Underwater Radiated Noise and Ship Energy Efficiency, this encouraged submission of best practices on implementation as guidance prior to the release of MEPC 85. Discussion included the flow chart of the noise management plan, the priority of noise reduction measures, the setting of underwater noise target values and the classification of underwater noise from ships. Currently, the impact of ship underwater noise on marine ecosystems remains an unresolved issue. More research is needed in the future to understand the impact of ship underwater noise on marine ecosystems and to develop more effective mitigation measures.

The ITTC Specialist Committee on Noise contributed by submitting the following document to IMO during the development of their circulars; ITTC 2023, “Review of full-scale ship noise measurement and estimation techniques”.

3. PROCEDURES

All the procedures and guidelines have been updated. The main task has been making all the documents consistent with each other. Therefore, a global document, based on the procedure 7.5-02-03-03.2, has been extensively updated to give a common base for all the other procedures and guidelines. It has been renamed “Visual description and measurement of cavitation events.” It proposes global features and a common description of the cavitation events that could be observed in many configurations. Specific aspects of a given configuration have been maintained in the other documents only if applicable for the procedure.

3.1 Model-scale cavitation test

The document 7.5-02-03-03.1 has been revised to ensure consistency with all other procedures and guidelines in terms of definitions and references.

3.2 Visual description and measurement of cavitation events

The procedure 7.5-02-03-03.2 includes the information that are common to all the other procedures or guidelines. The description of cavitation has been extended with super-cavitation. A section on cavitation observations on podded propulsors and a section on measurements of cavitation events have been added.

3.3 Cavitation induced pressure fluctuations: model scale experiments

The document 7.5-02-03-03.3 has been revised to ensure consistency with all other procedures and guidelines in terms of definitions and references. The discussion about the wake field has been updated.

3.4 Cavitation-induced pressure fluctuations: numerical prediction methods

The document 7.5-02-03-03.4 has been revised with different numerical approaches. Also, recent references have been added to illustrate the results obtained by the different methods.

3.5 Model experiments including numerical simulation guidance for propeller and rudder cavitation erosion

The document 7.5-02-03-03.5 combines the two previous rudder and propeller erosion procedures[1]. The numerical simulation has been extended to reflect current practice.

3.6 Podded propulsor model scale cavitation test

The document 7.5-02-03-03.6 has been revised to ensure consistency with all other procedures and guidelines in terms of definitions and references.

3.7 Modelling the behaviour of cavitation in waterjets

The procedure 7.5-02-03-03.8 has been reorganized and updated with the addition of more recent references, including experiments and simulations with the ONR AxWJ-2 axial flow waterjet pump geometry.

3.8 Model-scale propeller cavitation noise measurements.

The document 7.5-02-03-03.9 maintains most of the content of the previous guideline[2], except for some minor corrections and/or modifications to ensure consistency with other procedures and guidelines.

3.9 Underwater noise from ships, full scale measurements

The document 7.5-04-04-01 has been updated with a focus on special requirements for test sites and hydrophone deployment. The section on shallow water measurements includes propagation loss assessing methods for ship radiated noise source level estimation.

4. CAVITATION AND NOISE ACTIVITIES

4.1 Cavitation

4.1.1 Experimental model testing

A large number of recent publications on model scale cavitation tests deal with noise measurements which are treated in Section 4.2.1 of this report. The developments in the field of optical measurements and laser techniques are mainly dealt with in Section 4.1.2.

Measuring the flow field of the propeller is important to understanding the source of pressure fluctuations and noise to improve numerical modelling. Guangnian *et al.* (2020) measured the flow field near the blade tip using the 2D-PIV technique. They monitor the process of generation and shedding of the propeller tip vortex in real time and analyze the dynamic structure of the tip vortex.

Yilmaz *et al.* (2020) present further systematic measurements conducted in the Shanghai Jiao Tong University (SJTU) cavitation tunnel with “The Princess Royal” benchmark propeller in open water conditions, including cavitation observations with tests for tip vortex cavitation inception and desinence. The study also includes a computational fluid dynamics (CFD) investigation to discuss the results of the experiments, concentrating on comparing tip vortex cavitation.

[1] The two previous documents were the procedure 7.5-02-03-03.5 entitled Cavitation Induced Erosion on Propellers, Rudders and Appendages Model Scale Experiments and the procedure 7.5-02-03-03.7 entitled Prediction of Cavitation Erosion Damage for Unconventional Rudders or Rudders Behind Highly-Loaded Propellers

[2] Note that the previous, now obsolete, guideline was numbered as 7.5-02-01-5.

Mingtai *et al*. (2022) use acoustics for determination of cavitation inception. Classic noise spectrum analysis is compared to the continuous wavelet transform and DEMON spectrum analysis.

Chao *et al*. (2022) present a case study on waterjet system cavitation and pressure fluctuations. Wavelet Packet Transform and Fractal Dimension Exponent to analyze the features of cavitation pressure pulsation signals. The methods can be used for detection of cavitation inception and performance loss due to cavitation.

Wu *et al* (2022) study short-term pressure pulses caused by propeller-hull vortex (PHV). This is a common phenomenon when a highly loaded propeller works in an ice-blocked stern wake field. Since the fluctuating pressure signal is not repeated in a periodic manner, it is necessary to analyze the frequency characteristics in different time of the fluctuating pressure signal. The authors use short-term Fourier transform (STFT) to analyze the time-frequency characteristics of the fluctuating pressure induced by propeller cavitation in the ice-breaking condition.

Krasilnikov *et al*. (2022) address the challenge of propeller noise predictions in a paper with rich data comparisons EFD/CFD.

Aktas *et al*. (2020) study different paint types and application methods for the soft paint technique for cavitation erosion in model scale. This is an interesting comparison since most facilities paint composition is kept secret.

Abbasi *et al*. (2022) present an experimental case study on blade root cavitation erosion where they use the soft paint technique and high-speed video. This research addresses two main aims: broadening the knowledge about hydrodynamic mechanisms responsible for cavitation erosion occurring at the blade root, and assessing a simple experimental procedure able to measure the erosion risk associated with cavitation to create a correlation with full scale data.

Özsayan *et al*. (2022) compare numerical methods with model scale data using the soft paint method. Erosion formation on the propeller was estimated using the Erosive Power Method (EPM).

Dong *et al*. (2022) study cavitation impact load and pitting in brass using FEM. They compare experimental tests using magnetostrictive ultrasonic vibration cavitation erosion apparatus (ASTM G32). The load distribution corresponding to the deformation is deduced by using the finite element method (FEM). The predicted cavitation impact load is correlated with the parameters describing the cavitation flow erosiveness of the hydrofoil. On this basis, the cavitation depth distribution on the surface of a NACA0015 hydrofoil is preliminarily predicted.

Usta *et al*. (2023) study erosion in marine propeller materials using the cavitating jet technique (ASTM G134).

Ju and Choi (2022) present a systematic study on pitting/material loss in full-scale for small ship propellers. They quantify the damage by weighting and liquid penetrant testing (PT) was used for the non-destructive examination of propeller erosion damage. An image processing technique is applied to the PT images to quantify the amount of pitting.

4.1.2 Measurement techniques

Experimental techniques have been developed to provide quantitative and accurate information about cavitation. Such information is crucial for the validation of cavitation computations, and for the understanding of propeller performance, as well as for addressing critical topics such as cavitation-induced vibrations and radiated noise. Visualization using optical devices has been at the centre of these approaches for decades as cavitation is an extremely visual phenomenon.

Still pictures using standard film photography or digital devices such as charge-coupled devices (CCDs), CMOS or other modern technologies, have been constant and reliable tools in cavitation testing, both at model and full scales. The methodology can provide high quality pictures that can be a useful tool to document the cavitation occurrence in classical propeller performance testing. Regarding the use of digital technologies, significant improvement can be attained by synchronizing the digital devices with the rotation of the propeller, with a once-per-revolution (OPR) pulse, and coupling it with a stroboscopic light. With the addition of a constant delay generator, it becomes possible to make pseudo-video recordings of the cavitation pattern at different angular positions, which can be useful to explore the range of variability of the cavitation extension during the rotation An implementation of this measurement approach is depicted in Figure 2.

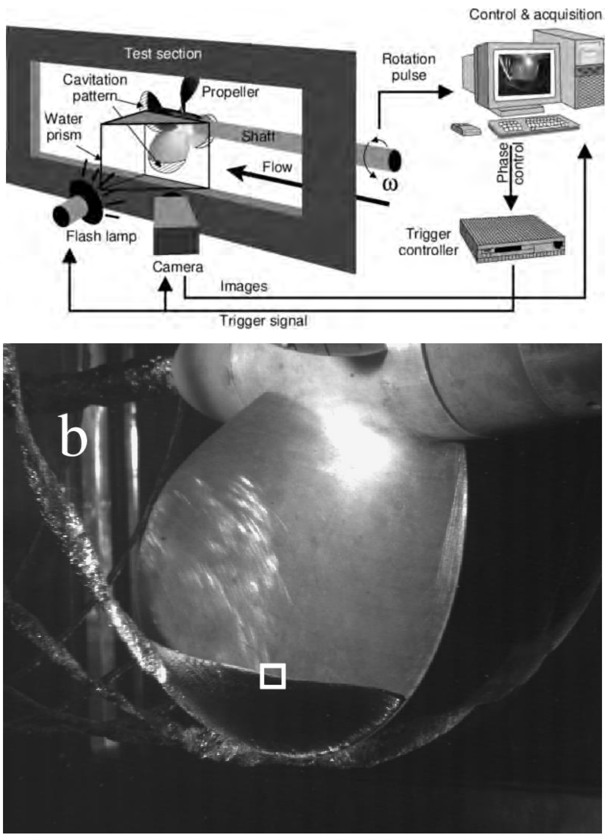

Figure 2: Setup for synchronized image recording using a digital camera and stroboscopic light (top); sample image (Pereira *et al*, 2004)

Technical developments have made possible by the time-resolved recording of cavitation using high-speed cameras, thus allowing the visual analysis of unsteady cavitation typical of a propeller operating in e.g. non-uniform flows deriving from off-design conditions. Guidelines for the operation of these techniques can be found in the ISO 22098:2020 document “Ships and marine technology - Full-scale test method for propeller cavitation observation and hull pressure measurement.”

However, still pictures, time-lapse or high-speed movies are not sufficiently informative for the purpose of computational validation, or for the purpose of correlating the visualizations with other quantities such as pressure fluctuations or noise data. Specifically, experimental methodologies and analysis tools are needed to retrieve quantitative information about the cavitation, either from visualization images or from other sources of information.

Lehman (1966) is, to our knowledge, the first to attempt the measurement of cavity volumes on a rotating propeller, using a laser-based technique. Ukon and Kurobe (1981), followed by Kurobe *et al* (1983) developed a similar approach to measure the cavity thickness at model and full scales. Pereira *et al* (1998) developed a four-camera tomographic system to capture cloud cavitation, enabling the definition of a size spectrum used to quantify the erosion potential. This complex technique is however not fully adequate for the measurement of attached cavities, such as leading-edge cavitation, since the three-dimensional reconstruction of the vapor volumes requires at least two sufficiently different viewing points to make measurements, with accuracy increasing with the number of views. Implementing computer vision algorithms based on the principles of triangulation and applied to stereo-vision, Savio *et al* (2009) used two cameras and laser beam projection to determine the cavitation bubble thickness over the blades as well as to spatially localize the cavitating tip vortex and measure its diameter. Shiraishi *et al* (2017,2022) implemented a variant of this approach based on a combination-line CCD camera measurement method to measure cavity shape and volume, see Figure 3. This measurement method also makes it possible to measure tip vortex cavitation, which has been difficult to determine in the past.

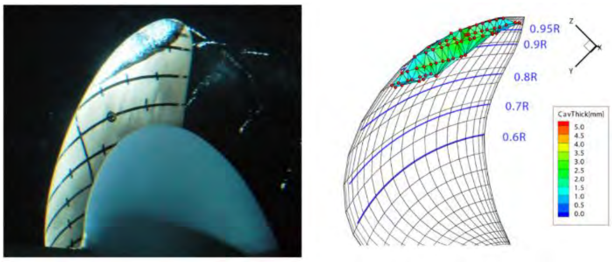

Figure 3: Combination-line technique to measure cavity volume and tip vortex size at model scale (Shiraishi *et al*, 2017, 2022)

The main disadvantage of these multiple-view systems is their requirement of significant optical access, since depth resolution is typically dependent on the separation between the viewing systems and on their distance to the object point, i.e. to the cavitation on the propeller blades. To remediate this problem, Felici *et al* (2013) proposed to use ultrasound pulsed echography (UPE) for the same purpose and applied it to leading-edge cavitation on a two-dimensional hydrofoil for validation, further comparing the results with the laser-line projection approach. The practical implementation of UPE is simple as it uses off-the-shelf instrumentation and is suitable for space-constrained configurations, or where optical access is limited or even non-existent. Processing of UPE data is also much faster since the operations measure the Doppler shift by a simple peak detection, and can therefore be performed in real-time. The main limitations of the UPE approach regard its large and distance-dependent measurement volume, the relatively low acquisition rate, and its sensitivity to background scatter noise such as the acoustic scattering from gas bubbles in the bulk of the fluid. In addition, and because it is based on a time-of-flight principle, its application to rotating machinery would require high-repetition rate pulse generation, which is limited by the speed of sound in water, as well as specific synchronization hardware.

Simple imaging of cavitation, done through still photography or synchronized digital recordings coupled with flash illumination, was exploited by Pereira *et al* (2004) to extract the area of the cavitation extension over the blades. Using image processing techniques based on established de-warping algorithms, and provided a dedicated but simple optical calibration, it was shown that accurate area measurements could be obtained. Inviscid flow boundary element method (BEM) computations of cavitation in uniform flow were validated through this data. A further step in this direction (Alves Pereira *et al*, 2016) was taken using one high-speed camera and continuous lighting. The same algorithmic approach was followed, allowing the possibility to explore and quantify unsteady cavitation, specifically the periodic variation of the cavity extension over the blade in a non-uniform wake presenting a typical skeg-like narrow pressure gradient. The mean and fluctuation of the cavity area could be determined, see Figure 4.

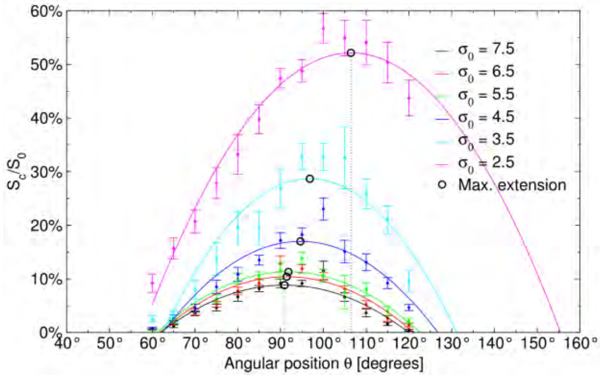

Figure 4: Cavity extension and corresponding root-mean-square fluctuations as a function of the propeller angle θ, for different cavitation numbers σ_0, with quadratic fit curves and indication of the location of the cavity maximum extension (circle markers) (Alves Pereira *et al*, 2016)

Cao *et al*. (2022) introduces an image-based experimental method for cavitation pattern analysis and pressure fluctuations. The method is based on the grey level frequency analysis of cavitation images from high-speed video.

Recent developments have demonstrated the application of Laser Doppler Velocimetry (LDV) to the simultaneous measurement of cavitation volume and of flow velocity on a rotating propeller, see Capone *et al* (2024). One major advantage of this approach is that the technique is insensitive to the light scattering typical of cavitation interfaces. The other unique advantage is its ability to access the inter-blade region, which is extremely difficult to probe using other velocimetry techniques such as Particle Image Velocimetry (PIV). The technique measures the three-component velocity field at a point of the fluid. The velocity field in a volume is reconstructed by traversing the microscale measurement point across this volume in an automated manner. The part of this volume where no velocity information is available represents either a solid boundary, such as the blade surface, or the cavitating domain. Therefore, it becomes possible to estimate the cavity volume from the missing LDV data. LDV has the major advantage that it can be built into an integrated system, compact, easy to setup and robust against vibrations. Feasibility has been demonstrated at model scale (Capone *et al* 2024), see Figure 5, however full-scale cavitation measurement has yet to be assessed.

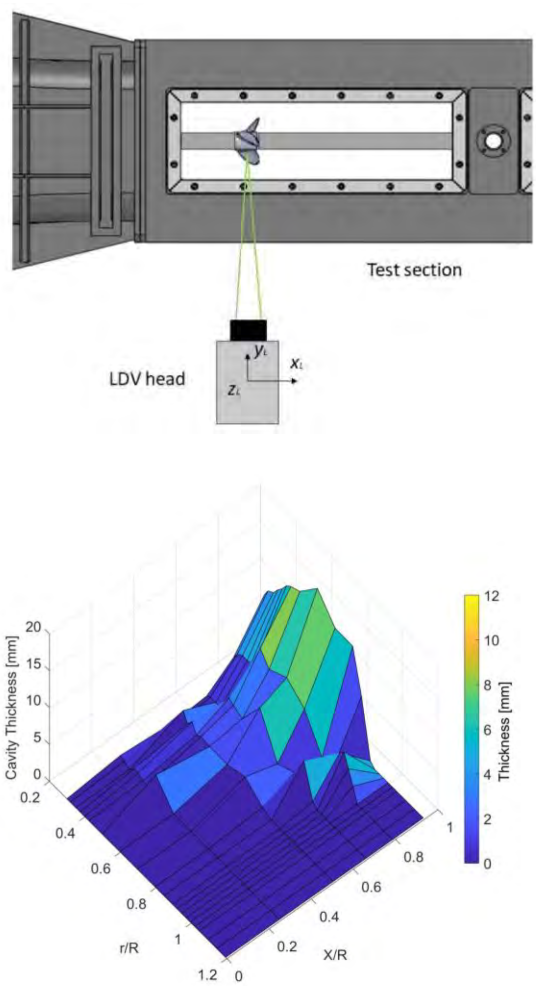

Figure 5: Cavity volume measurement using LDV: basic setup in tunnel (top); cavity shape (bottom) (Capone *et al*, 2024)

Recent works have considered the indirect measurement of cavitation from the radiated pressure field emitted by a cavity. On the assumption that a pulsating cavitation void behaves as a monopole source, the sound pressure radiated by this monopole is directly proportional to the acceleration of the pulsating cavity volume:

$$\Delta p \propto \frac{\partial^2 V_c}{\partial t^2}$$

The soundness of this principle has been demonstrated at model scale (Alves Pereira *et al*, 2016), showing that a measure of the cavity volume can provide accurate information about the radiated pressure field, see Figure 6.

Figure 6: Comparison between reduced-order Δp from measurements (-) and computed Δp from volume

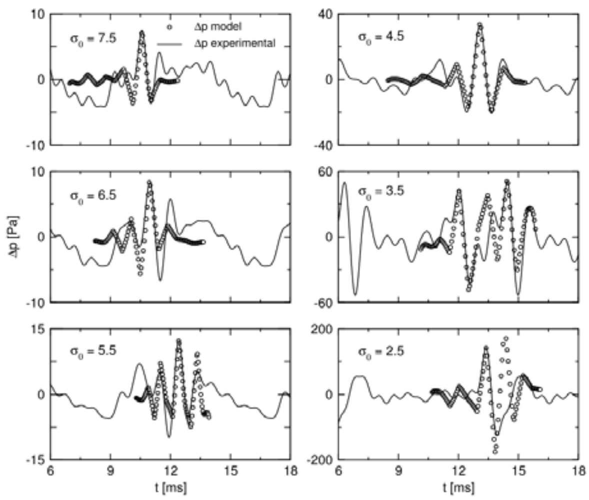

acceleration (o) (Alves Pereira *et al*, 2016)

Recently, Fohring *et al* (2023) have proposed to reverse the principle by determining the cavity volume from the measured pressure fluctuations, and applied the approach to full-scale data obtained on a 3,600 TEU container vessel, see Figure 7. Fluctuations of the cavity volumes could be estimated as well.

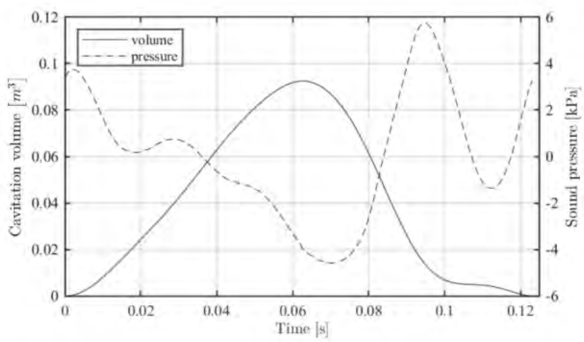

Figure 7: Representative sound pressure and cavitation volume of one blade passage (Fohring *et al*, 2023)

These authors point out that this reverse acoustic approach cannot "generally distinguish between cavitation types, so the calculated volume may well comprise a combination of sheet and tip vortex cavitation or other types." Moreover, the methodology is applicable if cavitation occurs on one single blade only.

Inukai (2019) implemented a technique called Multi-Layered Doppler Sonar (MLDS) to measure the flow velocity at the stern of a 14000 TEU container ship. The principle relies on the scattering of particles or bubbles in the flow field, thus creating a Doppler shift that is measurable and directly related to the particle/bubble velocity. The technique requires a limited amount of instrumentation and minimum intrusiveness into the ship structure:

Figure 8: MLDS equipped on 14,000TEU container ship (Left: the gate valve for the transducer of the MLDS at the bottom, Right: the transceiver of the MLDS and PC for analysis in the steering gear room) (Inukai 2019)

Although similar to the UPE approach used by Felici *et al* (2013), the authors did not explore the possibility of measuring the cavity volume.

Particle Image Velocimetry (PIV) is another advanced non-intrusive velocimetry technique that has been applied in different test cases of interest. Atsavapranee *et al* (2008) have been among the first to make full scale PIV measurements, by installing PIV cameras in underwater cases to investigate the viscous roll-damping around the bilge keel of a 88.6 m long navy ship. Kleinwächter *et al* (2014, 2015) improved the concept using onboard cameras, see Figure 9, and performed full scale velocity measurements on a 186.22 m long ConRo-ship. Hiroi *et al* (2019) used the same concept on a 63000 DWT bulk carrier. Birvalski *et al* (2023) devised a different implementation to measure the propeller inflow on a 50000 DWT tanker, with the PIV system being mounted externally and inside a rotating underwater case, adding some flexibility to the concept.

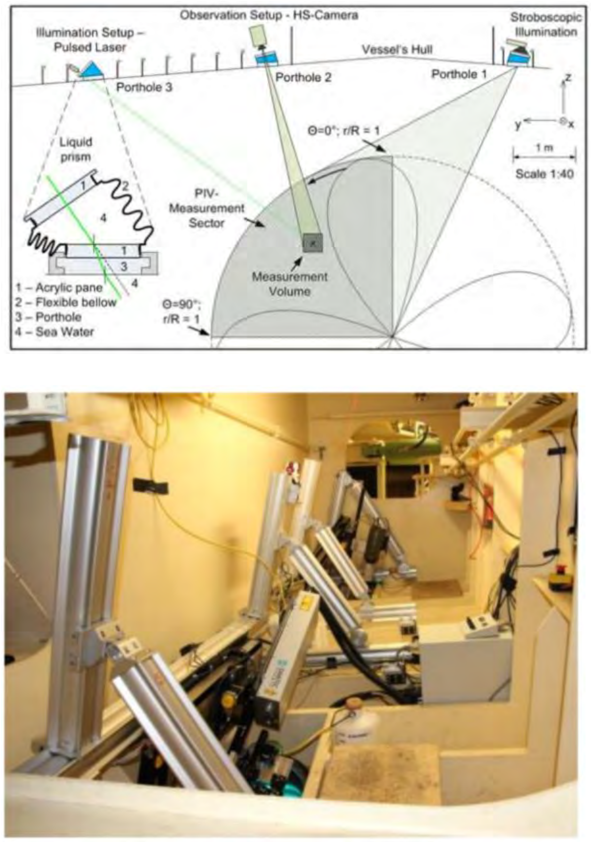

Figure 9: Schematic measurement setup (top) and actual setup (bottom) (Kleinwächter *et al* 2015)

Although PIV could potentially be used for cavitation volume measurement, as with LDV (Capone *et al*, 2024), the technique presents important challenges, such as limited access to the inter blade region, very limited flexibility due to critical alignment and space requirements, dangerous laser scattering on cavitation interfaces, etc.

Grasso *et al* (2019) developed a methodology to optically measure the hydro-elastic response of flexible propellers in non-uniform flow, and applied it at model scale in the cavitation tunnel and at full scale on a ship. The deformation of the propeller blades was measured optically with Digital Image Correlation (DIC) and two underwater cameras installed on the vessel's rudder, see Figure 10.

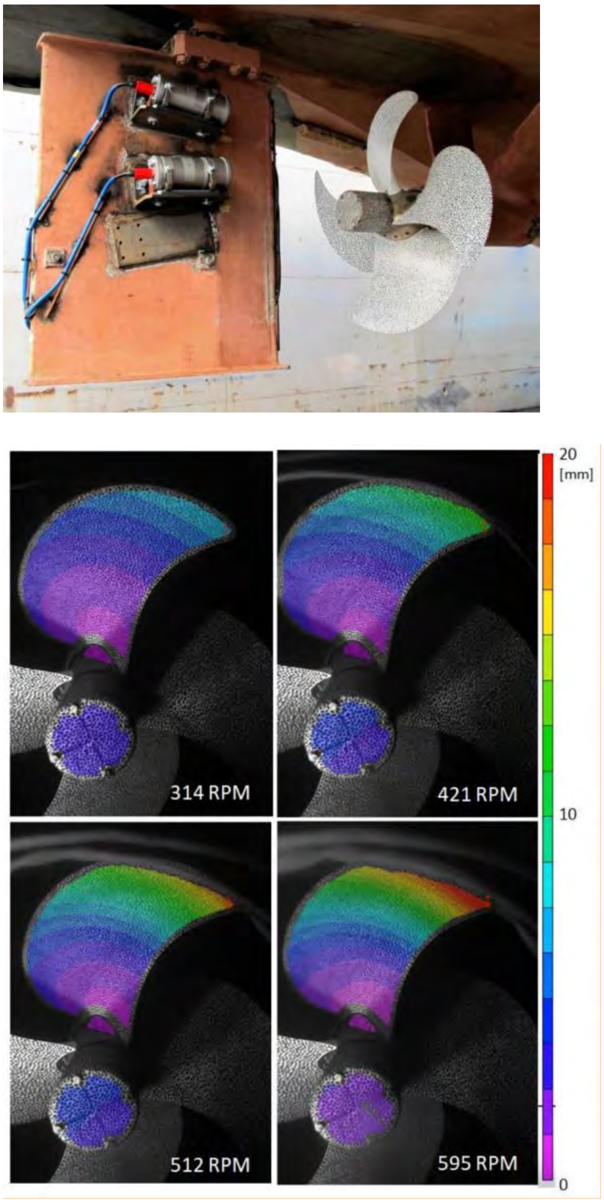

Figure 10: Full-scale setup (top) and deflection results (bottom) (Grasso *et al* 2019)

4.1.3 Numerical methods for cavitation induced pressure fluctuations

CFD has been widely utilized to simulate cavitation phenomena, from single cavitation bubble dynamics to macro scale behaviour like cavitation surge in hydraulic machinery. For marine propellers, nowadays CFD with cavitation modelling is adopted for predicting macro behaviour or appearance of cavitation and propeller performance, pressure fluctuation, erosion, and radiated noise.

Cavitation in marine propellers exists with wide spatial-and-time scale phenomena (i.e., from single bubble generation and collapse to extent or shedding of sheet or cloud cavitation on blade). Dealing with this multi-scale problem directly is difficult, especially in engineering applications. Therefore, most cavitation modelling for marine propellers is based on a mixture model, which treats cavitating flow as a mixture of water and vapour macroscopically, without directly modelling individual bubbles or interfaces between phases. This model is simplified in comparison with other types of methods like two-fluid models (simulate each phase's velocity and momentum independently) or Lagrangian models, but is widely used not only for marine propellers but also for other hydro-machines (for example, Nohmi *et al*. (2003)). This macroscopic modelling is also utilized for predicting cavitation erosion risk, although erosion basically comes from the collapsing of bubbles near the blade. For example, Hasuike *et al*. (2009) adopted indexes based on macro behaviour of cavitation and pressure from CFD to discuss erosion risk. Recently, Melissaris *et al*. (2018) applied an idea of potential power of macroscale propeller cavitation, related to time derivatives of pressure and vapour volume, to assess erosion risk on propellers based on URANS simulations. Similar methods were applied by Köksal *et al*. (2021) using URANS and DES results. The numerical results were compared to visual observations of cavitation paint tests. Figure 11 shows a visual comparison of a paint test result to a DES solution.

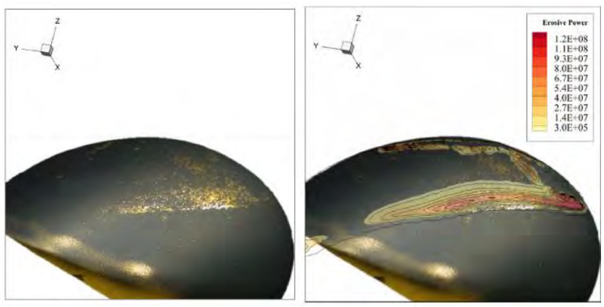

Figure 11: Visual comparison of paint test (left) and DES (right) (Köksal *et al*, 2021).

A hybrid approach with Eulerian mixture treatment along with Lagrangian bubble transportation has been studied to tackle the multi-scale problem. Tian *et al*. (2022) applied this approach to a cavitating hydrofoil. They adopted the Eulerian approach with VOF (Volume of Fluid) for large scale phenomena and the Lagrangian approach with a discrete bubble model for small scale phenomena simultaneously (Figure 12). This type of approach seems to have the potential to deal with erosion or noise with modelling individual bubble collapse.

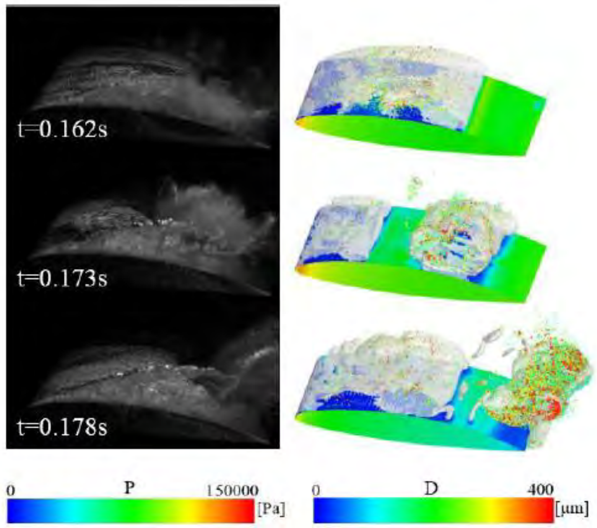

Figure 12: Cavitating flow around a hydrofoil (Tian *et al.* (2022))

To describe mass transfer between water and vapour (i.e., vaporization and condensation), several models have been developed and used. Most of these models basically apply the local pressure difference from vapor pressure to describe the mass transfer rate, but their theoretical origins and details are different. For example, Schnerr and Sauer (2001) derived their model from a simplified Rayleigh-Plesset equation, which describes single bubble dynamics. Other examples of relatively popular models can be found in, Singhal *et al*. (2002), Kunz *et al*. (2000), Zwart *et al*. (2004), etc. In another type of approach, Mike *et al*. (2022) tried to adopt a "Multi-process cavitation model" which is based on the moment method and solves detailed information of cavitation like number of bubbles, radius, surface, volume and mass. They applied this model to cavitating flow in a twisted hydrofoil and saw reasonable results in predicting cavitation shedding frequency.

Turbulence modelling is also an issue common to other CFD applications. Bensow (2011) studied the influence of the turbulence model on cavitation around a twisted hydrofoil. In his study, LES and DES could predict cavitation shedding behaviour and its frequency reasonably, but there is discrepancy in their lift. Also the Spalart-Almaras RANS model with eddy viscosity correction based on void fraction could predict the shedding, although a normal RANS model without the correction could not show shedding. Viitanen *et al*. (2020) studied the difference between model scale and full scale using DDES and RANS with/without a transition model. Two propellers, both in uniform flow, were simulated and there was little difference between the turbulence models. Geese *et al*. (2022) also studied using transition models with a propeller in uniform flow, and found that the model did not affect the overall behaviour of cavitation but there was some difference in radiated noise. Sezen *et al*. (2021) conducted a comparison between RANS and DES for a cavitating propeller in uniform flow. In this case, the difference in sheet cavitation was small, but the length of tip vortex cavitation agreed better in DES. Viitanen & Siikonen (2017) studied a model scale propeller in uniform flow using RANS, Reynolds stress and DES methods. While propeller performance and cavitation phenomena near the blades were similar between the models, wake flow and tip vortex cavitation extent were more dependent on the choice of the model. Additionally, they showed that using a compressive limiter for the convective terms in the void fraction equation resulted in an improved vortex cavitation prediction (Figure 13).

LES and DES approaches are generally better for simulating unsteady or unstable cavitation like cavitation shedding or vortex structures, but require greater computational resources (computational power and time) compared to the RANS approach. The appropriate approach should be chosen considering focusing phenomena simulations and allowable computational resources.

Figure 13: Comparison of computed cavitation extents with the different flux limiters (bottom) and experimental photograph (top) (Viitanen & Siikonen, 2017).

To reproduce the hull wake field, there are two types of methods similar to model tests. One is setting the hull shape in the calculation domain and calculating the wake development directly. The other is giving a prescribed wake distribution at the inlet as a velocity boundary condition. Many studies have been conducted with both methods (some of them are referenced later) but no significant difference in calculated cavitation extent or pressure fluctuation was suggested in this review. Also, there are some cases with an inclined shaft arrangement without wake, to realize the same condition as the corresponding model test.

Early application of CFD to cavitating propellers can be found in Watanabe *et al.* (2003) with good agreement between CFD and model tests of sheet cavitation in a uniform flow. Subsequently the application was expanded to predicting unsteady cavitation in a wake and its pressure fluctuation. Sato *et al.* (2009) studied CFD's applicability in ten different propellers for various merchant ships and found that the appearance of sheet cavitation and its difference between propellers were well predicted. The tendency of the 1st order component of pressure fluctuation above the propeller centre was relatively well predicted. The 2nd order components were underestimated, with rough time stepping being indicated as one of the reasons for the variation. Hasuike *et al.* (2015) conducted calculations for twenty propellers and obtained 1st order comparisons, as shown in Figure 14. In addition, they attempted to calculate 2nd order components from the 2nd order time derivative of the cavity volume and this resulted in decreasing the discrepancy between CFD and model tests.

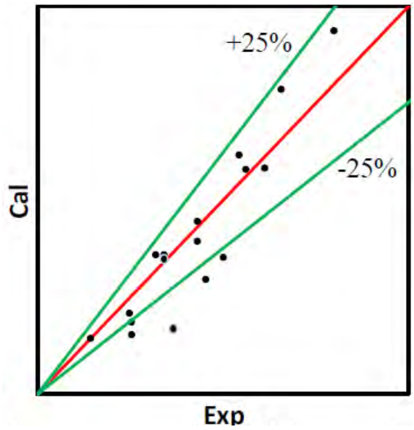

Figure 14: Comparison of 1s order component of pressure fluctuations. (Hasuike *et al.* (2015)

Paik *et al.* (2013) conducted simulation for two propellers with the hull present and compared the cavitation appearance and pressure fluctuation distribution on the hull with model tests. Good agreement of the two propellers 1st order components was found when comparing various locations on hull, as shown in Figure 15. On the other hand, 2nd order components had relatively large discrepancies. Similar results can be seen in works by Park *et al.* (2018) (Figure 16), Deng *et al.* (2022), Viitanen *et al.* (2022) and Zhen *et al.* (2022).

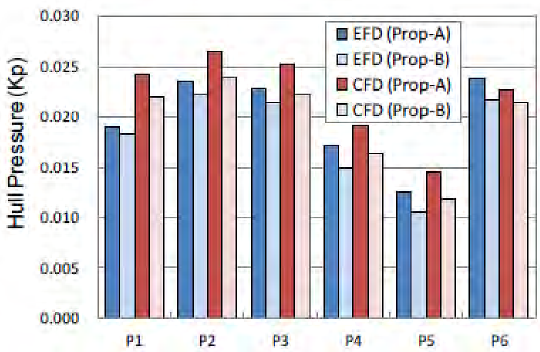

Figure 15: Comparison of pressure fluctuations in 1st order. (Paik *et al.* (2013))

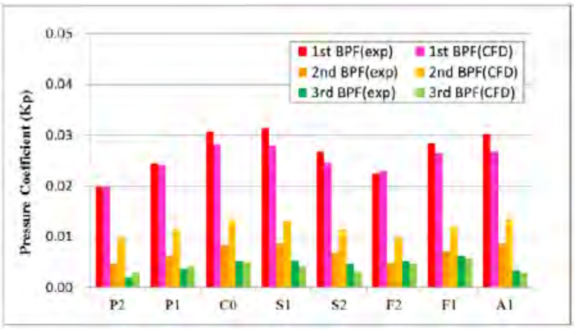

Figure 16: Comparison of pressure fluctuations (Park *et al*. (2018))

Fujiyama (2015) adopted adaptive mesh refinement[3] (AMR) for tip vortex cavitation and had good results in presenting cavitation extent. In addition, a discrete wavelet analysis was applied to the cavitation surface pressure and indicated cavitation behaviour around the trailing edge of the tip has a relatively strong relation to 2nd order pressure fluctuations (Figure 17).

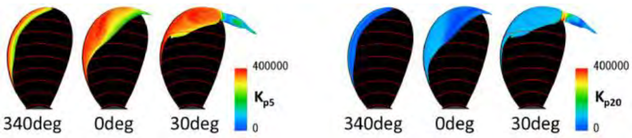

Figure 17: Contribution of cavitation to pressure fluctuation. (Left : 1st order, Right : 2nd order) (Fujiyama (2015)

AMR technique was studied by Yilmaz *et al.* (2019) and resulted in a good prediction of detailed tip vortex cavitation appearance, for a propeller in uniform flow (Figure 18).

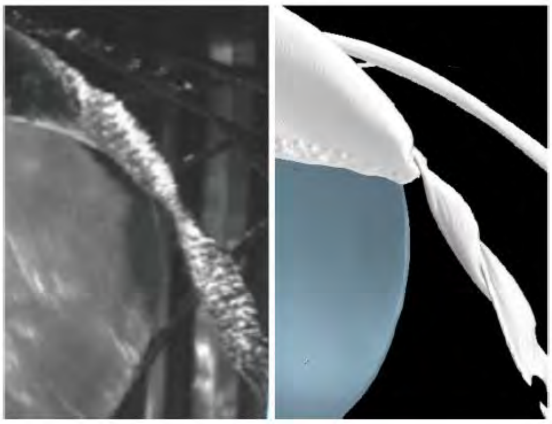

Figure 18: Comparison of tip vortex cavitation roll-up (Yilmaz *et al*. (2019))

Regarding the influence of turbulence modelling, Chaosheng (2017) applied an eddy viscosity correction to RANS (SST k-ω). This approach is similar to Bensow (2011) which showed a positive effect on cavitation shedding on a hydrofoil, but in this case the influence on pressure fluctuation was small (Figure 19).

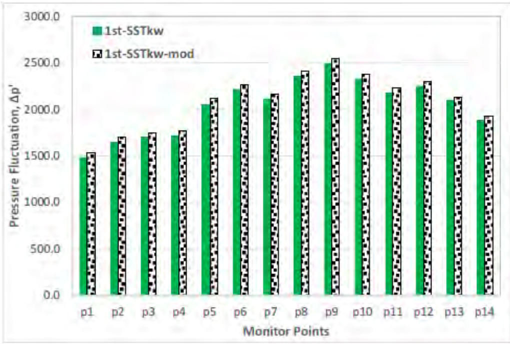

Figure 19: Comparison of pressure fluctuation with viscosity correction (Chaosheng (2017))

Kimmerl *et al.* (2022) conducted comparisons between RANS, LES and LES with AMR for tip vortex cavitation. In cavitation appearance, the difference between RANS and LES was small but improvement in vortex cavitation representation was shown with AMR (Figure 20, here "QRef" means "with AMR"). Regarding pressure fluctuation, LES showed good agreement with model tests in the 1st order component, but the improvement was not clear in higher order components (Figure 21).

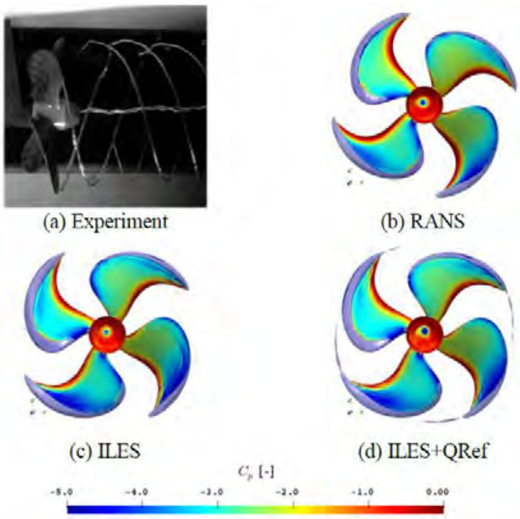

Figure 20: Cavitation appearance in several turbulence modelling (Kimmerl *et al*. (2022))

[3] Adaptive mesh refinement is local mesh refinemnet by cell size adjustment based on calculated flow characteristics like pressure or velocity.

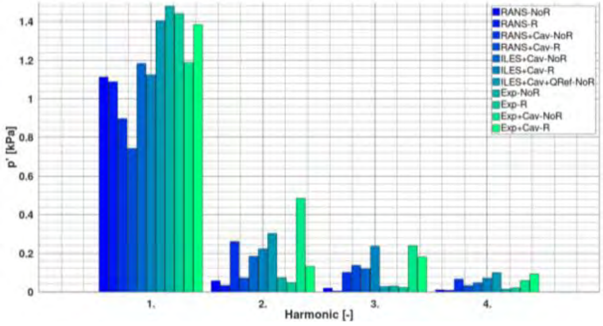

Figure 21: Comparison of pressure fluctuations (Kimmerl *et al*. (2022))

From these studies, the current state of CFD predictions for cavitation extent and pressure fluctuations is summarized below.

- The extent of sheet cavitation on a propeller operating in a wake can be predicted well. Sometimes the tip vortex cavitation appearance is also well predicted with an AMR technique or high-resolution mesh.

- Regarding pressure fluctuations, the 1st blade passing frequency component is predicted reasonably. Although, it is still difficult to predict the 2nd order and higher components.

To obtain reasonable results, careful consideration when utilizing CFD is necessary. Further discussion can be found in ITTC Recommended Procedures and Guidelines 7.5-02-03-03.4 “Procedure for Cavitation-Induced Pressure Fluctuations: Numerical Prediction Methods.”

As the pressure fluctuation is related not solely to cavitation extent, but also to the 2nd derivative of cavitation volume variation, much higher accuracy is required. To improve the accuracy of predicting higher harmonics, improvement in predicting tip vortex cavitation or other complicated phenomena like cloud cavitation or bursting might be needed. At the same time, the importance of validation or uncertainty analysis in model tests, especially for higher order pressure fluctuations should be noted.

4.1.4 Dummy models

A dummy model is used to provide a representative hull wake field for testing propellers in a cavitation test. The shape of the dummy model is usually different from a geometrically similar full scale ship (e.g. Figures 22 and 23), but the method for designing or evaluating a dummy model has not been clarified and generalized as a recommended procedure or guideline.

Figure 22: An example of dummy model and its setting in cavitation tunnel (in INM)

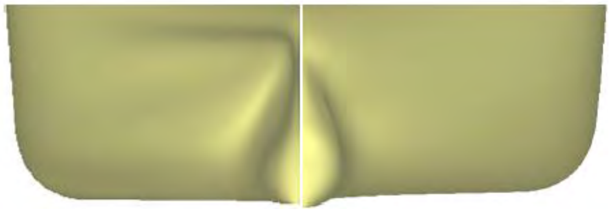

Figure 23: An example of designed dummy model (Left: designed dummy model, Right: original geosim hull) (Schiling *et al*. (2011))

To understand the facilities’ experiences with dummy models, a questionnaire was distributed to twenty-seven organizations using cavitation tunnels, sixteen organizations kindly provided their answers.

An overview of the results is provided in the following sections.

4.1.4.1.Fundamental information of facilities and test objectives.

Nine out of the 16 facilities use dummy models, and many of them (7 out of 9, hereafter simply “7/9”) are using dummy models as established practice.

Six facilities use dummy models although their test sections are relatively large, i.e. their width and height are over 1.0m, and might be able to use a fully geometrically similar hull model.

Typical model propeller diameters used are around 250mm, similar to common cavitation tests without dummy models.

Regarding water quality control, upstream microbubble injection and/or adjustment of gas content are widely adopted similar to common cavitation tests. Using an electrolysis device on the dummy model is not common practice (3/9).

The objective of the cavitation test with a dummy model is similar to standard cavitation tests: cavitation observation, measurement of pressure fluctuation, URN, investigation of inception, erosion, etc.

4.1.4.2. Target wake and evaluation of simulated wake

Many of facilities (7/9) using dummy models attempt to simulate an estimated full scale wake, and approximately half of facilities (5/9) intend to simulate full 3D velocity components including radial and tangential at the propeller disk plane. On the other hand, turbulence intensity and pressure distribution are rarely (1/9) part of the simulation.

There are two methods for evaluation, i.e. by experimental measurement in tunnel, or/and numerical prediction, but experimental measurement is dominant (7/9). Almost half of facilities (4/9) have some clear criteria for wake simulation. The criteria between facilities vary widely (e.g. less than 15% use a 3-dimensional velocity, less than 5% in velocity amplitude difference) to more qualitative ones like “width of the low-speed areas,” “phase angle of wake field” and “visual comparison of curves”. It appears difficult to find common criteria for this part of the survey.

4.1.4.3.Details of dummy models and their design

The dummy model shape for (7/9) facilities models the aft hull section as geometrically similar with full scale. When deviating from a geometrically similar aft end hull shape, some points like tip clearance, configuration of shaft bracket and rudder are maintained to directly scale with full scale. Also the stern tube shape is sometimes modified to accommodate. In some cases, where the aft hull shape is maintained with full scale, there are cases where the hull’s beam must be adjusted to fit the tunnel. Also, many facilities (7/9) adopt appendages, e.g. rudder, shaft, shaft brackets, ESD such as pre-swirl fins, thruster housing, ducts, bilge keel, sonar dome and stabilizer.

There are not many descriptions or comments on fore hull shape, but one facility indicated that fore shape also affects the wake meaning the bow geometry should be geometrically similar to full scale.

In addition to dummy models, some facilities (2/9) adopt an additive wire mesh to obtain the required wake. One facility adopts flow liners on the wall of the cavitation tunnel, to shrink the wake distribution.

Criteria on blockage against the tunnel section varies from 10% to 30% depending on the facility. One participant commented that the effect is taken into account in CFD simulations for designing their model.

In designing the dummy model, both experimental measurement and numerical simulation are commonly used, but which type is adopted is dependent on the facility. All numerical simulation methods used are RANS type CFD, and most of them (5/6) are commercial codes. Using RANS, some facilities conduct unsteady simulations, but the results are utilized as time averaged mean flow information. No facility considers unsteadiness or unstableness directly. Regarding the components predicted or evaluated by numerical simulation, most facilities (5/6) consider not only axial velocity distribution but also tangential or/and radial velocity distribution. Checking for the occurrence of unintended flow separation or other flow modes is also in the scope (3/6). Some facilities also consider turbulent intensity or pressure distribution. The typical accuracy of these CFD simulations for dummy models is not clarified in this survey, but one facility commented that the outer area is usually well predicted but not always the inner radius, especially if there is flow separation.

Using these numerical simulations, one facility indicated that the dummy model hull shape is parametrized and iteratively adjusted to obtain the target wake, but generally no special optimization system is utilized.

4.1.4.4.Problems utilizing the dummy model

A main concern raised when using a dummy model is the difficulty of simulating the tangential and radial components of the wake. One facility does not feel this is a problem but several other facilities consider it difficult to achieve sufficient results and it can be very time consuming. This indicates that the design method for dummy models is not well established between facilities and requires further research and discussion to determine the key components that affect results.

Other problems indicated in this survey are more specific to each facility's situations. For example, time and cost consuming risk comes from their model manufacturing. Also, one facility expects cost reduction by using dummy models with a common fore body with modifications in the aft hull section only, but this assumes the fore body shape does not affect the wake into the prop plane.

4.1.4.5.Recommendation for a new guideline

Currently it is difficult to provide a procedure for defining the shape of dummy models, as the survey highlights many variations between facilities. Ideally the new guideline will provide fundamental ideas and examples of the shape and its evaluation.

The contents might include points like following.

- The typical shape of dummy models is a shortened hull where the aft part is geometrically similar to the full scale ship. The aft hull sometimes requires modifications due to limitations from model test equipment like the dynamometer.

- The fore hull shape can affect the wake into the propeller plane, so the shape of fore hull should be discussed carefully.

- Appendages like the shaft bracket, rudder etc. should be adopted.

- In addition to the hull, wire-mesh may be adopted to improve the wake quality. Also, a liner on the tunnel walls may be used to shrink the hull's wake.

- The resulting design should be evaluated with measurement or numerical prediction. In addition to axial wake, tangential and radial components might be in scope. Other flow characteristics like static pressure and turbulence intensity could also be discussed.

- The design might be run iteratively until the target wake is obtained.

- There is no separate criteria for wake simulation with a dummy model, and it will follow the discussion of wake simulation without a dummy model. (see ITTC Recommended Procedures and Guide-lines 7.5-02-03-03.1 "Procedure for Model-Scale Cavitation Test")

- As numerical simulations, typically RANS-type CFD are utilized for design and evaluation both steady and unsteady simulations (with its results time averaged) are used.

4.2 Noise

4.2.1 Model-scale measurement

Considering the recent growing importance of shipping noise, the specialist committee on hydrodynamic noise of the 27th, 28th and 29th ITTC had reviewed the model-scale noise measurement techniques in detail. ITTC guideline 7.5-02-03-03.9 on Model-Scale Propeller Cavitation Noise Measurements had also been updated to the latest reviewed knowledge.

The 30th ITTC specialist committee on cavitation and noise has reviewed the latest aspects of model-scale measurements more specifically on reverberation, tip vortex scaling, water quality, and its effect on uncertainty.

Facility reverberation has been widely recognized as a main cause of adverse effects on the reliable source level estimation of cavitating propellers at model-scale. The previous hydrodynamic noise committee mainly dealt with transfer function measurement techniques including the type of source signals (Tani *et al.*, 2019a,b; Park *et al.*, 2018b), transducer positions (Briançon *et al.*, 2013; Tani *et al.*, 2019b) and post-processing techniques to remove unrealistic humps and hollows in the measured transfer functions (Briançon *et al.*, 2013; Tani *et al.*, 2019b; Harrison & Harrison, 1995[4]). Demodulation techniques (Boucheron, 2019) to identify the mode characteristics inside the test sections were also examined in the previous report.

The acoustic characteristics of the test facility can also be studied by using numerical simulations. Way *et al.* (2021) proposed an adapted image source model to analyze reverberation effects in the towing tank at which noise measurements are performed. Figure 24 shows the lattice of image sources where their locations are controlled by vectors $\underline{u}$ and $\underline{l}$. This model includes volumetric absorption and the use of spherical wave reflection coefficients at the tank boundaries. The plane wave reflection coefficients only agree with spherical coefficients at near vertical incidence ($\leq 20°$) as shown in Figure 25. Three periodicities were identified in the frequency variation of the transfer function. The periodicities arise from Lloyd's mirror effect (1 in Figure 26), cut on of transverse modes between the sides of the tank and between the tank floor and free surface (2 in Figure 26), and interference between axial standing waves between the two end walls of the tank (3 in Figure 26).

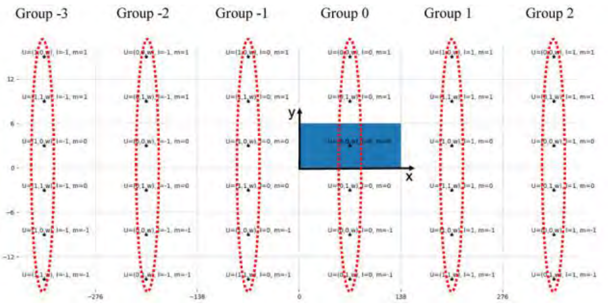

Figure 24: Lattice of image source in the x-y planes for a towing tank in which the position of each source is controlled by vectors $\underline{u}$ and $\underline{l}$ (Way *et al.*, 2021).

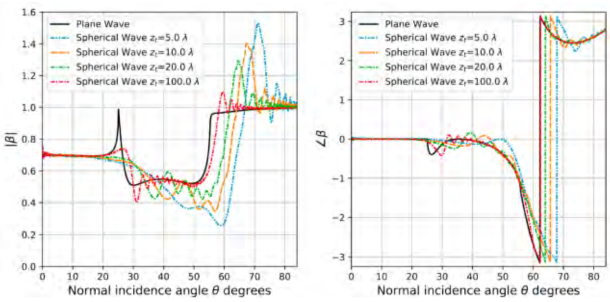

Figure 25: Examples of calculated reflection coefficients of plane and spherical waves (Way *et al.*, 2021).

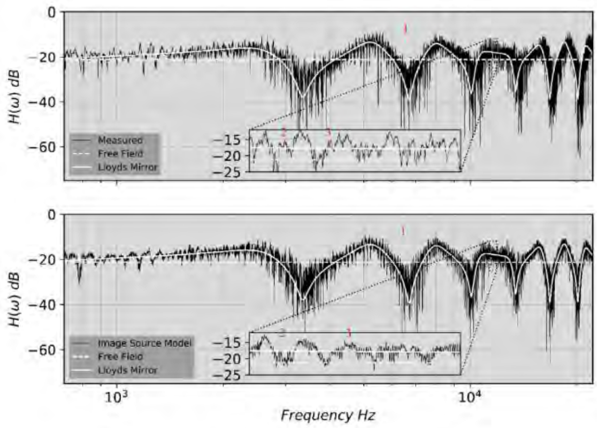

Figure 26: A comparison between measured (top) and simulated (bottom) transfer function (Way *et al.*, 2021). The analytical free field and Lloyd's mirror transfer functions are overlaid in white in the figure.

Boucheron (2023a) studied the scattering effects of the acoustic sources (typically spherical and cylindrical shaped projectors used for the transfer function measurements in the test section of a cavitation tunnel) using numerical simulations. The reflections from the surrounding walls are incorporated using the image method, the principles of which are similar to Figure 24. The scattered fields of

[4] The problem of smoothing is also well known in ocean acoustics

spherical and cylindrical projectors are simulated with spherical and cylindrical Bessel functions, respectively. Figure 27 shows a comparison between the simulated transfer functions with and without the scattering effects from a spherical shaped source. The values in the figure were picked from the points with maximum power. It was observed that the scattering effect can be neglected in the low frequency domain ($kR < 1$), however, it becomes significant as the frequency increases.

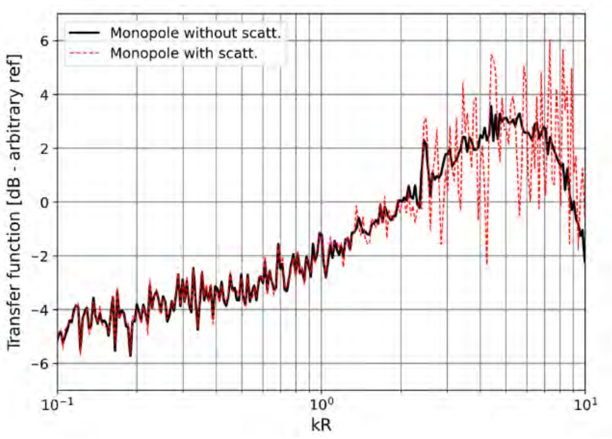

Figure 27: A comparison between simulated transfer functions with- and without the scattering effects of a spherical shaped acoustic source (Boucheron, 2023a).

It is noted that the transfer function measurement is not required if hydrophones or pressure sensors are used as onboard sensors (Foeth & Bosschers, 2016). Examples of estimating model-scale source strength with onboard sensors using array signal processing techniques[5] can be found in Foeth & Bosschers (2016) and Jeong *et al.* (2021). It is noted that those two references also dealt with full-scale measurements.

Foeth & Bosschers (2016) applied near-field beamforming to estimate source strength as well as source location. In order to validate the proposed method, they formed an array with flush-mounted pressure transducers embedded on the model ship and used a transducer fitted within the wake field measurement equipment as shown in Figure 28. Figure 29 presents a comparison between the nominal source strength and the estimates using array processing and two hydrophones[6]. It was observed that the estimates by the array processing shows good agreements with the nominal source levels except for the lower frequencies (≤ 5 kHz) due to the low transmitting power of the transducer. It was also noted that the relatively larger discrepancies above 15 kHz might come from reflections by the shaft, struts and traversing mechanism.

Figure 28: Model test setup used by Foeth & Bosschers (2016).

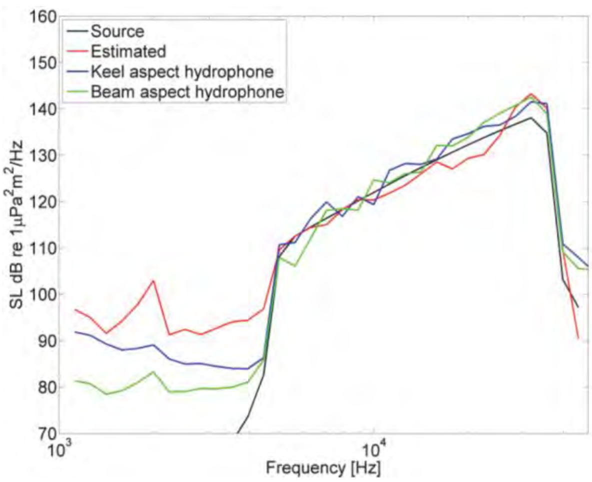

Figure 29: A comparison of estimated source levels to the nominal ones emitted by the source at the bottom of the propeller disc position (Foeth & Bosschers, 2016).

Jeong *et al.* (2021) also applied a simple beamforming method[7] to monitor the propeller

[5] The array signal processing technique was also used in wind tunnel aeroacoustic measurements (see Muller (Ed.), 2002).

[6] The source levels were obtained after applying corrections for the surface reflection (Lloyd's mirror effect) and for the distance between the source and the hydrophone to the sound pressure levels measured at an additional two hydrophones.

[7] The given method is similar with Foeth & Bosschers (2016) in principle.

noise in a model-scale measurement. They calculated an estimated source level at each source grid point using noise data measured at the hydrophone array in Figure 30 and the source strength was determined where the beamforming power was at its maximum. From the comparison between measured[8] and calculated source levels in Figure 31, it was confirmed that the proposed method can estimate the source level to a good degree.

Figure 30: Model test setup used by Jeong *et al*. (2021).

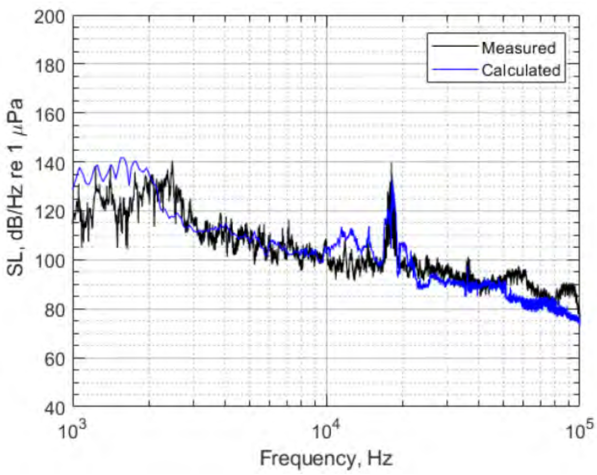

Figure 31: A comparison between measured and estimated source levels (Jeong *et al*., 2021).

The modal characteristics due to facility reverberation can be used for the localization of acoustic sources. Boucheron (2023b) proposed a demodulation technique for this purpose. It was shown through numerical simulations that the proposed method gives good performance especially for the lower frequency domain (between the two dashed lines in Figure 32) at which conventional array signal processing is not appropriate due to lower resolution.

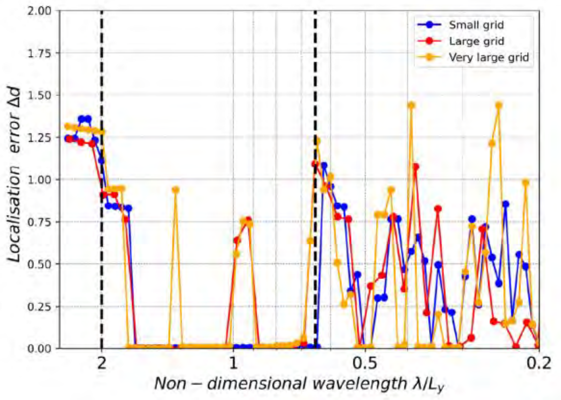

Figure 32: Localization accuracy against the non-dimensional wavelength for various grid size (Boucheron, 2023b).

After earlier publications to address the effect of Reynolds number on the noise of tip vortex cavitation (Strasberg, 1977; Baiter, 1989; Oshima, 1990, 1994; Blake, 2017), a few publications dealing with its scaling were reviewed in the report of the previous committee including Park & Seong (2017), Park *et al*. (2019, 2020), and Bosschers (2018, 2020).

Recently, Lee *et al*. (2024) proposed a scaling technique for tip vortex cavitation noise and presented scaling results from model-scale experiments. In this study, a relationship between tip vortex cavity size and cavitation model, which provides information on the equivalent cavitation number for the model test condition to ensure the same non-dimensionalized radius of the TVC as the full-scale one, was derived from the empirical vortex model proposed by Proctor *et al*. (2010). A new scaling exponent, k_{ce}, was introduced in this study based on the assumption that the exponent relating the cavitation number (σ) and Reynolds number (Re) of the model-scale (m) and the full-scale (s) varies according to cavitation growth:

$$\frac{f_s}{f_m} = \frac{n_s}{n_m}\left(\frac{Re_s}{Re_m}\right)^{0.5k_{ce}} \quad (1)$$

$$\Delta L_s = 10log_{10}\left[\left(\frac{r_m}{r_s}\right)^2\left(\frac{n_s D_s}{n_m D_m}\right)^3\left(\frac{D_s}{D_m}\right)^3\left(\frac{Re_s}{Re_m}\right)^{1.5k_{ce}}\right] \quad (2)$$

[8] The source level was measured using the transfer function correction.

$$k_{ce} = \frac{log_{10}\left(\frac{\sigma_s/\sigma_{i,s}}{\sigma_m/\sigma_{i,m}}\right)+log_{10}\left(\frac{\sigma_{i,s}}{\sigma_{i,m}}\right)}{log_{10}\left(\frac{Re_s}{Re_m}\right)} \quad (3)$$

Figure 33 shows an example of the scaling exponent, k_{ce}, derived from the equivalent cavitation number for two test conditions. Figure 34 presents a comparison between the full-scale measurements and the scaled source levels.

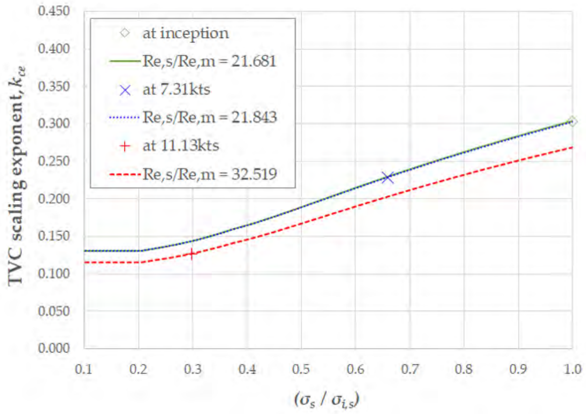

Figure 33: Scaling exponent, k_{ce}, derived from the equivalent cavitation number for two test conditions (Lee *et al.*, 2024).

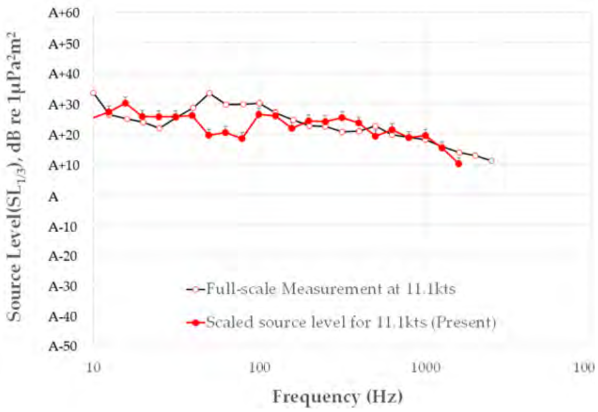

Figure 34: A comparison between the measured and the scaled source levels (Lee *et al.*, 2024).

The effect of water quality, generally quantified by dissolved gas content, was reviewed in detail in the report of the previous hydrodynamic noise committee.

Khoo *et al.* (2021) recently investigated the effect of nucleation on tip vortex cavitation dynamics and noise. Two different nuclei populations, denoted as ‘monodisperse’ and polydisperse’ in Figure 35, were used for measuring TVC inception of NACA0012 hydrofoil. Both the nuclei population and the ambient pressure were observed to affect the inception event rate significantly as shown in Figure 36. However, tip vortex kinematics and acoustics were influenced more by changes in local pressure (cavitation number) than by nuclei population and initial nucleus size (see Figure 37 for the effects on the acoustics). Khoo *et al.* (2021) noted the relative independence of nuclei size on cavity kinematics and acoustics might be due to the similarity of the bubble critical pressures in the 50-100 μm diameter range (see Figure 36 for the bubble diameter distribution).

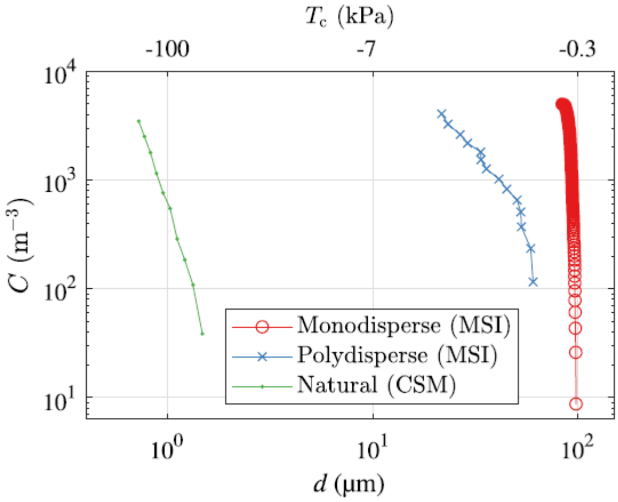

Figure 35: Injected nuclei populations used by Khoo *et al.* (2021).

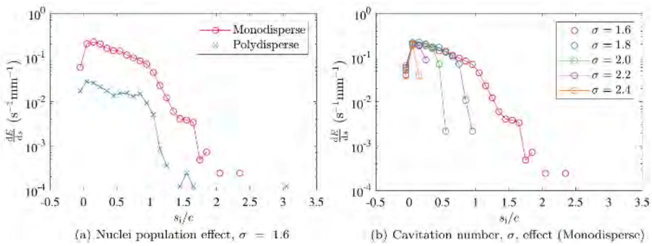

Figure 36: Effects of (a) nuclei population and (b) cavitation number on inception events rate density (Khoo *et al.* 2021).

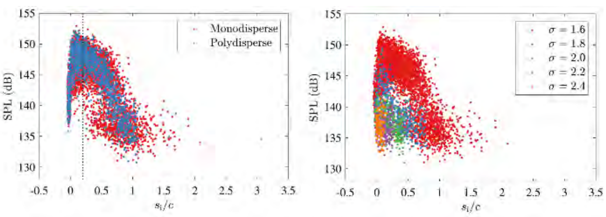

Figure 37: Effects of (left) nuclei population and (right) cavitation number on the sound pressure level (SPL) of inception events (Khoo *et al.* 2021).

4.2.2 Full-scale noise

A number of international committees and organizations have published or are drafting various standards to provide guidance on procedures and methodologies for measuring underwater noise from surface vessels, as shown in Figure 38.

Ship classifications societies, such as American Bureau of Shipping (ABS), Bureau Veritas (BV), Det Norske Veritas Germanischer Lloyd (DNV), Lloyd's Register (LR), Registro Italiano Navale (RINA), China Classification Society (CCS), and Korean Register (KR), have published underwater radiated noise guidelines and notations. In addition, International Organization for Standardization (ISO) is developing international standards for measuring URN in deep water (ISO 17208-1:2016; ISO 17208-2:2019) and shallow water (ISO 17208-3/DIS:2024).

Figure 38: Guidelines and standards for URN measurement

However, these guidelines do not follow consistent methods for ship noise measurements, analysis, and reporting procedures. Therefore, certificates provided by different societies cannot be directly compared as shown in Figure 39, which hinders the determination of relative noise.

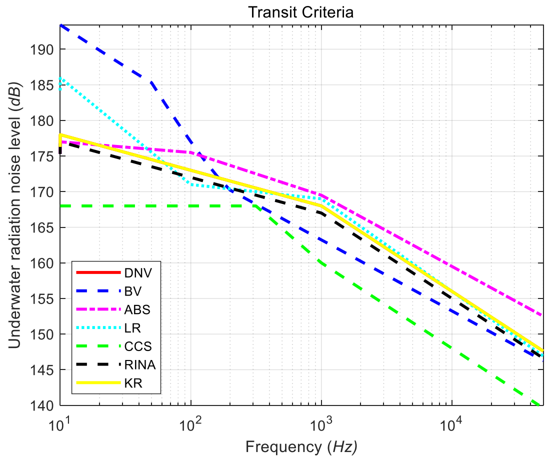

Figure 39: Limitation criteria for URN for Transit Condition of different classification societies. (Hannay *et al*, 2018)

To improve standard procedures for URN measurements in shallow water, the EU and Canada have launched several projects.

SATURN is an EU-funded project that develops URN standards and produces recommendations for effective underwater sound management. SATURN defines standards for terminology, methodology, tools and metrics for measuring, assessing and comparing the impacts of noise from shipping and boats. In the SATURN project, URN and background noise was collected for approximately 190 and 80 vessels respectively. Data was collected according to different procedures at water depths ranging from 50m to 200m using different instrumentation deployment strategies such as the drifting buoys, the moored surface buoys and two hydrophone seabed configurations. Figure 40 shows an example of reported differences of URN levels between ISO 17208-1 and other procedures.

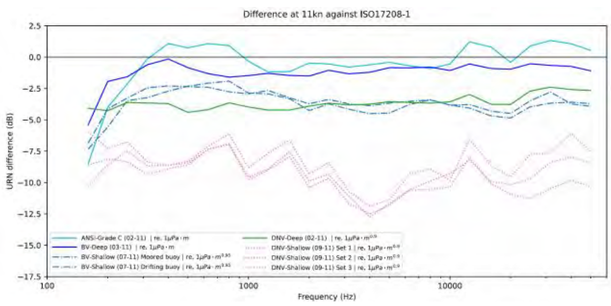

Figure 40: Difference of reported URN levels between ISO 17208-1 and the other procedures (Yubero de Diego *et al* 2023)

Transport Canada and VFPA (Vancouver Fraser Port Authority) initiated the 'URN Standardization Support' project to improve harmonization of URN measurement procedures, and to support the International Organization for Standardization (ISO) to develop a shallow-water URN measurement standard. The Enhancing Cetacean Habitat and Observation (ECHO) Program, initiated a second project concerning the alignment of URN measurement and analysis procedures used by ship classification societies for quiet ship certification.

Source level measurements using a drifting hydrophone array were analyzed separately from the other measurements (Figure 41). The overall quality of the drift measurements was poorer than the static measurements. This was partly due to increased self-noise, caused by wave-induced surface motion and currents, and partly due to difficulties controlling the measurement geometry caused by the relative motion of the source vessel and the measurement vessel.

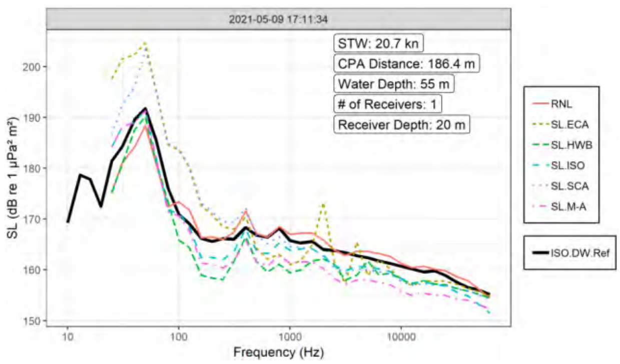

Figure 41: Source level (SL) measurements of vessel are performed at the shallow site using the drifting hydrophone array compared to the deep-water reference source level (Ainslie *et al* 2021).

ISO has recently been developing a standard for URN measurements in shallow water (ISO 17208-3/DIS:2024), which is also described in the ITTC Recommended Procedures and Guidelines 7.5-04-04-01, investigating the shallow water sound interacting with the seabed characteristics which are rarely known with accuracy. Depending on the water depth, sound may reflect one or more times from the seabed before arriving at the measurement points. Facilitating repeatable measurements in shallow water is expected to reduce the cost of obtaining quiet certifications (by reducing sailing time to a measurement location) and hence increase the proportion of the global fleet. To address the guideline for measurements in shallow water, the special requirements such as characteristic length, test site and hydrophone deployment, as well as various methods for assessing propagation loss are described below.

Since underwater ship noise is mainly due to machinery and propeller noise contributions, the ship characteristic length may be reduced to the distance between the machinery room and the propeller (Figure 42), rather than overall ship length. It is required in ISO 17208-3/DIS:2024 that length L is greater than 1/3 of the overall length of the ship L_{OA}.

$$L \leq L_{OA} \text{ and } L > L_{OA}/3 \qquad (4)$$

The ship source length L is also defined to solve the problem that the CPA (Closest Point of Approach) distance is too large for the measurements to get high enough SNR.

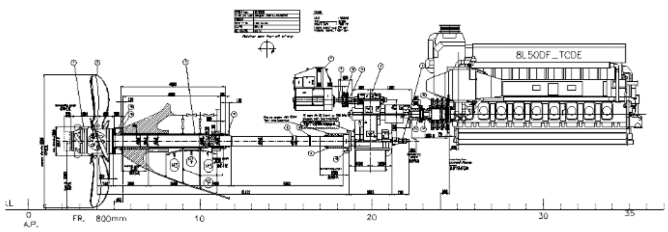

Figure 42: The dominant source of sound is main engine and propeller

For the test site, if the water depth is much smaller than the CPA distance, the water depth and seabed properties should be such that the lowest frequency of interest is at or greater than the shallow water cut-off frequency $f_{\min}$.The document 7.5-04-04-01 pointed out that shallow water effects can affect ship resistance and hence have influence on the ship radiated sound. This requires that the minimum water depth H_{min} for a ship of width B and draft T should be larger than $3\sqrt{BT}$. Figure 43 shows the minimum water depths according to ships overall lengths which were obtained from the marine AIS (Automatic Identification System) for vessels operating in the North Sea.

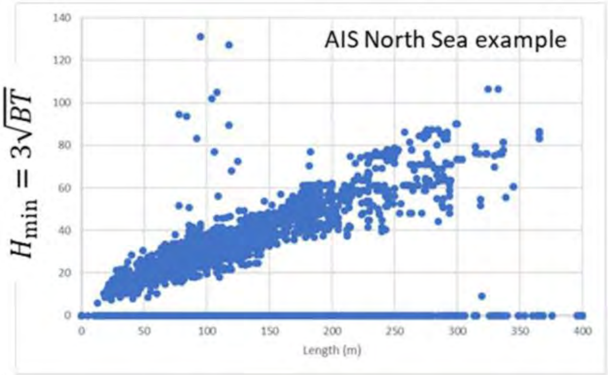

Figure 43: Minimum water depth according to ship length.

For water depths greater than the CPA distance, the hydrophone configuration specified in ISO 17208-1 applies. In water depths smaller than the CPA distance, a vertical array of at least three hydrophones, distributed over the water depth (Figure 44) is preferred.

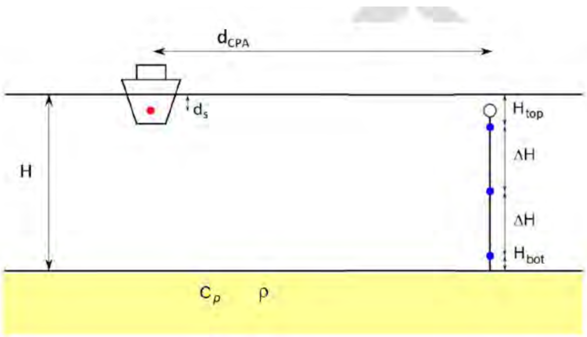

Figure 44: Proposed configuration for a vertical array in shallow water

For surface deployment, the wave drift will lead to a significant increase in low-frequency background noise. Also, the hydrophone deployed underwater is impacted by the water flow, and there is a strong flow noise interference. It is appropriate to apply measures to reduce the flow noise interference, such as those shown in Figure 45.

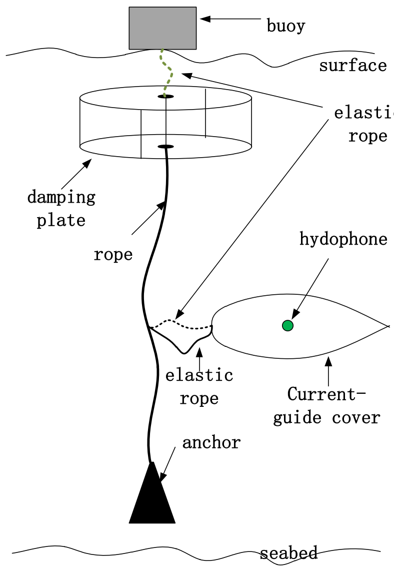

Figure 45: Measures to deploy hydrophone reducing the flow noise interference

Multiple methods for assessing propagation loss are provided: Seabed-critical angle (SCA) method (MacGillivray *et al*, 2023); Application of an empirical formula (as in ISO 17208-2) (Audoly *et al*, 2017; MacGillivray *et al*, 2023). The propagation loss assessment with an empirical formula is supported by measurements at the test site with a controlled acoustic source, as shown in Figure 46 (Pang *et al*, 2023).

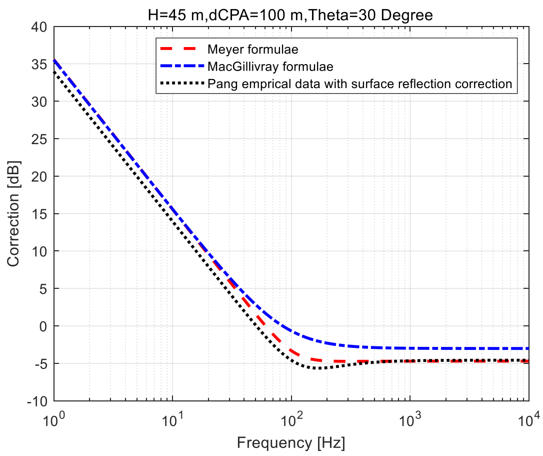

Figure 46: The empirical propagation loss corrections are compared (Pang *et al* 2023)

In addition to direct full-scale measurement in both deep and shallow waters, noise level evaluation methods based against on-board monitoring have been developed. Real-time evaluation of underwater radiated noise of merchant ships through on-board monitoring is a beneficial application that can reduce URN testing costs and is easily acceptable to ship owners. Meanwhile, it can monitor the ship's radiated noise for a long time and enrich the operational database, helping to optimize the design and operation.

Current on board methods used to estimate far-field noise from ships include: direct prediction methods based on hydrophones above the propellers; transfer functions derived from the relationship between measured vibration levels and sound source levels to optimize the number of sensors selected based on the contribution of the ship's sound sources, non-negative least squares (NNLS) methods (Basten 2015, Mulders 2018, Graeme *et al* 2021), the Operational Transfer Path Analysis (OTPA) method (Zerbs and Pascher, 2016); Average Quadratic Velocity (AQV) method based on the relationship between shell mean square vibration velocity and radiated noise transfer (Cintosun 2021); Energy Transfer Path Analysis (ETPA) method; Sound source level estimation from propeller characteristics (Bosschers 2017). These methods are known to be valid for propellers with or without cavitation.

Graeme *et al*. (2021) reported that ship's URN can be accurately estimated using NNLS values from on board accelerometers installed on the hull above the propellers and on possible machinery noise sources such as engines, generators and pumps. Figure 47 shows that the reconstructed URN using data from on board sensors agrees very well with off-board measured results.

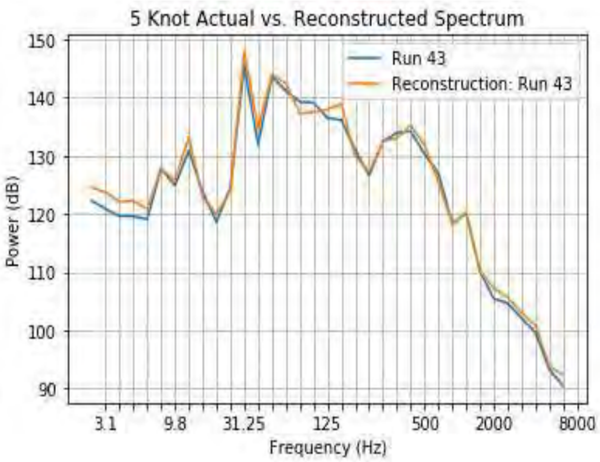

Figure 47: Ship radiation noise prediction results based on NNLS method (Cintosun *et al* 2021).

The OTPA-based method can be applied to submarine and surface vessel radiated noise prediction, but the prediction results can show a large deviation when there is a lack of certain equipment information, such as a source not equipped or not available as input to the method.

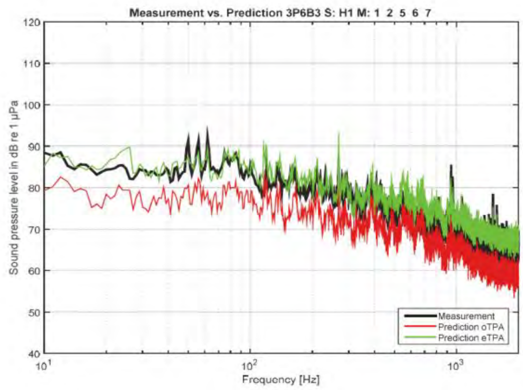

Figure 48: Ship radiation noise prediction results based on OTPA method (Zerbs and Pascher 2016)

4.2.3 Methods for hydro-acoustic modelling of noise

<u>Cavitation noise prediction</u>

Typically, propulsors are analyzed in open-water conditions, such as in a tunnel or in a free-field. Analyzes are commonly carried out at model scale. Some recent studies have considered the effects of the hull wake on the propeller hydrodynamics and acoustics, that is, by simulating propeller operation in the behind-the-hull condition. For most cases, validation data in terms of noise measurements is available. To capture the hydrodynamic sound sources, key physics need to be resolved, that is, flow turbulence and multiphase phenomena. The acoustics modelling approach should account for the propagation of the sound waves in the fluid medium, as well as the effects of the environment, such as the boundary conditions imposed by solid walls (hull, propulsor) or the free surface. The acoustic characteristics of the noise may also differ depending on whether the analysis is performed in a free-field or in a tunnel configuration.

Regarding turbulence modelling, the RANS approximation is frequently used in propeller analyzes. While propeller performance can be predicted well using RANS-based models, unsteady flow features, vortical flow and wake flow in general can suffer from a lack of detail. Tonal noise should be adequately predicted using RANS methods, but higher frequency noise content and the range of cavitation phenomena are usually more poorly represented, since these methods have limitations due to their averaging nature in resolving the turbulence fields and thus predicting broad-banded excitation. Scale-resolving models, such as large eddy simulation (LES) or hybrid RANS-LES based methods, such as detached eddy simulation (DES) or scale adaptive simulation (SAS) techniques, can resolve a part of the turbulent flow fluctuation spectra and thus also capture broadbanded sources of sound. In predictions of propeller cavitation performance and related sound levels, methods belonging to the DES category, such as delayed DES (DDES) or improved DES (IDDES), appear preferred and are frequently applied.

Most viscous CFD methods are based on a homogeneous mixture approximation that employs a volume-of-fluid (VOF) method to account for the water and vapour phases. Phase change is accounted for by mass-transfer models that are primarily driven by isothermal and incompressible pressure differences. The inability of mixture VOF models to resolve cavitation structures on small scales (on practical numerical grids), such as bubble growth and collapse, leads to the under prediction of the high-frequency content of the sound level spectra. Vapour structures resolution and turbulent flow are interconnected and high-fidelity cavitation modelling should be employed together with an appropriate turbulence modelling approach. A multi-scale multiphase modelling technique, such as the Eulerian-Eulerian two-fluid method (e.g., Li & Carrica, 2021; Viitanen & Peltola, 2021) or Eulerian-Lagrangian method (e.g., Wang *et al*., 2021; Lidtke *et al*., 2016), is likely needed for a more complete representation of various cavitation types and dynamics. These currently remain as research topics, although some applications have been reported. An Eulerian-Eulerian two-fluid method has been recently applied to study cavitation noise on static hydrofoils (Hynninen *et al*., 2023), and the results were compared to those with the VOF method and experimental measurements. Ku *et al*. (2022) applied a sequential, one-way coupled Eulerian-Lagrangian bubble model to predict tip vortex cavitation inception and noise. They performed an unsteady RANS simulation to obtain tip vortex trajectories where they inserted Lagrangian bubbles to predict TVC inception and resulting noise (Figure 49). Cavitation noise was predicted by modelling the bubbles as point monopoles, and the resulting pressure spectra were compared with measurements (Figure 50).

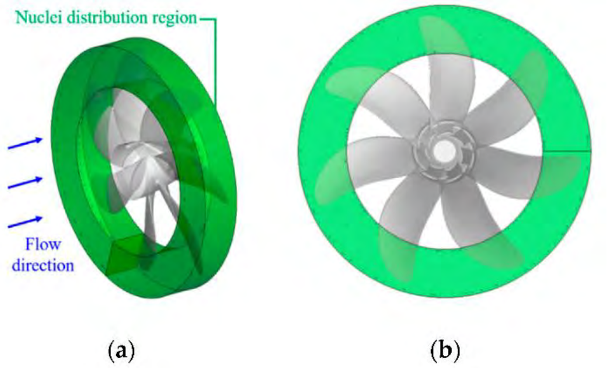

Figure 49: Distribution domains of nuclei (Ku *et al.* 2022).

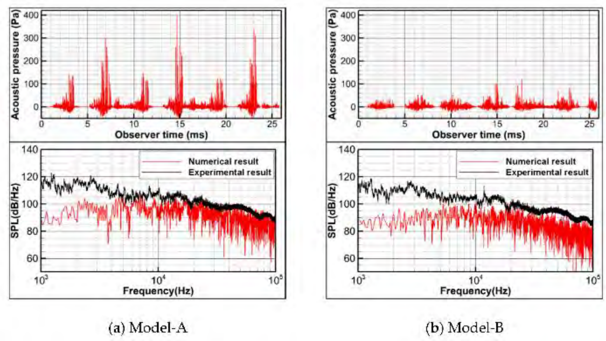

Figure 50: Acoustic pressure due to tip vortex cavitation in the time and frequency domains (Ku *et al*. 2022).

Typically, cavitation propeller noise predictions using CFD and CHA (computational hydroacoustics) methods are based on the Ffowcs Williams Hawkings (FWH) acoustic analogy (e.g., Fujiyama & Nakashima (2017), Li *et al*., (2018), Sezen *et al*., (2020, 2021a, 2021b), Ku *et al*. (2021), Lidtke *et al*., (2022)). There are variations in specific numerical techniques applied in this CHA class, frequently referred to as direct and permeable (or porous) formulations for the acoustic analogy (Wang *et al*., 2022). With the direct method, one evaluates the Lighthill stress tensor directly with a volumetric integration. The permeable formulation closes the main sound sources with a data surface, and noise generation within this surface is idealised by virtual sources on the surface. The latter approach is most frequently used. As noted by Cianferra (2017), the permeable formulation predicted the main frequency components although with underpredicted amplitude and sensitivity to the position of the surface, while the direct approach provided a noise prediction very similar to reference data everywhere in the field. Recently, Wang *et al*. (2022) proposed an interesting dual-mesh technique for the direct FWH analogy for propeller noise simulation, that reduces the calculation time and required computer disk storage space (Figure 51). Lyu *et al* (2023) demonstrated that with careful positioning of the data surfaces for a cavitating propeller case, similar results can be predicted in terms of monopole noise spectra using the permeable formulation. On the other hand, Viitanen *et al*. (2018) have applied a FEM based Lighthill analogy for noise simulations of wetted and cavitating propellers, which utilised both volumetric sources near the propeller and a conformal surface enclosing the propeller, with source data from a DDES-based solution. This method was also used to predict non-cavitating noise from a thruster unit in-behind conditions and the results were compared to full-scale noise measurements (Viitanen *et al*., 2023).

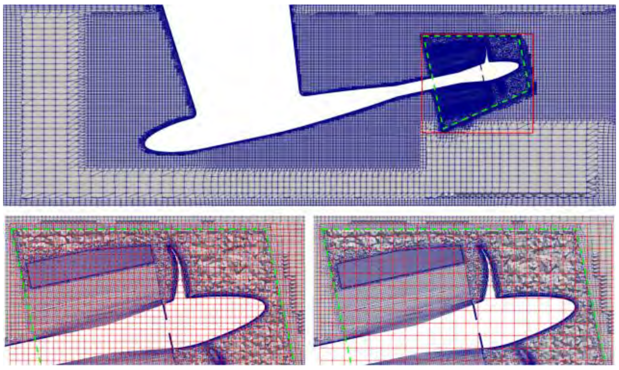

Figure 51: CFD (blue) and acoustic (red) meshes (Wang *et al*. 2022).

Li *et al*. (2018) applied a DDES based flow solution together with a permeable FWH formulation to predict URN. The results were compared to model-scale and full-scale noise measurements (Figures 52 & 53). They demonstrated that the numerically predicted pressure pulses and tonal noise closely correspond to the measured data for the first five orders of blade passing frequency. Low-frequency (< 112 Hz) broadband noise was underestimated, which was attributed to under-resolved tip vortex cavitation.

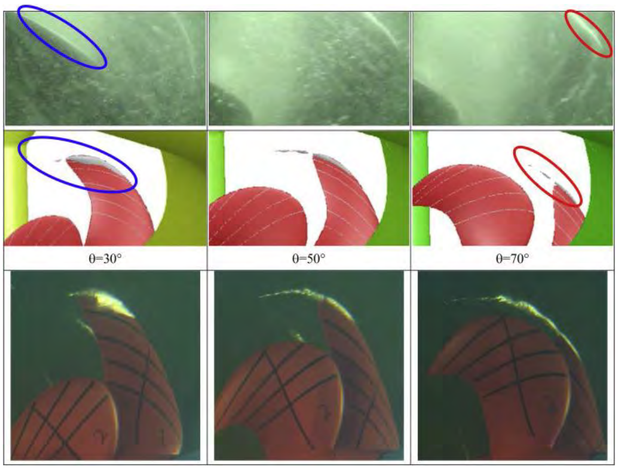

Figure 52: DDES prediction of cavitation (middle row) and comparison to sea trials (top) and model tests (bottom) (Li *et al*. 2018).

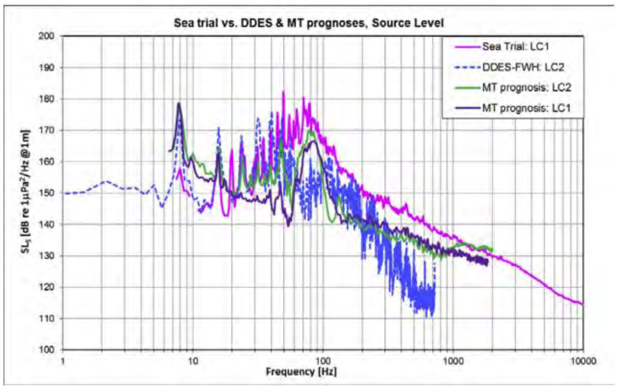

Figure 53: Full-scale noise source levels based on different methods (Li *et al*, 2018).

Lidtke *et al*. (2022) applied a permeable FWH acoustic analogy, using an IDDES method for the flow solutions to resolve part of the turbulence spectra and cavitation dynamics. They showed that low-frequency peak sound pressure levels can be predicted to within 5 dB of measurements, and that key features of the shape of the noise spectra can be well represented with the simulations. They also bring up an interesting point that has not been widely discussed, that is, the CFD method generates background noise that can be significant in certain conditions or frequency ranges. To address this, they propose that determination of numerical background noise should be a part of the URN assessment.

Sezen *et al*. (2021a) investigated the influence of several RANS-based turbulence models, and a permeable formulation for the FWH acoustic analogy was applied to evaluate the resulting noise. They noted that the RANS models predicted similar noise levels at low propeller loading, and that at high loading more discrepancies were seen.

Sakamoto & Kamiirisa (2018) applied two different noise prediction methods based on viscous CFD solutions with DES. In the first method, they used the time domain pressure predicted by the CFD solver at certain probe points, to resolve blade passing frequencies and a limited range of broadband noise. In the second method, they applied Brown's formula (Brown, 1976) together with the CFD simulation. The Brown's formula is an empirical relation with, e.g., the propeller diameter, number of blades and rate of revolution as parameters, and information of the cavitation volume predicted by the CFD solver was used. They concluded that methods estimate the tonal noise up to the 3rd blade frequency well, and that Brown's formula predicted the upper bound of broadband noise. A similar approach was also used by Fujiyama & Nakashima (2017), who also compared the results to the FWH acoustic analogy solution and to full-scale measurements. They noted that the results with the direct pressure analysis were in good agreement with measurements and with the FWH method. Comparison with experiments was favourable up to the 5th blade passing frequency in model-scale, and in full scale up to approximately the 2nd blade passing frequency due to challenges in resolving the tip vortex cavitation in full-scale simulations. It was challenging to reliably predict noise levels using CFD calculations alone at higher frequencies. Consequently, the empirical formula was suggested to be applied in conjunction with the CFD results.

<u>Noise propagation modelling, especially for shallow waters</u>

Several numerical methods exist for modelling noise propagation. Based on their accuracy and practicality, Etter (2009) and Farcas *et al*. (2016) have reviewed various propagation models that are currently in use. Underlying mathematical methods, including ray theory, normal modes, multipath expansion, wavenumber integration, and parabolic equation, have been used to divide the propagation models. The methods can be classified based on their ability to predict propagation in different depths and frequencies (Figure 54). The models can be further categorized as range-independent (depth-dependent) and range-dependent models. For instance, with ray theory applicability is better in deep water at low frequencies where there are less reflections from the bottom and the surface. At high frequencies in shallow water the applicability is worse in range-independent environments. Parabolic equation (PE) methods allow a weak range dependence, though at high frequencies, the model typically becomes impractical due to excessive execution times, especially in shallow water where the strong bottom interaction demands shorter range steps.

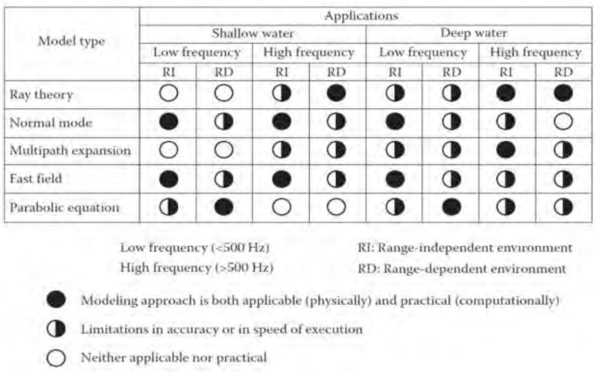

Model type	Applications							
	Shallow water				Deep water			
	Low frequency		High frequency		Low frequency		High frequency	
	RI	RD	RI	RD	RI	RD	RI	RD
Ray theory	○	○	◑	●	◑	◑	●	●
Normal mode	●	◑	●	◑	●	◑	◑	○
Multipath expansion	○	○	◑	◑	◑	◑	●	◑
Fast field	●	◑	●	◑	●	◑	◑	◑
Parabolic equation	◑	●	○	○	◑	●	◑	◑

Low frequency (<500 Hz)
High frequency (>500 Hz)
RI: Range-independent environment
RD: Range-dependent environment

● Modeling approach is both applicable (physically) and practical (computationally)
◑ Limitations in accuracy or in speed of execution
○ Neither applicable nor practical

Figure 54: Domains of applicability of different ocean-acoustic propagation models (Etter, 2009).

Deavenport *et al*. (2019) have developed a ray model with a convolution-based time-domain procedure to simulate transient signals that propagate in shallow-water environments. Zhou *et al*. (2021) developed a two-dimensional FEM for predicting propagation of sound. The method was applied to different environments, and results compared to other benchmarks, analytical and numerical solutions.

Liu *et al*. (2021) applied a few numerical methods to estimate transmission loss (TL) in shallow water with varying bathymetries, and compared the results to measurements (Figure 55). Forms of TL in different frequencies were analyzed with respect to the varying characteristics of the seabed and the underwater environment. Sipilä *et al*. (2019) applied a propagation model based on the PE method to predict transmission in very shallow waters (depth 25 m) and compared the results with full-scale noise measurements. They also investigated the sensitivity of transmission loss to bathymetry and seabed sediment characteristics (Figure 56). It was observed that the measured and simulated transmission loss levels were similar and showed an increasing trend towards higher frequencies.

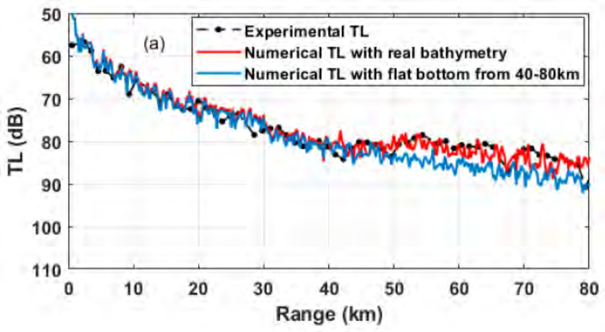

Figure 55: Comparisons of experimental and numerical TLs (Liu *et al*, 2021).

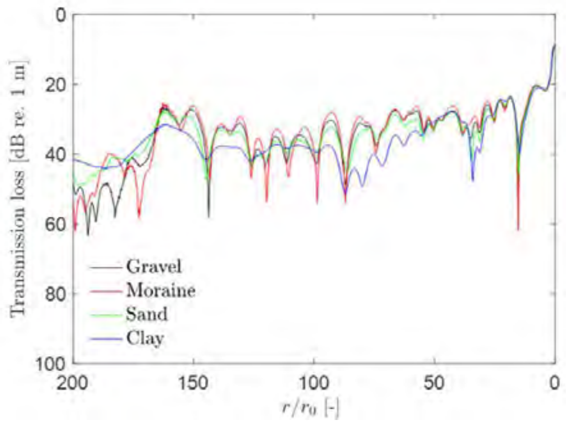

Figure 56: Comparisons numerical TLs for different bottom sediments (Sipilä *et al*, 2019).

Küsel & Siderius (2019) compared several different propagation models. They studied the same test cases as were applied in a sound mapping workshop (Colin *et al*., 2015), with range-independent and dependent cases, and comparisons of propagation loss (PL), sound exposure level (SEL), and pressure in the time domain (Figure 57). They noted that a PE would likely be a method of choice for a range-dependent environment, and that ray-based theory was not appropriate for shallow water waveguide based also on errors in broadband SEL. They also pointed out that experienced propagation modelers know intrinsic details of each model, however, for occasional users who want to know what the sound field looks like given a specific source and environment and if sound levels are too high such that they may harm marine organisms, many details regarding their model of choice may not be obvious or intuitive.

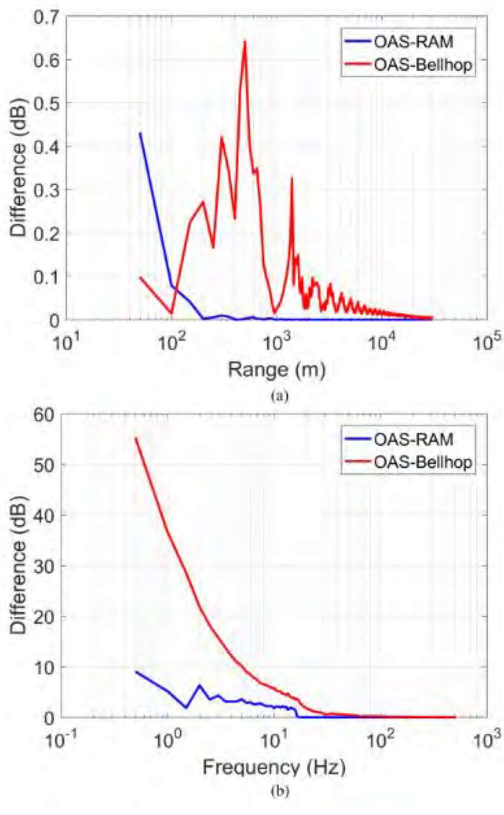

Figure 57: Mean absolute errors of sound exposure levels vs. range (a) and frequency (b) between different numerical methods (Küsel & Siderius, 2019).

Oliveira *et al*. (2019) presented a comparison of different methods in idealised cases (2D and 3D) with varying complexity (Figure 58). Moreover, the PE model was applied in a shallow water environment, with the environment being extremely complicated, especially the highly variable bathymetry. They noted that transmission loss (TL) results provided by the PE, normal mode, and beam tracing models tended to agree with each other, although differences can result with increasing the bathymetry complexity and expanding the range of propagation. The low-frequency cases of 500 Hz in such shallow water were below the threshold of a ray or beam model's validity. They noted that when choosing an underwater sound propagation model for practical applications in complex shallow water environments, a compromise must be made between numerical model accuracy, computational time, and validity.

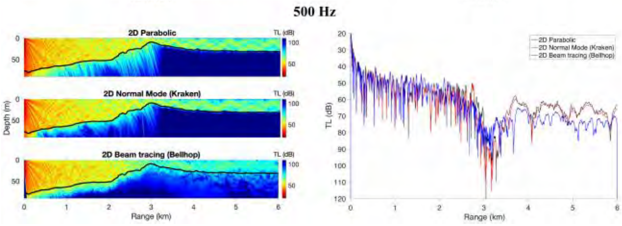

Figure 58: TLs based on different numerical methods (Oliveira *et al*, 2019).

4.2.4 Noise in ice conditions

The rapid loss of summer sea ice that's been observed in recent years has opened up ship traffic to this once nearly inaccessible region. Low-frequency sounds generated by ships propagate efficiently and travel long distances in deep marine environments such as polar regions.

<u>Noise propagation under ice condition</u>

Noise propagation in ice conditions is different from non-polar regions. At high latitudes, noise from a ship is particularly efficient at propagating over long distances due to the Artic sound channel (see Figure 59), similar to the SOFAR (Sound Fixing and Ranging) channel. Frequencies between 15 and 30 Hz travel most efficiently through the Arctic sound channel, and high frequency sounds do not propagate as far as lower frequency sounds. Sound propagates much farther in the SOFAR channel compared to the Arctic sound channel, because sound waves in the Arctic sound channel may also interact with the ice, and therefore increase attenuation. However, the Arctic sound channel allows for farther propagation distances at shallow depths (100 to 300 m) compared to non-polar regions.

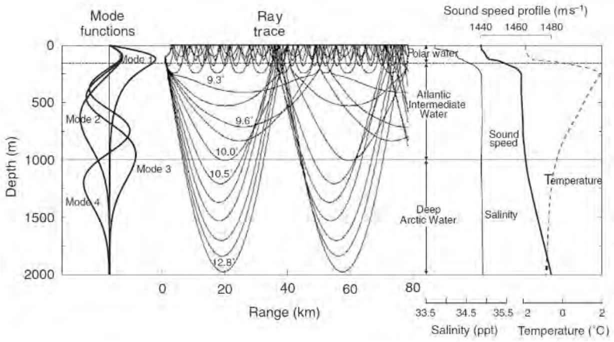

Figure 59. Ray trace in Arctic sound channel (Mikhalevsky, 2001).

<u>Noise from collision of propeller and ice</u>

According to available studies, the main noise source during icebreaking seems to be propeller cavitation (Almgren 1991; Erbe 2000; Roth 2013), icebreakers generate higher and more variable noise levels from propeller cavitation compared to other vessels due to the episodic nature of ice breaking, which often involves manoeuvres such as backing-and-ramming into the ice.

A study of the United States Coast Guard (USCG) Cutter Healy's URN signature during ice breaking operations was reported in Roth (2013). Compared to open-water transiting, the noise signature increased approximately 10 dB between 20 Hz and 2 kHz when breaking ice (Figure 60). Operating ahead, even when breaking ice, does not typically produce high noise levels. There are two scenarios that generate considerably higher noise levels, when propellers are operated in opposite directions; and during backing and ramming when the propellers are operated astern, particularly when the ship begins to impact the ice.

Some icebreakers are equipped with bubbler systems that blow high-pressure air into the water to push floating ice away from the ship, creating additional noise over short ranges (Roth, 2013; Erbe 2000). Its noise characteristics are temporary continuous with a white noise spectrum with most of its energy below 5 kHz. The reported source level spectra from ice-breaking operations (Roth, 2013; Erbe 2000) are typically 10 to 15 dB higher than what can be expected for a conventional LNGC in open water.

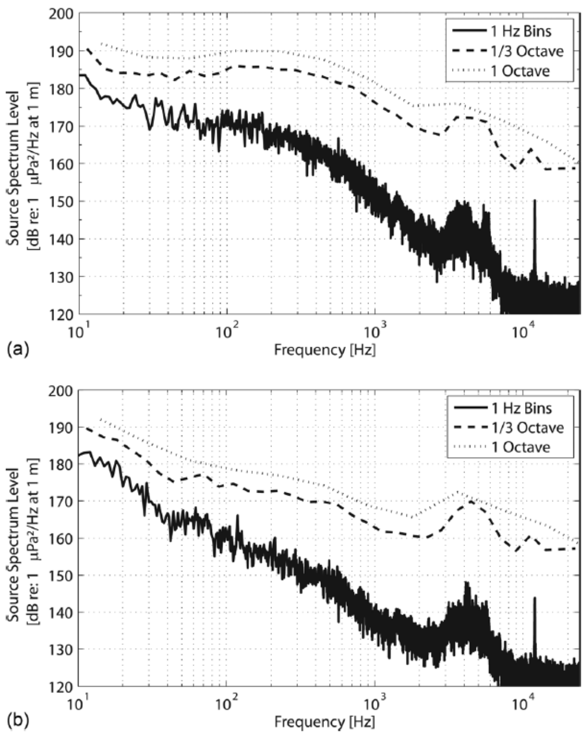

Figure 60. During August 27 transit: (a) estimated source level of Healy transiting in 8/10's ice cover at 05:26:30; range to the sonobuoy was approximately 2 km. (b) Estimated source level of Healy transiting in 3/10's ice cover at 05:51:20; range to the sonobuoy was approximately 4 km (Roth *et al* 2013).

Underwater noise from the Swedish icebreaker ODEN was measured east of Greenland in 1990, Almgren (1991). The propeller was found to be the primary acoustic source and the most intense noise levels were produced when the propeller nozzles clogged with ice causing stagnation of the inflow to the propellers, resulting in increased cavitation. The source levels, were reported to be roughly the same as from other icebreakers, but much higher than noise levels from ordinary ship operations in open water, as shown in Figure 61. The source levels also seem comparable to more recent studies, e.g. Roth (2013) and Erbe (2000).

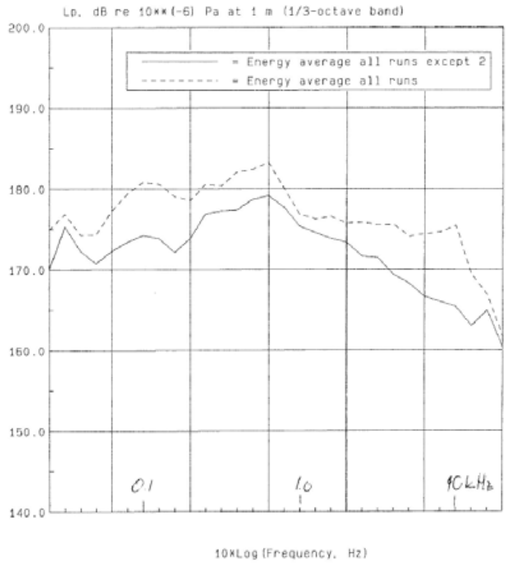

Figure 61. Source Level of Swedish icebreaker ODEN during ice-breaking operations in August 1990, with and without the two noisiest series (Almgren 1991).

The predicted receiver level at various distances is shown in Figure 62. At 1 and 10 km distances the sound pressure level is well above the ambient noise. The sound pressure level was found to be below the measured ambient noise at 100km distance, except in the range 20 to 40 Hz where the levels may be above the ambient noise also at 100 km; Only Baleen whales are known to produce sound in this frequency range.

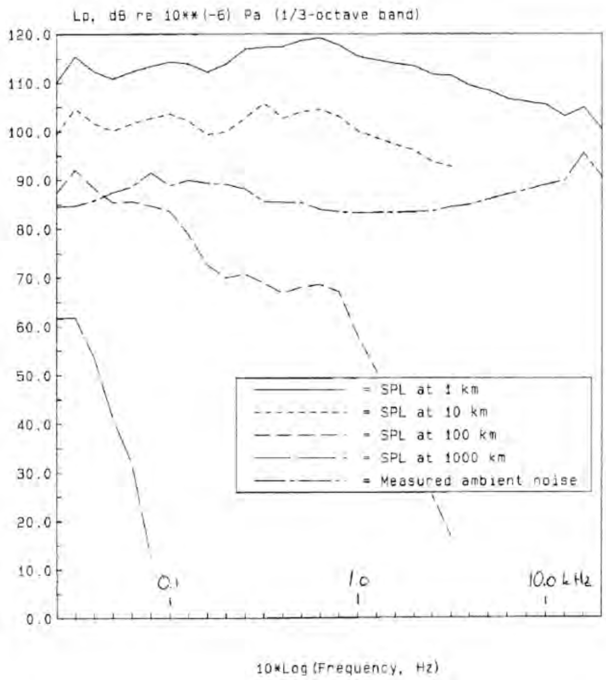

Figure 62. Prediction of ice-breaking noise from Swedish icebreaker ODEN at different distances (Almgren 1991).

4.3 Vibrations

Tor #8 was dedicated to the review of open literature dealing with the respective contributions of the hull vibrations and of the propeller in the ship radiated noise at full scale (frequency line and broad band spectrum) and investigate ways of assessing those contributions.

As previously reported in the 29th ITTC Specialist Committee on Hydrodynamic Noise Final report, the noise caused by vibrating machinery onboard a ship is called structural borne noise with the first path of vibrations being transmitted through the ship structure to the outer plating resulting in radiated noise. The secondary structural path is excited by the airborne noise that impinges at the compartment boundaries and excites the structure to vibrate. These vibrations propagate to the outer plating causing underwater noise.

The intent of the literature review is to understand the extent of full scale ship measurements undertaken to understand the contribution of hull vibrations and the propeller. In general propeller cavitation is the significant component of broadband noise and propeller singing (tonal type) and other ship sources are considered narrowband. Figure 63 taken from (Crocker, MJ, 1998) shows typical frequency contributions to ship acoustics.

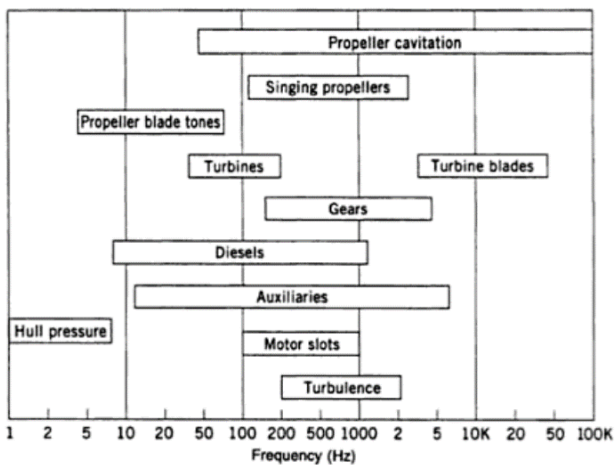

Figure 63: Ship Noise Sources (Crocker 1998).

There are a limited number of available papers in the open source domain looking at the contribution of structural borne noise from ships based on full scale ship trials. Zhang *et al* (2019) published a paper comparing different radiation modelling for the structural borne noise of an oil tanker. The paper discusses the three major contributions to underwater noise sources: mechanical noise, propeller noise and hydrodynamic noise of which the mechanical and propeller are most significant. The paper only considers underwater radiated noise from hull vibration due to the main power plants in the engine room. Foot vibration accelerations of the power plants were obtained on the full scale ship. In addition, vibrational acceleration measurements were acquired on local parts of the oil tanker for comparison with simulation results.

The structural borne component was compared using different acoustic models at low and mid-frequencies;

- The finite element and boundary element method (FE-BEM)
- Finite Element and infinite element method (FE-IFEM)
- Finite Element and automatic matching layer (FE-AML)

In the paper's conclusions it was found for this ship that the FE-BEM is the preferred method for estimating ship underwater radiated noise. The high frequency components performed using the statistical energy analysis (SEA)

The oil tanker vibration calculated values agree well with the measure values. Figure 64 shows the comparison of simulation and measured engine room vibrations.

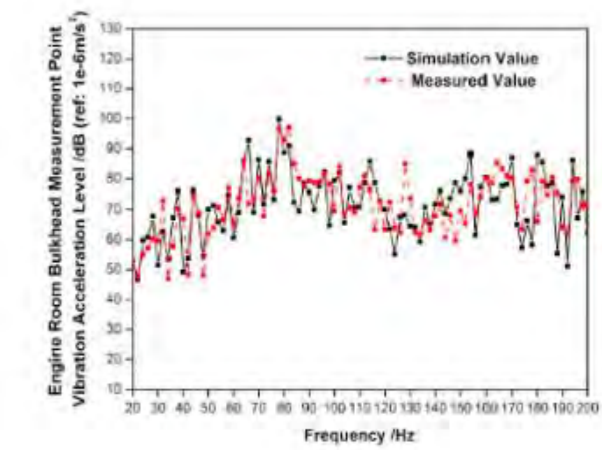

Figure 64: Comparison of simulated and measured values for Engine room measured location.

Rodrigo-Saura *et al* (2017) look at the transfer function (TF) of the structure-borne noise to underwater radiated noise for a vessel constructed of glass fiber reinforced plastics (GRP) and one constructed of steel.

Full scale measurements were obtained from two fishing boats, the GRP vessel being 23m length and the steel 24m. The vessels were instrumented up with accelerometers and data was acquired simultaneously with URN measurements.

Figure 65: Fishing boat full scale measurements.

The TF relates to the structure borne noise level of the hull with the underwater radiated noise (URN). The intent being the acoustic noise generated by the vibrations of the hull could be estimated from real time measurements of the structure-borne noise levels of the hull by applying the TF in real time. From the conclusions it verified that parameters such as the ambient noise, size of the vibrating panels and position of sensors must be taken into account to estimate the TF. Figure 66 compares the mean transfer functions for both hulls for both Broadband and Narrowband.

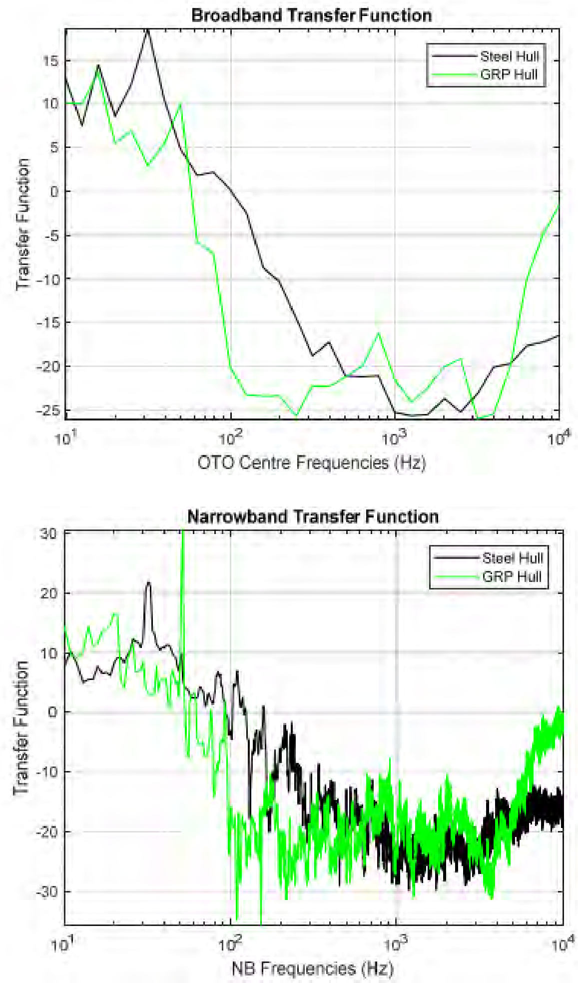

Figure 66: Broadband (top) and Narrowband (bottom) mean transfer function of the measurements of the ship with steel and GRP hulls.

A further paper (Lee *et al,* 2024) investigates experimental validation of a numerical procedure for estimating the structure-borne URN transfer function of a marine structure based on Statistical Energy analysis. (SEA). The transfer function method is considered as a countermeasure by classifying the URN generation mechanism into the sources and the propagation paths to predict the ship URN levels through a simple summation of various URN contributions. The experimental validation was originally undertaken on a fluid-loaded four-edge stiffened plate of 1.44m long and 0.71m wide as seen in Figure 67 and an exciter mid panel representing the mechanical power.

Figure 67: Stiffened plate fabricated for validation tests.

The results of the structure-borne URN TF's estimated by the SEA and experiments are shown in Figure 68.

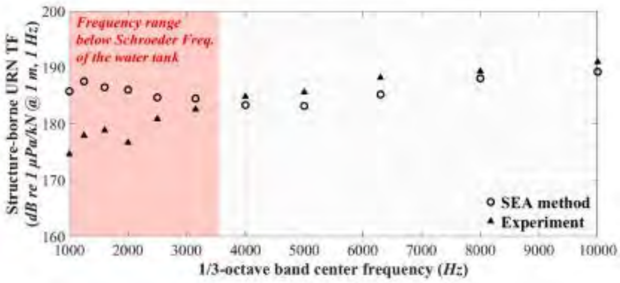

Figure 68: Structure Bourne URN TF's estimated by the SEA and experiment 1-10 kHz

Full scale measurements were conducted on a 65.4m Korean Research vessel, 'Cheong-Hae' to confirm the practicality of the proposed procedure. The structural borne URN of the vessel and the predicted measurements are shown in Figure 69.

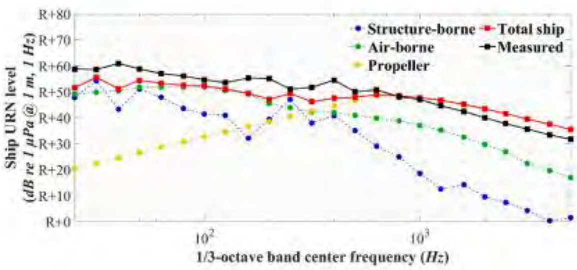

Figure 69 Total ship URN levels evaluated by the SEA and sea trail measurements. (25Hz-5kHz)

Under the collaborative project AQUO, (Achieve Quieter Oceans by shipping noise footprint reduction), a measurements task was undertaken (AQUO D3.3 2014). The contents of the paper details ship types and methods used to acquire accurate experimental data for analysis of the URN signatures of each vessel. The intent was to collect data for the contribution of each noise source on the vessel. Table 1 provides the list of full scale measurements made for the AQUO project.

Partner	Vessel type	Measurement Activities							
		Hull	Machinery	Calibration	URN	Directivity	Cavitation visualization	Power	AIS
TSI	FRV (FS1)	X	X	X	X	X		X	X
TSI	RV (FS2)	X	X	X	X	X			X
TSI	Commercial (FS3)	X	X	X	X	X		X	
TSI	FV (FS4)			X	X	X			
CTO	Research Vessel (FS5)	X*		X	X		X	X	X
SSPA	Coastal Tanker (FS6)	X*	X	X	X	X	X	X	

Table 1: Full scale measurement undertaken.

The aim of the hull and machinery vibration measurement is the correlation of the on board vibration phenomena with the narrow band spectra obtained during the URN measurements. The intent is to, in the future, report the different sources of the underwater footprint of the vessel. Therefore, the AQUO project should be monitored for any further open source literature by this ITTC committee.

From the open source data currently found, Figure 69 provides the only actual breakdown of components showing URN contributions. It is likely that with URN being of high priority for Naval vessels further work has been conducted assessing the contributions of structural acoustics but this data tends to be at a classification not available as open source information.

4.4 Benchmark tests

4.4.1 JoReS activity

CFD methods have been confirmed as a potential on ship hydrodynamic prediction. While being a flexible and low-cost tool, its results are subject to model test validation, as it offers a well-controlled, physical measured value.

Striving to increase confidence in numerical methods and create a basis to further ship performance improvement and industry digitalization, a group of key companies and research institutes have now stepped up to close this knowledge gap between model tests, CFD and full-scale reality and joined the Joint

Research Project: Development of an industry recognized benchmark for Ship Energy Efficiency Solutions (JoRes).

JoRes (www.jores.net) aims to increase the understanding of full-scale ship hydrodynamics by comparing the state-of-the-art ship hydrodynamic measurement techniques (model test results, CFD calculations and ship scale measurements including PIV propeller flow measurement).

One of the main tasks of the JoRes project is to develop a full set of industry recognized benchmark cases for full-scale and model-scale validation of CFD computations. The target goal is to increase knowledge on the important propeller/hull interaction effects, build confidence in ship scale CFD and assess their performance compared to traditional model testing.

The existing MV Regal vessel (Lpp=138 m) was selected as the first validation test case. The JoRes project organized several workshops to compare the full-scale results of CFD computations with the sea trial measurements conducted in September 2020 on the single screw general cargo vessel Regal. The primary objective is to assess and enhance the predictive capability of numerical simulation tools in ship scale.

Figure 70: Test (a) and simulation (b) geometry model of general cargo vessel REGAL; (Song *et al*., 2021)

Blind CFD computation results from different companies were compared either to empirical friction lines proposed by literature (flat plate and viscous hull resistance), calm water model tests (propeller open water data and cavitation), sea-trials data (hull and propeller roughness, resistance, and propulsion), direct and statistical comparison by the CFD data (resistance, propeller open water data and self-propulsion).

Although the presented CFD results were within the range of the experimental results, a big spread in the submitted data was shown between different numerical solvers. Therefore, it was suggested to investigate the details of all possible reasons that cause this difference. It was decided to investigate deeper every case separately and allocate a meeting to discuss the results for each case.

Flat plate simulation is the simplest form of the presented CFD simulations. The mesh error effect was excluded by asking the participants to compute using the same provided mesh. After discussing the results, a common relevant procedure (turbulence model, wall treatment and boundary conditions) to conduct CFD computations on a flat plate was established.

The second test was the ship resistance at full-scale without implementing hull roughness (smooth hull roughness). Similar to the smooth flat plate case, the results for the smooth resistance case showed a spread of about 40%.

To identify systematic deviations between the CFD-methods, it was proposed to conduct a series of mini workshops and evaluate the data (starting from the simplest to the most complex case) and make sure each step leads to an accurate procedure for resistance computation at full-scale. The new procedure is based on some predefined settings (excluding at this stage the superstructure and propeller blades). For this case, it was requested to generate the mesh individually, while respecting the imposed methodology; given domain size, thickness of the first cell on the hull and using the k-ω SST turbulence model. During the mini workshop dedicated to this first case, it was concluded that a proper procedure to conduct the smooth hull resistance at full-scale and improvement of the results was seen compared to the experimental data.

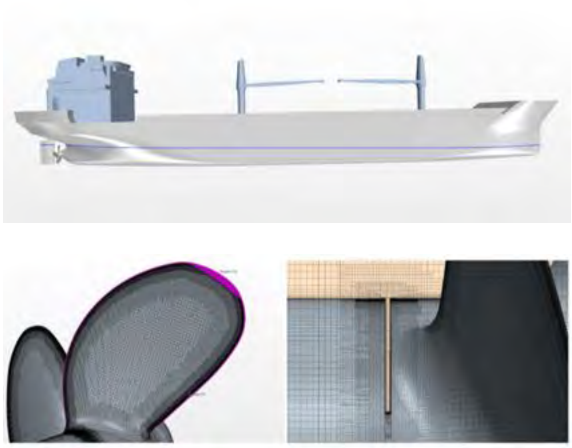

Figure 71: Geometry assembly of the MV REGAL used in self-propulsion simulations. Blue line shows the free surface level at the initial hydrostatic position; (Krasilnikov *et al*., 2023)

To simulate sea trials numerically in CFD, it is important to know the actual roughness characteristics of the hull and propeller. The JoRes team has been conducting a study on how to derive the roughness coefficients for the ship hull and propeller. Therefore, instructions and guidelines on numerical calculations have been shared with the working group.

The RANS self-propulsion simulation conducted with the measured hull roughness was extended with a cavitation simulation using a phase change model by Krasilnikov *et al*., 2023. The cavitation images obtained from the simulation were compared with borescope video taken during the sea trials.

After the first successful case, the JoRes 1 tanker (Lpp=178.5 m) has been selected as the second benchmark candidate. Similar exercises have been conducted and the computational speed/power results (Resistance, Torque, Thrust, Speed, Rpm, Cavitation observations and pressure pulse measurements) have been discussed in several CFD workshops.

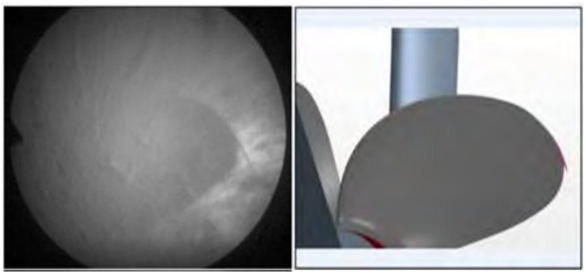

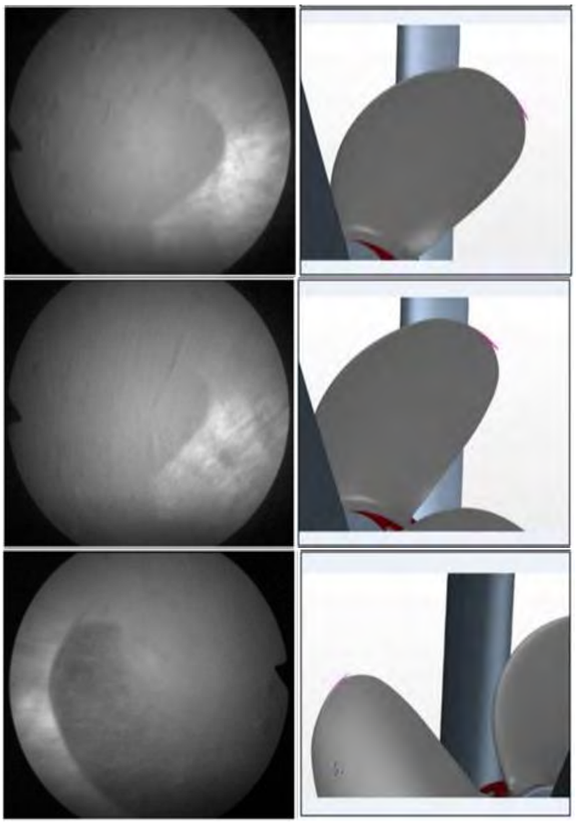

Figure 72: Comparison between the numerical simulation and full-scale observations on propeller cavitation; (Krasilnikov *et al*., 2023)

Direct comparison of the twin-screw propulsion performance is a good example to improve understanding of the model tests correlation and reduce the inherent numerical accuracy and uncertainties in modelling the exact trials conditions. The JoRes 2 ferry vessel, a twin-screw RORO ferry, is equipped with Controllable Pitch Propellers. so, there is always uncertainty about the actual pitch angle at the time of trials. Significant efforts were made to minimize this uncertainty, nevertheless, it is still not zero. That is why two sets of propellers with different pitch angles (-9.5 deg and -10.5 deg) have been offered.

To provide high-fidelity sea trial data for CFD validation, extra benchmark cases have been made available by the JoRes project, namely: the JoRes3 Cruise Liner (two 5-bladed fixed pitch propellers) and the JoRes4 Denis tugboat (two 4-bladed ducted propellers). For each benchmark case, the CAD geometry is cleaned and prepared for CFD validation along with providing the results of model tests and sea-trials data.

The JoRes Joint Industry project was successfully completed on the 1st of December 2023. Within the project 6 ship-scale validation cases were developed and all the results and geometries will be publicly available from the 1st of December 2024 (free registration on the JoRes website will be enabled).

As a follow-up to the success of the JoRes project, Chalmers University of Technology is introducing the seventh validation case and organizing a blind CFD workshop (Open Workshop on Ship Scale Resistance Prediction) full-scale and model-scale resistance prediction. The CFD results will be compared with measurements for different model scales and full-scale as well.

4.4.2 Round Robin Test on Cavitation Noise

The Round Robin Test Case, described briefly below, is the one selected by the previous 29th ITTC Specialist Committee on Noise.

Ship characteristics

In Figure 73 a photograph of the ship is reported, while the main ship characteristics are listed below.

Figure 73: Nawigator XXI Research Vessel

- Ship name: Nawigator XXI
- Type / Year of building: Research Vessel built in 1998
- Owner: Maritime University of Szczecin
- Length overall: 60.3 m (LOA)
- Beam: 10.5 m
- Draft: 3.15 m
- Displacement: about 1150 t
- Speed: 13 kn (max)

Propulsion plant and other machineries characteristics are listed below:

- 1 Controllable Pitch Propeller (CPP), D = 2.26 m, P/D(design) = 0.942, 4 blades
- Main Engine: SULZER Cegielski 8S20D (4 stroke, 8 cyl L) resilient mounted, 1120 kW, 900 RPM, reduction rate: 3.75
- Auxiliary Engines: Caterpillar SR4: (4 stroke, 8 cyl L) resilient mounted, 2 x 240 kW + 1 x 85 kW, 1500 RPM
- Bow thruster: 110 kW, abt. 500 RPM (propeller)

URN measurements at sea have been carried out during the EU-FP7 AQUO project; the campaign took place in the Baltic Sea and the following data was recorded:

- Shaft power, rpm, pitch, speed over ground
- Cavitation observations
- Vibrations
- URN
- Pressure pulses

Measurements have been performed at one ship draught (3.2 m at stern, 3.15 m at bow), propeller pitch was varied at constant RPM (8 different pitch settings); in addition to this, at one pitch setting two different propeller RPMs have been considered.

Documents for the benchmark have been written. It contains:

- Memo document with the presentation of the test cases
- ITTC Agreement that each participant is required to sign that they comply with the requirements of sharing results within ITTC
- Nawigator geometry
- Propeller at two different pitches
- Hull geometry

Three main conditions have been chosen for the propeller operating conditions. They are summarized in Table 2

Condition	P/D	K_T	$\sigma_{N\ (tip)}$
A1[9]	0.91	0.22	2.79
A2	0.91	0.26	2.79
A3	0.91	0.22	4.2

Table 2: Mandatory conditions for the proposed benchmark

The tests have to be performed in accordance with the participant's normal procedures.

4.4.3 Numerical benchmark possibilities

The Nawigator case has been recently chosen as the test case for the numerical benchmark Wageningen CFD 2025 workshop (as successor to previous CFD workshops). This benchmark appears to be a good opportunity to exchange results on the same test cases. Comparison of experimental results at model-scale, full-scale results and simulations is important.

5. SUMMARY AND CONCLUSIONS

The conclusions of the 30th Specialist Committee on Cavitation and Noise are presented here, ordered by the Terms of Reference.

1. All procedures and guidelines have been updated. A global document, based on the procedure 7.5-02-03-03.2, has been extensively updated to give a common base for all the other procedures and guidelines. It has been renamed "Visual description and measurement of cavitation events". It proposes global features and a common description of the cavitation events that could be observed in many configurations. Moreover, the two guidelines on erosion (7.5-02-03-03.5 and 7.5-02-03-03.7) have been merged into one document.

2. An extensive review of the recent studies dealing with cavitation has been presented. Most of them are dedicated to cavitation and noise measurements. Accuracy is generally not investigated by authors and remains an important task to conduct in the future.

3. A review of existing methods for cavitation simulations is presented. A questionnaire about dummy model practice has been distributed. Results obtained thanks to many institutes have been analyzed and are presented in this report. Due to the important differences between the practices, writing a guideline for "Dummy model practice" seems to be a difficult task.

4. Among all the benchmark data for CFD investigated, only JORES has been found available for sharing data (data available at end of 2024). Discussions with Wageningen Workshop 2025 for the definition of the test case on cavitation have been lead. The Nawigator XXI test case has been identified as a particularly interesting case and links with the Round Robin Test could be made between results at full-scale, model-scale and CFD.

5. A review of recent studies with different optical techniques using cameras and laser as well as non-optical approaches is presented. Applications of such techniques at full-scale have also been reported for cavitation and/or noise.

6. The process for the organization of the Round Robin Test proposed by 29th Specialist Committee on Hydrodynamic Noise has been defined. Formal agreement for sharing the hull geometry is still lacking (the only point that prevents launching the benchmark).

7. Some progress on acoustic features at model-scale have been reported. They concern particular aspects of acoustic or techniques with several sensors. It is worth noticing that a new method for scaling Tip Vortex Cavitation will be published in 2024.

[9] For this condition full scale measurements are available; propeller revolution rate at full scale was 230 RPM, with a correspondent $\sigma_{N\ (shaft)} = 3.09$

8. There are a limited number of available papers in the open domain looking at the contribution of structural borne noise from ships based on full scale ship trials. The review of these papers is presented.

9. An update of ISO and classification society rules has been made. The procedure for full-scale noise measurements has been updated thanks to the recent studies and methods developed for shallow water configurations.

10. A review of the recent studies and methods used for CFD noise prediction is presented in the report. Examples of recent literature are presented in this document focusing on the applicability of the method to the case investigated.

Finally, the ITTC Specialist Committee on Noise has submitted a document to IMO during the development of their circulars: “ITTC 2023, Review of full-scale ship noise measurement and estimation techniques”.

6. RECOMMENDATIONS

The 30th Specialist Committee on Cavitation and Noise recommends adopting the following guidelines:

- ITTC Guideline 7.5-02-03-03.6: Podded Propulsor Model Scale Cavitation Test
- ITTC guideline 7.5-02-03-03.9: Model-scale Propeller Cavitation Noise Measurements
- ITTC Guideline 7.5-04-04-01: Underwater Noise from Ships, Full Scale Measurements.

We also recommend adopting the following procedures:

- ITTC Procedure 7.5-02-03-03.1: Model-Scale Cavitation Test.
- ITTC Procedure 7.5-02-03-03.2: Visual Description and Measurements of Cavitation Events.
- ITTC Procedure 7.5-02-03-03.3: Cavitation Induced Pressure Fluctuations Model Scale Experiments.
- ITTC Procedure 7.5-02-03-03.4: Cavitation Induced Pressure Fluctuations: Numerical Prediction Methods.
- ITTC Procedure 7.5-02-03-03.5: Model Experiments including Numerical Simulation Guidance for Propeller and Rudder Cavitation Erosion
- ITTC Procedure 7.5-02-03-03.8: Modelling the behaviour of Cavitation in Waterjets.

The recommendations for future work are:

1. Continue to organize of the Round Robin Test: collect and analyze data. Summarize the main trends.
2. Investigate the possibility of launching a benchmark on CFD. Topics could be noise, wake simulation, Tip Vortex Cavitation (TVC), cavitation inception, “classical” CFD with the Nawigator XXI (study the possibility to liaise with Wageningen Workshop on CFD).
3. Review of wake’s evaluation in the state of the art.
4. Review URN measurements in ice conditions with a particular focus on accuracy
5. Continue monitoring the accuracy of URN measurements at model scale including the calibration, reverberation, and new methodologies (comprising instrumentations) for the measurement of propeller noise in tunnel facilities.
6. Monitor the progress of signal processing techniques in the two domains (cavitation, noise) and notably the use of data-machine learning and AI approaches (data-driven simulations).
7. Review of methods for cavitation noise mitigation, including bubble injection below the hull and its effect on URN.
8. Provide recommendation about cavitation testing of renewable energy devices (vertical or horizontal axis tidal turbines, etc.) and examine the possibility of a guideline.
9. Monitoring of energy saving devices for efficiency improvement and the way to

manage both objectives (energy saving efficiency and low noise emission).

7. REFERENCES

ABS Guide for the classification notation - Underwater Noise[S]. ABS 295-2018.2018.

Abbasi, A. A., Franzosi, G., Bartetta, D., Delucchi, M., Viviani, M. and Tani, G. 2022, "Model Scale Investigation of Blade Root Cavitation Erosion on a Set of Marine Propellers". 7th International Symposium of Marine Propulsors, smp'2022, Wuxi, China. https://www.marinepropulsors.com/proceedings/2022/2-2-3.pdf

Ainslie, M.A., Martin, S.B. and Deveau, T.J. *et al*., 2021, "Towards a standard for vessel urn measurement in shallow water: applying acoustical propagation modelling to inform the design of a measurement program that determines if shallow water urn measurements can be comparable to those from deep water". Document 02167, Version 1.0. White paper by JASCO Applied Sciences for Transport Canada Innovation Center.https://publications.gc.ca/collections/collection_2021/tc/T89-8-2021-eng.pdf

Aktas B., Usta O., Atlar M. 2020. "Systematic investigation of coating application methods and soft paint types to detect cavitation erosion on marine propellers". Applied Ocean Research, 94, art. no. 101868. https://doi.org/10.1016/j.apor.2019.101868

Almgren, M., Oden in polar expeditions – Environmental assessment – Underwater noise radiation, SSPA Report 6103-1, Appendix 3, Gothenburg, Sweden, 1991.

Alves Pereira, F., Di Felice, F. and Salvatore, F., 2016, "Propeller cavitation in non-uniform flow and correlation with the near pressure field", Journal of Marine Science and Engineering, 4, 70, DOI: https://doi.org/10.3390/jmse4040070

AQUO Collaborative Project WP3 Measurements, "D3.3 - On-site measurements experimental data for accurate identification and quantification of cavitation noise and other sources", 2014

Atsavapranee, P., Engle, A., Grant, D.J., Carneal, J.B., Beirne, T., Etebari, A., Percival, S., Rosario, J., Lugni, C. and Soave, M., "Full-scale investigation of viscous roll damping with particle image velocimetry", Proceedings of the 27th Symposium on Naval Hydrodynamics, Seoul, Korea, 5-10 October 2008.

Atsavapranee, P., "Full-scale PIV measurements at sea", Proceedings of the 25th International Towing Tank Conference, Fukuoka, Japan, 14-20 September 2008.

Audoly, C. and Meyer, V., "Measurement of radiated noise from surface ships – Influence of the sea surface reflection coefficient on the Lloyd's mirror effect". Proceedings of Acoustics, Perth, Australia, 2017.

Baiter, H.J., "On cavitation noise scaling with the implication dissimilarity in cavitation inception", ASME International symposium on cavitation noise and erosion in fluid systems, San Francisco, California, USA, 1989.

Basten, T., de Jong, C., Graafland, F. and Hof, J.V., "Acoustic signature monitoring and management of naval platforms", ICSV22, Florence, Italy, 12-16 July 2015.

Bensow, R.E., "Simulation of the unsteady cavitation on the Delft Twist 11 foil using RANS, DES and LES", 2nd International Symposium on Marine Propulsors (SMP'11), 2011.b https://www.marinepropulsors.com/proceedings/2011/I-2.1_Bensow.pdf

Birvalski, M., Struijk, G.D. and Ponkratov, D., "Full-scale PIV measurements of the propeller inflow", Proceedings of the 15th International Symposium on Particle Image

Velocimetry – ISPIV 2023. an Diego, California, USA, June 19–21, 2023.

Blake, W.K., 2017, "Mechanics of flow-induced sound and vibration". 2nd edition, Academic Press.

Bosschers, J. and van Wijngaarden, E., "Validation of the crs prediction methods for cavitation induced hull pressure fluctuations and underwater radiated noise of the DAMEN Combi freighter", Report No: 28040 5 RD, Cooperative Research Ships, May 2017.

Bosschers, J., 2018, "Propeller tip-vortex cavitation and its broadband noise". PhD Thesis, University of Twente, Enschede, The Netherlands.

Bosschers, J., "The effect of Reynolds number on a developed tip-vortex cavity and its radiated noise", 33rd Symposium on Naval Hydrodynamics, Osaka, Japan, 2020.

Boucheron, R., 2019, "Development of a demodulation method for acoustic propagation in ducts with unknown impedance conditions for both modal magnitude and wall impedance estimate", 26th International Congress on Sound and Vibration - ICSV26, Montreal, Canada, 2019.

Boucheron, R., 2023a, "Modelling the acoustic propagation in a test section of a cavitation tunnel: scattering issues of the acoustic source", Modelling, Vol. 4, pp. 650-665. DOI: https://doi.org/10.3390/modelling4040037

Boucheron, R., 2023b, "Localization of acoustic sources in water tunnel with a demodulation technique", Ocean Engineering, Vol. 281. DOI: https://doi.org/10.1016/j.oceaneng.2023.114891

Briançon, L., Fournier, P. and Frechou, D., "Marine propeller noise measurements techniques in hydro-acoustics tunnel", 3rd International Conference on Advanced Model Measurement Technology for the EU Maritime Industry AMT'13, 2013.

Brown, N. A., "Cavitation Noise Problems and Solutions", Proceedings of the International Symposium on Shipboard Acoustics, pp. 21-38, 1976.

Bureau Veritas (BV) "Underwater Radiated Noise (URN)". Bureau Veritas Rule Note NR614, 2014.

Cao, Y., Xu, L., Peng, X. 2022. "An Image Based Method to Quantify the Unsteady Cavitating Behavior around a Hydrofoil". 7th International Symposium of Marine Propulsors, smp'2022, Wuxi, China. https://www.marinepropulsors.com/proceedings/2022/4-3-3.pdf

Capone, A., Alves Pereira, F. and Di Felice, F. "Flow and cavity measurements in a super-cavitating propeller". J. Mar. Sci. Eng. 2024, 12, 243. DOI: https://doi.org/10.3390/jmse12020243

Chao, F., Zonglong, W., Yang, Y. Tengyan, L., Hualun Z. 2022. "Extraction of Cavitation Pressure Pulsation Feature of Mixed-flow Waterjet Pump Based on Wavelet Packet Energy and Fractal Dimension". 7th International Symposium of Marine Propulsors, smp'2022, Wuxi, China. https://www.marinepropulsors.com/proceedings/2022/3-1-2.pdf

Chaosheng, Z., "The numerical prediction of the propeller cavitation and hull pressure fluctuation in the ship stern using OpenFOAM", Proceedings of the Fifth International Symposium on Marine Propulsors (SMP'17), Espoo, Finland, June 2017. https://www.marinepropulsors.com/proceedings/2017/THA1-3.pdf

China Classification Society (CCS) "Guideline for ship underwater radiated noise". 2018.

Cintosun, E. and Gilroy, L. "Estimating ship underwater radiated noise from onboard vibrations". Paper presented at the SNAME Maritime Convention, Providence, Rhode

Island, USA. DOI: https://doi.org/10.5957/SMC-2021-114, October 2021.

Colin, M. E. G. D., Ainslie, M. A., Binnerts, B., de Jong C. A. F., Sertlek, H. Ö., Karasalo, I., Östberg, M., Folegot, T. & Clorennec, D., Definition and results of test cases for shipping sound maps. OCEANS 2015, Genova, Italy

Crocker, M J., 1998. "Handbook of Acoustics". Wiley-Interscience. 16 March 1998.

Deavenport, R. L., Gilchrest, M. J., & Thomson, D. J. 2019. Acoustic modelling of a transient source in shallow water. Applied Acoustics, 150, 227-235. DOI: https://doi.org/10.1016/j.apacoust.2019.01.028

Deng, L., Long, Y., & Ji, B., 2022, "Numerical analysis of cavitating flow around the propeller behind a hull with verification and validation procedures", 7th International Symposium on Marine Propulsors, Wuxi, China, October 2022 (smp'22) https://www.marinepropulsors.com/proceedings/2022/3-2-4.pdf

Det Norske Veritas and Germanischer Lloyd (DNV GL) "Rules for ships - silent class notation". 2010.

DNV CG 0313 "Rules for ships silent class notation measurement procedures for noise emission". Oslo: Det Norske Veritas (DNV AS), 2022.

Dong, J.-S., Li, Z.-R., He, W., Liu, Q. 2022. "Assessment of Cavitation Impact Load Based on Cavitation Erosion Pitting Test of Brass H62". 7th International Symposium of Marine Propulsors, smp'2022, Wuxi, China. https://www.marinepropulsors.com/proceedings/2022/4-3-4.pdf

Erbe,C. and Farmer, D. M., "Zones of impact around icebreakers affecting beluga whales in the Beaufort Sea", *J. Acoust. Soc. Am.*, 108 (3): 1332 – 1340, 2000. https://doi.org/10.1121/1.1288938

Etter, P.C., Review of ocean-acoustic models. Proc. OCEANS 2009, p 1-6, Biloxi, Mississippi, USA, 2009.

Farcas, A., Thompson, P. M., & Merchant, N. D. 2016. Underwater noise modelling for environmental impact assessment. Environmental Impact Assessment Review, 57, 114-122. DOI: https://doi.org/10.1016/j.eiar.2015.11.012

Felici, A., Di Felice, F. and Alves Pereira, F., 2013, "Measurement of the cavitation pattern by two non-intrusive techniques: laser imaging and ultrasound pulsed echography", Exp. Fluids, 54:1482, DOI: https://doi.org/10.1007/s00348-013-1482-x

Foeth, E.J. and Bosschers, J., "Localization and source-strength estimation of propeller cavitation noise using hull mounted pressure transducers", 31st Symposium on Naval Hydrodynamics, Monterey, California, 2016.

Föhring, L.S., Juhl, P.M. and Wittekind, D., 2023, "Cavitation volume behaviour derived from full-scale pressure fluctuations, Ships and Offshore Structures, Vol. 18, No. 4, Taylor & Francis, p. 541-549. DOI: https://doi.org/10.1080/17445302.2022.2053353

Fujiyama, K., 2015, "Numerical Simulation of Ship Hull Pressure Fluctuation Induced by Cavitation on Propeller with Capturing the Tip Vortex", 4th International Symposium on Marine Propulsors, Austin, Texas, USA, June 2015 (smp'15) https://www.marinepropulsors.com/proceedings/2015/WA4-1.pdf

Fujiyama, K., & Nakashima, Y. 2017. "Numerical prediction of acoustic noise level induced by cavitation on ship propeller at behind-hull condition". 5th International Symposium on Marine

Propulsors (SMP'17), 2017. https://www.marinepropulsors.com/proceedings/2017/THA1-2.pdf

Geese, J., Kimmerl, J., Nadler, M., & Abdel-Maksoud, M., 2022, "Acoustic Emissions and Cavitation Effects on Model Scale Propellers Using a Transition Model", 7th International Symposium on Marine Propulsors, Wuxi, China, October 2022 (smp'22) https://www.marinepropulsors.com/proceedings/2022/4-1-3.pdf

Grasso, N., Hallmann, R., Scholcz, T., Zondervan, G.J., Maljaars, P. and Schouten, R., "Measurements of the hydro-elastic behaviour of flexible composite propellers in non-uniform flow at model and full scale", Proceedings of the Sixth International Symposium on Marine Propulsors (SMP'19), Rome, Italy, May 2019. https://www.marinepropulsors.com/proceedings/2019/THA3-1.pdf

Guangnian L., Chen Q., Liu Y. 2020. "Experimental Study on Dynamic Structure of Propeller Tip Vortex". Polish Maritime Research, 27 (2), pp. 11 – 18. https://doi.org/10.2478/pomr-2020-0022

Hannay, D.E. A.O. MacGillivray, H. Frouin-Mouy, Z. Li, F. Pace, J. Wladichuk and Z. Alavizadeh. 2018. Study of Quiet Ship Certifications: Analysis using ECHO Ship Noise Database. JASCO Document 01737, Final Report Version 1.0. Technical report by JASCO Applied Sciences for Transport Canada. https://publications.gc.ca/collections/collection_2022/tc/T89-7-2021-eng.pdf

Harrison, C.H. and Harrison, J.S., 1995, "A simple relationship between frequency and range averages for broadband sonar", Journal of Acoustical Society of America, Vol. 97, no. 2, pp.1314-1317. DOI: https://doi.org/10.1121/1.412172

Hasuike, N., Yamasaki, S. and Ando, J, "Numerical Study on Cavitation Erosion Risk of Marine Propellers Operating in Wake Flow", 7th International Symposium on Cavitation (CAV2009), 2009.

Hasuike N., Kajihama, T. and Fukuda, K., "Numerical simulation of pressure fluctuation induced by cavitating propellers in wake flow", 18th Numerical Towing Tank Symposium (NuTTS2015), 2015.

Hiroi, T., Winden, B., Kleinwachter, A., Ebert, E., Fujisawa, J., Kamiirisa, H., Damaschke, N., and Kawakita, C., 2019, "Full-scale on-board measurements of wake velocity profiles, underwater noise and propeller induced pressure fluctuations", The Japan Society of Naval Architecture and Ocean Engineers, Vol. 29, pp 193-198.

Hu, J., Ning, X., Zhao, W., Li, F., Ma, J., Zhang, W., & Lin, C. 2021. Numerical simulation of the cavitating noise of contra-rotating propellers based on detached eddy simulation and the Ffowcs Williams–Hawkings acoustics equation. Physics of Fluids, 33(11). DOI: https://doi.org/10.1063/5.0065456

Hynninen, A., Viitanen, V., Tanttari, J., Klose, R., Testa, C., & Martio, J. 2023. Multiphase Flow Simulation of ITTC Standard Cavitator for Underwater Radiated Noise Prediction. Journal of Marine Science and Engineering, 11(4), 820. DOI: https://doi.org/10.3390/jmse11040820

ISO 17208-1. "Underwater acoustics – Quantities and procedures for description and measurement of underwater sound from ships – Part 1: Requirements for precision measurements in deep water used for comparison purposes". 2016.

ISO 17208-2. "Underwater acoustics – Quantities and procedures for description and measurement of underwater sound from ships – Part 2: Determination of source level from deep water measurements". 2019.

ISO/DIS 17208-3. "Underwater acoustics – Quantities and procedures for description and measurement of underwater sound from ships – Part 3: Requirements for measurements in shallow water". 2024.

ISO 22098:2020 "Ships and marine technology - Full-scale test method for propeller cavitation observation and hull pressure measurement", 2020.

Inukai, Y, "Full scale measurement of the flow field at the stern by using multi-layered doppler sonar (MLDS)", 6th International Symposium on Marine Propulsors (SMP'19), Rome, Italy, 2019. https://www.marinepropulsors.com/proceedings/2019/TB4-1.pdf

Jeong, H., Lee, J., Kim, Y. and Seol, H., 2021, "Estimation of the noise source level of a commercial ship using on-board pressure sensors", Applied Science, Vol. 11. https://doi.org/10.3390/app11031243

Ju H.-J., Choi J.-S. 2022. "Experimental Study of Cavitation Damage to Marine Propellers Based on the Rotational Speed in the Coastal Waters". Machines, 10 (9), art. no. 793. https://doi.org/10.3390/machines10090793

Khoo, M. T., Venning, J. A., Pearce, B. W. and Brandner, P. A., 2021, " Nucleation and cavitation number effects on tip vortex cavitation dynamics and noise", Experiments in Fluids, Vol. 62, art. 216. https://doi.org/10.1007/s00348-021-03308-2

Kimmerl, J., Abdel-Maksoud, M., Nataletti, M. and Savio, L., "Acoustic Comparison of a Ship-Propeller Model in Cavitating Conditions with LES and FWH-Method", 7th International Symposium on Marine Propulsors (SMP'22), 2022. https://www.marinepropulsors.com/proceedings/2022/5-3-2.pdf

Kleinwächter, A., Ebert, E., Kostbade, R., Hellwig-Rieck, K., Heinke, H.J. and Damaschke, N.A., "Full-scale total wake field PIV-measurements for an enhanced cavitation prediction", Proceedings of the 17th International Symposium on Applications of Laser Techniques to Fluid Mechanics, Lisbon, Portugal, 07-10 July, 2014.

Kleinwächter, A., Hellwig-Rieck, K., Ebert, E., Kostbade, R., Heinke, H.J. and Damaschke, N.A., "PIV as a novel full-scale measurement technique in cavitation research", Proceedings of the Fourth International Symposium on Marine Propulsors (SMP'15), Austin, Texas, USA, June 2015. https://marinepropulsors.com/proceedings/2015/TA4-2.pdf

Köksal, Ç. S., Usta, O., Aktas, B., Atlar, M., & Korkut, E. 2021. Numerical prediction of cavitation erosion to investigate the effect of wake on marine propellers. Ocean Engineering, 239, 109820.

Korean Register (KR) "Guidance for underwater radiated noise", 2021.

Krasilnikov, V., Savio, L., Koushan, K., Felli, M., Abdel-Maksoud, M., Kimmerl, J., Reichstein, N., Fageraas, A., Sun, J. 2022. "Towards Reliable Prediction of Propeller Noise: Challenges and Findings of the Project ProNoVi". 7th International Symposium of Marine Propulsors, smp'2022, Wuxi, China. https://www.marinepropulsors.com/proceedings/2022/2-3-1.pdf

Krasilnikov V., Skjefstad V.S., Koushan K., Rambech H.J. A 2023. " Calibration Study with CFD Methodology for SelfPropulsion Simulations at Ship Scale ". J. Mar. Sci. Eng. 2023, 11, 1342. https://doi.org/10.3390/jmse11071342

Ku, G., Cheong, C., Park, I., & Seol, H. 2020. Numerical investigation of tip vortex cavitation inception and noise of underwater propellers of submarine using sequential Eulerian–Lagrangian approaches. Applied Sciences, 10(23), 8721. https://doi.org/10.3390/app10238721

Ku, G., Cho, J., Cheong, C., & Seol, H. 2021. Numerical investigation of tip-vortex cavitation noise of submarine propellers using hybrid computational hydro-acoustic approach. Ocean Engineering, 238, 109693.DOI: https://doi.org/10.1016/j.oceaneng.2021.109693

Kunz, R., F., Boger D. A., Stinebring, D. R., Chyczewski, T. S., Lindau, J. W., Gibeling, H. J., Venkateswaran, S., & Govindan, T. R., 2000, "A preconditioned Navier-Stokes method for two-phase flows with application to cavitation prediction", Computers & Fluids, Vol. 29, pp. 849-875. DOI: https://doi.org/10.1016/S0045-7930(99)00039-0

Kurobe, Y., Ukon Y., Koyama K. and Makino M., 1983, "Measurement of cavity volume and pressure fluctuations on a model of the training ship "SEIUN-MARU" with reference to full scale measurement", Papers of Ship Research Institute, Vol. 20, No.6, pp 395-429.

Küsel, E. T., & Siderius, M. 2019. Comparison of propagation models for the characterization of sound pressure fields. IEEE Journal of oceanic engineering, 44(3), 598-610. DOI: https://doi.org/10.1109/JOE.2018.2884107

Lee, T., Ahn, B-K., Lee, K. and Lee, Y, "Noise Scaling Method and Applications for Marine Propeller with Isolated Tip Vortex Cavitation". Proceedings of the 8th International Symposium on Marine Propulsors (SMP'24), Berlin, Germany, March 17-20, 2024. DOI: https://doi.org/10.15480/882.9372

Lehman, A. F., "Determination of cavity volumes forming on a rotating blade", 11th International Towing Tank Conference (ITTC), Tokyo (Japan), pp. 250–253, 1966.

Li, J., & Carrica, P. M. 2021. "A population balance cavitation model". International Journal of Multiphase Flow, 138, 103617. DOI: https://doi.org/10.1016/j.ijmultiphaseflow.2021.103617

Li, D.Q., Hallander, J., Johansson, T. and Karlsson, R., "Cavitation dynamics and underwater radiated noise signature of a ship with a cavitating propeller", Proceedings of the VI International Conference on Computational Methods in Marine Engineering, Marine 2015.

Li, D. Q., Hallander, J., & Johansson, T. 2018. Predicting underwater radiated noise of a full scale ship with model testing and numerical methods. Ocean Engineering, 161, 121-135. DOI: https://doi.org/10.1016/j.oceaneng.2018.03.027

Lidtke, A. K., Turnock, S., & Humphrey, V. 2016. Multi-scale modelling of cavitation-induced pressure around the Delft twist 11 hydrofoil. In Proceeding of the 31st Symposium on Naval Hydrodynamics, Monterey, USA.

Lidtke, A. K., Lloyd, T., Lafeber, F. H., & Bosschers, J. 2022. Predicting cavitating propeller noise in off-design conditions using scale-resolving CFD simulations. Ocean Engineering, 254, 111176. DOI: https://doi.org/10.1016/j.oceaneng.2022.111176

Liu, D., Li, Z., Wang, G., & Liu, Y. 2021. Sound propagation with undulating bottom in shallow water. Journal of Marine Science and Engineering, 9(9), 1010. DOI: https://doi.org/10.3390/jmse9091010

Lloyd's Register (LR), "Shipright - design and construction - additional design and construction procedure for the determination of a vessel's underwater radiated noise". 2017.

Lyu, S. J., Ji, B., Wang, X. C., Zhan, Z. W., & Zhang, D. H. 2023. Numerical investigation of the cavitation noise around a marine propeller focusing on the influence of ventilation. Journal of Hydrodynamics, 35(4), 630-648. DOI: https://doi.org/10.1007/s42241-023-0055-6

MacGillivray, A.O., Martin, S.B., Ainslie, M.A., Dolman, J.N., Li, Z. and Warner, G.A. 2023. "Measuring vessel underwater radiated noise in shallow water". J. Acoust. Soc. Am. 153 (3), 1506–1524. DOI: https://doi.org/10.1121/10.0017433

Melissaris, T., Beerens, M., Oprea, I. and Bijlard, M., "Cavitation Erosion Risk Assessment on the Nozzle Surface of Ducted Propellers", Proceedings of the 7th International Symposium on Marine Propulsors (SMP'22), Wuxi, China, October 17-21, 2022. https://www.marinepropulsors.com/proceedings/2022/4-3-2.pdf

MEPC 58/19, "Minimizing the introduction of incidental noise from commercial shipping operations into the marine environment to reduce potential adverse impacts on marine life", IMO, 2008.

MEPC.1/Circ 883, "Guidelines for The Reduction of Underwater Noise from Commercial Shipping to Address Adverse Impacts on Marine Life", IMO, 2014.

MEPC 75/14, "Proposal for a new output concerning a review of the 2014 Guidelines for the reduction of underwater noise from commercial shipping to address adverse impacts on marine life (MEPC.1/Circ.833) and identification of next steps", IMO, 2019.

MEPC 76/12/1, "MITTEE AND SUBSIDIARY BODIES - Comments on document MEPC 75/14 – Proposal for a new output on underwater noise". IMO, 2021.

Mikhalevsky, P.N., Arctic Acoustics. Encyclopedia of Ocean Sciences, John H. Steele, Karl K. Turekian, Steve A. Thorpe (Eds.), Academic Press,1, pp. 53-61, 2001, courtesy of Academic Press.

Miki, T., Fujiyama, K., Tsuda, S. and Irie, T., "Cavitation analysis of a Delft twisted hydrofoil using multi-process cavitation model", 18th International Symposium on Transport Phenomena and Dynamics of Rotating Machinery (ISROMAC 18, online, November 23rd to 26th, 2020), Journal of Physics: Conference Series, 2021, DOI: https://doi.org/10.1088/1742-6596/1909/1/012014

Mingtai, S., Jiang, Lv., Xiangnan, G., Yihong, C., Denghai, T. 2022. "Detection of Propeller Cavitation Inception by the Acoustic Method". 7th International Symposium of Marine Propulsors, smp'2022, Wuxi, China. https://www.marinepropulsors.com/proceedings/2022/5-2-1.pdf

Mulders, I., F. Graafland, C. Bosschaart, and J. van't Hof, "Acoustic signature estimation for MCDV HMCS Glace Bay" TNO 2018 R11656, TNO VERTROUWELIJK August 2019.

Müller-BBM, "Acoustic signature management" GmbH (muellerbbm.com)

National Physical Laboratory (NPL), "Good Practice Guide No. 133, Underwater Noise Measurement", 2014.

Nohmi, M. and Goto, A., 2003, "Cavitation CFD in a Centrifugal Pump", 5th International Symposium on Cavitation, Osaka Japan, November 2003 (CAV2003)

Oliveira, T. C., Lin, Y. T., & Porter, M. B. 2021. Underwater sound propagation modeling in a complex shallow water environment. Frontiers in Marine Science, 8, 751327. DOI: https://doi.org/10.3389/fmars.2021.751327

Oshima, A., 1990, "A study on correlation of vortex cavitation noise of propeller measured in model experiments and full scale". Journal of the Society of Naval Architects of Japan, Vol. 168, no. 1, pp. 89–96. DOI: https://doi.org/10.2534/jjasnaoe1968.1990.168_89

Oshima, A., 1994, "Scaling of tip vortex cavitation noise of propeller", Technical report, Vol. 31, No. 3, Mitsubishi Heavy Industries, Ltd., Nagasaki, Japan.

Özsayan, S., Köksal, Ç. S., Usta, O., Çelik, C., Yilmaz, N., Korkut, E. 2022. "An Experimental and Numerical Investigation of the Cavitation Effects on Propeller Performance and Erosion on DTMB-5415 Propeller". 7th International Symposium of Marine Propulsors, smp'2022, Wuxi, China. https://www.marinepropulsors.com/proceedings/2022/2-2-1.pdf

Paik, K. J., Park, H. G. and Seo J., "URANS Simulations of Cavitation and Hull Pressure Fluctuation for Marine Propeller with Hull Interaction", 3rd International Symposium on Marine Propulsors (SMP'13), 2013. https://www.marinepropulsors.com/proceedings/2013/9A.1.pdf

Pang, Y. and Yu, M. 2023. "Source level measurement method of underwater radiated noise in shallow water based on regression propagation loss using multi-distance arrays". Journal of Ship Mechanics, 2023 (04):598-606.

Park, J. and Seong, W., 2017, "Novel scaling law for estimating propeller tip vortex cavitation noise from model experiment". Journal of Hydrodynamics, Vol. 29, no. 6, pp. 962–971. DOI: https://doi.org/10.1016/S1001-6058(16)60810-7

Park J. Y., Peric, M., Farrall, M. and Park C., "Numerical analysis for the prediction of hull pressure fluctuations and underwater radiated noise induced by marine propeller cavitation", 10th International Symposium on Cavitation (CAV2018), 2018a

Park, C., Kim, G.-D., Park, Y.-H., Jang, H.-G. and Jang, Y.H., 2018b, "A Study on the Model Test for the Twin Propeller Cavitation Noise" (in Korean). Journal of the Society of Naval Architects of Korea, Vol. 55, no. 1, pp. 28-36.

Park, C., Kim, G. D., Yim, G.-T., Park, Y., and Moon, I.-S., "The validation of model test method for propeller cavitation noise prediction". 6th International Conference on Advanced Measurement Technology for the Maritime Industry, AMT'19, Rome, Italy, 2019.

Park, C., Kim, G. D., Yim, G.-T., Park, Y., and Moon, I.-S., 2020, "A validation study of the model test method for propeller cavitation noise prediction", Ocean Engineering, Vol. 213, 107655. DOI: https://doi.org/10.1016/j.oceaneng.2020.107655

Pereira, F., Avellan. F. and Dupont, Ph., 1998, "Prediction of cavitation erosion: an energy approach", J Fluid Eng - T ASME, 120(4):719–727. DOI: https://doi.org/10.1115/1.2820729

Pereira, F., Salvatore, F. and Di Felice, F., 2004, "Measurement and modelling of propeller cavitation in uniform inflow", J Fluid Eng – T ASME, 126:671–679. DOI: https://doi.org/10.1115/1.1778716

Proctor, F., Ahmad, N., Switzer, G., Limon Duparcmeur, F., 2010, "Three-phased wake vortex decay",. AIAA Atmospheric and Space Environments Conference, 2010-7991, Toronto, Ontario, Canada.

Registro Italiano Navale (RINA). Amendments to Part A and Part F of "Rules for the Classification of Ships" - New additional class notation: "DOLPHIN QUIET SHIP" and "DOLPHIN TRANSIT SHIP". 2017

Rodrigo-Sauro, F . J., Ramis-Soriano, J., Fernandez-Perles, J., Carbajo-San Martin, J., Poveda-Martinez, Pedro., Segovia-Eulogio, E. G., 2017," Transfer Function of the structure-Borne noise to underwater radiated noise for ships with Hull of different material", European Symposium on Underwater Acoustics applications (Techni Acustica 2017)

Roth, E. H., Schmidt, V., Hildebrand, J. A. and Wiggins, S. M., "Underwater radiated noise levels of a research icebreaker in the central

Arctic Ocean", *J. Acoust. Soc. Am*. 133 (4): 1971-1980, 2013. https://doi.org/10.1121/1.4790356

Sakamoto, N., & Kamiirisa, H. 2018. "Prediction of near field propeller cavitation noise by viscous CFD with semi-empirical approach and its validation in model and full scale". Ocean Engineering, 168, 41-59. DOI: https://doi.org/10.1016/j.oceaneng.2018.08.061

Sato, K, Oshima, A., Egashira, H. and Takano, S., "Numerical Prediction of Cavitation and Pressure Fluctuation around Marine Propeller", 7th International Symposium on Cavitation (CAV2009), 2009.

Savio, L., Conti, F., Viviani, M. and Ferrando, M., "Application of computer vision techniques to measure cavitation bubble volume and cavitating tip vortex diameter", Proceedings of the 7th International Symposium on Cavitation (CAV2009), Ann Arbor, Michigan, USA, August 17-22, 2009.

Schnerr, G. H. and Sauer, J., "Physical and Numerical Modeling of Unsteady Cavitation Dynamics", 4th International Conference on Multiphase Flow (ICMF2001), 2001.

SDC 8/14, "Review of the guidelines for the reduction of underwater noise (mepc.1/circ.833) and identification of next steps - Outcome of MEPC 76 on the review of MEPC.1/Circ.833". IMO,2021.

SDC 9/5 "Review of the guidelines for the reduction of underwater noise (mepc.1/circ.833) and identification of next steps - Report of the Correspondence Group". IMO, 2021.

Sezen, S., Atlar, M., Fitzsimmons, P., Sasaki, N., Tani, G., Yilmaz, N., & Aktas, B. 2020. Numerical cavitation noise prediction of a benchmark research vessel propeller. Ocean Engineering, 211, 107549. DOI: https://doi.org/10.1016/j.oceaneng.2020.107549

Sezen, S., Cosgun, T., Yurtseven, A., and Atlar, M. 2021a. Numerical investigation of marine propeller underwater radiated noise using acoustic analogy Part 2: The influence of eddy viscosity turbulence models. Ocean Engineering, 220, 108353. DOI: https://doi.org/10.1016/j.oceaneng.2020.108353

Sezen, S., Atlar, M. and Fitzsimmons, P., 2021b, "Prediction of cavitating propeller underwater radiated noise using RANS & DES-based hybrid method", Ship and Offshore Structures, Vol. 16, sup1, pp.93-105. DOI: https://doi.org/10.1080/17445302.2021.1907071

Shiraishi, K., Sawada, Y. and Hoshino, K., "Cavity Shape Measurement Using Combination-Line CCD Camera Measurement Method", Proc. of the Fifth International Symposium on Marine Propulsion (SMP'17), Espoo, Finland, June 2017, n° 1214, 2017. https://www.marinepropulsors.com/proceedings/2017/TB4-2.pdf

Shiraishi, K., Sawada, Y., Kaneko, A., Arakawa D. 2022. "Development of Cavitation Shape Measurement Method Using Muti-View Line Sensing Method". 7th International Symposium of Marine Propulsors, smp'2022, Wuxi, China. https://www.marinepropulsors.com/proceedings/2022/3-1-1.pdf

Singhal, A. K., Athavale, M. M., Li, H., & Jiang, Y., 2002, "Mathematical Basis and Validation of the Full Cavitation Model", Journal of Fluids Engineering, Vol. 124, pp.617-624. DOI: https://doi.org/10.1115/1.1486223

Sipilä, T., Viitanen, V., Uosukainen, S. & Klose, R. 2019. "Shallow Water Effects on Ship Underwater Noise Measurements." In 48th International Congress and Exhibition on Noise Control Engineering, INTER-NOISE 2019 (p. 1707). Institute of Noise Control Engineering.

Song K., Guo Ch., Sun C., Wang Ch., Gong J., Li P. and Wang L., 2021. " Simulation strategy of the full-scale ship resistance and propulsion performance". Engineering Applications of Computational Fluid Mechanics, 15:1, 1321-1342, DOI: https://doi.org/10.1080/19942060.2021.1974091

Strasberg, M., "Propeller Cavitation Noise after 35 Years of Study", ASME Symposium on Noise and Fluids Engineering, Atlanta, USA, 1977.

Tani, G., Viviani, M., Ferrando, M. and Armelloni, E., 2019a, "Aspects of the measurement of the acoustic transfer function in a cavitation tunnel", Applied Ocean Research, Vol. 87, pp. 264–278. DOI: https://doi.org/10.1016/j.apor.2019.02.017

Tani, G., Aktas, B., Viviani, M., Yilmaz, N., Miglianti, F., Ferrando, M. and Atlar, M., 2019b, "Cavitation tunnel tests for "The Princess Royal" model propeller behind a 2-dimensional wake screen", Ocean Engineering, Vol. 172, pp. 829–843. DOI: https://doi.org/10.1016/j.oceaneng.2018.11.017

Tian, B., Li, L., Meng, Y. and Huang, B., "Numerical study of multiscale cavitating flow around a hydrofoil", 7th International Symposium on Marine Propulsors (SMP'2022), 2022. https://www.marinepropulsors.com/proceedings/2022/3-2-1.pdf

Ukon, Y. and Kurobe, Y., "Measurement of cavity thickness distribution on marine propellers by laser scattering technique", Proc. of the 16th ITTC, vol. 2, Leningrad (USSR), pp. 241–245, 1981.

Usta O., Köksal Ç.S., Korkut E. 2023. "A systematic study into the cavitation erosion test for marine propeller materials by cavitating jet technique". Ocean Engineering, 284. https://doi.org/10.1016/j.oceaneng.2023.115252

Viitanen, V. M., & Siikonen, T. 2017. Numerical simulation of cavitating marine propeller flows. In Proceedings of the 9th National Conference on Computational Mechanics (MekIT'17), Trondheim, Norway (pp. 11-12).

Viitanen, V. M., Hynninen, A., Sipilä, T., & Siikonen, T. 2018. DDES of wetted and cavitating marine propeller for CHA underwater noise assessment. Journal of Marine Science and Engineering, 6(2), 56. DOI: https://doi.org/10.3390/jmse6020056

Viitanen, V., Siikonen, T. and Sánchez-Caja, A., 2020, "Cavitation on model-and fullscale marine propellers: steady and transient viscous flow simulations at different reynolds numbers", Journal of Marine Science and Engineering, 8, 141: DOI: https://doi.org/10.3390/jmse8020141

Viitanen, V. and Peltola, J., "Hydrodynamic cavitation investigations with homogeneous and inhomogeneous multiphase flow models in OpenFOAM context". Proceedings of the 11th International Symposium on Cavitation (CAV2021): Online proceedings (pp. 618-624). Article P00191 The Society of Naval Architects of Korea. 2021.

Viitanen, V., Sipilä, T., Sánchez-Caja, A. and Siikonen T., 2022, "CFD predictions of unsteady cavitation for a marine propeller in oblique inflow", Ocean Engineering, Vol. 266. DOI: https://doi.org/10.1016/j.oceaneng.2022.112596

Viitanen, V., Hynninen, A., & Sipilä, T. 2023. Computational fluid dynamics and hydroacoustics analyzes of underwater radiated noise of an ice breaker ship. Ocean Engineering, 279, 114264. DOI: https://doi.org/10.1016/j.oceaneng.2023.114264

Wang, Z., Cheng, H., & Ji, B. 2021. Euler–Lagrange study of cavitating turbulent flow around a hydrofoil. Physics of Fluids, 33(11). DOI:

https://doi.org/10.1063/5.0070312

Wang, Y., Mikkola, T., & Hirdaris, S. 2022. A fast and storage-saving method for direct volumetric integration of FWH acoustic analogy. Ocean Engineering, 261, 112087. DOI: https://doi.org/10.1016/j.oceaneng.2022.112087

Yilmaz, N., Atlar, M., & Khorasanchi, M., 2019, "An improved mesh adaption and refinement approach to cavitation simulation (MARCS) of propellers", Ocean Engineering, Vol. 171, pp.139-150. DOI: https://doi.org/10.1016/j.oceaneng.2018.11.001

Yilmaz N., Dong X., Aktas B., Yang C., Atlar M., Fitzsimmons P.A. 2020. "Experimental and numerical investigations of tip vortex cavitation for the propeller of a research vessel, "The Princess Royal"". Ocean Engineering, 215. https://doi.org/10.1016/j.oceaneng.2020.107881

Yubero de Diego R., Ghasemi M., Pettersen O.S, D2.1 Final Report on Vessel URN Measurements，EU Saturn project report, 7 December 2023. SATURN - T2.2.1. Review fundamentals of URN measurement and acoustic field evaluation (http://saturnh2020.eu)

Zerbs C., Pascher I., 2016. "Monitoring of underwater radiated sound for ships using transfer path analysis models" Inter-noise, Hamburg.

Zhang, B., Xiang, Y., He, P., Zhang, G-J., 2019, "Study on prediction methods and characteristics of ship underwater radiated noise within full frequency", Ocean Engineering 174 (2019) 61-70. DOI: https://doi.org/10.1016/j.oceaneng.2019.01.028

Zheng, C., Hong, F., Zhang, Z., & Liu D., 2022, "The Numerical Investigation of Propeller Cavitation Benchmark Tests in Oblique Flow", 7th International Symposium on Marine Propulsors, Wuxi, China, October 2022 (smp'22). https://www.marinepropulsors.com/proceedings/2022/2-2-2.pdf

Zhou, Y. Q., & Luo, W. Y. 2021. A finite element model for underwater sound propagation in 2-D environment. Journal of Marine Science and Engineering, 9(9),DOI: https://doi.org/10.3390/jmse9090956

Zwart, P. J., Gerber, A. G. and Belamri, T., "A Two-Phase Flow Model for Predicting Cavitation Dynamics", International Conference on Multiphase Flow (ICMF2004), 2004.

ITTC2024

30TH INTERNATIONAL TOWING TANK CONFERENCE
22–27 SEPTEMBER 2024 | HOBART TASMANIA AUSTRALIA

REPORT OF THE SPECIALIST COMMITTEE ON OCEAN RENEWABLE ENERGY

SPECIALIST COMMITTEE ON OCEAN RENEWABLE ENERGY

1. INTRODUCTION

This report summarizes the work of the Specialist Committee on Ocean Renewable Energy for the 30th ITTC.

1.1 Membership and Meetings

The members of the Specialist Committee on Ocean Renewable Energy of the 30th ITTC has been organized into three focus group: Offshore wind turbines (OWT), current turbines (CT), and wave energy converters (WEC).

The committee consisted of the following members, divided into their respectively focus group:

Offshore Wind Turbines (OWT):

- Prof. Maurizio Collu (Chair)
  University of Strathclyde,
  Glasgow
  UK
- Dr. Petter Andreas Berthelsen (Secretary)
  SINTEF Ocean,
  Trondheim
  NORWAY
- Dr. Vincent Leroy
  École Centrale de Nantes,
  Nantes
  FRANCE
- Prof. Antonio Fernandes
  LOC/COPPE/UFRJ,
  Rio De Janeiro,
  BRAZIL
- Dr. Weiwen Zhao
  Shanghai Jiao Tong University,
  Shanghai
  P.R. CHINA

Wave Energy Converters (WEC):

- Prof. Motohiko Murai
  Yokohama National University,
  Yokohama
  JAPAN
- Dr. Giuseppina Colicchio
  CNR-INM,
  Rome
  ITALY
- Dr. Kyong-Hwan Kim
  KRISO,
  Daejeon,
  KOREA

Current Turbines (CT):

- Prof. Gustavo R. S. Assi
  University of São Paulo,
  São Paulo,
  BRAZIL
- Dr. Jean-Roch Nader
  Australian Maritime College,
  Launceston,

TASMANIA

Four committee meetings have been held during the work period:

- Online, 9-11 November 2021.
- Online, 23-25 August 2022.
- University of Strathclyde, Glasgow, UK, 9-11 May 2023.
- Online, 9-11January 2024.

1.2 Acknowledgements

The Committee would also like to acknowledge the contributions of Christopher Vogel, and Rodrigo Batista Soares.

1.3 Tasks

The recommendations for the work of the Specialist Committee on Ocean Renewable Energy as given by the 29th ITTC were as follows:

1.3.1 General recommendations

- Continue interactions with IEC.
- Review interactions between model scale and moderate/full scale test sites.
- Review of testing of deployment (transportation, installation) and O&M for marine renewable devices.
- Review testing of multipurpose platforms (e.g., combined WEC/OWT/ Solar/Aquaculture platforms).

1.3.2 Recommendations for wave energy converters (WECs)

- Continue to monitor development of new concepts of WECs.
- Continue to monitor developments in PTO modelling both for physical and numerical prediction of power capture.
- Assess the feasibility of developing specific guidelines for numerical and experimental survival testing of WECs.
- Assess support to using the benchmark round robin data for numerical comparison and/or for evaluating facility biases and scale related uncertainties.
- Update the uncertainty analysis of WEC testing to include the uncertainties of the power capture and potentially of a different type of device technology.
- Update and extend array section of the guidelines for numerical modelling of WECs.
- Review and report on the different PTO control strategies for power optimization and survivability modes.
- Review and report on comparisons between full scale data and numerical work/experimental model testing.

1.3.3 Recommendations for current turbines (CTs)

- Continue to monitor development in physical and numerical techniques for prediction of performance of current turbines
- Assess the support for round robin test of a 3-blade horizontal axis turbine (such as the DoE turbine). If there are enough willing participants develop a technical delivery plan.
- Review and report the techniques use for CFD modelling current turbines. This should include the use of combined EFD/CFD techniques for scaling and blockage corrections and methodologies for replicating environmental conditions.

1.3.4 Recommendations for offshore wind turbines (OWTs)

Continue monitoring and report on the development in full-scale installation of floating offshore wind turbines.
Report on possible full-scale measurement data available and address how these data can be

utilized for validation of simulation tools and evaluation of scaling effects from model scale tests.
Continue monitoring and report on the development in model testing methodology for offshore wind turbines.

- Review and report on recent development of physical wind field modelling in open space with application for wave tank testing of floating offshore wind turbines, including modelling of turbulence and measuring and documentation of the wind field.
- Review and report on the development of numerical offshore wind farm modelling.

2. PROCEDURES AND GUIDELINES

2.1 Existing guidelines

This committee is responsible for maintaining the following ITTC procedures and guidelines:

- 7.5-02-07-03.7 Wave Energy Converter Model Test Experiments

This procedure addresses designing and performing hydrodynamic model tests of wave energy converters. The guideline provides a careful consideration of the differences and complexities in testing a device at various TRLs where for example the power take-off (PTO) system should be representative of the full-scale PTO and survivability tests where extreme load fatigue analysis is required. No major revision has been performed during the 29th ITTC.

- 7.5-02-07-03.8 Model tests for Offshore Wind Turbines

This procedure addresses designing and performing hydrodynamic model tests of offshore wind turbines. The guideline describes different methods for modelling of the wind loads on the wind turbine in a hydrodynamic testing facility as well as test procedures for offshore wind turbines. No major revision has been performed during the 30th ITTC, but in addition to a general polishing and minor updates, the acronym list has been revised and the list of symbols has been added.

- 7.5-02-07-03.9 Model tests for Current Turbines

This procedure involves the design and execution of model tests for ocean and tidal current turbine devices across a range of scales in a reproducible environment, specifically at a hydrodynamic test facility. The primary objective is to assess the suitability of this facility for conducting comprehensive tests on ocean and tidal current turbine devices, ensuring accurate and reliable results. The procedure was revised to ensure conformity and consistency across ITTC guidelines. This revision has not introduced any new sections. Some sentences have been rewritten for clarity.

- 7.5-02-07-03.12 Uncertainty Analysis for a Wave Energy Converter

The procedure addresses guidelines for the application of uncertainty analysis to the small-scale testing of wave energy converters provided by ITTC procedure 7.5-02-07-03.7, “Wave Energy Converter Model Test Experiments”. Details about the energy capture performance have been added to the procedure. Because of the relative importance of the PTO system in the different stages of development, three macro categories for the applications of the uncertainty have been identified: the concept validation stages (TRL 1-3), the design validation stages (TRL 4-5) and the system validation, prototype, and demonstration stage (TRL 6-9). For each of these stages, the sources of uncertainty to consider are listed as well as guidelines for their reliable evaluation.

- 7.5-02-07-03.15 Uncertainty Analysis – Example for horizontal-axis current turbines

The procedure addresses guidelines for applying uncertainty analysis to the small-scale testing of horizontal-axis current turbines provided by ITTC procedure 7.5-02-07-03.9, “Model Tests for Current Turbines”. The guideline was revised for consistency, and some sentences were rewritten for clarity. Brief comments have been added on the uncertainty analysis for unsteady experiments as well as experiments with arrays of turbines in proximity (high blockage). The equations have been revised and corrected where necessary. The title of the document should be updated to “Uncertainty Analysis - Example for Horizontal-Axis Current Turbines”.

- 7.5-02-07-03.17 Uncertainty Analysis for Model Testing of Offshore Wind Turbines

The purpose of the guideline is to provide guidance on the application of uncertainty analysis to the model scale testing of offshore wind turbines following the ITTC Procedure 7.5-02-07-03.8, “Model Tests for Offshore Wind Turbines”. The model scale testing of offshore wind turbines focuses on the environmental loads and global response of the structure, similar to the testing of other offshore structures (floating or fixed). The section on uncertainty has been substantially revised, adding the GUM approach for evaluating and expressing uncertainty (and its limitation), and a section on the Monte Carlo approach.

- 7.5-02-07-03.18 Practical Guidelines for Numerical Modelling of Wave Energy Converters

The purpose of this guideline is to provide a methodology to assess the fidelity of the numerical simulation for Wave Energy Converters (WECs) at different stages of development, to set up numerical calculations and to analyse the obtained results. Therefore, they have been classified as a function of the objectives of the study, of the Technology Readiness level (TRL) of the WEC and the numerical facility on which they can be run has been detailed.

2.2 New guidelines

No new guidelines were developed during this term.

For the WEC focus group, it was suggested to *“Assess the feasibility of developing specific guidelines for numerical and experimental survival testing of WECs”*. It was discussed and agreed that the best course of action is, rather than developing a new guideline, to update and extend 7.5-05-07-03.7, section 2.7.4, and 7.5-05-07-03.18, section 2.5 (see relevant info in section 2.1).

3. COOPERATION WITH OTHER COMMITTEES

3.1 Collaboration with the International Electrotechnical Commission (IEC)

3.1.1 Description

The IEC is a key international body which addresses standards in all field of electrotechnology. The work is organized through technical committees (TCs). The TC of relevance for the ITTC SC on ORE are IEC TC88 (Wind Turbines) and IEC TC114 (Marine Energy – Wave, tidal and other water current converters).

3.1.2 Meetings and workshop

Through the previous ITTC term, an official type A liaison with the has been established with the IEC TC114, and Prof. Maurizio Collu (SC ORE chair) has been nominated to cover this role in March 2022. During the 29th ITTC term, at the IEC TC114 plenary meetings of March 2022 and April 2023, the ITTC SC on ORE chair presented the ITTC in general, and the aims and scope of the ITTC SC on ORE. This has been followed by a meeting between two chairs (IEC TC114 and ITTC SC on ORE) to define a collaboration strategy between the two committees, and a copy of the IEC TS 62600-103 Ed. 1 (WEC) and of the IEC TS 62600-202 Ed. 1 (CT) has been obtained, to be compared with the relevant procedures and guidelines of the present SC.

Furthermore, Dr. Thomas Davey, a member of the IEC TC114, has attended the 3rd committee meeting of the ITTC SC on ORE in Glasgow (May 2023). During this meeting, the work of the ITTC SC on ORE on WEC and CT has been presented more in details, and an approach to identify conflicts between ITTC procedures and guidelines and IEC guidelines has been defined.

3.1.3 Procedure to identify conflicts defined and trialled

The WEC and CT focus groups have performed a first pass at applying the approach defined to identify these conflicts comparing, respectively, the IEC TS 62600-103 Ed.1 vs 7.5-02-07-03.7 Wave Energy Converter Model Test Experiments, and IEC TS 62600-202 Ed. 1 vs 7.5-02-07-03.8 Model tests for Offshore Wind Turbines, and the work needs to be continued in the next term.

The chair of the ITTC SC on ORE is also working on establishing a type A liaison with the IEC TC88, which focusses on Offshore Wind Turbines, to apply the same approach.

4. STATE OF THE ART

4.1 Review of testing of deployment (transportation, installation) and O&M for OWT and WEC

4.1.1 Offshore wind turbines

Experimental and numerical testing, in the open literature, remains largely focused on operational and survival design load conditions for a fully installed and commissioned offshore wind turbines, although a few publications are starting to appear, illustrating the methodologies and results of investigations focused on deployment and maintenance phases.

Hyland et al. (2014) performed experimental towing tests analyses of the GICON TLP configuration, considering several operational and towing conditions – and observing Vortex-Induced Motion (VIM).

Buttner et al. (2022) performed an experimental analysis on the towing process of the Orthospar platform, subject to wave loads with different incoming directions, focusing on the towing line load imposed on the platform. Mas-Soler et al. (2021) experimentally investigated a Tension Leg Platform (TLP) towing characteristics, considering different towing configurations, both in calm water and under wave loads.

Le et al. (2021) investigated numerically and experimentally the dynamic response of two TLP configurations having a semisubmersible configuration during towing, measuring heave, pitch and roll under different significant heights. Bollard pull requirements for different towing scenarios are also investigated. More recently, Ramachandran et al. (2024) conducted a comprehensive experimental and numerical study on towing operations of the DeepCwind semisubmersible platform, highlighting the importance of the evaluation of viscous forces in numerical models, and other non-linear phenomena, such as VIM, fishtailing, galloping, and pitch-induced wave run-up, observed in the experiments.

4.1.2 Wave energy converters

Wave energy is not necessarily at a higher Technology Readiness Level (TRL) than other renewable energy sources. Research and development in this field is progressing rapidly, and new, more efficient devices are constantly being developed. It is estimated that more than 1,000 patents for wave energy converter (WEC) concepts have been granted annually worldwide, and thousands of existing patents have been registered. This indicates that WEC designs have not yet converged into a single type.

Existing WECs can be broadly classified into three types based on their basic operating principles: "overtopping devices", "oscillating bodies", and "oscillating water columns". Recently, point-absorption wave energy conversion devices, which are a type of oscillating body, have been attracting attention due to their relatively easy construction and expected lower overall cost if deployed in a wave energy farm.

The development of numerical techniques and tank testing to validate them are important for WEC R&D, which is still under development. Numerical and experimental test cases have been devised by the International Energy Agency's Ocean Energy Systems (IEA OES) in its Task 10 "Wave Energy Converters Modelling Verification and Validation", presenting comparisons among linear, weakly nonlinear, and fully nonlinear codes, as well as experimental data.

The latest open-source software for WEC simulation is the WEC-Sim series, developed in MATLAB/SIMULINK using the multi-body dynamic solver Simscape Multibody. The project team is planning to develop a code to obtain the hydrodynamic coefficients needed for the pre-processing of WEC-Sim based on the Boundary Element Method.

The European project MaRINET2, a network of 39 partners in 13 European countries, has been working to progress offshore renewable energy technologies such as wave, tidal, and offshore wind. The project focused on testing two kinds of WECs to identify the uncertainty deriving from facility bias, but no further updates on its progress have been publicized after 2019.

Similarly, the pan-European COST action WECANET had planned another round-robin test to contribute to large-scale WEC array deployment, but no further updates on its progress have been published after 2021.

Papers on numerical simulation of wave power generation have been published extensively, likely due to the proliferation of open-source codes and general-purpose software, which make it easier to obtain numerical solutions at a certain level. These include studies on arrays of more than 10 WECs, as well as the use of AI models to predict waves, motion, and control forces. However, different types of WEC technologies have different issues, and the validation of numerical models remains challenging in some respects.

In summary, while a great number of new ideas have emerged in wave power generation, and numerical calculations and tank experiments have been conducted on them, most are still commercially immature and not yet fully verified through numerical analysis, tank tests using scaled models, and intercomparisons of demonstration projects using full-scale devices. Developing basic tank test data that can validate numerical analyses may be necessary to advance the field.

4.2 Review testing of multipurpose platforms (MPPs)

While multi-purpose platforms (MPPs) hold great potential for the offshore industry, their technological readiness level is very low, requiring comprehensive experimental trials. These trials are usually complex due to the need to integrate various subsystems, each governed by its own set of physical laws.

Wan et al. (2016) conducted a comparative experimental study on the survivability of a combined wind-wave floating offshore energy converter, the spar-torus combination (STC), testing three possible survival strategies against extreme loads. The study described the two model tests and compared the measured responses for each survival mode. Sarmiento (2019) performed experimental testing of a wind-wave MPP floating platform, providing insights into its global response, mooring loads, and the performance of the integrated oscillating water column wave converters under different sea states. The wind turbine was simulated using a wind generator and a drag disk, while the

OWC dynamics were reproduced through different diameter openings.

Ruzzo et al. (2021) reviewed the scaling laws and strategies for physical modeling of MPPs, highlighting the higher conflicts of a Froude-scaling approach when considering different subsystems, and the limitations of small-scale modeling due to the generally larger size of MPPs. Modeling the forces on flexible aquaculture nets poses a substantial challenge, as aquaculture is often integrated into these platforms.

Konispoliatis (2021) proposed a TLP-type renewable energy multi-purpose (wind-wave) floating offshore system and conducted scaled-model experiments to validate the analytical and numerical models developed, focusing on the hydrodynamic aspects. Ohana et al. (2023) described an experimental campaign aimed at assessing the coupled dynamics of a wind-wave-aquaculture MPP and providing data for numerical models' validation. The tests were carried out with a 1:40 model in a large ocean basin, with the wind turbine represented using a Software-In-The-Loop approach. Ruzzo et al. (2023) presented an experimental set-up for an outdoor, field campaign on a 1:15 scale wind-wave-aquaculture MPP, including a large moonpool, over 11 months. The study provided details on the scaled platform, measurement systems, and data acquisition for various parameters.

4.3 Full-scale installations

4.3.1 Current turbines

Table 1 lists full-scale deployed or planned projects in the last five years (2018-2023). Very little information regarding long-term project survivability is available.

Table 1 Active current turbine projects deployed or planned between 2018 and 2023. Database collected and published by the PRIMRE Portal and Repository for Information on Marine Renewable Energy (https://openei.org/wiki/PRIMRE)

#	Start Year	Project Name	Project Manager	Country	Capacity (MW)	Project Scale	Devices	Number of Devices	Waterbody
1	Planned	FloWatt	Hydroquest SAS,Qair	France	17.5	Array	Hydroquest	7	Le Raz Blanchard, Normandie, France
2	Planned	MeyGen Pentland Firth Phase 2	SIMEC Atlantis Energy	United Kingdom	312	Array	Seagen S		Inner Sound of the Pentland Firth
3	Planned	Morecambe Bay and Duddon Estuary Tidal Lagoon	North West Energy Squared Limited,Northern Tidal Power Gateways	United Kingdom	3960	Array		132	Morecambe Bay and the Duddon Estuary, Irish Sea
4	Planned	Morlais	Menter Mon	United Kingdom	240	Array	O2 Turbine, Magallanes Renovables ATIR, Nova M100		Irish Sea, Wales, United Kingdom
5	Planned	SBS 1MW Pilot Project	SBS Intl Ltd	Indonesia	1	Array			
6	Planned	Uisce Tapa Project	DP Energy,Halagonia Tidal Energy Ltd	Canada	9	Array	HS1500	6	Minas Passage, Bay of Fundy, Atlantic Ocean
7	2022	Larantuka 10MW project	SBS Intl Ltd	Indonesia	10	Array			Larantuka Strait, Indonesia

8	2022	Pempa‚Äôq In-stream Tidal Energy Project	Sustainable Marine Energy Ltd,Fundy Ocean Research Center for Energy	Canada	9	Array	PLAT-I	20	Bay of Fundy, Nova Scotia, Canada
9	2022	Vestmanna Tidal Power Plant	Minesto AB	Denmark	1.4	Array	Minesto Dragon 4, Minesto Dragon 12	3	Vestmanna, Faroe Islands
10	2021	East Foreland Tidal Project	Ocean Renewable Power Company	United States	5	Array	Seagen S		Cook Inlet
11	2021	Green Hydrogen and Oxygen Supply from Tidal Energy	Nova Innovation Ltd	United Kingdom	3	Array	Nova M100	30	Yell, Scotland, United Kingdom
12	2021	Islay Community Demonstration	Flex Marine Power Ltd	United Kingdom	0.05	Single Device	FM-Swimmer Tidal Turbine	1	Sound of Islay, Scotland, United Kingdom
13	2021	Kootznahoo Inlet	Littoral Power Systems Inc,Barrett Energy Resources Group	United States	0.3	Single Device		1	Kootznahoo Inlet, AK, USA
14	2021	Orbital at PTEC	Scotrenewables	United Kingdom	15	Array	O2 Turbine	7	Isle of Wright, United Kingdom
15	2021	Perpetuus Tidal Energy Centre PTEC	Perpetuus Tidal Energy Centre Ltd	United Kingdom	30	Array	O2 Turbine		South coast of the Isle of Wight
16	2021	West Somerset Tidal Lagoon	Halcyon Tidal Power LLC	United Kingdom	3000	Array		960	Bristol Channel
17	2020	FORWARD2030	Scotrenewables	United Kingdom	10	Array	O2 Turbine	2	Fall of Warness, Scotland, United Kingdom
18	2020	Lashy Sound Phase 2	Orbital Marine Power	United Kingdom	20	Array	O2 Turbine	10	Lashy Sound, Orkney; Scotland, Orkney
19	2020	MeyGen Pentland Firth Phase 1b	SIMEC Atlantis Energy	United Kingdom	10	Array	Seagen S	6	Inner Sound of the Pentland Firth
20	2019	Blue Shark Power Djibouti 2	Blue Shark Power System	Djibouti	120	Array	Blue Shark	495	
21	2019	FORCE 9 MW Pre-Commerical Demo	ANDRITZ Hydro	Canada	9	Array	HS1500	6	Minas Basin
22	2018	Grand Passage	Sustainable Marine Energy Ltd	Canada	0.7	Single Device	PLAT-I	1	Grand Passage, Nova Scotia, Canada
23	2018	Holyhead Deep	Minesto AB	United Kingdom	80	Array	Deep Green Tidal Kite	20	Irish Sea, UK
24	2018	Majis	New Energy Corporation	Oman	0.005	Array			Port of Sohar, Oman

25	2018	MeyGen Pentland Firth Phase 1c	SIMEC Atlantis Energy	United Kingdom	6	Array	SIMEC AR1500,ANDRITZ Hydro HS1000	4	Inner Sound of the Pentland Firth
26	2018	P154 Guinard Demo	Guinard Energies Nouvelles	France	0.02	Single Device	MegaWattBlue	1	Atlantic Ocean
27	2018	Vestmanna DG100 Tidal Kite System	Minesto AB	Denmark	0.1	Array	Deep Green Tidal Kite		Vest-manna, Faroe Islands

4.3.2 Offshore wind turbines (Floating)

The global offshore wind industry has seen significant growth from 2021 to 2024. In 2021, the cumulative global offshore wind installed capacity grew to 50,623 MW from 257 operating projects, largely driven by China's commissioning of 13,790 MW. The size of offshore wind turbines has also increased, with the world's largest single-capacity 16 MW turbines now in operation in China. Floating offshore wind turbines have also seen progress, with the total installed capacity reaching 57.1 MW in 2021, including the largest floating offshore wind project in the UK and several demonstration projects in China. However, there are still many challenges to overcome, such as fully coupled performance analysis and lightweight design for cost reduction.

Table 2 List of floating offshore wind farm projects

PROJECT NAME	COUNTRY	COMMISSIONING	CAPACITY (MW)	OWNER
TetraSpar Demo	Norway	2021	3.8	Stiesdal
Three Gorges Leader Demo (Sanxia YingLing Hao)	China	2021	5.5	China Three Gorges
Haizhuang Fuyao Demo	China	2022	6.2	CSSC Haizhuang
Haiyou Guanlan Demo	China	2023	7.25	CNOOC
Hywind Tampen Norway	Norway	2023	88	Equinor
Les éoliennes flottantes du Provence Grand Large (PGL)	France	2024	24	SBM Offshore
Forthwind Demo	UK	2024	20	#N/A
Mingyang OceanX Demo	China	2024	16.6	Mingyang
EOLMed	France	2025	30	Ideol
Les éoliennes flottantes du Golfe du lion (EFGL)	France	2025	30	Principle Power
Pentland Deom (Dounreay Tri)	UK	2025	15	#N/A
Hainan Wanning Offshore Floating Phase I	China	2025	200	Power China
Flocan 5 Canary	Spain	2025	25	Grupo Cobra
Goto Sakiyama Oki Oki Huangdao Pilot A	Japan	2026	16.8	Toda
Goto Sakiyama Oki Oki Huangdao Pilot B	Japan	2026	5.2	Toda
Hainan Wanning Offshore Floating Phase II	China	2027	800	Power China

Oahu North, Hawaii	USA	2032	400	Principle Power
Oahu South, Hawaii	USA	2032	400	Principle Power

4.3.3 Wave energy converters

Worldwide, WEC full-scale tests are continuing, with wave power generation units of tens of kW to MW being developed. Most WECs are movable or OWC types, with full-scale deployments mainly in Europe and recent activity in the US and Asia. However, information on full-scale tests is limited, and meaningful power generation for commercialization has not been achieved. Overcoming survival at sea remains a key challenge, as it is directly related to cost and a barrier to commercialization. While full-scale tests are increasing, and the IEC is preparing a performance evaluation system, more disclosure of test information and technical progress is needed to advance the wave energy sector.

Table 3 List of the recent projects on WECs

PROJECT NAME	COUNTRY	YEAR ONLINE	DEVELOPMENT STATUS	DEVELOPER	Scale	RATED POWER [MW]	TYPE
LAMWEC	Belgium	2020/2021	At Sea Prototype	Laminaria	1:7	0.2	Point Absorber
Wavepiston	Denmark	2017-2019	Demonstration Scale	Wavepiston A/S	Full Scale	Unknown	Oscillating Wave Surge Converter
mWave	Wales	2021	Development	Bombora	1:7	1.5	Gravity Based Pressure Differential
King Island Project	Australia	2020	Installed Waiting Connection	Wave Swell Energy	Full Scale	0.2	Oscillating Water Column
OE Buoy	Ireland/USA	2020	Arrived at Hawaii Test Site	Ocean Energy (Ireland)	Full Scale	0.5	Oscillating Water Column
PowerBuoy	North Sea	2020	Operational	Ocean Power Technologies	Full Scale	0.003	Point Absorber
NEMOS Wave Energy Converter	Belgium	2019	At Sea Prototype	NEMOS	Large Scale	Unknown	Point Absorber
Tordenskiold	Denmark	2019	Half-Scale Open Sea	Crestwing	1:2	Funknown	Attenuator
WAVEGEM	France	2019	At Sea Prototype	GEPS Techno	Full Scale	0.15	Point Absorber
WaveSub	United Kingdom	2018	At Sea Prototype	Marine Power Systems	1:4	4.5 full scale (Proto-type rated power unknown)	Submerged Point Absorber
WaveRoller	Portugal	2018	At Sea Prototype	AW-Energy	unknown	0.25	Oscillating Wave Surge Converter
C4	Sweden	2018	At Sea Prototype	CorPower	Full Scale	0.3	Point Absorber

PROJECT NAME	COUNTRY	YEAR ONLINE	DEVELOPMENT STATUS	DEVELOPER	Scale	RATED POWER [MW]	TYPE
Oneka Buoy	Canada	2018	At Sea Prototype	Oneka	unknown	5-10 m^3 of fresh water per day	Point Absorber
Penguin	Finland	2017	Grid Con-nected Test	Wello Oy	Full Scale	1	Internal Rotating Mass
Wanshan 1 MW (2×500 kW) Wave Energy Demonstration Project	China	2023	Under Construc-tion	Guangzhou Institute of Energy Conversion (GIEC)	Full Scale	1	Oscillat-ing Wave Surge Converter
Exowave WEC	Denmark	2022	Operational	Exowave	Small Scale	0.001	Oscillat-ing Wave Surge Converter
Floating Power Plant A/S Com-mercial scale PTO dry test rig (PTO TWIN)	Denmark	2022	Under Construc-tion	Floating Power Plant A/S	Full Scale	0.2	Point Absorber
DIKWE	France	2022	At Sea Prototype	Geps Techno/Groupe LE-GENDRE	1:4	Unknown	Oscillat-ing Wave Surge Converter
REWEC3 @ Civi-tavecchia	Italy	2022	Operational	Mediterranean Uni-versity of Reggio Ca-labria	Full Scale	0.02	Oscillating Water Column
Overtopping Breakwater (OBREC)	Italy	2022	Operational	University of Campa-nia Luigi Vanvitelli	Full Scale	0.015	Wave Overtopping
ISWEC revamp	Italy	2022	Under Construc-tion	ENI, Wave for Energy, Politecnico di Torino	Full Scale	0.25	Internal Rotating Mass
Youngsoo OWC Pilot Plant	Korea	2022	Operational	KRISO	Full Scale	0.5	Oscillating Water Column
OWC WEC with Breakwater	Korea	2022	Operational	KRISO	Full Scale	0.03	Oscillating Water Column
Mutriku Wave Power Plant	Spain	2022	Operational	EVE	Full Scale	0.296	Oscillating Water Column
Ocean Energy Buoy (OE Buoy)	USA	2022	Under Construc-tion	Ocean Energy Ltd,	Full Scale	0.5	Oscillating Water Column
C-Power SeaRay Wave Power System (previ-ously planned as StingRAY WEC)	USA	2022	Under Construc-tion	C-Power	Full Scale	0.02	Oscillat-ing Wave Surge/Heave Con verter
Blue X	UK	2022	Operational	Mocean Energy	Full Scale	0.01	Attenuator

* Note: from the IEA OES Annual Report 2021, 2022 and 2023

4.4 Wave energy converters

4.4.1 New concepts

WECs can be categorized by the physical process used to extract energy (Falcão (2010)): "Oscillating Water Columns", "Oscillating bodies", and "Overtopping devices". Recent trends in numerical studies explore introducing AI techniques, such as machine learning, into control algorithms to improve efficiency. However, it is challenging to scale down and test the power take-off (PTO) mechanisms used in actual equipment. Examples include using AC control systems and simulating PTO systems for OWC and other pneumatic equipment using orifice loads during proof-of-concept testing to overcome this challenge.

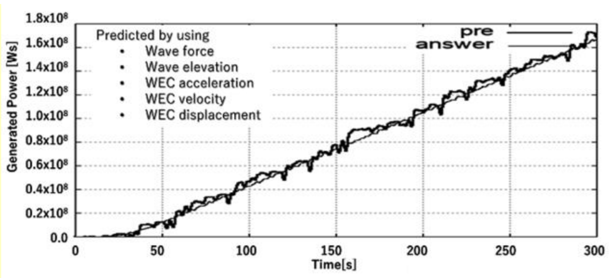

Figure 1: Comparisons of accumulated power generation: analytical result VS AI model (M. Murai, (2022))

4.4.2 Power take-off systems (PTO)

Scaling down and testing the power take-off (PTO) mechanisms used in actual wave energy converter (WEC) equipment is challenging. Examples include using AC control systems and simulating PTO systems with Coulomb or linear dampers, as well as simulating OWC and pneumatic PTO systems using orifice loads during proof-of-concept testing. The ITTC guideline 7.5-02-07-03.7 discusses various PTO systems for WEC model test experiments.

4.4.3 Physical and numerical modelling

Wave energy converter (WEC) problems often involve significant nonlinearities in fluid flow and fluid-structure/PTO interaction. However, for cases where the inviscid fluid hypothesis and small amplitude oscillations can be assumed, analytical solutions can be determined using the superposition principle to divide the problem into diffraction and scattering problems (Alves, 2016; Budan et al., 1975; Falnes et al., 1985). This allows the calculation of free surface oscillation, body motion, and potential hydrodynamic power extraction.

The ITTC guideline 7.5-02-07-03.18 Practical Guidelines for Numerical Modelling of Wave Energy Converters categorizes numerical modeling methods for WECs as potential flow models, CFD models, and hybrid models, providing considerations and a summary of the status and characteristics of each method in terms of Technology Readiness Level (TRL).

4.4.4 Control strategies

Recent years have seen an increase in numerical studies on the introduction of AI technologies, such as machine learning, into control strategies to improve wave energy converter (WEC) efficiency. Machine learning can be classified into methods like Deep Neural Network, Convolutional Neural Network, Recurrent Neural Network, and Long Short Term Memory. However, this classification may not remain appropriate as more branches and combinations of AI techniques continue to emerge for WEC applications.

4.4.5 Array of WECs

The hydrodynamic interactions between multiple WECs in a wave farm can significantly affect energy conversion. Incident waves are diffracted and refracted between devices, potentially reducing or increasing the total energy absorption of the WEC array.

The hydrodynamic interaction between WEC arrays is described by the multiple scattering model, as expressed by Kagemoto and Yue (1986). Within linear wave theory, this direct matrix model is considered rigorous. Li and Murai et al. (2018) evaluated the output performance of point absorber arrays, considering PTO copper losses. Their results showed that a transverse linear arrangement outperformed other configurations, with an optimal device spacing of around 50% of the significant wave period wavelength.

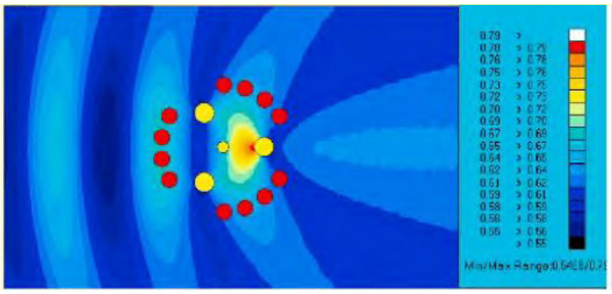

Figure 2: Wave forms around the DeepCwind semi-submersible with different PA-WECs arrangements (Hamid, R.G., et. al, (2021))

Potential flow theory cannot account for viscous effects such as boundary layer separation, turbulence, wave breaking, and wave overtopping. However, these phenomena are essential in predicting the hydrodynamic forces acting on the device. Therefore, CFD modelling based on the solution of the Navier-Stokes equations is starting to be employed. In recent years, the application of CFD methods to multi-point absorbing WECs has increased due to the rapid evolution of computational techniques. However, the computational cost is still too high to study arrays. At present, most CFD studies on multiple PA-WECs use finite volume methods, Li, et. al, (2012).

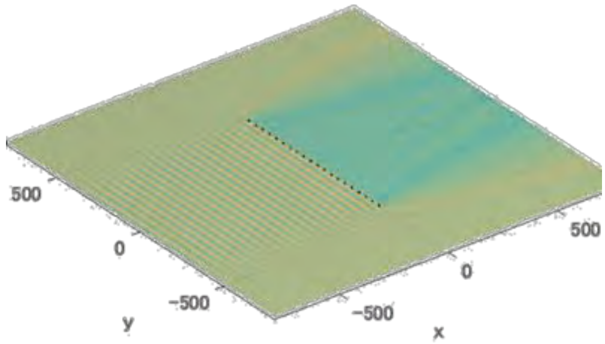

Figure 3: Example of the numerical simulation on arrayed 20 WECs and wave field around the array in regular waves (Murai et al, (2021))

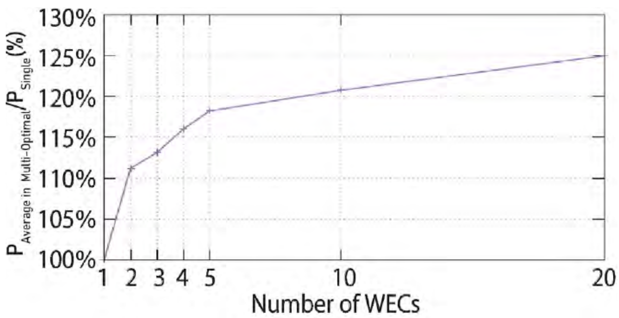

Figure 4: Increase rate of power generation of each PA-WEC number in the one direction irregular wave. (Murai et al, (2021))

Tank tests on arrays of multiple WECs can be broadly divided into cases where there is no common platform and cases where there is a common platform. In the former case, the focus is to optimize the layout configuration to maximize total output under different operating conditions, for example, considering regular or irregular waves and PTO system type. In the latter case, the focus is often on how the motion response of the platform is affected by controlling the WECs, for example, by assuming the attachment of multiple wave power generators to a floating wind turbine system.

Figure 5: Impression of a 2-WEC column array under regular waves, (V. Stratigaki, et al., (2014))

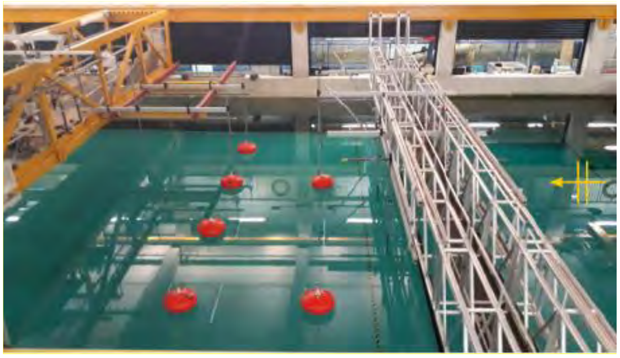

Figure 6: WECs’ array layout (M. Giassi, et al., (2020))

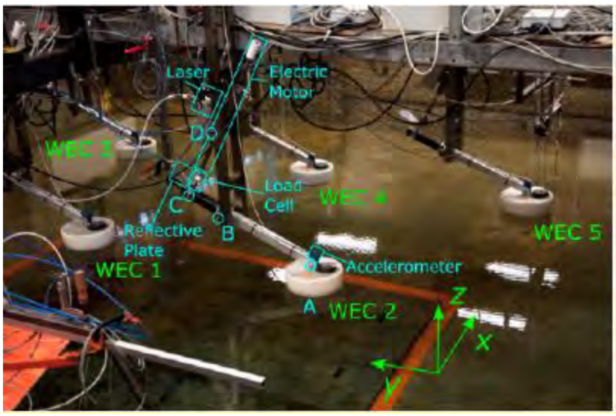

Figure 7: Model test (Mercad´e et al.(2017))

Figure 8: physical model Sketch of the wave basin (K. Sun, et al. (2021))

4.5 Current turbines

4.5.1 Physical and numerical techniques for prediction of performance

The performance of hydrokinetic turbines is often predicted using semi-analytical approaches, computational fluid dynamics, machine learning, and experiments, at either model or full scale, depending on available test facilities, financial support, and scale factors.

4.5.1.1 Model Scale Measurements

Ensuring accurate representation of the investigated phenomenon is essential when conducting model-scale tests for wave energy converters (WECs) and hydrokinetic turbines. The model scale must be carefully chosen to accommodate geometric, kinematic, and dynamic similitudes while avoiding scale effects that could disrupt the output parameter values.

Guidelines and recommended practices, such as the ITTC guideline 7.5-02-07-03.9 and the IEC guideline (IEC, 2022), provide extensive recommendations for model tests, test facilities, result reporting, and factors to consider during analysis. Additionally, JCGM 100:2008 offers valuable advice on representing experimental uncertainties.

Model studies have exemplified tests to reach the performance of hydrokinetic turbines. Tests at the Federal University of Rio de Janeiro (UFRJ) by Fernandes & Rostami (2015) determined the efficiency of a Vertical Axis Autorotation Current Turbine (VAACT) under different Reynolds numbers and dimensionless moments of inertia. The results showed a maximum efficiency of approximately 7% at Re=59,800 and I* in the range of 0.5-0.6 (Figure 9).

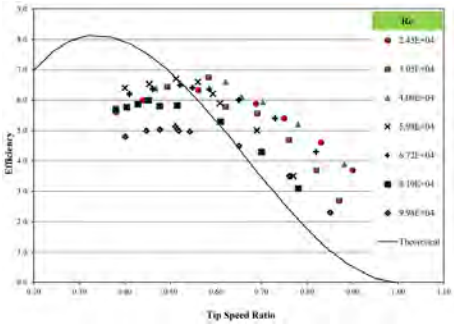

Figure 9: Experimental data for efficiency of flat plate model at I*=0.52 (Fernandes & Rostami, 2015). The theoretical curve (black line) is reported by (Manwell et al., 2002)

Rostami and Fernandes (2015) further experimented on a flapped VAACT turbine, achieving a maximum efficiency of around 33% when the Reynolds number was 20,900 and the dimensionless moment of inertia was 0.70 (Figure 10).

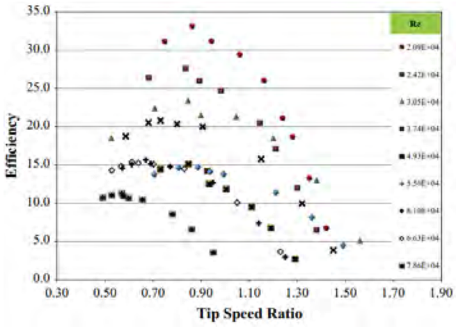

Figure 10: Experimental data for efficiency of flapped plate model at I*=0.70 (Rostami & Fernandes, 2015)

4.5.1.2 In-Situ Measurements

In-situ measurements are a valuable practice that helps understand hydrokinetic turbines' performance and external loads. Even though these measurements come with high costs, they provide insights into any issues that may arise during the installation and operation of turbines. Typically, these measurements are conducted using devices with power capacities in the magnitude of kilowatts. Niebuhr et al. (2019) provide, in Table 4, examples of in-situ measurements and prototypes that have been installed and presented in the literature. Depending on the generator's characteristics and environmental constraints, these devices are placed near the free surface or at the riverbed.

Table 4: Developments with hydrokinetic turbine prototypes (Niebuhr et al., 2019)

Device	Characteristics	Picture
Smart Duofloat	Power Capacity: 5 kW Flow Velocity: 2.8 m/s Diameter: 1 m	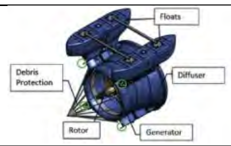
Smart Freestream	Power Capacity: 5 kW Flow Velocity: 3.1 m/s Diameter: 1 m	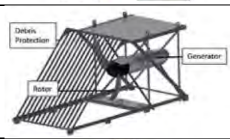
Hydroquest River 1.4	Power Capacity: 40 kW Flow Velocity: 3.1 m/s	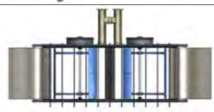

Device	Characteristics	Picture
Waterotor Energy Tech	Power Capacity: 1.1 kW Flow Velocity: 0.89 m/s	
Guinard Energies	Power Capacity: 130–3500 W Flow Velocity: 1 m/s	
EnviroGen Series	Power Capacity: 5 kW Flow Velocity: 3 m/s	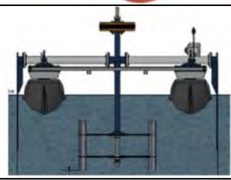
ORPC RivGen	Power Capacity: 15 kW Flow Velocity: 2.3 m/s	
HeliosAltas	Power Capacity: 100–500 W Flow Velocity: 1.8 m/s	
Instream energy system	Power Capacity: 25 kW Flow Velocity: 3 m/s	

4.5.1.3 Semi-Analytical Techniques

4.5.1.3.1 Blade Element Momentum (BEM) Theory

The blade element momentum theory is commonly used in designing horizontal axis turbines. This method divides the blades into two-dimensional sections to determine their torque and thrust. By integrating these properties along the blades, the total torque and thrust of the turbine can be calculated. BEM theory can be embedded in numerical codes for CFD simulations or numerical optimization (Yeo et al., 2022). It is a popular choice for designing turbine blades to improve their performance curves and determine their design point (El-Shahat et al., 2020). Additionally, this technique is precious for exploring new concepts and designs (Elfering et al., 2023).

4.5.1.3.2 Actuator Disc Model

The actuator disc model utilizes the one-dimensional momentum theory. This involves applying simple hypotheses and conserving linear momentum to the control volume. However, specific corrections have been used to the model, such as incorporating wake rotation for horizontal axis turbines (Manwell et al., 2002).

The theory's most significant finding is the calculation of the maximum power coefficient versus the tip speed ratio (TSR). For the classic one-dimensional momentum theory model, the maximum power coefficient (C_P) is 59%, regardless of the tip speed ratio. However, the wake rotation model introduces a dependency on TSR, causing the curve to tend towards the maximum from the ideal model as TSR increases.

Recent advances in wind turbine aerodynamics have been made using the actuator disc model. (Bastankhah & Porté-Agel, 2014) have developed dynamic models that simulate lateral and vertical wake motion, known as dynamic wake meandering. Similarly, (Howland et al., 2019) have explored wind turbine wake steering strategies using the actuator disc model to optimize turbine yaw angles. Additionally, (Baratchi et al., 2020) have utilized the blade element actuator disc method in CFD for simulations with ducted tidal turbines. Finally, (Behrouzifar & Darbandi, 2019) employed this model to predict a horizontal axis turbine's performance and wake region.

4.5.1.3.3 Quasi-Steady Models

Quasi-steady models are widely used to predict turbine response and performance while minimizing time expenditure with simulations. This method relies on an equation of motion that depends on hydrodynamic coefficients derived from experiments or numerical simulations using a static turbine. These coefficients are determined based on the Reynolds number and angle of attack, and the resulting method can be an efficient alternative for research in this field.

Leroux et al. (2019) compared experimental results with computational fluid dynamics simulations using transient and quasi-steady models to simulate a horizontal axis turbine. The analysis focused on velocity deficits in the wake at distances of 2D, 3D, 6D, and 10D behind the turbine. Although the quasi-steady model did not predict the turbulence intensity distribution correctly and did not reflect wake behaviour accurately, this model was consistent with experimental results for downstream distances greater than 6D (Figure 11).

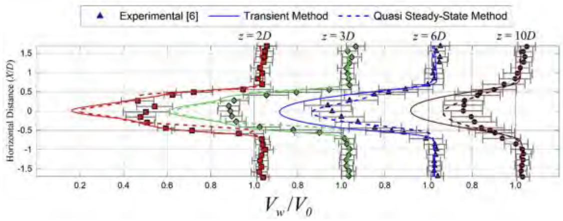

Figure 11: Normalized velocity comparison between experimental results and the transient-rotor simulation for the distance behind the turbine of 2D, 3D, 6D, and 10D (Leroux et al., 2019)

The stability, motions, and performance of flat plate turbines have also been explored in studies by (Fernandes & Mirzaeisefat, 2015; Mirzaeisefat & Fernandes, 2013; Soares et al., 2022b). These studies utilized numerical simulations to provide coefficients for the quasi-steady method to investigate turbine performance, showing that this methodology is feasible in studying hydrokinetic turbines.

Rostami & Fernandes (2017) performed an experimental and numerical study on the motion of flat plates in uniform flow. Their models showed excellent agreement, and the research indicated that a flat plate turbine performing fluttering must achieve a maximum efficiency of 19%. This efficiency is about 18% greater than that of autorotation.

4.5.1.4 Computational Fluid Dynamics (CFD)

One common method for simulating currents in turbines is to use computational fluid dynamics software. Typically, this involves a sliding-mesh approach, where the control volume is split into stationary and rotating regions. The rotating section includes the turbine geometry, which rotates with the turbine. Occasionally, remeshing techniques are used to generate a new mesh at each time step, but this is rare due to the high computational costs involved.

Turbulence models are used in CFD studies, and Reynolds numbers are usually in the turbulent range, making Direct Numerical Simulation impractical. Therefore, researchers focus on Reynolds-Averaged Navier-Stokes (RANS), Large Eddy Simulation (LES), and hybrid models like the Detached Eddy Simulation (DES). LES and DES models have good turbulence resolutions but require complex grid refinement. RANS models perform well with low grid refinement but fail to model high-gradient phenomena.

Kulkarni et al. (2022) reviewed CFD and Fluid-Structure Interaction (FSI) simulations to optimize tidal turbines. This technique allows researchers to determine how pressure and fluid flow affect structural deformations and how structural deformations affect pressure and flow.

The study by Niebuhr et al. (2022) on counter-rotating turbines employed the CFD technique to determine their performance and wake characteristics. To validate the rate of decay of turbulence intensity, the turbulence model was changed to decide which represented the wake characteristics more accurately (Figure 12). The experimental wake was compared to the results obtained from the turbulence models to interpret the BEM-CFD approach using RSM-LPS2. The findings revealed that the approach adheres closely to the experimental results and provides exemplary accuracy.

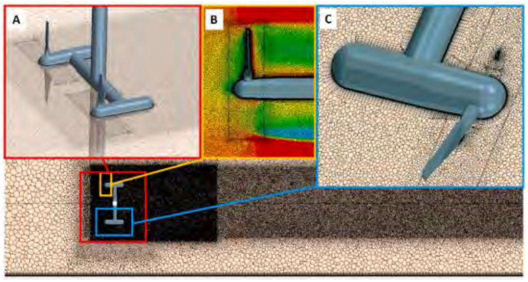

Figure 12: Schematic view of the grid for the axial hydrokinetic turbine (Niebuhr et al., 2022)

In (Wu et al., 2023), CFD techniques are used to evaluate a novel hydrokinetic turbine. The simulations model the power take-off mechanism and aim to obtain the optimized shape for the vertical turbine. The analyses have shown a significant effect of the turbine's flap angles and the inner length on the power coefficient.

Reddy et al. (2022) reviewed a couple of CFD studies to improve the efficiency of hydrokinetic turbines. These studies used geometric parameterization to analyze the power coefficient behavior based on fluid and geometric characteristics such as Reynolds number and tip speed ratio. Additionally, the researchers considered the turbine arrangements to account for the changes in performance due to device interactions. Table 2 provides a summary of the CFD studies conducted on lift-driven devices.

Table 5: Effect of various parameters on the lift-based hydrokinetic turbines (Reddy et al., 2022)

Reference	Parameter	Definition	Conceptualization	Performance Characteristic Curves
(Shiono et al., 2002)	Design parameters Solidity	Fraction of the circumference of the rotor covered by the blade σ = nC/πD (Gorlov, 1995) or σ = nC/D (Khanjanpour & Javadi, 2020).	The solidity definition illustrates that it depends on three geometric parameters: number of blades, chord length, and turbine diameter.	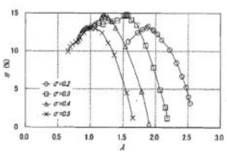

Reference	Parameter	Definition	Conceptualization	Performance Characteristic Curves
(Saini & Saini, 2018)	Blade Profile	NACA hydrofoils (symmetrical/ unsymmetrical) are used to design the rotor blades.	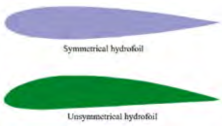	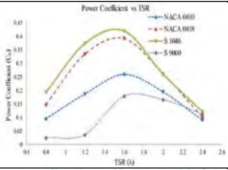
(R. Kumar & Sarkar, 2022)	Helicity	Blade made angle with the horizontal plane φ = tan− 1(nH /πD) (R. Kumar & Sarkar, 2022).	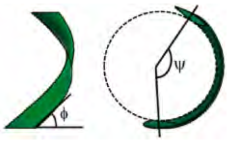	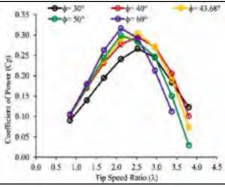
(Li et al., 2017)	Aspect Ratio	The ratio of turbine height to turbine diameter AR = H/D.	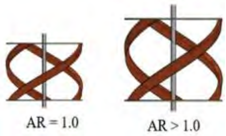	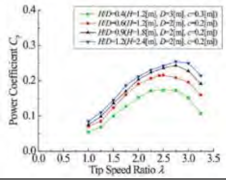
(Hwang et al., 2009)	Number of Blades	The number of blades is directly proportional to the solidity.	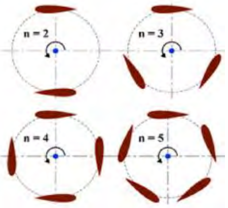	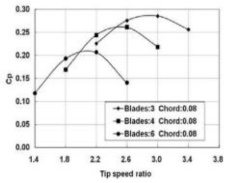
(R. Kumar & Sarkar, 2022)	Blade Pitch Angle	The angle between the blade chord and a tangential line is drawn to the circle of revolution of the turbine.	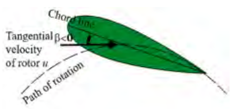	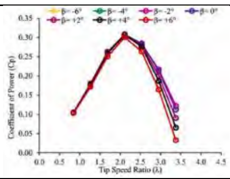
(Talukdar et al., 2017)	Number of Steps	Position of turbines one over the other.	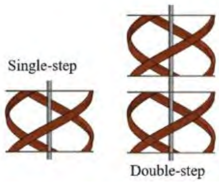	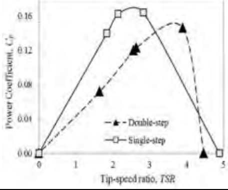
-	Mount Point Ratio	The ratio of position of chord to chord length MP = p/C.	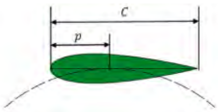	-
-	Struts/ End-plates	These are used to connect the blades to the turbine shaft.	-	-
(Kiho et al., 1996)	Reynolds number	As Reynolds number (Re) increases, the torque produced by the turbine increases. Re = (ρvD/μ).	-	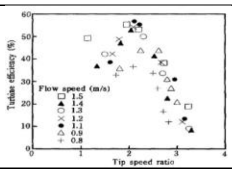

Reference	Parameter	Definition	Conceptualization	Performance Characteristic Curves
(Kirke, 2011)	Augmentation technique	This technique includes auxiliary devices such as duct/diffuser, placing foil in front of the turbine, and blocking the plate.	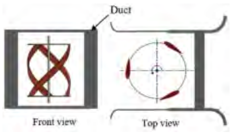	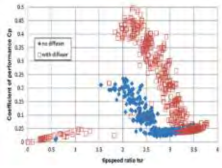
(Patel et al., 2017)	Turbine arrangement	Represents the arrangement of turbines in a strategic array to avoid undesirable turbine-wake interactions.	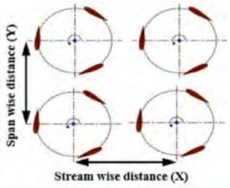	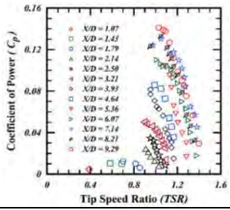
(Talukdar et al., 2018)	Turbine installation	The turbine can be installed in three different types of mounting schemes: bottom structure mounting, near-surface structure mounting, and floating structure mounting.	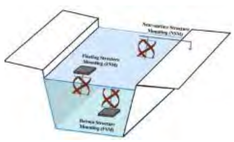	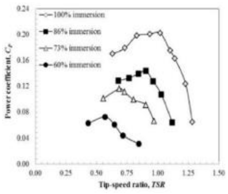

4.5.1.5 Machine Learning Approach

Although ML has been studied to improve performance, most research has focused on the predictive maintenance of power plants and microgrid operations. This allows for the early identification of potential equipment failures, reducing downtime and increasing overall efficiency (Arafat et al., 2024). Nonetheless, this technique can improve the accuracy of failure predictions, detect and diagnose faults in real-time, and assist with the operation and maintenance of power plants. Common machine learning methodologies include Support Vector Machine (SVM), Random Forest (RF), Artificial Neural Network (ANN), Fuzzy Expert Systems (FES), and Deep Learning approaches. Critical analyses of these machine-learning methods for power plant components can be found in (Arafat et al., 2024).

Kumar et al. (2024) have devised a statistical approach to predict the efficiency of a hydropower plant using a Kaplan turbine. Their methodology employs an Artificial Neural Network to develop models to estimate the turbine's maximum efficiency. The neural network is implemented using 17520 samples, divided into three parts: 80% for modelling, 10% for testing, and 10% for validation. The resulting model shows an excellent fit with the data, producing a coefficient of determination (R-squared) almost equal to 1.0.

Khani et al. (2024) utilized a combination of Catboost and standalone linear regression models to predict the power coefficient, maximum power coefficient, and the corresponding tip speed ratio of a Savonius turbine in straight and bend flumes. By implementing advanced optimization techniques such as whale optimization, grey wolf optimization, and Bayesian optimization, the hybrid models achieved Savonius performance.

The research findings reveal that the combination of CastBoost and Grey Wolf Optimization integration produces the most optimal adherence among the tested methods. The study also highlights the critical role of machine learning models in identifying the sensitivity of turbine performance to inserting a returning blade deflector and the position of the current turbine in the bend test facility. Furthermore, the study indicates that the number of turbine stages is crucial to the analysis.

In a similar investigation, Cheng et al. (2022) proposed a hybrid machine learning approach to evaluate the performance of a Dual Darrieus turbine. The prediction model involves the application of an artificial neural network, adaptive neuro-fuzzy interference system, and support vector machine to build the objective function. The optimization of the model is achieved using particle swarm optimization, simulated annealing method, and genetic algorithm. The training model incorporates an orthogonal test and computational fluid dynamics. The study demonstrates that applying hybrid machine-learning techniques yields promising results in predicting turbine performance (Cheng et al., 2022).

4.5.2 CFD modelling

This section review and report the techniques used for CFD modelling of current turbines. This includes the use of combined EFD/CFD techniques for scaling and blockage corrections and methodologies for replicating environmental conditions.

The Computational Fluid Dynamics approach has been extensively applied to study the blockage effect and wave effect on the performance of hydrokinetic turbines. The literature provides studies relating those factors to changes in power and thrust coefficients of harvesting devices. Moreover, a comprehensive wake analysis is accomplished to verify factors such as the velocity profile, the turbulence intensity, and the decay of the turbulence intensity downstream.

Schluntz & Willden (2015) analysed the effect of lateral blockage (ϵ) on a horizontal axis current turbine. They employed the blade element momentum (BEM) theory embedded into the Reynolds-Averaged Navier Stokes (RANS) solver to account for blockage ratios ranging from 0.1% to 31.4% (Figure 13). The study also examined the ratio between lateral intra-rotor spacing and the rotor diameter (s/d), which was tested between 0.25 and 100. The numerical model revealed that operating at higher blockage can lead to a more significant improvement compared to working at the turbine's design point. Therefore, the study suggests that the blockage ratio should be considered during the turbine design optimization.

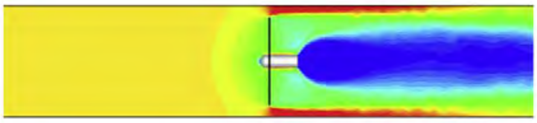

(a) $s/d = 0.25$; $\beta = 0.314$

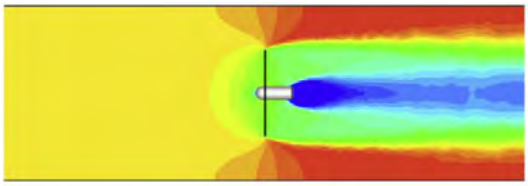

(b) $s/d = 1.0$; $\beta = 0.196$

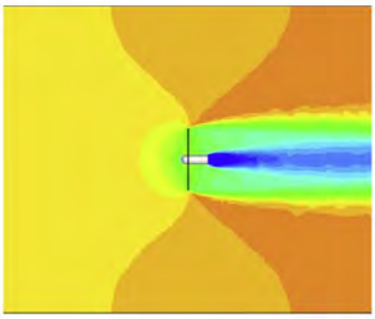

(c) $s/d = 4.0$; $\beta = 0.079$

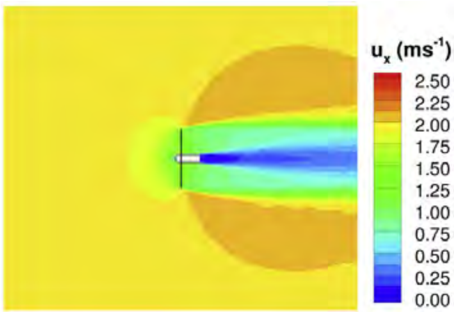

(d) $s/d = 100.0$; $\beta = 0.0001$

Figure 13: Ratio between the lateral intra-rotor spacing (s/d) and blockage ratio in the control volumes (Schluntz & Willden, 2015)

Kinsey & Dumas (2017) searched the impact of channel blockage on the performance of axial and cross-flow turbines. They employed a three-dimensional CFD model at high Reynolds numbers to achieve this. The study proposes blockage corrections for axial and cross-flow hydrokinetic turbines. These corrections enable the estimation of drag (C_D), power (C_P), and tip speed ratio (λ) for the theoretically unconfined turbine based on the results of the confined turbine. The linear momentum actuator disc theory, suitable for axial and low-solidity cross-flow turbines, was used to achieve this. Equation (1) shows the relevant details.

$$
\begin{aligned}
C_P' &= C_P \cdot \left(\frac{U}{U'}\right)^3 \\
C_D' &= C_D \cdot \left(\frac{U}{U'}\right)^2 \\
\lambda' &= \lambda \cdot \left(\frac{U}{U'}\right), \\
\forall \frac{U}{U'} &= \frac{\alpha_2}{\alpha_2^2 + C_D/4}
\end{aligned}
\qquad (1)
$$

The equation above distinguishes the properties denoted by the superscript "prime" as those belonging to an unconfined flow, while those without it refer to a confined flow. The findings indicate that the correction factor for the 3-bladed (high-solidity) cross-flow turbine is slightly underestimated by this method, especially for drag than for power. The methodology proposes the blockage correction presented in Equation (2), where the knowledge of the confined and unconfined properties enables estimating their values at another blockage condition. These adjustments are exemplified in Figure 14. Note that ϵ is another possible nomenclature for the blockage ratio.

$$
\begin{aligned}
C_D(\epsilon) &= \left(\frac{C_D(\epsilon_1) - C_D'}{\epsilon_1}\right) \cdot \epsilon + C_D' \\
C_P(\epsilon) &= \left(\frac{C_P(\epsilon_1) - C_P'}{\epsilon_1}\right) \cdot \epsilon + C_P' \\
\lambda(\epsilon) &= \left(\frac{\lambda(\epsilon_1) - \lambda'}{\epsilon_1}\right) \cdot \epsilon + \lambda'
\end{aligned}
\qquad (2)
$$

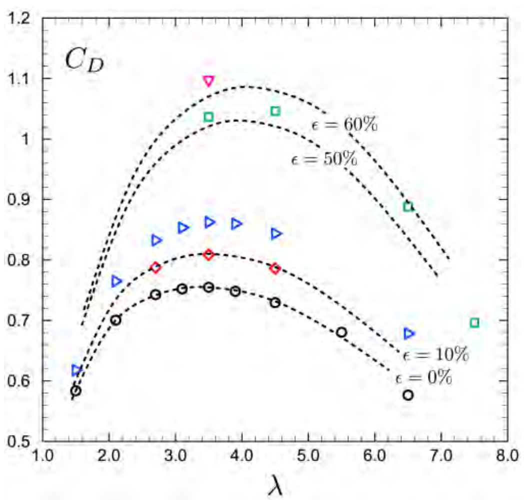

(a) Drag coefficient x Tip speed ratio

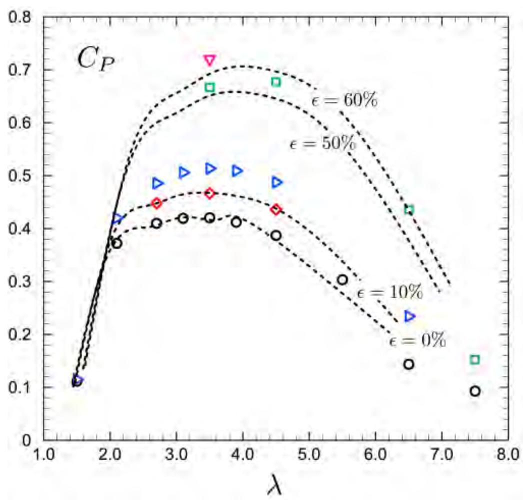

(b) Power coefficient x Tip speed ratio

Figure 14: Performance coefficients versus tip speed ratio (Kinsey & Dumas, 2017)

Koh and Ng (2017) studied tidal turbines using the actuator disk model and CFD simulations. They aimed to investigate the impact of various parameters on the thrust generated by the turbines. The turbines were placed in blocked conditions and exposed to a higher velocity than inflow. Results showed that the presence of boundary layers affected the thrust produced by the turbines. The turbines had less thrust when boundary layers were present in the simulation than when they were absent.

The study also revealed that an optimal aspect ratio can be achieved when boundary layers are present, leading to the maximum performance of a single turbine. This further demonstrated that the turbulence intensity and flow velocity influenced the turbine's predicted thrust. The rate of decay of turbulence intensity in the channel was found to be dependent on the channel depth, which may have affected the results.

The effect of channel depth on turbulence intensity and flow velocity can be observed in Figure 15, which compare them for experiments and turbulence models. The flow experiences a significant velocity drop ($u \,/\, u_0$ from 1.0 to 0.5) and a high turbulence intensity (TI = 30%) when reaching the turbine. The distance from the wake is fundamental in determining the decay in turbulence intensity, particularly at $y \,/\, D$ = 1.5, where the turbine is located. Velocity profile inflection minimizes as the downstream distance increases.

Birjandi et al. (2013) conducted a study to examine how the vertical blockage effect affects the performance of a squirrel cage turbine. The clearance coefficient, the ratio between the water height above the turbine and the turbine's diameter, is a critical parameter in this study. The clearance coefficient, denoted as C_h, can be calculated using Equation (3).

$$C_h = \frac{H}{D} \tag{3}$$

where H is the water height above the turbine and D is the turbine diameter. If C_h is negative, the water level is below the top of the rotor. Meanwhile, a positive clearance coefficient yields the water level above the turbine blades, meaning the model is submerged. The authors state this coefficient analyses the influence of both the blockage effect and free-surface effect for the power coefficient, especially in scenarios such as rivers where the water level may change throughout the year.

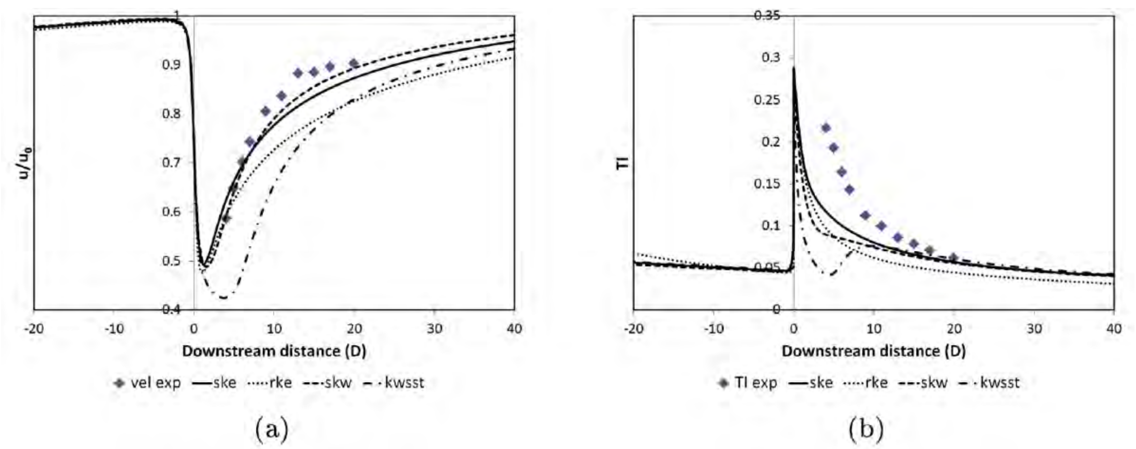

Figure 15: The a) centreline velocity and b) turbulence profiles of an actuator disk generated by the different turbulence models (Koh & Ng, 2017)

Figure 16 illustrates that the turbine performs better at slightly positive clearance coefficients. The research provides that a clearance coefficient between 0.0 and 0.2, installing the turbine a few distances from the free surface, leads to excellent performance improvement to the device, which not only overcomes the Betz limit but also almost reaches 100% efficiency by the graph. However, negative C_h values do not allow for accessing good power coefficient values, being advised to operate in the range of 0.0 to 0.2.

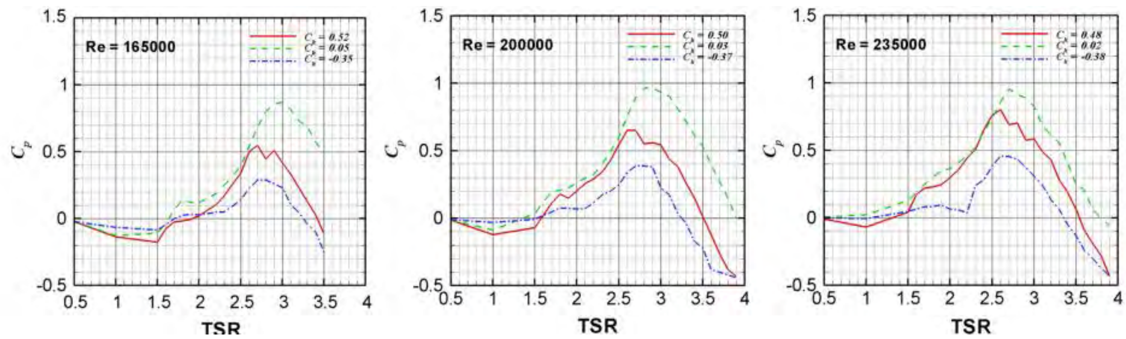

Figure 16: Power coefficient variation with clearance height at Reynolds number of (a) 165,000, (b) 200,000, and (c) 235,000 (Birjandi et al., 2013)

A study was accomplished by Kolekar & Banerjee (2015) on marine hydrokinetic turbines using numerical simulations in shallow water. The study revealed that when the turbine is positioned close to the free surface, the free-surface elevation rises, resulting in peak device performance. The device attains its highest performance, 40%, when the clearance coefficient is 0.20 (Kolekar & Banerjee, 2015). Furthermore, Zilic de Arcos et al. (2020) studied the blockage effect for axial-flow tidal turbines and compared the results to six blockage correction methods. Table 6 Blockage correction used in (Zilic de Arcos et al., 2020) displays the various blockage corrections utilized in the study.

Table 6 Blockage correction used in (Zilic de Arcos et al., 2020)

Reference	Equation	
(Glauert, 1933)	$\frac{U_T}{U_F} = \left(1 + \frac{\beta\, C_T}{4\sqrt{1 - C_T}}\right)^{-1}$	(4)
(Maskell, 1963)	$\frac{U_T}{U_F} = \sqrt{1 - \beta\, C_T (1 - k^2)^{-1}},$ $\forall (1 - k^2) = 0.3551 - 5.1050\beta$	(5)
(Pope & Harper, 1966)	$\frac{U_T}{U_F} = \frac{1}{1 + \epsilon_t}, \forall \epsilon_t = \frac{1}{4\beta}$	(6)
(Mikkelsen & Sørensen, 2002)	$\frac{U_T}{U_F} = \frac{1}{u + \frac{C_T}{4u}}$	(7)
(Bahaj et al., 2007)	$\frac{U_T}{U_F} = \frac{U_1/U_T}{(U_1/U_T)^2 + C_T/4}$	(8)

(Werle, 2010)	$\frac{U_T}{U_F} = 1 - \beta$ $C_{T_c} = \frac{(1-\beta)^2}{1+\beta} C_T$ $C_{P_c} = (1-\beta)^2 C_P$	(9)

where U_T and U_F are the channel undisturbed flow velocity and the equivalent free-stream velocity, respectively. U_1 is the velocity at the turbine plane according to the actuator disc model. In Equation (7), u depends on the axial induction factor, such as $u = 1 - a$.

The Glauert method, proposed in 1933, is usually employed for aircraft propellers, assuming an equivalent free-stream velocity at equal thrust in a flume or wind tunnel. However, it only applies to thrust coefficients less than 1 ($C_T < 1.0$). The Maskell proposal, introduced in 1965, is typically used for bluff bodies but has also been used for turbines and aerodynamic profiles. For low-speed wind tunnel tests with blockage ratios between 1% and 10%, the blockage correction described by Pope & Harper in 1966 is adopted. Wind turbines are typically corrected using the method proposed by Mikkelsen & Sørensen in 2002. Bahaj et al. proposed a correction method based on the actuator disc model, while Werle's method in 2010 has been considered for correcting the measurements near the maximum extractable power.

The research indicates that the Mikkelsen & Sørensen method is most suitable for horizontal axis turbines. The Bahaj correction can be used if the actuator disc model's induction factors are unavailable. The Maskell and Pope & Harper corrections are also recommended, but avoiding the Werle and Glauert methods for horizontal turbines is advisable.

Zhang et al. (2023) conducted tests and numerical simulations on three types of turbines - a ductless Archimedes screw hydrokinetic turbine (DAST), a Savonius turbine, and a high-solidity horizontal axis turbine - to investigate the correction methods available in the literature. Ross's bypass velocity method provided more accurate results for the DAST device. In the Savonius turbine case, Steiros's method (Steiros & Hultmark, 2018) was more suitable for corrections during operational states, while Alexander's method performed better at static states. Finally, Jeong's method was adequate for large blockage ratios, while Barnsley & Wellicome's method worked better for small blockage ratios in horizontal axis turbines.

A summary of research on blockage corrections for turbines is presented in Table 7, showing the device, the solidity ratio, the blockage ratio, and the correction factor employed in the analysis.

Table 7: Details of the correction factor in several turbines (D. Zhang et al., 2023)

Reference	**Device**	**Solidity Ratio**	**Blockage Ratio**	**Correction Factor**
(Kinsey & Dumas, 2017)[a]	Darrieus Turbine	0.25	13%, 265, 51%	7.36%, 14.2%, 37.3%
(Kinsey & Dumas, 2017)[a]	Horizontal Axis Turbine	0.17	20%, 50%, 60%	6.9%, 17.2%, 29.6%
(Ross & Polagye, 2020b)[a]	Horizontal Axis Turbine	0.16	35%	19.1%
(Ross & Polagye, 2020b)[a]	Darrieus Turbine	0.33	36%	27.6%
(Ryi et al., 2015)[a]	Horizontal Axis Turbine	0.06	8.1%, 18%, 48.1%	1.1%, 5.9%, 12.7%
(Abutunis et al., 2021)[a]	Horizontal Axis Turbine	0.2,0.3	19.3%	10.2%, 12.2%

(Bahaj et al., 2007)[a]	Horizontal Axis Turbine	0.07	7.5%, 17.5%	2.6%, 5.7%
(Zilic de Arcos et al., 2020)[b]	Horizontal Axis Turbine	0.06	10%, 20%, 40%	7.3%, 16%, 40.6%
(Jeon et al., 2015)[c]	Savonius Turbine	1.0	5.3%, 8.3%	6.9%, 9.5%
(Jeong et al., 2018)[c]	Darrieus Turbine	0.64	24.7%, 13.4%	9.1%, 26%
(Alexander & Holownia, 1978)[c]	Savonius Turbine	1.0	24.9%	37%
(Kinsey & Dumas, 2017)[a]	Horizontal Axis Turbine	0.17	10%, 20%, 50%, 60%	29.63%, 17.26%, 6.92%, 3.53%
(Zilic de Arcos et al., 2020)[d]	Horizontal Axis Turbine	0.06	40%	15.9%

a. Barnsley and Wellicome's method; b. Werle's method; c. Maskell's method; d. Pope and Harper's method

Note that Barnley and Wellicome's method is an iterative method to obtain the ratio between the stream-wise velocity through the rotor (u_T) and the confined condition with the flow speed (V_0) and depends on the bypass velocity (u_b). The methodology is expressed in Figure 17. The iterative process starts with a reasonable guess of u_b / u_w . After that, it solves u_T / u_w and V_0 / u_w and checks the error between two values of V_0 / u_w . Since this value minimizes, the method converges. Otherwise, new iterations are required to achieve convergence. This method is adequate for diffuser-augmented hydrokinetic turbines (DAHT) (Du et al., 2023).

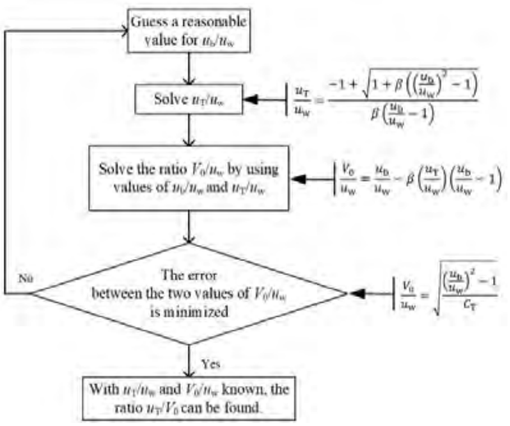

Figure 17: Flowchart of Barnsley and Wellicome's method (D. Zhang et al., 2023)

4.5.3 Modelling of arrays

Most research into turbine arrays has utilized computational fluid dynamics (CFD) techniques. These investigations examine how the interaction between turbines in a hydrokinetic farm can impact their performance, as well as the resulting changes in the flow (such as velocity profile, turbulence intensity, and blockage effect).

Chen et al. (2021) examined the interaction between the approaching flow and tidal turbine models in a multi-row array. Porous discs were used to represent the ten horizontal axis turbines arranged in a staggered configuration with four rows. The turbines' number decreased in the streamwise direction, forming an inverted triangle layout.

According to the study, the efficiency averaged over the rows mainly depends on the velocity of the approaching flow. This is due to the blockage effect, which increases the velocity but decreases because of the wake velocity deficit. However, the additional turbines deployed six turbine diameters downstream do not exhibit a local blockage effect. Consequently, the array performance does not improve as expected in a staggered configuration. When the wakes overlap, the disadvantage of the wake shelter is reinforced, while the advantage of the blockage acceleration is lost.

The study found that the load instability becomes significant as the shear-induced turbulence intensifies, primarily among the second-row turbines. However, instability is reduced by wake overlapping. In the end, the authors imply that this configuration resulted in an efficient array performance, as expected.

Figure 18 to Figure 20 demonstrate that the turbulence intensity notably affects the second row. The row notices a turbulence intensity of about 18%. As the distance from the first row increases, the decay rate gradually decreases to reach reasonable values, such as 13%. This setup positively impacts the overall performance of the first row, as shown in Figure 21.

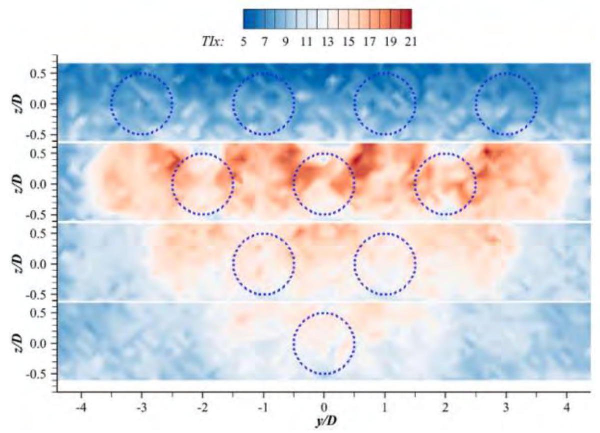

Figure 18: Streamwise turbulence intensity of approaching flow over the array cross-sections. From top to bottom, the cross-sections are located at 0D, 6D, 12D, and 18D, respectively. The blue dashed circles represent porous discs arrayed in each row (Chen et al., 2023)

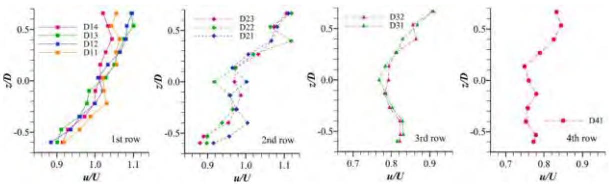

Figure 19: Vertical profiles of streamwise velocity along the vertical center axis of each disc in four rows array (Chen et al., 2023)

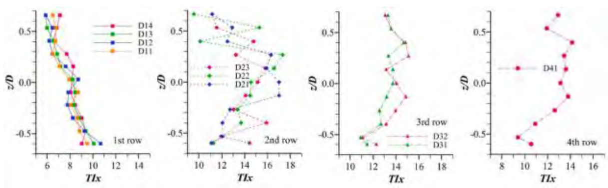

Figure 20: Vertical profiles of streamwise turbulence intensity along the vertical center axis of each disc in a rows array (Chen et al., 2023)

The data shows that the first row's thrust coefficient is significantly improved compared to a single disc with the same flow condition. With appropriate row configurations, this suggests that there is potential for more efficient energy capture. In the first row, D12 and D13 outperform D11 and D14. When an additional row is deployed downstream, the row-averaged thrust coefficient drops from 1.08 to 1.05. This is because the staggered discs in the second row block the flow passages between neighbouring discs upstream, causing an increase in the overall resistance of the array to the oncoming flow. Consequently, more mass flow bypasses the array, reducing the first row's performance.

Djama Dirieh et al. (2022) have developed a new methodology for designing tidal farm arrays, which utilizes the actuator disk method to simulate realistic flow fields around turbine arrays. However, this method does not consider the blockage effect, which may affect the power and thrust coefficients. To address this issue, the authors have integrated an analytical blockage correction into a three-dimensional model made in Telemac3D, which modifies these coefficients. According to their findings, the blockage corrections have resulted in a 3% increase in array production over a mean spring tidal cycle. Interestingly, the power production seems to decrease when the row number in the tidal farm is increased, as shown in Figure 22.

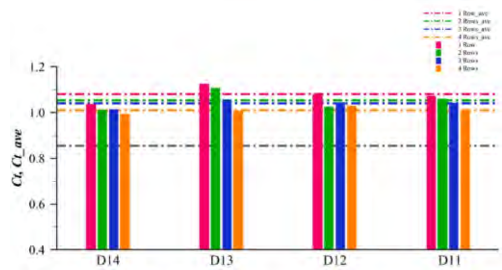

Figure 21: Thrust coefficient of each disc (bar chart) and averaged thrust coefficient of each row (dash-dotted line). The grey dash-dotted line indicates the thrust coefficient of a single disc installed in the flume. From top to bottom, the graphs show thrust coefficients for the first, second, third, and fourth rows respectively (Chen et al., 2023)

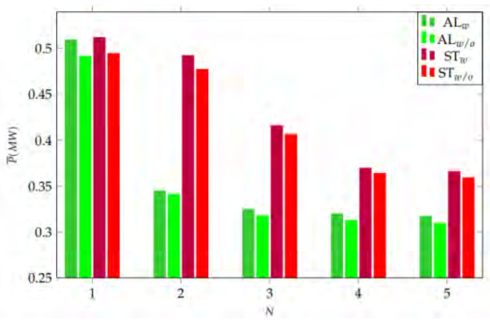

Figure 22: The mean production per row (N). For the aligned configuration, the lime green bar (ALw) corresponds to the case with blockage correction and the green bar (ALw/o) to the case without blockage correction. For the staggered configuration, the purple bar (STw) corresponds to the case with blockage correction, and the red bar (STw/o) to the case without blockage correction (Djama Dirieh et al., 2022)

Zhang et al. (2023) analyzed the wake interactions and performance in the twin-rotor configuration. According to their numerical analysis, the power fluctuation increases with the tip speed ratio. A single turbine's lateral velocity deficit cloud diagram is a half-elliptical contour with the hub at its center and the tip at its initial covertices. For twin turbines, these symmetric transversal distributions are broadly exhibited. Figure 23shows that high turbulence intensity values are computed six diameters (6D) downstream of the wake. This configuration causes symmetry in the wake, as illustrated by the graphs.

Similarly to the previous study, Soares et al. (2022) made two-dimensional simulations to estimate the efficiency of an S-shaped VAACT in a twin-rotor configuration. The results showed a 23% improvement in the turbine's performance (Soares et al., 2022a). Several new studies that model arrays of hydrokinetic turbines are presented in Table 8

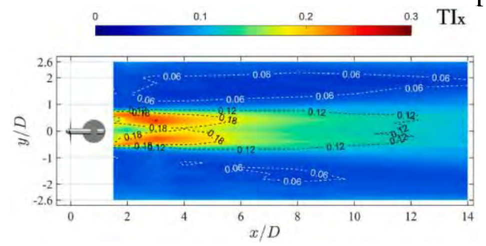

(a) Single-rotor

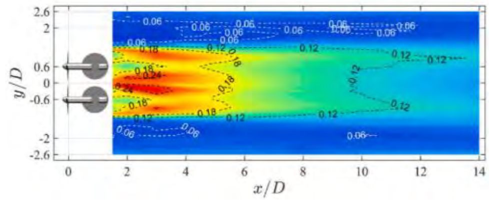

(b) 1.2D spacing

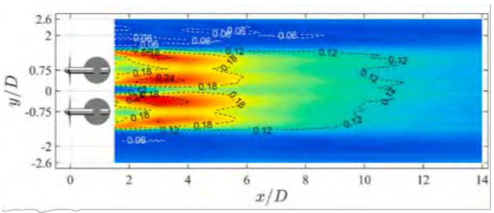

(c) 1.5D spacing

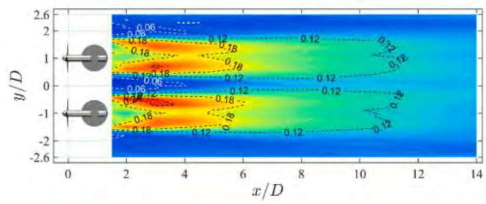

(d) 2.0D spacing

Figure 23: Horizontal wake TIx cloud diagram (Y. Zhang et al., 2023)

Table 8: Summary of modelling arrays (Nago et al., 2022)

Type	Author	Description
River	(Guerra & Thomson, 2019)	Experiment of a crossed flow turbine of 1.5m diameter, two rotors, and flow velocity of 2 m/s upstream in the river.
Tidal and	(Nuernberg & Tao, 2018)	Experimental study of four, three-blade tidal turbine systems testing several lateral and longitudinal distances between the turbines. V = 0.44 m/s (velocity near to average velocity) and D = 0.28m.

Type	Author	Description
Oce-anic	(Tedds, 2014)	An experiment in a channel with turbines of the horizontal axis of 3 blades, 0.5m diameter, and velocity equal to 0.9 m/s.
	(Tedds et al., 2014)	Experiment in a channel with horizontal axis turbines, 0.5m diameter, and an average velocity of 1 m/s.
	(Stallard et al., 2013)	Experiment with three blades and 0.27m diameter horizontal axis turbines. Longitudinal spacing between rows ranging from 4 to 10 D. V = 0.47 m/s.
	(Chawdhary et al., 2017)	A triangle diagram called Triframe is used in which a first turbine is positioned in the first row 2D away from the second row, which has two turbines. V = 0.27 m/s and D = 0.15m. It is an experimental and CFD investigation.
	(Hill et al., 2020)	Experimental study of a dual rotor tidal turbine model. V = 1.04 m/s and D = 0.5 m.
	(Ouro et al., 2019)	Study on a tidal turbine hydrokinetic park using the Large-Scale Simulation (LES) model associated with the actuator lines model to represent the various turbines of the hydrokinetic park. Depth-averaged velocity of 0.47 m/s.
	(Mycek et al., 2014b, 2014a)	Tests to evaluate the effects of the turbulence intensity on the wakes of a tidal turbine (isolated and with two associated turbines) of 0.7 m in diameter through experimental tests with an average current velocity of 0.8 m/s.

4.5.4 Blockage corrections for testing in water channels

To address blockage issues in hydrokinetic turbines, researchers have developed studies to obtain performance curves of the turbines at various test facilities. These tests are carried out at different blockage ratios, and the results are compared to analytical formulations from existing literature. This approach helps to identify potential blockage problems and find solutions to improve the turbines' performance.

Espina-Valdés et al. (2020) performed a numerical and experimental analysis on a small cross-flow turbine operating under high blockage effect conditions (β = 45% - 58%). The turbine's rotor, which measures 230 mm in chord and 300 mm in height, is connected to a timing pulley and extracts energy through a permanent magnet generator (PMG). The researchers employed an experimental setup, illustrated in Figure 24, which demonstrates that the significant blockage effect causes a deformation on the free surface, contributing to an improved turbine performance.

Analysis in Figure 25 compares the experimental and numerical results of model tests at a 306 m³/h flow rate. The numerical model doesn't account for mechanical losses, PMG performance, measurement errors, and turbulence model inaccuracies, resulting in slight differences in the results. Despite these factors, the experimental model performs well for tip speed ratios close to 1.0 - 1.5.

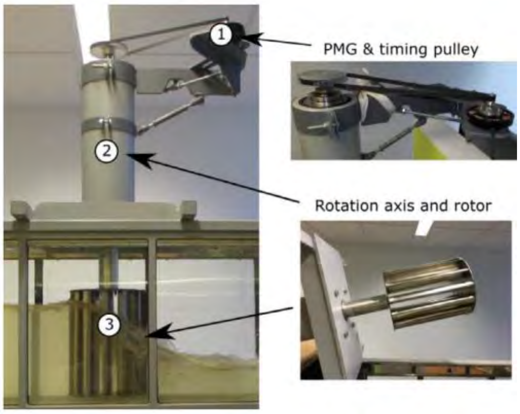

Figure 24: Experimental setup (Espina-Valdés et al., 2020)

Ross & Polagye (2020) examined blockage impact on the wake of a cross-flow turbine. The experiments were done at the University of Washington (UW). To measure the torque and forces experienced by the model test, two 6-axis load cells were placed at the top and bottom of the turbine's vertical axis. The rotational speed of the device was measured using a servo motor. Acoustic Doppler Velocimeters were installed at a gantry to capture the velocity pattern of the wake affected by the blockage effect of the test facilities in various cross-sections.

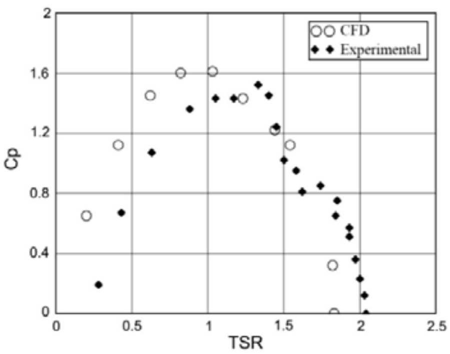

Figure 25: Power coefficient versus tip speed ratio at a flow rate of 306 m³/h (Espina-Valdés et al., 2020)

Figure 26 (a) presents the load cells, while Figure 26 (b) shows the velocity pattern. The experiments were conducted at BMSC and UW with 14% and 36% blockage ratios, respectively. The flumes were kept at the same water depth and temperature to ensure data consistency. Additionally, the experiments were designed to have equal chord-based Reynolds numbers and depth-based Froude numbers in both cases.

Note that this study presents similarities to the analysis done by (Ross & Polagye, 2020a). The study evaluated the effectiveness of several analytical blockage corrections for cross-flow and axial-flow turbines. The investigation found that increasing blockage improved turbine performance, resulting in higher thrust and power coefficients over a broader range of tip-speed ratios. The two corrections based on measured thrust performed the best, and these corrections were more effective for the cross-flow turbine than the axial-flow turbine. The corrections performed better for thrust than power, consistent with the analytical theory's assumptions.

(a) Schematic view

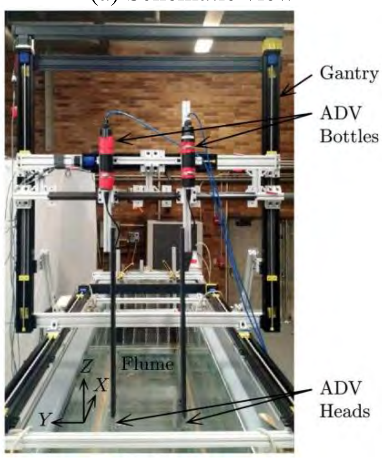

(b) Test setup

Figure 26: Experimental setup for the tests performed in (Ross & Polagye, 2020b)

Figure 28 displays the wake characteristics for two blockage ratios. These characteristics include mean streamwise velocity, turbulent kinetic energy (TKE), wake extent, and viscous dissipation. The bulk structure of the wake is similar for both blockage cases, and a noticeable wake recovery is observed in the vertical direction as the core flow reduces in size at increasing X/D. The velocity of both the core and bypass flows rises as the blockage ratio increases, as the graph in Figure 28 (a) indicates.

Figure 28 (b) displays TKE, which remains relatively low near the centre and edges of the measurement region, with a sharp increase in TKE at the shear layer regardless of the blockage ratio. As we move further downstream, the shear layer becomes less defined, and the TKE near the centre and edges of the profiles rises. The analysis indicates an increase in the magnitude of TKE in the shear layer at the higher blockage ratio. Still, the magnitude of TKE outside of the shear layer remains consistent.

The wake extent is shown in Figure 28 (c). The wake contracts vertically as the core and bypass flows mix but keep a constant width. The wake is smaller for the higher blockage case at each downstream position. Still, the size difference is primarily observed in the lateral direction, and the vertical extent is relatively independent of the blockage.

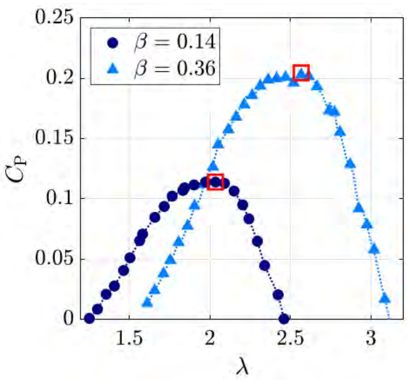

(a) Power coefficient curve

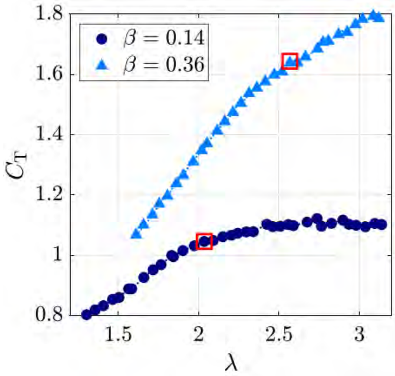

(b) Thrust coefficient curve

Figure 27: Results of power and thrust coefficients in the test facilities BMSC and UW (Ross & Polagye, 2020b)

Finally, Figure 28 (d) addresses the viscous dissipation rate. The dissipation rate is highest in the shear layer at X/D = 0.75 and X/D = 1.25 but is relatively uniform across the measurement region at X/D = 1.75 and X/D = 2.25. The magnitude of the dissipation rate increases with blockage. Closer to the turbine, this increase occurs primarily in the shear layer, while at further downstream positions, the dissipation rate increases throughout the measurement region. For a given blockage, the cross-sectional average dissipation rate remains relatively constant with the downstream position.

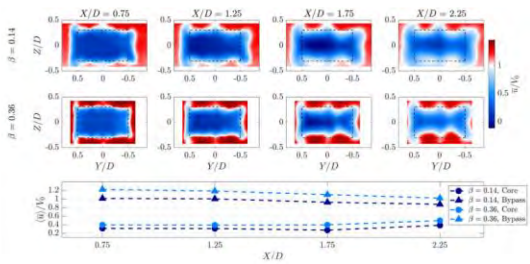
(a) Mean streamwise velocity profiles normalized by the free-stream velocity for both blockage ratios

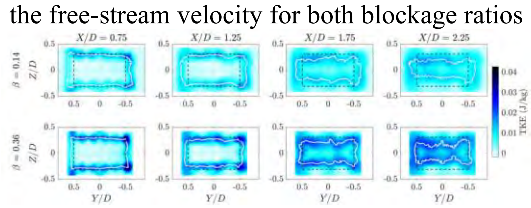
(b) Turbulent Kinetic Energy profiles for both blockage ratios

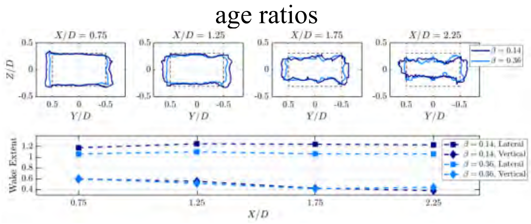

(c) Wake extent at both blockage ratios

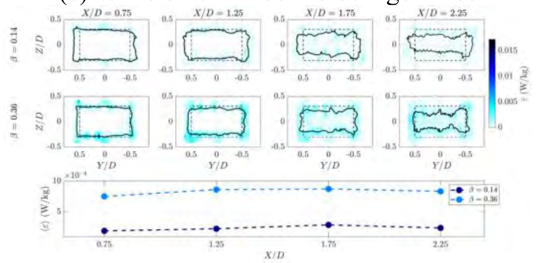

(d) Viscous dissipation rate profiles for both blockage ratios and dissipation rate averaged over each profile

Figure 28: Wake characteristics for both blockage ratios (Ross & Polagye, 2020b)

4.6 Offshore wind turbines

4.6.1 Development in model testing methodology

Reviews of the testing techniques employed for floating offshore wind turbines (FOWT) were recently published (Otter et al., 2021), (Chen et al., 2022), (Shi et al., 2023). They notably present the evolution of reproduction of aerodynamic loads on FOWTs in wave tank experiments, using either physical wind or real-time hybrid methods.

4.6.1.1 Real-Time Hybrid Model testing

Various works focusing on the real-time hybrid methods (RTHM), or software-in-the-loop (SIL), have been carried out over the last years in numerous wave tank testing facilities. These approaches have been developed in the last decade and aim at including the aerodynamic force acting on a turbine model using an actuator. This enables to overcome the difficulties in scaling down the aerodynamic loads with physical wind. The rotor is not represented with rotating blades generating aerodynamic loads, but with actuators (either cable driven robots or propellers), and the thrust can be calculated with a simple numerical model such as a drag disk model or a coupled servo-aerodynamic solver. The difficulties then lie primarily in the accuracy of the produced forces and in the speed of the real-time system.

(Bonnefoy et al., 2024) sorted existing hybrid systems for wave-tank testing according to a limited number of criteria. The following details the comparison of some of the systems presented in the recent literature, the overview is shown in Table 9.

4.6.1.1.1 Complexity of the aerodynamic model used in the real-time simulation

Some models use a simple formulation of a drag disk to represent the action of the wind on the rotor. The thrust is calculated in a very short time, with the simple use of thrust and possibly torque coefficient precomputed and stored in a look-up table, as a function of the tip speed ratio (TSR). This method is efficient, but the consideration of complex wind turbine controllers is not possible. Examples can be found in (Matoug et al., 2020), with a study on 10 MW horizontal and vertical axis wind turbines, or (Otter et al., 2022), with a study on the NREL 5 MW turbine.

Other models use a real-time servo-aerodynamic simulation of the rotor to calculate the force to be reproduced at model scale. The measured position and velocity of the physical model serve as inputs to the simulation, which can run at full scale, and the calculate force to be replicated is then Froude-scaled. A modified version of the NREL OpenFAST solver is for example used in (Azcona et al., 2019) or in (Bonnefoy et al., 2024). The simulation should be based on a simple model to be able to run in a very short time. The Blade Element Momentum is commonly used.

4.6.1.1.2 Number or components or dimensions of the reproduced force

In many studies, only the axial thrust force is being used. Consequently, the other forces induced on the rotor, e.g. aerodynamic yaw moment and gyroscopic effect, cannot be considered. This is for example the case in (Azcona et al., 2019), (Arnal, 2020), both with a propeller, and (Hall and Goupee, 2018), with a cable robot.

It is also possible to actuate a force with more than one dimension. This can include for example an asymmetrical thrust and the induced yaw moment (Ha et al, 2023). Other multi-component RTHM systems can include over two components, such as (Urbán and Guanche, 2019) that reproduces the thrust force, the rotor torque and the pitch and yaw moments, (Thys et al., 2018, Thys et al., 2021) that reproduce all force components (except for the vertical load) using a cable-driven parallel robot, or (Bonnefoy et al., 2024) that reproduce the same 5-component force using propellers.

4.6.1.1.3 The type of actuators

To date, most of the actuators make use of propellers but some use cable-driven parallel robots (Table 9). The latter makes it compulsory to implement a feedback loop to control the force applied by each winch.

4.6.1.1.4 The measurement and control of the actuated force

(Gueydon et al., 2023) emphasized the importance of the measurement of the applied force for the analysis of the measurements. (Bonnefoy et al., 2024) and (Mojallizadeh et al., 2024) present the strategy used to implement a feedback controller on a multi-component propeller-based actuator to improve the speed and accuracy of the RTHM system.

The cable-driven parallel robots are controlled with a feed-back loop, which is necessary with these systems (e.g. (Hall and Goupee, 2018), (Thys et al., 2018), (Thys et al., 2021), (Antonutti et al., 2020)), and most of the propeller-based RTHM systems use an open-loop control for more simplicity (e.g. (Urbán and Guanche, 2019), (Ha et al, 2023), (Azcona et al., 2019), (Vittori et al., 2022)), except (Bonnefoy et al., 2024) that implemented a feedback control loop as used in (Hegazy et al., 2024) to test and validate new control laws for FOWTs.

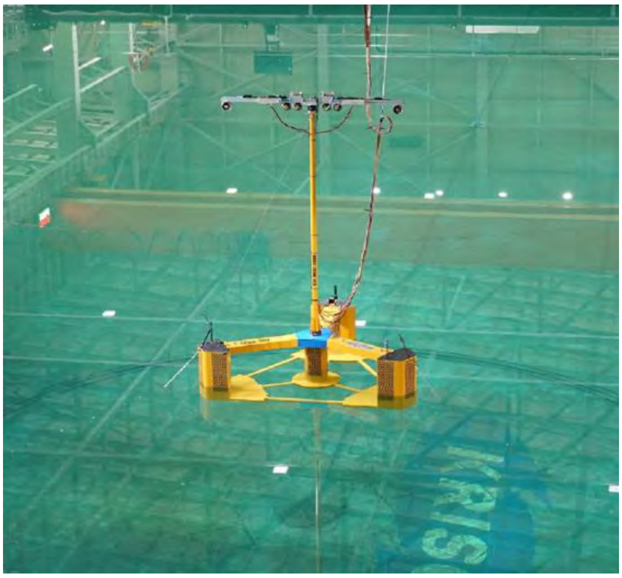

Figure 29: 10 MW class floating offshore wind turbine model with an actuator composed of ducted fans, able to reproduce thrust and yaw moments on the tower top, at the KRISO ocean engineering wave tank (Ha et al., 2023)

Table 9: Synthesis of the recent RTHM systems referenced in the literature (non-exhaustive). Fx corresponds to the axial thrust force, and Fz to the vertical force

Reference	Force calculation	Actuator	Force components						Force control
			Fx	Fy	Fz	Mx	My	Mz	
Hall and Goupee, 2018	RT simulation	Cables	x						Feedback
Thys et al., 2018	RT simulation	Cables	x	x		x	x	x	Feedback
Geydon et al., 2018	Look-up table	Cables	x				x	x	Feedback
Azcona et al., 2019	RT simulation	Propellers	x						open-loop
Urbán and Guanche, 2019	RT simulation	Propellers	x			x	x	x	open-loop
Arnal, 2020	RT simulation	Propellers	x						open-loop
Matoug et al., 2020	Look-up table	Propellers	x						open-loop
Antonutti et al., 2020	RT simulation	Cables	x				x	x	Feedback
Vittori et al., 2022	RT simulation	Propellers	x				x	x	open-loop
Otter et al., 2022	Look-up table	Propellers	x			x			open-loop
Ha et al., 2023	RT simulation	Propellers	x					x	open-loop
Bonnefoy et al., 2024	RT simulation	Propellers	x	x		x	x	x	Feedback

The delay can be defined as the time delay between the theoretical force that should ideally be applied at a given instant on the physical model and the force that is physically reproduced by an actuator. However, a generalized and common formulation of the force delay is still to be defined. In addition, the quantification of the total delay of the RTHM system is highly valuable in order to increase confidence in the fidelity of a RTHM system, notably for the reproduction of aerodynamic damping, which is critical for FOWTs.

The variety of developments in RTHM systems raises new questions. (Gueydon et al., 2023) points out the importance of the measurement of the force applied by the actuator. This enables a better understanding of the tests performed, identifying uncertainties and eventually a better comparison with numerical models. As pointed out in (Bonnefoy et al., 2024), a feedback controller on the applied force enables the system to reach an improved accuracy in the reproduced force (in both amplitude and delay reduction).

All actuators are limited in frequency. In most cases, they can follow the reference force on the low and wave frequency forces present in the aerodynamic force. Discrepancies arise for higher frequencies, including the 3P and the 1st tower bending mode frequencies when it is scaled on the physical model. This is notably where the presented RTHM systems may differ.

4.6.1.2 Physical wind

The testing of FOWTs with wind physical wind and rotor blades is also being carried out in different research facilities. As presented in (Chen et al., 2022), such realization of the aerodynamic loads on scaled models can be performed using either geometrical scaled blades or performance-matched blades. In the former case, the blades dimensions are scaled using the same scaling factor as for the rest of the geometry. The Reynolds numbers occurring on the blades are then much lower than on the full-scale blades, and the induced aerodynamic effects may not be well represented. In the latter case, the blades are scaled down with a geometry that replicates closer thrust and power curves for the considered rotor.

Design procedures for these performance-matched rotors are for instance presented in (Wen et al., 2020). (Chen et al., 2018) presented a comparative study of the dynamics observed during model tests of a platform with both approaches. Mainly, the two approaches reach a good agreement, but the performance-matched model leads to a better aerodynamic modelling than the geometry-scaled rotor (notably on the aerodynamic damping). The geometry and mass distribution however lead to differences in the gyroscopic effect, tower modes response, particularly since the 3P frequency of the geometrical-matched rotor is close to the tower eigen frequencies in the study from (Chen et al., 2018).

(Chen et al., 2022a) used a geometry-matched rotor to study the NREL 5 MW turbine supported by the OC3-Hywind spar platform at a scale 1/50. The control of the rotor was reproduced, but with a constant pitch angle for each test. The elastic properties of the tower were also captured. The analysis observed significant coupled motions between all platform rigid degrees of freedom, including a yaw response of the system. The nP harmonics in the aerodynamic force and the double frequency wave effects (second-order hydrodynamic loads) triggered the resonance of the tower bending. The latter was shown to be dominant in the resonance of the tower, highlighting the importance of high-frequency wave loads.

In (Wen et al., 2022), the analysis of the NREL 5 MW turbine supported by a spar platform with a reduced draft (50 m, full scale) was presented at scale 1/50. The spar is a redesign of the OC3-Hywind platform for moderate depth water. The blades of the rotor were geometrically scaled. The effects of the wind loads were investigated, for example by means of decay tests without wind, and with wind for a parked and rotating turbine. This shows the alteration of the surge natural frequency (mainly due to the altered mooring stiffness at a shifted position under the action of wind thrust) and damping by the aerodynamic loads. White noise wave tests were also performed without wind and with wind for an operating turbine. This exhibited that the presence of wind on the operating turbine increased the surge response, while strongly damping the pitch resonance. A significant yaw motion was also observed, probably due to the cumulated effects of imbalanced loads, mooring restoring force and gyroscopic effect as the turbine pitches.

(Madsen et al., 2020) makes the analysis of the DTU 10 MW turbine supported by a Tension Leg Platform (TLP), with a performance-matched and pitch-regulated rotor at scale 1/60. The collective blade pitch is dynamically controlled with an actuator. This experimental set-up allows the investigation of three controllers, including an open-loop controller (fixed pitch), a closed-loop controller tuned for an onshore turbine and a closed-loop controller tuned for a floating offshore wind turbine, all with collective blade pitch angle control. Their effects on the turbine dynamic response in different environmental conditions are studied. Therefore, the controllers are tuned to match the scaled thrust curve rather than the torque, as the response of the model rather than its power production is at stake in this study. The known phenomenon of negative damping with the onshore closed-loop controller was then observed during the wave tank testing, resulting in amplified motions of the turbine. The offshore controller led to a large surge displacement after shutdown, which was explained in terms of alteration of the aerodynamic damping. Amongst other conclusions, this work demonstrates that control algorithms for floating offshore wind turbines can be tested and validated with this type of experimental set-up, including Froude scaled floaters and performance-matched rotors at reduced scale.

(Yang et al., 2021) present a study on a 6 MW turbine supported by a spar platform of 76 m draft. The study considers a thrust-matched rotor. The study is made at scale 1/65.3 to match the full scale 100 m water depth in the wave tank. It focuses mostly on the low-frequency loads that would occur in an intermediate draft configuration (100 m). A comparison is made between the experimental measurements and FAST simulations. The study concludes on the importance of second order loads in the prediction of the low-frequency motions in both vertical and horizontal plane. In particular, the full QTF formulation improves the prediction of these loads and oscillations compared to Newman's approximation. The wind and current loads can typically decrease the low natural frequencies of the system and increase the low-frequency response of the platform. They however only have little effect on the wave frequency response, where the wave loads are dominant.

(Guo et al., 2024) analyses a 12 MW rotor supported by a semi-submersible platform (tri-floater) at scale 1/70. The scaled rotor is thrust-matched, and the tower is stiffness- and geometry-matched, with a use of a light foam ring around the stiffness-matched tower. This allows a better reproduction of the aerodynamic loads on the tower. No dynamic blade pitch control was considered, but a constant blade pitch angle was set at the start of each condition. The study focuses on various environmental conditions, including waves, wind and current. It is for example highlighted that the presence of current significantly decreases the pitch motion of the turbine and the tower base loads. With strong environmental conditions, it is observed that the standard deviation of mooring loads and motions increase notably when the wind exceeds the cut-out wind speed. In operating conditions, the tower top loads are driven by the 3P effects for the shear load, and by the 1P effect for the bending moment.

4.6.1.3 Structural elasticity and internal loads (floating)

The structural elasticity and internal loads of the platform of floating wind turbine are challenging to study. Experimentally, structural similarity is possible at model scale for the tower, choosing a material (with given density and Young's modulus) and a geometry (diameter and thickness distribution) that enables to reproduce the eigen frequencies and possibly the shapes of the first structural modes. This is however difficult for the support structure because the geometry is constrained by the Froude scaling of the hydrodynamic loads on the outer shell. It is also possible to investigate internal loads on a rigid structure (as done on ships for instance), but this requires a very stiff structure, to keep all eigen frequencies away from the frequency window of interest in the tests. For example, to investigate the vertical bending moment in the ITTC-ISSC container ship benchmark reported by (Kim and Kim, 2016), (Bouscasse et al., 2022) chose to have a natural frequency over 20 times larger than the wave frequency when $\lambda_{wave} = L_{pp}$ (λ_{wave} being the wavelength and L_{pp} the length between perpendiculars). This enabled an accurate analysis of strongly non-linear effects on the wave-structure interaction for this ship without the alteration of the measurements by the vibrations of the structure. This section presents a few studies made on elastic platforms for wind turbines.

A wind turbine supported by a lightweight semi-submersible was studied in (Suzuki et al., 2019) using an elastic model. The tower is supported by guywires for increased stiffness and mass reduction. The semi-submersible platform is composed of a central column carrying the turbine and three side columns on the side (at 120° from each other), connected with pontoons to the central column. Guywires connect the side columns to the tower top (the tension in the guywires is adjustable). The authors present a 1/80 elastically and dynamically scaled model of the turbine, scaling the bending stiffness of the pontoons. To do so, a segmented backbone (or skeleton) is designed as shown in Figure 30. The structural stiffness is scaled by the backbone and the geometry of the shell is scaled to respect the Froude scaling law. Strain gauges are mounted on the flexible beams. The model was tested in the Ocean Basin of University of San Paulo. The analysis is mostly focused on the effects of the side columns inclination and of the guy-wires tension on the dynamic response of the turbine.

Following a similar strategy, (Takata et al., 2021) designed a 1/50 scaled flexible semi-submersible tri-floater shown in Figure 31. The whole floater is made flexible thanks to an elastically scaled skeleton and geometrically scaled floaters. The skeleton (or backbone) was made of stainless steel, and the design of thin beams enabled to down-scale the bending stiffness modulus EI, where E is the Young's modulus and I the inertia of the beam section. Strain gauges are mounted at different positions on the backbone. The study focused primarily on regular waves, showing significant elastic response of the structure, and in particular a coupling between the bending of the pontoons and the heave response. This indicates the importance of elastic effects in the design of such a platform. Comparisons with a numerical Morison based model showed a good agreement with the experimental measurements.

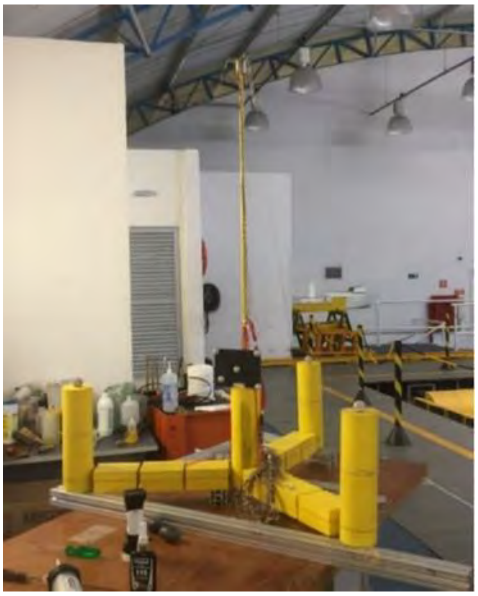

Figure 30: Flexible model presented in (Suzuki et al., 2019)

(Liu and Ishihara, 2021) also studied a flexible semi-submersible platform designed for a 2 MW turbine at a scale of 1/60. The flexibility of pontoons and braces is included in the model (green sections in Figure 32), where the bending stiffness modulus K=EI of the elements are scaled according to Froude scaling law, meaning $K_{ms} = \frac{K_{fs}}{\lambda^5}$, where *ms* and *fs* refer to model and full scale respectively, and λ is the scaling factor.

(Leroy et al., 2022) designed a flexible spar platform supporting a wind turbine at the scale 1/40. The FOWT model was tested in the ocean engineering wave tank of Ecole Centrale de Nantes in France. The platform was composed of a central backbone, providing a Froude-scaled 1st bending mode frequency, with light floaters mounted around to provide Froude-scaled hydrodynamic loads, as shown in Figure 33.

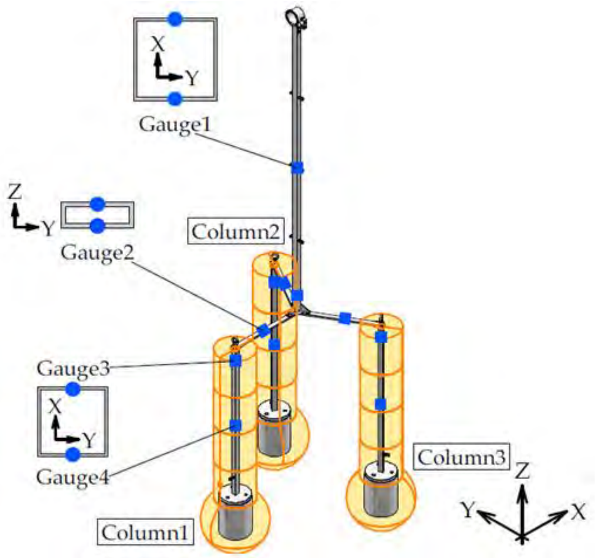

Figure 31: Flexible semi-submersible tri-floater modelled in Takata (et al. 2021)

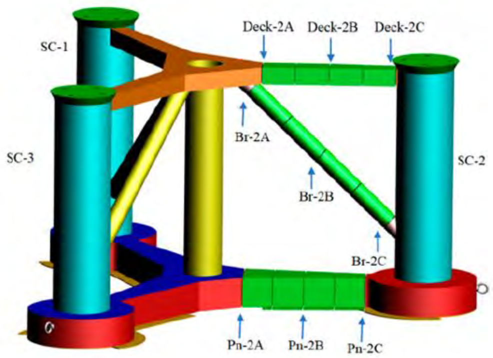

Figure 32: Flexible semi-submersible platform studied in (Liu and Ishihara, 2021)

The study includes decay tests, regular and irregular waves of various steepness. Studying the bending of the spar and its vibrations in various steep sea-states, the authors conclude on the importance of non-linear hydrodynamic loading in the emergence of resonant responses, as springing/ringing response of the structure is observed at the natural bending mode frequency. For example, Figure 34 shows the bending strain in the platform during an extreme sea-state (Hs

= 10.9 m and Tp = 13.8 s) at three different locations. The wave frequency response is clearly identified in the window [0.05; 0.18] Hz (at full scale), and the natural modes of surge and pitch are seen at lower frequencies. The peak at 0.38 Hz corresponds to the springing/ringing response occurring when steep wave packets reach the platform. No aerodynamic loads were considered in this study. The measurements have been published online as open-data (Leroy et al., 2024) and a comparison to low/intermediate fidelity numerical tools (based on linear potential flow and Morison equation) was also published (Ran et al., 2023).

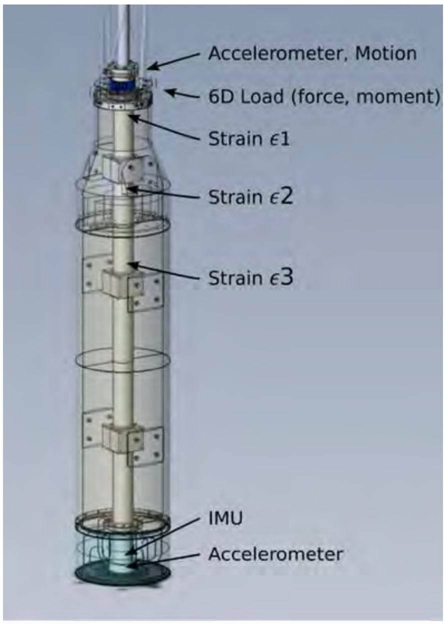

Figure 33: CAD view of the 1/40 scaled flexible spar designed and tested in (Leroy et al., 2022)

Lastly, (Hansen et al., 2024) presented an extensive analysis of high-order loads on a flexible semi-submersible platform. The model is a simplified semi-submersible presented in Figure 35. It is made of two columns, connected with a flexible pontoon beam. Two values of structural stiffness have been tested for the pontoon, leading to two different natural frequencies for the 1st flexible mode.

To the knowledge of the authors, the analysis presents a four-phase separation method applied for the first time for a floating body. This allows a decomposition of the response of the turbine into the 0th and four first harmonics from irregular wave measurements. The inertia- and drag-driven contributions to the response can then be identified. Linear and non-linear wave-structure interaction terms can then be studied, emphasizing the importance of quadratic drag second order forcing terms in the modelling of such structure. For the soft configuration, a second-order potential flow theory based numerical model with drag was able to calculate the system's response, after calibration of the damping coefficients. Some deviation remained because of a slightly wrong estimation of the even-harmonic content of the loads. For the stiffer case, with a natural bending mode larger than the wave frequency range, the resonant response observed in the tests was not accurately, even after calibration of the damping.

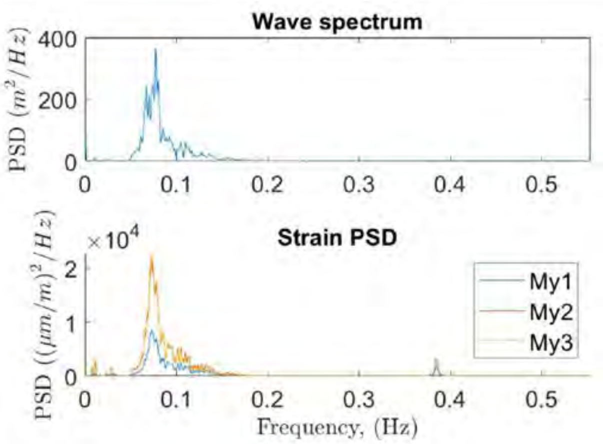

Figure 34: Bending strain power spectral density measured in the flexible platform in an extreme sea-states (Hs = 10.9 m and Tp = 13.8 s) in (Leroy et al., 2022)

The four-phase decomposition identified the forcing as third or higher harmonic in severe sea-state states. A second order based model was then unable to predict the bending resonance, even with drag. This study confirms the importance of experimental analysis on non-linear wave-structure interaction. Non-linear wave forcing terms could lead to resonant vibration outside the wave frequencies, and beyond 2nd order wave loads that can usually be included in numerical simulations.

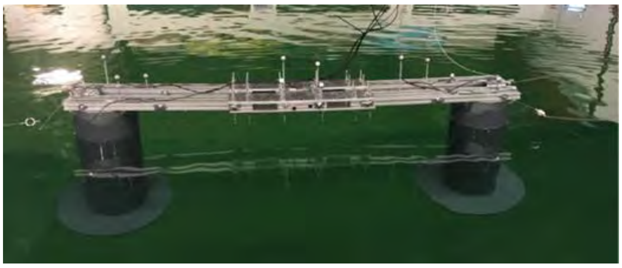

Figure 35: Simplified semi-submersible platform used in the DHI ocean tank in (Hansen et al., 2024)

4.6.2 Influence of the vertical wind profile on the operation and efficiency

The vertical wind shear profile is often modelled using a power law and a constant shear profile. However, the shape of the wind shear profile will vary, both in time and in location. The various wind profiles will influence both the power produced by the wind turbines and the loads on the wind turbine structures.

The vertical wind profile can vary for different reasons. Onshore, the different roughness in the terrain will have a great impact. However, offshore the sea is relatively smooth and the main driver for different wind shear profiles are temperature gradients. Inside the atmospheric boundary layer, the atmospheric stability is important for the shape of the vertical shear profile. The atmospheric stability is a measure of the vertical motion of air parcels. In unstable atmospheric conditions the air parcels will move upwards, while in stable atmospheric conditions these motions will be downwards. Normally one assumes that neither happens, so there is no vertical motion of the air parcels, this is neutral atmospheric conditions (Pérez Albornoz et al. 2022).

Typical wind shear profiles are shown in Figure 36. The profiles here are using the Monin-Obhukov similarity theory, which was developed for onshore but is shown to also be valid offshore (Edson and Fairall, 1998), and a log-law relationship for the vertical variations of mean wind speed (Alblas et al., 2014).

In the study by Sathe et al. (2013), wind shear for different stability conditions at 10 m/s was investigated for a 5.5 MW wind turbine at hub height 100 m. Considering the different atmospheric conditions at offshore wind sites, it was shown that it is not conservative to assume that the wind shear is always logarithmic when estimating fatigue lifetime for the blade root. Based on the findings, the largest fatigue is found for large wind shear conditions, which are often related to stable atmospheric conditions. Measurements from several offshore wind sites indicate that the stable atmospheric conditions occur often. Figure 37, taken from Alblas et al. (2014), shows the distribution of stability class at the two offshore windfarms Egmond aan Zee (OWEZ) and North Hoyle.

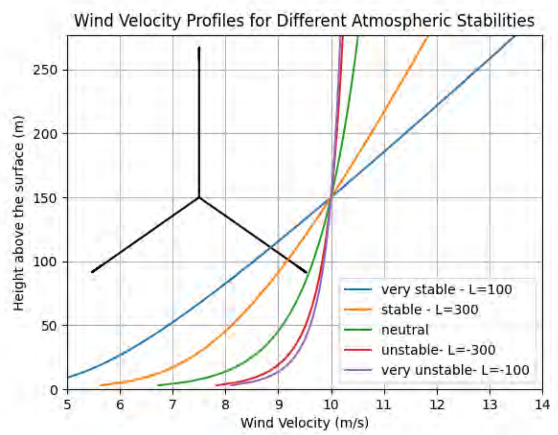

Figure 36: The vertical wind profile for different heights, considering five different stability conditions. The wind turbine in the back has the same dimensions as the IEA 15 MW, with hub height 150 m and blade length 117 m. The reference speed is 10 m/s at 150 m (hub height).

The wind shear does not have a direct impact on the power production, if one considers the wind speed at hub-height. If one considers wind speed measurements lower than hub height and extrapolate to hub height, the wind speed at hub height will depend on the wind shear and consequently the controller will behave differently depending on the wind shear (Lange et al. 2004; Motta et al. 2005).

It is important to note that the atmospheric stability also has an influence on the turbulence.

The stable conditions have typically low turbulence, while the unstable conditions have more turbulence. For a wind farm the turbulence is important for wake length. High turbulence has a shorter wake compared to the lower turbulence (Alblas et al., 2014). Figure 38 shows the simulated wake losses at OWEZ and North Hoyle, and it is seen that the very unstable conditions with high turbulence and little vertical shear have less wake loss and higher power production.

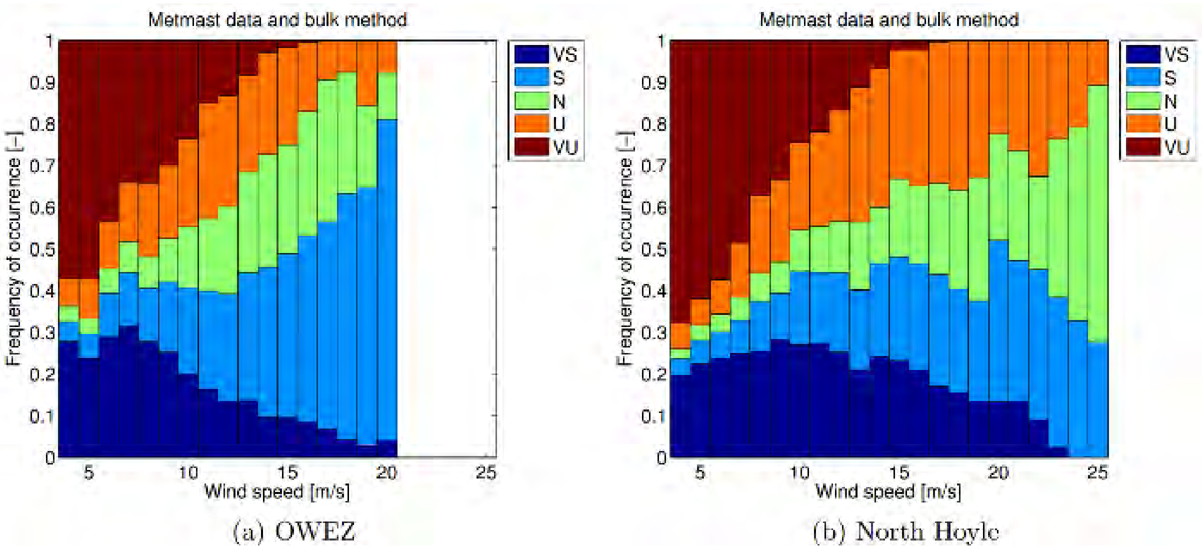

Figure 37: The distribution of stability classes versus wind speed at OWEZ and North Hoyle. VS=very stable, S=stable, N=Neutral, U=Unstable, VU=very unstable. Courtesy to Laurens Alblas, figure from Alblas et al. (2014).

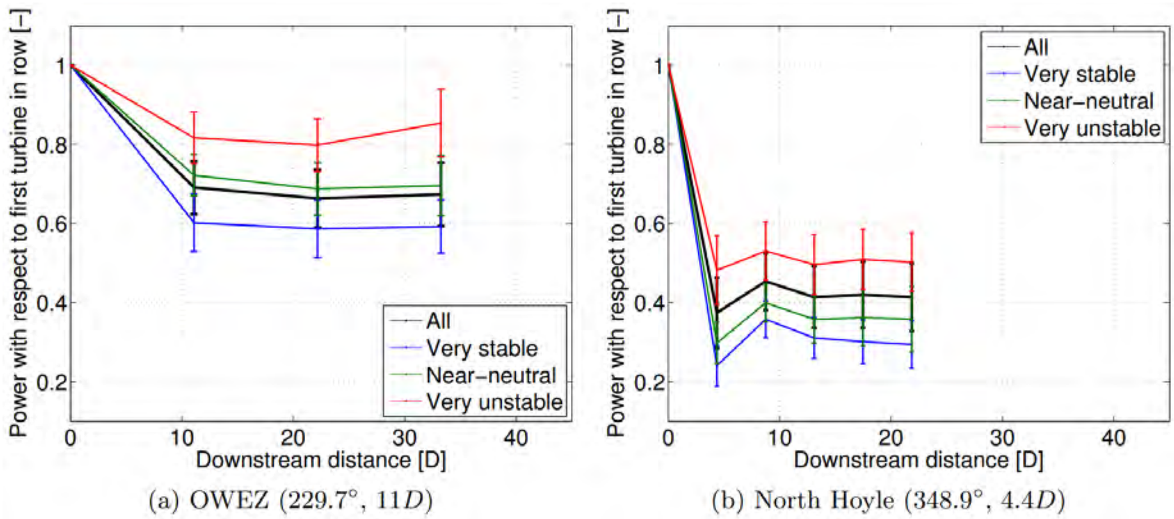

Figure 38: Simulated wake losses at (a) OWEZ and (b) North Hoyle at wind speed 8m/s. The error bars are one standard deviation. Courtesy to Laurens Alblas (Alblas et al., 2014).

Power production for wind farms is typically estimated using so-called actuator disc models. In these models the rotor is considered as a disc that extracts the energy from the incoming wind. The power produced by a wind turbine is proportional to the cube of the inflow wind speed, the disc area and a power coefficient, C_p, representing the efficiency of the turbine in extracting power from the wind. There exist various methods on how to formulate the inflow wind speed. The traditional approach is to consider the hub height wind speed (HHWS). However, the wind speed at hub height is not necessarily representative of the average wind speed across the rotor, especially offshore and for large wind turbines where there can be large variations in the wind profile across the rotor disc due to the atmospheric boundary layer. An alternative is to use a rotor-equivalent wind speed (REWS) model where the wind field is averaged over the area swept by the rotor blades. There are also modifications to these models that accounts for variations of wind direction, or wind veer, across the rotor disc. These methods have been applied in several studies to examine the importance of wind shear on power production, and an extensive review is given by Lopes (2021) who concluded that the choice of model will affect the estimate of power production. A few recent publications are summarized below.

Murphy et al. (2020) studied how wind speed shear and directional veer affected wind power production for a megawatt size wind turbine, employing various modelling strategies including different shear and veer metrics. Their conclusion was that REWS emerges as the most predictive metric, showcasing significant correlations with power production across a wide range of wind speeds for the specific site considered. Exploring wind power prediction at the Anholt Offshore Wind Farm in Denmark, Ryu et. al (2022) compared the effectiveness of REWS methods with the traditional HHWS method using two years of SCADA data. Results indicated that REWS tends to provide more accurate predictions than HHWS. However, this was not always consistent, likely due to variations in local atmospheric stability condition. It is therefore important to assess nearby atmospheric stability characteristics to determine whether REWS or HHWS will provide more reliable power output predictions.

The actuator disc model simplifies the representation of the rotor by treating it as a disc that extracts kinetic energy from the wind passing through it, while the BEM method divides the rotor blade into multiple elements along its length and calculates the aerodynamic forces acting on each element. The BEM method enhance the level of complexity and details in calculating the aerodynamic performance of the wind turbine. It is generally used for aerodynamic load calculation on rotor blades in design codes, but less applied for wind power production estimates as it is more computational demanding compared to the actuator disc model.

Mata et al. (2023) examined the impact of wind speed and direction shear on wind power production by analysing LiDAR measurements alongside SCADA power measurements. The study compared HHWS and REWS with a blade element momentum (BEM) model based on their ability to account for wind shear effects. The BEM model demonstrated the highest correlation and lowest overall error with the SCADA measurements. The research highlighted the importance of accurately modelling wind shear for wind energy resource assessment and turbine design. Sensitivity analysis of the BEM model revealed its dependence on factors such as induction and turbine control. Thus, future research should include refining aerodynamic models to better account for wind shear effects and improve the tip-speed ratio estimation based on the wind conditions.

The BEM method was applied by Li et al. (2018) when they investigated the effect of wind field on the power generation and aerodynamic performance of a 5MW floating wind turbine. Three different wind fields were considered, namely a uniform wind field, a steady wind field with wind shear, and a turbulent wind field. Six different load cases were studied with wind speeds both below and above rated wind speed. All the three wind fields had the same mean wind speed at the hub height. The result from the analysis showed that the wind shear had very limited effect on the power generation and thrust force compared to a uniform wind field. But the wind shear caused noticeable effect on the local aerodynamic loads applied on the individual blades. Introduction of turbulence had also little effect on the mean power production and mean thrust force. However, the standard deviation of both power generation and thrust force increase significantly with turbulent wind. They observed a difference in the reaction of the power generation due to low frequency turbulence depending on the operational state. This was attributed to the two different wind turbine controllers which are active in different operational states. Furthermore, the paper concluded that both fatigue and extreme loads increase with wind shear and inflow turbulence, and thus a uniform wind field is not sufficient for the analysis of the floating wind turbine behaviour.

For illustration purposes, the power production is simulated for the different shear profiles shown in Figure 36 using an aero-elastic code based on the BEM-method. A model of the IEA 15 MW (Gaertner et al. 2020) is used in the simulations.

Table 9 shows the results for the different shear profiles with a reference wind speed of 10 m/s at 150 m height. There are few differences seen in the mean values, but it is also important to consider how the loads will vary during the rotation of each blade. Figure 39 shows the blade root bending moment for different shear profiles. The very stable load case with high shear, gives a higher amplitude for the load cycle. The wind profile with the lowest shear gives a lower amplitude in the load cycle. Similar results were also found by (Sathe et al. 2013).

Table 10: Mean values of wind speed at hub, power produced, blade pitch and the out-of-plane bending of blades. *OOP stands for Out-Of-Plane, ** FA – fore-aft.

Parameter	Very stable	Stable	Neutral	Unstable	Very stable
U_hub [m/s]	10	10	10	10	10
Power [MW]	9.9	9.7	9.6	9.7	9.7
Blade pitch [deg]	3.4	3.4	3.4	3.4	3.4
Blade root bending moment (OOP*)	32.9	32.9	32.8	33.0	33.0
Blade tip displacement (OOP*) [m]	7.4	7.4	7.4	7.4	7.4
Tower base bending moment (FA)	-104	-99.6	-95.5	-94.7	-94.6

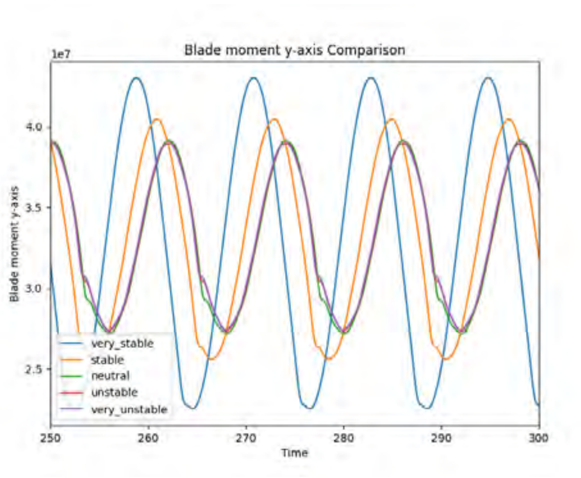

Figure 39: The blade root bending moment (OOP) with different shear profiles. The wind speed is 10 m/s at hub height for all load cases.

4.6.3 Offshore wind farm numerical modelling

Compared with onshore wind farm, floating offshore wind farm suffers more power deficit attributed by low turbulence intensity of high-quality wind resources (Xu et al, 2022). In addition, the tilting angle of FOWT will also affect the wake performance and velocity deficit (Wang et al, 2022). High-fidelity CFD simulations in combination with actuator disk or actuator line model were used, due to its computational efficiency, to reveal the underlying physical mechanism of wake interactions for floating offshore wind turbines.

Rezaeiha and Micallef (2021) utilized ANSYS Fluent in combination with an actuator disc model to investigate the aerodynamic wake interactions of two tandem NREL 5MW FOWTs. A prescribed surge motion was imposed on the upstream rotor while the downstream one was kept fixed. They revealed that the surging motion of the upstream rotor enhanced flow mixing in the wake, which accelerates the wake recovery of the downstream rotor. These findings suggest prospects for further research on the optimization of wind farm layouts for FOWTs, to achieve more compact arrangements.

Arabgolarcheh et al. (2022) developed an actuator line model (ALM) by implementing a dedicated C++ library with OpenFOAM for exploring the near wake characteristics of FOWTs. The implemented numerical approaches are a great advantage in terms of computational efficiency compared with blade-resolving CFD methods. They revealed that the distance between two successive vortex rings and their strength undergo periodic changes in accordance with the prescribed surge motion. These variations render the intermediate wake unstable due to the mutual interaction between neighboring vortices of varying strengths.

Zhang et al. (2022) conducted a systematic analysis of the performance of significant interactions between two FOWTs by CFD based on overset mesh model. This blade-resolving method requires approximately 32 million cell number with a small time step. They compared power output, torque and six degrees of freedom motion response under different scenarios. They revealed that tandem layout with a distance of 9.25*D* (*D* the rotor diameter) is the practical optimal parameter choice.

Huang, Zhao and Wan (2023) utilized an in-house CFD code FOWT-UALM-SJTU to study the coupled aero-hydrodynamic performance and wake interaction between two spar-type FOWTs with tandem and offset layouts under combined wind-wave conditions. The unsteady aerodynamic loads of the FOWT are calculated by the unsteady ALM. The dynamic responses of the FOWT, including aerodynamic loads, platform motions, and wake characteristics, are analysed in detail. Their study suggested that both platform motions and wake interaction contribute to an increased variation range of inflow wind speed experienced by the downstream FOWT, thereby increasing the instability of its aerodynamic loads. The platform motions also lead to an increase of turbulence intensity in the wake region, accelerating wake velocity recovery and widening the wake width. Figure 40 illustrates the vortex structures of the two spar-type FOWTs under different simulation conditions.

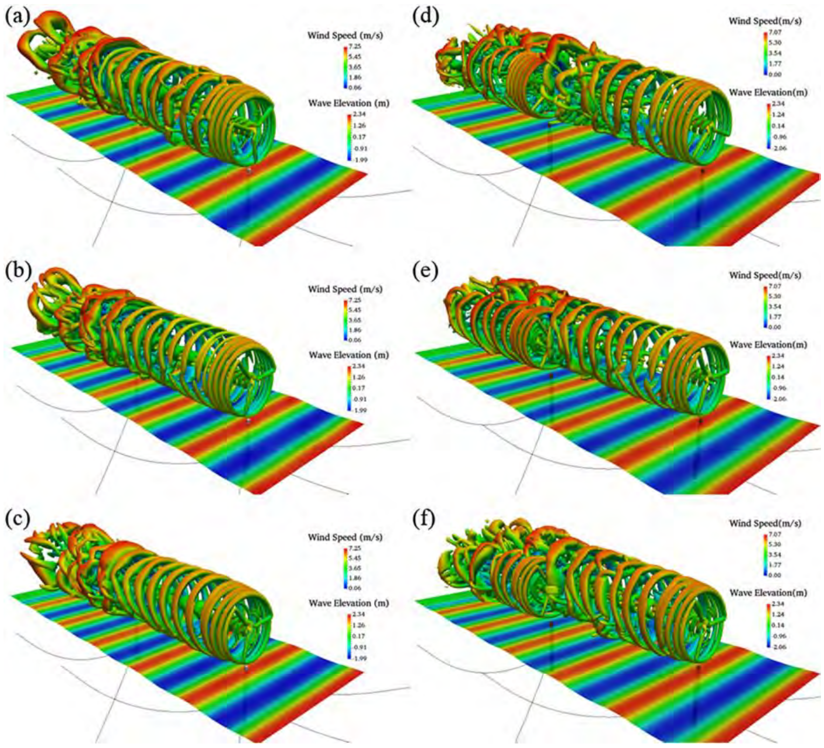

Figure 40: Vortex structures (Q=0.002) of two spar-type FOWTs under tandem and offset layout (Huang et al., 2023)

5. FINAL REPORT AND RECOMMENDATIONS TO THE 30TH ITTC

The 30th ITTC Specialist Committee on Ocean Renewable Energy recommends the following.

5.1.1 General recommendations

1. Continue interactions with IEC.
2. Continue the review of testing of deployment (transportation, installation) and O&M for marine renewable devices.
3. Continue reporting on full scale installation of CT, WEC, and floating OWT
4. Review of model and prototype experimental testing and numerical simulations for floating photovoltaics platforms and ocean thermal energy conversion platforms

5.1.2 Recommendations for wave energy converters (WECs)

The recommendations for future work relating to Wave Energy Converters (WECs):

1. Continue to monitor development of new concepts of WECs.
2. Continue to monitor development in PTO modelling both of physical and numerical prediction of power capture
3. Update the guidelines for numerical and experimental survival testing of WECs.
4. Update the uncertainty analysis of WEC testing include the uncertainties of the power capture and potentially of a different type of device technology.
5. Update and extend array section of guidelines for numerical modelling of WECs. (keep)
6. Review and report on the different control strategies including using AI for power optimization and survivability modes.

7. Review and report on comparisons between full scale data and numerical work/experimental model testing.

5.1.3 Recommendations for current turbines (CTs):

Some of the previous TOR could not be completed in this term due to the small number of specialists in current turbines currently assigned to the SC ORE. One key recommendation for ITTC is to assign more current turbine specialists to the SC ORE in the next term.

The recommendations for future work relating to current turbines (CTs):

1. Continue to investigate and assess data for current turbines from IEC.
2. Continue to monitor developments in physical and numerical techniques for prediction of performance of current turbines.
3. Assess support and if sufficient interest, develop specifications for a benchmark study of a horizontal axis turbine (for instance the 3-blade DoE turbine).
4. Continue review and report effects and reproduction at model scale of inflow turbulence and unsteadiness to the turbine including the effects of waves.
5. Continue review and report on the progress made on the modelling of arrays, elaborating on wake interactions and impact on performance.
6. Continue review and report blockage corrections for testing current turbines in water channels, and where necessary revise relevant guidelines and/or recommended procedures.
7. Improve procedure 7.5-02-07-03.9 Model Tests for Current Turbines, especially concerning: blockage corrections, device interference, PTO modelling, and crossflow turbines.
8. Continue monitoring the deployment of full-scale projects.
9. Review and report on methods to evaluate survivability of current turbines.

5.1.4 Recommendations for offshore wind turbines (OWTs):

The recommendations for future work relating to offshore wind turbines (OWTs):

1. Report on possible full-scale/prototype measurement data available in the public domain, assess their potential to be utilized for validation of simulation tools and evaluation of scaling effects from model scale tests.
2. Continue monitoring and reporting on the development in model testing methodology for single offshore wind turbines.
3. Review and report on model testing and numerical modelling techniques for offshore wind farms.
4. Review methodologies presented for major maintenance operations for floating wind turbines (e.g. high- and heavy lifting offshore, tow to shore, etc.).

6. CONCLUSIONS

6.1 Wave energy converters

The current level of development of large-scale wave energy generation is at a point where full-scale demonstrations are gradually beginning to take place. Commercial use of wave energy is only economically viable for off-grid applications where a small power supply is sufficient, such as the already proven light beacon buoys, or when WECs are used in multi-use coastal facilities such as breakwaters or deployed in large arrays.

In such offshore wave power farms, the interaction between WECs in close proximity (near-field effects) creates a complex wave field that affects the power extracted by each device and thus the total output of the wave power generation facility. In addition, if the farm is far from behind the WECs (far-field effects), the farm will alter the wave field and affect coastal processes such as other users at sea, coastal ecosystems, and shorelines. Numerical and experimental modelling of arrays have each made considerable progress over the past few years, but there are still challenges. The most important advances have been the introduction of optimization techniques that allow multi-criteria selection of the location of WECs in the array, mainly in numerical calculations, and the widespread use of CFD analysis methods.

In the modelling of PTO systems for WECs, more efforts have been made in recent years to identify nonlinear effects, transient characteristics, and viscous effects. Understanding the coupling effects between PTO system components is critical to improving performance assessment, and more attention has been given to developing integrated simulation tools that can include interactions between PTO components.

However, wave energy technologies are certainly the most diverse among marine renewable energy systems. Indeed, many projects and companies have proposed unique and different ways to harness ocean wave energy. This also means that the standardization of component manufacturing and equipment with respect to wave energy is not yet organized, suggesting that the current supply chain, component manufacturing, etc., for large-scale applications is not easy to transition from one device to another. In other words, the speed of development in this area is still less than a sense of acceleration to the top TRLs. To date, none of the companies have reached a fully commercial stage, and only the Mutriku wave power plant has demonstrated stable power generation that makes commercial sense. To become more competitive, companies are gradually moving toward niche markets, off-grid applications, and integration into current or future offshore structures (breakwaters, multi-purpose platforms, harbours etc.).

Therefore, it is important to ensure thorough guidelines and procedures to assist developers through TRLs. There are still many unknowns regarding scale effects, hydrodynamic PTO impacts, survivability testing, etc., and much of the available data is very new. As further information gradually becomes available, it will be important, if not necessary, to continually improve these guidelines and procedures.

6.2 Current turbines

The developments in current turbines today have typically been modelled using simulation through computational fluid dynamics (CFD). However, this analysis is not restricted to it. Hybrid techniques using CFD, machine learning, and semi-analytical methods support these studies for predicting current turbine performance and typical operational conditions. The experimental approach is also significant in this scenario, especially considering the analysis of small-scale current turbines, where it is worth mentioning the scale effects and uncertainty analysis. These follow the ITTC guideline 7.5-02-07-03.9 and IEC and JCGM guidelines to ensure the data repeatability and extrapolation for the full scale.

The key points in the experimental analysis consist of the limitations imposed by the test facility and the power take-off modelling. The test facility dimensions may affect the magnitude of the efficiency because of a high blockage ratio. The literature still notices the vertical blockage effect may disturb the turbine’s performance. This situation has been handled through the clearance coefficient, which has a similar role to the blockage ratio.

Regarding full-scale developments, the present document has shown that the current turbine prototypes are designed to operate with flow velocity in the range 1 m/s - 3 m/s and power capacity from 1 kW to 25 kW. This suggests the developments in current turbines must achieve higher maturity levels to make the technology economically feasible. Studies have suggested that this improvement in power capacity can be achieved by optimising the turbine arrays in current/tidal farms. Nowadays, this issue is carefully addressed because the turbulence effects of a turbine may affect other turbines downstream, decreasing their efficiency and, consequently, their power capacity.

The study of turbine layouts, especially by computational fluid dynamics, has shown that the turbine arrangement in staggered and twin rotor layouts provides promising results. According to the investigation, the turbine arrangements must be designed so that the turbulence intensity in the wake does not affect the incoming flow of the downstream turbines. Then, the challenge in modelling current turbine arrays has been to minimise the effect of the turbulence intensity at the flow and keep (or even increase) the device efficiency for the development of current turbine farms.

6.3 Offshore wind turbines

Recent studies have started to investigate experimental and numerical approaches to analyse the deployment and maintenance phases of offshore wind turbines, in addition to the traditional focus on operational and survival conditions. E experimental towing tests have observed phenomena like Vortex-Induced Motion (VIM) and analyzed towing line loads under wave conditions, numerical and experimental studies have examined the dynamic response, including heave, pitch, and roll, of semisubmersible platforms during towing, as well as bollard pull requirements, and comprehensive studies have highlighted the importance of accounting for viscous forces and non-linear effects, such as VIM, fishtailing, and pitch-induced wave runup, in numerical models of towing operations.

In terms of full-scale floating wind turbine installations, the global offshore wind installed capacity grew from 50,623 MW in 2021 to 57.1 MW for floating projects and saw the installation of the world's largest 16 MW offshore wind turbine in China, despite challenges in fully coupled performance analysis and lightweight design for cost reduction.

Reviews of the testing techniques employed for floating offshore wind turbines (FOWT) were recently published, presenting the evolution of reproduction of aerodynamic loads on FOWTs in wave tank experiments, using either physical wind or real-time hybrid methods.

Various works focusing on the real-time hybrid methods (RTHM), or software-in-the-loop (SIL), have been carried out over the last years in numerous wave tank testing facilities. These approaches have been developed in the last decade and aim at including the aerodynamic force acting on a turbine model using an actuator. This enables to overcome the difficulties in scaling down the aerodynamic loads with physical wind. In the present report, the complexity of the correct reproduction of the aerodynamic forces, the number and dimensions of the components necessary, the type of actuators, and the measurement and control of the actuated forces have been discussed.

The testing of FOWTs with wind physical wind and rotor blades is also being carried out in different research facilities. Such realization of the aerodynamic loads on scaled models can be performed using either geometrical scaled blades or performance-matched blades. In the former case, the blades dimensions are scaled using the same scaling factor as for the rest of the geometry. The Reynolds numbers occurring on the blades are then much lower than on the full-scale blades, and the induced aerodynamic effects may not be well represented. In the latter case, the blades are scaled down with a geometry that replicates closer thrust and power curves for the considered rotor.

Due to the increasingly larger size of offshore wind turbines, and in particular floating wind turbines, it is becoming important to reproduce the flexibility of the most elongated members of the structure. Nonetheless, studying the structural elasticity and internal loads of floating wind turbine platforms is challenging. At model scale, structural similarity for the tower can be achieved by selecting materials and geometries that replicate eigenfrequencies and structural modes. However, this is difficult for the support structure due to Froude scaling constraints on hydrodynamic loads. Investigating internal loads on a rigid structure is possible but requires an extremely stiff structure to keep eigenfrequencies outside the test frequency range. This approach is similar to methods used for ships but is complex and demanding in practice.

Modelling the vertical wind profile is important to capture its impact on the operation and efficiency of offshore wind turbines. The vertical wind shear profile, often modeled with a power law and constant shear, varies by time and location, impacting wind turbine power production and structural loads. Onshore, terrain roughness influences the profile, while offshore, temperature gradients and atmospheric stability are key factors. Atmospheric stability affects turbulence, with stable conditions leading to low turbulence and longer wakes. Traditional models use hub-height wind speed (HHWS), but rotor-equivalent wind speed (REWS) can offer more accurate predictions. Studies show that REWS better predicts power production under varying wind conditions. Accurate modeling of wind shear is crucial for turbine design and wind energy resource assessment.

In terms of wind-farm level analyses, compared with onshore wind farm, floating offshore wind farm suffers more power deficit attributed by low turbulence intensity of high-quality wind resources. In addition, the tilting angle of FOWT will also affect the wake performance and velocity deficit. High-fidelity CFD simulations in combination with actuator disk or actuator line model are used, due to its computational efficiency, to reveal the underlying physical mechanism of wake interactions for floating offshore wind turbines. However, present studies represent a wind farm with a limited number of turbines. The studies on the wake interactions of multi-FOWT wind farms are still scarce.

7. REFERENCES

Abutunis, A., Fal, M., Fashanu, O., Chandrashekhara, K., & Duan, L. (2021). Coaxial horizontal axis hydrokinetic turbine system: Numerical modeling and performance optimization. Journal of Renewable and Sustainable Energy, 13(2). https://doi.org/10.1063/5.0025492

Alblas, L., Bierbooms, W., Veldkamp, D., 2014, "Power Output of Offshore Wind Farms in Relation to Atmospheric Stability", Journal of Physics: Conference Series 555 (1): 012004, https://doi.org/10.1088/1742-6596/555/1/012004.

Alexander, A. J., & Holownia, B. P. (1978). Wind tunnel tests on a savonius rotor. *Journal of Wind Engineering and Industrial Aerodynamics*, *3*(4), 343–351. https://doi.org/10.1016/0167-6105(78)90037-5

Antonutti, R., Poirier, J. C., Gueydon, S., 2020, "Coupled testing of floating wind turbines in waves and wind using winches and software-in-the-loop", Offshore Technology Conference, p. D021S019R001

Arabgolarcheh A., Jannesarahmadi S., Benini E. (2022). Modeling of near wake characteristics in floating offshore wind turbines using an actuator line method. Renewable Energy, 185, 871-887. https://doi.org/10.1016/j.renene.2021.12.099

Arafat, M. Y., Hossain, M. J., & Alam, M. M. (2024). Machine learning scopes on microgrid predictive maintenance: Potential frameworks, challenges, and prospects. *Renewable and Sustainable Energy Reviews*, *190*, 114088. https://doi.org/10.1016/j.rser.2023.114088

Arnal, V., 2020 "Modélisation expérimentale d'une éolienne flottante par une approche "software-in-the-loop"". Ph.D. thesis. Ecole Centrale de Nantes.

Azcona, J., Bouchotrouch, F., Vittori, F., 2019, "Low-frequency dynamics of a floating wind turbine in wave tank-scaled experiments with SIL hybrid method", Wind Energy, Vol. 22, No. 10, p. 1402-1413.

Bahaj, A. S., Molland, A. F., Chaplin, J. R., & Batten, W. M. J. (2007). Power and thrust measurements of marine current turbines under various hydrodynamic flow conditions in a cavitation tunnel and a towing tank. Renewable Energy, 32(3), 407–426. https://doi.org/10.1016/j.renene.2006.01.012

Baratchi, F., Jeans, T. L., & Gerber, A. G. (2020). Assessment of blade element actuator disk method for simulations of ducted tidal turbines. Renewable Energy, 154, 290–304. https://doi.org/10.1016/j.renene.2020.02.098

Bastankhah, M., & Porté-Agel, F. (2014). A new analytical model for wind-turbine wakes. Renewable Energy, 70, 116–123. https://doi.org/10.1016/j.renene.2014.01.002

Behrouzifar, A., & Darbandi, M. (2019). An improved actuator disc model for the numerical prediction of the far-wake region of a horizontal axis wind turbine and its performance. Energy Conversion and Management, 185, 482–495. https://doi.org/10.1016/j.enconman.2019.02.005

Birjandi, A. H., Bibeau, E. L., Chatoorgoon, V., & Kumar, A. (2013). Power measurement of hydrokinetic turbines with free-surface and blockage effect. Ocean Engineering, 69, 9–17. https://doi.org/10.1016/j.oceaneng.2013.05.023

Bonnefoy, F., Leroy, V., Mojallizadeh, M. R., Delacroix, S., Arnal, V., Gilloteaux, J.-C., 2024, "Multidimensional hybrid software-in-the-loop modeling approach for experimental analysis of a floating offshore wind turbine in wave tank experiments", Ocean Engineering, Vol. 309, p, 118390, https://doi.org/10.1016/j.oceaneng.2024.118390.

Bouscasse, B., Merrien, A., Horel, B., De Hauteclocque, G., 2022, "Experimental analysis of wave-induced vertical bending moment in steep regular waves", Journal of Fluids and Structures , Vol. 111, p. 103547.

Büttner, T.; Pérez-Collazo, C.; Abanades, J.; Hann, M.; Harper, P.; Greaves, D.; Stiesdal, H., 2022. "OrthoSpar, a novel substructure concept for floating offshore wind turbines: Physical model tests under towing conditions", Ocean Eng., 245, 110508, https://doi.org/10.1016/j.oceaneng.2021.110508

Chawdhary, S., Hill, C., Yang, X., Guala, M., Corren, D., Colby, J., & Sotiropoulos, F. (2017). Wake characteristics of a TriFrame of axial-flow hydrokinetic turbines. Renewable Energy, 109, 332–345. https://doi.org/10.1016/j.renene.2017.03.029

Chen, C., Ma, Y., Fan, T., 2022, "Review of model experimental methods focusing on aerodynamic simulation of floating offshore wind turbines", Renewable and Sustainable Energy Reviews , Vol. 157, p. 112036.

Chen, J., Liu, Z., Song, Y., Peng, Y., Li, J., 2022a, "Experimental study on dynamic responses of a spar-type floating offshore wind turbine", Renewable Energy, Vol. 196, p. 560-578

Chen, J., Hu, Z., Wan, D., Xiao, Q., 2018, "Comparisons of the dynamical characteristics of a semi-submersible floating offshore wind turbine based on two different blade concepts", Ocean Engineering, Vol. 153, pp. 305-318

Chen, Y., Lin, B., & Liang, D. (2023). Interactions between approaching flow and hydrokinetic turbines in a staggered layout. Renewable Energy, 218, 119339. https://doi.org/10.1016/j.renene.2023.119339

Cheng, B., Du, J., & Yao, Y. (2022). Machine learning methods to assist structure design and optimization of Dual Darrieus Wind Turbines. Energy, 244, 122643. https://doi.org/10.1016/j.energy.2021.122643

Djama Dirieh, N., Thiébot, J., Guillou, S., & Guillou, N. (2022). Blockage Corrections for Tidal Turbines—Application to an Array of Turbines in the Alderney Race. Energies, 15(10), 3475. https://doi.org/10.3390/en15103475

Du, X., Tan, J., Yuan, P., Si, X., Liu, Y., & Wang, S. (2023). Research on the blockage correction of a diffuser-augmented hydrokinetic turbine. Ocean Engineering, 280, 114470. https://doi.org/10.1016/j.oceaneng.2023.114470

Edson, J.B., Fairall, C.W., 1998, "Similarity Relationships in the Marine Atmospheric Surface Layer for Terms in the TKE and Scalar Variance Budgets", Journal of the Atmospheric Sciences 55 (13): 2311–28, https://doi.org/10.1175/1520-0469(1998)055<2311:SRITMA>2.0.CO;2.

Elfering, K., Metoyer, R., Chatterjee, P., Mazzoleni, A., Bryant, M., & Granlund, K. (2023). Blade element momentum theory for a skewed coaxial turbine. Ocean Engineering, 269, 113555. https://doi.org/10.1016/j.oceaneng.2022.113555

El-Shahat, S. A., Li, G., Lai, F., & Fu, L. (2020). Investigation of parameters affecting horizontal axis tidal current turbines modeling by blade element momentum theory. Ocean Engineering, 202, 107176. https://doi.org/10.1016/j.oceaneng.2020.107176

Espina-Valdés, R., Fernández-Jiménez, A., Fernández Francos, J., Blanco Marigorta, E., & Álvarez-Álvarez, E. (2020). Small cross-flow turbine:Design and testing in high blockage conditions. Energy Conversion and Management, 213, 112863. https://doi.org/10.1016/j.enconman.2020.112863

Fernandes, A. C., & Mirzaeisefat, S. (2015). Flow induced fluttering of a hinged vertical flat plate. Ocean Engineering, 95, 134–142. https://doi.org/10.1016/j.oceaneng.2014.12.009

Fernandes, A. C., & Rostami, A. B. (2015). Hydrokinetic energy harvesting by an innovative vertical axis current turbine. Renewable Energy, 81, 694–706. https://doi.org/10.1016/j.renene.2015.03.084

Gaertner, E., Rinker, J., Sethuraman, L., Zahle, F., Anderson, B., Barter, G., Abbas, N, et al., 2020, "IEA Wind TCP Task 37: Defini-tion of the IEA 15-Megawatt Offshore Reference Wind Turbine", NREL/TP--5000-75698, 1603478. https://doi.org/10.2172/1603478.

Ghafari Hamid, R., Hassan, G., Guanghua, H., 2021, "Numerical study of the Wavestar wave energy converter with multi-point-absorber around DeepCwind semisubmersible floating platform", Ocean. Eng. 232, 109177

Giassi, M., et al., 2020, "Comparison of wave energy park layouts by experimental and numerical methods", J. Mar. Sci. Eng. 8 (10) 750

Glauert, H. (1933). Wind tunnel interference on wings, bodies and airscrews.

Gorlov, A. M. (1995). The helical turbine: A new idea for low-head hydro.

Guerra, M., & Thomson, J. (2019). Wake measurements from a hydrokinetic river turbine. Renewable Energy, 139, 483–495. https://doi.org/10.1016/j.renene.2019.02.052

Gueydon, S., Lindeboom, R., van Kampen, W., de Ridder, E.-J., 2018, "Comparison of Two Wind Turbine Loading Emulation Techniques Based on Tests of a TLP-FOWT in Combined Wind, Waves and Current", International Conference on Offshore Mechanics and Arctic Engineering, Vol. 51975, p. V001T01A012

Gueydon, S., Bayati, I., Bosman, R., van Kampen, W., de Ridde, E.-J., 2023, "Wind Turbine Load Monitoring During Model-Test in a Wave Basin", International Conference on Offshore Mechanics and Arctic Engineering, Vol. 86908, p. V008T09A040

Guo, J., Liu, M., Fang, Z., Chen, W., Pan, X., Yang, L., 2024, "An experimental study on the influence of wind-wave-current coupling effect on the global performance of a 12 MW semi-submersible floating wind turbine", Ocean Engineering , Vol. 304, p. 117795

Ha, Y.-J., Ahn, H., Park, S., Park, J.-Y., Kim, K.-H., 2023, "Development of hybrid model test technique for performance evaluation of a 10 MW class floating offshore wind turbine considering asymmetrical thrust", Ocean Engineering, Vol. 272, p. 113783

Hall, M., Goupee, A.J., 2018, "Validation of a hybrid modeling approach to floating wind turbine basin testing", Wind Energy, Vol. 21, pp. 391–408.

Hansen, C. L., Bredmose, H., Vincent, M., Steffensen, S. E., Pegalajar-Jurado, A., Jensen, B., Dixen, M., 2024, "Resonant response of a flexible semi-submersible floating structure: experimental analysis and second-order modelling", Journal of Fluid Mechanics, Vol 982, A7

Hegazy, A., Naaijen, P., Leroy, V., Bonnefoy, F., Pérignon, Y., van Wingerden, J. W., 2024, "The potential of wave feedforward control for floating wind turbines: A wave tank experiment", Wind Energy Science Discussions, pp. 1-30

Hill, C., Neary, V. S., Guala, M., & Sotiropoulos, F. (2020). Performance and Wake Characterization of a Model Hydrokinetic Turbine: The Reference Model 1 (RM1) Dual Rotor Tidal Energy Converter. Energies, 13(19), 5145. https://doi.org/10.3390/en13195145

Howland, M. F., Lele, S. K., & Dabiri, J. O. (2019). Wind farm power optimization through wake steering. Proceedings of the National Academy of Sciences, 116(29), 14495–14500. https://doi.org/10.1073/pnas.1903680116

Huang, Y., Zhao, W., & Wan D. (2023). Wake interaction between two spar-type floating offshore wind turbines under different layouts. Physics of Fluids, 35, 097102. https://doi.org/10.1063/5.0161759

Hwang, I. S., Lee, Y. H., & Kim, S. J. (2009). Optimization of cycloidal water turbine and the performance improvement by individual blade control. Applied Energy, 86(9), 1532–1540. https://doi.org/10.1016/j.apenergy.2008.11.009

Hyland, T.; Adam, F.; Dahlias, F.; Großmann, J. (2014), "Towing tests with the GICON®-TLP for wind turbines. In Proceedings of the ISOPE International Ocean and Polar Engineering Conference, Busan, Republic of Korea, 15–20 June 2014.

IEC. (2022). Marine energy - Wave, tidal and other water current converters - Part 202: Early stage development of tidal energy converters - Best practices and recommended procedures for the testing of pre-prototype scale devices.

IEA OES, 2021, Annual Report: An Overview of Ocean Energy Activities in 2021

IEA OES, 2022, Annual Report: An Overview of Ocean Energy Activities in 2022

IEA OES, 2023, Annual Report: An Overview of Ocean Energy Activities in 2023

JCGM. (2008). Evaluation of measurement data - Guide to the expression of uncertainty in measurement.

Jeon, K. S., Jeong, J. I., Pan, J.-K., & Ryu, K.-W. (2015). Effects of end plates with various shapes and sizes on helical Savonius wind turbines. Renewable Energy, 79, 167–176. https://doi.org/10.1016/j.renene.2014.11.035

Jeong, H., Lee, S., & Kwon, S.-D. (2018). Blockage corrections for wind tunnel tests conducted on a Darrieus wind turbine. Journal of Wind Engineering and Industrial Aerodynamics, 179, 229–239. https://doi.org/10.1016/j.jweia.2018.06.002

Junki, F., Murai, M., Qiao, L., 2020, "Research on how the arrangement of arrayed PAWECs influences to their electric power generation", J. Jpn. Soc. Nav. Archit. Ocean Eng. 31 (2020) 59–71

Kagemoto, H. and Yue D.,1986, "Interactions among multiple three-dimensional bodies in water waves: an exact algebraic method", J. Fluid Mech. 166 (1986) 189–209

Khani, M. S., Shahsavani, Y., Mehraein, M., Soleimani Rad, M. H., & Nikbakhsh, A. A. (2024). Evaluation of the performance of the Savonius hydrokinetic turbines in the straight and curved channels using advanced machine learning methods. Energy, 290, 130189. https://doi.org/10.1016/j.energy.2023.130189

Khanjanpour, M. H., & Javadi, A. A. (2020). Optimization of the hydrodynamic performance of a vertical Axis tidal (VAT) turbine using CFD-Taguchi approach. Energy Conversion and Management, 222, 113235. https://doi.org/10.1016/j.enconman.2020.113235

Kiho, S., Shiono, M., & Suzuki, K. (1996). The power generation from tidal currents by darrieus turbine. Renewable Energy, 9(1–4), 1242–1245. https://doi.org/10.1016/0960-1481(96)88501-6

Kim, Y., Kim, J.H., 2016, "Benchmark study on motions and loads of a 6750-TEU containership", Ocean Engineering, Vol 119, pp. 262–273

Kinsey, T., & Dumas, G. (2017). Impact of channel blockage on the performance of axial and cross-flow hydrokinetic turbines. Renewable Energy, 103, 239–254. https://doi.org/10.1016/j.renene.2016.11.021

Kirke, B. K. (2011). Tests on ducted and bare helical and straight blade Darrieus hydrokinetic turbines. Renewable Energy, 36(11), 3013–3022. https://doi.org/10.1016/j.renene.2011.03.036

Koh, W. X. M., & Ng, E. Y. K. (2017). A CFD study on the performance of a tidal turbine under various flow and blockage conditions. Renewable Energy, 107, 124–137. https://doi.org/10.1016/j.renene.2017.01.052

Kolekar, N., & Banerjee, A. (2015). Performance characterization and placement of a marine hydrokinetic turbine in a tidal channel under boundary proximity and blockage effects. Applied Energy, 148, 121–133. https://doi.org/10.1016/j.apenergy.2015.03.052

Kulkarni, S. S., Wang, L., Golsby, N., & Lander, M. (2022). Fluid-structure interaction based optimisation in tidal turbines: A perspective review. Journal of Ocean Engineering and Science, 7(5), 449–461. https://doi.org/10.1016/j.joes.2021.09.017

Kumar, K., Kumar, A., Saini, G., Mohammed, M. A., Shah, R., Nedoma, J., Martinek, R., & Kadry, S. (2024). Performance Monitoring of Kaplan Turbine Based Hydropower Plant under Variable Operating Conditions Using Machine Learning Approach. Sustainable Computing: Informatics and Systems, 100958. https://doi.org/10.1016/j.suscom.2024.100958

Kumar, R., & Sarkar, S. (2022). Effect of design parameters on the performance of helical Darrieus hydrokinetic turbines. Renewable and Sustainable Energy Reviews, 162, 112431. https://doi.org/10.1016/j.rser.2022.112431

Konispoliatis, D.N., Katsaounis, G.M., Manolas, D.I., Soukissian, T.H., Polyzos, S., Mazarakos, T.P., Voutsinas, S.G. and Mavrakos, S.A., 2021, "REFOS: a renewable energy multi-purpose floating offshore system. Energies", 14(11), p.3126. https://doi.org/10.3390/en14113126.

Lange, B., Larsen, S., Højstrup, J., Barthelmie, R., 2004, "Importance of Thermal Effects and Sea Surface Roughness for Offshore Wind Resource Assessment", Journal of Wind Engineering and Industrial Aerodynamics 92 (11): 959–88, https://doi.org/10.1016/j.jweia.2004.05.005.

Le, C.; Ren, J.; Wang, K.; Zhang, P.; Ding, H. (2021), "Towing Performance of the Submerged Floating Offshore Wind Turbine under Different Wave Conditions", J. Mar. Sci. Eng., 9, 633, https://doi.org/10.3390/jmse9060633.

Leroux, T., Osbourne, N., & Groulx, D. (2019). Numerical study into horizontal tidal turbine wake velocity deficit: Quasi-steady state and transient approaches. Ocean Engineering, 181, 240–251. https://doi.org/10.1016/j.oceaneng.2019.04.019

Leroy, V., Delacroix, S., Merrien, A., Bachynski-Polić, E. E., Gilloteaux, J.-C. 2022, "Experimental investigation of the hydro-elastic response of a spar-type floating offshore wind turbine", Ocean Engineering, Vol. 255, p. 111430

Leroy, V., Delacroix, S., Merrien, A., Bachynski-Polić, E. E., Gilloteaux, J.-C., 2024, "Hydroelastic response of the scaled model of a floating offshore wind turbine platform in waves: HELOFOW Project Database (1.0.1) [Data set]". Zenodo.

Li, L., Liu, Y., Yuan, Z., Gao, Y. 2018, "Wind field effect on the power generation and aerodynamic performance of offshore float-ing wind turbines". Energy 157:379–390. https://doi.org/10.1016/j.energy.2018.05.183.

Li, Q., Maeda, T., Kamada, Y., Shimizu, K., Ogasawara, T., Nakai, A., & Kasuya, T. (2017). Effect of rotor aspect ratio and solidity on a straight-bladed vertical axis wind turbine in three-dimensional analysis by the panel method. Energy, 121, 1–9. https://doi.org/10.1016/j.energy.2016.12.112

Li, Y., Yu, Y.H., 2012, "A synthesis of numerical methods for modeling wave energy converter-point absorbers", Renew. Sustain. Energy Rev. 16, 4352–4364

Liu, Y., Ishihara, T., 2021, "Numerical study on sectional loads and structural optimization of an elastic semi-submersible floating platform", Energies, Vol 14, No 1, 182

Lopes, P.E., 2021, "Improved Wind Power Estimation Method for Operation & Maintenance of Offshore Wind Farm", Master thesis, University of Stavanger, https://hdl.handle.net/11250/2786258.

Madsen, F. J., Nielsen, T. R. L., Kim, T., Bredmose, H., Pegalajar-Jurado, A., Mikkelsen, R. F., Lomholt, A. K., Borg, M., Mirzaei, M., Shin, P., 2020, "Experimental analysis of the scaled DTU10MW TLP floating wind turbine with different control strategies", Renewable Energy, Vol. 155, pp. 330-346

Magagna, D. 2019, Ocean Energy Technology Development Report, EUR 29907 EN, Joint Research Centre of the European Commission, Luxembourg, https://publications.jrc.ec.europa.eu/repository/bitstream/JRC118296/jrc118296_1.pdf

Mas-Soler, J.; Uzunoglu, E.; Bulian, G.; Soares, C.G.; Souto-Iglesias, A., 2021. "An experimental study on transporting a free-float capable tension leg platform for a 10 MW wind turbine in waves", Renew. En., 179, 2158–2173, https://doi.org/10.1016/j.renene.2021.08.009

Manwell, J. F., McGowan, J. G., & Rogers, A. L. (2002). Wind energy explained: theory, design and application (E. J. W. Press, Ed.).

Mata, S.A., Martínez, J.J.P., Quesada, J.B., Larrañaga, F.P., Yadav, N., Chawla, J.S., Howland, M.F., 2023, "Modeling the effect of wind speed and direction shear on utili-ty-scale wind turbine power production", arXiv:2309.15254 [physics.flu-dyn], https://doi.org/10.48550/arXiv.2309.15254

Matoug, C., Augier, B., Paillard, B., Maurice, G., Sicot, C., Barre, S. 2020, "An hybrid approach for the comparison of VAWT and HAWT performances for floating offshore wind turbines", Journal of Physics: Conference Series, Vol. 1618, No. 3, p. 032026.

Mercad´e Ruiz, P., Ferri, F., Kofoed, J.P., 2017, "Experimental validation of a wave energy converter array hydrodynamics tool", Sustainability 9 (1) 115

Mikkelsen, R., & Sørensen, J. N. (2002). Modelling of wind turbine blockage. 15th IEA Symposium on the Aerodynamics of Wind Turbines.

Mirzaeisefat, S., & Fernandes, A. C. (2013). Stability analysis of the fluttering and autorotation of flow-induced rotation of a hinged flat plate. Journal of Hydrodynamics, 25(5), 755–762. https://doi.org/10.1016/S1001-6058(13)60422-9

Motta, M., Barthelmie, R. J., Vølund, P., 2005. "The Influence of Non-Logarithmic Wind Speed Profiles on Potential Power Output at Danish Offshore Sites", Wind Energy 8 (2): 219–36, https://doi.org/10.1002/we.146.

Mojallizadeh, M. R., Bonnefoy, F., Ohana, J., Delacroix, S., Leroy, V., Bouscasse, B., Weber, M., 2024, "Control design for thrust generators with application to wind turbine wave-tank testing: a sliding-mode control approach with Euler backward time-discretization", Control Engineering Practice, Vol. 146, p. 105894

Murai, M., Qiao, L., Junki, F., 2019, "Study on the generated power changes by the relation between an arrangement of an array of point absorber type WECs and an incident wave angle", Proceeding International Conference on Offshore Mechanics and Arctic Engineering, vol. 58882, American Society of Mechanical Engineers, Glasgow, Scotland, UK, pp. 9–14

Murai, M., Junki, F., Qiao, L., 2020, "How the hydrodynamic response of PA-WECs' array, under maximizing the power generation by its arrangement and control force change?", in: Proceeding International Conference on Offshore Mechanics and Arctic Engineering, vol. 84362 American Society of Mechanical Engineers, Virtual, Online, pp. 3–7, https://doi.org/10.1115/omae2020-18189. August

Murai, M., Qiao, L., Junki, F., 2021, "Study on power generation of single point absorber wave energy converters (PA-WECs) and arrays of PA-WECs", Renew. Energy 164, 1121–1132

Murai, M. and Sakamoto, S., 2022, "A Fundamental Study on the Potential of AI Prediction in Control Force Estimation to Maximize Power Generation of PA-WECs in Irregular Waves", J.JASANAOE, Vol.35, pp.55-64

Murphy, P., Lundquist, J.K., Fleming, P., 2020, "How wind speed shear and directional veer affect the power production of a meg-awatt-scale operational wind turbine, Win Energ. Sci., 5, 1169-1190, https://doi.org/10.5194/wes-5-1169-2020.

Mycek, P., Gaurier, B., Germain, G., Pinon, G., & Rivoalen, E. (2014a). Experimental study of the turbulence intensity effects on marine current turbines behaviour. Part I: One single turbine. Renewable Energy, 66, 729–746. https://doi.org/10.1016/j.renene.2013.12.036

Mycek, P., Gaurier, B., Germain, G., Pinon, G., & Rivoalen, E. (2014b). Experimental study of the turbulence intensity effects on marine current turbines behaviour. Part II: Two interacting turbines. Renewable Energy, 68, 876–892. https://doi.org/10.1016/j.renene.2013.12.048

Nago, V. G., Santos, I. F. S. dos, Gbedjinou, M. J., Mensah, J. H. R., Tiago Filho, G. L., Camacho, R. G. R., & Barros, R. M. (2022). A literature review on wake dissipation length of hydrokinetic turbines as a guide for turbine array configuration. Ocean Engineering, 259, 111863. https://doi.org/10.1016/j.oceaneng.2022.111863

Niebuhr, C. M., Schmidt, S., van Dijk, M., Smith, L., & Neary, V. S. (2022). A review of commercial numerical modelling approaches for axial hydrokinetic turbine wake analysis in channel flow. Renewable and Sustainable Energy Reviews, 158, 112151. https://doi.org/10.1016/j.rser.2022.112151

Niebuhr, C. M., van Dijk, M., Neary, V. S., & Bhagwan, J. N. (2019). A review of hydrokinetic turbines and enhancement techniques for canal installations: Technology, applicability and potential. Renewable and Sustainable Energy Reviews, 113, 109240. https://doi.org/10.1016/j.rser.2019.06.047

Nuernberg, M., & Tao, L. (2018). Experimental study of wake characteristics in tidal turbine arrays. Renewable Energy, 127, 168–181. https://doi.org/10.1016/j.renene.2018.04.053

Ohana J., Horel B., Merrien A., Arnal V., Bonnefoy F., Brizzi G., Bouscasse B., 2022, Dataset: Wave tank testing of a multi-purpose platform with aquaculture, wind turbine and wave energy converters, https://doi.org/10.17882/88376.

Ohana J., Horel B., Merrien A., Arnal V., Bonnefoy F., Brizzi G., Bouscasse B., Ruzzo C., (2023), "Wave Tank Testing of a Multi-Purpose Floating Platform with Aquaculture, Wind Turbine and Wave Energy Converters", (2023) SSRN, http://dx.doi.org/10.2139/ssrn.4437075.

Otter, A., Desmond, C., Flannery, B., Murphy, J., 2022, "Combined current and wind simulation for floating offshore wind turbines", Journal of Physics: Conference Series, Vol. 2362, p. 012028.

Otter, A., Murphy, J., Pakrashi, V., Robertson, A., Desmond, C., 2021, "A review of modelling techniques for floating offshore wind turbines", Wind Energy, Vol. 25, No. 5, pp. 831-857.

Ouro, P., Ramírez, L., & Harrold, M. (2019). Analysis of array spacing on tidal stream turbine farm performance using Large-Eddy Simulation. Journal of Fluids and Structures, 91, 102732. https://doi.org/10.1016/j.jfluidstructs.2019.102732

Patel, V., Eldho, T. I., & Prabhu, S. V. (2017). Experimental investigations on Darrieus straight blade turbine for tidal current application and parametric optimization for hydro farm arrangement. International Journal of Marine Energy, 17, 110–135. https://doi.org/10.1016/j.ijome.2017.01.007

Pérez Albornoz, C., Escalante Soberanis, M.A., Ramírez Rivera, V., and Rivero, M., 2022, "Review of Atmospheric Stability Estimations for Wind Power Applications", Renewable and Sustainable Energy Reviews 163 (July): 112505, https://doi.org/10.1016/j.rser.2022.112505

Pope, A., & Harper, J. (1966). Low-speed wind tunnel testing. Wiley.

Qiao, L., Murai, M., Kuwada, S., 2018, "A study on electrical power for multiple linear wave energy converter considering the interaction effect", Energies 11 (11), 1–20, https://doi.org/10.3390/en11112964

Ramachandran, R.C., Serraris, J.J., Montfort, J.H., De Ridder, E.J., Desmond, C. and Murphy, J. (2024). Towing Analysis and Validation of a Fully Assembled Floating Offshore Wind Turbine Based on an Experimental Study. Journal of Marine Science and Engineering, 12(4), p.689. https://doi.org/10.3390/jmse12040689

Reddy, K. B., Bhosale, A. C., & Saini, R. P. (2022). Performance parameters of lift-based vertical axis hydrokinetic turbines - A review. Ocean Engineering, 266, 113089. https://doi.org/10.1016/j.oceaneng.2022.113089

Rezaeiha, A., Micallef, D, 2021, "Wake interactions of two tandem floating offshore wind turbines: CFD analysis using actuator disc model", Renewable Energy, Vol 179, pp 859–876.

Robert, M., Dezhi, N., Boyin, D., et al. 2022, "Wave energy converter systems-status and perspectives", in: D. Ning, B. Ding (Eds.), Modelling and Optimization of Wave Energy Converters, first ed., CRC Press, Boca Raton, pp.1-58, https://doi.org/10.1201/9781003198956

Ross, H., & Polagye, B. (2020a). An experimental assessment of analytical blockage corrections for turbines. Renewable Energy, 152, 1328–1341. https://doi.org/10.1016/j.renene.2020.01.135

Ross, H., & Polagye, B. (2020b). An experimental evaluation of blockage effects on the wake of a cross-flow current turbine. Journal of Ocean Engineering and Marine Energy, 6(3), 263–275. https://doi.org/10.1007/s40722-020-00172-w

Rostami, A. B., & Fernandes, A. C. (2015). The effect of inertia and flap on autorotation applied for hydrokinetic energy harvesting. Applied Energy, 143, 312–323. https://doi.org/10.1016/j.apenergy.2015.01.051

Rostami, A. B., & Fernandes, A. C. (2017). From fluttering to autorotation bifurcation of a flat plate in a current. Journal of the Brazilian Society of Mechanical Sciences and Engineering, 39(11), 4769–4784. https://doi.org/10.1007/s40430-017-0912-8

Ruzzo, C., Muggiasca, S., Malara, G., Taruffi, F., Belloli, M., Collu, M., Li, L., Brizzi, G. and Arena, F., (2021), "Scaling strategies for multi-purpose floating structures physical modeling: state of art and new perspectives", Applied Ocean Research, 108, p.102487, https://doi.org/10.1016/j.apor.2020.102487.

Ruzzo, C., Fiamma, V., Scialò, A., Arena, F., Santoro, A., Muggiasca, S., Taruffi, F., Di Carlo, S., Larrea, I., Corvaglia, P.A. and Zuccarino, A., 2022, "Field experimental campaign on a multi-purpose floating structure: Set-up description. Trends in Renewable Energies Offshore", pp.817-825.

Ryi, J., Rhee, W., Chang Hwang, U., & Choi, J.-S. (2015). Blockage effect correction for a scaled wind turbine rotor by using wind tunnel test data. Renewable Energy, 79, 227–235. https://doi.org/10.1016/j.renene.2014.11.057

Ryu, G.H., Kim, D., Kim, D.-Y., Kim, Y.-G., Kwak, S.J., Choi, M.S., Jeon, W., Kim, B.-S., Moon, C.-J., 2022, "Analysis of vertical wind shear effects on offshore wind energy prediction accuracy applying rotor equivalent wind speed and the relationship with atmospheric stability", Appl. Sci. 12, 6949, https://doi.org/10.3390/app12146949

Sarmiento, J., Iturrioz, A., Ayllón, V., Guanche, R. and Losada, I.J., 2019, "Experimental modelling of a multi-use floating platform for wave and wind energy harvesting", Ocean Engineering, 173, pp.761-773. https://doi.org/10.1016/j.oceaneng.2018.12.046

Saini, G., & Saini, R. P. (2018). Numerical Investigation of the Effect of Blade Profile of a Darrieus Hydrokinetic Turbine. 2018 5th IEEE Uttar Pradesh Section International Conference on Electrical, Electronics and Computer Engineering (UPCON), 1–6. https://doi.org/10.1109/UPCON.2018.8597073

Sathe, A., Mann, J., Barlas, T., Bierbooms, W.A.A.M., van Bussel, G.J.W., 2013, "Influence of Atmospheric Stability on Wind Turbine Loads", Wind Energy 16 (7): 1013–32, https://doi.org/10.1002/we.1528

Schluntz, J., & Willden, R. H. J. (2015). The effect of blockage on tidal turbine rotor design and performance. Renewable Energy, 81, 432–441. https://doi.org/10.1016/j.renene.2015.02.050

Shi, W., Fu, J., Ren, Z., Jiang, Z., Wang, T., Cui, L., Li, Xin, 2023, "Real-time hybrid model tests of floating offshore wind turbines: Status, challenges, and future trends", Applied Ocean Research, Vol. 141, p. 103796.

Shiono, M., Suzuki, K., & Kiho, S. (2002). Output Characteristics of Darrieus Water Turbine with Helical Blades for Tidal Current Generations. Proceedings of the International Offshore and Polar Engineering Conference, 859–864.

Soares, R. B., Fernandes, A. C., & Sales Junior, J. S. (2022a). Performance Improvement of Vertical Axis Autorotation Current Turbine through Twin-Rotors. 5th International Conference on Renewable Energies Offshore, Lisbon, Portugal

Soares, R. B., Fernandes, A. C., & Sales Junior, J. S. (2022b). Stability Analysis of Fluttering to Autorotation to Flat Plate Turbine. 5th International Conference on Renewable Energies Offshore

Stallard, T., Collings, R., Feng, T., & Whelan, J. (2013). Interactions between tidal turbine wakes: experimental study of a group of three-bladed rotors. Philosophical Transactions of the Royal Society A: Mathematical, Physical and Engineering Sciences, 371(1985), 20120159. https://doi.org/10.1098/rsta.2012.0159

Steiros, K., & Hultmark, M. (2018). Drag on flat plates of arbitrary porosity. Journal of Fluid Mechanics, 853, R3. https://doi.org/10.1017/jfm.2018.621

Stratigaki, V., et al., 2014, "Wave basin experiments with large wave energy converter arrays to study interactions between the converters and effects on other users in the sea and the coastal area", Energies 7 (2) 701–734

Sun, K., Yi, Y., Zheng, X., et al.2021," Experimental investigation of semi-submersible platform combined with point-absorber array", Energy Convers. Manag. 245, 114623

Suzuki, H., Xiong, J., Do Carmo, L. H. S., Vieira, D. P., De Mello, P. C., Malta, E. B., Simos, A. N., Hirabayashi, S., Gonçalves, R. T., 2019 "Elastic response of a light-weight floating support structure of FOWT with guywire supported tower", Journal of Marine Science and Technology, Vol 24, pp 1015-1028.

Takata, T., Takaoka, M., Gonçalves, R. T., Houtani, H., Yoshimura, Y., Hara, K., Oh, S., Dotta, R., Malta, E. B., Iijima, K., Suzuki, H., 2021, "Dynamic behavior of a flexible multi-column FOWT in regular waves", Journal of Marine Science and Engineering, Vol. 9, No. 2, 124

Talukdar, P. K., Kulkarni, V., Das, A. K., Dwivedy, S. K., Kakoty, S. K., Mahanta, P., & Saha, U. K. (2017, December 7). In-Situ Experiments to Estimate the Performance Characteristics of a Double-Step Helical-Bladed Hydrokinetic Turbine. Volume 2. https://doi.org/10.1115/GTINDIA2017-4572

Talukdar, P. K., Kulkarni, V., & Saha, U. K. (2018). Field-testing of model helical-bladed hydrokinetic turbines for small-scale power generation. Renewable Energy, 127, 158–167. https://doi.org/10.1016/j.renene.2018.04.052

Tedds, S. C. (2014). Scale model testing of tidal stream turbines: wake characterisation in realistic flow conditions. University of Liverpool

Tedds, S. C., Owen, I., & Poole, R. J. (2014). Near-wake characteristics of a model horizontal axis tidal stream turbine. Renewable Energy, 63, 222–235. https://doi.org/10.1016/j.renene.2013.09.011

Thys, M., Chabaud, V., Sauder, T., Eliassen, L., Sæther, L. O., Magnussen, Ø. B., 2018, "Real-time hybrid model testing of a semi-submersible 10MW floating wind turbine and advances in the test method", International Conference on Offshore Mechanics and Arctic Engineering, Vol. 51975, p. V001T01A013

Thys, M., Souza, C., Sauder, T., Fonseca, N., Berthelsen, PA., Engebretsen, E., Haslum, H., 2021, "Experimental investigation of the coupling between aero- and hydrodynamical loads on a 12 mw semi-submersible floating wind turbine", Proceedings of the ASME 2021 40th International Conference on Ocean, Offshore and Arctic Engineering. Volume 9: Ocean Renewable Energy. Virtual, Online. June 21–30, 2021. https://doi.org/10.1115/OMAE2021-62980

Urbán, A. M., Guanche, R., 2019, "Wind turbine aerodynamics scale-modeling for floating offshore wind platform testing", Journal of Wind Engineering and Industrial Aerodynamics, Vol. 186, pp. 49-57

Vittori, F., Azcona, J., Eguinoa, I., Pires, O., Rodríguez, A., Morató, Á., Garrido, C., Desmond, C., 2022, "Model tests of a 10 MW semi-submersible floating wind turbine under waves and wind using hybrid method to integrate the rotor thrust and moments", Wind Energy Science , Vol. 7, No. 5, p. 2149-2161

Wan, L., Gao, Z., Moan, T. and Lugni, C., 2016, "Comparative experimental study of the survivability of a combined wind and wave energy converter in two testing facilities", Ocean Engineering, 111, pp.82-94. https://doi.org/10.1016/j.oceaneng.2015.10.045

Wang, Y., Lin, J., Zhang, J., 2022, "Investigation of a new analytical wake prediction method for offshore floating wind turbines considering an accurate incoming wind flow", Renewable Energy, Vol 185, pp 827–849

Wen, B., Tian, X., Dong, X., Li, Z., Peng, Z., Zhang, W., Wei, K., 2020, "Design approaches of performance-scaled rotor for wave basin model tests of floating wind turbines", Renewable Energy, Vol. 148, pp. 573-584

Wen, B., Jiang, Z., Li, Z., Peng, Z., Dong, X., Tian, X., 2022, "On the aerodynamic loading effect of a model Spar-type floating wind turbine: An experimental study", Renewable Energy, Vol. 184, pp. 306-319

Werle, M. J. (2010). Wind Turbine Wall-Blockage Performance Corrections. Journal of Propulsion and Power, 26(6), 1317–1321. https://doi.org/10.2514/1.44602

Wu, H., Fernandes, A. C., Cao, R., & Wang, E. (2023). Performance evaluation and shape improvement of a novel vertical-axis autorotation current turbine. Ocean Engineering, 284, 115086. https://doi.org/10.1016/j.oceaneng.2023.115086

Xiaoming, R., Leroy, V., Bachynski-Polić, E. E., 2023, "Hydroelastic response of a flexible spar floating wind turbine: Numerical modelling and validation", Ocean Engineering, Vol. 286, p. 115635.

Xu, S., Xue, Y., Zhao, W., Wan, D., 2022, "A review of high-fidelity computational fluid dynamics for floating offshore wind turbines", Journal of Marine Science and Engineering, Vol 10(10), 1357

Yeo, E. J., Kennedy, D. M., & O'Rourke, F. (2022). Tidal current turbine blade optimisation with improved blade element momentum theory and a non-dominated sorting genetic algorithm. Energy, 250, 123720. https://doi.org/10.1016/j.energy.2022.123720

Yang, J., He, Y.-P., Zhao, Y.-S., Shao, Y.-L., Han, Z.-L., 2021, "Experimental and numerical studies on the low-frequency responses of a spar-type floating offshore wind turbine", Ocean Engineering, Vol. 222, p. 108571

Zhang, D., Guo, P., Cheng, Y., Hu, Q., & Li, J. (2023). Analysis of blockage correction methods for high-solidity hydrokinetic turbines: Experimental and numerical investigations. Ocean Engineering, 283, 115185. https://doi.org/10.1016/j.oceaneng.2023.115185

Zhang, L., Li, Y., Xu, W., Gao, Z., Fang, L., Li, R., Ding, B., Zhao, B.; Leng, J., He, F., 2022, "Systematic analysis of performance and cost of two floating offshore wind turbines with significant interactions". Applied Energy, Vol 321, 119341

Zhang, Y., Zhang, Z., Zheng, J., Zheng, Y., Zhang, J., Liu, Z., & Fernandez-Rodriguez, E. (2023). Research of the array spacing effect on wake interaction of tidal stream turbines. Ocean Engineering, 276.

Zilic de Arcos, F., Tampier, G., & Vogel, C. R. (2020). Numerical analysis of blockage correction methods for tidal turbines. Journal of Ocean Engineering and Marine Energy, 6(2), 183–197. https://doi.org/10.1007/s40722-020-00168-6

ITTC2024

30TH INTERNATIONAL TOWING TANK CONFERENCE
22–27 SEPTEMBER 2024 | HOBART TASMANIA AUSTRALIA

REPORT OF THE SPECIALIST COMMITTEE ON ICE

SPECIALIST COMMITTEE ON ICE

1. INTRODUCTION

1.1 Membership and Meetings

The members of the Specialist Committee on ice of the 30th ITTC are:

- Franz von Bock und Polach (Chair), Hamburg University of Technology, Germany
- Takatoshi Matsuzawa (Secretary), National Maritime Research Institute (NMRI), Japan
- Aleksei Alekseevich Dobrodeev, Krylov State Research Centre (KSRC), Russia (Secretary and member until May 2023)
- Nils Reimer, Hamburgische Schiffbau-Versuchsanstalt GmbH (HSVA), Germany
- John Wang, National Research Council of Canada, Canada
- Yukui Tian, China Ship Scientific Research Centre (CSSRC), China
- Yan Huang, Tianjin University, China
- Jinho Jang, Korea Research Institute of Ships and Ocean Engineering (KRISO), Korea
- Riikka Matala, Aker Arctic, Finland
- Otto Puolakka, Aalto University, Finland

The following committee meetings have been held during the work period:

- October 26, 2021, online meeting; Participants: Franz von Bock und Polach (Chair), Aleksei Dobrodeev (Secretary), John Wang Nils Reimer, Yan Huang, Takatoshi Matsuzawa, Jinho Jang, Otto Puolakka, Riikka Matala, Yukui Tian

- May 6, 2022, online meeting; Participants: Franz von Bock und Polach (Chair), Aleksei Dobrodeev (Secretary), John Wang Nils Reimer, Yan Huang, Takatoshi Matsuzawa, Riikka Matala, Yukui Tian Absent: Jinho Jang, Otto Puolakka,

- October 4, 2022, online meeting; Participants: Franz von Bock und Polach (Chair), Aleksei Dobrodeev (Secretary), Nils Reimer, Takatoshi Matsuzawa, Riikka Matala, Yukui Tian Absent: Jinho Jang, Otto Puolakka, Yan Huang, John Wang

- December 2, 2022, online meeting; Participants: Franz von Bock und Polach (Chair), Aleksei Dobrodeev (Secretary), Nils Reimer, Takatoshi Matsuzawa, Riikka Matala, Yukui Tian, John Wang

Absent: Jinho Jang, Otto Puolakka, Yan Huang

- February 22, 2023, online meeting; Participants: Franz von Bock und Polach (Chair), Nils Reimer (Acting Secretary), Takatoshi Matsuzawa, Riikka Matala, Yukui Tian Absent: Jinho Jang, Otto Puolakka, Yan Huang, Aleksei Dobrodeev (Secretary), John Wang

- May 12, 2023, online meeting; Participants: Franz von Bock und Polach (Chair), Takatoshi Matsuzawa (Secretary), Takatoshi Matsuzawa, Riikka Matala, Yukui Tian, Otto Puolakka, Yan Huang; Absent: Jinho Jang, John Wang

- July 4, 2023, online meeting; Participants: Franz von Bock und Polach (Chair), Takatoshi Matsuzawa (Secretary), Takatoshi Matsuzawa, Riikka Matala, Yukui Tian, Otto Puolakka, John Wang; Absent: Jinho Jang, Yan Huang

- November 14, 2023, online meeting; Participants: Franz von Bock und Polach (Chair), Takatoshi Matsuzawa (Secretary), Takatoshi Matsuzawa, Riikka Matala, Yukui Tian, John Wang; Absent: Jinho Jang, Yan Huang, Otto Puolakka

- January 30, 2024, online meeting; Participants: Franz von Bock und Polach (Chair), Takatoshi Matsuzawa (Secretary), Takatoshi Matsuzawa, Riikka Matala, Yukui Tian, John Wang Absent: Jinho Jang, Yan Huang, Otto Puolakka

- May 6-7, 2024, Hamburg; Participants: Franz von Bock und Polach (Chair), Takatoshi Matsuzawa (Secretary), Takatoshi Matsuzawa, Riikka Matala, Yukui Tian, John Wang Absent: Jinho Jang, Yan Huang, Otto Puolakka

1.2 Tasks

The recommendations for the work of the Specialist Committee on Ice as given by the 29th ITTC were the Terms of Reference (TORs):

1. Continue to maintain, review and update existing accepted procedures and guidelines in accordance with current practice.
2. Continue work on uncertainty analysis including conducting benchmarking study among ice model basins. Focus on the largest error sources is recommended such as the uncertainty related to the ice properties. Based on conducted measurement and analyses, include review how the findings may reflect ice measurements.
3. Develop Guideline 7.5-02-04-02.5 – Ice Property Tests, including findings related to the uncertainty analysis.
4. Revise the procedure 7.5-02-04.1 Ship Trials in Ice. Pay special attention to ice conditions (such as flexural strength, thickness, snow coverage / density and ice types).
5. Continue to develop Guideline for the Testing of Fixed Structures, including monopiles, based on prepared outline (Table of Content). Pay special attention to scaling issues for vertical structures where crushing strength is dominant.
6. Review State of the Art on numerical modelling.
7. Review and study current methods for testing Waves in Ice and based on this prepare outline for Guidelines.
8. Review State of the Art on underwater radiated noise (URN) in ice conditions with respect to the relevance of URN topic in general and in cooperation with the SC on Cavitation and Noise

In the process of the term it was decided to combine the tasks 2 & 3 and join them into one guideline.

2. STATE OF THE ART

This section resembles the TORs 6 & 8 which are state of the art reviews on numerical modelling and Underwater Radiated Noise.

2.1 Review State of the Art on numerical modelling (TOR6)

This paper contains a review and analysis of some numerical methods, which have found their application in modelling the ice–structure interaction process. It has to be emphasized that the suitability of certain methods may depend on the modelled scenario or purpose.

Recent comprehensive overviews and reviews for structure-ice interaction by Makarov et al. (2022), ships in ice (Xue et al. 2020) and specifically ships in broken ice (Li und Huang 2022) exist. This report provides an overview over the most relevant and frequently used models. Other approaches and methods are briefly stated in a subsection at the end of this section.

A significant aspect of ice-ship interactions is the determination of continuous and arbitrary fragmentation between computational elements. Various forms of rupture can occur when sea ice interacts with the hull of a ship. For example, local buckling damage or global cleavage damage depends on the nature of the ice cover contact, boundary conditions and geometry. Capturing these different failure modes in numerical simulations based on conventional continuum media mechanics can be quite challenging (Liu et al. 2018). In addition to the scenario also the scale of the scenario to be modelled might affect the suitability of the method.

2.1.1 Existing methods for numerical modelling of ice-structure and ship-ice interaction.

The following methods exist (Makarov et al. 2022; Xue et al. 2020) :

2.1.1.1 The Finite Element Method (FEM)

The finite element method is a start of the art method in structural engineering and is therefore often very suitable assessing the interaction of ice on a structure. This method solves partial differential equations. The modelled geometry model is discretized into finite elements and partial differential equations are solved.

Several FEM based models exist with different scopes and material models. One model that has been developed in connection with medium scale experiments and is also validated against third party experiments is the MCNS model (Herrnring und Ehlers 2022). This is a finite element based model, which uses a Mohr-Coulomb material model for the ice and a critical strain to split nodes between elements when failure occurs. This is currently one of the most used models due to satisfying experimental validation. This model has also been used for high impact loads (Müller et al. 2023) and was the basis for a model for propeller ice interaction (Böhm et al. 2024). In both of the latter cases experimental data are used for comparison and validation.

Other frequently used FEM models to asses ice loads are Dolney, J. and Daley, C.; Gagnon; Sazidy (2015; 2011; 2015). The model of Gagnon (2011) is a compressible foam model, which does not entirely reflect the phenomenological deformation of the ice, but resulting forces appear to correlate with measurements and observations made to some degree. The exact limitations of the above mentioned models remain to be investigated.

The cohesive element or cohesive zone method (CZM) is another approach for the division or separation of ice elements (Kellner et al. 2021; Konuk et al. 2009a, 2009b). It is often used with finite elements and is part of several solver, hence it is accommodated in this section. Those CZM models use, a traction–separation law (TSL) to capture the softening behaviour. The TSL curve process to cracking and employs one law to estimate both crack nucleation and propagation without any pre-set variables (Mulmule und Dempsey 1997; Xue et al. 2020). Important unknowns of any initial boundary value problem concerning fracture is on how to determine the crack propagation surface (Konuk et al. 2009a, 2009b). Therefore, it is of high importance to determine the traction–separation curve (Xue et al. 2020). The latter may be considered as critical parameters, which can however not be directly measured and may require an indirect calibration with measurements, which might limit the transferability of models to different scenarios.

A finite element model developed specifically for model-ice is found in von Bock und Polach; von Bock und Polach und Ehlers (2015; 2013), where the cracking and failure is modelled through element deletion. This violates the postulation of conservation of mass, however as the element size is aligned with grain sizes it was considered acceptable. The element size makes it also computationally very costly limiting it for practical applications.

2.1.1.2 Smoothed Hydrodynamic Particle method (SPH)

The smoothed particle hydrodynamic (SPH) method is meshless method developed as a meshless particle method (MPM) in a Lagrangian framework to overcome the reliance on meshes of traditional mesh-based methods and has been used in the fields of fluid mechanics, aerodynamics, astrophysics and deformable solid mechanics since its inception. The smoothed particle hydrodynamics approach involves dividing the region into individual particles. These particles have a spatial distance, called the smoothing length, at which their properties are 'smoothed' by a kernel function (Makarov et al. 2022). The effect of each particle on the material properties is assessed according to its density and distance from the associated particle.

The interaction of ships in ice is found in simulations of ship-horizontal ice interactions (Zhang et al. 2019). Similar to the FEM the SPH method allows the integration of specific material models. For example an elastic-plastic intrinsic model with a damage model and a Drucker-Prager yield criterion was introduced within the SPH framework to capture the plastic failure behavior of ice (Zhang et al. 2017). The fluid as an elastic basis is compared with the fluid-solid coupling interaction to investigate its effect on the ice-breaking resistance, i.e., the ice-breaking resistance and the submergence resistance during ice breaking. In the meantime, the SPH method is still in the early stages of development in ice simulation. and the aforementioned models also require an external crack expansion criterion to simulate damage (Zhang et al. 2019).

2.1.1.3 Discrete Element Method (DEM)

The DEM is primarily used for modeling discrete granular media (Cundall und Strack 1979). Among other meshless methods, DEM models have been used for various problems on ice mechanics summarized in Tuhkuri und Polojärvi (2018) and are recognized as an effective numerical method for analyzing ice ship interactions (Dempsey 2000). The main idea of the method is to represent the simulated medium as a set of computational elements with their own properties (density, elastic modulus, etc.). The method can describe the discrete nature of ice at the microscopic scale and reasonably model the ice-breaking phase in ship-ice interaction at the macroscopic scale representing the process of ice break-up transport and accumulation, and that this process will significantly influence later sea ice break-up events (Tuhkuri und Polojärvi 2018). Discrete elements can have different sizes and shapes, and forces are calculated based on Newton's law and contact force models (Makarov et al. 2022; Tuhkuri und Polojärvi 2018). The DEM-based approach allows for the simulation of broken ice in a non-bonded state, where discrete particles characterize broken sea ice elements individually, and the introduction of a spring bond model for modeling floating and level ice under multi-elements bonding. Especially for operations in ice floes this approach is suitable.

Oceanic Consulting Corporation developed a block-based discrete element approach (DECICE) based on the National Research Council of Canada (NRC) and carried out simulations of ship maneuverability (turning and zigzag maneuvers) (Lau et al. 2011).

The GEM (GPU-Event Mechanics) software from Memorial University of Newfoundland, Canada. This software has pre- and post-processing capabilities, uses a discrete quasi-3D model and block cells, is computationally efficient, and allows for large scale long time simulations in a GPU parallel environment, but the reliability of the computational results is low and the validation results are not very satisfactory (Daley et al. 2014). However, despite missing publications on the GEM insight from the SC members is that the tool has been developed further since 2014, but concluding remarks on capacity cannot be made.

The joining of discrete elements may be facilitated with a finite-element-discrete element coupling method (FEM-DEM). The interaction between the ice blocks is calculated using discrete elements and the internal forces and deformations of the ice blocks are calculated by finite elements. This allows the modelling of larger ice sheets, while accounting for subsequent interactions after initial breaking. Recent developments with in-house codes are made at Aalto University, Finland (Lilja et al. 2019; Ranta et al. 2017). Recent work conducted at the Hamburg University of Technology uses DEM for a ship in ice floes, where the elements themselves are broken as well by different analytical and semi-analytical models (Sapp 2023). The model of Sapp (2023) is as most other codes an in-house development using the earlier development of Erceg et al. (2022) as basis.

The simulation of ice floe fields appears to be the main domain of the DEM method (see also Xue et al. 2020).

2.1.2 Other Methods

The above list is not exhaustive as a high variety of numerical methods exist, but of reduced maturity and popularity than those mentioned above. Based on Makarov et al. (2022) the following methods are considered to be mentioned:

- Smoothed Particle Galerkin method (SPG)
- Galerkin Discontinuous Method
- Smoothed Particle Galerkin method (SPG)
- The Lattice Boltzmann Method (Janßen et al. 2015)
- Coupling of methods, such as *FEM–SPH–SPG*
- Ice breaking model (Erceg et al. 2022) based on infinite wedge theory (Nevel 1961)
- Phase field modelling (currently explored at Hamburg University of Technology)

2.1.3 Concluding remarks

In addition to the robustness of the theory also the computational costs need to be accounted for in simulating certain scenarios. The following conclusion is drawn by Xue et al. (2020) (Table 1). It is to be underlined that the analysis of Xue et al. (2020) focussed on ship-ice interaction such as icebreaking, but not the calculation of local loads.

Method	Computational cost	Theory Robustness
DEM	medium	Low
FEM	low	High
SPH	high	medium
Peri-Dynamics	high	high

Table 1: Evaluation of numerical methods for ship ice interaction.

With respect to ice-structure interaction FEM based models appear to be most frequently used. The modelling of ice structure interaction is usually a local modelling, where the impact of ice on certain hull regions is investigated. The application of FEM may refer to the quality of the models, but is certainly also attributed to the fact that FEM is the superior state of the art for structural analysis and consequently FEM models of ice are preferred to transfer ice induced loads to the structure. Furthermore, FEM has a low barrier for usage, as most material models are already available in different software.

Popular models are: Dolney, J. and Daley, C.; Gagnon; Herrnring und Ehlers; Sazidy (2015; 2011; 2022; 2015).

The potential of certain methods for simulating ice-ship interaction is strongly purpose bound.

2.2 Review State of the Art on underwater radiated noise (URN) in ice conditions with respect to the relevance of URN topic in general and in cooperation with the SC on Cavitation and Noise (TOR8)

Within the SC on Ice no experts on noise and cavitation are present. A cooperation with the SC on Cavitation and Noise could not be established. The review was done with best effort under the mentioned conditions.

2.2.1 Introduction

The situation of URN in ice-covered water is quite different from non-ice regions in such as noise sources, propagation, and impact on marine mammals. The Protection of the Arctic Marine Environment Working Group (PAME 2019) published a comprehensive report on URN with Arctic ship traffic analysis, calculation of underwater noise source levels of ships, noise propagation models, and acoustic overlap between Arctic marine mammals and URN (PAME 2019). The report refers to (Roth et al. 2013)describing a result of a full-scale URN measurement on USCG Healy. Although these works of literature partly reveal what URN is in ice-covered conditions, the data still needs to be sufficient to understand URN in ice to develop reasonable prediction models.

2.2.2 Propeller-induced URN in Ice

In general, propeller-induced noise is the most considerable in URN from ships. In view of engineering, the design of a propeller in ice differs from that of normal. The interference of ice results in variation of hydrodynamics and propulsion efficiency. The interaction of ice and propeller results in increase of loading characterized of strong randomness and non-linearity. There correspondingly presents the influence on structure response and strength.

The presence of ice changes the cavitation phenomena. Noise of low frequency liner spectrum and high frequency broadband correspondingly varies. Generally, the propeller noise level increases (Acoustics in ice).

How to test, capture and analyse the noise raises needs for new techniques.

Sound radiation in far field with ice would be more complicated. How to deal with it in time domain, spectral domain and spatial distribution would differ from normal.

Throughout the above topics, further studies on theory, mechanism, testing methods, analysis, and prediction seem to be necessary. Some of them can be jointly studied by the SC on Cavitation and Noise and the SC on Ice.

2.2.3 Literature Survey

The following sections contain comments and lists of literatures on acoustic studies in ice-covered water excluding for general URN.

2.2.3.1 Shipping Increase in Arctic Region

- PAME (2021) UNDERWATER NOISE POLLUTION FROM SHIPPING IN THE ARCTIC

ASTD (Arctic Ship Traffic Data) for the traffic and Wittekind model for noise level estimation were used and Geospatial noise impact distributions were introduced (PAME 2019). Jalkanen et al. (2022) stated that: "*Shipping noise emissions increase rapidly in Arctic areas and the Norwegian Sea. The largest contributors are the containerships, dry bulk and liquid tanker vessels which emit 75% of the underwater shipping noise source energy*." Furthermore, The STEAM (Ship Traffic Emission Abatement Model) by FMI, with Wittekind model inside, was used to estimate underwater noise, however it appears that this is not including ice (Jalkanen et al. 2022).

2.2.3.2 Soundscape of Arctic / Sound Propagation Models

During the 1960s – 1970s: ambient noise under ice was measured in a few field experiments in the Arctic.

- In the Canadian Arctic Archipelago with measurements of spectrum levels of ambient noise. The noise mechanism: cracking-noise, ice-fracturing noise (Milne und Ganton 1964).
- East Greenland Sea: The sound spectrum level under ice is lower than in open water areas and some acoustic propagation models with ice cover have been developed (Diachok und Winokur 1974).

- MIZ in 2013 were simulated and compared. The simulation with the OASES (Ocean Acoustic and Seismic Exploration Synthesis) model suggests that the roughness under ice causes the weakening of the wave (Hope et al. 2017).

- Simon et al. (2018) Modeling acoustic wave propagation and reverberation in an ice covered environment using finite element analysis. Simon et al. (2018) used a 3-D FEM and compared this with OASES (Hope et al. 2017). This appears to be a good background note. Full of model-related references.

- The Acoustical Society of America featured Arctic soundscape in the “Special Issue on Ocean Acoustics in the Changing Arctic” in their journal throughout 2022. According to the supplement of the journal, there existed some presentations relating to Arctic at the society’s meetings in 2022 as follows:

    - Heaney et al. (2022): The Arctic underwater soundscape today and as projected for 2030. Projections of ice cover and shipping routes along and between the northern borders of Arctic countries were used to forecast potential future (2030) Arctic soundscapes.

    - Webstey et al. (2022): Ship noise radiation characteristics observed from an Arctic acoustic array. The multi-channel acoustic recordings with a 48-hydrophone array mounted on the ship bottom were conducted in Arctic.

2.2.3.3 Noises in Icebreaking Operation

There is little knowledge of icebreaking noise itself, but the propulsor noise and the cavitation noise during icebreaking are seriously high shown in the following studies.

The Sparton AN/SSQ-57B sonobuoy was employed to record underwater noise in the ice operation of Healy (Roth et al. 2013). The noise sources are: propeller cavitation, propulsion machinery, and medium-speed diesels (operating at slow speeds). The sound scattering or reradiating from the water-ice interface is not thought to contribute meaningfully to the overall noise (Roth et al. 2013). Compared to open-water transit, Healy’s noise signature increased approximately 10 dB between 20 Hz and 2 kHz when breaking ice. High noise situations occurred in low speed and high RPM, propeller operating in opposing directions, backing and ramming, resulting in cavitation (Roth et al. 2013).

In Geyer et al. (2016) the noise sources are distinguished by the frequency using the same dataset as in Roth et al. (2013). The ship noise from icebreaking appears at the 25-50 Hz frequency band, while the engine noise appears at around 330 Hz, which is considerably high.

2.2.3.4 Experimental Study of Cavitation in Ice Blockage and Milling Condition

- Atlar, M. et al (2003) Cavitation in Ice-Milling with a Podded Propulsor. 4th ASME/JSME Joint Fluids Engineering Conference, 2003.

The advance coefficient of the propeller with high-speed operation during icebreaking navigation is low (Atlar et al. 2003). For the propeller under heavy load and being blocked by ice can easily cause the surface pressure of the blade to drop sharply and generate cavitation (Atlar et al. 2003).

3. PROCEDURES

The following Procedures were revised and updated. In addition to corrections and amendments the symbols in all Procedures were reviewed and corrected follow the ITTC Symbols and Terminology List, Version 2017.

3.1 Updates on the Reviewed and Revised Procedures

3.1.1 7.5-02-04-01 General Guidance and Introduction to Ice Model Testing

In this Guidelines there was only some minor spelling error corrections in Equations 1 and 2.

1. The General Guidance and Introduction to Ice Model Testing was reviewed and minor corrections were applied. Small additions were made in section 1 "Purpose of the Guideline" including information whom the guideline shall address.

2. Some language and refinement of terminology were made in section 2.1 "Facilities, Ice Conditions and Ship Model".

3. In section 2.2 "Model Ice Production" The definition of model ice "seeding" was corrected.

3.1.2 7.5-02-04-02 Test Methods for Model Ice Properties

The procedures and guidelines of test methods for model ice properties was reviewed and modified to better describe the current practices. Some editorial changes were done. The most significant changes in the guideline were as follows: When measuring flexural strength using cantilever beam test downwards in situ, it is notified that the force induced by submerging the beam in the water might need to be considered depending on the beam dimensions.

The method for determining level ice shear force is removed from the guideline because the current committee did not recognize the method.

The potential significance of friction coefficient between ice fragments (ice-ice friction) is recognized in the new revision. One method for its determination is provided.

3.1.3 7.5-02-04-02.1 Resistance tests in ice

In addition to minor editorial changes to wording/spelling, two main modifications were made in this procedure regarding:

1. the description of device for force measurement in test methods, and

2. the introduction of a new symbol for rest resistance related to ice and besides resistance due to breaking the ice in analysis of tests in intact level ice.

In Section 2.1 Test Methods, the apparatus for force measurement was modified from dynamometer to force transducer considering that dynamometer is not an optimal term for this part while force transducer is the most accurate one and practically used for ice model basins in resistance tests. "A dynamometer" or "dyno" for short, as known, is a device for simultaneously measuring the thrust, torque and rotational speed (RPM) of an engine, motor or other rotating prime mover so that its instantaneous power may be calculated, and suitable for the occasions of self-propulsion or towed-propulsion testing in ice. In total, three corrections in such a way of replacing dynamometer with force transducer were made where two were for explaining the alternative test setups in 2.1.1 and one was for noting measured towing force in 2.1.2.

In Section 2.2 Analysis of Results, R_r, ice resistance other than ice breaking component R_{br}, i.e. rest resistance containing submerging, clearing, etc., was originally given as part of the net ice resistance RI. However, Rr is defined as residual resistance in the current ITTC symbols. To avoid confusion, a new symbol R_{rR} was proposed and put instead in equation (8) and (9) in 2.2.1.3 elaborating correction of minor deviations in flexural strength for resistance. R_c, resistance for ice clearing, are also confusable, but no reaction was made because it is not conflicted with any existing ITTC symbols. (RC is used as steady turning radius, but the subscription C is capital in this case.)

3.1.4 7.5-02-04-02.3 Manoeuvring Tests in Ice

During ITTC29 this procedure received a substantial update. Consequently, no significant modifications are proposed.

3.1.4.1 Turning circle test

In this section, the following was added: "*Thruster angles and rudder position can be subjected to changes during the manoeuvre.*"

3.1.5 7.5-02-04-03 Guidelines for Modelling of Complex Ice Environments

This guideline addresses complex ice environments, including ridges, brash ice channels, rubble fields, managed ice, pack ice, compressive ice, and snow-covered ice. Some of these were not explicitly mentioned in the introduction and have been added.

In the previous guidelines, a statement could have been misinterpreted to mean that the crest edges of the ridge are always consolidated. They are not consolidated in some situations, so the description has been corrected as "the crest edges can be consolidated."

When reproducing the brash ice channel, the previous guidelines noted that the size of the ice pieces depends on the scale or scenario. However, what is essential is that the number and size of ice fragments in the reproduced brash ice channel reflect the actual interaction phenomena, so this was clearly stated in the description.

Grammatical errors and missing words were corrected. Sources for some figures and references were added, and the text became more accurate than the previous guidelines overall.

3.2 Revise the procedure 7.5-02-04.1 Ship Trials in Ice. Pay special attention to ice conditions (such as flexural strength, thickness, snow coverage / density and ice types) (TOR4)

The entire guideline was re-organised in sections reflecting the procedure and tasks applied on ice trials:

1. Purpose of this Guideline
2. Trial Conditions
3. Performance Tests
4. Manoeuvring Tests
5. Data Acquisition System
6. Data Analysis

In section 1 "Purpose of this Guideline" the text was modified with respect to the main objectives and focus of the guideline.

In section 3.3 "Tests in ridges" a passage was added describing the procedure and limitation for ridge tests astern. New figures have been added to the sections.

The entire section 4 "Manoeuvring Tests" was overworked and descriptions of further relevant manoeuvres such as break out tests and star manoeuvre were added. The figures have been replaced by ones of higher quality. New figures have been included to illustrate the additional described manoeuvres. The figures include definitions of the most relevant parameters that are to be determined.

The section 5.3 "Ice properties" has been extended significantly. The descriptions of each property measurement procedure is more detailed and figures are added to provide an impression of field work and illustrate the methods.

The list of data to be recorded was extended in section 5.5. "Initial conditions".

In Section 6 "Data Analysis" high level descriptions of correction methods and correlation factors are included in the revised guideline.

The language and formatting of the entire procedure is adjusted and revised.

4. FINAL REPORT AND RECOMMENDATIONS TO THE 30TH ITTC

4.1 Develop Guideline 7.5-02-04-02.5 – Ice Property Tests, including findings related to the uncertainty analysis. (TOR 3&2)

As mentioned previously this TOR3 is combined with TOR2 ("*Continue work on uncertainty analysis including conducting benchmarking study among ice model basins. Focus on the largest error sources is recommended such as the uncertainty related to the ice properties. Based on conducted measurement and analyses, include review how the findings may reflect ice measurements.*").

The draft of this procedure required significant work and interaction with various experts leading to a delay in finalizing the procedure in consequence of which the draft could not be published as procedure. The draft is submitted to the ITTC and available for future committees to finalize the process. A brief description is provided below:

1. This procedure is considered interim and is not being published at this time due to the lack of review time. The committee hopes that this procedure will be thoroughly reviewed and published in the next term. However, a brief overview is provided. This procedure follows the ITTC 7.5-02-01-01 (ITTC 7.5-02-01-01) Guide to the Expression of Uncertainty in Experimental Hydrodynamics, which is based on the International Organization for Standardization (ISO) Guide to the Expression of Uncertainty in Measurement, also called GUM (JCGM)

2. The primary sources of uncertainty from ice model tests could be the ice properties or repeatability of ice tests. This procedure provides an example of analysing the uncertainty of main ice properties such as ice thickness, ice flexural strength, and hull-ice friction. Repeatability was considered using previous repeat test data.

3. A generic ice resistance correction equation was developed and used for the uncertainty analysis. Type A and Type B uncertainties were considered. The uncertainty for each ice property and repeatability was calculated based on the published dataset, and the total uncertainty results were determined.

4.2 Continue to develop Guideline for the Testing of Fixed Structures, including monopiles, based on prepared outline (Table of Content). Pay special atten-

tion to scaling issues for vertical structures where crushing strength is dominant (TOR5)

Especially with respect to the shift towards renewable energies, the topic of fixed structures in ice is considered highly relevant.

The committee prepared a draft submitted to the ITTC. However, within the SC committee it is concluded that the state of the art is not mature enough to propose a procedure. For fixed and vertical structures different scaling principles are needed which are not developed yet as well as the current state of the art model ice is not suitable for vertical and fixed structures. Attempts to for new developments are made, but not fully explored and are rather at trial stage. GESA developed a new model ice with focus on the crushing properties and a high flexural strength. The model ice is produced similar as ice at sea with a water surface excited by a wavemaker. A proof of principle was established, but neither scalability nor scaling laws are explored or defined. The committee agrees that such a guideline is needed especially with respect to offshore wind energy, but more development is needed so that the state of the art is suitable for a guideline.

4.3 Review and study current methods for testing Waves in Ice and based on this prepare outline for Guidelines (TOR7)

Currently world-wide three facilities that can produce waves in ice:

- Aalto University (granular model ice),
- HSVA (columnar model ice)
- University of Melbourne (no model ice, frozen water, fresh water ice).

Consequently, the state of the art is slim and it was decided that the state of the art is not mature enough to compile a guideline or significant content. However, it is acknowledged that experimental wave-ice investigation is key to understand the behaviour of such as waves in ice and wave induced break-up.

At this current stage, focus was put on focus on those as those are considered being base cases. In recent works it was identified for wave-level ice interaction especially wave steepness, elastic modulus and the flexural strength are important and on this basis scaling similitudes are developed with a focus on the elastic properties of the ice (Colin Fox 2001; von Bock und Polach et al. 2021a). However, model ice tends to have flexural rigidity or elastic modulus which is not in scale (von Bock und Polach et al. 2019). As already indicated above this might require alternative scaling approaches (case based scaling, von Bock und Polach et al. (2021b).

On this basis in von Bock und Polach et al. (2021a) the Model Ice of Virtual Equivalent Thickness (MIVET) is introduced which is thinner, but with a higher elastic modulus as postulated by introduced scaling laws. It could be shown that the excessive damping in classic model ice is significantly reduced (von Bock und Polach et al. 2021a).

For the testing of waves in ice observing non-linear relationships (Hartmann et al. 2019), damping (Passerotti et al. 2022) or both also the visco-elastic properties must be set in scale as those appear relevant for the progression of waves in ice (K K Dharma Sree et al. 2019).

It appears that the damping and apparent visco-elastic properties are exaggerated in model ice due to non-linear material behaviour and cross-coupling effects with the low elastic modulus, but to date no validated method exists measuring visco-elastic properties in model ice and scaling those with respect to full-scale values.

Consequently, testing waves in model ice still requires work on fundamentals from ice property testing methods to scaling. Especially practical limitations might require *case based scaling*.

5. CONCLUSIONS

5.1 State of the Art

The state of the art of underwater radiated noise in ice is beyond the expertise of the SC on Ice. It is acknowledged that it is a topic of relevance, but in future considerations, the SC on Ice should rather act as a consultant to the SC of experts on noise and cavitation.

The state of the art on numerical modelling is rather well described in various review papers and methods appear at least theoretically explored. The next necessary step would be numerical benchmark studies in order to assess the quality of results between the different methods.

The state of the art review indicated furthermore overlap with activities of the ISSC (International Ship Structures Committee) and a joint coordination of ISSC and ITTC activities seems reasonable.

5.2 Future Work

Review of the state-of the-art: maintain, revise, and update existing procedures and guidelines in accordance with current practice.

Fundamental uncertainty analysis of model ice properties: benchmark study among ice tanks is preferable.

Members suggest topics to be discussed in the next Committee on Ice as below:

- Guidelines for performance prediction in various ice conditions such as broken, rafted, or deformed ice.
- Knowledge accumulation of snow on ice, which impacts resistance.
- Underwater radiated noise is a hot topic, but testing is inauspicious.
- Scaling of ice-propulsor interaction.
- Uncertainty assessment or more consistent guidelines of brash ice test.
- Fundamental uncertainty analysis of model ice properties: benchmark study among ice tanks is preferable.
- Standardize the simple ice-breaking resistance model to verify the ice tank characteristics.

6. REFERENCES

Atlar, Mehmet; Prasetyawan, Ika; Aryawan, Wasis Dwi; Wang, Dazheng; Sasaki, Noriyuki (2003): Cavitation in Ice-Milling With a Podded Propulsor. In: Volume 1: Fora, Parts A, B, C, and D. ASME/JSME 2003 4th Joint Fluids Summer Engineering Conference. Honolulu, Hawaii, USA, 06.07.2003 - 10.07.2003: ASMEDC, S. 269–278.

Böhm, Angelo; Sapp, Lina; von Bock und Polach, Rüdiger Ulrich Franz (2024): Derivation of a numerical propeller-ice interaction model. Norwegian University of Science and Technology, Department of Marine Technology. Unter Mitarbeit von TUHH Universitätsbibliothek. In: Technische Universität Hamburg, Port Said University (Hg.): 8th International Symposium on Marine Propulsors, smp 2024. Unter Mitarbeit von TUHH Universitätsbibliothek. Berlin.

Colin Fox (2001): A Scaling Law for the Flexural Motion of Floating Ice. In: J P Dempsey und H H Shen (Hg.): Springer Netherlands, S. 135–148.

Cundall, P. A.; Strack, O. D. L. (1979): A discrete numerical model for granular assemblies. In: *Géotechnique* 29 (1), S. 47–65. DOI: 10.1680/geot.1979.29.1.47.

Daley, Claude; Alawneh, Shadi; Peters, Dennis; Colbourne, Bruce (2014): GPU-Event-Mechanics Evaluation of Ice Impact Load Statistics. In: OTC Arctic Technology Conference. OTC Arctic Technology Conference. Houston, Texas, 2/10/2014 - 2/12/2014: OTC.

Dempsey, John P. (2000): Research trends in ice mechanics. In: *International Journal of Solids and Structures* 37 (1-2), S. 131–153. DOI: 10.1016/S0020-7683(99)00084-0.

Diachok, O. I.; Winokur, R. S. (1974): Spatial variability of underwater ambient noise at the Arctic ice-water boundary. In: *The Journal of the Acoustical Society of America* 55 (4), S. 750–753. DOI: 10.1121/1.1914594.

Dolney, J. and Daley, C. (2015): ONR Ice Capability Assessment & Experimental Planning – Deliverable #2: Advanced Modeling and Re-assessment of NSWCCD HULL 3000. Unter Mitarbeit von ABS Technical Report prepared for ONR.

Erceg, Sandro; Erceg, Boris; Bock und Polach, Franz von; Ehlers, Sören (2022): A simulation approach for local ice loads on ship structures in level ice. In: *Marine Structures* 81, S. 103117. DOI: 10.1016/j.marstruc.2021.103117.

JCGM, 2008: Evaluation of measurement data - Guide to the expression of uncertainty in measurement.

Gagnon, R. E. (2011): A numerical model of ice crushing using a foam analogue. In: *Cold Regions Science and Technology* 65 (3), S. 335–350. DOI: 10.1016/j.coldregions.2010.11.004.

Geyer, Florian; Sagen, Hanne; Hope, Gaute; Babiker, Mohamed; Worcester, Peter F. (2016): Identification and quantification of soundscape components in the Marginal Ice Zone. In: *The Journal of the Acoustical Society of America* 139 (4), S. 1873. DOI: 10.1121/1.4945989.

ITTC 7.5-02-01-01, 2014: Guide to the Expression of Uncertainty in Experimental Hydrodynamics,, zuletzt geprüft am 2023.

Hartmann, Moritz; von Bock und Polach, R. U. Franz; Ehlers, Sören; Hoffmann, Norbert; Onorato, Miguel; Klein, Marco (2019): Numerical Study on Nonlinear Wave-Ice-Interaction. In: Volume 8: Polar and Arctic Sciences and Technology; Petroleum Technology. ASME 2019 38th International Conference on Ocean, Offshore and Arctic Engineering. Glasgow, Scotland, UK, 09.06.2019 - 14.06.2019: American Society of Mechanical Engineers.

Heaney, Kevin D.; Verlinden, Christopher; Seger, Kerri D.; Brandon, Jennifer; Hatch, Leila; Schönau, Martha; Heaney, Andrew (2022): The Arctic underwater soundscape today and as projected for 2030. In: *The Journal of the Acoustical Society of America* 151 (4_Supplement), A189-A189. DOI: 10.1121/10.0011059.

Herrnring, Hauke; Ehlers, Sören (2022): A Finite Element Model for Compressive Ice Loads Based on a Mohr-Coulomb Material and the Node Splitting Technique. In: *Journal of Offshore Mechanics and Arctic Engineering* 144 (2), Artikel 021601. DOI: 10.1115/1.4052746.

Hope, Gaute; Sagen, Hanne; Storheim, Espen; Hobæk, Halvor; Freitag, Lee (2017): Measured and modeled acoustic propagation underneath the rough Arctic sea-ice. In: *The Journal of the Acoustical Society of America* 142 (3), S. 1619. DOI: 10.1121/1.5003786.

Jalkanen, Jukka-Pekka; Johansson, Lasse; Andersson, Mathias H.; Majamäki, Elisa; Sigray, Peter (2022): Underwater noise emissions from ships during 2014-2020. In: *Environmental pollution (Barking, Essex : 1987)* 311, S. 119766. DOI: 10.1016/j.envpol.2022.119766.

Janßen, Christian; Mierke, Dennis; Überrück, Micha; Gralher, Silke; Rung, Thomas (2015): Validation of the GPU-Accelerated CFD Solver ELBE for Free Surface Flow Problems in Civil and Environmental Engineering. In: *Computation* 3 (3), S. 354–385. DOI: 10.3390/computation3030354.

K K Dharma Sree; L W K Adrian; H H Shen (2019): An experimental study on surface wave attenuation by floating viscoelastic segments. In:, 2019-June. Online verfügbar unter https://www.scopus.com/inward/record.uri?eid=2-s2.0-85070834298&partnerID=40&md5=9a35c6382529843a4c2afb920915f012.

Kellner, Leon; Lu, Wenjun; Ehlers, Sören; Høyland, Knut V. (2021): Study on the cohesive edge crack in a square plate with the cohesive element method. In: *Int J Fract*. DOI: 10.1007/s10704-021-00560-9.

Konuk, Ibrahim; Gu¨rtner, Arne; Yu, Shenkai (2009a): A Cohesive Element Framework for Dynamic Ice-Structure Interaction Problems—Part I: Review and Formulation. In: Offshore and Arctic Engineering Corporate Author International Conference on Ocean (Hg.): ASME 2009 28th International Conference on Ocean, Offshore and Arctic Engineering. May 31-June 5, 2009, Honolulu, Hawaii, USA. Volume 5, Polar and arctic sciences and technology ; CFD and VIV. ASME 2009 28th International Conference on Ocean, Offshore and Arctic Engineering. Honolulu, Hawaii, USA, 5/31/2009 - 6/5/2009: ASME, S. 33–41.

Konuk, Ibrahim; Gu¨rtner, Arne; Yu, Shenkai (2009b): A Cohesive Element Framework for Dynamic Ice-Structure Interaction Problems—Part II: Implementation. In: Offshore and Arctic Engineering Corporate Author International Conference on Ocean (Hg.): ASME 2009 28th International Conference on Ocean, Offshore and Arctic Engineering. May 31-June 5, 2009, Honolulu, Hawaii, USA. Volume 5, Polar and arctic sciences and technology ; CFD and VIV. ASME 2009 28th International Conference on Ocean, Offshore and Arctic Engineering. Honolulu, Hawaii, USA, 5/31/2009 - 6/5/2009: ASME, S. 185–193.

Lau, Michael; Lawrence, Karl P.; Rothenburg, Leo (2011): Discrete element analysis of ice loads on ships and structures. In: *Ships and Offshore Structures* 6 (3), S. 211–221. DOI: 10.1080/17445302.2010.544086.

Li, Fang; Huang, Luofeng (2022): A Review of Computational Simulation Methods for a Ship Advancing in Broken Ice. In: *JMSE* 10 (2), S. 165. DOI: 10.3390/jmse10020165.

Lilja, Ville-Pekka; Polojärvi, Arttu; Tuhkuri, Jukka; Paavilainen, Jani (2019): Effective material properties of a finite element-discrete element model of an ice sheet. In: *Computers & Structures* 224, S. 106107. DOI: 10.1016/j.compstruc.2019.106107.

Liu, R. W.; Xue, Y. Z.; Lu, X. K.; Cheng, W. X. (2018): Simulation of ship navigation in ice rubble based on peridynamics. In: *Ocean Engineering* 148, S. 286–298. DOI: 10.1016/j.oceaneng.2017.11.034.

Makarov, Oleg; Bekker, Alexander; Li, Liang (2022): Comparative analysis of numerical methods for the modeling of ice–structure interaction problems. In: *Continuum Mech. Thermodyn.* 34 (6), S. 1621–1639. DOI: 10.1007/s00161-022-01152-1.

Milne, A. R.; Ganton, J. H. (1964): Ambient Noise under Arctic-Sea Ice. In: *The Journal of the Acoustical Society of America* 36 (5), S. 855–863. DOI: 10.1121/1.1919103.

Müller, Franciska; Böhm, Angelo; Herrnring, Hauke; Bock und Polach, Rüdiger U. Franz von; Ehlers, Sören (2023): Experimental and Numerical Analysis of Ice Crushing Tests With Different Shaped Ice Specimens. In: Proceedings of ASME 2023 42nd International Conference on Ocean, Offshore & Arctic Engineering (OMAE 2023). June 11-16, 2023, Melbourne, Australia. ASME 2023 42nd International Conference on Ocean, Offshore and Arctic Engineering. Melbourne, Australia, 6/11/2023 - 6/16/2023. New York, N.Y.: the American Society of Mechanical Engineers.

Mulmule, S. V.; Dempsey, J. P. (1997): Stress-Separation Curves for Saline Ice Using Fictitious Crack Model. In: *J. Eng. Mech.* 123 (8), S. 870–877. DOI: 10.1061/(ASCE)0733-9399(1997)123:8(870).

Nevel, Donald E. (1961): The narrow free infinite wedge on an elastic foundation.

PAME (2019): Underwater Noise in the Arctic: A State of Knowledge Report. Hg. v. Protection of the Arctic Marine Environment (PAME) Secretariat, zuletzt geprüft am 2019.

Passerotti, Giulio; Bennetts, Luke G.; von Bock und Polach, Franz; Alberello, Alberto; Puolakka, Otto; Dolatshah, Azam et al. (2022): Interactions between Irregular Wave Fields and Sea Ice: A Physical Model for Wave Attenuation and Ice Breakup in an Ice Tank. In: *Journal of Physical Oceanography* 52 (7), S. 1431–1446. DOI: 10.1175/JPO-D-21-0238.1.

Ranta, Janne; Polojärvi, Arttu; Tuhkuri, Jukka (2017): The statistical analysis of peak ice loads in a simulated ice-structure interaction process. In: *Cold Regions Science and Technology* 133, S. 46–55. DOI: 10.1016/j.coldregions.2016.10.002.

Roth, Ethan H.; Schmidt, Val; Hildebrand, John A.; Wiggins, Sean M. (2013): Underwater radiated noise levels of a research icebreaker in the central Arctic Ocean. In: *The Journal of the Acoustical Society of America* 133 (4), S. 1971–1980. DOI: 10.1121/1.4790356.

Sapp, Lina (2023): Development of a floe-ice breaking simulation for the generation of propeller–ice load spectra. TUHH Universitätsbibliothek.

Sazidy, M. S. (2015): Development of velocity dependent ice flexural failure model and application to safe speed methodology for polar ships. PhD thesis. Memorial University of Newfoundland.

Simon, Blake; Isakson, Marcia; Ballard, Megan (2018): Modeling acoustic wave propagation and reverberation in an ice covered environment using finite element analysis. In:. 175th Meeting of the Acoustical Society of America. Minneapolis, Minnesota, 7–11 May 2018: Acoustical Society of America (Proceedings of Meetings on Acoustics), S. 70002.

Tuhkuri, Jukka; Polojärvi, Arttu (2018): A review of discrete element simulation of ice-structure interaction. In: *Philosophical transactions. Series A, Mathematical, physical, and engineering sciences* 376 (2129). DOI: 10.1098/rsta.2017.0335.

von Bock und Polach, Franz; Klein, Marco; Hartmann, Moritz (2021a): A New Model Ice for Wave-Ice Interaction. In: *Water* 13 (23), S. 3397. DOI: 10.3390/w13233397.

von Bock und Polach, R. U. Franz; Ziemer, Gesa; Klein, Marco; Hartmann, Moritz C. N.; Toffoli, Alessandro; Monty, Jason (2021b): Case Based Scaling: Recent Developments in Ice Model Testing Technology. In: AMERICAN SOCIETY OF MECHANICAL ENGINEERS (Hg.): ASME 2020 PROCEEDINGS OF THE ASME 39TH INTERNATIONAL CONFERENCE ON OCEAN, OFFSHORE AND… ARCTIC VOLUME 7. Polar and arctic sciences and tec. ASME 2020 39th International Conference on Ocean, Offshore and Arctic Engineering. Virtual, Online, 8/3/2020 - 8/7/2020. [S.l.]: AMER SOC OF MECH ENGINEER.

von Bock und Polach, Rüdiger; Ehlers, Sören (2013): Model scale ice — Part B: Numerical model. In: *Cold Regions Science and Technology* 94, S. 53–60. DOI: 10.1016/j.coldregions.2013.06.009.

von Bock und Polach, Rüdiger U. Franz (2015): Numerical analysis of the bending strength of model-scale ice. In: *Cold Regions Science and Technology* 118, S. 91–104. DOI: 10.1016/j.coldregions.2015.06.003.

von Bock und Polach, Rüdiger U. Franz; Ettema, Robert; Gralher, Silke; Kellner, Leon; Stender, Merten (2019): The non-linear behavior of aqueous model ice in downward flexure. In: *Cold Regions Science and Technology* 165, S. 102775. DOI: 10.1016/J.COLDREGIONS.2019.05.001.

Webstey, Aaron; Thomson, Dugald; Barclay, David R.; Topple, Jessica (2022): Ship noise radiation characteristics observed from an Arctic acoustic array. In: *The Journal of the Acoustical Society of America* 152 (4_Supplement), A200-A200. DOI: 10.1121/10.0016023.

Xue, Yanzhuo; Liu, Renwei; Li, Zheng; Han, Duanfeng (2020): A review for numerical simulation methods of ship–ice interaction. In: *Ocean Engineering* 215, S. 107853. DOI: 10.1016/j.oceaneng.2020.107853.

Zhang, Ningbo; Zheng, Xing; Ma, Qingwei (2017): Updated Smoothed Particle Hydrodynamics for Simulating Bending and Compression Failure Progress of Ice. In: *Water* 9 (11), S. 882. DOI: 10.3390/w9110882.

Zhang, Ningbo; Zheng, Xing; Ma, Qingwei; Hu, Zhenhong (2019): A numerical study on ice failure process and ice-ship interactions by Smoothed Particle Hydrodynamics. In: *International Journal of Naval Architecture and Ocean Engineering* 11 (2), S. 796–808. DOI: 10.1016/j.ijnaoe.2019.02.008.

ITTC2024

30TH INTERNATIONAL TOWING TANK CONFERENCE
22–27 SEPTEMBER 2024 | HOBART TASMANIA AUSTRALIA

APPENDIX 1
COMMITTEE MEMBERS

EXECUTIVE COMMITTEE	
Dr. Kourosh Koushan (Chair)	SINTEF Ocean (formerly MARINTEK)
Geographical Area Representatives	
Art Reed (rep. Americas)	Naval Surface Warfare Center, Carderock Division
Dr. Claus D. Simonsen (rep. Northern Europe)	FORCE Technology
Lanfranco Benedetti (rep. Southern Europe)	CNR-INM
Dr. Janou Hennig (rep. Central Europe)	Hamburgische Schiffbau-Versuchsanstalt GmbH (HSVA)
Prof. Yonghwan Kim (rep. South and East Asia)	Seoul National University
Chunrong He (rep. North and West Asia)	China Ship Scientific Research Centre (CSSRC)
Prof. Toru Katayama (rep. Pacific Islands)	Osaka Metropolitan University
Ex Officio Members	
Prof. Gerhard Strasser (Advisory Council Chairman)	Schiffbautechnische Versuchsanstalt in Wien
Dr. Didier Fréchou (29th Conference Chairman)	DGA Hydrodynamics
Michael Woodward (30th Conference Chairman)	Australian Maritime College
Secretary	
Mr. Aage Damsgaard (EC Secretary)	FORCE Technology
John Koch Nielsen	Future EC Secretary

ADVISORY COUNCIL

Ilkka Saisto	Aker Arctic Technology Inc.
Takashi Mikami	Akishima Laboratories (Mitsui Zosen) Inc.
Gregor Macfarlane	Australian Maritime College
Ms. Marta Pedisic Buca	Brodarski Institute, Ship Hydrodynamics and Physical Modelling
Prof. Dr. Rumen Kishev	Bulgarian Ship Hydrodynamics Centre
Francisco J. Pérez Villalonga	Canal de Experiencias Hidroninámicas de El Pardo (CEHIPAR)
Wentao Wang	China Ship Scientific Research Centre (CSSRC)
Lanfranco Benedetti	CNR-INM
Young Bum Lee	Hanwa Ocean (formerly DSME, Daewoo)
Prof. Dr. Ing. Bettar Ould el Moctar	Development Centre for Ship Technology and Transport Systems
Dr. Didier Fréchou	DGA Hydrodynamics
Prof. Pierre Ferrant	École Centrale de Nantes
Dr. Claus D. Simonsen	FORCE Technology
Dr. Janou Hennig	Hamburgische Schiffbau-Versuchsanstalt GmbH (HSVA)
Hyun-ho Lee	Hyundai Heavy Industries Co. Ltd.
Hideo Orihara	Japan Marine United Corporation
Keyyong Hong	Korea Research Institute of Ships and Ocean Engineering (KRISO, formerly MOERI)
Viacheslav Magarovskii	Krylov State Research Centre
Carlos Levi	LabOceano - Brazilian Ocean Technology Laboratory
Sujun Yang	Marine Design and Research Institute of China (MARIC)
Adam Grzonka	Maritime Advanced Research Centre (CTO S.A.)
Dr. Bas Buchner	Maritime Research Instutute Netherlands (MARIN)
Takayuki Mori	Meguro Model Basin
Daisuke Matsumoto	Mitsubishi Heavy Industries, Ltd.
Masaru Tsujimoto	National Maritime Research Institute
Ayhan Akinturk	National Research Council of Canada
Dr. Martin J. Donnelly	Naval Surface Warfare Center, Carderock Division
Pengfei Liu	Newcastle University
In Won Lee	Pusan National University
Andrew Peters	QinetiQ
Yong Chul Lee	Samsung Heavy Industries
Dr. Christian Masilge	Schiffbau Versuchsanstalt Potsdam GmbH
Prof. Gerhard Strasser	Schiffbautechnische Versuchsanstalt in Wien
Prof. Yonghwan Kim	Seoul National University
Decheng Wan	Shanghai Jiao Tong University (SJTU)
Guoxiang Dong	Shanghai Ship and Shipping Research Institute (SSSRI)
Dr. Kourosh Koushan	SINTEF Ocean (formerly MARINTEK)
Lars T. Gustafsson	RISE (formerly SSPA Sweden AB)
Prof. Robert F. Beck	University of Michigan
Daisuke Kitazawa	University of Tokyo
Dr. Seppo Kivimaa	VTT

SPECIALIST COMMITTEE ON ICE

R.U.Franz von Bock und Polach (Chair)	Hamburg University of Technology
John Wang	National Research Council of Canada
Nils Reimer	Hamburgische Schiffbau-Versuchsanstalt GmbH (HSVA)
Prof. Yan Huang	Tianjin University
Takatoshi Matsuzawa	National Maritime Research Institute
Jinho Jang	Korea Research Institute of Ships and Ocean Engineering (KRISO, formerly MOERI)
Otto Puolakka	Aalto University (1)
Riikka Matala	Aker Arctic Technology Inc.
Yukui Tian	China Ship Scientific Research Centre (CSSRC)

SPECIALIST COMMITTEE ON CAVITATION AND NOISE

Romuald Boucheron (Chair)	DGA Hydrodynamics
Kei Sato	Mitsubishi Heavy Industries, Ltd.
Yezhen Pang	China Ship Scientific Research Centre (CSSRC)
Cheolsoo Park	Korea Research Institute of Ships and Ocean Engineering (KRISO, formerly MOERI)
Ville Viitanen	VTT
Przemyslaw Krol	Maritime Advanced Research Centre (CTO S.A.)
Djahida Boucetta	Flanders Maritime Laboratory
Crispin Fetherstonhaugh	QinetiQ
Francisco Alves Pereira	CNR-INM
Thad Michael	Naval Surface Warfare Center, Carderock Division

SPECIALIST COMMITTEE ON COMBINED CFD/EDF METHODS

Kevin Maki (Chair)	University of Michigan
Feng Zhao	China Ship Scientific Research Centre (CSSRC)
Peter Horn	Hamburgische Schiffbau-Versuchsanstalt GmbH (HSVA)
Joe Banks	University of Southampton
Jussi Martio	VTT
Bram Starke	Maritime Research Instutute Netherlands (MARIN)
Diego Villa	Università de Genova
Yichen Jiang	Dalian University of Technology
Shoji Shingo	Shipbuilding Research Centre of Japan
Riccardo Broglia	CNR-INM
Hyunse Yoon	IIHR-Hydroscience & Engineering

RESISTANCE AND PROPULSION COMMITTEE

Nikolaj Lemb Larsen (Chair)	FORCE Technology
Bryson Metcalf	Naval Surface Warfare Center, Carderock Division
Yasuhiko Inukai	Japan Marine United Corporation
Tokihiro Katsui	Kobe University
Nicholas Dawson	QinetiQ
Kwang-Soo Kim	Korea Research Institute of Ships and Ocean Engineering (KRISO, formerly MOERI)
Renchuan Zhu	Shanghai Jiao Tong University (SJTU)
Matteo Diez	CNR-INM
Stefano Gaggero	Università de Genova
Weichao Shi	University of Strathclyde
Byong Guk Kim	Hanwa Ocean (formerly DSME, Daewoo)

FULL SCALE SHIP PERFORMANCE COMMITTEE

Hideo Orihara (Chair)	Japan Marine United Corporation
Sebastian Bielicki	Maritime Advanced Research Centre(CTO S.A.)
Se-Myun Oh	Samsung Heavy Industries
Gongzhen Xin	China Ship Scientific Research Centre (CSSRC)
Gijs Struijk	Maritime Research Instutute Netherlands (MARIN)
Giuliano Vernengo	Università de Genova
Stephen Minnich	Naval Surface Warfare Center, Carderock Division
Peiyuan Feng	Marine Design and Research Institute of China (MARIC)
Mariko Kuroda	National Maritime Research Institute
Min Woo Kim	Hyundai Heavy Industries Co. Ltd.

SPECIALIST COMMITTEE ON WIND POWERED AND WIND ASSISTED SHIPS

Sofia Werner (Chair)	SSPA Sweden AB
Sverre Anders Alterskjær	SINTEF Ocean
David Trodden	Newcastle University
Rogier Eggers	Maritime Research Instutute Netherlands (MARIN)
Yeongyu Kim	Korea Research Institute of Ships and Ocean Engineering (KRISO, formerly MOERI)
Yuling Gao	Shanghai Ship and Shipping Research Institute (SSSRI)
Xinshu Zhang	Shanghai Jiao Tong University (SJTU)
Kenichi Kume	National Maritime Research Institute

MANOEUVRING COMMITTEE

Xide Cheng (Chair)	Wuhan University of Technology
Janne F. Otzen	FORCE Technology
Zhiming Yuan	University of Strathclyde
Takashi Kishimoto	Akishima Laboratories (Mitsui Zosen) Inc.
Maciej Reichel	Gdansk University of Technology
Dobrin Efremov	Bulgarian Ship Hydrodynamics Centre
Shawn Aram	Naval Surface Warfare Center, Carderock Division
Hether Peng	Memorial University of Newfoundland
Young-Jae Sung	Hyundai Heavy Industries Co. Ltd.
Andrea Serani	CNR-INM
Dong Jin Yeo	Korea Research Institute of Ships and Ocean Engineering (KRISO, formerly MOERI)

SEAKEEPING COMMITTEE

Frederik Gerhardt (Chair)	SSPA Sweden AB
Munehiko Minoura	Osaka University
Benjamin Bouscasse	École Centrale de Nantes
Ole Andreas Hermundstad	SINTEF Ocean
Bo-Woo Nam	Korea Research Institute of Ships and Ocean Engineering (KRISO, formerly MOERI)
Kay Domke	Schiffbau Versuchsanstalt Potsdam GmbH
Antonio Souto-Iglesias	Escuela Técnica Superior de Ingenieros Navales (ETSIN)
Wenyang Duan	Harbin Engineering University
Yulin Pan	University of Michigan
Bertrand Malas	École Centrale de Nantes

STABILITY IN WAVES COMMITTEE

Vadim Belenky (Chair)	Naval Surface Warfare Center, Carderock Division
Mr. Akihiko Matsuda	National Research Institute of Fisheries Engineering
Evangelos Boulougouris	University of Strathclyde
Jean-Francois Leguen	DGA Hydrodynamics
Taeyoung Kim	Samsung Heavy Industries
Shuxia Bu	China Ship Scientific Research Centre (CSSRC)
Yi Liu	Marine Design and Research Institute of China (MARIC)
Claudio Rodríguez	LabOceano - Brazilian Ocean Technology Laboratory

OCEAN ENGINEERING COMMITTEE

Longfei Xiao (Chair)	Shanghai Jiao Tong University (SJTU)
Yasunori Nihei	Osaka Metropolitan University
Nuno Fonseca	SINTEF Ocean
Narakorn Srinil	Newcastle University
Nick Markov	Bulgarian Ship Hydrodynamics Centre
Guillaume Ducrozet	École Centrale de Nantes
Hasanat Zaman	National Research Council of Canada
Kwang-Hyo Jung	Pusan National University
Pedro Mello	University of São Paulo

SPECIALIST COMMITTEE ON OCEAN RENEWABLE ENERGY

Maurizio Collu (Chair)	University of Strathclyde
Petter Berthelsen	SINTEF Ocean
Giuseppina Colicchio	CNR-INM
Gustavo Assi	University of São Paulo
Antonio Fernandes	LOC/COPPE/UFRJ
Kyung-Hwan Kim	Korea Research Institute of Ships and Ocean Engineering (KRISO, formerly MOERI)
Weiwen Zhao	Shanghai Jiao Tong University (SJTU)
Jean-Roch Nader	Australian Maritime College
Motohiko Murai	Yokohama National University
Vincent Leroy	École Centrale de Nantes

QUALITY SYSTEMS GROUP

Marco Ferrando (Chair)	Università de Genova
Joel Sales Sena Jr.	LabOceano - Brazilian Ocean Technology Laboratory
Weimin Chen	Shanghai Ship and Shipping Research Institute (SSSRI)
Gregory Grigoropoulos	National Technical University of Athens
Cheirdaris Spyridon	Aalto University (1)
Kwang-Jun Paik	Inha University
Chengsheng Wu	China Ship Scientific Research Centre (CSSRC)
Daisuke Kitazawa	University of Tokyo
Joel Park	Naval Surface Warfare Center, Carderock Division
Tahsin Tezdogan	University of Southampton

ITTC2024

30TH INTERNATIONAL TOWING TANK CONFERENCE
22–27 SEPTEMBER 2024 | HOBART TASMANIA AUSTRALIA

APPENDIX 2 TASKS AND STRUCTURE OF TECHNICAL COMMITTEES AND GROUPS OF THE 31ST ITTC

1. STRUCTURE OF THE TECHNICAL COMMITTEES AND GROUPS FOR 31ST ITTC

1.1 Technical Committees

As decided by the 29th Full Conference, there is no longer a distinguishment between the permanent committees and Specialist Committees. They are all named Technical Committees. The following Technical Committees are proposed for the 31st ITTC:

- Resistance
- Propulsion
- Manoeuvring
- Seakeeping
- Ocean Engineering
- Stability in Waves
- Full Scale Ship Performance
- Cavitation and Noise
- Ice
- Wind Powered and Wind Assisted Ships

1.2 Groups

- Quality Systems Group
- Group on Overlap

2. TERMS OF REFERENCE FOR THE TECHNICAL COMMITTEES AND GROUPS

2.1 Technical Committees

Each Technical Committee will be responsible for its specified subject area. It will review the state-of-the-art, identify the need for research and development, and carry out longer term studies with broad impact.

Each Technical Committee will submit a report on the results of its work to the Full Conference. The conclusions and the recommendations of the Technical Committee report should be structured as follows:

1. General technical conclusions
2. Recommendations to the Full Conference, which require actions such as, e.g., adopting ITTC procedures.

In addition, each Technical Committee shall submit proposals for future work of the Technical Committee and identification of tasks, which may be appropriate for new Technical Committees. These proposals shall be submitted to the Advisory Council which will compile the proposals and present them to the Full Conference.

2.2 Groups

Groups may be established from time to time by the Executive Committee to carry out specific tasks for the Conference, which are generally not technical issues.

Each Group will present a final report on the results of its work to the Full Conference. The conclusions and the recommendations of the Group report should be structured as follows:

1. General conclusions
2. Recommendations to the Full Conference, which require actions such as, e.g., adopting ITTC procedures.

In addition, each Group shall submit proposals for future work and identification of tasks, which may be appropriate for Technical Committees. These proposals shall be submitted to the Advisory Council which will compile the proposals and present them to the Full Conference.

3. MECHANISM FOR IDENTIFYING NEW TECHNICAL COMMITTEES

As part of their Terms of Reference, the Technical Committees shall consider the need for new tasks and include appropriate proposals in their technical reports. If the Advisory Council identifies a need for a new Technical Committee when it reviews the draft recommendations of the Technical Committees, the Advisory Council will prepare and agree on a statement of the technical aims and objectives for the work of the new Technical Committee.

Independent of the proposals of the Technical Committees, the Advisory Council will keep the requirement for new Technical Committees under continuous review.

When the Advisory Council has agreed on the need for a new Technical Committee, the draft statement of technical aims and objectives will be presented to the Executive Committee for endorsement. If the Executive Committee approves the formation of a new Technical Committee, it will present the proposal to the Full Conference for approval.

4. TASKS OF THE TECHNICAL COMMITTEES AND GROUPS OF THE 31ST ITTC

4.1 General Terms of Reference

1. All committees shall observe the Terms of Reference and general obligations. The committees are expected to perform all the tasks defined in this document. However, should a committee be unable to do this, it shall consult the Advisory Council with regard to reduction of the work.

2. All committees shall identify areas of mutual interest with other committees and the concerned committees shall establish active co-operation/liaison in these areas.

3. All committees shall cooperate with the Group on Overlap.

4. All committees shall endeavour to identify benchmark data and submit these to the ITTC Secretary for inclusion in the benchmark data repository on the ITTC website. Each committee shall appoint a member responsible for this.

5. In their work, the committees shall follow the guidelines given in ITTC Recommended Procedure 1.0-03, General Guideline for the Activities of Technical Committees, Liaison with the Executive Committee and Advisory Council.

6. All committees shall monitor and propose possible application of combined CFD/EFD methods.

7. Committee reports to the Conference should be structured in line with the Terms of Reference of the committee and in accordance with Recommended Procedure 4.2.3-01-02, Guidelines for Preparation of Committee and Group Reports.

4.2 Requirements to new and revised Recommended Procedures and Guidelines

In the preparation of new or revision of existing Recommended Procedures and Guidelines, the committees shall observe the following:

1. Some committees are given the task to either write a new procedure or guideline on a specific subject, or to update an existing procedure or guideline with regard to a specified subject. When this is the case, the new or updated procedure or guideline shall follow the structure and instructions given in procedure 4.2.3-01-01, Guide for the Preparation of ITTC Recommended Procedures, follow the instructions given in 4.2.3-01-03, Work Instruction for Formatting ITTC Recommended Procedures, and use the template given in the same Work Instruction.

2. The annex of these Terms of Reference contains a list of existing Recommended Procedures and Guidelines with the identification of which committee is responsible for maintaining each procedure or guideline. The committees are not obliged to review and update all the procedures and guidelines they are responsible for. However, if a committee finds that a revision is recommended, it shall describe the recommended revision and seek approval from the Advisory Council to implement the recommended revision. Recommendations for modifying procedures or guidelines shall preferably be sent together with the first committee progress report so that the modifications may be implemented during the second year, if approved by the Advisory Council.

4.3 Terms of Reference for the Technical Committees

Resistance Committee

1. Update the state-of-the-art for predicting the performance of different ship concepts emphasizing developments since the 30th ITTC Conference. The committee report should include sections on:

   a. The potential impact of new technological developments on the ITTC, including, for example new types of hull coatings, appendages and rudders.
   b. New experimental techniques and extrapolation methods.
   c. New benchmark data.
   d. The practical applications of computational methods to performance predictions and scaling.
   e. The need for R&D for improving methods for model experiments, numerical modelling and full-scale measurements.

2. Monitor the experience of ITTC members using CFD-based form factors and continue comparative studies on CFD methods for form factor derivation. Investigate the use of CFD and combined CFD/EFD methods in scaling processes for a more precise speed/power prediction including correlation with sea-trial data and numerical friction line. Pay special emphasis on the scaling of transom flow (wetted, dry and partially dry). Update the Recommended Procedures related to CFD-based form factor and transom scaling.

3. Investigate the requirements for testing and numerical evaluation of high-speed marine vessels. Address the need of updating 7.5-02-05-01, HSMV Resistance Test.

4. Investigate the use of CFD and combined CFD/EFD methods in scaling processes for a more precise speed power prediction. The issue with high priority is scaling of transom flow (wetted, dry and partially dry).

5. Investigate scaling of sinkage and trim in deep water, as well as their effect on the form factor.

6. Investigate the scale effects for ships advancing through shallow/restricted waters.

7. Review and analyze state of the art and advances in CFD methods for roughness allowance treatment (for both wall resolved and wall function RANS), recommend best practices and propose incorporation in ITTC Procedures and Guidelines. Promote adoption of the revised 7.5-03-01-01, gather feedback related to its use, and summarize conclusions along with possible further improvements.

8. Evaluate the guideline 7.5-02-02-03 for the determination of the frictional drag reduction factor α. Investigate new techniques for the determination of C_F for surfaces with reduced skin friction and extrapolation methods for different Reynolds numbers, for example friction test tunnels using the pressure loss along the test section to determine the wall shear stress and, finally, the frictional resistance coefficient. Evaluate the model test procedure for flat plates with an Air Lubrication System at different Reynold numbers. Collect examples of air lubrication practice in model tests as well as full-scale data, if available. Develop a guideline for establishing the injection pressure and air- flow rate scaling approach.

Propulsion Committee

1. Update the state-of-the-art for predicting the performance of different ship concepts emphasizing developments since the 30th ITTC Conference. The committee report should include sections on:
   a. The potential impact of new technological developments on the ITTC, including, for example new types of propulsors, rudders and hull and propeller coatings.
   b. New experimental techniques and extrapolation methods.
   c. New benchmark data.
   d. The practical applications of computational methods for performance predictions and scaling.
   e. The need for R&D for improving methods of model experiments, numerical modelling and full-scale measurements.

2. Conduct a benchmark study on propellers focusing on the effect of Re at model scale and scaling methods for full-scale predictions. CFD calculations would be run at a range of Re at model scale and full scale, along with open-water model tests at a range of Re. The study could use the two propellers that were provided for the previous benchmark study run by the 28th ITTC.

3. Investigate the issue of laminar flow effects in self-propulsion tests of propeller with low blade area.
   a. Review literature on the subject.
   b. Conduct a survey how ITTC members tackle this issue, and which scaling method they use for low blade area propellers.
   c. Investigate whether it is sufficient to conduct the open water test at only two different Reynolds numbers for full scale extrapolation.
   d. Suggest modification to Recommended Procedures 7.5-02-03-01.1, 7.5-02-03-01.3, 7.5-02-03-01.4 and 7.5-02-03-02.1 with regard to these effects.
   e. Investigate how CFD can be used to improve scaling methods or used in combination with EFD.

4. Investigate the issue of extrapolation of model tests with ducted propellers to full scale taking into account the different Re-numbers. Identify the need and change the procedures mentioned under 3.d, if necessary.
   a. Update Load variation test method in 7.5–02-03–01.4, 1978 ITTC Performance Prediction Method. Review the Load Variation Test contained in procedure 7.5-02-03-01.4 and harmonise it with the Propulsion Test Procedure 7.5-02-03-01.1 and procedure 7.5-04-01-01.1. Take into account that the load variation test at present is applied for two different tasks:

i. for the correction of the external tow force (skin friction force) during the propulsion test with small difference of the resistance-ratios. No added resistance is taken into account.

ii. as preparation for the analysis of speed power trials (7.5-04-01-01.1, Appendix D, Chapter J.2 and ISO 15016) where the difference of the resistance-ratios is much bigger, and which should be included in the performance prediction method. The dependencies of propulsion efficiencies and rate of revolution with power increase apply to this case. The purpose of this task should be clearly stated. Co-operate with the Full-Scale Ships Performance Committee. Supply a calculated Example as given in Appendix A of Procedure 7.5-02-03-01.4.

iii. To avoid further confusion, it should be considered to rename task ii as e.g., "Determination of overload factors".

b. Review the effectiveness of the Load Variation Test method in shallow water and develop a new method, if necessary.

5. Continue work on updating the guideline for correlation factors developed by the AC WG on Correlation during the 30th ITTC. Cooperate with the Full-Scale Ship Performance Committee. *(AC may decide to continue the WG in which case this task is deleted)*.

6. Investigate the requirements for testing and numerical evaluation of high-speed marine vessels. Address the need of updating 7.5-02-05-02, HSMV Propulsion Test.

7. Investigate the use of CFD methods in scaling processes for a more precise speed power prediction. The issues with high priority are:
   a. Effective-wake scaling
   b. Energy-saving devices

8. Develop a guideline for conducting full-scale performance evaluations for energy saving methods (ESM).

Manoeuvring Committee

1. Update the state-of-the-art for predicting the manoeuvring behaviour of ships, emphasizing developments since the 30th ITTC Conference. The committee report should include sections on:
   a. the potential impact of new technological developments on the ITTC, such as unmanned ship and autonomous navigation
   b. new propulsion and steering technologies and their impact
   c. AI and data-based technology and their application to ship manoeuvring.

2. Update procedure 7.5-02-06-02, Captive Model Test, with regard to hexapod tests.

3. Update procedure 7.5-02-06-04, Uncertainty Analysis for Manoeuvring Predictions, based on Captive Manoeuvring Tests and 7.5-02-06-03, Validation of Manoeuvring Simulation Models, reflecting the outcome of SIMMAN and any other new developments.

4. For procedure 7.5-03-04-01, Guideline on Use of RANS Tools for Manoeuvring Prediction,
   a. update numerical simulation procedure in calm water and in waves,
   b. update the example on simulation based on derivatives in calm water,
   c. add an example of direct manoeuvring simulation in waves.
   d. Ask the Seakeeping Committee to review the updated procedure and reflect their comments on the procedure.

5. Update procedure 7.5-03-04-02, Validation and Verification of RANS Solutions in the

Prediction of Manoeuvring Capabilities. Add an example of manoeuvring in waves, if possible.

6. Liaise with the authorities/organizations/associations on marine autonomous vessels, check the validity of existing ITTC procedures for standard manoeuvring trials when applied to maritime autonomous surface ships (MASS).

7. Collect model- and full-scale benchmark data for surface and underwater vehicles and include the benchmark data in procedure 7.5-02-06-06, Benchmark Data for Validation of Manoeuvring Predictions. Liaise with Full-Scale Ship Performance Committee, review and collect benchmark data for full-scale manoeuvring tests.

8. Review the guidelines for low-speed manoeuvring tests and full-scale manoeuvring trials, and, if needed, update procedures 7.5-02-06-01, Free Running Model Tests, and 7.5-04-02-01, Full Scale Manoeuvring Trials, implementing the low-speed tests and/or bow-thruster test procedures.

Seakeeping Committee

Note: The Seakeeping Committee is primarily concerned with the behaviour of ships underway in waves. The Ocean Engineering Committee covers moored and dynamically positioned ships. For the 31st ITTC, the modelling and simulation of waves, wind and current is the primary responsibility of the Ocean Engineering Committee, with the cooperation of the Seakeeping and the Stability in Waves Committees.

1. Update the state-of-the-art for predicting the behaviour of ships in waves, emphasizing developments since the 30th ITTC Conference. The committee report should include sections on:
   a. the potential impact of new technological developments on the ITTC
   b. new experimental techniques and extrapolation methods
   c. new benchmark data
   d. On-board and real time data collection, including collection system, data quality, ocean environmental data, monitoring system.

2. Complete collection and analysis of the benchmark test data for added resistance in waves, acquired in the 30th ITTC, and utilize this data to update or generation of the related ITTC procedure or guideline. Focus shall be on oblique waves where data is scarce.

3. Update ITTC procedure 7.5-02-07-02.1, Seakeeping Experiments, including the standardized number(s) of encounter waves in model-scale and full-scale measurements.

4. Collect numerical simulation data to investigate the topic of 'voluntary' speed reduction for vessels smaller than 100m in length and recommend the sea state for the computation of Weather factor *fw* for small ships.

5. Finish and publish the draft "Guideline for determining Minimum Propulsion Power to Maintain the Manoeuvrability of Ships in Adverse Conditions" prepared by the 30th ITTC Seakeeping Committee. Investigate whether there are any technical issues or shortcomings in MEPC.1/Circ.850/Rev.3 and, if so, prepare a submission to IMO MEPC on the subject.

6. Create a new guideline for verification and validation of CFD methods for seakeeping analysis.

Ocean Engineering Committee

Note: The Ocean Engineering Committee covers moored and dynamically positioned ships and floating structures. For the 31st ITTC, the modelling and simulation of waves, wind and current is the primary responsibility of the Ocean Engineering Committee with the cooperation of the Seakeeping and the Stability in Waves Committees.

1. Provide a survey of the state-of-the-art of the relevant developments in the field of

ocean engineering and ocean renewable energy, emphasizing developments since the 30th ITTC Conference. The committee report should include sections on:
   a. the potential impact of new technological developments on the ITTC
   b. new experimental techniques
   c. new benchmark data
   d. the practical applications of computational methods to prediction
   e. the need for R&D for improving methods of model experiments and numerical modelling.

2. Consider whether floating solar (photovoltaics platforms), ocean thermal energy and deep-sea mining require specific guidelines beyond the present guidelines for wave energy, current energy and offshore wind (for instance deep water large diameter risers).

3. Review and report on specific AI developments and applications in this field.

4. Review and report on comparisons between full-scale measurements, model-scale measurements, and numerical predictions.

5. Review and report on the way arrays of ocean energy systems can be tested and simulated.

6. Review and report on how the hydro-elasticity of ocean energy systems can be evaluated experimentally and simulated computationally.

7. Review and report on wind, current and sea state modelling in model tests and simulations for ocean energy systems.

8. Finalise the general guideline on modelling wind and wind loads for ships and offshore structures started by the Seakeeping Committee of the 30th ITTC. Wind loads shall in principle be in all six degrees-of-freedom, but may be reduced to those modes of motion relevant for the specific applications.

Stability in Waves Committee

Note: The Stability in Waves Committee covers the stability of intact and damaged ships in waves. For the 31st ITTC, the modelling and simulation of waves, wind and current is the primary responsibility of the Ocean Engineering Committee with the cooperation of the Seakeeping and the Stability in Waves Committees.

1. Update the state-of-the-art for evaluating the stability of ships in adverse weather conditions, emphasizing developments since the 30th ITTC conference. The committee report should include sections on:
   a. the potential impact of new technological developments on the ITTC
   b. new experimental techniques
   c. new benchmark data
   d. the practical applications of computational methods to prediction
   e. the need for R&D for improving methods of model experiments, numerical modelling.

2. Develop a new procedure for the qualitative validation of time-domain simulation tools for direct stability assessment under the IMO Second Generation Intact Stability Criteria (IMO 2020, MSC.1/Circ. 1627), particularly including
   a. calculation of backbone and roll repose curves,
   b. finding surf-riding equilibrium
   c. evaluation of heel during a turn in calm water
   d. simulation of a straight captive run in stern quartering waves
   e. calculation of a heel angle caused by drift and wind.

3. Update of procedure 7.5-02-07-04.6 with Extrapolation Methods, particularly addressing the technical issues which are not covered by current ITTC procedures.

4. In the current procedures, check the format of the parts that are too descriptive and revise the procedures to conform to the current format.

Full-Scale Ship Performance Committee

1. Update the state-of-the-art for investigation of full-scale ship performance, emphasizing developments since the 30th ITTC Conference. The committee report should include sections on:
   a. the potential impact of new technological developments on the ITTC
   b. new measuring techniques
   c. new benchmark data
   d. the practical applications of numerical simulation to full scale ship performance
   e. the need for R&D for improving methods of full-scale measurements and numerical modelling.

2. Focus on the short wave issue and further investigate the quadratic transfer function (QTF) extrapolation method in short waves for the evaluation of added resistance in waves (ARW).

3. Conduct a sensitivity study on the influence of discrepancies in evaluation of ARW on final corrections to the sea trials; study how ARW affects the final speed-power curves. Perform a comparative study of the influence of directional energy spreading on the wave correction in speed/power trials.

4. Carry out a comparison of validated methods on the larger set of ship types by using real-ship parameters. It should not be limited to organisations performing model tests. Consider the possibility of selecting among the methods for wave, wind and current corrections in speed/power trials depending on the availability of ship form data.

5. Monitor and explore further measurement techniques applicable in speed/power trials and in-service monitoring: Lidar wind measurements, thrust measurement and wave spectra measurement.

6. Provide technical support to ISO and IMO in furthering development of approaches to in-service performance monitoring.

7. Collect the full-scale data to evaluate the frictional resistance reduction by air lubrication system and validate correlation of actual reduction rate (ADR) and estimated reduction rate (EDR) to predict performance at full loading conditions.

8. Investigate cases with crosswind in head/following waves to find the necessity of correcting the issue of ship running with stable drift angles.

9. Investigate the effect of bio-fouling related roughness, monitoring effect of roughness and analyse methods for evaluating ship performance in service.

10. Extend the sea trial procedure to include new metrics such as ADR and EDR, along with the methodologies for measurements.

Cavitation and Noise Committee

1. Update the state-of-the-art for evaluating cavitation and hydrodynamic noise, emphasizing developments since the 30th ITTC conference. The committee report should include sections on:
   a. the potential impact of new technological developments on the ITTC
   b. new experimental techniques
   c. new benchmark data
   d. the practical applications of computational methods to prediction
   e. The need for R&D for improving methods of model experiments, numerical modelling.

2. Review and update the current ITTC Guidelines / Procedures on Noise model and full-scale measurement with focus on calibration, reverberation and instrumentation.

3. Review the state of the art on cavitation model testing (cavitation appearance, hull pressure fluctuation, thrust break down, cavitation erosion, bubble injection for noise reduction) and noise model testing

with a special focus on propellers operating in ice conditions.

4. Conduct Round Robin Test on the basis of Nawigator XXI (as organized within the 30th ITTC Conference)- collect and analyze data, summarizing the main findings.

5. On the basis of the findings from the Round Robin Test, propose improvements to the accuracy for underwater radiated noise (URN) measurements at model scale for the measurement of propeller noise in tunnels or towing tank facilities.

6. Review the current CFD methods for cavitation and noise. Prepare data and launch a CFD benchmark test campaign (noise, wake simulation, tip vortex cavitation, cavitation inception) possibly within Nawigator XXI.

7. Monitor progress for signal processing in two domains (cavitation and noise) and use of data, machine learning, and AI approaches (data driven simulations).

8. Monitor the use of energy saving devices for efficiency improvement and ways to manage both propulsion efficiency and noise generation simultaneously (energy saving devices and noise emissions).

9. Revise methods (CFD or empirical) for improved scaling of propeller inflow / wake evaluation methods such as dummy model technique.

10. Review state of the art on cavitation and noise measurements at full scale taking into account different requirements from different Classification Societies (Silencing Notations).

11. Monitor and review studies on the cavitation and noise of wind powered ships.

Ice Committee

1. Update the state-of-the-art for investigation of ship performance in ice, emphasizing developments since the 30th ITTC Conference. The committee report should include sections on:
   a. the potential impact of new technological developments on the ITTC
   b. new experimental techniques
   c. new benchmark data
   d. numerical modelling of ice resistance and ice-ship interaction
   e. the need for R&D for improving methods of measurements and numerical modelling.

2. Revise and finalize interim Guideline 7.5-02-04-02.5, Experimental Uncertainty Analysis for Ship Resistance in Ice Tank Testing, including review done by external experts concerning general uncertainty.

3. Establish and conduct simple benchmark test in order to investigate fundamental uncertainty analysis of model ice properties (flexural strength and other ice properties), collect and summarize findings.

4. Establish standard for simple ice-breaking model (possibly cone) for resistance measurements to verify ice tank characteristics.

5. Develop a Guideline related to testing fixed structures in ice. The Guideline should include subdivision such as: pile foundation structures, shallow foundation structures and ice induced vibration tests and encompass scaling issues for vertical structures.

6. Monitor advances on performance prediction in deformed ice (especially brash ice) including high uncertainty following TraFi Guidelines (Finnish Swedish Ice Class Rules) and report in a form of outline for a guideline.

7. Review State of the Art on numerical modelling of ice resistance and ice-ship interaction.

8. Monitor advances related to snow ice features including surface interaction between ship and hull.

9. Monitor and review methods for propulsor (propeller) - ice interaction.

Wind Powered and Wind Assisted Ships Committee

1. Update the state-of-the-art for investigation of wind powered and wind assisted ships, emphasizing developments since the 30th ITTC Conference. The committee report should include sections on:
   a. the potential impact of new technological developments on the ITTC
   b. new measuring techniques
   c. new benchmark data
   d. numerical modelling of wind powered and wind assisted ships

2. Review and monitor new wind propulsion technologies·

3. Review and align the use of terminology and definitions to ensure consistent alignment with industry as the technologies evolve.

4. Review and monitor the progress in developing performance prediction methods for wind powered/wind assisted ships.

5. Continue to improve Recommended Procedure 7.5-04-01-02 (sea trial). Perform uncertainty analysis and sensitivity analysis of various models and assumptions. Collect experience on the use of sea trials for wind powered/wind assisted ships in practice, including uncertainty analysis.

6. Continue to improve Guideline 7.5-02-03-01.9, Predicting the Power Saving of Wind Assisted Ships. Perform uncertainty and sensitivity analysis of the various models and assumptions. Recommend one source for wind statics and routing methods for the voyage simulations.

7. Review and assess experimental and numerical methods for seakeeping and manoeuvring assessment of wind assisted ships. Develop Guidelines on manoeuvring and seakeeping tests of wind assisted ships including Software-in-the-loop (SIL), roll damping effects, uncertainty. Liaise with other committees.

8. Review the development of methods for full-scale force measurements for wind propulsion devices, onboard and on land.

9. Review and assess wind tunnel tests of wind propulsion technologies including methods, data, experiences, scale effects. Give recommendations as to necessary requirement for wind tunnel set-up (wind speed, Reynolds number, blockage).

10. Monitor and support the development of regulations affecting the design and operation of wind powered ships, such as EEDI, Colreg, class rules etc.

11. Review and monitor the use of anti-heel and anti-drift devices on wind powered ships.

12. Continue to review and collect data on empirical corrections: effect of leeway and heel on resistance components and propulsive efficiency, effect of reduced propeller flow on rudder effectiveness.

4.4 Terms of Reference for the Groups

Quality Systems Group

1. Support the Technical Committees in their work on Recommended Procedures and Guidelines. Supply the chairmen of the new committees with the MS Word versions of the relevant documents.

2. Maintain the Register of ITTC Recommended Procedures and Guidelines.

3. Introduce New Uncertainty Analyses Guidelines to include data anomalies in Machine Learning Algorithms.

4. Follow the development or revision of ISO Standards regarding Quality Control.

5. Update the ITTC Symbols and Terminology List.

6. Harmonize the uncertainty symbols list with Annex J of JCGM 100:2008.

7. Update the ITTC Dictionary of Hydromechanics.

8. Support the technical committees dealing with stochastic processes with guidance on development, revision, and update of procedures for the inclusion of confidence bands on their computational and experimental results.

9. Observe BIPM/JCGM standards for uncertainty analysis, in particular the uncertainty analysis terminology.

10. Review developments in metrology theory and uncertainty analysis and issue appropriate procedures.

11. Upload all the collected and verified benchmark data into the ITTC benchmark data repository.

12. Cooperate with technical committees to establish the ITTC benchmarks, including definition, raw data, data format, etc.

13. Before publication of new and revised procedures and guidelines:
    a. Perform a detailed review of all new and revised ITTC Recommended Procedures and Guidelines for compliance with ITTC quality requirements with regard to format, references, symbols, terminology, uncertainty analysis and parameter lists
    b. Either update the procedures in these aspects or cooperate with the relevant committee on these updates.

Group on Overlaps

1. Identify and record overlaps in the ITTC Recommended Procedures and Guidelines. In particular those listed below.

2. Waves
    a. Identify overlaps on phenomena and mathematical description and modelling of waves in the ITTC Recommended Procedures contained in the following chapters of the Register of the ITTC Recommended Procedures and Guidelines:
        i. Seakeeping
        ii. Environmental Modelling
        iii. Ocean Engineering
        iv. Manoeuvring
        v. Stability
        vi. Speed and Power Trials
        vii. High Speed Marine Vehicles
        viii. 1978 ITTC Performance Prediction Method (7.5-02-03-01.4)
    b. Merge the identified Recommended Procedures (Guidelines) on the description of waves and/or applicable parts of them into a Guideline to which the above identified Recommended Procedures in future can refer to.
    c. Merge the identified Recommended Procedures (Guidelines) on the modelling of waves (physically) and/or applicable parts of them into a Guideline to which the above identified Recommended Procedures and Guidelines in future can refer to.

3. Wind and current
    a. Identify and record overlaps regarding phenomena and description of wind and air resistance in the ITTC Recommended Procedures contained in the following chapters of the Register of the ITTC Recommended Procedures and Guidelines:

    i. Performance
    ii. High Speed Marine Vehicles
    iii. Environmental Modelling
    iv. Ocean Engineering
    v. Speed and Power Trials
  b. Merge the identified Recommended Procedures (Guidelines) on the description of wind and/or applicable parts of them into a Guideline to which the above identified Recommended Procedures in future can refer to.
  c. Merge the identified Recommended Procedures (Guidelines) on the modelling of wind (physically) into a Recommended Guideline to which the above identified Recommended Procedures and Guidelines in future can refer to.

4. CFD
  a. Identify and record overlaps on CFD in the ITTC Recommended Procedures and Guidelines.
  b. Merge the identified Recommended Procedures (Guidelines) containing overlapping CFD issues and/or applicable parts of them into Guidelines to which the above identified Recommended Procedures in future can refer to.

ITTC2024

30TH INTERNATIONAL TOWING TANK CONFERENCE
22–27 SEPTEMBER 2024 | HOBART TASMANIA AUSTRALIA

APPENDIX 3 STATUTES AND ARTICLES OF ITTC-ASSOCIATION - PROPOSED REVISIONS 2024

I Preamble

0. The International Towing Tank Conference was founded in 1932 and the first Conference of Tank Superintendents was held in 1933. To give continuity from one Conference to another, the 5th Conference appointed a "Standing Committee", and agreed that the Chairperson would be the representative of the country arranging the next Conference. It was in the next Conference celebrated in Washington in 1951 when the Standing Committee suggested that a three-year interval between the Sixth and the Seventh Conference would be desirable. From then on, every three years the Conference has taken place. In 1954 the name "International Towing Tank Conference" was adopted for future conferences.

   In 2017 the Full Conference decided to transform the ITTC into a legal entity the ITTC Association (ITTC.A).

II Name and Location

1. The International Towing Tank Conference Association (ITTC.A) is a non-commercial association according to art. 60 of the Swiss Civil Code. ITTC.A is politically and religiously neutral.

2. The International Towing Tank Conference (ITTC.A) is a worldwide independent association of hydrodynamics research organisations that support the designers, builders and operators of ships and marine installations by giving advice and information regarding the performance, safety and environmental impact of ships and marine installations using the results of physical model tests, numerical modelling and full-scale measurements.

3. The domicile of ITTC.A is, as of 20.09.2019:

c/o Forum Rechtsanwälte
Dr. iur. Diego R. Gfeller
Universitätsstrasse 100
8006 Zürich

4. The rules and regulations of the ITTC are relevant by-laws of ITTC.A.

III Aims

5. The aims of the ITTC.A are:

a) To stimulate progress in solving the technical problems which are of importance to its members;
b) To stimulate research in areas in which a better knowledge is required in order to improve methods of predicting the full-scale hydrodynamic performance of ships and marine installations;
c) To stimulate the improvement of methods of model experiments, numerical modelling and full-scale measurements;
d) To recommend procedures for carrying out physical model experiments, numerical modelling and full-scale measurements of ships and marine installations;
e) To validate the accuracy of full-scale predictions for quality assurance;
f) To formulate collective policy on matters of common interest;
g) To provide an effective organisation for the interchange of information;
h) To be a contact point to other international organisations such as IMO, ISO, etc. on aspects related to the aims of the association.

IV Activities

6. The aims of ITTC.A shall be pursued by

   a) Stimulating research into specific topics;
   b) Organizing and encouraging meetings to review progress in this research;
   c) Making such recommendations and decisions on joint action and policy as seem desirable to the members of the ITTC.A;
   d) Establishing procedures and guidelines to help the member organisations of the ITTC.A to maintain their institutional credibility with regard to quality assurance of products and services, such as, performance prediction and evaluation of designs by either experimental or computational means.
   e) Recording and publishing discussions taking place at ITTC meetings.

V Membership

Note: unless otherwise stated, whenever the term 'member' is used in these Statutes, it refers to both 'Full membership' and 'Advisory Council membership'.

7. Membership of ITTC.A is open to all members of ITTC (Full Membership) fulfilling the requirements of ITTC Rules for membership.

8. Membership of ITTC.A is furthermore open to all members of the Advisory Council of the ITTC (Advisory Council Membership) fulfilling the requirements of the ITTC Rules for Advisory Council Membership.

9. Commercial, financial and other pressures shall not compromise technical judgements of the members and its staff.

10. Applications for membership shall be made to the Chairperson of ITTC.A.

11. The financial year runs from 1 October to 30 September the following year.

12. A membership fee shall be payable by all members. The membership fees of the different membership-categories can diverge. The amount of the membership fee is proposed triennially by the Executive Committee to be approved by the General Assembly.

13. A member, who has not paid the fee by March 31st in the year of the date of payment, shall no longer be a member organisation of ITTC.A and the name of the organisation shall be removed from the membership list. The Executive Committee may extend this deadline if unusual financial or administrative circumstances delay payment of the fee.

14. Membership in ITTC.A expires in case of

    a) withdrawal by the member;
    b) expulsion;
    c) demise or default of the member organisation.

15. The withdrawal by the member shall be made by means of a written declaration to the Executive Committee. It may only take place at the end of the calendar year subject to a six-month notice period.

16. The Executive Committee shall declare any expulsion. The decision is binding. Exclusion may occur without giving reasons. The association, its governing bodies, and its members are not liable for any loss, which might result directly or indirectly from the exclusion pronounced to the statutes.

17. Those members resigning, or considered as resigning, or excluded or their rightful claimants have no right whatsoever to the association's assets. They cannot claim reimbursement of any subscriptions made whatsoever.

VI Adherence

18. Each member is obliged to adhere to the statutes, to the Internal Rules and to all those regulations and decisions made in pursuance of the Statutes or the Internal rules.

VII Governing Bodies

19. The governing bodies of ITTC.A are:

   a) General Assembly
   b) Executive Committee
   c) Advisory Council

20. ITTC.A opts out of the limited audit. The General Assembly appoints two internal auditors from its members for a period of three years and not more than three years to monitor the financial activities of the organisation.

VIII General Assembly

21. The General Assembly is held every third year. It shall be held at the location of the Conference of ITTC.

22. The Executive Committee shall make the invitation at least 20 days in advance, either in writing or by e-mail, specifying the agenda items. Application to the General Assembly must be addressed in writing to the Chairperson no shorter than 10 days in advance.

23. Extraordinary General Assemblies shall be convened by resolution of the Executive Committee when the interests of the Association shall demand such, or upon the request of 1/3 of the members of the Advisory Council, or 1/5 of the ITTC.A Full members. However, such a request will only be valid if submitted in writing and signed by all petitioners, and only if it sets out in clear and precise terms the object of the proposed extraordinary meeting. The Executive Committee shall make the invitation at least 20 days in advance, either in writing or by e-mail, specifying the agenda items.

24. A Global General Assembly may be held at any time without prior specifying the items of the agenda.

25. Powers:

The General Assembly of members decides on all matters that are not reserved to other governing bodies of the association. Its resolutions, adopted in accordance with these statutes are mandatory for all members of the association, including absent, defaulting and dissenting members.

It supervises the activities of the governing bodies and may at any time dismiss members of the latter without prejudice to any contractual rights of those dismissed.

The right of dismissal exists by law whenever justified by good cause

26. Resolutions on matters for which prior proper notice has not been given may be adopted only where the articles of the association expressly permit this.

27. The general assembly passes resolutions with simple majority of the members present. In calculating the vote, the votes of those members abstaining are not included except where quorums of those present or a specified majority are required.

28. All members of the association may attend the meetings of the General Assembly and participate in discussions, which may be initiated by the General Assembly, either in an ordinary or extraordinary meeting of the General Assembly. All members have equal voting rights at the General Assembly.

29. Only members are eligible to vote. The vote shall be exercised by the designated representative, but may be delegated to another staff member of the same organisation. A member organisation that is unable to attend the meeting can delegate the voting rights of the member to another member. The designated representative must inform the chairperson of the Executive Committee of the name of the alternate before the start of the General Assembly at which the vote will take place. Postal or email votes shall not be allowed.

30. Voting may be by secret ballot or a show of hands as determined by the Executive Committee.

31. Each member is by law excluded from voting on any resolution concerning a transaction or dispute between the association on the one part and the member on the other part.

IX Executive Committee

32. The Executive Committee consists of twelve or more members.

33. There shall be one representative from each of the seven geographic areas listed in Annex A of the rules of ITTC (the area representative). Where at all possible, the area representative shall represent a member organisation of the Advisory Council. The Executive Committee may approve exceptions to the area representative being from a member organisation of the Advisory Council. Each area representative shall normally serve for two terms of three years each. The area representatives shall be appointed at least one-half year prior to the Conference by the member organisations of that area. Each region shall decide on its own procedure for selection (election) of its area representative.

34. The Executive Committee consists of

a) The chairperson of ITTC.A
b) The chairperson of the ITTC Conference. The chairperson of the ITTC Conference could, but must not necessarily, be the chair of ITTC.A. In case not being ITTC.A chair, the chairperson of ITTC Conference has no voting right.
c) The ITTC Secretary. The ITTC Secretary need not be member of ITTC.A. The ITTC Secretary has no voting right.
d) The AC chairperson. The AC chairperson has no voting right.
e) The chairperson of the previous ITTC Conference has no voting right.
f) The representatives of the geographical regions defined in the ITTC Rules.

35. The Executive Committee shall:

a) Elect a Vice Chairperson among the EC members.
b) Implement the decisions of the General Assembly;
c) Represent the ITTC, delegate representation of ITTC in special cases;
d) Accept new members;
e) Manage the income;
f) Appoint committees of ITTC.A and members to such committees as needed;
g) Define the triennial membership fee.

36. The chairperson of ITTC.A of the next Executive Committee shall be appointed by the Full Conference at the end of the conference and act as chairperson until the end of the next Conference.

37. The chairperson of ITTC Conference is usually the designated representative of the member organisation that will host the next Conference, but the Executive Committee may propose as its chairperson the designated representative of any member organisation in the area where the next conference will be held. He is responsible for the organisation of the next ITTC Conference.

38. The members of the Executive Committee act as a corporate body; they incur no personal obligation whatsoever for the liabilities of the association. They are responsible only for executing their mandate.

39. Votes by the Executive Committee may be by a show of hands or secret ballot at the call of the chairperson. A simple majority shall carry a motion. Any member of the Executive Committee unable to attend can, by written confirmation, confer upon another member the power to act and vote in his name, for that meeting only. A member can only represent one other member. For decisions of the Executive Committee to be valid, at least six members shall be present or represented, except in case of extreme urgency, in which case decisions may be made irrespective of the number of members present or represented.

40. In special cases also virtual meetings of the Executive Committee, such as Audio meetings or Internet meetings can be arranged.

41. Signatory power:

Two members of the Executive Committee who are not accountable to third parties for a previous decision of the Executive Committee (Chairperson and Vice-chairperson) sign all transactions concerning the association, all letters of procuration, and all transactions requiring the assistance of a public official. Documents concerned with routine management, receipts from and credits to third parties, the railways, the post, telegraph and telephone services, giro accounts and all other government services and their internal administrative divisions and international or supranational bodies are signed by those people, to whom the Executive Committee has granted, by a special decision, such powers within the limits and conditions determined by it.

42. All signed expenses not prior approved by the Executive Committee need afterwards to be justified to the Executive Committee.

43. The ITTC Secretary shall undertake all administrative and secretarial tasks in support of the operation of ITTC.A.

44. The duties of the ITTC Secretary may include maintaining lists of members, publishing Newsletters and maintaining the website. The ITTC Secretary provides secretarial support to the Executive Committee and the Advisory Council.

45. The ITTC Secretary shall be responsible for the administration of ITTC.A funds. The ITTC Secretary shall:

a) set up a bank account for ITTC.A funds;
b) collect ITTC.A membership fees;
c) make records of income and expenditure;
d) prepare proposed budgets and financial reports for the Executive Committee and General Assembly;
e) make authorized withdrawals from the account;
f) finish the accounting every year;
g) keep the minutes of the meetings

X Advisory Council

46. The Advisory Council proposes to the Executive Committee the topics that should be addressed by the ITTC, bearing in mind that the primary aim of the ITTC is to solve technical problems of importance to its members. It proposes new technical committees and recommends terms of reference for all technical committees based on input from technical committees, ITTC members at large and the expertise and priorities of Advisory Council members.

    The Advisory Council proposes recommended procedures and guidelines to the Executive Committee based on proposals by technical committees and groups.

    The Advisory Council may provide advice or recommendations to the Executive Committee on any other topics agreed by the Chairmen of the Executive Committee and Advisory Council

    The Advisory Council may set up mechanisms to support and monitor the work of Technical Committees. The Advisory Council may communicate with technical committees through the ITTC Secretary.

    Votes on matters other than the appointment of the Chairperson or Vice Chairperson may be by show of hands or secret ballot at the call of the Chairperson. A simple majority shall carry a motion.

    The Advisory Council shall meet at least three times between Conferences at times and places coordinated with meetings of the Executive Committee.

47. Advisory Council members between one year and one-half year prior to the next Conference shall elect the Chairperson and Vice Chairperson of the Advisory Council. The election shall be by secret ballot, the candidate with the maximum number of votes shall be elected. The Chairperson shall take office immediately following the end of this Conference. In the absence of the Chairperson, the Vice Chairperson shall conduct the meetings of the Advisory Council.

48. The ITTC Secretary shall provide secretarial support to the Advisory Council.

XI Liability

49. ITTC.A is liable for its obligations with its assets. Such liability is limited to the assets (Art. 75a Swiss Civil Code).

XII Amendments to the Articles/Dissolution

50. The General Assembly shall approve amendments to the Articles of association with the exception of changes in the aims of the association or the dissolution of the association, with the absolute majority of the votes cast. In the event of a tie, the amendment shall be deemed to have been rejected.

51. The General Assembly of the ITTC Association may, if half of the members present representing at least two-thirds of the member votes are in favour of the move, change the aims or dissolve the Association. If this quorum is not represented in the General Assembly, a second meeting is convened with the same agenda, after at least three weeks prior notice, this meeting with two-thirds majority of votes being valid regardless of the number of members represented.

52. In the event of the voluntary dissolution of this association, the General Assembly in deciding on such dissolution will determine at the same time the conditions for liquidation. It will appoint one or more liquidators who will act in accordance with those conditions, will determine his/her or their powers and will determine the disposal of assets remaining after the settlement of the liabilities.

The Chairperson: The ITTC Secretary:

ITTC2024

30TH INTERNATIONAL TOWING TANK CONFERENCE
22–27 SEPTEMBER 2024 | HOBART TASMANIA AUSTRALIA

APPENDIX 4 DESCRIPTION AND RULES OF THE ITTC PROPOSED FOR ACCEPTANCE BY 30TH FULL CONFERENCE 2024

Table of Contents

Description and Rules of the ITTC (International Towing Tank Conference)

1. DESCRIPTION

The International Towing Tank Conference (ITTC) is a world-wide independent association of hydrodynamics research organizations that support the designers, builders and operators of ships and marine installations by giving advice and information regarding the performance, safety and environmental impact of ships and marine installations using the results of physical model tests, numerical modelling and full-scale measurements.

2. AIMS

The aims of the ITTC are:

A) To stimulate progress in solving the technical problems which are of importance to the member organisations;
B) To stimulate research in areas in which a better knowledge is required in order to improve methods of predicting the full-scale hydrodynamic performance of ships and marine installations;
C) To stimulate the improvement of methods of model experiments, numerical modelling and full-scale measurements;
D) To recommend procedures for carrying out physical model experiments, numerical modelling and full scale measurements of ships and marine installations;
E) To validate the accuracy of full-scale predictions for quality assurance;
F) To formulate collective policy on matters of common interest;
G) To provide an effective organization for the interchange of information.

3. ACTIVITIES

The aims of the ITTC shall be pursued by:

A) Stimulating research into specific topics;
B) Organising and encouraging meetings to review progress in this research;
C) Making such recommendations and decisions on joint action and policy as seem desirable to the members of the ITTC;
D) Establishing procedures and guidelines to help the member organizations to maintain their institutional credibility with regard to quality assurance of products and services, such as, performance prediction and evaluation of designs by either experimental or computational means;
E) Recording and publishing discussions taking place at ITTC meetings.

4. COPYRIGHT AND PUBLICATION

ITTC.A shall hold the copyright to all reports, procedures, and guidelines (hereafter 'reports') produced by ITTC Technical Committees, Groups, and ad-hoc Working Groups as part of the work performed to fulfil the Terms of Reference assigned to them by the Full Conference, the Executive Committee, or the Advisory Council.

No papers or reports intended for the public domain that are based on an ITTC report(s), which are or will be copyrighted by ITTC, shall be published until said ITTC report(s) have been presented at an ITTC Conference. Papers and reports intended for the public domain shall properly cite and reference the ITTC reports used and shall not extensively quote ITTC reports.

However, there are no restrictions on the use of existing data or data acquired by any organization independently, in support of ITTC activities.

5. MEMBERSHIP

Membership of the ITTC shall be open to all organisations that carry out hydrodynamic work in support of the designers, builders and operators of ships and marine installations, and to other organisations that contribute to the aims of the ITTC.

Applications for membership shall be made to the Executive Committee through the ITTC Secretary. Each such organisation shall satisfy the Executive Committee that it is eligible for membership.

Each member organisation shall be represented by its director or other senior officer having the authority to bind the member organisation in matters relating to the ITTC (the designated representative).

A membership fee shall be payable by all member organisations. The Executive Committee shall propose the annual fee for the next three years for approval by the Full Conference. The fee shall be payable annually by October 1st. Member organisations may choose to pay annually or once for all three years. Members admitted during an ITTC period shall pay the full membership fee for the year they are admitted and for the following years.

A member organisation, which has not paid the fee by March 31st the following year shall no longer be a member organisation of ITTC and the name of the organisation shall be removed from the membership list. The Executive Committee may extend this deadline if unusual financial or administrative circumstances delay the payment of the fee.

6. FULL CONFERENCE

The Full Conference comprises the designated representatives of member organisations eligible to vote and present at general sessions that take place during the Conference.

6.1 Roles and responsibilities

The Full Conference shall:

A) Determine the policies of the ITTC;
B) Approve changes to the rules of the ITTC;
C) Appoint the Chairman of the Executive Committee and the ITTC Secretary;
D) Appoint the Chairman and members of each technical committee or group;
E) Approve financial reports and plans and the ITTC membership fee;
F) Approve the host organisation and chairman for the next Conference;
G) Approve terms of reference for technical committees and groups;
H) Approve recommended procedures and guidelines.

Only member organisations are eligible to vote. The vote shall be exercised by the designated representative of the organisation and no organisation shall be entitled to more than one vote. A designated representative who is unable to attend the meeting may choose to delegate the voting rights of the member organisation to another employee of the organisation or to the designated representative of another member organisation. The designated representative must inform the Chairman of the Executive Committee of the name of the alternate before the start of the general session at which the vote will take place. Postal or email votes shall not be allowed.

Voting may be by secret ballot or a show of hands as determined by the Executive Committee. An affirmative vote of at least 2/3 of members present shall be required to carry a motion.

A record of the decisions of the Full Conference shall be published in the proceedings of the Conference.

6.2 Decision making between Full Conferences

If for any reason a decision is required in the time gap between Full Conferences with regard to the items listed in 5.1, the Executive Committee unanimously and supported by a majority of the Advisory Council is mandated to make such decision. If a unanimous decision cannot be made, a decision shall be made in accordance with a procedure approved by the Full Conference.

Any decisions made in accordance with 5.2 shall be reported to the Full Conference and recorded in the proceedings of the Conference.

7. EXECUTIVE COMMITTEE

7.1 Roles and responsibilities

The Executive committee shall:

A) Implement the decisions of the Full Conference;
B) Represent the ITTC between Conferences;
C) Replace members of technical committees or groups as necessary between Conferences;
D) Accept new member organisations to the ITTC;
E) Manage the income from the ITTC and Advisory Council membership fees.
F) Approve the arrangements and associated costs and registration fees for the Conference;
G) Prepare a report on its activities for presentation at a general session of the Conference.

The Executive Committee shall propose the following for approval by the Full Conference:

A) The Executive Committee Chairman, ITTC Secretary and members and Chairmen of technical committees and groups;
B) The terms of reference of technical committees and groups;
C) Recommended procedures and guidelines
D) The host organisation and chairman for the next Conference;
E) A financial plan and the ITTC membership fee.

In order to pursue the aims of the ITTC the Executive Committee may initiate formal interactions or collaborations between the ITTC and other organisations (for example the IMO or ISSC). The Executive Committee may require technical committees to carry out specific tasks in support of such interactions.

Votes by the Executive Committee may be by a show of hands or secret ballot at the call of the Chairman. A simple majority shall carry a motion.

The Executive Committee shall meet at least three times between Conferences.

7.2 Membership

The Executive Committee shall normally consist of eight full-voting members including the Chairman.

A) There shall be one representative from each of the seven geographic areas listed in Appendix A. (the area representative). Where at all possible, the area representative shall represent a member organisation of the Advisory Council. The Executive Committee may approve exceptions to the area representative being from a member organisation of the Advisory Council. Each area representative shall normally serve for two terms of three years each. The area representatives shall be appointed at least one-half year prior to the Conference by the member organisations of that area. Each region shall decide on its own procedure for selection (election) of its area representative.
B) The Chairman of the next Executive Committee shall be appointed by the Full Conference at the end of the Conference and act as Chairman until the end of the next Conference. The Vice Chairman of the Executive Committee shall be elected by the Executive Committee from its members.

The following shall be ex-officio non-voting members of the Executive Committee:

A) The Chairman of the Advisory Council
B) The ITTC Secretary
C) The past Conference Chairman. If the past Conference Chairman is the representative of a geographic area, that person shall be a

full voting member of the Executive Committee.

D) The Chairman of the next Conference, if that person is not a member of the Executive Committee.

In the absence of the Chairman, meetings of the Executive Committee shall be conducted by the Vice Chairman.

8. ADVISORY COUNCIL

8.1 Roles and responsibilities

The Advisory Council proposes to the Executive Committee the topics that should be addressed by the ITTC, bearing in mind that the primary aim of the ITTC is to solve technical problems of importance to the member organisations. It proposes new technical committees and recommends terms of reference for all technical committees based on input from technical committees, ITTC members at large and the expertise and priorities of Advisory Council members.

The Advisory Council proposes recommended procedures and guidelines to the Executive Committee based on proposals by technical committees and groups. The Advisory Council may provide advice or recommendations to the Executive Committee on any other topics agreed by the Chairmen of the Executive Committee and Advisory Council.

The Advisory Council may set up mechanisms to support and monitor the work of Technical Committees. The Advisory Council may communicate with technical committees through the ITTC Secretary.

Votes on matters other than the appointment of the Chairman or Vice Chairman may be by a show of hands or secret ballot at the call of the Chairman. A simple majority shall carry a motion.

The Advisory Council shall meet at least three times between Conferences at times and places coordinated with meetings of the Executive Committee.

8.2 Membership

The Executive Committee appoints members to the Advisory Council. Applications for membership shall be made to the Executive Committee through the area representative. Each such organisation must satisfy the Executive Committee that:

A) The purpose of the organisation is the prediction of performance of marine vehicles, marine structures and marine installations. The organisation provides information, on a fee-for-service basis, to clients who are the designers, builders, owners or operators of these assets. The work is directed and executed by full time professional staff. The organisation may also conduct research, technology development, and education activities, provided the funding for these is secondary to its client revenue.

B) It has a long history of work in support of the ITTC as evidenced by membership of Committees and Groups, providing data in support of committee and group work, or making written contributions to committees and groups;

C) It operates at least two model test facilities and has the capability of performing a variety of experimental and numerical investigations within the scope of the ITTC.

No limit shall be put on the total number of members. However, the Executive Committee shall confirm the membership of each member of the Advisory Council once every six years. In order to remain a member of the Advisory Council members must demonstrate to the Executive Committee that they meet the criteria A), B) and C) and that in addition, they have had a record of regular attendance at meetings of the Advisory Council and the Full Conference and have made meaningful contributions to the Advisory Council. Half the Advisory Council member organisations shall be confirmed every three years.

The Advisory Council shall recommend the process for confirmation to the Executive Committee.

Member organisations appointed to the Advisory Council shall be represented on the Advisory Council by their designated ITTC representative. In the event of the designated representative being unable to attend a meeting, the member organisation may send an alternate who shall be a senior technical member of the management of the member organisation, able to contribute to technical discussions on hydrodynamic testing, numerical modelling and full-scale measurement.

Each member of the Executive Committee shall be an ex-officio member of the Advisory Council if he/she is not already a member in his own right as a representative of a member organisation.

The Chairman and Vice Chairman of the Advisory Council shall be elected by its members between one year and one-half year prior to the next Conference. The election shall be by secret ballot, the candidate with the maximum number of votes shall be elected. The Chairman shall take office immediately following the end of this Conference. In the absence of the Chairman, the meetings of the Advisory Council shall be conducted by the Vice Chairman.

Secretarial support to the Advisory Council shall be provided by the ITTC Secretary.

8.3 Advisory Council fee

Advisory Council members shall pay a fee to provide sufficient money to cover the cost of the additional workload on the ITTC Secretary of performing secretarial duties directly for the Advisory Council. The fee shall be approved by the Advisory Council and paid at the same time and under the same conditions as the ITTC membership fee. The Advisory Council shall be responsible for managing the income from the Advisory Council fee.

9. TECHNICAL COMMITTEES

9.1 Roles and responsibilities

The technical committees carry out the technical work of the ITTC defined in their terms of reference. The results shall be documented in reports published in the proceedings of the Conference.

Technical committees shall develop detailed plans in accordance with their terms of reference. The work of all technical committees shall be directed towards the techniques and understanding of physical and numerical modelling as a means of predicting full-scale behaviour. While maintaining an awareness of progress, fundamental theoretical studies and fundamental aspects of numerical fluid computation shall be covered by other forums, such as the ONR Symposium on Naval Hydrodynamics or Conference on Numerical Ship Hydrodynamics.

Technical committees may contact member organisations to request assistance (for example, by completing a questionnaire, participating in comparisons of the results of experiments or calculations or providing other information) or accept offers assistance from member organisations or individuals to help them carry out their work. Written contributions to the program of work of a technical committee may be submitted to its chairman by any member organisation or individual. The technical committee may include a short abstract of any such contribution in its report, with an indication of the source from which the full document may be obtained. The conclusions and recommendations published in the committee report are the sole responsibility of the committee.

A technical committee may make informal contact with technical committees of other organisations which may be working in areas of interest to the ITTC committee.

The report of a technical committee shall reflect the opinion of the complete committee. If the committee is unable come to a consensus, the different opinions of committee members shall be published. The length, structure and format of the report shall be in accordance with guidelines set by the Executive Committee. The report shall include a general technical conclusion and recommendations for future work.

Technical committees may make proposals for future work in the subject area covered by the committee. Such proposals shall be communicated to the Advisory Council through the ITTC Secretary.

Reporting schedules for the technical committees shall be set by the Executive Committee and communicated by the ITTC Secretary.

Technical committees shall meet no more than four times in person between Conferences. Use of virtual meetings is encouraged.

9.2 Membership

Each technical committee shall normally consist of not more than eight members, including the chairman. The chairman and members shall in all cases be selected for their personal contributions to, interest in, and ability to contribute to the subject area of that technical committee. Formal qualifications and a balanced geographic representation shall also be considered in the selection process. The organisation sponsoring the candidate must have agreed to support the candidate financially in carrying out his/her committee work and travel to committee meetings.

The membership of each technical committee shall be reviewed by the Full Conference at intervals of not more than three years. A person shall not serve on technical committees for more than a total of four three-year terms, and shall not be a member on any one technical committee for more than three terms.

A member of a technical committee who is unable to continue in committee work shall be replaced by a qualified expert from a member organisation.

10. GROUPS

The Executive Committee may establish groups to carry out specific non-technical tasks for the ITTC. Examples of groups are the Symbols and Terminology Group and the Quality Systems Group. Groups may have fewer members than the technical committees. Membership on a group shall normally not exceed three consecutive terms of three years, but the Executive Committee may make exceptions. Groups shall be disbanded upon completion of their tasks. Groups shall meet no more than four times in person between Conferences. Use of virtual meetings is encouraged.

11. SERVING IN MORE THAN ONE CAPACITY

No person shall serve in more than one official capacity, or on more than one technical committee, at the same time. The official capacities are:

A) Membership of the Executive Committee;
B) Chairman of the Advisory Council;
C) Chairman of a technical committee or group.

A member of the Executive Committee or the Chairman of the Advisory Council shall not also be a member of a technical committee or group except for short periods of time at the expressed recommendation of the Executive Committee.

12. ITTC SECRETARY

12.1 Roles and responsibilities

The ITTC Secretary shall undertake all administrative and secretarial tasks in support of the operation of the ITTC.

The duties of the ITTC Secretary may include maintaining lists of ITTC memberships, publishing the ITTC Newsletter and maintaining the ITTC website. The ITTC Secretary provides secretarial support to the Executive Committee and the Advisory Council and is the primary point of contact for communications within the ITTC and between outside organisations and the ITTC.

The ITTC Secretary shall be responsible for the administration of ITTC funds. The ITTC Secretary shall:

A) set up a bank account for ITTC funds;
B) collect ITTC membership fees and Advisory Council fees;
C) Perform accounting and arrange auditing of the accounts
D) prepare proposed budgets and financial reports for ITTC and ITTC Association;
E) make authorized withdrawals from the account.

12.2Selection of the ITTC Secretary

The ITTC Secretary shall be employed by or in the case of a retiree, directly supported by a member organisation of the Advisory Council which undertakes to provide necessary services such as office space, internet, email etc. (The host organisation for the ITTC Secretary). The Secretary shall have experience as a representative on the Advisory Council or as a member of a technical committee.

The Advisory Council shall give the name of a qualified person willing to become ITTC Secretary for the next ITTC period to the Executive Committee between one year and one-half year prior to the next Conference. The name shall be chosen by secret ballot and the candidate with the maximum number of votes shall be passed on to the Executive Committee. The Executive Committee shall propose the ITTC Secretary to the Full Conference for appointment.

The ITTC Secretary shall normally serve for at least two terms.

The remuneration for the ITTC Secretary shall be decided by the Executive Committee.

13. MANAGEMENT OF ITTC FUNDS

The Executive Committee shall be responsible for the management of income from ITTC and Advisory Council membership fees. Income from membership fees shall be used to cover the costs of the ITTC organisation, including the remuneration of the ITTC Secretary, part of the cost of producing the proceedings of the Conference and other costs approved by the Executive Committee.

Once each year the Executive Committee shall review and approve the budget. The budget shall show actual income and expenditures to date, including any balance or deficit remaining from previous ITTC periods, and income and expenditures planned for the remainder of the current ITTC period.

The ITTC Secretary shall set up a separate bank account for ITTC funds. The ITTC membership fees and Advisory Council fees may be kept in the same bank account (the ITTC Account). Withdrawals from the account shall be made only by the ITTC Secretary with the written authority of the Chairman of the Executive Committee.

A financial report shall be included in the Executive Committee Report to the Conference. The Executive Committee shall also present an outline financial plan for the upcoming period including a proposal for the ITTC membership fee, for approval by the Full Conference. The financial reporting period for the ITTC is from October 1st to September 30th in the following year.

14. THE CONFERENCE

The Conference shall be held at three-year intervals.

Invitations from organisations to host the Conference of the next interval must be sent to the Executive Committee, through the area representative, at least one year before the Conference of the current interval.

The Executive Committee and the Full Conference shall ensure a balanced rotation of the Conference venue among the seven geographic areas. Each area shall decide on its own procedure for the rotation of venue among the countries in the area.

The host organisation for the Conference may be either an ITTC member organisation or an association whose mandate or aims are relevant to the aims of the ITTC, such as the American Towing Tank Conference, the Society of Naval Architects of Japan or the British Marine Hydrodynamics Panel.

The host organisation shall have overall responsibility for the organisation of the Conference.

When the host organisation is an ITTC member, the Conference organiser shall be the designated representative of the host organisation. When the host is a local association, the Conference organiser shall be the designated representative of an ITTC member organisation chosen by the association.

The Conference organiser shall be responsible for the detailed arrangements for the Conference including the preparation and publication of the Conference proceedings.

ITTC Association shall have the copyright to the Proceedings of the conference.

The arrangements, associated costs and registration fees for the Conference must be proposed by the host organisation for approval by the Executive Committee.

Participation in the Conference is by invitation only. The host organisation shall invite designated representatives of ITTC member organisations and members of technical committees and groups to the Conference. The host organisation may also invite observers and seniors to attend. The names of observers shall be proposed by their area representative. Seniors are persons now retired who have had a long association with the ITTC and whose attendance is proposed by their area representative and endorsed by the Executive Committee. The host organisation shall offer reduced registration fees to seniors.

14.1 Conference arrangements

The Conference shall include general and technical sessions.

General Sessions shall include discussion of the report of the Executive Committee and presentations of proposals from the Executive Committee for decisions by a vote of the Full Conference. The agenda and decision record of the general sessions shall be published in the proceedings of the Conference. General Sessions shall be chaired by the Chairman of the Executive Committee.

Technical sessions shall discuss the reports and recommendations of the technical committees. No discussion shall be permitted that is not directly related to the report and recommendations under consideration. The Conference proceedings shall not be used as vehicles for disseminating technical papers. Technical sessions shall be chaired by members of the Executive Committee or Advisory Council.

The Conference may also include group discussions, to provide opportunity for discussion of topics of current interest to members. The Advisory Council shall propose topics for group discussions to the Executive Committee. The Executive Committee shall choose suitably qualified individuals to organise and chair the group discussions. A summary of the discussion shall be published in the proceedings.

Designated representatives, members of technical committees and groups, observers and seniors may participate in discussions at technical sessions (including submitting written discussion) and in group discussions. Designated representatives may submit written discussion on behalf of colleagues from their organisation. Presentation of written discussion during the technical session shall be at the discretion of the session chairman. Only designated representatives of member organisations may participate in discussions at general sessions.

15. COMMUNICATIONS

The Executive Committee shall regularly communicate with member organisations on activities relating to the work of the Executive Committee, the Advisory Council and technical committees and groups and any other matters judged by the Executive Committee to be of concern to ITTC member organisations. The communications may be through the use of a web site, the publication of a newsletter or any other means chosen by the Executive Committee.

Member organisations may bring issues to the attention of the ITTC through their area representative. Members of the Advisory Council may do so at a meeting of the Advisory Council.

15.1ITTC Website

There shall be only one ITTC web site. The ITTC Secretary shall maintain the site.

The ITTC website shall provide access to:

A) Membership information, rules, procedures and guidelines, and the archive of Conference proceedings;
B) Information relating to the upcoming Conference, including location, hotels, travel, technical and social programs, and committee reports, and other documentation for discussion at the Conference.

15.2ITTC Newsletter

A newsletter may be used to communicate with member organisations. The newsletter shall be published twice a year. It shall be edited and produced by the ITTC Secretary. The newsletter may be published in paper or electronic form.

Appendix A.

Geographic areas

Area	Countries Included
Americas	Argentina, Brazil, Canada, Chile, Ecuador, Mexico, USA, Venezuela
Central Europe	Austria, Belgium, Germany, The Netherlands, United Kingdom Ireland
North and West Asia	China, Iran, Israel
Northern Europe	Denmark, Finland, Norway, Poland, Russia, Sweden Estonia
Pacific Islands	Australia, Indonesia, Japan,
Southern Europe	Bulgaria, Croatia, France, Greece, Italy, Portugal, Romania, Spain, Turkey
South and East Asia	Korea India Malaysia Vietnam Singapore

Countries not listed will be placed in an area to be decided by the Executive Committee

Appendix B.

B.1. Notes on the organisation and operation of the ITTC

This Appendix provides information to help new members of ITTC or members joining committees for the first time, understand the workings of the ITTC organisation. It includes background information, explains some rules in more detail than is appropriate in the formal rules document and includes brief descriptions of current practice.

The Appendix is supplementary to the Rules, and does not take the place of the Rules. In case of a perceived conflict between this Appendix and the Rules, the Rules shall be followed.

B.2. Definitions

In previous versions of the Rules and colloquially, the words 'International Towing Tank Conference', its initials, ITTC, and shortened form, 'Conference' have been used to mean different things depending on the context. The present Rules attempt to avoid this confusion by using these words with specific meanings:

The four letters **ITTC** means the association of organisations which functions according to these rules.

The Conference means the tri-annual meeting of ITTC member organisations.

The Full Conference means the representatives of member organisations with authority to vote.

The name "**International Towing Tank Conference**" is not used in the Rules except as the title. In other documents it may be used to mean the organisation (ITTC) or the tri-annual meeting (the Conference), depending on the context.

In addition the following three words are used in the Rules:

Shall: Conveys commitment to doing something. Of these three words, shall is used in the Rules in paragraphs which describe the operation of the ITTC.

Must: The action is mandatory; there are no alternatives; gives emphasis; stronger than shall.

May: The action is optional; the choice is up to the person performing the action.

These definitions are also used in this Appendix.

B.3. Brief history of the ITTC

In 1933 23 representatives of tanks from 10 countries including the superintendents of 9 tanks met in The Hague, to “confer in an open and confidential manner on their own methods and also on the manner of publication of tank results.” The program for the new Conference of Ship Tank Superintendents was focused on the everyday business of tanks. The conference appointed a committee to work out “in a more definite way the general conclusions.” This was the forerunner of the technical committees we have today. All decisions were made by all those present at the “the conference”.

This simple organisation continued until 1948, when a Standing Committee of six regional members was formed to give continuity from one Conference to another. it later became the Executive Committee. Up until 1948 individual Conference attendees made presentations, but from 1948 discussions at the Conference were based on reports of the technical committees. This continues to be the structure of the ITTC Conferences.

As the size and number of topics considered by the ITTC increased, there was concern that the ITTC should not evolve into a diffuse organisation loosely concerned with ship hydrodynamics. In addition, the member organisations whose primary business was model testing for clients were worried that they would be outnumbered by the tanks operated by educational and research institutions which did not share the same responsibilities to customers. There was a possibility that ITTC might adopt procedures and policies that would be harmful to the relationships between the more commercial facilities and their customers. The Advisory Council was formed at the 13th ITTC in 1972 in response to these concerns. The purpose of the Advisory Council was (and still is) to recommend the subjects to be considered “bearing in mind the primary aim of the conference is to solve technical problems of importance to tank superintendents.” Organisations represented on the Advisory Council were selected from member organisations which met criteria chosen to show that their primary business was model testing for clients. In many ways the Advisory Council represents the community of Tank Superintendents which first met in 1933.

In 2005, ITTC was granted consultative status to IMO as a Non-Government-Organisation and several ITTC technical committees have contributed to the regulation issued by IMO..

In 2017, the Full Conference decided to create an association, ITTC.A, registered in Switzerland. ITTC.A is essentially identical to ITTC in structure and ways of working, but the formal status as a legal entity enables ITTC among others to enter into cooperation with organisations such as ISO and IEC.

B.4. Aims of the ITTC

The Aims of the ITTC written in the Rules have changed very little from the aims of the ITTC expressed in the first meetings in the 1930’s. Over the years, they have been revised to keep them up to date by including numerical modelling and full-scale trials and work done by ITTC members on marine installations other than ships. The aims include stimulating relevant research in hydrodynamics, but the exchange of information concerning research in theoretical hydrodynamics and fundamental aspects of numerical fluid computations are not included. These are covered by other forums, such as the ONR Symposium on Naval Hydrodynamics or Conference on Numerical Ship Hydrodynamics. The ITTC establishes the need for research, encourages research and provides for coordination of research carried out by its members, but does not, as an organisation, fund or carry out research. The aims are written to ensure that the ITTC continues to focus on its unique role of meeting the needs of its members for giving advice and information on full-scale performance to the designers, builders and operators of ships and marine installations based on physical and numerical modelling.

B.5. The ITTC Organisation

Members

Members of the ITTC are organisations that satisfy the Executive Committee that they meet the criteria for membership stated in the Rules. (The ITTC does not have individual memberships; people participate in ITTC activities as representatives of member organisations).

Designated representatives

Designated representatives are directors or senior officers of member organisations who have authority to bind the organisation in matters relating to ITTC. Each member organisation has one designated representative.

Full Conference

Decision making authority for the ITTC rests with its member organisations. The Full Conference is the collective name of the designated representatives from member organisations present at general sessions held during the Conference. Votes taken during general sessions at the Conference are recorded as decisions of the Full Conference.

Executive Committee

The Executive Committee is in effect, the ‘governing body’ of the ITTC. The Chairman is elected by the Full Conference and is chairman of both ITTC and ITTC.A. The Executive Committee members are representatives from each of seven geographic areas. The Executive Committee implements decisions of the Full Conference and may take actions between Conferences. The agenda of the Executive Committee includes applications for membership of the ITTC, membership of technical committees, arrangements for the next Conference, financial matters and relationships with other organisations.

Chairman of the Executive Committee

The Chairman of the Executive Committee is the leader of the ITTC and chairs general sessions at the Conference.

Advisory Council

The Advisory Council drives the technical agenda of the ITTC. It is comprised of about 40 of the larger member organisations whose primary business is model testing for clients and have had a long history of involvement with the ITTC. The Advisory Council identifies topics of importance to the ITTC, drafts terms of reference for the technical committees and groups and provides ongoing support and monitoring of the technical committees as they carry out the work. It reviews proposed recommended procedures in detail, and ensures they are appropriate for practical application in work for clients. It reviews annual progress reports from technical committees.

Advisory Council Working Groups

To do its work effectively, the Advisory Council has set up four working groups. Each working group has responsibility for a technical area of importance to the ITTC. Members of the working groups are members of the Advisory Council who have an expertise or particular interest in the subjects covered by the group. The working groups take the lead in dealing with technical matters in their area of expertise and report at meetings of the Advisory Council.

Technical Committees

Technical committees carry out the technical work of the ITTC. Members of the technical committees are chosen for their ability to carry out the work. The Executive Committee chooses the Chairmen. The scope of work is defined in the terms of reference for the committee. All the technical committees have equivalent responsibilities. There is no hierarchy between technical committees. The reports of technical committees primarily contain reviews of research relevant to ITTC members and are not comparable in format or content with publications in technical journals or at other conferences.

Groups

Groups are similar to technical committees except that their work is primarily non-technical (for example symbols, quality control).

The ITTC Secretary

The ITTC Secretary is a central point of contact for communications between ITTC members and to and from organisations outside the ITTC. The ITTC Secretary undertakes secretarial tasks in support of the operation of the ITTC. The duties of the Secretary include maintaining lists of memberships, the administration and collection of membership fees, accounting and arrangement of auditing of the accounts, publishing the ITTC newsletter, maintaining the ITTC website and preparing agenda and minutes of meetings of the Executive Committee and the Advisory Council.

The Conference

The Conference is held once every three years, usually in September. The Conference agenda is based on the presentation and discussion of reports of technical committees, not presentations of papers by individuals. The plenary or general sessions are the opportunity for representatives of ITTC member organisations to discuss and for the Full Conference to vote on recommendations from the Executive Committee.

The Conference venue and host organisation are chosen to ensure a balanced rotation between geographic areas. The host organisation has overall responsibility for ensuring the Conference meets the requirements of the ITTC as described in the Rules and communicated by the Executive Committee. The detailed arrangements for the Conference are the responsibility of the Conference Organiser who is the designated representative of the host organisation. The Executive Committee must approve the arrangements and associated costs for the Conference.

Participation in the Conference is by invitation only. Invitations are sent to all designated representatives and members of technical committees and groups. In addition, area representatives may propose observers and seniors to attend. Employees of ITTC member organisations who are neither designated representatives nor members of technical committees or groups may attend the Conference as observers. Observers may also be persons with an interest in the work of the ITTC who are not affiliated with ITTC member organisations. Examples are representatives from ship designers and builders, classifications societies or other marine research organisations. Representatives of commercial companies with an interest in marketing to ITTC members may attend the Conference as observers, but no provision is made at most venues for the distribution of advertising material or product demonstrations.

Meetings

ITTC committees (including the Executive Committee and Advisory Council) meet three or four times between Conferences. The cost of attending these meetings is a significant cost to committee members' organisations and every effort is taken to minimize them. Meetings are often scheduled to coincide with major conferences likely to be attended by several committee members and the cost to the host is kept small by using in non-commercial facilities whenever possible. The high cost of long-distance air travel is distributed among members by holding meetings in different geographic areas.

ITTC Fees

Member organisations pay a membership fee by which ITTC funds are raised. The ITTC funds are used to cover the cost of the ITTC organisation, including paying for the ITTC Secretary and a proportion of the cost of publishing the proceedings of the Conference. (Conference proceedings are distributed to all members, whether they attend the Conference or not). Registration fees paid by Conference attendees cover the cost of the Conference and the remainder of the cost of the Proceedings.

Decision making process

The Full Conference is the decision-making authority for the ITTC. Decisions by technical committees, the Advisory Council and Executive Committee (other than those concerning only the internal operation of these committees or otherwise mandated by these Rules) are made as recommendations for adoption to the next level on the organisation as follows:

1) Technical committees or groups
2) Advisory Council
3) Executive Committee
4) Vote by the Full Conference

ITTC2024

30TH INTERNATIONAL TOWING TANK CONFERENCE
22–27 SEPTEMBER 2024 | HOBART TASMANIA AUSTRALIA

APPENDIX 5 MEMBER ORGANISATIONS

ARGENTINA

University de Buenos Aires

Canal de Ensayos de Arquitectura Naval (CEAN), Paseo Colón 850, Buenos Aires C1063ACV, Argentina

www.fi.uba.ar

AUSTRALIA

Australian Maritime College

National Centre for Maritime Engineering and Hydrodynamics, University of Tasmania, Locked Bag 1395, Launceston, Tasmania 7250, Australia

www.amc.edu.au

AUSTRIA

Schiffbautechnische Versuchsanstalt in Wien

Brigittenauerlände 256, A-1200 Wien, Austria

www.sva.at

BELGIUM

Flanders Maritime Laboratory

Berchemlei 115B, 2140 Antwerp, Belgium, Belgium

www.waterbouwkundiglaboratorium.be

University of Liege - ANAST

Department ArGEnCo - Sector: TLU+C, Instutut du Genie Civil, Bat. B52/3 (Niv. +1) Chemin des Chevreuils 1, B-4000 Liege 1, Belgium

www.ulg.ac.be/anast

BRAZIL

Instituto de Pesquisas Tecnológicas do Estado de São Paulo - IPT

Centro de Engenharia Naval e Oceânica, Av. Prof. Almeida Prado, 532, Cidade Universitária, Butantã, São Paulo, SP, CEP: 01333-030, Brazil

www.ipt.br

LabOceano - Brazilian Ocean Technology Laboratory

Parque Tecnológico - Quadra 07, Ilha do Fundão - Cidade Universitária, Caixa Postal: 68508, CEP: 21945 - 970 Rio de Janeiro, Brazil

www.laboceano.coppe.ufrj.br

LOC/COPPE/UFRJ

Av. Athos da Silveira Ramos, Block I, Room 104, University City, Rio de Janeiro, Brazil

joel@oceanica.ufrj.br

Numerical Offshore Tank, University of São Paulo

Av. Prof. Mello Moraes, 2231 Cidade Universitária, São Paulo, SP, Brazil - CEP05508-030, Brazil

www.tpn.usp.br

Technomar Engenharia LTDA

Avenida Pedroso de Morais, 631, CJ112- Pinheiros, São Paolo/SP, CEP: 05419-905, Brazil

ribollamasetti@technomar.com.br

BULGARIA

Bulgarian Ship Hydrodynamics Centre

William Froude Str. 1, P.O. Box 58, 9003 Varna, Bulgaria

www.bshc.bg

CANADA

Memorial University of Newfoundland

Ocean Engineering Research Centre, Faculty of Engineering and Applied Science, St. John's, NF A1B 3X5, Canada

www.engr.mun.ca/research/ocean.php

National Research Council of Canada

Ocean, Coastal and River Engineering, Arctic Avenue, P.O. Box 12093, St. John's, Newfoundland A1B 3T5, Canada

www.nrc.ca

CHILE

Universidad Austral de Chile

Campus Miraflores, General Lagos 2086, Valdivia, Chile, Chile

gonzalo.tampier@uach.cl

CHINA

China Ship Scientific Research Centre (CSSRC)

P.O. Box 116, Wuxi, Jiangsu 214082, China

www.cssrc.com.cn

Dalian University of Technology

School of Naval Architecture and Ocean Engineering, 2 Ling-gong Road, Dalian 116024, China

www.dlut.edu.cn

Harbin Engineering University

College of Shipbuilding Engineering, 145 Nantong Street, Nangang District, Harbin, Heilongjiang 150001, China

www.hrbeu.edu.cn

Huazhong University of Science and Technology

School of Naval Architecture and Ocean Engineering, Wuhan, Hubei 430074, China

www.hust.edu.cn

Jiangsu University of Science and Technology

School of Naval Architecture and Ocean Engineering, No. 2 Mengxi Road, Zhenjiang 212003, China

zhurq@just.edu.cn

Marine Design and Research Institute of China (MARIC)

1688 Xizangnan Road, Shanghai 200011, China

www.maric.com.cn

Shanghai Jiao Tong University (SJTU)

School of Naval Architecture, Ocean and Civil Engineering, 800 Dong Chuan Road, Shanghai 200240, China

www.sjtu.edu.cn

Shanghai Ship and Shipping Research Institute (SSSRI)

600 Minsheng Road, Shanghai 200135, China

www.sssri.com

Tianjin University

Ice Engineering Laboratory, Weijin Road 92, Nankai District, Tianjin 300072, China

www.tju.edu.cn

Wuhan University of Technology

School of Transportation, Yujiatou, Wuchang District, Wuhan, Hubei 430063, China

www.whut.edu.cn

Zhejiang Ocean University

Towing Tank, No. 18 Haiyuan Rd., Dinghai Dist., Zhoushan, Zhejiang Province, China

cyxy.zjou.edu.cn/info/2757/7279.htm

CROATIA

Brodarski Institute, Ship Hydrodynamics and Physical Modelling

Ave. V. Holjevca 20, HR.10020 Zagreb, Croatia

www.hrbi.hr

DENMARK

FORCE Technology

Division for Maritime Industry, Hjortekaersvej 99, 2800 Kgs. Lyngby, Denmark

www.forcetechnology.com/en

ESTONIA

Tallinn University of Technology

Ehitajate tee 5,, 19086 Tallinn, Harjumaa, Estonia

tarmo.sahk@taltech.ee

FINLAND

Aalto University

P.O.Box 5300, 02015 TKK, FIN-02015 TKK, Finland

www.tkk.fi/Units/Ship

Aker Arctic Technology Inc.

Sjöfaragatan 6, FI-00980 Helsinki, Finland

www.akerarctic.fi

VTT

Vuorimiehentie 3, Espoo, P.O. Box 1000, FIN-02044 VTT, Finland

www.vtt.fi

FRANCE

DGA Hydrodynamics

Chaussée du Vexin, BP 510, F-27105 Val de Reuil, France

www.bassin.fr

École Centrale de Nantes

LHEEA Lab., 1 Rue de la Noë, B.P. 92101, F-44321 Nantes Cedex 3, France

www.ec-nantes.fr

GERMANY

Development Centre for Ship Technology and Transport Systems

Oststrasse 77, D-47057 Duisburg, Germany

www.dst-org.de

Hamburg University of Technology

Am Schwarzenberg Campus 4C, 21073 Hamburg, Germany

www.tuhh.de/alt/skf/research-areas/ice-loads.html

Hamburgische Schiffbau-Versuchsanstalt GmbH (HSVA)

Bramfelder Strasse 164, D-22305 Hamburg, Germany

www.hsva.de

Schiffbau Versuchsanstalt Potsdam GmbH

Marquardter Chaussee 100, D-14469 Potsdam, Germany

www.sva-potsdam.de

Technische Universität Berlin

Fachgebiet Dynamik Maritimer, Systeme Institut für Land- und Seeverkehr - Bereich Schiffs- und Meerestechnik, Sekr. SG 17, Salzufer 17-19, 10587 Berlin, Germany

www.tu-berlin.de

GREECE

National Technical University of Athens

Department of Naval Architecture and Marine Engineering, 9 Heroon Polytechniou Str., Zografou, Athens, 157-73, Greece

www.naval.ntua.gr

INDIA

Naval Science and Technological Laboratory

Defence R&D Organisation, Govt of India, Vigyan Nagar, NAD Kotha Road, Visakhapatnam 530 027, Andhra Pradesh, India

www.drdo.gov.in

INDONESIA

Hydrodynamic Laboratory BRIN

Jl. Hidrodinamika, Kompleks ITS, Sukolilo, Surabaya 60002, Indonesia

www.bth.bppt.go.id

IRAN

National Iranian Marine Laboratory (NIMALA)

Babaie Highway, Tehran, I.R. Iran, Iran

www.nimala.ir

ISRAEL

CAMERI - Coastal and Marine Engineering Research Institute

Technion City, Haifa 32004, Israel

sea21@technion.ac.il

ITALY

Centro Esperienze Idrodinamiche Marina Militare (CEIMM)

Ministero Difesa Marina, Via di Vallerano 149, I-00196 Roma, Italy

www.marina.difesa.it/ceimm

Centro per gli Studi di Tecnica Navale (CETENA)

Via Ippolito d'Aste 5, I-16121 Genova, Italy

www.cetena.it

CNR-INM

Via di Vallerano 139, I-00128 Roma, Italy

www.inm.cnr.it

Università de Genova

Dipartimento di Ingegneria Navale,Elettrica, Elettronica e delle Telecomunicazioni-DITEN, Via all'Opera Pia 11A, I-16145 Genova, Italy

dinav.unige.it

Università di Napoli

Dipartimento di Ingegneria Industriale (Sezione Navale), Via Claudio 21, I-80125 Napoli, Italy

www.din.unina.it

Università di Trieste

Department of Engineering and Architecture, Building C5, University of Trieste, Via A. Valerio 10, I-34127 Trieste, Italy

www.dinma.univ.trieste.it

JAPAN

Akishima Laboratories (Mitsui Zosen) Inc.

1-1-50, Tsutsujigaoka, Akishima City, Tokyo 196-0012, Japan

www.mes.co.jp/Akiken/index-j.html

Hiroshima University

Department of Social & Environmental Engineering, 1-4-1, Kagamiyama, Higashi-Hiroshima 739-8527, Japan

www.naoe.hiroshima-u.ac.jp

Imabari Ship Model Basin

Showa-Cho 30, Marugame, Kagawa Pref., 763-8511, Japan

shimizu.nobuyuki@imazo.com

Japan Marine United Corporation

Technical Research Center, Hydrodynamics Research Group 1-3, Kumozukokan-cho, Tsu-City, Mie-pref. 514-0398, Japan

www.jmuc.co.jp/en/

Kawasaki Marine Engineering Co. Ltd., Akashi Ship Model Basin

3-1, Kawasaki-cho, Akashi-City, 673-0014, Japan

www.asmb.co.jp

Kobe University

Graduate School of Marine Sciences, 5-1-1 Fukoeminami, Higashinadaku, Kobe 658-0022, Japan

www.maritime.kobe-u.ac.jp

Kyushu University - NAMS

Department of Naval Architecture and Marine Systems Engineering, 744 Motooka, Nishishi-ku, Fukuoka 819-0395, Japan

www.nams.kyushu-u.ac.jp

Kyushu University - Research Institute for Applied Mechanics

6-1 Kasuga-koen, Kasuga-Shi, Fukuoka 816–8580, Japan

hu@riam.kyushu-u.ac.jp

Meguro Model Basin

Naval Sytstems Research Center, Technical Research and Development Institute, Ministry of Defense, 2-2-1 Nakameguro, Meguro-Ku, Tokyo 153-8630, Japan

cs.trdi.mod.go.jp

Mitsubishi Heavy Industries, Ltd.

Nagasaki Experimental Tank, 3-48 Bunkyo-machi, Nagasaki 852-8131, Japan

www.mhi.com

Nagasaki Institute of Applied Science

536 Amiba-cho Nagasaki-shi, Nagasaki 851-0193, Japan

www.nias.ac.jp

National Maritime Research Institute

6-38-1 Shinkawa, Mitaka-City, Tokyo 181-0004, Japan

www.nmri.go.jp

National Research Institute of Fisheries Engineering

Fishing Research Agency, 7620-7 Hasaki Kamisu Ibaraki, Ibaraki 314-0408, Japan

www.nrife.affrc.go.jp

Osaka Metropolitan University

Department of Marine System Engineering, 1-1 Gakuen-cho, Nakaku, Sakai, Osaka 599-8531, Japan

www.marine.osakafu-u.ac.jp

Osaka University

Department of Naval Architecture and Ocean Engineering, 2-1 Yamadaoka, Suita, Osaka 565-0871, Japan

www.naoe.eng.osaka-u.ac.jp

Shipbuilding Research Centre of Japan

KICHIJOJI SUBARU Building, 1-6-1 Kichijoji minamimachi-cho, Musashino, Tokyo 180-0003, Japan

www.srcj.or.jp

Sumitomo Heavy Industries

Marine&Engineering Co., Ltd., 19, Natsushima-cho, YOKOSUKA, Kanagawa 237-8555, Japan

www.shi.co.jp

Tokyo University of Marine Science and Technology

2-1-6 Etchujima,Koto-ku, Tokyo 135-8533, Japan

www.kaiyodai.ac.jp

University of Tokyo

Institute of Industrial Science, Common Research Laboratory, Research and Testing Complex II, Kashiwanoha 5-1-5, Kashiwa-shi, Chiba 277-8574, Japan

mefe.iis.u-tokyo.ac.jp/daisuke_e.html

Yokohama National University

Department of Naval Architecture and Ocean Engineering, 79-5 Tokiwadai, Hodogaya-ku, Yokohama 240-8501, Japan

www.ynu.ac.jp

KOREA

Changwon National University

Building 56,, 20 Changwondaehak-ro, Uichang-gu, Changwon-si, Gyeongsagnam-do, Korea

hkyoon@changwon.ac.kr

Hanwha Ocean

96, Baegot 2-ro, Siheung-si, Gyeonggi-do, Korea

yblee@hanwha.com

Hyundai Heavy Industries Co. Ltd.

Hyundai Maritime Research Institute, 1000, Bangeojinsunhwan-doro, Dong-gu, Ulsan 44032, Korea

www.hhi.co.kr

Inha University

Department of Naval Architecture and Ocean Engineering, 253-Yonghyun-Dong, Nam-Ku, Inchon 402-751, Korea

www.naoe.inha.ac.kr

Korea Research Institute of Ships and Ocean Engineering (KRISO, formerly MOERI)

1312-32 Yuseong-daero, Yuseong-gu, Daejeon 34103, Korea

www.kriso.re.kr

Pusan National University

Department of Naval Architecture and Ocean Engineering, San 30 Changjon-Dong, Kumjong-Ku, Pusan 609-735, Korea

www.pusan.ac.kr

Research Institute of Medium & Small Shipbuilding (RIMS)

23, Mieumsandan, 5-ro 42beon-gil, Gangseo-gu, Busan, Korea

csshin@rims.re.kr

Samsung Heavy Industries

Samsung Heavy Industries Co. Ltd., 103-28, Munji-dong, Yuseong-gu, Daejeon, 305-380, Korea

www.shi.samsung.co.kr

Seoul National University

Department of Naval Architecture and Ocean Engineering, 1 Gwanak-ro, Gwanak-gu, Seoul 151-744, Korea

naoe3.snu.ac.kr

University of Ulsan

School of Naval Architecture and Ocean Engineering, San 29 Moogeo-Dong, Nam-Ku, Ulsan 680-749, Korea

naoe.ulsan.ac.kr

MALAYSIA

Universiti Teknologi Malaysia

Marine Technology Centre, 81300 Skudai, Johore, Malaysia

www.fkm.utm.my/marine

NORWAY

SINTEF Ocean (formerly MARINTEK)

P.O. Box 4125, Valentinlyst, N-7002 Trondheim, Norway

www.sintef.no

Stadt Towing Tank

N-6718 Deknepollen, Norway

www.stadttowingtank.no

POLAND

Gdansk University of Technology

Faculty of Mechanical Engineering and Ship Technology, ul. Gabriela Narutowicza 11/12, 80-233 Gdansk, Poland

www.wimio.pg.edu.pl

Maritime Advanced Research Centre(CTO S.A.)

65 Szczecinska St, 80-392 Gdansk, Poland

www.cto.gda.pl

ROMANIA

University of Galati

Domneasca Street 47, 800008 Galati, Romania

florin.pacuraru@ugal.ro

SINGAPORE

Technology Centre for Offshore and Marine, Singapore (TCOMS)

12, Prince George's Park, #04-01, Singapore 118411, Singapore

kylim@tcoms.sg

SPAIN

Canal de Experiencias Hidroninámicas de El Pardo (CEHIPAR)

Carretera de la Sierra s/n, 24048 El Pardo-Madrid, Spain

www.inta.es/icts-cehipar/es/inicio/

Escuela Técnica Superior de Ingenieros Navales (ETSIN)

Universidad Politécnica de Madrid, Avda Arco de la Victoria s/n, 28040 Madrid, Spain

www.etsin.upm.es

SWEDEN

Kongsberg Hydrodynamic Research Centre

P.O. Box 1010, SE-68129 Kristinehamn, Sweden

www.rolls-royce.com

RISE

P.O. Box 24001, SE-400 22 Göteborg, Sweden

www.sspa.se

THE NETHERLANDS

Maritime Research Instutute Netherlands (MARIN)

P.O. Box 28, NL-6700 AA Wageningen, The Netherlands

www.marin.nl

TURKEY

Istanbul Technical University

Naval Architecture and Ocean Engineering, 34469 Maslak Istanbul, Turkey

nutkulab.itu.edu.tr

UNITED KINGDOM

Newcastle University

School of Marine Science and Technology, Armstrong Building, Queen Victoria Road, Newcastle Upon Tyne, NE1 7RU, United Kingdom

www.ncl.ac.uk/engineering

QinetiQ

Maritime Platforms, Haslar Marine Technology Park, Haslar Road, Gosport, Hampshire, PO12 2AG, United Kingdom

www.qinetiq.com

University College London

Torrington Place, London WC1E 7JE, United Kingdom

www.ucl.ac.uk

University of Southampton

B176, 3027 Boldrewood Innovation Campus, Faculty of Engineering and Environment, University of Southampton, Southampton, SO16 7QF, United Kingdom

www.southampton.ac.uk/research/facilities/towing-tank

University of Strathclyde

Department of Naval Architecture, Ocean and Marine Engineering, HD3.19, Henry Dyer Building, 100 Montrose Street, Glasgow, G4 0LZ, United Kingdom

www.strath.ac.uk/naome/

USA

Applied Research Labratory

Pennsylvania State University, P.O. Box 30, Mailstop 3300B, State College, PA, 16801-0030, USA

www.arl.psu.edu

IIHR-Hydroscience & Engineering

University of Iowa, Iowa City, IA 52242-1585, USA

www.iihr.uiowa.edu

Naval Surface Warfare Center, Carderock Division

David Taylor Model Basin, 9500 MacArthur Blvd., W. Bethesda, MD 20817-5700, USA

www.dt.navy.mil

United States Naval Academy

Hydromechanics Laboratory, 590 Holloway Road, Annapolis, MD 21402, USA

www.usna.edu/Hydromechanics/index.php

University of Michigan

Department of Naval Architecture and Marine Engineering, 2600 Draper Road, Ann Arbor, MI 48109-2145, USA

www.mhl.engin.umich.edu

University of New Orleans

School of Naval Architecture and Marine Engineering, 2000 Lakeshore Drive, Engineering Building 911, New Orleans, LA 70148, USA

www.uno.edu/~engr/towtank

ITTC2024

30TH INTERNATIONAL TOWING TANK CONFERENCE
22–27 SEPTEMBER 2024 | HOBART TASMANIA AUSTRALIA

APPENDIX 6
ITTC MEMBERS AND OBSERVERS INVITED TO ATTEND THE 30TH ITTC CONFERENCE

Ayhan	Akinturk	National Research Council of Canada	Canada
Patrik	Almstroem	Qualisys AB	Sweden
Francisco	Alves Pereira	Institute of Marine Engineering	Italy
Jun	Ando	Kyushu University	Japan
Hiroshi	Arai	Japan Marine United Corporation	Japan
Shawn	Aram	Naval Surface Warfare Center Carderock Division	United States
Joseph	Banks	University of Southampton	United Kingdom
Vadim	Belenky	NSWCCD	United States
Trystan	Bennett	hr wallingford	United Kingdom
Petter Andreas	Berthelsen	SINTEF Ocean	Norway
Jonathan	Binns	Defence Science and Technology Group	Australia
Pavel	Bogachko	Qualisys AB	Singapore
Romuald	Boucheron	DGA Techniques Hydrodynamiques	France
Evangelos	Boulougouris	University of Strathclyde	United Kingdom
Riccardo	Broglia	CNR-INM	Italy
Shuxia	Bu	China Ship Scientific Research Center	China
Shuling	Chen	Jiangsu University of Science and Technology	China
Weimin	Chen	Shanghai Ship and Shipping Research Institute	China
Xide	Cheng	Wuhan University of Technology	China
Soonho	Choi	Samsung Heavy Industries	South Korea
Maurizio	Collu	University of Strathclyde	United Kingdom
Corino	Corver	Van Halteren Technologies B.V.	Netherlands
Paul	Crossland	QinetiQ Ltd	United Kingdom
Aage	Damsgaard	Force Technology	Denmark

Johan	De Jong	Marin	Netherlands
Martin	Donnelly	NSWCCD	United States
Peiyuan	Feng	Marine Design and Research Institute of China	China
Didier	Frechou	DGA Techniques Hydrodynamiques	France
Yoshitaka	Furukawa	Kyushu University	Japan
Stefano	Gaggero	University of Genoa	Italy
Yuling	Gao	Shanghai Ship and Shipping Research Institute	China
Frederik	Gerhardt	Research Institutes of Sweden	Sweden
Davide	Grande	University College London	United Kingdom
Gregory	Grigoropoulos	NTUA	Greece
Lars	Gustafsson	Research Institutes of Sweden	Sweden
Chunrong	He	China Ship Scientific Research Center	China
Ole Andreas	Hermundstad	SINTEF Ocean	Norway
Keyyong	Hong	KRISO	South Korea
Peter	Horn	Hamburgische Schiffbau Versuchsanstalt	Germany
Qiaogao	Huang	Northwestern Polytechnical University	China
Dominic	Hudson	University of Southampton	United Kingdom
Ahmed	Ibrahim	United States Naval Academy	United States
Takuro	Ikebuchi	Imabari Shipbuilding Co Ltd	Japan
Takehiro	Ikeda	Akishima Laboratories (Mitsui Zosen) Inc	Japan
Yasuhiko	Inukai	Japan Marine United Corporation	Japan
Yichen	Jiang	Dalian University of Technology	China
Xue	Jiang	Zhejiang Ocean University	China
Sun	Jianglong	Huazhong University of Science and Technology	China
Carolyn	Judge	United States Naval Academy	United States
Kwanghyo	Jung	Pusan National University	South Korea
Toru	Katayama	Osaka Metropolitan University	Japan
Tokihiro	Katsui	Kobe University	Japan
Byoungguk	Kim	Hanwha Ocean	South Korea
Minwoo	Kim	Hyundai Heavy Industries	South Korea
Dong-jin	Kim	Korea Research Institute of Ships and Ocean Engineering	South Korea
Kyong-Hwan	Kim	KRISO	South Korea
Taeyoung	Kim	Samsung Heavy Industries	South Korea
Yonghwan	Kim	Seoul National University	South Korea
Takashi	Kishimoto	Akishima Laboratories (Mitsui Zosen) Inc	Japan
Daisuke	Kitazawa	The University of Tokyo	Japan
Seppo	Kivimaa	VTT Technical Research Centre of Finland Ltd	Finland
Kourosh	Koushan	SINTEF Ocean	Norway
Niklas	Kühl	Hamburg Ship Model Basin	Germany

Kenichi	Kume	National Maritime Research Institute	Japan
Mariko	Kuroda	National Maritime Research Institute	Japan
Youngbum	Lee	Hanwha Ocean Limited	South Korea
Hyun-ho	Lee	HD Hyundai Heavy Industries	South Korea
Inwon	Lee	Pusan National University	South Korea
Jean-Francois	Leguen	DGA Techniques Hydrodynamiques	France
Zeng	Liu	Huazhong University of Science and Technology	China
Yi	Liu	Marine Design and Research Institute of China	China
Yang	Luo	Northwestern Polytechnical University	China
Gregor	Macfarlane	Australian Maritime College	Australia
Kevin	Maki	University of Michigan	United States
Hayden	Marcollo	AMOG Consulting	Australia
Nikolay	Markov	Bulgarian Ship Hydrodynamics Centre	Bulgaria
Jussi	Martio	VTT Technical Research Centre of Finland Ltd	Finland
Christian	Masilge	Schiffbau-Versuchsanstalt Potsdam GmbH	Germany
Reeta Riikka Inkeri	Matala	Aker Arctic Technology Inc	Finland
Akihiko	Matsuda	National Research Institute of Fisheries Engineering	Japan
Daisuke	Matsumoto	Mitsubishi Heavy Industries Ltd	Japan
Bryson	Metcalf	NSWCCD	United States
Thad	Michael	NSWCCD	United States
Takashi	Mikami	Akishima Laboratories (Mitsui Zosen) Inc	Japan
Munehiko	Minoura	Osaka University	Japan
Takayuki	Mori	Meguro Model Basin	Japan
Motohiko	Murai	Yokohama National University	Japan
Bo Woo	Nam	Seoul National University	South Korea
John Koch	Nielsen	Force Technology	Denmark
Semyun	Oh	Samsung Heavy Industries	South Korea
Hideo	Orihara	Japan Marine United Corporation	Japan
Michelle	Otero	NSWCCD	United States
Janne Flensborg	Otzen	Force Technology	Denmark
Kwang-Jun	Paik	Inha University	South Korea
Joel	Park	NSWCCD	United States
Neil	Patterson	Defence Science and Technology Group	Australia
Marta	Pedisic Buca	Croatian Shipbuilding Corporation (Brodarski Institute)	Croatia
Heather	Peng	Memorial University	Canada
Francisco Javier	Pérez Villalonga	INTA/CEHIPAR	Spain
Luis	Perez-rojas	Universidad Politécnica de Madrid. ETSI Navales	Spain
Andrew	Peters	QinetiQ	United Kingdom
Wei	Qiu	Memorial University	Canada

Arthur	Reed	NSWCCD	United States
Martin	Renilson	University of Tasmania	Australia
Claudio	Rodríguez	LabOceano - Brazil / Fundação COPPETEC	Brazil
Shaun	Ross	hr wallingford	United Kingdom
Pedro Luis	Sanchez Gonzalez	INTA/CEHIPAR	Spain
Ilkka	Saisto	Aker Arctic Technology Inc	Finland
Kei	Sato	Mitsubishi Heavy Industries Ltd	Japan
Daniel	Sgarioto	Defence Science and Technology Group	Australia
Weichao	Shi	Newcastle University	United Kingdom
Nobuyuki	Shimizu	Imabari Ship Model Basin	Japan
Shoji	Shingo	Shipbuilding Research Centre of Japan	Japan
Claus	Simonsen	Force Technology	Denmark
Lei	Song	Huazhong University of Science and Technology	China
Callum	Stevens	AMOG Consulting	Australia
William	Straka	Applied Research Laboratory - Penn State University	United States
Gerhard	Strasser	ITTC	Austria
Clemens	Strasser	Vienna Model Basin Ltd	Austria
Gijs	Struijk	Marin	Netherlands
Jianglong	Sun	Huazhong University of Science and Technology	China
Jianqiao	Sun	Tianjin University	China
Gonzalo	Tampier	Universidad Austral De Chile	Chile
Neil	Thompson	QinetiQ	United Kingdom
Yukui	Tian	China Ship Scientific Research Center	China
Masaru	Tsujimoto	National Institute of Maritime, Port and Aviation Technology	Japan
Stephen	Turnock	University of Southampton	United Kingdom
Naoya	Umeda	Osaka Metropolitan University	Japan
I Ketut Aria Pria	Utama	Institut Teknologi Sepuluh Nopember	Indonesia
Shotaro	Uto	Hokkaido University	Japan
Thibaut	Van Zwijnsvoorde	Flanders Hydraulics	Belgium
Michiel	Verhulst	Marin	Netherlands
Diego	Villa	University of Genova	Italy
Decheng	Wan	Shanghai Jiao Tong University	China
Zhaohui	Wang	Directorate Navy Engineering	Australia
Jungyong	Wang	National Research Council Canada	Canada
Sofia	Werner	Research Institutes of Sweden	Sweden
Michael	Woodward	University of Tasmania	Australia
Chengsheng	Wu	China Ship Scientific Research Center	China
Rui	Wu	Shanghai Ship and Shipping Research Institute	China
Longfei	Xiao	Shanghai Jiao Tong University	China

Gongzheng	Xin	China Ship Scientific Research Center	China
Sujun	Yang	Marine Design and Research Institute of China	China
Pengcheng	Ye	Northwestern Polytechnical University	China
Dong Jin	Yeo	Korea Research Institute of Ships and Ocean Engineering	South Korea
Zhiming	Yuan	University of Strathclyde	United Kingdom
Zhicheng	Zhang	Huazhong University of Science and Technology	China
Jian	Zhang	Jiangsu University of Science and Technology	China
Xinshu	Zhang	Shanghai Jiao Tong University	China
Feng	Zhao	China Ship Scientific Research Center	China
Weiwen	Zhao	Shanghai Jiao Tong University	China
Renqing	Zhu	Jiangsu University of Science and Technology	China
Renchuan	Zhu	Shanghai Jiao Tong University	China

VOLUME 1

ISBN 978-3-03931-000-5